Volume 51 Numbers 17–19 2004 ISSN 0967-0645

SEVIER

DEEP-SEA RESEARCH

PART II

n D. Milliman

Editors:
. Hofmann
. Wiebe
. Costa
. Torres

Integrated Ecosystem Studies of Western Antarctic Peninsula Continental Shelf Waters and Related Southern Ocean Regions

Library
Pacific Islands Fisheries Science Center
Nat'l Marine Fisheries Service
Received Feb 2005

DEEP-SEA RESEARCH II

http://www.elsevier.com/locate/dsr2

Editor

PROFESSOR JOHN D. MILLIMAN: *Virginia Institute of Marine Science, School of Marine Science, The College of William and Mary, P.O. Box 1346, Gloucester Point, VA 23062–1346, USA*
E-mail: milliman@vims.edu

Associate Editors

J.W. MURRAY (*Chemistry*): *School of Oceanography, WB-10, University of Washington, Seattle, WA 98195, U.S.A. E-mail: jmurray@ocean.washington.edu*

FRIEDRICH A. SCHOTT: *Institut für Meereskunde an der Universität Kiel, Düsternbrooker Weg 20, D-24105 Kiel, Germany. E-mail: fschott@ifm.uni-kiel.de*

SHARON L. SMITH: *The Rosenstiel School, University of Miami, 4600 Rickenbacker Causeway, Miami, FL 33149, USA. E-mail: ssmith@rsmas.miami.edu*

Founder Editor: DR. MARY SEARS

Publishing Offices Elsevier Ltd, The Boulevard, Langford Lane, Kidlington, Oxford OX5 1GB, UK. Tel: +44(0) 1865 843000; Fax: + 44(0) 1865 843010.

Advertising information. Advertising orders and enquiries can be sent to: ***USA, Canada and South America:*** Mr Tino DeCarlo, The Advertising Department, Elsevier Inc., 360 Park Avenue South, New York, NY 10010-1710, USA; phone: (+1) (212) 633 3815; fax: (+1) (212) 633 3820; e-mail: t.decarlo@elsevier.com. ***Europe and ROW:*** Katrina Barton, Advertising Department, Elsevier Ltd., 84 Theobald's Road, London WC1X 8RR, UK; phone (+44) 207 611 4117; fax: (+44) 207 611 4463; e-mail: k.barton@elsevier.com

USA mailing notice: *Deep-Sea Research II* (ISSN 0967-0645) is published annually in 26 issues by Elsevier Ltd. (P.O. Box 211, 1000 AE Amsterdam, The Netherlands). Annual subscription price in the USA US$ 3152 (valid in North, Central and South America), including air speed delivery.
USA POSTMASTER: Send address changes to *Deep-Sea Research II*, 655, Avenue of the Americas, New York, NY 10010.
AIRFREIGHT AND MAILING in the USA by Publications Expediting Inc., 200 Meacham Avenue, Elmont, NY 11003. Periodical postage rate paid at Jamaica, NY 11431.

Subscription Information

Published annually in 26 issues. Information on published and forthcoming issues can be found at the journal website.

Publication information: *Deep-Sea Research Part II* (ISSN 0967–0645). For 2004, volume 51 is scheduled for publication. Subscription prices are available upon request from the Publisher or from the Regional Sales Office nearest you or from this journal's website (http://www.elsevier.com./locate/dsr2). Further information is available on this journal and other Elsevier products through Elsevier's website: (http://www.elsevier.com). Subscriptions are accepted on a prepaid basis only and are entered on a calendar year basis. Issues are sent by standard mail (surface within Europe, air delivery outside Europe). Priority rates are available upon request. Claims for missing issues should be made within six months of the date of despatch.

Author enquiries. For enquiries relating to the submission of articles (including electronic submission), the preparation of electronic artwork, the status of accepted articles, author Frequently Asked Questions and any other enquiries relating to Elsevier, please consult http://authors.elsevier.com
Contact details for questions arising after acceptance of an article, especially those relating to proofs, are provided when an article is accepted for publication. Authors can also keep a track on the progress of their accepted article, and set up e-mail alerts informing them of changes to their manuscripts status, by using the "Track a paper" feature of Elsevier's Author Gateway (http: //authors.elsevier.com).

Orders, claims, and journal enquiries: please contact the Customer Service Department at the Regional Sales Office nearest you:
Orlando: Elsevier, Customer Service Department, 6277 Sea Harbor Drive, Orlando, FL 32887-4800, USA; phone: (+1) (877) 8397126 [toll free number for US customers], or (+1) (407) 3454020 [customers outside US]; fax: (+1) (407) 3631354; e-mail: usjcs@elsevier.com
Amsterdam: Elsevier, Customer Service Department, PO Box 211, 1000 AE Amsterdam, The Netherlands; phone: (+31) (20) 4853757; fax: (+31) (20) 4853432; e-mail: nlinfo-f@elsevier.com
Tokyo: Elsevier, Customer Service Department, 4F Higashi-Azabu, 1-Chome Bldg, 1-9-15 Higashi-Azabu, Minato-ku, Tokyo 106-0044, Japan; phone: (+81) (3) 5561 5037; fax: (+81) (3) 5561 5047; e-mail: jp.info@elsevier.com
Singapore: Elsevier, Customer Service Department, 3 Killiney Road, #08-01 Winsland House I, Singapore 239519; phone: (+65) 63490222; fax: (+65) 67331510; e-mail: asiainfo@elsevier.com

♾The paper used in this publication meets the requirements of ANSI/NISO Z39. 48-1992 (Permanence of Paper).

© **2004 Elsevier Ltd. All rights reserved.**

Back Issues: Back issues of all previously published volumes are available direct from Elsevier Offices. Complete volumes and single issues can be purchased for 1999–2003. Earlier issues are available in high quality photo-duplicated copies as complete volumes only. Back volumes on microfilm are available from UMI, 300 North Zeeb Road, Ann Arbor, MI 48106-1346, USA.

Cover image: These seven images illustrate the breath and integrated multidisciplinary nature of the Southern Ocean Global Ocean Ecosystem Dynamics (SO GLOBEC) program that is reflected in the papers in this volume, and are from left to right, top row: a crabeater seal (*Lobodon carcinophagus*) with a Platform Transmitter Terminal satellite tag attached, the program target species Antarctic krill (*Euphausia superba*); an Adélie penguin (*Pygoscelis adeliae*) with an attached satellite transmitter tag; the two research vessels used for the U.S. SO GLOBEC program, the ARSV *Laurence M. Gould* (foreground) and the RVIB *Nathaniel B. Palmer* (background); the Bio-optical Multifrequency Acoustical and Physical Environmental Recorder (BIOMAPER-II) that was used for hydroacoustic surveys; the sea ice measurement team working at a process station site; and deployment of the Rosette/conductivity-temperature-depth instrument to obtain environmental measurements. Photographs were provided by D. Costa (panels 1, 4 and 6), S. Nicol (panel 2), B. Salihoğlu (panel 3), G. Lawson (panel 5), and K. Daly (panel 7).

DEEP-SEA RESEARCH

PART II

Topical Studies in Oceanography

Integrated Ecosystem Studies of Western Antarctic Peninsula Continental Shelf Waters and Related Southern Ocean Regions

Guest Editors

Eileen E. Hofmann
Center of Coastal Physical Oceanography
Old Dominion University
Norfolk, VA 23529, USA

Peter H. Wiebe
Department of Biology
Woods Hole Oceanographic Institution
Woods Hole, MA 02543, USA

Daniel P. Costa
Department of Biology
University of California, Santa Cruz
Santa Cruz, CA 95064, USA

Joseph J. Torres
College of Marine Science
University of South Florida
140 Seventh Avenue South
St. Petersburg, FL 33701, USA

ELSEVIER

STATEMENT POLICY

Deep-Sea Research Part II: Topical Studies in Oceanography Publishes the topical issues arising from the many international and interdisciplinary projects which are undertaken.

Shorter research papers are welcomed for *Deep-Sea Research Part I: Oceanographic Research Papers*. Acceptable topics for papers include:

(1) the results of original scientific research
(2) theoretical work of evident oceanographic applicability
(3) the solution of some instrumental or laboratory problem with evidence of its successful use, and
(4) applications of oceanography.

Papers dealing with research on continental shelves (water depths shallower than 100–200 m) in most cases should be submitted to our sister journal *Continental Shelf Research*.

Progress reports and review articles may be invited by the Editor but these are generally more appropriate for *Progress in Oceanography*.

© **2004 Elsevier Ltd. All rights reserved.**

This journal and the individual contributions contained in it are protected under copyright by Elsevier Ltd, and the following terms and conditions apply to their use:

Photocopying
Single photocopies of single articles may be made for personal use as allowed by national copyright laws. Permission of the publisher and payment of a fee is required for all other photocopying, including multiple or systematic copying, copying for advertising or promotional purposes, resale, and all forms of document delivery. Special rates are available for educational institutions that wish to make photocopies for non-profit educational classroom use.

Permissions may be sought directly from Elsevier Global Rights Department, P.O. Box 800, Oxford OX5 1DX, UK; phone: (+44) 1865 843830, fax: (+44) 1865 853333, e-mail: permissionselsevier.co.uk. You may also contact Global Rights directly through Elsevier's home page (http://www.elsevier.com), by selecting 'Obtaining Permissions'.

In the USA, users may clear permissions and make payments through the Copyright Clearance Center, Inc., 222 Rosewood Drive, Danvers, MA 01923, USA; phone: (+1) (978) 7508400, fax: (+1) (978) 7504744, and in the UK through the Copyright Licensing Agency Rapid Clearance Service (CLARCS), 90 Tottenham Court Road, London W1P 0LP, UK; phone: (+44) 20 7631 5555; fax: (+44) 20 7631 5500. Other countries may have a local reprographic rights agency for payments.

Derivative Works
Subscribers may reproduce tables of contents or prepare lists of articles including abstracts for internal circulation within their institutions. Permission of the publisher is required for resale or distribution outside the institution.

Permission of the publisher is required for all other derivative works, including compilations and translations.

Electronic Storage or Usage
Permission of the Publisher is required to store electronically any material contained in this journal, including any article or part of an article.

Except as outlined above, no part of this publication may be reproduced, stored in a retrieval system or transmitted in any form or by any means, electronic, mechanical, photocopying, recording or otherwise, without prior written permission of the publisher.

Address permissions requests to: Elsevier Global Rights Department, at the mail, fax and e-mail addresses noted above:

Notice
No responsibility is assumed by the Publisher for any injury and/or damage to persons or property as a matter of products liability, negligence or otherwise, or from any use or operation of any methods, products, instructions or ideas contained in the material herein. Because of rapid advances in the medical sciences, in particular, independent verification of diagnoses and drug dosages should be made.

Although all advertising material is expected to conform to ethical (medical) standards, inclusion in this publication does not constitute a guarantee or endorsement of the quality or value of such product or of the claims made of it by its manufacturer.

Integrated Ecosystem Studies of Western Antarctic Peninsula Continental Shelf Waters and Related Southern Ocean Regions

Volume 51 Nos. 17–19, 2004

CONTENTS

		Editorial
E.E. Hofmann, P.H. Wiebe, D.P. Costa and J.J. Torres	1921	An overview of the Southern Ocean Global Ocean Ecosystems Dynamics program
		The Physical/Biological Setting
J.M. Klinck, E.E. Hofmann, R.C. Beardsley, B. Salihoglu and S. Howard	1925	Water-mass properties and circulation on the west Antarctic Peninsula Continental Shelf in Austral Fall and Winter 2001
R.C. Beardsley, R. Limeburner and W.B. Owens	1947	Drifter measurements of surface currents near Marguerite Bay on the western Antarctic Peninsula shelf during austral summer and fall, 2001 and 2002
S.L. Howard, J. Hyatt and L. Padman	1965	Mixing in the pycnocline over the western Antarctic Peninsula shelf during Southern Ocean GLOBEC
Y.M. Serebrennikova and K.A. Fanning	1981	Nutrients in the Southern Ocean GLOBEC region: variations, water circulation, and cycling
M.S. Dinniman and J.M. Klinck	2003	A model study of circulation and cross-shelf exchange on the west Antarctic Peninsula continental shelf
D.K. Perovich, B.C. Elder, K.J. Claffey, S. Stammerjohn, R. Smith, S.F. Ackley, H.R. Krouse and A.J. Gow	2023	Winter sea-ice properties in Marguerite Bay, Antarctica
G.L. Lawson, P.H. Wiebe, C.J. Ashjian, S.M. Gallager, C.S. Davis and J.D. Warren	2041	Acoustically-inferred zooplankton distribution in relation to hydrography west of the Antarctic Peninsula
C.J. Ashjian, G.A. Rosenwaks, P.H. Wiebe, C.S. Davis, S.M. Gallager, N.J. Copley, G.L. Lawson and P. Alatalo	2073	Distribution of zooplankton on the continental shelf off Marguerite Bay, Antarctic Peninsula, during Austral Fall and Winter, 2001
M. Zhou, Y. Zhu and J.O. Peterson	2099	In situ growth and mortality of mesozooplankton during the austral fall and winter in Marguerite Bay and its vicinity
		Krill feeding, growth, development, and overwintering studies
M. Zhou and R.D. Dorland	2119	Aggregation and vertical migration behavior of *Euphausia superba*

K.L. Daly	2139	Overwintering growth and development of larv *Euphausia superba*: an interannual comparis under varying environmental conditions west the Antarctic Peninsula
R.M. Ross, L.B. Quetin, T. Newberger and S.A. Oakes	2169	Growth and behavior of larval krill (*Euphaus superba*) under the ice in late winter 2001 west the Antarctic Peninsula
E.A. Pakhomov, A. Atkinson, B. Meyer, B. Oettl and U. Bathmann	2185	Daily rations and growth of larval krill *Euphaus superba* in the Eastern Bellingshausen Sea durin austral autumn
S.-J. Ju and H.R. Harvey	2199	Lipids as markers of nutritional condition and die in the Antarctic krill *Euphausia superba* an *Euphausia crystallorophias* during austral winter
S. Nicol, P. Virtue, R. King, S.R. Davenport, A.F. McGaffin and P. Nichols	2215	Condition of *Euphausia crystallorophias* off Eas Antarctica in winter in comparison to othe seasons
J. Donnelly, H. Kawall, S.P. Geiger and J.J. Torres	2225	Metabolism of Antarctic micronektonic crustace across a summer ice-edge bloom: respiration composition, and enzymatic activity
		Krill predator studies: seabirds, seals, whales, an midwater fish
T.M. Lancraft, K.R. Reisenbichler, B.H. Robison, T.L. Hopkins and J.J. Torres	2247	A krill-dominated micronekton and macrozoo plankton community in Croker Passage, Antarc tica with an estimate of fish predation
E.W. Chapman, C.A. Ribic and W.R. Fraser	2261	The distribution of seabirds and pinnipeds i Marguerite Bay and their relationship to physica features during austral winter 2001
J.M. Burns, D.P. Costa, M.A. Fedak, M.A. Hindell, C.J.A. Bradshaw, N.J. Gales, B. McDonald, S.J. Trumble and D.E. Crocker	2279	Winter habitat use and foraging behavior o crabeater seals along the Western Antarctic Peninsula
N.J. Gales, W.R. Fraser, D.P. Costa and C. Southwell	2305	Do crabeater seals forage cooperatively?
D. Thiele, E.T. Chester, S.E. Moore, A. Širovic, J.A. Hildebrand and A.S. Friedlaender	2311	Seasonal variability in whale encounters in the Western Antarctic Peninsula
A. Širović, J.A. Hildebrand, S.M. Wiggins, M.A. McDonald, S.E. Moore and D. Thiele	2327	Seasonality of blue and fin whale calls and the influence of sea ice in the Western Antarctic Peninsula

CONTENTS Direct

This journal is part of **ContentsDirect**, the ***free*** alerting service which sends tables of contents by e-mail for Elsevier books and journals. You can register for **ContentsDirect** online at: **www.elsevier.com/locate/contentsdirect**

ELSEVIER

Deep-Sea Research II 51 (2004) 1921–1924

DEEP-SEA RESEARCH
PART II

www.elsevier.com/locate/dsr2

Editorial

An overview of the Southern Ocean Global Ocean Ecosystems Dynamics program

1. Introduction

The Southern Ocean Global Ocean Ecosystems Dynamics (SO GLOBEC) program is an international multidisciplinary effort focused on understanding the physical and biological factors that influence growth, reproduction, recruitment, and survival of Antarctic krill (*Euphausia superba*). The program uses a multi-trophic level approach that includes the predators and competitors of Antarctic krill, represented by other zooplankton, fishes, penguins, seals, and cetaceans. Extensive studies describing the ecology and physiology of important species at all trophic levels contributed to the ecosystem approach that is GLOBEC's trademark.

During the planning of SO GLOBEC, it became obvious that the processes allowing Antarctic krill and other species to survive the austral winter were poorly understood. Thus, an extensive field program was developed that would provide observations and measurements during the transition from austral summer to fall, during the austral winter, and during the winter to spring transition at several sites around the Antarctic. The first series of SO GLOBEC field studies were centered on Marguerite Bay along the west Antarctic Peninsula (Fig. 1).

This special volume of *Deep-Sea Research* is comprised of papers representing the initial results of the SO GLOBEC field program, most of which are from studies that took place during the field seasons in April–June 2001 and July–September 2001 along the west Antarctic Peninsula. The field season began with a cruise in March–April that was done as part of the German SO GLOBEC program aboard the F.S. *Polarstern*. Following this cruise, a process cruise aboard the A.R.S.V. *Laurence M. Gould* and a survey cruise aboard the R.V.I.B. *Nathaniel B. Palmer* took place in April–June 2001 as part of the U.S. SO GLOBEC field program. The process and survey cruises were repeated about six weeks later in July–September 2001. The five cruises in 2001 provided coverage from the late fall, through the winter, and into the beginning of spring, which is the first time for such observations in Antarctic continental shelf waters. In 2002, the U.S. SO GLOBEC program once again went to sea on survey and process cruises in Marguerite Bay during April–May and in July–September.

During the U.S. SO GLOBEC survey cruises bottom mapping was done using the Sea-Beam system aboard the R.V.I.B. *Nathaniel B. Palmer*. These bathymetry data were combined with historical data from the region and with high-resolution bathymetry measurements made during British Antarctic Survey cruises aboard the R.R.S. *James Clark Ross* in February and March of 2001 and 2002 (Pudsey and Morris, 2001; Pudsey, 2002), as described in Bolmer et al. (2004). The resulting high-resolution bathymetry for the Marguerite Bay region of the west Antarctic Peninsula (Fig. 2) shows deep channels and troughs that connect the outer and inner continental shelf. As reported in several papers in this volume, these

0967-0645/$ - see front matter © 2004 Elsevier Ltd. All rights reserved.
doi:10.1016/j.dsr2.2004.08.007

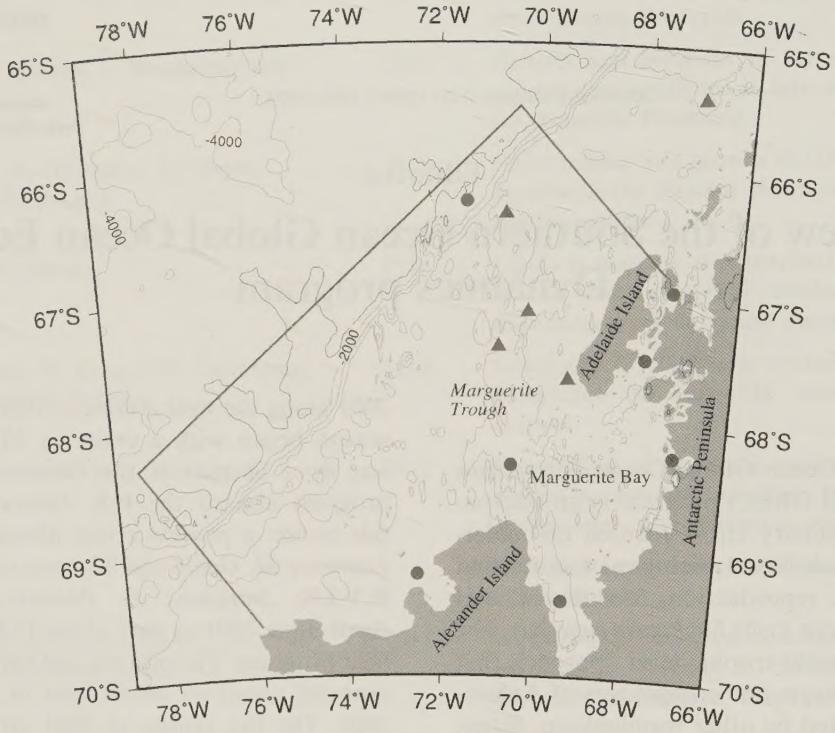

Fig. 1. Map showing the SO GLOBEC study region (solid line box) along the western Antarctic Peninsula. The process station sites occupied as part of the U.S. SO GLOBEC field program during April–June 2001 (●) and July–September 2001 (▲) are indicated. The 500, 1000, 2000, 3000, and 4000-m bathymetry contours are shown.

connections, especially Marguerite Trough, are important in determining physical and biological structure and dynamics in this region.

Our understanding of structure and function in the winter Antarctic marine food web is considerably enhanced by the papers in this volume. In keeping with the GLOBEC philosophy of understanding effects of environmental variability on marine populations, the first nine papers in the volume provide the physical and biological setting of the west Antarctic Peninsula continental shelf. The results reported in these papers highlight the contribution of a particular water mass, Circumpolar Deep Water, to the hydrography, circulation, sea ice, and biological environments of this region. The next seven papers present results from different seasons and areas of the Antarctic that advance understanding of marine zooplankton processes. The first five papers in this group focus on behavior, growth, feeding, nutrition, and overwintering strategies of Antarctic krill. The sixth paper in this group provides comparisons of winter processes for another krill species from a different area of the Antarctic. The final paper in this section provides a summer counterpoint to winter data via measurements of metabolism, composition, and enzymic activity in krill and other Antarctic micronekton. The SO GLOBEC program has a large component studying top predators, reflected in the last six papers of the volume that are centered on fish, seabirds, seals, and cetaceans. Cetacean observations were the result of a partnership with the International Whaling Commission. The SO GLOBEC field program provided some of the first austral winter measurements of the distribution and abundance of seabirds and marine mammals. This field effort was the first to obtain data on the diving behavior and movement patterns of crabeater seals (*Lobodon carcinophagus*) and reports the first use of a

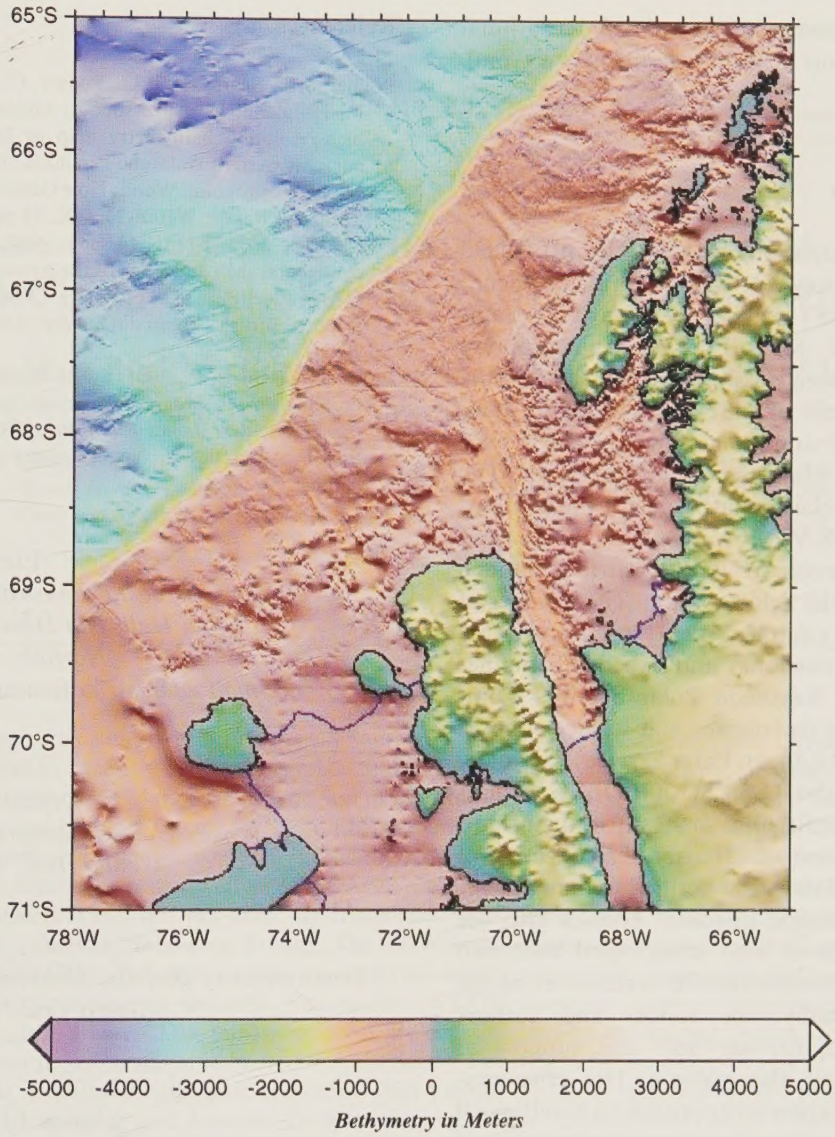

Fig. 2. High-resolution bathymetry of the SO GLOBEC study region. The blue lines indicate permanent ice shelves. Geographic names are given in Fig. 1. The data used to construct the bathymetry are available at: http://globec.whoi.edu/jg/serv/globec/soglobec/bathy.html0. Bathymetry figure provided by T. Bolmer, Woods Hole Oceanographic Institution.

bottom-mounted acoustic observatory to record marine mammal calls. The acoustic records confirm a year-round presence of minke whales (*Balaenoptera acutorostrata*) in the west Antarctic Peninsula region.

This is the first of several anticipated volumes dedicated to results of the SO GLOBEC effort. The continued synthesis and integration of the many data sets collected during SO GLOBEC will provide a basis for planning future efforts directed at studying the physics and biology of the Antarctic marine food web. Additional information about the SO GLOBEC and U.S. National GLOBEC programs is available at: http://www.

usglobec.org. Information on the International GLOBEC program is found at http://www.pml.ac.uk/globec.

Acknowledgments

The U.S. participation in the SO GLOBEC field program was supported by the National Science Foundation (NSF) Office of Polar Programs (OPP). The U.S. SO GLOBEC field program would not have been possible without the support and encouragement of NSF OPP program managers, P. Penhale and B. Lettau, and NSF OPP Ocean Projects Manager, A. Sutherland. The professional and cheerful attitudes of the captains and crews of the R.V.I.B. *Nathaniel B. Palmer* and the A.R.S.V. *Laurence M. Gould* contributed much to the success of the field program. The logistics of undertaking a complex field program were handled in a professional and expedient manner by A. Doyle of Raytheon Polar Services Company. The marine technicians and science support personnel from Raytheon Polar Services Company who sailed on the U.S. SO GLOBEC cruises deserve much credit and thanks for their hard work and dedication which made the collection of the high quality data sets described in many of the papers in this volume possible. Thanks also are due to the reviewers who contributed time and expertise to the comprehensive evaluations of the manuscripts. Finally, the editors and authors thank J. Morgan for her help and support as technical editor of this volume. Her efficiency, organization and cheerful approach to handling all the details associated with manuscript reviews and processing made this volume possible. This is contribution number 491 of the U.S. GLOBEC program funded by the National Science Foundation and contribution 11241 of the Woods Hole Oceanographic Institution.

References

Bolmer, S.T., Beardsley, R.C., Pudsey, C., Morris, P., Wiebe, P., Hofmann, E., Anderson, J., Maldonado, A., 2004. A high-resolution bathymetry map of Marguerite Bay and adjacent western Antarctic Peninsula shelf Southern Ocean GLOBEC program. Woods Hole Oceanographic Institution Technical Report WHOI-2004-02, 76 pp.

Pudsey, C., 2002. Marine geology and geophysics on the continental shelf and slope of the Antarctic Peninsula in the NW Weddell Sea. R.R.S. *James Clark Ross* JR 71 Cruise Report, British Antarctic Survey Reference No. ES6/1/2002/1, 66 pp.

Pudsey, C., Morris, P., 2001. Swath bathymetry and TOPAS profiling on the Antarctic Peninsula margin and in Drake Passage. R.R.S. *James Clark Ross* JR 59 Cruise Report, British Antarctic Survey Reference No. ES6/1/2001/1, 36 pp.

Eileen E. Hofmann
Center for Coastal Physical Oceanography, Crittenton Hall, Old Dominion University, Norfolk, VA 23529, USA
E-mail address: hofmann@ccpo.odu.edu

Peter H. Wiebe
Department of Biology, Woods Hole Oceanographic Institution, Woods Hole, MA 02543, USA

Daniel P. Costa
Department of Biology, University of California, Santa Cruz, CA 95064, USA

Joseph J. Torres
College of Marine Science, University of South Florida, 140 Seventh Avenue South, St. Petersburg, FL 33701, USA

ELSEVIER

Deep-Sea Research II 51 (2004) 1925–1946

DEEP-SEA RESEARCH
PART II

www.elsevier.com/locate/dsr2

Water-mass properties and circulation on the west Antarctic Peninsula Continental Shelf in Austral Fall and Winter 2001

John M. Klinck[a,*], Eileen E. Hofmann[a], Robert C. Beardsley[b], Baris Salihoglu[a], Susan Howard[c]

[a]*Center for Coastal Physical Oceanography, Crittenton Hall, Old Dominion University, Norfolk, VA 23529, USA*
[b]*Woods Hole Oceanographic Institution, Clark 343, MS 21 Woods Hole, MA 02543, USA*
[c]*Earth and Space Research, 1910 Fairview Avenue E., Suite 102, Seattle, WA 98102, USA*

Accepted 13 July 2004

Abstract

Hydrographic measurements made during the US Southern Ocean Global Ocean Ecosystem Dynamics cruises, which took place from April to June and July to September 2001, provide a description of changes in water-mass distributions and circulation patterns in the Marguerite Bay region of the west Antarctic Peninsula continental shelf that result from seasonal variability and offshore forcing by the southern boundary of the Antarctic Circumpolar Current (ACC). The primary seasonal change in water-mass properties is the reduction in Antarctic Surface Water and replacement by a thick Winter Water layer. The primary effect of the ACC is to pump warm (> 1.5 C), salty (34.65 34.7), and nutrient-rich Circumpolar Deep Water (CDW) onto the continental shelf below 200 m at specific sites that correspond to bathymetric features, such as Marguerite Trough. The CDW intruded onto the continental shelf, moved across shelf, and entered Marguerite Bay. This flow pattern was observed during both cruises, suggesting that onshelf intrusions of CDW are a regular occurrence on this shelf. The number of CDW intrusions observed suggests that 4–6 events can occur in a year. Regions where CDW intrusions occur are characterized by surface waters that are above freezing in winter. Diffusive heat fluxes based on estimated diffusivities are insufficient for the observed rate of temperature decay of CDW intrusions. Localized, bathymetrically controlled vertical mixing is suggested as the primary heat transfer mechanism. The hydrographic and Acoustic Doppler Current Profiler measurements show a southwesterly flowing coastal current along Adelaide Island that enters the north side of Marguerite Bay and exits around Alexander Island. This current, which may result from seasonal, coastal buoyancy forcing, was present in fall and winter, but was better developed in fall. This current may be part of a larger cyclonic gyre that overlies the northern part of the area surveyed during the two cruises.
© 2004 Elsevier Ltd. All rights reserved.

*Corresponding author. Tel.: +1-757-683-6005; fax: +1-757-683-5550.
E-mail address: klinck@ccpo.odu.edu (J.M. Klinck).

0967-0645/$ - see front matter © 2004 Elsevier Ltd. All rights reserved.
doi:10.1016/j.dsr2.2004.08.001

1. Introduction

The hydrographic structure of the water overlying the central western Antarctic Peninsula (WAP) continental shelf (Fig. 1) results primarily from forcing at the air-sea boundary and at the outer continental margin. Sea-ice cover in this region melts completely during the austral summer (Stammerjohn and Smith, 1996), leaving the shelf waters exposed to atmospheric forcing. Air-sea exchange contributes to the large seasonal variations in the thermohaline properties in Antarctic Surface Water (AASW) in the upper 100–120 m overlying the continental shelf (Hofmann et al., 1996; Smith et al., 1999). This water mass is replaced in the austral fall and winter by near-freezing Winter Water (WW). Beneath the AASW and WW is warmer ($\theta > 1\,^{\circ}C$) and saltier ($S > 34.64$) water that covers the shelf below the permanent pycnocline at 150–200 m (Smith et al., 1999). This deep water mass derives from Circumpolar Deep Water (CDW), which is present at the outer edge of the WAP continental shelf at depths of 200–600 m (Hofmann and Klinck, 1998a; Smith et al., 1999).

The WAP outer continental shelf break and slope has no Antarctic Slope Front (Whitworth et al., 1998; Smith et al., 1999) associated with sharp horizontal gradients in temperature, salinity, and density (Jacobs, 1991), which is typical of the shelf break in other parts of the Antarctic. Thus, there is no dynamic barrier to block flow of CDW from the deep ocean onto the continental shelf (Talbot, 1988). Consequently, the outer WAP shelf region is directly affected by the northeastward flowing Antarctic Circumpolar Current (ACC), with its southern boundary located on the upper continental slope along the 750–1000 m isobath (Hofmann and Klinck, 1998a).

The presence of the southern boundary of the ACC along the outer WAP continental shelf produces subsurface, onshelf intrusions of CDW (Hofmann and Klinck, 1998a; Dinniman and Klinck, 2004), which in turn affects the thermohaline properties of the subpycnocline waters (Klinck, 1998; Smith et al., 1999), nutrient and phytoplankton distributions (Prézelin et al., 2000, 2004), and sea-ice concentration (Smith and Klinck, 2002) of the shelf waters. The subsurface CDW intrusions tend to occur at preferred sites along the WAP shelf that are associated with bathymetric variations (Hofmann and Klinck,

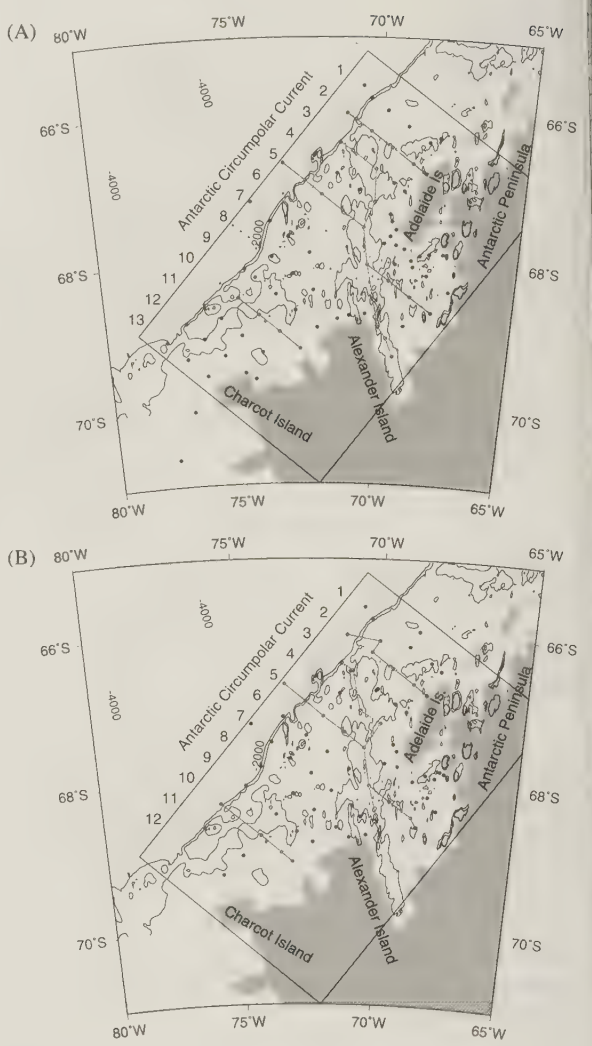

Fig. 1. Map of study area showing the location of the hydrographic (circles) stations occupied during the (A) April–May 2001 and (B) July–August 2001 cruises. The across-shelf transects are numbered from north to south and the lines indicate the sampling locations used to construct the across-shelf vertical hydrographic distributions described in the text. Geographic locations are identified and bottom bathymetry contours are 500, 1000, 2000, 3000 and 4000 m. Marguerite Bay is the indentation in the Antarctic Peninsula coastline between Adelaide and Alexander Islands. The large box is the domain used in Figs. 7–10.

1998a; Dinniman and Klinck, 2004). In addition, shelf-scale cyclonic gyres, with length scales of 200–400 km alongshelf and 100–150 km across-shelf, have been observed on the WAP continental shelf (Stein, 1992; Smith et al., 1999).

This study uses extensive hydrographic and direct velocity measurements obtained from two cruises in the austral fall (April–May) and winter (July–August) of 2001, which were part of the US Southern Ocean Global Ocean Ecosystems Dynamics (SO GLOBEC) field program (Hofmann et al., 2002), to extend the description of the water-mass properties and circulation of WAP continental shelf. These measurements covered the south-western portion of the WAP shelf in the region of Marguerite Bay and extended north and south of Adelaide and Alexander Islands, respectively (Fig. 1). The large spatial scale and repeated measurements allow descriptions of changes in water mass distributions, estimation of the frequency and duration of CDW intrusions, and a description of variability of the shelf-wide circulation. These data also represent the first high-resolution and coincident hydrographic and current measurements for this region.

The following section provides a description of the hydrographic and Acoustic Doppler Current Profiler (ADCP) velocity measurements used in this study. This is followed by analyses and descriptions of these data and a discussion and summary of the effect of CDW intrusions on the heat budget of this region and the circulation of the WAP continental shelf.

2. Data sources and methods

2.1. Hydrographic data distribution

The hydrographic data used in this analysis were collected during two cruises aboard the United States icebreaker RVIB *Nathaniel B. Palmer*. The stations occupied during the austral fall cruise (Fig. 1A) provide coverage of the continental shelf to the north and south of Marguerite Bay. Those occupied during the austral winter cruise (Fig. 1B) covered essentially the same area, but with fewer stations in the southern part of the study region and within Marguerite Bay. For both cruises, the individual stations, with spacing ranging from 10 to 40 km, were aligned in across-shelf transects with 40-km spacing that ran perpendicular to a baseline situated along the coast (Fig. 1).

The April–May survey grid consisted of thirteen across-shelf transects and 81 stations (Fig. 1A, Table 1). Thirteen of the originally planned stations in the central portion of the survey region were not occupied because of weather conditions. The outer-most stations on some southern transects were not occupied because of time constraints; instead, eXpendable Conductivity-Temperature-Depth (XCTD) probes were used (Table 1). The stations were occupied from north to south, starting with the outer-most station on survey transect 1.

On the July–August cruise, only 69 of the planned survey stations were occupied either because of time constraints or sea ice conditions (Fig. 1B, Table 1). The stations that were occupied coincided with the April–May station locations, and the winter survey also was run from north to south. No XCTDs were used on this cruise.

2.2. Hydrographic data collection

The hydrographic measurements were collected using a SeaBird 911+ Niskin/Rosette conductivity-temperature-depth (CTD) sensor system, which included dual sensors for temperature and conductivity. Other sensors mounted on the CTD-Rosette system measured dissolved oxygen concentration, transmission, fluorescence, and photosynthetically active radiation. The 24-place Rosette was equipped with 10-L Niskin bottles, and water samples were taken at the surface and bottom, above, within and below the oxygen-minimum layer that characterizes CDW, throughout the subpycnocline waters, and at a series of standard depths between 100 m and the surface. All hydrographic casts were done to within 5–20 m of the bottom, depending on weather and sea-state conditions. The CTD measurements were processed using the procedures and algorithms given in UNESCO (1983).

On each CTD cast, water samples were taken at several depths for salinity determinations to

Table 1
Summary of the hydrographic stations occupied during the 2001 austral fall and winter Southern Ocean GLOBEC cruises

Cruise	Dates	Sampling time	CTD stations	XCTD stations
April–May	24 April–5 June	29 April–2 June	81	16
July–August	24 July–31 August	27 July–25 August	69	0

Table 2
Summary of the differences in the salinity (S) values obtained from the primary (0) and secondary (1) CTD conductivity sensors and differences between the CTD sensor values and those measured from bottle salinity (Sb) samples for the April–May and July–August 2001 Southern Ocean GLOBEC cruises

Cruise	S0-S1 (psu)	S0-Sb (psu)	S1-Sb (psu)	T0-T1 (°C)
April–May	-0.009 ± 0.0047 (413)	-0.0002 ± 0.0053 (388)	-0.0007 ± 0.0053 (390)	0.0013 ± 0.0047 (399)
July–August	-0.00354 ± 0.106 (334)	0.0034 ± 0.0058 (296)	0.00272 ± 0.0053 (294)	0.00082 ± 0.0106 (339)

The difference in the primary (0) and secondary (1) CTD temperature (T) sensors is also given. The number of samples on which the differences are based is shown in parentheses.

provide calibration of the conductivity sensors on the CTD. The conductivities of the discrete salinity samples were measured during the cruise, usually within 72 h of collection, using a Guildline AutoSal 8400B Number 2 laboratory salinometer and converted to salinity. The primary and secondary CTD conductivity sensors were compared for internal consistency, and the salinity values computed using the sensors were then compared with the bottle salinities (Table 2). Details of the salinity calibrations for the fall and winter cruises are given in US SO GLOBEC Report Number 2 (2001) and US SO GLOBEC Report Number 3 (2001), respectively.

2.3. Acoustic Doppler current profiler data

The RDI 150 kHz Acoustic Doppler Current Profiler (ADCP) system mounted in the hull of the RVIB *Nathaniel B. Palmer* was configured to acquire velocity measurements with an 8-m pulse length, in fifty 8-m depth bins using five-minute ensemble averages. This configuration provided velocity measurements from the first bin, at 31 m, to 300 m and sometimes 350 m. Depth bins 4–12 were used as the reference layer. Data collection started once the ship was past the 200-mile limit of the Argentine Exclusive Economic Zone (Table 1) and continued until this boundary was again reached at the end of the cruise.

For most of the cruise, the ADCP was run in bottom tracking mode as the water was less than 500 m deep (Fig. 1). Bottom tracking was disabled when the ship was in water deeper than 500 m for more than a few hours. While the ship moved through sea ice, the ADCP was unable to receive sufficient samples to generate proper statistics. During these times, accurate current measurements were made only while the ship was stationary or moving slowly. Such conditions occurred only during the winter cruise. Storms during the fall cruise interfered with accurate ADCP measurements.

Preliminary processing of the ADCP data was done during the cruise using an automated version of the Common Oceanographic Data Access System (CODAS) developed by Firing and Hummon from the University of Hawaii. Following the cruises, final processing and quality control of the ADCP data was performed by Hummon. The data were calibrated and edited using CODAS. Heading corrections were made using data collected by the Ashtech ADU-2 GPS system onboard the RVIB *Nathaniel B. Palmer*.

3. Results

3.1. Water mass structure

The potential temperature-salinity (θ-S) diagram constructed from the April–May CTD and XCTD observations (Fig. 2A) shows AASW with temperatures of −1.5–1.0 °C and salinities of 33.0–33.7 at σ_θ values less than 27.4. The large scatter in AASW properties reflects the temporal changes in near-surface water due to seasonal heating and cooling during the summer and fall.

The temperature minimum at −1.6 to −1.7 °C at a salinity of 34.1 was associated with the remnant WW produced during the previous winter, which had undergone mixing with AASW and subpycnocline waters (Fig. 2A). By the austral winter, WW with temperatures less than −1.8 °C at a salinity of 34.1 was formed by local cooling. The AASW layer was greatly reduced and this water was on or near the freezing line (Fig. 2B), indicating that the upper waters were in the winter state throughout the July–August cruise. However, the large variability in salinity seen in the AASW indicates that the salt increase due to sea-ice freezing was not yet complete and that not all of the upper water-column water had been converted to WW.

Water with temperatures of 1.0–2.0 °C and salinities of 34.6–34.74 represents CDW, which is composed of two varieties: Upper and Lower CDW. The Upper CDW (UCDW) is characterized by a temperature maximum at a potential density of 27.72. Lower CDW (LCDW) is characterized by a salinity maximum of 34.74 at a potential density of 27.8. These water masses were present off the shelf in the fall and winter (Figs. 2A, B) and showed little variability between the two seasons.

A water mass that is intermediate between AASW and CDW, characterized by temperatures of 1.0–1.5 °C and salinities of 34.3–34.6, was observed during these cruises (Figs. 2A, B). This water is a mixture of UCDW and AASW (Klinck, 1998; Smith et al., 1999; Smith and Klinck, 2002), which forms a cooler and less saline water mass, which has been referred to as modified CDW water (Hofmann and Klinck, 1998b).

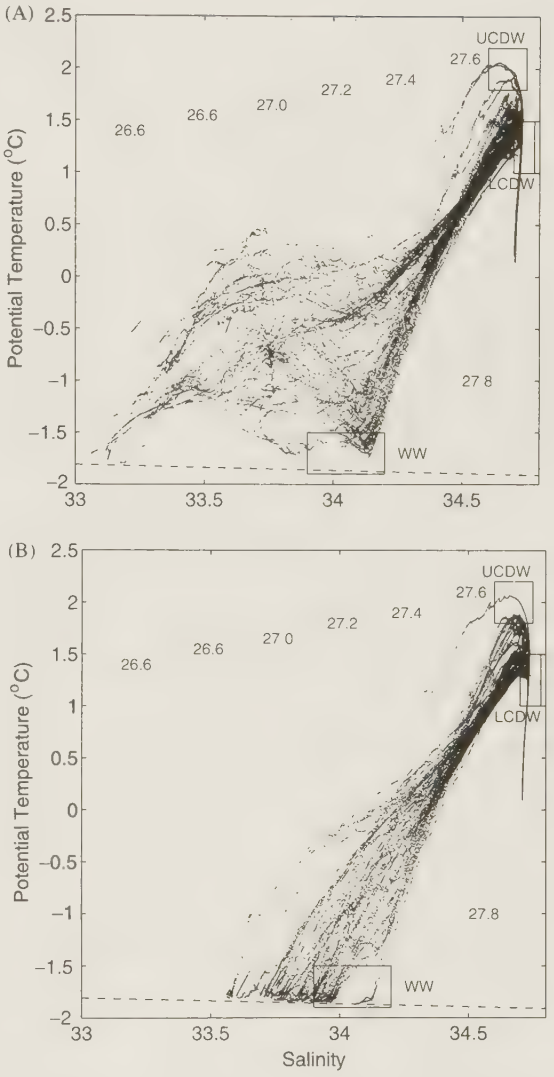

Fig. 2. Potential temperature-salinity diagram constructed from (A) April–May 2001 and (B) July–August 2001 hydrographic observations. The temperature and salinity ranges that characterize UCDW, LCDW and WW water masses are shown by the boxes. The potential density at the surface for the indicated temperature and salinity is indicated by the dotted lines. The freezing point of seawater is indicated by the dashed line.

An additional water type, seen in the fall, is characterized by temperatures of −1.7–−1.8 °C and salinities of 33.1–33.2 (Fig. 2A). This water was observed at the surface in the CTD casts from inshore waters near the ice shelves on Adelaide

Island in the northern part of the study region (Fig. 1).

3.2. Hydrographic observations

3.2.1. Vertical structure

The vertical distributions of potential temperature, salinity, and potential density along across-shelf transects from different parts of the study region provide a description of the water-mass structure and changes in this structure between the two survey periods. These sections illustrate specific features of the WAP continental shelf thermohaline distributions and the extent of the onshelf flow of oceanic waters.

The vertical temperature distribution along line 2 in the northern part of the study region (Fig. 1) during April–May 2001 (Fig. 3A) showed a maximum of 1.8 °C centered at 300 m at the outer edge of the continental shelf. This water has a salinity of 34.7–34.72 (Fig. 3C) indicating that it was UCDW. The 1.8 °C isotherm at the outer shelf edge indicates the presence of the Southern ACC Front (Orsi et al., 1995). Below 300 m at the outer shelf, temperature decreased and salinity increased to a maximum of 34.74 at 1200 m (not shown), which is characteristic of LCDW. Above 300 m, temperature decreased to a minimum of 1.5 °C (Fig. 3A) and salinity decreased to 34.1 (Fig. 3C) at about 100 m, which is the core of the WW layer. Above the WW layer was AASW.

Water warmer than 1.0 °C flooded the shelf below 200 m across the entire section (Fig. 3A). The salinity below 200 m was greater than 34.65 (Fig. 3C) which indicates the offshore origin of this water. The potential density surfaces below 200 m (Fig. 3E) sloped upward from the shelf edge onto the shelf, indicating onshelf movement and cooling of oceanic CDW. The temperature and salinity distributions above 200 m (Figs. 3A, C) show that the remnant WW layer extended across the shelf. There was a warmer, less saline and lower density layer in the upper 100 m at the two inner-most stations on line 2 (Figs. 3A, C, E), representing a low salinity coastal current.

In July–August, the vertical property distributions along line 2 still showed the presence of the ACC at the outer shelf edge, flooding of warm and salty water below 200 m, and upward sloping density surfaces below 200 m (Figs. 3B, D, F). The primary differences were in the waters above 200 m, which were colder than −1.8 °C over most of the section. Salinity and density of the water above 100 m increased relative to the April–May observations, likely as the result of cooling and brine rejection during sea-ice formation. The surface waters not at freezing were found at the two inner-most stations on the transect.

The property distributions along the across-shelf transect constructed from the outer stations on line 5 and the inner stations on line 6 (cf. Fig. 1) are similar to those seen along the section to the north. The southern boundary of the ACC was present at the shelf edge in fall (Fig. 4A) and winter (Fig. 4B), warm salty water flooded the shelf below 200 m (Figs. 4C, D), and the potential density surfaces slope upwards at the outer shelf edge (Figs. 4E, F). The waters above 100 m showed the transition from AASW in the fall to WW in the winter. The WW layer in fall was more eroded along this section than along the line 2 section. At the stations inside Marguerite Bay, the WW layer was completely gone and water near 0 °C extended from about 175 m to the surface.

In the southern part of the study region, along line 10 (Fig. 1), the across-shelf temperature and salinity distributions in the fall (Figs. 5A, C) showed modified CDW and shelf water below 200 m and AASW above. The WW layer was eroded, although there is a suggestion of this layer in the temperature distribution at the outer part of the section (Fig. 5A). The density surfaces sloped downwards towards the inner portion of the section, which suggests flow to the south–southwest on the inner shelf. In winter, 1.5 °C water was observed at the outer shelf below 300 m, and the surface waters were near freezing at the outer two station locations (Fig. 5B). Salinity in the upper 100 m decreased onshore, and the offshore salinity below 200 m was characteristic of UCDW (Fig. 5D). The potential density surfaces above 200 m reflect the colder and more saline water present in winter relative to the fall (Fig. 5F versus Fig. 5B). Below 200 m the density structure in the two seasons was similar (Figs. 5E, F).

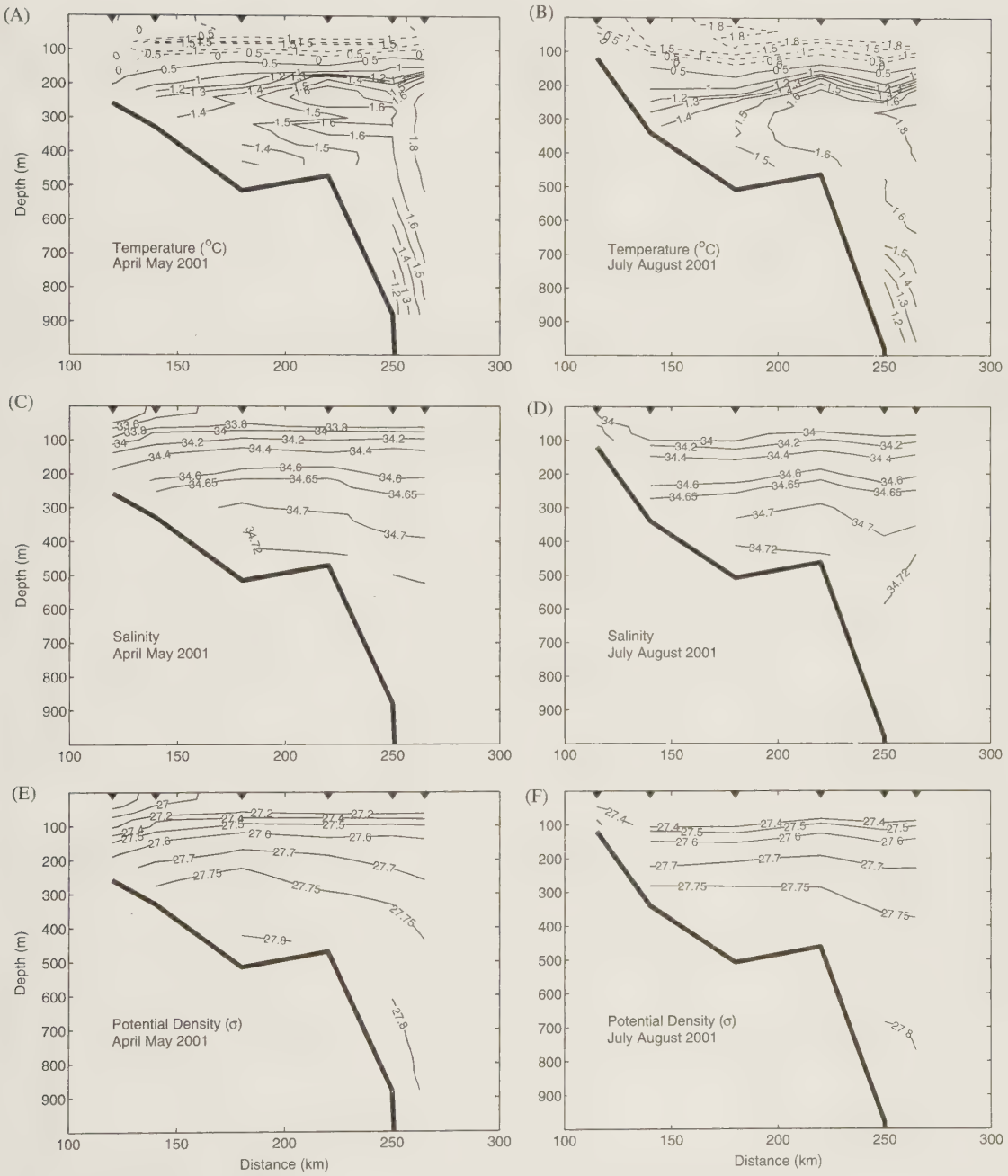

Fig. 3. Vertical across-shelf sections of potential temperature, salinity, and potential density constructed from measurements made during April–May 2001 (A, C, E) and July–August 2001 (B, D, F) along line 2 in the northern portion of the study region. The station locations used to construct the sections are shown on Fig. 1 and the station spacing along the transect is indicated by the triangles.

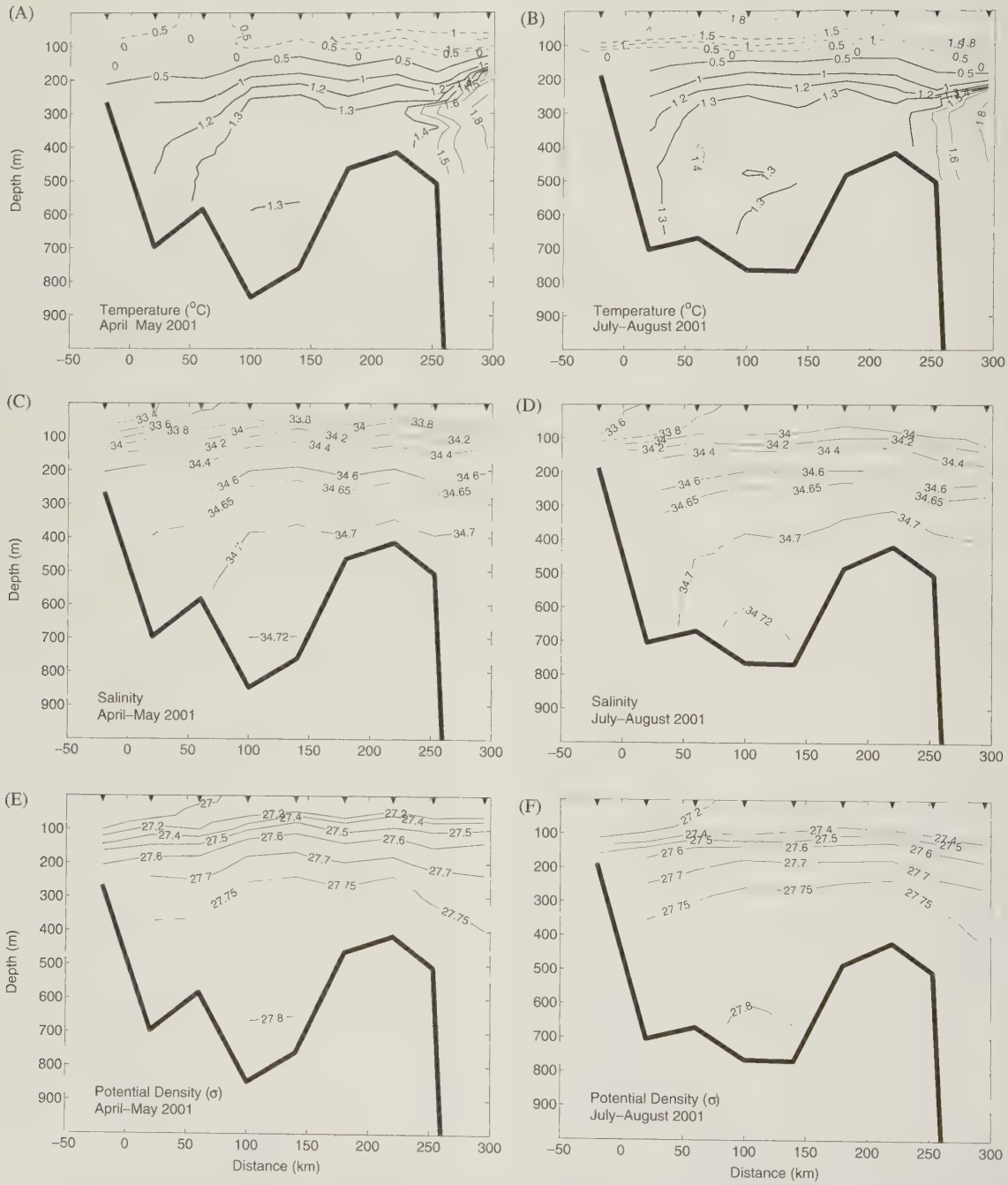

Fig. 4. Vertical sections of potential temperature, salinity, and potential density constructed from measurements made during April–May 2001 (A, C, E) and July–August 2001 (B, D, F) along the outer portion of line 5 and the inner portion of line 6. The station locations used to construct the sections are shown on Fig. 1 and the station spacing along the transect is indicated by the triangles.

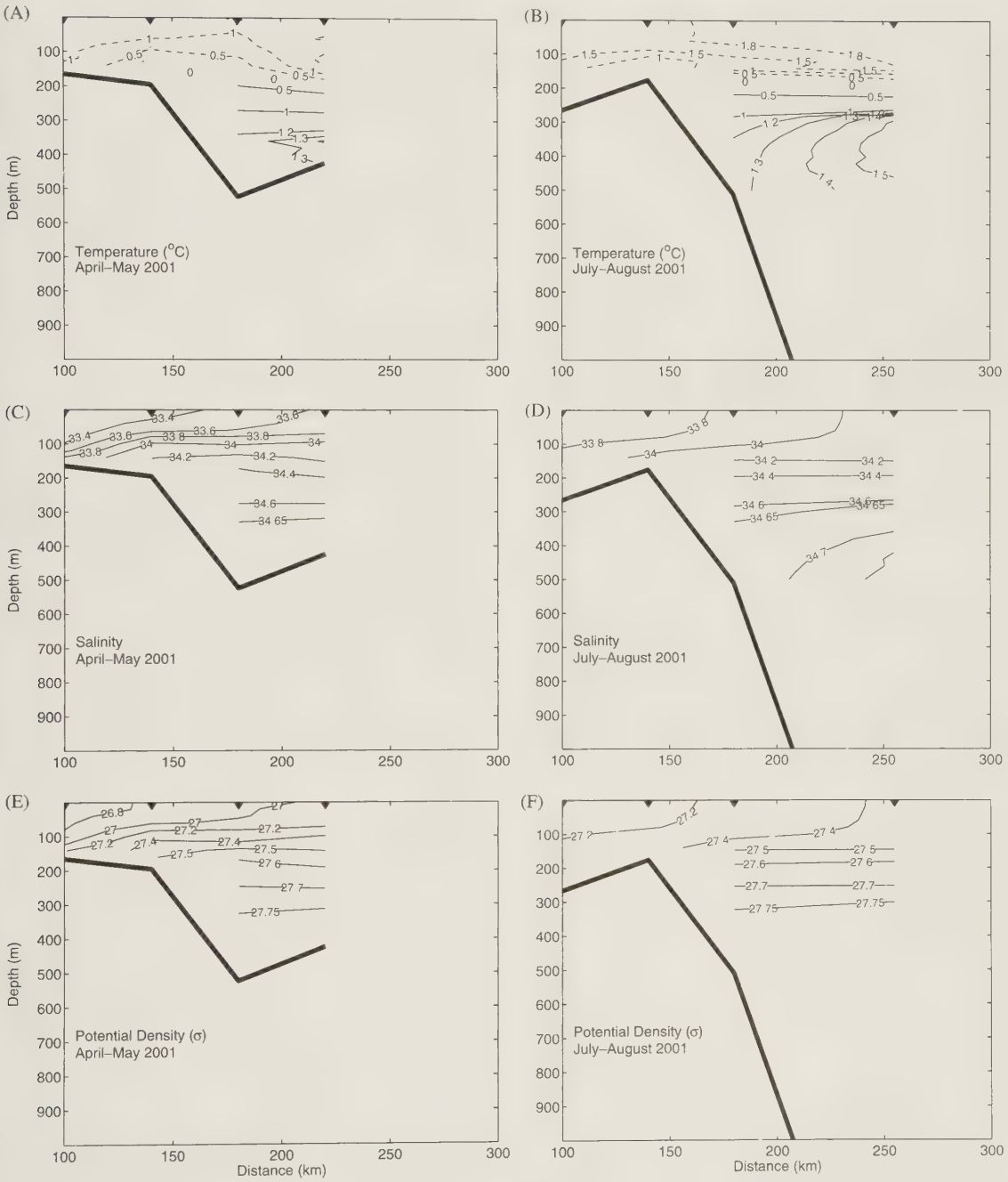

Fig. 5. Vertical across-shelf sections of potential temperature, salinity, and potential density constructed from measurements made during April May 2001 (A, C, E) and July–August 2001 (B, D, F) along line 10. The station locations used to construct the sections are shown on Fig. 1 and the station spacing along the transect is indicated by the triangles.

The hydrographic section along the axis of Marguerite Trough (Fig. 1) shows oceanic water along this deep connection from the outer WAP shelf and into inner Marguerite Bay (Fig. 6). In April–May, an isolated region of 1.5 °C water was observed between 250 and 400 m (Fig. 6A) with cooler water on either side. Salinity along Marguerite Trough below 200 m was 34.7–34.72 (Fig. 6C) with potential densities of 27.75–27.8 (Fig. 6E). The WW layer was eroded and surface temperature and salinity decreased inside Marguerite Bay (Figs. 6A, C). In the winter, the thermohaline properties below 200 m were similar to those observed in the fall (Figs. 6B, D, F), but the temperature below 200 m was only 1.4 °C. The surface waters were near freezing except for a small region around a shallow bank, at about 75 km along the transect, where surface waters were above freezing.

3.2.2. Surface temperature and salinity

The temperature distribution at 10 m from April to May (Fig. 7A) shows the progressive cooling of the surface waters that occurred over the course of the cruise. Surface waters in the northern part of the study region, which were sampled first, ranged from −0.4 to −1.0 °C, while surface water in the southern part of the survey grid had cooled to −1.2 to −1.4 °C by the end of the cruise. The salinity distribution at 10 m (Fig. 7C) showed highest salinities (33.8–33.6) at the shelf edge in the northern part of the study region, which extended onto the shelf and into Marguerite Bay along the axis of Marguerite Trough. Low salinities of 33.4–33.2 were found on the inner shelf around the northern side of Adelaide Island, along Alexander Island, and near Charcot Island (Fig. 7C).

Near-surface water temperature in winter is near freezing throughout the study region, which gives little horizontal contrast. However, the difference between the temperature at 10 m and the freezing temperature at the ambient salinity (Fig. 7B) does show large-scale patterns. Departures from freezing of 0.06–0.08 °C were found throughout the northern part of the study region, especially along the axis of Marguerite Trough. A second area above freezing by 0.06 °C was found along the northern tip of Adelaide Island. Departures from freezing of 0.02–0.04 °C occurred along the outer shelf. The largest departures from freezing of 0.1 °C occurred at the entrance to Marguerite Bay along the southern flank of Marguerite Trough and along the southern side of Adelaide Island (Fig. 7B). The salinity distribution in winter at 10 m showed the highest salinities (34.0–33.9) along the outer shelf edge and along the axis of Marguerite Trough (Fig. 7D). Lowest salinities were on the inner shelf and inside Marguerite Bay.

3.2.3. Temperature maximum below 200 m

The distribution of the temperature maximum below 200 m (Fig. 8) provides a way to track movement of CDW and modified CDW on the WAP shelf. This approach assumes that the isotherm patterns can be used to approximate the current flow. Also, the southern boundary of the ACC is denoted by the 1.6 °C isotherm and the Southern ACC Front is denoted by the 1.8 °C isotherm below 200 m (Orsi et al., 1995), which allows these features to be located.

In April–May, the 1.8 and 1.6 °C isotherms were present along the outer edge of the continental shelf over the entire study region (Fig. 8A), indicating that the ACC was situated along the shelf edge. Temperatures greater than 1.6 °C extended onto the WAP shelf in the northern end of the survey grid and between survey transects 6 and 7. The onshelf movement of the 1.6 °C isotherm in the northern study region was associated with a meander in the southern ACC boundary, which was aligned with the northeastern side of Marguerite Trough. The temperature section along Marguerite Trough (cf. Fig. 6A) clearly shows the intrusion as water below 200 m warmer than 1.5 °C.

The 1.4 °C isotherm forms the boundary between the CDW and modified CDW that is found on the WAP continental shelf (Smith et al., 1999). This isotherm extended to the inner shelf in the northern study region, towards the shelf break in the central region, and along the outer shelf in the southern region (Fig. 8A). This pattern suggests that there were two regions of onshelf flow separated by offshelf flow.

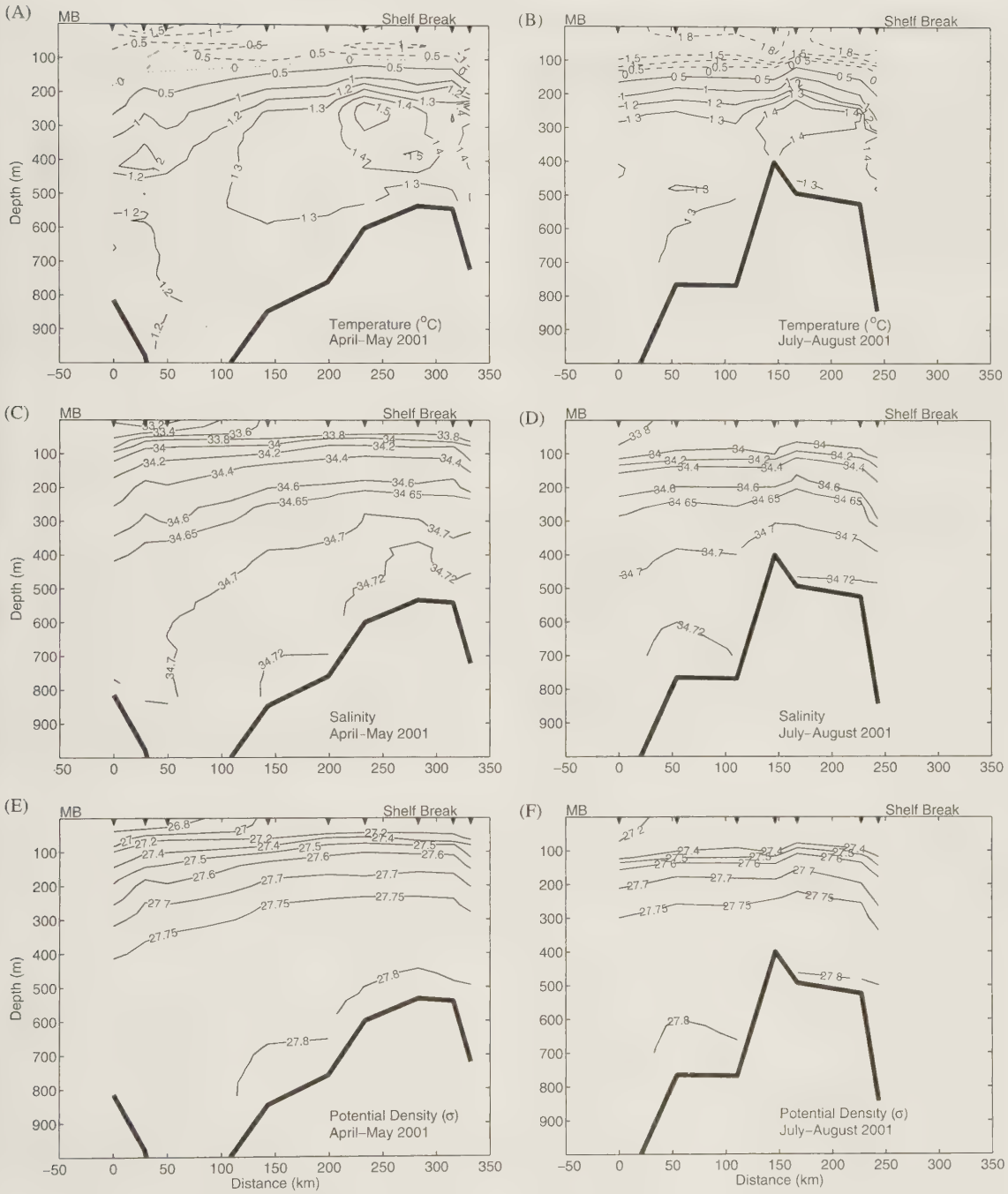

Fig. 6. Vertical sections of potential temperature, salinity, and potential density constructed from measurements made during April–May 2001 (A, C, E) and July–August 2001 (B, D, F) along a transect that runs along the axis of Marguerite Trough. The station locations used to construct the sections are shown on Fig. 1 and the station spacing along the transect is indicated by the triangles. Marguerite Bay is indicated by MB.

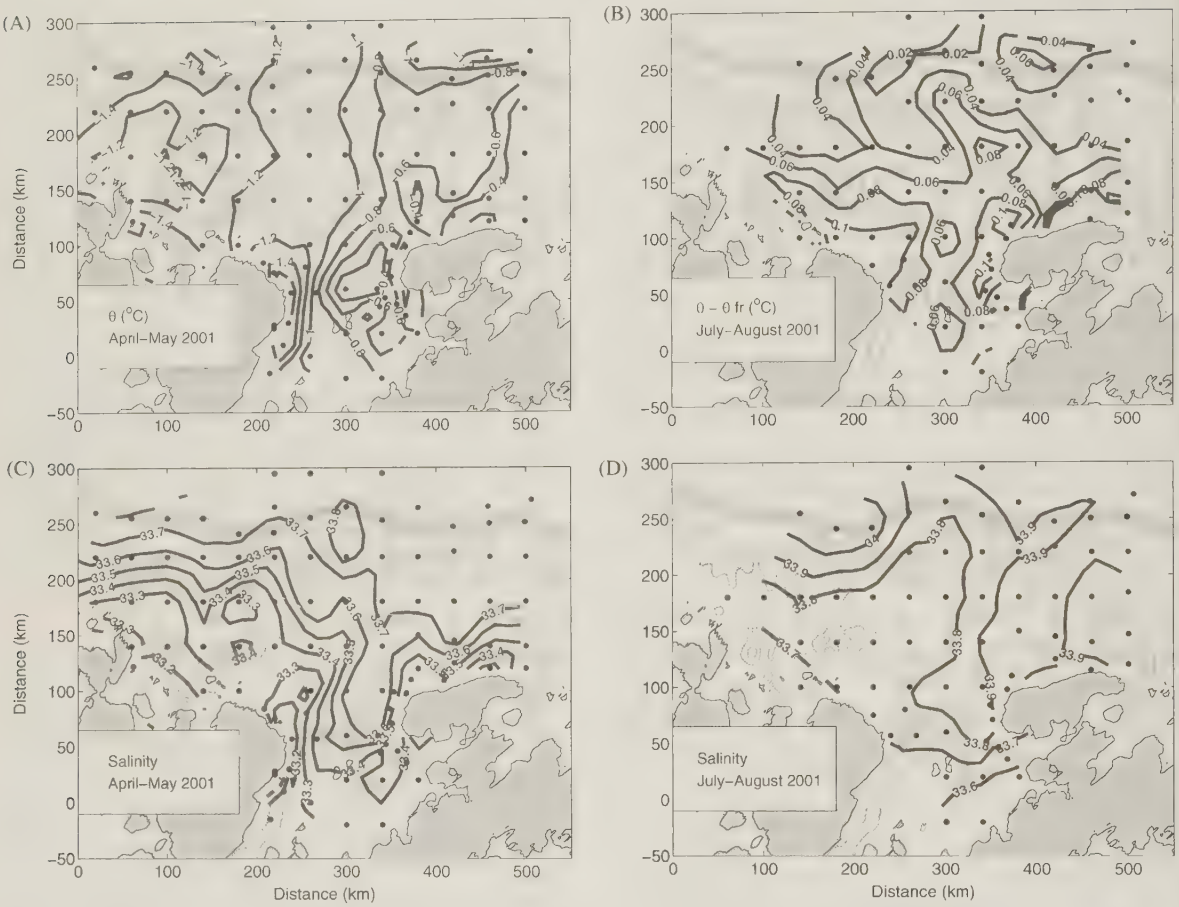

Fig. 7. Distribution of potential temperature (θ) and salinity at 10 m constructed from the April–May 2001 observations (A, C), the difference between the observed water temperature and freezing temperature (θ fr) at the ambient salinity (B), and salinity (D) constructed from the July–August 2001 observations. Station locations used to construct the distributions are shown and bathymetry contours are 500, 1000, and 1500 m. Light shading shows land and geographical names are given on Fig. 1.

The 1.2 °C isotherm is the edge of the colder inner shelf waters along the western sides of Adelaide and Alexander Islands. The only exception was in the mid-portion of the study region, where this isotherm extended into Marguerite Bay aligned with Marguerite Trough. The isotherm pattern suggests flow from the outer WAP in the northern study region, extending along Marguerite Trough, and into inner Marguerite Bay. In the southern study region, this isotherm extends across the shelf, reaching to within 40 km of the shelf edge. Water below 200 m in the inner reaches of Marguerite Bay in April–May was warmer than 0 °C.

During July–August 2001, the pattern of the temperature maximum below 200 m (Fig. 8B) is similar to that seen in the fall. The 1.6 and 1.8 °C isotherms were again along the shelf break indicating the presence of the ACC. The two regions of onshelf isotherm deflection were still evident near transects 2 and 3 and transects 6 and 7, respectively, with the intervening region of offshelf isotherm deflection. An isolated region of water warmer than 1.4 °C occurred in Marguerite Trough at the entrance to Marguerite Bay. The 1.3 and 1.4 °C isotherms extended about 50 km further off the shelf in the southern study region than observed in April–May (Fig. 8B versus Fig. 8A).

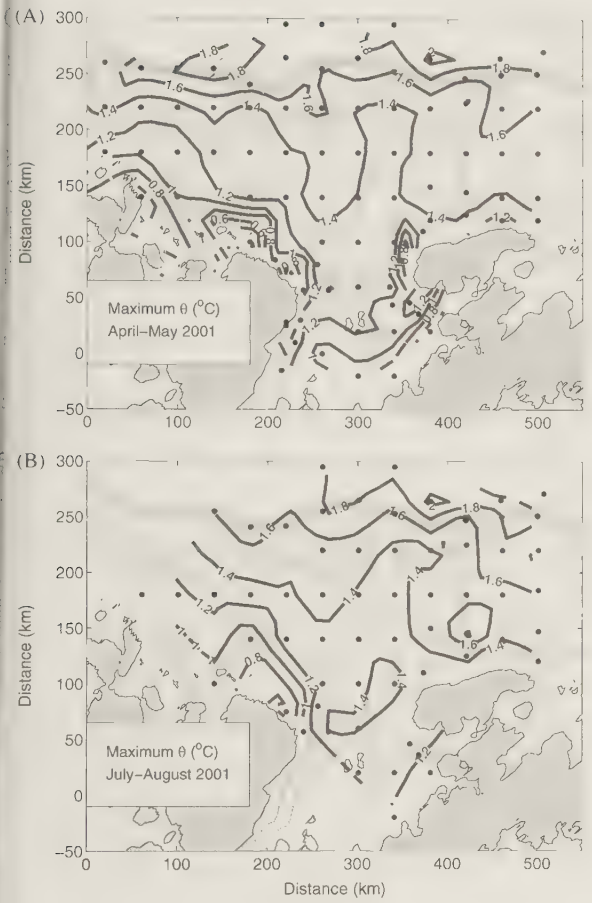

Fig. 8. Horizontal distribution of the maximum in potential temperature (θ) below 200 m constructed from the (A) April–May 2001 and (B) July–August 2001 observations. Station locations used to construct the distributions are shown and bathymetry contours are 500, 1000, and 1500 m. Light shading shows land and geographical names are given on Fig. 1.

3.2.4. Temperature and salinity anomaly

The range of temperature and salinity below 200 m was small, so differences across the study region and between the two cruises are best seen as anomalies. Thus, an average temperature and salinity vertical profile was calculated for each cruise using the observed values. This average profile was then subtracted from each observed profile and the resulting anomaly field at specific depths was plotted. The temperature and salinity anomaly fields at 300 m (Fig. 9) provided the best contrast.

In April–May 2001 the temperature and salinity anomalies at 300 m were positive over the northern and central portions of the survey region (Figs. 9A, C), showing clearly the onshelf movement of warm, salty UCDW. Positive anomalies coincided with locations of ACC meanders onto the shelf and Marguerite Trough. Negative temperature and salinity anomalies occur along the southern tip of Adelaide Island, along Alexander Island and across the continental shelf in the southern part of the survey region.

Temperature and salinity anomalies at 300 m in July–August (Figs. 9B, D) are similar to those seen in the fall, with positive anomalies in the north and central parts of the study region and negative anomalies in the southern region. Two distinct positive anomalies occur along the axis of Marguerite Trough with a possible third region at the outer shelf edge. These potentially represent three separate UCDW intrusions that moved onto the WAP via Marguerite Trough. The inner-most feature, along the inner parts of transects 5 and 6, had the lowest temperature and salinity anomalies, suggesting that the intruded UCDW had cooled and freshened as it moved onshore.

3.2.5. Dynamic height

Stratification of the WAP continental shelf waters is weak (Smith et al., 1999; Smith and Klinck, 2002), so the baroclinic velocity based on dynamic topography does not represent all of the flow. One measure of the stratification is the buoyancy frequency squared ($N^2 = -g\frac{\partial \rho}{\partial z}$) which was estimated for individual stations and average conditions for each cruise. The near-surface N^2 can reach $10^{-4}\,s^{-2}$ but maximum values in the pycnocline are around $5 \times 10^{-5}\,s^{-2}$ with deeper values a factor of 10 or more smaller. Dynamic mode calculations result in first internal radii of deformation of around 5 ± 1 km for any station on either cruise.

The dynamic topography at the surface relative to 400 m, constructed from the vertically integrated density anomaly, represents the baroclinic circulation (Fig. 10). The dynamic topography for April–May (Fig. 10A) showed a cyclonic gyre over the northern part of the study region between

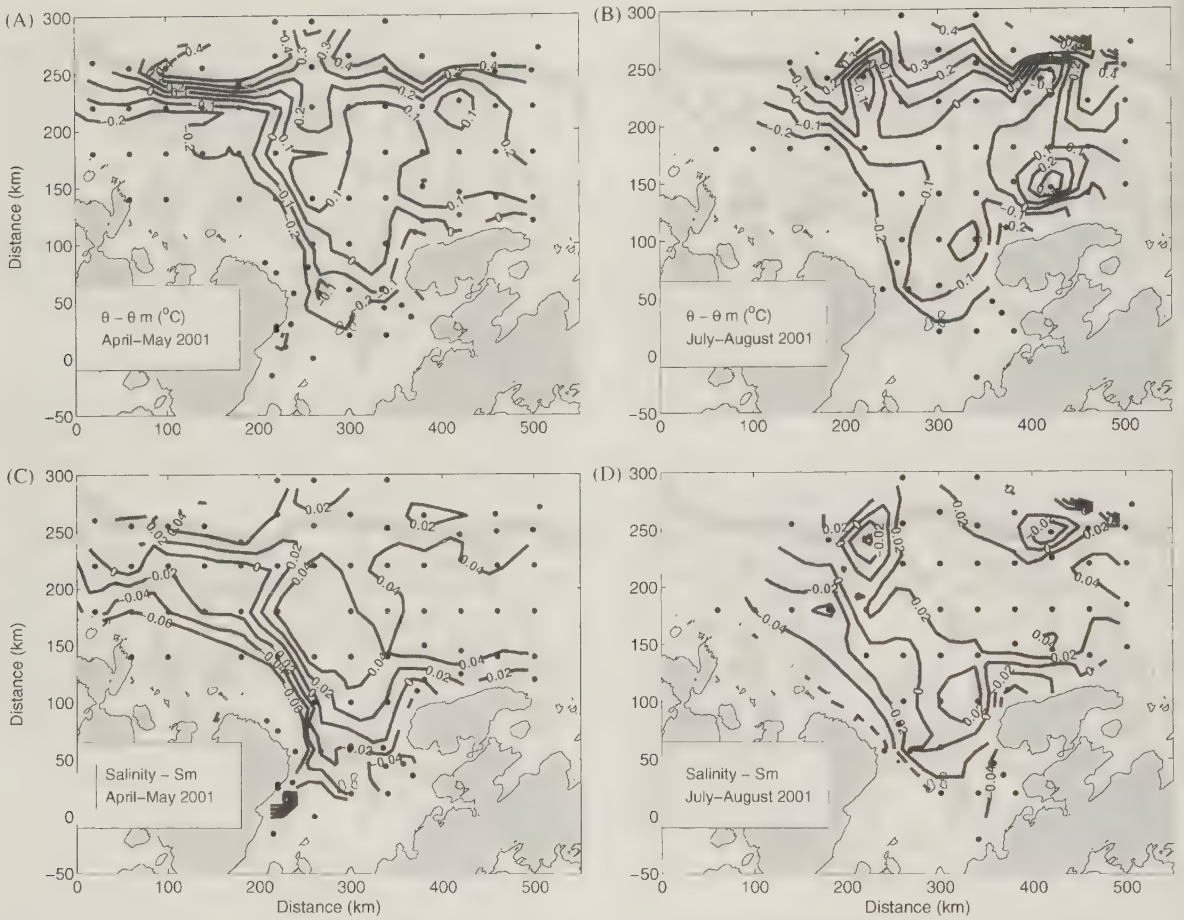

Fig. 9. Horizontal distribution of the potential temperature (θ) and salinity anomaly fields at 300 m constructed from the April–May 2001 (A, C) and July–August 2001 (B, D) observations. The spatial average of potential temperature (θ m) and salinity (Sm) at 300 m was subtracted to construct the anomaly distribution. Station locations used to construct the distributions are shown and bathymetry contours are 500, 1000, and 1500 m. Light shading shows land and geographical names are given on Fig. 1.

transects 1 and 7. This flow extended along Marguerite Trough and into Marguerite Bay.

The southwesterly flow along the offshore side of Adelaide Island turned around the southern tip of the Island and flowed into Marguerite Bay. On the other side of the Bay near Alexander Island, the flow was outward, suggesting that there is a general cyclonic circulation within Marguerite Bay. The outward flow from Marguerite Bay joined with the southerly flow which dominated the continental shelf in the southern third of the study region. This southerly flow is consistent with the slope of the isopycnals observed along the inner part of transect 10 (cf. Figs. 5E, F).

In July–August the cyclonic gyre in the northern part of the study region (Fig. 10B) was still present, although weaker than in April–May. The offshelf flow in the southern third of the study region was still apparent. A suggestion remains of southwesterly flow along the offshore side of Adelaide Island that turns into Marguerite Bay and of southward flow over the continental shelf in the southern part of the study region. However, the reduced number of stations occupied during the July–August cruise (cf. Table 1) does not allow full resolution of these features.

The dynamic height difference over 100 km across the onshelf limb of the circulation is

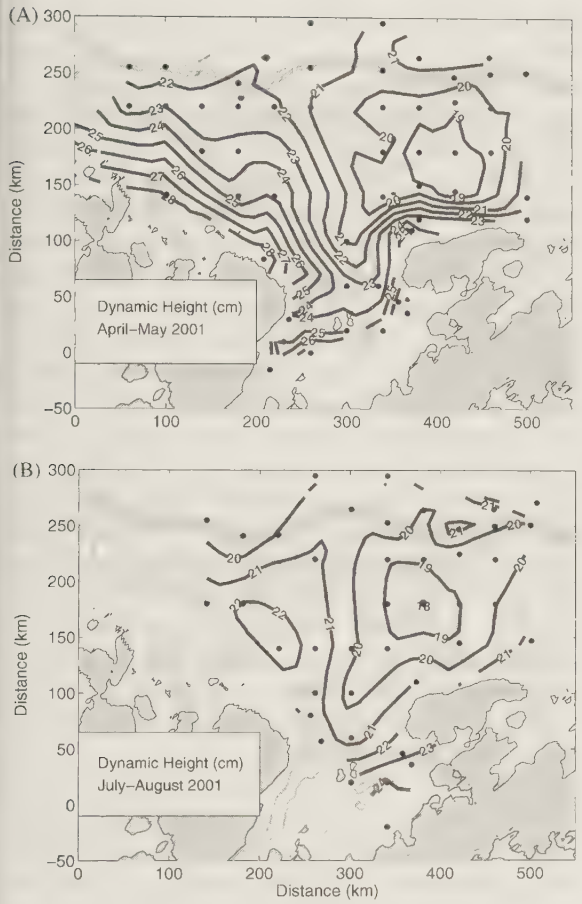

Fig. 10. Dynamic topography at the surface relative to 400 m constructed from the (A) April–May and (B) July–August 2001 observations. Station locations used to construct the distributions are shown and bathymetry contours are 500, 1000, and 1500 m. Light shading shows land and geographical names are given on Fig. 1.

0.03 m (0.21–0.18 dynamic meters) in both realizations of the gyre. This difference corresponds to a velocity of $0.03\,m\,s^{-1}$ or $2.6\,km\,d^{-1}$ at 67 °S. This weak circulation would move water parcels from the outer to inner WAP continental shelf, a distance of about 130 km, in about 50 days.

The surface flow based on drifters (drogued at 15 m) is consistent with this described flow along Adelaide Island, through Marguerite Bay and southwestward along Alexander Island (Beardsley et al., 2004). Surface flow is estimated to be $0.1\,m\,s^{-1}$ with peak speeds twice this during stronger winds. ADCP measurements of sub-pycnocline flow (discussed in the next section) show that deep flow is consistent in speed and direction with these surface drifters. Thus the dynamic topography is a reliable indicator of the flow direction but a poor indicator of speed.

3.2.6. *ADCP-derived velocity measurements*

The ADCP-derived currents are available along the cruise track for both cruises, although the data recovery is reduced during July–August due to sea ice. Tidal flow is not removed from these observations because it is only of order $1–5\,cm\,s^{-1}$ in this area (Amos, 1993; Klinck, 1995); and is not a primary component of the total flow. More problematic are the strong inertial oscillations due to strong and frequent wind events (Howard et al., 2003; Beardsley et al., 2004), which are difficult to remove due to their episodic nature. To reduce the influence of these oscillations, the 5-minute average ADCP measurements were depth averaged from 183 m to the deepest good measurement (to a maximum depth of 423 m) and gridded into boxes that were 16.7 km on a side. Averaging onto a spatial grid has the effect of time averaging the 5-minute data thus reducing the influence of the inertial oscillations. Nevertheless, there are occasional vectors that do not follow the pattern of the rest of the flow due to these oscillations.

The ADCP-derived vertically averaged currents below 183 m along the April–May cruise track (Fig. 11A) showed sub-pycnocline current patterns that are generally consistent with those suggested by the hydrography and dynamic topography (Figs. 7–10), although the ADCP currents show variability. The general pattern of the flow is onto the shelf off Adelaide Island, a cyclonic circulation through Marguerite Bay and offshore flow in the center of the sampling region. There is indication of two gyres within Marguerite Bay: one south of Adelaide Island and the other over Marguerite Trough east of Alexander Island. These flows are consistent with the flow suggested by the temperature maximum (Fig. 8A) and dynamic topography (Fig. 10A) distributions.

There is a region of onshore flow at the shelf break off Alexander Island, which is not indicated in the dynamic topography. The temperature

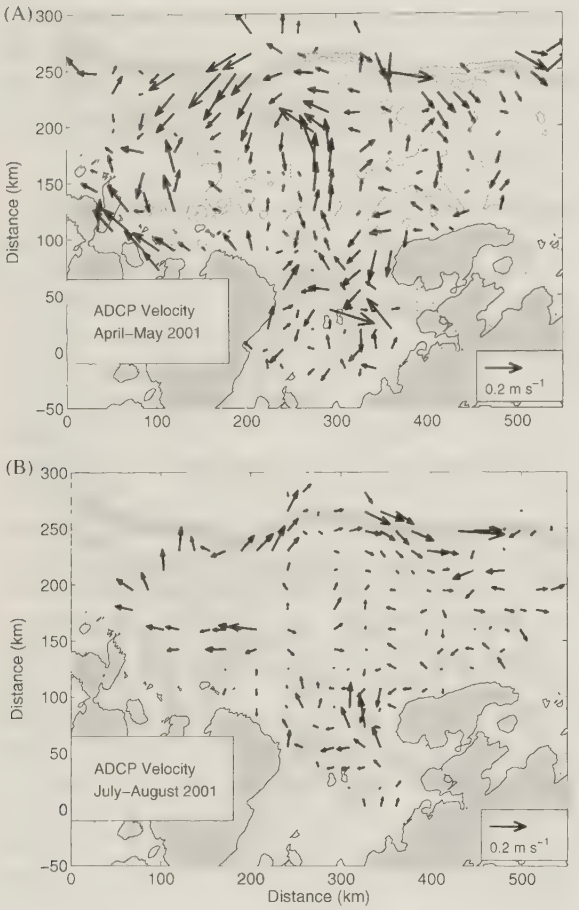

Fig. 11. Acoustic Doppler Current Profiler-derived velocity distributions for the (A) April–May 2001 and (B) July–August 2001 cruises. The ADCP records were averaged in depth from 183 to 423 m (bins 20–50) and over a spatial grid with 16.7 km spacing. Bathymetry contours are 500, 1000, and 1500 m. Light shading shows land and geographical names are given on Fig. 1.

maximum distribution has a weak plume of warm (1.6 °C) water associated with these currents (Fig. 8A) so this may be the beginning of an intrusion of UCDW onto the shelf in this area.

The more prominent flow vectors during the April–May cruise are 0.05–0.20 m s^{-1}, which is faster than indicated by the dynamic topography but consistent with velocity estimates from the surface drifters (Beardsley et al., 2004). There are only a few vectors at the shelf break indicating strong northeastward flow associated with the ACC, which may indicate that the ACC was offshore during the time that these measurements were made.

The ADCP-derived currents from the July–August survey (Fig. 11B) had reduced coverage because of interference from sea ice. Flow speeds are 0.1–0.15 m s^{-1} which are higher than indicated by the dynamic topography (Fig. 10B). A more consistent ACC occurred along the shelf break with an offshore meander near the center of the study area and an onshore meander off Adelaide Island along Marguerite Trough. Offshore flow at 0.05 m s^{-1} away from the mouth of Marguerite Bay is indicated. There is no clear indication of flow along Adelaide Island or of cyclonic flow within Marguerite Bay.

The weaker flow is consistent with the weaker dynamic topography (Fig. 10B). The plume of warm (1.6 °C) water at the shelf break off Adelaide Island is consistent with the measured flow.

4. Discussion and summary

4.1. Contribution of LCDW

The water mass structure in the Southern Ocean GLOBEC study region is relatively simple, consisting of AASW, WW, UCDW, and a modified (cooled) form of UCDW. However, one issue that is not clear is the contribution of LCDW to the water mass properties on the WAP continental shelf. LCDW water is present at the outer shelf edge and in deep depressions, such as Marguerite Trough, that intersect the WAP continental shelf. These depressions can provide pathways for this water to move onto the shelf. It is important to determine how much LCDW is present on the WAP continental shelf because of its effect on heat and salt budgets (discussed below). Also, LCDW is characterized by a silicate maxima (Smith et al., 1999; Serebrennikova and Fanning, 2004) and is thus a potential source of nutrients to the shelf.

Water with temperatures of 1.3–1.4 °C, which is characteristic of LCDW (cf. Fig. 2), fill the deeper parts of Marguerite Trough (Figs. 6A, B). However, this temperature range is also characteristic of the modified form of UCDW that floods the WAP shelf below 200 m (cf. Fig. 2). The LCDW

salinity maximum (34.74) provides a better way to locate this water. The excess salt of the LCDW should remain discernible because the deep salinity gradients everywhere are weak (Figs. 6C, D) and the vertical diffusivity is small, about $10^{-5}\,m^2\,s^{-1}$ (Howard et al., 2004).

LCDW is clearly seen in the potential temperature-salinity diagrams for sections that extended beyond the shelf break. However, only stations in Marguerite Trough showed the presence of LCDW on the WAP continental shelf (Fig. 12). In April–May, the salinity maximum associated with LCDW was present, but weak (Fig. 12A). The potential temperature-salinity diagram from the July–August cruise shows clearly the presence of LCDW in Marguerite Trough (Fig. 12B). The stations at which LCDW was present are those in the deeper part of the Trough, which is near the entrance to Marguerite Bay.

The presence of LCDW in Marguerite Trough might be expected because this bathymetric feature provides a deep connection between the outer and inner shelf. However, the depth of Marguerite Trough at the shelf edge is about 750 m, which is shallower than the core of LCDW which is near 900–1000 m. Thus, how LCDW gets into Marguerite Trough is not immediately apparent. One possibility is that there is another connection without a shallow sill at the shelf edge between the outer shelf and Marguerite Trough that is not resolved in the current bathymetry for this area. This could account for the presence of LCDW along the inner part of the hydrographic section that runs along the Trough and not along the outer portion. A second possibility is that meandering of the ACC at the shelf edge pumps LCDW over the sill and into Marguerite Trough. This would require that the LCDW be lifted about 200–300 m. The dynamics of how this might occur must await the development of high resolution numerical models or other theoretical studies for this shelf region.

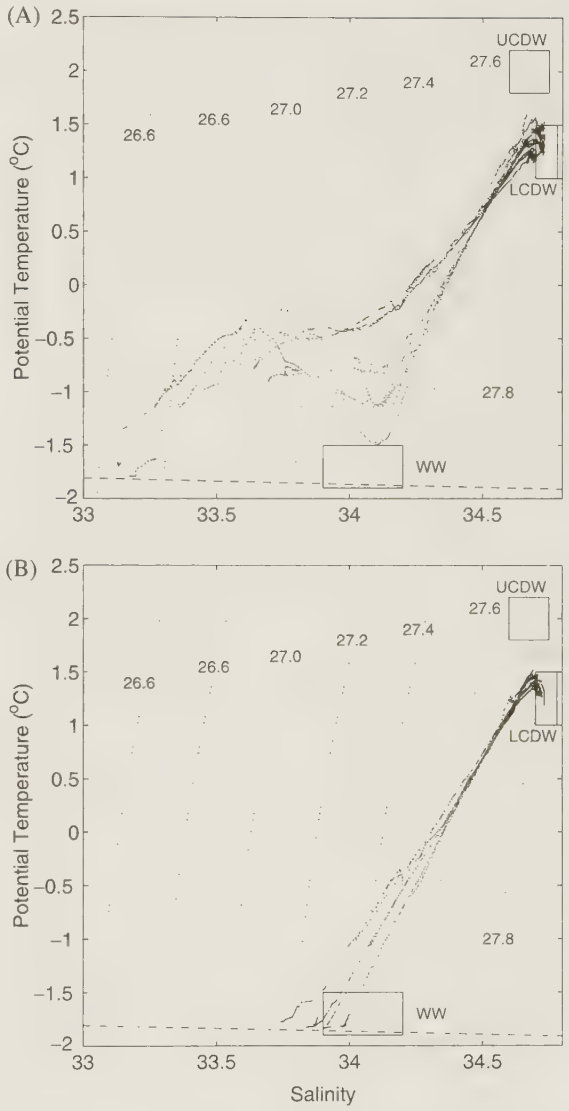

Fig. 12. Potential temperature-salinity diagrams from the stations occupied along the axis of Marguerite Trough in (A) April–May 2001 and (B) July–August 2001. The temperature and salinity ranges that characterize UCDW, LCDW and WW water masses are shown by the boxes. The potential density at the surface for the indicated temperature and salinity is shown dotted lines. The freezing point of seawater is indicated by the dashed line.

4.2. *UCDW intrusions*

The onshelf movement of CDW along the WAP continental shelf was described earlier (e.g., Potter and Paren, 1995; Talbot, 1988; Domack et al., 1992) but the extent to which these events occur along the WAP continental shelf was not appreciated until repeated measurements were made in this region, such as those described in Prézelin

et al. (2004) and those from Southern Ocean GLOBEC. Dinniman and Klinck (2004) discuss the dynamics underlying the movement of CDW onto the WAP within the context of a numerical circulation model developed for this region. Their analysis indicates that movement of CDW onto the WAP occurs when the ACC flows along the outer shelf edge and is deflected offshore by the variable topography. As the topography turns in front of the ACC, some of the water continues in a straight line onto the shelf. Thus, the introduction of CDW requires the presence of the ACC and variable topography.

Intrusions of CDW onto the WAP continental shelf are certainly related to the presence of the ACC, the location of which is determined by the 1.8 °C isotherm (Orsi et al., 1995). Thus, monitoring the location of this isotherm provides a means for inferring areas where CDW intrusions can occur. Also, movement of this isotherm away from the WAP shelf edge, perhaps due to changes in the location of the core of the ACC (Hofmann and Whitworth, 1985) or changes in the ACC transport (e.g., Whitworth, 1983), would prevent the onshelf movement of CDW, which in turn will alter heat, salt and nutrient distributions, as well as biological production on this shelf.

4.3. UCDW intrusion frequency

The temperature and salinity anomaly (Fig. 9) provide an approach to determine the number of UCDW intrusions for the period covered by the 2001 cruises. In April–May positive temperature and salinity anomalies of 0.15 °C and 0.05, respectively, were observed along the inner part of transect 4 (Figs. 9A, C), indicating the presence of warmer and saltier UCDW. The temperature maximum below 200 m showed onshelf deflection of isotherms (Fig. 8A). A second area of positive temperature and salinity anomalies occurred at the outer end of the transects 2 and 3, suggesting that one UCDW intrusion was already on the continental shelf during the April–May survey and that a second was beginning at the outer shelf in the northern part of the study region.

The temperature and salinity anomalies for the July–August cruise (Figs. 9B, D) showed positive anomalies over Marguerite Trough at the entrance to Marguerite Bay, along the inner parts of the across-shelf transects 3 and 4, and along the outer portion of transect 3 in the northern part of the survey region. This pattern suggests that the UCDW intrusion on the continental shelf in April–May moved further onto the shelf and that the intrusion that was beginning at the outer shelf in April–May moved farther onto the shelf. The displacement of the UCDW intrusion on the shelf between April–May and July–August was about 100–125 km. The time between the two surveys is about 45 days, which gives an average speed of about 0.026 m s^{-1}, which is consistent with the dynamic topography but slow compared to the surface drifter and ADCP velocity measurements. A third intrusion may have started at the outer shelf in July–August.

The hydrographic distributions indicate that two and possibly three UCDW intrusions occurred on the WAP continental shelf during the 5–6 months encompassed by the two survey cruises. If this is representative of the frequency of these events, then 4–6 UCDW intrusions could occur on this part of the WAP shelf in a year. Intrusions of UCDW are known to occur on other parts of the WAP continental shelf (e.g., Smith et al., 1999; Prézelin et al., 2000). Thus, if the frequency of occurrence observed in the Southern Ocean GLOBEC study region is assumed to be representative of that in other areas, then these events control the thermohaline characteristics of this shelf. Moreover, more than one UCDW intrusion can be present at a given time, each being in a different stage of decay (e.g., releasing heat and nutrients).

The South Atlantic Bight on the southeast US continental shelf, is similarly influenced by episodic inputs of oceanic waters (Atkinson, 1977; Atkinson et al., 1985). The Gulf Stream flows along the shelf break and meanders in response to wind forcing and bottom variations. Gulf Stream-derived water moves onto the shelf via bottom intrusions during the summer when shelf waters are stratified and winds are upwelling favorable (Atkinson, 1985; Atkinson et al., 1987). Onshelf movement of oceanic water at other times occurs via Gulf Stream frontal eddies (e.g., Lee et al.,

1991). The frequency of bottom intrusions for the South Atlantic Bight shelf was estimated to be 4–6 per year (Atkinson et al., 1987), which is similar to the CDW intrusion frequency for the Southern Ocean GLOBEC study region. The area included in these estimates is similar for both systems.

4.4. UCDW intrusion heat flux and mixing estimates

The intrusion of UCDW across the shelf break displaces shelf water and constitutes a heat flux to the WAP shelf. The temperature of the oceanic water decreases to that of the shelf in a few months (Figs. 3–6) either by vertical mixing into the surface layers and to the atmosphere or by lateral mixing with shelf water.

A volume integral of the advective-diffusive equation (Gill, 1982, Section 4.4) is used to estimate the eddy diffusivities required for this transfer. The region used for this calculation is the northeastern half of the cyclonic gyre (Fig. 10) where the movement of oceanic water onto the WAP continental shelf is most pronounced. A region 100 km on a side and 400 m deep (from the permanent pycnocline to the bottom at about 600 m) was chosen; similar results were obtained with different size regions.

Average temperature and salinity profiles were constructed from the hydrographic observations, with a 2-m resolution, for the oceanic, mid-shelf and inner-shelf (Marguerite Bay) areas. The assumption in this calculation is that mid-shelf water in the volume is replaced with oceanic water by advection. The volume looses heat by either vertical or horizontal diffusion. The specific heat, c_p, was calculated at each depth from temperature and salinity. Due to the small variation in water properties, there was little change in c_p which had a value of approximately $3999\,\mathrm{J\,kg^{-1}\,^{\circ}C^{-1}}$. Therefore, ρ and c_p can be factored from the vertical integrals with little error in the result.

The volume and time averaged heat budget is

$$\rho c_p \left[\frac{u}{L} \overline{T_o - T_m} - \frac{k}{H} \left. \frac{\partial T}{\partial z} \right|_{top} - \frac{K}{L} \left. \frac{\partial T}{\partial x} \right|_{s} \right] = 0,$$

where u is the advective speed, T_o is the oceanic temperature profile, T_m is the mid-shelf temperature profile, $L = 100\,\mathrm{km}$ is the horizontal size of the volume, $H = 400\,\mathrm{m}$ is the thickness of the volume, k and K are the vertical and horizontal diffusivities, respectively. The overbar indicates a vertical average of the temperature difference. This budget is used to estimate the horizontal and vertical eddy diffusivities based on the assumption of complete water modification either by vertical or horizontal flux every 60 d.

The vertical average temperature change between the ocean and mid-shelf is 0.3 °C. The average vertical temperature gradient in the pycnocline is $0.03\,^{\circ}\mathrm{C\,m^{-1}}$. Balancing advection and vertical diffusion requires a vertical diffusivity $k = 7.7 \times 10^{-4}\,\mathrm{m^2\,s^{-1}}$, which is similar to the values found by Smith and Klinck (2002). However, recent estimates of vertical heat diffusivity are 70 times smaller ($k = 1 \times 10^{-5}\,\mathrm{m^2\,s^{-1}}$, Howard et al., 2004). If the smaller diffusivity is correct, then it should take 70 times longer to dissipate the temperature anomaly of UCDW, which means that an intrusion should last a decade or more ($70 \times 60\,\mathrm{d} = 11\,\mathrm{yr}$).

An alternative is for heat to diffuse laterally to the rest of the shelf, especially the cooler parts of the inner shelf. The lateral temperature gradient between the mid- and inner-shelf is 0.18 °C over a distance of L. Balancing advection and lateral diffusion requires that $K = 1600\,\mathrm{m^2\,s^{-1}}$. There are no direct estimates of lateral diffusivity in this region, but a value this large would remove all horizontal gradients; which is not observed.

The above calculation shows that background levels of turbulent diffusion of heat are not sufficient to cool the intrusions of UCDW in the time that is observed, which suggests that other processes must be active to accomplish this mixing. One possibility is that localized mixing over shallow and variable topography accomplishes the heat transfer. This mixing is most easily seen in the winter when surface temperature should be at the freezing point for the given salinity, but it is not always so (Fig. 7). Certain areas near southern Adelaide Island (Fig. 7B) and along the coast of Alexander Island have water temperature 0.1 °C above freezing. Such exposure of the deep warm

water is accomplished by breeching the cold WW layer which is seen at some stations (Fig. 4A, at a distance of 50 km). Such areas will have thinner sea ice in winter and because they are tied to bathymetry, will occur with some certainty from year-to-year.

4.5. Regional circulation

The ADCP flow measurements show a southwesterly flow along the west side of Adelaide Island (Figs. 10, 11). This current is associated with salinity less than 33.6 (Figs. 3C, 7C) in the fall and slightly higher salinity (33.9) in winter. This current is likely a continuation of the southwesterly flow on the inner shelf that exists north of the study region (Smith et al., 1999). The low salinity suggests that this current results from buoyancy forcing due to sea ice melt near the coast. The southwest coast of Adelaide Island is characterized by a coastal polynya in winter, which may contribute to the higher salinity. The effect of the polynya on the coastal flow is unknown.

Flow over most of the shelf tends to be south-southwestward (Figs. 10, 11). However, in the central study region the flow turns offshore to form a closed cyclonic gyre, which is consistent with observations on other parts of the WAP continental shelf (Stein, 1992; Smith et al., 1999). The southerly flow along the western side of Adelaide Island may represent the inner limb of this larger shelf-wide flow or a separate buoyancy-driven southerly flowing coastal current or both. The cyclonic gyre is potentially important in retaining planktonic organisms on the shelf and for providing a connection between the inner and outer shelf environments (Lawson et al., 2004; Chapman et al., 2004).

ADCP-derived velocity measurements on the outer shelf indicate the northeasterly flowing ACC, which is influenced by meanders and instabilities. Offshore flows and flow reversals, such as those seen in the northern part of the study region, are consistent with an offshelf meander that then turns southward over the continental shelf. These meanders are likely persistent features of the flow that are associated with bathymetric variations. Time changes in the ACC transport are likely to contribute to these flow variations.

Acknowledgements

This research was supported by the U.S. National Science Foundation, Office of Polar Programs by grant No. OPP 99-09956 to EEH and JMK and grant No. OPP 99-10092 to RCB. Support for S. Howard was provided by grant No. OPP 99-10102 to Earth and Space Research. We thank the hydrographic team members on the two cruises, Sue Beardsley, Rosario Sanay, Aparna Sreenivasan, Sinan Husrevoglu, Jason Hyatt, and Hae-Cheol Kim, for their efforts in ensuring that the hydrographic data sets were of the highest quality. We also thank the Captains and crew of the RVIB *Nathaniel B. Palmer* and the Raytheon Support personnel on the April–May and July–August 2001 cruises for their help and assistance in acquiring the hydrographic data used in this analysis. Computer facilities and support used for the hydrographic data analyses were provided by the Commonwealth Center for Coastal Physical Oceanography at Old Dominion University. This is US GLOBEC contribution number 448.

References

Amos, A.F., 1993. RACER: The tides at Palmer Station. Antarctic Journal of the US 28, 162–164.

Atkinson, L.P., 1977. Modes of Gulf Stream intrusion into the South Atlantic Bight shelf waters. Geophysical Research Letters 4, 583–586.

Atkinson, L.P., 1985. Hydrography and nutrients of the southeastern U.S. continental shelf. In: Atkinson, L.P., Menzel, D.W., Bush, K.A. (Eds.), Oceanography of the Southeastern US Continental Shelf, American Geophysical Union, Coastal and Estuarine Sciences, vol. 2. Washington, DC, pp. 77–92.

Atkinson, L.P., Menzel, D.W., Bush, K.A. (Eds.), 1985. Oceanography of the Southeastern US Continental Shelf, American Geophysical Union, Coastal and Estuarine Sciences, vol. 2. Washington, DC, 156pp.

Atkinson, L.P., Lee, T.N., Blanton, J.O., Paffenhöfer, G.-A., 1987. Summer upwelling on the southeastern continental shelf of the USA during 1981, Hydrographic observations. Progress in Oceanography 19, 231–266.

Beardsley, R.C., Limeburner, R., Owens, W.B., 2004. Drifter measurements of surface currents near Marguerite Bay on

the western Antarctic Peninsula shelf during austral summer and fall, 2001 and 2002. Deep-Sea Research II, this issue [doi:10.1016/j.dsr2.2004.07.031].

Chapman, E.W., Ribic, C.A., Fraser, W.R., 2004. The distribution of seabirds and pinnipeds in Marguerite Bay and their relationship to physical features during austral winter 2001. Deep-Sea Research II, this issue [doi:10.1016/j.dsr2.2004.07.005].

Dinniman, M.S., Klinck, J.M. 2004. A model study of circulation and cross-shelf exchange on the west Antarctic Peninsula continental shelf. Deep-Sea Research II, this issue [doi:10.1016/j.dsr2.2004.07.030].

Domack, E.W., Schere, E., McClennen, C., Anderson, J., 1992. Intrusion of Circumpolar Deep Water along the Bellingshausen Sea continental shelf. Antarctic Journal of the United States 27, 71.

Gill, A.E., 1982. Atmosphere-Ocean Dynamics. Academic Press, New York, 662pp.

Hofmann, E.E., Klinck, J.M., 1998a. Thermohaline variability of the waters overlying the west Antarctic continental shelf. In: Jacobs, S.S., Weiss, R.F. (Eds.), Ocean, Ice, and Atmosphere: Interactions at the Antarctic Continental Margin, Antarctic Research Series, vol. 75. American Geophysical Union, pp. 67–81.

Hofmann, E.E., Klinck, J.M., 1998b. Hydrography and circulation of the Antarctic continental shelf: 150°E eastward to the Greenwich Meridian. In: Robinson, A.R., Brink, K.H. (Eds.), The Sea, The Global Coastal Ocean, Regional Studies and Synthesis, vol. 11. pp. 997–1042.

Hofmann, E.E., Whitworth III, T., 1985. A synoptic description of the flow through Drake Passage from year-long measurements. Journal of Geophysical Research 90, 7177–7187.

Hofmann, E.E., Klinck, J.M., Lascara, C.M., Smith, D.A., 1996. Water mass distribution and circulation west of the Antarctic Peninsula and including Bransfield Strait. In: Ross, R.M., Hofmann, E.E., Quetin, L.B. (Eds.), Foundations for Ecological Research west of the Antarctic Peninsula, Antarctic Research Series, vol. 70. American Geophysical Union, pp. 61–80.

Hofmann, E.E., Costa, D.P., Daly, K.L., Klinck, J.M., Fraser, W.R., Torres, J.J., 2002. US Southern Ocean Global Ocean Ecosystems Dynamics Program. Oceanography 15, 64–74.

Howard, S.L., Padman, L., Hyatt, J., 2004. Mixing in the pycnocline over the western Antarctic Peninsula shelf during Southern Ocean GLOBEC. Deep-Sea Research II, this issue [doi:10.1016/j.dsr2.2004.08.002].

Jacobs, S.S., 1991. On the nature and significance of the Antarctic Slope Front. Marine Chemistry 35, 9–24.

Klinck, J.M., 1995. Palmer LTER: Comparison between a global tide model and observed tides at Palmer Station. Antarctic Journal of the US 30, 263–264.

Klinck, J.M., 1998. Heat and salt changes on the continental shelf west of the Antarctic Peninsula between January 1993 and January 1994. Journal of Geophysical Research 103, 7617–7636.

Lawson, G.L., Wiebe, P.H., Ashjian, C.J., Gallager, S.M., Davis, C.S., Warren, J.D., 2004. Acoustically-inferred zooplankton distribution in relation to hydrography west of the Antarctic Peninsula. Deep-Sea Research II, this issue [doi:10.1016/j.dsr2.2004.07.022].

Lee, T.N., Yoder, J.A., Atkinson, L.P., 1991. Gulf Stream frontal eddy influence on productivity of the southeast U.S. continental shelf. Journal of Geophysical Research 96, 22191–22205.

Orsi, A.H., Whitworth III, T., Nowlin Jr., W.D., 1995. On the meridional extent and fronts of the Antarctic Circumpolar Current. Deep-Sea Research I 42, 641–673.

Potter, J.R., Paren, J.G., 1985. Interaction between ice shelf and ocean in George VI Sound, Antarctica. In: Jacobs, S.S. (Ed.), Oceanology of the Antarctic Continental Shelf, Antarctic Research Series, vol. 43. American Geophysical Union, pp. 35–58.

Prézelin, B.B., Hofmann, E.E., Mengelt, C., Klinck, J.M., 2000. The linkage between Upper Circumpolar Deep Water (UCDW) and phytoplankton assemblages on the west Antarctic Peninsula continental shelf. Journal of Marine Research 58, 165–202.

Prézelin, B.B., Hofmann, E.E., Moline, M., Klinck, J.M., 2004. Recognizing physical forcing of phytoplankton community structure and primary production in continental shelf waters of the western Antarctic Peninsula: Synthesis and analyses of five seasonal cruises. Journal of Marine Research 62, 419–460.

Serebrennikova, Y.M., Fanning, K.A., 2004. Nutrients in the Southern Ocean GLOBEC region: variations, water circulation, and cycling. Deep-Sea Research II, this issue [doi:10.1016/j.dsr2.2004.07.023].

Smith, D.A., Klinck, J.M., 2002. Water properties on the west Antarctic Peninsula continental shelf: A model study of effects of surface fluxes and sea ice. Deep-Sea Research II 49, 4863–4889.

Smith, D.A., Hofmann, E.E., Klinck, J.M., Lascara, C.M., 1999. Hydrography and circulation of the west Antarctic Peninsula continental shelf. Deep-Sea Research 46, 951–984.

Stammerjohn, S., Smith, R.C., 1996. Spatial and temporal variability in west Antarctic sea ice coverage. In: Ross, R.M., Hofmann, E.E., Quetin, L.B. (Eds.), Foundations for Ecological Research west of the Antarctic Peninsula, Antarctic Research Series, vol. 70. American Geophysical Union, pp. 81–104.

Stein, M., 1992. Variability of local upwelling off the Antarctic Peninsula, 1986–1990. Archiv Fischereiwissenschaft 41, 131–158.

Talbot, M.H., 1988. Oceanic environment of George VI Ice Shelf, Antarctic Peninsula. Annals of Glaciology 11, 161–164.

UNESCO, 1983. Algorithms for computation of fundamental properties of seawater. In: Fofonoff, N.P., Millard, R.C., Jr. (Eds.), Technical Papers in Marine Science 44, 53pp.

US SO GLOBEC Report Number 2, 2001. Report of RVIB Nathaniel B. Palmer Cruise 01-03 to the Western Antarctic

Peninsula, 24 April to 5 June 2001. Available from U.S. Southern Ocean GLOBEC Planning Office, Old Dominion University, Norfolk, VA, 198pp.

US SO GLOBEC Report Number 3, 2001. Reports of RVIB Nathaniel B. Palmer Cruise NBP01-03 and R/V Lawrence M. Gould Cruise LMG01-06 to the Western Antarctic Peninsula, 24 July to 31 August 2001 and 21 July to 1 September 2001. Available from U.S. Southern Ocean GLOBEC Planning Office, Old Dominion University, Norfolk, VA, 340pp.

Whitworth III, T., 1983. Monitoring the transport of the Antarctic Circumpolar Current at Drake Passage. Journal of Physical Oceanography 13, 2045–2057.

Whitworth, T., III, Orsi, A.H., Kim, S.-J., Nowlin, W.D., Jr., Locarnini, R.A., 1998. Water masses and mixing near the Antarctic Slope Front. In: Jacobs, S.S., Weiss, R.F. (Eds.), Ocean, Ice, and Atmosphere: Interactions at the Antarctic Continental Margin, Antarctic Research Series, vol. 75. American Geophysical Union, pp. 1–27.

ELSEVIER

Deep-Sea Research II 51 (2004) 1947–1964

DEEP-SEA RESEARCH
PART II

www.elsevier.com/locate/dsr2

Drifter measurements of surface currents near Marguerite Bay on the western Antarctic Peninsula shelf during austral summer and fall, 2001 and 2002

Robert C. Beardsley*, Richard Limeburner, W. Brechner Owens

Department of Physical Oceanography, Woods Hole Oceanographic Institution, Woods Hole, MA 02543, USA

Accepted 9 July 2004

Abstract

We deployed 24 satellite-tracked surface drifters near Marguerite Bay on the western Antarctic Peninsula shelf during March–May 2001 and February–April 2002. The WOCE-style drifters featured holey sock drogues centered at 15 m and were located about 20 times per day by Service ARGOS.

Analyses of the drifter tracks show a coastal current that flows toward the southwest along the west coast of Adelaide Island and into Marguerite Bay near the southern tip of Adelaide Island, then flows clockwise around the Bay near the coast, and finally exits the Bay near Alexander Island. This coastal current flowed along the eastern boundary of Marguerite Bay in 2001, but across the central part of the Bay in 2002 due to the early presence of sea ice in the southern half of the Bay. The outflow from the Bay continued along the coast of Alexander Island toward the southwest in 2001, but was directed northwestward across the shelf in 2002 due to the sea ice coverage to the south. A mean drifter current speed of about 10 cm s^{-1} was observed in the coastal current with a maximum speed of about 20 cm s^{-1} during periods of strong wind stress. An intermittent northeastward current was observed near the shelf break.

The drifter tracks also show that intermittent near-inertial currents are common in Marguerite Bay and over the adjacent shelf during ice-free conditions. These counterclockwise oscillations had periods near the local inertial period (roughly 13.0 h) and speeds of 5–20 cm s^{-1}, with a tendency for smaller amplitudes within Marguerite Bay.
© 2004 Elsevier Ltd. All rights reserved.

1. Introduction

The US Southern Ocean Global Ocean Ecosystem Dynamics (SO GLOBEC) program is a collaborative effort designed to study physical and biological factors that contribute to the enhanced growth, reproduction, recruitment, and survivorship of Antarctic krill (*Euphausia superba*) on the central western Antarctic Peninsula (WAP) shelf (Fig. 1). One primary SO GLOBEC hypothesis is that offshore forcing by the Antarctic

*Corresponding author. Tel.: +1 508 289 2536; fax: +1 508 457 2181.

E-mail address: rbeardsley@whoi.edu (R.C. Beardsley).

0967-0645/$ - see front matter © 2004 Elsevier Ltd. All rights reserved.
doi:10.1016/j.dsr2.2004.07.031

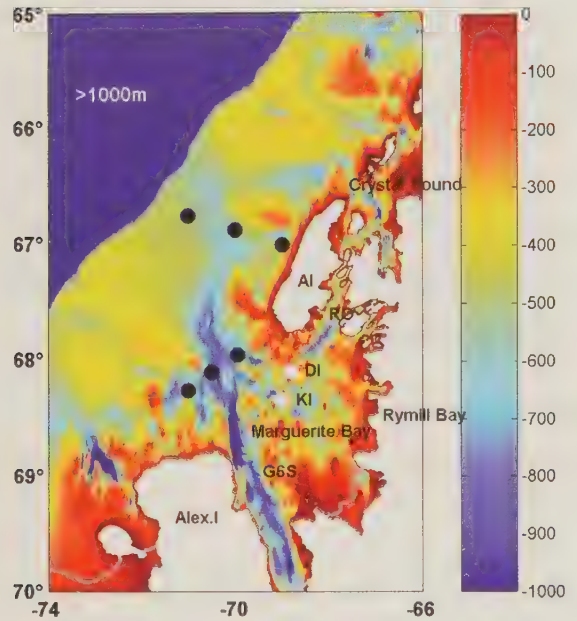

Fig. 1. SO GLOBEC study area. Location code from north to south: Crystal Sound; Adelaide Island (Al); Rothera (RO); Dismal Island (DI); Kirkwood Island (KI); Rymill Bay; Marguerite Bay; George VI Sound (G6S); and Alexander Island (Alex. I). The bathymetry color scale is shown to the right, with depths greater than 1000 m denoted by the 1000-m deep blue. The six solid black dots shown the locations of WHOI current meter moorings deployed in March 2001, and the two hollow diamonds the locations of the University of Wisconsin Automatic Weather Stations (AWSs) deployed in May 2001.

Circumpolar Current (ACC) and atmospheric surface forcing in combination with the regional topography produce a clockwise (cyclonic) circulation over the shelf that helps make the Marguerite Bay and adjacent shelf especially well suited to support large populations of krill and their primary upper trophic-level predators (seals, whales, penguins, and birds). Since this region had almost no prior direct measurements of currents, a modest program using satellite-tracked drifters to observe the near-surface Lagrangian currents was conducted to investigate the regional circulation and possible presence of a cyclonic gyre off Marguerite Bay. These drifters were deployed from SO GLOBEC cruises during the austral summer and early fall of 2001 and 2002. Since most drifters had either left the study area or failed by winter, they describe the circulation only for the austral summer and fall. The results from this drifter study are presented here.

2. Background

The bathymetry in the SO GLOBEC study region is quite variable, especially within Marguerite Bay where many shallow reefs and small islands occur in addition to a deep trough (Fig. 1) (Hofmann et al., 2004). The average bottom depth over the shelf is roughly 460 m, while the mean depth of the shelf break is about 500 m. A deep trough starting near the shelf break runs southeastward across the shelf off Adelaide Island, crosses Marguerite Bay, and continues southward around Alexander Island as George VI Sound. The maximum depth of this trough is about 1600 m, located within Marguerite Bay near Alexander Island. The presence of this trough plus several shallower cross-shelf channels and distinct protrusions of the shelf break are thought to influence the regional circulation (Klinck et al., 2003).

Recent hydrographic data provide a clear picture of the seasonal evolution of stratification over the central WAP shelf region (Hofmann et al., 1996; Smith et al., 1999). An on-shelf flow of Upper Circumpolar Deep Water (UCDW) from the ACC maintains a relatively warm, salty, nutrient-rich lower layer over the shelf beneath an upper layer of relatively cooler, fresher Antarctic Surface Water (AASW). The two layers, separated by a permanent pycnocline and centered between 150 and 200 m, provide a vertical flux of heat and salt into the upper layer (Klinck, 2001; Smith and Klinck, 2002). Over much of the shelf, net surface heating in austral spring through fall ($\sim +80\,W/m^2$) warms the upper water column to depths of 50–100 m, while increased wind mixing, surface cooling ($\sim -80\,W/m^2$), and brine rejection during ice formation in fall through winter creates a 100-m deep surface mixed layer.

In comparison, our present knowledge of flow over the WAP shelf is quite limited, being based

primarily on one First GARP Global Experiment (FGGE) drifter track from 1979, limited drifter deployments in the Bransfield and Gerlache Straits farther to the northeast (Zhou et al., 2002), recent hydrographic data (Hofmann et al., 1996; Hofmann and Klinck, 1998), incomplete knowledge of regional wind forcing, and regional tidal models (Padman et al., 2002). The FGGE drifter moved northeastward along the shelf break during austral spring, then crossed the shelf near 65.5°S and moved southwestward to Adelaide Island in summer (mean speed 6 cm s^{-1}) before failing. The mixed layer drifters deployed in the Bransfield and Gerlache Straits exhibited a regional northeastward current along the deep channel to the southern continental margin of the South Shetland Islands and cyclonic eddies over the deep basins. The 1993 summer and fall salinity sections off Adelaide Island show a coastal band of fresher (lighter) water, which increased in depth, width and salinity contrast into fall, when it extended roughly 50-m deep and 70 km offshore with a salinity difference of 0.5 psu from adjacent water (Smith et al., 1999). These observations suggest the formation of a buoyant coastally trapped current near Adelaide Island during spring and summer melt, which continued to strengthen into fall towards the southwest. Monthly mean winds over the Marguerite Bay/WAP shelf region derived using data from the National Aeronautics and Space Administration Scatterometer NSCAT were southwestward from spring into fall during ice-free conditions (M. Caruso, personal communication). These downwelling favorable winds should help drive and maintain a coherent buoyant coastal current along Adelaide Island during these seasons.

3. The drifter data set

A total of 24 World Ocean Circulation Experiment (WOCE) Surface Velocity Program (SVP) drifters were deployed near Marguerite Bay during the March–May 2001 and February–April 2002. The SVP drifter consists of a relatively small (0.5-m diameter) surface buoy housing an Service ARGOS radio transmitter, antenna, sea surface temperature sensor, battery, submergence sensor to monitor drogue presence, a tether line, and a 1-m diameter by 7-m tall holey sock drogue centered at a depth of 15 m (Sybrandy and Niiler, 1991). The drifter was designed with a 40:1 minimum drag ratio between the drogue and the surface buoy and underwater components to optimize the drifter's water-following response and minimize slippage due to wind forcing. Slippage has been estimated to be about 1 cm s^{-1} in 10 m s^{-1} winds. Each drifter was located about 20 times per day in the study area with an rms accuracy of about 0.7 km for each fix, with the drifter data transmitted to the Woods Hole Oceanographic Institution (WHOI) via ARGOS and the Internet (Appendix A). The drifter position data were first edited to remove clearly bad points and then averaged in 1-h time bins and linearly interpolated in space and time to form a basic 1-h position time series. The hourly drifter position data were then low-pass filtered with a linear-parabolic filter to remove tidal and near-inertial oscillations with periods less than 33 h (Flagg et al., 1976). High-frequency position data were computed by subtracting the low-pass-filtered drifter position data from the 1-h interpolated position data. The drifter east and north velocities were computed used centered differences. The final drifter data set and animations are available at http://www.whoi.edu/science/PO/so_globec/

The drifters were deployed in two sets each year. The first sets of drifters were deployed near the WHOI mooring sites during the summer SO GLOBEC mooring cruises abroad the ARSV *L.M. Gould* (March–April 2001; February 2002) while the second sets were launched during the subsequent fall broad-scale survey cruises on the RVIB *N.B. Palmer* (May 2001; April 2002). The initial deployment positions were chosen in 2001 to sample near the moorings on the shelf west of Adelaide Island and in the mouth of Marguerite Bay. As these drifters began to show the existence of a coherent coastal flow into Marguerite Bay, the second set of drifters was deployed to further explore this coastal current. A total of 14 drifters were deployed in 2001, and 10 in 2002.

4. Background meteorological and sea ice conditions

As part of the SO GLOBEC program, Raytheon Polar Services Corporation (RPSC) technicians deployed two Automatic Weather Stations (AWSs) provided by the University of Wisconsin Antarctic Meteorological Research Center (AMRC) on Kirkwood and Dismal Islands (small low islands located near the center of Marguerite Bay) during the May, 2001 fall survey cruise (Fig. 1). These stations transmitted vector-averaged wind speed and direction, air temperature, relative humidity and barometric pressure data back to AMRC via ARGOS, where the raw data were decoded and sent to WHOI for final processing. Both AWSs produced high-quality data through September 2002, with only a few short periods of zero wind speed or constant wind direction thought due to anemometer icing. The AWS data are self-consistent, and compare favorably with that from the British research station Rothera located on the southeastern side of Adelaide Island (Fig. 1), except for wind speed and direction at Rothera which differ strongly by from the AWS winds due to the rugged topography around Rothera.

Ocean surface wind stress was estimated using the Large and Pond (1981) neutral drag formula and the AWS sensor height above sea level. While the resulting wind stress estimates at Dismal Island exceed those at Kirkwood by roughly 13% on average (due partly to uncertainties in the effective sensor heights), the AWS stress estimates provide a good proxy for the local wind stress in Marguerite Bay. The AWS monthly averaged wind stresses are primarily southward, with an apparent increase in magnitude during austral fall and winter to values in the range 0.05–0.1 $\mathrm{N\,m^{-2}}$ (Fig. 2). The wind stress is highly variable on synoptic time scales, with the monthly mean rms magnitude generally exceeding the monthly mean wind stress throughout the measurement period. The monthly mean AWS and Rothera air

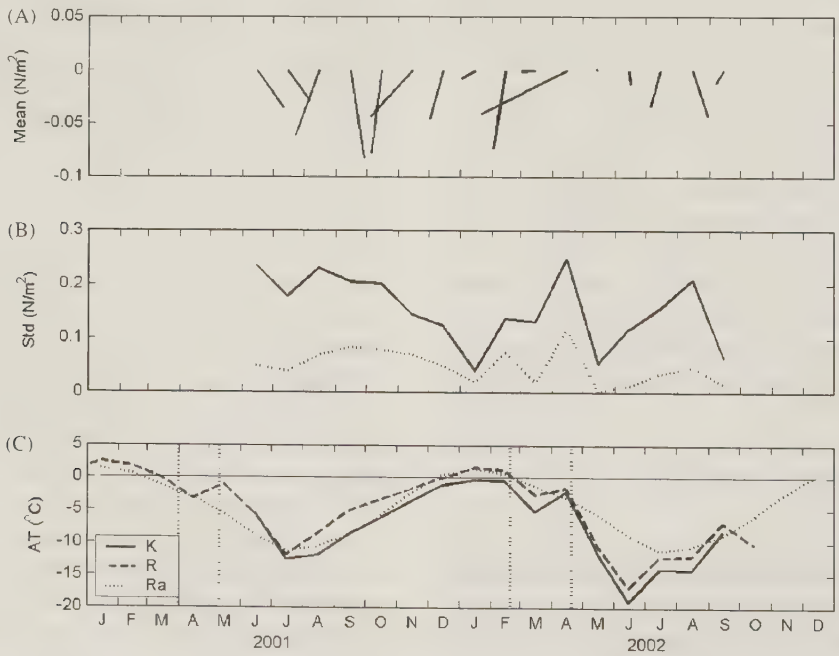

Fig. 2. (A) Monthly mean vector wind stress, (B) the monthly mean wind stress magnitude (dotted) and wind stress standard deviation (solid), and (C) air temperature (solid) measured at the Kirkwood Island (K) AWS. (The Dismal Island AWS results are similar and not shown to simplify this figure.) Rothera air temperature (R: dashed) and the 1977–2001 average mean seasonal cycle (R_a: dotted) are also shown in panel C. The vertical lines in C indicate the approximate times when the two sets of drifters were deployed each year.

temperatures track closely, and show that May and June 2002 were much colder (roughly 5 and 3 °C, respectively) than the previous year and the long-term seasonal cycle at Rothera, which contributed to the early onset of ice cover in Marguerite Bay in 2002. These 2 months were the coldest June and second coldest May on record at Rothera since 1977.

Sea ice distribution was examined using two remote sensing products. The Danish Center of Remote Sensing (http://www.dcrs.dtu.dk/sea-ice/new.antarctica/) posts daily maps of sea ice concentration based on Special Sensor Microwave Imager (SSM/I) data collected aboard Defense Meteorological Satellite Program (DMSP) satellites, while NASA (http://rapidfire.sci.gsfc.nasa.gov/production/) posts daily Moderate-resolution Imaging Spectroradiometer (MODIS) images taken on the Terra satellite. The MODIS data were limited by cloud cover, especially in winter, but have higher spatial resolution (~250 m) than the SSM/I data and showed extensive leads in the sea ice structure that were not observed with the lower resolution (~25 km) SSM/I data. In general, the sea ice concentration in Marguerite Bay is minimal in early May, and by early June, sea ice first appears at the shelf break and further offshore. In early July 2001, Marguerite Bay was relatively ice free, but sea ice was observed at the shelf break at 66°S, 400 km north of Alexander Island. In early July 2002, all of Marguerite Bay was covered with sea ice that extended beyond the shelf break at 64°S. The initial sea ice distribution during austral fall appears to be strongly influenced by advection of sea ice towards the northeast near the 1000-m isobath in addition to local heat loss.

5. Description of low-frequency drifter motion

The low-pass-filtered drifter tracks are shown next in a sequence of monthly panels in Figs. 3 and 4 for the two field years. The tracks are color-coded to show each drifter track for days 1–10 (red), days 11–20 (green), and the remaining days (blue) during each month. Since the presence of sea ice appears to reflect in part the surface circulation, the sea ice distribution at the beginning of each month is shown in light blue. Note that the sea ice in 2002 was more extensive than in 2001. One interesting characteristic of the drifter tracks over the WAP shelf is that the tracks were often not coherent with each other over separations as short as 20–30 km. The internal Rossby deformation scale L^1 is roughly 10–15 km in the study area.

5.1. 2001

During 2001, six drifters (A1–A6) were deployed in late March/early April and eight more drifters (A7–A14) were deployed in May. The deployments were generally made near Adelaide Island or near the six WHOI mooring sites (Fig. 1). In March, Marguerite Bay was generally ice free and the first drifter (A1) deployed closest to Adelaide Island moved rapidly (mean speed 22 cm s^{-1}) towards the southwest roughly parallel with the coast and local topography for 2 days just after deployment before turning more westward. The wind stress during this period was strong (0.1–0.3 N m^{-2}) towards the southwest. The other four drifters set later in March moved little during this period.

In April, the two drifters (A4, A5) deployed in the central WAP shelf moved slowly towards the southwest, remaining over the central shelf. Drifter A6 moved little before failing 5 days after launch. Both drifters (A2, A3) deployed in the central mouth of the Bay initially moved further into the Bay before turning west and exiting near Alexander Island. During April 5–10, A2 was in a strong boundary current along the northeast coast of Alexander Island, covering a distance of roughly 115 km with a mean speed of 26 cm s^{-1} and maximum speed of 43 cm s^{-1}.

[1]For a two-layer fluid, the internal Rossby radius of deformation $L = g(\Delta\rho/\rho_0)(h_1h_2/(h_1+h_2))^{2]m}/f$, where h_1 and h_2 are the upper and lower layer thicknesses, $\Delta\rho$ the layer density difference, ρ_0 the mean density, g gravitational acceleration, and f the Coriolis parameter. With $h_1 = 100$ m, $h_2 = 400$ m, $\Delta\rho = 3$ kg/m^3, and $f = 1.3 \times 10^{-4}$ s^{-1} as typical values for the study region, $L = 11$ km. Given observed stratification during summer and fall and the large variation in bottom depth, estimates of L range from 10 to 15 km.

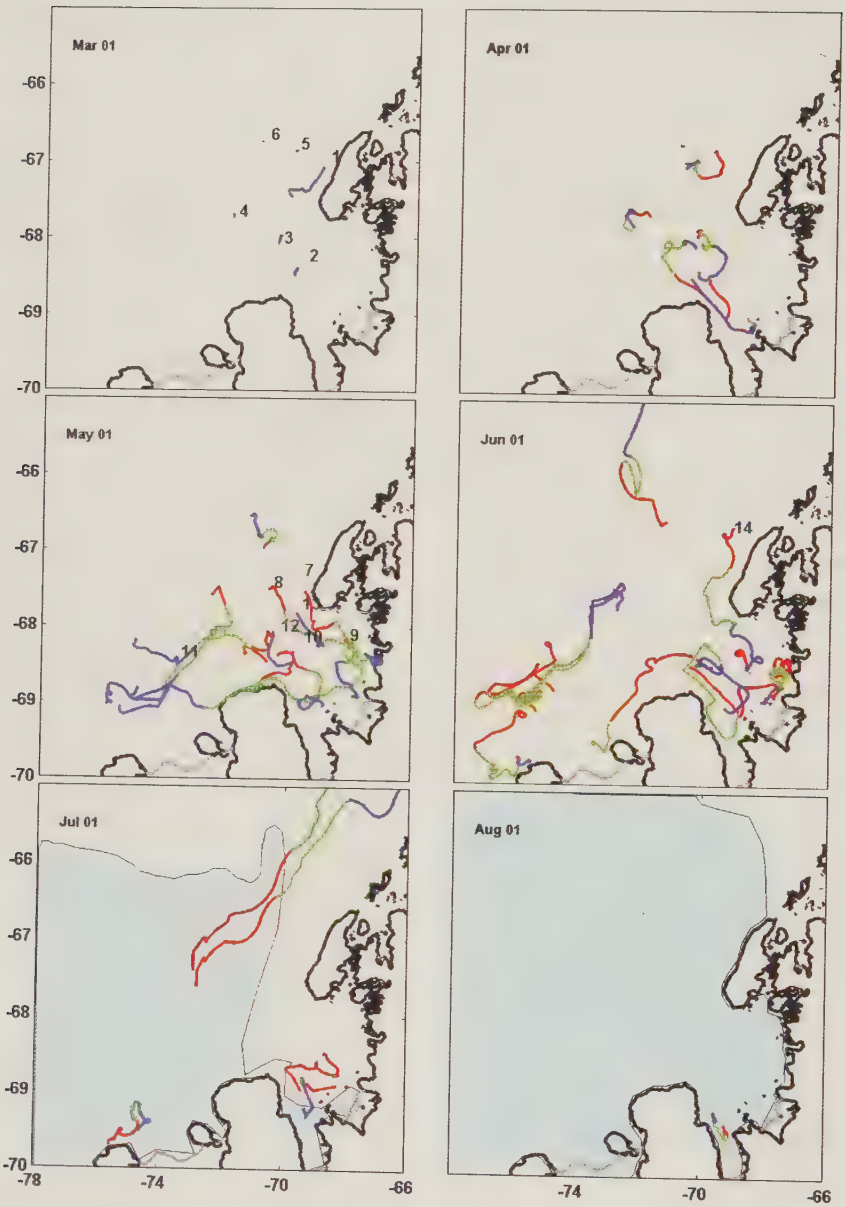

Fig. 3. Low-pass drifter trajectories during March through August 2001. In each monthly panel, the drifter track(s) is drawn using the color code red for days 1–10, green for days 11–20, and blue for days >21. The blue shading indicates sea ice cover on the first of the month for that panel.

Drifter A1 stopped transmission March 31 but was located deep within Marguerite Bay on April 21 when transmission returned. This drifter then followed A2 in the boundary current along the northeast coast of Alexander Island, with a mean speed of 28 cm s^{-1} and a maximum speed of 34 cm s^{-1} during the 5-day exit.

In May, three new drifters (A7, A8, and A13) deployed within 50 km of the west coast of Adelaide Island all moved to the southeast into

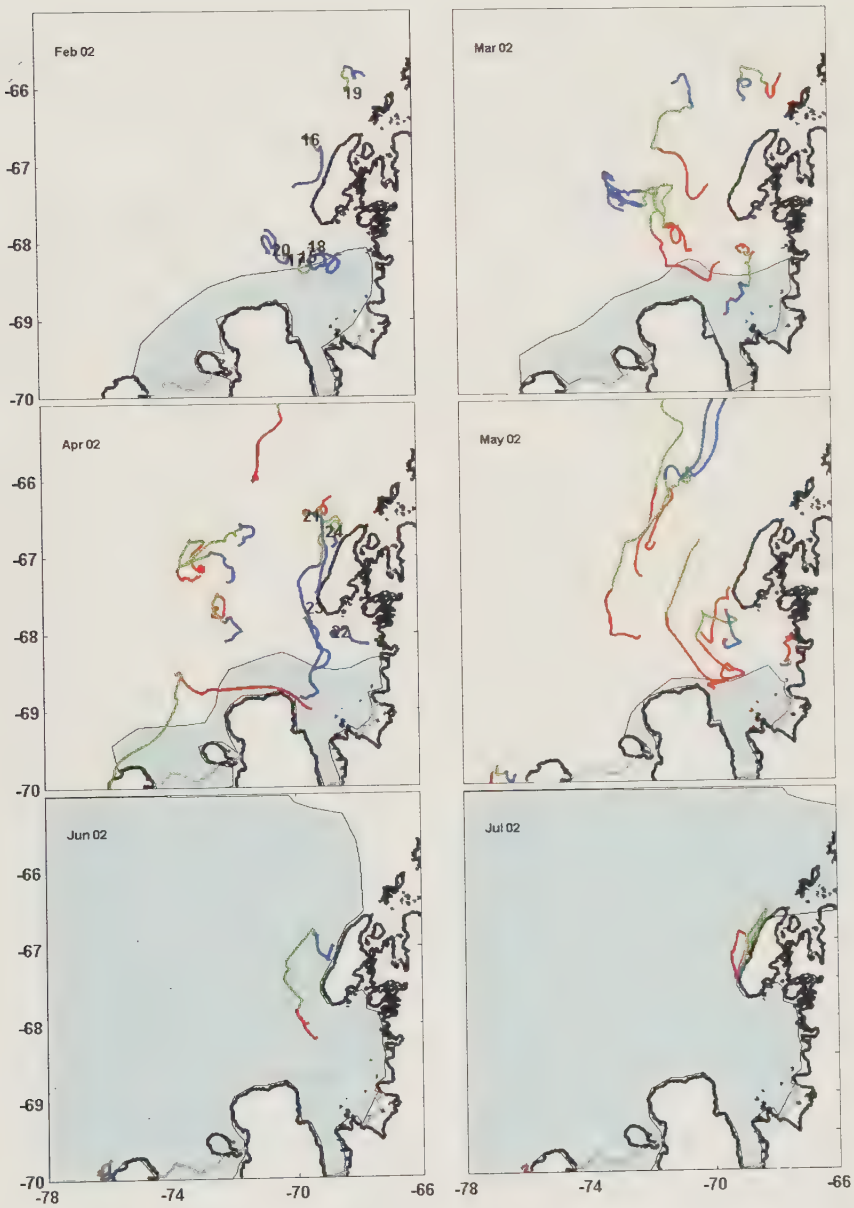

Fig. 4. Low-pass drifter trajectories during February through July 2002. In each panel, the drifter track(s) is drawn using the color code red for days 1–10, green for days 11–20, and blue for days >21. The blue shading indicates sea ice cover on the first of the month for that panel.

Marguerite Bay. While A13 failed after 17 days, A7 and A8 penetrated deep into the Bay, with A7 making a complex looping path near the coast at 68.5°S for 38 days before moving towards the southwest along the coast in June. Drifter A8 made a large clockwise path through the Bay before exiting in the boundary current off Alexander Island June 19, only to then turn northeastward and re-enter the Bay in late May. Drifter A9, deployed in the northeast corner of Marguerite Bay, also followed a large clockwise path before exiting the Bay near Alexander Island before

failing. Drifter A10, deployed in the central mouth of the Bay, moved into the Bay and then turned clockwise before exiting off Alexander Island. Drifter A14, deployed off northern Adelaide Island in early June, moved south and deep into the Bay where it failed July 6. Both A7 and A8 were also deep within the Bay when they failed in mid-June, presumably due to becoming caught in the sea ice filling in the southern end of the Bay.

Over the shelf, A5 moved so slowly during parts of April and May that we wondered if it was still working. Its mean low-pass vector speed for the 63-day period from deployment through May was only $1\,cm\,s^{-1}$ towards the northeast (its mean scalar speed was only $6\,cm\,s^{-1}$). In May, A2 and A4 continued to move slowly towards the southwest along the mid- and outer shelf, as did A11 and A12, which were deployed near the outer and mid-shelf off Marguerite Bay in late May. In June, while A3, A11, and A12 failed near or south of 69°S, presumably due to sea ice, A2 and A4 turned and followed quite similar paths up the outer shelf towards the northeast for roughly 580 km until their tracks diverged in mid-July north of 66°S. One drifter trailed the other by roughly 24 h and followed paths separated by only 20 km during this period of parallel flow, with a mean scalar speed of $22\,cm\,s^{-1}$. By July 1, the northern boundary of sea ice (based on SSM/I data) was located near 66°S over the shelf break while A2 and A4 were on the outer shelf near 67.5°S (Fig. 3). These two drifters were thus in sea ice from late June into mid-July, but did not appear to be slowed, suggesting that the sea ice was unconsolidated.

The 2001 drifter tracks show the following key features. Drifters deployed over the inner shelf west of Adelaide Island tended to move southwest in a broad coastal current that turned and entered Marguerite Bay, where these drifters generally moved around the Bay in a large clockwise flow. Outflow from Marguerite Bay tended to be concentrated in a strong narrow boundary current along the northeast coast of Alexander Island, with some drifters continuing towards the northwest out to the mid-shelf while other drifters turned towards the southwest and continued along the northwestern coast of Alexander Island. Drifters deployed over the mid- and outer shelf tended to move down-coast towards the southwest until late May when the drifters started to move northeast along the shelf in advance of sea ice.

5.2. 2002

During 2002, six drifters (A15–A20) were deployed in February and four more drifters (A21–A24) were deployed in April. These deployments were generally made at the mooring locations and north of Adelaide Island, in part because the southern half of Marguerite Bay remained covered with sea ice (formed the previous winter) through well into May.

Four drifters were deployed in mid-to-late February in open water in the northern half of the mouth of Marguerite Bay. A17 and A20 moved directly across the shelf towards the northwest, arriving near the 1000-m isobath by early April. Deployed deeper in the Bay, A15 wandered northeast and then southwest before exiting the Bay quickly along the northeastern tip of Alexander Island in early March. This drifter continued to move northwestward across the shelf, arriving near the 1000-m isobath in early April. A18, deployed about 6 h before and 19 km northeast of A20, drifted slowly clockwise around Marguerite Bay before moving rapidly out of the Bay and along the northern coast of Alexander Island to near 76°W during April 1–18, having a mean and maximum speed of 24 and $57\,cm\,s^{-1}$, respectively. Both MODIS and SSM/I sea ice data suggest that A18 was in open water surrounded by sea ice during part of its passage out of the Bay and westward. There is no obvious symptom of the ice in the drifter data. A21, deployed even farther into the Bay in April, moved eastward and south along the coast until failing in mid-May.

The remaining six drifters were deployed to the west and north of Adelaide Island, to investigate the coastal current identified in the 2001 drifter data. Both A16 and A19, set in February, moved generally towards the south, but neither entered Marguerite Bay. A16 reached 67.5°S before turning towards the northwest, nearing the 1000-m isobath in mid-March and then following the continental margin northeastward. A19 followed a looping path generally towards the southwest over

the mid-shelf until it headed south before failing near Adelaide Island on April 22. A19 had a mean speed over its 70-day life of 9 cm s^{-1} and a maximum speed of 27 cm s^{-1}, with a mean vector speed of only 2 cm s^{-1} southward towards Adelaide Island.

A22 and A24, set 39 km and 9 h apart on April 16, both drifted directly south into the mouth of the Bay. Over its 20-day life, A22 had mean and maximum speeds of 15 and 41 cm s^{-1}, respectively, with a mean vector speed of 10 cm s^{-1}. A24, starting closer to Adelaide Island, moved south to 68.5°S in just 15 days, with a mean speed of 19 cm s^{-1} and a maximum speed of 42 cm s^{-1}, with a mean vector speed of 15 cm s^{-1}. Then A24 made a large slow counterclockwise turn and moved back west and north. A23, deployed April 22 close to the southwestern tip of Adelaide Island, moved generally southward into the Bay, reaching 68.8°S off Alexander Island before turning northwest in early May. During this 8-day period, A23 had a mean speed of 19 cm s^{-1} and a maximum speed of 34 cm s^{-1}, with a mean vector speed of 16 cm s^{-1}. The southward motion of A19, A22, A23, and A24 towards or into Marguerite Bay during April 19–May 1 is evidence of a strong coherent southward coastal current along Adelaide Island during this period.

Remote sensing and observations during the *Palmer* fall 2002 broad-scale survey cruise suggest a rapid advance of sea ice towards the northeast over the shelf in early May. During May 10–14, A17, A23, and A24 moved first northwest and then turned and moved northeastward as a coherent flow spanning the shelf (with A17 nearest the shelf break and A24 nearest the mouth of Marguerite Bay). On May 15, A24 appeared to become stuck in ice while the other two drifters continued unhindered northeastward along the shelf.

In summary, a strong southward surface current was observed along the west coast of Adelaide Island in late April, but this current veered offshore in early May and moved across the shelf rather than flowing deep into the northern part of Marguerite Bay. Three of the four drifters deployed in late February near the center of the mouth of Marguerite Bay moved across the shelf towards the northwest in March, before eventually moving northeastward along the shelf break and leaving the study area by mid-May. While two drifters left Marguerite Bay along the northeast end of Alexander Island, only one continued along the northern coast of Alexander Island towards the southwest.

6. Statistical properties of the low-frequency drifter motion

In an attempt to describe the spatial structure of the surface circulation in Marguerite Bay and adjacent shelf, spatial (bin) and temporal averaged statistics for the drifters were computed for the domain 66–70°S, 66–72°W. Because the character of the trajectories appeared to differ significantly in 2001 and 2002, temporal averages were made for each year rather than for the combined data set. For each year, means and principal axes of the low-passed drifter velocities were computed for 1/4° latitude by 1/2° longitude (~24 km) boxes. To estimate the uncertainties in the mean currents, the number of degrees of freedom (ndof) for each box was computed assuming that each drifter followed independent tracks and a Lagrangian integral time scale of one day for both east (u) and north (v) velocity components (estimated from the drifter Lagrangian velocity autocorrelation functions). The number of ndof was calculated for each individual drifter track within a defined bin by dividing the length of time the drifter was in the bin by twice the Lagrangian integral time scale and rounding up to the nearest integer. The total ndof for each bin was the sum of the ndof's for each track within the bin. The ndof varied from one (only one independent observation within the box) to a maximum of 34. The 95% confidence limits for u and v were then computed as $\pm 1.96 \times \sigma_u/\sqrt{\text{ndof}}$ and $\pm 1.96 \times \sigma_v/\sqrt{\text{ndof}}$. These statistics cover the period March 26–August 31 in 2001 and February 12–July 11 in 2002.

The resulting mean currents and principal axes for both years are shown in the upper two panels in Fig. 5 for all boxes containing at least 36 hourly observations. In the lower two panels in Fig. 5 are plotted the mean currents which have one or both

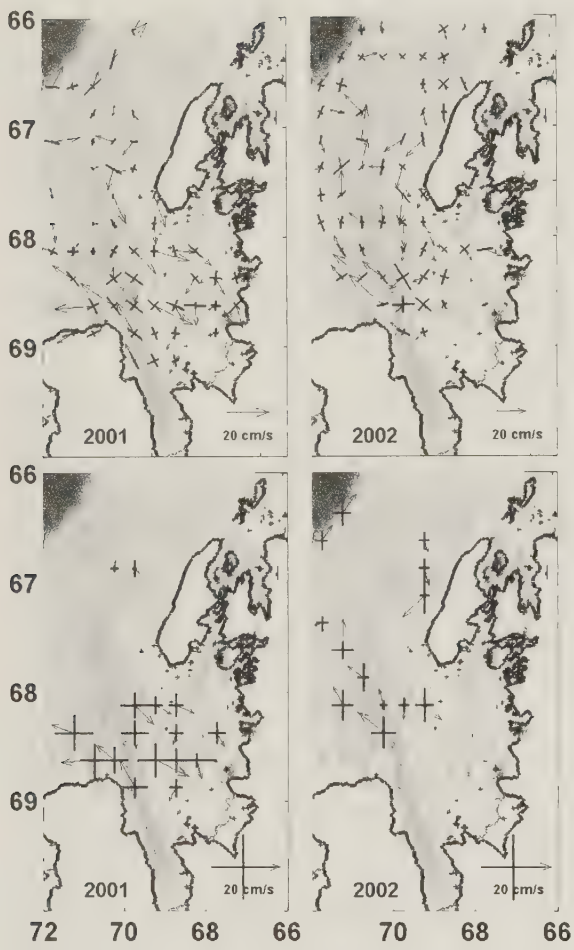

Fig. 5. Upper row shows the mean Eulerian current vectors and principal axes based on low-passed drifter motion during March–August 2001 (upper left) and February–July 2002 (upper right). Results are shown for bins with a minimum of 36 h of drifter observations. Lower row shows for the same time periods the mean Eulerian current vectors in bins where the east or north or both current components exceed the 95% confidence limits and ndof >3. The velocity scale is given in the lower right of each panel.

components exceed the 95% confidence limits in boxes with ndof>3. Despite the relative uncertainties, the mean currents show a significant and consistent pattern of surface circulation in the study area. In both years, there is a clear indication of outflow from the southern end of Marguerite Bay, with mean speeds above 10 cm s^{-1} near the northeastern tip of Alexander Island, and weaker inflow into the Bay around the southern end of Adelaide Island. The mean velocities over the inner shelf west of Adelaide Island are weak but generally have a southward component, while those over the outer shelf and shelf break are generally northeastward. The principal axes tend to be polarized near the mouth of Marguerite Bay, with the major axis oriented northwest–southeast in both years. The major axes varied in amplitude from roughly 10 to 20 cm s^{-1}.

7. Mesoscale eddy variability

The low-frequency drifter tracks show relatively little mesoscale eddy variability over the WAP shelf. The primary features of the surface flow (e.g., the coastal current off Adelaide Island, the inflow and outflow from Marguerite Bay) appear to have horizontal scales well in excess of the local Rossby deformation scale L (~10–15 km during austral summer and fall). However, two drifters within Marguerite Bay showed intense eddy activity over 2–6 weeks beginning May 2001. Each drifter suddenly began repeated cyclonic (clockwise, CW) and anticyclonic (counterclockwise, CCW) looping, making separate closed loops with diameters less than 20 km and periods of 2–5 days. None of the other drifters showed any indication of such mesoscale eddy motion over the WAP shelf.

Drifter A13 was located in Marguerite Bay and moving towards the southeast without any appreciable eddy motion during mid-May. On May 26, this drifter suddenly began a series of 5 consecutive CW loops over the next 12 days with radii of 3–6 km and a mean speed of 12 cm s^{-1} (Fig. 6). The eddy motion was centered over a 400-m east–west channel between two shallow (<300-m) ridges, and ended abruptly on June 6 when the drifter again headed southeast in deeper water. The AWS data from nearby Kirkwood Island show storms on May 25 and 27, with wind stresses of about 0.3 N m^{-2}. The origin of this eddy motion is unknown, although it is possible that the eddy motion may have been generated by the interaction of the wind-driven flow with the local topography.

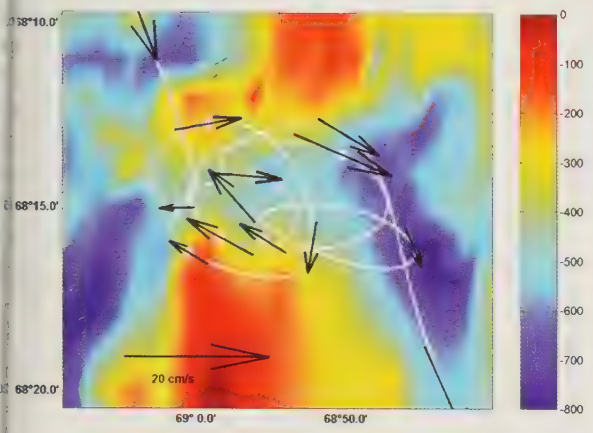

Fig. 6. Drifter A13 low-pass filtered track near Kirkwood Island during May 29–June 24, 2001. White dots are plotted every 24 h along the track, and the black velocity vector plotted every 60 h. The bottom depth color scale in m is shown to the right.

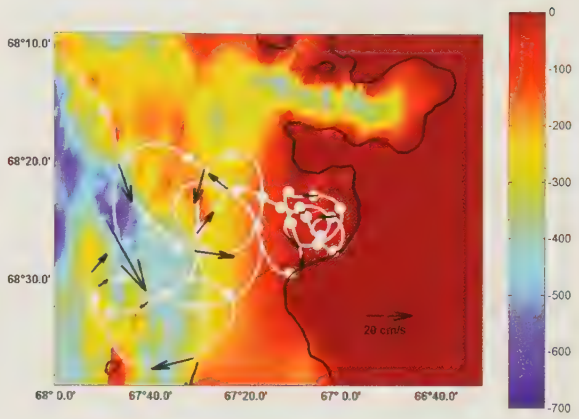

Fig. 7. Drifter A7 low-pass filtered track in and near Rymill Bay during May 29–June 10, 2001. White dots and black velocity vectors are plotted every 24 h along the track. The drifter entered the region from the northwest and exited to the south. The depth color code is shown to the right.

Drifter A7 was also moving smoothly southeastward in mid-May before suddenly starting looping on May 20 in Rymill Bay, located along the central eastern coast of Marguerite Bay (Fig. 7). The drifter made 3 CCW circuits with periods of about 2 days and radii of 3–6 km within Rymill Bay before moving westward 20 km in front of Rymill Bay. The drifter then made 2 more CCW loops with longer time scales (2–5 days) and larger radii (10–20 km). Finally the drifter completed 2 CW loops over the next 10 days before leaving the region, moving southward parallel to the coast with no more eddy motion. The mean drifter speed during the looping motion was 12 cm s^{-1}, with a standard deviation of 7 cm s^{-1}. The minimum eddy speed was 7 cm s^{-1} (loop 2) and the maximum speed was 21 cm s^{-1} (loop 5).

The Rymill Bay region is relatively unexplored and little bathymetric data exist except for some soundings on the western side of Fig. 7. A storm passed the region on May 21, perhaps forcing the coastal current and generating eddies through the interaction of the coastal current with the local headlands. In general, too few drifters were deployed to properly resolve the mesoscale variability within Marguerite Bay, but these two drifters did demonstrate the existence of eddy motion on the Rossby deformation scale.

8. High-frequency motion

The hourly unfiltered drifter position data reveal intermittent high-frequency oscillatory motion that is more noticeable when the drifter's low-frequency motion was slower. The track of A5 (Fig. 8) for the 60-day period March 31–May 30, 2001 nicely illustrates this behavior. While the drifter moved generally towards the west and north over the shelf west of Adelaide Island, it made several distinct series of CCW loops with diameters up to 6 km. The rotary kinetic energy spectrum for this period (Fig. 9) shows that most of the high-frequency current variability occurred in the CCW inertial/semidiurnal tidal (I/SD) frequency band (periods between 15.4 and 11.4 h), with the largest contribution near the local inertial period at 13.1 h. Since the rotary spectra for most other drifters also exhibit a clear CCW peak near the local inertial period, simple complex demodulation was used to generate time series of amplitude and phase of the dominant oscillatory motion for each drifter. A single CCW-rotating current mode with period T was fit using least squares to the high-passed drifter velocity over a window of fixed length W that was advanced in time. An example of this demodulation is given next.

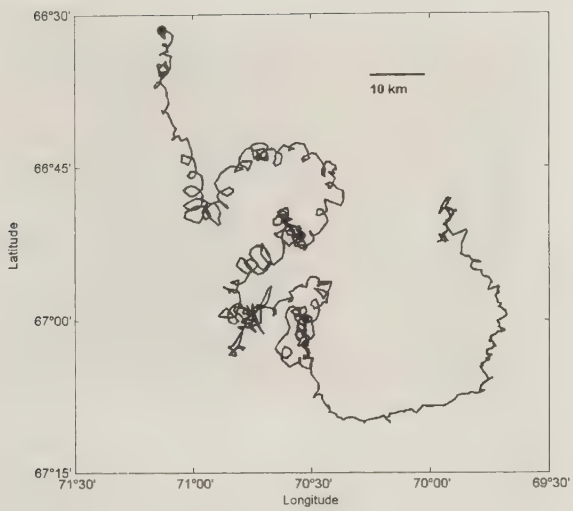

Fig. 8. Track of drifter A5 for period March 31–May 30, 2001, when the drifter moved generally towards the northwest. A 10-km scale is shown in the upper right for comparison.

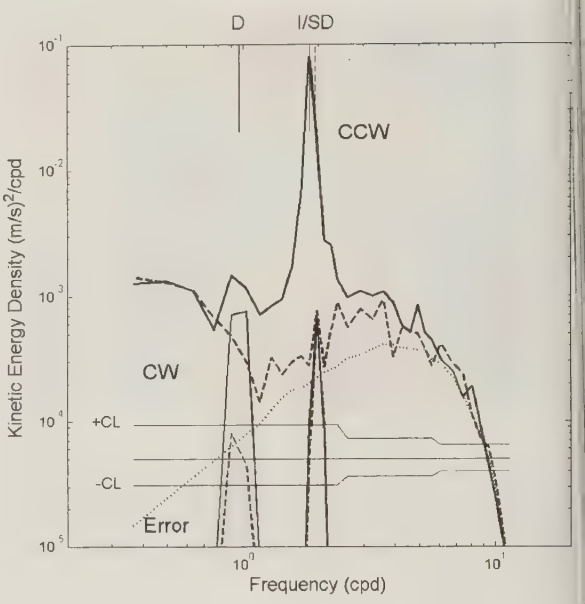

Fig. 9. Drifter A5 rotary kinetic energy spectrum for 60-day period March 31–May 30, 2001. The counterclockwise (CCW) and clockwise (CW) components denoted by solid and dashed curves. The dotted curve represents the ensemble-average CW and CCW contributions due to the random position errors added to the raw position data. Solid vertical lines show the center of the diurnal tidal band (24.8 h) and local inertial period (13.0 h), while a vertical dotted line shows the center of the semidiurnal tidal band at 12.2 h. The lower shaded peaks show the CCW barotropic diurnal and semidiurnal tidal contributions predicted using the Padman et al. (2002) tidal model with realistic topography along the path of A5 during this period. The 95% confidence limits are plotted along the bottom of the figure for reference.

By March 28, 2002, three drifters (A15, A17, and A20) had moved across the shelf to within 25 km of each other and the shelf break west of Adelaide Island (Fig. 10). Over the next 7 days, the CCW mode for each drifter (computed with T and W equal 13 h) exhibited different behavior (Fig. 11). By early March 30, all three drifters showed an onset of I/SD-band motion, with amplitudes about 5–20 cm s^{-1} and relative phases within 30°. During April 1, the CCW mode amplitude for A17 increased to about 30 cm s^{-1} and remained above 15 cm s^{-1} for the next 3 days, while the A15 and A20 amplitudes decreased to <15 cm s^{-1}. During this period, when A17 moved onshelf away from A15 and A20, the phase difference between A17 and the other two increased to 50–70°. During March 30–31, the low-frequency motion of A15 was northeastward while that of A20 was in the opposite direction (Fig. 10); the resulting horizontal shear (7 cm s^{-1} over 6 km) was 0.9% of the Coriolis parameter f, suggesting that the relative vorticity ζ (due to the local mesoscale shear) may be large enough to cause significant spatial and temporal variations in the effective Coriolis parameter $f_{\text{eff}} = f + 0.5\zeta$ that governs the dynamics of the local inertial flow (Kunze, 1985; Kunze and Boss, 1998).

These two examples show that near-inertial oscillations occur intermittently over the WAP shelf near Marguerite Bay during austral summer. Rotary spectra for most other drifters also exhibit a clear CCW peak near the local inertial period, indicating that near-inertial waves occur in the surface flow in the SO GLOBEC study area during summer and fall ice-free conditions. While peak CCW I/SD-band velocities reached 30 cm s^{-1} for several days over the shelf and in the mouth of Marguerite Bay, the rms high-frequency velocity (computed over 15-day segments) ranged from 10 to 12 cm s^{-1}, with the rms CCW I/SD-band velocity varied from 5 to 10 cm s^{-1} (Fig. 12). The few drifters that penetrated deep into Marguerite Bay exhibited less high-frequency variability, with

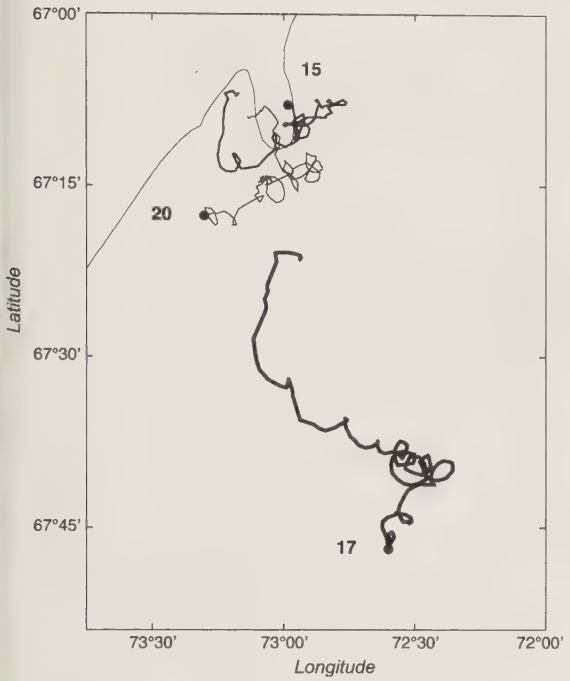

Fig. 10. Tracks of drifters A15, A17, and A20 during March 29–April 4, 2002. The large circle indicates the last position of each track. The 1000-m isobath indicates the approximate position of the shelf break in the northwest corner of the figure.

rms velocities generally less than $6\,cm\,s^{-1}$ and CCW I/SD-band velocities less than $3\,cm\,s^{-1}$.

Over the shelf and in the mouth of Marguerite Bay where the bottom topography is relatively well known, the observed high-frequency currents far exceed the total diurnal and semidiurnal barotropic tidal currents predicted at the drifter positions using the state-of-the-art tidal model of Padman et al. (2002). An example of this is shown in Fig. 9, where the tidal kinetic energy spectrum for A5 exhibits clear peaks in the diurnal and semidiurnal bands, however, the tidal semidiurnal peak is roughly two orders of magnitude smaller than the observed CCW peak near the local inertial period, and the tidal CCW diurnal peak, while roughly 70% of the measured diurnal peak, contributes relatively little to the overall high-frequency current variance. This suggests that the observed I/SD-band currents over the shelf are not due primarily to the barotropic tides nor to the baroclinic tides forced by the weak barotropic tidal flow over the shelf topography (this may be less true near the shelf break where barotropic diurnal tidal currents can force trapped topographic vorticity oscillations, see Howard et al., 2004).

One likely candidate for exciting the near-inertial oscillations is wind forcing. While several examples of storm passage nearly coincident with the onset of strong CCW I/SD-band motion could be found, the existing AWS surface wind data are too limited spatially to investigate this hypothesis in any detail

9. Ice drift

Drifters deployed in both years generally stopped transmitting within 2–4 months of launch, presumably due to the formation of sea ice and the surface floats being either crushed or submerged under the ice. However, in 2002, one drifter (A24) transmitted data during the entire winter (Fig. 13). This drifter was located in sea ice near Adelaide Island from mid-May through January 2003. Sea ice in this area is constantly influenced by the surface wind stress, with the formation of very large solid sheets caused by convergent and/or onshore winds while divergence and/or offshore winds can create large cracks (leads) and open water regions (polynyas). While SSM/I images of sea ice generally cannot resolve leads due to poor spatial resolution, they can be observed in high-resolution MODIS images like Fig. 14, taken on September 6, 2002. This image shows the ice covered shelf region just west of Adelaide Island. The Fuchs ice piedmont, mountains, and sun shadows of the mountains on Adelaide Island are clearly visible in the image. The region west of Adelaide Island has broken ice with large leads and a large region of open water near the southern coast of the island.

Drifter A24 was deployed on March 15 northwest of Adelaide Island and moved into and clockwise around Marguerite Bay until the end of May, at which time the Bay had become covered with ice (Fig. 13). A24 then moved northward with the sea ice in June almost back to its initial deployment position. During June through

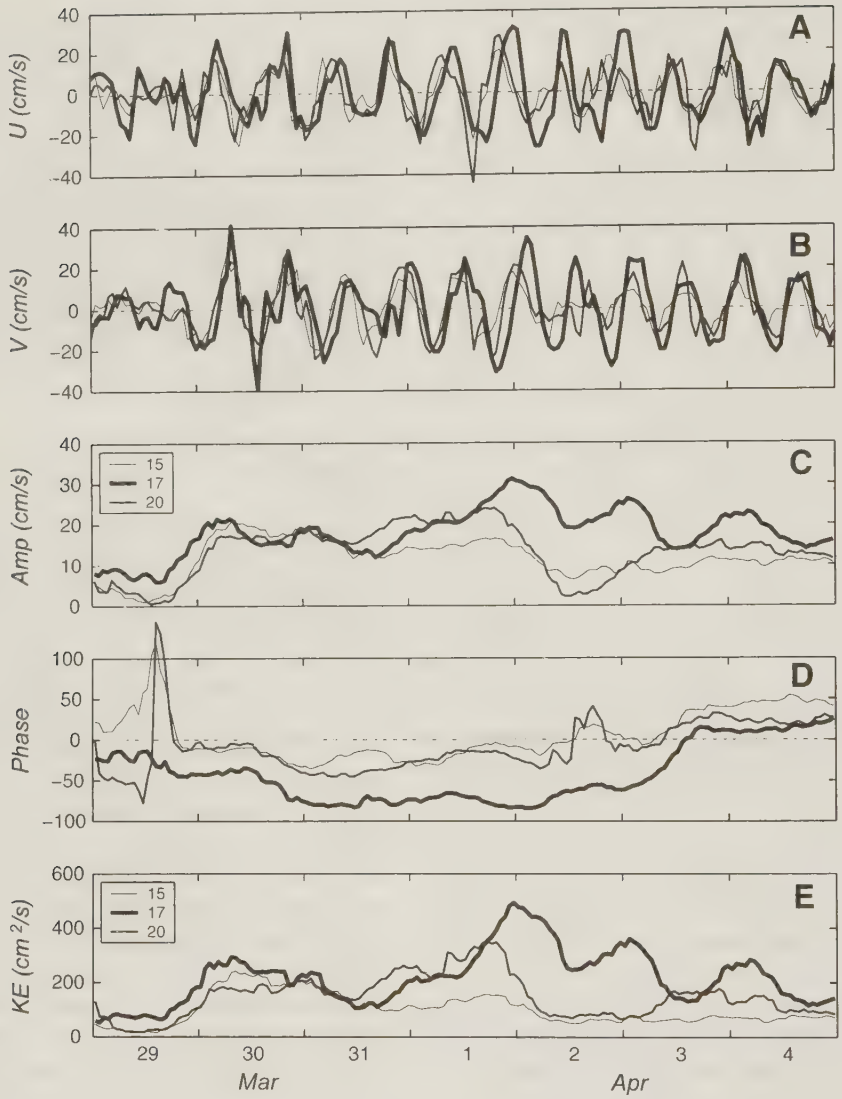

Fig. 11. High-frequency currents of drifters A15 (thin), A17 (thick), and A20 (medium) during March 29–April 4, 2002. East and north components are shown in panels (A) and (B), the CCW I/SD mode amplitudes and phases in panels (C) and (D), and the total high-frequency kinetic energies in panel (E). These demodulation results were computed using the CCW mode period T and window W equal to 13 h (the local inertial period) and a window advance of 1 h. Computations with slightly different T and $W=26$ h gave quite similar results.

September, the drifter moved back and forth about 60 km, northeastward and southwestward, roughly parallel to the west coast of Adelaide Island. A24 stopped moving near the southeast coast of Adelaide Island for the first 3 weeks in August, apparently stuck in fast ice, then began moving again in late August. Finally, during October, A24 began to move offshore although the drifter was still located within sea ice at the end of October.

The position of A24 on September 6 is shown in Fig. 14. Based on this and other high-resolution images, we think that A24 moved with the ice or in leads after mid-May. In particular, the rapid

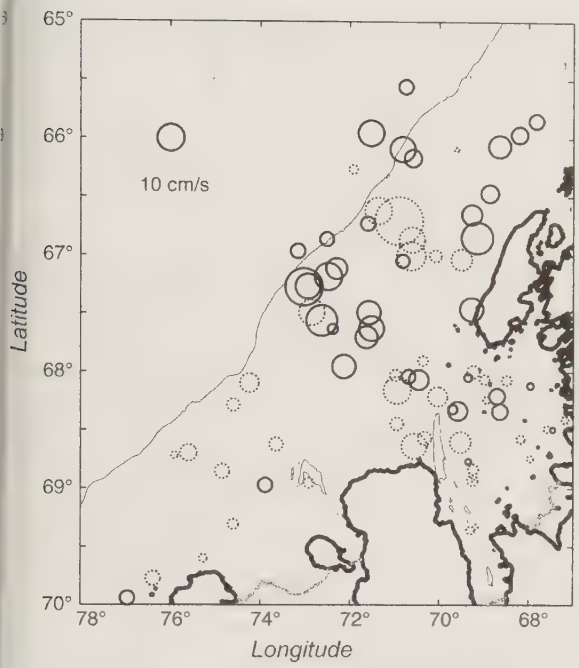

Fig. 12. Map of CCW I/SD-band rms speed computed in 15-day non-overlapping segments along each drifter's track in 2001 (dashed) and 2002 (solid). The 1000-m isobath is shown by the thin line.

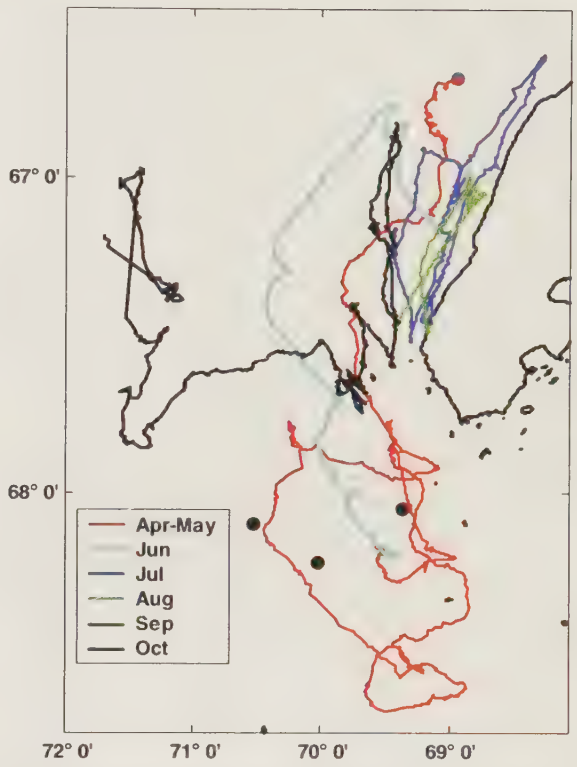

Fig. 13. Track of drifter A24 during 2002. A24 entered the sea ice around May 15. The coastline of Adelaide Island and the three C mooring sites are plotted in black.

back-and-forth movement close to Adelaide Island probably occurred in the relatively open water region frequently seen there and may be locally wind-driven.

10. Summary and conclusions

As part of the US Southern Ocean GLOBEC program, we deployed 24 satellite-tracked surface drifters near Marguerite Bay on the WAP shelf during the 2001 and 2002 austral summer and fall. Since most of these drifters had either left the study area or failed by winter, they provide an initial description of the near-surface (15-m) circulation for austral summer and fall only.

Analysis of the drifter tracks suggests the existence of a persistent coastal current flowing southward along the west coast of Adelaide Island and into Marguerite Bay near the southern tip of Adelaide Island, then flowing clockwise around the Bay near the coast, and finally exiting the Bay near Alexander Island. This coastal current flowed along the eastern boundary of Marguerite Bay in 2001, but across the central part of the Bay in 2002 due to the early presence of ice in the southern half of the Bay. The outflow from Marguerite Bay continued along the coast of Alexander Island toward the southwest in 2001, but was directed northwestward across the shelf in 2002 because of the early ice coverage. A mean drifter current speed of about $10\,\mathrm{cm\,s^{-1}}$ was observed in the coastal current with maximum speeds of about $20\,\mathrm{cm\,s^{-1}}$ during periods of strong favorably directed wind stress.

Hydrographic data collected both prior to and during the 2001–2002 SO GLOBEC field program by Klinck et al. (2003) show a surface band of fresher (lighter) water along the west coast of Adelaide Island during austral summer and fall. This observation, combined with the drifter data

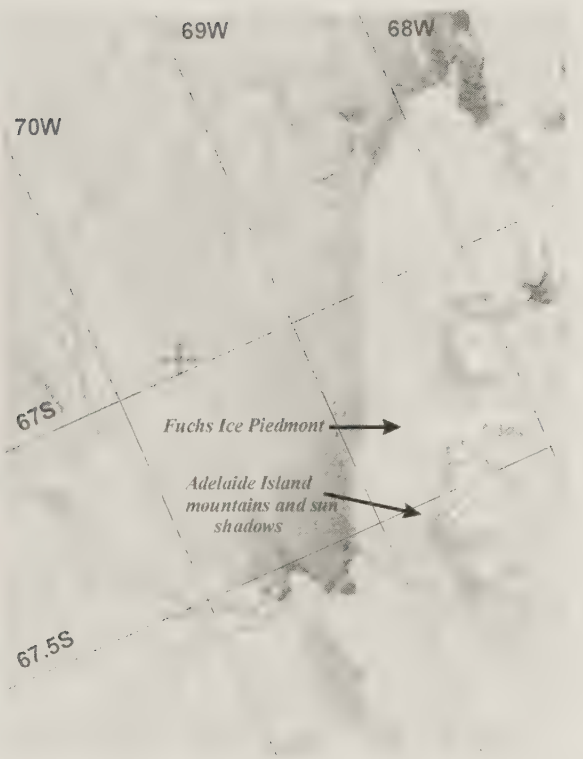

Fig. 14. MODIS image on September 6, 2002, showing the sea ice distribution west and south of Adelaide Island. The red cross shows the location of drifter A24 on this date.

and the AWS measurements indicating mean southward wind stress in Marguerite Bay, suggest that the observed coastal current is surface-intensified and driven by both buoyancy and winds. The mean southward wind stress is downwelling-favorable, which helps keep the fresher surface water near the west coast of Adelaide Island and the coastal current spatially coherent. The upstream source of this fresher water is thought to be Crystal Sound and the more northern inner shelf, where significant sea ice and glacier melt presumably occurs in summer through fall.

Drifters that reached the outer shelf near Marguerite Bay generally moved towards the northeast parallel to the shelf break until eventually turning more northward and leaving the shelf. This northeastward flow over the outer shelf combines with the southward coastal current to form a regional clockwise circulation. While most of the drifters in the coastal current that exited Marguerite Bay eventually moved across the shelf and turn northeastward, none left the outer shelf and shelf break region to re-enter the coastal flow along Adelaide Island. This suggests that the regional clockwise surface circulation is not a closed gyre, but is open at its northeast end.

The large number of drifter position fixes (~20) per day plus their relative accuracy (± 0.7 km) allows analysis of drifter motion in the study area on tidal and inertial time scales. Drifter tracks generally showed intermittent periods of distinct high-frequency looping motion, and kinetic energy rotary spectra have a distinct single peak near the local inertial period (~13 h) in the counterclockwise inertial/semidiurnal tidal band. This is direct evidence of near-inertial current oscillations which can last several days or more and have near-surface speeds of 5–20 cm s^{-1} in ice-free conditions. These oscillations are presumed to be generated by surface forcing, but we cannot demonstrate this with the available wind data. The observed high- and low-frequency current variability are comparable, and only two clear examples of coherent mesoscale flow were observed, both within Marguerite Bay.

The drifter data provide crude estimates of residence times within Marguerite Bay. Defined as the time between when a drifter enters and leaves the Bay (i.e., crossing the shortest straight line between Adelaide and Alexander Islands), the greatest drifter residence times within the Bay were about 40 days. This means that a drifter entering the Bay near Adelaide Island and moving clockwise around the Bay and exiting near Alexander Island during ice-free conditions takes roughly 40 days to make this circuit. In contrast, one drifter which entered the ice field in mid-May 2002 remained over the shelf west of Adelaide Island through January, 2003. In addition, two ice stations deployed on ice floes on the shelf in August–September 2001 continued to transmit their positions through November and remained over the shelf west of Adelaide Island (D. Pevovich, personal communication). If the motion of our drifter and the two ice stations are at all representative of the water and ice near them, then the residence time of young krill that spend much

f the winter just under the ice may extend through he winter in the Marguerite Bay and adjacent helf area.

Acknowledgments

We want to thank A. Doyle (RPSC) and the crews of the research vessels *L.M. Gould* and *N.B. Palmer* for their significant help in this work. P. Wiebe (WHOI) helped deploy drifters during NBP02-04. P. Niiler (SIO) and C. Engler (NOAA) kindly supplied four SVP drifters for our use in 2001. C. Stearns, G. Weidner, M. Lazzara, and J. Thom (U. Wisconsin—Madison Antarctic Meteorological Research Center) provided the two AWSs and critical support monitoring the ARGOS data quality throughout their deployment. The AWSs were successfully installed in difficult sea conditions by J. Otten, J. Doren, and D. Green (all of RPSC). D. Perovich (CRREL) generously provided data from the autonomous ice stations that his group deployed during cruise LMG0204 plus ideas about ice formation and movement. Discussions with L. Padman (ESR) and J. Hyatt (WHOI) and feedback from two reviewers helped clarify and improve this manuscript. This work was supported by the National Science Foundation Office of Polar Programs through US Southern Ocean GLOBEC grant OPP 99-10092. This is WHOI contribution number 11070 and US GLOBEC contribution number 449.

Appendix A. Drifter position and velocity accuracy

In the SO GLOBEC study area, each drifter was located about 20 times per day on average. The fixes were not spaced uniformly in time, but occurred on average roughly every 2 h during the 11-h period 10–21 GMT and every hour during the rest of the day. Comparisons of position data recorded by 5 drifters collocated in Punta Arenas for 3 days prior to the February 2002 mooring deployment cruise indicated that individual ARGOS position fixes had uncorrelated rms errors of ± 560 m in longitude and ± 310 m in latitude. These position errors cause irregular trajectories in the 1-h interpolated drifter time series since a drifter with a speed of 0.1 m s^{-1} moves only 360 m in 1 h. To estimate the effects of these position errors on the high-frequency velocity time series computed using the 1-h interpolated drifter position, a simple bootstrap approach was used. Independent Gaussian random errors in longitude and latitude were added to the raw drifter data, and the combined time series used to compute east (u) and north (v) velocity components as before. The difference time series between the original u and v and those computed with the added random position error represent the velocity error series. Ensemble averages of these series yield a mean rms velocity error of about 7 cm s^{-1}, with most of the error kinetic energy occurring at frequencies above the inertial/semidiurnal band. The low-pass filtered drifter position and velocity data were essentially unaffected by the ARGOS position error.

References

Flagg, C.N., Vermersch, J.A., Beardsley, R.C., 1976. 1974 MIT New England shelf dynamics experiment (March 1974) data report—Part II: the moored array. GFD Lab Report 76-1, Meteorology Department, MIT.

Hofmann, E.E., Klinck, J.M., Lascara, C.M., Smith, D.A., 1996. Water mass distribution and circulation west of the Antarctic Peninsula and including Bransfield Strait. In: Ross, S.M., Hofmann, E.E., Quetin, L.B. (Eds.), Foundation for Ecological Research West of the Antarctic Peninsula. Antarctic Research Series, vol. 70. American Geophysical Union, Washington, DC, pp. 61 80.

Hofmann, E.E., Klinck, J.M., 1998. Thermohaline variability of the waters overlying the West Antarctic Peninsula continental shelf. Ocean, Ice, Atmosphere, Interactions at the Antarctic Continental Margin, Antarctic Research Series, vol. 75, pp. 67–81.

Hofmann, E.E., Wiebe, P.H., Costa, D.P., Torres, J.J., 2004. An overview of the Southern Ocean Global Ocean Ecosystem Dynamics program. Deep-Sea Research II, this issue [doi:10.1016/j.dsr2.2004.08.007].

Howard, S.L., Hyatt, J., Padman, L., 2004. Mixing in the pycnocline over the western Antarctic Peninsula shelf during Southern Ocean GLOBEC. Deep-Sea Research II, this issue [doi:10.1016/j.dsr2.2004.08.002].

Klinck, J.M., 2001. Heat and salt changes on the continental shelf west of the Antarctic Peninsula between January 1993 and January 1994. Journal of Geophysical Research 103, 7617–7636.

Klinck, J.M., Hofmann, E.E., Beardsley, R.C., Salihoglu, B., Howard, S., 2004. Water-mass properties and circulation on the west Antarctic Peninsula Continental Shelf in Austral Fall and Winter 2001. Deep-Sea Research II, this issue [doi:10.1016/j.dsr2.2004.08.001].

Kunze, E., 1985. Near-inertial wave propagation in geostrophic shear. Journal of Physical Oceanography 15, 544–565.

Kunze, E., Boss, E., 1998. A model for vortex-trapped internal waves. Journal of Physical Oceanography 28, 2104–2115.

Large, W.G., Pond, S., 1981. Open ocean flux measurements in moderate to strong winds. Journal of Physical Oceanography 11, 324–336.

Padman, L., Fricker, H.A., Coleman, R., Howard, S., Erofeeva, S., 2002. A new tidal model for the Antarctic ice shelves and seas. Annals of Glaciology 34, 247–254.

Smith, D.A., Hofmann, E.E., Klinck, J.M., Lascara, C.M., 1999. Hydrography and circulation of the west Antarctic Peninsula continental shelf. Deep-Sea Research II 46, 925–949.

Smith, D.A., Klinck, J.M., 2002. Water properties on the west Antarctic Peninsula continental shelf: a model study of effects of surface fluxes and sea ice. Deep-Sea Research II 49, 4863–4886.

Sybrandy, A., Niiler, P.P., 1991. WOCE/TOGA Lagrangian drifter construction manual. SIO Reference 91/6, Scripps Institution of Oceanography, University of California, San Diego.

Zhou, M., Niiler, P.P., Hu, J.-H., 2002. Surface currents in the Bransfield and Gerlache Straits. Deep-Sea Research II 49, 267–280.

ELSEVIER

Deep-Sea Research II 51 (2004) 1965–1979

DEEP-SEA RESEARCH
PART II

www.elsevier.com/locate/dsr2

Mixing in the pycnocline over the western Antarctic Peninsula shelf during Southern Ocean GLOBEC

S.L. Howard[a,*], J. Hyatt[b], L. Padman[a]

[a]*Earth & Space Research, 1910 Fairview Ave E., Suite 210, Seattle, WA 98102, USA*
[b]*MIT-WHOI Joint Program in Oceanography, Department of Physical Oceanography, Woods Hole Oceanographic Institution, Woods Hole, MA 02543, USA*

Accepted 8 July 2004

Abstract

The Southern Ocean Global Ecosystem Dynamics program studied the continental shelf region in the vicinity of Marguerite Bay, on the western side of the Antarctic Peninsula, to determine the factors that contribute to Antarctic krill survival over winter. Subsurface intrusions of upper circumpolar deep water (UCDW) onto the shelf provide much of the nutrient flux into the region. Here we describe the small-scale processes that contribute to upward diapycnal fluxes of heat, salt, and nutrients from the UCDW to the surface-mixed layer. The study makes use of conductivity–temperature depth and vessel-mounted acoustic Doppler current profiler data collected during three research cruises between April and September 2001. Near-inertial baroclinic waves generated by wind stress provide most of the shear across the sharp pycnocline at the base of the mixed layer. The mean vertical diffusivity associated with shear instability is estimated at $\leqslant 1 \times 10^{-5}\,m^2\,s^{-1}$, corresponding to a heat flux into the base of the mixed layer of $< 2\,W\,m^{-2}$. A previous suggestion that double-diffusive convection (DDC) provides significant upward heat fluxes (of order $10\,W\,m^{-2}$) in a nearby region is not supported by our analyses of the present data set, which indicates almost no contribution to diapyncal fluxes from DDC.
© 2004 Elsevier Ltd. All rights reserved.

1. Introduction

The western Antarctic Peninsula (WAP) shelf region (Fig. 1) is an area of unusually high krill production and thus a favorable habitat for krill predators such as Adélie penguins and Crabeater seals. The Southern Ocean Global Ecosystem Dynamics (SO GLOBEC) program examined the unique physical and biological factors that contribute to enhanced krill growth, reproduction, recruitment and survivorship in this region throughout the year (see Hofmann et al., 2004).

In this paper we identify and attempt to quantify the fluxes associated with the small-scale physical oceanographic processes that facilitate the supply of heat, salt, and nutrients to the upper

*Corresponding author. Tel.: +1-206-726-0501x15; fax: +1-206-726-0524.
E-mail address: howard@esr.org (S.L. Howard).

0967-0645/$ - see front matter © 2004 Elsevier Ltd. All rights reserved.
doi:10.1016/j.dsr2.2004.08.002

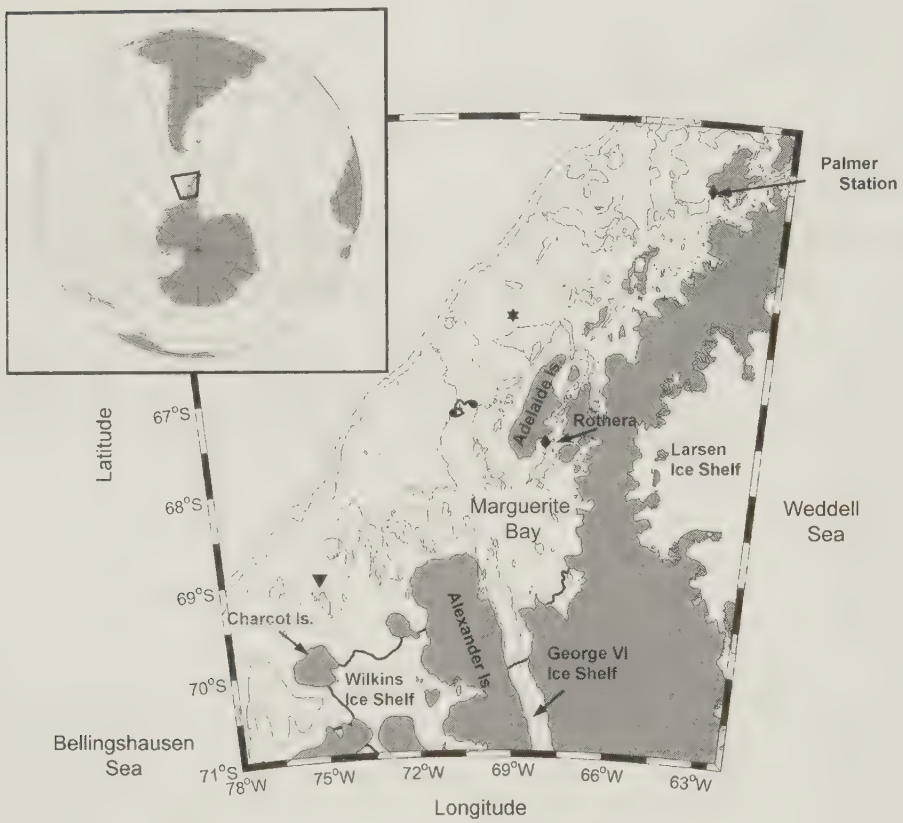

Fig. 1. Map of the study area surrounding Marguerite Bay on the western side of the Antarctic Peninsula. Thin black lines are the 500 and 2000 m isobaths based on the Smith and Sandwell ETOPO2 dataset updated with GLOBEC bathymetry data. Bold black lines indicate fronts of major ice shelves. The location of survey station 3 near 66.2°S, 69.1°W (see Fig. 2) is indicated by a star, while CTD 76 near 69°S, 75°W from the fall 2001 survey cruise (see Fig. 6) is indicated by a filled triangle. The drift track for the section of the winter process cruise on *L. M. Gould* used in Fig. 4 is also indicated (centered near 67.2°S, 70.5°W).

ocean over the WAP shelf. The principal pathway for these fluxes to the shelf is via large-scale lateral subsurface intrusions of warm, salty, nutrient-rich upper circumpolar deep water (UCDW). The UCDW is derived from the Antarctic circumpolar current (ACC) (Prézelin et al., 2000; Smith and Klinck, 2002) and flows shoreward along bathymetric features such as the Marguerite Trough (Klinck et al., 2004). Over the shelf, the UCDW typically lies below about 200 m, well below the less dense surface waters that are formed from ocean/atmosphere buoyancy exchange and sea-ice processes. In a plot (not shown) of potential temperature (θ) against salinity (S), the transition region between the UCDW and the surface waters (roughly the depth range 80–200 m in Fig. 2) is fairly linear, suggesting that the θ–S relationship in this depth range is set by diapycnal mixing between the end-member water types. Our goal is to determine the processes that drive this mixing.

The most likely candidates for pycnocline mixing processes in this environment are shear-driven instability (SDI) and double-diffusive convection (DDC). In turn, the most likely sources of energy for SDI are from wind stress and tides (e.g., Munk and Wunsch, 1998). The mixing rates associated with these processes can be estimated in three ways: a box-model of heat and salt budget calculations for the surface-mixed layer (e.g.,

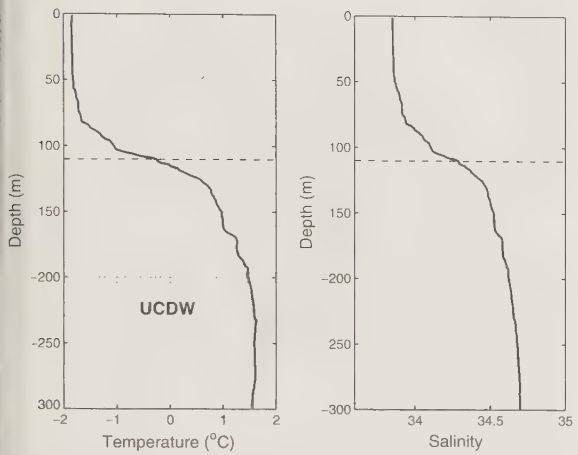

Fig. 2. Profiles of temperature (left) and salinity (right) at survey station 3 from the fall (gray line) and winter (black line) survey cruises (see Fig. 1 for location). The profiles were separated by ~89 days. Upper circumpolar deep water (UCDW) that has intruded onto the shelf occupies the water column below about 200 m. On the assumption that lateral advection is negligible (Smith and Klinck, 2002), the heat and salt flux divergences associated with the change in heat and salt content of the profiles above 110 m (indicated by the horizontal dashed line) are $-72\,W\,m^{-2}$ and $0.7\,mg\,m^{-2}\,s^{-1}$, respectively.

Smith and Klinck, 2002); measurements of scalars or velocity shear that fully resolve the turbulent microscales of order 1–10 cm (see Gregg, 1987); or by invoking parameterizations that relate mixing rates to measured "large-scale" quantities.

The difficulty of a box-model approach for the WAP region is illustrated in Fig. 2. For a representative site (survey station 3; see Fig. 1 for location) over the central WAP shelf, the change in upper-ocean heat and salt content between the austral fall and winter 2001 survey cruises is consistent with net vertical flux divergences of heat and salt across the mixed layer of $-72\,W\,m^{-2}$ and $0.7\,mg\,m^{-2}\,s^{-1}$, respectively. In contrast, the mean upward fluxes from below the mixed layer are likely of order $1–10\,W\,m^{-2}$ and $0.01\,mg\,m^{-2}\,s^{-1}$ (Smith and Klinck, 2002), implying that the upper-ocean heat and salt budgets are dominated by the seasonal cycles of heat and fresh water exchange at the ocean surface. Attempts to estimate the diffusivities in the pycnocline from box-model studies of surface-mixed layer heat and fresh water budgets are therefore subjected to the significant errors associated with parameterizations of the large surface fluxes.

No microstructure data are available from SO GLOBEC year 1 cruises, hence the direct measurement of diffusivity in the pycnocline is not possible. Instead, for the present paper we concentrate on the third approach; using fine-scale hydrographic and velocity data to identify mixing processes in the pycnocline. The data we analyze consist of hydrographic profiles from conductivity–temperature–depth (CTD) recorders and acoustic Doppler current profilers (ADCPs). The CTD resolution is ~1 m when sea-state is not severe, and the ADCP collects velocity profiles at a vertical resolution of ~10 m.

2. Data

The SO GLOBEC program collected data in the WAP area during the austral fall and winter seasons of 2001 and 2002 using four survey cruises and four process cruises. Three additional cruises to deploy, service and recover moorings took place in the austral late summers of 2001–2003. For this study, we concentrate on data from CTD profiles and the vessel-mounted ADCP during the fall and winter 2001 survey cruises on the RVIB *N. B. Palmer* (US SO GLOBEC, 2001b, c) and the winter 2001 process cruise on the ARSV *L. M. Gould* (US SO GLOBEC, 2001c) (Table 1). Vertical profiles of temperature (T) and conductivity (C) as functions of pressure (P) were obtained on a grid pattern (Fig. 3) on the survey cruises using a SeaBird SBE 911^+ CTD system. Additional CTD profiles were obtained from the *L. M. Gould* process cruise using a similar CTD

Table 1
Summary of 2001 SO GLOBEC cruises discussed in this paper. Dates and types of cruises are included

Year 1 cruises	Type	Date
NBP01–03	Fall survey	April 23–June 6
NBP01–04	Winter survey	July 22–August 31
LMG01–06	Winter process	July 21–August 31

LMG—ARSV *L. M. Gould*.
NBP—RVIB *N. B. Palmer*.

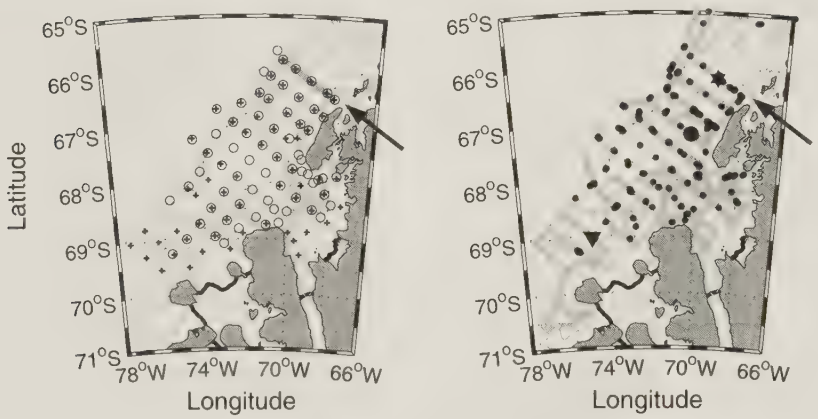

Fig. 3. Left: Locations of CTD stations during the 2001 SO GLOBEC survey cruises. Fall stations are shown as plus symbols (+). Winter stations are shown as circles (o). Right: Location of useable vessel-mounted ADCP data collected by the RVIB *N.B. Palmer* for the same cruises. Fall survey data are shown as gray dots. Winter survey data are shown as black dots. Large symbols indicate the locations of the same sites shown in Fig. 1. The cross-shelf transect 1 (Fig. 5), is indicated by an arrow.

system. Salinity (S) and potential density (σ_θ) were derived from C, T, and P. Accuracies of T and S are $\sim 10^{-4}$ °C and $\sim 10^{-3}$ practical salinity units (psu), respectively, after post-calibration. The data that we use here were averaged initially over 1-m vertical bins: additional averaging used in our analysis is described where necessary. The cruise reports (US SO GLOBEC 2001a–c) and Klinck et al. (2004) provide more details about the CTD data set and the general hydrographic structure and circulation that it reveals.

Vertical profiles of upper-ocean horizontal current ($\mathbf{U}(z) = u(z)\mathbf{i} + v(z)\mathbf{j}$) were obtained from each vessel with RDI 150 kHz vessel-mounted ADCPs. The ADCP systems were set for 8-m vertical bins, 8-m pulse length, and an ensemble averaging period of 5.0 min for all SO GLOBEC cruises except the 2001 mooring deployment and 2001 fall process cruises on the *L. M. Gould*. These two cruises used a 16-m pulse length. The resultant nominal accuracy of each estimate of $\mathbf{U}(z)$ is $\sim 1\,\mathrm{cm\,s^{-1}}$, per the manufacturer's design error estimate. The ADCP on the *N. B. Palmer* measures currents from 31 m to ~300–350 m depths. Quoted depths refer to the center of the 8-m vertical bins. The ADCP on the *L. M. Gould* measures currents from 26 to ~300–350 m depths. Navigation data were obtained with an Ashtech 3D GPS system and were used in the processing of the ADCP data. Bottom tracking was used when the ship was in water less than 500 m deep. Fig. 3 (right panel) shows the location of usable ADCP data from the 2001 *N. B. Palmer* survey cruises. Sea state and ice cover both interfered with collection of ADCP data. Sea-state effects can be seen as gaps in the grid for the fall survey cruise. Sea ice interferes with ADCP data collection while the ship is underway. During the winter cruise, therefore, data were acquired only as time series at fixed sites while the vessel was stopped during CTD and other station operations. These measurements lasted for as long as the on-station work, which typically took a few hours depending on water depth and sampling activities.

3. Vertical mixing processes

3.1. Shear-driven instability

The SDI is the primary source of mixing in the World Ocean pycnocline. The source of energy for SDI is a combination of atmospheric forcing (primarily wind stress, but also surface buoyancy fluxes) and tides: Munk and Wunsch (1998) and Wunsch (2000) suggest that about 50% of the globally integrated mixing is associated with each source. This ratio is, however, strongly dependent

on local conditions. Tides can be the dominant source of mixing via production of baroclinic tides and higher frequency internal waves in regions where strong barotropic tidal currents flow across steep topography; see Padman and Dillon (1991) and Wijesekera et al. (1993) for high-latitude examples. The spatial distribution of shear is complicated by the propagation of super-inertial waves away from the energy source (Dushaw et al., 1995; Muench et al., 2002; Lozovatsky et al., 2003). Thus for any particular location, determining the likely strength of mixing through SDI requires knowledge not only of the local strength of forcing of baroclinic waves but also the potential for wave energy to propagate from elsewhere to the observation site.

For reasons explained below, we believe that the dominant source of shear in the WAP pycnocline is associated with wind-forced near-inertial waves. Baroclinic tides may provide additional shear in certain localized regions. We discuss each of these shear sources separately.

3.1.1. Near-inertial waves

At process site 3 from the winter process cruise while the *L. M. Gould* drifted in pack ice, we observed persistent shear in the ADCP data, with the shear being concentrated across the sharp pycnocline at the base of the mixed layer (Fig. 4). The dominant signal in this record is a semidiurnal oscillation, where the current vectors in the layers above and below the sharp pycnocline rotate

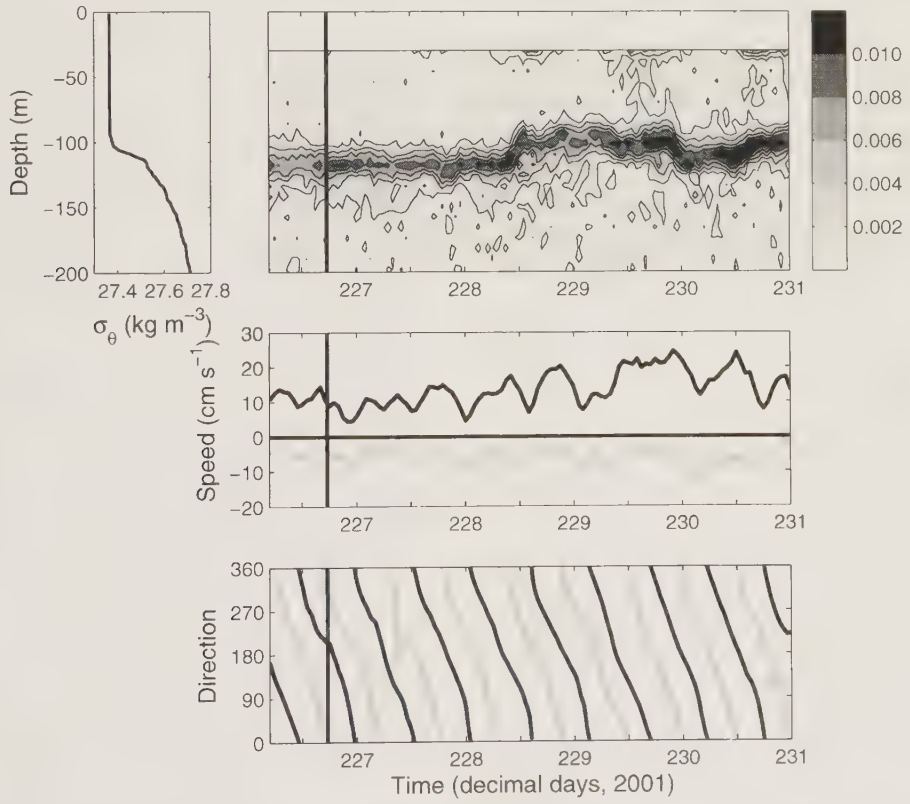

Fig. 4. Density and velocity fields for process site 3 from the winter process cruise on *L. M. Gould* (see Fig. 1 for location). Vertical profile of potential density for CTD 227 (upper left), time series of shear magnitude $\langle |U_z| \rangle$ (s^{-1}) calculated from ADCP data (upper right), time series of current speed (cm s^{-1}) at 50 m depth (black line) and the negative of the speed at 154 m depth (gray line) from the vessel-mounted ADCP (central right), and time series of current direction for 50 m depth (black line) and 154 m depth (gray line) (lower right). The solid vertical lines on the right-hand panels show the time of CTD 227. The fundamental periodicity of the phase lines is ~12.9 h (~f), and the surface layer is roughly 180° out of phase with the deeper layer for the entire time period.

anticlockwise but are roughly 180° out of phase with each other. Current speeds are up to $24\,cm\,s^{-1}$ in the upper mixed layer, and weaker but still significant in the lower layer. Although the ADCP record does not reach full depth (~500–650 m) in this region, the impression is that the net depth-integrated flow is small, with the volume flux in the faster and thinner surface layer being compensated for by the opposing flux in the thicker but slower-moving lower layer.

The duration of this record at a fairly constant location allows us to identify the semidiurnal signal, on the basis of its dominant periodicity, ellipticity and rotation direction (counter-clockwise), as being near-inertial (period $\sim 2\pi/f \approx 13.0$ h at 67 °S) rather than tidal: the principal semidiurnal tidal constituents, M_2 and S_2, have periods of ~12.42 and 12.00 h, respectively. Analyses of satellite-tracked drifter paths (Beardsley et al., 2004) indicate that near-inertial surface currents are frequently energetic over the WAP shelf and into the mouth of Marguerite Bay. Near-inertial oscillations are commonly associated with rapid changes in wind stress, i.e., the passage of storm fronts, and such events are frequent in this region (US SO GLOBEC, 2001a, b, c). The shear across the sharp pycnocline associated with the near-inertial currents is strong (Fig. 4), suggesting that these waves may provide sufficient energy for SDI mixing to be significant.

3.1.2. Tides

A second plausible source of shear and turbulence for the pycnocline in the study area is from tides, specifically baroclinic tides generated as the barotropic tide flows across sloping topography; see Levine et al. (1997) and Muench et al. (2002) for two Antarctic examples. The two principal tidal species, semidiurnal and diurnal, behave very differently in the Antarctic (Foldvik et al., 1990): in the WAP region, $\omega_{tide} > f$ for all semidiurnal tidal harmonics, whereas $\omega < f$ for the diurnal tides. Super-inertial baroclinic semidiurnal tides can be easily generated and propagate freely away from the generation sites, whereas the sub-inertial diurnal tides are much more restricted in their ability to support shear and will be constrained to topographic wave guides such as the shelf break.

There are few existing current meter data sets for the WAP region, hence we base our knowledge of tides on a numerical model, the Circum-Antarctic Tidal Simulation, version 02.01 (CATS02.01) (Padman et al., 2002). This model predicts that the barotropic semidiurnal tidal kinetic energy on the WAP shelf is very small. Indeed, Beardsley et al. (2004) show that, over the mid-shelf, predicted tidal current speeds are only ~1/10 of the surface near-inertial currents. Thus, it is unlikely that significant shear can be generated by semidiurnal tides, and this hypothesis is confirmed by a primitive-equation numerical model that we have run of the three-dimensional structure of M_2 tides for the region offshore of Marguerite Bay. In contrast, CATS02.01 predicts that the time-averaged diurnal tidal current speed exceeds $10\,cm\,s^{-1}$ at a few locations along the WAP shelf break. Maximum tidal current speeds ("spring" tides) usually exceed mean speeds by a factor of ~2. The strong currents are associated with diurnal-band topographically trapped vorticity waves (DTVWs), which are known to have a significant cross-slope component over the upper slope and shelf break in many locations around Antarctica (Middleton et al., 1987; Padman and Kottmeier, 2000; Padman et al., 2003). For a variety of reasons the energy of DTVWs are difficult to accurately model (Foldvik et al., 1990; Padman and Kottmeier, 2000; Cummins et al., 2000), and so we only use CATS02.01 to indicate the approximate magnitude of currents. Some support for the model is provided, however, by observations of the diurnal-band variability of velocity evaluated from surface drifters (Beardsley et al., 2004). The diurnal-band velocity of one of these drifters that spent significant time over the outer continental shelf was up to $\sim 15\,cm\,s^{-1}$, broadly consistent with model predictions. These data, and studies of DTVWs in the Arctic Ocean (Padman and Dillon, 1991; Padman et al., 1991; Padman et al., 1992) support our hypothesis that barotropic tidal energy in the form of DTVWs may result in mixing near the shelf break. Further work is required to determine whether a significant fraction of the energy in the primarily barotropic DTVWs can be transferred to higher-frequency baroclinic motions capable of inciting the growth

of shear instabilities in the pycnocline. While the previously cited studies support this energy pathway to mixing for the Arctic Ocean, the weaker stratification of the WAP region may preclude significant baroclinic wave generation associated with DTVWs.

3.1.3. Mixing rates associated with shear

In the absence of microstructure measurements, estimates of pycnocline mixing rates due to SDI only can be made through parameterizations based on larger-scale features of the hydrographic and velocity structure. Such parameterizations fall into two broad categories; schemes based on Richardson number Ri (Pacanowski and Philander, 1981; hereinafter called PP-81) and those based on energy flux to smaller scales via wave–wave interactions in an internal wave field frequency–wavenumber spectrum (Gregg, 1989; Wijesekera et al., 1993; Levine et al., 1997). Parameterizations of vertical diffusion in numerical models tend to be based on Ri, e.g., Large et al. (1994). However, the relationship between Ri and the turbulent diffusivity K_v in the ocean is not well constrained (Peters et al., 1988), and any Ri-based estimate of K_v will have large errors associated with it. Nevertheless, it is instructive to see what value of K_v would be predicted by physical or coupled physical ecological models that attempt to reproduce the SO GLOBEC data sets.

The Richardson number is defined as $N^2/|\partial \mathbf{U}/\partial z|^2$, where N is the buoyancy frequency. We define a "mean" gradient Richardson number $\overline{Ri}$, as

$$\overline{Ri} = \frac{\langle N^2 \rangle}{\langle U_z^2 \rangle}, \tag{1}$$

where angle brackets $\langle \ldots \rangle$ indicate averaging in space and/or time and $\langle U_z^2 \rangle = (\partial u/\partial z)^2 + (\partial v/\partial z)^2$. The overbar on $\overline{Ri}$ reminds the reader that this parameter is based on averaged $\langle N^2 \rangle$ and $\langle U_z^2 \rangle$. Values of Ri based on fully resolved density and velocity fields can be used to identify when the necessary condition for dynamic instability of the shear flow is met. Values of $Ri < 0.25$ are generally taken to indicate that shear instabilities are likely to occur according to linear theory for two-dimensional stratified shear flow, while $Ri < 1$ indicates that the potential exists for advective instabilities (Orlanski and Bryan, 1969). The interpretation of $\overline{Ri}$ is, however, intimately related to the vertical and temporal averaging scales for density and velocity gradients (Padman and Jones, 1985). In this view, $\overline{Ri}$ is some measure of the probability of shear instabilities occurring at time and/or space scales smaller than the averaging scales, not a threshold criterion separating fully turbulent from laminar flow.

Velocity shear ($\mathbf{U}_z = \partial \mathbf{U}/\partial z$) is approximated in the ADCP ensemble data as

$$\langle \mathbf{U}_z \rangle = \left(\frac{\Delta \langle u \rangle}{\Delta z}, \frac{\Delta \langle v \rangle}{\Delta z} \right), \tag{2}$$

where $\Delta \langle u \rangle$ and $\Delta \langle v \rangle$ are the differences in east and north velocity components between adjacent ADCP depth bins separated by Δz m. As before, angle brackets $\langle \ldots \rangle$ denote averaging over space and/or time scales. Here, u and v are averaged over an ADCP depth bin that is Δz (8 m) thick and over times as described herein, typically of order 1 h.

Large values of shear magnitude, $\langle \mathbf{U}_z \rangle$, were frequently found in the upper water column on the WAP shelf. Fig. 5 shows a cross-shelf plot of $|\langle \mathbf{U}_z \rangle|$ for transect line 1 from the fall survey cruise on *N. B. Palmer* (see Fig. 3 for location). The "on-station" data were removed from the total transects record prior to making this figure. There is a strong shear layer ($\langle \mathbf{U}_z \rangle > 0.01\ \mathrm{s}^{-1}$) in the 70–80 m depth range, coincident with the strong stratification at the base of the surface-mixed layer. Throughout the study region, the strongest shears tended to occur in this portion of the water column, although there are also several occurrences of relatively strong shear in the deeper pycnocline. The transect shown in Fig. 5 took ~26 h to complete (~2 inertial, and ~1 or ~2 tidal periods), and so the plotted variability is a combination of both spatial and temporal changes in currents.

We can only calculate $\overline{Ri}$ from (1) with on-station data, where measurements of $\langle N^2 \rangle$ and $\langle U_z^2 \rangle$ are simultaneously available. The value of $\langle N^2 \rangle$ in (1) is based on potential density $\sigma_\theta(z)$ from a single CTD profile. For consistency with the estimation of $\langle U_z^2 \rangle$, we first average σ_θ in the

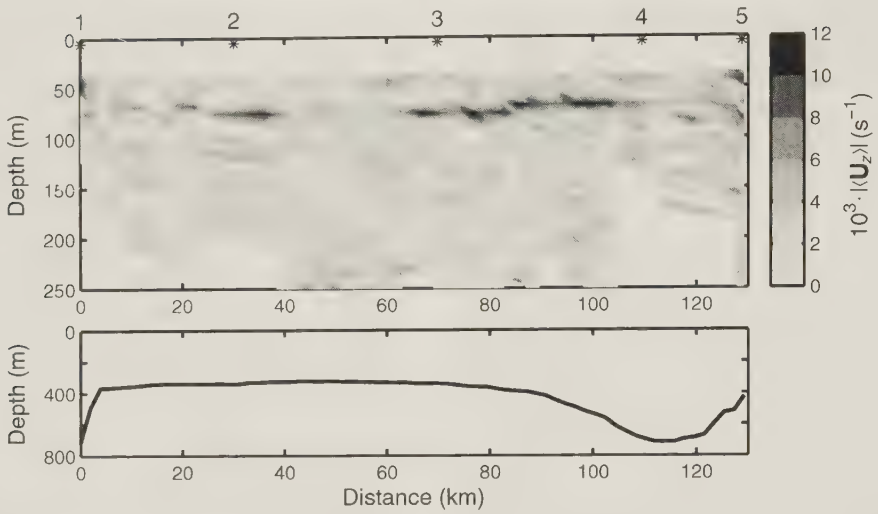

Fig. 5. Upper panel: transect of shear magnitude $\langle U_z \rangle$ (s^{-1}) calculated from ADCP data collected on the fall survey cruise transect 1 (see Fig. 3 for location). Station locations are shown at the top of the plots. Station 1 is at the shelf break and station 5 is nearest to the coast. The transect took ~26 h to complete. The water depth along this transect is shown in the lower panel.

same 8-m depth bins used for ADCP-based velocity, and then calculate $\langle N^2 \rangle$ from

$$\langle N^2 \rangle = \frac{g}{\rho_0} \frac{\Delta \langle \sigma_\theta \rangle}{\Delta z}, \tag{3}$$

where $\Delta \langle \sigma_\theta \rangle$ is the potential density difference between adjacent 8-m ADCP-based depth bins and ρ_0 is a characteristic density. The averaging time for $\langle U_z^2 \rangle$ is taken as the duration of the CTD cast, up to a maximum of 2.7 h centered on the mean time of the cast. With $\Delta z = 8$ m and $\Delta t = 0.5$–2.7 h, we cannot fully resolve the expected shear and density gradient joint frequency-wavenumber spectrum (Wijesekera et al., 1993). These averaging scales are, however, of the same order of magnitude as the time step and vertical resolution in regional numerical models, and thus our interpretation of mixing based on $\overline{Ri}$ emulates mixing parameterizations in those models.

In Fig. 6 we show an example of the steps in calculating $\overline{Ri}$ for one station; station 76 during the fall 2001 survey cruise on *N. B. Palmer*. Well-defined shear layers were present at the base of the mixed layer and between ~150 and ~210 m within the main pycnocline (Fig 6C). Values of $\overline{Ri}$ within the latter shear layer are near unity (Fig. 6F). We have applied these methods to create profiles of $\overline{Ri}$ for all on-station data obtained during the 2001 fall and winter *N. B. Palmer* survey cruises. Very few profiles show $\overline{Ri} < 0.25$ and the fraction of the total data set with $\overline{Ri} < 1$ is also low, indicating that parameterized occurrences of energetic mixing by SDI is rare.

The mean diffusivity $\overline{K_v}$ that would be predicted by the turbulence parameterizations in general circulation models can be estimated by applying the same algorithms to our profiles of $\overline{Ri}$. We report this calculation for just one such scheme (PP-81). The PP-81 scheme is based on matching numerical model predictions with observations of the Pacific Ocean Equatorial Undercurrent, and so may have little relevance to a high-latitude coastal-ocean pycnocline. Nevertheless, Muench et al. (2002) used this model to obtain predictions of mixing rates that were consistent with the expected dissipation of internal tides generated along the South Scotia Ridge. That paper describes in detail how CTD and ADCP data can be used with PP-81 to make predictions of $\overline{K_v}$, although note that Eq. (2) ($K_v = f(Ri)$) in Muench et al. (2002) is incorrectly printed.

Most estimates of $\overline{Ri}$, in both the sharp pycnocline and the more weakly stratified "deep" part of the pycnocline, are sufficiently large that

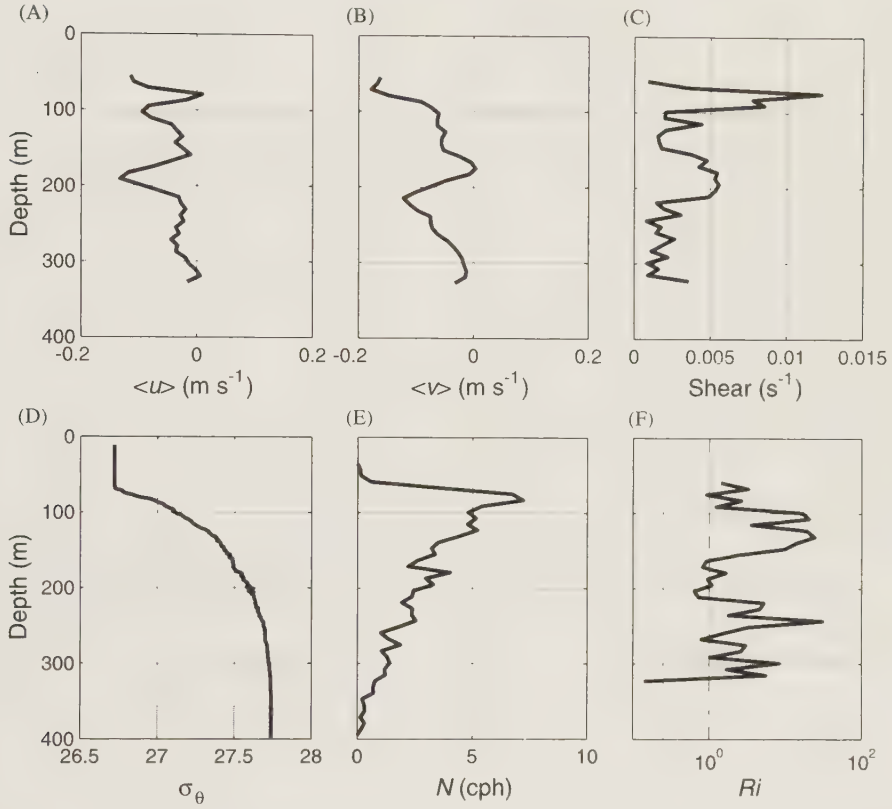

Fig. 6. Example showing results of mixing parameter calculations from the CTD and ADCP for station 76 from the fall survey cruise (see Fig. 3 for location): (A) east component of time-averaged velocity $\langle u \rangle$; (B) north component of time-averaged velocity $\langle v \rangle$; (C) time-averaged shear magnitude $<|\boldsymbol{U}_z|>$; (D) potential density σ_θ; (E) Buoyancy frequency, $\langle N \rangle$; (F) Richardson number (vertical dashed lines indicate $\overline{Ri} = 1/4$ and $\overline{Ri} = 1$).

PP-81 predicts values of K_v that are close to the asymptotic lower limit of $1 \times 10^{-5}\,\mathrm{m^2\,s^{-1}}$. That is, there is no significant difference between PP-81 and using a constant diffusivity of $1 \times 10^{-5}\,\mathrm{m^2\,s^{-1}}$, this constant being consistent with values found in the mid-latitude main thermocline (Ledwell et al., 1993; Ruddick et al., 1997). The heat fluxes F_H associated with this value of K_v in the sharp pycnocline and the deep pycnocline are about 1–2 and $<0.5\,\mathrm{W\,m^{-2}}$, respectively. A more recent, "modified" form of PP-81 (R. Houghton, personal communication, 2003) has a lower asymptotic limit for K_v at high $\overline{Ri}$, thus the mean value of F_H may be $<1\,\mathrm{W\,m^{-2}}$.

There are, however, a few areas where $\overline{Ri}$ was low enough to indicate mixing (e.g., the two depth ranges of relatively low $\overline{Ri}$ in Fig. 6F). Shear associated with the near-inertial currents at process site 3 (Fig. 4) of the winter process cruise leads to low $\overline{Ri}$ at the time of the CTD cast shown in the figure. When the heat flux is averaged vertically over the entire sharp pycnocline (the region in which N exceeds 3 cph), the estimated average pycnocline flux at this time is $\sim 5\,\mathrm{W\,m^{-2}}$. The shear is clearly stronger later in the time series, but no CTD data are available for further calculations of K_v and F_H. Intermittent but relatively energetic events such as this may be the dominant contributors to mean turbulent diapycnal fluxes.

Our focus in this paper is on mixing in the main pycnocline as a mechanism for transporting the

scalar properties of UCDW into the surface layer through the intervening pycnocline. Nevertheless, as we have previously noted (see Fig. 2), the variability of mixed layer properties is dominated by the seasonal cycle associated with surface buoyancy fluxes. Surface stress also contributes to the seasonal cycling of the upper ocean. M. McPhee (personal communication, 2004) has run a one-dimensional local turbulence closure (LTC) model (McPhee, 1999) for the winter process site 3 data set reported herein (see Fig. 4). His model successfully reproduces the ice drift velocity, which provides some support for other predictions of the LTC model. Strong upward heat flux ($\sim$10 W m^{-2} averaged over the 4 days) is predicted in the center of the surface layer near 55 m depth from $t \approx 227.5$ to 231.5 days. This average is, however, dominated by a short period of intense mixing from $t \approx 230.4$ to 230.8 days in which the modeled F_H exceeds 50 W m^{-2}. The modeled 4-day average flux of $\sim$10 W m^{-2} for the center of the surface-mixing layer is close to our estimate of the flux through the sharp pycnocline based on ADCP and CTD data at the time of the single CTD profile for this site. Wind stress clearly contributes to the transfer of heat from the upper pycnocline to the ocean surface. Importantly, the model results also confirm our data-based view that rare but energetic events may dominate the mean mixing rates and associated fluxes in the upper ocean. That is, it is quite possible that our mean flux values based on field data are lower than the true mean values because of inadequate sampling of these important events.

3.2. Double-diffusive convection

The DDC is a process that is driven by the different molecular diffusivities of T and S in a stratified fluid where both properties increase with depth (Turner, 1973). Such stratification is frequently found in high-latitude oceans where a cold, fresh surface layer formed by local air/sea/ice interactions overlies warmer and saltier water that has been advected into these regions from lower latitudes (Padman and Dillon, 1987; Robertson et al., 1995). Where DDC is active, the process forms a "thermohaline staircase", a vertical sequence of quasi-homogeneous layers separated by sharp interfaces in which vertical gradients of T and S are large. This feature allows us to identify, from high-resolution CTD or scalar microstructure profiles, where DDC is likely to be a significant contributor to total vertical scalar fluxes.

Smith and Klinck (2002) estimated that, for a region of the west Antarctic Peninsula continental shelf just north of the SO GLOBEC study region, $\sim$5–10 W m^{-2} of upward vertical heat flux across the pycnocline was required to balance the total heat budget of the upper ocean in their one-dimensional vertical numerical model of this region. They also concluded that they needed a higher effective pycnocline diffusivity for T than for S, which is consistent with DDC being the dominant source of mixing. These authors noted the presence of steppiness in many of the CTD profiles from their study region: the vertical scale of this finestructure was consistent with DDC layer heights that would be required to reconcile laboratory-based DDC flux formulas with the heat and salt fluxes determined by their model-based analyses.

Our inspection of the "raw" (24 Hz) SO GLOBEC CTD profiles from the winter 2001 survey cruise identified a few profiles containing finestructure that was reminiscent of thermohaline steps, suggesting that DDC may occasionally contribute to vertical fluxes in the study area and that further study of DDC is warranted. However, in general, the observed "interfaces" were much thicker than we would expect for DDC ($\sim$1–10 cm: Padman and Dillon, 1987). We therefore believe that the steppy hydrographic structure is generally associated with non-DDC processes such as intrusive activity near the coast and ice fronts, and the finestructure remnants of shear-driven mixing.

In keeping, however, with our goal of investigating fluxes that would arise from the application of one-dimensional turbulence parameterizations such as Large et al. (1994), we apply models of DDC fluxes to the CTD data collected in 2001 during the winter survey cruise on *N. B. Palmer*. The fundamental parameter describing DDC activity is the density ratio R_ρ (Turner, 1973),

given by

$$R_\rho = \frac{\beta \partial S/\partial z}{\alpha \partial \theta/\partial z}, \quad (4)$$

where β (psu^{-1}) is the haline contraction coefficient and α ($^\circ\mathrm{C}^{-1}$) is the thermal expansion coefficient. To create profiles of R_ρ, $\theta(z)$ and $S(z)$ were first filtered over a 30-m vertical scale, which was chosen to be much larger than likely DDC layer heights of ~1 10 m. The mean gradients of the filtered T and S were then calculated over the high-gradient core of the pycnocline separating the surface-mixed layer from the depth of the UCDW temperature maximum. The DDC instability cannot occur below the depth of maximum temperature due to the change in sign of $\partial\theta/\partial z$. Values of R_ρ slightly above 1 indicate strong double diffusion. As R_ρ increases above 2, DDC fluxes become quite small. Estimates of DDC heat fluxes in polar oceans range from $<0.1\,\mathrm{W\,m^{-2}}$ in the Canada Basin in the Arctic ($R_\rho > 4$; Padman and Dillon, 1987) to $\sim 20\,\mathrm{W\,m^{-2}}$ in the central Weddell Sea ($R_\rho \approx 1$; Muench et al., 1990).

We calculated R_ρ over the winter survey cruise to estimate the possible strength of DDC processes on the WAP shelf. We concentrated on this survey because the seasonal upper-ocean stratification that is present throughout much of the fall survey cruise complicates automated detection of the core of the pycnocline below the Winter Water, the subsurface temperature-minimum layer representing the remnant of the previous winter's near-freezing surface-mixed layer. Furthermore, CTD profiles taken while the vessel is becalmed in ice are of much higher quality than the wave-influenced "open ocean" profiles obtained during the fall survey cruise. Some steppiness is seen in profiles from the winter survey cruise when R_ρ is low, ~2. This relatively low value of R_ρ indicates the potential for DDC to occur; however, inspection of the raw (24 Hz) CTD profiles of T and C confirm that sharp steps are rare. Most of the profiles in the WAP region have higher R_ρ values (typically ~3.6) in the pycnocline, indicating only weak DDC.

Several models have been developed to estimate DDC heat fluxes. Robertson et al. (1995) provide an overview and comparison (their Fig. 7) of these models. In the present study, we use the Kelley (1990) heat flux parameterization, defined as

$$F_{H-K} = 0.0032\rho_0 c_p \alpha^{-1} \exp[4.8 R_\rho^{-0.72}] \times (g\kappa_t^2 \upsilon^{-1})^{1/3} (\alpha \Delta\theta)^{4/3}, \quad (5)$$

where ρ_0 is the mean density, c_p is the specific heat capacity of seawater at constant pressure ($\sim 4.0 \times 10^3\,\mathrm{J\,kg^{-1}\,K^{-1}}$), κ_t is the molecular diffusivity for heat, υ is the kinematic viscosity of seawater, and $\Delta\theta$ is the thermal step between adjacent well-mixed layers. The thermal step is estimated by first obtaining the DDC layer height, H, using a relationship based on large-scale stratification parameters proposed by Kelley (1984);

$$H = [0.25 \times 10^9 R_\rho^{1.1} \upsilon \kappa_t^{-1} (R_\rho - 1)]^{0.25} \times (\kappa_t \langle N^{-1} \rangle)^{0.5}. \quad (6)$$

The thermal step is then obtained using

$$\Delta\theta = \langle \partial\theta/\partial z \rangle H, \quad (7)$$

where the temperature gradient $\langle \partial\theta/\partial z \rangle$ is the average gradient over the depth range in which evidence of DDC is sought.

Heat fluxes were estimated by applying (5)–(7) to all stations from the winter 2001 survey cruise. The area-averaged heat flux due to DDC was ~ 0.2–$0.4\,\mathrm{W\,m^{-2}}$ over the central and inner continental shelf, and ~ 0.4–$0.9\,\mathrm{W\,m^{-2}}$ over the continental slope where the average value of R_ρ was smaller than for the central shelf. The error bars associated with these values are uncertain. Another DDC heat flux model developed by Marmorino and Caldwell (1976) predicts values up to a factor of 2 greater than F_{H-K} for R_ρ values between 1.4 and 1.5 (Robertson et al., 1995). However, as R_ρ increases, the differences between the estimates from the various analytical models decrease (see also, Fig. 4b in Large et al., 1994). Note, however, that all models of DDC assume that the hydrography has organized into a thermohaline staircase, in which a continuous upward flux of heat is maintained by molecular diffusion through extremely sharp interfaces ("sheets") ~1–10 cm thick and buoyancy-driven convection in the adjacent layers ~1–10 m thick (see Padman and Dillon, 1987). When these sheets

and layers are not present, as in the present data set, expected heat fluxes will be less than the models predict.

Assuming, however, that these fluxes do at least represent some potential level of DDC activity, we can estimate the thermal diffusivities associated with these heat fluxes from

$$K_v^T = \frac{F_{H-K}}{\rho_0 c_p \langle \partial\theta/\partial z \rangle} \quad (\mathrm{m^2\,s^{-1}}), \tag{8}$$

where $\langle \partial\theta/\partial z \rangle$ is again averaged over the pycnocline. Using this method, the average DDC thermal diffusivity in the main pycnocline on the continental slope is $\sim 0.5 \times 10^{-5}\,\mathrm{m^2\,s^{-1}}$, and $\sim 0.3 \times 10^{-5}\,\mathrm{m^2\,s^{-1}}$ over the central and inner continental shelf.

The diffusivity for salt, K_v^S, is lower than K_v^T for DDC (see Fig. 2 in Kelley, 1984). The ratio of the two diffusivities is given by

$$K_v^S / K_v^T = R_F R_\rho^{-1}, \tag{9}$$

(Kelley, 1984), where the buoyancy flux ratio R_F is given by

$$R_F = \frac{R_\rho + 1.4(R_\rho - 1)^{3/2}}{1 + 14(R_\rho - 1)^{3/2}} \tag{10}$$

(Kelley, 1990). Based on (9) and (10), K_v^S is $\sim 0.5 \times 10^{-6}\,\mathrm{m^2\,s^{-1}}$ over the continental slope and $\sim 0.1 \times 10^{-6}\,\mathrm{m^2\,s^{-1}}$ over the central and inner continental shelf. The salt fluxes associated with these diffusivities are $\sim 0.002\,\mathrm{mg\,m^{-2}\,s^{-1}}$ over the continental slope and $\sim 0.001\,\mathrm{mg\,m^{-2}\,s^{-1}}$ over the shelf.

It remains an open question whether DDC fluxes in the ocean can be correctly parameterized by formulas developed in laboratory studies. For example, Padman (1994) suggested that the addition of mean shear to thermohaline steps can increase the vertical momentum and scalar fluxes relative to unsheared steps. A fundamental assumption in the Padman (1994) model was that the applied shear was "relatively" weak (incapable of causing mixing in the absence of the finestructure established by DDC), and the sharp DDC interfaces were, therefore, not significantly disrupted by the applied shear. We reiterate that very few cases of sharp interfaces separating truly homogeneous layers were found in the SO GLOBEC data, which implies that DDC was not active at the time the observations were made. There are several plausible explanations for the observed steppy fine structure in some CTD profiles, however, it is possible that some of this finestructure points to prior double-diffusive activity that has since been partially erased by more recent shear-driven turbulence.

4. Discussion and conclusions

We used CTD and ADCP data from the first year (2001) of Southern Ocean GLOBEC field work to study diapycnal mixing processes in the pycnocline separating UCDW from the surface layer over the WAP continental shelf near Marguerite Bay. Based on a recent box-model study of a region of the WAP shelf just north of the SO GLOBEC study area (Smith and Klinck, 2002), our a priori expectation was that DDC would be the dominant process driving the upward flux of heat, salt and nutrients from the UCDW, with an additional contribution from SDI.

Detailed examination of high-resolution CTD profiles from the winter 2001 survey cruise on *N. B. Palmer*, combined with the application of common parameterizations of DDC fluxes to the observed hydrographic profiles, suggest that DDC was either not active or was very weak during this cruise. The maximum likely DDC heat flux is $< 1\,\mathrm{W\,m^{-2}}$, compared with Smith and Klinck's estimate of order $10\,\mathrm{W\,m^{-2}}$.

We attribute most of the velocity shear observed in the pycnocline with hull-mounted ADCP to wind forcing. With the exception of small regions near the shelf break, the tidal currents predicted from an Antarctic tide model (CATS02.01) are an order of magnitude weaker than typical wind-forced, near-inertial oscillations of the upper ocean. A simple parameterization of vertical mixing due to SDI, following Pacanowski and Philander (1981), suggests that the mean vertical diffusivity (K_v) in the pycnocline in winter 2001 was $\sim 1 \times 10^{-5}\,\mathrm{m^2\,s^{-1}}$ with a corresponding upward heat flux from the UCDW of $\sim 1\,\mathrm{W\,m^{-2}}$. We caution, however, that this parameterization was

developed for oceanic conditions (the mean-sheared Equatorial Undercurrent) that are quite different from the WAP region.

The pycnocline fluxes that we estimate are two orders of magnitude less than those required to explain the loss of heat from the surface-mixed layer between the fall and winter survey cruises: as expected, surface buoyancy fluxes are the primary causes of the strong seasonal cycle in the upper ocean. The destabilizing buoyancy flux in fall and winter, as a source of entrainment of the pycnocline at the base of the mixed layer, is augmented by the turbulent stress penetrating the ice pack.

We conclude that the downward flux of momentum originating in the wind-stress field is the dominant process driving diapycnal fluxes in the pycnocline through downward propagation of near-inertial internal waves, and is also a critical component of upper-ocean seasonal variability. There are several practical consequences to this observation. First, since the actual stress transmitted to the upper ocean through the sea ice (when present) depends on the roughness, thickness and mobility of the sea ice, mixing in the pycnocline cannot be evaluated in isolation from either accurately prescribed or modeled sea ice conditions. Second, since the wind stress in this region is extremely variable (US SO GLOBEC, 2001a–c), we risk undersampling the rare but energetic events that might dominate mean mixing rates, and so may significantly underestimate mean pycnocline diffusivity. Third, generating realistic near-inertial behavior in a model of the upper ocean requires atmospheric model forcing fields with high resolution in both time and space. The output from global atmospheric models is typically every 6–12 h and on a coarse spatial grid; thus a new high-resolution regional atmospheric model will be required before WAP shelf circulation models can hope to capture the physics of mixing.

We hypothesize that, given the importance of wind forcing, coastal upwelling could be a significant factor contributing to the upward flux of UCDW properties. Upwelling may raise UCDW into the depth range affected directly by surface stress. Given the short Rossby radius (~5 km) in high-latitude coastal seas, sampling very close to the coast under upwelling-favorable wind conditions would be required to test this hypothesis.

Finally, we note that the study period covers only the fall and winter of 1 year, 2001, whereas we expect that both SDI and DDC could be sensitive to interannual variability of stratification. The Amundsen–Bellingshausen Sea sector of Antarctica experiences significant El Niño–Southern Oscillation (ENSO) atmospheric and sea-ice variability (Kwok and Comiso, 2002), while the Antarctic Circumpolar Wave (ACW) provides an additional multi-year signal (White and Peterson, 1996). It is possible that quite different annual-mean fluxes in the pycnocline occur during appropriate phases of the ENSO and ACW cycles.

Acknowledgements

This work was supported by NSF Grant OPP-9910102 to ESR, and OPP–9910092 to WHOI. We thank the crews of *N. B. Palmer* and *L. M. Gould* and the Raytheon Polar Services seagoing personnel for their considerable logistic support for this study. The efforts of E. Firing, J. Hummon, and T. Chereskin in managing the ADCP systems on the *L. M. Gould* and *N. B. Palmer*, including post-processing, were critical to creating a high quality ADCP data set for SO GLOBEC. We gratefully acknowledge R. Limeburner's provision of drifter position data for our analyses of diurnal tidal current variability. R. Beardsley, J. Klinck, M. McPhee, V. Strass, and editor E. Hofmann provided valuable suggestions for improvements of the original manuscript. We particularly wish to thank M. McPhee for providing the results of his 1-D local turbulence closure model for analyzing upper-ocean and sea ice behavior due to wind stress. This is U.S. GLOBEC contribution number 450.

References

Beardsley, R.C., Limeburner, R., Owens, W.B., 2004. Drifter measurements of surface currents near Marguerite Bay on the western Antarctic Peninsula shelf during austral summer and fall, 2001 and 2002. Deep-Sea Research II, this issue [doi: 10.1016/j.dsr2. 2004.07.031].

Cummins, P.F., Masson, D., Foreman, M.G.G., 2000. Stratification and mean flow effects on diurnal tidal currents off Vancouver Island. Journal of Physical Oceanography 30, 15–30.

Dushaw, B.D., Cornuelle, B.D., Worcester, P.F., Howe, B.W., Luther, D.S., 1995. Barotropic and baroclinic tides in the central North Pacific Ocean determined from long-range reciprocal acoustic transmissions. Journal of Physical Oceanography 25, 631–647.

Foldvik, A., Middleton, J.H., Foster, T.D., 1990. The tides of the southern Weddell Sea. Deep-Sea Research 37 (8), 1345–1362.

Gregg, M.C., 1987. Diapycnal mixing in the thermocline: a review. Journal of Geophysical Research 92, 5249–5286.

Gregg, M.C., 1989. Scaling turbulent dissipation in the thermocline: a review. Journal of Geophysical Research 94, 9686–9698.

Hofmann, E.E., Wiebe, P.H., Costa, D.P., Torres, J.J., 2004. An overview of the Southern Ocean Global Ocean Ecosystems Dynamics program. Deep-Sea Research II, this issue [doi: 10.1016/j.dsr2.2004.08.007].

Kelley, D., 1984. Effective diffusivities within thermohaline staircases. Journal of Geophysical Research 89, 10484–10488.

Kelley, D., 1990. Fluxes through diffusive staircases: a new formulation. Journal of Geophysical Research 95, 3365–3371.

Klinck, J.M., Hofmann, E.E., Beardsley, R.C., Salihoglu, B., Howard, S., 2004. Water-mass properties and circulation on the west Antarctic Peninsula continental shelf in austral fall and winter 2001. Deep-Sea Research II, this issue [doi: 10.1016/j.dsr2.2004.08.001].

Kwok, R., Comiso, J.C., 2002. Southern Ocean climate and sea ice anomalies associated with the southern oscillation. Journal of Climate 15, 487–501.

Large, W.G., McWilliams, J.C., Doney, S.C., 1994. Oceanic vertical mixing: a review and a model with a nonlocal boundary layer parameterization. Reviews of Geophysics 32 (4), 363–403.

Ledwell, J.R., Watson, A.J., Law, C.S., 1993. Evidence for slow mixing across the pycnocline from an open-ocean tracer-release experiment. Nature 364, 701–703.

Levine, M.D., Padman, L., Morison, J.H., Muench, R.D., 1997. Internal waves and tides in the western Weddell Sea: observations from ice station Weddell. Journal of Geophysical Research 102, 1073–1089.

Lozovatsky, I.D., Morozov, E.G., Fernando, H.J.S., 2003. Spatial decay of energy density of tidal internal waves. Journal of Geophysical Research 108 (C6), 3201.

Marmorino, G.O., Caldwell, D.R., 1976. Heat and salt transport through a diffusive thermohaline interface. Deep-Sea Research 23, 59–67.

McPhee, M.G., 1999. Parameterization of mixing in the ocean boundary layer. Journal of Marine Systems 21, 55–65.

Middleton, J.H., Foster, T.D., Foldvik, A., 1987. Diurnal shelf waves in the southern Weddell Sea. Journal of Physical Oceanography 17, 784–791.

Muench, R.D., Fernando, H.J.S., Stegen, G.R., 1990. Temperature and salinity staircases in the northwestern Weddell Sea. Journal of Physical Oceanography 20, 295–306.

Muench, R.D., Padman, L., Howard, S.L., Fahrbach, E., 2002. Upper ocean diapycnal mixing in the northwestern Weddell Sea. Deep-Sea Research II 49, 4843–4861.

Munk, W., Wunsch, C., 1998. Abyssal recipes II: energetics of tidal and wind mixing. Deep-Sea Research I 45, 1977–2010.

Orlanski, I., Bryan, K., 1969. Formation of the thermocline step structure by large-amplitude internal gravity waves. Journal of Geophysical Research 74, 6975–6983.

Pacanowski, R.C., Philander, S.G.H., 1981. Parameterization of vertical mixing in numerical models of tropical oceans. Journal of Physical Oceanography 11, 1443–1451.

Padman, L., 1994. Momentum fluxes through sheared oceanic diffusive–convective steps. Journal of Geophysical Research 99, 22491–22499.

Padman, L., Dillon, T.M., 1987. Vertical heat fluxes through the Beaufort Sea thermohaline staircase. Journal of Geophysical Research 92, 10799–10806.

Padman, L., Dillon, T.M., 1991. Turbulent mixing near the Yermak Plateau during the Coordinated Eastern Arctic Experiment. Journal of Geophysical Research 96, 4769–4782.

Padman, L., Jones, I.S.F., 1985. Richardson number statistics in the seasonal thermocline. Journal of Physical Oceanography 15, 844–854.

Padman, L., Kottmeier, C., 2000. High-frequency ice motion and divergence in the Weddell Sea. Journal of Geophysical Research 105, 3379–3400.

Padman, L., Dillon, T.M., Wijesekera, H.W., Levine, M.D., Paulson, C.A., Pinkel, R., 1991. Internal wave dissipation in a non-Garrett–Munk ocean. Proceedings of the Aha Huliko'a Hawaiian Winter Workshop, University of Hawaii at Manoa, Honolulu, pp. 31–51.

Padman, L., Plueddemann, A.J., Muench, R.D., Pinkel, R., 1992. Diurnal tides near the Yermak Plateau. Journal of Geophysical Research 97, 12,639–12,652.

Padman, L., Fricker, H.A., Coleman, R., Howard, S., Erofeeva, S., 2002. A new tidal model for the Antarctic ice shelves and seas. Annals of Glaciology 34, 247–254.

Padman, L., Erofeeva, S., Joughin, I., 2003. Tides of the Ross Sea and Ross Ice Shelf cavity. Antarctic Science 15 (01), 31–40.

Peters, H., Gregg, M.C., Toole, J.M., 1988. On the parameterization of equatorial turbulence. Journal of Geophysical Research 93, 1199–1218.

Prézelin, B.B., Hofmann, E.E., Klinck, J.M., Menglet, C., 2000. The linkage between Upper Circumpolar Deep Water (UCDW) and phytoplankton assemblages on the west Antarctic Peninsula continental shelf. Journal of Marine Research 58, 165–202.

Robertson, R., Padman, L., Levine, M.D., 1995. Finestructure, microstructure, and vertical mixing processes in the upper ocean in the western Weddell Sea. Journal of Geophysical Research 100, 18517–18536.

Ruddick, B.R., Walsh, D., Oakey, N., 1997. Variations in apparent mixing efficiency in the North Atlantic central waters. Journal of Physical Oceanography 27, 2589–2605.

Smith, D.A., Klinck, J.M., 2002. Water properties on the west Antarctic Peninsula continental shelf: a model study of effects of surface fluxes and sea-ice. Deep-Sea Research II 49, 4863–4886.

Turner, J.S., 1973. Buoyancy Effects in Fluids. Cambridge University Press, New York, 368pp.

US SO GLOBEC, 2001a. Reports of R/V *Lawrence M. Gould* Cruises LMG01-03 and LMG01-04 to the Western Antarctic Peninsula, 18 March to 13 April 2001 and 23 April to 6 June 2001. US Southern Ocean GLOBEC Report Number 1, 94pp.

US SO GLOBEC, 2001b. Reports of RVIB *Nathaniel B. Palmer* Cruise NBP01-03 to the Western Antarctic Peninsula, 24 April to 5 June 2001. US Southern Ocean GLOBEC Report Number 2, 189pp.

US SO GLOBEC, 2001c. Reports of RVIB *Nathaniel B. Palmer* Cruise NBP01-04 and R/V *Lawrence M. Gould* Cruise LMG01-06 to the Western Antarctic Peninsula, 24 July to 31 August 2001 and 21 July to 1 September 2001. US Southern Ocean GLOBEC Report Number 3, 240pp.

White, W.B., Peterson, R., 1996. An Antarctic circumpolar wave in surface pressure, wind, temperature, and sea ice extent. Nature 380, 699–702.

Wijesekera, H., Padman, L., Dillon, T., Levine, M., Paulson, C., Pinkel, R., 1993. The application of internal-wave dissipation models to a region of strong mixing. Journal of Physical Oceanography 23, 269 286.

Wunsch, C., 2000. Moon, tides and climate. Nature 405, 743–744.

ELSEVIER

Deep-Sea Research II 51 (2004) 1981–2002

DEEP-SEA RESEARCH
PART II

www.elsevier.com/locate/dsr2

Nutrients in the Southern Ocean GLOBEC region: variations, water circulation, and cycling

Yulia M. Serebrennikova, Kent A. Fanning*

College of Marine Science, University of South Florida, 140 7th Avenue South, St. Petersburg, FL 33701, USA

Accepted 14 July 2004

Abstract

As part of the US Southern Ocean Global Ecosystem Dynamics (SO GLOBEC) study on the West Antarctic Peninsula (WAP) continental shelf, four surveys were conducted along a grid of close-spaced stations lying within an area composed of Marguerite Bay (MB) and the adjacent continental margin. The surveys occurred in the autumn and winter of both 2001 and 2002. A detailed repetitive plan of the SO GLOBEC surveys permitted the delineation of the important features of nutrient processes. Horizontal intrusions of Upper Circumpolar Deep Water onto the WAP continental shelf do not appear to produce fluxes of nitrate and phosphate onto the shelf but appear to lead to a dilution of the silica inventory on the shelf. High silica concentrations ($>115\,\mu M$) observed in the near-bottom waters on the shelf were most likely generated locally through dissolution of opal in sediments.

Nutrient deficits and net community production (NCP) were calculated by the integration of decreases in nutrient concentrations in the mixed-layer below corresponding values in the underlying remnant Winter Water layer. Waters in MB and other coastal areas were strongly depleted in nutrients—deficits of total inorganic nitrogen ($TIN = NO_3^- + NO_2^- + NH_4^+$) and silica were $>0.6\,mol\,m^{-2}$ and $>2.5\,mol\,m^{-2}$, respectively—and enriched in ammonium stocks ($>0.25\,mol\,m^{-2}$) relative to other parts of the grid, especially in the autumn of 2001. Autumn NCP values calculated from TIN deficits in MB equaled or exceeded autumnal NCP values from the Joint Global Ocean Flux Study Ross Sea study in 1997. Observed $\Delta N/\Delta P$ and $\Delta Si/\Delta N$ removal ratios were 12.4 ± 1.6 and 3.9 ± 1.2, respectively, in 2001; and 11.1 ± 1.3 and 4.1 ± 1.1, respectively, in 2002. These results strongly suggest the dominance of diatoms in the study region. Co-location of maxima in ammonium stocks with the areas of the highest TIN and silica deficits indicated a spatial coupling between primary and heterotrophic production in both years. This co-location highlights the finding that temporal trends in ammonium were usually the opposite of trends in the other nutrients.
© 2004 Elsevier Ltd. All rights reserved.

1. Introduction

The water mass structure on or adjacent to the West Antarctic Peninsula (WAP) continental shelf consists of several components. For much of the

*Corresponding author. Tel.: 1-727-553-1594; fax: 1-727-553-1189.

E-mail address: kaf@seas.marine.usf.edu (K.A. Fanning).

0967-0645/$ - see front matter © 2004 Elsevier Ltd. All rights reserved.
doi:10.1016/j.dsr2.2004.07.023

year, Antarctic Surface Water (AASW) occupies the upper 100–150 m. It is replaced by Winter Water (WW) in the autumn and winter and overlies a modified form of Upper Circumpolar Deep Water (UCDW) (Klinck et al., 2004). Modified UCDW (MUCDW) results from mixing of UCDW and AASW (Smith et al., 1999). UCDW and Lower Circumpolar Deep Water (LCDW) are the largest water masses in the Antarctic Circumpolar Current (ACC), which flows along the WAP shelf break (Smith et al., 1999).

Dissolved inorganic nutrients on the WAP shelf are the focus of this study. Since the WAP continental shelf is important in the life cycle of Antarctic krill *Euphausia superba* (Quetin and Ross, 2003), nutrient dynamics should play a reasonably direct role in that cycle. Prézelin et al. (2000), e.g., stated that the lower ratios of silica to nitrate concentrations in the regions influenced by the ACC compared to the rest of the WAP continental shelf indicate a silica drawdown due to an intensive phytoplankton activity, most probably by the diatoms that are a primary food source for krill. Other features of these nutrients, such as distributions and variations, can be equally informative.

Several nutrient-related questions are considered in this study, which was conducted as a part of the US Southern Ocean Global Ocean Ecosystem Dynamics (SO GLOBEC) program in the austral autumns and winters of 2001 and 2002. First, variability in the ACC results in frequent on-shelf intrusions of the UCDW and LCDW that are thought to deliver nutrients (nitrate, phosphate and silica) onto the shelf (Prézelin et al., 2000; Klinck et al., 2004). After an evaluation of nutrient water-mass structure and variations in nutrient distributions, this claim is examined using data most closely associated with the Marguerite Bay (MB) region of the WAP (Fig. 1). Second, magnitudes and annual variability of primary productivity in the study area on the WAP continental shelf are evaluated by estimating net community production (NCP) for comparison with other areas of the Southern Ocean. We utilize the concept that seasonal depletions in nutrients such as silica, phosphate, and total inorganic nitrogen (TIN) (nitrate + nitrite + ammonium) may be considered to be measures of NCP (Bates et al., 1998).

A "peculiarity" of the Southern Ocean is the occurrence of high ammonium concentrations in its upper water column. Ammonium concentrations 4.5–10 μM on the WAP (Koike et al., 1986; Owens et al., 1991; Karl et al., 1996; Garibotti et al., 2003), 3 μM in Pridz Bay in the Indian sector of the SO (Semeneh et al., 1998), and 4 μM in the Ross Sea (Gordon et al., 2000) were measured in the summer time. Winter values up to 1 μM were found in the Weddell Sea (Cota et al., 1992; Nöthig et al., 1991). Thus, our third goal is to evaluate the geographical and annual variability of the occurrence of the high ammonium pool, expressed as the total standing ammonium stocks in the study area. This approach provides a more complete picture by correcting for the fact that physical dispersion may alter the ammonium concentration near the sea surface. Also, this study examines a possible relationship between net production and ammonium stock accumulation in the MB region that may serve as a model for other near-shore areas of the Southern Ocean.

2. Field and analytical methods

Nutrient data were collected abroad the R.V.I.B *Nathaniel B. Palmer* during four US SO GLOBEC surveys (Table 1). The study area covered MB and the adjacent WAP continental shelf from the northern tip of Adelaide Island to Charcot Island (Fig. 1A–D). The basic SO GLOBEC grid consisted of 13 across-shelf transects with 40-km along-shelf spacing and 10–40 km spacing between individual stations. The total number of hydrostations occupied during each survey varied from 50 to 96 (Fig. 1A–D, Table 1). Fewer stations were occupied on SO GLOBEC winter cruises II and IV (Fig. 1B,D) than on SO GLOBEC autumnal cruises I and III (Fig. 1A, C).

Water samples were taken at discrete depths using the 10-l Niskin bottles attached to a 24-bottle CTD rosette. Measurements of nitrate, nitrite, phosphate, and silicic acid were performed

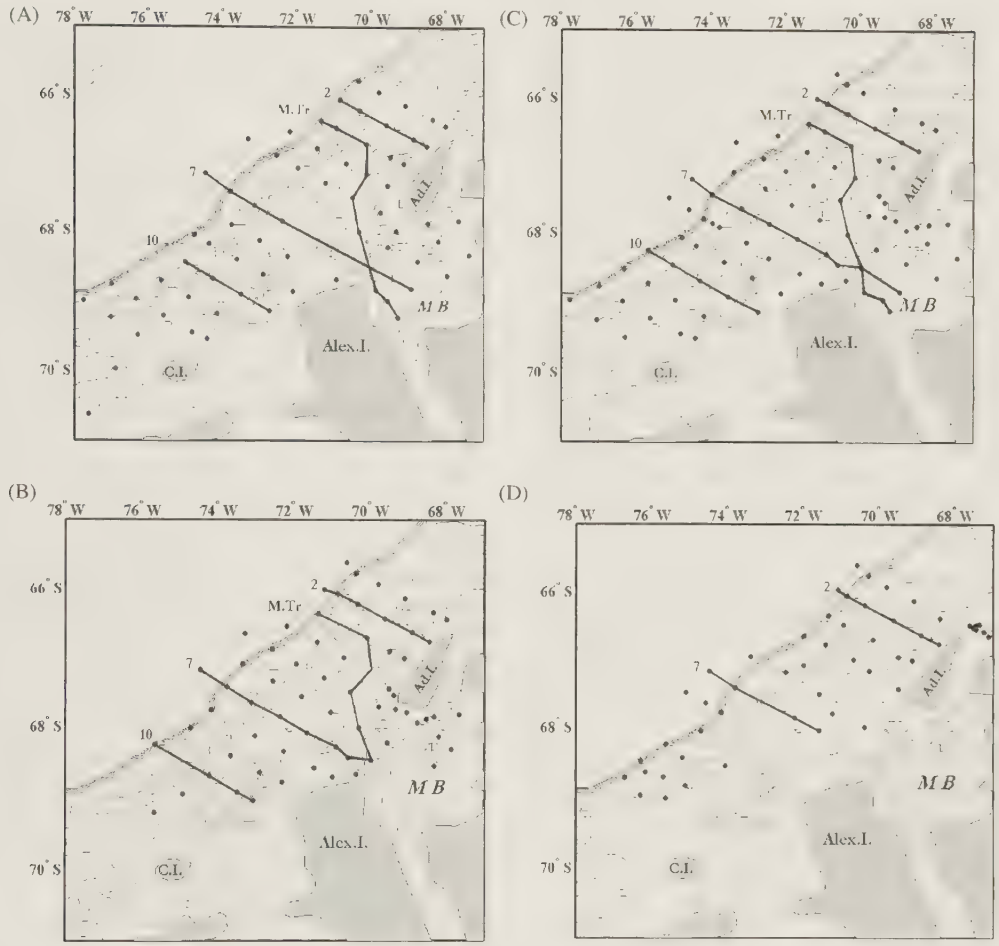

Fig. 1. Map of MB and the adjacent WAP continental shelf showing the CTD station locations for the SO GLOBEC surveys: (A) SO GLOBEC I, (B) SO GLOBEC II, (C) SO GLOBEC III, and (D) SO GLOBEC IV. The numbered across-shelf transects indicate the sampling locations used to construct the across-shelf nutrient distribution sections (Figs. 3–8). The location of the section along Marguerite Trough from the shelf break into MB is designated as "M.Tr". The bottom bathymetry contour inside MB indicates the 500 m depth. Bathymetry contour interval is 500 m. Key to island names: Ad. I.—Adelaide Island; Alex. I.—Alexander Island; C. I.—Charcot Island

Table 1
Summary of SO GLOBEC cruise designations, dates, and stations for the 2001 and 2002 austral autumn and winter field seasons

Survey	R.V.I.B N.B. *Palmer* cruise	Dates	Number of stations occupied
SO GLOBEC I	NBP0103	April 21–June 5, 2001	84
SO GLOBEC II	NBP0104	July 21–September 1, 2001	64
SO GLOBEC III	NBP0202	April 9–May 19, 2002	96
SO GLOBEC IV	NBP0204	July 31 September 19, 2002	50

on a 5-channel Technicon AutoAnalyzer II following the recommendations of Gordon et al. (1993) for the World Ocean Circulation Experiment Hydrographic Program. The fifth channel on the AutoAnalyzer was used for the determination of dissolved ammonium concentrations. A

modification of the indophenol-blue ammonium method suggested by Grasshoff (1976) was employed. Analytical precisions were as follows: ±0.06 μM for nitrate + nitrite, ±0.01 μM for nitrite, ±0.34 μM for silicic acid, ±0.04 μM for ammonium, and ±0.02 μM for phosphate.

Reagent blanks for nitrate + nitrite, nitrite, silicic acid and phosphate were obtained by using deionized water. However, the deionized water had higher signals in the ammonium channel than many samples of Antarctic seawater being analyzed, especially those below the pycnocline. Therefore, the ammonium reagent blank for the CTD-rosette casts was obtained by assuming that the deep seawater sample in each cast that gave the lowest signal had an ammonium concentration of zero. This procedure for determining the ammonium blank is consistent with the very low ammonium values of 0.04–0.06 μM reported below 2000 m in the North Atlantic by Woodward and Rees (2001) using a high sensitivity method (Jones, 1991) and also with the approach of Gordon et al. (2000).

All of our nutrient data have been placed in the US SO GLOBEC Data Archive (http://globec.whoi.edu/jg/dir/globec/soglobec/)

3. Results

3.1. Nutrients and water mass structure

This section describes the nutrient signatures of the different water masses occupying the SO GLOBEC study region using the plots of silicic acid and nitrate versus hydrographic properties (temperature and salinity). Since phosphate closely followed nitrate in a least-square distribution ($r^2 = 0.98$), phosphate was not needed to define water-mass nutrient signatures.

UCDW, characterized by maxima in temperature (Orsi et al., 1995; Smith et al., 1999) and nitrate (Fig. 2A, B), appears on the silica-temperature diagram as a leg of 80–100 μM silicic acid associated with temperatures above 1.6 °C (Fig. 2A) and on a nitrate-salinity diagram as having high nitrate concentrations, 33–36 μM, at salinities of 34.6–34.72 (Fig. 2B). Corresponding phosphate concentrations are 2.4–2.7 μM.

LCDW is characterized by higher silicic acid concentrations than UCDW (>100 μM in Fig. 2A) and a local nitrate minimum (32 μM) associated with a salinity maximum of >34.73 in Fig. 2B (Smith et al., 1999). LCDW phosphate is

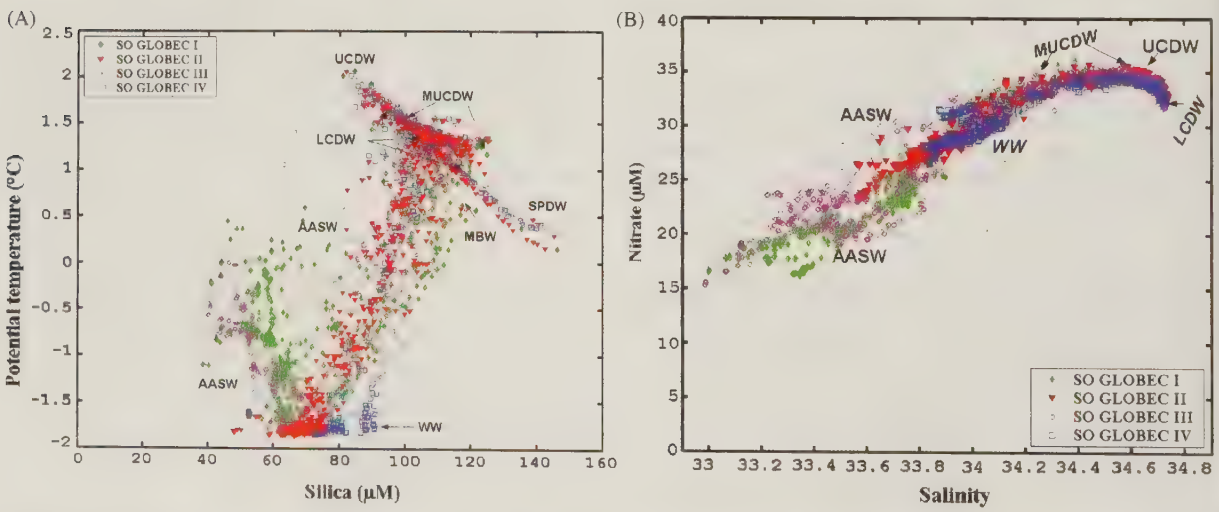

Fig. 2. (A) Silica (μM) versus potential temperature (°C) and (B) nitrate (μM) versus salinity diagrams constructed from observations during SO GLOBEC I–IV surveys. Abbreviations: UCDW—Upper Circumpolar Deep Water, LCDW—Lower Circumpolar Deep Water, MBW—Marguerite Bay bottom Water, SPDW—South Pacific Deep Water, MUCDW—Modified Upper Circumpolar Deep Water, AASW—Antarctic Surface Water, and WW—Winter Water.

2.15 μM. The highest silicic acid concentrations (>130 μM on Fig. 2A) denote South Pacific Deep Water (SPDW) (Smith et al., 1999) and were found at depths below 2500 m.

A cluster of points on the silica-temperature diagram with 100–125 μM silica values and a 1–1.5 °C temperature range (Fig. 2A) appears to be modified UCDW. It is slightly fresher than UCDW but has the same high nitrate concentration range (Fig. 2B). The bottom water of Marguerite Bay (MBW in Fig. 2A) has high silicic acid concentrations (110–125 μM) and lower temperatures (0.4–1.0 °C) than MUCDW on the shelf.

AASW, a water mass with temperatures of −1.5 °C to 1 °C and salinity of 33.0–33.7, is characterized by wide concentration ranges, 16–27 μM nitrate and 40–74 μM silica (Fig. 2A,B). Colder (−1.8 °C to −1.5 °C) and saltier (34.0–34.2) than AASW, WW is characterized by 24–31 μM nitrate and 48–90 μM silica concentrations (Fig. 2A, B). Corresponding phosphate values are 1.3–2.2 μM.

3.2. Nutrient transects

Figs. 3–8 illustrate the spatial and temporal variations in the distributions of silica and nitrate for four SO GLOBEC surveys on three across-shelf transects representing the northern, central, and southern parts of the study area (2, 7, and 10 in Fig. 1A–D) and a section along Marguerite Trough (M.Tr. in Fig. 1A–C). An important point

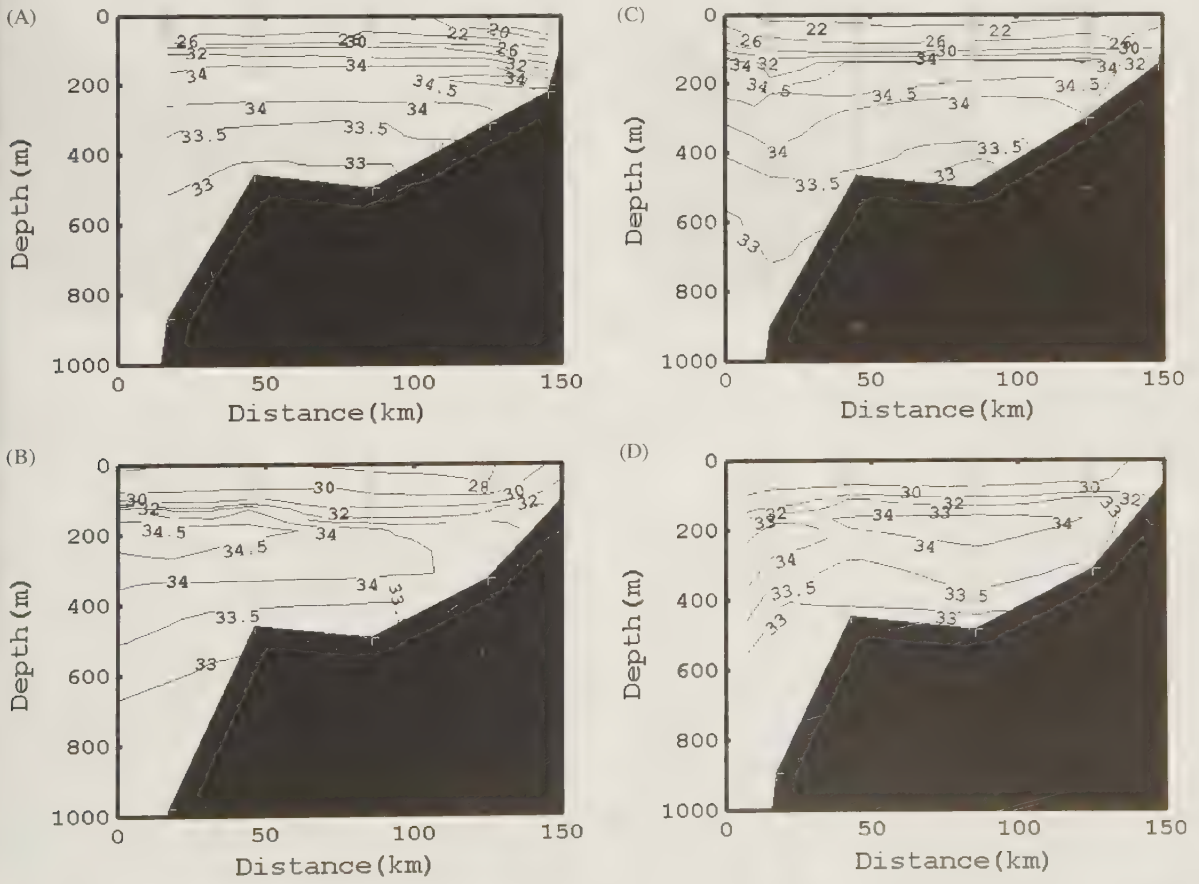

Fig. 3. Vertical sections of the distribution of nitrate concentration (μM) along transect #2 (see Fig. 1 for the location) on (A) SO GLOBEC I, (B) SO GLOBEC II, (C) SO GLOBEC III, and (D) SO GLOBEC IV. Zero distance denotes the location of the most seaward station of the sections.

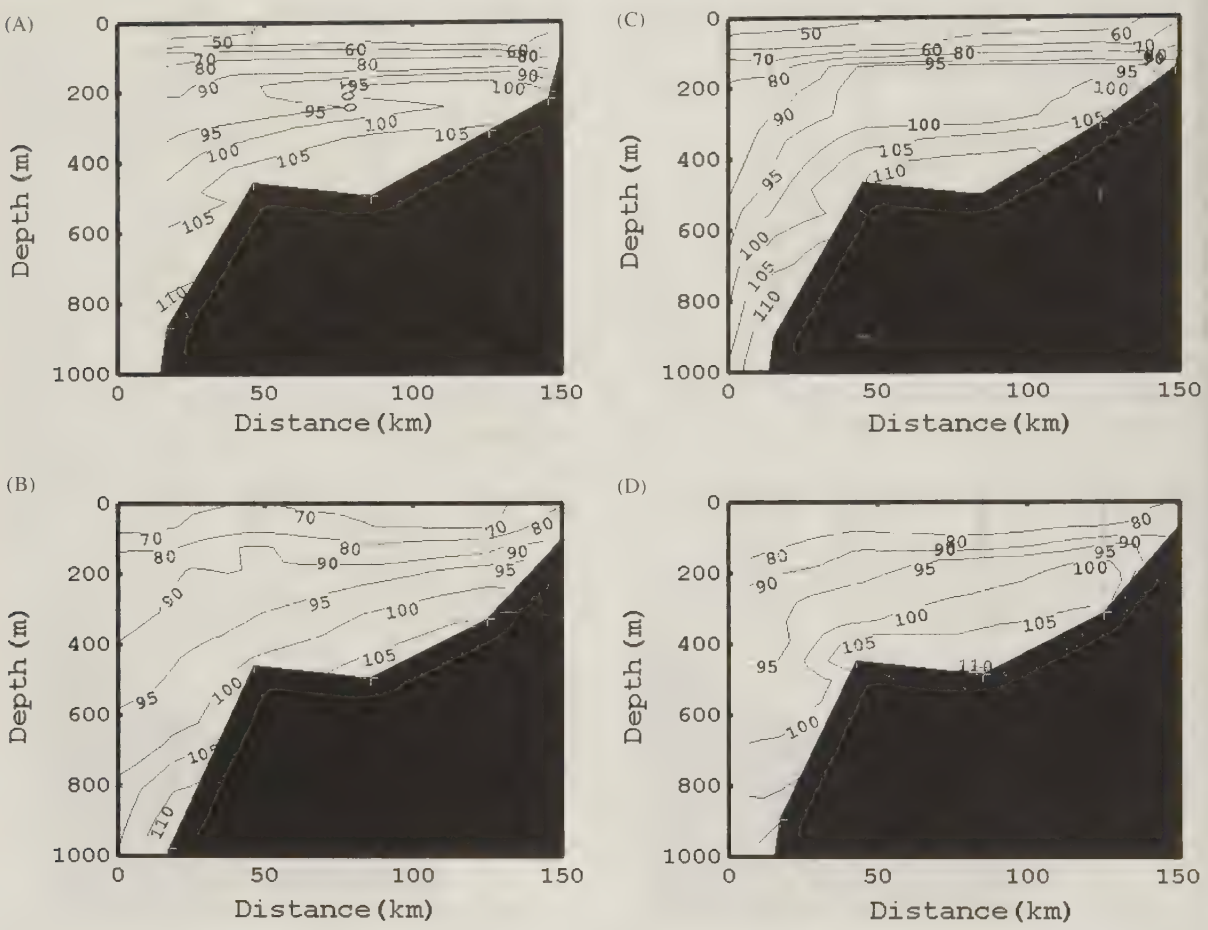

Fig. 4. Vertical sections of the distribution of silica concentration (μM) along transect #2 (see Fig. 1 for the location) on (A) SO GLOBEC I, (B) SO GLOBEC II, (C) SO GLOBEC III, and (D) SO GLOBEC IV. Zero distance denotes the location of the most seaward station of the sections.

to note is that the combination of both nutrients describes the distribution of the major water masses on the WAP shelf much more effectively than either nutrient by itself.

Along transect 2, e.g., the following features were found. Nitrate concentrations $>33\,\mu M$ could denote either UCDW or MUCDW between 200 and 500 m on all SO GLOBEC surveys (Fig. 3). Nitrate alone cannot distinguish between them. However, based on Fig. 2A, the boundary between the two water masses is the $100\,\mu M$ silicic acid isopleth. Thus the UCDW silica signature ($<100\,\mu M$ below 200 m) was fairly shallow (200–300 m) over the shelf on SO GLOBEC I (Fig. 4A) but appeared to deepen somewhat on the succeeding surveys (Fig. 4B–D), indicating that a larger portion of the water column below 200 m was filled with UCDW, possibly due to a closer proximity of the ACC to the shelf. Another interesting feature involves LCDW (with nitrate concentration $<33\,\mu M$ in Fig. 3 and silica concentration $>100\,\mu M$ in Fig. 4). It was seen below 600 m offshore, and the nitrate and silica patterns suggest that LCDW was present in a thin bottom layer over most of the shelf on transect 2 (Figs. 3 and 4).

Above 200 m, nutrient concentrations within the AASW decrease upward and reach their lowest

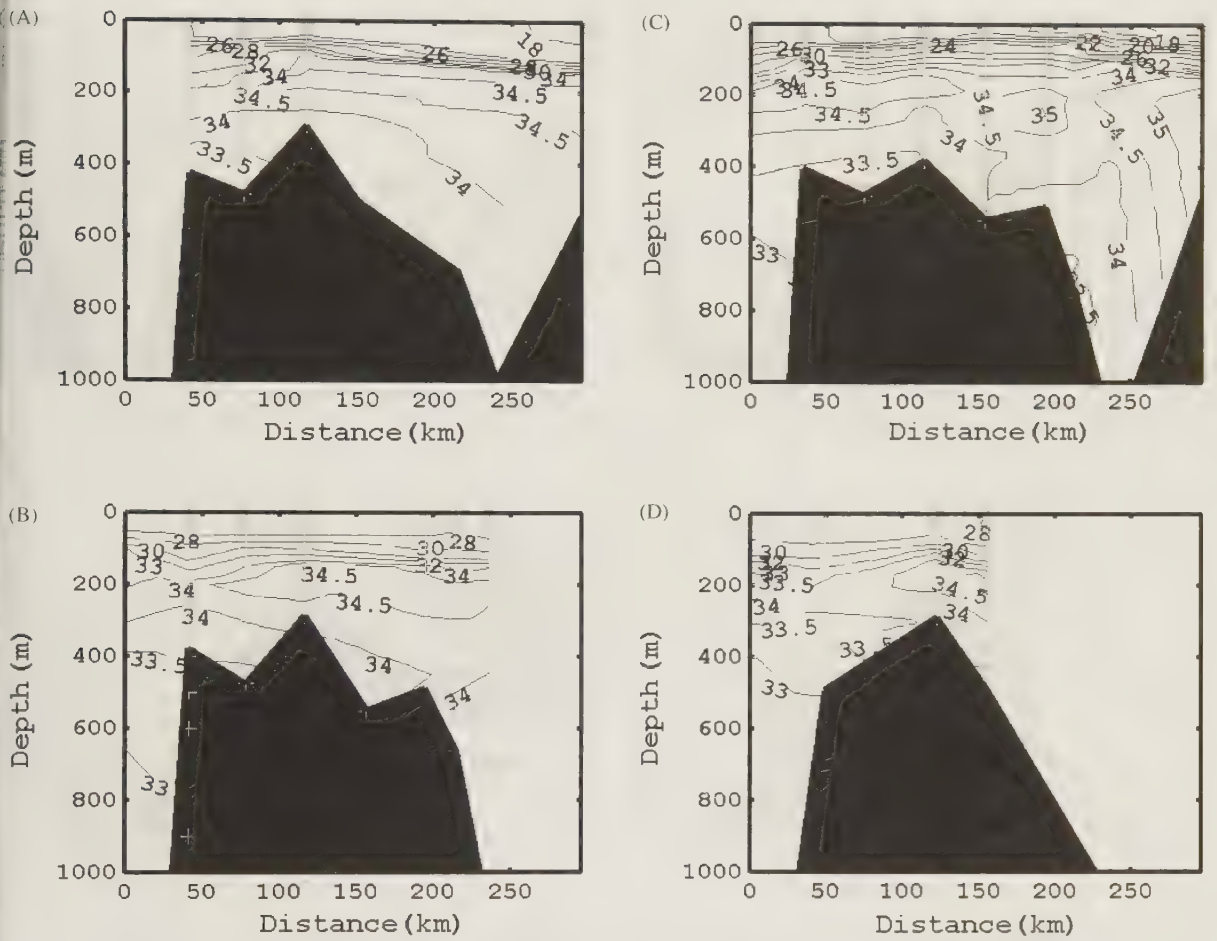

Fig. 5. Vertical sections of the distribution of nitrate concentration (μM) along transect #7 (see Fig. 1 for the location) on (A) SO GLOBEC I, (B) SO GLOBEC II, (C) SO GLOBEC III, and (D) SO GLOBEC IV. Zero distance denotes the location of the most seaward station of the sections.

values—$[NO_3]$ <26 μM and $[SiO_2]$ <60 μM—in the surface mixed layer on the autumn sections, SO GLOBEC I and III (Figs. 3A, C, and 4A, C). On wintertime surveys, SO GLOBEC II and IV, AASW was being replaced by WW and nutrient concentrations above 200 m were higher (WW nitrate concentrations range between 26 and 31 μM and silica concentrations range between 60 and 90 μM—Figs. 3B, D and 4B, D). Nutrient concentrations were reasonably uniform in the mixed layer (i.e., above 100 m) at all stations on all surveys.

The distributions of nitrate and silica below 200 m along across-shelf transects 7 and 10 (see Fig. 1A–D for location) were consistent with those observed along transect 2 (Figs. 5-7). Nitrate maxima (>33 μM) were approximately centered at 200 m on both transects (Figs. 5 and 7A–C). The 100 μM silica isopleth was definitely shallow (<200 m) on both transects during SO GLOBEC I (Figs. 6A and 7D) and deeper (>200 m) on most of the other transects (Figs. 6B, D and 7E, F). Thus, autumn 2001 was different from the other surveys, showing less penetration of UCDW onto the shelf on transects 7 and 10 just like on transect 2. Likewise the deepening of the 100 μM isopleth on most of the other transects suggests a greater presence of UCDW on most of the other surveys

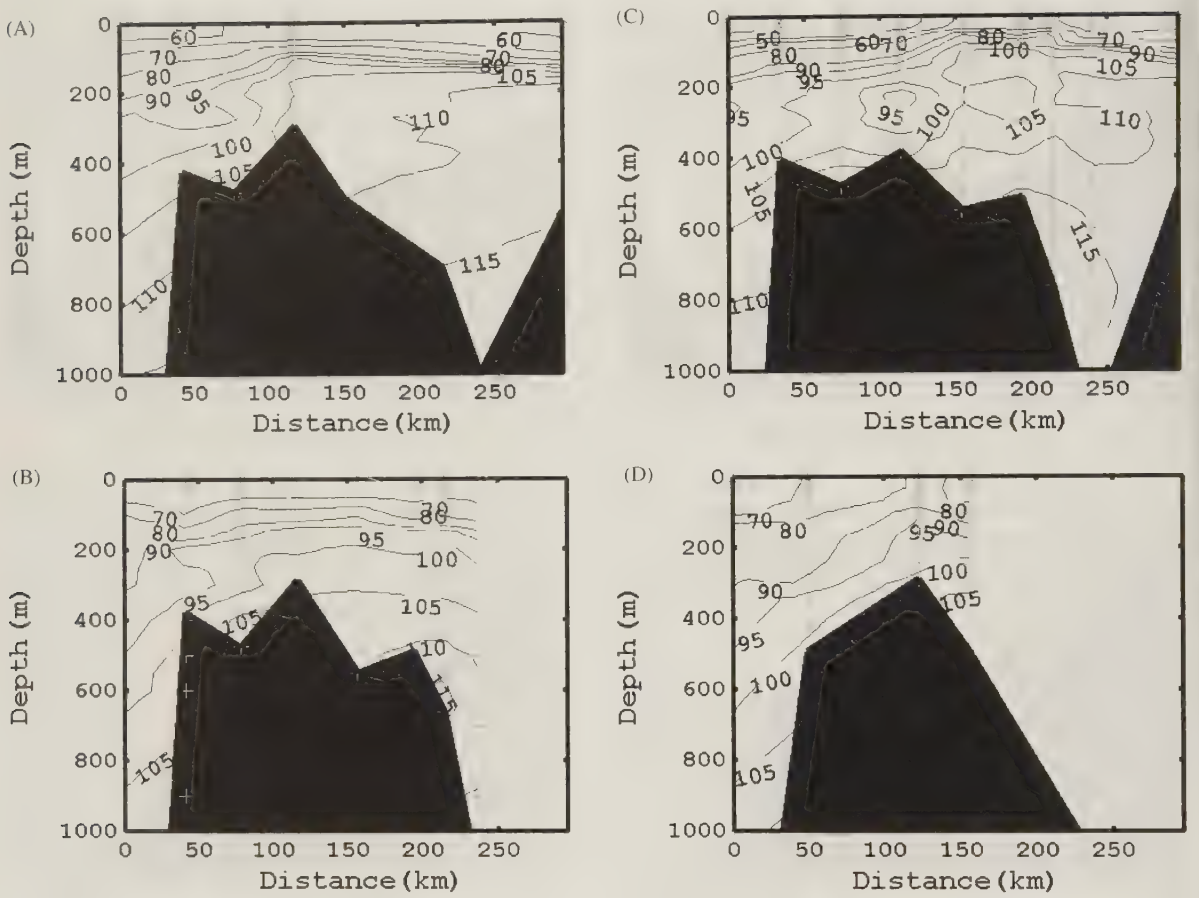

Fig. 6. Vertical sections of the distribution of silica concentration (μM) along transect #7 (see Fig. 1 for the location) on (A) SO GLOBEC I, (B) SO GLOBEC II, (C) SO GLOBEC III, and (D) SO GLOBEC IV. Zero distance denotes the location of the most seaward station of the sections.

along transects 7 and 10. Autumn 2002 (SO GLOBEC III) was somewhat anomalous on transect 7 (Fig. 6C). Over most of the shelf the 100 μM silica isopleth was quite shallow, suggesting a smaller presence of UCDW than on transect 2 in autumn 2002 (see Fig. 4C). However, slightly below 200 m at a distance of 100 km from the seaward end of transect 7 is a bolus of lower-silica water that appears to be UCDW (Fig. 6C). The water surrounding the bolus has silica characteristics more like MUCDW (>100 μM). This distribution suggests that the influx of UCDW, which was quite strong in autumn 2002 on transect 2, was weaker on transect 7.

On all four SO GLOBEC surveys, nitrite and ammonium concentrations were approximately uniform throughout the mixed layer at each station and then rapidly decreased with depth to zero, which was defined by detection limit of the analytical methods employed.

3.3. Nutrient delivery to the shelf

Based on salinity and temperature distributions, Klinck et al. (2004) showed that the intrusions of CDW onto the shelf occur most strongly along a bathymetric depression, Marguerite Trough (see Fig. 1A–C for the location). In order to study how

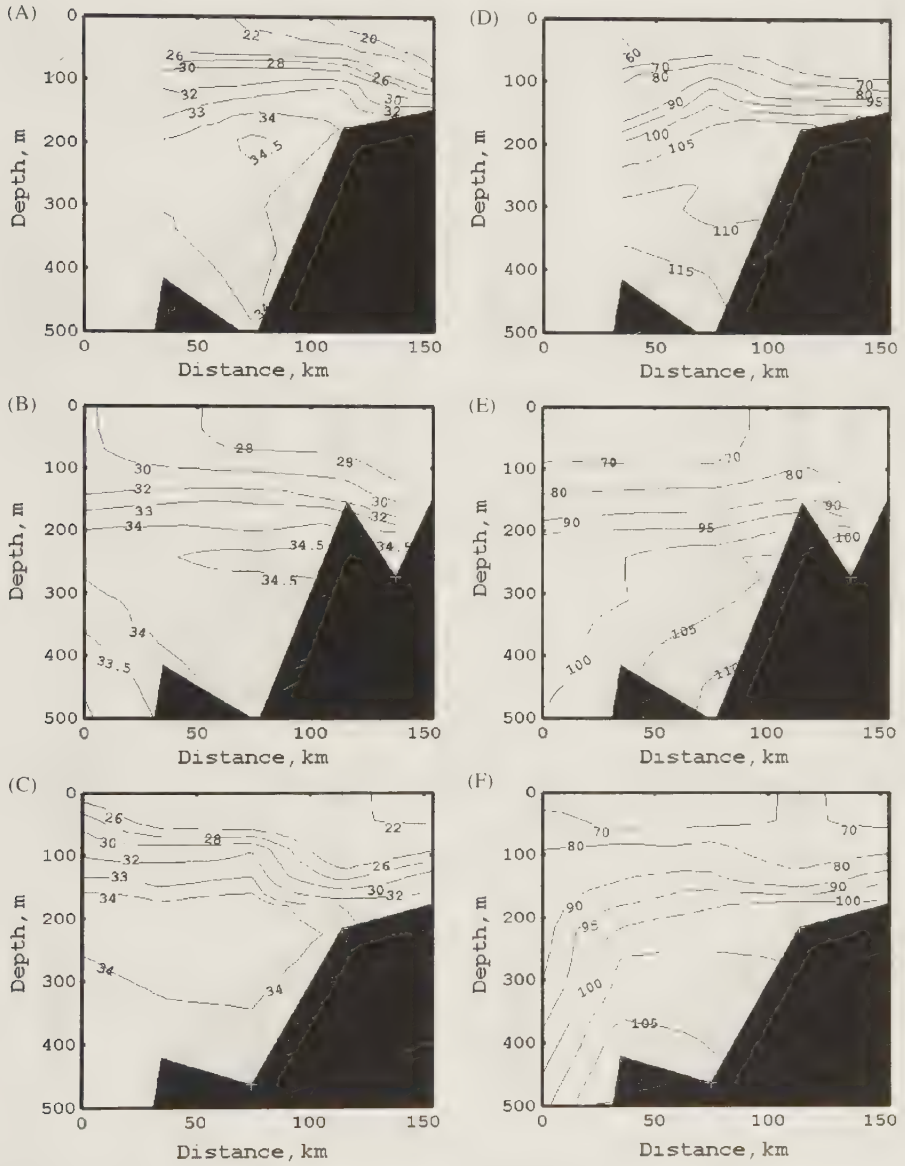

Fig. 7. Vertical sections of the distribution of nitrate concentrations (μM) on (A) SO GLOBEC I, (B) SO GLOBEC II, and (C) SO GLOBEC III and vertical sections of the distribution of silica concentrations (μM) on (D) SO GLOBEC I, (E) SO GLOBEC II, and (F) SO GLOBEC III along transect #10 (see Fig. 1A–C for the location). Insufficient data were obtained on SO GLOBEC IV. Zero distance denotes the location of the most seaward station of the sections.

the movement of CDW affects the distribution of nutrients on the shelf, we constructed sections along Marguerite Trough for the SO GLOBEC I–III surveys (Fig. 8). Due to heavy sea ice in winter 2002, the number of stations occupied along Marguerite Trough on SO GLOBEC IV was insufficient to construct a similar transect. The nitrate distribution along the Trough was similar to that along the other across-shelf transects, showing a maximum of $>33\,\mu M$ centered at approximately 200 m (compare Fig. 8A–C with Figs. 3, 5, and 7A–C). There was no apparent

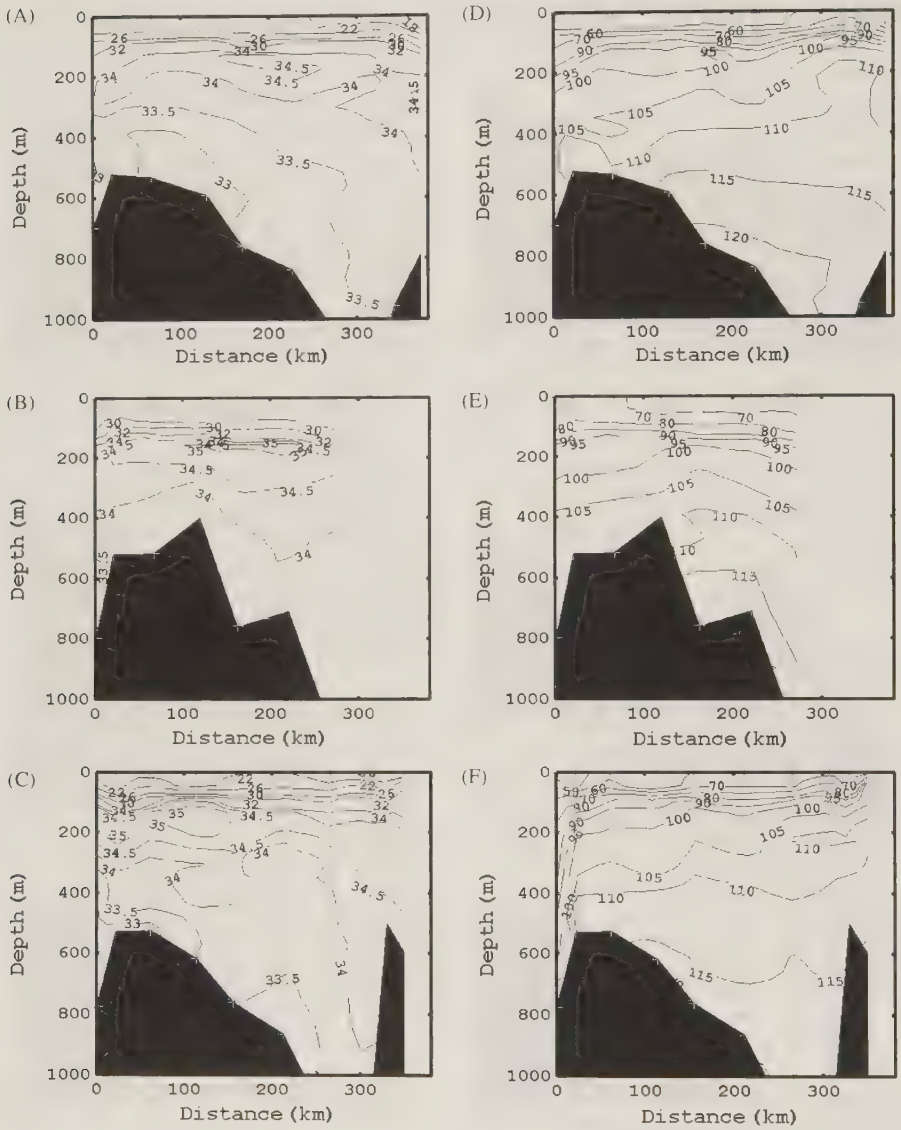

Fig. 8. Vertical sections of the distribution of nitrate concentrations (μM) on (A) SO GLOBEC I, (B) SO GLOBEC II, and (C) SO GLOBEC III and vertical sections of the distribution of silica concentrations (μM) on (D) SO GLOBEC I, (E) SO GLOBEC II, and (F) SO GLOBEC III along the Marguerite Trough section (see Fig. 1A–C for the location). Insufficient data were obtained on GLOBEC IV. Zero distance denotes the location of the most seaward station of the sections.

trend in the distribution of nitrate that would indicate net enrichment in nitrate of the shelf waters by offshore-to-inshore flow (Fig. 8A–C). No evidence was found for an offshore source of higher nitrate concentrations in the upper 600 m. Fig. 8D–F shows that silica concentrations were those of MUCDW (>100 μM) below 200 m along Marguerite Trough. MUCDW is a shelf phenomenon and is not found beyond the shelf break (Klinck et al., 2004). This idea is strongly supported by the SO GLOBEC III Marguerite Trough section, which exhibited a sharp horizontal gradient in silica concentration between offshore low-silica UCDW (<100 μM) and silica-rich

MUCDW (>100 μM) at the shelf break (Fig. 8F). This feature indicates little possibility of offshore-to-onshore net silica transport along the Trough, such as suggested by rising isopleths of 90–100 μM silica along the across-shelf transects 2, 7 and 10 (Figs. 4, 6, and 7D–F). In fact, the higher silica concentrations (>115 μM) in the bottom water of the Trough appear to be generated in place.

3.4. Nutrient deficit calculations

In order to estimate NCP in the WAP study area, we focused on the period of greatest biological activity (i.e., spring-autumn) and began by calculating nutrient deficits using the method of Rubin et al. (1998) and Ishii et al. (2002). These deficits were then used to estimate NCP values for that period. The deficit calculations were based on vertically integrated depletions of nutrients in the surface layer down to the depths of a layer of remnant WW, which is the only part of AASW that remains the same regardless of season (Hofmann et al., 1996) and was distinguished by a subsurface temperature minimum and salinity around 34 (Klinck et al., 2004) during both SO GLOBEC autumn surveys. Since this layer forms at the end of the winter every year, its properties, which are still present in the autumn, are reasonable approximations of the entire mixed layer in the early spring (Ishii et al., 2002). Thus, WW layer nutrient concentrations can be considered the starting values before the subsequent spring and summer primary production and nutrient uptake occur, and vertically integrated reductions in nutrient concentrations below those in the underlying remnant WW layer indicate the magnitudes of the nutrient deficits produced during the growing season.

This method of calculating nutrient deficits assumes that the changes of nutrient concentrations within the WW layer from spring to autumn were negligible. Possible causes, if any, for such changes would be photosynthesis and/or remineralization of organic matter within the WW layer, vertical and lateral mixing, and dilution by ice meltwater. Mixing and dilution by ice-melt can affect the overlying mixed layer as well. There are few data on biological activity (photosynthesis, remineralization) in the WW layer, but it was not considered to be important because of a comparison between the properties of the WW layer in autumn 2001 with the same properties of the WW layer earlier in the year. Long Term Ecological Research (LTER) data in the SO GLOBEC region showed that salinities (34.0±0.1), nitrate concentrations (31.6±0.8 μM), and phosphate concentrations (2.08±0.04 μM) in the WW layer in January 2001 (Vernet, 2001), when it had temperatures of −1.6 °C±0.2 °C (Martinson, 2001), were not statistically different from those observed in this layer in the following autumn 3 months later, during SO GLOBEC I (Table 2). This suggests that the remnant WW layer present in the autumn had not undergone any significant changes in its salinity or other chemical properties during the growing season. The remnant WW layer in autumn 2002 (SO GLOBEC III) was assumed to have been similarly unchanged during the 2002 growing season.

The temperature of the remnant WW layer was −0.9 °C±0.5 °C during autumn 2001 (SO GLOBEC I) and autumn 2002 (SO GLOBEC III). The fact that this temperature range is larger and slightly more positive than the "typical" WW temperature range of −1.0 °C to −1.8 °C (Hofmann et al., 1996) suggests that the layer may have been eroded by mixing with warmer deep water from below and/or warmer near-surface waters from above before the two autumn SO GLOBEC cruises. Since nutrient concentrations increase with

Table 2
The remnant Winter Water (WW) layer properties in the SO GLOBEC region including the average depth of the layer, the range in silica concentration and average salinity, phosphate, and total inorganic nitrogen (TIN = $[NO_3]+[NO_2]+[NH_4]$) observed in the layer

Year	WW layer depth (m)	Salinity	Silica range (μM)	Phosphate (μM)	TIN (μM)
2001	100±40	34.0±0.1	55.5–95.2	2.16±0.04	31.1±0.8
2002	85±50	33.9±0.3	60.0–96.0	2.18±0.6	30.8±1.0

depth, mixing with waters from below the WW layer would tend to increase the nutrient concentrations within the layer, while mixing with the waters from above would tend to decrease them. However, the potential impact on nutrient concentrations in either the WW or the overlying mixed layer is difficult to ascertain. The overall net effect, if any, of this vertical mixing of nutrients from below the WW layer into the surface mixed layer would probably be to cause our nutrient deficit estimates to be too low, i.e., minima. At this point, we cannot predict the error in those estimates that might result, but, because of the above-mentioned agreement between LTER WW layer data and our WW layer data (Table 2), we assume it to be slight. Inshore areas of the WAP continental shelf are more productive and therefore more nutrient depleted than offshore areas (Moline and Prézelin, 1996; Smith et al., 1998; Prézelin et al., 2000; Garibotti et al., 2003). Lateral transport of offshore waters inshore also might be expected to lead to an underestimation of the actual inshore nutrient deficits. It will be shown later that nutrient deficit isopleths were nearly parallel to the coast. Thus, alongshore lateral transport should have led to negligible changes in nutrient deficits as it would have brought in waters with approximately the same nutrient deficit values.

The evidence that we could find does not indicate that the nutrient deficit calculations (and resulting NCP estimates) were significantly affected by mixing or variations in WW nutrient concentrations during the WAP growing season. The impact of dilution of mixed-layer nutrient concentrations by meltwater was also minimal. When those nutrient concentrations were scaled to a constant salinity of 34.0, nutrient deficits changed by about 2%.

Estimates of nutrient deficits (and the resulting NCP values) for the winter surveys were not possible because WW and its nutrient signatures from the preceding winter could not be identified.

3.5. Nutrient deficit relationships

Nutrient deficit calculations were made for TIN ($TIN = [NO_3^-] + [NO_2^-] + [NH_4^+]$), silica ($SiO_2$), and phosphate ($PO_4$) at all autumn stations in 2001 and 2002. Regressions between deficits showed linearity for both autumns, especially between the TIN and PO_4 regressions ($r^2 > 0.9$, Fig. 9A). Net consumptions of TIN and PO_4 are *well* correlated. Averages of the ratios of the individual TIN deficits to the corresponding PO_4 deficits provide measures of the net N:P incorporation ratios, which can be compared to the classical Redfield $\Delta N/\Delta P$ ratio of 16. Those averages (12.4 ± 1.6 for

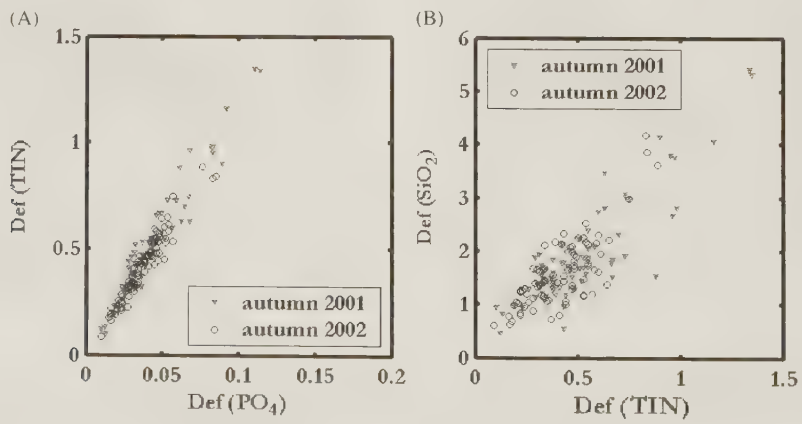

Fig. 9. (A) The relationships between deficits of TIN and phosphate for autumn 2001 and autumn 2002. For autumn 2001, $r^2 = 0.94$, $n = 65$, Def (TIN) = 11.6 (± 0.8)* Def (PO_4) + 0.03 (± 0.04). For autumn 2002, $r^2 = 0.92$, $n = 88$, Def (TIN) = 10.8 (± 0.7)* Def (PO_4) + 0.01(± 0.02). (B) The relationships between silica and TIN deficits for the autumn of 2001 and autumn of 2002. For autumn 2001, $r^2 = 0.76$, $n = 65$, Def (SiO_2) = 3.3 (± 0.5)* Def (TIN) + 0.2 (± 0.3). For autumn 2002, $r^2 = 0.62$, $n = 88$, Def (SiO_2) = 3.3 (± 0.6)* Def (TIN) + 0.2 (± 0.2). All units are in mol m^{-2}.

autumn 2001 and 11.1±1.3 for autumn 2002) are lower than Redfield, and a potential reason was provided by Sweeney et al. (2000a), who reported ΔN/ΔP utilization ratios of 10.0±0.7 for diatoms in the Ross Sea. The similarity between the Sweeney et al. (2000a) ratios and those of the autumn SO GLOBEC surveys suggests a dominance of diatoms in the MB region preceding the autumn surveys. To investigate this possibility further, we examined the relationships between silica and TIN deficits for both autumns (Fig. 9B). The two parameters increase together, although with more variability in the form of scatter than the correlation between TIN and PO_4 deficits showed. Values of r^2 for Fig. 9B varied from 0.6 to 0.8, indicating a reasonable degree of correlation. Averages of individual ratios of SiO_2 deficit to TIN deficit were 3.9±1.2 for autumn 2001 and 4.1±1.1 for autumn 2002. Assuming NCP: $\Delta N = 7\,mol\,mol^{-1}$ (Rubin et al., 1998), these averages convert to 0.56±0.18 and 0.59±0.16 $mol\,mol^{-1}$, respectively, and reflect the average net incorporation ratios of silica to carbon in the WAP plankton during the two growing seasons. These ratios are consistent with the high values measured in the Pacific sector of the Southern Ocean, where Def(SiO_2):NCP is 0.66±0.2 (Rubin et al., 1998), and high values in this ratio are indicators of diatom domination according to Sweeney et al. (2000a). A possible contributing factor to high $\Delta SiO_2/\Delta N$ ratios is that soft-tissue nitrogen is more labile than frustule silica (DeMaster et al., 1996). Soft-tissue remineralization within the surface mixed layer, coupled with export of silica frustules from the mixed layer, could thus help to cause an increase in the net $\Delta SiO_2/\Delta N$ ratios (Ishii et al., 2002).

3.6. Nutrient deficit distributions

In autumn 2001 (SO GLOBEC I), the TIN and silica deficits exhibited strong offshore/inshore trends. The lowest values (<0.2 and $<1.5\,mol\,m^{-2}$, respectively) were near the shelf break, and the largest values (>1 and $>3.5\,mol\,m^{-2}$, respectively) were found inside MB and between Alexander and Charcot Islands (see Fig. 10A for the TIN deficit distribution and Fig. 10B for the silica deficit distribution). The highest phosphate deficit was $0.12\,mol\,m^{-2}$ (Table 3).

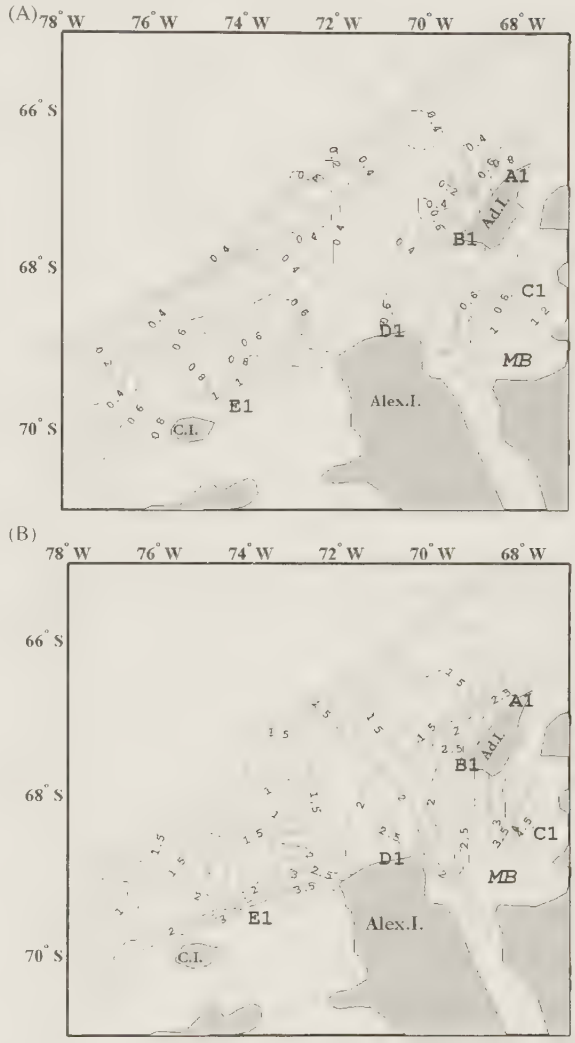

Fig. 10. (A) Distribution of the TIN deficit, mol m $^{-2}$, and (B) silica deficit, $mol\,m^{-2}$, in autumn 2001. Regions of high TIN and silica deficits are indicated by letters A1–E1. Station locations are indicated by dots. Bathymetry contours are 500, 1000, 1500, and 2000 m, with the contour in MB being 500 m.

An interesting pattern of along-shore variability in the distribution of the nutrient deficits in the autumn of 2001 also was found. Five regions of high nutrient deficit values were identified (A1–E1 in Fig. 10A, B): A1 and B1 were located along the Adelaide Island coast; the largest one, C1, was

Table 3
Averages and ranges for the deficits of TIN, phosphate, silica and NCP estimates integrated to the depths of the remnant WW layer for autumn 2001 and 2002

	Autumn 2001	Autumn 2002	Ross Sea (autumn)
TIN	0.54±0. 26	0.41±0.30	0.46±0.17
TIN range	0.1–1.37	0.09–0.91	—
Phosphate	0.04±0.02	0.04±0.02	0.02±0.01
Phosphate range	0.01–0.12	0.01–0.09	—
Silica	2.0±1.0	1.6±1.3	0.49±0.22
Silica range	0.5–5.5	0.6–4.2	—
NCP	3.8±1.9	2.8±2.3	3.9±0.9
NCP range	0.7–9.6	0.6–6.3	—

Uncertainties represent the standard deviation for all stations occupied on each survey. Nutrient deficits and NCP values from the autumnal 1997 JGOFS survey in the Ross Sea, which are reported in Sweeney et al. (2000b), are given for a reference. All units are in mol m^{-2}.

inside MB; and D1 and E1 were found near Alexander and Charcot Islands south of MB.

The actual number of high nutrient deficit regions may have been less than five. The ADCP-derived currents and drifter measurements from SO GLOBEC I revealed a pronounced coastal current (10–25 cm s^{-1}) moving southward along Adelaide Island and into MB. It then flowed clockwise around the bay near the coast and continued southward along Alexander and Charcot Islands (Klinck et al., 2004; Beardsley et al., 2004). Interestingly, the high nutrient deficit regions (see A1–E1 in Fig. 10A, B) lay along the path of this current. Since we sampled each east–west grid line in Fig. 1 beginning at #1 and moving south to #13 we may have actually resampled one or more of these regions as they moved with the coastal current. For example, during the time that the research vessel moved along the sampling grid transects 8–10 (Fig. 1), a high nutrient deficit region could have drifted with the current from position D1 to position E1. From the elapsed time between samplings and the distance along the most likely path of the coastal current between the positions of D1 and E1, the estimate of the travel speed of that region would have been 16 cm s^{-1}. Since that estimate approximates the surface current (10–25 cm s^{-1}) obtained from the ship ADCP (Klinck et al., 2004), then we most likely sampled the same region twice and probably no more than four high nutrient deficit regions of TIN or silica existed along the coast in autumn 2001.

In the autumn of 2002 (SO GLOBEC III), the distribution of the deficits was somewhat different from those in autumn 2001 (Fig. 11A, B). Although the averages and ranges in the deficits were not significantly different between the two autumns (Table 3), the trends in the horizontal distribution of the TIN and silica deficits were not strong, and the highest TIN deficit (>0.6 mol m^{-2}) and silica deficit (>2.5 mol m^{-2}) were found in a narrow region between the southern tip of Adelaide Island and the central part of MB (Fig. 11A, B). The highest phosphate deficit was 0.09 mol m^{-2} (Table 3).

3.7. Ammonium stocks

As mentioned, a complete picture of the total ammonium in the system is best achieved by calculating standing ammonium stocks. The procedure was to integrate the ammonium concentration profile at each hydrostation from the surface down to the depth of zero ammonium concentration (approximately 100 m).

The usefulness of this approach can be illustrated by an example from the Ross Sea Joint Global Ocean Flux Study (JGOFS) Antarctic Environment and Southern Ocean Process Study (AESOPS) summer and autumnal data. Although the highest AESOPS ammonium concentrations

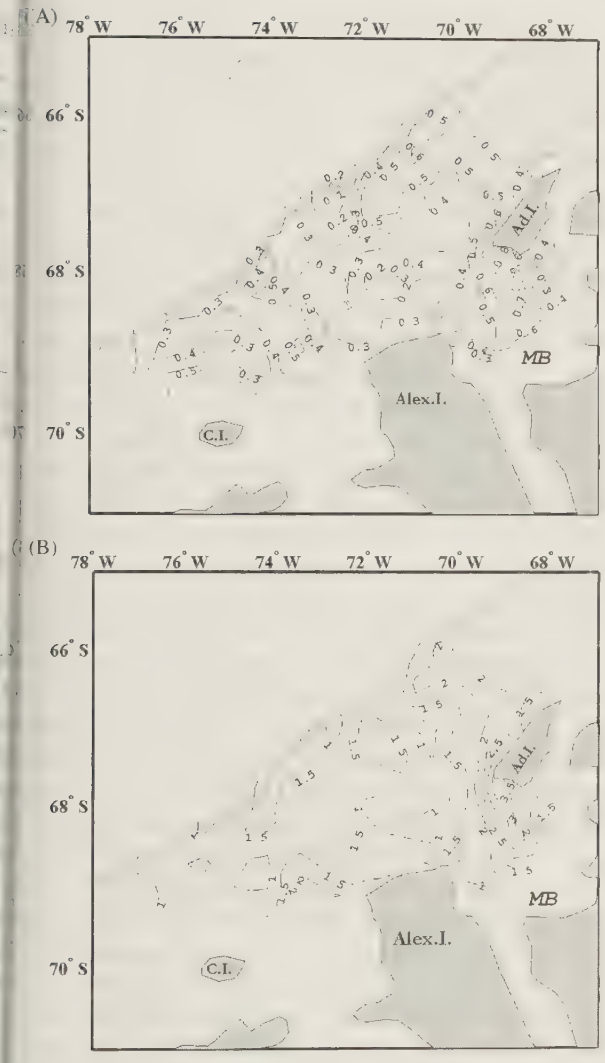

Fig. 11. (A) Distribution of the TIN deficit, mol m^{-2}, and (B) silica deficit, mol m^{-2}, in autumn 2002. Station locations are indicated by dots. Bathymetry contours are 500, 1000, 1500, and 2000 m, with the contour in MB being 500 m.

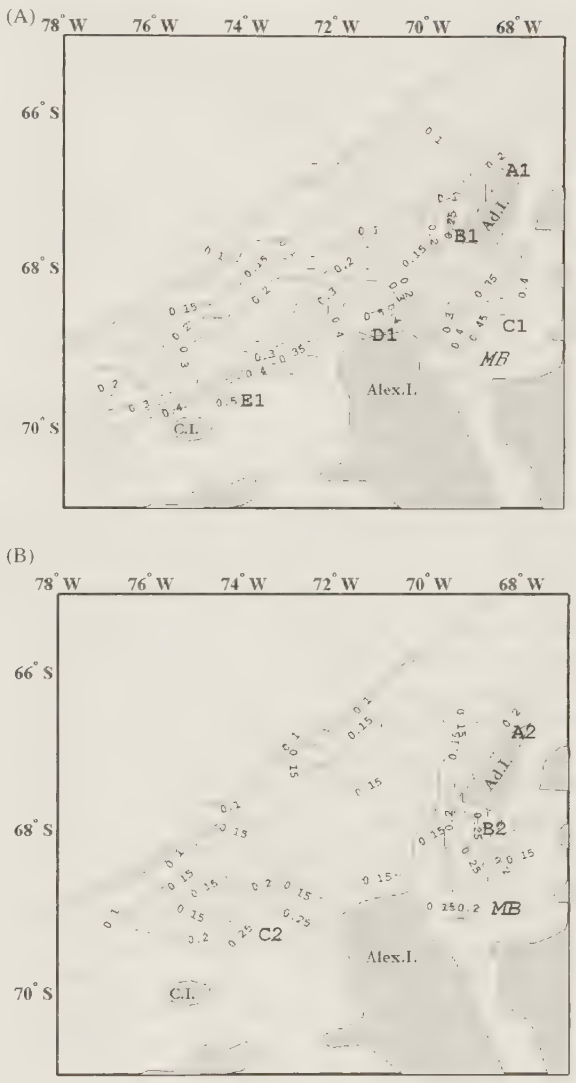

Fig. 12. Distribution of the ammonium stocks, mol m^{-2}, in (A) autumn 2001 and (B) autumn 2002. Regions of high ammonium stocks are indicated by letters A1–E1 for autumn 2001 and A2–C2 for autumn 2002. Station locations are indicated by dots. Bathymetry contours are 500, 1000, 1500, and 2000 m, with the contour in MB being 500 m.

were lower in autumn (2.5 μM) than in summer (4 μM), the dispersion of ammonium in the surface-mxed layer in autumn caused standing stocks to be higher in autumn (~0.6 mol m^{-2}) than in summer (~0.3 mol m^{-2}) (Codispoti, 1997). A focus on ammonium concentration exclusively can be misleading.

During SO GLOBEC I (autumn 2001), the highest ammonium stocks, >0.45 mol m^{-2}, were found inside MB and near Alexander and Charcot Islands. The lowest stocks (<0.1 mol m^{-2}) covered the northern and central part of the study region (Fig. 12A). The high ammonium standing stocks found in MB region are comparable to ammonium stocks of ~0.6 mol m^{-2} calculated for the autumnal Ross Sea JGOFS (AESOPS) data (Codispoti,

1997). Interestingly, the locations of the regions of high ammonium stocks (A1–E1 in Fig. 12A) coincided with the locations of the regions of high nutrient deficit (A1–E1 in Fig. 10A, B) observed during SO GLOBEC I.

Lower ammonium stocks were observed on subsequent SO GLOBEC surveys. Although the SO GLOBEC II (winter 2001) data are not shown, MB remained the region of the highest ammonium stocks, 0.18 mol m^{-2}, consistent with the horizontal distributions in the autumn 2001. However, these ammonium stocks were essentially only 35% of the autumn 2001 values. The lowest ammonium stocks, 0 01–0.02 mol m^{-2}, were found in the western and northeastern parts of the grid.

Overall, the ammonium stocks observed during SO GLOBEC III (autumn 2002) were comparable with those found on SO GLOBEC II (winter 2001), but were significantly lower than those in the previous autumn. There were three regions of high ammonium stocks (>0.2 mol m^{-2}, A2–C2 in Fig. 12B), but only two were matched by high nutrient deficit regions. The region designated by B2, located within MB (Fig. 12B), was matched by peaks of the highest TIN and silica deficits (Fig. 11A, B). The region designated as C2, located between Alexander and Charcot Islands (Fig. 12B), was matched only by a high silica deficit region (Fig. 11B). The lowest stocks, <0.1 mol m^{-2}, were found beyond the shelf break (Fig. 12B). During SO GLOBEC IV (winter 2002), ammonium stocks were slightly lower than those found at the same locations in the previous winter (not shown).

4. Discussion

4.1. General deep water summary—nutrients and CDW intrusions

Both analyses of nutrient water mass structure (Fig. 2) and vertical nutrient distribution (Figs. 3–8) lead to the same conclusions about the chemical effects of CDW intrusions onto the WAP continental shelf. UCDW and MUCDW (which is the WAP shelf water) have essentially the same range of nitrate concentrations- –33–36 μM (Fig. 2A). Vertical sections of nitrate (Figs. 3, 5, 7A–C, 8A–C) show that the nitrate isopleths are virtually horizontal as they extend from offshore onto the shelf. Thus, the flow of UCDW onto the WAP continental shelf does not result in nitrate (and therefore phosphate) enrichment of MUCDW.

The silica versus temperature diagram (Fig. 2A) indicates that UCDW possesses silica concentrations that are too low to enrich MUCDW. In addition, several patches of low-silica UCDW, like one shown on Fig. 6C, were found far inshore from the shelf break. These features suggest that the UCDW intrusions would more likely lead to dilution of the shelf-water silica inventory.

This finding poses the question: what processes produce the silica enrichment of WAP continental shelf waters? One possible pathway is through a LCDW contribution to the shelf water formation (Klinck et al., 2004). Indeed, the characteristic LCDW salinity of >34.73 and nitrate minimum (<33 μM) were detected on the shelf near the shelf break at depths of approximately 500 m along transects 2 (Fig. 3) and 7 (Fig. 5) and the Marguerite Trough section (Fig. 8A–C). Beyond the shelf break, such salinity and nitrate were found only below 600 m. The silica concentrations (105–110 μM) corresponding to the LCDW salinity maximum and nitrate minimum were also found at those depths (Figs. 4, 6, 8D–F). The vertical distribution of the silica isopleths suggests the upwelling of LCDW onto the shelf bottom. The pathways by which this water might get onto the shelf are likely to be associated with the ACC meanders at the shelf (Klinck et al., 2004).

However, the LCDW contribution does not account for the highest near-bottom silica concentrations (>115 μM) found in the inner parts of the shelf, along the Marguerite Trough (Fig. 8D–F) and in MB bottom water (Fig. 2A). The salinities of near-bottom waters of the Marguerite Trough were 34.7–34.725. Such salinities and silica concentrations (115–125 μM) are found only below 1500 m beyond the shelf break. An upwelling of water from such great depth onto the shelf is unlikely. The salinities of MB bottom Water (MBW) were less than 34.7, which is below the LCDW salinity range (34.7–34.74). This fact argues against any possibility of offshore

origin of the MBW high silica concentrations (110–125 μM).

Another possible source of silica is the regeneration of biogenic silica deposits (DeMaster et al., 1996; Ragueneau et al., 2000). Although, to our knowledge, no studies on the WAP have considered the composition of the sediments, the bottom accumulation of opal might be expected given the dominance of diatoms in the phytoplankton communities (Moline et al., 1996; Prézelin et al., 2000; Garibotti et al., 2003) and the high rates of the downward export fluxes from the mixed layer on the WAP continental shelf (Karl et al., 1996).

To sum up then, the nutrient data presented here do not make a strong case for fluxes from offshore enriching the nutrients on the WAP continental shelf. No evidence was found for offshore-to-onshore nitrate injection in intruding LCDW at least for the times of our surveys. Since phosphate follows nitrate, we would not anticipate much phosphate injection either. The only effect for silica due to UCDW seems to be a dilution of silica already on the WAP shelf. Some silica might reach the shelf if an upwelling mechanism for LCDW can be established, but the highest near-bottom silica concentrations in the MB or Marguerite Trough seem to be generated locally.

4.2. Net community production in the autumns of 2001 and 2002

From the calculated nutrient deficits for the autumns of 2001 and 2002, we can estimate NCP. There are some important considerations. First, as mentioned, we assumed that the changes in the nutrient content in the surface layer above the remnant WW layer between early spring and autumn in both years were largely the results of biological activity, not physical mixing. Second, NCP values are commonly presented as carbon deficits. Thus, we needed to convert the nutrient deficits by employing a stoichiometric carbon-to-nutrient ratio. The C/P and C/Si ratios have been shown to exhibit a considerable variability depending on the dominant phytoplankton group in the Southern Ocean (Bates et al., 1998; Rubin et al., 1998; Sweeney et al., 2000a). The C/N ratio has been found not to vary significantly and thus seems to be an appropriate ratio to use (Bates et al., 1998; Rubin et al., 1998; Sweeney et al., 2000a). We used a stoichiometric C/N ratio of 7 observed in the Pacific sector of the Southern Ocean to convert TIN deficits to carbon deficits (Rubin et al., 1998).

The NCP values calculated as described above ranged from 0.7 to 9.6 mol m^{-2} in the autumn of 2001 (Table 3). Based on the distribution of TIN deficits shown in Fig. 10A, in the autumn of 2001 the highest NCP values (>4.2 mol m^{-2}) should have been nearshore and located in one or more of five areas, A1–E1. The lowest NCP values (<2 mol m^{-2}) should have been beyond the shelf break. This finding is consistent with the results of the summer studies on the WAP shelf that found primary production to be the highest in the inshore areas (Moline and Prézelin, 1996; Smith et al., 1998; Garibotti et al., 2003).

A combination of several factors supports high production in the nearshore areas. Nearshore phytoplankton are less likely to be carried to depth out of the euphotic zone because of greater stability of the upper water column nearshore. Melt water from sea and glacial ice enhances the seasonal pycnocline at the base of the mixed layer, and protection from winds and storms by the continental land mass slows vertical mixing (Moline and Prézelin, 1996; Smith et al., 1998).

In 2002, the picture was different. The average nutrient deficits and NCP values (2.8 ± 2.3 mol m^{-2}) in the autumn of 2002 were about the same as in the autumn of 2001 (3.7 ± 1.9 mol m^{-2}); however, both the high-end and low-end values in autumn 2002 were lower than those in autumn 2001 (Table 3). The most pronounced decrease in NCP between the 2 years occurred in the inner part of MB and along the coasts of Alexander and Charcot Islands since NCP is calculated from TIN deficits, e.g., compare TIN deficit distributions in Figs. 10A and 11A.

The distribution of the highest TIN deficits went from five areas in 2001 (A1–E1 in Fig. 10A) to essentially only one area near the southern tip of Adelaide Island in 2002 (Fig. 11A). In both years, the highest NCP values had to follow the maximal TIN deficit distributions because of the method of NCP calculation. However, silica deficits are

independent of TIN deficits, and since the nutrient concentrations and ratios point toward a diatom-dominated phytoplankton population, we might expect that the silica deficit distributions in 2001 and 2002 would follow those of the TIN deficits. Figs. 10B and 11B show that silica deficits in 2001 and 2002 followed TIN deficits very well, leading to a consistent picture of the changes in nutrients and NCP between 2001 and 2002.

A possible explanation for the decrease in nutrient drawdown values, and therefore in NCP values, in 2002 versus 2001 is the difference in environmental conditions, in particular, sea-ice cover. In 2001, the MB region was practically ice free by mid-summer, while in 2002 MB and the southeastern part of the study region were partly ice-covered through summer into autumn. The ice-cover most likely restricted light availability for the water-column phytoplankton and thus, prevented high phytoplankton bloom development in the inner part of MB and between Charcot and Alexander Islands. Those were the areas where the highest nutrient deficits were found in autumn 2001 (Fig. 10A, B). The decrease in the summer-time phytoplankton biomass would have resulted in the lower nutrient deficits observed in those areas in the autumn of 2002 (Fig. 11A, B). An influence of sea-ice dynamics on phytoplankton biomass variability has been found in the previous observations on the WAP (Smith et al., 1998).

The NCP values we estimated cannot be easily compared to the primary production rates observed in the MB region in summer. Measured primary production rates reflect principally autotrophic production at a fixed point in time, whereas, our autumnal NCP estimates represent the net production of the entire community over the period of time from the end of winter to autumn. Respiration should have had a stronger effect in this period than during fixed times of sampling in the summer. To our knowledge, no previous estimates of NCP exist for the MB region.

However, we can compare our estimates of NCP (and nutrient deficits) to values obtained in the oligotrophic Pacific sector of the Southern Ocean (Rubin et al., 1998) and the highly productive Ross Sea (Sweeney et al., 2000a,b). Although Sweeney et al. (2000a,b) used different approaches to calculate nutrient deficits (differences between profiles integrated to a depth not necessarily related to the presence of WW) and NCP values (depth-integrated CO_2 drawdown), their results could be compared to ours, *especially* for the autumn. Averaged SO GLOBEC TIN deficits and NCP estimates for the autumns of 2001 and 2002 were similar to those of Sweeney et al. (2000b) for the Ross Sea in the autumn of 1997 (Table 3). However, the Marguerite Bay region is very heterogeneous. TIN deficits $<0.3\,mol\,m^{-2}$ and NCP estimates $<2\,mol\,m^{-2}$ observed beyond the shelf break in the region were rather similar to the NCP values in low-productivity High Nutrient Low Chlorophyll waters of the southern Pacific ($0.8–2.8\,mol\,m^{-2}$; Rubin et al., 1998). SO GLOBEC TIN deficits $>0.6\,mol\,m^{-2}$ and NCP estimates $>4.2\,mol\,m^{-2}$ found inshore were greater than the autumnal estimates from the Ross Sea and were closer to the summertime Ross Sea NCP estimates by Sweeney et al. (2000a): $4.4–10.8\,mol\,m^{-2}$. Silica deficits in the MB region in the autumns of 2001 and 2002 (2.0 ± 2.0 and $1.6\pm1.3\,mol\,m^{-2}$) showed a tendency to be larger than those from the Ross Sea in both summer and autumn (0.3 ± 0.29 and $0.49\pm0.22\,mol\,m^{-2}$; Sweeney et al., 2000b), supportive of the greater importance of diatoms and silica utilization in the MB region as outlined above.

4.3. Nutrient utilization ratios

Interestingly, despite high spatial variability in the magnitude of nutrient drawdown, the linear relationships between TIN, phosphate, and silica deficits (Fig. 9A, B) imply a rather uniform structure of phytoplankton communities in the entire study area. Diatoms appear to dominate.

Although there was a decrease in the nutrient drawdown in the autumn of 2002, the nutrient utilization ratios suggest a considerable similarity in phytoplankton community structure between 2 years. The averages of the Def (TIN):Def (PO_4) and Def (SiO_2):Def (TIN) ratios for autumn 2002 were not significantly different from those for autumn 2001 ($p=0.37$ and 0.8, respectively). The interannual variability in the magnitude of the

phytoplankton bloom (i.e. NCP) apparently had little impact on the composition of phytoplankton population.

During SO GLOBEC, the WAP continental shelf appeared to differ from other regions of the Southern Ocean, such as the Ross Sea, where distinct biogeochemical regions dominated by different phytoplankton groups (e.g., *Phaeocystis* spp.) can be distinguished based on the nutrient-deficit relationships (Arrigo et al., 1999; Sweeney et al., 2000a). Some local dominance of phytoplankton groups other than diatoms has been reported for the WAP shelf from summer-time studies (Prézelin et al., 2000; Garibotti et al., 2003). However, these reports are not supported by our observations. Non-diatomaceous phytoplankton groups seemed less important in nutrient utilization in the MB region.

4.4. Ammonium puzzles

The sources of high ammonium stocks found in the MB region and the dominant factors influencing ammonium distribution are not clearly established. Zooplankton biomass was low to moderate on the shelf and relatively high inside and along the coast south of MB (Ashjian et al., 2004). An offshore/inshore gradient in zooplankton biomass was evident (Lawson et al., 2004) and was similar to that of ammonium stocks. This apparent correlation between zooplankton biomass and ammonium stocks suggests that the accumulation of the ammonium pool could be due to ammonium excretion by zooplankton. When taking into account the maximal net zooplankton biomass of $130\,g\,m^{-2}$ that was observed in MB in autumn 2001 (Ashjian et al., 2004) integrated from the surface to the bottom (600 m), its contribution to the ammonium pool would be 5 mmol $(NH_4)\,m^{-2}\,d^{-1}$. This production rate was obtained by using the ammonium excretion rate for mixed zooplankton of $1.6\,\mu mol\ (NH_4)\,(g\ wet\ wt)^{-1}\,h^{-1}$, given by Biggs (1982). This production rate could produce the range of ammonium standing stocks in MB in autumn 2001 (Fig. 12A) in 60–100 days, which is not unreasonable.

However, the vertical distributions of ammonium and zooplankton did not correlate well. The highest ammonium concentrations were found in the mixed-layer (upper 30–70 m), while most of zooplankton biomass was found below the pycnocline (Ashjian et al., 2004). The vertical migration of zooplankton was not clearly evident; so we cannot be certain that they were responsible for the production of high ammonium stocks.

An alternative explanation of the high ammonium concentrations and stocks observed during the autumnal SO GLOBEC cruises is the activity of smaller plankton (excretion, sloppy feeding) and bacterial remineralization of particulate material in the preceding summers. Although heterotrophic pico-and-nanoplankton may be responsible for approximately 80% of ammonium stock production in other Antarctic waters (Koike et al., 1986; Goeyens et al., 1991; Semeneh et al., 1998), such data are not available for our field studies.

The locations of the regions of high nutrient deficits and high ammonium stocks were the same in autumn of 2001 (Figs. 12A and 10A, B). This suggests an extended role of summer biological activity into the fall. The higher the nutrient deficits were, the more organic matter should have accumulated. Greater abundances of organic matter in the inner shelf and MB at the end of summer could have led to a greater degree of ammonification in those areas, thus producing the observed ammonium maxima. The autumn of 2002 somewhat followed the trend: the location of the highest ammonium stocks (B2 in Fig. 12B) matched the location of the highest nutrient deficit peaks, but there were no other distinct peaks of nutrient deficits corresponding to the ammonium stocks peaks A2 and C2 (Figs. 12B and 11A, B).

Both physical and biochemical processes could have produced the winter decline in ammonium. High ammonium waters in the mixed layer near the coastline can be diluted by horizontal mixing with offshore low-ammonium waters and/or vertical mixing with deeper low-ammonium waters from below the mixed layer. Low irradiance levels in the wintertime could well have permitted nitrifying bacteria to oxidize the ammonium to nitrate since photoinhibition of their activity should have been reduced (Olson, 1981). However, despite this fact, nitrification rates measured in the

Antarctic coastal waters appear to be very low—less than a few nM d^{-1} (Olson et al., 1981; Priscu et al., 1990; Karl et al., 1996). Another possible sink for ammonium, uptake by phytoplankton, was small because primary production is negligible on WAP continental shelf in austral autumn and winter (Prézelin et al., 2004) Metabolic studies on biological ammonium consumption, principally by bacterial nitrification, in the region are needed to resolve this issue.

Overall, ammonium in the SO GLOBEC region has some interesting features. Its high mixed-layer concentrations fall within the range found in high-latitude oceans elsewhere. Yet the changes in ammonium concentration generally run opposite to those of other nutrients. Mixed-layer concentrations of other nutrients (nitrate, phosphate, and silica) are higher in winter than in autumn; whereas winter mixed-layer ammonium concentrations are much lower than in autumn. Further, at the end of the growing season, our autumnal data show that mixed-layer nutrient levels have declined, while mixed-layer ammonium levels have increased. Yet the maximum autumnal standing stocks of ammonium are found in the same mixed-layers as the maximum autumnal deficits of other nutrients. These features are found even when comparing ammonium (associated with tissues) to silica, which is associated with frustules.

5. Conclusions

In this study, conducted during a series of four surveys as a part of SO GLOBEC program in the region of MB on the WAP continental shelf in the austral autumns and winters of 2001 and 2002, we investigated chemical effects of the CDW intrusions onto the shelf, spatial and annual variability in the autumnal nutrient deficits, NCP, and ammonium stocks.

Horizontal intrusions of UCDW onto the WAP shelf do not result in any changes in MUCDW nitrate or phosphate concentrations but lead to a dilution of the MUCDW silica inventory. The highest silica concentrations observed in MUCDW most likely result from the dissolution of opal sediments.

Deficits of TIN (nitrate + nitrite + ammonium), phosphate, and silica were computed as vertically integrated depletions of these nutrients from surface down to the base of the WW layer, which retained its early spring chemical properties during the growing season. The average NCP values calculated from TIN deficits by employing $\Delta C/\Delta N$ ratio of 7 were 3.8 ± 1.9 and 2.8 ± 2.3 mol m^{-2} during the autumns of 2001 and 2002, respectively. These values were similar to those observed in the Ross Sea in autumn of 1997 (Sweeney et al., 2000b). The highest nutrient deficits and NCP values were found in the nearshore parts of the MB region. Despite the fact that the averages of the nutrient deficits and NCP values were not significantly different between 2001 and 2002, the inshore nutrient deficits and NCP values showed a considerable interannual variability that was most likely related to the differences in sea ice dynamics between the 2 years. Maxima in ammonium stocks tended to be co-located with the regions of the highest nutrient deficit, indicating spatial coupling between primary and heterotrophic production in both years.

Net nutrient utilization ratios showed a remarkable consistency between the 2 years. $\Delta N/\Delta P$ and $\Delta Si/\Delta N$ removal ratios were 12.4 ± 1.6 and 3.9 ± 1.2, respectively, in autumn 2001 and 11.1 ± 1.3 and 4.1 ± 1.1, respectively, in autumn 2002. These results suggest the dominance of diatoms in the study region. The relatively high $\Delta Si/\Delta N$ removal ratios observed also may be a result of preferential remineralization of nitrogen relative to silica in the surface layer during the growing season.

Acknowledgements

This study was supported by the US National Science Foundation, Office of Polar Programs, Award No. OPP 99-10100. We thank the nutrient team members, Robert Masserini, Howard Rutherford, Steve Bell, and Rebecca Conroy, for the highest-quality nutrient data set. We also thank L. Codispoti and Maria Vernet for providing nutrient data from JGOFS AESOPS study in the Ross Sea and Long Term Ecological Research (LTER) study on the WAP shelf.

References

Arrigo, K.R., Worthen, D.L., Robinson, D.H., Dunbar, R.B., DiTullio, G.R., VanWoert, M., Lizotte, M.P., 1999. Phytoplankton community structure and the drawdown of nutrients and CO_2 in the Southern Ocean. Science 283, 365–367.

Ashjian, C.J., Rosenwaks, G.A., Wiebe, P.H., Davis, C.S., Gallager, S.M., Copley, N.J., Lawson, G.L., Alatalo, P., 2004. Distribution of zooplankton on the continental shelf off Marguerite Bay, Antarctic Peninsula, during Austral Fall and Winter, 2001. Deep-Sea Research II, this issue [doi:10.1016/j.dsr2.2004.07.025].

Bates, N.R., Hansell, D.A., Carlson, C.A., 1998. Distribution of CO_2 species, estimates of net community production, and air–sea CO_2 exchange in the Ross Sea polynya. Journal of Geophysical Research 103, 2883–2896.

Beardsley, R.C., Limeburner, R., Owens, W.B., 2004. Drifter measurements of surface currents near Marguerite Bay on the western Antarctic Peninsula shelf during austral summer and fall, 2001 and 2002. Deep-Sea Research II, this issue [doi:10.1016/j.dsr2.2004.07.031].

Biggs, D.C., 1982. Zooplankton excretion and NH_4^+ cycling in near-shore waters of the Southern Ocean. I. Ross Sea, Austral Summer 1977–1978. Polar Biology 1, 55–67.

Codispoti, L., 1997. Temperature, salinity, nutrients from Niskin bottles for the AESOPS/NBP9703 Ross Sea cruise. US JGOFS data system, online, dataset, http://usjgofs.whoi.edu/jg/dir/jgofs/southern/.

Cota, G.F., Smith, W.O., Nelson, D.M., Muench, R.D., Gordon, L.I., 1992. Nutrient and biogenic particulate distributions, primary productivity and nitrogen uptake in the Weddell–Scotia Sea marginal ice zone during winter. Journal of Marine Research 50, 155–181.

DeMaster, D.J., Ragueneau, O., Nittrouer, C.A., 1996. Preservation efficiencies and accumulation rates for biogenic silica and organic C, N, and P in high-latitude sediments: The Ross Sea. Journal of Geophysical Research 101 (C8), 18501–18518.

Garibotti, I.A., Vernet, M., Ferrario, M.E., Smith, R.C., Ross, R.M., Quetin, L.B., 2003. Phytoplankton spatial distribution patterns along the western Antarctic Peninsula (Southern Ocean). Marine Ecology Progress Series 261, 21–39.

Goeyens, L., Treguer, P., Lancelot, C., Mathot, S., Becquevort, S., Morvan, J., Dehairs, F., Baeyens, W., 1991. Ammonium regeneration in the Scotia–Weddell Confluence area during spring 1988. Marine Ecology Progress Series 78, 241–252.

Gordon, L.I., Jennings Jr., J.C., Ross, A.A., Krest, J.M., 1993. A suggested protocol for continuous flow automated analysis of seawater nutrients, in WOCE Operation Manual, WHP Office Report 77 No. 68/91, pp. 1–52.

Gordon, L.I., Codispoti, L.A., Jennings Jr., J.C., Millero, F.J., Morrison, J.M., Sweeney, C., 2000. Seasonal evolution of hydrographic properties in the Ross Sea, Antarctica, 1996–1997. Deep-Sea Research II 47, 3095–3117.

Grasshoff, K., 1976. Methods of Seawater Analysis. Verlag Chemie, Weinhem, Germany and New York, NY, p. 317.

Hofmann, E.E., Klinck, J.M., Lascara, C.M., Smith, D.A., 1996. Water mass distribution and circulation west of the Antarctic Peninsula and including Bransfield Strait. In: Ross, R.M., Hofmann, E.E., Quetin, L.B. (Eds.), Foundation for Ecological Research West of the Antarctic Peninsula, Antarctic Research Series 70. American Geophysical Union, Washington, DC, pp. 61–80.

Ishii, M., Inoue, H.Y., Matsueda, H., 2002. Net community production in the marginal ice zone and its importance for the variability of the oceanic pCO_2 in the Southern Ocean south of Australia. Deep-Sea Research II 49, 1691–1706.

Jones, R.D., 1991. An improved fluorescence method for the determination of nanomolar concentrations of ammonium in natural waters. Limnology and Oceanography 36, 814–819.

Karl, D.M., Christian, J.R., Dore, J.E., Letelier, R.M., 1996. Microbiological oceanography in the region west of the Antarctic Peninsula: microbial dynamics, nitrogen cycle and carbon flux. In: Ross, R.M., Hofmann, E.E., Quetin, L.B. (Eds.), Foundation for Ecological Research west of the Antarctic Peninsula, Antarctic Research Series 70. American Geophysical Union, Washington, DC, pp. 303–332.

Klinck, J.M., Hofmann, E.E., Beardsley, R.C., Salihoglu, B., Howard, S., 2004. Water-mass properties and circulation on the west Antarctic Peninsula Continental Shelf in Austral Fall and Winter 2001. Deep-Sea Research II, this issue [doi:10.1016/j.dsr2.2004.08.001].

Koike, I., Holm-Hansen, O., Biggs, D.C., 1986. Inorganic nitrogen metabolism by Antarctic phytoplankton with special reference to ammonium recycling. Marine Ecology Progress Series 30, 105–116.

Lawson, G.L., Wiebe, P.H., Ashjian, C.J., Gallager, S.M., Davis, C.S., Warren, J.D., 2004. Acoustically-inferred zooplankton distribution in relation to hydrography west of the Antarctic Peninsula. Deep-Sea Reseach II, this issue [doi:10.1016/j.dsr2.2004.07.022].

Martinson, D.G., 2001. Temperature and salinity for the LTER LMG01-01 Annual Cruise. LTER data system, online, dataset, http://pal.lternet.edu/cgi-bin/ucmbo-cgi/studycatalog03.cgi.

Moline, M.A., Prézelin, B.B., 1996. Long-term monitoring and analyses of physical factors regulating variability in coastal Antarctic phytoplankton biomass, in situ productivity and taxonomic composition over subseasonal, seasonal and interannual time scales. Marine Ecology Progress Series 145, 143–160.

Nöthig, E.-M., Bathmann, U., Jennings Jr., J.C., Fahrbach, E., Gradinger, R., Gordon, L.I., Makarov, R., 1991. Regional relationships between biological and hydrographical properties in the Weddell Gyre in late austral winter 1989. Marine Chemistry 35, 325–336.

Olson, R., 1981. ^{15}N tracer studies of the primary nitrite maximum. Journal of Marine Research 39, 203–226.

Orsi, A.H., Whitworth III, T., Nowlin Jr., W.D., 1995. On the meridional extent of the Antarctic Circumpolar Current. Deep-Sea Research I 42 (5), 641–673.

Owens, N.J.P., Priddle, J., Whitehouse, M.J., 1991. Variations in phytoplanktonic nitrogen assimilation around South Georgia and the Bransfield Strait (Southern Ocean). Marine Chemistry 35, 287–304.

Prézelin, B.B., Hofmann, E.E., Mengelt, C., Klink, J.M., 2000. The linkage between Upper Circumpolar Deep Water (UCDW) and phytoplankton assemblages on the west Antarctic Peninsula continental shelf. Journal of Marine Research 58, 165–202.

Prézelin, B.B., Hofmann, E.E., Moline, M., Klinck, J.M., 2004. Physical forcing of phytoplankton community structure and primary production in continental shelf waters of the western Antarctic Peninsula. Journal of Marine Research 62, 419–460.

Priscu, J.C., Dowes, M.T., Priscu, L.R., Palmisano, A.C., Sullivan, C.W., 1990. Dynamics of ammonium oxidizer activity and nitrous oxide (N_2O) within and beneath Antarctic sea ice. Marine Ecology Progress Series 62, 37–46.

Quetin, L.B., Ross, R.M., 2003. Episodic recruitment in Antarctic krill *Euphausia superba* in the Palmer LTER study region. Marine Ecology Progress Series 259, 185–200.

Ragueneau, O., Treguer, P., Leynaert, A., Anderson, R.F., Brzezinski, M.A., DeMaster, D.J., Dugdale, R.C., Dymond, J., Fischer, G., Froncois, R., Heinze, C., Maier-Reimer, E., Martin-Jezequel, V., Nelson, D.M., Queguiner, B., 2000. A review of the Si cycle in the modern ocean: recent progress and missing gaps in the application of biogenic opal as a paleoproductivity proxy. Global and Planetary Change 26, 317–365.

Rubin, S.I., Takahashi, T., Chipman, D.W., Goddard, J.D., 1998. Primary productivity and nutrient utilization ratios in the Pacific sector of the Southern Ocean based on seasonal changes in seawater chemistry. Deep-Sea Research I 45, 1211–1234.

Semeneh, M., Dehairs, F., Elskens, M., Baumann, M.E.M., Kopczynska, E.E., Lancelot, C., Goeyens, L., 1998. Nitrogen uptake regime and phytoplankton community structure in the Atlantic and Indian sectors of the Southern Ocean. Journal of Marine Systems 17, 159–177.

Smith, R.C., Baker, K.S., Vernet, M., 1998. Seasonal and interannual variability of phytoplankton biomass west of the Antarctic Peninsula. Journal of Marine Systems 17, 229–243.

Smith, D.A., Hofmann, E.E., Klink, J.M., Lascara, C.M., 1999. Hydrography and circulation of the West Antarctic Peninsula Continental Shelf. Deep-Sea Research I 46, 925–949.

Sweeney, C., Hansell, D.A., Carlson, C.A., Codispoti, L.A., Gordon, L.I., Marra, J., Millero, F.J., Smith, W.O., Takahashi, T., 2000a. Biogeochemical regimes, net community production and carbon export in the Ross Sea, Antarctica. Deep-Sea Research II 47, 3369–3394.

Sweeney, C., Smith, W.O., Hales, B., Bidigare, R.R., Carlson, C.A., Codispoti, L.A., Gordon, L.I., Hansell, D.A., Millero, F.J., Park, M., Takahashi, T., 2000b. Nutrient and carbon removal ratios and fluxes in the Ross Sea, Antarctica. Deep-Sea Research II 47, 3395–3421.

Vernet, M., 2001. Nutrient data for the LTER LMG01-01 Annual Cruise. LTER data system, online, dataset, http://pal.lternet.edu/cgi-bin/ucmbo-cgi/studycatalog03.cgi.

Woodward, E.M.S., Rees, A.P., 2001. Nutrient distribution in an anticyclonic eddy in the northeast Atlantic Ocean, with reference to nanomolar ammonium concentrations. Deep-Sea Research II 48, 775–793.

ELSEVIER

Deep-Sea Research II 51 (2004) 2003–2022

DEEP-SEA RESEARCH
PART II

www.elsevier.com/locate/dsr2

A model study of circulation and cross-shelf exchange on the west Antarctic Peninsula continental shelf

Michael S. Dinniman*, John M. Klinck

Center for Coastal Physical Oceanography, Old Dominion University, Norfolk, VA 23529, USA

Accepted 10 July 2004

Abstract

Exchange of warm, nutrient-rich Circumpolar Deep Water (CDW) onto Antarctic continental shelves and coastal seas has important effects on physical and biological processes in these regions. The present study investigates the locations of this exchange and their dynamics in the west Antarctic Peninsula with a high-resolution three-dimensional numerical model. The model circulation is forced by daily wind stress along with heat and salt fluxes calculated by bulk formulae. All surface fluxes are modified by an imposed climatological ice cover.

The model circulation compares favorably to general schematics of the flow based on dynamic topography, water properties from recent hydrography, and ADCP measurements. The sea-surface temperature is similar to satellite estimates except that the model temperatures are slightly higher than observations in the summer and lower in the winter. The seasonal variation of the depth and temperature of the model mixed layer matches observations reasonably well. Sub-pycnocline temperature shows evidence of persistent intrusion of warm CDW onto the shelf, for example, at the shelf break offshore of Adelaide Island. There is a significant correlation between the curvature of the shelf break and the volume transport across the shelf break, indicating that circulation crosses the shelf break in places where the tendency of the flow to maintain a given direction would have it cross a strongly curved bathymetric contour. A momentum term balance shows that momentum advection helps to force flow across the shelf break in specific locations due to the curvature of the bathymetry. For the model to create a strong intrusion of CDW onto the shelf, it appears two mechanisms are necessary. First, CDW is driven onto the shelf at least partially due to momentum advection and the curvature of the shelf break. Then, the general shelf circulation pulls the CDW into the interior.
© 2004 Elsevier Ltd. All rights reserved.

1. Introduction

The Southern Ocean is a heterogeneous system composed of a variety of sub-regimes, each with its own characteristic physical, biological and chemical features (Tréguer and Jacques, 1992). For

*Corresponding author. Tel.: +1 757 683 5559; fax: +1 757 683 5550.
E-mail address: msd@ccpo.odu.edu (M.S. Dinniman).

0967-0645/$ - see front matter © 2004 Elsevier Ltd. All rights reserved.
doi:10.1016/j.dsr2.2004.07.030

example, the West Antarctic Peninsula (WAP) region is thought to have little or no bottom water formation, large populations of Antarctic krill (*Euphausia superba*) and an active circulation including interactions with the southern boundary of the Antarctic Circumpolar Current (ACC) (Marr, 1962; Hofmann et al., 1996; Hofmann and Klinck, 1998a). In contrast, the Ross Sea produces bottom water (although the amount is uncertain), is the most biologically productive region of the Antarctic, and has generally sluggish sub-tidal circulation (Arrigo et al., 1998; Jacobs and Giulivi, 1998). In order to address fundamental questions on the controls of phytoplankton productivity and growth in these two systems, a suite of physical and biological models is being developed and used in both locations (Dinniman et al., 2003; Smith et al., 2003). Physical forcing, which includes advective circulation, vertical mixing, vertical stratification, and irradiance availability, may be the primary factor producing the observed vertical and horizontal variability in phytoplankton distribution and primary production in the WAP region. Oceanic Circumpolar Deep Water (CDW), a relatively warm, salty and nutrient-rich water mass that is part of the ACC, flows along the shelf break in the WAP region. This water occasionally intrudes onto the continental shelf (Hofmann and Klinck, 1998a) where it moderates the ice cover through heat flux, provides a relatively warm subsurface environment for some animals, and provides nutrients to stimulate primary production (e.g., Prézelin et al., 2000). CDW exchange is known to be episodic, but persistent, and is thought to occur at specific locations due to bottom topography. This study analyzes the exchange of CDW.

The WAP region has been studied intermittently for many years with an accumulated understanding of the physics, chemistry and biology in the area (cf. Ross et al., 1996; Hofmann et al., 2004). The area contains a relatively deep continental shelf (200–500 m) about 200 km wide with rugged bottom topography. The major circulation features in the WAP shelf area are the northeasterly flowing ACC close to the shelf break and a southward flowing coastal current (Hofmann et al., 1996; Klinck et al., 2004). The coastal current is thought to turn into and flow cyclonically around Marguerite Bay. ADCP measurements (S.L. Howard, personal communication) as well as satellite-tracked drifters (Beardsley et al., 2004) also show a current turning into Marguerite Bay just south of Adelaide Island and flowing clockwise around the Bay. Dynamic topography for the WAP shelf suggests that the circulation is largely cyclonic with perhaps one or more subgyres on the shelf (Stein, 1992; Smith et al., 1999; Klinck et al., 2004). The ADCP and drifter measurements also indicate locations where the flow is directed more across the shelf than along it, suggesting gyral circulation on the shelf.

Tidal flow on this shelf is rather weak (a few $cm\,s^{-1}$) based on limited observations and a local tidal model (Padman et al., 2002). Internal tides are thought to be important for straining sea ice (Howard et al., 2004). The continental shelf in this area is mostly ice free in summer and ice covered in winter, with the sea ice developing rapidly from May to July, reaching a peak in August, and declining slowly from September through January (Stammerjohn and Smith, 1996).

The water mass structure on the west Antarctic Peninsula shelf is described in detail in Smith et al. (1999). As a reminder, water structure from top to bottom is composed of Antarctic Surface Water (−1.8 to 1.0 °C, 33.0–33.7 psu), Winter Water (−1.5 °C, 33.8–34.0 psu), and CDW, which has several sub-types. There is no cold, salty, dense water on this shelf of the kind observed in the Weddell and Ross Seas.

Off of the shelf, CDW has two types associated with either a temperature maximum (Upper CDW) with relatively high temperatures (1.6–2.0 °C) or a salinity maximum (Lower CDW) of 34.73. UCDW occupies a depth range of 300–600 m and is relatively easily transported across the shelf break. LCDW occurs between 700 and 1000 m and is less frequently seen on the shelf. A modified (cooled) form of UCDW is seen on the west Peninsula shelf, with temperatures between 1.2 and 1.5 °C and only slightly reduced salinity.

For the purposes of this paper, the temperature of the water below the permanent pycnocline (below 200 m) is a good indicator of recent exchange of CDW across the shelf break. Water

above 1.5 °C is considered to be oceanic water that recently intruded onto the shelf. The rate of cooling of UCDW on the WAP shelf is not known, but measurements from successive cruises (Klinck, 1998) indicate that 2–3 months is enough to convert UCDW into modified CDW.

The goal of this study is to examine the exchange between the shelf and the open ocean as part of a larger effort to determine the effect of circulation and nutrient dynamics on phytoplankton growth on Antarctic continental shelves. A finite difference primitive equation model is used to simulate the circulation in the WAP region in order to analyze the cross-shelf-break exchange of UCDW. Several results from the model are compared to different observations to show the validity of the model for examining the cross-shelf-break physics. These results lead to a discussion of the cross-shelf-break heat, salt and volume transport.

2. Model configuration

The Rutgers/UCLA Regional Ocean Model System (ROMS) was used for this study. The model domain (Fig. 1) is located along the west side of the Antarctic Peninsula from about 70°S to just past the northern tip, covers the entire continental shelf and extends ≈ 500 km seaward of the shelf break. The eastern boundary of the model is a closed solid wall (no direct connection to the Weddell Sea) with a free-slip condition. All the other three boundaries are partially or completely open, depending on the coastline (Fig. 1). The horizontal grid spacing (5 km) was chosen to allow as much topographic detail as possible. A dynamic vertical mode calculation based on horizontally averaged density from measurements on this shelf results in a first internal radius of deformation of 4.7 (winter) to 5.3 km (fall). The model marginally resolves baroclinic eddies for this region. There are 24 vertical levels that are concentrated towards the top and bottom of the model domain. The gridded bathymetry used is derived from the Smith and Sandwell (1997) ETOPO2 global 2 min resolution bathymetry with modifications made around Marguerite Bay based on chart data (R.C. Beardsley, personal communication). The bathymetry is artificially "straightened" for the last few grid-points (isobaths set normal to the boundary) at every open-boundary to improve performance of open-boundary conditions. The bathymetry was somewhat smoothed with a modified Shapiro filter which has been designed to selectively smooth areas where the changes in bathymetry are large with respect to the total depth (Wilkin and Hedström, 1998). Therefore, much of the smoothing was on the shelf and there was less smoothing over the shelf break. The model setup is similar to that for the circulation model of the Ross Sea described in Dinniman et al. (2003) and several other details are described there.

Open boundaries use a two-dimensional radiation scheme combined with adaptive nudging (Marchesiello et al., 2001), except for the temperature and salinity. Several radiation schemes were tried for the tracers on the open boundaries, and all of them had problems where the shelf-break intersected the northern boundary. Instead, the temperature and salinity were relaxed to values from the World Ocean Atlas 98 (WOA98) climatology over the 10 grid points closest to the open boundary using the flow relaxation scheme of Martinsen and Engedahl (1987). The model setup at the boundaries for the velocities differed from that in Marchesiello et al. (2001) for their US West Coast experiment only in that no nudging is used for the baroclinic velocities and the component of the barotropic velocity parallel to the boundary, τ_{out} (the time scale for nudging for outgoing waves) is 4 years and τ_{in} (the time scale for nudging for incoming waves) is 4 years/30 (= 48.7 days). The barotropic velocities were relaxed to monthly values of depth-averaged circulation from the Parallel Ocean Circulation Model (POCM) global 0.25° resolution model (Semtner and Chervin, 1992).

The model is initialized with horizontally uniform temperature and salinity and a vertical structure obtained from the average of the WOA98 values in the model domain. In order to lessen the shock from the initial geostrophic adjustment, the horizontal variation is ramped in by running the model for five days with the

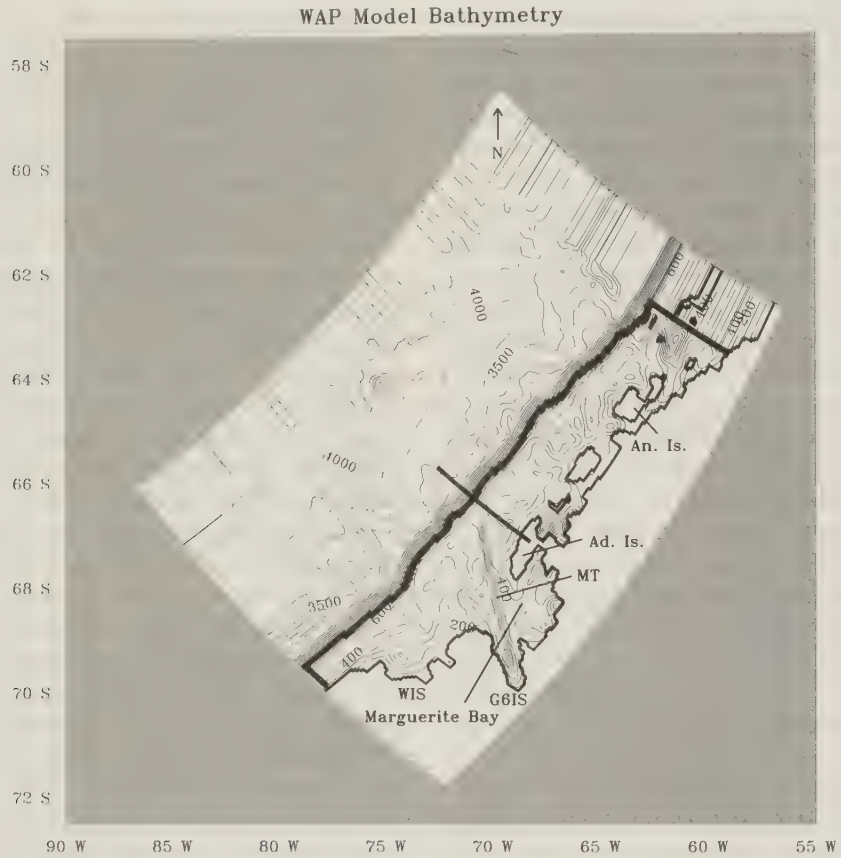

Fig. 1. Model domain and bathymetry. The contour interval for the bathymetry is 50 m up to 1000 m depth and 250 m below 1000 m. 'Ad. Is.' is Adelaide Island and 'An. Is.' is Anvers Island. The solid line from Adelaide Island across the shelf break represents the section covered in Fig. 9. The thick line around the shelf represents the enclosed shelf region discussed in Section 4.1. The line in Marguerite Bay labeled 'MT' shows the location of the Marguerite Trough. 'G6IS' shows the location of the George VI Ice Shelf and 'WIS' represents the Wilkins Ice Shelf.

stratification strongly relaxed to the gridded temperature and salinity climatology. The non-linear equation of state is used. Silicate, nitrate and chlorophyll are also simulated in the model as passive tracers but will not be discussed here.

Daily values of wind stress and wind speed were obtained from a blend of NSCAT and ERS-2 scatterometer data and NCEP analyses to give a repeatable annual cycle from August 1996 through July 1997 (Milliff et al., 1999). The wind stress is applied as a body force over the top three layers of the model. Instead of using a fully dynamic sea-ice model, ice concentrations from a climatology derived from the special sensor microwave imager (SSM/I) are imposed. The model surface heat flux is then calculated as a linear combination of heat flux due to ice cover and the open-water heat flux with the ratio determined by the ice concentration in that grid cell (Markus, 1999). The open-water heat flux was calculated with the COARE bulk flux algorithm (Fairall et al., 1996), with most of the necessary atmospheric data coming from monthly climatologies from either the NCEP reanalysis (air pressure, humidity and air temperature) or the ISCCP cloud climatology. Daily winds were used for the open-water heat flux calculation. The model surface freshwater flux (imposed as a salt flux) is also calculated as a linear combination of open-water evaporation minus precipitation and that due to ice melting or freezing (Markus,

1999). Precipitation was taken from the Xie and Arkin (1997) climatology. There is no relaxation term for the surface temperature or salinity except at the open boundaries. None of the cavities under ice shelves in the region (primarily the George VI and Wilkins Ice Shelves) are included.

ROMS has a terrain following vertical coordinate system, and these types of models have a well-known problem with their discrete approximation of horizontal pressure-gradient force (Haney, 1991; Mellor et al., 1994, 1998; Song, 1998; Shchepetkin and McWilliams, 2003). A large error was not expected here due to the relatively weak stratification in much of the model domain, and a simple experiment verified this. A simulation was run with the model initialized with a representative vertical temperature and salinity profile with no horizontal variability and all the surface fluxes and boundary relaxation terms set to zero. The resulting flow should be zero, so that any circulation is due, at least initially, to errors due to the vertical discretization (pressure gradient, non-uniform vertical mixing, etc.). As expected, the error flow is very small. After 5 days, the rms velocity for the entire model domain is $0.18\,cm\,s^{-1}$ (maximum: $2.5\,cm\,s^{-1}$) compared with $6.57\,cm\,s^{-1}$ (maximum: $66.9\,cm\,s^{-1}$) for the forced flow.

After the 5-day spin-up of the stratification, the model is initialized to start in late austral winter (September 15). Model simulations have been run successfully for slightly longer than two years and all results presented here will be from the second year unless explicitly stated otherwise.

3. Results

3.1. Circulation

The model circulation along the outer shelf must be representative of the observations if this model is to be used to study the interaction of the shelf and the open ocean. The circulation on the shelf in the west Antarctic Peninsula region is usually described in terms of the northeasterly flowing ACC along the shelf break and a southward flowing coastal current with perhaps some gyral circulation between the two. However, it has also been suggested that the shelf circulation is not coherent over large distances (Hofmann and Klinck, 1998a), but instead is composed of localized gyres with length scales that appear to be determined by the rugged bottom topography. In order to estimate the circulation below the surface, a map of ADCP measurements (see Howard et al., 2004, for details on the ADCP data) at 200 m was made (Fig. 2). The ADCP data come from seven cruises during austral fall and winter of 2001 and 2002 as part of the Southern Ocean Global Ecosystem Dynamics (SOGLOBEC) program (Table 1). All the available 1-h measurements at the appropriate depth bin from all seven cruises were simply averaged in 0.50° longitude by 0.20° latitude boxes (approximately 22 km on a side). This is obviously not a synoptic picture, but it can give an idea of the sub-surface circulation in this area. The flow along the shelf break is primarily, although not exclusively, to the northeast with large velocities that may indicate the ACC against the shelf break. There is a weak indication of a coastal current to the south along Adelaide Island, although it is much more visible at 50 m (not shown) implying that the coastal current is a surface feature. Beardsley et al. (2004) also suggest that the coastal current is at least "surface-intensified". There is a noticeable circulation turning into the north side of Marguerite Bay along the north side of Marguerite Trough (MT), flowing cyclonically around the depression in the mouth of the bay and back out on the south side of the Trough. There are also several other small-scale circulation features on the shelf. For example, note the cyclonic circulation around trenches that open up into the shelf break at 66.5° and 65.1°S with flow onto the shelf on the north side and off the shelf on the south.

A temporal average of the model circulation over mid-March–mid-September of year 2 (model days: 550–730, Fig. 3) shows the flow over the shelf to be similar to the estimated circulation. Much of the model flow is constrained to follow bottom topography. Point comparisons of flow vectors are problematic because the small scale and strongly topographically forced nature of the flow means than small errors in the modeled topography can lead to large differences in flow velocity at a

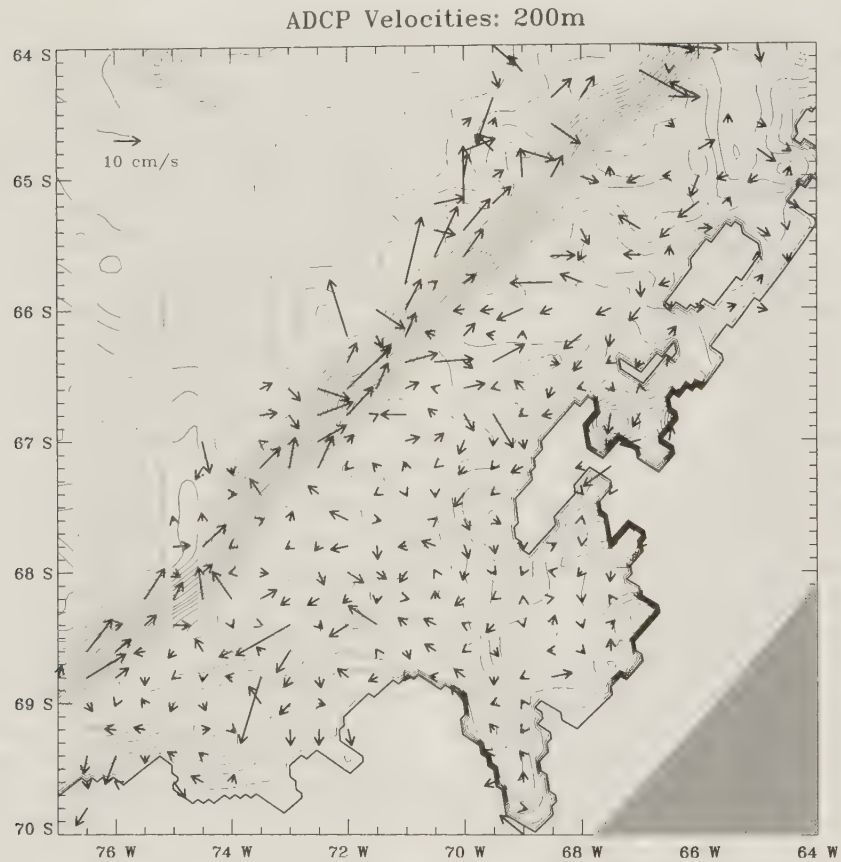

Fig. 2. ADCP measurements of velocity at 200 m along the WAP shelf from seven cruises during austral fall and winter (see text). The bathymetry is that used in the model and the contour interval is the same as for Fig. 1.

Table 1
S.O. GLOBEC cruises that produced ADCP data used here

Cruise	Date
NBP0103	Apr 23–June 6 2001
NBP0104	July 21–Sept 6 2001
LMG0103	Mar 18–Apr 13 2001
LMG0104	Apr 23–June 6 2001
LMG0106	July 21–Sept 6 2001
NBP0202	Apr 9–May 21 2002
NBP0204	July 31–Sept 18 2002

LMG—R/V Laurence M. Gould. NBP—R/V Nathaniel B. Palmer.

specific location. Also, the time scales of the measurements are quite different. With these in mind, the comparison to actual ADCP measurements is quite reasonable. There is a current to the northeast along the shelf break, although the velocities along the break itself are a little weak (compared to the ADCP data) with the model ACC core located off the shelf break. The model does not have an average southward coastal current along Adelaide Island, although (not shown) one does show up from time to time depending on the local winds. A possible reason for this could be that the model does not have accurate fresh water processes at the coastal boundaries, and it is known that this can be very important dynamically at high latitudes (Royer, 1998; Bacon et al., 2002). Large quantities of fresh water enter the system from the melting of glaciers and ice sheets in the area. For example, the net freshwater flux from basal melting of the George VI Ice Shelf into the sound directly beneath it has

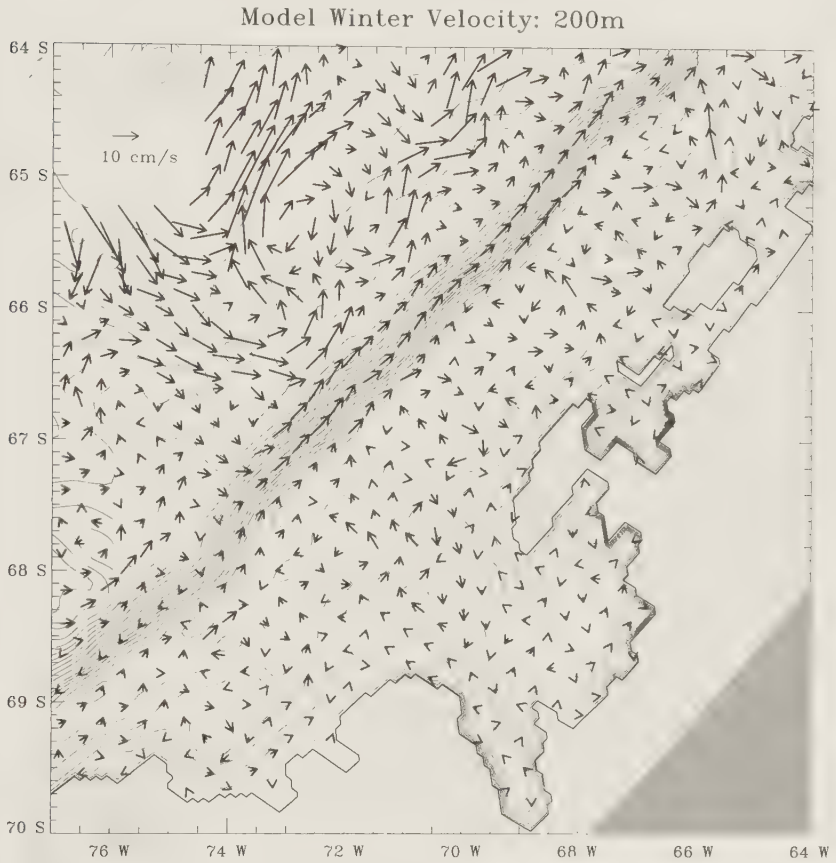

Fig. 3. Total flow at 200 m averaged over model day 550–730 (mid-March–mid-September of year 2). The contour interval for the bathymetry is the same as for Fig. 1. Every fourth model vector is plotted.

been estimated to be 2.1 m year^{-1} (Potter and Paren, 1985). The coastal current in the model should be significantly improved by having more realistic fresh water sources near the coast, especially freshwater melt from ice shelves and we plan to add this in the future.

The model does have a current turning into the north side of Marguerite Bay along the north side of the trench, flowing cyclonically around the depression in the mouth of the bay and back out on the south side of the bay very similar to that in the observations. It appears that in both the model and the observations much of the water flowing into the north side of Marguerite Bay comes from the north side of the MT at 66.5°S. The flow into and around the trenches that cut into the shelf at 66.5° and 65.1°S is also very similar to the ADCP data. It is this cross-shelf circulation near the shelf break that will be important for CDW intrusions.

In order to make a more quantitative comparison between the ADCP observations and the model output, the model velocities were horizontally averaged into the same boxes as the measurements and then compared in any box where there were observations. The comparison was done at 200 m to remain below the layer directly forced by the wind, thus avoiding oscillations in the measured velocity due to wind variability. Although the ADCP measurements were taken over several months, most of the horizontal boxes only have measurements from one or two individual cruises. Therefore, it is more appropriate to use snapshots of the model velocity for the comparison instead of using a temporal

average even though no individual snapshot will be representative of the time period over which the observations were gathered. The mean ADCP velocity at the comparison points at 200 m was 7.3 cm s^{-1}. A comparison was made using snapshots every 10 days over mid-March–mid-September of year 2 (model days: 550–730). The average model velocity magnitude at the same points was a little less than observations (6.4 cm s^{-1}) with an average difference between the two of 0.9 cm s^{-1} and an average rms error of 6.8 cm s^{-1}.

The intrusion of CDW onto the west Antarctic Peninsula continental shelf has been consistently observed to occur at specific locations over the years. For example, the maximum temperature (below the surface layer) observed over the shelf for the period Apr 23–June 6, 2001 (Fig. 4) show a strong plume of intruding warm CDW along the north side of MT northwest of Adelaide Island. Warmer water also can be seen going into Marguerite Bay. There is a second possible intrusion across the center of the grid, but the signature is weak. Klinck et al. (2004) estimate that 4–6 intrusions of CDW occur per year on this part of the WAP continental shelf, with the water moving on the shelf at a speed of about 2.5 cm s^{-1}. Episodic intrusions also occur in the model. For example, 3–5 (depending on the level of the temperature anomaly that defines an intrusion) separate intrusions can be found in the same area in the model during model year 2. In late August of model year 2 (Fig. 5) an intrusion of CDW can

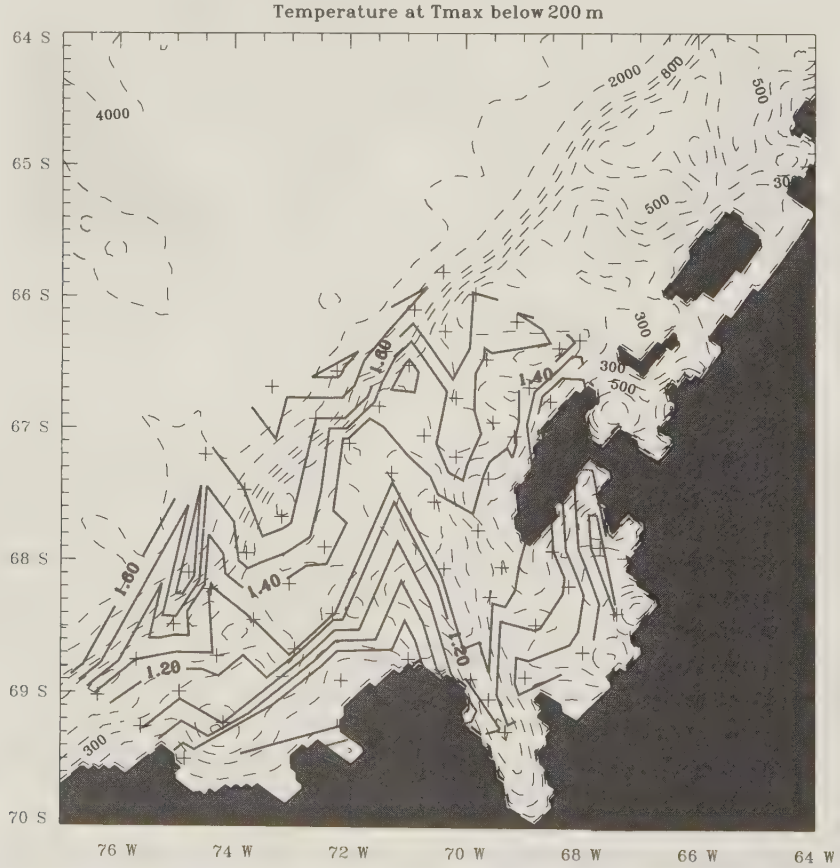

Fig. 4. Distribution of the temperature maximum (°C) below 200 m constructed from CTD temperature observations during May, 2001. The crosses represent station locations. The contour interval is 0.2 °C except between 1.2 and 1.6 °C where it is 0.1. The thin dotted lines in the background are model bottom topography.

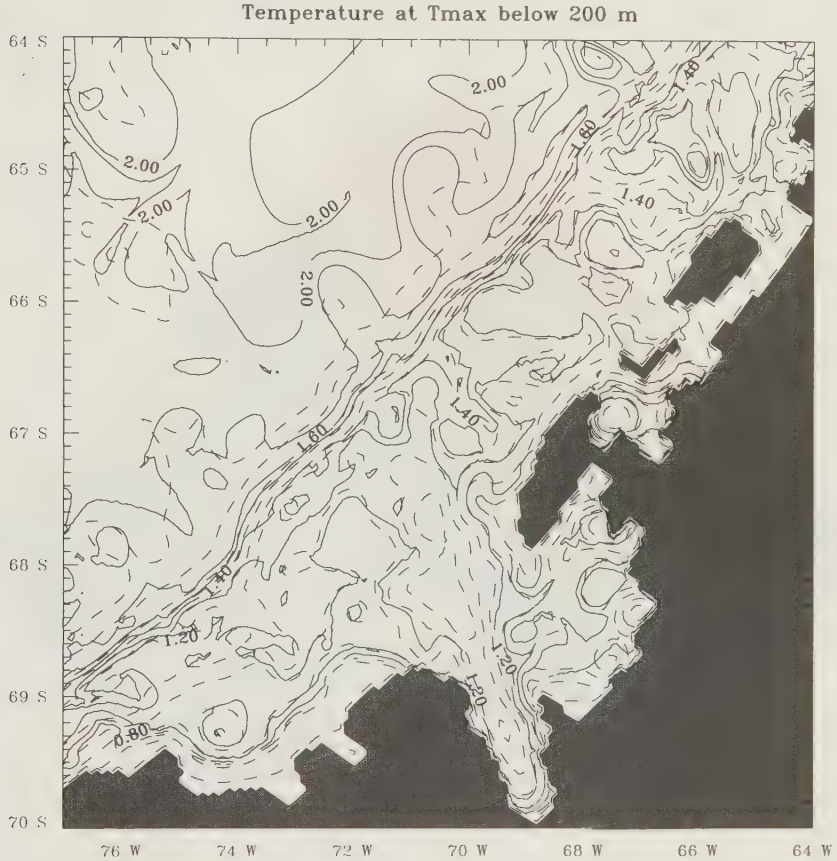

Fig. 5. Model maximum temperature (°C) below 200 m at model day 710 (late August). The contour interval is the same as for Fig. 4.

clearly be seen in the same location (north side of MT) where it occurs in the observations. The influence of the circulation into Marguerite Bay can also be seen in the maximum temperature.

3.2. Temperature

In order to use the model to assess the importance of cross-shelf-break transport on heat budgets on the shelf, it is necessary to examine how well the model is moving heat between the atmosphere, the surface ocean and the interior. One test of the accuracy of the model's surface processes is a comparison of the model sea-surface temperature (SST) to satellite estimates. Since there is no relaxation to a pre-defined temperature, SST accuracy is a check on several processes including the open-water surface heat flux, heat transfer between the ice and the water, penetration of the solar heating below the surface, horizontal advection and vertical mixing.

A climatology of Advanced Very High-Resolution Radiometer (AVHRR) satellite SST covering 1985–2000 with 9 km resolution, averaged over 5-day periods (Casey and Cornillon, 1999) and interpolated onto the model grid, is compared to model SST. Most of the model domain is ice free in austral summer, and much of it has high ice concentrations in winter leading to significant surface temperature changes ($>3.0\,^{\circ}C$ for 85% of the model grid) over the year. The model SST displays mesoscale variability (Fig. 6) that is not apparent in the observed climatology. However, the model SST has a realistic seasonal cycle when compared with the satellite estimates (Figs. 7 and 8). To quantify the SST comparison, the model

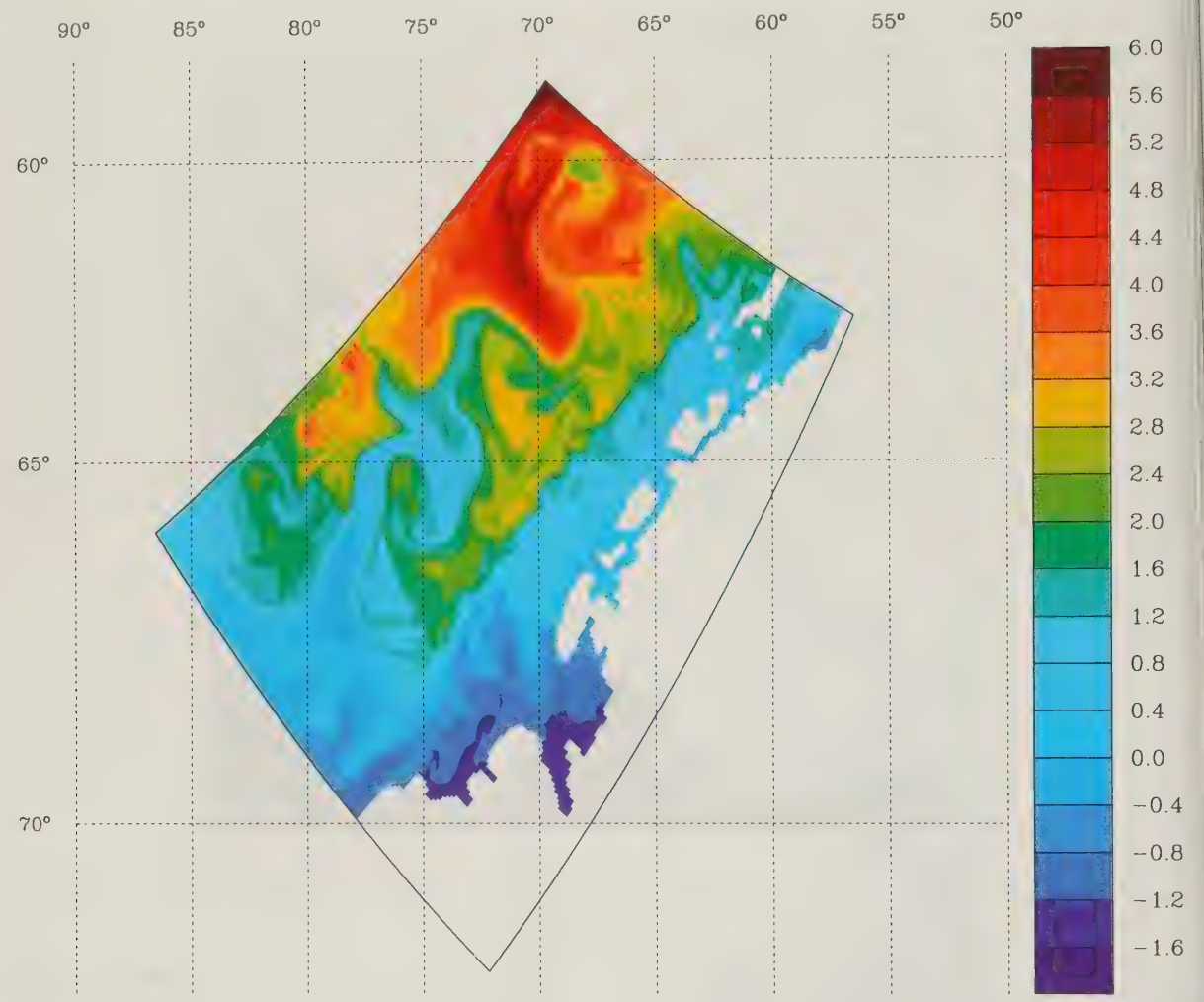

Fig. 6. Model top layer temperature (°C) at model day 510 (February 6).

values for the second year of the simulation are compared to observations at every grid point where AVHRR data were available (low or no sea ice) every 10 days. The average rms error over this period was 0.72 °C with a maximum of 0.97 °C in late March. Some of this error is due to the mesoscale variability in the model that is not in the climatology. The errors are somewhat compensated over the model grid at any given time, with the model SST warm in austral spring and late summer (max error 0.56 °C) and slightly cool in winter (max error −0.24 °C). The annual error over the entire year balances out to be only 0.09 °C. Note that it is also thought the AVHRR Pathfinder SST has a cold bias at high latitudes although the amount is uncertain (K.S. Casey, personal communication). In order to obtain an estimate of the scale of the error due to the mesoscale variability, a climatology of the model SST was created over the entire model run (except the first 90 days). Even though the climatology only extends over 2 years, the average rms error was reduced to 0.60 °C, with a maximum of 0.83 °C in mid-April and an annual error over the entire year of only 0.07 °C. The reduction in rms error due to time averaging of the model SST

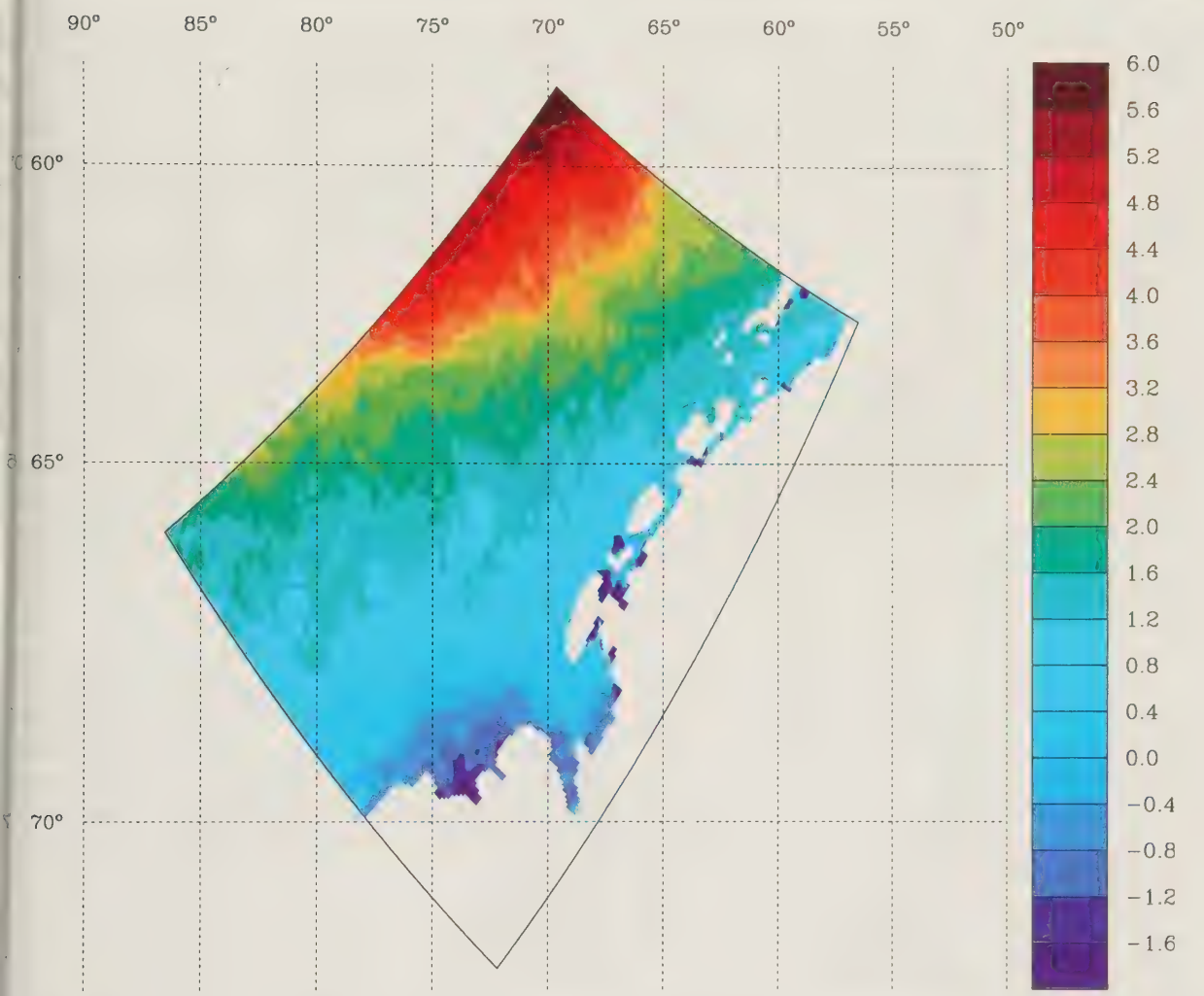

Fig. 7. Satellite (AVHRR) SST (°C) climatology (1985–2000) for the period February 5–9.

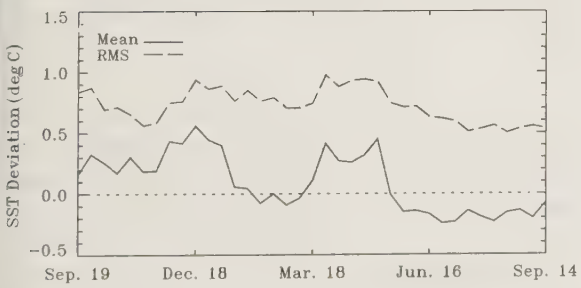

Fig. 8. Comparison between model and AVHRR SST over model year 2. The annual average deviation is 0.09 °C and annual average RMS error is 0.72 °C.

with little change in the mean error indicates that small-scale (mesoscale) variability of the model is the source of much of the rms error.

The model does a reasonable job of estimating the SST. However, two general problems could produce the excess heating in the summer and cooling in the winter. The open-water heat flux formulas were derived for tropical regions and may not be appropriate in high latitudes. Note that different bulk algorithms vary significantly in their calculation of heat flux (Zeng et al., 1998). A related problem could be the cloud-correction algorithm; different cloud-cover algorithms have

a wide variety of effects in the Antarctic (Kim and Hofmann, manuscript in preparation).

The second problem is the magnitude of vertical mixing, which is estimated from a turbulence parameterization (Large et al., 1994). The coefficients in the turbulence model may need to be adjusted for high latitudes and are a current topic of study. Double diffusive mixing, which may (Smith and Klinck, 2002) or may not (Howard et al., 2004) be important, was not used. Tidal mixing, which was not included in the model, can be important in the Antarctic (Levine et al., 1997, Muench et al., 2002) although it is uncertain whether it is significant in the WAP region (Padman et al., 2002; Howard et al., 2004). There also may be problems with the vertical mixing on the inner shelf due to inaccurate surface forcing related to the coast (coastal ice melt and winds). Double diffusive mixing and tidal circulation (driven at the open boundaries) will be added to the model in the future.

Cross sections of the model temperature just north of Marguerite Bay in late January and late July (Fig. 9) show the seasonal cycle of the mixed layer. In late January of model year 2, the temperature matches reasonably well with observations at the same time and location. Water is warmer than 1.25 °C at depth, although the core of the ACC does seem to be farther offshore in the model than in the observations. Cool winter water is centered near 100 m. There is also a shallow layer of warm water at the surface, although the off-shelf surface temperature is too warm (as much as 1 °C) in the model compared to observations. The same section in late July has a 75 m thick very cold mixed layer, with the temperature increasing monotonically with depth below the mixed layer over most of the shelf in both the model and observations. The −1.5 °C contour is at about 80–100 m in both the model and observations while the 0 °C is at 150 m in both. The model does not have the very warm water (>1.75 °C) up against the coast at 200–350 m that appears in the observations. However, the warm water in this location was probably the result of an intrusion of CDW passing by this station. Observations along the same line a couple of months earlier (May 3–4, 2001, not shown) have a maximum temperature of 1.4 °C in the location of the maximum on July 31. The model does show evidence of a intrusion of warm CDW near 350 m.

Note that the temperature of the very cold mixed layer in late July in the model is a couple of deci-degree below freezing. This happens because of the imposed ice cover. The model surface heat flux is calculated as a linear combination of heat flux due to ice cover and the open-water heat flux. The heat flux due to the ice cover is a function of the difference between the mixed layer temperature and the freezing point of sea water (Markus, 1999), which means that this heat flux term will not force the temperature below freezing. However, the open-water heat flux can be strongly negative (heat leaving the water) even with the water at the freezing point. At this location in late July, the imposed sea-ice is not 100%, so the heat flux is a combination of the ice cover term and the open-water flux term. The open-water heat flux here is strongly negative leading to strong cooling. Since the rapid cooling cannot directly lead to ice formation (which would reduce the contribution of the open water term) due to the ice cover being imposed, the surface temperature is cooled excessively. This problem will be fixed by adding a dynamic sea-ice model in the future.

4. Discussion

A primary motivation for this model is the study of exchange of water masses across the shelf break and its effect on biological processes. For example, CDW is shown to be important, due to its temperature, to the reproductive cycle of Antarctic krill (Hofmann et al., 1992). The specifics of cross-shelf nutrient transport, as part of CDW intrusions, are important for biological production (Prézelin et al., 2000). Also, the rate and timing of vertical diffusion providing heat and nutrients to the surface layer affect annual cycles of sea ice and summer production.

4.1. Shelf budgets

In order to study exchange across the shelf break, an enclosed "shelf" is defined by the 1000 m

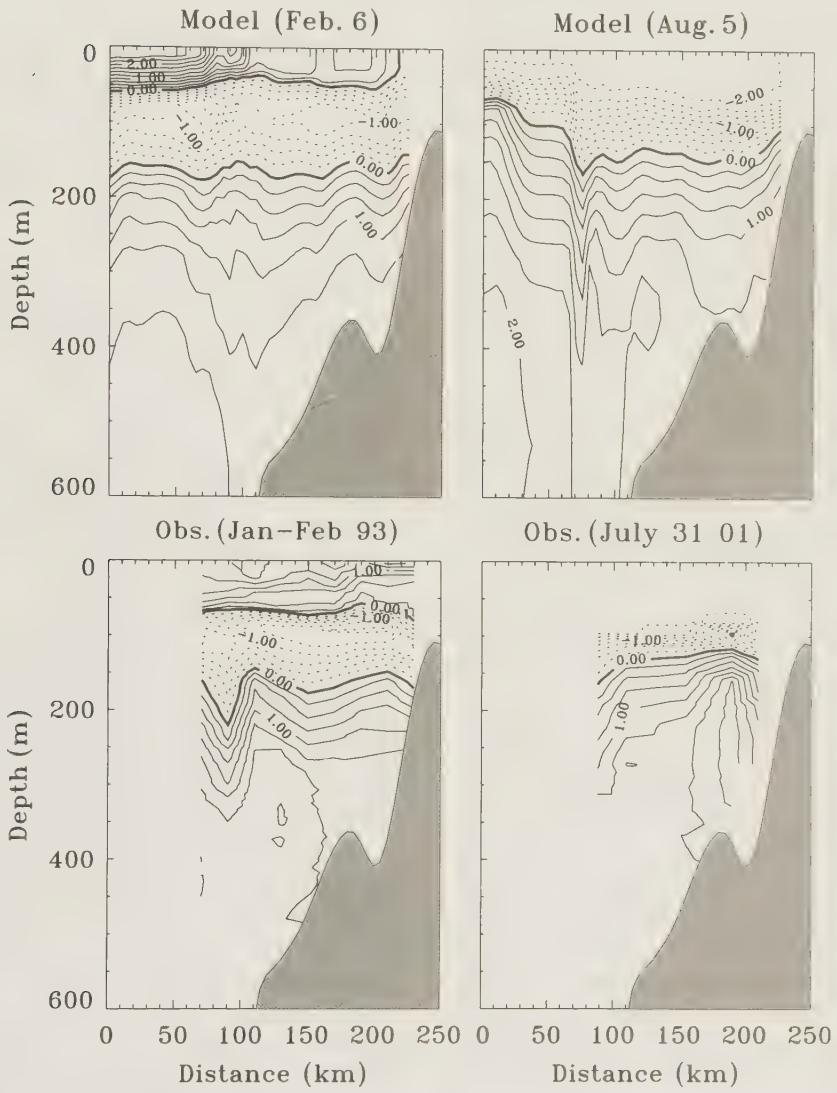

Fig. 9. Modeled and observed temperature cross-sections across the shelf and shelf break across from Adelaide Island (see Fig. 1). The top two figures are from the model at model days 510 (February 6) and 690 (August 5). The bottom two figures are observations from late January to early February 1993 and on July 31, 2001. Temperatures below 0 °C are represented with dashed lines and the contour interval is 0.25 °C.

isobath from near the south end of the model domain to the south end of Bransfield Strait and then to land at each end (Fig. 1). Because of model variability, instantaneous snapshots are not adequate for flux estimates. Instead, accumulated totals of volume and tracer fluxes in each horizontal direction are calculated in the model to increase the accuracy of the computed net flux. A budget of the volume flux onto the shelf computed from 5-day averages over model year 2 shows the mean total transport onto the shelf to be extremely small ($\approx 1400\,m^3\,s^{-1}$ on average). Note that the total horizontal transport onto the shelf does not have to be exactly zero due to the free surface. Although the volume flux is basically zero, there is a small net on-shelf transport of heat

(1.78 TW, heat content here is calculated with respect to the surface freezing point) and salt (0.16 psu-Sv.). If the average temperature (0.7 °C) and salinity (34.5 psu) along the shelf border are used, then the heat flux just due to the mean total transport onto the shelf is 0.014 TW and the salt flux is 0.048 psu-Sv, indicating that the net on-shelf transport of heat and salt is not simply due to the mass imbalance on the enclosed shelf. There is not much of a seasonal signal in the heat flux, instead there are episodic pulses of on and off-shelf heat transport.

The total advective heat flux into the enclosed region normalized by the surface area (1.86×10^{11} m^2) is equivalent to a vertical heat flux of 9.6 W m^{-2}. Using hydrographic observations on and off the shelf from Marguerite Bay north to Anvers Island over 1993 and 1994, Klinck (1998) estimated an annual average equivalent vertical heat flux due to transport of heat across the shelf break in subpycnocline waters to be 4.3 W m^{-2}. The model equivalent salt flux is 0.85 mg salt m^{-2} s^{-1}, while the Klinck estimate is 0.36 mg salt m^{-2} s^{-1}. The model fluxes are within a factor of two of the changes estimated from hydrographic measurements.

The average time rate of change of the heat and salt content on the shelf, normalized by the surface area, can also be computed as an equivalent vertical flux. The change in the heat content in the top 150 m (Fig. 10) shows the expected strong annual cycle with heating in austral spring and early summer and cooling in fall and early winter. However, the annual average change was close to zero (0.3 W m^{-2}). The water below 150 m on the shelf does not have an apparent seasonal cycle and has an annual net loss (2.6 W m^{-2}) of heat, which may be due to winter mixing below 150 m since much of the heat loss occurs in early austral winter. The total change in heat on the shelf is significantly smaller than the advective heat transport onto the shelf.

The change in salt content in the top 150 m on the shelf shows a general trend of freshening in summer and adding salt in fall and winter which is what one would expect from the melting and creation of sea ice. However, there is non-seasonal variability that is due to the precipitation climatology, open-water evaporation, and advection from off the shelf. The annual average increase in the top 150 m is 0.75 mg salt m^{-2} s^{-1}. The change in salt content below the top 150 m is small (annual average 0.07 mg salt m^{-2} s^{-1}), and the annual mean total increase in salt on the shelf (0.82 mg salt m^{-2} s^{-1}) is very close to the total advective transport onto the shelf. For the model, the advective transport is a very important part of the heat and salt budgets on the shelf.

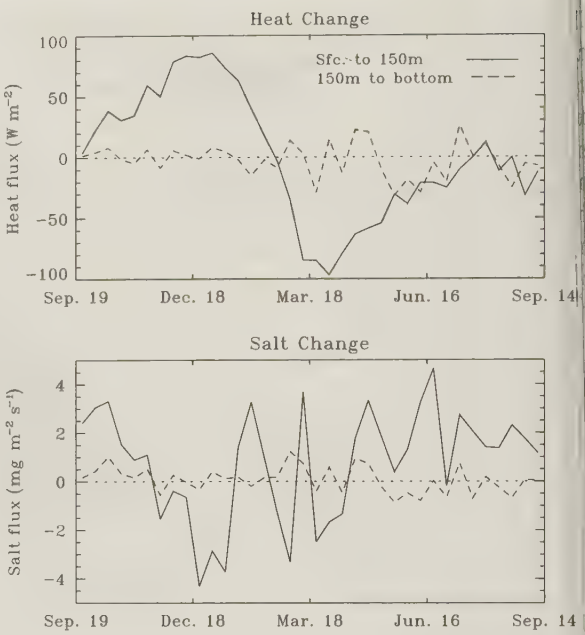

Fig. 10. Time history of change in heat and salt content for the second model year. The two lines in each plot represent the average above and below 150 m for the enclosed area shown in Fig. 1.

There is not much cross-shelf-break transport in either frictional layer represented by the top three model layers (directly forced by the wind stress) or the bottom model layer (over which the bottom friction in the model is directly applied as a body force).

The cross-shelf-break transport of CDW, defined as water below 150 m with a temperature above 1.0 °C, is time variable but averages 0.20 Sv onto the shelf. This water brings in substantial quantities of heat (22 W m^{-2}) and salt (41 mg salt m^{-2} s^{-1}). The equivalent vertical heat and salt fluxes show that advective transport of

CDW is very important to heat and salinity budgets on the WAP shelf. The cross-break transport of CDW accounts for much of the flux below 150 m as the advective heat flux onto the shelf of all waters below 150 m is 25 W m^{-2} and that of salt is 65 mg salt m^{-2} s^{-1}. Much of this on-shelf heat and salt transport is balanced in the model by atmospheric exchange and off-shelf transport of near-surface waters below the top three model layers.

Little Antarctic Bottom Water (AABW) is thought to form in the west Antarctic Peninsula shelf region (Hofmann and Klinck, 1998b; Orsi et al., 1999; Smith et al., 1999). If we define AABW here as water below the permanent pycnocline (150 m) with a temperature below −0.50 °C and a salinity above 34.6 psu, then no Bottom Water is found on or advected onto or off of the shelf.

4.2. Shelf-break exchange processes

Transport of CDW across the shelf break is thought to be tied to certain bathymetric features. For example, a linkage has been proposed between topographically induced upwelling of nutrient-rich CDW (primarily at sites of shallow topography near the shelf break) onto the shelf and the presence of diatom-dominated phytoplankton assemblages on the WAP continental shelf (Prézelin et al., 2000). A cross-section (not shown) of the time-mean cross-slope velocity along a section of the shelf-break across from Marguerite Bay shows the strongest flow generally at the surface, with alternating vertical sections of on and off-shelf transport. The cross-slope velocity at each individual grid point along the shelf break is calculated as

$$U_{\text{cross}} = \vec{U} \cdot \left(\frac{\nabla H}{|\nabla H|} \right),$$

where H is the depth.

Even though the total model cross-shelf volume transport is very close to zero, there are several locations that have relatively large and variable transport consistently on or off the shelf. It appears that many of the locations of cross-shelf transport can be related to the curvature of the shelf break (Fig. 11). This curvature can be numerically computed as the change along the shelf break (where s is the distance along the shelf break) of the unit gradient of the bathymetry:

$$\left| \frac{\mathrm{d}}{\mathrm{d}s} \left(\frac{\nabla H}{|\nabla H|} \right) \right|.$$

The curvature is defined to be positive when, going from southwest to northeast, the shelf-break rotates counter-clockwise. Since the flow along the shelf break is primarily from southwest to northeast, positive curvature rotates the bathymetry so that inertia would tend to drive water onto the shelf. When the annual mean cross-shelf-break volume flux (over model year 2) as a function of position along the shelf break is compared to the curvature (Fig. 12), there is an obvious lagged correlation over much of the shelf break. Note that at the southern end of the shelf break (approximately up to grid index 70), where the volume flux seems to lead instead of lag the curvature, the flow along the shelf break is directed more southwestward (Fig. 3). The correlation is at a maximum at a lag of either 1.5 ($r = 0.481$) or 2.5 ($r = 0.448$) gridpoints, corresponding to 7.5–12.5 km in distance along the shelf break (note that the curvature locations are one-half grid point removed from the cross shelf flow locations). The large-lag standard error (Sciremammano, 1979) is computed to be 0.110, so these correlations are easily statistically significant at the 99% level (2.6σ). Physically, this indicates that circulation crosses the shelf break in places where the tendency of the flow to maintain a given direction would have it cross a bathymetric contour that is rapidly changing direction. The maximum cross-shelf-break flux occurs about 10 km after the maximum change in the shelf-break direction. No significant lagged correlation was found between the cross-shelf-break flux and either the magnitude of the bottom slope or the depth. This indicates that there is no relationship in the model between transport and the depth or sharpness of the shelf break, contradicting earlier suggestions that water moved on the shelf over banks and off the shelf in troughs.

The terms in the momentum acceleration equation were calculated from time-averaged quantities at each level, summed over the entire

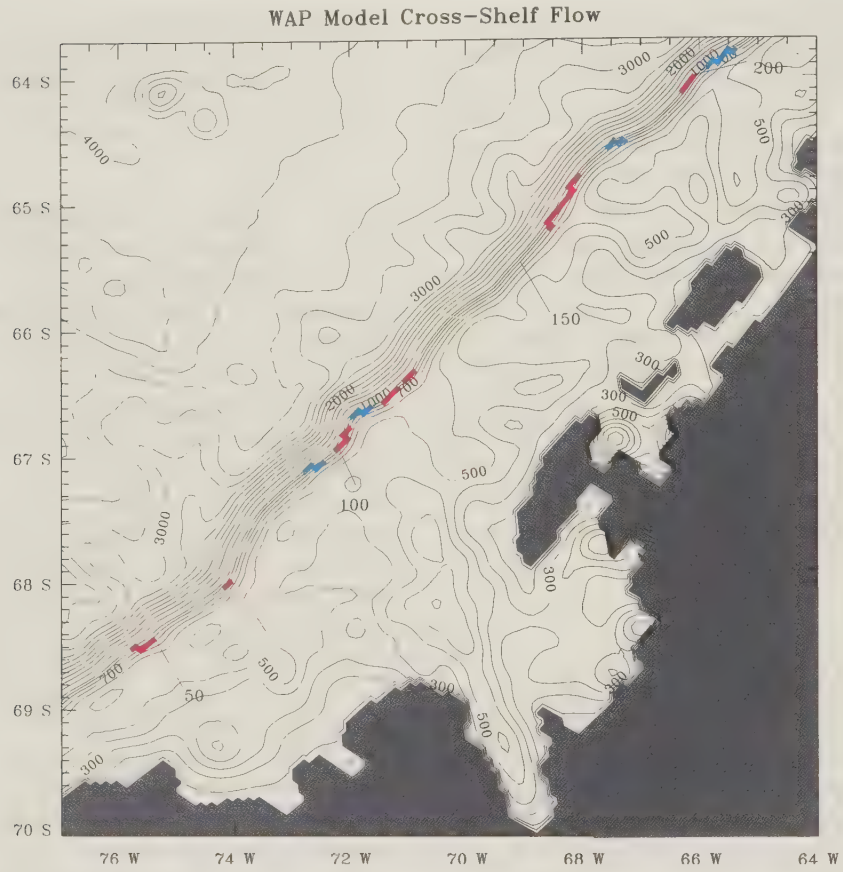

Fig. 11. Magnified view of the model domain and bathymetry around Marguerite Bay. The bathymetry contours are the same as for Fig. 1. Red (blue) lines along the shelf break represent sections where the total cross-shelf-break transport averaged over a year is largely onto (off) the shelf (see Section 4.2). The numbers are indices for a line defined along the shelf break (also see Section 4.2).

water column and then rotated at each grid point into across shelf break and along shelf-break components. Over the shelf break, the dominant terms in the annual average momentum balance in the cross-shelf-break direction are the Coriolis, the pressure gradient force, and the horizontal momentum advection terms, with the surface wind stress contributing but less important. The bottom drag, while important in the bottom boundary layer, does not have a large impact on the vertically integrated cross-shelf acceleration. The momentum advection term is greater than, or at least comparable to, the residual (sum of Coriolis, pressure gradient force, horizontal momentum advection and surface wind stress) over all of the shelf-break edge.

The cross-shelf-break momentum advection term (Fig. 12) is significantly correlated along the shelf break with the cross-shelf-break transport with a lag of either 0 ($r = 0.416$) or 1 ($r = 0.420$) grid points (large-lag standard error 0.124). This implies that on an annual average, some of the forcing of water across the isobaths is due to the non-linear advection of momentum. The momentum advection term is very strongly correlated with the shelf-break curvature ($r = 0.757$), implying that much of the momentum advection in the cross-shelf-break direction is just due to the rotation of the isobaths as one moves along the shelf break. Inertia causes the water to try to travel in a straight line, which will force water onto or off of the shelf when the shelf-break curves. The

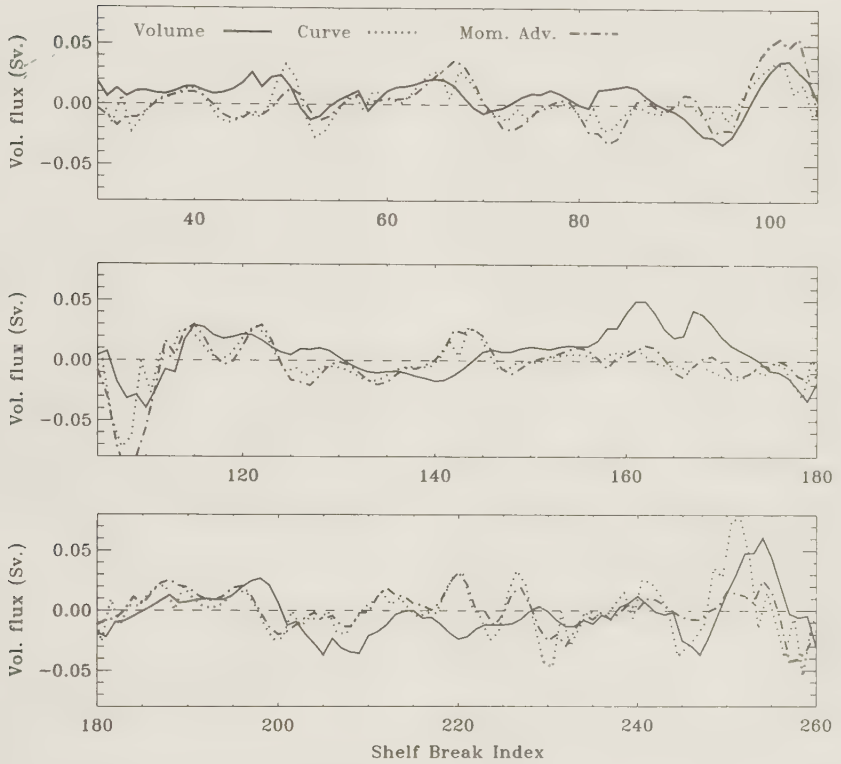

Fig. 12. Cross-shelf-break volume flux (Sv.), shelf-break curvature (normalized units * 0.25) and cross-shelf-break momentum advection term for the entire grid cell volume of water (10^5 m^4 s^{-2}). These are averaged values over model days 365–730. The x-axis is grid number along the defined shelf break.

annual average cross-shelf-break surface Ekman flux (not shown) is primarily on-shore southwest of grid index 180 and offshore to the northeast, and is significantly weaker than the momentum advection term over most of the shelf-break edge. However, there is somewhat of a correlation of surface Ekman flux with the cross-shelf-break transport ($r = 0.375$) along the break that is just barely significant at the 99% level (large-lag standard error 0.131).

Along the shelf break where there is mean on-shelf flow, the deeper CDW driven upward by the shallowing bathymetry raises nutrients that could support a localized increase in biological production. Note that of the four outer shelf-break locations where Prézelin et al. (2000 - Figure 9a) found a diatom-dominated phytoplankton community indicative of nutrient-rich upwelled water, three of them (Prézelin 200, 300 and 600 lines) correspond to locations in this model (shelf edge grid indices 102, 121 and 197) where there is on-shelf flow that is highly correlated to the bathymetric curvature.

However, how many of these locations of strong on-shore flow lead to CDW being transported well onto the shelf? It was noted previously that much of the cross-shelf circulation over the shelf in the model and observations was along bathymetric contours. Warm CDW was shown to intrude onto the shelf in some specific areas (e.g., along the northern side of MT). For example, the on-shelf flux around shelf edge grid indices 115–125 can be carried into the interior of the shelf by the general circulation of the shelf. Note that this is also where the strong intrusion showed up in the observations (Fig. 4). Conversely, the on-shelf flux around indices 85 or 100 does not intrude very far (Fig. 4) because of the mean circulation on the shelf. Also

note that observations show a weak intrusion at this location (index number 85). For the model to create a strong intrusion of CDW onto the shelf, it appears two mechanisms are necessary. Much of the CDW first appears on the shelf due to momentum advection and the curvature of the shelf break. Then, the general circulation on the shelf, which in this case is strongly influenced by bathymetric variations, pulls the CDW into the interior or back off the shelf.

5. Conclusions

A circulation model has been created for the west Antarctic Peninsula region in order to study the exchange of warm nutrient-rich CDW onto the continental shelf in this region. The model circulation is forced by daily wind stress along with heat and salt fluxes calculated by bulk formulae. All surface fluxes are modified by an imposed climatological sea-ice concentration.

The model circulation compares favorably to general schematics of the flow based on dynamic topography, water properties from recent hydrography and ADCP measurements. There are some problems with the circulation in the model near the coast, likely due to incorrect specification of ice-shelf melting. However, the circulation along the shelf break and outer shelf appears to be realistic, which is important for studying the exchange of CDW onto the shelf. The sea-surface temperature is similar to satellite estimates except that the model temperatures are slightly higher than observations in the summer and lower in the winter. Better agreement can be obtained by increasing the mixing across the pycnocline. The seasonal variability of the depth and temperature of the model mixed layer matches observations reasonably well. Sub-pycnocline temperature shows evidence of persistent intrusion of warm CDW onto the shelf, for example, at the shelf-break offshore of Adelaide Island.

Calculations of the advective transport of heat and salt onto the shelf and of the heat and salt budgets on the shelf show that the cross-shelf-break transport of CDW is very important to heat and salinity budgets on the WAP shelf. There is a significant correlation between the curvature of the shelf break and the volume transport across the shelf break, indicating that circulation crosses the shelf break in places where the tendency of the flow to maintain a given direction would have it cross a curving bathymetric contour. A balance of the terms in the momentum equation shows that momentum advection helps to force flow across the shelf break in specific locations due to the curvature of the bathymetry. For the model to create a strong intrusion of CDW onto the shelf, it appears two mechanisms are necessary. First, CDW is driven onto the shelf at least partially due to momentum advection and the curvature of the shelf break. Then, the general circulation on the shelf pulls the CDW into the interior.

Acknowledgements

We thank the Office of Computing and Communications Services at Old Dominion University for the use of the Sun HPC 10000 on which the simulations were run. Comments from Dr. David Musgrave, Dr. Peter Wiebe and an anonymous reviewer were very helpful. Dr. Hernan Arango provided the Beta 1.0 release of ROMS. The AVHRR SST data were provided by Dr. Kenneth Casey. The POCM model output fields were provided by Dr. Ricardo Matano. ADCP data are courtesy of Ms. Susan Howard and Earth and Space Research. Computer facilities and support were provided by the Commonwealth Center for Coastal Physical Oceanography. This work was supported by the US National Science Foundation Grant OCE-99-11731. This is US GLOBEC contribution no. 452.

References

Arrigo, K.R., Weiss, A.M., Smith Jr., W.O., 1998. Physical forcing of phytoplankton dynamics in the western Ross Sea. Journal of Geophysical Research 103, 1007–1022.

Beardsley, R.C., Limeburner, R., Owens, W.B., 2004. Drifter measurements of surface currents near Marguerite Bay on the western Antarctic Peninsula shelf during austral summer and fall, 2001 and 2002. Deep-Sea Research II, this issue [doi:10.1016/j.dsr2.2004.07.031].

Bacon, S., Reverdin, G., Rigor, I.G., Snaith, H.M., 2002. A freshwater jet on the east Greenland shelf. Journal of Geophysical Research 107, 10.1029/2001JC000935.

Basey, K.S., Cornillon, P., 1999. A comparison of satellite and in situ based sea surface temperature climatologies. Journal of Climate 12, 1848–1863.

Dinniman, M.S., Klinck, J.M., Smith Jr., W.O., 2003. Cross shelf exchange in a model of the Ross Sea circulation and biogeochemistry. Deep-Sea Research II 50, 3103–3120.

Fairall, C.W., Bradley, E.F., Rogers, D.P., Edson, J.B., Young, G.S., 1996. Bulk parameterization of air–sea fluxes for Tropical Ocean-Global Atmosphere Coupled-Ocean Atmosphere Response Experiment. Journal of Geophysical Research 101, 3747–3764.

Haney, R.L., 1991. On the pressure gradient force over steep topography in sigma coordinate ocean models. Journal of Physical Oceanography 21, 610–619.

Hofmann, E.E., Klinck, J.M., 1998a. Thermohaline variability of the waters overlying the west Antarctic Peninsula continental shelf. In: Jacobs, S.S., Weiss, R.F. (Eds.), Ocean, Ice and Atmosphere Interactions at the Continental Margin. Antarctic Research Series, vol. 75. American Geophysical Union, Washington, DC, pp. 67–81.

Hofmann, E.E., Klinck, J.M., 1998b. Hydrography and circulation of the Antarctic continental shelf: 150°E eastward to the Greenwich Meridian. In: Robinson, A.R., Brink, K.H. (Eds.), The Sea, vol. 11. Wiley, New York, pp. 997–1042.

Hofmann, E.E., Capella, J.E., Ross, R.M., Quetin, L.B., 1992. Models of the early life history of *Euphausia superba* I. Temperature dependence during the descent-ascent cycle. Deep-Sea Research 39A, 1177–1200.

Hofmann, E.E., Klinck, J.M., Lascara, C.M., Smith, D.A., 1996. Hydrography and circulation west of the Antarctic Peninsula and including Bransfield Strait. In: Hofmann, E.E., Quetin, L.B. (Eds.), Foundations for Ecological Research West of the Antarctic Peninsula. Antarctic Research Series, vol. 70. American Geophysical Union, Washington, DC, pp. 61–80.

Hofmann, E.E., Wiebe, P.H., Costa, D.P., Torres, J.J., 2004. An overview of the Southern Ocean Global Ocean Ecosystems Dynamics program. Deep-Sea Research II, this issue [doi:10.1016/j.dsr2.2004.08.007].

Howard, S.L., Padman, L., Hyatt, J., 2004. Mixing in the pycnocline over the western Antarctic Peninsula shelf during Southern Ocean GLOBEC. Deep-Sea Research II, this issue [doi:10.1016/j.dsr2.2004.08.002].

Jacobs, S.S., Giulivi, C.F., 1998. Interannual ocean and sea ice variability in the Ross Sea. In: Jacobs, S.S., Weiss, R.F. (Eds.), Ocean, Ice and Atmosphere Interactions at the Continental Margin. Antarctic Research Series, vol. 75. American Geophysical Union, Washington, DC, pp. 135–150.

Klinck, J.M., 1998. Heat and salt changes on the continental shelf west of the Antarctic Peninsula between January 1993 and January 1994. Journal of Geophysical Research 103, 7617–7636.

Klinck, J.M., Hofmann, E.E., Beardsley, R.C., Salihoğlu, B., Howard, S., 2004. Water-mass properties and circulation on the west Antarctic Peninsula Continental Shelf in Austral Fall and Winter 2001. Deep-Sea Research II, this issue [doi:10.1016/j.dsr2.2004.08.001].

Large, W.G., McWilliams, J.C., Doney, S.C., 1994. Oceanic vertical mixing: a review and model with a nonlocal boundary layer parameterization. Reviews of Geophysics 32, 363–403.

Levine, M.D., Padman, L., Morison, J.H., Muench, R.D., 1997. Internal waves and tides in the western Weddell Sea: observations from Ice Station Weddell. Journal of Geophysical Research 102, 1073–1089.

Marchesiello, P., McWilliams, J.C., Shchepetkin, A., 2001. Open boundary condition for long-term integration of regional oceanic models. Ocean Modelling 3, 1–20.

Markus, T., 1999. Results from an ECMWF-SSM/I forced mixed layer model of the Southern Ocean. Journal of Geophysical Research 104, 15603–15620.

Marr, J.W.S., 1962. The natural history and geography of the Antarctic krill (*Euphausia superba* Dana). Discovery Report 32, 37–465.

Martinsen, E.H., Engedahl, H., 1987. Implementation and testing of a lateral boundary scheme as an open boundary condition in a barotropic ocean model. Coastal Engineering 11, 603–627.

Mellor, G.L., Ezer, T., Oey, L.-Y., 1994. The pressure gradient conundrum of sigma coordinate ocean models. Journal of Atmospheric and Oceanic Technology 11, 1126–1134.

Mellor, G.L., Oey, L.-Y., Ezer, T., 1998. Sigma coordinate pressure gradient errors and the seamount problem. Journal of Atmospheric and Oceanic Technology 15, 1122–1131.

Milliff, R.F., Large, W.G., Morzel, J., Danabasoglu, G., Chin, T.M., 1999. Ocean general circulation model sensitivity to forcing from scatterometer winds. Journal of Geophysical Research 104, 11337–11358.

Muench, R.D., Padman, L., Howard, S.L., Fahrbach, E., 2002. Upper ocean diapycnal mixing in the northwestern Weddell Sea. Deep-Sea Research II 49, 4843–4861.

Orsi, A.H., Johnson, G.C., Bullister, J.L., 1999. Circulation, mixing, and production of Antarctic Bottom Water. Progress in Oceanography 43, 55–109.

Padman, L., Fricker, H.A., Coleman, R., Howard, S.L., Erofeeva, S., 2002. A new tidal model for the Antarctic ice shelves and seas. Annals of Glaciology 34, 247–254.

Potter, J.R., Paren, J.G., 1985. Interaction between ice shelf and ocean in George VI Sound, Antarctica. In: Jacobs, S.S. (Ed.), Oceanology of the Antarctic Continental Shelf. Antarctic Research Series, vol. 43. American Geophysical Union, Washington, DC, pp. 35–58.

Prézelin, B.B., Hofmann, E.E., Mengelt, C., Klinck, J.M., 2000. The linkage between Upper Circumpolar Deep Water (UCDW) and phytoplankton assemblages on the west Antarctic Peninsula continental shelf. Journal of Marine Research 58, 165–202.

Ross, R.M., Hofmann, E.E., Quetin, L.B., (Eds.), 1996. Foundations for Ecological Research West of the Antarctic

Peninsula. Antarctic Research Series, vol. 70. American Geophysical Union, Washington DC.

Royer, T.C., 1998. Coastal processes in the northern North Pacific. In: Robinson, A.R., Brink, K.H. (Eds.), The Sea, vol. 11, Wiley, New York, pp. 395–414.

Sciremammano Jr., F., 1979. A suggestion for the presentation of correlations and their significance levels. Journal of Physical Oceanography 9, 1273–1276.

Semtner, A.J., Chervin, R.M., 1992. Ocean general circulation from a global eddy-resolving model. Journal of Geophysical Research 97, 5493–5550.

Shchepetkin, A.F., McWilliams, J.C., 2003. A method for computing horizontal pressure-gradient force in an oceanic model with a nonaligned vertical coordinate. Journal of Geophysical Research 108, doi:10.1029/2001JC001047.

Smith, W.H., Sandwell, D.T., 1997. Global sea floor topography from satellite altimetry and ship depth soundings. Science 277, 1956–1962.

Smith, D.A., Klinck, J.M., 2002. Water properties on the west Antarctic Peninsula continental shelf: a model study of effects of surface fluxes and sea-ice. Deep-Sea Research II 49, 4863 -4886.

Smith, D.A., Hofmann, E.E., Klinck, J.M., Lascara, C.M., 1999. Hydrography and circulation of the west Antarctic Peninsula continental shelf. Deep-Sea Research I 46, 925–949.

Smith Jr., W.O., Dinniman, M.S., Klinck, J.M., Hofmann, E.E., 2003. Biogeochemical climatologies of the Ross Sea, Antarctica. Deep-Sea Research II 50, 3083 -3101.

Song, Y.T., 1998. A general pressure gradient formulation for ocean models. Part 1: scheme design and diagnostic analysis. Monthly Weather Review 126, 3213–3230.

Stammerjohn, S.E., Smith, R.C., 1996. Spatial and temporal variability in the west Antarctic Peninsula sea ice coverage. In: Hofmann, E.E., Quetin, L.B. (Eds.), Foundations for Ecological Research West of the Antarctic Peninsula. Antarctic Research Series, vol. 70. American Geophysical Union, Washington, DC, pp. 81–104.

Stein, M., 1992. Variability of local upwelling off the Antarctic Peninsula. Archiv für Fischereiwissenschaft 41, 131–158.

Tréguer, P., Jacques, G., 1992. Dynamics of nutrients and phytoplankton and fluxes of carbon, nitrogen and silicon in the Antarctic Ocean. Polar Biology 12, 149–162.

Wilkin, J., Hedström, K.S., 1998. User's manual for an orthogonal curvilinear grid-generation package. Technical report (available from Institute of Marine and Coastal Sciences, Rutgers University), 31pp.

Xie, P., Arkin, P.A., 1997. Global precipitation: a 17-year monthly analysis based on gauge observations, satellite estimates, and numerical model outputs. Bulletin of the American Meteorological Society 78, 2539–2558.

Zeng, X., Zhao, M., Dickinson, R.E., 1998. Intercomparison of bulk aerodynamic algorithms for the computation of sea surface fluxes using TOGA COARE and TAO data. Journal of Climate 11, 2628–2644.

ELSEVIER

Deep-Sea Research II 51 (2004) 2023–2039

DEEP-SEA RESEARCH
PART II

www.elsevier.com/locate/dsr2

Winter sea-ice properties in Marguerite Bay, Antarctica

D.K. Perovich[a,*], B.C. Elder[a], K.J. Claffey[a], S. Stammerjohn[b], R. Smith[c], S.F. Ackley[d], H.R. Krouse[e], A.J. Gow[a]

[a]*US Army Engineer Research and Development Center, Cold Regions Research and Engineering Laboratory, 72 Lyme Road, Hanover, NH 03755-1290, USA*

[b]*Lamont–Doherty Earth Observatory, Columbia University, 61 Route 9W, Palisades, NY 10964, USA*

[c]*Geography Department, University of California, Santa Barbara, Santa Barbara, CA 93106-4060, USA*

[d]*Civil and Environmental Engineering Department, Clarkson University, Potsdam, NY 13699, USA*

[e]*Physics and Astronomy Department, University of Calgary, Calgary, Alta, Canada T2N 1N4*

Accepted 11 July 2004

Abstract

During the winter 2001 and 2002 cruises of the SO-GLOBEC experiment, we investigated the morphological properties, growth processes, and internal permeability of sea ice in the Marguerite Bay area of the Western Antarctic Peninsula. There was considerable interannual variability in ice thickness with, average values of 62 cm in 2001 and 102 cm in 2002, with medians of 43 and 68 cm, respectively. Snow depth averaged 16 cm in 2001 and 21 cm in 2002. At 40% of the thickness holes in 2001 and 17% in 2002, a combination of deep snow and thin ice resulted in negative freeboard and the potential for surface flooding. Ice production was strongly influenced by the snow cover. Deep snow resulted in negative freeboard, surface flooding, and the formation of snow–ice, but also limited columnar ice growth on the bottom of the ice. A stratigraphic analysis of ice thin sections showed that more than half of the ice sampled was granular and that virtually all of the upper 20 cm of the ice cover was granular. Stable isotope ($\delta^{18}O$) analysis of samples from 2001 indicated that snow ice formation at the surface contributed significantly to ice formation. Two-thirds of the cores had some snow–ice and 15% of the ice sampled in 2001 was snow–ice. For 95% of the ice sampled the combination of warm ice temperatures and large salinities resulted in brine volumes that were greater than the percolation threshold of 5%. Autonomous mass balance buoys indicated that the ice was above the percolation threshold throughout late winter and spring. The exceeding of the percolation threshold allows continuous flooding to occur throughout the late winter–spring period. The WAP sea-ice therefore represents a warm "end-member" of the sea-ice covers of Antarctica. An expected consequence of the lengthy flooding condition at the snow ice interface is an earlier onset of an algal bloom in the flooded snow than elsewhere in Antarctic sea ice.

© 2004 Elsevier Ltd. All rights reserved.

*Corresponding author. Tel.: +603 646 4255; fax: +603 646 4644.
E-mail address: perovich@crrel.usace.army.mil (D.K. Perovich).

0967-0645/$ - see front matter © 2004 Elsevier Ltd. All rights reserved.
doi:10.1016/j.dsr2.2004.07.024

1. Introduction

The snow and sea-ice cover of the Antarctic marine ecosystem is a dynamic and important component that is sensitive to interactions with the atmosphere and ocean. The sea-ice cover provides a complex habitat for marine microalgae (Ackley et al., 1979; Palmisano and Sullivan, 1983; Eicken, 1992; Horner et al., 1992; Legendre et al., 1992), krill (Siegel and Loeb, 1995; Quetin et al., 1996), and higher organisms (Ainley and DeMaster, 1990; Trivelpiece and Fraser, 1996). Interactions of different trophic levels with sea ice have been hypothesized and outlined (Ackley and Sullivan, 1994; Smith et al., 1995). Of particular concern to the US Southern Ocean GLOBEC (SO-GLOBEC) program are potential relationships between krill survival and the sea-ice cover (Quetin and Ross, 1991; Quetin et al., 1994; Siegel and Loeb, 1995). The morphology of the sea-ice cover is an important element of the physical environment that strongly influences both the distribution of and the amount of resources available to Antarctic krill (Marschall, 1988; Daly, 1998). The presence of a sea-ice cover also strongly affects the transfer of heat, salt, and momentum between the atmosphere and ocean.

The spatial distribution and temporal evolution of snow depth, ice thickness, and freeboard are complex. Ice deformation results in great variability in ice thickness. Heavy snows can result in flooding of the ice surface with the eventual formation of snow–ice. Studies have indicated that, because of ample snowfall and large ocean heat fluxes, Antarctic sea ice can be melting on the bottom, while it is growing on the surface through snow–ice formation (Lytle and Ackley, 2001). The permeability of the sea ice strongly influences the exchange of salt and nutrients between the ice and upper ocean. Above the critical percolation threshold of 5% brine volume, the ice becomes permeable to rapid fluid transport (Golden et al., 1998; Golden, 2001). The morphology of the ice cover also affects the light regime in and under the ice, which in turn influences the snow algae, ice algae, and water column productivity, as well as the visibility for both predator and prey.

There have been numerous previous studies of physical and morphological properties of Antarctic sea ice and snow (Jeffries et al., 1998; Massom et al., 1997; Sturm et al., 1998; Worby et al., 1998). Granular ice has long been recognized as an abundant structural component of sea ice in the Western Weddell Sea found in amounts roughly equal to or greater than columnar congelation ice (Gow et al., 1982, 1987; Lange, 1988; Lange et al., 1989; Eicken and Lange, 1989; Lange and Eicken, 1991; Ackley et al., 1992; Gow et al., 1992; Lytle and Ackley, 1992). Formation of very significant amounts of granular ice also has been observed in the sea ice of the Western Ross Sea by Jeffries and Weeks (1993); in the eastern Ross, Amundsen, and Bellingshausen Seas by Jeffries et al. (1994); and in the Indian Ocean sector by Allison and Qian (1985), Jacka et al. (1987), and Tison and Haren (1989). Worby et al. (1998) summarized results from several cruises in the East Antarctic region, while Jeffries et al. (1998) reported findings from the Bellingshausen Sea, Amundsen Sea, and Ross Sea. Generally speaking, Antarctic studies have shown a preponderance of deformed first-year ice, considerable surface flooding, large ice salinities, predominantly granular crystal structure, and significant amounts of snow–ice formation.

The Marguerite Bay region was the focus of US Southern Ocean GLOBEC field studies in August and September of 2001 and 2002. Prior to the experiment little was known about the ice properties in this region. Our work was directed at remedying this lack and answering three science questions: (1) what are the basic morphological properties of the ice cover; (2) what are the ice production mechanisms; and (3) was the ice above the percolation threshold? Answering these questions is of importance not only to SO-GLOBEC research, but also to other issues such as the exchange of heat and salt between the atmosphere and ocean and the mass balance of the ice.

2. Instruments and methods

The three science questions were addressed through observations made during the 2001 and 2002 winter cruises of the R.V. *Laurence M. Gould.*

Observations were conducted from the bridge while the ship was en route, surveys of snow and ice thickness and properties were performed from the surface, and measurements were made using autonomous mass balance buoys. The morphological properties of the ice cover were investigated by measurements of the distribution of snow depth, ice thickness, and flooded ice. Observations of the crystallographic structure of the ice were used to gain insight about ice production. Autonomous buoys investigated ice production by monitoring the accretion and ablation at the surface and bottom of the ice. Measurements of ice temperature and salinity were used to compute the brine volume to determine whether the ice was above the percolation threshold.

When the ship was underway, hourly ice observations were made from the bridge using the ASPECT protocol (Worby, 1999). The ice concentration, thickness, ice type, and snow type were recorded for the primary, secondary, and tertiary ice types. These observations provided an estimate of the ice thickness and concentration over the large area of the ship cruise tracks (Fig. 1).

When the ship was stopped it was possible to conduct surface-based surveys of snow and ice morphology. This was done on 10 floes in 2001 and eight floes in 2002. The locations of these measurements sites are shown in Fig. 1 and the dates are listed in Table 1. The 2002 cruise was slightly later, with sites visited between 5 August and 5 September, compared to 28 July–23 August in 2001. Time on station ranged from 1 to 6 days and the level of detail of the measurements varied accordingly. The central element of the snow and ice morphology characterization was surveys of snow depth and ice thickness. Survey lines were selected to include a representative sample of ice conditions. We attempted to make the lines at least 50 m long, but often the floes were small and consequently line lengths ranged from 12 to 126 m. Measurements were made at a 1-m horizontal spacing along these survey lines. First snow depth and flooded layer depth were measured along the entire line. After these measurements were completed, holes were drilled using a 5-cm-diameter auger and ice thickness was measured along the line. Measurements were made using tapes and rulers and had an accuracy of ± 0.5 cm. Twelve survey lines were measured in 2001 and 15 in 2002. In some cases there was sufficient time on station that made it possible to repeat the survey lines to examine ice production and evolution over a 3- to 6-day period.

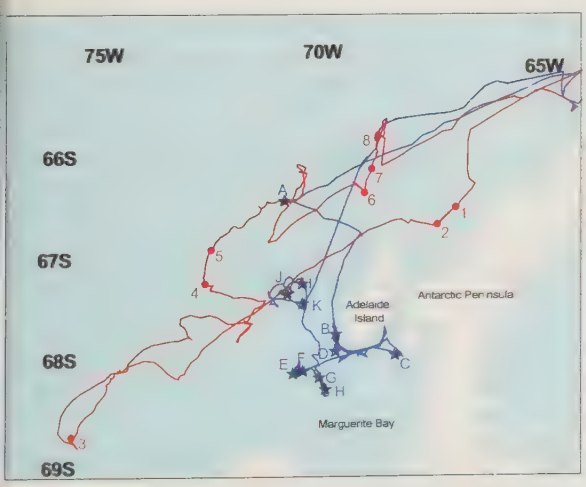

Fig. 1. Map showing cruise tracks and ice study sites of 2001 (blue) and 2002 (red) of the R.V. *Laurence M. Gould.*

Several sites were selected along the survey lines for a more detailed analysis of the snow and ice cover. The presence of ice layers or slush in the snow cover was noted. Typically, four ice cores were taken at each site: one to measure vertical profiles of temperature, salinity, and oxygen isotopes; one to examine the crystal texture and stratigraphy of the ice; and two for biological analysis. The cores were drilled by hand using a 7.25-cm core barrel to avoid contamination by oil and gasoline. Small holes were drilled in the ice properties core at 5- to 10-cm intervals immediately after the core was removed. Ice temperatures were then measured in these holes using a digital thermometer with an accuracy of $\pm 0.1\,^{\circ}$C. One core was sliced into 5- to 10-cm sections, which were placed into separate containers, returned to the ship, and melted. After melting, the salinity was measured using a YSI Model 30 salinometer with an accuracy of 0.1 psu. Measured temperature and salinities were used to compute the brine volume using the relationship of Frankenstein and Garner (1967). Thin sections were made parallel to

Table 1
Summary of thickness survey results

Ice station	Floe ID	Date	Length	Snow				Ice						Freeboard				% Below sea level
				Mean	Std. Dev.	Min	Max	Mean	Std. dev.	Coef. var.	Floe type	Min	Max	Mean	Std. Dev.	Min	Max	
2001																		
Site 1, Floe 1	A	28 Jul	12	18.6	3.7	13	26	65.3	19.3	0.30	Y	49	103	0.1	1.3	−2	3	31
Site 1, Floe 2	A	28 Jul	25	5.7	0.5	5	7	32	0.4	0.01	X	31	33	0.8	0.4	0	2	0
Arched Ice Berg	B	30 Jul	69	15.3	12.1	1	47	60.3	44.6	0.74	Z	17	214	−1.3	7.6	−17	22	37
Leopard Seal	C	1 Aug	10	10.8	5.6	3	19	51.3	22.3	0.43	X	29	95	2.9	7	−6	15	45
Flooding return	D	2 Aug	24	14.4	8.6	4	36	33	9.9	0.30	Y	10	54	−0.3	3	−8	5	48
Robert	E	5 Aug	126	22.7	9.6	4	57	71.4	50.3	0.70	Z	19	235	−2.6	10.6	−17	36	67
Robert	E	9 Aug	32	16.1	5.4	8	32	57.5	19.7	0.34	Y	43	142	0.5	1.5	−3	3	21
Fernando	F	11 Aug	35	23.3	7.5	7	33	43	8.2	0.19	X	33	74	−10.2	7.4	−20	17	89
Backbend	H	12 Aug	15	20.5	11.5	7	38	50.8	16.6	0.33	Y	33	97	−4.8	7.8	−16	15	69
Billy	I	15 Aug	76	6.4	3.9	1	22	75	57.1	0.76	Z	23	280	5.9	10.5	−1	80	1
Billy	I	19 Aug	44	12.8	7	2	31	62.1	46.2	0.74	Z	27	179	3	6.2	−1	32	7
Yoga	J	23 Aug	20	18.3	5.5	8	29	76.8	21.2	0.28	Y	41	119	−1.5	4.8	−8	12	57
All 2001 sites		7/28–8/23	488	16	11	1	57	62	44	0.71		10	280	−0.9	9.5	−20	80	40
2002																		
Levy	1	5 Aug	25	22	2.9	17	27	61.1	7.9	0.13	X	43	75	0.6	2	−3	5	23
Bergie Bit	2	5 Aug	35	44	15.7	21	89	189	85.8	0.45	Z	55	323	9.4	16.7	−14	63	14
Sparky	3	11 Aug	64	10.7	5.6	0	31	79.2	65.4	0.83	Z	22	320	4.9	9.7	−19	40	23
Sparky	3	11 Aug	30	19.5	12.1	7	58	173.2	116.3	0.67	Z	27	388	7.4	19.3	−28	52	26
Sparky	3	17 Aug	9	5	1.4	3	8	34.4	2.7	0.08	X	29	38	1.8	1.5	0	4	0
Minke	4	20 Aug	40	15	9.3	4	45	191.8	56.7	0.30	Y	38	295	14.2	8.6	0	40	0
Minke	4	20 Aug	30	10.8	3	3	19	74.1	30.1	0.41	Z	31	191	3.2	4.2	0	24	0
Rodin	5	22 Aug	100	10.4	7.7	1	41	56.1	39.9	0.71	Z	21	202	3.6	5..9	0	52	0
Rodin	5	22 Aug	30	8.7	4.2	4	17	85.4	68.4	0.80	Z	32	221	5.7	4.8	1	18	0
Rodin	5	25 Aug	60	7.7	5.4	2	27	39.3	8.3	0.21	Y	31	65	2.8	1.3	0	5	0
Rodin	5	28 Aug	50	7	1.2	5	10	38.5	3.1	0.08	X	32	48	2.2	1.1	0	5	0
Free Floater	6	1 Sep	20	32.2	13.3	15	55	50	15.1	0.30	Y	22	87	−9.5	1.5	−12	−6	100
Neptune	7	2 Sep	21	28.2	14.5	15	66	127.7	44.2	0.35	Y	57	185	1.1	8.1	−4	34	55
Deep Dish	8	5 Sep	25	72.9	7.9	50	83	213.8	64.7	0.30	Y	83	333	0.9	9.4	−7	37	73
Deep Dish	8	5 Sep	25	90.3	26.4	37	140	305.9	120.7	0.39	Y	160	565	13.4	32.5	−4	110	40
All 2002 sites[a]		8/5–9/5	564	20.9	23.6	0	140	102.1	92.1	0.90		21	565	4.5	11.5	−28	134	17

All thicknesses and depths are in cm. Floe type refers to the classification system of Jeffries et al. (1998).
[a]except for Deep Dish.

.e vertical axis of the structure cores. These thin ections were photographed in both transmitted natural light and between crossed polarizers to etermine the ice type and crystallographic struc- ure. Samples from the snow and the ice sections so were used for a post-experiment oxygen otope analysis. Delta ^{18}O determinations used ne traditional method of CO_2 equilibration with ater (Epstein and Mayeda, 1953). After one day f equilibration at 25 °C, the CO_2 was analyzed ith a dual inlet triple ion collection (masses 44, 5, and 46) mass spectrometer built with Micro- ass components. Laboratory working standards alibrated using IAEA reference waters were easured with the samples daily. Isotope data re reported using the conventional delta notation n terms of the standard V-SMOW (Coplen, 1996). he standard deviation of the measurements was ±0.2‰.

In addition to the surveys, we installed two ustom-made CRREL ice mass balance buoys in 001 and two in 2002 (Perovich and Elder, 2001; Morison et al., 2002). These buoys provided a means to obtain temporal information on ice production and on percolation in the ice. Fig. 2 presents a schematic of a mass balance buoy plus a photograph of an installed buoy. The buoys had a thermistor string that measured a vertical profile of temperature, at 5-cm spacing, from the air, through the snow and ice, and into the upper ocean. There were acoustic sensors measuring the positions of the snow surface and ice bottom. Barometric pressure, position, and air temperature also were measured. All buoy data were transmitted via Service ARGOS. The combination of thin ice, high winds, and considerable ice deformation made this a harsh environment for these mass balance buoys. However, in each year one mass balance buoy survived for more than 3 months, providing a temporal record of the ice evolution.

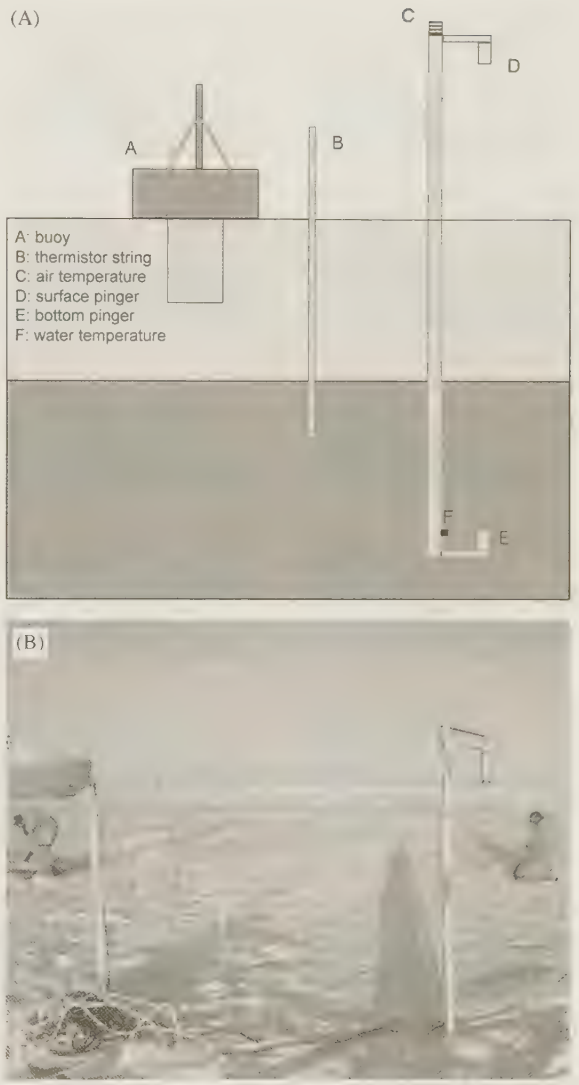

Fig. 2. The autonomous mass balance buoy: (A) buoy schematic and (B) photograph of an installed buoy.

3. Results

3.1. The morphological properties of the ice cover

The basic morphological properties of the ice cover include the ice extent, ice thickness, snow depth, and freeboard. The overall development of the ice cover was markedly different in 2001 and 2002. (Fig. 3). There was more ice present in 2002 throughout the entire fall–winter period in the Western Antarctic Peninsula region. During 2002 there was ice present in Marguerite Bay even in March, and there was ample ice coverage in the entire region by late June. In contrast, in 2001, the Western Antarctic Peninsula region into Marguerite Bay was open until late June. These differences

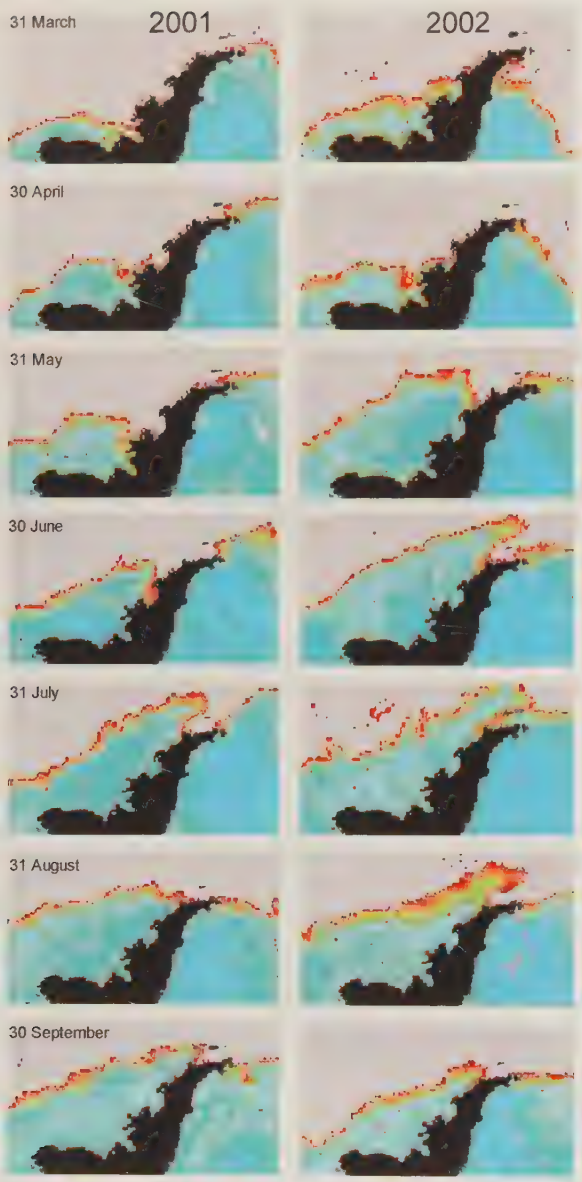

Fig. 3. Regional ice extent and concentration as a function of time for 2001 and 2002 as derived from Special Sensor Microwave Imager (SSM/I) satellite data (NOAA Web site).

are consistent with our experience cruising in the pack in 2001 and 2002. In 2001 with the ice edge closer to mainland Antarctica, south of Palmer Station, we were able to maneuver in the coastal leads and polynas into the northern reaches of Marguerite Bay with little difficulty. In contrast, during 2002 we encountered the ice edge north of Palmer Station and the Antarctic Peninsula, making passage more difficult. The larger extent of the ice created more forcing on the ice from the winds, creating higher amounts of ridged ice and an ice pack that was frequently under pressure, preventing us from even entering Marguerite Bay. Therefore, our 2002 studies were farther offshore than in 2001, but still well within the ice pack.

Each year hourly ice observations were made while the ship was underway in the ice. The average ice thickness derived from these measurements, not including areas of open water, was 46 cm in 2001 and 56 cm in 2002. The distribution of ice thickness, grouped into 10-cm bins, is presented in Fig. 4. Although in both years the peak of the ice thickness distribution was the 40- to 50-cm bin, there were distinct differences. In 2001 there was more ice thinner than 40 cm and less ice thicker than 60 cm.

When the ship was stopped, it was possible to get on the ice and make detailed surveys of the snow depth, freeboard, and ice thickness. During the two field campaigns, we measured a total of 27 thickness survey lines; 12 in 2001 and 15 in 2002, for a total of 1052 points. Table 1 summarizes the results from individual surveys and cumulative averages for each year. In 2002, there was a search for an extremely thick floe. This floe, "Deep Dish," was not representative of the general ice pack, and results from the surveys on it are not included in the summary statistics. Results from

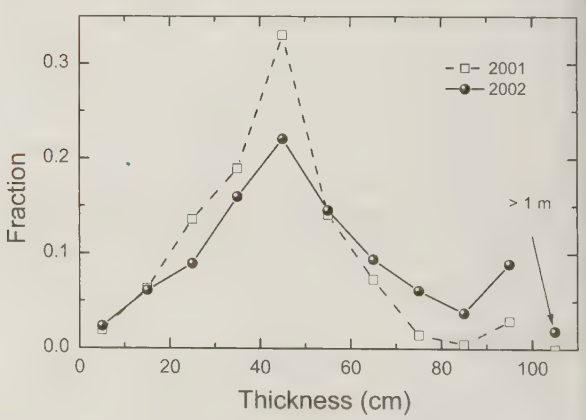

Fig. 4. Probability distributions of ice thickness grouped into 10-cm bins in 2001 and 2002 determined from bridge observations made while the ship was en route in the ice.

individual measurements were combined to calculate probability distributions of ice thickness, snow depth, and freeboard (Fig. 5). Data were grouped using 5-cm bins for snow depth and ice thickness and 1-cm bins for freeboard. Though 2 years do not make a climatology, the comparisons between 2001 and 2002 provide a limited, but still useful, perspective on the interannual variability of ice conditions in the Marguerite Bay region.

The ice was much thicker in 2002, with an average value of 102 cm compared to 62 cm in 2001. This is consistent with the earlier ice formation in 2002 and with the fact that the 2002 measurements were made later in the growth season. The 2001 ice thickness distribution has a sharp peak at 30–35-cm, with over half of the thicknesses between 30 and 50 cm (Fig. 5B). The 2002 peak was also 30–35 cm, but it was much less pronounced than in 2001 and only 27% of the thicknesses were between 30 and 50 cm. There was more thick ice (>1 m) in 2002, implying greater deformation that year.

A key difference between the 2 years was in the average freeboard: −1 cm in 2001, compared to 5 cm in 2002. The freeboard probability distribution is centered around 0–1 cm, tapering off towards negative and positive values. In 2001, the negative portion of the distribution is larger than the positive, while in 2002 the opposite is true. Indeed, 52% of the ice had a freeboard $\leqslant 0$ in 2001, compared to only 20% in 2002, implying a greater opportunity for surface flooding and snow–ice formation in 2001.

The average snow depth was 21 cm in 2002 compared to 16 cm in 2001. In both years the snow depth distribution had a broad peak in the 5- to 30-cm range. There was more deep snow in 2002, with 11% of the snow depths being greater than 50 cm, compared to less than 1% in 2001. However, it should be noted that in 2001 over half the ice had negative freeboard and considerable surface flooding was observed. It is possible that this flooding and the subsequent formation of snow–ice, reduced the depth of the snow cover in 2001 (Jeffries et al., 2001).

The roughness of the ice is an important consideration for the redistribution of windblown snow, for ice production, and for the underice

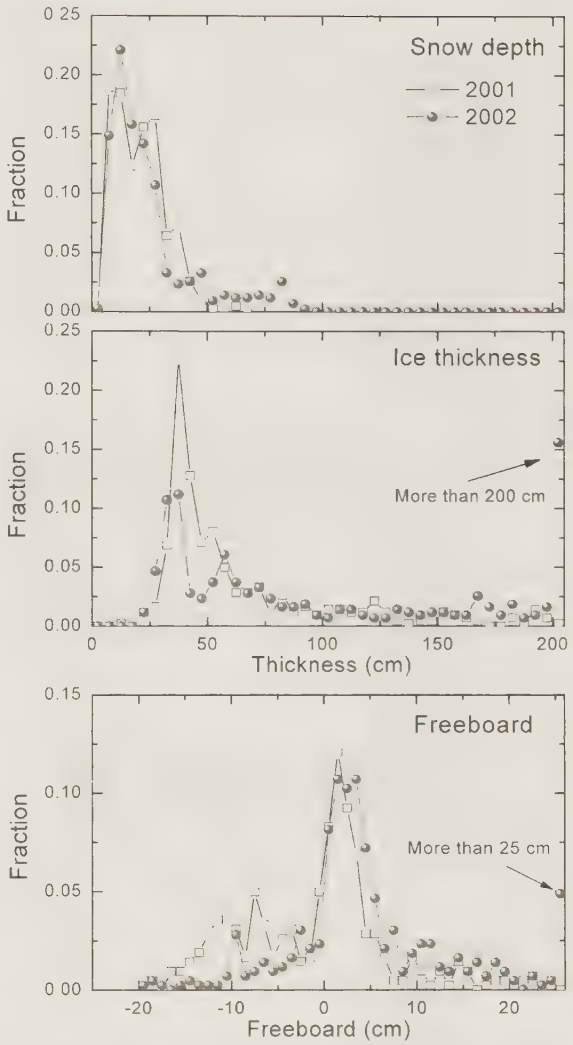

Fig. 5. Probability distributions of (A) snow depth, (B) ice thickness, and (C) freeboard for 2001 and 2002 determined from survey profiles.

habitat. Jeffries et al. (1998) classified floes into three basic categories based on ice roughness and ridging. The categories were defined using the ratio of the standard deviation (σ_i) and mean ice thickness (μ_i) and corresponded to σ_i/μ_i ranges of 0–0.19 (X), 0.2–0.39 (Y), and above 0.4 (Z). Applying this criterion to our data (Table 1), there were 6 X areas (22%), 11 Y areas (41%), and 10 Z areas (37%). Compared to the Jeffries et al. (1998) results from the Amundsen and Ross Seas, the Marguerite Bay region had fewer smooth areas (X)

and more rough areas (Y, Z). We believe that the greater spatial variability in ice thicknesses in Marguerite Bay was a result of an ice pack that was more broken up, with smaller floes, and more deformed ice.

Detailed transect data are presented in Fig. 6 for ice floes representing these three types. Floe A was one of only a few X-type floes we encountered, where the ice appeared smooth and there were no signs of deformation (Fig. 6A). The snow depth was 5–8 cm and the entire transect had positive freeboard. Fig. 6B presents a profile of a Y-type floe, the unusually thick, 2002 cruise "Deep Dish" floe. This was the thickest floe sampled, with an average thickness of 305 cm and a range from 15 to 450 cm. This floe also had the deepest snow averaging 90 cm and ranging from 37 to 140 cm. As the snow profile in Fig. 6B indicates, the large pressure ridge acted as a collector, building a snowdrift. This was not surprising as high winds and blowing snow were frequently observed during the experiment. Because of this deep snow even though this was the thickest ice measured, 40% of the transect line was below sea level and flooded. Typical of the most common floes encountered was the Z-type floe measured on Floe E (Fig. 6C). The 50-cm-thick ice has undergone considerable ridging, forming several 1- to 2-meter keels and 0.2- to 0.5-m sails that were effective in collecting snow. This floe had the deepest snow of the 2001 field experiment. This resulted in a 10-cm-thick flooded layer that covered two-thirds of the transect line.

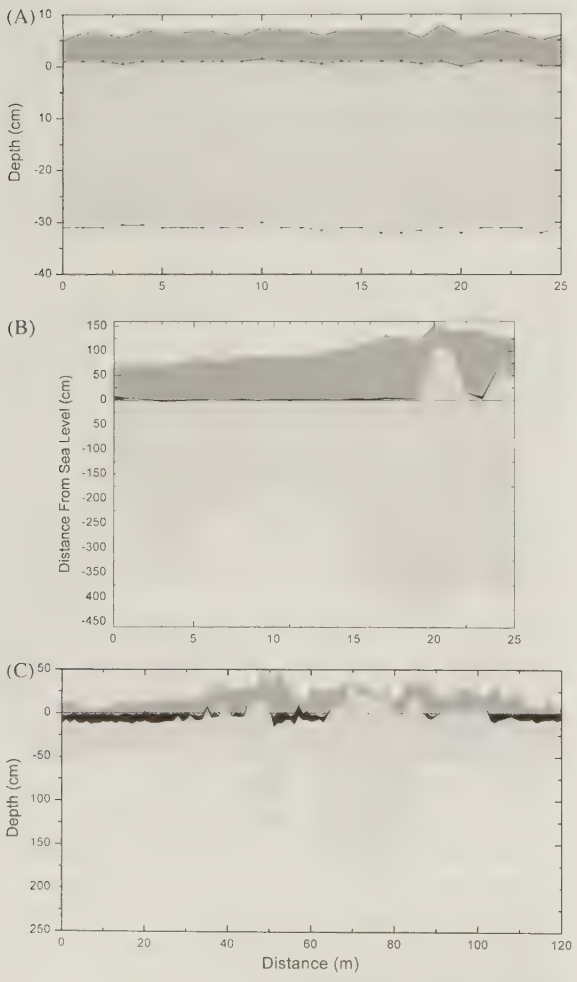

Fig. 6. Selected profiles from ice thickness surveys illustrating (A) undeformed ice (type X), (B) thick ice (type Y), and (C) highly deformed ice (type Z). Dark gray is snow, light gray is ice, black is flooded ice and snow, and white is the air (above) and the ocean (below).

3.2. Ice production

The ship- and surface-based surveys provide a broad picture of the ice cover—its thickness and snow depth, and whether there is flooding. However, by nature, these surveys were snapshots in time, and did not provide information on the formation and evolution of the ice cover. The crystallography of the ice provides a window into its origin and formation. There were 31 such windows in 2001 and 20 in 2002, where an ice core was removed for detailed crystallographic analysis.

The ice core analysis included vertical thin sections photographed under natural and polarized light plus profiles of temperature, salinity, brine volume, and $\delta^{18}O$. The two major components of sea ice are granular ice and columnar congelation ice. Congelation ice is formed by direct freezing of seawater to the underside of an existing ice sheet under quiescent conditions. Granular ice includes frazil ice and snow–ice. Frazil ice forms under turbulent conditions when there is wind- or wave-driven mixing. Frazil ice production is usually more rapid than columnar congelation growth. Snow–ice formation occurs

when snow is infiltrated by water that freezes. It is not possible to distinguish accurately between frazil ice and snow–ice by visual inspection under either natural or polarized light. However, the two granular ice components can be readily identified by their differing stable isotopic composition. $\delta^{18}O$ values trend towards more negative values in snow–ice relative to frazil ice, which generally possesses slightly positive values. Following the established protocol (Jeffries et al., 2001), negative $\delta^{18}O$ values were assumed to be snow–ice and positives values frazil ice. The snow–ice fraction was estimated from ice core samples that were melted and returned to the laboratory for $\delta^{18}O$ analysis.

Results from three examples representing cores with small, moderate, and large amounts of granular ice are presented in Fig. 7. The first core had a large amount of columnar ice and was indicative of ice grown under quiescent conditions (Fig. 7A). At this site the ice was 31 cm thick and the snow was 7 cm deep. The top 7 cm of the ice was coarse-grained granular ice and the remainder was columnar. All of the $\delta^{18}O$ samples were $>0‰$, indicating that no snow–ice was present and that the granular ice was frazil. This core was unusual in its relative lack of granular ice (23%). The second example (Fig. 7B) was similar in crystal structure to the first from a depth of 10 cm to the bottom. The difference was in the top 10 cm, where the fine-grained granular ice and the $\delta^{18}O$ values of -2 to $-8‰$ indicate that it was snow–ice. Indeed, snow–ice formation was continuing at this site during the measurements. The ice freeboard was negative and the bottom 8 cm of the snowpack was wet and slushy. Fig. 7C shows results from 48-cm-thick ice that consisted entirely of granular ice, aside from the bottom few centimeters that were columnar ice. This ice was warm (-2 to $-3\,^{\circ}C$) and nearly isothermal. Brine volumes were quite large, 20–24% near the surface and 10% at depth. Once again the freeboard was negative and the bottom of the snowpack was wet and slushy. The $\delta^{18}O$ values indicate that the top 22 cm were snow–ice and the remainder of the granular ice was frazil.

Ice core results are summarized in Table 2. Analyzing all the cores indicated that there was a

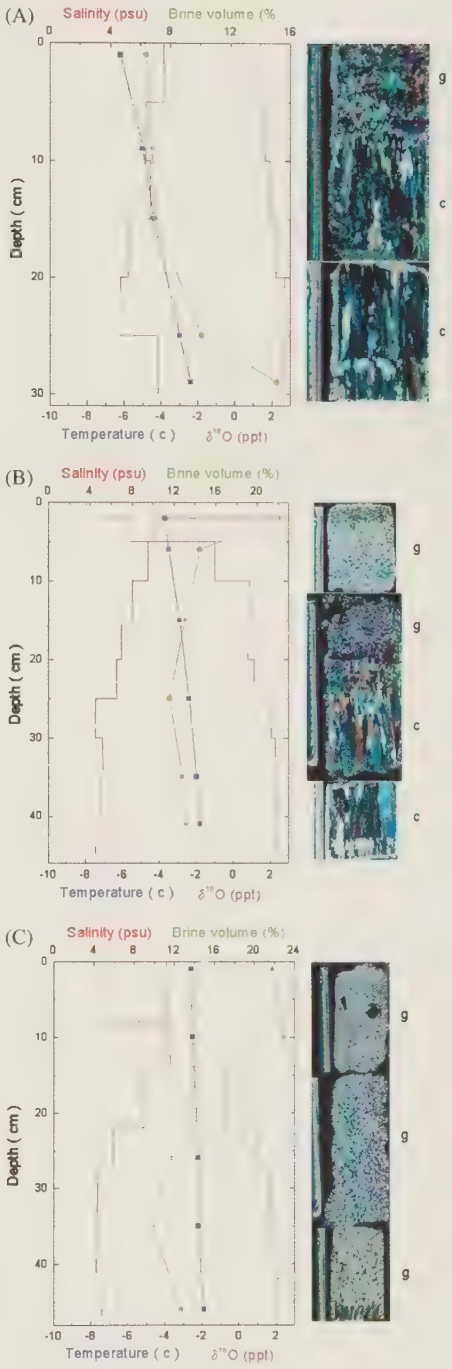

Fig. 7. Typical ice core results from cores that were (A) primarily columnar (18 August 2001; 67°13′ S, 70° 33′ W), (B) granular and columnar with a surface layer of snow–ice (9 August 2001; 68° 02′ S, 70° 07′ W), and (C) snow–ice and granular (12 August 2001; 68° 12′ S, 69° 31′ W).

Table 2
Summary of ice physical properties cores

Date	Latitude (S)	Longitude (W)	Length	H_i	F_b	S_b	Granular (%)	Columnar (%)	Snow–ice (%
7/28/2001	66 21.3′	70 43.1′	50			5.4	40	60	0
7/28/2001	67 21.6′	71 43.1′	33			5.8	53	47	0
7/30/2001	68 39.5′	70 20.0′	33	32	1	8.9	40	60	15
7/30/2001	67 39.8′	69 20.4′	45	40	1	6.2	73	27	33
8/1/2001	67 49.2′	67 48.0′	30	31	1	6.7	68	32	30
8/2/2001	67 49.5′	69 18.8′	35	34	2	7.5	37	63	31
8/6/2001	68 04.1′	70 11.2′	86	86	7.5	7.7	25	75	0
8/6/2001	68 04.2′	70 11.9′	32	29	−7	6.7	59	41	
8/6/2001	68 04.4′	70 13.2′	167	183	14	6.6	76	24	0
8/7/2001	68 01.2′	70 20.2′	40	39	−8	7.0	58	42	10
8/7/2001	68 01.2′	70 20.2′	52			6.8	80	20	0
8/7/2001	68 01.2′	70 20.2′	47	47	13	4.6	100	0	0
8/7/2001	68 01.2′	70 20.2′	28	33	3	6.3	100	0	53
8/7/2001	68 01.2′	70 20.2′	147	165	12	7.4	48	52	7
8/7/2001	68 01.2′	70 20.2′	52	51	4	8.2	54	46	49
8/7/2001	68 01.2′	70 20.2′	44	47	3	7.4	43	57	35
8/9/2001	68 02.1′	70 06.8′	42	42	0		43	57	13
8/9/2001	68 02.1′	70 06.8′	44	44	0	7.4			27
8/11/2001	68 05.5′	69 41.5′	54	52	1	8.8	28	72	24
8/11/2001	68 05.5′	69 41.5′	44				40	60	
8/12/2001	68 12.3′	69 31.1′	50	49	2	7.4	95	5	47
8/16/2001	67 08.5′	70 14.6′	24	25	0	6.7	69	31	14
8/16/2001	67 08.5′	70 14.6′	36	40	−3	5.6	84	16	0
8/16/2001	67 08.5′	70 14.6′	30	33	3	7.8	19	81	13
8/16/2001	67 08.5′	70 14.6′	46			7.2	100	0	41
8/16/2001	67 08.5′	70 14.6′	115	142	5	8.7	86	14	22
8/16/2001	67 08.5′	70 14.6′	49		3	7.3	97	3	0
8/18/2001	67 12.9′	70 33.0′	30	30	0	6.3	65	35	0
8/19/2001	67 17.1′	70 35.1′	34	35	0	8.7			41
8/16/2001	67 08.5′	70 14.6′	31	32	0	5.9	66	34	16
8/20/2001	67 11.3′	70 49.2′	64	64	20	6.1	47	53	0
8/21/2001	67 24.8′	70 49.6′	164	164	−3	5.5	84	16	6
8/23/2001	67 22.3′	70 11.8′	76		3	7.4			10
8/5/2002	66 20.4′	66 40.8′	58	59	0	6.2	92	8	
8/6/2002	66 31.2′	67 04.8′	108	119	1	6.9	62	38	
8/11/2002	68 40.2′	76 10.8′	31			7.9	100	0	
8/11/2002	68 40.2′	76 10.8′	180	179	19	5.5	92	8	
8/14/2002	68 10.2′	75 11.4′	177			7.1	73	27	
8/15/2002	68 05.4′	75 01.2′	70	72	1	8.6	92	8	
8/16/2002	68 01.8′	74 51.0′	34	31	1	7.3	100	0	
8/19/2002	67 30.0′	71 30.0′	117	141	25	6.4	86	14	
8/21/2002	68 05.4′	72 39.6′	31			6.0	88	12	
8/21/2002	68 05.4′	72 39.6′	166	206	15	6.9	47	53	
8/23/2002	66 42.6′	72 10.2′	221	255	7	8.8	—	—	
8/24/2002	66 38.4′	71 58.8′	300			7.9	100	0	
8/26/2002	66 23.4′	71 09.6′	72	66	0	6.5	37	63	
9/1/2002	66 15.6′	68 52.2′	63	60	−6	6.8	35	65	
9/2/2002	66 01.8′	68 44.4′	64	64	−3	6.8	75	25	
9/2/2002	66 01.2′	68 44.4′	152	173	6	7.1	78	22	
9/4/2002	65 46.2′	68 40.2′	75	72	−6	8.6	100	0	
9/6/2002	65 42.6′	68 43.2′	60	67	2	11.5	86	14	
9/7/2002	65 37.2′	68 36.0′	87	88	5	5.9	—	—	
9/7/2002	65 37.2′	68 36.0′	83	80	2	5.8	95	5	
9/8/2002	65 31.2′	68 29.4′	44	79	2	7.6	79	21	

Length is the core length (cm), H_i theice thickness (cm), F_b the freeboard (cm), and S_b the bulk salinity (psu).

reponderance of granular ice, consistent with the ndings of earlier studies (Gow et al., 1987; Lange, 988; Eicken and Lange, 1989; Lange and Eicken, 991; Jeffries and Weeks, 1993; Jeffries et al., 1994; Vorby et al., 1998). There was more granular ice n 2002 (78%) than in 2001 (66%). Overall the ranular fraction of individual cores ranged from 0% to 100%. In 2002, 85% of the cores were nore than half granular ice compared to 65% of he cores in 2001. Many of the cores, 20% in 2002 nd 10% in 2001, were composed entirely of granular ice. The abundance of granular ice confirms our qualitative observation that growth conditions in the study area typically were urbulent, favoring frazil production over congelation growth. Also, a significant portion of the ice surface was flooded, leading to snow–ice formation.

The frequency distribution of $\delta^{18}O$ values for the samples taken in 2001 is plotted in Fig. 8A. Most of the samples (85%) had positive $\delta^{18}O$ values, though 15% had negative values, implying that it was snow–ice. Examining the $\delta^{18}O$ results on a core-by-core basis indicated that 32% of the cores had no snow–ice, 23% had a small amount in the top few centimeters of ice, and 45% were at least 15% snow–ice. Fig. 8B displays all the measured $\delta^{18}O$ values for 2001 as a function of depth within the ice. Most of the negative $\delta^{18}O$ values were from the top 10 cm of the ice and virtually all were from the top 20 cm. The one exception was a negative value found at a depth of 50 cm. This was in a core that showed strong evidence of ice deformation and a likelihood that the 50-cm-deep sample was once at the surface.

At a few sites, we were able to obtain a brief glimpse of the temporal evolution of the ice cover by repeating the thickness survey along the same transect a few days later. Fig. 9A shows results from a 30-m transect made on 5 August 2001 and repeated on 9 August 2001. Initially, the entire transect was below freeboard and the surface was flooded with a 5- to 10-cm slush layer. After 5 days of air temperatures between −10 °C and −4 °C, this slush layer froze, forming snow–ice (Fig. 9B). However, there was essentially no bottom growth of the ice cover during this period. The heat lost from the ice cover to the atmosphere resulted in

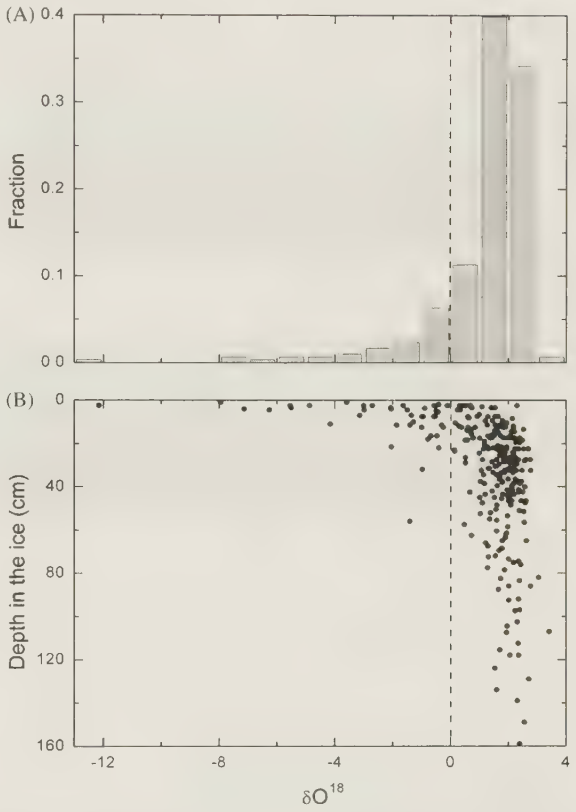

Fig. 8. $\delta^{18}O$ results from samples taken from the 2001 ice cores: (A) probability distribution of $\delta^{18}O$ values and (B) scattergram of $\delta^{18}O$ versus sample depth within the ice.

freezing of the slush layer, not bottom growth. There was evidence of modest deformation around 15 m and significant ridging at 28–30 m, illustrating the important of ice dynamics in this region. In 2002, repeat measurements were made at a 30–40-cm-thick floe that had a thin 5–10-cm snow cover. On 22 August 2002 the freeboard was positive along the entire transect and there was no surface flooding (Fig. 9C). Six days later on 28 August 2002, the repeat of the transect (Fig. 9D) showed an accumulation of a few centimeters of new snow bottom ice growth of 3–5 cm everywhere along the line. Air temperatures ranged from −25 to −4 °C, averaging −13 °C during this period. In this case, with no flooded layer to freeze, there was columnar ice growth at the bottom.

The autonomous mass balance buoys also provide information on the formation and

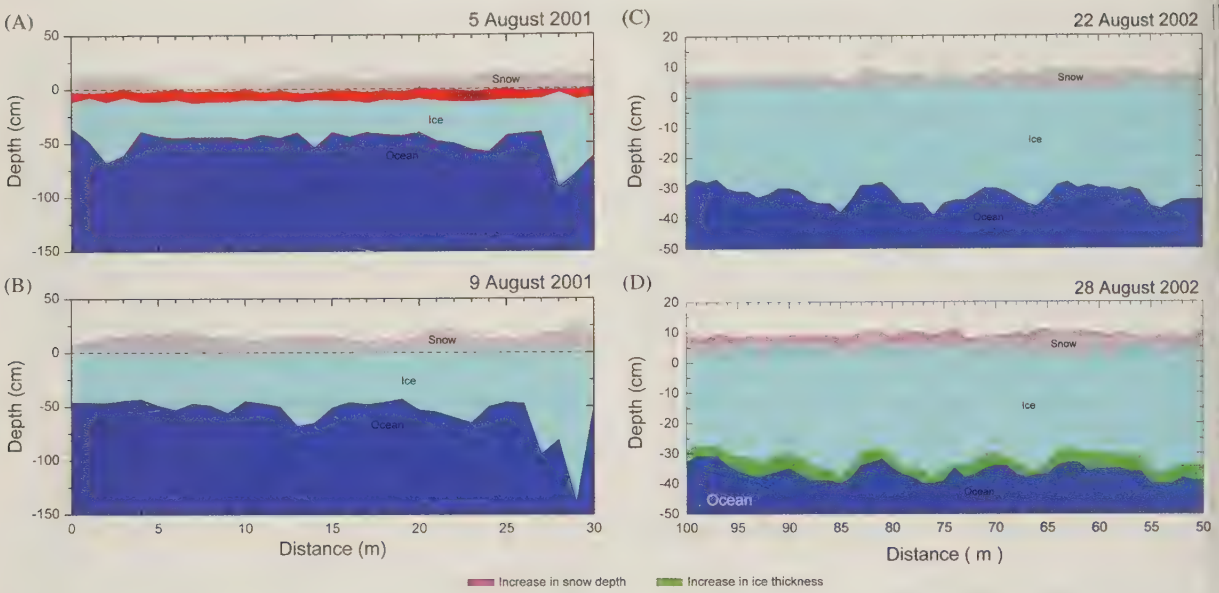

Fig. 9. Before and after repeat thickness surveys in 2001 showing freezing of flooded layer and in 2002 showing bottom growth. The panels are (A) 5 August 2001, (B) 9 August 2001, (C) 22 August 2002, and (D) 28 August 2002.

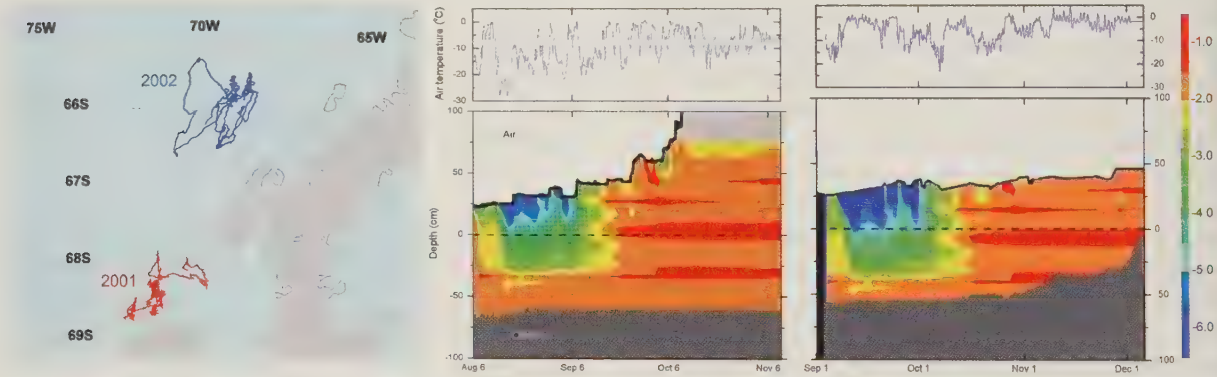

Fig. 10. Time series results from the autonomous mass balance buoys of (A) drift tracks and mass balance from (B) 6 August to 10 November 2001, and (C) 4 September to 5 December 2002. Internal ice temperature is displayed using color contours, with blue being cold (−6 °C) and red warm (0 °C). The black/white interface denotes the changing position of the snow surface, the dashed black line the original position of ice surface, and the bottom boundary between orange and gray the ice/ocean interface. The gray portion in panel (B) is snow where there were not any temperature measurements. The ice bottom sensor in 2001 failed on 20 September and a flat line is plotted after this date.

evolution of the ice. Results from the two longest lasting mass balance buoys in 2001 and 2002 are presented in Fig. 10. The data record for each buoy was approximately 3 months long, with a period of data overlap between 4 September and 10 November for the 2 years. We believe that the 2001 buoy was destroyed during an ice deformation event, while in 2002 the buoy was lost when the ice melted.

The defining feature of the 2001 time series was the heavy snowfall. When the buoy was installed there were 25 cm of snow, 65 cm of ice, and a

freeboard of −1 cm. The snow depth increased by more than 1 m between 6 August and 6 November. The temperature record indicates the ice was warm and, given the initial ice salinity of 5–10 psu, the brine volume was large. The temperature record also shows warm intrusions (red bands in Fig. 10B), presumably due to surface flooding. With air temperatures below freezing, this flooding could lead to substantial snow–ice formation. Assuming that (1) as the snow depth increases, the floe sinks to remain in hydrostatic equilibrium; (2) there is brine percolation in the ice; (3) the surface floods as the floe sinks; and (4) if the flooded snow freezes into ice, then there would be 68 cm of snow–ice formation at this site. This would double the initial ice thickness of 67 cm. In contrast, there was only 20 cm of snow accumulation at the buoy in 2002 and no evidence of snow ice formation.

There was little growth (< 5 cm) at the bottom of the ice in either year. The bottom record from 2001 is limited, since the under-ice sensor failed midway through the experiment. However, to this point there had been no bottom ice growth and approximately 5 cm of bottom ablation. In addition, the temperature profiles exhibited very weak thermal gradients limiting ice growth. The 2002 bottom sensor record is complete and shows no bottom growth and two periods of significant bottom ablation. The first was between 1 November and 11 November, when the ice thinned by 13 cm from 49 to 36 cm. The second was the final melting of the floe, which began on 25 November, ending with the demise of the buoy on 2 December 2002. Overall the buoy results indicate that there was little columnar ice growth, but there was considerable slush formation with some snow–ice formation.

Ice production in Marguerite Bay was similar to that found in other Antarctic sea-ice regions. There was a highly variable mix of granular and columnar ice, but overall a preponderance of granular ice. The granular ice was primarily frazil, but snow–ice was significant, comprising from 0% to 41% of individual cores and 15% overall. Ice production was strongly influenced by the snow cover. Deep snow resulted in negative freeboard, surface flooding, and the formation of slush and snow–ice. Surface flooding stopped the growth of columnar ice at bottom of the ice. In some cases there was even bottom ablation, which tended to reduce the relative amount of columnar ice.

3.3. Percolation in the ice

When the brine volume of the ice exceeds a critical threshold of 5%, the sea ice becomes permeable enough that percolation can occur and the transport of brine within the ice matrix is greatly enhanced (Golden et al., 1998; Golden, 2001). This transport is of great importance, as it contributes to the flooding of the ice surface as well as affecting the distribution of nutrients within the ice. The ice core measurements of temperatures and salinities along with the computed brine volumes provide insight on the amount of ice above the percolation threshold. Even though air temperatures were cold during the cruises, the combination of deep snow and thin ice resulted in warm temperatures throughout the ice. As was noted earlier, ice salinities were large, typically ranging from 5 to 9 psu. The brine volumes of the ice sampled were typically above the critical percolation threshold regardless of the ice thickness or crystallography. For example, the ice crystallography of the three cores in Fig. 7 was quite different, but their temperatures, salinities, and consequently brine volumes were similar. The three cores were above the percolation threshold at all depths. Analyzing the brine volume profiles from all the ice cores showed that in 2001 the mean brine volume was 12.9%, with a range from 2.9% to 31.5%. Results from 2002 were roughly comparable, with a mean brine volume of 16% and a range from 1% to 37%. Most important, in 2001, 95% of the ice sampled was above the critical threshold and 97% was above in 2002.

The mass balance buoys were used to extend the percolation data set. When the buoys were installed the ice salinities ranged from 5 to 10 psu. The ice temperatures measured by the buoys were used to calculate the brine volume, with the assumption that the initial ice salinity profile did not change appreciably over time. From August to December, air temperatures typically ranged from −20 to 0 °C, with changes

of 15 °C in a day common. Even though air temperatures were as cold as −20 °C, temperatures in the ice were warm in both years, ranging from 0 to −6 °C as a result of the combination of thin ice and deep snow. From mid-September on, ice temperatures were never colder than −2.5 °C. These temperatures translated to brine volumes ranging from 5% to 30%. The brine volumes were above 5% percolation threshold throughout the ice for the entire lifetime of the buoys. The in situ measurements and the results from the autonomous buoys indicate that the vast majority of the ice sampled in the Marguerite Bay region in late winter and early spring was above the percolation threshold, allowing rapid transport of brine, and of nutrients, within the ice matrix.

4. Discussion

Two-thirds of the cores had some snow–ice and 15% of the ice sampled in 2001 was snow–ice, i.e., an average of ~10 cm in a core of ~60-cm length. Although significant, the high incidence of surface flooding at the time of observation (40%) suggests snow–ice formation is potentially higher. This is also seen by the mass balance buoy observations where flooding and warm temperatures coupled with more than 1 m of snow accumulation showed that an additional 67 cm of snow was flooded at that location. As well, we found that for 95% of the ice sampled at other locations, the combination of warm ice temperatures and large salinities resulted in brine volumes that were greater than the percolation threshold of 5%. Time series from the autonomous mass balance buoys confirmed that high temperatures, consistent with percolation and surface flooding, prevailed at the ice surface throughout late winter and spring.

In comparison, the Weddell Sea pack ice has substantially different character for both the older ice in the western Weddell Sea and the first-year ice in the eastern Weddell Sea. In the eastern part, intermittent flooding is observed during winter. Ice surface temperatures cycle between just above and just below percolation in the winter there (Golden et al., 1998). This case leads to cycling of flooding and snow–ice formation on periods of a few days as air temperature rises and falls with the storm cycle. Coupled with this flooding is the melting of ice from the bottom because of upwelled ocean heat flux (McPhee et al., 1996). This coupled cycle of melting from below (keeping the freeboard near zero) and freezing of flooded snow from the top can lead to the whole vertical profile being composed of snow–ice (Lytle and Ackley, 2001), i.e. 100% snow–ice rather than the 15% snow–ice we observed here.

In the western Weddell Sea, a cold extreme is observed. Ice lasting through the summer has flooded surfaces that freeze up quickly in fall. The freezeup institutes convective overturning of seawater in the near-surface ice and the upwelling of nutrients in the seawater triggers a fall algal bloom in the ice near the surface. Once frozen, however, ice surface temperatures there are below the percolation threshold until well into spring (Lytle and Ackley, 1996). Snow–ice formation is therefore limited to the fall freezeup with no percolation in the winter because of low temperatures, followed by flooding in late spring. No additional snow–ice formation takes place then because of the general increase in air temperatures assisted by high incident solar radiation after the equinox. Instead, some melting in the snow leads to the formation of superimposed ice on the top of the flooded seawater layer (Haas et al., 2001).

The Western Antarctic Peninsula sea ice can therefore be considered as the "warm end member" in the spectrum of flooding and snow–ice formation in the Antarctic sea ice zone. The combination of thin ice, enough snow, and cold air temperatures that allow snow–ice formation apparently exists only in the late fall–early winter period, leading to flooding and snow–ice formation accumulating to the 15% of the vertical ice cover observed in our core profiles. In mid-late winter, heavy snowfall continues to depress the surface below sea level (e.g., >1 m at the mass balance buoy site) and leads to substantial flooding, for example, an additional 67-cm-thick flooded layer at the mass balance site. At the same time, however, the slightly warmer air temperatures and increased snow depth keep ice surface temperatures high enough to prevent additional snow ice formation and to also allow continuous

flooding (as observed where 95% of the ice cover is above the percolation threshold).

The extended "spring" of the WAP sea ice, in having a substantial flooded layer from early August to December, can lead to higher sustained levels of algal production in the snow–ice community (Ackley and Sullivan, 1994) than observed elsewhere in the Antarctic sea ice. Access to this algal production by juvenile krill also may be better here than elsewhere because of the substantially porous nature of the ice, indicated by its high percentage above the percolation threshold.

6. Conclusions

At the beginning of this paper, three questions were posed concerning the ice morphology, the formation processes of the ice, and percolation in the ice. The sea ice in this region can be considered as the "warm end member" in the spectrum of flooding and snow–ice formation in the Antarctic sea ice zone. In the late fall–early winter period there is a combination of thin ice, enough snow, and cold air temperatures leading to flooding and snow–ice formation, accumulating to the 15% of the vertical ice cover observed in our core profiles. In mid-late winter, heavy snowfall continues to depress the surface below sea level and leads to substantial flooding. However, the slightly warmer air temperatures and increased snow depth keep ice surface temperatures high enough to prevent additional snow–ice formation and to allow continuous flooding (as observed where 95% of the ice cover is above the percolation threshold). There was considerable interannual variability in ice thickness, with average values of 62 cm in 2001 and 102 cm in 2002. The mean snow depth was 16 cm in 2001 and 21 cm in 2002. At 40% of the thickness holes in 2001 and 17% in 2002, a combination of deep snow and thin ice resulted in negative freeboard and surface flooding.

A stratigraphic analysis of ice thin sections showed that more than half of the ice cover was granular and that virtually all of the upper 20 cm of the ice cover was granular. There was little bottom ice accretion observed, even though air temperatures were as cold as −20 °C. There were indications that snow–ice formation at the surface contributed significantly to ice formation. At most sites the base of the snow cover was wet and saline, indicating flooding. A $\delta^{18}O$ analysis of ice cores taken in 2001 indicated that 15% of the samples had negative values, implying that the sample was snow–ice. Between August and November 2001, mass-balance buoy results indicated over 1 m of snowfall, resulting in considerable snow–ice formation.

Ice core observations indicated that, as a result of a combination of warm ice temperatures and large salinities, brine volumes were typically greater than the critical percolation threshold of 5%. Over 95% of the ice sampled was in a percolation regime, creating the potential for rapid transport of brine and nutrients within the ice matrix. Also, results from the mass-balance buoys indicated that the ice sampled was always above the percolation threshold from mid-August to early December. Ice above the percolation threshold, combined with negative freeboard, facilitated surface flooding of the sea ice cover.

The description of the sea-ice cover presented in this paper captures much of its character as a habitat. However, even our dense thickness surveys provide only a one-dimensional point-by-point description of the ice. Under-ice video revealed regions where extensive ice rafting created an intricate habitat consisting of a three-dimensional maze of ice pieces and blocks. These regions are difficult to characterize from the surface and are potentially an important component of the under-ice habitat. More work needs to be done using divers and under-ice video to characterize this component in terms of its areal extent and morphological characteristics.

Acknowledgments

This work was funded by the National Science Foundation, Office of Polar Programs Antarctic Program. Special thanks to C. Fritsen, members of the ice sampling team, Raytheon support staff, and the crew of the R.V. *Laurence M. Gould*. We deeply appreciate the constructive and

considerable contributions made by two anonymous reviewers.

References

Ackley, S.F., Sullivan, C.W., 1994. Physical controls on the development and characteristics of Antarctic sea ice biological communities—a review and synthesis. Deep-Sea Research 41, 1583–1604.

Ackley, S.F., Buck, K.R., Taguchi, S., 1979. Standing crop of algae in the sea ice of the Weddell Sea region. Deep-Sea Research 26 (3A), 269–281.

Ackley, S.F., Gow, A.J., Lytle, V.I., Darling, M.N., Yankielun, N.E., 1992. Sea ice investigations on Nathaniel B. Palmer, Cruise 92-2. Antarctic Journal of the United States 27 (5), 87–88.

Ainley, D.G., DeMaster, D.P., 1990. The upper trophic levels in polar marine ecosystems. In: Smith, W.O. (Ed.), Polar Oceanography. Stanford University. Press, San Diego, pp. 599–630.

Allison, I., Qian, S., 1985. Characteristics of sea ice in the Casey Region. ANARE Research Notes 28, 47–56.

Coplen, T.B., 1996. New guidelines for reporting hydrogen, carbon, and oxygen isotope ratio data. Geochemist Cosmochimica Acta 60, 3359–3360.

Daly, K.L., 1998. Physioecology of juvenile Antarctic krill (*Euphausia superba*) during spring in ice-covered seas. In: Lizotte, M.P., Arrigo, K.R. (Eds.), Antarctic Sea Ice: Biological Processes, Interactions and Variability. Antarctic Research Series, Washington, DC, pp. 183–198.

Eicken, H., 1992. The role of sea ice in structuring Antarctic ecosystems. Polar Biology 12, 3–13.

Eicken, H., Lange, M.A., 1989. Development and properties of sea ice in the coastal regime of the southeastern Weddell Sea. Journal of the Geophysical Research 94 (C6), 8193–8206.

Epstein, S., Mayeda, T., 1953. Variations of 18O content of waters from natural sources. Geochemist Cosmochimica Acta 4, 213–224.

Frankenstein, G.E., Garner, R., 1967. Equations for determining the brine volume of sea ice from −0.5 °C to −22.9 °C. Journal of Glaciology 6, 943–944.

Golden, K.M., 2001. Brine percolation and the transport properties of sea ice. Annals of Glaciology 33, 28–33.

Golden, K.M., Ackley, S.F., Lytle, V.I., 1998. The percolation phase transition in sea ice. Science 282 (5397), 2238–2241.

Gow, A.J., Ackley, S.F., Weeks, W.F., Govoni, J.W., 1982. Physical and structural characteristics of Antarctic sea ice. Annals of Glaciology 3, 113–117.

Gow, A.J., Ackley, S.F., Buck, K.R., Golden, K.M., 1987. Physical and structural characteristics of Weddell Sea pack ice. CRREL Report 87–14.

Gow, A.J., Lytle, V.I., Bell, D., Ackley, S.F., 1992. Ice core studies in the western Weddell Sea. Antarctic Journal of the United States 27 (5), 89–90.

Haas, C., Thomas, D.N., Bareiss, J., 2001. Surface properties and processes of perennial Antarctic sea ice in summer. Journal of Glaciology 47 (159), 613–626.

Horner, R., Ackley, S.F., Dieckmann, G.S., Gulliksen, B., Hoshiai, T., Legendre, L., Melnikov, I.A., Reeburg, W.S., Spindler, M., Sullivan, C.W., 1992. Ecology of sea ice biota, 1, Habitat, terminology, and methodology. Polar Biology 12, 417–427.

Jacka, J.H., Allison, I., Thwaites, R., Wilson, J.C., 1987. Characteristics of the seasonal sea ice of East Antarctica and comparisons with satellite observations. Annals of Glaciology 9, 85–91.

Jeffries, M.O., Weeks, W.F., 1993. Structural characteristics and development of sea ice in the western Ross Sea. Antarctic Science 5 (1), 23–25.

Jeffries, M.O., Shaw, R.A., Morris, K., Veazey, A.L., Krouse, H.R., 1994. Crystal structure, stable isotopes ($\delta^{18}O$) and development of sea ice in the Ross, Amundsen, and Bellingshausen Seas, Antarctica. Journal of Geophysical Research 99 (C1), 985–995.

Jeffries, M.O., Li, S., Jana, R.A., Krouse, H.R., Hurst-Cushing, B., 1998. Late winter first-year ice floe thickness variability, seawater flooding and snow–ice formation in the Amundsen and Ross Seas. In: Jeffries, M.O. (Ed.), Antarctic Sea Ice: Physical Processes, Interactions and Variability. American Geophysical Union, Antarctic Research Series, Washington, DC, pp. 89–122.

Jeffries, M.O., Roy Krouse, H., Hurst-Cushing, B., Maksym, T., 2001. Snow–ice accretion and snow cover depletion on Antarctic first year sea ice floes. Annals of Glaciology 33, 51–59.

Lange, M.A., 1988. Basic properties of Antarctic sea ice as revealed by textural analysis of ice cores. Journal of Glaciology 10, 95–101.

Lange, M.A., Eicken, J., 1991. Textural characteristics of sea ice and major mechanisms of ice growth in the Weddell Sea. Annals of Glaciology 15, 210–215.

Lange, M.A., Ackley, S.F., Wadhams, P., Dieckmann, G.S., Eicken, H., 1989. Development of sea ice in the Weddell Sea, Antarctica. Annals of Glaciology 12, 92–96.

Legendre, L., Ackley, S.F., Dieckmann, G.S., Gulliksen, B., Horner, R., Hoshiai, T., Melnikov, I.A., Reeburgh, W.S., Spindler, M., Sullivan, S.W., 1992. Ecology of sea ice biota, 2, Global significance. Polar Biology 12, 429–444.

Lytle, V.I., Ackley, S.F., 1992. Snow properties and surface elevation profiles in the western Weddell Sea. Antarctic Journal of the United States 27 (5), 93–94.

Lytle, V.I., Ackley, S.F., 1996. Heat flux through sea ice in the western Weddell Sea: Convective and conductive transfer processes. Journal of Geophysical Research 101 (C4), 8853–8868.

Lytle, V.I., Ackley, S.F., 2001. Snow–ice growth: A fresh water flux inhibiting deep convection in the Weddell Sea, Antarctica. Annals of Glaciology 33, 45–50.

Marschall, H-P., 1988. The overwintering strategy of Antarctic krill under the pack-ice of the Weddell Sea. Polar Biology 9, 129–135.

assom, R.A., Drinkwater, M.R., Haas, C., 1997. Winter snow cover on sea ice in the Weddell Sea. Journal of Geophysical Research 102 (C1), 1101–1117.

cPhee, M.G., et al., 1996. Antarctic Zone flux experiment. American Meteorological Society 77 (6), 1221–1232.

orison, J.A., Aagaard, K., Falkner, K.K., Hatakeyama, K., Moritz, R., Overland, J.E., Perovich, D.K., Shimada, K., Steele, M., Takizawa, T., Woodgate, R., 2002. North Pole Environmental Observatory delivers early results, EOS. Transactions of the American Geophysical Union 83 (357), 360–361.

OAA Web site, http://polar.wwb.noaa.gov/pub/ice/sh/2001/.

lmisano, A.C., Sullivan, C.W., 1983. Sea ice microbial communities (SIMCO), 1, Distribution, abundance, and primary production of ice microalgae in McMurdo Sound, Antarctica in 1980. Polar Biology 2, 171–177.

erovich, D.K., Elder, B., 2001. Temporal evolution and spatial variability of the temperature of Arctic sea ice. Annals of Glaciology 33, 207–212.

uetin, L.B., Ross, R.M., 1991. Behavioral and physiological characteristics of the Antarctic krill, *Euphausia superba*. American Zoologist 31, 49–63.

uetin, L.B., Ross, R.M., Clarke, A., 1994. Krill energetics: Seasonal and environmental aspects of the physiology of *Euphausia superba*. In: El-Sayed, S.Z. (Ed.), Southern Ocean Ecology: The BIOMASS Perspective. Cambridge University Press, Cambridge, pp. 165–184.

uetin, L.B., Ross, R.M., Fraser, T.K., Haberman, K.L., 1996. Factors affecting distribution and abundance of zooplankton, with an emphasis on Antarctic krill *Euphausia superba*. In: Ross, R.M., Hofmann, E.E., Quetin, L.B. (Eds.), Foundations for Ecological Research West of the Antarctic Peninsula. American Geophysical Union, Antarctic Research Series, Washington, DC, pp. 357–371.

Siegel, V., Loeb, V., 1995. Recruitment of Antarctic krill *Euphausia superba* and possible causes for its variability. Marie Ecology Progress Series 123, 45–56.

Smith, R.C., Baker, K.S., Fraser, W.R., Hofmann, E.E., Karl, D.M., Klinck, J.M., Quetin, L.B., Prezelin, B.B., Ross, R.M., Trivelpiece, W.Z., Vernet, M., 1995. The Palmer LTER: A long-term ecological research program at Palmer Station, Antarctica. Oceanography 8, 77–86.

Sturm, M., Morris, K., Massom, R., 1998. Winter snow cover of the west Antarctic pack ice: Its spatial and temporal variability. In: Jeffries, M.O. (Ed.), Antarctic Sea Ice: Physical Processes, Interactions and Variability. American Geophysical Union, Antarctic Research Series, Washington, DC, pp. 89–122.

Tison, J.L., Haren, J., 1989. Isotropic, chemical, and crystallographic characteristics of first-year sea ice from Breid Bay. Antarctic Science 1, 106–125.

Trivelpiece, W.Z., Fraser, W.R., 1996. The breeding biology and distribution of Adelie Penguins: Adaptations to environmental variability. In: Ross, R.M., Hofmann, E.E., Quetin, L.B. (Eds.), Foundations for Ecological Research West of the Antarctic Peninsula. American Geophysical Union, Antarctic Research Series, Washington, DC, pp. 273–285.

Worby, A.P., 1999. Observing Antarctic Sea Ice: A Practical Guide for Conducting Sea Ice Observations from Vessels Operating in Antarctic Pack Ice. ASPECT CD-ROM.

Worby, A.P., Massom, R.A., Allison, I., Lytle, V.I., Heil, P., 1998. East Antarctic sea ice: a review of its structure, properties, and drift. In: Jeffries, M.O. (Ed.), Antarctic Sea Ice: Physical Processes, Interactions and Variability. American Geophysical Union, Antarctic Research Series, Washington, DC, pp. 41–67.

ELSEVIER

Deep-Sea Research II 51 (2004) 2041–2072

DEEP-SEA RESEARCH
PART II

www.elsevier.com/locate/dsr2

Acoustically-inferred zooplankton distribution in relation to hydrography west of the Antarctic Peninsula

Gareth L. Lawson[a,b,*], Peter H. Wiebe[b], Carin J. Ashjian[b], Scott M. Gallager[b], Cabell S. Davis[b], Joseph D. Warren[c]

[a]*MIT/Woods Hole Oceanographic Institution Joint Program in Oceanography, Woods Hole, USA*
[b]*Biology Department, Woods Hole Oceanographic Institution, Woods Hole, MA 02543, USA*
[c]*Southampton College, 239 Montauk Hwy, Southampton, NY 11968, USA*

Accepted 12 July 2004

Abstract

The relationship between the distribution of zooplankton, especially euphausiids (*Euphausia* and *Thysanoessa* spp.), and hydrographic regimes of the Western Antarctic Peninsula continental shelf in and around Marguerite Bay was studied as part of the Southern Ocean GLOBEC program. Surveys were conducted from the RVIB *N.B. Palmer* in austral fall (April–June) and winter (July–August) of 2001. Acoustic, video, and environmental data were collected along 13 transect lines running across the shelf and perpendicular to the Western Antarctic Peninsula coastline, between 65°S and 70°S. Depth-stratified net tows conducted at selected locations provided ground-truthing for acoustic observations. In fall, acoustic volume backscattering strength at 120 kHz was greatest in the southern reaches of the survey area and inside Marguerite Bay, suggestive of high zooplankton and micronekton biomass in these regions. Vertically, highest backscattering was in the 150–450 m depth range, associated with modified Circumpolar Deep Water (CDW). The two deep troughs that intersect the shelf break were characterized by reduced backscattering, similar to levels observed off-shelf and indicative of lower zooplankton biomass in recent intrusions of CDW onto the continental shelf. Estimates of dynamic height suggested that geostrophic circulation likely caused both along- and across-shelf transport of zooplankton. By winter, scattering had decreased by an order of magnitude (10 dB) in the upper 300 m of the water column in most areas, and high backscattering levels were found primarily in a deep (>300 m) scattering layer present close to the bottom. The seasonal decrease is potentially explained by advection of zooplankton, vertical and horizontal movements, and mortality. Predictions of expected backscattering levels based on net samples suggested that large euphausiids were the dominant source of backscattering only at very particular locations and depths, and that copepods, siphonophores, and pteropods were more important in many locations.
© 2004 Elsevier Ltd. All rights reserved.

*Corresponding author. Tel.: +1 508 289 3649; fax: +1 508 457 2134.
E-mail address: glawson@whoi.edu (G.L. Lawson).

0967-0645/$ - see front matter © 2004 Elsevier Ltd. All rights reserved.
doi:10.1016/j.dsr2.2004.07.022

1. Introduction

Zooplankton play a pivotal role in the antarctic continental shelf ecosystem, providing both a trophodynamic link between phytoplankton and higher predators, and, via their faecal pellets, a mechanism by which newly fixed carbon can be exported from the euphotic zone (Priddle et al., 1992). Historically, much attention has focused on Antarctic krill (*Euphausia superba*) due to its status as a key prey item for many whales, birds, seals, and fishes (Laws, 1985) and as the subject of a commercial fishery (Ichii, 2000). Although less studied, other zooplankton also represent important ecosystem members: copepods, for example, frequently exceed Antarctic krill in abundance and are the main prey of invertebrates, sei whales, and fish (Voronina, 1998), while salps may account for more carbon export to depth than Antarctic krill (Le Fèvre et al., 1998).

High-frequency acoustic sensors are often used in the study of zooplankton distribution, due to their high sampling rates and concomitant ability to survey the entire water column over large areas (Foote and Stanton, 2000). In the Antarctic, acoustic techniques are used routinely to survey the biomass and distribution of Antarctic krill (see review by Hewitt and Demer, 2000), but have been used much less frequently to study other zooplankton taxa (Weeks et al. 1995; Brierley et al., 1998). Substantial progress has been made in discriminating Antarctic krill from other acoustic scatterers that may be present (Madureira et al., 1993; Brierley et al., 1998; Watkins and Brierley, 2002; Hewitt et al., 2003). Historically, however, many Southern Ocean acoustic studies have simply assumed that all volume backscattering strength measurements above some minimum threshold stemmed from Antarctic krill (e.g., Macaulay et al., 1984; Lascara et al. 1999; Nicol et al., 2000). The contribution to acoustic observations from other zooplankton taxa often has been assumed to be negligible, which discards potential information on the biomass and distribution of such taxa, and may result in an overestimation of Antarctic krill abundance.

The continental shelf region in and around Marguerite Bay, west of the Antarctic Peninsula (Fig. 1), is hypothesized to be an important over-wintering ground for Antarctic krill, and may act as a source for the down-stream krill population in the Bransfield Strait and at South Georgia (Atkinson et al., 2001; Fach et al., 2002). Little is known about the winter distribution of Antarctic krill or other zooplankton in this area, however although studies of the nearby Bransfield Strait region have been more numerous (e.g., Siegel 1989; Zhou et al., 1994). In the only previous acoustic survey of the region, Lascara et al. (1999) examined Antarctic krill distribution in Marguerite Bay and the region immediately to the north, and found distinct seasonal variability in biomass and vertical distribution, with krill more abundant and shallower during the summer and spring than fall and winter. The acoustic system employed reached to only 189 m in depth, and so this study was unable to conclude whether the seasonal decrease in biomass resulted from vertical or horizontal movements. Given the dearth of previous studies, the US Southern Ocean GLOBal ECosystems Dynamics (SO GLOBEC) program has targeted austral fall and winter as periods for detailed study of the Marguerite Bay region (Hofmann et al., 2002). The program's primary objective is to understand the physical and biological factors that contribute to Antarctic krill over-wintering success. As such, one goal of the program is to link physical processes with the distribution of Antarctic krill and other members of the zooplankton community, and ultimately with higher predators.

In this paper, we describe measurements of acoustic volume backscattering strength made over most or all of the water column during austral fall and winter of 2001, in relation to hydrography in the vicinity of Marguerite Bay. We then use depth-stratified net samples and taxon-specific models of acoustic target strength to predict the likely sources of acoustic backscattering, with particular emphasis on understanding the contribution of zooplankton taxa other than Antarctic krill. On the basis of these measurements and predictions, we make certain inferences concerning seasonal and spatial variability in zooplankton and micronekton biomass in the region.

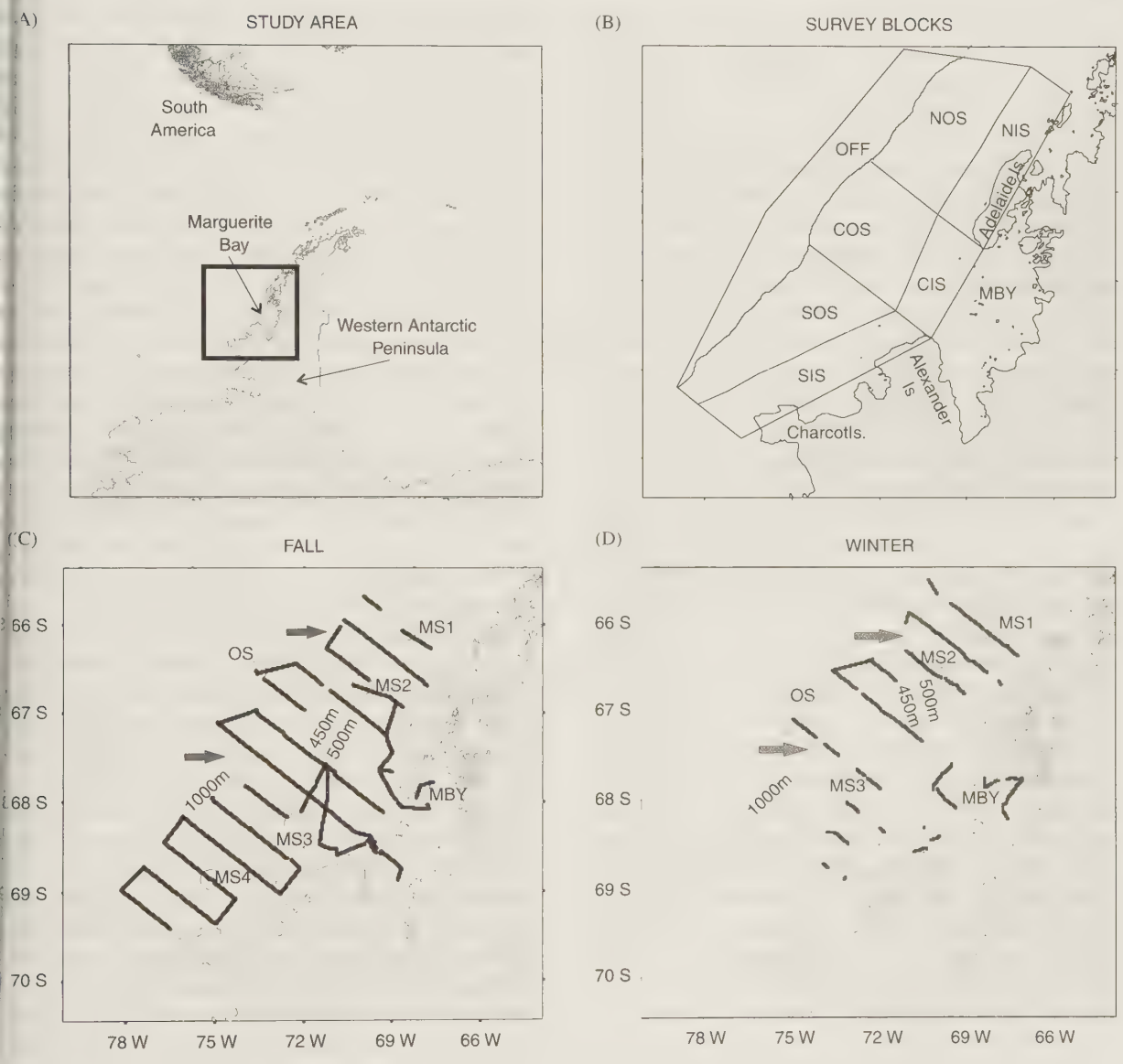

Fig. 1. US SO GLOBEC survey area. Shown are (A) the overall geographical context of the survey area, (B) the location of survey blocks, and the cruise tracks in (C) fall and (D) winter 2001. The latter show only those portions of the overall cruise-track where acoustic data were collected. Note the lower survey coverage in winter relative to fall. Block name abbreviations are: Northern Outer-Shelf (NOS), Northern Inner-Shelf (NIS), Central Outer-Shelf (COS), Central Inner-Shelf (CIS), Southern Outer-Shelf (SOS), Southern Inner-Shelf (SIS), Off-Shelf (OFF), and Marguerite Bay (MBY). Circles indicate where the MOCNESS tows analyzed here were conducted, with tow locations abbreviated as mid-shelf 1-4 (MS1-4), off-shelf (OS), and Marguerite Bay (MBY). Gray arrows show where the deep troughs that run diagonally across the continental shelf meet the shelf break.

2. Methods

2.1. Study area

The US SO GLOBEC Program study site was located on the continental shelf to the west of the Western Antarctic Peninsula, extending from the northern tip of Adelaide Island to the southern portion of Alexander Island and including Marguerite Bay (Fig. 1). Two cruises were conducted in the area on the RVIB *Nathaniel B. Palmer*: an austral fall cruise from April 23 to June 6, 2001 (cruise number NBP0103), and a winter cruise from July 21 to September 6, 2001 (cruise number NBP0104). The fall cruise track was determined by the position of 84 station locations distributed along 13 transect lines running across the continental shelf and perpendicular to the Peninsula coastline. On the winter cruise, eight additional stations were added to the survey grid and the entire grid was shifted south by 2 km so that acoustic mapping of the sea floor would take place over unmapped sea floor. In order to allow spatial comparisons across the region, the overall study area was subdivided into eight functional blocks (Fig. 1B). The survey region first was subdivided from northeast to southwest into three sectors (southern, central, and northern), each of which was divided into inner-shelf (i.e. coastal) and outer-shelf blocks. An off-shelf block was defined as the region beyond the 1000 m isobath, and a final block corresponded to the interior of Marguerite Bay.

2.2. BIOMAPER-II

The BIo-Optical Multi-frequency Acoustical and Physical Environmental Recorder, or BIOMAPER-II, is a towed system designed to conduct quantitative surveys of the spatial distribution of plankton and nekton (Wiebe et al., 2002). The system consists of a multi-frequency echosounder, a Video Plankton Recorder (VPR, Davis et al., 1992), and an environmental sensor package (Conductivity, Temperature, and Depth sensor (CTD); fluorometer; transmissometer). To enhance the performance of the BIOMAPER-II in high sea states, a slack tensioner was used to damp the motion of the ship (see Wiebe et al., 2002 for additional details).

2.2.1. Acoustic data collection

The BIOMAPER-II collected acoustic data from five pairs of transducers, with frequencies of 43, 120, 200, 420, and 1000 kHz. All transducers had 3° half-power beamwidths, with the exception of the 43 kHz transducers, which had beamwidths of 7°. One of each pair of transducers was mounted on the top of the tow-body looking upward, while the other was mounted on the bottom looking downward. This arrangement allowed acoustic data to be collected over most or all of the water column as the instrument was 'towyoed' obliquely up and down through the water column between 20 and 300 m depth. The vessel proceeded along the track-line between stations at 4–6 knots, and surveying was conducted around the clock.

Multi-frequency acoustic data were collected over much of both surveys, although prohibitively thick pack ice in portions of the survey area led to the area surveyed in winter being less than in fall (Figs. 1C and D). Due to episodic malfunctions at the different acoustic frequencies, 120 kHz represents the frequency at which data were collected with the greatest spatial coverage. In order to allow examinations of the seasonal distribution of zooplankton over the broadest scales possible and best complement the scales at which data were collected by other projects conducted during the cruises (e.g., top predator surveys), this paper deals only with acoustic data collected at 120 kHz. Analyses of the multi-frequency data will be the subject of future papers.

Volume backscattering strength, S_v (where $S_v = 10 \log_{10} s_v$ in units of decibels, and s_v is the observed volume backscattering coefficient), is a measure of the intensity of emitted sound that is reflected back to the source per cubic meter. For simplicity, this quantity will be referred to as 'backscattering.' Backscattering is related to both the number and size of scatterers in the path of the incident sound, to the efficiency with which these scatterers reflect sound, and thereby to their taxonomic composition. Although the relationship

tween backscattering and the biomass of scatrers is thus highly complex, we assume that the rge spatial and temporal differences in backattering observed in the present study are related differences in zooplankton and micronekton omass. In the discussion we show how the nfounding influences of animal size, sound attering efficiency, and taxonomic composition, e minimized in this study.

Backscattering data at 120 kHz were collected in 5-m-deep bins, starting at 6 m from the transduer face (the end of the acoustic near-field) and xtending to a maximum range of 300 m from the strument. A 10 kHz bandwidth chirp pulse was sed (Ehrenberg and Torkelson, 2000), with an ffective pulse duration of 0.18 ms, and a ping rate f 0.3 pings s $^{-1}$. The system's dynamic range llowed these data to be collected between −100 nd −40 dB. Profiles of noise levels (ship's noise, mbient noise, and system noise combined) vs. epth were made in situ near the start of each ruise. Backscattering levels in each ping were ompared to these profiles, and those bins where ackscattering did not exceed noise levels were set o zero. Backscattering data were echo-integrated ver 4-ping intervals (i.e., ~35 m along-track).

All transducers were acoustically calibrated by he manufacturer (Hydroacoustic Technologies nc., Seattle, WA, USA) prior to each cruise for ource level, receive sensitivity, as well as transmit nd receive beam patterns. An in situ calibration lso was performed at the end of the winter cruise with a 38 mm tungsten carbide (6% cobalt) standard target, following established practices Foote et al., 1987). This calibration indicated that he standard target was approximately 6 dB lower n the down-looking 120 kHz transducer than it should have been, and the data therefore were corrected for this offset. Although there is no reason to doubt the validity of the calibration, 6 dB is a large correction and it must be noted that he absolute levels of backscattering reported here hus may contain some bias. The relative changes n backscattering that are the focus of this paper nd our conclusions would not be affected by any such bias. After backscattering data were corected for the results of these calibrations, there was evidence of higher backscattering levels observed by the up-looking 120-kHz transducer relative to the down-looking transducer in some portions of the water column (Fig. 2). This discrepancy was particularly evident in low-scattering areas such as the northern portion of the survey area in fall, and much of the continental shelf during winter; in high-scattering areas like Marguerite Bay, no such difference was evident. Furthermore, the enhanced backscattering levels in the up-looking data were restricted to the pycnocline and were especially prominent in regions of rapid vertical changes in density. We believe that these enhancements do not represent scattering from biological sources, but rather represent an as-yet unexplained artifact. They may result from sound reflecting off vortices shed by the tow cable as it passes through the pycnocline. Since the tow cable extends above the towed body, only the up-looking transducer would observe such artifactual backscattering. It therefore was excluded from all quantitative analyses, representing a 7% reduction in data (varying from 0% to 24% on a by-transect basis), primarily between 0 and 200 m.

2.2.2. Acoustic data post-processing

Acoustic data from the up- and down-looking transducers were combined to provide a vertically continuous acoustic record extending from the surface to at least 300 m, and at most 550 m, depending on the position of the BIOMAPER-II along its towyo path. This acoustic record then was edited using custom MATLAB-based routines to remove unwanted returns from the surface bubble layer and the bottom, as well as noise spikes from the ship's engines or ice-breaking.

For many of the following spatial analyses, measurements of integrated backscattering in each 1.5-m depth bin were averaged over 1-km along-track intervals and also over depth, in intervals of 25–100 m (shallow layer), 100–300 m (mid-water layer), and 300–500 m (deep layer). These depth ranges were chosen since the surface bubble layer obscured most measurements shallower than 25 m, the mixed-layer depth was generally around 100 and 300 m represents the depth to which the BIOMAPER-II always made acoustic observations despite being towyoed up and down through

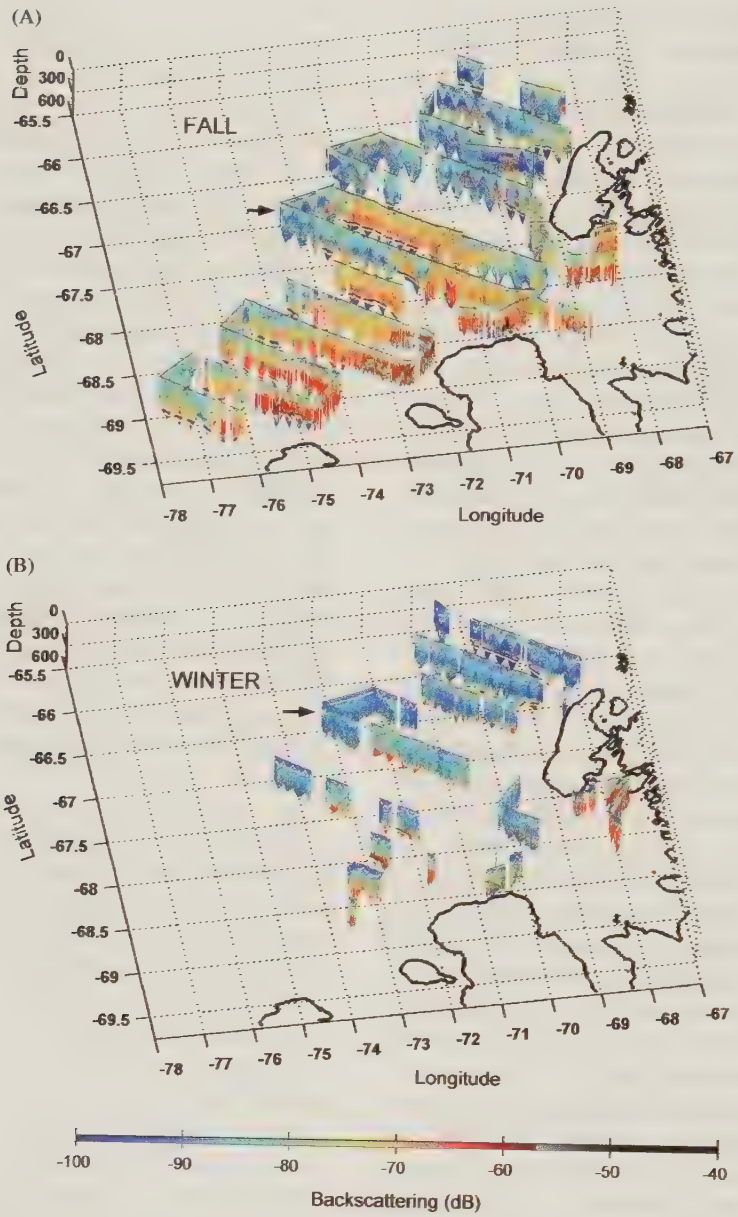

Fig. 2. Acoustic data collected in (A) fall and (B) winter 2001. Backscattering levels are plotted on the color scale in decibels, according to the depth and position of measurement. Blue indicates low levels of zooplankton backscattering, while red to black indicate high levels. High backscattering near the surface corresponds to the surface bubble layer. Strong (i.e. black) returns at depth are from the strongly reflecting bottom. Both the bottom and surface layer were edited out for quantitative analyses. The V-shape of the maximum depth of observation is due to the BIOMAPER-II being towyoed up and down through the water column as the vessel proceeded along-track. Arrows indicate typical regions of the pycnocline where enhanced backscattering measured by the up-looking transducer (i.e. in the upper portion of the towyo's V) was believed to represent an artifact rather than scattering from biological sources.

e water column. These averages, as well as all her simple descriptive statistics, were calculated ing the arithmetic form of backscattering (s_v). ne arithmetic form also was used in between-ock statistical comparisons, since the tests nployed were rank-based (see below) and so sensitive to whether the data were transformed not. The decibel form of backscattering (S_v) was ed in regression analyses, since this test is arametric and the log-transformed data better proximated a normal distribution. The decibel rm is also used in figures and in the text.

3. Environmental analyses

Acoustic data were combined with environmen-l data to examine the association of back-cattering with environmental properties and ater masses. Depth, temperature, conductivity, uorescence, and transmissometry data were ollected by the BIOMAPER-II along its towyo ath at 4-s intervals. In order to provide details of he environmental structure at greater depths than ampled by the towed body, however, data from TD casts made at the survey stations by Klinck t al. (2004) were used as the primary source for uantitative analyses. The CTD rosette package nade measurements of salinity, fluorescence, ransmittance, photosynthetically active radiation PAR), potential temperature, and oxygen con-entration at 1-m depth intervals from the surface o between 5 and 20 m off the bottom. In analyses f backscattering in relation to environmental conditions, each environmental measurement was associated with the acoustic measurement aver-aged in 1-km intervals made nearest to that depth and location.

2.4. MOCNESS

A 1-m^2 Multiple Opening/Closing Net and Environmental Sensing System (MOCNESS; Wiebe et al., 1985) was used to sample the zooplankton at selected stations distributed throughout the survey grid (24 locations in fall and 17 in winter). The MOCNESS was equipped with nine 335-μm mesh nets, a suite of environmental sensors including temperature, conductivity, fluorescence, and light transmission, and a strong strobe light, that flashed at 4-s intervals. The rationale behind the strobe system was to shock or blind the animals temporarily so that the net would not be perceived and avoided, and catches of large euphausiids were significantly enhanced when using the strobe (Sameoto et al., 1993; Wiebe et al., 2004). The MOCNESS was towed obliquely from near-bottom to the surface, sampling eight depth intervals on the up-cast. The deepest tows sampled to 1000 m. Typically, the upper 100 m were sampled in 25-m intervals, with 50-m intervals at intermediate depth ranges, and greater intervals (150- or 200-m) for the deepest depth ranges (see Ashjian et al., 2004, for additional details). The depth-specific samples were preserved upon recovery in 4% buffered formalin.

The size distributions of plankton for six MOCNESS tows from each of the two cruises have been analyzed to date (Ashjian et al., 2004). Following the nomenclature of Ashjian et al. (2004), tow locations will be referred to as off-shelf, Marguerite Bay, and mid-shelf 1–4 (Figs. 1C,D). Note that no acoustic data were collected in the vicinity of the winter mid-shelf 4 site. Lengths of individuals of each sampled taxon were determined for an aliquot of each net sample using the silhouette method of Davis and Wiebe (1985).

2.5. Taxonomic composition of zooplankton and micronekton

The ultimate goal of our research is to use VPR observations and taxon-specific differences in backscattering at increasing frequencies, in addition to net catches, to partition accurately our measurements of backscattering among taxonomic groups, and then to make biomass estimates for each taxon. Here, we make preliminary inferences concerning the sources of acoustic backscattering measurements by conducting the forward problem: an exercise where predictions are made of expected levels of backscattering based on MOCNESS catches and models of the backscattering from individual sampled animals (Wiebe et al., 1996). By comparing these predictions to observed

backscattering levels, it is possible to assess whether the animals collected by the nets could account for measured levels of backscattering. Provided that this assessment is favorable, inferences can then be made about the likely relative contributions of different taxa to observed backscattering levels in the vicinity of each tow.

In addressing the forward problem, predicted backscattering levels for each depth stratum sampled by the MOCNESS were calculated as the linear (i.e. incoherent) sum of expected echo intensities from each captured animal. Expected echo intensities, or backscattering cross-sections $\langle \sigma_{bs} \rangle$ were estimated based on the length of each individual determined by silhouette analysis and models of acoustic scattering appropriate to the individual's taxonomic group. These models were developed by Stanton et al. (1994, 1998), are reviewed in Stanton and Chu (2000), and are sensitive to numerous parameters in addition to animal length, including animal orientation and material properties (Chu et al., 2000; Table 1). Discrete values were used for all parameters other than animal orientation (Table 1). For the latter, scattering from each animal was averaged over some distribution of orientations, to allow for the fact that the animals are oriented at a range of angles as they move through the water.

Estimates of expected backscattering cross-sections for each *j*th individual were summed over all individuals in each *i*th taxon and then over all taxa to yield an estimate of the total expected volume backscattering strength (S_v, in dB) in the volume (V) defined by the depth range sampled by each *k*th net:

$$S_{v_k} = 10 \log_{10} \left[\frac{1}{V_k} \sum \sum \langle \sigma_{bs} \rangle_{ij} \right].$$

Since the BIOMAPER-II and the MOCNESS could not be towed concurrently, comparisons of predicted backscattering levels could not be made to observations of backscattering made at the identical time and location. Comparisons were thus made to acoustic observations made in the appropriate depth interval and averaged over a spatial area within no more than 17 km of each of the 11 MOCNESS tows. At all but two MOCNESS tow locations, acoustic data were collected within no more than 5 h of the net tow as the vessel approached or departed the station. At the mid-shelf 1 and 2 stations in winter, however, MOCNESS tows and acoustic data collection were separated in time by approximately four weeks due to instrument problems. Predictions of backscattering from each taxon were still calculated based on these tows, in order to shed light on the sensitivity of the predicted to observed backscattering comparison to temporal variation.

3. Results

Backscattering during fall generally was enhanced within Marguerite Bay and in the southern portion of the survey area (Fig. 2A). Large subsurface patches of intensified backscattering that stood out markedly from background scattering levels were observed primarily in coastal regions of complex bathymetry, and at depth in the northern portion of the continental shelf. The term 'patch' is used here to denote a recognizable feature in the acoustic record, but does not imply any particular aggregative behavior on the part of the zooplankton or micronekton comprising these features. Smaller such patches also were evident within the mixed layer across the shelf. In winter, the most striking feature was a dramatic decrease in backscattering relative to fall levels throughout most of the water column (Fig. 2B); backscattering in winter was high only within Marguerite Bay and in the bottom scattering layer, which was present on both cruises.

3.1. Environmental setting

The continental shelf in this region is characterized by intrusions of oceanic Circumpolar Deep Water (CDW; salinity (S) 34.6–34.74, potential temperature (θ) 1.0–2.0 °C), pumped up onto the shelf at depth by the action of the Antarctic Circumpolar Current (see Klinck et al., 2004; and Smith et al., 1999, for further water mass definitions and descriptions of hydrography). As this warm and salty CDW interacts with cooler and fresher shelf waters, it forms a water mass that has been referred to as modified-Circumpolar Deep

ater (mCDW, *sensu* Hofmann and Klinck, 1998; 34.0–34.6, θ −1.8 to 1.5 °C). Such mCDW was e primary water mass observed through the rcnocline and below in the study area, often with DW present at greater depths (Table 2). During l, the water column at shallow depths contained ntarctic Surface Water (AASW, Table 2; S .0–33.7, θ −1.5 to 1.0 °C). In winter, AASW as mostly replaced near the surface in all survey ocks by Winter Water (WW; S 33.8–34.1, θ −1.8 − 1.5 °C). Water properties differed between gions. The mCDW found during fall in the more rthern and more offshore blocks was generally armer and saltier (i.e. less-modified) than elsehere in the study area, suggesting more recent trusions of CDW onto the shelf. The more astal regions typically had warmer and fresher ASW present at shallow depths, particularly in larguerite Bay.

2. Vertical distribution of backscattering

Seasonal and spatial differences were observed n the vertical distribution of backscattering Fig. 3). In fall, backscattering was strongest etween 150 and 450 m in all of the inner-shelf nd southern blocks. Scattering in the northern nd central outer-shelf blocks was more constant ith depth. A slight enhancement in backscatterng was observed in all blocks at shallower depths 15–95 m, depending on block), corresponding o the influence of episodic patches of high ackscattering present within the mixed layer. he decrease in backscattering from fall to winter as also evident in the vertical distribution of ackscattering. Backscattering throughout the pper 300 m of the water column in winter was ery low in all blocks except Marguerite Bay nd the two southern blocks. Below 300 m, owever, backscattering generally increased rapidly, and in all but one block reached evels higher than those observed at comparable depths during fall. This increase at depth was due to the influence of the deep scattering layer associated with the bottom, which was present during both surveys, but more intense in winter (Fig. 2).

3.3. Horizontal distribution of backscattering

The horizontal distribution of backscattering was examined via comparisons between geographically defined spatial blocks and spatial interpolations of backscattering data between transect lines using linear kriging (Chu, 2000; Fig. 4). During fall, backscattering in the mid-water (100–300 m) and bottom (300–500 m) depth ranges spatially averaged over 1-km intervals differed significantly between survey blocks (Kruskal-Wallis non-parametric one-way analysis of variance (Sokal and Rohlf, 2000), $\chi^2 = 809$, $p < 0.001$, $n = 1932$, and $\chi^2 = 573$, $p < 0.001$, $n = 1030$, respectively; Table 2), with highest levels in the southern inner-shelf and Marguerite Bay and lowest off-shelf (Tukey-Kramer post-hoc tests (Sokal and Rohlf, 2000), $p < 0.05$). Within the shallow layer (25–100 m), backscattering was reduced relative to the deeper layers, but showed similar enhancements in coastal areas, as well as significant differences between blocks ($\chi^2 = 367$, $p < 0.001$, $n = 1385$).

Marguerite Trough is the deep trough that cuts diagonally across the continental shelf, meeting the shelf break at approximately 66.5°S (Figs. 1C,D and 4A,C); interpolations show that backscattering at depth was very low in the vicinity of this meeting point. A second trough meets the shelf break at approximately 67.75°S (Fig. 1C,D). Backscattering near this point was very low in the 100–300 m depth range, and reduced relative to nearby levels in the 300–500 m range. Hydrographic observations suggest that CDW intrudes on to the shelf at these locations (Figure 9 in Klinck et al., 2004; Dinniman and Klinck, 2004); the low observed backscattering levels are suggestive of low zooplankton biomass in these recently intruded waters. Contours of dynamic height relative to 400 m calculated by Klinck et al. (2004) indicate a cyclonic gyre situated in the northern portion of the survey area, and a coastal current moving along the shelf towards the southwest (Fig. 4E). Enhanced backscattering was evident in all three depth ranges at the southern end of this gyre, where water was flowing in an offshelf direction. Scattering also was enhanced in the vicinity of the coastal current off Alexander Island.

Table 1
Scattering models employed in forward calculations of backscattering levels expected based on MOCNESS catches

Taxon	Scattering model (Ref. in parentheses)	Parameter values		
		Orientation (Ref.)	Density contrast (g) (Ref.)	Sound speed contrast (h) (Ref.)
Copepods*	Distorted-Wave Born Approximation (DWBA)-Based Fluid-Like Deformed Cylinder (1)	N(0,30)	1.02 (7)	1.058 (14)
Large Euphausiids* and Mysids (>15 mm)	DWBA Deformed Cylinder (1)	N(20,20) (6)	$g = 5.485 \times 10^{-4} \times \mathrm{L(mm)} + 1.002$ (8)	$h = 5.942 \times 10^{-4} \times \mathrm{L(mm)} +$ 1.004 (8)
Small Euphausiids and Mysids (<15 mm)	DWBA Deformed Cylinder (1)	N(20,20) (6)	1.016 (8)	1.019 (8)
Amphipods	DWBA Deformed Cylinder (1)	N(0,30)	1.058 (9)	1.058 (9)
Chaetognaths and Polychaetes	DWBA Deformed Cylinder (1)	N(0,30)	1.03 (7)	1.03 (7)
Ostracods	DWBA Deformed Cylinder (1)	N(0,30)	1.03 (7)	1.03 (7)
Fish	DWBA Deformed Cylinder (1)	N(0,30)	1.03 (7)	1.03 (7)
Salps*	DWBA Deformed Cylinder (1)	N(0,30)	1.004 (10)	1.004 (10)
Gymnosome Pteropods	DWBA Deformed Cylinder (1)	N(0,30)	1.03 (7)	1.03 (7)
Larval Crustaceans	DWBA Deformed Cylinder (1)	N(0,30)	1.058 (9)	1.058 (9)
Eggs	High-Pass Fluid Sphere (2)	—	0.979 (11)	1.017 (11)
Thecosome Pteropods (*Limacina* spp.)*	High-Pass Fluid Sphere (2)	—	1.732 (10)	1.732 (10)
Radiolarians	High-Pass Fluid Sphere (2)	—	2.147 (12)	3.979 (12)
Medusae*	DWBA-based Model of Two Spheroidal Interfaces (3)	Broad-side only	1.02 (3)	1.02 (3)
Siphonophore Bracts and Nectophores	Scattering proportional to the volume of a fluid-filled sphere of equivalent volume (4)		1.02 (7)	1.02 (7)
Siphonophore Pneumatophores*	Carbon Monoxide-filled Sphere (5)	—	$g = g_{\mathrm{surface}}(1 + 0.1\mathrm{Depth(m)})$, where $g_{\mathrm{surface}} = 0.0012$ (13)	0.22 (15)

Asterisks (*) indicate those models that have been validated through comparisons of model predictions to laboratory measurements of scattering from the animal of interest; elsewhere, models were deemed appropriate on the basis of what is known about the animal's physical structure, but not on experimental verifications. Each model involves a number of parameters, describing the animal's shape, orientation, and acoustic material properties. The latter include the ratio of the animal's density to that of the surrounding water (g) and the ratio of the speed of sound in the animal to that in the surrounding water (h). Parameter values were drawn from a number of sources. All necessary shape parameters (e.g., length:width and length:volume ratios) were measured empirically for a sub-sample of captured animals. An average backscattering cross-section was calculated for each animal, based on a distribution of orientations. Where there was little or no information available on orientation, a normal distribution with a mean of 0° and a standard deviation of 30° was assumed (i.e. N(0,30)), where an angle of 0° indicates sound striking the animal in dorsal aspect. The taxa listed constituted the majority of sampled animals. Certain rare taxa (<3% of net abundance) were excluded from forward calculations; these included

thecosome *Styliola*-like pteropods, foraminifera, larval polychaetes, and ctenophores. Sensitivity analyses using scattering models for taxa comparable to these rare animals suggested that they were very minor contributors to overall backscattering levels (not shown).

(1) Equation (5) of Stanton et al. (1998), and see Stanton and Chu (2000) and references therein.

(2) Equation given in Stanton et al. (1994), p. 507.

(3) D. Chu. Unpublished Data.

(4) D. Chu. and A. Lavery, Pers. Comm.; Fluid-filled sphere model is derived from Anderson (1950).

(5) Derived from Anderson (1950).

(6) Chu et al. (1993).

(7) D. Chu. Pers. Comm.

(8) D. Chu. Unpublished Measurements; preliminary descriptions of results are found in US SO GLOBEC (2002). Measurements were performed only on animals larger than 20 mm.For animals smaller than this length (e.g., the 'small euphausiid' category), the g and h predicted by the regression equations for a 20 mm animal were assumed to apply.

(9) Inferred for shrimp based on model-fits to direct observations by Stanton et al. (1994), and very comparable to values measured by Chu et al. (2000) for the decapod shrimp *Palaemonetes vulgaris*. Assumed here to also apply to certain other crustacean taxa.

(10) Inferred based on model-fits to empirical observations, Stanton et al. (1994).

(11) Measured by Chu et al. (2003).

(12) Based on the density and sound speed of fused silica ($2.2\,g\,m^{-3}$ and $5968\,m\,s^{-1}$, respectively), and assuming the speed of sound in seawater is $1500\,m\,s^{-1}$, and the density of seawater is $1.025\,g\,m^{-3}$.

(13) A. Lavery. Pers. Comm.; based on pressure-related increases in density and thereby g in depth (Medwin and Clay, 1998). $g_{surface}$ is the density contrast for carbon monoxide at the surface (1 atmospheric pressure).

(14) Measured by Chu et al. (2000) for Gulf of Maine calanoid copepods.

(15) Sound speed contrast for carbon monoxide at surface pressure of 1 atmosphere.

Table 2
Between-block comparisons of environmental properties and backscattering

Block	Pot. temperature (Std Deviation)			Salinity			Mean (dB), Median (dB), and CV of backscattering			Day vs. night mean backscattering (dB)		
	25–100 m	100–300 m	300–500 m	25–100 m	100–300 m	300–500 m	25–100 m	100–300 m	300–500 m	25–100 m	100–300 m	300–500 m
Fall												
Northern Outer-Shelf	−0.84 (0.43)	1.02 (0.65)	1.44 (0.11)	33.95 (0.21)	34.57 (0.13)	34.71 (0.01)	Mean = −76.2 Med = −80.1 CV = 3.09	Mean = −70.9 Med = −76.1 CV = 1.33	Mean = −75.8 Med = −78.2 CV = 1.29	D = −74.4 N = −79.2	D = −70.5 N = −70.7	D = −74.3 N = −77.9
Northern Inner-Shelf	−0.33 (0.50)	0.70 (0.62)	1.37 (0.05)	33.74 (0.25)	34.45 (0.23)	34.69 (0.02)	Mean = −78.6 Med = −79.7 CV = 0.76	Mean = −68.6 Med = −72.8 CV = 1.49	Mean = −71.0 Med = −73.6 CV = 1.53	D = −79.4 N = −78.0	D = −69.1 N = −68.5	D = −72.6 N = −70.8
Central Outer-Shelf	−1.02 (0.26)	0.68 (0.81)	1.47 (0.08)	33.92 (0.19)	34.51 (0.16)	34.70 (0.01)	Mean = −72.2 Med = −73.2 CV = 0.88	Mean = −69.7 Med = −70.1 CV = 0.78	Mean = −67.8 Med = −68.4 CV = 0.72	D = −72.4* N = −71.8	D = −70.1* N = −69.4	D = −69.5* N = −67.2
Central Inner-Shelf	−0.44 (0.44)	0.49 (0.55)	1.27 (0.13)	33.74 (0.23)	34.38 (0.23)	34.67 (0.04)	Mean = −74.7 Med = −77.5 CV = 0.86	Mean = −64.6 Med = −71.2 CV = 4.52	Mean = −68.3 Med = −72.8 CV = 2.71	D = −72.0* N = −76.4	D = −59.2* N = −70.8	D = −65.1* N = −71.0
Southern Outer-Shelf	−1.24 (0.30)	0.09 (0.95)	1.31 (0.17)	33.75 (0.22)	34.40 (0.19)	34.68 (0.03)	Mean = −75.2 Med = −76.7 CV = 0.85	Mean = −69.6 Med = −70.6 CV = 0.90	Mean = −67.8 Med = −69.1 CV = 0.88	D = −76.8* N = −74.7	D = −70.4 N = −69.2	D = −68.4 N = −67.5
Southern Inner-Shelf	−0.99 (0.29)	−0.20 (0.64)	0.91 (0.16)	33.52 (0.23)	34.23 (0.23)	34.58 (0.05)	Mean = −71.0 Med = −74.0 CV = 2.42	Mean = −59.9 Med = −63.5 CV = 2.03	Mean = −64.2 Med = −64.1 CV = 0.46	D = −73.0 N = −70.3	D = −56.4 N = −62.9	D = −64.4 N = −64.1
Marguerite Bay	−0.42 (0.27)	0.38 (0.44)	1.07 (0.13)	33.48 (0.09)	34.28 (0.29)	34.61 (0.04)	Mean = −71.4 Med = −75.1 CV = 1.88	Mean = −67.4 Med = −67.6 CV = 0.49	Mean = −65.4 Med = −65.5 CV = 1.31	D = −77.4 N = −71.2	D = −71.4 N = −67.4	D = N.D. N = −65.3
Off-shelf	−1.05 (0.53)	1.11 (1.03)	1.78 (0.20)	33.92 (0.19)	34.51 (0.15)	34.69 (0.02)	Mean = −78.9 Med = −79.2 CV = 0.61	Mean = −73.2 Med = −77.0 CV = 1.25	Mean = −74.9 Med = −77.6 CV = 0.46	D = −77.7* N = −79.8	D = −77.2 N = −72.3	D = −73.7 N = −76.0

Winter

Northern Outer-Shelf	−1.70 (0.30)	0.90 (0.79)	1.49 (0.14)	33.96 (0.07)	34.22 (0.16)	34.71 (0.02)	Mean = −79.9 Med = −83.5 CV = 2.74	Mean = −82.7 Med = −83.4 CV = 0.66	Mean = −73.9 Med = −77.3 CV = 1.39	D = −82.9* N = −78.8	D = −83.6* N = −82.3	D = −74.0 N = −73.7
Northern Inner-Shelf	−1.08 (0.84)	0.77 (0.58)	1.45 (0.04)	33.98 (0.17)	34.49 (0.16)	34.69 (0.01)	Mean = −84.2 Med = −86.9 CV = 1.10	Mean = −81.5 Med = −85.5 CV = 1.64	Mean = −74.2 Med = −74.7 CV = 0.72	D = −84.3 N = −83.9	D = −86.2 N = −79.9	D = −74.9 N = −72.1
Central Outer-Shelf	−1.51 (0.40)	0.78 (0.65)	1.36 (0.06)	33.92 (0.12)	34.53 (0.16)	34.70 (0.05)	Mean = −83.4 Med = −84.5 CV = 1.07	Mean = −78.6 Med = −79.4 CV = 0.68	Mean = −65.7 Med = −65.9 CV = 0.45	D = −87.2* N = −83.0	D = −79.1 N = −78.0	D = N.D. N = −65.5
Central Inner-Shelf	−1.50 (0.39)	0.80 (0.66)	1.38 (0.04)	33.90 (0.11)	34.52 (0.17)	34.70 (0.01)	Mean = −78.4 Med = −84.8 CV = 4.66	Mean = −77.6 Med = −80.8 CV = 1.92	Mean = −74.6 Med = −77.6 CV = 0.94	D = −83.5* N = −75.5	D = −74.1 N = 79.2	D = −71.1 N = −76.9
Southern Outer-Shelf	−1.68 (0.22)	0.31 (0.68)	1.24 (0.08)	33.79 (0.07)	34.40 (0.20)	34.67 (0.02)	Mean = −88.4 Med = −91.5 CV = 1.18	Mean = −73.0 Med = −75.7 CV = 1.00	Mean = −61.8 Med = −61.2 CV = 0.47	D = −91.2 N = −85.6	D = −76.1 N = −69.1	D = −62.3 N = N.D.
Southern Inner-Shelf	−1.62 (0.22)	–		33.78 (0.05)		-	Mean = −81.6 Med = −80.6 CV = 0.72	Mean = −71.0 Med = −71.1 CV = 0.42	Mean = −67.2 Med = −67.8 CV = 0.80	D = N.D. N = −81.6	D = N.D. N = −71.0	D = N.D. N = −67.2
Marguerite Bay	−1.54 (0.35)	0.53 (0.58)	1.16 (0.04)	33.70 (0.12)	34.39 (0.24)	34.64 (0.01)	Mean = −78.6 Med = −82.5 CV = 1.18	Mean = −64.5 Med = −64.5 CV = 0.57	Mean = −61.3 Med = −61.7 CV = 0.59	D = −85.7* N = −76.9	D = −64.5 N = −64.2	D = −62.3 N = −60.5
Off-shelf	−1.56 (0.76)	0.77 (1.15)	1.71 (0.22)	33.97 (0.12)	34.47 (0.20)	34.69 (0.04)	Mean = −83.7 Med = −85.2 CV = 1.95	Mean = −82.6 Med = −82.6 CV = 0.45	Mean = −78.7 Med = −79.5 CV = 0.53	D = −85.2* N = −82.1	D = −83.5* N = −81.8	D = −78.5 N = −80.8

Mean potential temperature and salinity are shown, with standard deviations in parentheses. Mean, median, and coefficient of variation (CV) of backscattering were all calculated from backscattering measurements (arithmetic form, s_v) averaged over 1-km spatial intervals, and then over the three depth layers. Comparisons were made of mean day (D) and night (N) backscattering levels. In some cases, no data (N.D.) were collected during one or the other of the day/night periods in a given block. Asterisks (*) indicate instances where day backscattering within a given depth layer and block differed significantly ($p<0.05$) from night levels (Mann-Whitney non-parametric t-test equivalent, with significance levels Bonferroni-corrected for multiple tests). Note that the proportion of total survey time conducted during the day or night varied between blocks and seasons.

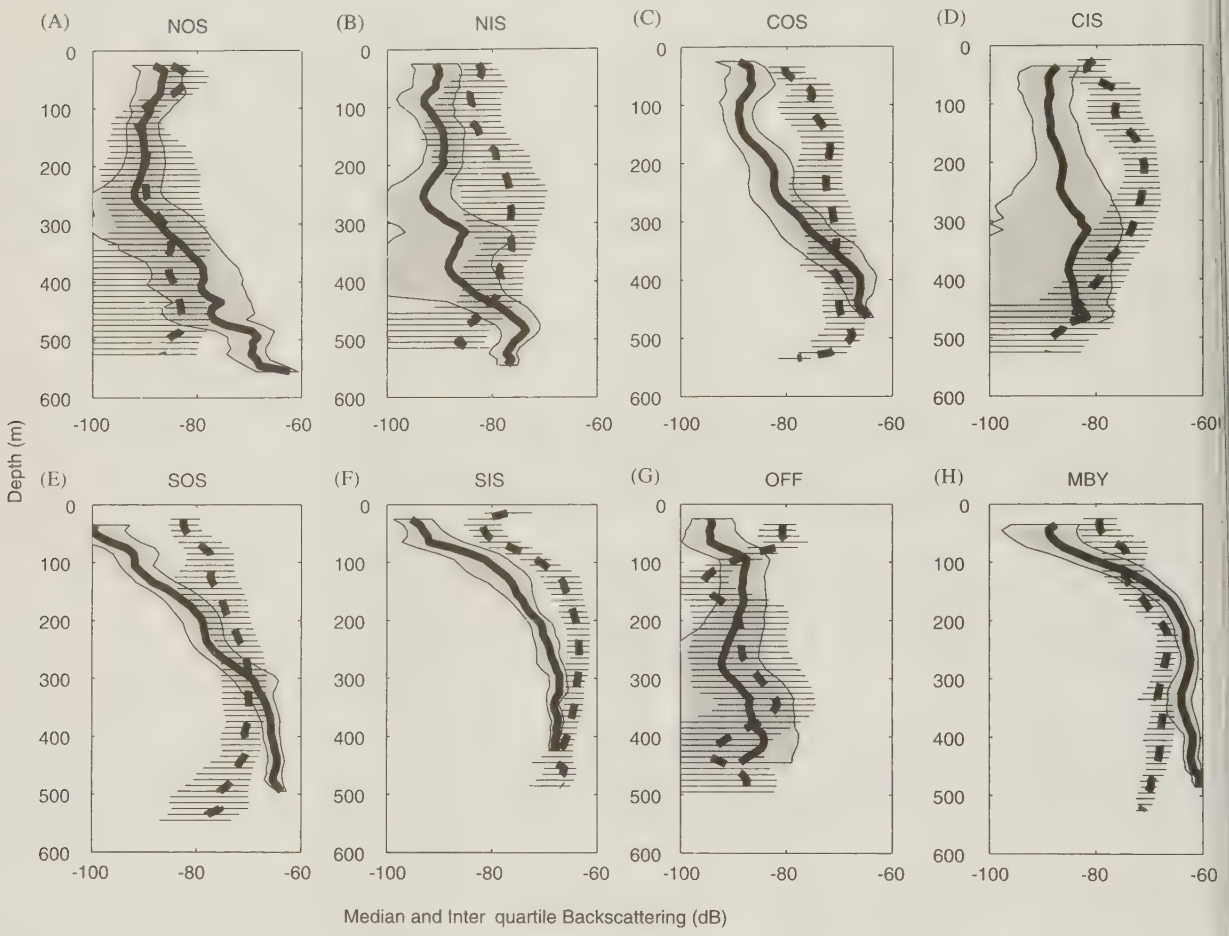

Fig. 3. Vertical distribution of backscattering in each survey block, during fall (dashed line) and winter (solid line), in the (A) Northern Outer-Shelf, (B) Northern Inner-Shelf, (C) Central Outer-Shelf, (D) Central Inner-Shelf, (E) Southern Outer-Shelf, (F) Southern Inner-Shelf, (G) Off-Shelf, and (H) Marguerite Bay blocks. Block name abbreviations are as in Fig. 1. Median and inter-quartile range (indicated by black error bars in fall and gray shading in winter) of backscattering were calculated in 10-m depth intervals over all observations in each block.

In winter, backscattering decreased by an order of magnitude (i.e. ~10 dB) relative to fall levels within the shallow and middle-depth layers, except in the mid-water layer of Marguerite Bay (Fig. 4B,H and Table 2; Friedman non-parametric two-way analysis of variance test for the effect of season (Sokal and Rohlf, 2000), shallow layer: $\chi^2 = 8$, $p = 0.005$, mid-water layer: $\chi^2 = 4.5$, $p = 0.03$). Significantly different scattering between blocks (Kruskal-Wallis test, $\chi^2 = 510$, $p < 0.001$, $n = 748$) was driven primarily by high scattering in Marguerite Bay and low scattering in

Fig. 4. Interpolated backscattering during fall and winter. Data used for interpolations are the backscattering levels averaged over 1-km along-track intervals. (A,B) Interpolated backscattering 100–300 m. Overlain are contours of bathmetry, showing the 450 and 1000 m isobaths. (C,D) Interpolated backscattering 300–500 m, with bathymetric contours again overlain. (E,F) Interpolated backscattering 100–300 m. Overlain are contours of dynamic height (from Klinck et al., 2004) relative to 400 m. Lows (L) and highs (H) in dynamic topography are indicated, and arrows show the direction of geostrophic flow. (G,H) Interpolated backscattering 25–100 m, with dynamic height contours overlain.

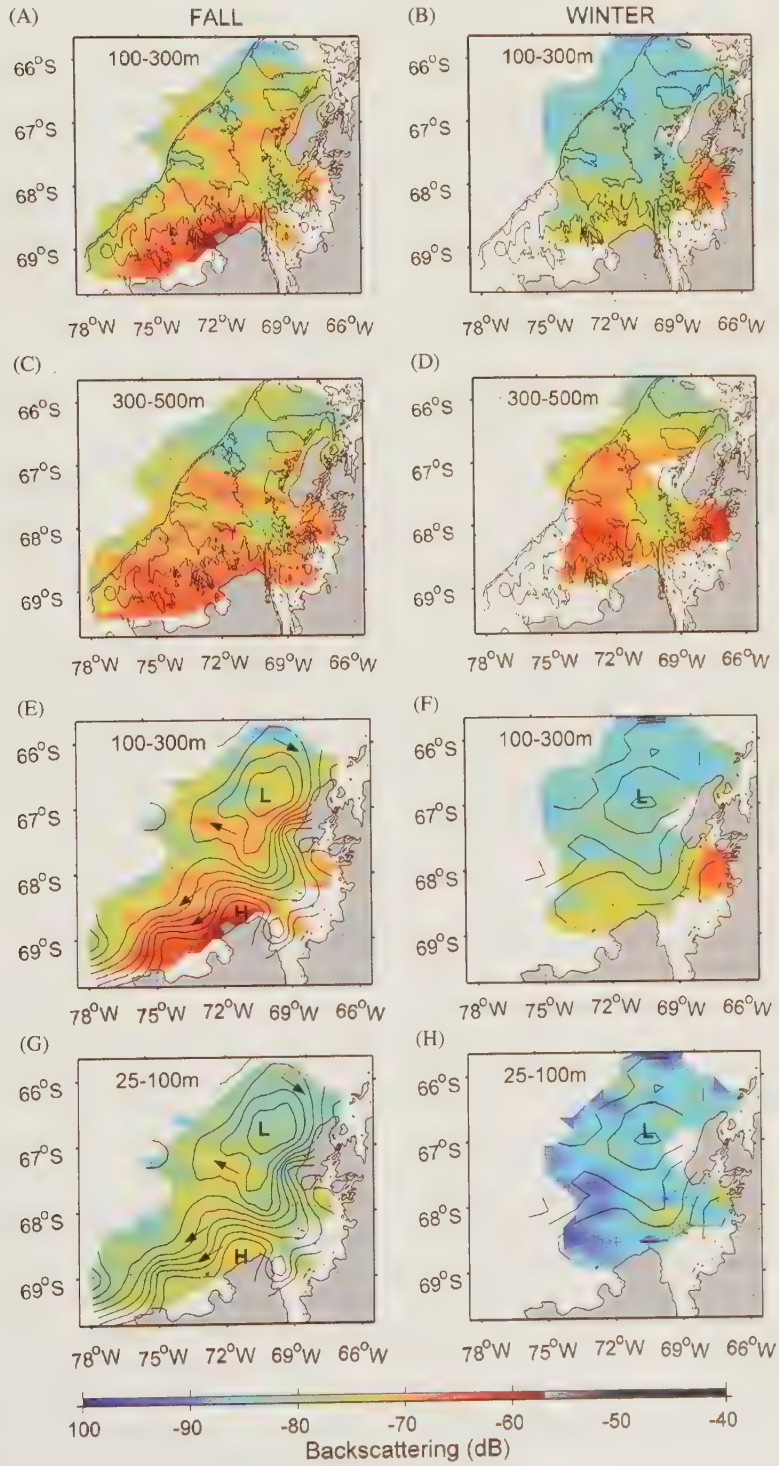
(A)
FALL
100-300m
(B)
WINTER
100-300m
(C)
300-500m
(D)
300-500m
(E)
100-300m
L
H
(F)
100-300m
L
(G)
25-100m
L
H
(H)
25-100m
L
66°S
67°S
68°S
69°S
78°W 75°W 72°W 69°W 66°W
100 -90 -80 -70 -60 -50 -40
Backscattering (dB)

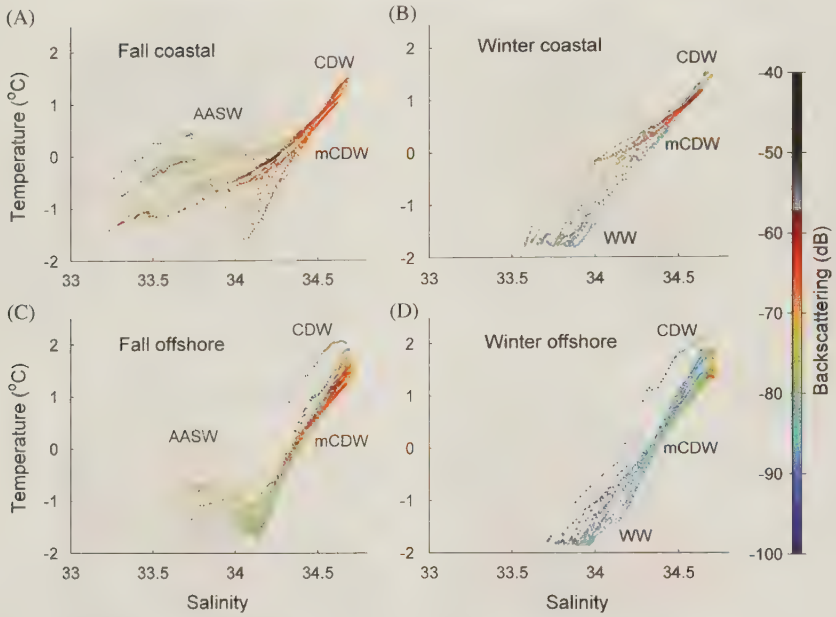

Fig. 5. Potential temperature-salinity diagrams, with dot color indicating backscattering intensity (dB). Data are plotted separately for the (A) fall coastal, (B) winter coastal, (C) fall offshore, and (D) winter offshore blocks. The 'coastal' category includes the three inner-shelf blocks and Marguerite Bay, while the 'offshore' blocks include the outer- and off-shelf blocks. Environmental data were collected at CTD stations (see Klinck et al., 2004). Acoustic backscattering levels represent the acoustic observation (backscattering averaged over 1-km intervals) made nearest to the depth and location of each CTD measurement of temperature and salinity. Note that due to the high sample sizes (9246 in fall, and 6481 in winter), some dots were plotted on top of one another and so low values are somewhat obscured. The water masses present were Antarctic Surface Water (AASW), Circumpolar Deep Water (CDW), modified Circumpolar Deep Water (mCDW), and Winter Water (WW).

the northern and off-shelf blocks (Tukey-Kramer post-hoc tests, $p<0.05$). In the bottom layer (300–500 m; Fig. 4D), backscattering was high over much of the continental shelf, as well as within Marguerite Bay, and did not differ between blocks (Friedman test non-significant; Table 2). Winter backscattering levels showed less of a clear association with the deep troughs across the shelf (Fig. 4B,D). Although there was still evidence from dynamic topography of a weakened gyre in the northern portion of the survey area and a coastal current, there was little evidence of any enhanced backscattering at depth associated with these features (Fig. 4F,H).

3.3.1. Potential impact of vertical migrations on horizontal patterns

In order to determine whether the observed trends in horizontal distribution were confounded by diel vertical migration of the zooplankton responsible for measured backscattering, mean daytime and nighttime backscattering levels in each block were compared within the shallow (25–100 m), mid-water (100–300 m), and deep (300–500 m) layers. Day was defined as 0900–1500, and night as 1700–0700, with dawn and dusk excluded from analysis in order to examine solely whether day or night backscattering differed from one another. If the zooplankton were migrating upwards at night one might expect to see an increase in backscattering in the shallower depth layers from day to night, associated with decreases in the deeper strata. No such pattern consistent with diel vertical migration was observed: comparable backscattering levels were measured in each layer during both day and night in most blocks (Table 2; Mann-Whitney tests $p>0.05$).

4. Backscattering relative to water masses

The association between backscattering and particular water masses was explored using observations of potential temperature and salinity from CTD casts (Fig. 5). During fall, highest backscattering levels were associated with modified-CDW. Episodic high values of backscattering also were observed in association with AASW, corresponding to the occasional presence of dense patches in surface waters. Warmer (i.e. less-modified) CDW present in areas farther offshore was typified by generally reduced backscattering, again suggestive of low zooplankton biomass in offshore waters and recent intrusions of CDW on to the continental shelf. In winter, backscattering was lower than in fall, particularly in the more offshore waters and in the WW and colder ($<0.5\,^{\circ}C$) mCDW present at shallower depths (Fig. 5). CDW and warmer mCDW present at depth showed some enhanced scattering, as would be expected from the deep scattering layer observed during the winter survey.

3.5. Multi-variate analyses

Multiple regression analysis with backward step-wise elimination of variables was used to examine how backscattering averaged in 1-km intervals was associated with salinity, fluorescence, transmittance, photosynthetically active radiation (PAR), bottom depth, bottom complexity, distance along-shelf, and distance across-shelf. The standard deviation of the nearest 20 measurements of bottom depth (i.e. within a horizontal distance of ~400 m) was used as a proxy for bottom complexity. Potential temperature, oxygen concentration, and depth were highly correlated with one another and with salinity during both cruises ($r \geqslant 0.8$), and so only salinity was used in the analysis. In fall, distance along-shelf, distance across-shelf, and salinity were the most strongly associated with backscattering levels (standardized partial regression coefficients of −0.53, −0.41, and 0.31, respectively, all p's <0.001). The former two variables had negative effects, indicating that backscattering increased farther in on the shelf and farther along the shelf towards the southwest. Increasing backscattering was associated with increasing salinity, but note that the latter's influence may be due to an association of the zooplankton with salinity itself, or due to the influence of one of its correlates, such as depth. Overall, only 34% of the variation in fall backscattering was accounted for by the selected independent variables ($n = 9246$). In winter, distance along-shelf and salinity were the two most important explanatory variables (standardized partial regression coefficients of −0.50 and 0.46, respectively, p's <0.001), and 41% of the total variation in backscattering was explained by the selected variables ($n = 6481$).

3.6. Taxonomic composition

In general, small (< 2.5 mm in length) and large copepods (>2.5 mm) dominated MOCNESS catches in terms of both numbers and estimated biomass. From qualitative examinations, small copepods were dominated by *Metridia gerlachei* copepodites, with cyclopoids (e.g., *Oithona* and *Oncaea* spp.) also abundant at some locations. The large copepod group was composed of mostly *Calanoides acutus*, *Calanus propinquus*, *Gauidius* spp., adult *M. gerlachei*, *Rhincalanus gigas*, and *Paraeuchaeta* spp. (Ashjian et al., 2004).

Our silhouette method for identifying net catches was not able to identify euphausiids to the level of species. Microscopic examination of a subset of the net catches indicated that the euphausiid community consisted of *E. superba*, *E. crystallorophias*, *E. frigida*, *E. triacantha*, and *Thysanoessa macrura*. For the remainder of this paper, we will group these species together and refer to them simply as euphausiids. Small euphausiids (all individuals <15 mm in length, corresponding to larval stages) often contributed substantially to total zooplankton abundance and biomass, though less than copepods. Large (>15 mm, juveniles and adults) euphausiids made important contributions to sampled biomass, but typically not to abundance. Other taxa, such as pteropods, chaetognaths, amphipods, mysids, siphonophores, other jellies, and micronektonic fishes, were proportionally important only at limited depth ranges and particular locations.

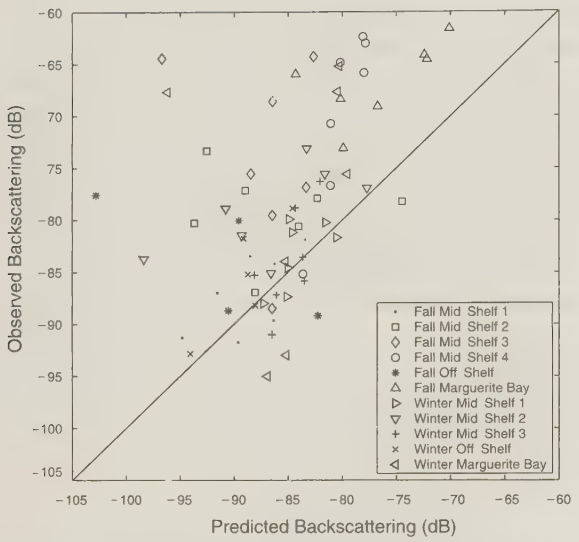

Fig. 6. Comparison of backscattering observed acoustically and that predicted based on the composition of the MOCNESS catches. Observed backscattering levels represent averages over depth ranges equivalent to those sampled by the nets, with individual symbols representing each MOCNESS tow. Acoustic observations were made within 17 km and 5 h of the net tows.

Detailed analyses of MOCNESS catches were performed in a companion study (Ashjian et al., 2004), and the emphasis here is on using these catches to interpret acoustic observations.

Forward calculations of expected backscattering based on net catches showed a positive correlation with observed backscattering levels (Fig. 6; $n = 58$, $r^2 = 0.43$, $p < 1 \times 10^{-7}$). Observed backscattering was generally greater than predicted backscattering, particularly at high levels. The average deviation from a one-to-one relationship was 6.8 dB.These analyses excluded the winter mid-shelf 1 and 2 stations, the two locations where net tows and acoustic data collection were separated in time by approximately a month. Interestingly, however, the predicted backscattering levels for the mid-shelf 1 station fell very close to the 1:1 line. Furthermore, while the predicted backscattering levels for the mid-shelf 2 station were generally lower than observed levels, they were certainly not the most extreme outliers.

The ratios of predicted backscattering for each of the various taxa to total predicted backscattering provide some insight into the possible biological sources of backscattering in the vicinity of each MOCNESS tow. The full set of backscattering predictions for each taxon in each net and tow can be found in Fig. 7; here, only the more noteworthy features will be highlighted.

3.6.1. Fall sources of backscattering

Based on fall net catches and taxon-specific acoustic scattering models, large euphausiids were the predicted source of the majority of predicted backscattering at only a few locations and depths: in the mid-water at the mid-shelf 1 and 2 stations (at 22–240 m, and 149–344 m, respectively), at depths where large and diffuse patches were present (Fig. 2A), as well as in the very high scattering and patchy 50–198 m depth range in Marguerite Bay (Fig. 7A). Elsewhere, large euphausiids were either absent or constituted only a minor component of predicted backscattering. Small euphausiids were estimated to make their most important contributions at shallow depths (25–100 m).

Aside from euphausiids, the remainder of the fall predicted backscattering stemmed from a mixture of taxa (Fig. 7A). Large copepods were an important predicted constituent at many stations, particularly below 100 m. Despite never contributing more than 11% of net-sampled biomass (Ashjian et al., 2004), pteropods were occasionally responsible for the majority of predicted backscattering (up to 69%). This is due to the hard shell and associated strong scattering intensity of pteropods in comparison to the more weakly-scattering taxa like euphausiids or copepods (Stanton et al., 1994). Similarly, at certain depths and locations, pneumatophore-bearing siphonophores explained the majority of backscattering. For instance, in the 99–145 m depth stratum at mid-shelf station 3, 66% of backscattering was estimated to result from siphonophores, even though catch biomass in this layer was still dominated by copepods (47%) and the contribution of siphonophores to biomass was negligible (~1%). The pneumatophore structure of siphonophores is a gas-filled sac that scatters a great deal of sound (Warren et al., 2001), evidently overwhelming the contribution to observed backscattering of the biomass-dominating copepods.

Fig. 7. Predictions of the sources of backscattering based on MOCNESS catches during (A) fall and (B) winter. The percent of total predicted backscattering accounted for by each taxon is shown relative to the depth interval sampled by each net of each tow. The 'pteropod' category refers only to thecosomes (*Limacina* spp.). The 'other' category includes small (<2.5 mm) copepods, medusae, polychaetes, ostracods, eggs, salps, crustacean larvae, radiolarians, mysids, and gymnosome pteropods.

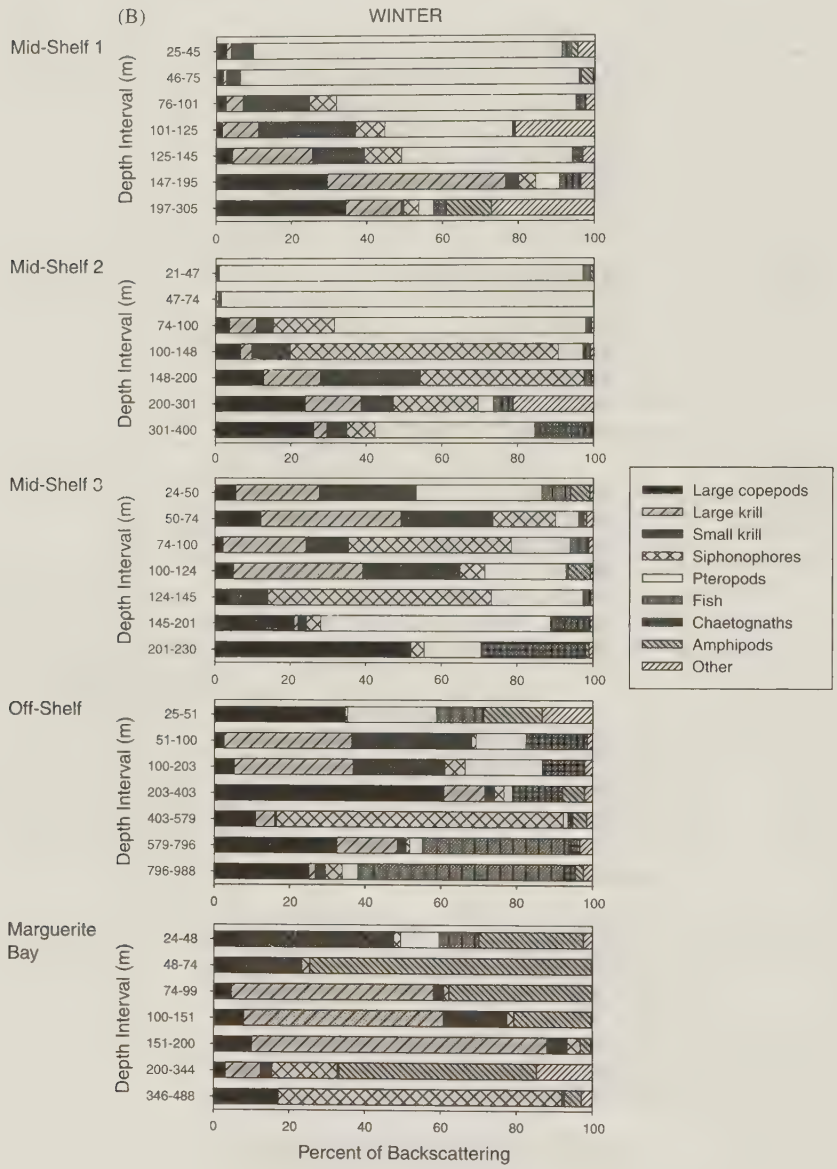

Fig. 7. (*Continued*)

Small copepods frequently dominated catches (up to 72% of biomass), but this taxon never explained more than 19% of predicted backscattering, due to their small size and concomitant weak target strength at 120 kHz.

3.6.2. *Winter sources of backscattering*

In winter, the sources of backscattering predicted from net samples differed from fall (Fig. 7B). The dominant feature observed acoustically in winter was the deep scattering layer found close to the bottom over much of the continental shelf. Unfortunately, difficulties associated with towing the MOCNESS through the pack ice led to problems in sampling this layer. At the mid-shelf 1 station, the deepest net sampled to within 40 m of the bottom. Acoustic data were collected in this region 30 days prior to the net

w, and at that time, a deep scattering layer was esent extending 20–100 m above the bottom. edictions from the catch composition in this net ggested that large copepods and radiolarians ncluded in the 'other category' of Fig. 7B) were e dominant contributors to expected backscattering levels in the layer, with smaller contributions from amphipods and large euphausiids. At e mid-shelf 2 station, a scattering layer was esent extending 100–150 m off the bottom. edictions from the deepest net in a tow made 4 days later to within 90 m of the bottom dicated that expected backscattering in the layer as accounted for primarily by pteropods and rge copepods. At the mid-shelf 3 station, the eepest net only sampled to within 95 m of the ottom, and therefore passed 25 m above the deep cattering layer observed acoustically. Backscattering in this sampled region immediately above e deep scattering layer was predicted to stem redominantly from copepods and chaetognaths.

Catches from shallower sampled strata suggested that the low backscattering observed outside the deep scattering layer stemmed from a ighly complex mixture of taxa (Fig. 7B). Where hey were present, siphonophores and pteropods often accounted for most of the predicted backcattering levels. In Marguerite Bay, amphipods were the dominant scatterer in two of the sampled lepth intervals, while large euphausiids dominated predicted backscattering in the acoustically intense 51–200 m depth range and in the less intense 74–151 m layer.

4. Discussion

Distinct spatial and seasonal patterns were evident in backscattering levels across the Marguerite Bay continental shelf study area. Clear associations also were observed between backscattering and particular water masses and dynamic topography, which is an indicator of flow. Together with the information derived from net samples on the taxonomic composition of the zooplankton and micronekton responsible for the backscattering, these observations permit important inferences concerning the seasonal distribution, transport, and retention of zooplankton and micronekton biomass in the region.

4.1. Potential limitations of the acoustic technique

The relationship between backscattering at a single frequency and zooplankton biomass is highly complex, and in order to draw any conclusions about biomass on the basis of our acoustic measurements, a number of potentially confounding factors first must be taken into account. Backscattering depends on a number of factors, including the abundance or biomass, taxonomic composition, size, and orientation of scatterers (Stanton and Chu, 2000). In linear echo-integration theory, the echoes from individual animals within the acoustic beam are assumed to sum incoherently, such that echo-integrated backscattering increases with animal abundance. This assumption is valid provided that animal densities are not so high as to cause acoustic attenuation or multiple scattering, and targets can be assumed to be distributed randomly within the beam (MacLennan and Simmonds, 1992); this is likely to be the case here. Inasmuch as biomass increases with abundance, backscattering therefore will also increase with biomass.

Different anatomical classes of zooplankton scatter sound with very different efficiencies, and the taxonomic composition of scatterers has a substantial impact on backscattering. The echo energy scattered per unit biomass of a pteropod, for example, can be 70 times greater than that from a decapod or pneumatophore-bearing siphonophore (Stanton et al., 1994). An observed increase in backscattering therefore could result either from an increase in the biomass of a given taxon of zooplankton, or from a shift in taxonomic composition towards stronger scatterers like pteropods; such a shift even could be accompanied by a decrease in biomass. In the present study, predictions based on net catches of the likely relative contributions of different taxa to observed backscattering levels suggest a highly heterogeneous composition of animals (Fig. 7; note that Section 4.3.1 acknowledges certain limitations of these predictions). There is little evidence that changes in taxonomic composition

might confound our interpretation that the major observed seasonal and spatial differences in backscattering are related to concomitant changes in biomass. The strong-scattering pteropods were predicted to account for more of the backscattering in winter than in fall, suggesting that the decrease in backscattering between the two seasons may be due to an even-larger decrease in biomass than if the taxonomic composition had remained the same. During fall, there was evidence of greater contributions of pneumatophore-bearing siphonophores to backscattering at depths below 100 m in the southern reaches of the survey area and in Marguerite Bay, and an increased importance of euphausiids towards the north. Although backscattering was lower in the north, echo energy per unit biomass is comparable for siphonophores and euphausiids (Stanton et al., 1994), and so this backscattering decrease is more likely related to a difference in biomass than to spatial patterns in community composition.

For the most part, backscattering increases with animal size. Since biomass also increases with size, backscattering should increase with biomass irrespective of whether biomass increases are related to size or abundance. There do exist, however, size ranges for which backscattering and size are negatively related, such that slightly larger (higher biomass) animals have lower backscattering than smaller ones (Stanton and Chu, 2000). For single pings and individual animals, such 'dips' in the scattering vs. size relationship can be quite pronounced, and have the potential to confound the relationship between backscattering and biomass. In this study, however, we integrate backscattering over large depth ranges and horizontal intervals, and thereby average over a very large number of animals. When scattering is averaged over a distribution of animal lengths, the dips in backscattering at particular size ranges are substantially reduced in magnitude, to 5 dB or less (Stanton et al., 1998; Stanton and Chu, 2000). What's more, the sizes of animals encountered in this study mostly avoid the problem of animal size confounding the relationship between backscattering and biomass: the lengths of most of the net-sampled taxa (e.g., copepods, pteropods, siphonophores, and small euphausiids) were much smaller than the length at which the first dip in the backscattering vs. size relationship occurs. Large euphausiids are the only taxon sampled by the nets whose sizes might have been expected to fall within this first dip, but examining the length distributions of this group in net catches suggests that most animals fell on either side of the requisite range of lengths (Ashjian et al., 2004).

Similarly, animal orientation can have a substantial impact on backscattering for individual animals and single realizations, but this effect is much reduced when scattering is averaged over a distribution of aspects. It also seems unlikely that the observed spatial and seasonal patterns in backscattering can be explained simply by variability in the orientation of animals, as this would require complicated spatial and seasonal changes in orientation that are less plausible than differences in biomass.

Animal taxonomic composition, size, and orientation certainly introduce imprecision into the relationship between backscattering and zooplankton and micronekton biomass, and it therefore is not possible to relate backscattering uniquely to biomass. Nonetheless, the present analyses have revealed large spatial and temporal differences in backscattering (greater than 5 dB), which should exceed any imprecision introduced by these confounding factors, allowing us to attribute coarsely these differences to changes in biomass.

There also exists the possibility that some of the observed backscattering stemmed from sources other than zooplankton or micronekton, such as nekton or non-biological sources. It is unlikely that any animals larger than micronekton (e.g., large fishes) contributed substantially to backscattering measurements. Larger animals would be expected to appear in the acoustic record as distinct and recognizable targets, associated with very high backscattering levels. Very few such targets were evident, however, and backscattering levels seldom exceeded −50 dB. Aside from the artifactual backscattering excised from the up-looking transducer's acoustic record described above, we have little information on the possibility of scattering from non-biological sources. Work in the Gulf of Maine has demonstrated that small-scale variations in the temperature and salinity

ucture of the water column (i.e. microstructure) y at times scatter sound at levels comparable to ckscattering from zooplankton (Warren et al., 03). Preliminary examinations of acoustic data lected concurrent to casts with a microstructure obe during a later cruise suggest that thin and v-intensity backscattering layers may be asso- ted at times with regions of high microstructure, t such weak scattering is unlikely to contribute bstantially to the averages of backscattering der examination in the present study.

Finally, diel vertical migrations by the animals sponsible for observed backscattering may in- oduce uncertainty into our interpretations of stribution. Comparisons of mean backscattering thin the different depth strata between day and ght do not support this notion, other than rhaps in the shallow layer during winter. Even this depth range, since the position of the ship in lation to time of day was effectively random, any el changes in vertical position should simply troduce random error into the acoustic measure- ents. Diel vertical migration of some component the zooplankton community undoubtedly does cur (e.g. Zhou and Dorland, 2004 observed stinct diel vertical migrations by individual euphausiid aggregations), but it seems that the influence of such migrations on our large-scale analyses is minor.

4.2. Seasonal changes in backscattering

One of the most striking patterns observed in backscattering levels was the decrease in scattering from fall to winter evident in the upper 300 m of the water column throughout the survey area, other than in Marguerite Bay. In contrast, backscattering below 300 m remained high even in winter, and in fact increased relative to fall levels in Marguerite Bay and the northern and southern outer-shelf. Comparing backscattering levels averaged over the entire sampled depth range (25–500 m) suggests that water-column backscattering in Marguerite Bay and the outer- and off-shelf areas during winter was comparable to or exceeded fall levels (Fig. 8). Over the inner-shelf, winter backscattering was reduced to 6–19% of fall levels. Mean winter backscattering averaged over the entire surveyed area and water column was −69.6 dB, accounting for 32.5% of the backscattering present during fall (mean −64.8 dB). This is indicative of a seasonal decrease in

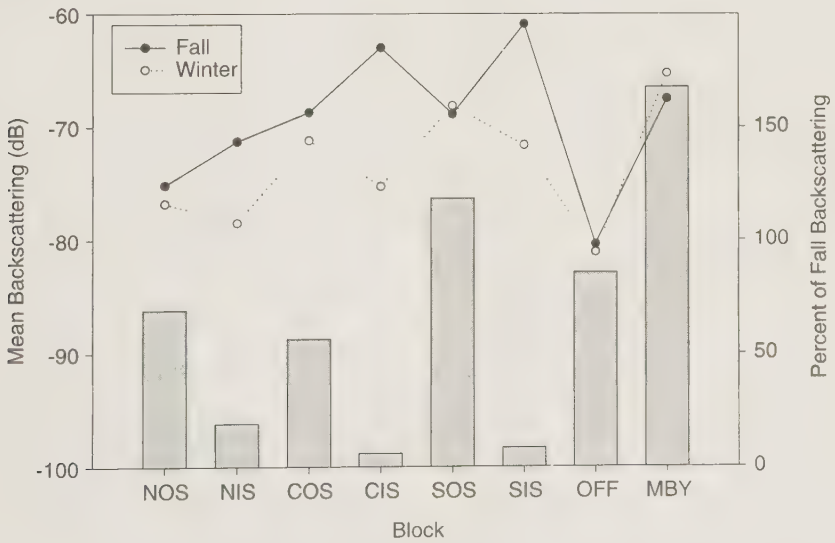

Fig. 8. Mean backscattering levels observed in the entire sampled portion of the water column (25–500 m) in each block, during fall and winter (left y-axis). Vertical bars indicate the percent of fall total backscattering in each block that can be accounted for by winter backscattering levels (right y-axis). Averages and percentages were calculated using the arithmetic form of backscattering (s_v).

zooplankton biomass, and correspondingly, a decrease in zooplankton biomass between the two seasons also was observed by other instruments. Biomass sampled in the MOCNESS tows described above decreased from fall to winter by approximately 60% (Ashjian et al., 2004). Analyses of optical plankton counter-derived zooplankton size spectra likewise suggested that particle abundance between 0.25 and 14 mm in equivalent spherical diameter decreased between fall and winter of 2002 by 82% (Zhou et al., 2004).

Similar seasonal reductions in the biomass of zooplankton have been observed in studies of other regions of the antarctic continental shelf (e.g. copepods; Schnack-Schiel et al., 1998), and for Antarctic krill in particular (Heywood et al., 1985; Siegel, 1988, 1989; Lascara et al., 1999; and see review in Siegel, 2000). A seasonal decrease in Antarctic krill biomass may not be a consistent feature across all regions, however, as South Georgia typically supports a strong krill fishery during winter (e.g. Murphy et al., 1997). In repeat surveys that overlapped during fall and summer with the northern end of the SO GLOBEC study area, and that in winter and spring covered the continental shelf farther north, Lascara et al. (1999) observed an order of magnitude decrease from spring and summer Antarctic krill biomass levels (32 and 95 g m^{-2}, respectively) to fall and winter (12 and 8 g m^{-2}, respectively). In the latter survey, mean biomass was driven primarily by one high-biomass station; biomass was zero at most other stations. These authors calculated biomass by assuming that all backscattering at 120 kHz in excess of −81 dB and above 189 m in depth was Antarctic krill. Although we do not make this scaling from backscattering to biomass, winter backscattering in the present study frequently exceeded −81 dB, and so would have resulted in non-zero biomass estimates by the Lascara et al. (1999) method. However, backscattering levels higher than −81 dB typically were found below 189 m, possibly explaining the many zero winter biomass estimates made in this earlier study.

A number of factors may explain the decrease in zooplankton backscattering from fall to winter. These include vertical and horizontal movements, mortality, and advection of the zooplankton and micronekton in question. It also must be noted in considering these explanations that we are dealing with backscattering as a whole, and that different factors may explain changes in the biomass and distribution of individual taxa.

4.2.1. Vertical movements

Downwards seasonal migrations may have contributed to the decrease in overall backscattering levels. Certain taxa, including the large copepods *C. acutus* and *R. gigas*, are known to undergo ontogenetic migrations to deeper waters during winter (Ross et al., 1996). Migration below the depth ranges normally sampled by nets and acoustics has been hypothesized to be a possible cause of apparent seasonal changes in the biomass of Antarctic krill in the present study area (Lascara et al., 1999). Euphausiid biomass at depths below 400 m has typically been found to be low in all seasons (Marin et al., 1991; Ross et al., 1996; Ashjian et al., 2004). There is some evidence, however, that Antarctic krill on occasion may be associated with the bottom, from a bottom-mounted light trap in a shallow water region under fast ice (Kawaguchi et al., 1986), acoustic observations in conjunction with trawl catches (Heywood et al., 1985), and two observations made by a remote-operated vehicle (ROV) within 1 m of the bottom (Gutt and Siegel, 1994).

In the present study, due to the use of a chirp pulse (Ehrenberg and Torkelson, 2000) and to the ability of the BIOMAPER-II to be towed at depths up to 300 m, we were consistently able to sample acoustically to 500 m, occasionally reaching as deep as 550 m. Depending on bathymetry, this allowed us to sample all the way to the bottom over much of the continental shelf. In certain portions of the study area, backscattering in the deepest portions of the water column increased from fall to winter, suggestive of a downwards movement of zooplankton. Overall, however, even including backscattering at the deepest depths surveyed, winter backscattering in the surveyed water column accounted for only 32.5% of observed fall levels. Downwards vertical movements alone therefore may not account for the seasonal decrease in backscattering.

Upwards migration of the zooplankton responsible for backscattering above the minimum sampled range of the acoustic system (25 m) also does not explain the fall to winter decrease. Analyses of MOCNESS catches do not indicate that total zooplankton biomass increased in the 0–25 m depth stratum (Ashjian et al., 2004). Concurrent ROV surveys did observe high abundances of larval euphausiids immediately under the pack ice in many locations during winter, suggesting that larval euphausiids may have migrated to the underside of the ice (Gallager et al., 2002). Since the present analyses indicate that small euphausiids are minor contributors to overall backscattering, such a migration is unlikely to have affected observed backscattering levels.

4.2.2. Horizontal migrations

Horizontal migrations to preferred over-wintering habitats by zooplankton or micronekton may explain some of the winter decrease in backscattering. Adult Antarctic krill are capable of sustained swimming at speeds of 10–15 cm s^{-1} (Kils, 1981), and so in the eight weeks between the fall and winter surveys, could have migrated as far as 725 km. Siegel (1988) hypothesized that adult Antarctic krill migrate offshore in spring, returning to coastal areas for the winter perhaps following a food gradient, and an association of zooplankton with coastal waters during winter has been observed in other shelf regions (Siegel, 1988, 1989; Zhou et al., 1994; Lascara et al., 1999). In the present study, we penetrated through the ice close to shore during winter on only limited occasions. On one of those instances, in Laubeuf Fjord at the northern end of Marguerite Bay, high backscattering was observed, and according to our net-based predictions, much of this backscattering came from large euphausiids. It thus seems possible that large euphausiids may have migrated out of the surveyed area between fall and winter, into the many un-surveyed coastal fjords of Marguerite Bay and its surrounding islands. It appears unlikely, however, that a preference for a particular water mass and a change in the distribution of that water mass would be involved in such a horizontal movement. Temperature-salinity diagrams indicated that backscattering in fall was highest in modified CDW, and similar diagrams from winter data indicate that abundant modified CDW was still present on the shelf.

4.2.3. Mortality

Large zooplanktivorous predators are common in the Marguerite Bay region, and include whales (Thiele et al., 2004), seals (Burns et al., 2004), and birds (Chapman et al., 2004). Such predators may have been responsible for high levels of mortality. Until we gain a detailed understanding of the sources of backscattering and the population dynamics of the various zooplankton taxa, the contribution of mortality to the decrease in backscattering remains unclear.

4.2.4. Transport and retention of zooplankton and micronekton

Advection may have transported zooplankton and micronekton out of the study area, accounting for some of the observed decrease in backscattering between the two seasons. In fall, contours of dynamic height indicated the presence of a large gyre situated over the northern portion of the continental shelf study area; previous studies of the area and analyses of historical datasets suggest that this is a persistent feature of the region (Hofmann et al., 1996; Smith et al., 1999). The southern end of this gyre contained elevated backscattering, suggesting that zooplankton were being transported in an off-shelf direction. Current speeds in the gyre were on the order of 3–15 cm s^{-1} (from ADCP and dynamic height calculations, respectively; Klinck et al., 2004), and in the eight weeks between the two cruises, could have transported the zooplankton between 145 and 725 km in a straight-line direction. Where the southern end of the gyre reached the shelf break and turned towards the north, zooplankton may either have been entrained into the fast-flowing (up to 30 cm s^{-1}, Klinck et al., 2004) Antarctic Circumpolar Current (ACC) and transported to regions farther north, or retained within the gyre structure.

Dynamic height estimates, ADCP measurements, and drifter tracks indicated the presence during fall of a strong coastal current moving towards the southwest along Adelaide and

Alexander Islands (Beardsley et al., 2004; Klinck et al., 2004). High zooplankton backscattering was associated with this physical feature. Although the coastal current passes through areas of complex bathymetry where zooplankton could potentially find refuge, it still likely transported much of the zooplankton found during fall in the southern shelf region towards the southwest and out of the study area. At ADCP-measured speeds of 10–25 $cm\,s^{-1}$ (Klinck et al., 2004), this current could have transported plankton between 480 and 1210 km.

On-shelf flow also may account for some of the seasonal decrease. Hydrographic observations and modeling exercises indicate that warm oceanic CDW is pumped up onto the continental shelf primarily at points where the deep troughs bisecting the shelf meet the shelf break and where the shelf break is strongly curved (Klinck et al., 2004; Dinniman and Klinck, 2004). Maps of interpolated backscattering relative to bathymetry, low levels of backscattering observed in the off-shelf block, analyses of the association between backscattering and water masses, as well as low net-sampled biomass at the off-shelf station (Ashjian et al., 2004), suggest that the oceanic waters being pumped onto the shelf were relatively low in zooplankton. The waters replacing those lost from the study area through other advective features thus may have contributed to the overall decrease in zooplankton and micronekton biomass.

Retentive processes may partially explain why water column backscattering in Marguerite Bay increased from fall to winter: ADCP measurements made by other SO GLOBEC investigators (Zhou et al., 2004; Klinck et al., 2004) suggest the possible existence of a small gyre in the northern end of Marguerite Bay, a notion that is supported by the dynamic height contours presented here. Such a gyre could serve to retain zooplankton in this region, keeping backscattering levels high in both fall and winter.

4.3. Sources of acoustic backscattering

4.3.1. Accuracy of forward calculations

Any inferences about the sources of acoustic backscattering rely on the accuracy of our forward calculations. Forward predictions of backscattering based on net samples were generally lower than observed backscattering levels, particularly at high intensities. A number of factors may have contributed to this discrepancy. First, MOCNESS tows and acoustic samples could not be made at exactly the same times and locations. High spatial and temporal variability in the abundance and composition of zooplankton may have resulted in the two systems sampling different communities. This is particularly true for sparsely or patchily distributed organisms like euphausiids, which may have contributed to the acoustic measurements but been missed by the nets. It is pertinent that in temperate waters typified by generally higher zooplankton densities and where net and acoustic sampling were co-located, forward calculations have yielded more favorable comparisons than seen here (Wiebe et al., 1996; Bucklin et al., 2002). Furthermore, net studies have led to the suggestion that although the absolute biomass of a particular taxon may vary dramatically in space or time, its proportional contribution to total zooplankton biomass is generally much less variable (Wiebe et al., 1992). While spatial and temporal variability thus might contribute to the discrepancy in magnitude between predicted and observed backscattering, the predicted relative contributions of individual taxa may be less subject to such error.

Second, biological characteristics such as length distribution can vary dramatically between even closely spaced Antarctic krill swarms, and a single tow may not provide an unbiased estimate of the length distribution of krill in a given region (Watkins et al., 1986, 1990). Some degree of uncertainty thus will certainly be propagated into our predictions of the sources of backscattering due to error in the net catch data themselves. During the surveys, it generally was not possible to conduct replicate tows in order to quantitatively constrain this error. At the Marguerite Bay station in fall, however, three separate tows were made through a series of dense euphausiids swarms over the course of 18 h and over a spatial area of $16 \times 4.5\,km^2$ (Wiebe et al., 2004). Analysis of the catches indicated a marginally non-significant ($p = 0.065$) difference between tows in euphausiid length.

Third, some of the animals present may have voided the oncoming net. Larger taxa in particular might have been capable of avoidance, despite our use of a strobe light to reduce such an effect. Larger animals also would produce higher observed backscattering levels, and the greater offset between observed and predicted backscattering at higher scattering levels may support the notion that avoidance partially explains the difference between the two. Similar to the present results, Zhou et al. (1994) found that backscattering levels predicted from net catches of euphausiids became increasingly smaller than levels observed with an ADCP for higher observed values, which they attributed to avoidance on the part of the euphausiids.

Finally, some of the models and parameters used in making forward predictions may not have been appropriate in all instances. For most of the dominant taxa, the models of acoustic scattering used here have been experimentally validated through comparisons of model predictions to measured target strengths of actual individual organisms (Stanton et al., 1998; Table 1). Model parameter values (e.g., animal orientation), however, were occasionally chosen on the basis of very little information (see Table 1). Sensitivity analyses suggest that changing parameter values, while still keeping them within biologically plausible ranges, would increase predicted backscattering by only one to five decibels. Model parameter values alone therefore do not appear to explain fully the difference between predicted and observed backscattering.

4.3.2. *Taxonomic composition of zooplankton and micronekton*

Given the preceding discussion, and since only five or six tows were available per cruise to describe such a large study area, any conclusions concerning the sources of observed backscattering must be approached with caution. Performing the forward calculations furthermore only provides an indication of the relative contribution of each zooplankton and micronekton taxon to total backscattering in a given region, and does not allow the conclusion that these relative contributions have been uniquely determined. Nonetheless, these analyses do allow certain broad inferences.

Backscattering in the study area was found in two general forms: dense patches of elevated backscattering intensity, and more elongated and homogenous layers. In fall, dense and discrete patches were observed primarily in Marguerite Bay, contributing to the high mean backscattering levels and enhanced coefficients of variation in backscattering observed in this region. Forward predictions suggest that these patches were composed of large euphausiids. Large but more diffuse patches also were observed at depth over the northern shelf. The composition of these deep patches is less certain, as we can not be certain that the fall mid-shelf 1 MOCNESS tow actually passed through one of these patches. The catch data do suggest the presence of euphausiids, but myctophid fishes are also known to inhabit these areas. Dense patches were less evident in Marguerite Bay in winter, but the MOCNESS tow suggested that large euphausiids and amphipods made up the majority of the intense scattering layer present below 150 m in this area. Outside of these very distinct patches, the analysis of net samples indicated that the sources of backscattering likely included a complex and variable mixture of taxa.

The dominant backscattering feature in winter was the dense bottom scattering layer. Copepods were predicted to be the dominant scatterer in this layer, although two of the three MOCNESS tows that sampled this layer were the two instances where net tows were separated in time from acoustic data collection by as much as 30 days. It is also possible that some taxa were undersampled to a greater extent by the nets than others, leading to an apparent dominance of these other taxa (e.g., copepods in this instance). This may particularly be the case since predicted backscattering levels were low in comparison to measured levels in the bottom scattering layer, suggesting that some component of the animals scattering sound may have been undersampled. There is, however, little evidence from the current analyses to support the notion that large euphausiids migrated to depth during winter.

4.3.3. Implications to acoustic surveys

An important finding of the present study is that euphausiids accounted for the majority of predicted backscattering only at certain depths and locations within the survey area. Backscattering more typically was predicted to be dominated by copepods, pneumatophore-bearing siphonophores, pteropods, or a complex mixture of taxa. Where they were present, the relatively rare and low-biomass but strongly scattering pteropods and siphonophores appeared to overwhelm the contributions to backscattering of more weakly scattering taxa (similar to observations in the Gulf of Maine and on Georges Bank; Wiebe et al., 1996; Benfield et al., 2003). At 120 kHz, small fluid-like animals like copepods scatter near the transition between the Rayleigh and geometric scattering regions, and so in our predictions from net catches, copepod contributions to overall backscattering never exceeded −80 dB.Although copepod backscattering thus can be filtered out via thresholding if larger animals like euphausiids are of sole interest, such levels are certainly measurable and of consequence in generally low-scattering regions such as the present study site. Furthermore, copepods frequently dominate the zooplankton community in terms of abundance and biomass (Ashjian et al., 2004), and it is noteworthy that acoustic data potentially can provide information on their distribution.

Acoustic surveys in the Antarctic have employed a number of techniques to discriminate euphausiid backscattering from that arising from other scatterers. Often it has been assumed that all measured zooplankton backscattering above some minimum threshold (generally ca. −80 dB) stemmed from Antarctic krill (e.g., Macaulay et al., 1984; Lascara et al., 1999; Nicol et al., 2000). This assumption would lead to over-estimates of Antarctic krill biomass in the present study area, at least. In other instances, visual scrutiny and/or some degree of trawling has been employed to distinguish Antarctic krill patches from other sources of backscattering such as myctophid fishes (Sahrhage, 1989; Sprong and Schalk, 1992; Murray et al., 1995; Pauly et al., 2000), but this approach discards a great deal of potential information on the abundance of taxa other than krill.

Differences in backscattering at two or more discrete frequencies have been used with a great deal of success to identify euphausiid backscattering and filter out returns from other taxa. The range of differences in scattering attributable to particular euphausiid species has been based either on analyses of patches known from net samples to be predominantly mono-specific (Madureira et al., 1993; Brierley et al., 1998; Watkins and Brierley, 2002), in one instance in conjunction with analyses of swarm energetic and shape characteristics (Woodd-Walker et al., 2003), or on theoretical predictions from target strength models (e.g., Hewitt et al., 2003). Such multi-frequency analyses are very promising, and perhaps could be expanded to account for rare, but strongly scattering taxa like pteropods and gas-bearing siphonophores, where they are present.

5. Summary

Distinct spatial and seasonal patterns were evident in zooplankton backscattering across the Marguerite Bay continental shelf study area. During fall, backscattering was highest in the southern reaches of the survey area and inside Marguerite Bay, regions also associated with high abundances of whales, seals, and birds (Thiele et al., 2004; Burns et al., 2004; Chapman et al., 2004, respectively). In winter, the dominant scattering feature was a bottom scattering layer covering much of the continental shelf. Downwards vertical migrations of zooplankton into this bottom layer may have contributed to the observed decrease in backscattering levels from fall to winter in the mid-water, but may not account fully for the decrease in backscattering for the water column as a whole. The latter was probably due to vertical migrations plus a combination of advection out of the survey area, mortality, and horizontal movements. Advection could have occurred either via zooplankton in the northern shelf gyre becoming entrained into the ACC or via the southwest-flowing coastal current. Although the results from the present study concerning the advection of zooplankton are equivocal, the possibility that zooplankton from

e Marguerite Bay region become entrained o the ACC and transported to regions farther rth is tantalizing, and would support the pothesis that Marguerite Bay helps to sustain e large downstream euphausiid populations in e Bransfield Strait and South Georgia regions tkinson et al., 2001; Fach et al., 2002). Predicons based on net catches of the sources of served backscattering levels suggest that euausiids were the dominant scatterer only at very rticular locations and depths. Antarctic acoustic rveys should take care to account for other atterers, including the abundant, but weakly attering copepods, and the relatively rare, but rongly scattering pteropods and gas-bearing phonophores.

cknowledgments

We gratefully acknowledge the support of all fficers and crew of the RVIB *N. B. Palmer* and ne staff of Raytheon Polar Services. The tireless fforts of all members of the BIOMAPER-II and OCNESS teams were greatly appreciated: P. latalo, M. Butler, M. Dennett, K. Fisher, A. irard, J. Peterson, and M. Taylor. We also thank . Alatalo, N. Copley, P. Hull, and G. Rosenwaks or lab analyses of MOCNESS catches, E. ofmann, J. Klinck, and all the members of the TD group for the use of their data and dynamic eight estimates, and Sam Johnston of HTI for etting up the acoustic data collection system. D. hu, A. Lavery, and T. Stanton provided much ppreciated assistance with acoustic models, as well as advice concerning the assumptions of the single-frequency technique. Earlier versions of the manuscript benefited substantially from the comments of Jon Watkins and an anonymous reviewer. This project was supported by NSF US Antarctic Program Grant OPP-9910307 to P. Wiebe, C. Ashjian, C. Davis, and S. Gallager. G. Lawson was supported by a Fulbright Scholarship, a Natural Sciences and Engineering Research Council of Canada Post-Graduate Scholarship, and an Office of Naval Research Graduate Traineeship Award in Ocean Acoustics (Grant N00014-03-1-0212). This is GLOBEC contribution number 431 and Woods Hole Oceanographic Institution contribution number 11124.

References

Anderson, V.C., 1950. Sound scattering from a fluid sphere. Journal of the Acoustical Society of America 22, 426–431.

Ashjian, C.J., Rosenwaks, G.A., Wiebe, P.H., Davis, C.S., Gallager, S.M., Copley, N.J., Lawson, G.L., Alatalo, P., 2004. Distribution of zooplankton on the continental shelf off Marguerite Bay, Antarctic Peninsula, during Austral Fall and Winter, 2001. Deep-Sea Research II, this issue [doi:10.1016/j.dsr2.2004.07.025].

Atkinson, A., Whitehouse, M.J., Priddle, J., Cripps, G.C., Ward, P., Brandon, M.A., 2001. South Georgia, Antarctica: a productive, cold water, pelagic ecosystem. Marine Ecology Progress Series 216, 279–308.

Beardsley, R.C., Limeburner, R., Owens, W.B., 2004. Drifter measurements of surface currents near Marguerite Bay on the western Antarctic Peninsula shelf during austral summer and fall, 2001 and 2002. Deep-Sea Research II, this issue [doi:10.1016/j.dsr2.2004.07.031].

Benfield, M.C., Lavery, A., Wiebe, P.H., Greene, C.H., Stanton, T.K., Copley, N.C., 2003. Distributions of physonect siphonulae in the Gulf of Maine and their potential as important sources of acoustic scattering. Canadian Journal of Fisheries and Aquatic Sciences 60, 759–772.

Brierley, A.S., Ward, P., Watkins, J.L., Goss, C., 1998. Acoustic discrimination of Southern Ocean zooplankton. Deep-Sea Research II 45, 1155–1173.

Bucklin, A., Wiebe, P.H., Smolenack, S.B., Copley, N.J., Clarke, M.E., 2002. Integrated biochemical, molecular genetic, and bioacoustical analysis of mesoscale variability of the euphausiid *Nematoscelis difficilis* in the California Current. Deep-Sea Research I 49, 437–462.

Burns, J.M., Costa, D.P., Fedak, M., Bradshaw, C.J.A., Hindell, M.A., McDonald, G., Trumble, S.J., Chittick, E., Gray, M., Gales, N., Barnes, J., Shaffer, S., Kuhn, K., Lovell, P., Crocker, D., 2004. Winter habitat use and foraging behavior of crabeater seals along the Western Antarctic Peninsula. Deep-Sea Research II, this issue [doi:10.1016/j.dsr2.2004.07.021].

Chapman, E.W., Ribic, C.A., Fraser, W.R., 2004. The distribution of seabirds and pinnipeds in Marguerite Bay and their relationship to physical features during austral winter 2001. Deep-Sea Research II, this issue [doi:10.1016/j.dsr2.2004.07.005].

Chu, D., 2000. The GLOBEC Kriging Software Package - EasyKrig2.1, May 1, 2000. WWW Page, http://globec.whoi.edu/software/kriging/easy_krig/easy_krig.html.

Chu, D., Foote, K.G., Stanton, T.K., 1993. Further analysis of target strength measurements of Antarctic krill at 38 and 120 kHz: Comparison with deformed cylinder model and inference of orientation distribution. Journal of the Acoustical Society of America 93, 2985–2988.

Chu, D., Wiebe, P.H., Stanton, T.K., Hammar, T.R., Doherty, K.W., Copley, N.J., Zhang, J., Reeder, D.B., Benfield, M.C., 2000. Measurements of the material properties of live marine organisms and their influence on acoustic scattering. Proceedings of the OCEANS 2000 MTS/IEEE International Symposium, Sept. 11–14, 2000, Providence, RI, Vol. 3, pp. 1963–1967

Chu, D., Wiebe, P.H., Copley, N.J., Lawson, G.L., Puvanendran, V., 2003. Material properties of North Atlantic cod eggs and early stage larvae and their influence on acoustic scattering. ICES Journal of Marine Science 60, 508–515.

Davis, C.S., Wiebe, P.H., 1985. Macrozooplankton biomass in a warm-core Gulf Stream ring: Time series changes in size structure, taxonomic composition, and vertical distribution. Journal of Geophysical Research 90, 8871–8882.

Davis, C.S., Gallager, S.M., Solow, A.R., 1992. Microaggregations of oceanic plankton observed by towed video microscopy. Science 257, 230–232.

Dinniman, M.S., Klinck, J.M., 2004. A model study of circulation and cross-shelf exchange on the west Antarctic peninsula continental shelf. Deep-Sea Research II, this issue [doi:10.1016/j.dsr2.2004.07.030].

Ehrenberg, J.E., Torkelson, T.C., 2000. FM slide (chirp) signals: a technique for significantly improving the signal-to-noise performance in hydroacoustic assessment systems. Fisheries Research 47, 193–199.

Fach, B.A., Hofmann, E.E., Murphy, E.J., 2002. Modeling studies of antarctic krill *Euphausia superba* survival during transport across the Scotia Sea. Marine Ecology Progress Series 231, 187–203.

Foote, K.G., Stanton, T.K., 2000. Acoustical methods. In: Harris, R.P., Wiebe, P.H., Lenz, J., Skjoldal, H.R., Huntley, M. (Eds.), ICES Zooplankton Methodology Manual. Academic Press, Boston, pp. 223–258.

Foote, K.G., Knudsen, H.P.,Vestnes, G., MacLennan, D.N., Simmonds, E.J., 1987. Calibration of acoustic instruments for fish density estimation: a practical guide. ICES Cooperative Research Report 144.

Gallager, S.M., Daly, K., Fisher, K., Lawson, G., Davis, C.S., Ashjian, C., Wiebe, P.H., 2002. Seasonal changes in the association of larval krill with its potential microplankton food resource along the Western Antarctic Peninsula. Eos, Transactions of the American Geophysical Union, 84, Ocean Sciences Meeting Supplement, Abstract OS51A-13.

Gutt, J., Siegel, V., 1994. Benthopelagic aggregations of krill (*Euphausia superba*) on the deeper shelf of the Weddell Sea (Antarctic). Deep-Sea Research I 41, 169–178.

Hewitt, R.P., Demer, D.A., 2000. The use of acoustic sampling to estimate the dispersion and abundance of euphausiids, with an emphasis on Antarctic krill, *Euphausia superba*. Fisheries Research 47, 215–229.

Hewitt, R.P., Demer, D.A., Emery, J.H., 2003. An 8-year cycle in krill biomass density inferred from acoustic surveys conducted in the vicinity of the South Shetland Islands during the austral summers of 1991 1992 through 2001–2002. Aquatic Living Resources 16, 205–213.

Heywood, R.B., Everson, I., Priddle, J., 1985. The absence of krill from the South Georgia zone, winter 1983. Deep-Sea Research 32, 369–378.

Hofmann, E.E., Klinck, J.M., 1998. Hydrography and circulation of the Antarctic continental shelf: 150°E eastward to the Greenwich Meridian. In: Robinson, A.R., Brink, K.H. (Eds.), The Sea, The Global Coastal Ocean, Regional Studies and Synthesis, Vol. 11, pp. 997–1042.

Hofmann, E.E., Klinck, J.M., Lascara, C.M., Smith, D.A., 1996. Water mass distribution and circulation west of the Antarctic Peninsula and including Bransfield Strait. In: Ross, R.M., Hofmann, E.E., Quetin, L.B. (Eds.), Foundations for ecological Research West of the Antarctic Peninsula, American Geophysical Union, Washington, DC, Antarctic Research Series, Vol. 70, pp. 61–80.

Hofmann, E.E., Klinck, J.M., Costa, D.P., Daly, K.D., Torres, J.J., Fraser, W.R., 2002. US Southern Ocean Global Ocean Ecosystem Dynamics Program. Oceanography 15, 64–74.

Ichii, T., 2000. Krill harvesting. In: Everson, I. (Ed.), Krill: Biology, Ecology and Fisheries. Blackwell Science, Oxford, pp. 228–261.

Kawaguchi, K., Matsuda, O., Ishikawa, S., Naito, Y., 1986. A light trap to collect krill and other micronektonic and planktonic animals under the Antarctic coastal fast ice. Polar Biology 6, 37–42.

Kils, U., 1981. Swimming behavior, swimming performance and energy balance of Antarctic krill *Euphausia superba*. BIOMASS Scientific Series 3, 1–122.

Klinck, J.M., Hofmann, E.E., Beardsley, R.C., Salihoglu, B., Howard, S., 2004. Water-mass properties and circulation on the west Antarctic Peninsula Continental Shelf in Austral Fall and Winter 2001. Deep-Sea Research II, this issue [doi:10.1016/j.dsr2.2004.08.001].

Lascara, C.M., Hofmann, E.E., Ross, R.M., Quetin, L.B., 1999. Seasonal variability in the distribution of Antarctic krill, *Euphausia superba*, west of the Antarctic Peninsula. Deep-Sea Research I 46, 951 984.

Laws, R.M., 1985. The ecology of the Southern Ocean. American Scientist 73, 26–40.

Le Fèvre, J., Legendre, L., Rivkin, R.B., 1998. Fluxes of biogenic carbon in the Southern Ocean: roles of large microphagous zooplankton. Journal of Marine Systems 17, 325–345.

Macaulay, M.C., English, T.S., Mathisen, O.A., 1984. Acoustic characterization of swarms of Antarctic krill (*Euphausia superba*) from Elephant Island and Bransfield Strait. Journal of Crustacean Biology 4 (Spec. No. 1), 16–44.

MacLennan, D.N., Simmonds, E.J., 1992. Fisheries Acoustics. Chapman & Hall, London.

Madureira, L.S.P., Ward, P., Atkinson, A., 1993. Differences in backscattering strength determined at 120 and 38 kHz for three species of Antarctic macroplankton. Marine Ecology Progress Series 93, 17–24.

Marin, V.H., Brinton, E., Huntley, M., 1991. Depth relationships of *Euphausia superba* eggs, larvae and adults near the Antarctic Peninsula, 1986–87. Deep-Sea Research 38, 1241 1249.

Medwin, H., Clay, C.S., 1998. Fundamentals of Acoustical Oceanography. Academic Press, Boston.

Murphy, E.J., Trathan, P.N., Everson, I., Parkes, G., Daunt, F., 1997. Krill fishing in the Scotia Sea in relation to bathymetry, including the detailed distribution around South Georgia. CCAMLR Science 4, 1–17.

Murray, A.W.A., Watkins, J.L., Bone, D.G., 1995. A biological acoustic survey in the marginal ice-edge zone of the Bellingshausen Sea. Deep-Sea Research II 42, 1159–1175.

Nicol, S., Pauly, T., Bindoff, N.L., Wright, S., Thiele, D., Hosie, G.W., Strutton, P.G., Woehler, E., 2000. Ocean circulation off east Antarctica affects ecosystem structure and sea-ice extent. Nature 406, 504–507.

Pauly, T., Nicol, S., Higginbottom, I., Hosie, G., Kichener, J., 2000. Distribution and abundance of Antarctic krill (*Euphausia superba*) off East Antarctica (80–150 E) during the Austral summer of 1995/1996. Deep-Sea Research II 47, 2465–2488.

Priddle, J., Smetacek, V., Bathmann, U., 1992. Antarctic marine primary production, biogeochemical carbon cycles and climatic change. Philosophical Transactions: Biological Sciences 338, 289–297.

Ross, R.M., Quetin, L.B., Lascara, C.M., 1996. Distribution of Antarctic krill and dominant zooplankton west of the Antarctic Peninsula. In: Ross, R.M., Hofmann, E.E., Quetin, L.B. (Eds.), Foundations for Ecological Research west of the Antarctic Peninsula, American Geophysical Union, Washington DC, Antarctic Research Series, vol. 70, pp. 199–218.

Sahrhage, D., 1989. Hydroacoustic detection of krill during "Polarstern" cruises ANT V/1 and ANT VI/2 (1987). Archiv für Fischereiwissenschaft 39, 73–80.

Sameoto, D., Cochrane, N., Herman, A.W., 1993. Convergence of acoustic, optical, and net-catch estimates of euphausiid abundance: use of artificial light to reduce net avoidance. Canadian Journal of Fisheries and Aquatic Science 50, 334–346.

Schnack-Schiel, S.B., Hagen, W., Mizdalski, E., 1998. Seasonal carbon distribution of copepods in the eastern Weddell Sea, Antarctica. Journal of Marine Systems 17, 305–311.

Siegel, V., 1988. A concept of seasonal variation of krill (*Euphausia superba*) distribution and abundance west of the Antarctic Peninsula. In: Sarhage, D. (Ed.), Antarctic Ocean and Resources Variability. Springer, Berlin, Heidelberg, pp. 219–230.

Siegel, V., 1989. Winter and spring distribution and status of the krill stock in Antarctic Peninsula waters. Archiv für Fischereiwissenschaft 39, 45–72.

Siegel, V., 2000. Krill (Euphausiacea) demography and variability in abundance and distribution. Canadian Journal of Fisheries and Aquatic Sciences 57 (Suppl. 3), 151–167.

Smith, D.A., Hofmann, E.E., Klink, J.M., Lascara, C.M., 1999. Hydrography and circulation of the west Antarctic Peninsula continental shelf. Deep-Sea Research I 46, 925–949.

Sokal, R.R., Rohlf, F.J., 2000. Biometry: The Principles and Practice of Statistics in Biological Research. W.H. Freeman and Co., New York.

Sprong, I., Schalk, P.H., 1992. Acoustic observations on krill spring-summer migration and patchiness in the northern Weddell Sea. Polar Biology 12, 261–268.

Stanton, T.K., Chu, D., 2000. Review and recommendations for the modelling of acoustic scattering by fluid-like elongated zooplankton: euphausiids and copepods. ICES Journal of Marine Science 57, 793–807.

Stanton, T.K., Wiebe, P.H., Chu, D., Benfield, M.C., Scanlon, L., Martin, L., Eastwood, R.L., 1994. On acoustic estimates of zooplankton biomass. ICES Journal of Marine Science 51, 505–512.

Stanton, T.K., Chu, D., Wiebe, P.H., 1998. Sound scattering by several zooplankton groups. II. Scattering models. Journal of the Acoustical Society of America 103, 236–253.

Thiele, D., Chester, E., Moore, S., Širovic, A., Hildebrand, J., Friedlaender, A., 2004. Seasonal variability in whale encounters in the Western Antarctic Peninsula. Deep-Sea Research II, this issue [doi:10.1016/j.dsr2.2004.07.007].

US Southern Ocean GLOBEC, 2002. Report of the RVIB Nathaniel B. Palmer Cruise 02-02 to the Western Antarctic Peninsula, 9 April to 21 May 2002. United States Southern Ocean Global Ocean Ecosystems Dynamics Program Report Number 9. Old Dominion University, Norfolk, VA. 190pp.

Voronina, N.M., 1998. Comparative abundance and distribution of major filter-feeders in the Antarctic pelagic zone. Journal of Marine Systems 17, 375–390.

Warren, J.D., Stanton, T.K., Benfield, M.C., Wiebe, P.H., Chu, D., Sutor, M., 2001. In situ measurements of acoustic target strengths of gas-bearing siphonophores. ICES Journal of Marine Science 58, 740–749.

Warren, J.D., Stanton, T.K., Wiebe, P.H., Seim, H.E., 2003. Inference of biological and physical parameters in an internal wave using multiple-frequency, acoustic-scattering data. ICES Journal of Marine Science 60, 1033–1046.

Watkins, J.L., Brierley, A.S., 2002. Verification of the acoustic techniques used to identify Antarctic krill. ICES Journal of Marine Science 59, 1326–1336.

Watkins, J.L., Morris, D.J., Ricketts, C., Priddle, J., 1986. Differences between swarms of Antarctic krill and some implications for sampling krill populations. Marine Biology 93, 137–146.

Watkins, J.L., Morris, D.J., Ricketts, C., Murray, A.W.A., 1990. Sampling biological characteristics of krill: effect of heterogeneous nature of swarms. Marine Biology 107, 409–415.

Weeks, A.R., Griffiths, G., Roe, H., Moore, G., Robinson, I.S., Atkinson, A., Shreeves, R., 1995. The distribution of acoustic backscatter from zooplankton compared with physical structure, phytoplankton and radiance during the spring bloom in the Bellingshausen Sea. Deep-Sea Research II 42, 997–1019.

Wiebe, P.H., Morton, A.W., Bradley, A.M., Backus, R.H., Craddock, J.E., Cowles, T.J., Barber, V.A., Flierl, G.R., 1985. New developments in the MOCNESS, an apparatus for sampling zooplankton and micronekton. Marine Biology 87, 313–323.

Wiebe, P.H., Copley, N.J., Boyd, S.H., 1992. Coarse-scale horizontal patchiness and vertical migration of zooplankton in Gulf Stream warm-core ring 82-H. Deep-Sea Research 39 (Suppl. 1), S247 S278.

Wiebe, P.H., Mountain, D., Stanton, T.K., Greene, C., Lough, G., Kaartvedt, S., Manning, J., Dawson, J., Martin, L., Copley, N., 1996. Acoustical study of the spatial distribution of plankton on Georges Bank and the relation of volume backscattering strength to the taxonomic composition of the plankton. Deep-Sea Research II 43, 1971–2001.

Wiebe, P.H., Stanton, T.K., Greene, C.H., Benfield, M.C., Sosik, H.M., Austin, T., Warren, J.A., Hammar, T., 2002. BIOMAPER II: An integrated instrument platform for coupled biological and physical measurements in coastal and oceanic regimes. IEEE Journal of Oceanic Engineering 27, 700–716.

Wiebe, P.H., Ashjian, C., Gallager, S., Davis, C., Lawson, G.L., Copley, N., 2004. Using a high powered strobe light to increase the catch of Antarctic krill. Marine Biology 144, 493–502.

Woodd-Walker, R.S., Watkins, J.L., Brierley, A.S., 2003. Identification of Southern Ocean acoustic targets using aggregation backscatter and shape characteristics. ICES Journal of Marine Science 60, 641–649.

Zhou, M., Dorland, R.D., 2004. Aggregation and vertical migration behavior of *Euphausia superba*. Deep-Sea Research II, this issue [doi:10.1016/j.dsr2.2004.07.009].

Zhou, M., Nordhausen, W., Huntley, M., 1994. ADCP measurements of the distribution and abundance of euphausiids near the Antarctic Peninsula in winter. Deep-Sea Research I 41, 1425–1445.

Zhou, M., Zhu, Y., Peterson, J.O., 2004. In situ growth and mortality of mesozooplankton during the austral fall and winter in Marguerite Bay and its vicinity. Deep-Sea Research II, this issue [doi:10.1016/j.dsr2.2004.07.008].

ELSEVIER

Deep-Sea Research II 51 (2004) 2073–2098

DEEP-SEA RESEARCH
PART II

www.elsevier.com/locate/dsr2

Distribution of zooplankton on the continental shelf off Marguerite Bay, Antarctic Peninsula, during Austral Fall and Winter, 2001

Carin J. Ashjian*, Gaelin A. Rosenwaks[1], Peter H. Wiebe, Cabell S. Davis, Scott M. Gallager, Nancy J. Copley, Gareth L. Lawson, Philip Alatalo

Department of Biology, Woods Hole Oceanographic Institution, Woods Hole, MA 02543, USA

Accepted 12 July 2004

Abstract

The Marguerite Bay region of the Western Antarctic Peninsula is known to support a large population of krill during the summer and is hypothesized to be a site of successful overwintering of krill. The distributions of zooplankton biomass, abundance, and taxonomic composition at six locations on or near the continental shelf at Marguerite Bay were determined for fall and winter, 2001, as a part of the Southern Ocean GLOBEC program. Water column zooplankton were sampled using a 1-m^2 MOCNESS. Samples were analyzed for taxonomic composition, size, and estimated biomass using silhouette analysis. Characteristics of four categories (small and large copepods, small and large krill) were described in detail.

Total biomass and abundance were markedly reduced in winter relative to fall. The vertical distributions of total abundance and biomass, and of taxonomic composition, were associated with the hydrographic structure of the water column. Larger larval krill were observed at all locations during winter than during fall. Krill were relatively unimportant to total biomass and abundance at most locations, while copepods frequently dominated both biomass and abundance. In fall, greatest abundance and biomass of larval krill were observed on the continental shelf in association with a persistent clockwise gyre located to the west of Adelaide Island. During winter, much lower abundances of larval krill were present in the water column throughout the study region. High abundance and biomass of juvenile and adult krill were observed only in Laubeuf Fjord (Marguerite Bay) during fall.
© 2004 Elsevier Ltd. All rights reserved.

1. Introduction

Krill are considered key members of the Antarctic ecosystem, often dominating biomass and abundance and providing an essential food

*Corresponding author. Tel.: +1 508 289 3457; fax: +1 508 457 2169.
E-mail address: cashjian@whoi.edu (C.J. Ashjian).
[1]Present address: 224 East 67th St., New York, NY 10021, USA.

0967-0645/$ - see front matter © 2004 Elsevier Ltd. All rights reserved.
doi:10.1016/j.dsr2.2004.07.025

supply to a rich, upper trophic level community including seabirds, seals, and whales (Marr, 1962; Laws, 1985). Because of their pivotal importance in the ecosystem and their potential commercial value, considerable study has been devoted to understanding the life histories and ecology of krill in different regions of the Antarctic (e.g., Smith and Schnack-Schiel, 1990; El-Sayed, 1996; Everson, 2000). However, because of the difficulties in accessing and sampling these ice-covered regions during winter, understanding of the overwintering strategies, including the distributions and habitat utilizations of krill, is limited (Hofmann et al., 2002). The Antarctic Peninsula is believed to be a source of krill populations for regions to the north and east. Krill are hypothesized to spawn offshore along the western continental shelf of the Peninsula in summer, with the resulting larval krill spreading across the shelf in the next year and moving northwards to replenish populations from the Gerlach Straits to as far north as South Georgia Island (Hofmann et al., 1988; Siegel, 1988; Ross and Quetin, 2000; Atkinson et al., 2001; Fach et al., 2002).

The Southern Ocean Global Ocean Ecosystems Dynamics (GLOBEC) program was a 2-year field program to elucidate the overwintering strategies of krill (Hofmann et al., 2002). Marguerite Bay, Antarctic Peninsula was chosen as the focus of the Southern Ocean GLOBEC program, because it was characterized by several factors thought to be important to successful overwintering of krill: regular and persistent winter sea-ice cover, physical oceanographic features (gyre) that promote retention of krill locally, and input of nutrient-rich Upper Circumpolar Deep Water (UCDW) onto the shelf (Hofmann et al., 1996; Smith et al., 1999). Marguerite Bay contains a rich and diverse krill predator community that must be supported by a persistent krill population (Costa and Crocker, 1996; Fraser and Trivelpiece, 1996). It was hypothesized that the gyre system present on the shelf serves as a retention mechanism for krill in this region, permitting high abundances of krill to overwinter there and allowing the Marguerite Bay region to be a source of krill for the Antarctic Peninsula.

Although krill are perceived to be the dominant component of the zooplankton in the Antarctic, few reports on the relative abundances and biomass of non-krill taxa are available. Many zooplankton studies in the Southern Ocean have been conducted using estimates of biomass derived from backscatter intensity; these biomass estimates usually have assumed that krill are the primary scatterers (Daly and Macaulay, 1988; El-Sayed, 1994; Sprong and Shalk, 1992; Lascara et al., 1999; Hewitt and Demer, 2000; Pauly et al., 2000; reviewed in Hewitt and Demer, 2000, but see Brierley et al., 1998). There have been reports, however, that krill may not always dominate the zooplankton, particularly when salps are present (Voronina, 1983, 1998; Loeb et al., 1997). Understanding of the Southern Ocean ecosystem requires descriptions of the abundance of all taxonomic categories, including copepods and other diverse taxa.

During 2001, two broad-scale cruises were conducted to Marguerite Bay and the adjacent shelf as part of the Southern Ocean GLOBEC program to survey physical and biological characteristics of the ecosystem during fall and winter. The net component of the project had two main objectives: (1) to determine the vertical distribution, abundance, and size structure of the dominant zooplankton, especially krill, at selected locations across the survey region; and (2) to collect information on the taxonomic composition and size distribution of the zooplankton in order to ground-truth the acoustic data collected using the BIOMAPER-II multi-frequency acoustic system (Wiebe et al., 2002) and the video data collected by the Video Plankton Recorder (VPR, Davis et al., 1992) mounted on the BIOMAPER-II. The purpose of this paper is to describe distributions of zooplankton biomass, abundance, taxonomic composition, and their relationship to the vertical and hydrographic structure at the selected locations.

2. Methods

The two 6-week cruises were conducted on the RVIB *Nathaniel B. Palmer* from April 24 to June 5

and from July 24 to August 31, 2001. During each cruise, a broad-scale grid of stations encompassing the shelf to the north and south of Marguerite Bay, from the offshore deep water (>1000 m) to nearshore including Marguerite Bay, was surveyed using along-track and on-station measurement systems. The grid was laid out in 13 NW-SE transects, orthogonal to the shelf-break, with additional tracks inside Marguerite Bay.

Net sampling for zooplankton was conducted using a 1-m^2 Multiple Opening/Closing Net and Environmental Sensing System (MOCNESS) equipped with nine 335 μm mesh nets and a suite of environmental sensors including temperature and conductivity probes (Wiebe et al., 1976, 1985). The MOCNESS also was equipped with a strong strobe light that flashed at 4-s intervals (Wiebe et al., 2004). Because krill are strong swimmers and may see slow-moving nets such as the MOCNESS, krill frequently avoid being captured by net systems. The rationale behind the strobe system was to shock or blind the krill temporarily so that the net would not be perceived and avoided. Use of the strobe light resulted in significantly enhanced catches of krill larger than 15 mm relative to when the strobe was not used (Wiebe et al., 2004). No significant differences in the catch of krill less than 15 mm were observed with or without the strobe flashing, demonstrating that avoidance of the MOCNESS by larval krill, even without the strobe, was not a problem. These results suggested that avoidance of the net by large krill was decreased when the strobe was flashing and that the MOCNESS equipped with a strobe is an effective instrument for sampling krill.

Tows were conducted at selected sites across the shelf, off the shelf in deep (>1000 m) water, and in Marguerite Bay. Twenty-four tows were conducted during the fall 2001 and 17 during the

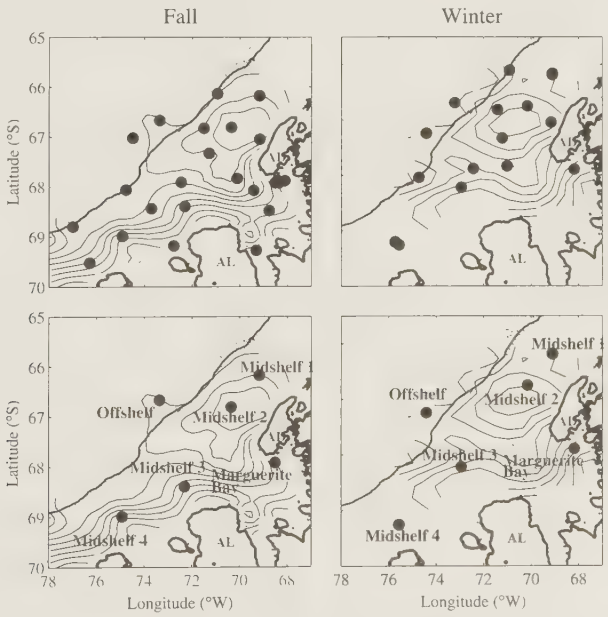

Fig. 1. Locations where MOCNESS tows were conducted on the Antarctic Peninsula. Upper panels: Locations of all tows conducted during fall (left) and winter (right) relative to bottom and dynamic height topographies. Solid, heavy contours show coastline and 2000 m isobath; dashed contours show 1000 and 3000 m isobaths. Solid, thin contours show dynamic height, relative to 400 dbars (Klinck et al., 2004). The gyre in the northern region is a dynamic low so that circulation flows clockwise (cyclonic) around the approximate location of the Midshelf 2 station. Contours of flow along Adelaide Island, through Marguerite Bay, and along the southern shelf show advection from north to south with higher dynamic heights further inshore. (AD = Adelaide Island, AL – Alexander Island). Lower panels: Locations and site names of each pair of MOCNESS tows analyzed during this study; this nomenclature is used throughout the paper.

winter 2001 (Fig. 1). Tow locations were selected based on bathymetry and hydrographic location. Several tows were conducted off of the continental shelf in water of >1000 m depth where the Antarctic Circumpolar Current impinges on the shelf (Hofmann et al., 1996; Smith et al., 1999). Several tows were located within the geographic confines of Marguerite Bay itself. The other tows were dispersed approximately evenly across the shelf, with a line of tow locations extending from north to south along the axis of the shelf and intersecting the center of the reported cyclonic gyre on the shelf (Smith et al., 1999). Tows were conducted without regard to time of day. Resource limitations dictated that only a subset of the tows could be analyzed. Six from each season were selected, again based on bathymetry and hydrography, as follows: one tow from the deep water off the shelf, one tow from within Marguerite Bay, and four tows from along the axis of the shelf (Fig. 1, Table 1). These 12 tows (six from each season) were analyzed for total biomass and taxonomic abundance and composition. The six winter tows were conducted under ice of 6/10s or greater total cover (Table 1). At most locations, oblique tows were conducted from the surface to near bottom, sampling the entire water column on the down cast with the first net and selected depths on the up cast with the remaining eight nets. Typically, the upper 100 m was sampled at 25 m intervals, with 50 m intervals in the intermediate depth ranges and greater intervals (150, 200 m) in the deepest depth ranges. Unpredictable and uneven topography limited the maximum depths of some tows during both seasons (Table 1). During the winter, considerable difficulty was encountered while towing in ice so that the portion of the water column near the bottom often could not be sampled and the upper 10 m typically was not sampled because considerable quantities of broken pack ice were present in that depth interval. Samples were preserved upon recovery in 4% buffered formalin seawater.

Biomass (wet weight) and abundance were determined principally by silhouette digitization of taxa lengths and conversion to equivalent wet weights according to the equations and methods adapted from Davis and Wiebe (1985) and Wiebe et al. (2004). New formulas were calculated for Southern Ocean krill because the length–weight relationship ($\text{Wet Weight} = 0.0054 \times \text{Length}^{3.214}$) differed from that of the North Atlantic euphausiids ($\text{Wet Weight} = 0.0138 \times \text{Length}^{3.071}$; Davis and Wiebe, 1985).

Table 1
Summary of locations, times, and depths for the 12 net tows

Cruise	Region	Tow number	Date	Time (local)	Light	Latitude (°S)	Longitude (°W)	Tow depth (m)	Bottom depth (m)	Ice cover (tenths)
Fall	Offshore	6	05/04/01	1332	D	66° 40.17	73° 22.08	0–1001	3650	0
	Midshelf 1	1	04/30/01	2050	N	66° 10.80	69° 10.47	0–306	360	0
	Midshelf 2	3	05/02/01	0320	N	66° 48.53	70° 21.42	0–348	600	0
	Midshelf 3	12	05/13/01	1830	N	68° 23.62	72° 18.44	0–356	400	0
	Midshelf 4	16	05/18/01	0854	N	68° 59.43	74° 55.77	0–340	350	0
	Marguerite Bay	24	05/29/01	0300	N	67° 55.33	68° 30.69	0–602	690	0
Winter	Offshore	11	08/11/01	0918	T	67° 14.69	74° 25.27	0–989	2917	10
	Midshelf 1	17	08/26/01	0306	N	66° 11.13	69° 06.21	7–305	346	6
	Midshelf 2	4	07/31/01	0949	D	66° 45.18	70° 09.64	11–413	501	8
	Midshelf 3	13	08/17/01	2117	N	68° 13.21	72° 56.53	0–230	325	10
	Midshelf 4	14	08/21/01	1136	D	69° 15.55	75° 34.00	20–290	~340	7
		15	08/22/01	0327	N	69° 12.30	75° 43.90	0–91	~350	9
	Marguerite Bay	9	08/08/01	0215	N	67° 53.74	68° 10.82	0–488	600+	9

Light conditions are designated as "D" = day, sunlight present; "N" = night, darkness; "T" = twilight.

Silhouette photographs were first obtained from each sample; the photographs were then scanned with an Epson Expression 1600 scanner at 1200 dpi to produce Tagged Image File Format (TIFF) images. Identification and measurement of organisms from the TIFF image were accomplished manually using the specialized MATLAB (Mathworks, Inc.) routine, the WHOI Silhouette DIGITIZER (v 1.0) (Little and Copley, 2003). A scanned photographic image of an aliquot of a sample was displayed with a superimposed reference grid on the computer screen. The operator identified each organism to taxonomic and/or size category by selecting the appropriate category button. Organism lengths (both straight and curved) then were measured by the operator using the cursor on the computer screen. Although the nominal resolution of the measurement is 0.02 mm, in practice the resolution was ~0.05 mm. In instances where there were too many organisms of a given type to justify measuring every individual organism, the DIGITIZER routine generated a list of cells to produce a stratified random sub-sample of the overall image. Each organism's biomass was calculated automatically from its length measurement using the appropriate length–weight relationship.

Total biomass also was estimated by determining the displacement volume of each preserved sample using methods modified from Ahlstrom and Thrailkill (1963) and then converting the displacement volume to equivalent wet weight (mg m^{-3}) using the functional regressions of Wiebe et al. (1975) and Wiebe (1988). The two methods for measuring zooplankton biomass were compared. Total water-column biomass (g wet weight m^{-2}) estimated from displacement volume was greater than that estimated from silhouette analysis for all times and locations except one (Fig. 2; Wilcoxon signed rank test, $p<0.001$). However, as described below, the seasonal and regional patterns observed in the displacement-volume-estimated biomass were the same as those observed using the silhouette analysis, so that the two methods yield the same relative patterns in biomass. The discrepancy may have resulted (1) from retention of liquid in the sample during the displacement volume estimate so that the volume

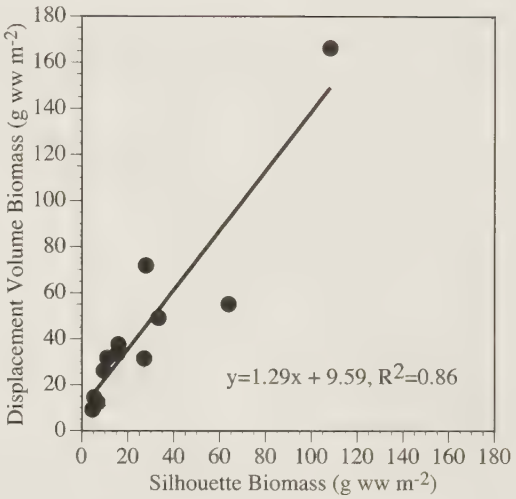

Fig. 2. Comparison of total water column wet weight biomass estimated from silhouette analysis and from displacement volume estimates. The functional regression (solid line, equation) and the 1:1 correspondence (dashed line) are shown.

was overestimated, (2) from different weight:volume ratios for the separate taxa that cannot be accounted for in the displacement volume to biomass calculation, or (3) from not all the biomass in the samples being accounted for in the silhouette measurements. Silhouette biomass estimates are used in this paper. Conversion between the two estimates can be done using the functional regression: displacement volume biomass (g ww m^{-3}) = 1.392 × (silhouette biomass, g ww m^{-3}) + 6.81.

For most taxa, all size categories were considered together. Large (2.5–10 mm) and small (0.001–2.499 mm) copepods and large (15–100 mm) and small (1.00–14.99 mm) euphausiids/krill were enumerated separately. Thirty-one taxonomic or size categories were identified in the images (Table 2), although only nine (large copepods, small copepods, large krill, small krill, ostracods, *Limacina* spp., amphipods, chaetognaths, polychaetes) were observed in abundance. Krill lengths were measured as Standard Length 3, from the posterior base of the eye stalk to the posterior margin of the sixth abdominal segment (Mauchline, 1980). Although not frequently used in measuring Antarctic krill, this length measurement is standard for the CalCOFI program (Isaacs

Table 2
Taxonomic and size categories used in the silhouette analysis

Diatoms	Copepod Nauplii
Foraminifera	Ostracods
Radiolarians	Euphausiids < 15.0 mm
Ctenophores	Euphausiids ≥ 15.0 mm
Medusae	Crustacean larvae
Siphonophore bracts	Mysids
Siphonophore nectophores	Isopod
Siphonophore pneumatophores	Amphipods
Clione	Chaetognaths
Pteropods—type *Styliola*	Salps
Pteropods—type *Limacina*	Larvaceans
Polychaete fragment	Fish
Polychaete larvae	Egg Sacs
Polychaetes	Eggs
Cladoceran	Sphere—large (≥0.5 mm)
Copepods < 2.5 nm	Sphere—small (<0.5 mm)
Copepods ≥ 2.5 nm	

Small and large spheres may be eggs or diatoms.

et al., 1969) and is appropriate for the length:biomass relationships used here to estimate krill biomass. Conversion from Standard Length 3 to the more common Standard Length 1 can be accomplished using a linear relationship established by measuring the two different lengths on 100 individuals $SL1 = (1.25 \times SL3) - 0.469$, $r^2 = 0.99$, where SL = Standard Length. The lengths and abundances were then used to estimate the total biomass in each taxonomic category for each sample. Common Antarctic copepod species that correspond to the two copepod size categories are *Metridia gerlachei*, *Oithona* spp., *Calanus propinquus*, *Microcalanus pygmaeus*, and *Oncaea* spp. for the small copepods and *Calanoides acutus*, *Rhincalanus gigas*, and *Paraeuchaeta antarctica* for the large copepods (Hopkins, 1985a; Smith and Schnack-Schiel, 1990; Atkinson and Shreeve, 1995; Ross et al., 1996; Schnack-Schiel et al., 1998; Voronina, 1998; Cabal et al., 2002). Silhouette images were qualitatively examined to determine the dominant copepod genera present. Common krill species in this region include *Euphausia superba*, *E. crystallorophias* (a coastal species), *E. frigida*, *E. triacantha* (an offshore species), *and Thysanoessa macrura* (e.g., Dzik and Jazdzewski, 1978; Ross et al., 1996; Smith and Schnack-Schiel, 1990). Based on known size distributions of the life stages of krill (Makarov, 1980), the small krill should be considered to be larval stages and the large krill to be juvenile and adult stages. Small krill are hence referred to as "larval krill" and large krill as "krill" for the remainder of this paper. Larval krill and krill from each category's depth of maximum abundance (not necessarily the same depth) from each tow were identified to species and life stage (larvae) by P. Hull.

For taxonomic composition of total abundance, eight taxonomic or size categories (Small Copepods, Large Copepods, Larval Krill, Krill, Chaetognaths, *Limacina* spp., Ostracods, Polychaetes) were dominant. For biomass composition, ten taxonomic or size categories (Small Copepods, Large Copepods, Larval Krill, Krill, Amphipods, Chaetognaths, Gelatinous Zooplankton, *Limacina* spp., Mysids, Polychaetes) comprised significant portions of the total biomass in many nets. Taxa present in low abundance or biomass were combined into a single category (Other) to reduce complexity. Four taxonomic/size categories (large copepods, small copepods, krill and larval krill) were targeted for separate consideration based on their relative importance to the overall biomass and abundance and to the understanding of the ecosystem. Mean depths of these four categories were calculated to represent their vertical distribution (Roe et al., 1984). The mean depth was calculated for each tow as

$$\text{mean depth} = \frac{\sum_{i=1}^{8} n_i z_i}{\sum_{i=1}^{8} n_i}$$

where n_i = abundance for the ith net (# m^{-3}), z_i = mean depth for the ith net, and there are eight nets.

3. Results

3.1. Hydrography

Dynamic height topographies calculated from CTD profiles from throughout the study area demonstrated mesoscale physical features (Fig. 1). Because of limited CTD sampling in the southern

region, dynamic height contours were not calculated to as far south in winter as during the fall. During each cruise, a mesoscale clockwise (cyclonic) gyre occupied much of the northern portion of the shelf (Fig. 1; Klinck et al., 2004). Advection was from north to south along the coast of Adelaide Island, into Marguerite Bay. During both seasons, a southwestward current extending from Marguerite Bay across the southern portion of the surveyed shelf region was present. The presence of these mesoscale features was supported by surface drifters that were deployed during the study period and by acoustic Doppler current profiler (ADCP) velocities measured from the ship (Beardsley et al., 2004; Klinck et al., 2004). The Antarctic Circumpolar Current (ACC) ran from SW to NE offshore of the shelf break.

Density was strongly influenced by salinity so that the vertical distribution of density closely resembled that of salinity. A strong pycnocline was observed in the upper water column at all locations (Fig. 3). The pycnocline was overlain by a mixed layer that varied with locations, being shallowest offshore and at the Midshelf 2 station during the fall. Hydrographic structure was influenced both by location and time since sampling occurred over an ~4-week period from north to south (Table 1). During the fall, seasonal cooling was observed in the upper water column temperatures and progressed with time as the shelf was surveyed from north to south. Remnants of the prior year's winter water (~ −1.5°C, Hofmann et al., 1996; Smith et al., 1999; Klinck et al., 2004) were observed as temperature minima located just below the mixed layer. This temperature minimum eroded with time, and hence location, as the upper water column cooled during the onset of winter and as a result of wind-induced deepening of the mixed layer. By contrast, mixed-layer temperatures (~−1.8°C) on the shelf during winter were far more consistent between locations. Variation in salinity structure was related to water mass changes and mixing. Vertical profiles of temperature and salinity at the Midshelf 2 site in fall resembled those observed at the offshore location; input of UCDW from offshore to the shelf occurred at this site (Klinck et al., 2004). The quite fresh salinities observed in Marguerite Bay

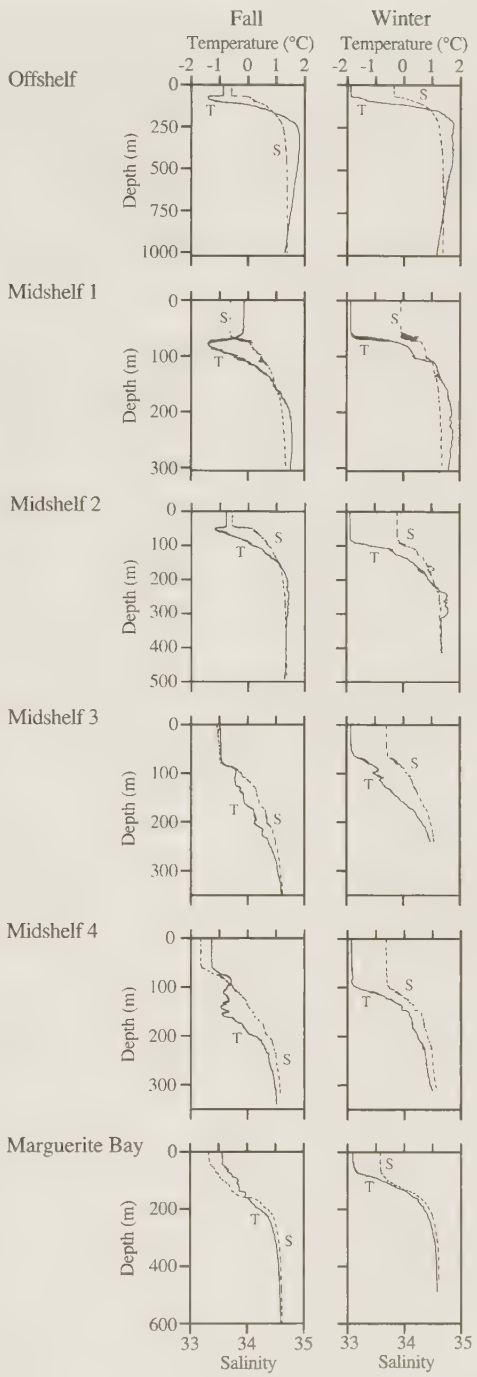

Fig. 3. Temperature and salinity characteristics of the water column at each location for fall (left column) and winter (right column) from the MOCNESS sensors. Temperature (°C) shown as the solid line; salinity shown as the dotted line. Depth scales are consistent for each location between the two seasons.

and on the southern shelf during fall in the MOCNESS environmental data (Fig. 3) likely resulted from the fresh, cold coastal current that ran south along Adelaide Island into Marguerite Bay and exited across the shelf to the south of the Bay in this current (Klinck et al., 2004).

3.2. Total water column biomass, abundance, and taxonomic composition

Water column plankton abundance (total biomass, total abundance) decreased substantially between fall and winter (Fig. 4; Wilcoxon signed rank test, $p<0.05$). Average abundances across the region decreased by 57%, from ~18,200 individuals m^{-2} to ~7800 individuals m^{-2}, while the decrease in average biomass was even greater (63%), from ~40.2 g wet weight m^{-2} in fall to ~14.8 g wet weight m^{-2} in winter.

Much greater biomass was found during the fall in Marguerite Bay than at shelf locations or offshore, whereas in winter biomass in Marguerite Bay was only slightly greater than in other areas. Elevated biomass also was found at the most southerly shelf location (Midshelf 4) during both seasons and was similar to the biomass in Marguerite Bay during winter. Biomass offshore was similar for both seasons and exceeded midshelf biomass at most locations in winter. No distinct regional patterns in abundance were observed (Fig. 4, lower panel).

Copepods and krill dominated biomass (62–93%) at most locations and times, with the exception of Midshelf 2 in winter (44%) (Fig. 5). Copepod biomass was closely correlated to total biomass ($r=0.90$, $p<0.01$) and represented 43% of total biomass on average. Krill biomass also was well correlated with total biomass when all tows are included ($r=0.87$, $p<0.01$) and represented 28% of total biomass on average. However, this correlation was strongly influenced by the high biomass of krill in Marguerite Bay during fall; the correlation between krill biomass and total biomass was much reduced ($r=0.27$) and not significant when this one tow is excluded. The elevated biomass observed during both fall and winter in Marguerite Bay (Fig. 4) was because of the high proportion of krill, both large and small,

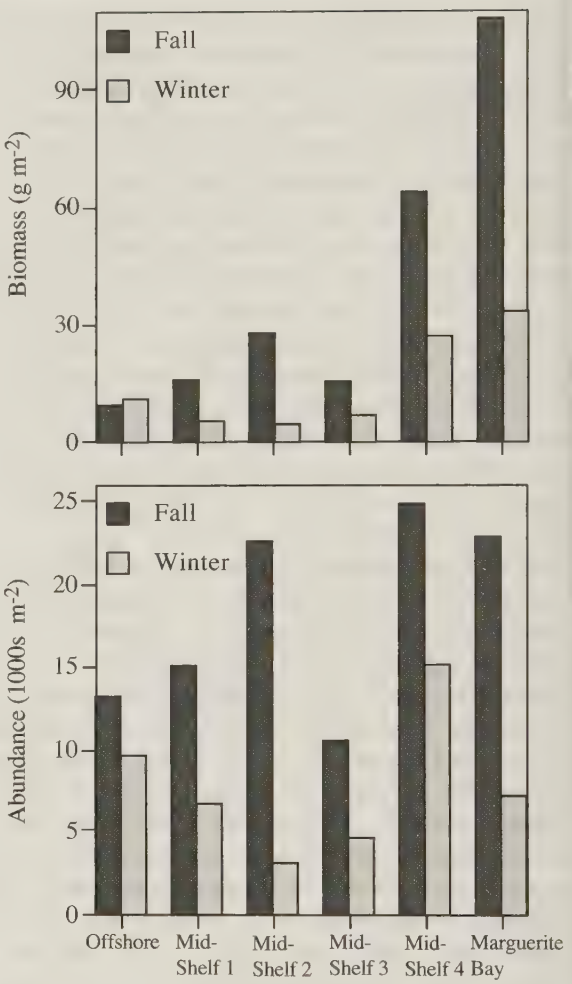

Fig. 4. Total water column wet weight biomass and zooplankton abundance for each fall–winter pair of tows at each location.

observed there. Large copepods also were important components of the total biomass in Marguerite Bay and the southern portion of the midshelf during the fall and at all locations in winter. The contribution of other taxa to the total biomass was 20% and 30% on average during fall and winter, respectively, and was spatially variable. It was greatest (~56%) at the Midshelf 2 location in winter and least (~8%) at the Midshelf 3 location in fall.

Total water-column abundance was dominated by the copepods, with larval krill numerically important only offshore and at the northern

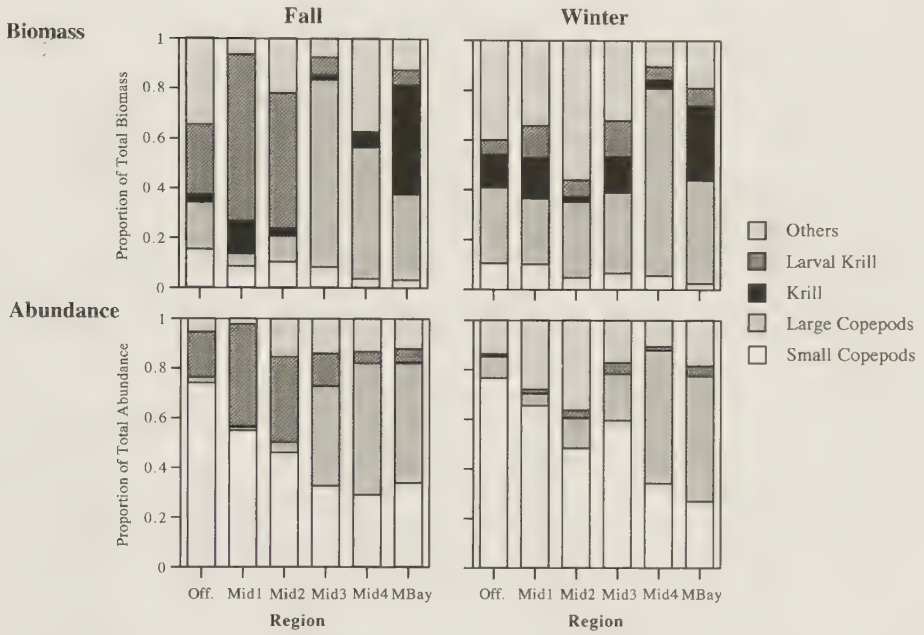

Fig. 5. Relative taxonomic composition of total water column wet weight biomass from silhouette analysis (upper row) and total water column abundance (lower row) for fall (left column) and winter (right column) at each location. The relative compositions of four important taxonomic groups (small and large copepods, small and large krill) are presented individually; all other taxa are combined into a single category (others). Total biomass and abundance for each time/location presented in Fig. 4.

midshelf locations during the fall (Fig. 5). Large krill were never significant numerically despite their great impact on total biomass at some locations. Small copepods dominated offshore and decreased in numerical importance moving from offshore (~70%) to Marguerite Bay (~30%) and also from north (60%) to south (~30%) along the axis of the shelf. In Marguerite Bay and on the southern portion of the shelf, the lower abundances of small copepods were accompanied by an increase in abundances of large copepods. Other taxa usually represented less than 20% of total numbers during the fall, except at the offshore location, but were relatively more abundant during the winter (~25–30%) when total abundances were reduced (Fig. 4).

3.3. Regional and seasonal variation in biomass and abundance of dominant taxa

Both total water-column biomass and abundance of the four important groups, large and small copepods and large and small krill, were greater during fall than during winter at most locations, although significantly greater only for small copepods and larval krill (Figs. 6 and 7, Wilcoxon signed rank test, $p<0.05$; note, because of the low number of data pairs (6), biomass or abundance at all six locations must be greater for a season in order to be significant). In addition, there were marked regional differences in the total water-column biomass and abundance of all groups except small copepods. For large copepods, greater biomass and abundance were found at the southernmost shelf location (Midshelf 4) and in Marguerite Bay. Large krill were most abundant and of greatest biomass in Marguerite Bay in the fall with elevated abundance but low biomass at the two northern midshelf locations. Larval krill were most abundant, and of greatest biomass, at the northern two shelf locations during fall.

3.4. Vertical distributions—biomass

Regional and seasonal differences in the vertical distribution of biomass and taxa were observed

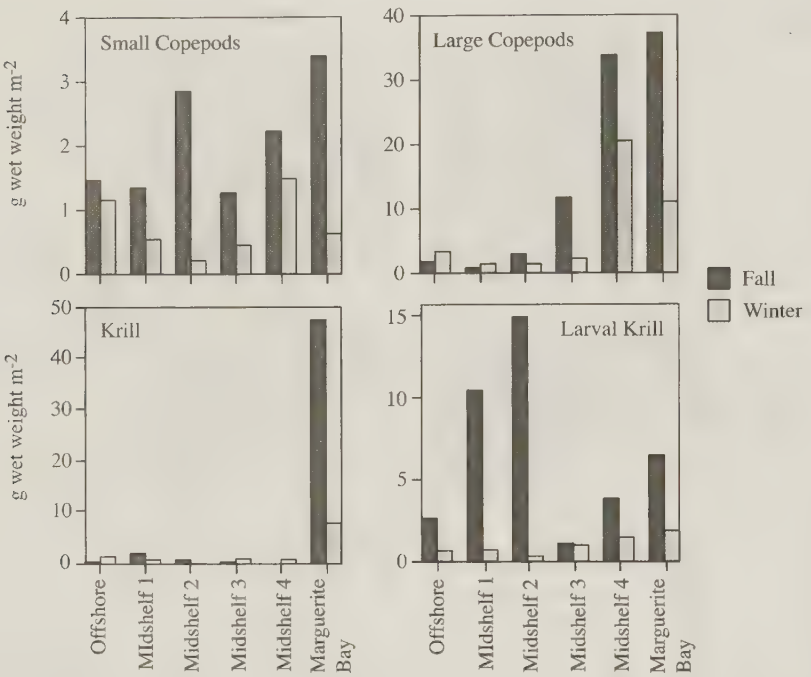

Fig. 6. Total water column wet weight biomass from silhouette analysis from each region and season for the four target taxonomic groups.

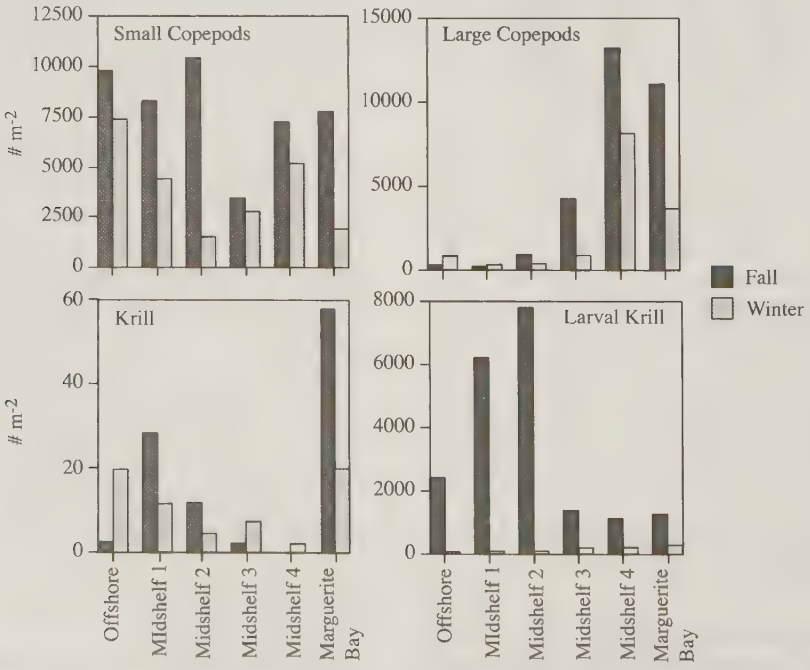

Fig. 7. Total water column abundance from each region and season for the four target taxonomic groups.

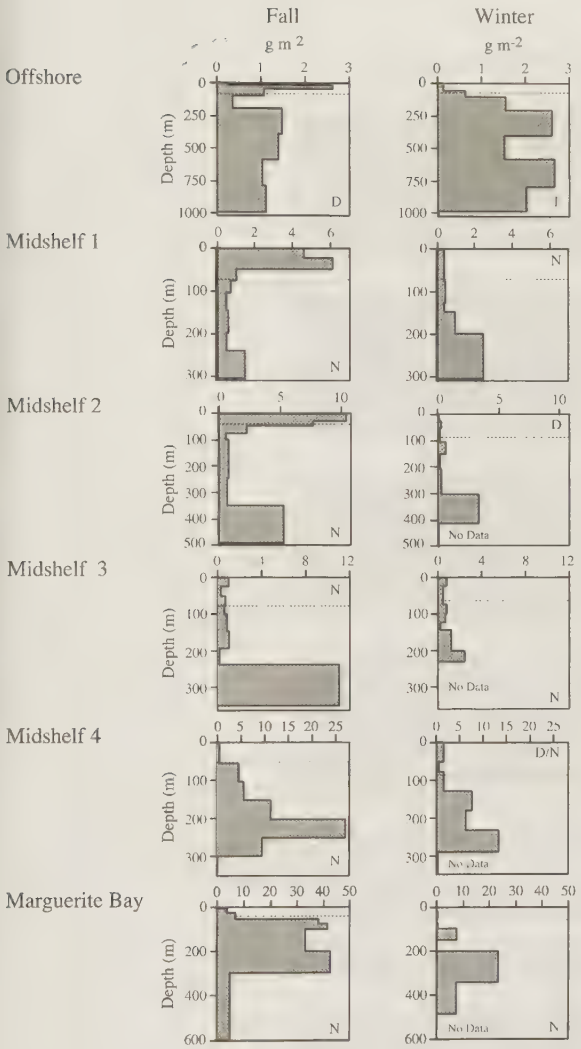

Fig. 8. Vertical distribution of wet weight biomass ($g m^{-2}$) from silhouette analysis at each location for fall (left column) and winter (right column). The maximum depth of the mixed layer is shown as the dotted horizontal line for each tow. Time of day (D(ay), N(ight), T(wilight)) indicated for each tow. At one location, designated as D/N, the upper 91 m was sampled during the night, while the lower depths were sampled during the day.

(Figs. 8, 9A and B). Generally, the proportion of biomass composed of larval krill decreased with depth while the proportion of large copepods and krill increased. Proportions of small copepods usually remained fairly constant throughout the water column. At most locations except Marguerite Bay, chaetognaths represented a significant proportion of the biomass at most depths. Gelatinous taxa also were important at some depths. At the offshore site, biomass was distributed nearly uniformly below the pycnocline. A biomass peak that was observed near the surface in fall had disappeared by winter. The taxonomic composition in terms of biomass was quite diverse, with most of the abundant taxa present.

At both of the more northern midshelf locations, minimum biomass was observed at mid-depths with greater biomass at depth. A prominent biomass peak of larval krill was present at both locations in and above the pycnocline during fall, which was not present during winter. *Limacina* spp. were important in the upper 100 m at both sites in winter and at Midshelf 2 in fall. Small fish and ostracods also were important at these locations in winter. Low biomass was observed throughout the upper water column at the Midshelf 3 location during both seasons, with a large biomass peak composed mainly of large copepods in the deepest depth interval during fall (note that the winter tow could not sample to closer than ~100 off the bottom because of ice; Table 1). At the southernmost shelf location, low biomass was observed in the mixed layer and much greater biomass occurred below, composed of large copepods and, in the fall at one depth, fish. Biomass was minimal near the bottom (note again that the winter tow did not extend to the bottom).

In Marguerite Bay, the vertical distributions differed between fall and winter. For both seasons, low biomass with a high proportion of larval krill was observed in the mixed layer above the pycnocline (~0–50 m). During fall, a prominent peak in biomass was observed below the pycnocline that was dominated by krill. A secondary peak in the bottom 200 m (~400–600 m) was dominated by large copepods (Fig. 9A). By contrast, in winter greatest biomass was observed from 200 to 488 m composed of large copepods, krill, and, at the deepest depth interval (346–488 m), gelatinous taxa (medusae).

3.5. *Vertical distributions—abundance*

The vertical distribution of abundance and taxa varied between seasons at the different sites and

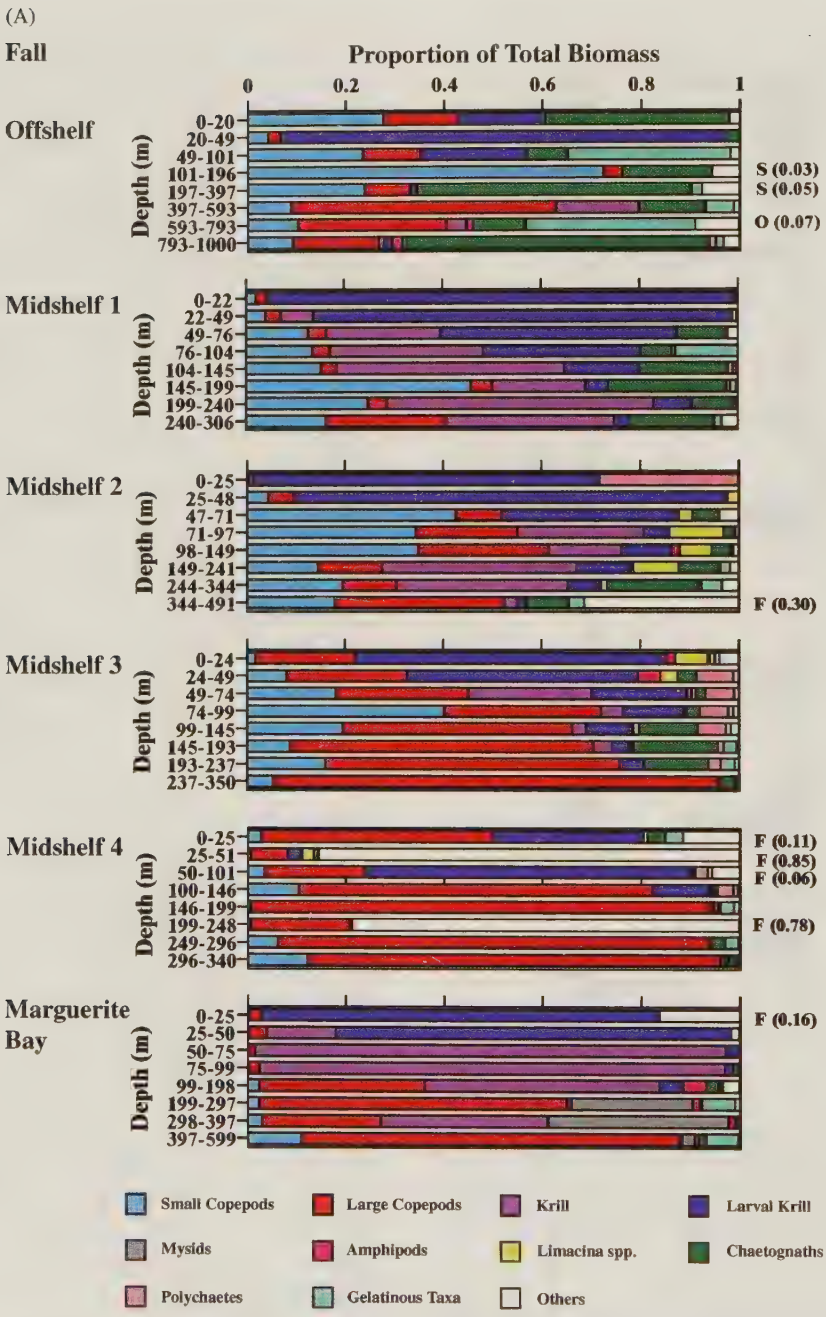

Fig. 9. Taxonomic composition as relative proportions of total wet weight biomass from silhouette analysis for each depth interval sampled at each location in (A) fall and (B) winter. Dominant taxa and proportions of the total biomass in the "other" category are identified for depths where the "other" category exceeded 5% of the total biomass (F = Fish, O = Ostracods, S = Salps).

even between sites within a season (Figs. 10, 11A and B). At the offshore location, greatest abundance was seen above 400 m during the fall. This peak was dominated by small copepods and larval krill. During winter, there was a much lower abundance of copepods and krill in the mixed

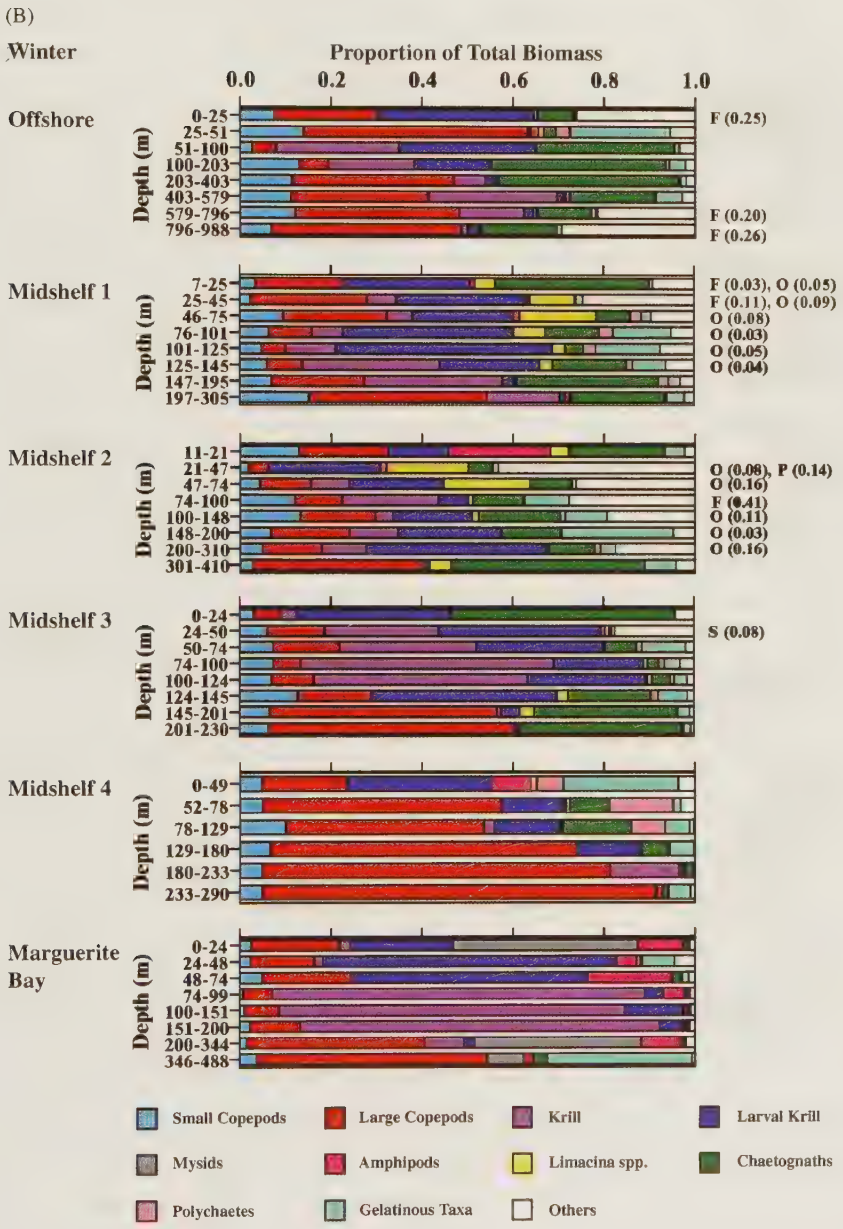

Fig. 9. (*Continued*)

layer. Small copepods dominated below the pycnocline during both seasons; however, large copepods and krill were relatively more important during winter. Chaetognaths, polychaetes, and, during winter, ostracods and *Limacina* spp. also were present at the offshore site in some abundance.

Midshelf locations in the north (Midshelf 1 and 2) had similar vertical patterns during fall, with elevated abundance in the pycnocline dominated by larval krill. A deeper abundance peak was dominated by small copepods. At Midshelf 2, *Limacina* spp. were abundant from 25 to 344 m and large copepods were present in moderate

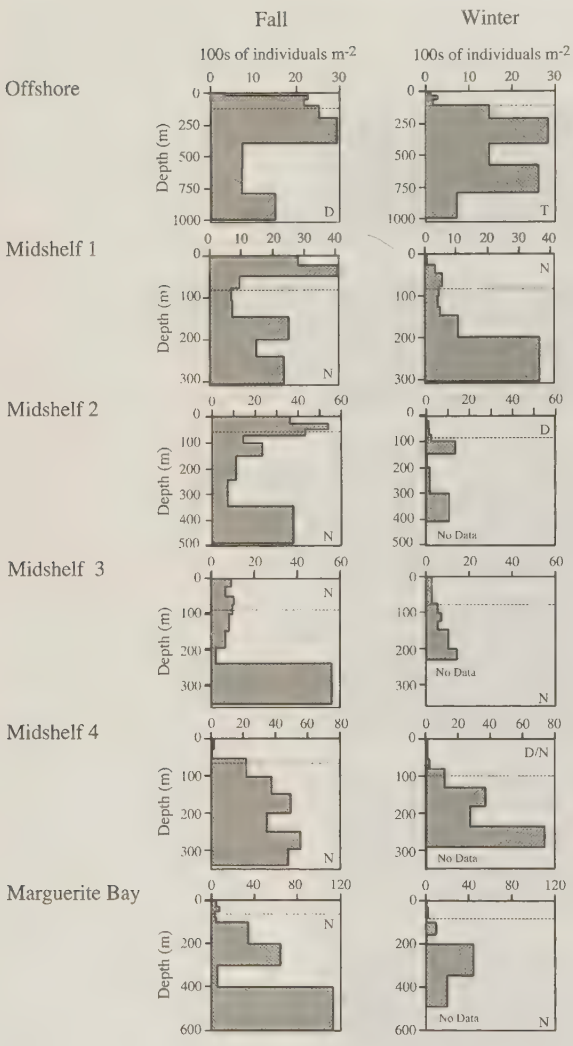

Fig. 10. Vertical distribution of zooplankton abundance ($100\,s\,m^{-2}$) at each location for fall (left column) and winter (right column). The maximum depth of the mixed layer is shown as the dotted horizontal line for each tow. Time of day (D(ay), N(ight), T(wilight)) indicated for each tow.

abundances at depth. The vertical distribution of abundance during winter at the Midshelf 1 site was dramatically different from that observed during the fall, with low abundance in the upper 150 m. The very low abundance consisted of larval krill, polychaetes, and other taxa and few copepods. The abundance peak near bottom (197–305 m) was comprised mainly (80%) of small copepods. Mid-depths (25–195 m) contained diverse taxa in low abundance, including *Limacina* spp. (~50%). At Midshelf 2 in winter, low abundances were observed throughout the water column, with no deep abundance peak. The composition was more diverse than usually observed on the shelf, with relatively low proportions of copepods (50–60%) and higher proportions of other taxa including *Limacina* spp., chaetognaths, and ostracods (10–35%).

Similarities between seasons at each site, but not between sites, were observed at the two southern midshelf sites (Midshelf 3 and 4). Low abundances were observed in the upper 225 m of the Midshelf 3 site during both seasons; the near-bottom depths, where elevated abundances were seen in fall, could not be sampled during the winter. Although the vertical patterns in total abundance were similar between seasons, taxonomic composition differed. Small copepods were more important during winter than fall. Large copepods were important at depth, especially during the fall. Polychaetes and *Limacina* spp. were found throughout the water column during both seasons. At Midshelf 4, diverse taxa (copepods, *Limacina* spp., polychaetes, others) were seen in low abundance above the pycnocline, with greater abundances of large and small copepods from 100 to 300 m during both seasons.

Marguerite Bay also had relatively low abundances above the pycnocline during both seasons and greater abundances below (Fig. 9). Abundances above the pycnocline were dominated by copepods and larval krill. Small copepods dominated abundances at depth in the fall. Greater proportions of large copepods, larval krill, and ostracods were observed throughout the sub-pycnocline water column in winter. The abundance peak at 200–488 m was dominated by large copepods (Fig. 10).

3.6. *Vertical distribution of copepods and krill*

The mean depth of a taxonomic category represents the central distribution of abundance in the water column and is useful as a single statistic to represent vertical distribution (Fig. 12) when the vertical distribution is mostly monotonic.

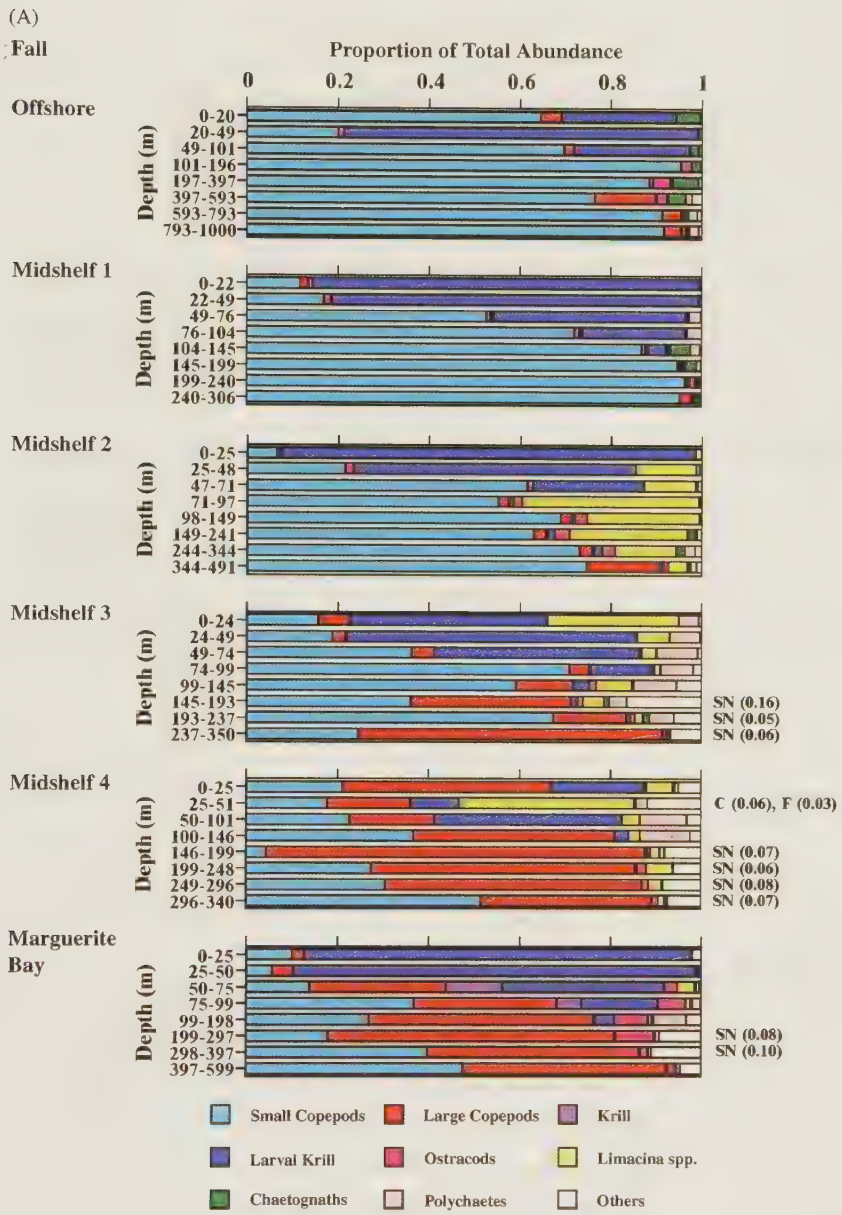

Fig. 11. Taxonomic composition as relative proportions of total zooplankton abundance for each depth interval sampled at each location in (A) fall and (B) winter. Dominant taxa and proportions of the total biomass in the "other" category are identified for depths where the "other" category exceeded 5% of the total abundance (C = Cladocerans, L = Larvaceans, R = Radiolarians, S(B)(N)(P) = Siphonophore Bracts and/or Nectophores and/or Pneumatophores).

Of the four target taxonomic categories, larval krill had the shallowest distribution (Wilcoxon signed rank, $p<0.05$ in comparison with the mean depths of the large copepods, larval krill, or juvenile/adult krill), with mean depths usually in the upper 100–150 m of the water column. Small copepods usually were shallower than large copepods (Wilcoxon signed rank, $p<0.05$).

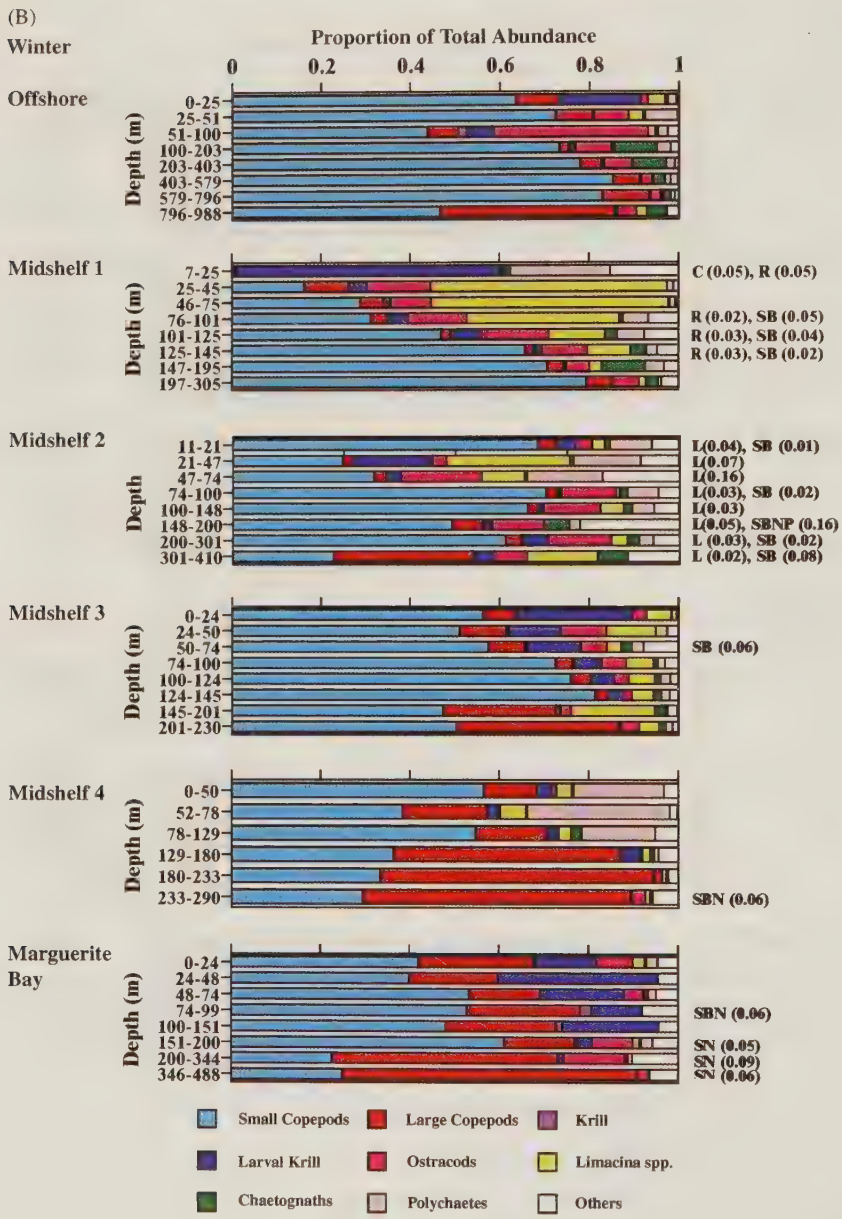

Fig. 11. (*Continued*)

3.7. Dominant copepod and krill species

Although quantitative descriptions of species distributions were not possible, qualitative evaluation of the copepod species or genera yielded some interesting insights. The small copepod fraction of the community everywhere was dominated by *M. gerlachei* copepodites, with cyclopoids (e.g., *Oncaea* spp., *Oithona* spp.) also abundant at the offshore site during both seasons. Large copepods were dominated by *C. acutus*, *C. propinquus*, *Gaedius* spp., adult *M. gerlachei*, *R. gigas*, and

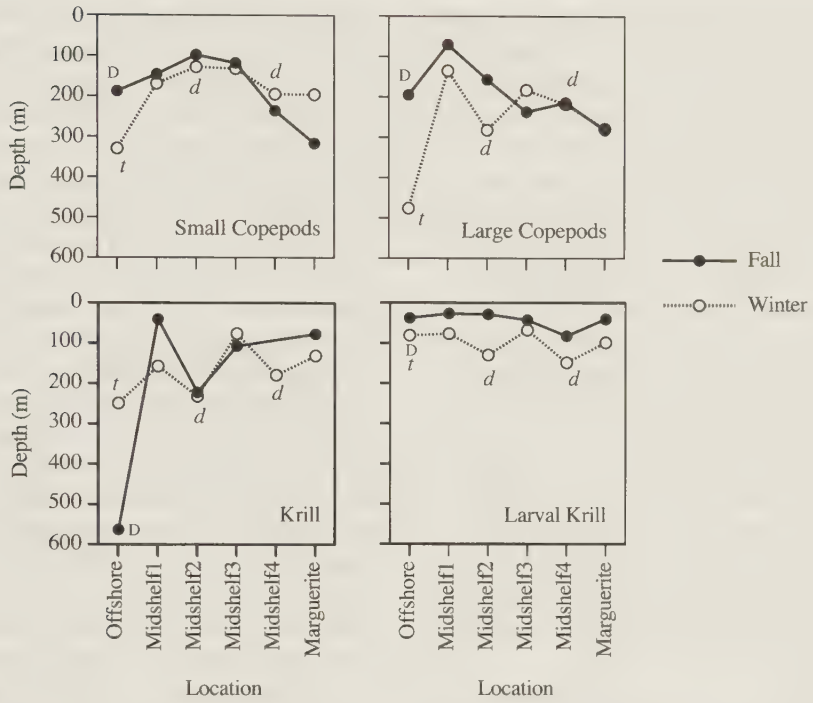

Fig. 12. Mean depth for each of four important taxonomic groups at each location during fall and winter. No krill were collected at the Midshelf 4 location in fall. All tows were conducted during night, except where noted by plain, upper case letters for fall tows and italic, lower case letters for winter tows as D/*d* = day and T/*t* = twilight (Table 1).

Paraeuchaeta spp. *R. gigas* was found in abundance below the pycnocline offshore and also at northern shelf locations where upwelling of deep water onto the shelf from offshore had occurred (Klinck et al., 2004). This species may be a useful indicator of the presence of offshore water on the shelf.

Qualitative analysis of the krill species was more limited, being confined only to the depth of maximum abundance for each category. Larval krill everywhere were dominated by *E. superba*, with the exception of the southernmost shelf station (Midshelf 4) during fall, where *E. crystallorophias* was dominant. *E. crystallorophias* was present in low proportions in Marguerite Bay and at the Midshelf 3 station also. Larval krill stage composition spanned a broad range of stages during fall, with the exception of Marguerite Bay where Furcilia 6 were predominant. During winter, a narrower range of life stages was observed, with Furcilia 6 predominant at most locations. For large krill, *E. superba* was dominant only in Marguerite Bay. *T. macrura* was present in fairly high proportions at all other locations during both seasons. The offshore species *E. triacantha* was dominant at the offshore station and present at the Midshelf 2 station during fall, also indicative of the intrusion of offshore water. During winter, the coastal species *E. crystallorophias* was present in Marguerite Bay and also at the southern two shelf stations.

3.8. Size distribution of copepods and krill

For krill and larval krill, all individuals in a sample frequently were measured. For copepods (large and small), subsets of the total usually were measured. Size frequencies were extrapolated to $\# m^{-3}$, integrated over the depth interval, and then summed over the water column to $\# m^{-2}$ for each size class. Size frequencies from the two size categories measured in the silhouette analysis are

plotted on the same plot for both copepods and krill; however, all statistical analysis and comparisons were conducted separately for small copepods, large copepods, larval krill, and krill.

The clearest pattern for copepods was the greater frequency of larger copepods at the southern shelf locations and in Marguerite Bay for both fall and winter. The relative paucity of larger copepods in northern shelf locations and offshore resulted in smaller overall means and a single peak in the frequency distribution, centered between 1 and 2 mm. By contrast, two peaks were observed in the size distribution at southern shelf locations and in Marguerite Bay; one centered at ~1–1.5 mm and a second at ~3.2–3.5 mm. Based on the qualitative assessment of the copepod species composition, these should correspond to *M. gerlachei* copepodites (~1 mm) and *C. acutus* and *C. propinquus* (~3.5 mm). Larger copepods (>4 mm) likely correspond to *R. gigas* and *P. antarctica*.

The most striking pattern for krill was the greater frequency of large krill (>15 mm) in Marguerite Bay relative to other locations for both fall and winter, resulting in larger mean sizes for these older stage krill. For the smaller, larval krill (<15 mm), mean size was greater at all locations in winter than in fall (Wilcoxon signed rank, $p<0.05$). Larval krill were largest in Marguerite Bay during fall, but of similar size at all locations in winter.

4. Discussion

4.1. Relation of taxa to hydrography

The dynamic height topography provides a context for many of the spatial patterns observed in total abundances and biomass, taxonomic composition, and size distributions (Fig. 1). During fall, the northern locations in the cyclonic gyre (Midshelf 1 and 2) shared many characteristics (low total abundances and biomass; dominance by larval krill; low abundances of large copepods; presence of *R. gigas* at depth) that were distinct from the other shelf locations and similar to the offshore location. Large *T. macrura* and the offshore *E. triacantha* also were present on the northern shelf and offshore. The larval krill, *R. gigas*, *T. macrura*, and *E. triacantha* may have been advected onto the shelf either in the UCDW or at shallower depths where the clockwise circulation of the gyre intersects with the ACC. The southern two shelf locations, located in the southwestward-flowing current, also were similar (e.g., low abundances of larval krill, elevated quantities of large copepods; presence of *E. crystallorophias* larvae). Marguerite Bay was distinct in many characteristics, in particular the high abundances and biomass of large krill (*E. superba*) and the larger size of krill. Drifter observations suggest the presence of small gyres in Marguerite Bay (especially Laubeuf Fjord) that may retain krill populations there (Beardsley et al., 2004). The northern shelf, southern shelf, and Marguerite Bay also were distinct during winter, although the patterns were not as closely associated with the location of the gyre. The presence of large *E. crystallorophias*, the coastal species, in both Marguerite Bay and on the southern shelf during winter, suggested advection of populations from Marguerite Bay to the southern shelf in the southwestward-flowing current.

4.2. Seasonal and regional biomass and abundance change

Marked regional and seasonal differences were observed for both total water-column biomass and abundance. The most dramatic pattern observed was the reduction in both biomass and abundance of ~60% in both during the winter relative to the fall at all locations that was seen also in backscatter intensity collected during these cruises (Lawson et al., 2004). A similar reduction in biomass of krill during winter was observed previously in this region by Lascara et al. (1999), based on acoustic observations, and at other shelf locations (Marr, 1962; Heywood et al., 1985; Siegel, 1988, 1992). This reduction in plankton between the two seasons may be a consequence of mortality, advection of populations out of the study area, or behavioral changes such as changes in vertical distribution or horizontal migration. Characteristics of the life history of several of the

major taxonomic groups suggest that such behavior may account for part of the seasonal change in water-column abundance.

Seasonal changes in vertical distribution are known for several taxa. The large copepods *C. acutus* and *R. gigas* migrate ontogenetically to depth during the winter (Smith and Schnack-Schiel, 1990; Atkinson et al., 1995; Ross et al., 1996; Schnack-Schiel et al., 1998). Because the net tows could not sample near the bottom in the present study, especially during winter, it is possible that significant abundances of these large copepods were not quantified. Elevated backscatter intensity was observed 100–200 m above the bottom in winter, which did not appear to be caused by krill aggregations, but rather by other zooplankton such as large copepods (Lawson et al., 2004). For the two tows that sampled to within 100 m of the bottom (Midshelf 1 and 4) during winter, a biomass and abundance peak dominated by large copepods was observed in the deepest net. Krill have been observed at some locations to aggregate near the bottom (within several meters) (Heywood et al., 1985; Kawaguchi et al., 1986; Gutt and Siegel, 1994); in the present study, such aggregations if they occurred could not be captured because the net tows did not sample near the bottom. Lascara et al. (1999) suggested that the decrease in krill biomass was because of migration of krill to greater depths than the sampling range of the transducer (~200 m). However, the present study sampled much greater depths than 200 m and found few krill there, indicating that the middle water column was not the winter habitat of krill. Larval krill, but not older life stages, migrate to the ice underside during winter, where adequate food (algae, detritus, microzooplankton) presumably is present (Garrison et al., 1986; Daly and Macaulay, 1988; Marschall, 1988; Stretch et al., 1988; Hamner et al., 1989; Daly, 1990; Nordhausen, 1994; Quetin et al., 1994, 1996; Frazer et al., 1997, 2002; Kawaguchi et al., 1999). Larval krill were observed under the ice using a remotely operated vehicle during the winter cruise of this study (Gallager et al., 2002). Thus, decreased abundances of water column larval krill may have resulted from migration of the larval krill out of the water column to the ice underside. Siegel et al. (1990) and Frazer et al. (2002) concluded that larval krill occupied both the sea ice and water-column habitats at similar abundance. Similar life history or ontogenetic habitat shifts that might contribute to the reduced winter abundances and biomass have not been observed for the small copepods (Figs. 13 and 14).

Identifying whether horizontal migration, advection, or mortality accounts for the dramatic reduction in plankton and krill biomass is more difficult. Horizontal migration may account for the drastically reduced abundances and biomass, although such migration may be effective only for the faster swimming older krill (Trathan et al., 1993; Lascara et al., 1999). Calculations by Lascara et al. (1999) support the possibility that horizontal migration of krill off the shelf in this region may be accomplished within the time interval between the two cruises in the present study. Some aspects of the krill life cycle are consistent with the depletion of krill on the shelf in winter, since spawning in spring is believed to occur primarily off the shelf over the slope and adjacent basin (Marr, 1962; Quetin and Ross, 1984; Siegel, 1988) and the krill must migrate off the shelf at some time prior to reproduction (Sprong and Shalk, 1992). Elevated abundances of krill have been found offshore at the ice edge at other locations on the Antarctic Peninsula (Daly and Macaulay, 1991). However, few adult/subadult or larval krill were observed at the offshore site during either fall or winter, so it is questionable if the low abundances of krill on the shelf can be attributed an offshore migration. Horizontal migration inshore to fjords and neritic regions also may result in reduction of krill abundance on the shelf (Siegel, 1988). The elevated abundance of krill observed in Marguerite Bay/Laubeuf Fjord in fall suggests inshore movement of krill prior to the sampling period. Larval krill are thought to migrate onto the shelf from offshore during development (Siegel, 1988); it was surprising that so few larval krill were present in the water column on the shelf during the winter.

Advection of zooplankton off the shelf may occur via the mesoscale physical features observed in the dynamic height topography and surface

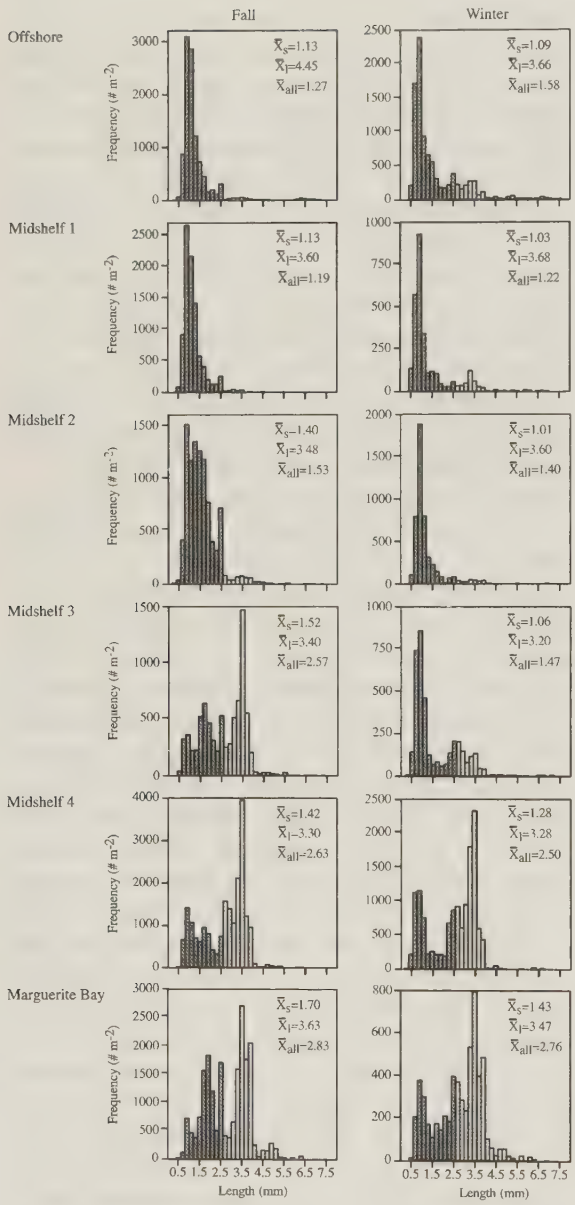

Fig. 13. Size distributions (# m^{-2} per size bin) of small and large copepods at the six locations for fall (left column) and winter (right column), with small copepods plotted in the darker shading. The grand mean for each size class (small = s; large = l) and for all copepods combined is shown for each region and season.

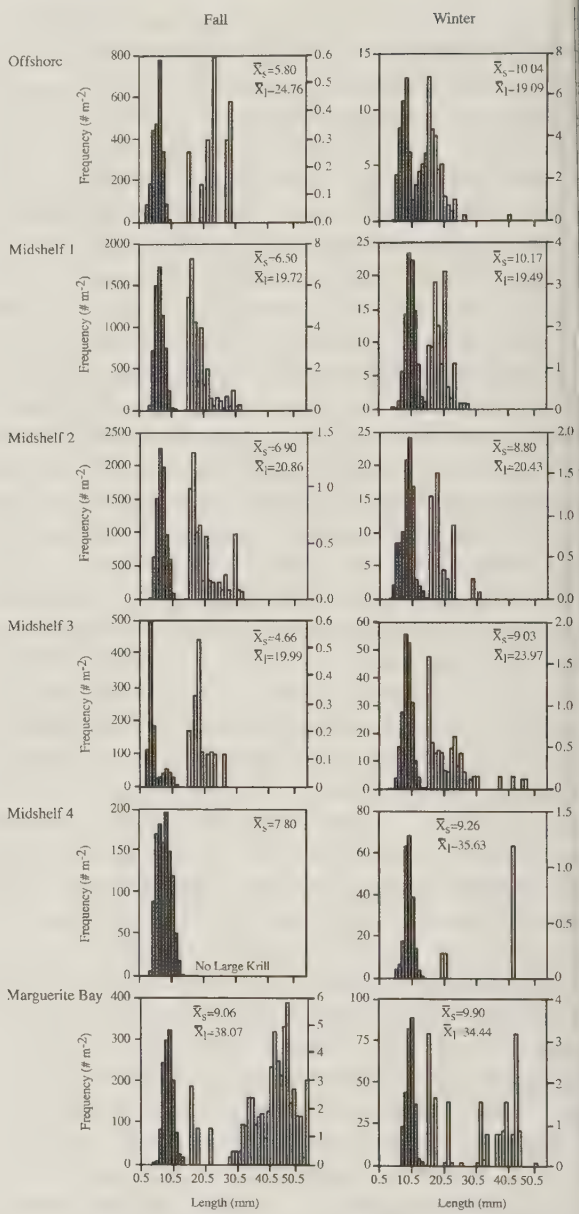

Fig. 14. Size distributions (# m^{-2} per size bin) of krill measured at the six locations for fall (left column) and winter (right column), with small, larval krill plotted in the darker shading. The grand mean for each size class (small = s; large = l) is shown for each region and season.

drifter tracks (Beardsley et al., 2004; Klinck et al., 2004). Zooplankton entrained in the cyclonic gyre or in the southwestern flow on the southern portion of the shelf may be advected into the Antarctic Circumpolar Current that flows northward along the shelf break. This has been

hypothesized to replenish krill populations in the northern Peninsula region. (Siegel, 1988; Hofmann et al., 1998; Fach et al., 2002). However, Lascara et al. (1999) estimated that the magnitude of the velocities present on the shelf ($\sim$10 cm s^{-1}), based on historical data, would be insufficient to transport krill out of the region. Preliminary estimates of the currents on the shelf measured using the hull-mounted 150 kHz Acoustic Doppler Current Profiler are consistent with these historic estimates (US Southern Ocean GLOBEC, 2001; Howard et al., 2002; Klinck et al., 2004). Greater velocities were measured in the coastal current along Adelaide Island and the southwestward current flowing across the shelf to the south of Marguerite Bay (15–25 cm s^{-1}), as well as in the northward Antarctic Circumpolar Current along the shelf edge (up to 40 cm s^{-1}) (Howard et al., 2002; Klinck et al., 2004). These higher velocity currents could contribute to the depletion of plankton populations on the shelf, if the populations are entrained in these features. During a 6-week period, a 25 cm s^{-1} current can transport water, and intrinsic plankton, $\sim$900 km or a considerably greater distance than that required to advect zooplankton from most shelf locations to offshelf. The resulting abundance of zooplankton on the shelf will depend on the abundance in the water input to replace that lost via the currents. Much of the input to the shelf in this region occurs via movement of Upper Circumpolar Deep Water onto the shelf (Hofmann et al., 1996; Smith et al., 1999; Klinck et al., 2004) that contained low abundances and biomass of plankton. Advection may be sufficient to deplete zooplankton populations on the shelf between fall and winter, depending on the path of the currents and the concentration of zooplankton in the water input to the shelf.

Mortality estimates of zooplankton based on biomass size spectra from the fall and winter of 2002 on the continental shelf adjacent to and in Marguerite Bay suggest that mortality rates could be significant, resulting in a reduction of 82% of zooplankton biomass between the fall and winter of that year (Zhou et al., 2004). Krill may utilize smaller zooplankton as prey during winter and reduce zooplankton abundance (Hopkins, 1985b; Hopkins and Torres, 1989; Price et al., 1988; Lancraft et al., 1991; Nordhausen et al., 1992; Huntley et al., 1994; Pakhamov et al., 1998). Elevated abundances of krill predators such as penguins and crabeater seals are common in Marguerite Bay, so that krill abundances there may have been depleted by predation in the fall prior to ice cover (Costa and Crocker, 1996; Fraser and Trivelpiece, 1996; Burns et al., 2004; Chapman et al., 2004).

4.3. Relation of krill to other zooplankton taxa

Although krill usually are perceived to be the dominant taxa in the plankton community in the Antarctic (Marr, 1962; Laws, 1985; Hopkins, 1985a), and indeed they are critical to the success of the higher trophic levels, several studies have shown that copepods can dominate biomass, abundance, and secondary production (Voronina, 1983, 1998; Chojnacki and Weglenska, 1984; Hopkins and Torres, 1988; Ward, 1989; Boysen-Ennen et al., 1991; Voronina et al., 1994). For the Marguerite Bay region, few if any reports exist that compare the relative abundance and biomass of krill and other taxonomic groups. In the present study, krill were relatively unimportant to total biomass and abundance at most locations, while copepods (large and small) frequently dominated both biomass and abundance. Krill or larval krill were important only in fall at two midshelf locations in the north of the region (larval krill) and in Marguerite Bay itself. Furthermore, copepods were relatively more important than krill to both biomass and abundance at depth. Although it is possible that some large krill avoided the net, despite the use of the strobe system, catches of larval krill were not enhanced with the strobe flashing (Wiebe et al., 2004), suggesting that net avoidance for the larval krill was not a problem. Also, large dense krill aggregations such as those seen in Marguerite Bay in backscatter data were observed rarely on the shelf or offshore (Lawson et al., 2004). Copepods (large and small) were more numerous and of greater biomass than larval krill at most locations. The present study confirms the importance of copepods in the Antarctic ecosystem relative to other taxa.

Zooplankton communities in Antarctica may be dominated by one of three general taxonomic groups, salps, krill, or copepods (Siegel and Piatkowski, 1990; Siegel and Loeb, 1995; Loeb et al., 1997; Hosie et al., 2000; Nicol et al., 2000). The presence of each type of community results both from environmental (e.g., ice) and life-history factors. The offshore and shelf locations in this study were characterized by different taxonomic compositions that were typical of Antarctic open-ocean and shelf communities (Siegel and Piatkowski, 1990; Ross et al., 1996). Greater relative abundances of taxa other than copepods and krill, such as chaetognaths, polychaetes, and, in winter, *Limacina* spp. were observed at the offshore site compared to shelf locations. On the shelf, elevated abundances and biomass of *Limacina* spp. and other taxa as well as larval krill were observed at some locations, although this was not consistent within a season. Most locations were copepod dominated during both seasons. Notable exceptions are Marguerite Bay and the northern shelf during fall with greater proportions of krill present.

4.4. Changes in body size between fall and winter

In the present study, larger larval krill were observed during winter relative to fall. Both this study and Daly (2004) observed that younger furcilia stages disappeared from the population in this region between fall and winter, resulting in an older life stage composition for the larval krill that would be reflected in the observed larger mean size. Previous investigations have suggested that shrinkage of body size during periods of starvation is a characteristic of overwintering juvenile and adult krill (Ikeda and Dixon, 1982; Nicol et al., 1992; Quetin and Ross, 1991), while others (Huntley et al., 1994) demonstrated that this did not occur. The large krill did not change significantly in size between the two sampling times and it did not appear that shrinkage had occurred. By contrast, larval krill appear to utilize a wider range of food types to survive such as ice biota (Daly, 1990, 2004; Meyer et al., 2002), and have not been observed to shrink.

The dramatically different sizes observed for both larval and subadult/adult krill in Marguerite Bay relative to other regions may have resulted from different life stage compositions, different species compositions, or a better food environment in that region relative to the other locations. Large krill in Marguerite Bay were dominated by *E. superba* while other species (*T. marcura*, *E. crystallorophios*, *E. triacantha*) dominated at most other locations. Although *E. superba* dominated larvae at all locations, the stage composition was more mature in Marguerite Bay during the fall than during the winter (see also Daly, 2004).

4.5. Overwintering potential for krill

The present study did not find a large population of krill overwintering on the shelf in this region. The very low abundances of large krill found at almost all times and locations and the extremely reduced abundances of larval krill in the water column in winter relative to fall suggest a decline of the krill population during winter and overall low abundances of krill during both seasons except at isolated locations. Alternatively, krill may utilize components of the environment such as the under-ice surface and the benthic boundary layer as winter refuges that were not sampled adequately in the present, water-column-based study. However, these results together with those of Lascara et al. (1999) confirm that the observed decrease in krill, and plankton, populations on the shelf during winter is a persistent characteristic.

In summary, dramatic differences were observed in total water-column biomass, abundance, and taxonomic composition between different regions and the two seasons. Krill or larval krill did dominate the zooplankton at a few times and locations. Large and small copepods with significant contributions by other diverse taxa were, however, most often dominant. Any assessment of Antarctic food webs must include consideration of the non-krill taxa, since significant portions of the primary production in this region may cycle through these components of the ecosystem. Zooplankton abundances and biomass were depleted during winter relative to fall. The cyclonic

gyre on the shelf apparently brought offshore zooplankton, especially larval krill, onto the continental shelf in the northern portion of the study region.

Acknowledgements

We thank the officers and crew of the RVIB *Nathaniel B. Palmer*, and the shipboard and onshore staff from Raytheon Polar Services, especially A. Doyle, J. Doren, J. Szelag, E. Horgan, R. LaRiviera, and J. Ardai, C. Macdonald, and J. White, who revived the MOCNESS after a near catastrophic ice collision. Many thanks also to our shipmates who assisted with the MOCNESS sampling including J. Peterson, M. Butler, M. Dennett, K. Fisher, A. Girard, M. Taylor, and J. Warren and to the CTD group for their efforts in collecting those data. E. Hoffman and J. Klinck generously shared their CTD dynamic height topography. T. Bolmer greatly improved the bottom topography data for this region. A. Solow provided statistical advice. Special thanks to P. Hull who identified krill species and life stages as part of her Summer Student Fellowship project at the Woods Hole Oceanographic Institution. Thanks also to our collaborators in the Southern Ocean GLOBEC program for sharing their ideas and inspirations. We gratefully acknowledge the insightful and helpful comments of two anonymous reviewers and K. Daly. This work was supported by NSF Grant OPP-9910307 to P. Wiebe, C. Ashjian, C. Davis, and S. Gallager. This is GLOBEC contribution number 454 and Woods Hole Oceanographic Institution Contribution number 11129.

References

Ahlstrom, E.H., Thrailkill, T.R., 1963. Plankton volume loss with time of preservation. CalCOFI Report 9, 57–73.

Atkinson, A., Shreeve, R.S., 1995. Response of the copepod community to a spring bloom in the Bellingshausen Sea. Deep-Sea Research II 42, 1291–1311.

Atkinson, A., Whitehouse, M.J., Priddle, J., Cripps, G.C., Ward, P., Brandon, M.A., 2001. South Georgia, Antarctica; a productive, cold water, pelagic ecosystem. Marine Ecology Progress Series 216, 279–308.

Beardsley, R.C., Limeburner, R., Owens, W.B., 2004. Drifter measurements of surface currents near Marguerite Bay on the western Antarctic Peninsula shelf during austral summer and fall, 2001 and 2002. Deep-Sea Research II, this issue [doi:10.1016/j.dsr2.2004.07.031].

Boysen-Ennen, E., Hagen, W., Hubold, G., Piatkowski, U., 1991. Zooplankton biomass in the ice-covered Weddell Sea, Antarctica. Marine Biology 111, 227–235.

Brierley, A.S., Ward, P., Watkins, J.L., Goss, C., 1998. Acoustic discrimination of Southern Ocean zooplankton. Deep-Sea Research II 45, 1155–1173.

Burns, J.M., Costa, D.P., Fedak, M.A., Hindell, M.A., Bradshaw, C.J.A., Gales, N.J., McDonald, B., Trumble, S.J., Crocker, D.E., 2004. Winter habitat use and foraging behavior of crabeater seals along the Western Antarctic Peninsula. Deep-Sea Research II, this issue [doi:10.1016/j.dsr2.2004.07.021].

Cabal, J.A., Alvarez-Marqués, F., Acuña, J.L., Quevedo, M., Gonzalez-Qirós, R., Huskin, I., Fernández, D., Rodriguez del Valle, C., Anadón, R., 2002. Mesozooplankton distribution and grazing during the productive season in the Northwest Antarctic Peninsula (FRUELA cruises). Deep-Sea Research II 49, 869–881.

Chapman, E.W., Ribic, C.A., Fraser, W.R., 2004. The distribution of seabirds and pinnipeds in Marguerite Bay and their relationship to physical features during austral winter 2001. Deep-Sea Research II, this issue [doi:10.1016/j.dsr2.2004.07.005].

Chojnacki, J., Weglenska, T., 1984. Periodicity of composition, abundance, and vertical distribution of summer zooplankton (1977/1978) in Ezcurra Inlet, Admiralty Bay (King George Island, South Shetland). Journal of Plankton Research 6, 997 1018.

Costa, D.P., Crocker, D.E., 1996. Marine mammals in the Southern Ocean. In: Ross, R.M., Hofmann, E.E., Quetin, L.B. (Eds.), Foundations for Ecological Research West of the Antarctic Peninsula, Antarctic Research Series, vol. 70. American Geophysical Union, Washington, DC, pp. 287–301.

Daly, K.L., 1990. Overwintering development, growth, and feeding of larval *Euphausia superba* in the Antarctic marginal ice zone. Limnology and Oceanography 35, 1564–1576.

Daly, K.L., 2004. Overwintering growth and development of larval *Euphausia superba*: an interannual comparison under varying environmental conditions west of the Antarctic Peninsula. Deep-Sea Research II, this issue [doi:10.1016/j.dsr2.2004.07.010].

Daly, K.L., Macaulay, M.C., 1988. Abundance and distribution of krill in the ice edge zone of the Weddell Sea austral spring. Deep-Sea Research I 35, 21–41.

Daly, K.L., Macaulay, M.C., 1991. The influence of physical and biological mesoscale dynamics on the seasonal distribution and behavior of *Euphausia superba* in the Antarctic marginal ice zone. Marine Ecology Progress Series 79, 37–66.

Davis, C.S., Wiebe, P.H., 1985. Macrozooplankton biomass in a warm-core Gulf Stream ring: time series changes in size structure, taxonomic composition, and vertical distribution. Journal of Geophysical Research 90, 8871–8882.

Davis, C.S., Gallager, S.M., Berman, M.S., Haury, L.R., Strickler, J.R., 1992. The video plankton recorder (VPR): design and initial results. Archiv für Hydrobiologie Heiheft, Ergebnisse der Limnologie 36, 67–81.

Dzik, J., Jazdzewski, K., 1978. The euphausiid species of the Antarctic region. Polskie archiwum hydrobologii 25, 589 605.

El-Sayed, S.Z., 1994. History, organization and accomplishments of the BIOMASS program. In: El-Sayed, S.Z. (Ed.), Southern Ocean Ecology: the BIOMASS Perspective. Cambridge University Press, Cambridge, pp. 1–8.

El-Sayed, S.Z., 1996. Historical perspective of research in the Antarctic Peninsula region. In: Ross, R.M., Hofmann, E.E., Quetin, L.B. (Eds.), Foundations for Ecological Research west of the Antarctic Peninsula, Antarctic Research Series, vol. 70. American Geophysical Union, Washington, DC, pp. 1–13.

Everson, I. (Ed.), 2000, Krill: Biology, Ecology, and Fisheries. Blackwell Science Ltd., Oxford, 372pp.

Fach, B.A., Hofmann, E.E., Murphy, E.J., 2002. Modeling studies of Antarctic krill *Euphausia superba* survival during transport across the Scotia Sea. Marine Ecology Progress Series 231, 187–203.

Fraser, W.R., Trivelpiece, W.Z., 1996. Factors controlling the distribution of seabirds: winter–summer heterogeneity in the distribution of Adélie penguin populations. In: Ross, R.M., Hofmann, E.E., Quetin, L.B. (Eds.), Foundations for Ecological Research West of the Antarctic Peninsula, Antarctic Research Series, vol. 70. American Geophysical Union, Washington, DC, pp. 257–272.

Frazer, T.K., Quetin, L.B., Ross, R.M., 1997. Abundance and distribution of larval krill, *Euphausia superba*, associated with annual sea ice in winter. In: Battaglia, B., Valencia, J., Walton, D.W.H. (Eds.), Antarctic Communities. Cambridge University Press, Cambridge, pp. 108–111.

Frazer, T.K., Quetin, L.B., Ross, R.M., 2002. Abundance, sizes and developmental stages of larval krill, *Euphausia superba*, during winter in ice-covered seas west of the Antarctic Peninsula. Journal of Plankton Research 10, 1067–1077.

Gallager, S.M., Daly, K., Fisher, K., Lawson, G., Davis, C.S., Ashjian, C., Wiebe, P.H., 2002. Seasonal changes in the association of larval krill with its potential microplankton food resource along the Western Antarctic Peninsula. Eos, Transactions of the American Geophysical Union, 84, Ocean Sciences Meeting Supplement, Abstract OS51A-13.

Garrison, D.L., Sullivan, S.W., Ackley, S.F., 1986. Sea ice microbial communities in Antarctica. BioScience 36, 243–250.

Gutt, J., Siegel, V., 1994. Benthopelagic aggregations of krill (*Euphausia superba*) on the deeper shelf of the Weddell Sea (Antarctic). Deep-Sea Research I 41, 169–178.

Hamner, W.M., Hamner, P.P., Obst, B.S., Carleton, J.H., 1989. Field observations on the ontogeny of schooling *Euphausia superba* furcilia and its relationship to ice in Antarctic water. Limnology and Oceanography 24, 451–456.

Hewitt, R.P., Demer, D.A., 2000. The use of acoustic sampling to estimate the dispersion and abundance of euphausiids with an emphasis on Antarctic krill, *Euphausia superba*. Fisheries Research 47, 215–229.

Heywood, R.B., Everson, I., Priddle, J., 1985. The absence of krill from the South Georgia zone, winter 1983. Deep-Sea Research I 32, 369–378.

Hofmann, E.E., Klinck, J.M., Locarnini, R.A., Fach, B.A., Murphy, E.J., 1988. Krill transport in the Scotia Sea and environs. Antarctic Science 10, 210–231.

Hofmann, E.E., Klinck, J.M., Lascara, C.M., Smith, D.A., 1996. Water mass distribution and circulation west of the Antarctic Peninsula and including Bransfield strait. In: Ross, R.M., Hofmann, E.E., Quetin, L.B. (Eds.), Foundations for Ecological Research West of the Antarctic Peninsula, Antarctic Research Series, vol. 70. American Geophysical Union, Washington, DC, pp. 61–80.

Hofmann, E.E., Klinck, J.M., Costa, D.P., Daly, K.D., Torres, J.J., Fraser, W.R., 2002. US Southern Ocean Global Ocean Ecosystems Dynamics Program. Oceanography 15, 64–74.

Hopkins, T.L., 1985a. The zooplankton community of Croker Passage, Antarctic Peninsula. Polar Biology 4, 161–170.

Hopkins, T.L., 1985b. Food web of an Antarctic midwater ecosystem. Marine Biology 89, 197–212.

Hopkins, T.L., Torres, J.J., 1989. Midwater food web in the vicinity of a marginal ice zone in the western Weddell Sea. Deep-Sea Research I 36, 543–560.

Hosie, G.W., Schultz, M.G., Kitchener, J.A., Cochran, T.G., Richards, K., 2000. Macrozooplankton community structure off east Antarctica (80–150°E) during the Austral summer of 1995/1996. Deep-Sea Research II 47, 2437–2463.

Howard, S.L, Padman, L, Muench, R.D., Gunn. J.T., 2002. Circulation and mixing on the Western Antarctic Peninsula Shelf: a component of Southern Ocean GLOBEC. Eos, Transactions of the American Geophysical Union, 84, Ocean Sciences Meeting Supplement, Abstract OS41C-19.

Huntley, M.E., Nordhausen, W., Lopez, M.D.G., 1994. Elemental composition, metabolic activity and growth of Antarctic krill *Euphausia superba* during winter. Marine Ecology Progress Series 107, 23–40.

Ikeda, T., Dixon, P., 1982. Body shrinkage as a possible overwintering mechanisms of the Antarctic krill, *Euphausia superba* Dana. Journal of Experimental Marine Biology and Ecology 62, 143–151.

Isaacs, J.D., Fleminger, A., Miller, J.K. 1969. Distributional atlas of zooplankton biomass in the California Current region: Spring and Fall 1955–1959. California Cooperative Fisheries Investigations Atlas Number 10, 276pp.

Kawaguchi, K., Ishikawa, S., Matsuda, O., 1986. The overwintering of Antarctic krill (*Euphausia superba* Dana) under the coastal fast ice off the Ongul Islands in Lutzow-Holm Bay, Antarctica. Memoirs of National Institute of Polar Research (Special Issue) 44, 67–85.

Kawaguchi, S., Ichii, T., Naganobu, M., 1999. Green krill, the indicator of micro- and nano-size phytoplankton availability to krill. Polar Biology 22, 133–136.

Klinck, J.M., Hofmann, E.E., Beardsley, R.C., Salihoglu, B., Howard, S., 2004. Water-mass properties and circulation on the west Antarctic Peninsula Continental Shelf in Austral Fall and Winter 2001. Deep-Sea Research II, this issue [doi:10.1016/j.dsr2.2004.08.001].

Lancraft, T.M., Hopkins, T.L., Torres, J.J., Donnelly, E., 1991. Oceanic micronekton/macrozooplanktonic community structure and feeding in ice covered Antarctic waters during the winter (AMERIEZ 1988). Polar Biology 11, 157–167.

Lascara, C.M., Hofmann, E.E., Ross, R.M., Quetin, L.B., 1999. Seasonal variability in the distribution of Antarctic krill, *Euphausia superba*, west of the Antarctic Peninsula. Deep-Sea Research I 46, 951–984.

Laws, R.M., 1985. The ecology of the Southern Ocean. American Scientist 73, 26–40.

Lawson, G.L., Wiebe, P.H., Ashjian, C.J., Gallager, S.M., Davis, C.S., Warren, J.D., 2004. Acoustically-inferred zooplankton distribution in relation to hydrography west of the Antarctic Peninsula. Deep-Sea Research II, this issue [doi:10.1016/j.dsr2.2004.07.022].

Little, W.S., Copley, N.J., 2003. WHOI Silhouette Digitizer version 1.0 User's Guide. Woods Hole Oceanographic Institution Technical Report # 2003-05, 63pp.

Loeb, V., Siegel, V., Holm-Hansen, O., Hewitt, R., Fraser, W., Trivelpiece, W., Trivelpiece, S., 1997. Effects of sea-ice extent and krill or salp dominance on the Antarctic food web. Nature 287, 897–900.

Makarov, R., 1980. Larval development of the Antarctic euphausiids. BIOMASS Handbook No. 3, 13pp.

Marr, J.W.S., 1962. The natural history and geography of the Antarctic krill (*Euphausia superba*). Discovery Report 32, 33–464.

Marschall, H.-P., 1988. The overwintering strategy of Antarctic krill under the pack-ice of the Weddell Sea. Polar Biology 9, 129–135.

Mauchline, J., 1980. Measurement of body length of *Euphausia superba* Dana. BIOMASS Handbook No. 4, 4–9.

Meyer, B., Atkinson, A., Stübing, D., Oettl, B., Hagen, W., Bathmann, U.V., 2002. Feeding and energy budgets of Antarctic krill *Euphausia superba* at the onset of winter—I. Furcilia III larvae. Limnology and Oceanography 47, 943–952.

Nicol, S., Stolp, M., Cochran, T., Geijsel, P., Marshall, J., 1992. Growth and shrinkage of the Antarctic krill *Euphausia superba* from the Indian Ocean sector of the Southern Ocean during summer. Marine Ecology Progress Series 89, 175–181.

Nicol, S., Pauly, T., Bindoff, N.L., Wright, S., Thiele, D., Hosie, G.W., Strutton, P.G., Woehler, E., 2000. Ocean circulation off east Antarctica affects ecosystem structure and sea-ice extent. Nature 406, 504–507.

Nordhausen, W., 1994. Winter abundance and distribution of *Euphausia superba*, *E. crystallorophias*, and *Thysanoessa macrura* in Gerlache Strait and Crystal Sound, Antarctica. Marine Ecology Progress Series 109, 131–142.

Nordhausen, W., Huntley, M., Lopez, M.D.G., 1992. RACER: carnivory by *Euphausia superba* during the antarctic winter. Antarctic Journal of the United States 27, 181–183.

Pakhamov, E.A., Perissinotto, R., Froneman, P.W., 1998. Abundance and trophodynamics of *Euphausia crystallorophias* in the shelf region of the Lazarev Sea during austral spring and summer. Journal of Marine Systems 17, 313–324.

Pauly, T., Nicol, S., Higginbottom, I., Hosie, G., Kitchener, J., 2000. Distribution and abundance of Antarctic krill (*Euphausia superba*) off East Antarctica (80–150°E) during the Austral summer of 1995/1996. Deep-Sea Research II 47, 2465–2488.

Price, H.J., Boyd, K.R., Boyd, C.M., 1988. Omnivorous feeding behavior of the Antarctic krill *Euphausia superba*. Marine Biology 97, 67–77.

Quetin, L.G., Ross, R.M., 1984. School composition of the Antarctic krill *Euphausia superba* in the waters west of the Antarctic Peninsula in the austral summer of 1982. Journal of Crustacean Biology 4, 96–106.

Quetin, L.B., Ross, R.M., 1991. Behavioral and physiological characteristics of the Antarctic krill *Euphausia superba*. American Zoologist 31, 49–63.

Quetin, L.B., Ross, R.M., Clarke, A., 1994. Krill energetics: seasonal and environmental aspects of the physiology of *Euphausia superba*. In: El-Sayed, S.Z. (Ed.), Southern Ocean Ecology: the BIOMASS perspective. Cambridge University Press, Cambridge, pp. 165–184.

Quetin, L.B., Ross, R.M., Frazer, T.K., Haberman, K.L., 1996. Factors influencing distribution and abundance of zooplankton, with an emphasis on Antarctic krill, *Euphausia superba*. In: Ross, R.M., Hofmann, E.E., Quetin, L.B. (Eds.), Foundations for Ecological Research West of the Antarctic Peninsula, Antarctic Research Series, vol. 70. American Geophysical Union, Washington, DC, pp. 357–372.

Roe, H.S.J., Angel, M.V., Badcock, J., Domanski, P., James, P.T., Pugh, P.R., Thurston, M.H., 1984. The diel migrations and distributions within the pelagic community in the northeast Atlantic. 1. Introduction and sampling procedures. Progress in Oceanography 13, 245–268.

Ross, R.M., Quetin, L.B., 2000. Reproduction in Euphausiids. In: Everson, I. (Ed.), Krill: Biology, Ecology, and Fisheries. Blackwell Science Ltd., Oxford, pp. 150–181.

Ross, R.M., Quetin, L.B., Lascara, C.M., 1996. Distribution of Antarctic krill and dominant zooplankton west of the Antarctic Peninsula. In: Ross, R.M., Hofmann, E.E., Quetin, L.B. (Eds.), Foundations for Ecological Research west of the Antarctic Peninsula, Antarctic Research Series, vol. 70. American Geophysical Union, Washington, DC, pp. 199–218.

Schnack-Schiel, S.B., Hagen, W., Mizdalski, E., 1998. Seasonal carbon distribution of copepods in the eastern Weddell Sea, Antarctica. Journal of Marine Systems 17, 305–311.

Siegel, V., 1988. A concept of seasonal variation of krill (*Euphausia superba*) distribution and abundance west of the

Antarctic Peninsula. In: Sarhage, D. (Ed.), Antarctic Ocean and Resources Variability. Springer, Berlin, Heidelberg, pp. 219–230.

Siegel, V., 1992. Assessment of the krill (*Euphausia superba*) spawning stock off the Antarctic Peninsula. Archiv für Fishereiwissenschaft 31, 101–130.

Siegel, V., Loeb, V., 1995. Recruitment of Antarctic krill *Euphausia superba* and possible causes for its variability. Marine Ecology Progress Series 123, 45–56.

Siegel, V., Piatkowski, U., 1990. Variability in the macrozooplankton community off the Antarctic Peninsula. Polar Biology 10, 373–386.

Siegel, V., Bergström., B., Strömberg, J.O., Schalk, P.H., 1990. Distribution, size frequencies, and maturity stages of krill, *Euphausia superba*, in relation to sea-ice in the Northern Weddell Sea. Polar Biology 10, 549–557.

Smith, S.L., Schnack-Schiel, S.B., 1990. Polar Zooplankton. In: Smith, Jr., W.O. (Ed.), Polar Oceanography, Part B: Chemistry, Biology, and Geology. Academic Press, San Diego, CA, pp. 527–598.

Smith, D.A., Hofmann, E.E., Klink, J.M., Lascara, C.M., 1999. Hydrography and circulation of the west Antarctic Peninsula continental shelf. Deep-Sea Research I 46, 925–949.

Sprong, I., Shalk, P.H., 1992. Acoustic observations on krill spring–summer migration and patchiness in the northern Weddell Sea. Polar Biology 12, 261–268.

Stretch, J.J., Hamner, P.P., Hamner, W.M., Michel, W.C., Cook, J., Sullivan, C.W., 1988. Foraging behavior of Antarctic krill, *Euphausia superba*, on sea ice microalgae. Marine Ecology Progress Series 44, 130–131.

Trathan, P.M., Priddle, J., Watkins, J.L., Miller, D.G.M., Murray, A.W.A., 1993. Spatial variability of Antarctic krill in relation to mesoscale hydrography. Marine Ecology Progress Series 98, 61–71.

Voronina, N.M., 1983. Biomass and production of Antarctic krill (*Euphausia superba* Dana). Oceanology of the Academy of Sciences of the USSR 23, 760–762.

Voronina, N.M., 1998. Comparative abundance and distribution of major filter-feeders in the Antarctic pelagic zone. Journal of Marine Systems 17, 375–390.

Voronina, N.M., Kosobokova, K.N., Pakhomov, E.A., 1994. Composition and biomass of summer metazoan plankton in the 0–200 m layer of the Atlantic sector of the Antarctic. Polar Biology 14, 91–95.

Ward, P., 1989. The distribution of zooplankton in an Antarctic fjord at South Georgia. Antarctic Science 1, 141–150.

Wiebe, P., 1988. Functional regression equations for zooplankton displacement volume, wet weight, dry weight, and carbon: a correction. Fishery Bulletin 86, 833–835.

Wiebe, P.H., Boyd, S., Cox, J.L., 1975. Relationships between zooplankton displacement volume, wet weight, dry weight, and carbon. Fishery Bulletin 73, 777–786.

Wiebe, P.H., Burt, K.H., Boyd, S.H., Morton, A.W., 1976. A multiple opening/closing net and environmental sensing system for sampling zooplankton. Journal of Marine Research 34, 341–354.

Wiebe, P.H., Morton, A.W., Bradley, A.M., Backus, R.H., Craddock, J.E., Barber, V., Cowles, T.J., Flierl, G.R., 1985. New developments in the MOCNESS, an apparatus for sampling zooplankton and micronekton. Marine Biology 87, 313–323.

Wiebe, P.H., Stanton, T.K., Green, C.H., Benfield, M.C., Sosik, H.M., Austin, T.C., Warren, J.D., Hammar, T., 2002. BIOMAPER-II: an integrated instrument platform for coupled biological and physical measurements in coastal and oceanic regimes. IEEE Journal of Oceanic Engineering 27, 700–716.

Wiebe, P.H., Ashjian, C.J., Gallager, S.M., Davis, C.S., Lawson, G.L., Copley, N.J., 2004. Using a high powered strobe light to increase the catch of Antarctic krill. Marine Biology 144 (3), 493–502.

Zhou, M., Zhu, Y., Peterson, J.O., 2004. In situ growth and mortality of mesozooplankton during the austral fall and winter in Marguerite Bay and its vicinity. Deep-Sea Research II, this issue [doi:10.1016/j.dsr2.2004.07.008].

ELSEVIER

Deep-Sea Research II 51 (2004) 2099–2118

DEEP-SEA RESEARCH
PART II

www.elsevier.com/locate/dsr2

In situ growth and mortality of mesozooplankton during the austral fall and winter in Marguerite Bay and its vicinity

Meng Zhou*, Yiwu Zhu, Jay O. Peterson

Department of Environmental, Coastal & Ocean Sciences, University of Massachusetts Boston, 100 Morrissey Blvd., Boston, MA 02125-3393, USA

Accepted 14 July 2004
Available online 18 October 2004

Abstract

Zooplankton play a critical role in the austral winter ecosystem of the Southern Ocean, transporting biomass from lower to higher trophic level organisms through their consumption and growth, and ultimately determining the survival of marine animals such as sea birds and mammals. Previous studies have provided evidence that krill utilize zooplankton through austral winter when the primary production is negligible. Though they are different, all survival strategies produce the same result, a decrease in total zooplankton biomass. It is difficult to examine the total zooplankton biomass balance and process rates from traditional net tow samples because of the spatial variation in zooplankton distribution and the lack of applicable mathematical methods to estimate population process rates. This study focuses on short-term (overnight) loss rates of mesozooplankton associated with adult krill grazing in austral fall and the long-term (winter) body growth and removal rates of mesozooplankton in austral winter based on measurements of zooplankton size structures obtained using an Optical Plankton Counter (OPC) mounted on a Multiple Opening and Closing Nets and Environmental Sensing System (MOCNESS). In order to target an adult *Euphausia superba* aggregation for a short period, a 153 kHz Vessel-Mounted (VM) Acoustic Doppler Current Profiler (ADCP) was used for the acoustic backscattering. The in situ process rates of growth and mortality are estimated based on the biomass balance and biomass spectrum theory. The overnight in situ grazing by adult *E. superba* on mesozooplankton is examined based on the in situ measurements of mesozooplankton biovolume within the water where an adult *E. superba* aggregation remained during a short study period in late April. The measurements show that approximately 16% of the existing mesozooplankton biovolume was removed in 4 h, which leads to an average specific daily grazing rate of $0.96\,day^{-1}$ assuming a daily feeding period of 16 h from dusk to dawn. From the amount of biovolume removed and the abundance of adult euphausiids of approximately 3 individuals m^{-3} estimated from the volume backscattering strength and the size of adult euphausiids, the daily ration for an adult euphausiid is approximately equal to 7% body biovolume or biomass day^{-1}. The total mesozooplankton biovolume decreased at a specific rate of $0.017\,day^{-1}$ over the austral winter 2002, while the specific individual body growth was approximately $0.045\,day^{-1}$. The sum of these two rates leads to the specific mortality rate equal to approximately $0.07\,day^{-1}$ for the winter. These rates lead to a system efficiency of 67% for recycling the biomass during the winter. The measurements

*Corresponding author. Tel.: +1-617-287-7419; fax: +1-617-287-7474.
E-mail address: meng.zhou@umb.edu (M. Zhou).

0967-0645/$ - see front matter © 2004 Elsevier Ltd. All rights reserved.
doi:10.1016/j.dsr2.2004.07.008

indicate that approximately 90% of biovolume (biomass) was removed in the period between the fall cruise in April–May and the winter cruise in August–September 2002.
© 2004 Elsevier Ltd. All rights reserved.

1. Introduction

Zooplankton mediate the biomass flow from primary producers to upper trophic level organisms in most aquatic systems. Typically there are several trophic links involved in this process, but in the Southern Ocean euphausiids (krill) occupy a unique position, directly mediating the biomass flow from phytoplankton to birds and mammals (Bargmann, 1945; Marr, 1962; Mauchline and Fisher, 1969). During the long dark austral winter, photosynthetic processes and phytoplankton biomass are at a minimum and the ecosystem must be supported by existing bio-energy (biomass) reservoirs. This reduction in energy input into the system is reflected in survival strategies of many organisms. For krill in particular, considered to be phytoplankton feeders in spring, summer and fall, a number of hypotheses and observations have been made on their overwintering strategies: (1) krill may feed on sea-ice algae (Daly, 1990; Daly and Macaulay, 1988; Fraser and Ainley, 1986); (2) krill may feed on smaller zooplankton (Hopkins et al., 1993a; Huntley et al., 1994; Atkinson et al., 2002); (3) krill may combust their stored lipids leading to body shrinkage (Hagen et al., 1996; Ikeda and Dixon, 1982; Nicol et al., 1992); and (4) krill may reduce their metabolism (Torres et al., 1994a,b). Most of these results are based on specific laboratory experiments. In recent studies by Atkinson et al. (2002), effects of capture stress and container size, comparison between methods used in previous studies and size-species specific feeding behavior of euphausiids were addressed. There is still a lack of in situ studies of krill grazing on other zooplankton, which requires either gut content analysis or direct measurements of the zooplankton biomass balance based on direct measurements, both of which are difficult to obtain.

The importance of observed overwintering strategies to krill survivorship may vary based on the specific physical and biological environment and their particular life history stages being considered. Results from the 1992 Research on Antarctic Coastal Ecosystem Rates (RACER) VI winter cruise and US Southern Ocean Global Ocean Ecosystem Dynamics Program (GLOBEC) fall and winter cruises in 2001 and 2002 provide little evidence that krill feed on ice biota even though a significant amount of potential food resources (brown ice) was found (Torres et al., 2001, 2002). Observations during the last four US Southern Ocean GLOBEC cruises (2001–2002) indicate that adult krill actively aggregated, vertically migrated, and fed in the water column where the phytoplankton biomass was extremely low. Through studies of smallscale and mesoscale distributions of krill and copepods, negative correlations between krill and copepod abundances were found, suggesting that *Euphausia superba* (krill) is a major control on copepod abundance (Atkinson and Snyder, 1997; Atkinson et al., 1999). Laboratory feeding experiments have proven what krill are capable of feeding on, which foods are energetically more desirable, and how these can vary with ontogeny (Atkinson et al., 2002). The difficulty is to extrapolate these results from laboratory experiments to actual in situ rates of krill growth, carnivory and their feeding behavior.

We have taken an alternative approach using a size-based automated sampling device, the biomass spectrum theory, and simple biomass balance relations (Platt and Denman, 1977; Sheldon and Parsons, 1967; Sheldon et al., 1972; Zhou and Huntley, 1997). A biomass spectrum classifies plankton biomass by plankton body sizes. The biomass spectrum theory uses allometrically scaled rates of individual growth and population change. In recent studies of mesozooplankton distribution and population processes, the size based measurements using Optical Plankton Counters (OPCs; Focal Technologies Inc., Dartmouth, Nova

Scotia) have been used to perform both high-resolution surveys of mesozooplankton abundance (Herman et al., 1993; Huntley et al., 1995; Pollard et al., 2002), and population dynamics processes (Edvardsen et al., 2002; Heath, 1995; Zhou and Huntley, 1997).

Early studies of marine animal abundance versus their size (individual length or biomass) show a similar trend: the abundance spectrum has a peak at the small-size end, and decreases to relatively minuscule values at the large-size end (Rodríguez and Mullin, 1986; Sheldon et al., 1972; Sprules and Munawar, 1986). A number of studies focused on the slope of a plankton biomass spectrum (biomass sorted into and normalized by a weight interval) as a means of measuring the relationship between growth, mortality, and respiration of a population or community (Heath, 1995; Platt and Denman, 1978; Silvert and Platt, 1978; Zhou and Huntley, 1997). In inland lakes, the slopes of biomass spectra vary from −0.90 to −1.16 (Sprules and Munawar, 1986). In the north Pacific Central Gyre, the slopes of biomass spectra vary from −1.23 for microplankton to −1.13 for macrozooplankton, and from −1.32 at the surface to −1.13 at a depth of 100–120 m (Rodríguez and Mullin, 1986). In later studies, the advances in instrumentation now allow us to examine changes in biomass spectra over a time period so that population dynamics process rates can be estimated (Edvardsen et al., 2002; Heath, 1995; Zhou and Huntley, 1997).

The goal of this study is to extend the use of the size-based measurements, the biomass spectrum theory and biomass balance relations to the process rate estimates of the mesozooplankton communities within the OPC measured size range, specifically examining the short-term grazing rate of adult krill on mesozooplankton and the long-term growth and mortality rates of mesozooplankton during austral winter. Taking advantage of the known taxonomy of mesozooplankton and their sizes (Hardy and Gunther, 1935; Voronina, 1966a,b), our rate estimates can be applied to different mesozooplankton species and then used to evaluate their functional roles in the ecosystem.

2. Materials and methods

2.1. Instruments and data

Data used in this paper were collected during the 2002 austral fall cruise on the A.S.R.V. *Laurence M. Gould* and the 2002 winter cruise on the R.V. *Nathaniel B. Palmer* of the Southern Ocean GLOBEC project in Marguerite Bay and its vicinity (Fig. 1). Process studies were conducted at sites in Crystal Sound, over the shelf break, and in Marguerite Bay during the 2002 fall process cruise between April 7 and May 20, and during the 2002 winter combined survey and process cruise between July 31 and September 18. The sampling stations during both 2002 cruises are shown in Fig. 1. In general, the process study areas cover Matha Strait entering Crystal Sound, the shelf-break near the deep canyon on the shelf, Laubeuf Fjord in the northern part of Marguerite Bay, and the deep canyons in the southern part of Marguerite Bay and on the shelf.

The size-based mesozooplankton measurements were taken using an Optical Plankton Counter (OPC; Focal Technologies, Dartmouth, Nova Scotia) mounted on the top of a Multiple Opening and Closing Nets and Environmental Sensing System (MOCNESS; B.E.S.S. Inc., Falmouth, MA). The data were transmitted to the data acquisition computer through conducting wires in the tow cable at real-time. Several publications outline the technical details of the OPC (e.g. Herman, 1992; Herman et al., 1993) and the MOCNESS (Wiebe et al., 1976, 1985). In a brief summary, the OPC uses optical sensors to measure the Equivalent Spherical Diameter (ESD) of particles passing through the flow-through tunnel. A particle with a size between 250 μm and 14 mm is classified into one of 3494 digital size classes. A depth sensor and a flowmeter (General Oceanics; Miami, FL) were integrated into the OPC to provide depth and flow information. The Global Positioning System (GPS) data were integrated into OPC data strings by the OPC data acquisition software through a serial port on the PC. Using elapsed time marks recorded in OPC data strings, the cross-sectional area of an OPC aperture ($0.005\,m^2$) and the flow speed, the water volume

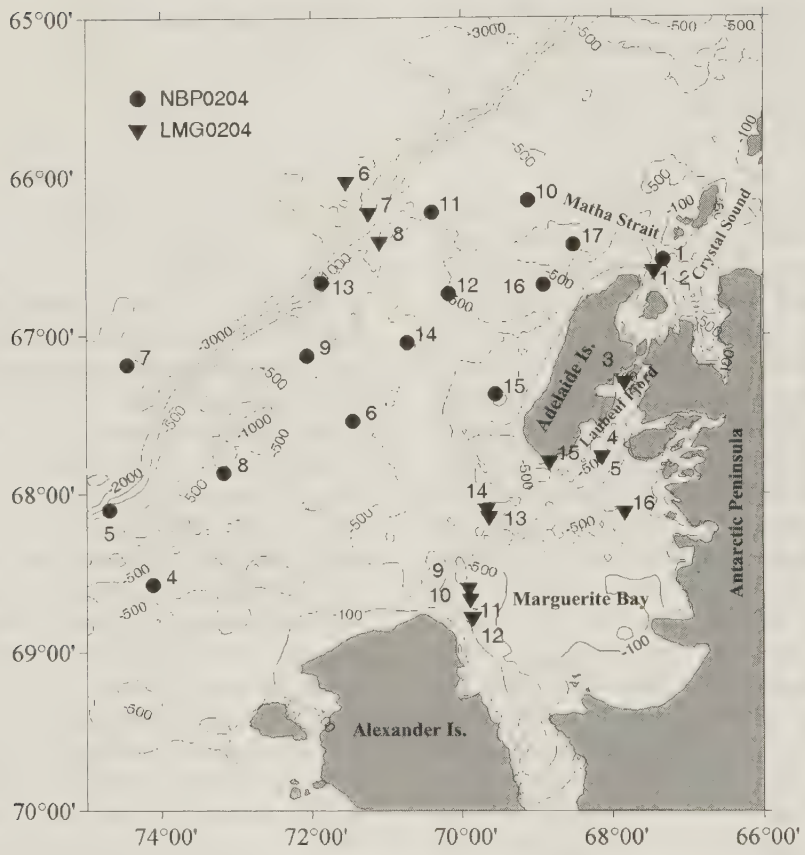

Fig. 1. The bathymetry of the study regions and MOCNESS-OPC stations during the April May austral fall cruise (solid dots) and the August–September austral winter cruise (solid triangles). The numbers next to the stations are MOCNESS tow numbers.

filtered by the OPC was calculated and used to normalize the OPC counts for absolute plankton abundance estimates.

The nets on the MOCNESS were closed and opened based on either predesigned depth intervals or acoustic layers on the echogram displayed at real-time from the single-ping backscattering measurements of a 153 kHz Vessel Mounted (VM) Narrow Band (NB) Acoustic Doppler Current Profiler (ADCP; RD Instruments, San Diego, CA). The single-ping data of the ADCP were transferred through the network at real time, and processed based on the standard method (RDI, 1992; Zhou and Dorland, 2004). The vessel was moving at a speed of approximately 3 knots during the net tows. The vertical angle of the tow cable varied but was approximately between 45°and 50°. The positions of a sampling net in the echogram were estimated based on its depth, cable length and a fixed 45° angle (Fig. 2).

Raw OPC data were processed by integrating measurements into depth intervals associated with the individual MOCNESS nets for each tow. The water volume filtered by the OPC in a depth interval from 25 to 250 m is approximately from 1 to 10 m^3. Taking an average mesozooplankton abundance of 2×10^3 individuals m^{-3} within the size range from 250 μm to 14 mm, the total zooplankton counted in a depth interval are approximately 2×10^3–10^4 individuals. This amount of zooplankton is not enough to allow all 3494 size classes to be adequately represented

statistically. Hence, the OPC data were integrated into 50 size classes on an equal $\log_{10}$ basis and normalized by both the size interval and the water volume filtered at each depth interval. With this integration, the variance produced by the undersampling is statistically reduced and the meaningful differences between measurements can be statistically identified (Figs. 3 and 4).

We choose the body volume of a zooplankter as its size for all computations in this paper because it is equal to the equivalent spherical volume that can be directly calculated from the measured ESD of that zooplankter. The other advantages include the nearly linear relations between biovolume and wet weight, and between wet weight and body carbon (Wiebe, 1988). The 50 size classes are occupied by different zooplankton species and stages. The mean size of the smallest class among the 50 size classes is 0.014 mm^3 in body volume or 0.3 mm in ESD. Assumptions of body aspect ratios are made to understand where a specific species will be on the biovolume coordinate. However, the computation of growth and mortality rates does not require any aspect ratios. For example, the body volume of 1 mm^3 is equivalent to 1.3 mm in ESD, 2.1 mm in length assuming a length to width aspect ratio of approximately 2.5 for a copepod, or 4.3 mm in length assuming a length to width aspect ratio of approximately 8 for a euphausiid (Ashjian et al., 2004; Nordhausen, 1994). The size range from 0.014 to 1 mm^3 should cover most copepod species, and the size range close to 1 mm^3 also should include krill larvae (nauplii, calyptope and furcilia). The size range between 1 and 10 mm^3 corresponds to an ESD range between 1.3 and 2.6 mm, or a length range between 2.1 and 4.2 mm taking an aspect ratio of 2.5, or between 4.3 and 9.3 mm taking an aspect ratio of 8. This size range should include large copepods, and krill calyptopes and furcilia. The size range larger than 10 mm^3 should include krill juveniles and adults with body lengths longer than 9.3 mm. The largest size measured by an OPC is approximately 14 mm in the ESD, which is equivalent to 22.5 mm in length, which is in the range of adult euphausiids.

We did not intend to sample adult euphausiids using the OPC because of their known capability of avoidance. For 3–5 cm adult euphausiids, their escape velocity is approximately 15–30 $cm\,s^{-1}$, 5–6 times their body length per second (Swartzman, 1991; Zhong et al., 1996). The aperture of the OPC is only 2.5 cm high and 20 cm wide. It takes less than 0.2 s for an adult euphausiid to swim a distance equivalent to the aperture height. When the MOCNESS was towed at 3 knots, the net travelled 30 cm in 0.2 s. An adult euphausiid can easily escape from an OPC if the euphausiid starts to escape more than 30 cm ahead of the OPC, well within their capability (Brinton, 1967; Everson and Bone, 1986; Sameoto et al., 1993).

Large numbers of aggregated adult *E. superba* and top predators were present in open water with small ice floes during our study in Crystal Sound in fall 2002 (Zhou and Dorland, 2004). We were able to use the volume backscattering strength measurements of the 153 kHz NB ADCP on the ASRV Gould to track the adult *E. superba* aggregation for conducting targeted measurements. Because we successfully followed the same aggregation for a short period, we were able to use the data for estimating the short-term grazing rate of *E. superba* on mesozooplankton. The long-term process rates were estimated based on averaged measurements from both cruises.

2.2. Mathematical methods

We take the definition of a normalized biomass spectrum (simply referred to as a biomass spectrum) from previous literature (Sheldon and Parsons, 1967; Platt and Denman, 1978; Silvert and Platt, 1978; Zhou and Huntley, 1997) that is,

$$\text{Biomass spectrum} = \frac{\text{Biomass in the size interval } \Delta w}{\text{The size interval } \Delta w}, \quad (1)$$

where the size (w) of zooplankton is the body biomass in carbon. Because an OPC provides ESD measurements of zooplankton, the body volumes of zooplankton can be converted directly from ESD. The biovolume spectrum (b) is defined as,

$$\text{Biovolume spectrum}(b) = \frac{\text{Biovolume in the size interval } \Delta v}{\text{The size interval } \Delta v}, \quad (2)$$

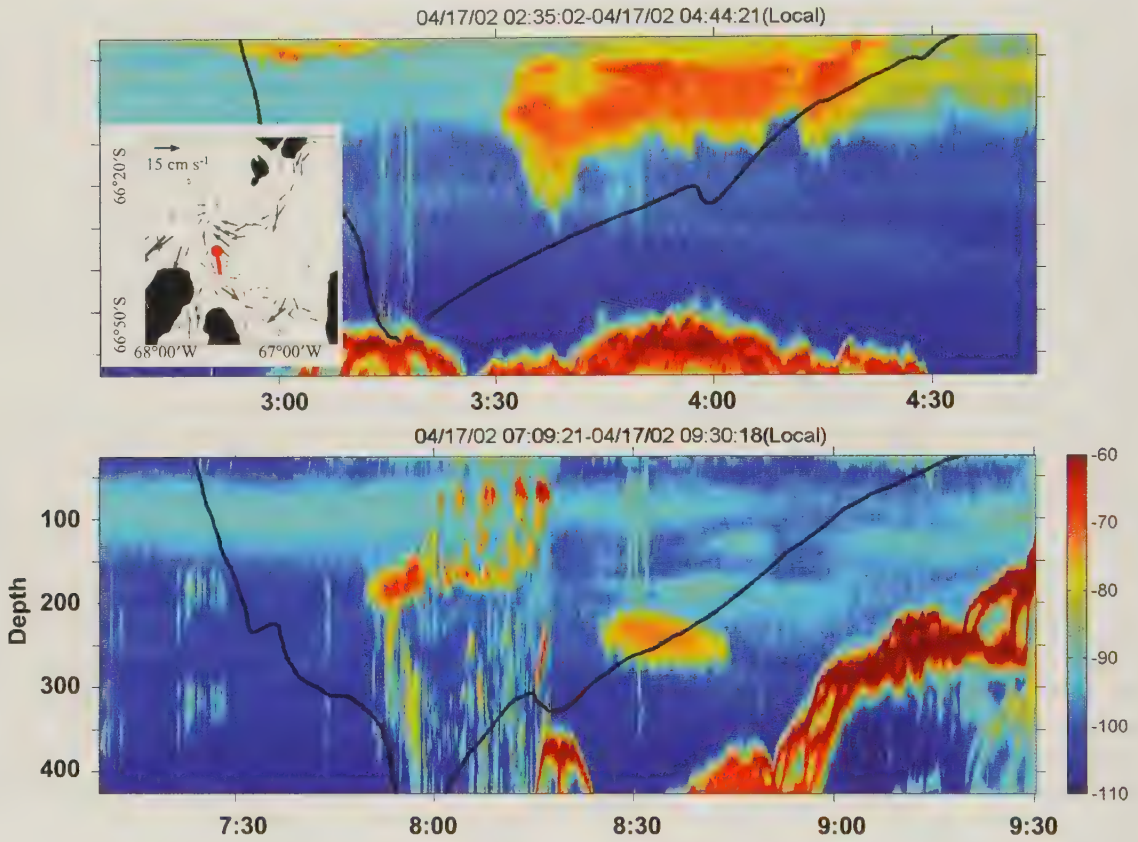

Fig. 2. ADCP echo intensity transects during the periods of the night MOCNESS tow (upper panel) and the day tow (lower panel) in Matha Strait. The solid black lines indicate the MOCNESS tow tracks. The inserted figure shows the ADCP current measurements at 34 m. The red dot and solid line in the inserted figure indicate the starting point and tow track of MOCNESS tows. The local timing information is indicated on the figure titles and horizontal axes.

where the size (v) of zooplankton is the body volume in mm^3. Though the relation between the body biomass and volume can vary from one species to another species, the biovolume spectrum should be equivalent to the biomass spectrum on the 1st-order approximation. To avoid further complication and uncertainty in the relations between the body biomass and volume for different species compositions, we simply use biovolume and biovolume spectra in our computations and discussion.

The specific individual growth (g) is defined as,

$$g = \frac{1}{v}\frac{\mathrm{d}v}{\mathrm{d}t}, \tag{3}$$

where v is the individual volume, and t is the time. Integrating Eq. (3) over a time period (Δt) from t_1 to t_2 by assuming g_c is a constant, or the mean value between t_1 and t_2, we have

$$g_c = \frac{\ln v(t_2) - \ln v(t_1)}{\Delta t}. \tag{4}$$

Using Eq. (4) for individual growth estimates, the error progress due to errors in v-estimates can be analyzed by taking the differentiation of Eq. (4), and then obtaining the upper limit, i.e.,

$$\left|\frac{\delta g_c}{g_c}\right| \leqslant \frac{\tau_g}{\Delta t}[|\delta \ln v(t_1)| + |\delta \ln v(t_2)|] + \left|\frac{\delta t}{\Delta t}\right| \leqslant \frac{2\tau_g}{\Delta t}\left|\frac{\delta v}{v}\right|_{\max} + \left|\frac{\delta t}{\Delta t}\right|, \tag{5}$$

where δg_c is the error of the growth rate, τ_g is the time scale of individual growth equal to $1/g_c$, and

δt is the time uncertainty. $\delta[\ln v(t_1)]$ and $\delta[\ln v(t_2)]$ are the errors of $v(t_1)$ and $v(t_2)$ on the natural logarithmic coordinate, respectively. The upper limit of δg_c can be estimated by taking the maximum measurement error of $|\ln v|_{\max}$. Eq. (5) indicates that the relative error of an individual growth rate ($\Delta g_c/g_c$) is amplified by a factor of ($2\tau_g/\Delta t$) from the relative error of the size measurements ($\Delta v/v$). To reduce the sensitivity of Eq. (4) in estimating individual growth rate, the time duration (Δt) between two measurements should be made equivalent to τ_g.

As individuals grow, the biomass flows from small to large sizes representing the energy flow in the ecosystem food web. In our case, we simply use the biovolume. The rate of change in a biovolume spectrum defined in Eq. (2), within a body biovolume class (v), can be written as,

$$\frac{\partial b}{\partial t} + \frac{\partial (vgb)}{\partial v} = (\mu + g)b, \tag{6}$$

where g is the mean specific body volume growth rate of zooplankton at size v defined as in Eq. (3), and μ is the mean specific population mortality rate of zooplankton at the size of v. Eq. (6) is an exact solution from the biomass (biovolume) balance. On the left of Eq. (6), the first term is the specific rate of change in biovolume at a given size, and the second term is the propagation of biovolume crossing the size classes at a rate equivalent to the body growth rate. The first term on the right represents the mortality, and the second term represents the individual growth. We will use Eq. (6) as the basis for mortality estimates.

Because most biovolume (biomass) spectra are expressed in logarithmic coordinates, normalizing Eq. (6) by the biovolume spectrum (b), and rearranging after taking partial derivatives of the second term on the left side, we have

$$\frac{\partial \ln b}{\partial t} + g\frac{\partial \ln b}{\partial \ln v} = \mu - \frac{\partial g}{\partial \ln v}. \tag{7}$$

The scales of each term in Eq. (7) can be estimated based on specific processes. The growth rate of mesozooplankton at $-1\,^{\circ}\mathrm{C}$ is less than $0.04\,\mathrm{day}^{-1}$, corresponding to a time scale of 25 days (Huntley, 1996; Huntley and Lopez, 1992). The temporal scales of a disturbance in physical processes at the high latitudes are approximately 1–5 days, corresponding to a spatial scale of 5–20 km (Huntley and Niiler, 1995; Pedlosky, 1987; Zhou et al., 2002), and the grazing period on mesozooplankton by adult euphausiids, if there is any, should be on a time scale from hours to a couple of days at a given location. The time scales of both physical processes and adult euphausiid grazing are much shorter than the growth scale. Thus, the variations in biovolume spectra at a given region represent short-term physical and biological processes such as advection and grazing, while the difference in total biovolume of mesozooplankton between two seasons may indicate fundamental biomass flows and population processes.

The shape of a biovolume spectrum can be used to interpret both individual body growth and mortality rates. For example, at a steady state condition, the slope of a biovolume spectrum on a logarithmic chart is equal to the ratio of population mortality to individual growth rates (Heath, 1995; Platt and Denman, 1978; Silvert and Platt, 1978; Zhou and Huntley, 1997; Zhou et al., 2001). In such a case, it is assumed that there is a net flux of smaller zooplankton constantly entering the spectrum from the left side, and propagating to larger ones at a rate equivalent to the body growth. It requires both the generation of small zooplankton entering the smallest size category represented by the spectrum and propagating from smaller sizes to larger sizes to balance the biomass or biovolume loss at one given size class due to mortality. Such an assumption may not be valid in some cases, for example, when the predation mortality suddenly increases as a patch of predators move into a steady-state system, when the reproduction stops in austral winter and there is a lack of small zooplankton entering the spectrum, or when we examine the seasonal variation in the primary production and zooplankton size structure. Therefore, the steady state solution cannot generally be applied to our biovolume spectra, and our discussion will be based on the realistic nonsteady state cases (Edvardsen et al., 2002; Zhou and Huntley, 1997).

Assuming the individual body growth rate to be estimated from Eq. (4), the mortality rate can then be computed based on Eq. (7), noting that the last term on the right side is dropped because g is

assumed to be a constant between $v(t_1)$ and $v(t_2)$ in Eq. (4), i.e.,

$$\mu \approx \frac{\ln b(t_2) - \ln b(t_1)}{\Delta t} + g_c \frac{\Delta_v \ln b(t_2) + \Delta_v \ln b(t_1)}{2\Delta_v \ln(v)}, \quad (8)$$

where $b(t_1)$ and $b(t_2)$ are biovolume spectra measured at time t_1 and t_2, Δ_v represents the substitution of central finite differences to differentiations against v in Eq. (7) and the last term is the time average of the central finite difference between t_1 and t_2. The error progress can be estimated by taking the differentiation of Eq. (8), and then normalizing, i.e.,

$$\begin{aligned}\frac{\delta\mu}{\mu} \leqslant & \frac{\tau_m}{\Delta t}[|\delta \ln b(t_1)| + |\delta \ln b(t_2)|] \\ & + \left|\frac{\ln b(t_2) - \ln b(t_1)}{\Delta t}\right|\left|\frac{\delta t}{\Delta t}\right| \\ & + \left(\frac{\tau_m}{\tau_i}\right)\left|\frac{\delta g}{g}\right|\left|\frac{\Delta_v \ln b(t_2) + \Delta_v \ln b(t_1)}{2\Delta_v \ln(v)}\right| \\ & + \frac{1}{\Delta_v \ln(v)}\left(\frac{\tau_m}{\tau_g}\right)[|\Delta_v(\delta \ln b(t_1))| \\ & + |\Delta_v(\delta \ln b(t_2))|], \end{aligned} \quad (9)$$

where $\delta\mu$ is the error of mortality rate, τ_m is the time scale of mortality equal to $1/\mu$, and δt is the time uncertainty. $\delta \ln b(t_1)$ and $\delta \ln b(t_2)$ are the errors of $b(t_1)$ and $b(t_2)$ on the logarithmic coordinate, respectively. The first error term on the right side of Eq. (9) is due to the measurement error of biovolume spectra, the second term is produced by the time uncertainty, the third term is produced by the error of growth rate estimates, and the fourth term is the error between size classes transported by growth. The equation can be simplified by assuming the slope of a biomass spectrum is less than -2 for the second term, and taking the maximum error in biovolume spectrum estimates, i.e.,

$$\begin{aligned}\frac{\delta\mu}{\mu} \leqslant & \left|\frac{\ln b(t_2) - \ln b(t_1)}{\Delta t}\right|\left|\frac{\delta t}{\Delta t}\right| \\ & + \left[\frac{2\tau_m}{\Delta t} + \frac{4}{\Delta_v \ln(v)}\left(\frac{\tau_m}{\tau_g}\right)\right]\left|\frac{\delta b}{b}\right|_{\max} \\ & + 2\left(\frac{\tau_m}{\tau_g}\right)\left|\frac{\delta g}{g}\right|. \end{aligned} \quad (10)$$

This equation indicates the mortality estimate should have a greater error if animals are classified into finer size classes. The error has a progressive relation with the errors in biovolume spectrum and growth rate estimates. During the winter season, if the growth is suppressed by the coldness, lack of food and reduced metabolism, the growth time scale should be much longer than the mortality time scale, and then Eq. (8) can be further reduced, i.e.

$$\mu = \frac{\partial \ln(b)}{\partial t} \approx \frac{\ln b(t_2) - \ln b(t_1)}{\Delta t}. \quad (11)$$

The error of Eq. (11) is then equal to,

$$\frac{\delta\mu}{\mu} \leqslant \frac{2\tau_m}{\Delta t}\left|\frac{\delta b}{b}\right|_{\max} + \left|\frac{\delta t}{\Delta t}\right|, \quad (12)$$

where the error introduced by the time uncertainty (δt) is included. The applicability of Eq. (11) to mesozooplankton in austral winter will be further addressed in the discussion section. An argument can be raised that zooplankton may still grow though there is no reproduction. In this case, we can integrate Eq. (6) over all size classes with a boundary condition at the smallest size class that there is no flux of any small animals into any size classes. The integration leads to

$$\frac{dB}{dt} = \bar{g}\left(1 + \frac{\bar{\mu}}{\bar{g}}\right)B, \quad (13)$$

where B is the total biovolume by integrating b over the entire size range, $\bar{g}$ is the mean specific growth rate and $\bar{\mu}$ is the mean specific mortality rate. In Eq. (13), $\bar{\mu}B$ is removed either efficiently (recycled) to produce body growth ($\bar{g}B$), or inefficiently to sink out of the system. Hence, the ratio of $-\bar{g}/\bar{\mu}$ should be the efficiency of the ecosystem.

3. Results

The study of *E. superba* potential grazing on mesozooplankton in the natural environment was conducted in Matha Strait at the entrance of Crystal Sound (Figs. 1 and 4). Instead of creating an assemblage of *E. superba* and mesozooplankton in an incubator, we used an ADCP to locate a natural aggregation of adult *E. superba* in situ, and followed it for a period of 7 h. Two

MOCNESS-OPC tows were conducted at the beginning and end of this period (Fig. 2). The study area was located a few km south of a coastal current with a velocity of approximately 15 cm s^{-1} (Zhou and Dorland, 2004). The flow field in the study area was sluggish, approximately 5 cm s^{-1}. The advection of water is estimated to be 1.3 km in 7 h. Each 2 h net tow covered 11 km at a tow speed of 3 knots. Because the area sampled was much larger than the extent of the current advection, we can assume that we measured the same water column and the same zooplankton community in these two net tows. Analysis of the net tow samples revealed that the zooplankton biomass was overwhelmingly dominated by adult *E. superba* of 4 cm in length.

Biovolume spectra are generated from the data collected during two tows at the beginning (night) and end (day) of the 7 h period (Fig. 3). Because there were only two tows, the confidence intervals of these spectra are not known. To examine the potential vertical migration of zooplankton, the spectra are averaged between 350 and 150 m, and between 150 m and the surface, respectively. It is evident that the mean biovolume spectrum from the morning tow is systematically lower than the mean of the night tow within the upper water column, while little change is found in the biovolume spectra between the night and morning tows in the deep water. The mortality rates and errors are calculated based on Eqs. (11) and (12) within the upper water column (Table 1).

The mean seasonal biovolume spectra and their 95% confidence intervals in the 2002 austral fall and winter cruises are shown in Fig. 4, which show a significant difference in biovolume spectra. Both mean biovolume spectra have similar characteristics, i.e. there are more mesozooplankton within the small-size range than those within the large-size range. The 95% confidence intervals increase from the small to large sizes, representing the undersampling problem of the OPC and the presence of relatively few large zooplankton compared to small ones. The species composition cannot be identified on these spectra because of the overlaps between different species and stages, which also vary between locations and in different time periods. The growth and mortality rates and

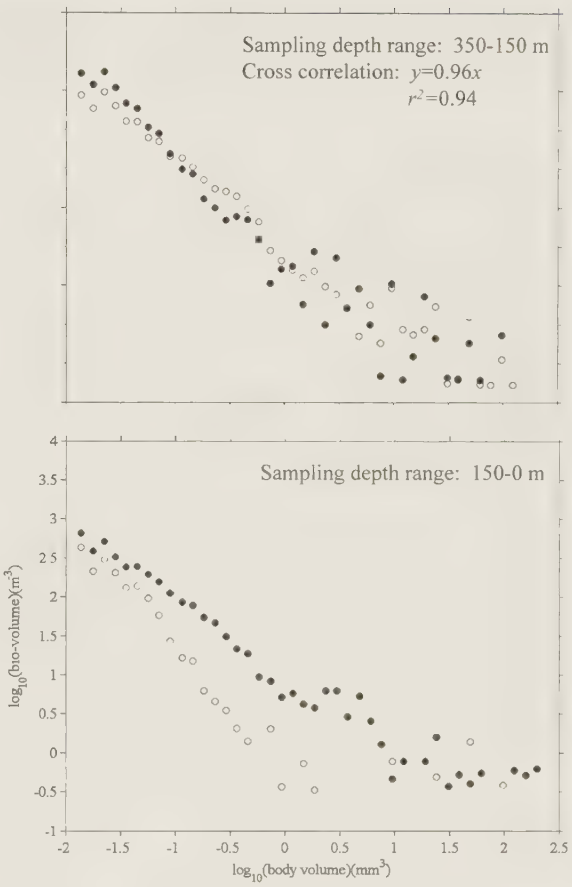

Fig. 3. The mean biovolume spectra measured by the OPC during the night (solid dots) and during the day (open circles) in Matha Strait. See text and Fig. 2 for the timing information.

their errors are calculated based on Eqs. (4), (5), (11) and (12) and listed in Table 1.

The biovolume spectra at selected stations during the 2002 austral fall and winter cruises are shown in Figs. 5 and 6, respectively, which provide general views of mesozooplankton distributions in two seasons. The lowest total biovolume was found in Matha Strait (Tow 1) during the 2002 austral fall cruise where large adult euphausiid aggregations were found. In an adjoining area, Laubeuf Fjord, the biovolume of tow 5 from the same cruise is two times higher than that of tow 1. Though there is a significant spatial variability, there is no large-scale trend in biovolume distribution within Marguerite Bay and

its shelf region. The mean biovolume spectra from these two cruises are significantly different (Fig. 4). The overall biovolume in the austral winter was 1 order of magnitude less than the overall biovolume in the austral fall.

Table 1
Measured values and estimated rates

	Late austral fall[a]	Austral winter
Measurements		
Time interval	4±2 (h)	90±18 (day)
Initial total biovolume ($mm^3\ m^{-3}$)	126	449±210
End total biovolume ($mm^3\ m^{-3}$)	106	83±39
Length of night (h)	16	N/A
Estimates		
Individual growth rate (day^{-1})	N/A	0.045±0.015
Mortality rate (day^{-1})	2.0±1.7	0.07±0.13
Net biovolume reduction rate (day^{-1})		0.017±0.014

[a]A euphausiid aggregation was present during the measurements.

4. Discussion

4.1. Short term mortality and carnivory by adult *E. superba*

Are adult *E. superba* carnivorous in austral winter? Previous studies have found body parts of copepods in adult euphausiid guts, high metabolic rates of adult *E. superba* in austral winter, and *E. superba* feeding on copepods (Atkinson et al., 2002; Hopkins et al., 1993b; Huntley et al., 1994). Though these facts proved adult *E. superba* are, at times, carnivorous, it is difficult to quantitatively measure their grazing on mesozooplankton. To estimate the potential grazing of adult *E. superba* on other zooplankton, we examined two biovolume spectra from an area with adult *E. superba* aggregations. The measurements were obtained within a period of 7 h in Matha Strait entering Crystal Sound (Figs. 1 and 3).

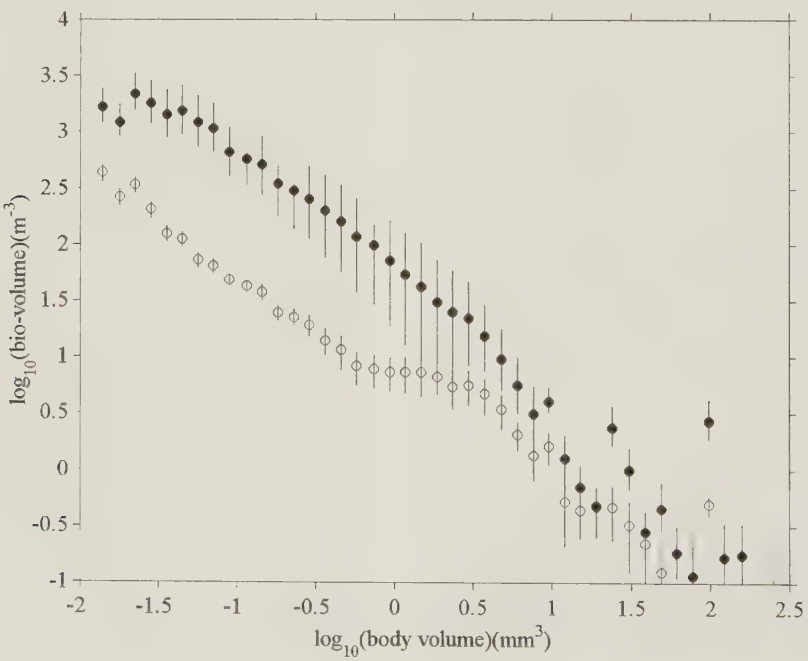

Fig. 4. The mean biovolume spectra measured in the austral fall from April 17, 2002 to May 10, 2002 (Tows 1–16; solid dots); and the austral winter from August 7, 2002 to September 11, 2002 (Tows 1–19; open circles). The vertical solid bars crossing the means are the 95% confidence intervals.

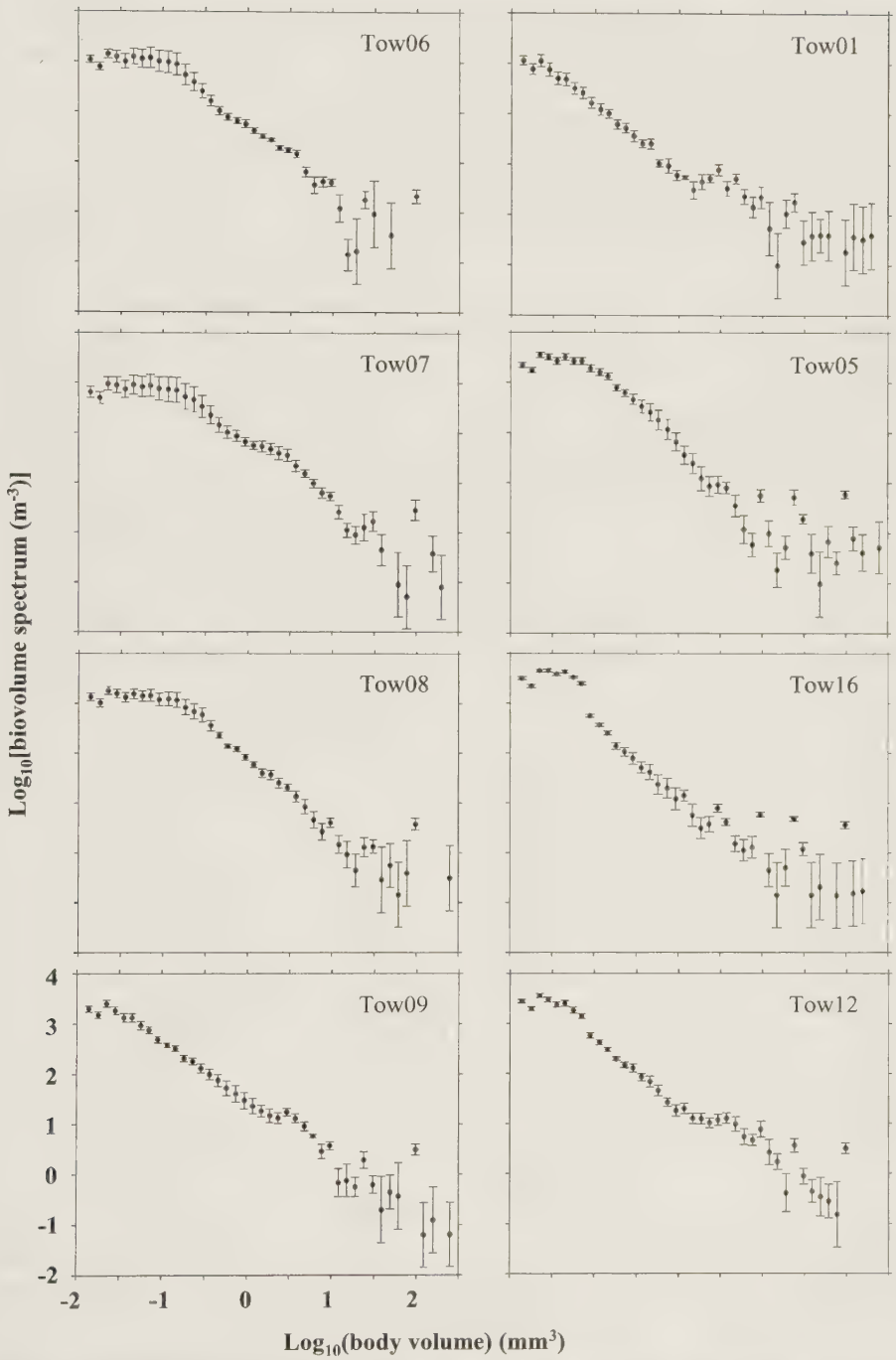

Fig. 5. Biovolume spectra at selected MOCNESS tow stations during the 2002 fall cruise. In each panel, the solid dots represent the mean biovolume spectrum, and the vertical solid bars through each dot represent the standard deviations derived from eight biovolume spectra corresponding to eight depth intervals during a net tow (see Ashjian et al., 2004).

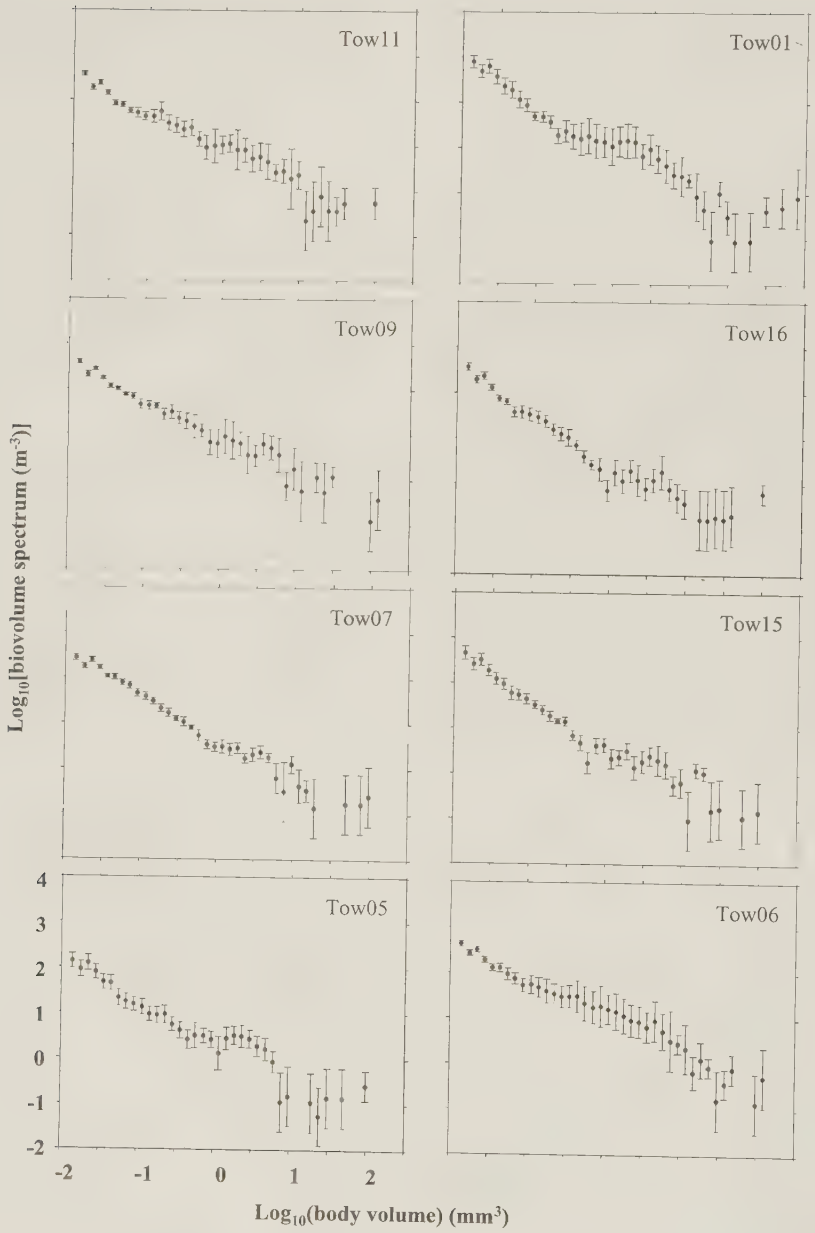

Fig. 6. Biovolume spectra at selected MOCNESS tow stations during the 2002 winter cruise. In each panel, the solid dots represent the mean biovolume spectrum, and the vertical solid bars through each dot represent the standard deviations derived from eight biovolume spectra corresponding to eight depth intervals during a net tow (see Ashjian et al., 2004).

The diel vertical migration of adult euphausiids is clearly depicted in the two ADCP transects and two net tows in Fig. 2. Euphausiids stayed in the upper water column, presumably feeding actively during the night. The dawn was at approximately 8 a.m. local time, and the measurements show a

downward movement of euphausiids during that period, ultimately remaining at depth during the day.

The OPC measurements reveal a 76% decrease of the biovolume in the upper 150 m between night and morning tows (the lower panel in Fig. 3). The causes for the decrease of biovolume in the upper water column could include spatial variability, diel vertical migration, and mortality associated with euphausiid grazing. The sluggish flow field ($5\,cm\,s^{-1}$) in the area eliminates advection as a likely factor. It was observed that the euphausiids fed in the upper 150 m water column during the night, and formed a smaller and denser aggregation in the deep water during the day (Zhou and Dorland, 2004). Because the morning tow was conducted during the downward migration period, the effect of euphausiid grazing on the zooplankton biovolume estimate in the deep water is negligible even if euphausiids were grazing in the deep water. Only spatial variability and vertical migration should be the primary causes for changes of the biovolume spectra in both upper and deep waters. However, the biovolume in the deep water changed only less than 1% between the night and morning tows, and the linear regression between the two biovolume spectra from these two tows has a slope of 0.96 and an r^2 of 0.94. This small change of the biovolume spectrum in the deep water implies that the spatial variability and diel vertical migration were negligible within the scope of the OPC measurements, and the decrease of biovolume in the upper 150 m between the night and morning tows primarily resulted from euphausiid grazing.

To estimate the specific mortality rate in the upper 150 m, we assume that the estimated time scale of individual growth is on the order of 50 s of days (see the estimation of individual growth rate in the next section) and the change of the biovolume spectrum occurred in the same water column over only several hours. Eq. (11) can be applied to estimate the mortality rate. Because the 95% confidence intervals of the biovolume spectra cannot be estimated from one measurement, the error contributed by δb is ignored in Eq. (12) during the following calculations. The 95% confidence intervals of the time interval can be approximated by the time duration of a tow. We take the median time interval between these two tows as approximately 4 h, and the time uncertainty (δt) is then approximately 2 h, the time duration of a net tow (Figs. 2 and 3). Neglecting the individual growth, we have the mean specific mortality rate ($\bar{\mu}$) and the absolute error based on Eqs. (11) and (12), respectively, i.e.,

$$\bar{\mu} = -0.13 \pm 0.11 \quad (h^{-1}). \tag{14}$$

If we assume that the decrease in biovolume at night was associated with grazing on mesozooplankton, and the feeding period of adult euphausiids is equal to the length of night (16 h) during our survey period, the specific daily mortality rate ($\bar{\mu}_d$) should be equal to

$$\bar{\mu}_d = -2.0 \pm 1.7 \quad (day^{-1}). \tag{15}$$

The time scale of the short term removal is approximately equal to 0.5 day, i.e., 87% of mesozooplankton biovolume in the upper water column will be removed by these adult *E. superba*. The total biovolume in tow 1 is approximately $73\,mm^3\,m^{-3}$ in the upper water column after summing all size classes. On the 1st order approximation, using the ratio of carbon (mg C) to wet weight (mg) of 0.03 and the specific weight of zooplankton of approximately 1.1 (Wiebe et al., 1975), we have the rate of decrease in biovolume and carbon equal to $150\,mm^3\,day^{-1}\,m^{-3}$ and $4.5\,mg\,C\,day^{-1}\,m^{-3}$, respectively. If we assume that *E. superba* started to feed at 4 p.m., and net tow 1 was conducted at 3:30 a.m., the median time of the tow, the initial biovolume (biomass) in the water column before the grazing should be approximately $410\,mm^3\,m^{-3}$ ($12\,mg\,C\,m^{-3}$), which is close to the mean of $449 \pm 210\,mm^3\,m^{-3}$ during the austral fall.

Taking the individual target strength at −70 dB for a euphausiid of 4 cm, and the volume backscattering strength of −65 dB from the ADCP echo intensity measurements, the abundance of adult euphausiids was approximately 3 individuals m^{-3} (Everson et al., 1990; Greene et al., 1991; Zhou et al., 1994; Zhou and Dorland, 2004). Converting to the biovolume based on a cylinder model with an aspect ratio of 8, a euphausiid of 4 cm in length is equal to $785\,mm^3$ and the

total biovolume of euphausiids is equal to 2355 $mm^3 m^{-3}$. The biovolume of other mesozooplankton is approximately 410 $mm^3 m^{-3}$ within the OPC size range. In our sampling area with adult euphausiid aggregations, the biovolume in the water column was dominated by adult euphausiids. The seasonal mean mortality is estimated to be approximately $-0.07\,day^{-1}$ (see Section 4.2), much smaller than that of the mortality of $-2.0\,day^{-1}$ around the adult euphausiid aggregations. The excessive mortality to mesozooplankton can be potentially partly caused by adult euphausiid grazing. The decrease in mesozooplankton biovolume around a euphausiid aggregation provides supportive evidence that adult euphausiids feed on other mesozooplankton.

The biomass needed for a *E. superba* to balance its respiration can be estimated as approximately 2% of the body biomass day^{-1} at $-1\,°C$ (Huntley and Boyd, 1984; Huntley et al., 1994). Recently studies indicate the ration is approximately 0.5–10% of body carbon day^{-1} during the autumn (Atkinson et al., 2002; Atkinson and Snyder, 1997). Thus, a 4 cm *E. superba* consumes 4–80 $mm^3\,day^{-1}$ or 0.12–2.4 mg C day^{-1} using the carbon to biovolume ratio of 0.03 (Wiebe et al., 1975) and the aspect ratio of 8. The amount of biovolume in the upper water column lost over night is approximately 393 $mm^3 m^{-3} day^{-1}$, which can support the energy requirement from 98 to 5 adult euphausiids m^{-3} if the ration is approximately 0.5–10% of body carbon day^{-1}. However, if we assume an adult euphausiid abundance of 3 individuals m^{-3}, and these adult euphausiids are fully responsible for the decrease in biovolume in the water column, the ration for an adult euphausiid is approximately 131 $mm^3\,day^{-1}$ $individual^{-1}$, or 17% of body volume (carbon) day^{-1} $individual^{-1}$. If considering a lower aspect ratio of 7, the body volume of a 4 cm euphausiid increases to 1025 mm^3, and the ration is only reduced to 13% of body volume. These estimates of rations exceed the literature values of 0.5–10% of body carbon day^{-1}, which implies other animals might also contribute to the morality of zooplankton in the water column. The decrease of biovolume occurred over all size classes, which may indicate that adult *E. superba* feed non-selectively on whatever is available in the water column.

4.2. Seasonal population process rates

The biovolume (biomass) of mesozooplankton decreased approximately 82% from the austral fall to the austral winter, 2002 when comparing the mean biovolume spectra from the fall and winter cruises (Fig. 4). The 95% confidence intervals of these two biovolume spectra in Fig. 4 indicate the differences are statistically significant. The loss of biovolume in the system clearly indicates that the ecosystem in austral winter has a negative net production, and most of the biovolume was dissipated by mortality through either being consumed or through natural death. The loss due to diapausing zooplankton in the deep water is minimal at best, with the vertical seasonal migration ending earlier than our survey periods (Ashjian et al., 2004). We believe that these estimates are not biased by sampling and advection effects (see discussion in Section 4.3).

If we assume that the growth had been zero during that period, the decrease in biomass would have been primarily caused by mortality. From Eqs. (11) and (12) the mean specific mortality rate ($\bar{\mu}$) based on the decrease in the biovolume spectrum (b) and absolute error are

$$\bar{\mu} = -0.017 \pm 0.014 \quad (day^{-1}), \tag{16}$$

where the average is taken over the entire OPC size range, τ_m is equal to $1/|\bar{\mu}|$ or approximately 59 days, the time interval between the two cruises (Δt) is equal to 90 days, the time uncertainty is equal to 18 days, half the cruise period, and the mean $(\delta b/b)_{max}$ through all size classes is equal to 0.47 (Table 1). The standard deviation (σ_μ) of the mortality variation over all size classes is equal to

$$\sigma_\mu = 0.009 \quad (day^{-1}). \tag{17}$$

The mortality rate estimated from the OPC data is similar to spring and summer values reported between 0.03 and 0.38 at high latitudes (Edvardsen et al., 2002; Eiane, 1999; Lopez, 1991), which contradicts the concept of high mortality rates in winter due to a lack of primary production, and grazing on zooplankton. Taking the temperature

in the upper water column as −1 °C, previous studies indicate that the maximum value of zooplankton growth is approximately $0.04\,day^{-1}$, though it is doubtful that zooplankton would grow at their maximum rate during periods without optimal food supplies (Huntley and Boyd, 1984; Huntley and Lopez, 1992). Examining the difference in the biovolume spectra from austral fall and winter (Fig. 4), the zooplankton larger than $1.8\,mm^3$ have little or no decrease compared to those smaller than $1.8\,mm^3$. It is hard to imagine that the mortality rate is equal to zero for the zooplankton larger than $1.8\,mm^3$. It is more likely that any decrease in biovolume is balanced by individual growth, i.e. smaller organisms grow into the larger size classes at a rate similar to the removal of larger organisms, thereby leading to little or no-change in the biovolume spectrum.

We notice that the change in a biovolume spectrum can be associated with three processes by examining the features of the biovolume spectra in Fig. 4: a significant reduction of small zooplankton at the left end of the spectrum, the growth of zooplankton from small to large size classes, and the mortality. The reduction in abundance of small zooplankton can be caused by a lack of reproduction during the austral winter. Because the mortality in a particular size class and the flux growing out of the size class are balanced by the flux growing into it, a lack of reproduction will lead to a decrease in the biovolume starting from small size classes and propagating towards the large ones at a rate equivalent to the body growth. The size range affected by the lack of reproduction is limited by the rate of body growth. In the affected range, the decrease in biovolume is caused by both mortality and a lack of reproduction. Out of the affected range, the decrease is only caused by mortality. Hence, the amount of biovolume reduced should be relatively greater in the affected range than the amount reduced in the non-affected range. These two body size ranges in Fig. 4 can be easily distinguished by comparing the difference between the austral fall and winter spectra. The boundary between these two ranges is approximately $1.8\,mm^3$ on the winter biovolume spectrum. On the left side of this boundary, the decrease in biovolume is approximately 90%, and on the right side, the decrease is approximately 60%. On the fall biovolume spectrum, the decline of the biovolume spectrum towards smallest body size classes between 0.01 and $0.03\,mm^3$ indicates the reduced flux into these classes affected by the reduction of productivity. Thus, assuming that the peak of zooplankton propagates from 0.03 to $1.8\,mm^3$ in approximately 90 days between the fall and winter cruises, we have the specific propagation rate of $0.045 \pm 0.015\,day^{-1}$ from Eq. (4), which is equal to the specific body growth rate similar to the estimate based on the temperature only (Huntley and Boyd, 1984; Huntley and Lopez, 1992). The error of the estimate can be evaluated by Eq. (5). If we take τ_g as being approximately equal to 50 days ($1/g$), Δt equal to 90 days, δt equal to 18 days, and δv equal to the size interval of $0.5\,mm^3$ for the $1.8\,mm^3$ sizeclass, the estimated relative error is equal to 34%. Thus, the estimated individual growth rate and absolute error are equal to

$$g = 0.045 \pm 0.015 \quad (day^{-1}). \tag{18}$$

Though the difference between 0.03 and $1.8\,mm^3$ is used for estimating the growth rate, there is no assumption that a zooplankter grows from 0.03 to $1.8\,mm^3$ in 90 days. It means that there are many zooplankton in different size classes moving biovolume from small sizes to large ones, which leads to the biovolume propagation. Such a process also can be interpreted from the point of view that zooplankton are just carriers of biovolume, like carts carrying material. Imagine that a cart carries zooplankton from size class 1 to size class 2 at a particular rate. Some zooplankton are removed by mortality during the transport. In size class 2, the cart is repacked with some of those carried in from size class 1 and those already in size class 2. Then, this cart moves into size class 3. We do not track one specific group of zooplankton because in each size class the cart will be repacked. Assuming there is a train of carts equivalent to a set of size classes, we now only examine the rate of motion and the number of zooplankton in each cart without following individuals. The rate of motion of a cart is the mean growth rate.

Eq. (8) can be used to calculate the mortality rate when the individual body growth rate can be estimated independently. We assume the individual body growth rate to be $0.045\,\mathrm{day}^{-1}$ for all body size classes on the first-order approximation, and compute the mortality rates at different sizes. The error of the estimate can be analyzed by Eq. (10). Taking τ_g equal to 22 days $(1/g)$, τ_m equal to 15 days $(1/|\bar{\mu}|)$, Δt equal to 90 (days), and $\Delta_v \ln(v)$ equal to 0.46, which is 2 times the size interval due to the use of the central difference, we have two scalars of 2.7 and 1.3 for the errors of biovolume spectra and growth rates, respectively.

$$\frac{\delta\mu}{\mu} \leqslant 2.7 \times \left|\frac{\delta b}{b}\right|_{\max} + 1.3 \times \left|\frac{\delta g}{g}\right| + \left|\frac{\delta t}{\Delta t}\right|. \tag{19}$$

Averaging Eq. (19), and using 0.47 for the mean $(\delta b/b)_{\max}$ and Eq. (18) for the mean $(\delta g/g)$, the seasonal mean mortality rate and its error are equal to

$$\bar{\mu} = -0.07 \pm 0.13 \quad (\mathrm{day}^{-1}). \tag{20}$$

The use of size independent specific growth is not ideal for the computation in Eq. (8), though there is no other in situ method available in this study. We argue that efficient grazers at a given size class will be limited by available prey in the water column and inefficient grazers at a given class will be replaced by efficient grazers growing into their size class from smaller ones. From the transport argument of a moving train, all carts will move at an average rate. Thus, the specific growth rate is uniform over all size classes.

The slopes of biovolume spectra in Fig. 4 are approximately equal to -1. The biovolume spectrum reaches a steady state when the propagation of biovolume due to body growth matches the mortality due to predation and death. The slope of a biovolume spectrum under the steady state assumption or time average is equal to the ratio of mortality to individual growth rates and is approximately between -0.9 and -1.3 (Platt and Denman, 1978; Rodríguez and Mullin, 1986; Sprules and Munawar, 1986; Zhou and Huntley, 1997; Zhou et al., 2001). That is, the magnitude of the mortality rate is approximately equivalent to the body growth rate. In our case, this ratio is nearly equal to -2. The difference between the slope of the biovolume spectra and the ratio can be explained by Eq. (8), which indicates that the absolute value of the mortality rate is equal to the sum of the body growth rate and the absolute rate of decrease in biovolume. The latter one is equal to zero when the biovolume spectrum reaches a steady state. If the high mortality rate in the austral winter could be attributed to starvation, we would expect the body growth rate to be small and negligible, which is not the case because the estimated value is approximately $0.045\,\mathrm{day}^{-1}$, similar to the optimal growth rate without food limitation (Huntley and Lopez, 1992). However, if zooplankton were feeding solely on other zooplankton during the winter when phytoplankton were not available, the mortality rate would be higher and therefore the slope of a biovolume spectrum would be more negative, as we see in the results of this study.

Without the input or flux of energy from phytoplankton to zooplankton in the austral winter, maintenance of the zooplankton population would depend on energy recycling within the zooplankton community. In Eq. (13), $\bar{\mu}B$ is the total amount of zooplankton removed from the OPC size range either to produce body growth $(\bar{g}B)$, or to be buried out of the system $(\bar{\mu}B - \bar{g}B)$. Hence, the ratio of $-\bar{g}/\bar{\mu}$ can be considered as a measure of the efficiency of the ecosystem. Taking the mortality rate of $0.07\,\mathrm{day}^{-1}$ (Eq. (20)) and the growth rate of $0.045\,\mathrm{day}^{-1}$, the efficiency is approximately 67% in austral winter.

4.3. Spatial variability and advection

It is important to evaluate the spatial sampling bias on the winter zooplankton process rate estimates in the Marguerite Bay shelf region because the significant variability in OPC zooplankton biovolume estimates was found, which is consistent with the biovolume estimates from other net samples and acoustic backscattering measurements (Ashjian et al., 2004; Lawson et al., 2004; Zhou and Dorland, 2004). Such variability in zooplankton distribution is associated with physical features. For example, the total biovolume, excluding adult euphausiids, from tow 1 in Matha Strait is the lowest measured value

among tows during the 2002 fall cruise, but it is the highest value among tows during the 2002 winter cruise. In an adjoining area, Laubeuf Fjord, the biovolume from tow 5 obtained during the austral fall cruise is 10 times higher than that of tow 1 while no adult euphausiid aggregations were found. The differences between the biovolume spectra from tows 6, 7 and 8 off and on the shelf break from the austral fall cruise may be associated with shelf break fronts and jets (Figs. 1 and 5). The biovolume spectrum from tow 8 is elevated to $2 \times 10^3\,m^{-3}$ between body sizes 10^{-2} and $10^{-0.5}\,mm^3$ compared to $1 \times 10^3\,m^{-3}$ from tows 6 and 7, and the biovolume spectrum from tow 7 is elevated to $4 \times 10^1\,m^{-3}$ centered at the body size of $10^{0.5}\,mm^3$, compared to $2 \times 10^1\,m^{-3}$ from tows 6 and 8. A difference in biovolume estimates crossing an ice edge exists and can be examined from tow 9 conducted at the ice edge and tow 12 conducted in solid pack ice during the 2002 austral fall cruise (Figs. 1 and 5). The effect of ice on the distribution of mesozooplankton may be significant to some mesozooplankton species at particular stages when ice provides shelter and potential food resources (ice algae) that significantly affect zooplankton aggregation behavior. Acoustic backscatter measurements and net tow samples also indicate that the distribution of adult *E. superba* is patchy, with the scale of their aggregations approximately 5–10 km, and there are cross-shelf and along-shelf gradients of zooplankton biomass(Ashjian et al., 2004; Lawson et al., 2004; Zhou and Dorland, 2004). From the net tow samples collected during the 2001 cruises, a large trend from higher zooplankton biomass on the shelf to lower zooplankton biomass off the shore, and high variability in the zooplankton biomass on the shelf along the southwest–northeastern direction were found (Ashjian, et al., 2004). These results from different stations, seasons and years certainly indicate the spatial variability in zooplankton distributions.

The sampling bias in the estimate of seasonal mean biovolume spectra due to spatial variability should be addressed because the net tow stations in the austral fall cruise covered a much different area from the area covered in the austral winter cruise. From net tow samples from the 2001 austral fall cruises, Ashjian et al. (2004) indicate that the highest zooplankton biomass is found in Laubeuf Fjord, and the lowest is found off the shelf break. Assuming that this conclusion is still applicable to the 2002 case, any biovolume spectra in the southwestern shelf region should be bounded between the lower limit off the shelf region and the upper limit in Laubeuf Fjord. The variability of biovolume spectra from the 2002 austral winter cruise is much smaller than that of the 2002 austral fall cruise though stations covered a larger area in the winter cruise than that of the fall cruise. The difference in zooplankton biomass between the 2002 austral fall and winter cruises is one order of magnitude. Hence, the seasonal difference is much higher than the regional difference, which is consistent with the findings from net tow samples (Ashjian et al., 2004). The error ranges in the rate estimates should be adequate to cover the spatial sampling bias.

The reduction of zooplankton biomass on the shelf can be produced by the advection of zooplankton off the shelf by mesoscale and large-scale circulations (Ashjian et al., 2004). Studies of the circulation based on hydrographic and ADCP data in the vicinity of Marguerite Bay indicate that the currents on most shelf areas are within 5–10 $cm\,s^{-1}$, forming mesoscale and large scale eddies, coastal currents are within narrow coastal areas, and the Antarctic Circumpolar Current (ACC) is found near the shelf break (Lascara et al., 1999; Torres et al., 2002.). Within those slow moving eddies, the transport of zooplankton would be insignificant. Most of the strong currents were found parallel to coasts and are localized, not transporting water off the shelf. At the shelf break, though strong currents up to 20–40 $cm\,s^{-1}$ were found primarily parallel to the shelf break, mesoscale eddies containing the Upper Circumpolar Deep Water (UCDW) were found on the shelf, and the UCDW entered the shelf region. Because there is no strong cross-shelf current, zooplankton are transported onto or off the shelf primarily by mesoscale eddies.

The area intruded by the UCDW can be examined from the temperature and salinity characteristics (i.e., Fig. 2 in Ashjian et al., 2004). The surface seasonal mixed layer was

between 50 and 100 m in both onshelf and offshelf regions. Significant heat loss from the surface cooling occurred during the austral winter based on the decrease in the temperature within the surface mixed layer. Below the mixed layer, both temperature and salinity can be used as the traces to identify water types. The UCDW off the shelf are typically warm in temperature and low in salinity, distinctly different from those shelf waters. In both seasons, the temperature and salinity profiles at Midshelf 1 noted in Ashjian et al. (2004) resemble those off the shelf, that is the water on the northeastern shelf region is of the UCDW type. The influence of UCDW can still be found in the Midshelf 2 water, and vanish in the Midshelf 3 and 4 waters, and Marguerite Bay water. Hence, the replacement of shelf waters by the UCDW only occurred in limited regions, and the shelf waters in most shelf regions still remained during the winter.

5. Conclusions

We have developed mathematical equations to estimate errors associated with these process rates. Different from the variation between size classes and geographic locations, the original errors are produced by sampling frequencies, resolutions and instrument accuracies and propagate into our final estimates. In most of our cases, the progressive error ranges exceed the natural variations. The equations used for growth and mortality rate estimates are based on general definitions, and the error analysis can generally be applied in similar studies. These equations for process rate estimates and error analysis can be used to guide experimental settings and cruise design.

Short- and long-term zooplankton population process rates were estimated from the in situ OPC biovolume data of the austral fall and winter cruises in 2002. Because of the limited data, these estimates bear significant uncertainties, though they are statistically meaningful. The short-term mesozooplankton mortality rate is approximately equal to $2.0\,day^{-1}$. If zooplankton were grazed only by a krill aggregation with a concentration of 3 adult euphausiid m^{-3}, the ration for a euphausiid is 13–17% of the body biovolume or biomass, which exceeds the literature values between 0.5% and 10%. Other animals may also prey on zooplankton during winter. The winter season individual growth and population mortality rates are approximately equal to 0.045 and $-0.07\,day^{-1}$, respectively. The total biovolume within the OPC size range decreases at a specific rate of $0.02\,day^{-1}$. If we assume that zooplankton survival entirely depends upon their consumption of other zooplankton through winter, the assimilation efficiency is approximately 67%. Because the ecosystem loses 33% every time the bio-energy is recycled without any source to balance the loss, the total biovolume must decrease during the winter season.

Acknowledgements

We would like to acknowledge Raytheon Polar Service Co. for assisting all our activities and solving technical difficulties during our cruises. Special thanks due to Ryan D. Dorland and Joseph P. Smith at the University of Massachusetts Boston for their help to collect field samples and data. The field research is supported by the National Science Foundation Grant number OPP-9910263 to M. Zhou. This is contribution No. 455 of the US GLOBEC Program.

References

Ashjian, C.J., Rosenwaks, G.A., Wiebe, P.H., Davis, C.S., Gallager, S.M., Copley, N.J., Lawson, G.L., Alatalo, P., 2004. Distribution of zooplankton on the continental shelf off Marguerite Bay, Antarctic Peninsula, during austral fall and winter, 2001. Deep-Sea Research II, this issue [doi:10.1016/j.dsr2.2004.07.025].

Atkinson, A., Snyder, R., 1997. Krill-copepod interactions at South Georgia, Antarctica, I. Omnivory by *Euphausia superba*. Marine Ecology Progress Series 160, 63–76.

Atkinson, A., Ward, P., Hill, A., Brierley, A.S., Cripps, G.C., 1999. Krill-copepod interactions at South Georgia, Antarctica, II. *Euphausia superba* as a major control on copepod abundance. Marine Ecology Progress Series 176, 63–79.

Atkinson, A., Meyer, B., Stubing, D., Hagen, W., Schmidt, K., Bathmann, U., 2002. Feeding and energy budgets of Antarctic krill *Euphausia superba* at the onset of

winter-II. Juveniles and adults. Journal of Limnology and Oceanography 47, 953–966.

Bargmann, H.E., 1945. The development and life-history of adolescent and adult krill *Euphausia superba*. Discovery Reports 23, 103–176.

Brinton, E., 1967. Vertical migration and avoidance capability of euphausiids in the California Current. Journal of Limnology and Oceanography 12, 451–483.

Daly, K.L., 1990. Overwintering development, growth, and feeding of larval *Euphausia superba* in the Antarctic marginal ice zone. Limnology and Oceanography 35, 1564–1576.

Daly, K.L., Macaulay, M., 1988. Abundance and distribution of krill in the ice edge zone of the Weddell Sea, austral spring 1983. Deep-Sea Research I 35, 21–41.

Edvardsen, A., Zhou, M., Tande, K.S., Zhu, Y., 2002. Zooplankton population dynamics, Measuring in situ growth and mortality rates using an Optical Plankton Counter. Marine Ecology Progress Series 227, 205–219.

Eiane, K., 1999. Stage specific mortality of *Calanus* spp. under different predation regimes. In, Pelagic food webs, structuring effects of different environmental forcing. D.Sc. Thesis, University of Bergen, Bergen.

Everson, I., Bone, D.G., 1986. Effectiveness of the RMT8 system for sampling krill (*Euphausia superba*) swarms. Polar Biology 6, 83–90.

Everson, I., Watkins, J.L., Bone, D.G., Foote, K.G., 1990. Implications of a new acoustic target strength for abundance estimates of Antarctic krill. Nature 345, 338–340.

Fraser, W.R., Ainley, D.G., 1986. Ice edges and seabird occurrence in Antarctica. Bioscience 36, 258–263.

Greene, C.H., Stanton, T.K., Wiebe, P.H., McClatchie, S., 1991. Acoustic estimates of Antarctic krill. Nature 349, 110.

Hagen, W., Van Vleet, E.S., Kattner, G.S., 1996. Seasonal lipid storage as overwintering strategy of Antarctic krill. Marine Ecology Progress Series 134, 85–89.

Hardy, A.C., Gunther, E.R., 1935. The plankton of the South Georgia whaling grounds and adjacent waters. Discovery Reports 11, 1–456.

Heath, M.R., 1995. Size spectrum dynamics and the planktonic ecosystem of Loch Linnhe. ICES Journal of Marine Science 52, 627–642.

Herman, A.W., 1992. Design and calibration of a new optical plankton counter capable of sizing small zooplankton. Deep-Sea Research 39, 395–415.

Herman, A.W., Cochrane, N.A., Sameoto, D.D., 1993. Detection and abundance estimation of euphausiids using an optical plankton counter. Marine Ecology Progress Series 94, 165–173.

Hopkins, T.L., Ainley, D.G., Torres, J.J., Lancraft, T.M., 1993a. Trophic structure in open waters of the marginal ice zone in the Scotia-Weddell confluence region during spring (1983). Polar Biology 13, 389–397.

Hopkins, T.L., Lancraft, T.M., Torres, J.J., Donnelly, J., 1993b. Community structure and trophic ecology of zooplankton in the Scotia Sea marginal ice zone in winter (1988). Deep-Sea Research I 40, 81–105.

Huntley, M.E., 1996. Temperature and copepod production in the sea, a reply. American Naturalist 148, 407–420.

Huntley, M., Boyd, C., 1984. Food-limited growth of marine zooplankton. American Naturalist 124, 455–478.

Huntley, M.E., Lopez, M.D.G., 1992. Temperature-dependent production of marine copepods, a global synthesis. American Naturalist 140, 201–242.

Huntley, M.E., Niiler, P.P., 1995. Physical control of population dynamics in the Southern Ocean. ICES Journal of Marine Science 52, 457–468.

Huntley, M.E., Nordhausen, W., Lopez, M.D.G., 1994. Elemental composition, metabolic activity and growth of Antarctic krill, *Euphausia superba* Dana, during winter. Marine Ecology Progress Series 107, 23–40.

Huntley, M.E., Zhou, M., Nordhausen, W., 1995. Mesoscale distribution of zooplankton in the California Current in late spring, observed by Optical Plankton Counter. Journal of Marine Research 53, 647–674.

Ikeda, T., Dixon, P., 1982. Body shrinkage as a possible overwintering mechanism of the Antarctic krill, *Euphausia superba* Dana. Journal of Experimental Marine Biology and Ecology 62, 143–151.

Lascara, C.M., Hofmann, E.E., Ross, R.R., Quetin, L.B., 1999. Seasonal variability in the distribution of Antarctic krill, *Euphausia superba*, west of the Antarctic Peninsula. Deep-Sea Research 46, 925–949.

Lawson, G.L., Wiebe, P.H., Ashjian, C.J., Gallager, S.M., Davis, C.S., Warren, J.D., 2004. Acoustically inferred zooplankton distribution in relation to hydrography west of the Antarctic Peninsula. Deep-Sea Research II, this issue [doi:10.1016/j.dsr2.2004.07.022].

Lopez, M.D.G., 1991. Molting and mortality depend on age and stage in naupliar *Calanus pacificus*, implication for development time of field cohorts. Marine Ecology Progress Series 75, 79–89.

Marr, J.W.S., 1962. The natural history and geography of the Antarctic krill (*Euphausia superba* Dana). Discovery Reports 322, 33–464.

Mauchline, J., Fisher, L.R., 1969. The biology of euphausiids. Advances in Marine Biology 7, 1–454.

Nicol, S., Stolp, M., Cochran, T., Geijsel, P., Marshall, J., 1992. Growth and shrinkage of Antarctic krill *Euphausia superba* from the Indian Ocean sector of the Southern Ocean during summer. Marine Ecology Progress Series 89, 175–181.

Nordhausen, W., 1994. Winter abundances and distribution of *Euphausia superba*, *E. crystallorophias* and *Thysanoessa macrura* in Gerlache Strait and Crystal Sound. Marine Ecology Progress Series 109, 131–142.

Pedlosky, J., 1987. Geophysical Fluid Dynamics. Springer, New York, 624pp.

Platt, T., Denman, K., 1977. Organisation in the pelagic ecosystem. Helgoländer wissenschaftliche Meeresuntersuchungen 30, 575–581.

Platt, T., Denman, K., 1978. The structure of pelagic marine ecosystems. Rapports et Proces-Verbaux des Réunions/ Conseil International pour l'Exploration de la Mer 173, 60–65.

Pollard, R.T., Bathmann, U., Dubischar, C., Read, J.F., Lucas, M., 2002. Zooplankton distribution and behavior in the Southern Ocean from surveys with a towed Optical Plankton Counter. Deep-Sea Research II 49, 3889–3915.

Rodríguez, J., Mullin, M.M., 1986. Relation between biomass and body weight of plankton in a steady state oceanic ecosystem. Limnology and Oceanography 31, 361–370.

Sameoto, D., Cochrane, N., Herman, A., 1993. Convergence of acoustic, optical and net-catch estimates of euphausiid abundance, use of artificial light to reduce net avoidance. Canadian Journal of Fisheries and Aquatic Science 50, 334–346.

Sheldon, R.W., Parsons, T.R., 1967. A continuous size spectrum for particulate matter in the sea. Journal of the Fisheries Research Board of Canada 24, 909–915.

Sheldon, R.W., Prakash, A., Sutcliffe, W.H.J., 1972. The size distribution of particles in the ocean. Limnology and Oceanography 17, 327–340.

Silvert, W., Platt, T., 1978. Energy flux in the pelagic ecosystem, a time-dependent equation. Limnology and Oceanography 23, 813–816.

Sprules, W.G., Munawar, M., 1986. Plankton size spectra in relation to ecosystem productivity, size, and perturbation. Canadian Journal of Fisheries and Aquatic Sciences 43, 1789–1794.

Swartzman, G., 1991. Fish school formation and maintenance, a random encounter model. Ecological Modelling 56, 63–80.

Torres, J.J., et al., 1994a. Metabolism of Antarctic micronektonic crustacea as a function of depth of occurrence and season. Marine Ecology Progress Series 113, 207–219.

Torres, J.J., et al., 1994b. Proximate composition and overwintering strategies of Antarctic micronektonic Crustacea. Marine Ecology Progress Series 113, 221–232.

Torres, J.J., et al., 2001. ASRV Laurence M. Gould Cruise LMG01-04: To the Western Antarctic Peninsula (23 April – 6 June 2001). U.S. Southern Ocean GLOBEC Report #1.

Torres, J.J., et al., 2002. ASRV Laurence M. Gould Cruise LMG02-03: To the Western Antarctic Peninsula (9 April to 21 May 2002). U.S. Southern Ocean GLOBEC Report #5.

Voronina, N.M., 1966a. Distribution of zooplankton biomass in the Southern Ocean. Oceanology 6, 836–846.

Voronina, N.M., 1966b. The zooplankton of the Southern Ocean, some study results. Oceanology 6, 557–563.

Wiebe, P.H., 1988. Functional regression equations for zooplankton displacement volume, wet weight, dry weight, and carbon, a correction. Fishery Bulletin 86, 833–835.

Wiebe, P.H., Boyd, S., Cox, J.L., 1975. Relationships between zooplankton displacement volume, wet weight, dry weight, and carbon. Fishery Bulletin 73, 777–786.

Wiebe, P.H., Burt, K.H., Boyd, S.H., Morton, A.W., 1976. A multiple opening-closing net and environmental sensing system for sampling zooplankton. Journal of Marine Research 34, 313–325.

Wiebe, P.H., et al., 1985. New developments in the MOCNESS, an apparatus for sampling zooplankton and micronekton. Marine Biology 87, 313–323.

Zhong, X., Huntley, M.E., Zhou, M., 1996. The influence of animals on turbulence in the sea. EOS 76 (suppl.), 150.

Zhou, M., Dorland, R.D., 2004. Aggregation and migration behavior of *Euphausia superba*. Deep-Sea Research II, this issue [doi:10.1016/j.dsr2.2004.07.009].

Zhou, M., Huntley, M.E., 1997. Population dynamics theory of plankton based on biomass spectra. Marine Ecology Progress Series 159, 61–73.

Zhou, M., Nordhausen, W., Huntley, M.E., 1994. ADCP measurements of the distribution and abundance of euphausiids near the Antarctic Peninsula in winter. Deep-Sea Research I 41, 1425–1445.

Zhou, M., Zhu, Y., Putnam, S., Peterson, J.O., 2001. Mesoscale variability of physical and biological fields in southeastern Lake Superior. Limnology and Oceanography 46, 679–688.

Zhou, M., Niiler, P.P., Hu, J., 2002. Surface current in the Bransfield and Gerlache Straits measured by surface Lagrangian drifters. Deep-Sea Research I 46, 267–280.

ELSEVIER

Deep-Sea Research II 51 (2004) 2119–2137

DEEP-SEA RESEARCH
PART II

www.elsevier.com/locate/dsr2

Aggregation and vertical migration behavior of *Euphausia superba*

Meng Zhou*, Ryan D. Dorland

Department of Environmental, Coastal and Ocean Sciences, University of Massachusetts Boston, 100 Morrissey Blvd., Boston, MA 02125-3393, USA

Accepted 11 July 2004
Available online 18 October 2004

Abstract

Aggregation and vertical migration behavior of *Euphausia superba* were studied in Marguerite Bay and its vicinity west of the Antarctic Peninsula using a vessel-mounted, Acoustic Doppler Current Profiler, and a Multiple Opening and Closing Nets and Environmental Sensing System, during the 2001 and 2002 fall US Southern Ocean GLOBEC project cruises. The kinematics of aggregation behavior of *E. superba* associated with diel migration is studied using observations of their abundance and swimming velocities: during the day, *E. superba* reduce their swimming at a depth of 250 m; and at night, they swim randomly at their cruising speed in the upper part of an aggregation near the surface, and coherently as schooling in the lower part of an aggregation. The causes for the aggregation behavior and vertical migration of krill are explored by examining the relationship with ice coverage and presence of predators. The motion of euphausiids is further analyzed in terms of kinetic energy and force balance, leading to new considerations of mathematical theories and models of aggregation behavior. The results show a diel variation of the energy demand for maintaining their locomotion. The horizontal scale of an aggregation is studied in conjunction with horizontal gradients of currents. Results indicate that the swimming capability of euphausiids determines the maintenance of an aggregation in the mesoscale circulation field.
© 2004 Elsevier Ltd. All rights reserved.

1. Introduction

Euphausiids have a fundamental position in polar marine food webs (Bargmann, 1945; Marr, 1962; Mauchline and Fisher, 1969; Pearcy et al., 1979). Especially in the Southern Ocean, euphausiids directly link the primary production to the higher trophic levels, such as birds and mammals. *Euphausia superba* may be the largest and arguably the most abundant species in Antarctic waters though in coastal waters of the Antarctic Peninsula other euphausiid species can sometimes outnumber *E. superba* (Brinton and Townsend, 1991; Everson et al., 1990; Marr, 1962). Marguerite Bay

*Corresponding author. Tel.: +1-617-287-7419; fax: +1-617-287-7474.
E-mail address: meng.zhou@umb.edu (M. Zhou).

0967-0645/$ - see front matter © 2004 Elsevier Ltd. All rights reserved.
doi:10.1016/j.dsr2.2004.07.009

and its adjacent areas support a large standing stock of both reproducing and nonreproducing Antarctic krill (Lascara et al., 1999; Marr, 1962). Thus, the study of *E. superba* is one of the critical components in understanding krill overwintering strategies and the austral winter ecosystem within the U.S. Global Ocean Ecosystem Dynamics Program (GLOBEC) Southern Ocean Project.

Aggregation and vertical migration behavior of euphausiids has been well recognized in determining the fate of natural populations within a dynamic physical and biological environment. Adult *E. superba* have a maximum length of approximately 6 cm, and have strong swimming capability (Hamner et al., 1983; Hamner, 1984; Hopkins et al., 1984; Zhou et al., 1994). Vertical migration has been intensively studied using both net tow samples and acoustic surveys (Demer and Hewitt, 1995; Hopkins et al., 1978; Kalinowski, 1978; Tarling et al., 2002). The most accepted cause for euphausiids to migrate down to deep water during the day is to avoid visual predators (Ritz, 1994). Aggregation behavior, i.e., active swimming to form aggregations, confers advantages in avoiding predation (Brock and Riffenburgh, 1960; Clark, 1974; Pitcher, 1983; Swartzman, 1991) and in utilizing food resources (Cowles et al., 1993; Duffy and Wissel, 1988; Ritz, 1994).

Studies of aggregation and vertical migration behavior are important to understand euphausiid swarming and schooling in all seasons, especially in late fall and winter because few observations are available. Most studies of krill aggregations and patchiness have used bioacoustical methods that employed volume backscattering strength or visual methods that employed SCUBA diving (Burcynski, 1973; Everson et al., 1990; Greene et al., 1991; Hamner et al., 1983; Miller and Hampton, 1989; Zhou et al., 1994). Results focused on packing densities, and statistical description of horizontal and vertical scales of aggregations. For example, during the austral summer season krill were generally found in the upper 200 m, forming dense aggregations at depth during the daytime and dispersing at night in the upper water column (Kalinowski, 1978; Tomo, 1983). These aggregations, with abundances as high as 1000s individuals m^{-3}, ranged from 10s m to several km in horizontal extent (Hamner et al., 1983; Macaulay et al., 1984; Watkins et al., 1992). Similar results also were found in austral winter, except that there was no obvious diel vertical migration pattern or diel change of aggregation behavior within ice-covered regions (Zhou et al., 1994).

The euphausiid aggregation shape and density, and the individual's activities may be specific under a given physical and biological environment. Beyond the descriptive differences in shapes, sizes, abundances and species composition of euphausiid aggregations, efforts were made to investigate general aggregation theories. These have described the relationship between abundance, swimming velocities, and aggregation sizes of animals, and how their behavior will change responding to variation of the physical and biological environment, such as currents, light, food sources, and predators (Anderson, 1981; Okubo, 1980; Zhou and Huntley, 1996).

Early studies of patch dynamics of animals emphasized the role of intraspecific autocoherence on the patch size (Anderson, 1981; Okubo, 1980; Parr, 1927). The autocoherence is balanced by stochastic random motion or diffusion (Anderson, 1981; Okubo, 1980). The patch dynamics theory was further developed to a group of deterministic conservation equations using macro-variables that represent statistical means of random phenomena (Zhou and Huntley, 1996). These theories are general because they are only based on the Newton's second law, i.e., $F = ma$, where the total forces (F) acting on an animal is proportional to the product of the mass (m) of the animal and the rate (a) of change in motion.

The central difference between aggregated and non-aggregated animals is the behavior to form aggregations. Such behavior is often called autocoherence or the biological attraction force between animals. The biological attraction force between animals can be analyzed from the relative motion between animals and their spatial distribution in an aggregation. This is an analogue of the inherent behavior using observable variables, such as abundance (individuals m^{-3}), mean swimming velocities ($m\,s^{-1}$), kinetic energy of random swimming velocities per unit mass ($m^2\,s^{-2}$), and

scales (m) (Okubo, 1986; Okubo and Anderson, 1984; Zhou and Huntley, 1996). The linkages between an aggregation and swimming velocities of animals are the random motion that disperses the aggregation and the physiological rate required to maintain the swimming (Torres and Childress, 1983). Most of the results are theoretical, that demonstrate the fundamental relations between abundance, motion and shapes of animal aggregations. Observations of these variables are rarely made.

In situ measurements of abundance, mean swimming velocities, kinetic energy of random swimming velocities and scales of an animal aggregation are needed to understand the kinetics and kinematics of aggregations based on mathematical theories and models, and in turn to apply these theories to future behavior studies. Visual observations of swimming and the corresponding abundance of euphausiids were made either at points or in small aggregations using SCUBA diving (Hamner et al., 1983; Hamner, 1984). Measurements of overall swimming patterns in a euphausiid aggregation of several km and their mean and random velocities have not been made in the past because of the lack of instruments, but with the Acoustic Doppler Current Profiler (ADCP; RD Instruments, San Diego, CA, USA) such measurements are possible. Advantages of an ADCP are its non-invasive remote sensing (which minimizes the external interference to euphausiid behavior), its high resolution measurements of both mean and random velocities (which allow identifying differences of abundance and velocities within an aggregation), and the fast survey capability at a speed of 4–10 knots (which provides synoptic maps of a euphausiid aggregation). During the Southern Ocean GLOBEC cruises, detailed measurements of abundance and both mean and random swimming velocities were made over euphausiid aggregations. Based on these observations, we provide a description of the kinematics of euphausiid aggregation and vertical migration behavior and the variation in aggregations associated with different physical and biological environments. In addition, we examine the dynamics processes and physical controls on aggregations and aggregation scales.

2. Methods

2.1. Study sites and surveys

The shelf region around Marguerite Bay and Crystal Sound (Fig. 1) is considered where krill aggregations are consistently found in late austral fall and austral winter (Lascara et al., 1999; Marr, 1962). This region also supports large populations of top predators that depend on krill as a food source (Costa and Crocker, 1996; Fraser and Trivelpiece, 1996). Physical settings favorable to high productivity in this region include, but are not limited to, deep canyons over 400 m deep connecting the shelf to offshelf nutrient-rich waters, mesoscale eddies in fjords and around islands promoting long residence times of

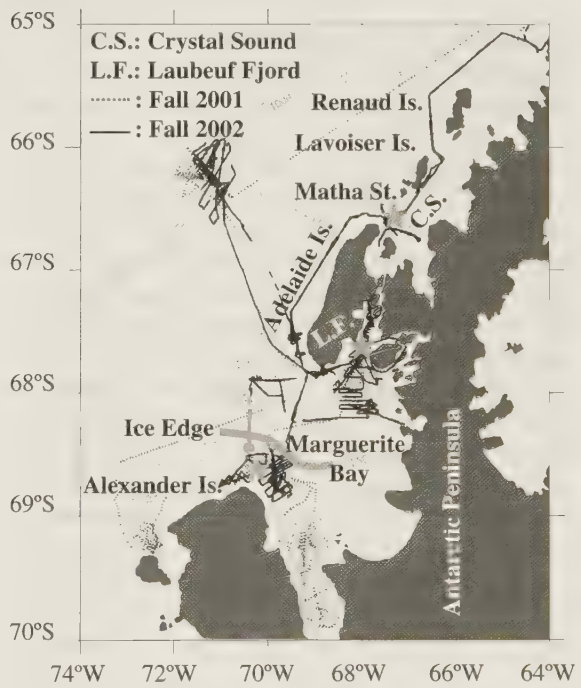

Fig. 1. The bathymetry in the shelf region around Marguerite Bay and Crystal Sound shown by gray contours. Cruise tracks are indicated by solid black lines for the 2002 austral fall cruise and dashed black lines for the 2001 austral fall cruise. The gray stars indicate the process stations in Crystal Sound, Laubeuf Fjord and north of Alexander Island. The thick solid black line and solid dot indicate the acoustic transect and start point in Fig. 8, respectively. The thick gray solid line indicates the ice edge.

populations, and ice coverage providing ice-biota food resources (Daly, 1990; Daly and Macaulay, 1991; Hofmann et al., 1996; Lascara et al., 1999; Marr, 1962). The deep canyons are typically associated with fjords and straits; for example, the deep canyons and basins in Matha Strait, Laubeuf Fjord, and George VI Sound.

Process studies were conducted at sites in Crystal Sound, over the shelf break and in Marguerite Bay during the 2001 Southern Ocean GLOBEC cruise between April 20 and June 6 and the 2002 cruise between April 7 and May 20. Three cases are presented based on observations made in Laubeuf Fjord from the 2001 fall process cruise, in Crystal Sound from the 2002 fall process cruise, and in the deep canyon north of Alexander Island from the 2002 fall process cruise. Large numbers of aggregated euphausiids and top predators were present in open water with small ice floes during our study in Crystal Sound. This setting provided an opportunity to study euphausiid aggregation and vertical migration behavior when predators were present. A number of euphausiid aggregations and top predators were found along the ice edge in the deep canyon north of Alexander Island. A comparison of euphausiid behavior can be made between aggregations in open water and in pack ice. Large numbers of euphausiids aggregated in open water in Laubeuf Fjord where a mesoscale eddy field provided a case for studying the effects of horizontal velocity shear on the horizontal scale of euphausiid aggregations.

Currents and euphausiid distributions in the study sites were first determined by small-scale surveys of several 10^1 km transects using a 153 kHz Vessel Mounted (VM) Narrow Band (NB) ADCP. Data were processed to identify mesoscale eddy features and euphausiid aggregations (e.g. Figs. 2 and 3). When aggregations were found, we conducted targeted tows using a Multiple Opening and Closing Nets and Environmental Sensing System (MOCNESS; B.E.S.S., Falmouth, MA, USA) for species information (Figs. 4 and 5) (Wiebe et al., 1976, 1985). Zooplankton samples were initially inspected visually for dominant species and size information before they were preserved.

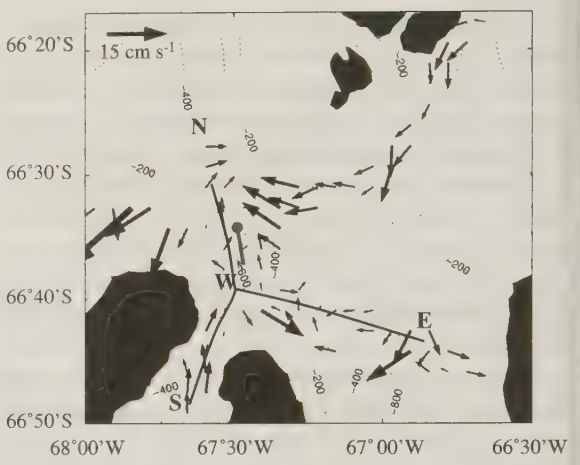

Fig. 2. The ADCP horizontal current measurements at 98 m in Matha Strait and Crystal Sound. Two black solid lines indicate the west–east and south–north transects in Fig. 3. The gray thick solid line indicates the ADCP transects and MOCNESS tows shown in Fig. 4. The solid dot indicates the starting point of a MOCNESS tow.

2.2. Instrumentation and measurements

A NB ADCP uses the acoustic Doppler technology and zooplankton as backscatterers to examine the Doppler shift on the frequency spectrum of volume backscattering (RDI, 1989). In the Southern Ocean, euphausiids can be the principal backscatters for a 153 kHz ADCP when euphausiid aggregations are present (Flagg and Smith, 1989b; Zhou et al., 1994). The power spectrum of acoustic backscattering is obtained by applying a Fast Fourier Transform (FFT). The first moment of a power spectrum reflects the mean Doppler shift produced by coherent motion of backscatterers, the mean height of a power spectrum reflects the echo intensity or volume backscattering (S_v), and the second moment of a power spectrum, the spectrum width, reflects both the finite length of an acoustic ping and the randomness of motion of backscatterers. ADCPs were primarily developed to use the mean Doppler shift for measuring ocean currents (RDI, 1989). The volume backscattering measurements of an ADCP have also been used to analyze abundance, distribution and migration of zooplankton and fish (Ashjian et al., 1998; Demer et al., 2002; Flagg and Smith, 1989b; RDI, 1990; Smith et al., 1989;

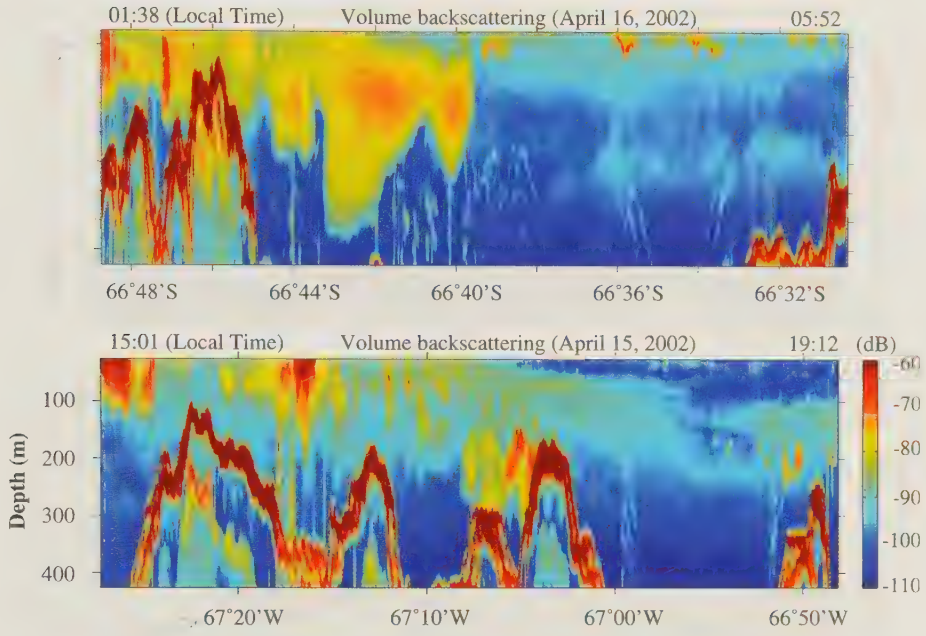

Fig. 3. The ADCP volume backscattering strength transects in Matha Strait and Crystal Sound, along the south–north track between S and N (upper panel) and the east–west track between W and E (lower panel) marked in Fig. 2. The thick solid black lines indicate the bottom.

Zhou et al., 1994). Recently, the mean Doppler shift measurements have been used to interpret movements of zooplankton and fish (Demer et al., 2002; Tarling et al., 2002; Zhou and Huntley, 1996). It should be noted that there is no direct method to separate the movement of the backscatterers from the currents. The separation can only be done by analyzing the echo intensity measurements for the presence of fish and euphausiids, and comparing velocity measurements in an aggregation to those in the water surrounding the aggregation.

The only two studies to use Doppler spectra for movement of acoustic backscatterers were made by Holliday (1974, 1977). The spectrum width measurements of an ADCP have not been used for any studies. To clarify the meaning of a spectrum width measurement, we assume that a random motion component (u') of backscatterers along the acoustic beam direction can be written as

$$u' = u'_{\mathrm{T}} + u'_{Z}, \tag{1}$$

where u'_{T} represents the contribution made by turbulence in the water volume, and u'_{Z} is the random swimming velocities of backscatterers, which are mesozooplankton and micronekton, often euphausiids in the Southern Ocean. Because the pulse length (τ) of a ping is finite, the time series of backscattering can be written as the product of a box function $B(t)$ with a window length of τ, that is

$$u'B(t) = u'_{\mathrm{T}}B(t) + u'_{Z}B(t). \tag{2}$$

The Fourier Transform of Eq. (2) is equal to the convolution of u and $B(t)$,

$$F(u')*F(B) = F(u'_{\mathrm{T}})*F(B) + F(u'_{Z})*F(B). \tag{3}$$

The spectrum width, the second moment, is equal to

$$\mathrm{SW}^2 = \frac{1}{W}\int_{R(f)} (f - f_0)^2 \times \left\| F(u'_{\mathrm{T}})*F(B) + F(u'_{Z})*F(B) \right\| \mathrm{d}f, \tag{4}$$

where f is the acoustic frequency, f_0 is the mean frequency of backscattering, $||\cdot||$ represents the mean modulus of $F(u)$, SW is the spectrum width, and W is the zeroth moment of the modulus of $F(u)$. The accuracy of spectrum width is similar to

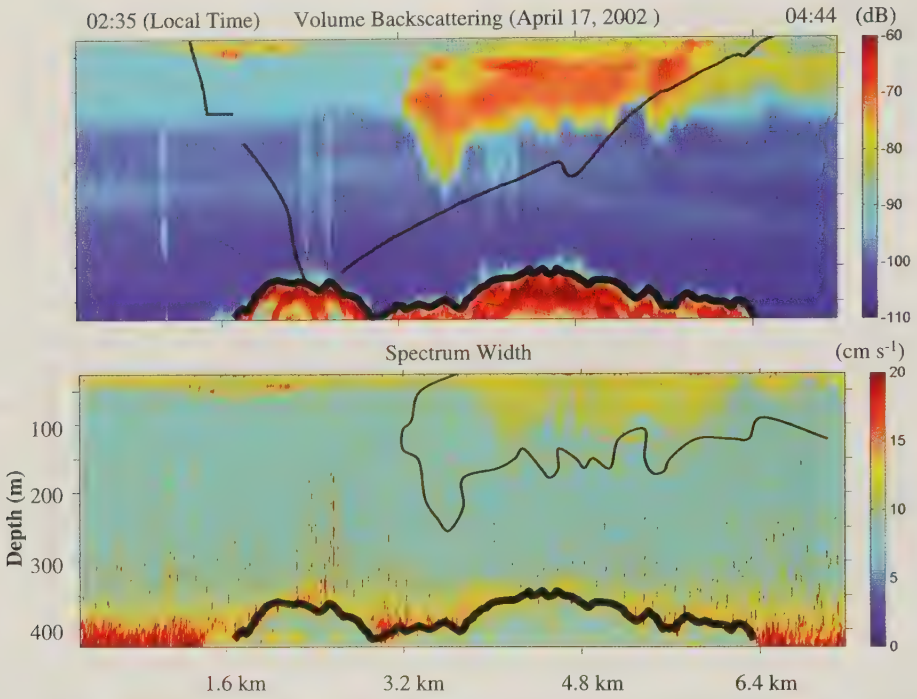

Fig. 4. The ADCP volume backscattering strength transect (upper panel) and spectrum width transect (lower panel) during the night MOCNESS tow in Matha Strait. The solid black line in the upper panel indicates the MOCNESS tow trajectory, and the solid black line in the lower panel indicates the edge of the euphausiid aggregation shown in the upper panel. The thick solid black lines indicate the bottom.

that of velocity measurements because they are processed in the same way.

Eq. (4) can be used to study random swimming of mesozooplankton by examining the anomaly of SW measurements to the background SW contributed only by the first term, $F(u'_T)^*F(B)$. Adult euphausiids are strong swimmers, and they can easily overcome turbulence (Hamner, 1984). In a euphausiid aggregation, randomly swimming euphausiids will lead to a positive anomaly in SW measurements, and coherently swimming euphausiids will lead to a negative anomaly.

An ADCP provides measurements of multiple variables. The volume backscattering measurements provide the abundance estimates when species and sizes of mesozooplankton are verified from net tows. The mean Doppler shift measures mean motion of currents and mesozooplankton. The spectrum width measurements provide estimates of random motion of mesozooplankton. These measurements can be directly used in mesozooplankton locomotion and aggregation processes (Okubo, 1986; Okubo and Anderson, 1984; Zhou and Huntley, 1996), and in physiological rates (Torres and Childress, 1983).

A 153 kHz VM NB ADCP was mounted on the ARSV L.M. Gould. The bin length was set at 8 m, the pulse length was set to be equal to the bin length, and the blank after transmission was set to 4 m. The echo intensity measurements have an accuracy of 1 dB for a single ping (RDI, 1990). The absolute volume backscattering can be made from echo intensity measurements using the standard sonar equation that contains corrections for physical environment parameters such as temperature, range dependence, spherical expansion, absorption, and noise level (Flagg and Smith, 1989a, b; RDI, 1990). Because the transducers of the ADCP were mounted at the bottom of the vessel, they were not calibrated in situ using standard targets. Thus, the volume backscattering

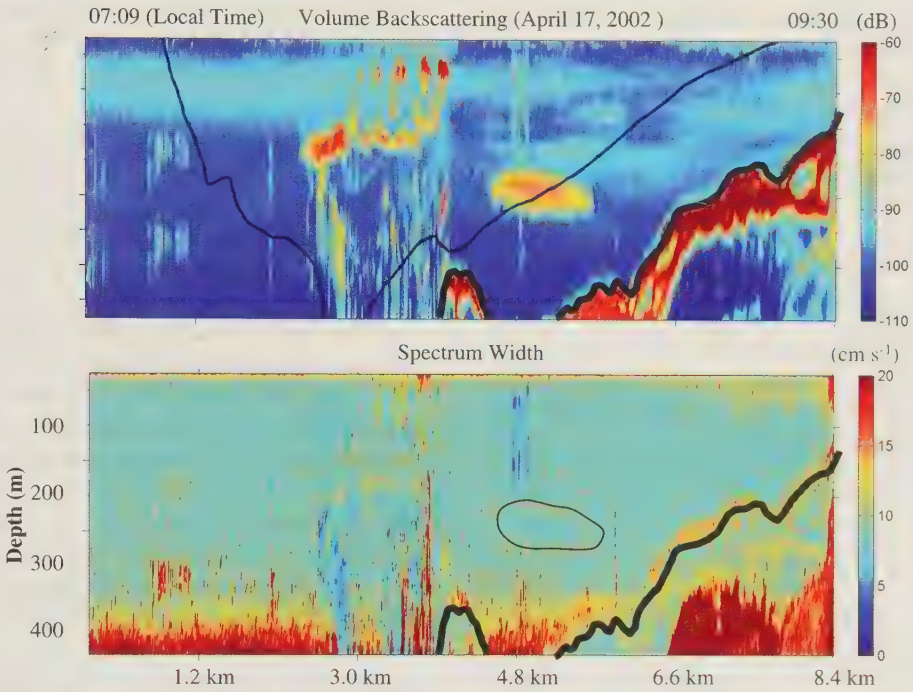

Fig. 5. The ADCP volume backscattering strength transect (upper panel) and spectrum width transect (lower panel) measurements during the day MOCNESS tow in Matha Strait. The solid black line in the upper panel indicates the MOCNESS tow trajectory, and the solid black line in the lower panel indicates the edge of the euphausiid aggregation shown in the upper panel. The thick solid black lines indicate the bottom.

estimates from this ADCP should be used with reservation.

The standard deviation of velocity measurements for a single ping at a 8-m pulse length is equal to 13 cm s^{-1} (RDI, 1992). During data processing, the fish rejection algorithm was set to a maximum tolerance of 63 dB between adjacent bins. A 5-min average is made for the velocity measurements by following the instrument specifications, by which the corresponding error is reduced to approximately 1.1 cm s^{-1} in a calm sea (RDI, 1989). Broadening of a spectrum width due to the finite ping length is within 7 cm s^{-1} along the beam direction for the 8-m pulse length at 153 kHz.The measurements of spectrum width are averaged every 8 pings between 4 transducers during post data processing. The accuracy of an averaged spectrum width measurement should be approximately 1.3 cm s^{-1}.

The intercomparison between estimates of zooplankton biomass based on ADCP volume backscattering and net-tow samples could be done though it might be fruitless simply due to the capability of *E. superba* to avoid plankton nets (Sameoto, 1980; Everson and Bone, 1986; Zhou et al., 1994). The discrepancy between net tow estimates and acoustic estimates can be approximately one order of magnitude or higher in the size range of adult *E. superba*. The net tow samples will better serve the purpose of determining which species might be responsible for the volume backscattering. In our case, the net tow samples will be used only to confirm that adult *E. superba* are the primary constituent of the acoustic layers and patches we used for aggregation studies.

The length of an adult *E. superba* is approximately 4–5 cm. Their cruising swimming velocity is approximately 2–3 times their body length per second, or 8 to 15 cm s^{-1} (Kils, 1979, 1983; Lochhead, 1961; Torres, 1984). The measurements of an ADCP with accuracies of 1.1 cm s^{-1} for velocities and 1.3 cm s^{-1} for spectrum width

should resolve currents and euphausiid swimming. It should be noted that the broadening of spectrum width ($7\,\mathrm{cm\,s^{-1}}$) due to the finite ping length should serve as a baseline because turbulence and random swimming of mesozooplankton always broaden the spectrum width.

2.3. Aggregation theories

The aggregation theories for zooplankton have been developed based on swimming velocities and their interference between individuals during swimming (Anderson, 1981; Zhou and Huntley, 1996). The general equations that can be used to described their abundance and swimming velocities are

$$\frac{\partial \rho}{\partial t} + \nabla \cdot (\mathbf{u}\rho) = r_n(\text{birth}, \text{death}), \tag{5}$$

$$\frac{\partial \mathbf{u}}{\partial t} + \mathbf{u} \cdot \nabla \mathbf{u} + \frac{1}{\rho}\nabla p = \frac{1}{\rho}(\mathbf{F}_I + \mathbf{F}_E), \tag{6}$$

where t is the time, ∇ is the three-dimensional gradient operator, ρ is animal abundance (individuals $\mathrm{m^{-3}}$), $\mathbf{u}$ is the mean swimming velocity ($\mathrm{m\,s^{-1}}$) of mesozooplankton, p is defined as the mean autocorrelation between random components of swimming velocities (individuals $\mathrm{m^{-1}\,s^{-2}}$), r_n is the rate of change in animal abundance related to population dynamics, $\mathbf{F}_I$ is the internal autocoherence forces between individuals, and $\mathbf{F}_E$ is the external force acting on individuals in a unit volume ($\mathrm{N\,kg^{-1}\,m^{-3}}$). The mean autocorrelation p can be simplified as

$$p = \rho\theta, \tag{7}$$

where θ is the mean kinetic energy of the random motion of animals. The detailed deduction for these equations can be found in Zhou and Huntley (1996).

The population change associated with mortality is critical to the overall survivorship of a euphausiid aggregation in austral winter facing both starvation and predation. The time scale associated with the mortality is approximately from several to 10s of days, which is much longer than the time needed to form a sharp edge of a swarm in minutes to hours. Thus, in the study of aggregation behavior the total number of euphausiids in an aggregation can be simply assumed to be a conservative constant, e.g., $r_n = 0$.

3. Results

The current fields and acoustic backscattering data were acquired along the entire cruise tracks during the two cruises (Fig. 1). The current measurements were five-minute averaged, and ship motion was removed using CODAS software developed by Eric Firing at the University of Hawaii. The echo intensity and spectrum width measurements of single pings were saved to harddrives and processed to absolute volume backscattering strength (S_v) and speeds of random velocities (SW) in real time. The color images of S_v and SW were displayed on a data processing personal computer, and updated approximately every 2 min. Many aggregations of euphausiids and probably micronekton were measured along survey tracks. A detailed description of findings from these cruises can be found in the Southern Ocean GLOBEC Cruise Reports (http://www.ccpo.odu.edu/Research/globec_menu.html). Only a few of the current fields and the backscattering and spectrum width data are selected here for describing physical and biological processes.

The current fields in Crystal Sound revealed a complicated mesoscale circulation pattern including a southward flow along the shelf of Lavoisier Island, a northward flow in the channel between Adelaide and Liard Islands, and an outflow along the deep canyon in Matha Strait (Fig. 2). The volume backscattering measurements clearly indicate that the euphausiid aggregations were more concentrated in the deep canyons, especially in Matha Strait and the channel between Adelaide and Liard Islands (Fig. 3).

Two MOCNESS tows targeting at the aggregation in Matha Strait were conducted at the same location for species information (Figs. 4 and 5). The Global Positioning System (GPS) was used to ensure we were following the same track, and the volume backscattering measurements from the ADCP were displayed in real time to ensure we would catch the euphausiid aggregations. High

topographic variation seen as the many sharp pinnacles and cliffs over 100s m (Figs. 3–5) caused considerable difficulties and risk in making the tows.

The diel vertical migration and night-day difference in aggregation behavior of euphausiids are shown in Figs. 4 and 5. A euphausiid aggregation of approximately 4 km in the upper water column was found during the dark period. The second net tow over the same location was designed in such a way that the down-cast and part of the up-cast of the tow in the deep water were during the dark and transition (dawn) period, and the up-cast of the tow in the upper 200 m was in the day, which measured both the downward diel migration and aggregation during the day. It is not known whether the second transect caught the same euphausiid aggregation as the first transect because an aggregation could have moved 3 km from its original location in 4 h at a mean velocity of 20 cm s^{-1}. Because there was no other similar sized aggregations in the nearby area (Fig. 3), it is very likely that we did measure the same aggregation. Because of a number of floes and limited visibility at night in our study area, the survey of euphausiids and currents was done at the speed of 4 knots. Because of time constraints, evaluation of the absolute shape of the euphausiid aggregation was not possible. Hence, it is not known which parts of the aggregation these two transects crossed.

Zooplankton samples from net tows were visually inspected for preliminary species and size information before they were preserved. The results confirm that these aggregations measured by the ADCP consisted of adult *E. superba* of approximately 4 cm. Detailed taxonomy and size analyses are currently being conducted. The individual target strength of a euphausiid at 4 cm is approximately equal to −70 dB (Greene et al., 1991; Zhou et al., 1994). The volume backscattering strength measurements within aggregations (Figs. 4 and 5) were less than −65 dB, leading to a maximum abundance estimate of adult euphausiids of approximately 3 individuals m^{-3}.

An ADCP uses zooplankton as Doppler backscatterers. Mean Doppler shifts represent the absolute mean velocities of backscatterers due to both currents and their swimming (Figs. 6 and 7). The empirical separation between currents and mean swimming can only been done by comparing the velocities in an aggregation to those surrounding it. Spectrum width measurements in an aggregation are highlighted by outlining the edges of an aggregation (Figs. 4 and 5). The variations of both mean and random velocities within aggregations and diel change of these velocities can been easily seen in these figures.

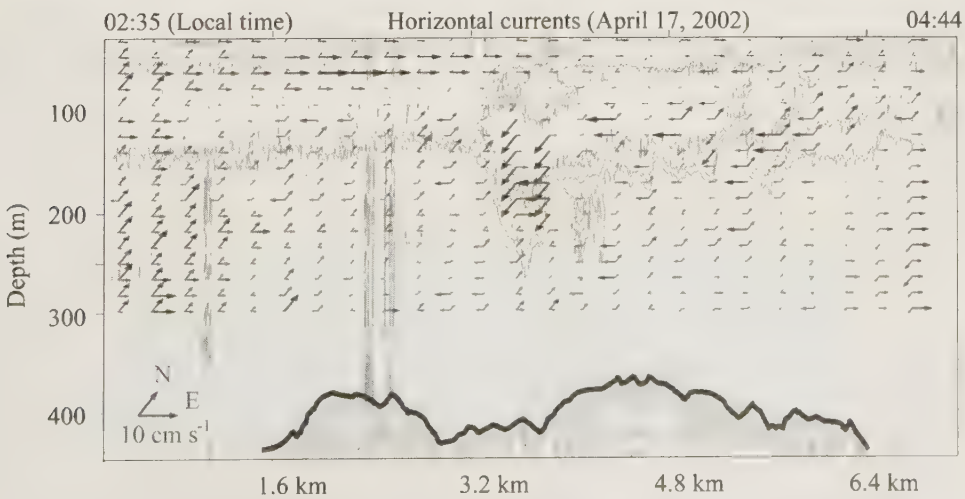

Fig. 6. The ADCP horizontal current measurements along the transect shown in Fig. 4. The black arrows are the 5 min averaged horizontal currents. Black contour lines are volume backscattering strength shown in Fig. 4.

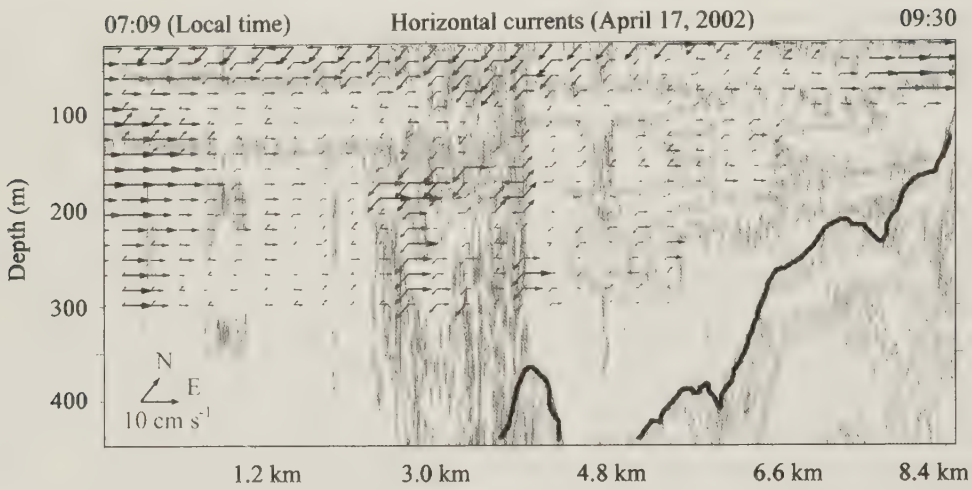

Fig. 7. The ADCP horizontal current measurements along the transect shown in Fig. 5. The black arrows are the 5 min averaged horizontal currents. Black contour lines are volume backscattering strength shown in Fig. 5.

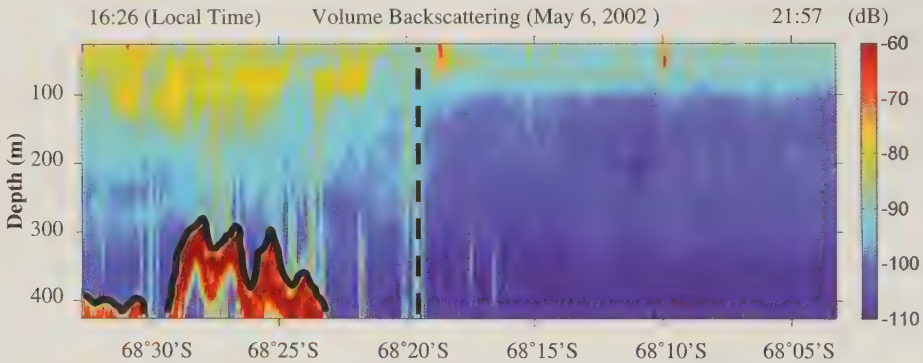

Fig. 8. The ADCP volume backscattering strength transect crossing the ice edge north of Alexander Island. The thick dash line indicates the location of the ice edge. The geographic location of the transect is indicated by the thick solid black line in Fig. 1.

The spatial variation in the distribution of euphausiid aggregations relative to the ice edge is demonstrated in Fig. 8. The measurements were taken 1.5 h after sunset. Thus, the measurements should reflect the vertical and horizontal distribution of euphausiids and zooplankton in the water column after the completion of vertical migration. A trend from the relatively less dense but spatially larger aggregations in the ice covered region to denser, but spatially smaller aggregations in the open water is clearly shown in Fig. 8.

The interaction between mesoscale circulation fields and spatial scales of euphausiid aggregations is further examined in the Laubeuf Fjord where several mesoscale eddies and dense euphausiid aggregations were found during the 2001 fall cruise (Figs. 9 and 10). MOCNESS tow samples and ADCP data indicated that most of adult *E. superba* aggregated in the upper 150 m. The existing large number of adult *E. superba* formed several aggregations of less than several km in size instead of forming one large aggregation. These results together with current measurements provide us a good case to study the interaction between circulation and euphausiid aggregation fields.

4. Discussion

4.1. Aspect ratios of aggregations

The spatial distribution of euphausiids in an aggregation reflects the activities and behavior of euphausiids described by Eqs. (5) and (6). The vertical and horizontal scales of an aggregation at night shown in Crystal Sound are approximately 100 m and 2 km, respectively (Fig. 4). Because the distance between euphausiids directly reflects the interaction between euphausiids during swimming, the ratio of the vertical to horizontal scales of approximately 0.05 is a reflection of a euphausiid preference to swim in horizontal more than they do in vertical (Zhou and Huntley, 1996). In the morning, a part of an aggregation was measured with the vertical and horizontal scales of approximately 50 m and 1.2 km, respectively (Fig. 5), a ratio of approximately 0.04. The aspect ratios of aggregations are similar between day and night. The horizontal and vertical scales of aggregations found in Crystal Sound and Marguerite Bay during the 2002 fall cruise follow a linear relation (Fig. 11). The mean aspect ratio is approximately 0.05 with $R^2 = 0.87$.

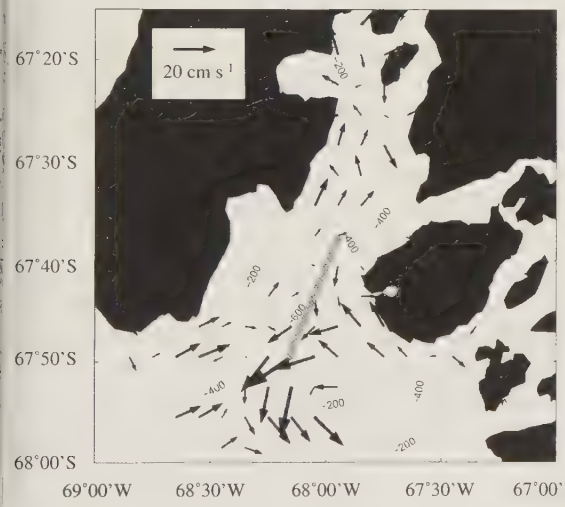

Fig. 9. The ADCP horizontal currents at 98 m in the Laubeuf Fjord. The gray solid line indicates the ADCP volume backscattering strength transect in Fig. 10.

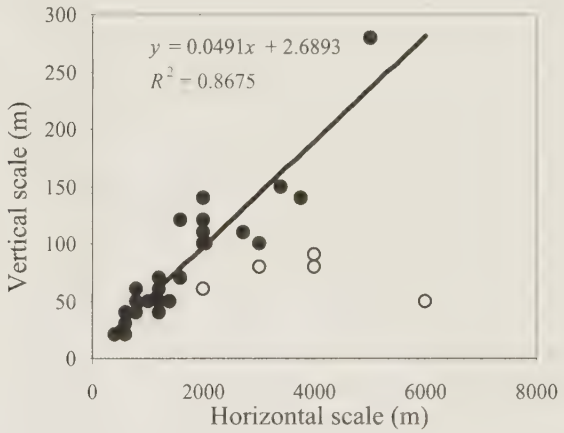

Fig. 11. The scattering plots of horizontal scales vs vertical scales of euphausiid aggregations. Black solid dots are data collected in Crystal Sound and north of Alexander Island during the 2002 fall cruise ($n = 25$), and circles are data collected in Laubeuf Fjord during 2001 fall cruise ($n = 5$).

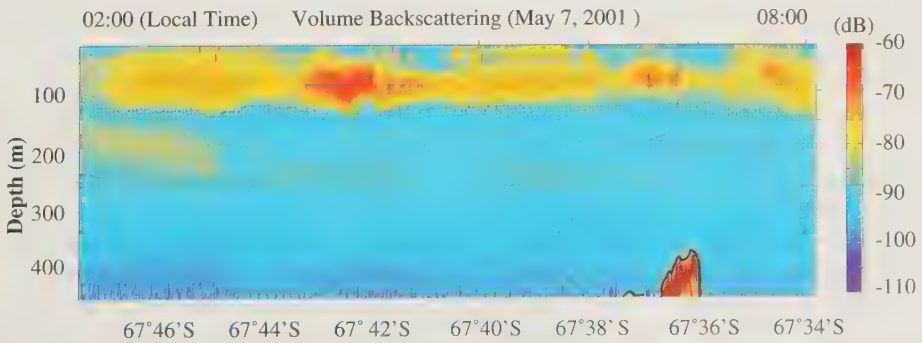

Fig. 10. The ADCP volume backscattering strength transect in the Laubeuf Fjord. The track is indicated by the gray solid line in Fig. 9.

The aspect ratios of aggregations in Laubeuf Fjord from the 2001 fall cruise, however, are different from those of the 2002 fall cruise. The horizontal scales of aggregations from the 2001 fall cruise are larger than those of the 2002 fall cruise while the vertical scales remained constant (Figs. 10 and 11). One possible mechanism for a large horizontal scale aggregation is the advection and convergence of horizontal current fields. The mechanism is explored later by using ADCP current measurements in the study area.

4.2. Day–night difference in aggregation scales

The night time aggregation in Crystal Sound was larger than the daytime one (Figs. 4 and 5). The layer thickness of the aggregation was more than 100 m in the upper water column at night. The interaction between euphausiids is directly caused by attraction and avoidance during swimming, which produces the randomness. The spectrum width measurements represent the random swimming, and are plotted against the volume backscattering in Figs. 4 and 5. In most parts of these figures, the spectrum width measurements are approximately 6–8 $cm\,s^{-1}$, representing the background spectrum width broadened by the finite pulse length and the background turbulence. Within the upper part of the aggregation in Fig. 4, the spectrum width measurements are approximately 12 to 16 $cm\,s^{-1}$, which are significantly larger than the background spectrum width. In the lower part, the spectrum width measurements are less than the background indicating the euphausiids swam coherently overcoming the turbulence. These results indicate that in an aggregation, some euphausiids are swarming (swimming randomly) while others are schooling (swimming coherently).

In the daytime aggregation, euphausiids showed less randomness in their velocities (Fig. 5). From this, we can argue that euphausiids are more active at night, swimming randomly while searching for food, and are less active when hiding from predators in deep waters during the day. Thus, the spectrum width measurements of the daytime aggregation are equal to or less than the background. The cause for less spectrum width is simply that euphausiids formed a coherent swimming pattern, i.e. schooling behavior, described in past studies (Hamner et al., 1983, 1989; Hamner, 1984). When euphausiids form a more coherent swimming pattern with less randomness, the possibility of collision will be reduced, and the size of an aggregation can become more compact during the day.

4.3. Vertical migration pattern

The diel vertical migration of euphausiids was clearly demonstrated from these two ADCP transects and two net tows (Figs. 4 and 5). Dawn was at approximately 8 am local time, and the measurements indicate a downward movement of euphausiids during that period. Sunset was at approximately 4 pm, and the euphausiids showed a upward movement between 4 and 5 pm (Fig. 3), which suggests that the upward migration was triggered by the light field.

It has been long recognized that visual predator avoidance during the day is the main cause for vertical migration of euphausiids. Euphausiids appeared to exhibit strong vertical migration between the surface and 250 m in Crystal Sound where numerous top predators were present, and weak migration between the surface and 100 m in Laubeuf Fjord and under the ice in the deep canyon north of Alexander Island where top predators were relatively few. Because both predators and euphausiids use visual sensors, the visible light in water column is critical for foraging and avoidance. It has been reported that euphausiids can see in a light field as low as $10^{-6}\,\mu Einstein\,cm^{-2}\,s^{-1}$ (Onsurd and Kaartvedt, 1998). The Photosynthetically Active Radiation (PAR) measured in the visible wave lengths between 400 and 700 nm was approximately $0.019\,\mu Einstein\,cm^{-2}\,s^{-1}$ at the surface and $1.14 \times 10^{-4}\,\mu Einstein\,cm^{-2}\,s^{-1}$ at the depth of 250 m in Crystal Sound during the day. Thus, the light level at 250 m was within the visual detection limit of euphausiids. The visual sensitivity of euphausiids may not be the only determinant of the vertical migration depth. If the primary cause for the diel vertical migration of euphausiids is to avoid predation, the diving depth of predators should be a key factor. In Crystal Sound, the mean

foraging diving depth of tagged Crabeater seals during our survey was approximately 140 m and 25% of dives were over 200 m (Burns et al., 2004), which matches the vertical migration range of euphausiids. In areas where euphausiids were protected from predators by ice, or there were less predators, euphausiid migration depths were relatively shallow. Thus, the migration depth of euphausiids appears to be a function of light and also the diving depth of predators.

The vertical swimming significantly affects the aggregation during a vertical migration period when euphausiids form much smaller irregular aggregation shapes (Fig. 5). The dynamics for the change can be examined from horizontal aggregation scales and swimming capability based on Eq. (6). When euphausiids contribute most of their swimming in the vertical during vertical migration, their horizontal aggregation capacity is reduced. Examining the horizontal force balance in Eq. (6), the second term on the left side is proportional to $[u]^2/L$ contributed by mean horizontal motion (u) and horizontal scale (L), and the third terms is proportional to $[u']^2/L$ contributed by random motion. During the downward migration, euphausiids moved 250 m in a half hour, inferring a downward velocity of approximately $14\,\mathrm{cm\,s^{-1}}$, i.e., the euphausiids contributed their swimming capacity to the vertical migration. Because of the reduction of horizontal swimming, the horizontal scale L must reduce so that the magnitudes of terms 2 and 3 can be maintained for the horizontal force balance. Studies of aggregation behavior for northern boreal euphausiids indicate that small aggregations will reform as a big aggregation at the depth after ceasing their vertical migration (Zhou et al., 2003).

4.4. Mean and random velocities of euphausiids

The observations of euphausiid swimming velocities are important not only because their aggregation behavior is ultimately expressed through their swimming, but also their swimming is directly associated with their energy budget and physiologic rates (Hamner et al., 1983; Hamner, 1984; Torres, 1984). Many marine animals swim at a cruising speed of 2–3 times their body length per second, though they can swim at 5–6 times their body length per second over short periods during escape movement (Kils, 1979, 1983; Lochhead, 1961; Torres, 1984). If euphausiids maintain swimming at a cruising speed regardless of the randomness or cohesiveness, the total kinetic energy of their swimming should be nearly constant, that is

$$\tfrac{1}{2}\mathbf{u}\cdot\mathbf{u}+\tfrac{1}{2}\mathbf{u}'\cdot\mathbf{u}'\approx\text{constant}, \tag{8}$$

where $\mathbf{u}$ and $\mathbf{u}'$ are the mean and random velocities of euphausiids. This relation will not be valid when external forcing such as predators is present and euphausiids are escaping. This relation can be examined by comparing the spectrum width measurements in Fig. 4 and the corresponding mean velocity measurements in Fig. 6. The velocity measurements show a clear contrast between mean velocities inside and outside the aggregation. The background velocities surrounding the aggregation are small, less than $5\,\mathrm{cm\,s^{-1}}$ below 75 m. There is a layer between 50 and 60 m on the left side of the aggregation in Fig. 4 where the velocities are up to $10\text{–}15\,\mathrm{m\,s^{-1}}$ and overlap a weak backscattering layer. We cannot determine if these fast velocities indicate a subsurface current, or simply some schooling fish or mesozooplankton. These velocities vanished in the aggregation. Compared to the background velocities in the lower part of the aggregation, the velocities jumped to $10\text{–}20\,\mathrm{cm\,s^{-1}}$ where the spectrum width measurements were at the minimum. In the upper part, the mean velocities vanished while the spectrum width increased to $12\text{–}16\,\mathrm{cm\,s^{-1}}$. Thus, the total kinetic energy of euphausiids remained constant. Recalling the relationship between kinetic energy of random velocities and p given by Eq. (7), and $\theta=\frac{1}{2}\mathbf{u}'\cdot\mathbf{u}'$, Eq. (8) is the Bernoulli Equation (Batchelor, 1967), i.e.,

$$\tfrac{1}{2}\mathbf{u}\cdot\mathbf{u}+p/\rho=\text{constant}. \tag{9}$$

This relation greatly simplifies the euphausiid energy balance equation, requiring that euphausiids simply remain at their cruising speed during night. It also provides a simple analogue for studying the interference between aggregated euphausiids by measuring the mean velocities. In the center of an aggregation, the interaction

between euphausiids is higher and motion is more random, and at the edge of an aggregation, the interaction between euphausiids is lower, and motion is more coherent (Figs. 4 and 6).

The relation between internal aggregation behavior and external forces can be explored by examining the dot product of $\mathbf{u}$ and Eq. (6), combined with Eq. (5), which yields

$$\frac{\mathrm{d}}{\mathrm{d}t}\left(\frac{1}{2}\rho\mathbf{u}\cdot\mathbf{u}+p+G\right)=\mathbf{u}\cdot\mathbf{F}_{\mathrm{E}}, \tag{10}$$

where G is the potential of the inherent aggregation force and $\mathbf{F}_{\mathrm{E}}$ is the external force (Okubo, 1986; Zhou and Huntley, 1996). The left-side of Eq. (10) represents the internal balance of total kinetic energy and internal force, and the right-side represents the work done by external force which is contributed only through the mean motion. Hence, the absence of mean motion implies the absence of external force. When the total kinetic energy and abundance remain uniform and constant, the work done by their mean swimming forced by external force is balanced by their internal aggregation force, i.e., $\mathrm{d}G/\mathrm{d}t=\mathbf{u}\cdot\mathbf{F}_{\mathrm{E}}$. The internal aggregation force is coupled with external forces through the mean motion of euphausiids. A strong mean swimming velocity at the lower part of an aggregation implies the existence of strong external forces.

4.5. *Effect of circulation fields on aggregation scales*

Horizontal scales of euphausiid aggregations observed during our surveys vary from 1 to several km (Fig. 11). Though several aggregations were adjacent to each other (Figs. 3, 8 and 10), no aggregation with scales larger than 10^1 km was observed. One of the scale control mechanisms is the advection of currents, especially convergent and shear currents. The convergent component is typically less than $1\,\mathrm{cm\,s^{-1}}$, one order of magnitude smaller than the geostrophic component (Pedlosky, 1987). Small zooplankton could be affected by the convergence and divergence. However, adult euphausiids swim at a speed of $10–15\,\mathrm{cm\,s^{-1}}$. The convergent component of $1\,\mathrm{cm\,s^{-1}}$ should not directly affect euphausiid aggregations. The horizontal shear current has a typical scale of $20–30\,\mathrm{cm\,s^{-1}}$ over 5–10 km in our study areas, which is comparable to a euphausiid aggregation of 2–6 km with a swimming speed of $10–15\,\mathrm{cm\,s^{-1}}$. Taking current advection into the governing Eqs (5) and (6) for euphausiids, the equations can be rewritten as

$$\frac{\partial\rho}{\partial t}+\nabla\cdot[(\mathbf{u}+\mathbf{u}_{\mathrm{c}})\rho]=r_n(\text{birth},\text{death}), \tag{11}$$

$$\frac{\partial\mathbf{u}}{\partial t}+\mathbf{u}\cdot\nabla\mathbf{u}+\mathbf{u}_{\mathrm{c}}\cdot\nabla\mathbf{u}+\mathbf{u}\cdot\nabla\mathbf{u}_{\mathrm{c}}+\frac{1}{\rho}\nabla p=\frac{1}{\rho}(\mathbf{F}_{\mathrm{I}}+\mathbf{F}_{\mathrm{E}}), \tag{12}$$

where $\mathbf{u}_{\mathrm{c}}$ is the current field, and other variables are same as those in Eqs. (5) and (6). In addition to those terms in Eq. (6), the third term in Eq. (12) is the mean current advection, and the fourth term is the rate of change in swimming velocities due to the nonuniform current field. The mean current only moves an aggregation from one place to another, but the shear will cause differential advection, which has to be compensated by active swimming of euphausiids to maintain the aggregation. Thus, in the second term, the differential swimming has to be larger than the differential advection due to shear currents in the fourth term in order to maintain an aggregation. Comparing the scales of these terms, i.e.

$$[\mathbf{u}][\mathbf{u}]L_{\mathrm{e}}^{-1}\sim[\mathbf{u}][\mathbf{u}_{\mathrm{c}}]L_{\mathrm{c}}^{-1}, \tag{13}$$

where $[\mathbf{u}]$ represents the scale of mean swimming velocities of euphausiids, $[\mathbf{u}_{\mathrm{c}}]$ represents the scale of currents, L_{e} is the spatial scale of a euphausiid aggregation, and L_{c} is the spatial scale of currents. Note that the scale of a gradient operator $[\nabla]$ is equal to $[\mathbf{x}]^{-1}$, inversely proportional to a spatial scale, where $\mathbf{x}$ is the horizontal coordinate. By rearranging Eq. (13), the critical horizontal scale (L_{e}^{*}) for euphausiids to maintain an aggregation is

$$L_{\mathrm{e}}^{*}=L_{\mathrm{c}}\frac{[\mathbf{u}]}{[\mathbf{u}_{\mathrm{c}}]}. \tag{14}$$

An aggregation with a horizontal scale larger than L_{e}^{*} cannot be maintained because their swimming capacity cannot match the current shear. The spatial scale of a mesoscale current field is determined by the internal Rossby Radius

(Huntley and Niiler, 1995; Pedlosky, 1987). The magnitude of currents in Crystal Sound is approximately 10–15 cm s^{-1} (Fig. 2), equivalent to the cruising speed of adult euphausiids. The internal Rossby Radius is approximately 5 km in the Southern Ocean (Huntley and Niiler, 1995). Thus, the spatial scale of euphausiid aggregations should be equivalent or smaller than 5 km. In our study areas, the horizontal scale of a euphausiid aggregation is equal to 2 ± 1.4 km (Fig. 11).

The scale analysis (Eq. (14)) can be used to examine the scales of euphausiid aggregations found in Laubeuf Fjord (Fig. 10). Several aggregations were found within the upper 150 m, which were confirmed by net tows to be primarily adult *E. superba*. The current measurements showed that the magnitude of the currents was approximately 20 cm s^{-1} and the spatial scale was approximately 5 km. From Eq. (14), the critical scale of a euphausiid aggregation should be on the order of 4 km assuming the swimming velocities of 15 cm s^{-1}. This scale is comparable to the horizontal scales of 1–6 km found from those aggregations in Laubeuf Fjord. When the shear current controls the scales of euphausiid aggregations, aggregations can be stretched to extra lengths that may explain the relative small aspect ratios of the vertical to horizontal scales for aggregations in Laubeuf Fjord.

4.6. *Effect of sea ice on aggregation behavior*

The variations in aggregation scales and abundance can be caused by external forces such as current fields, food sources or the presence of predators. Sea ice has been considered to play an important role in krill ecology by providing food resources and protection from predators during the austral winter (Daly, 1990; Daly and Macaulay, 1988; Kawaguchi et al., 1986; Marschall, 1988). In recent studies of krill distributions, acoustic surveys using an Autonomous Underwater Vehicle (AUV) revealed an increase in krill concentration within a narrow band along the ice edge (Brierley et al., 2002). To investigate changes in aggregation behavior across open water and solid ice in an ice edge is hence important for understanding environmental forcing on euphausiids and for predicting their behavior.

The transect crossing the ice edge was nearly 100 km, within which nearly 30 km was in packed ice (Figs. 1 and 8). The effects of ice noise on acoustic measurements can be seen from the vertical strips in Fig. 8. Clearly, the VM ADCP was performing very robustly. The disadvantage of using a VM ADCP is that we do not have any measurements within the first 16 m where euphausiids interact with ice. Our net tows in this area did not reveal any significant euphausiid aggregations within the upper 25 m, which also was found in other studies (Brierley et al., 2002). Thus, our ADCP surveys should reflect distributions of euphausiids in the water column.

Crossing the ice edge north of Alexander Island (Figs. 1 and 8), the euphausiid abundance increased from the ice edge 10–20 km into the pack ice, and then decreased. The elevation of euphausiid abundance in a band of 10–20 km along ice edge has been interpreted as the optimal physical and biological settings for euphausiids near ice edges in terms of food resources and refuge from predators. (Brierley et al., 2002). Algae concentrations in ice and water column were insignificant food sources for euphausiids during our study period (Daly, 2004). In regions of open water and small floes, euphausiid predators (Crabeater seals, whales, and penguins) were observed frequently during our cruises (Southern Ocean GLOBEC Cruise Reports, http://www.ccpo.odu.edu/Research/globec_menu.html). Whether euphausiids fed on other food sources during our survey period in addition to algae needs further analysis. It is fair to say that pack ice provided the euphausiids with protection from the numerous predators in the study area.

The scales and shapes of euphausiid aggregations vary from smaller size aggregations with a higher abundance in the ice free region to larger size aggregations with a lower abundance in the ice covered region. Studies indicate that individuals may leave an aggregation because the returns per individual are reduced in an overly dense aggregation when food sources become limited (Ritz, 1994). Observations also show that an aggregation

will be more packed in the presence of predators than one in the absence of predators. Thus, under pack ice, being protected from predation, euphausiids were likely exploring food sources in a much extended area. It can also be considered that in such an environment without external stimulation such as food or predators, the existence of euphausiid aggregations demonstrates their inherent aggregation behavior, that is, they prefer to stay together.

5. Summary

Euphausiids were found to form aggregations actively during late fall and winter. They aggregated more densely in the presence of predators than they did in the absence of predators. Abundant euphausiids were found associated with ice edges while pack ice prevented top predator from accessing water. There was no evidence that euphausiid aggregations were associated with sea-ice biota. They vertically migrated to a depth most likely associated with the diving depth of predators during the day. Though the aggregation scales change significantly corresponding to diel migration, a linear relation is found between horizontal and vertical scales with a mean aspect ratio approximately 0.05 ($R^2 = 0.87$). The aspect ratios decreased in Laubeuf Fjord where several aggregations were packed closely and sheared horizontally by mesoscale eddies. Analysis of dynamic balance for an aggregation in a current field indicates that the upper limit of horizontal scales of the euphausiid aggregation is determined by the product of the horizontal scale of a sheared current field and the ratio of euphausiid swimming to current speeds.

Euphausiids reduce their swimming at the depth during the day when they presumably stop feeding. They swim actively at their cruising speed in the upper water column during their feeding period at night. Velocity measurements show that they swim randomly in the upper part of an aggregation near the surface, and swim coherently, schooling in the lower part of an aggregation. Theoretical analysis indicates that the lower mean swimming velocities in an aggregation implies a lack of external forcing, and strong mean swimming velocities in an aggregation implies the existence of strong external forces.

The phenomenon of attraction has been widely observed among animals from zooplankton to mammals in waters, and from insects to other terrestrial animals on land. It is well documented that animals use chemical, acoustic, or visual sensing to communicate between individuals. From individual attractions to a social aggregation, the order of freedom within the system increases as a function of the number of animals in the aggregation. Recognizing the stochastic nature of animal aggregation behavior, we proposed a statistical dynamics approach by examining ensemble means of swimming velocities, means of random kinetic energy, scales of aggregations and interaction with current fields. These results are those very first to describe integrated swimming, aggregation shapes and current fields at the scale of an entire aggregation under different physical and biological environments. Though the importance of these observations and analyses will be further tested, such an approach is a step toward understanding animal aggregation dynamics and a mathematical description of the aggregation behavior.

Acknowledgement

This project is supported by the National Science Foundation grant number OPP-9910263 to M. Zhou. We thank Dr. Eric Firing at the University of Hawaii for configuring the ADCP settings and data acquisition. We acknowledge Raytheon Polar Service Co. for assisting networking, data transferring and net tows, and solving all technical difficulties. Special thanks due to Daniel Mertes at the Large Lakes Observatory, University of Minnesota, Jay O. Peterson, Yiwu Zhu, and Joseph P. Smith at the University of Massachusetts Boston for their helps in collecting field samples and data. We also would like to acknowledge two anonymous reviewers and Dr. Peter Wiebe for invaluable comments. This is contribution No. 456 of the US GLOBEC Program.

References

Anderson, J.J., 1981. A stochastic model for the size of fish schools. Fishery Bulletin of the United States 19, 315–323.

Ashjian, C.J., Sharon, L.S., Flagg, C.N., Wilson, C., 1998. Patterns and occurrence of diel vertical migration of zooplankton biomass in the Mid-Atlantic Bight described by an acoustic doppler current profiler. Continental Shelf Research 18, 831–858.

Bargmann, H.E., 1945. The development and life-history of adolescent and adult krill *Euphausia superba*. Discovery Reports 23, 103–176.

Batchelor, G.K., 1967. An introduction to fluid dynamics. Cambridge University Press, Cambridge, 615pp.

Brierley, A.S., et al., 2002. Antarctic krill under sea ice, elevated abundance in a narrow band just south of ice edge. Science 295, 1890–1892.

Brinton, E., Townsend, A., 1991. Development rates and habitat shifts in the Antarctic neritic euphausiid *Euphausia crystallorophias*, 1986–87. Deep-Sea Research 38, 1195–1211.

Brock, V.E., Riffenburgh, R.H., 1960. Fish schooling, a possible factor in reducing predation. Journal du Conseil Internationale et Permanent pour l'Exploration de la Mer 25, 307–317.

Burcynski, J., 1973. Hydroacoustic research system of R.V. *Professor Siedlecki*. Polish-USNF Highseas Fisheries Research Project, Gdynia, 33pp.

Burns, J.M., Costa, D.P., Fedak, M., Bradshaw, C.J.A., Hindell, M.A., McDonald, G., Trumble, S.J., Chittick, E., Gray, M., Gales, N., Barnes, J., Shaffer, S., Kuhn, K., Lovell, P., Crocker, D., 2004. Winter habitat use and foraging behavior of crabeater seals along the Western Antarctic Peninsula. Deep-Sea Research II, this issue [doi:10.1016/j.dsr2.2004.07.021].

Clark, C.W., 1974. Possible effects of schooling on the dynamics of exploited fish populations. Wiley-Interscience, New York, 322pp.

Costa, D.P., Crocker, D.E., 1996. Marine mammals in the Southern Ocean. In: Ross, R., Hofmann, E., Quetin, L. (Eds.), Foundations for Ecological Research West of the Antarctic Peninsula. Antarctic Research Series. American Geophysical Union, Washington, D.C., pp. 287–301.

Cowles, T.J., Desiderio, R.A., Neuer, S., 1993. In situ characterization of phytoplankton from vertical profiles of fluorescence emission spectra. Marine Biology 115, 217–222.

Daly, K.L., 1990. Overwintering development, growth, and feeding of larval *Euphausia superba* in the Antarctic marginal ice zone. Limnology and Oceanography 35, 1564–1576.

Daly, K.L., Macaulay, M., 1988. Abundance and distribution of krill in the ice edge zone of the Weddell Sea, austral spring 1983. Deep-Sea Research I 35, 21–41.

Daly, K.L., Macaulay, M.C., 1991. The influence of physical and biological mesoscale dynamics on the seasonal distribution and behavior of *Euphausia superba* in the Antarctic marginal ice zone. Marine Ecology Progress Series 79, 37–66.

Demer, D., Hewitt, R., 1995. Bias in acoustic biomass estimates of *Euphausia superba* due to diel vertical migration. Deep-Sea Research I 42, 455 475.

Demer, D.A., Barange, M., Boyd, A.J., 2002. Measurements of three-dimensional fish school velocities with an acoustic Doppler current profiler. Fisheries Research 47, 201–214.

Duffy, D.C., Wissel, C., 1988. Models of fish school size in relation to environmental productivity. Ecological Modelling 40, 201–211.

Everson, I., Bone, D.G., 1986. Effectiveness of the RMT8 system for sampling krill (*Euphausia superba*) swarms. Polar Biology 6, 83–90.

Everson, I., Watkins, J.L., Bone, D.G., Foote, K.G., 1990. Implications of a new acoustic target strength for abundance estimates of Antarctic krill. Nature 345, 338–340.

Flagg, C.N., Smith, S.L., 1989a. Zooplankton abundance measurements from acoustic Doppler current profilers, Oceans '89. Marine Technology Society and I.E.E.E., Seattle, WA.

Flagg, C.N., Smith, S.L., 1989b. On the use of the acoustic Doppler current profiler to measure zooplankton abundance. Deep-Sea Research 36 (3), 455–474.

Fraser, W.R., Trivelpiece, W.Z., 1996. Factors controlling the distribution of seabirds, winter-summer heterogeneity in the distribution of Adelaide penguin populations. In: Ross, R., Hofmann, E., Quetin, L. (Eds.), Foundations for Ecological Research West of the Antarctic Peninsula. Antarctic Research Series. American Geophysical Union, Washington, D.C., pp. 257–272.

Greene, C.H., Stanton, T.K., Wiebe, P.H., McClatchie, S., 1991. Acoustic estimates of Antarctic krill. Nature 349, 110.

Hamner, W.M., 1984. Aspects of schooling in *Euphausia superba*. Journal of Crustacean Biology 4 (Spec. No. 1), 67–74.

Hamner, W.H., Hamner, P.P., Strand, S.W., Gilmer, R.W., 1983. Behavior of Antarctic krill, *Euphausia superba*, chemoreception, feeding, schooling and moulting. Science 220, 433–435.

Hamner, W.M., Hamner, P.P., Obst, B.S., Carleton, J.H., 1989. Field observations on the ontogeny of schooling of *Euphausia superba* furciliae and its relationship to ice in Antarctic waters. Limnology and Oceanography 34, 451–456.

Hofmann, E.E., Klinck, J.M., Lascara, C.M., Smith, D.A., 1996. Water mass distribution and circulation west of the Antarctic Peninsula and including Bransfield Strait. In: Ross, R., Hofmann, E., Quetin, L. (Eds.), Foundations for Ecological Research West of the Antarctic Peninsula. Antarctic Research Series. American Geophysical Union, Washington, D.C., pp. 61–80.

Holliday, D.V., 1974. Doppler structure in echoes from schools of pelagic fish. Journal of the Acoustical Society of America 55, 1313 1322.

Holliday, D.V., 1977. Two applications of the Doppler effect in the study of fish schools. Rapports et Proces-verbaux du

Conseil Permanent et Internationale pour l'Exploration de la Mer 170, 21–30.

Hopkins, C.C.E., Falk-Petersen, Tande, K., Eilertsen, H.C., 1978. A preliminary study of zooplankton sound scattering layers in Balsfjorden: Structure, energetics, and migrations. Sarsia 63, 255–264.

Hopkins, C.C.E., Tande, K.S., Grönvik, S., Sargent, J.R., 1984. Ecological investigations of the zooplankton community of Balsfjorden, northern Norway, an analysis of growth and overwintering tactics in relation to niche and environment in *Metridia longa* (Lubbock), *Calanus finmarchicus* (Gunnerus), *Thysanoessa inermis* (Kröyer), and *T. raschii* (M. Sars). Journal of Experimental Marine Biology and Ecology 82, 77–99.

Huntley, M.E., Niiler, P.P., 1995. Physical control of population dynamics in the Southern Ocean. ICES Journal of Marine Science 52, 457–468.

Kalinowski, J., 1978. Vertical migration of krill in the region of South Georgia, February–March, 1976. Polish Archives of Hydrobiology 25, 573–583.

Kawaguchi, K., Ishikawa, S., Matsuda, O., 1986. The overwintering strategy of Antarctic krill (*Euphausia superba* Dana) under the coastal fast ice off the Ongul Islands in Lützow–Holm Bay, Antarctica. Memoirs of the Institute of Polar Research of Japan 44, 67–85.

Kils, U., 1979. Swimming speed and escape capacity of Antarctic krill, *Euphausia superba*. Meeresforschung 27, 264–266.

Kils, U., 1983. Swimming and feeding of Antarctic krill, *Euphausia superba*—some outstanding energetics and dynamics—some unique morphological details. Berichte zur Polarforschung 4, 130–155.

Lascara, C.M., Hofmann, E.E., Ross, R.R., Quetin, L.B., 1999. Seasonal variability in the distribution of Antarctic krill, *Euphausia superba*, west of the Antarctic Peninsula. Deep-Sea Research 46, 925–949.

Lochhead, J.H., 1961. Locomotion. In: Waterman, T.H. (Ed.), The physiology of Crustacea. Academic Press, New York, pp. 313–364.

Macaulay, M.C., English, T.S., Mathisen, O.E., 1984. Acoustic characterization of swarms of Antarctic krill (*Euphausia superba*) from Elephant Island and Bransfield Strait. Journal of Crustacean Biology 4, 16–44.

Marr, J.W.S., 1962. The natural history and geography of the Antarctic krill (*Euphausia superba* Dana). Discovery Reports 322, 33–464.

Marschall, H.-P., 1988. The overwintering strategy of Antarctic krill under the pack-ice of the Weddell Sea. Polar Biology 9, 129–135.

Mauchline, J., Fisher, L.R., 1969. The biology of euphausiids. Advances in Marine Biology 7, 1–454.

Miller, D.G.M., Hampton, I., 1989. Krill aggregation characteristics, spatial distribution patterns from hydroacoustic observations. Polar Biology 10, 125–134.

Okubo, A., 1980. Diffusion and ecological problems, Mathematical Models, Biomathematics. Springer, Berlin, 254pp.

Okubo, A., 1986. Dynamical aspects of animal swarming, swarms, schools, flocks and herds. Advances in Biophysics 22, 1–94.

Okubo, A., Anderson, J.J., 1984. Mathematical models for zooplankton swarms, their formation and maintenance. EOS 65, 731–732.

Onsurd, M.S.R., Kaartvedt, S., 1998. Diel vertical migration of the krill *Meganyctiphanes norvegica* in relation to physical environment, food and predators. Marine Ecology Progress Series 171, 209–219.

Parr, A.E., 1927. A contribution to the theoretical analysis of the schooling behavior of fishes. Occasional Papers, Bingham Oceanographic College, pp. 32.

Pearcy, W.G., Hopkins, C.C.E., Gronvik, S., Evans, R.A., 1979. Feeding habits of cod, capelin, and herring in Balsfjorden, northern Norway, July–August 1978, the importance of euphausiids. Sarsia 64, 269–277.

Pedlosky, J., 1987. Geophysical Fluid Dynamics. Springer, New York, 624pp.

Pitcher, T.J., 1983. Heuristic definitions of fish shoaling behavior. Animal Behavior 31, 611–613.

RDI, 1989. Acoustic Doppler current profilers. Principles of Operation, a practical primer. RD Instruments, 36pp.

RDI, 1990. Calculating absolute backscatter. RD Instruments.

RDI, 1992. Acoustic Doppler Current Profilers, Technical Manual, RD Instruments, San Diego.

Ritz, D.A., 1994. Social aggregation in pelagic invertebrates. Advanced Marine Biology 30, 155–216.

Sameoto, D.D., 1980. Quantitative measurement of euphausiids using a 120-kHz sounder and their in situ orientation. Canadian Journal of Fisheries and Aquatic Sciences 37, 693–702.

Smith, P.E., Ohman, M.D., Eber, L.E., 1989. Analysis of the patterns of distribution of zooplankton aggregations from an acoustic Doppler current profiler. CalCOFI Reports 30, 88–103.

Swartzman, G., 1991. Fish school formation and maintenance, a random encounter model. Ecological Modelling 56, 63–80.

Tarling, G.A., Jarvis, T., Emsley, S.M., Matthews, J.B., 2002. Midnight sinking behaviour in Calanus finmarchicus, a response to satiation or krill predation? Marine Ecology Progress Series 240, 183–194.

Tomo, A.P., 1983. Study on the diurnal migration of *Euphausia superba* and the formation of shoals. Berichte zur Polarforschung 4, 191–195.

Torres, J.J., 1984. Relationship of oxygen consumption to swimming speed in *Euphausia pacifica*. II. Drag, efficiency and a comparison with other swimming organisms. Marine Biology 78, 231–237.

Torres, J.J., Childress, J.J., 1983. Relationship of oxygen consumption to swimming speed in *Euphausia pacifica* I. Effects of temperature and pressure. Marine Biology 74, 79–86.

Watkins, J.L., Buchholz, F., Priddle, J., Morris, D.J., Ricketts, C., 1992. Variation in reproductive status of Antarctic krill swarms; evidence for a size-related sorting mechanism? Marine Ecology Progress Series 82, 163–174.

Wiebe, P.H., Burt, K.H., Boyd, S.H., Morton, A.W., 1976. A multiple opening-closing net and environmental sensing system for sampling zooplankton. Journal of Marine Research 34, 313–325.

Wiebe, P.H., et al., 1985. New developments in the MOCNESS, an apparatus for sampling zooplankton and micronekton. Marine Biology 87, 313–323.

Zhou, M., Huntley, M.E., 1996. The principle of biological attraction, demonstrated by the bio-continuum theory of zooplankton patch dynamics. Journal of Marine Research 54, 1017–1037.

Zhou, M., Nordhausen, W., Huntley, M.E., 1994. ADCP measurements of the distribution and abundance of euphausiids near the Antarctic Peninsula in winter. Deep-Sea Research I 41, 1425 -1445.

Zhou, M., Zhu, Y., Tande, K., 2003. Circulation and behavior of euphausiids in Norwegian sub-Arctic fjords. Marine Ecology Progress Series, in revision.

ELSEVIER

Deep-Sea Research II 51 (2004) 2139–2168

DEEP-SEA RESEARCH
PART II

www.elsevier.com/locate/dsr2

Overwintering growth and development of larval *Euphausia superba*: an interannual comparison under varying environmental conditions west of the Antarctic Peninsula

Kendra L. Daly*

College of Marine Science, University of South Florida, St. Petersburg, FL 33701, USA

Accepted 8 July 2004

Abstract

Growth, molting, and development of larval Antarctic krill were investigated near Marguerite Bay during four cruises in austral autumn and winter 2001 and 2002, as part of the US Southern Ocean GLOBEC program. Overwintering survival of larvae has been linked to annual sea-ice formation and extent, as sea-ice biota may provide food when other sources are scarce in the water column. During autumn 2001, larvae were very abundant (1–19 individuals m^{-3}), with younger stages dominant offshelf and older stages dominant on-shelf. On-shelf larvae were in better condition than offshore larvae. During autumn 2002, larvae again were abundant offshelf (0.01 110 m^{-3}), whereas all stages were scarce on-shelf. Declining diatom and radiolarian blooms were present during autumn in both years. Average chlorophyll concentrations were low (0.10 vs. 0.22 $\mu g l^{-1}$) in autumn and an order of magnitude lower in winter. Carbon content of larvae during autumn 2001 and 2002 (41% vs. 38% C of DW) suggested that lipid storage was moderate. The median autumn larval growth rate (0.027 mm d^{-1}) was lower and the intermolt period (19 d) longer than reported summer values. During winter, larvae appeared to be food-limited based on the following observations: (1) the median growth rate decreased (0.00 mm d^{-1}) and the intermolt period increased (40 d), (2) larval length-specific dry weight (DW) and % carbon and nitrogen of DW decreased, and (3) 88% of furcilia 6 did not develop to the juvenile stage, but remained at the same stage after molting. Experimental results demonstrated that some larvae could survive starvation for a month by combusting body reserves (ca. 1% decrease in DW and body C and N d^{-1}), implying that a portion of the population was resilient to the suboptimal food supply. Although sea ice formed up to 2 months earlier in 2002, ice algae at the ice–water interface, where it is accessible to krill, was not an abundant food source in either year (0.05 vs. 0.07 μg chl l^{-1}). In winter 2001, furcilia were commonly observed near the undersurface of sea-ice, but only rarely in 2002 until mid-September, when ice algae began to accumulate. Low gut fluorescence values also indicate that little nutrition was derived from autotrophs in winter. Instead, larvae were likely opportunistic scavengers exploiting all available food sources, including microzooplankton, benthic larvae, detritus, scarce phytoplankton and sea-ice biota. In summary, larval krill exhibited several overwintering behaviors: (1) flexible feeding, (2) flexible morphology (i.e., delayed development), (3) flexible physiology (i.e., increased intermolt period, reduced growth), (4) moderate lipid

*Tel.: +1-727-553-1041; fax: +1-727-553-1189.
E-mail address: kdaly@marine.usf.edu (K.L. Daly).

0967-0645/$ - see front matter © 2004 Elsevier Ltd. All rights reserved.
doi:10.1016/j.dsr2.2004.07.010

storage, and (5) ability to withstand starvation by combusting body C and N. Because most larvae did not shrink i length, this measure may not be a good indicator of the body combustion strategy. At these high latitudes, sea-ice biot may not be a primary source of food during winter, but progressively more important in spring as irradiance level increase. Winter survivors during 2001 resulted in a significant recruitment to the juvenile size class during spring.
© 2004 Elsevier Ltd. All rights reserved.

1. Introduction

High concentrations of Antarctic krill, *Euphausia superba*, occur along the western side of the Antarctic Peninsula and eastward into the Scotia Sea (Marr, 1962). The suite of environmental and biological factors that sustain this persistent stock and the processes that lead to its considerable interannual variability remain poorly known. One critical period in the krill life cycle is during the first autumn and winter. Young larvae must survive a long period when much of the Southern Ocean is covered by sea-ice and primary production in the water column is extremely low. Observations and field experiments within the pack ice zone during the 1980s led to the hypothesis that the overwintering survival and recruitment of young krill are related to the timing and extent of sea-ice and its associated biota (Guzman, 1983; Daly and Macaulay, 1988; Marschall, 1988; Daly, 1990; Smetacek et al., 1990). Sea-ice biota, which is composed of ice algae (often dominated by pennate diatoms), bacteria, protozoans, and small metazoans, can have relatively high concentrations from late autumn to spring (Hoshiai, 1985; Garrison and Close, 1993). Sea-ice primary production is estimated to be ca. 66 Tg C per year, which is about 5% of the total annual primary production in the Southern Ocean (Lizotte, 2001). Much of that production, however, occurs in late autumn or spring when phytoplankton production in the water column is negligible. Hence, extensive sea-ice coverage in winter may act to dampen the strong seasonal oscillation in food supply and promote ecosystem stability.

Subsequent studies reported correlations between recruitment indices of krill and sea-ice conditions (Kawaguchi and Satake, 1994; Siegel and Loeb, 1995), where years with extensive ice cover were often followed by higher recruitment of larvae to the juvenile class than during years with little or no ice cover. Because females reproduce over several years, Siegel and Loeb (1995) noted that on average the krill stock appeared to remain relatively stable despite 1–2 years of poor recruitment. However, they predicted that reduced ice cover for 3 or more years would significantly impact densities. The implication being that larval survival or mortality overwinter was more important than reproductive success in determining recruitment success or failure.

High-latitude zooplankton have evolved life history strategies to accommodate the large seasonal oscillation in environmental conditions. In the last two decades, *E. superba* was reported as having a suite of overwintering behaviors, including feeding on sea-ice biota (Daly and Macaulay, 1988; Marschall, 1988), carnivory (Hopkins et al., 1993), utilizing sequestered lipids to support metabolism (Hagen et al., 1996), body shrinkage (combustion of body carbon and nitrogen to support metabolism, Ikeda and Dixon, 1982), and reduced metabolism (Quetin et al., 1994; Torres et al., 1994). Recent findings suggest that behavior in larval krill may vary. For example, Meyer et al. (2002a) did not observe a decrease in respiration rate and enzyme activity between summer and autumn in furcilia stage 3 (F3). Frazer et al. (2002a), however, measured decreased respiration rates for F4–F6 during winter, which appeared to be sensitive to decreasing temperature and food supply. Due to the limited number of investigations on larval krill physiology, the relative importance of different behaviors under varying environmental conditions remains poorly known.

The strategy of body shrinkage, in particular, has received considerable attention. Euphausiids are obligate molters; molting throughout their lifespan and during all seasons. The results from several laboratory and field studies suggest that

E. superba larvae (Ross and Quetin, 1991) and juveniles and adults (Ikeda and Dixon, 1982; Sun et al., 1995; McGaffin et al., 2002) shrink in length at molting when food limited, which would confound estimates of growth and longevity based on net sample length–frequency data. The extent to which body shrinkage occurs in the field is currently being debated (Buchholz, 1991; Nicol, 2000). Nicol (2000) recommended integrating field sampling with short-term shipboard experiments to measure instantaneous or finite growth rates, and noted that standardization of growth rate measurements was needed to improve confidence in the interpretation of morphometric relationships and to compare results among different investigations. Variations in larval growth, development, and nutritional condition are the result of an integration of genetic, physiology, and environmental effects, with temperature and food quality and quantity being the primary environmental factors influencing larval physiology. Thus, growth (or shrinkage) is a measure of the net integration of overwintering strategies that larvae may employ to mitigate unfavorable winter conditions. A mechanistic understanding of larval krill behavior in relation to individual variability in growth (or shrinkage) and development is necessary to understand population size structure, secondary production, as well as fluctuations in recruitment.

As part of the US Southern Ocean GLOBEC program, the overwintering behaviors of larval *E. superba* were investigated along the western Antarctic Peninsula in the vicinity of Marguerite Bay. One objective of this program was to test the hypothesis that early and long-lasting ice cover provides a dependable food supply and enhanced survival of larvae. Here I report the development and growth of larval krill in relation to sea-ice dynamics during austral autumn and winter in 2001 and 2002. Two methods to experimentally measure growth rates are compared, as well as growth rates in terms of length and biomass (dry weight and body carbon and nitrogen) based on short-term shipboard experiments and field samples to determine whether larval growth or shrinkage occurs during winter in this region of the Southern Ocean.

2. Methods

Larval and Year 0 (Y0) juvenile *Euphausia superba* were collected during austral autumn and winter on four cruises between April 2001 and September 2002 in the vicinity of Marguerite Bay west of the Antarctic Peninsula as part of the US Southern Ocean GLOBEC Program (Figs. 1 and 2). This program had two ships operating simultaneously, one for process studies (Fig. 2A) and the other for surveys (Fig. 2B) of the study area. The observations reported here were obtained aboard the process ship on the autumn cruises and aboard the survey vessel during winter, hence the different station patterns. In the first year, field observations were made aboard the R.V. *Lawrence M. Gould* between 23 April and 6 June 2001 and aboard the R.V.I.B. *Nathaniel B. Palmer* between 24 July and 31 August 2001. In the second year, field observations were made aboard the R.V. *L. M. Gould* between 7 April and 20 May 2002 and aboard the R.V.I.B. *N. B. Palmer* between 31 July and 18 September 2002.

Surface chlorophyll samples were collected from the ship's flow-through seawater system, which have seawater intake between 5 and 7 m depth on both ships. Water-column chlorophyll was collected during CTD casts using 10-l Niskin bottles mounted on a rosette. Sea-ice biota were collected from the undersurface of ice floes at the ice–water interface by divers using a suction sampler. About 175 cm^2 of the under-ice surface area were simultaneously scraped and suctioned into a 1-l container. A variety of ice types were sampled, including where krill were observed feeding, such as surface ice slush, under first and second year ice, and new grease ice. Phytoplankton or sea-ice biota were filtered into GF/F filters, passively extracted in 7 ml of 90% acetone at −20 °C in the dark for at least 24 h, then chlorophyll fluorescence was measured on a Turner Design Digital 10-AU-05 fluorometer calibrated prior to the cruise. Particulate organic carbon (POC) and nitrogen (PON) samples collected by Niskin bottles and by the under-ice sampler were filtered through combusted (450 °C for 2 h) GF/F filters under low vacuum and frozen at −80 °C. Samples were analyzed at the University of California Santa Barbara,

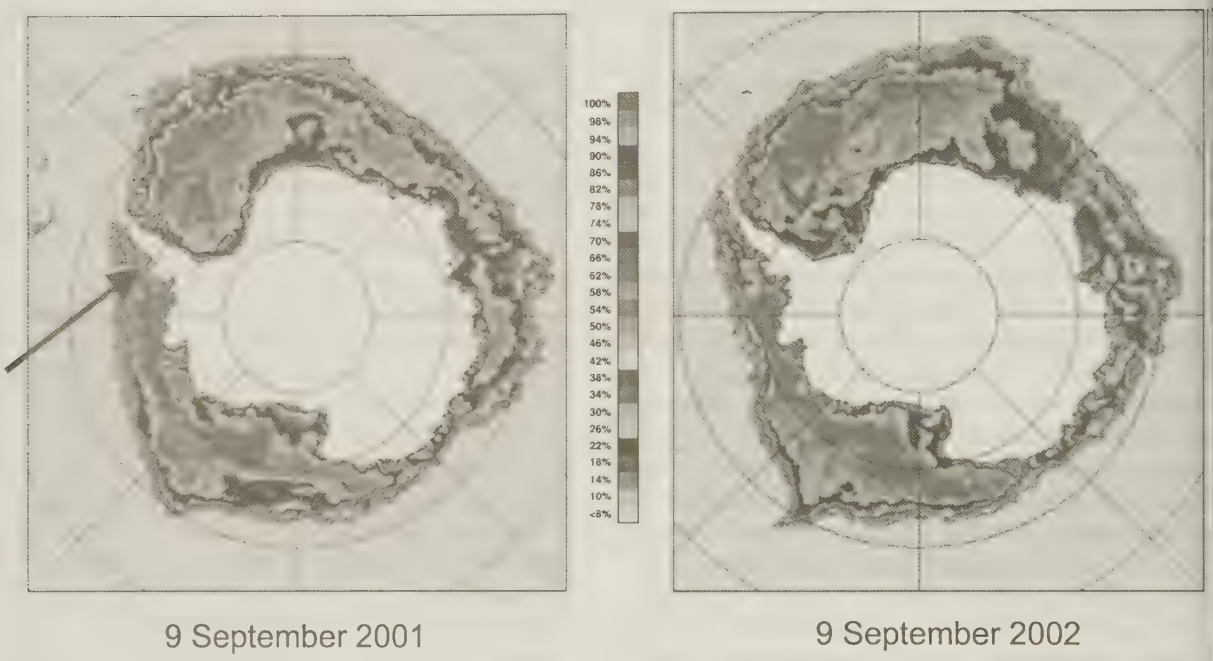

Fig. 1. Sea-ice concentration maps during winter maximum of the sea-ice extent in 2001 (left) and 2002 (right). Arrow shows location of the study area. Satellite images courtesy of J. Comiso.

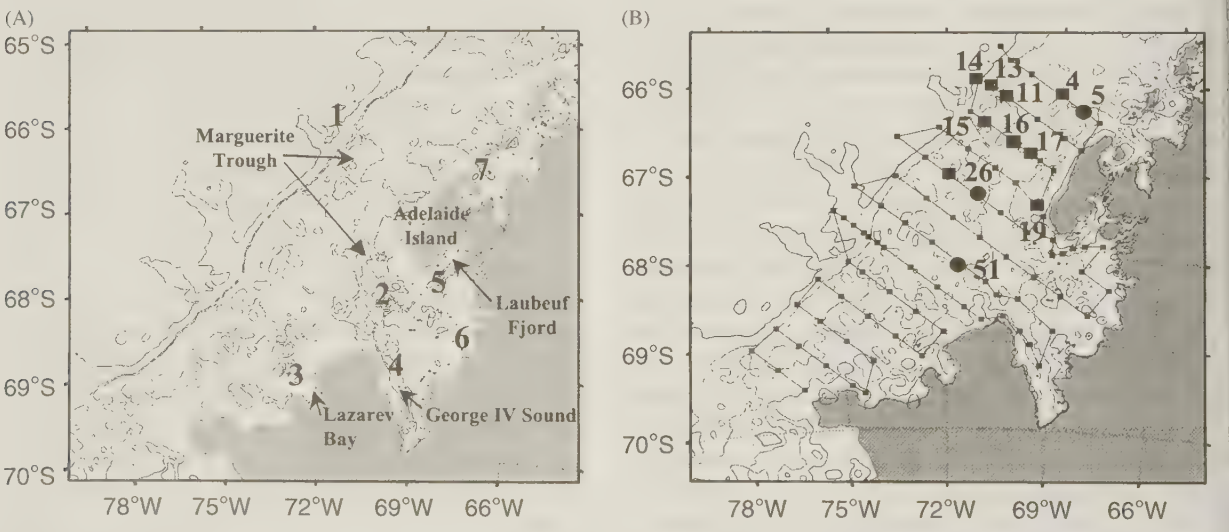

Fig. 2. Station locations during the austral autumn (A) and winter (B) cruises. Autumn stations are designated by numbers. The small dots on the grid in (B) show the survey sampling scheme; circles designate the 2001 stations and squares the 2002 stations mentioned in the text.

Marine Science Institute Analytical Laboratory using the high-temperature combustion Dumas method and an organic elemental analyzer.

For physiology experiments, larval krill were collected either from the upper 100 m of the water column using a 1.5-m^2 Tucker Trawl, having a

1/4 in mesh graded down to a 707 μm mesh with a protected cod-end; or larvae were collected under sea-ice by divers. On the second winter cruise, larvae were collected primarily using a 1-m diameter Reeve Net with a 333 μm mesh net having a 20 l protected cod end, in tandem with a 1-m diameter Ring Net (333 μm mesh). The heavy Reeve net cod-end was kept afloat using syntactic foam. The Reeve Net was hung about 3–5 m below the Ring Net, and both were deployed off the stern at about 10 and 15 m in depth, respectively. The propellers were run at 5–25% to keep water circulating into the nets, but with little to no forward ship movement or ice sweep-down under the hull. This method collected larvae in excellent shape. In addition larvae were collected at discrete depth intervals to assess their distribution in the water column during autumn using a 1-m^2 MOCNESS net with 333 μm mesh.

Larvae were identified to life history stage (Calyptopis I–III, Furcilia I-IV, or juvenile) after Makarov (1980). Direct or indirect development determinations were based on variant forms of telson morphology following Fraser (1936). Individuals were then measured for length from the base of the eye to the tip of the telson, excluding setae. Freshly collected and undamaged individuals also were measured for dry weight and carbon and nitrogen content. These larvae were rinsed briefly with distilled water to remove salts, blotted dry, then placed either individually, or in small groups for the younger stages, on a weighed combusted GF/F filter and dried in a combusted shell vial at 60 °C. Dry weights were measured on a Mettler UMX2 microbalance. A subset of these larvae was analyzed for carbon (C) and nitrogen (N) content by the UCSB Analytical Laboratory.

The effect of food limitation on dry weight and body C and N content of winter larvae was examined in 2001. Several hundred F4–F6 larvae, 6.5–14 mm in length, were collected from under sea-ice at Sta. 5 on July 28 and held in filtered (0.1 μm) seawater in two 20 l containers at about −1.0 °C. Container water was changed regularly and unhealthy-looking or dead individuals were removed. About every 3–5 days, 20 active individuals were removed and frozen, until August 24 when all remaining larvae were frozen. In the laboratory, slightly thawed larvae were measured for length and for dry weight. Larvae for CN measurements were placed directly on weighed, combusted GF/F filters to avoid any loss of material such as lipids. They were then dried, weighed, and analyzed for CN.

Gut fluorescence was measured by placing 1–30 larvae immediately upon collection in vials containing 90% acetone. Gut pigments were passively extracted in the dark at −20 °C for at least 24 h, then measured for fluorescence (Daly, 1990). Pigment content is expressed as total pigment (chlorophyll a + phaeopigments), with no correction factor for an unknown degradation loss. Larval stages for gut fluorescence included F4–F6 during autumn and primarily F6 during winter.

In situ molting rates were assessed using about 100 individuals in each experiment. Immediately after collection larvae were sorted into separate 28–129 ml jars containing filtered (1 μm) seawater and held in a water bath or large flow-through aquaria at in situ sea surface temperature (−0.59 to −1.82 °C) for 4–5 days. Water was changed every 1–2 days. Individuals were checked for molts every 12 h and dead, damaged, or molted individuals were removed. Larvae must be checked at least at that frequency and then separated from their molts if they are not measured immediately, as they often ingest their molts. For each experiment, the intermolt period (IMP) in days was calculated as the inverse of the average of the proportion of individuals molting each day of the experiment:

$$\mathrm{IMP} = \frac{1}{\frac{\sum(M_i/K_i)}{n}}$$

where M_i is the number of individuals molted per day, K_i is the number of individuals available to molt each day, and n is the number of days.

Growth rates were measured following the methods of Poleck and Denys (1982) as updated by Nicol (2000). Individuals that molted in the above experiments were removed and measured within a few hours for total length, then the length of the telson (Fig. 3A) and the exopodite of the right uropod (Fig. 3B) was measured on both the molted larvae and the molt under a dissecting

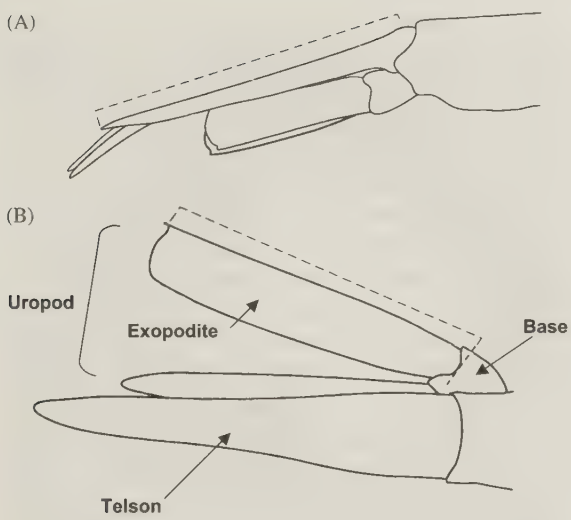

Fig. 3. Illustration of the distal portion of a furcilia 6 abdomen showing the location of growth measurements on the (A) telson in lateral view and on the (B) exopodite of the right uropod in dorsal view. The slightly flexed telson was measured from the middle of the small rise at the anterior end of the telson to the posterior end, excluding the telson spines. The exopodite was placed at about a 35° angle to the telson, then measured from the lowest point of the base to the distal end of the exopodite at the base of the spine.

microscope using a micrometer. If the right uropod was damaged, the left one was measured. Both the uropod and telson were measured for several reasons: (1) to provide a comparison with other studies. Most krill growth investigations are based on uropod measurements (e.g., Poleck and Denys, 1982; Buchholz, 1985; Ikeda and Thomas, 1987; Nicol et al., 1992; Daly, 1998; Pakhomov et al., 2004), but a few are based on telson length (Ross et al., 2000, 2004); (2) uropods are not present on Calyptopis I and II; (3) if either the telson or uropod was damaged, the other could be used to predict growth; and (4) to provide a comparison of both measurements within one data set. The telson was measured in lateral view and the uropods in dorsal view. Care was taken to ensure that the telson and uropod were consistently at the same angle relative to the abdomen as this can affect measurements. All measurements were made by only one person (Daly) to further reduce measurement error. Samples were not preserved because formalin may cause a greater shrinkage in body length relative to uropod length (Miller, 1983).

Growth rates were expressed in several ways to facilitate comparison with other published values. The percent change in uropod or telson length between the post-molt krill and its molt was based on direct measurements and, thus, has the least amount of associated error. The change in body length ($mm\,d^{-1}$) over the intermolt period was determined from a Model I linear regression of body length (BL) on uropod (UL) or telson length (TL) for the post-molt krill. Because regressions for each experiment were not significantly different ($p > 0.05$), length measurements from all experiments were pooled. The regression based on uropod length was

$$BL = 7.11\ UL + 1.08,$$

where r^2 was 0.99 ($n = 260$). The regression using telson length was

$$BL = 4.44\ TL + 0.021,$$

where $r^2 = 0.97$ ($n = 146$). The premolt body length was estimated by substituting in molt values for *UL* or *TL*. The finite growth rate (d^{-1}) was calculated as the difference between the premolt and post-molt body lengths divided by the intermolt period (days). Growth rate in terms of dry weight and carbon and nitrogen also were calculated using the relationships shown in Table 1.

Prior to statistical analyses, data were tested for normality, and then appropriate parametric or non-parametric tests were used (Zar, 1984) and noted in the text or figure legends. Many of the data reported here were not normally distributed; therefore the median and range were used to describe the average or central trend of these data. This was particularly important for the growth measurements, where the mean often represented a negative growth rate when the central trend was zero growth or slightly positive. Where the mean is reported there was no difference between measures of central trend. The geometric mean was used for averaging percentage and ratio data (Zar, 1984).

Table 1
The seasonal relationships between body length (L), dry weight (DW), and body carbon (C) and nitrogen (N) of larval (C2–F6) *E. superba*

Season & year	Equation	r^2	n
	L vs. DW		
Fall 2001	$DW = 3.35 \times 10^{-3} L^{2.47}$	0.93	131
Winter 2001	$DW = 2.35 \times 10^{-3} L^{2.48}$	0.46	159
Fall 2002	$DW = 4.51 \times 10^{-2} L^{1.55}$	0.93	16
Winter 2002	$DW = 4.24 \times 10^{-3} L^{2.38}$	0.52	68
	DW vs. Carbon		
Fall 2001	$C = 418\,DW + 0.467$	0.99	52
Winter 2001	$C = 405\,DW - 34.4$	0.98	34
Fall 2002	$C = 406\,DW - 37.2$	0.98	9
Winter 2002	$C = 206\,DW + 54.8$	0.72	15
	DW vs. Nitrogen		
Fall 2001	$N = 85.2\,DW + 4.68$	0.99	52
Winter 2001	$N = 88.9\,DW - 7.01$	0.97	34
Fall 2002	$N = 83.3\,DW - 1.10$	0.99	9
Winter 2002	$N = 55.7\,DW + 15.0$	0.74	15

Length in mm, dry weight in mg, body carbon and nitrogen in μg, n is sample size.

3. Results

3.1. Seasonal and interannual environmental conditions

Sea-ice: During austral fall 2001, most of the study area was ice free except for the most southerly stations. By 13 May, Sta. 4 in George VI Sound had unconsolidated brash ice and many icebergs present, with some new grease ice being formed. Similarly at Sta. 3 in Lazarev Bay (21 May), new sea-ice formation was observed among the glacial rubble and brash ice. Some sea-ice was forming in other parts of the study area by the end of the cruise on 29 May. By the time we returned for the winter cruise on 27 July, most of the study area was covered by first year sea-ice, except for a small polynya (open area surrounded by sea-ice) to the southeast of Adelaide Island, which remained open much of the time.

In contrast, during autumn 2002 some sea-ice still remained from the previous winter, especially in the southern regions of Marguerite Bay, and new ice started forming in the southern end of the bay (Sta. 4) by 1 May. Much of the study area was covered with new and second year ice by the end of the cruise on 13 May. During the winter cruise, satellite images indicated that most of the study area was covered by ice; however, the stations in the inner bay were unobtainable due to ice conditions. Relatively large leads were observed throughout the area, and a small coastal polynya was encountered in the vicinity of Sta. 19 at the southwest end of Adelaide Island. Winter sea-ice extended northeast up along the Antarctic Peninsula and well out over the Drake Passage in both years (Fig. 1).

Seawater temperatures: Temperature variation, either spatially or between autumn and winter, probably did not strongly influence changes in larval physiology. During both fall cruises, sea-surface temperature varied less than 2 °C (−0.59 to −1.82 °C) at all locations where larval krill were collected for growth experiments, with relatively warmer temperatures being at Sta. 1 offshelf in Antarctic Circumpolar Current waters (Figs. 4 and 5). During winter, near-surface temperatures were similar (−1.75 to −1.82 °C) at all locations and between years. In both seasons, temperature increased with depth. The largest temperature gradient that larvae would experience if they occurred throughout the water column would be about 3 °C between surface and deep water.

Food availability: Chlorophyll concentrations in the water column were regionally and seasonally variable. A declining bloom was observed at several locations in both autumn 2001 (Stas 1 and 5) and 2002 (Stas 1, 2, and 4). The bloom species were primarily phaeodarian radiolarians and the diatoms, *Chaetoceros criophilum* and *Synedra antarctica*. The diatoms, *Fragilariopsis kerguelensis*, *Corethron criophilum*, and *Rhizosolenia hebetata*, also were present. In general, however, chlorophyll concentrations were relatively low in the water column during autumn in both years (Table 2). During autumn 2001, the median chlorophyll *a* concentration in the upper 100 m for all stations was $0.10\,\mu g\,l^{-1}$ (range: $0.02–0.52\,\mu g\,chl\,l^{-1}$), but if phaeopigments are included that value doubles (median: 0.23; range: $0.04–1.39\,\mu g$ pigment l^{-1}). On average about 60% of the total pigment was phaeopigments, indicative of phytoplankton senescence and grazing activity.

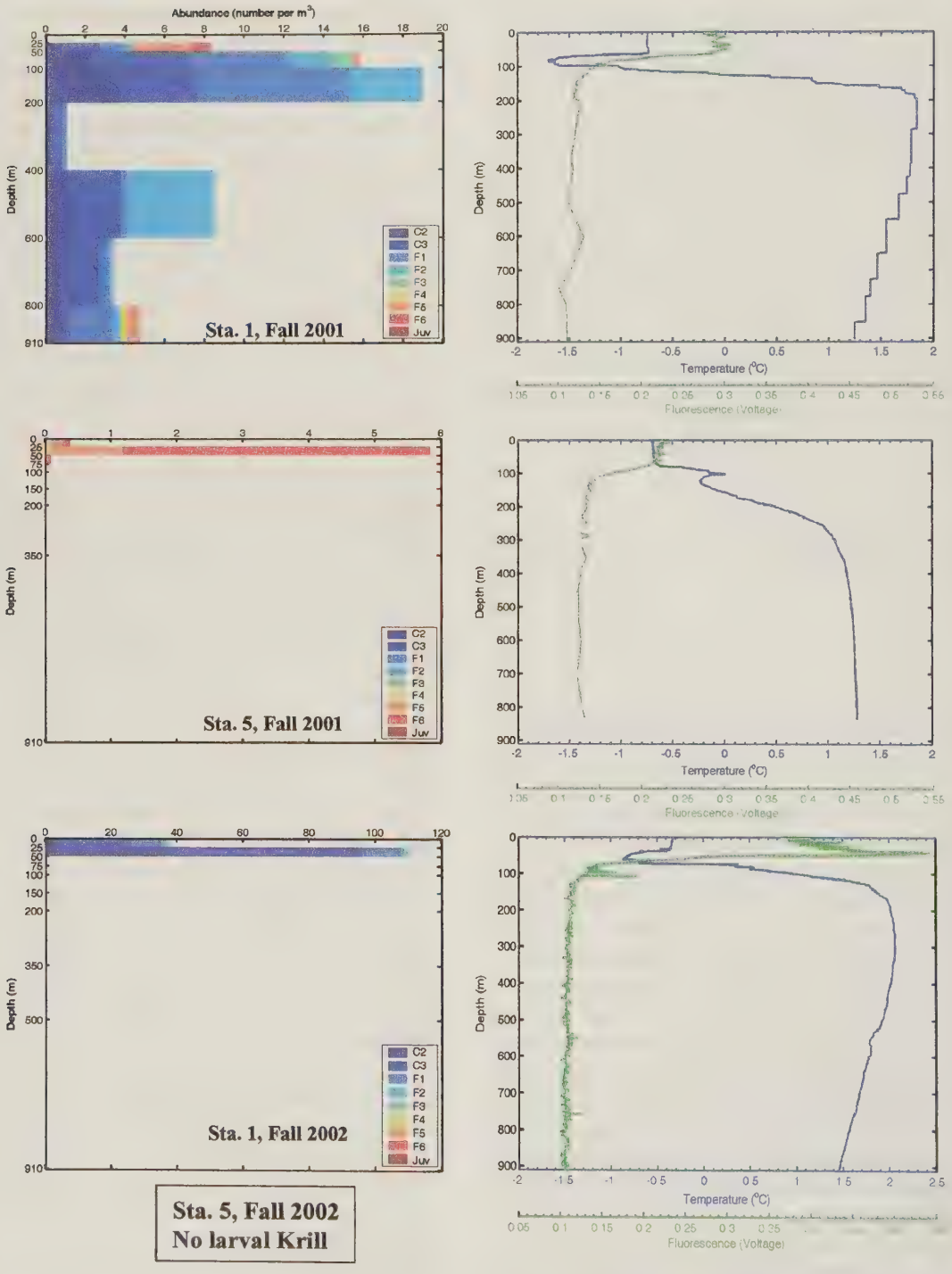

Fig. 4. Vertical distribution of larval stages of *E. superba* (left) in relation to seawater temperature and fluorescence (right) at Sta. 1 (offshelf) and Sta. 5 (inside Marguerite Bay) during autumn.

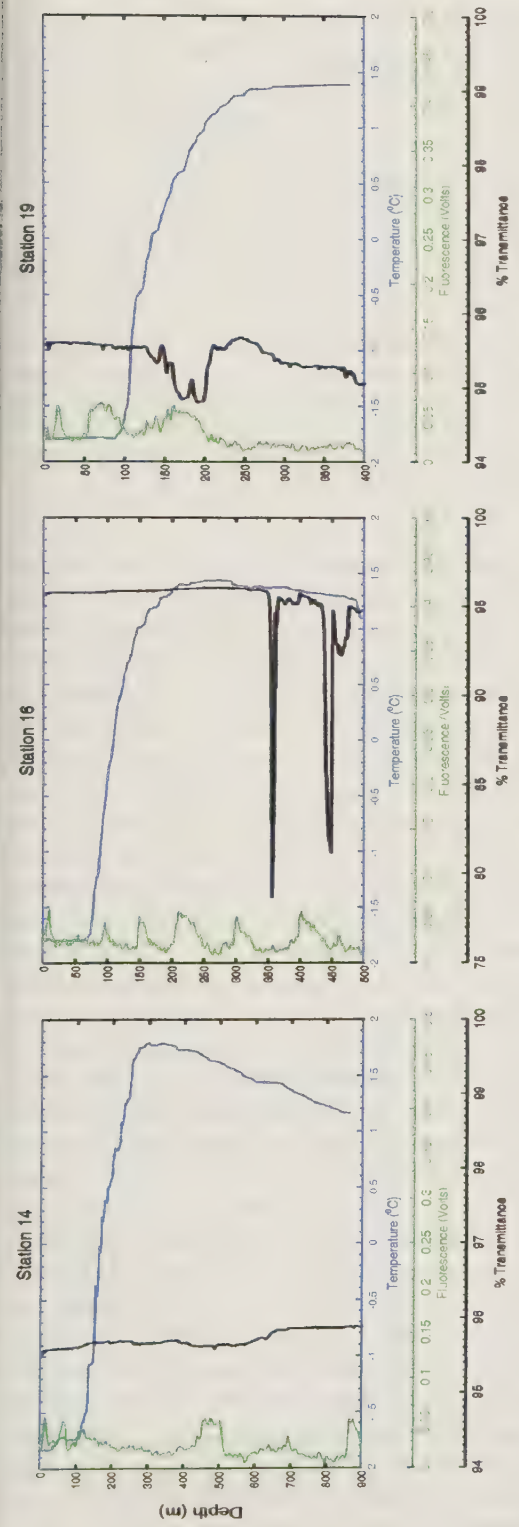

Fig. 5. Vertical profiles of temperature, fluorescence, and particle abundance from CTD casts at three stations across the northern shelf region of the study area in winter 2002. Transmissometer data was used to indicate particle density. Note the change in vertical scale between stations.

Table 2
Median integrated chlorophyll and phaeopigment concentrations ($mg\,m^{-2}$) within the study area during fall

Station	Fall 2001[a]			Fall 2002		
	n	Chl	Phaeo	*n*	Chl	Phaeo
1	6	18.4	29.7	3	35.7	12.2
2	3	4.47	9.76		0.61[b]	0.35[b]
3	3	4.87	11.7			
4	5	6.32	10.6	5	29.1	67.8
5	5	14.9	17.9	4	26.2	156
6				3	16.8	44.5
7				5	12.8	8.30

Pigments integrated 0–100 m, *n* is number of CTD profiles, Chl is chlorophyll *a*, Phaeo is phaeopigments *a*.
[a]Data provided by C. Fritsen.
[b]Surface concentrations ($\mu g\,l^{-1}$).

Integrated chlorophyll concentrations (0–100 m) were highest offshelf at Sta. 1, with the largest diatom concentration in the upper 25 m, and at Sta. 5 in Laubeuf Fjord (Table 2). Integrated pigment values were an order of magnitude lower at the more southerly stations. During autumn 2002, the median chlorophyll concentration in the upper 100 m of the water column was $0.22\,\mu g\,l^{-1}$ (range: 0.04–$1.50\,\mu g\,chl\,l^{-1}$), with phaeopigments averaging about 70% of the total pigment. Average integrated chlorophyll values were higher at all locations than those in 2001, possibly because sampling was about 2 weeks earlier in 2002. At the northern end of the study area, chlorophyll and total pigment maxima occurred below 500 m suggesting that a significant portion of the bloom had sunk out of the water column.

Winter chlorophyll concentrations were an order of magnitude lower throughout the water column than in autumn (Fig. 4 vs. Fig. 5). Median concentrations were $0.017\,\mu g\,chl\,l^{-1}$ (range: 0.001–$0.05\,\mu g\,chl\,l^{-1}$) in 2001 and $0.027\,\mu g\,chl\,l^{-1}$ (range: 0.001–$0.18\,\mu g\,chl\,l^{-1}$) in 2002, with phaeopigments concentrations about 50% and 38% of the total pigment in respective years. The vertical distribution of fluorescence in relation to temperature is shown for three stations across the northern shelf in 2002 to represent conditions in the study area (Fig. 5). Fluorescence was near the limit of sensor detection. In addition to phytoplankton,

detritus, glacial flour (24–260 μm), the pilidium stage of benthic nemerteans (0.5–1 mm diameter; 13–88 individuals $10\,m^{-3}$), larval polychaetes (1–2.5 mm in length), small larvaceans, fish larvae, ostracods, small pteropods, foraminifera, small amphipods, and large and small copepods were present in the 5–25 m depth interval under sea-ice where furcilia also occurred.

Food availability for larval krill on the undersurface of sea-ice also was assessed. During autumn 2001 there was little sea-ice in the study area. In contrast during autumn 2002, ice from the previous winter was still present in some locations and under some second year ice floes there was considerable accumulation of algal biomass as evidenced by golden coloration. Median ice algal chlorophyll concentrations in all types of sea-ice were about an order of magnitude higher (2.29 μg chl l^{-1}, range: 0.601–50 μg chl l^{-1}) than that found in the water column. During winter 2001, chlorophyll concentrations under sea-ice were relatively low (median: 0.05; range: 0.02–0.48 μg chl l^{-1}) and similar to that in the water column. During winter 2002, even though sea-ice formed much earlier in the autumn, chlorophyll concentrations on the undersurface of sea-ice, on average, were still relatively low at stations on the shelf outside the bay, with a median concentration of 0.07 μg chl l^{-1} (range: 0.016–3.14 μg chl l^{-1}). Because we were unable to sample the inner bay it is not known what ice algal concentrations were under that sea-ice. Total pigment (chlorophyll *a* + phaeopigments) concentrations in sea-ice biota tended to increase toward the northern end of the study area west of Adelaide Island, with the date of collection and latitude explaining about 40% of the variation in ice chlorophyll concentrations over the study area (Fig. 6).

Particulate organic carbon (POC) and nitrogen concentrations (PON) during autumn 2001 at the depth of the chlorophyll maximum were highest at Sta. 1 (range: 84.8–586 μg Cl^{-1}) and 4.52–46.3 μg Nl^{-1} and Sta. 5 (range: 56.2–156 μg Cl^{-1} and 8.94–28.5 μg Nl^{-1}) and lower at the more southern stations (Stas 3 and 4, range: 24.3–93.9 μg Cl^{-1} and 6.3–11.3 μg Nl^{-1}), following a pattern similar to that of chlorophyll. The median concentrations

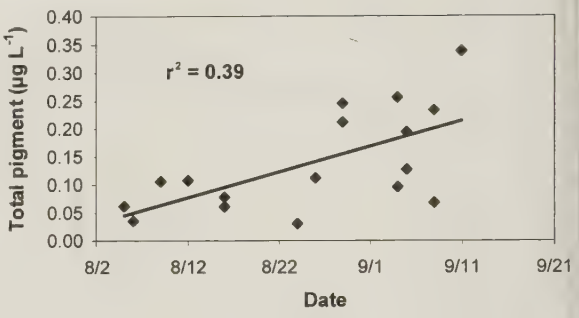

Fig. 6. The relationship between total pigment (chlorophyll + phaeopigment) concentrations on the undersurface of sea-ice and time of year (2002). Sampling was from southwest to northeast along the shelf, so that more northerly stations were sampled in late winter/early spring (i.e. September). Simple linear regression; $p < 0.05$.

for all samples were 56.3 μg Cl^{-1} and 9.59 μg Nl^{-1}, with an average C:N ratio of 6.9. During winter, the median POC and PON concentrations ($n = 7$) of water collected from the depths of particle maxima (determined by a transmissometer) were 262 μg Cl^{-1} and 11.7 μg Nl^{-1}. The concentrations in sea-ice biota, scraped from the undersurface of sea-ice where larval krill were feeding, were substantially higher (median: 544 μg Cl^{-1} and 33.7 μg Nl^{-1}). The highest concentration of larvae observed by divers was at Sta. 26 where POC/N concentrations in sea-ice biota also were highest (1225 μg Cl^{-1} and 27.2 μg Nl^{-1}). Winter C:N ratios were high (geomean: 27.8) in both the water-column and sea-ice samples and were significantly higher than ratios during autumn.

Particulate organic concentrations are only available from surface samples during autumn 2002. The median for all locations was 135 μg Cl^{-1} (range: 76.4–316) and 11 μg Nl^{-1} (range: 2.90–29.6). In contrast, the median concentration under year-old sea-ice, brash ice, and newly formed ice was 457 μg Cl^{-1} (range: 162–2076) and 71.8 μg Nl^{-1} (range: 18.7–291), with an average C:N ratio of 9.0. Larvae were only observed feeding under sea-ice at one location (Sta. 4) out of six dives. The winter vertical distribution of particulate material in relation to temperature and fluorescence are shown for three stations across the northern shelf in 2002 (Fig. 4). Particulate concentrations, as assessed by a

ransmissometer, were generally very low, with nost depths having a greater than 90% light ransmittance. Transmissometer maxima, and oc-asionally fluorescence maxima, were associated vith density features. Sampling of particle maxima rom a few stations showed a range of relatively ow values (35–200 μg Cl^{-1} and 2.83–13.6 μg Nl^{-1}). The median concentrations under sea-ice were 252 μg Cl^{-1} (range: 54–454) and 23.8 μg Nl^{-1} (range: 3.16–42.6). The average C:N ratio for he water column and sea-ice was 13.6 (geomean).

3.2. Larval abundance and distribution

The seasonal stage composition of larvae was similar between 2001 and 2002, but the abundance and depth distribution of stages varied by location in the study area and between years. Larval depth distributions based on discrete-depth 1 m^2 MOCNESS tows at Stas 1 and 5 are shown for autumn 2001 and 2002 to illustrate the contrast between offshelf and on-shelf stations and the difference between years (Fig. 4). During autumn 2001, larvae were very abundant throughout the study area where densities were on the order of 1–19 individuals m^{-3}. At the offshelf station (Sta. 1) where densities were highest (5627 individuals m^{-2}), younger stages (C2–F2) were nine times more abundant than older larvae (F3–F6). C3–F1 and F5 were the dominant modes suggesting that there were at least two reproductive pulses during the previous summer. Larvae were found in net samples between 25 and 910 m (the 0–25 m tow malfunctioned); however, the highest densities of younger stages were concentrated between 50 and 200 m in relatively warmer water but lower chlorophyll concentrations. The older stages were most abundant between 25 and 100 m. Many small larvae in the 800–910 m net appeared to have died prior to net collection, based on observations of an intact exoskeleton with internal body deterioration, and may have been sinking into deep water. These individuals were not included in the figure.

Onshore and inside Marguerite Bay, older larvae were more common and often concentrated in a narrow layer near surface. For example at Sta. 5 in Laubeuf Fjord, only F4–F6 larvae were found in net samples, with F6 having five-fold higher densities. Larvae were collected between 0 and 75 m, but were most abundant (ca. 6 m^{-3}) in the 25–50 m net in association with colder water and higher chlorophyll concentrations (Fig. 4). *E. superba* larvae were the dominant component of this sample both numerically (62%) and by weight (78%). Acoustic echograms give a more detailed picture of larval distribution in this depth interval, suggesting that most furcilia occurred in a highly aggregated, narrow layer at about 30 m depth, vertically separated from other deeper scattering organisms (Fig. 7). Because this spatial pattern was observed at many locations in the bay, food concentrations at these shallow depths were likely to be the most critical for larval growth rates during autumn 2001.

During winter 2001, F6 was the dominant stage. Furcilia were observed feeding on the undersurface of sea-ice at all seven dive sites, with the highest densities at Stas 5 and 26 at the northern end of the study area. The 2001 winter depth distributions of euphausiids are reported in Ashjian et al. (2004).

In general, larval densities were substantially lower throughout the study area during 2002. Although high densities were observed offshelf in

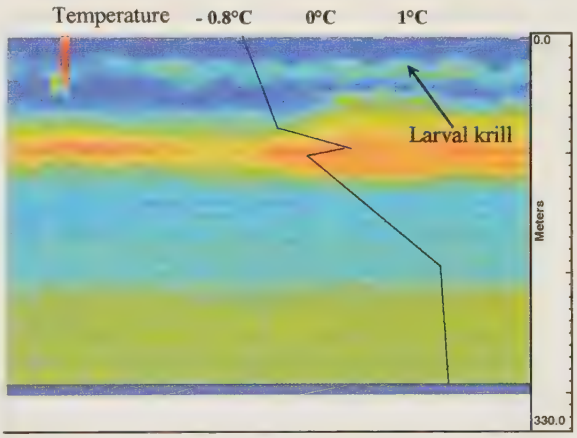

Fig. 7. Acoustic volume backscattering shows the narrow depth distribution of larval *E. superba* in relation to seawater temperature at Sta. 5 in Laubeuf Fjord during austral autumn 2001. Backscattering data were collected using a 120 kHz Hydroacoustic Technology Inc. Model 244 split-beam echosounder (Daly, unpublished). Depth scale, surface to 330 m. Net tows confirmed that the layer was primarily composed of krill larvae.

the Antarctic Circumpolar Current (Sta. 1), larvae were scarce at most locations on the shelf (Fig. 4). During autumn, C3 was the dominant stage offshelf and densities of the C2–F4 larvae were somewhat higher than in 2001 (0.01–110 m^{-3}; 3731 individuals m^{-2}). In contrast to the dispersed vertical distribution in 2001, larvae were concentrated near surface where the late fall diatom bloom was located. Many dead larvae were observed again, but this time in the 0–25 m net samples, along with larvae in good condition. The depth of maximum larval abundance was 25–50 m, in colder surface water and higher fluorescence. No *E. superba* larvae were found at Sta. 5 inside Marguerite Bay. The dominant overwintering stage was again F6; however, the 2002 individuals were not strongly associated with the undersurface of sea-ice. Krill larvae were observed near the undersurface of sea-ice in relatively low densities at only six out of nine dives. When few larvae were observed under sea-ice or in MOCNESS tows, we deployed Reeve and Rings nets in the upper 25 m where larvae were likely under-sampled by the MOCNESS. These net samples showed that *E. superba* larvae occurred consistently between 5 and 25 m in depth, albeit at low densities (2–23 furcilia $10\,m^{-3}$), coincident with benthic larvae, diatoms, and radiolarians. Larval densities were generally higher at the northern end of the study area (Stas 4, 13, 17, 26), west of Adelaide Island, than in the southern region.

3.3. Feeding behavior

Many furcilia had green or dark-colored guts and hepatopancreas during autumn, implying that they were feeding on plant material, while other larvae had off-white colored guts, presumably from feeding on microzooplankton or detritus. During winter, furcilia gut color ranged from no color (i.e. empty) to light green and off-white. Since chlorophyll *a* is not a conservative tracer of gut processes in *E. superba* (Daly, 1998), gut pigment values reported here are only intended to be a relative index of herbivory to assess potential feeding on phytoplankton and/or sea-ice algae. During autumn 2001, furcilia collected in the upper 50 m of the water column throughout the study area on average contained 7.62 ng pigmen individuals^{-1} (range: 1.92–54.3 ng pigment in dividuals^{-1}, $n = 58$). Furcilia collected feeding under recently formed pancake ice at Sta. 3 had lower gut fluorescence (3.47 ng pigment in dividuals^{-1}, range: 1.56–6.46, $n = 25$). Winter values were even lower and were similar for furcilia collected from the water column and from under sea-ice [1.57 ng pigment individuals^{-1} (range: 0.52–7.44, $n = 23$) versus 1.63 ng pigment individuals^{-1} (range: 0.57–3.16, $n = 21$)]. During autumn 2002, average gut pigment was 28.4 ng individuals^{-1} for only two groups measured since larvae were scarce. During winter 2002, most furcilia were collected in the upper 25 m of the water column. Furcilia gut pigment was relatively low in most locations (2.27 ng pigment individuals^{-1}, range: 0.86–5.67, $n = 5$), but much higher at Stas 11 and 13 (51.3 ng pigment individuals^{-1}, range: 19.8–70.7, $n = 4$) in early September, when ice algal concentrations were increasing (Fig. 6). The few groups of larvae collected feeding on the undersurface of ice averaged 2.48 ng pigment individuals^{-1} (range: 0.62–4.61, $n = 3$).

Observations from experiments and microscopic examination of gut and fecal pellet contents suggest that furcilia are efficient scavengers, capable of ingesting most available small particles in the water column or under sea-ice, including phytoplankton, sea-ice biota, molt exuviae, detritus, and microzooplankton. Because much of the detritus was aggregated and sticky, many small particles such as glacial flour also were ingested.

3.4. Length, dry weight, and carbon and nitrogen content of larval stages

The average size of larval stages varied between seasons (Table 3). Mean lengths of F4–F6 were significantly larger ($p<0.05$) during autumn (April–May) than during winter (August) in both years, but were similar between years for respective seasons. Dry weights also showed a significant decrease ($p<0.05$) between autumn and winter in both years as a function of both larval stage (Table 4) and length (Fig. 8A and B). Larval dry weights, however, were significantly higher

Table 3
Comparison of mean (± SD or range) length (mm) of *E. superba* calyptopis (C), furcilia (F), and Y0 juvenile (<14 mm) stages between seasons and years

Location, season & year	Stage								
	C2	C3	F1	F2	F3	F4	F5	F6	Juvenile
This study									
Fall 2001	3.00±0.39 (23)	3.72±0.49 (66)	4.42±0.71 (55)	5.53±1.01 (36)	7.43±1.21 (21)	8.85±1.22 (43)	9.99±1.15 (77)	11.68±1.58 (107)	0
Winter 2001						7.56±0.89 (5)	8.57±1.54 (58)	10.4±1.4 (268)	11.9±1.4 (66)
Fall 2002	2.41±0.37 (38)	3.21±0.35 (48)	5.19±0.94 (40)	6.38±0.69 (36)	7.32±0.62 (45)	8.85±0.94 (22)	9.84±0.56 (16)	11.0±0.0 (4)	0
Winter 2002						7.21±0.64 (28)	8.23±0.73 (37)	9.82±1.43 (27)	11.5 (1)
Other published data									
Lab[a]	2.90±0.14	4.26±0.00	5.38±0.29	6.65±0.35	8.24±0.06	8.82±0.18	9.60±0.23	10.66±0.23	
Gerlache St.,[b] Jan.–Mar. 1987		4.4	6.1	7.1	8.2	9.7			
Bransfield St.,[b] Jan.–Mar. 1987		4.0	5.5	6.9	7.8	9.0			
Drake Passage,[b] Jan.–Mar. 1987		3.81	4.9	6.2	7.4	8.3			
Marguerite Bay,[c] Feb–Mar, 2000		4.7±0.1	6.1±0.2	7.2±0.1					
Bransfield St.,[d] March 1984	3.35±0.02	4.21±0.35	5.33±0.26	6.35±0.62	7.11±0.41	7.75±0.18	9.30		
Scotia Sea,[d] March 1984	2.99±0.35	4.35±0.40	5.42±0.48	6.80±0.29	7.78±0.27	7.64			
N Elephant Is.,[d] March 1984	3.08±0.23	4.32±0.36	5.50±0.64	6.39±0.56	7.37±0.48	8.05±0.34	9.09±0.06		
Scotia Sea,[e] April 1928	2.88 (2.5–3.07)	4.15 (3.77–4.67)	5.15 (4.17–6.00)	6.32 (5.33–6.87)	7.46 (6.33–8.50)	8.37 (6.67–9.46)	9.45 (8.25–10.83)	10.49 (9.25–11.96)	
Circumpolar,[e] August 1928								10.11 (8.00–11.00)	
Scotia Sea,[f] August 1988						7.00	8.40±0.54	10.17±0.97	

Sample size in parentheses.
[a]Ikeda (1984).
[b]Huntley and Brinton (1991).
[c]Meyer et al. (2003).
[d]Brinton et al. (1986).
[e]Fraser (1936).
[f]Daly (1990).

Table 4
Comparison of mean (± SD) or range of dry weights (mg) of *E. superba* calyptopis (C), furcilia (F), and Y0 juvenile (<14 mm) stages between seasons and years

Location, season & year	Stage								
	C2	C3	F1	F2	F3	F4	F5	F6	Juvenile
This study									
Fall 2001		0.150±0.030 (18)	0.277±0.247 (9)	0.247±0.057 (8)	0.684±0.239 (10)	0.811±0.303 (36)	1.15±0.35 (34)	2.04±0.75 (32)	
Winter 2001						0.378±0.091 (3)	0.321±0.131 (15)	0.892±0.435 (103)	1.79±0.32 (3)
Fall 2002	0.180±0.067 67 (2)	0.358±0.11 (2)		0.488 (1)	0.770±0.304 (2)	1.17±0.082 (3)	1.92±1.92 (3)	2.27±0.22 (2)	
Winter 2002						0.514±0.274 (8)	0.809±0.416 (10)	1.08±0.51 (26)	2.1 (1)
Other published data									
Gerlache St.,[a] Jan.–Mar. 1987		0.437	0.500	0.706	0.882	1.12	1.25		
Bransfield St.,[a] Jan.–Mar. 1987		0.059	0.323	0.397	0.500	0.823			
Drake Passage,[a] Jan.–Mar. 1987		0.058	0.059	0.323	0.353	0.529			
Marguerite Bay,[b] Feb.–Mar. 2000		0.219±0.039	0.340±0.061	0.509±0.084					
Lazarev Sea,[c] Apr. 1999					0.335–0.400				

Sample size in parentheses is the number of groups of individuals measured for C2 F3, or number of individuals for F4–F6.
[a]Huntley and Brinton (1991).
[b]Meyer et al. (2003).
[c]Meyer et al. (2002).

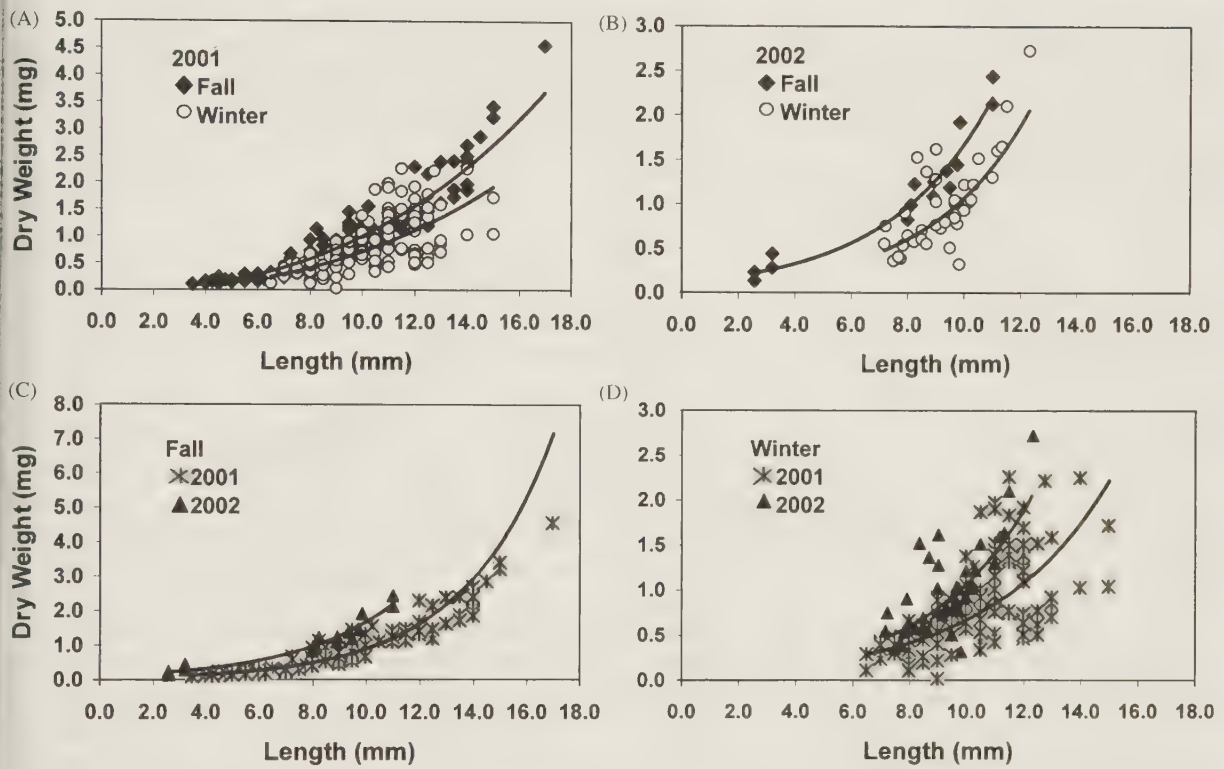

Fig. 8. Comparisons of the relationships between dry weight and length of larval *E. superba* between fall and winter in 2001 (A) and 2002 (B), and between both autumns (C) and winters (D) in each year. Regression relationships are shown in Table 1.

($p<0.05$) in 2002 compared to weights of larvae in 2001 (Fig. 8C and D). The similarity of F4 and F5 weights in winter 2001 (Table 4) was probably due to the small sample sizes as larvae were scarce and the broad range of winter weights. Fig. 8 data also suggest that the seasonal weight decrease was greater for larger larvae. Based on seasonal dry weight to length regressions (Table 1), the decline in dry weight for a 10 mm individual over 91 days, using 15 May and 15 August as arbitrary seasonal midpoints, was on the order of 0.003 mg DW d^{-1}, or about 0.3% of body DW d^{-1}, in 2001 and almost twice that in 2002.

Body carbon and nitrogen, as a percent of dry weight, was similar among larval stages C3–F6 (no data for C2) within each season, so stage data were pooled. The geometric mean percent C significantly decreased ($p<0.05$) between autumn and winter in both years, while N significantly decreased between seasons in 2001 but not in 2002 (Table 5). The percent decline in C and N between seasons was similar to that of dry weight. The mean percent C and N for all stages was not significantly different between fall 2001 and 2002, but percent C was significantly lower during winter 2002 than in 2001 ($p<0.05$), while nitrogen was not. The effects of starvation on dry weight and body C and N of winter F4–F6 were experimentally determined (Fig. 9). A substantial number of larvae (>30) survived and continued to molt for a 27-day period during which they were held without food. Numerous individuals were frozen at regular intervals throughout the experiment. Mortality did occur, but was not quantified. On average a starved 10-mm larva decreased 0.009 mg DW d^{-1}, 6.49 μg C d^{-1}, and 0.927 μg N d^{-1}. This is equivalent to about 1% of body DW, 1% of body C, and 1% of body N d^{-1}. Larger larvae experienced a greater weight loss than smaller larvae, similar to that observed in the 2001 field samples.

Table 5
Mean seasonal body carbon and nitrogen content and the C:N ratios for larval *E. superba*

	Fall 2001	Winter 2001	Fall 2002	Winter 2002
n	52	35	24	38
% Carbon	41.2	34.7	37.5	28.2
	(32.6–63.6)	(26.4–45.7)	(35.5–42.2)	(21.2–40.9)
% Nitrogen	9.21	7.66	8.27	7.52
	(7.59–12.1)	(5.00–9.00)	(7.73–8.73)	(5.36–9.86)
C:N	4.47	4.53	4.49	3.74
	(3.44–5.60)	(4.10–6.56)	(4.35–5.17)	(3.55–4.63)

C and N given as percent of dry weight, *n* is sample size, range in parentheses.

3.5. Larval development

Larval krill showed evidence of delayed development, especially during winter. During autumn, almost all of the youngest stages (C2–Fl, and F3) developed to the next larval stage when molting (Table 6). Very few showed indirect development to an intermediate or variant form based on telson spine morphology. However, older furcilia (F2, F4–F5) occasionally remained at the same stage when they molted even during autumn. This indirect or delayed development was most prevalent in F6 individuals during autumn, and the dominant behavior during winter. Even though larvae continued to molt in winter, 87% and 88% of the F6s in 2001 and 2002, respectively, did not develop to the juvenile stage during the study period.

Incomplete molting may have been an important source of mortality for C2–F5 stages, where the molt remained partially attached to the larvae and often resulted in death after several days. Incomplete molting occurred in 12% of the larvae (F1–F5) in growth experiments during autumn 2001 and in 50% of the larvae (C2–F3) during autumn 2002 at the offshelf station. No F6 showed evidence of incomplete molting.

3.6. Molting and growth rates

Larval krill continue to molt during autumn and winter. The intermolt period (IMP) varied, but in general the number of days between molting was shorter during autumn and increased during winter (Table 7). The median IMP for both years was 19 days in autumn and 40 days in winter. Multiple linear regression analysis ($p<0.001$) indicated that about 43% of the variation in the IMP between seasons was explained by sea-surface temperature and surface chlorophyll concentrations.

Both uropod and telson measurements were evaluated in order to determine their usefulness in estimating larval growth or shrinkage and to determine whether the results of the two methods were comparable. Uropods were less frequently damaged (ca. 2%) than the telson (ca. 18%) during molting, thus making uropods a more reliable measure. Telson and uropod lengths were compared for 56 larvae (F4–F6 and Y0 juveniles) during winter, when accurate measurements are critical to determine whether growth or shrinkage occurs. Both the right and left uropod exopodites also were measured on 21 of these larvae to assess the variability of that measure. The results show that the percent change in telson length was not correlated with the percent change in length of either uropod (left: Spearman $r_s = 0.13$, $p = 0.57$; right: $r_s = -0.21$, $p = 0.40$), whereas the percent change in right and left uropods was highly correlated ($r_s = 0.90$, $p<0.001$). The average difference in the percent change in length between the right and left uropod was 1.5% (range: 0–2.3%). The telson measurements also indicated negative growth 7% more frequently than did the uropod. These differences may be explained by the fact that the telson of the post-molt krill has a larger volume than the telson of the molt, while the uropods are relatively flat in both. Consequently, it is more difficult to accurately measure a small

change in length on a telson. Although the differences between telson and uropod measurements were relatively modest, small differences may result in very different interpretations of larval growth, particularly in winter. Lastly, uropod length was consistently a better predictor of total body length, based on R^2 values from Model I linear regressions (see Methods section). For these reasons and because the uropod was used more frequently in published growth studies, I used uropod length to estimate growth.

Larval growth rates were variable during autumn and were significantly lower ($p<0.001$) in winter, decreasing to near zero in both years (Fig. 10). Because larvae were scarce in 2002, there were only three growth experiments. The rates measured in the last experiment in September were significantly higher ($p<0.001$) than other winter rates. There was no significant difference ($p>0.05$) in growth rates, based either on percent change in uropod length or on calculated growth (mm d^{-1}), among stages or length of larvae within seasons.

Table 6
Percentage of larval *E. superba* following direct and indirect developmental pathways

Larval stage	Fall 2001		Winter 2001		Fall 2002		Winter 2002	
	%D	%I	%D	%I	%D	%I	%D	%I
C2					100			
C3					100			
F1	100				100			
F2	67	33			100[a]			
F3	100							
F4	92	8						
F5	91	9	100[a]				67	33
F6	4	96	13	87			12	88

D is direct development to the next stage (i.e., F4→F5) and I is indirect development to the same stage or an intermediate form (i.e., F4→F4) when molting. C is calyptopis, F is furcila.
[a]One individual.

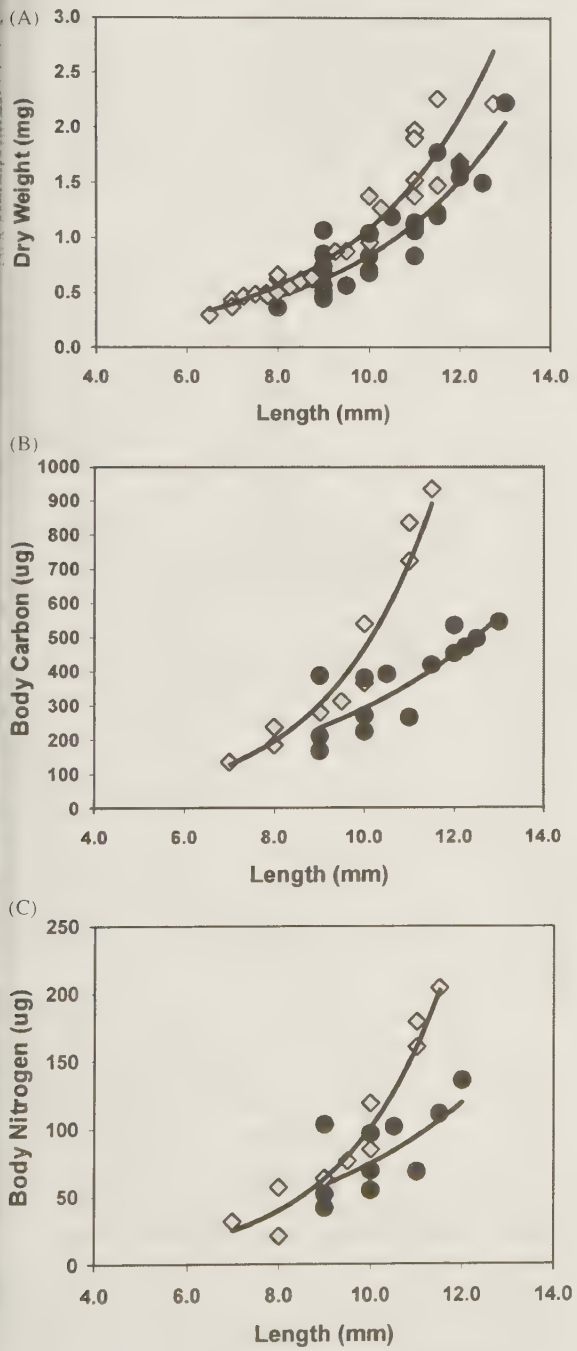

Fig. 9. Decrease in dry weight (A), body carbon (B), and body nitrogen (C) of starved larval *E. superba*. Initial condition of furcilia 4–furcilia 6 larvae on 28 July (diamonds) contrasted with larval condition on 24 August 2001 (circles). Regression relationships for Day 1 and Day 27 are: (A) $DW_{t1} = 0.039e^{0.332L_{t1}}$ ($r^2 = 0.95$, $n = 29$) and $DW_{t27} = 0.042e^{0.298L_{t27}}$ ($r^2 = 0.76$, $n = 31$), (b) $C_{t1} = 6.24e^{0.431C_{t1}}$ ($r^2 = 0.95$, $n = 10$), $C_{t27} = 33.4e^{0.217C_{t27}}$ ($r^2 = 0.63$, $n = 10$), and (c) $N_{t1} = 0.965e^{0.465N_{t1}}$, ($r^2 = 0.86$, $n = 10$), $N_{t27} = 7.01e^{0.236N_{t27}}$ ($r^2 = 0.42$, $n = 10$).

Table 7
Growth and intermolt period (IMP) for larval and first-year (Y0) juvenile *E. superba*

Sta.	SST (°C)	Chl ($\mu g l^{-1}$)	Larval stages	*n*	IMP (d)	% Change in uropod length	Growth rate ($mm d^{-1}$)
Fall 2001							
1	−0.59	0.37	F1–F6	13	19	8.5	0.030
1	−0.59	0.37	F1–F2	3	—	—	—
2	−0.82	0.22	F5–F6	16	17	8.31	0.020
2	−0.82	0.22	F2–F5	6	18	8.01	0.020
3	−1.75	0.08	F5–F6	20	20	7.02	0.036
4	−0.87	0.08	F4–F6	11	40	1.62	0.013
5	−0.64	0.09	F5–F6	16	18	5.94	0.030
Fall 2002							
	−0.20	0.35	C2–F3	16	21	6.9[a]	0.013
Fall median for both years				82	19	6.52	0.027
Winter 2001							
5	−1.75	0.05	F6	15	23	0.00	0.000
17							
26	−1.79	0.04	F5–F6	10	51	0.00	0.000
51	−1.81	0.04	F5–Juv	11	31	1.63	0.005
Winter 2002							
	−1.83	0.05	F6–Juv	12	40	4.25	0.013
	−1.82	0.03	F4–Juv	9	61	0.00	0.000
Winter median for both years					40	0.00	0.00

Growth is given as the median percent change in the length of uropods on all pairs (a krill and its molt) of molted individuals over the IMP and as the median daily growth rate. Sea-surface temperature (SST) and chlorophyll (Chl) concentrations at each location are shown. Larval stage *F* is furcilia, Juv is juvenile, *n* is number of molted individuals.

[a]Uropods damaged, used telson length.

There also was no significant difference in rates between years for each season (e.g., autumn 2001 vs. autumn 2002), therefore the rates from the 2 years were combined. The median IMP and growth rates for autumn and winter are shown in Table 7. The percent uropod change in length is shown because it is a direct measurement of growth, whereas the growth in terms of $mm d^{-1}$ was calculated and therefore subject to additional uncertainty. Using the relationships in Table 1 and the average daily growth rate ($0.027 mm d^{-1}$), the estimated daily weight increase for a 10 mm furcilia in autumn 2001 is about $6.75 \mu g DW d^{-1}$, $2.82 \mu g C d^{-1}$, and $0.575 \mu g N d^{-1}$.

Because the variance in field rates is likely more important than an average rate in understanding population dynamics, the histograms of growth rates for autumn and winter are shown in Fig. 11. Only a small percentage of the larval population had negative growth (1.3%) during autumn, while 37% showed a 0–5% increase in uropod length and the majority (55%) had a 6–15% increase in

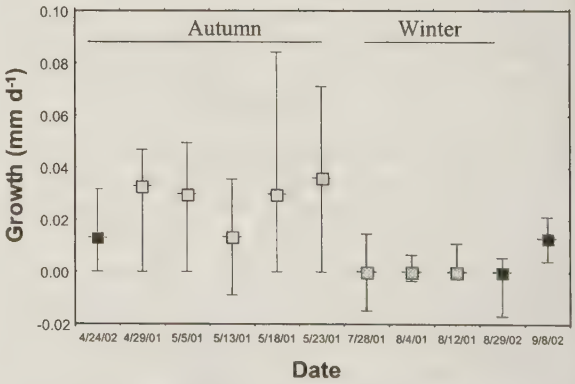

Fig. 10. Seasonal change in median growth rates for larval *E. superba* during autumn and winter in 2001 (gray boxes) and 2002 (black boxes). The vertical bars indicate the range.

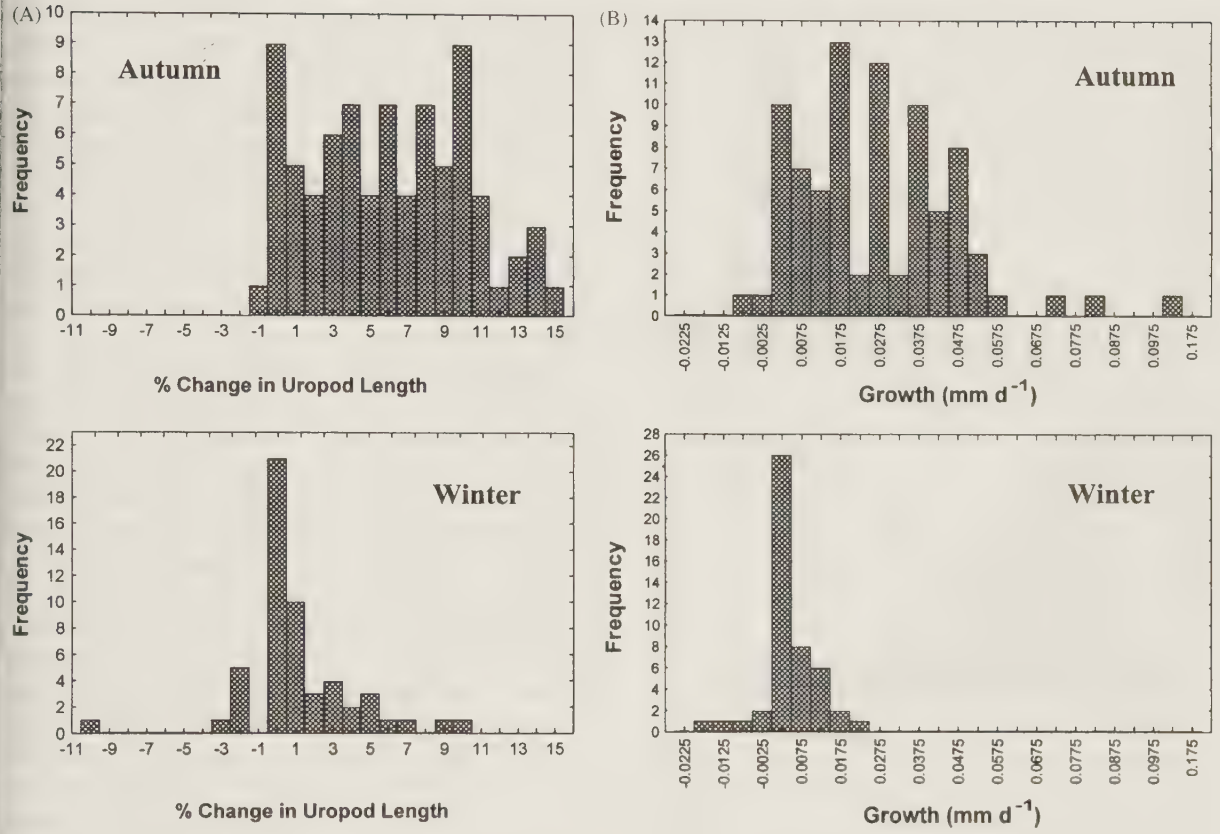

Fig. 11. Histograms of growth rates of larval *E. superba* to show the seasonal variation and range of values for (A) percent change in uropod length and (B) calculated growth rates (mm d^{-1}) during autumn and winter.

uropod length upon molting. During winter about 13% of the larvae had negative growth, 57% showed 0–1% growth, and 30% had a 2–10% increase in uropod length.

3.7. Recruitment

A substantial number of larvae appeared to survive overwinter and recruit to the juvenile class during spring 2001. The evidence for recruitment is that during autumn and winter 2001 there were few intermediate sized krill (20–40 mm) in the study area and all of these were immature adults and therefore probably not recruits in their second year; none were juveniles (Fig. 12). During autumn and winter 2002, however, there were a significant number of small to intermediate sized krill and many of these were juveniles, as well as immature adults. Although we do not know with certainty that these juveniles came from Marguerite Bay, their presence indicates that larvae survived overwinter somewhere in the general vicinity.

4. Discussion

Juvenile recruitment of *E. superba* in spring on the western Antarctic Peninsula shelf depends on several factors: (1) successful adult reproduction and larval survival during the prior summer, (2) entrainment onto the shelf of young larvae spawned offshore, (3) larvae retained on-shelf, and (4) survival of older larvae overwinter. In both autumn 2001 and 2002, larval abundances at the

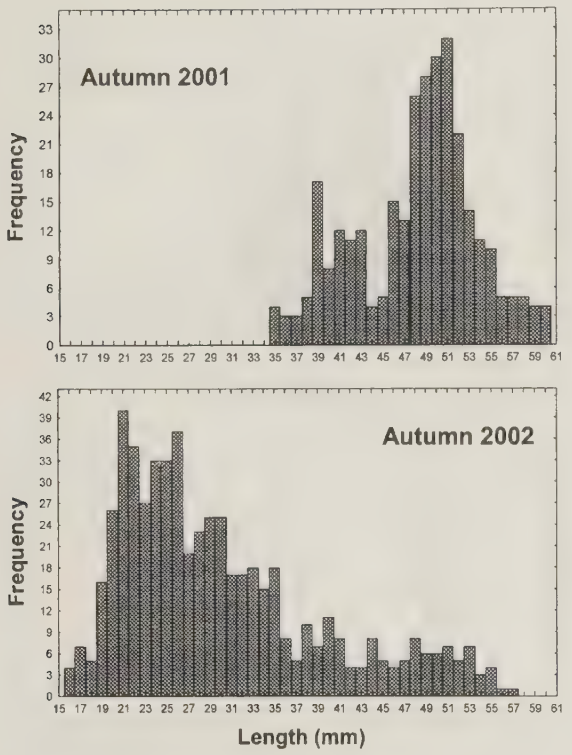

Fig. 12. Length-frequency of *E. superba* collected in net tows in autumn 2001 and autumn 2002 to show the recruitment of juvenile krill (15–30 mm in length) in 2002 resulting from overwintering 2001 larvae.

offshelf station in the Antarctic Circumpolar Current (ACC) are within the range of those reported for 1980–1981 (Brinton et al., 1986; Kittel and Jażdżewski, 1982), a year noted for high krill recruitment (Siegel and Loeb, 1995). Our larval densities suggest that there was successful adult reproduction during both summers prior to the GLOBEC cruises, but the timing and extent of summer reproduction may have varied between the two years. *E. superba* undergo a long, complex larval development (Fraser, 1936). Based on a laboratory study (Ikeda, 1984), calyptopis I (CI) larvae appear about 30 days and furcilia 6 (F6) larvae appear about 120 days after hatching. In April and May 2001, late stage furcilia were common throughout the study area, indicating that reproduction probably started in December and that larvae were retained on the shelf. A second mode of smaller larvae occurred offshelf suggesting that spawning continued into March. Pakhomov et al. (2004) observed higher larval densities, but a similar distribution of stages (i.e. later stages dominant over the shelf) a few weeks earlier in April. The lack of larvae on-shelf and the dominance of small larvae (C3) offshelf in April 2002 indicate that spawning may have started late in 2002, that earlier spawned larvae had poor survival, or that larvae were advected downstream in the ACC.

During our cruises, the ACC was observed to pump circumpolar deep water onto the shelf where the Marguerite Trough intersects the shelf break (Klinck et al., 2004). This episodic exchange was detected previously in this region (Hofmann and Klinck, 1998) and may be one mechanism whereby krill are entrained onto Antarctic shelves in general (Prézelin et al., 2000; Endo et al., 2002). The highest concentrations of larvae during winter 2002 were found on the shelf west of Adelaide Island. Another winter study noted a similar distribution pattern, with the highest concentrations of larvae along the outer shelf west of Adelaide Island and along the shelf break to the northeast (Siegel, 1989). There also was a large gyre on-shelf in the study area and sluggish circulation in the middle of the bay, which may act to retain larvae (Klinck et al., 2004; Beardsley et al., 2004). The combination of physical and biological processes that led to enhanced larval abundance in the study area during autumn 2001 may not have been as strongly developed or occurred at different times in 2002. Even though larvae were abundant during autumn 2001, net densities (Ashjian et al., 2004) and acoustic backscattering (Lawson et al., 2004) indicate that the abundance of all zooplankton in the study area significantly decreased between autumn and winter possibly due to advection and/or mortality.

4.1. Autumn and winter food limitation

Many factors influence krill overwintering survival. The ability of an individual furcilia to withstand a suboptimal winter environment, in part, will be a function of its body size, weight, and composition (e.g., lipid storage) at the end of the

productive season. Larger, more developed larvae with considerable lipid storage should be in better condition or more robust than smaller individuals with little lipid. Growth and development rates, as well as an assessment of an individual's condition at any point in time, reflect an integration of the environment experienced by that individual over a period of weeks prior to collection. Huntley and Brinton (1991) provided evidence from a summer field investigation that regional variability in larval body size, weight, growth, and development was positively correlated with higher food concentrations. Since chlorophyll concentrations are typically higher on-shelf than offshelf west of the Antarctic Peninsula during summer (Huntley and Brinton, 1991; Smith et al., 1996), on-shelf larvae may be in better condition to overwinter in this region.

Body length and weight: A comparison of body length (Table 3) and body weight (Table 4) among larvae collected during late summer, autumn, and winter in different locations, or raised in a laboratory supports this hypothesis and indicates that GLOBEC larvae collected over the shelf were in better than average condition prior to winter. Larvae with the largest size and highest dry weights were collected from Gerlache Strait (north end of the Antarctic Peninsula) during March, where integrated (0–50 m) chlorophyll *a* values averaged about 150 mg m^{-2} between January and March (Huntley and Brinton, 1991), and from inner Marguerite Bay (5–25 μg chl *a* l^{-1}) in February and March (Meyer et al., 2003). Furcilia collected from Bransfield Strait and the Drake Passage, however, had lower dry weights, concomitant with a substantially lower food supply (integrated chlorophyll $\leqslant$50 mg m^{-2}). F3s collected during April in the Lazarev Sea had dry weights similar to those from the Drake Passage, although April chlorophyll concentrations in the surface mixed layer were substantially lower (0.06–0.09 μg chl *a* l^{-1}) and more typical of winter concentrations (Meyer et al., 2002b). The dry weights of these larvae suggest that food availability may have been higher during the preceding summer. Pakhomov et al. (2004) found integrated chlorophyll values during early April 2001 ranging from 15 to 165 mg m^{-2}, with the highest values occurring over the shelf. They also estimated relatively high carbon ingestion rates (16.5–44.5% body C d^{-1}) for larval krill. Thus, summer chlorophyll values in Marguerite Bay may be similar to those in Gerlache Strait, providing a favorable environment for larval growth. Late April and May chlorophyll values in Marguerite Bay were an order of magnitude higher than those in the Lazarev Sea during April, which is at a higher latitude than Marguerite Bay.

During GLOBEC, young (C2–F1) larvae were collected primarily offshelf and were either similar to or smaller than individuals collected by other investigators in the Scotia Sea and from the northern Antarctic Peninsula region during March and April. The dry weight of these young larvae provides further confirmation of poor feeding conditions offshelf. Based on both length and weight, the larger GLOBEC furcilia (F4–F6), which were collected primarily on-shelf, appeared to be in similar or better condition than larvae reported from other regions or from the lab study, except for the Gerlache larvae or Marguerite Bay larvae collected during late summer 2000. The higher gut pigment values in autumn compared to that in winter suggest that the declining bloom and prevalent microzooplankton on the shelf may have further enhanced late summer and fall larval growth and development prior to overwintering.

There are few winter data to compare larval size or weight, particularly in relation to food availability. The length of winter F6 larvae (the dominant stage), collected from the water column and under sea-ice, either were similar to or slightly smaller than larvae reported from other winter studies at more northern Southern Ocean latitudes (Table 3). Both the average water-column (0.1 μg l^{-1}) and sea-ice (7.0 μg l^{-1}) chlorophyll concentrations in the Scotia–Weddell study (Daly, 1990) were higher than in Marguerite Bay. The very low chlorophyll concentrations in Marguerite Bay were similar to other Antarctic Peninsula winter values (Kottmeier and Sullivan, 1987). Chlorophyll on the undersurface of sea-ice was much more variable, but on average also very low and the same order of magnitude as values in the water column. The low gut pigment in winter suggests that little nutrition was derived from autotrophs either in the water column or under

sea-ice, consistent with measured chlorophyll concentrations. Average Marguerite Bay gut pigments during August were lower than values (4.0–21.0 ng individual^{-1}) for F6 larvae collected under sea-ice in the Scotia–Weddell seas, even after correcting Marguerite Bay larval values for a 32% degradation loss assumed in the Scotia–Weddell study (Daly, 1990). The higher gut pigments in September on the northern shelf of Marguerite Bay, coincident with increasing chlorophyll concentrations under sea-ice (Fig. 6), suggest that ice algal biomass was starting to accumulate and be utilized as a food source.

Few studies have investigated alternative food sources that may be exploited by larval krill during winter. Although ice algae may not have been prevalent on the undersurface of sea-ice in either year, heterotrophs are another important component of sea-ice assemblages (Palmisano and Garrison, 1993). Indeed, ciliates and other heterotrophs were relatively abundant in diver-collected sea-ice samples, near surface, and at the pycnocline during 2001, but not 2002 (S. Gallager, personal communication). Winter particulate organic concentrations in both years were higher on the undersurface of sea-ice than in the water column, even directly below sea-ice, possibly due to detritus. C:N concentrations and microscopic examination of samples from under ice and from the water column indicated a significant detrital component. Microzooplankton and detritus, in the water column and in sea-ice biota, may have been the most abundant food sources in 2001. In August 2002, when microzooplankton were scarce, other potential food sources included sparse diatoms, small benthic larvae, other small zooplankton, and detritus aggregated in the upper 25 m along with larval krill. Although alternative food sources may have been exploited during winter, the decrease in larval length-specific dry weights between autumn and winter during GLOBEC suggest that most furcilia were food limited (Fig. 8). Length-specific dry weights also were more variable in winter than fall, indicative of the variation in the ability of individuals to cope with a low-food environment.

One other study (Frazer et al., 2002b) reported size of larvae during early spring (September 1991 and 1993) from net and dive collections in th vicinity of the GLOBEC study area, but not i terms of larval stage, so the data were not include in Table 4. Chlorophyll also was not measured These authors observed that the mean size o larvae collected by divers was larger (1991 10.1 mm; 1993: 9.12 mm) than those collected b nets between 0 and 300 m (1991: 9.46 mm; 1993 8.30 mm). The GLOBEC larvae were similar to o slightly larger in size by comparison.

Body composition: Body carbon (C) and nitrogen (N) may be better predictors of larva robustness than weight or length. Pakhomov e al. (2004) observed comparable larval C:N ratios and percent body carbon in early April 2001; therefore, these body parameters did not appear to substantially change between April and May. The average C and N content of fall larvae also is similar to that measured for CIII, FI, and FII larvae from Marguerite Bay during late summer, with lipid concentrations between 13.8% and 19.7% DW (Meyer et al., 2003). Protein and lipids usually account for most of the body C and N in zooplankton, with carbohydrates being generally negligible (<5% of dry weight; Kolakowski and Szyper-Machowska, 1989). Since the C:N ratio for protein is about 3, the average C:N ratio of larvae from this study (4.47; Table 5) indicates that lipid storage was moderate during autumn and winter. Ju and Harvey (2004) also found low lipid storage in larval krill. Similarly, Stübing et al. (2003) measured a total lipid content in F3–F4 larvae of about 12% DW and F4–F6 had a mean lipid content of about 20% DW in this region during early April 2001. Relatively low lipid levels were reported for calyptopis (15% DW) and furcilia (18% DW) collected during autumn from the Weddell Sea (Hagen et al., 2001). Meyer et al. (2002b) also found a lipid level of 15% DW and a C body content of 36% DW in autumn F3s from the Lazarev Sea. Thus lipid storage appears to be variable and moderate in larval krill prior to overwintering. The decrease in C and N in Marguerite Bay larvae between autumn and winter, particularly in 2002, supports the observation of food limitation in winter; however, this measure is uncertain. If larvae were not retained in the study area, then the same population may not

have been sampled in both seasons. Additional data on dry weight, proximate composition, and lipids are needed to adequately assess regional and interannual differences.

Larval development: The delayed development of F6 larvae (Table 6) provides additional verification of suboptimal food and was a dominant behavior during both winters. Larval *E. superba*, like many invertebrate larvae, are characterized by phenotypic plasticity and demonstrate functional flexibility in the timing of molting and metamorphosis and the modes of development in response to changing environmental conditions. For example, indirect larval development or delayed development is believed to be evidence of food limitation (Brinton et al., 1986). Furthermore, the high mortality of younger stages in autumn due to incomplete molting and the appearance of dead larvae (deteriorated body within the exoskeleton) in net samples may have been due to food limitation or a higher age-specific mortality. Pakhomov et al. (2004) noted this phenomenon as well. Our combined observations suggest that the high mortality started at least by April and continued during May, and occurred in both years. Fraser (1936) describes in detail the variable or intermediate forms of furcilia. In Marguerite Bay, the younger stages (C2–F1, F3) that did not die when molting, all developed directly to the next stage. The fact that variant forms occurred in F2, F4, and F5 larvae, plus the delayed development of F6, may reflect an increasing flexibility by larvae to withstand poor food conditions with age.

The results of Melnikov and Spiridonov (1996) offer further support for the delayed development strategy. They reported that krill sampled under sea-ice in the western Weddell Sea (72–63 °S) during austral summer and autumn (early February–June) were mainly F6. They concluded that these larvae must have originated in the southeastern Weddell Sea during the previous summer (thus, 1+ age group) and that they had very low growth rates due to low food concentrations. Chlorophyll concentrations in the water column were less than 0.1 $\mu g\,l^{-1}$ and sea-ice biota was not well developed under sea-ice. In contrast, Daly (1990) observed continued larval development from F4 to juveniles between June and August within the pack ice at about 60 °S in the Scotia–Weddell confluence. This more northerly location was characterized by similar low chlorophyll concentrations in the water column, but with a visible and measurable accumulation of sea-ice biota on the undersurface of first-year sea-ice as noted above.

Larval growth: Lastly, growth and molting rates offers strong evidence that Marguerite Bay larvae were food-limited overwinter, with a significant part of the variability of the intermolt period (IMP) explained by seasonal decreases in temperature and surface chlorophyll. Buchholz (1991) reviewed laboratory studies of juvenile and adult krill, as well as his own findings, and concluded that the molting rate in older life history stages decreased with temperature, whereas growth rates were more sensitive to the quality and quantity of food and were not well correlated with temperature. The intermolt period also varies for body size as small larvae have a shorter IMP than adults during summer. A seasonal comparison of larval and Y0 juvenile growth rates and IMP from field and laboratory investigations (Table 8) show that my average IMP in autumn was similar to other reported rates for summer. The larvae having the longest fall IMP (i.e., Sta. 4; 40 d) may have already adjusted to a winter mode (Table 7). Larval molting rates decreased about two fold between autumn and winter; consequently, less energy was invested in molting.

Marguerite Bay larval growth increments during autumn (percentage change in uropod length; Fig. 11) are within the range of other published values (−15% to 21%, Buchholz, 1991; also see Table 8). The measured growth rates (mm d^{-1}) of larvae and Y0 juveniles in autumn and early spring were generally lower than published summer rates, and winter rates were near zero. Ross et al. (2004) measured even lower (−1.49% IMP^{-1}) growth increments during winter within the study area. In contrast to the consistently low winter growth rates, my September rate (Fig. 10) was similar to fall rates and suggests that larvae were responding to improved food conditions in early spring. Larval gut pigments also increased in September. These larvae were collected at the northern end of the study area (Stas 11, 13, 17), where the ciliate,

Table 8
Seasonal comparison of growth rates and intermolt period for furcilia stages 3–6 and Year 0 juvenile *E. superba*

Month season	Growth (mm d^{-1})	% Growth	IMP (d)	Measurement	References
Summer	0.06	9[c]	13–15	Lab experiment	Ikeda (1984)
Feb.–Mar.	0.082	18.3[c]	18	Field experiment	Huntley and Brinton (1991)
April–May	nd	10.2–18.5[a]	6–17	Field experiment	Pakhomov et al. (2004)
April–May	0.027	6.52[a]	19 (17–40)	Field experiment	This study
Fall/winter	0.047	nd	nd	Field samples	Hosie and Stolp (1989)
Winter	0.017[d]	5.43[b]	nd	Field experiment	Ross and Quetin (1991)
Winter	nd	−3.42[b]	nd	Field experiment	Ross and Quetin (1991)
Winter	0.020[d]	nd	48 (28–80)	Field experiment	Quetin et al. (1994)
Winter	−0.001 to −0.006	−1.6[b]	31 (22–115)	Field experiment	Ross et al. (2004)
August	0.070	14[c]	20	Field experiment	Daly (1990)
August	0.00	0.00[a]	40 (23–61)	Field experiment	This study
September	0.013	4.25[a]	40	Field experiment	This study
November	0.049	6.4[a]	33	Field experiment	Daly (1998)
Dec.–Jan.	0.07	2–10[b]	18 (7–40)	Field experiment	Ross et al. (2000)

IMP is the intermolt period (range in parentheses), nd is no data. Percentage growth is represented by the percent change over the intermolt period between a krill and its molt for:
[a]uropod length,
[b]telson length,
[c]total length.
[d]Elias (1990) cited in Quetin et al. (1994).

Mesodinium sp., was present in higher concentrations in the sea-ice biota than previously observed (S. Gallager, personal communication) and chlorophyll in sea-ice biota was relatively high (ca. 0.23 μg l^{-1}, Fig. 6).

It is not known whether the younger stages of larvae found in autumn can survive until winter. Fraser (1936), Daly (1990), and Frazer et al. (2002b), as well as this study, observed that F4–F6 larvae were the most common stages in early winter, with F6 being the dominant stage by late winter. Assuming that my average IMP is representative for April through June, the C3 larvae observed in late April could develop to the F3 stage by mid-June. Given food limitation, evidence of indirect or delayed development, increasing IMP and decreasing growth rates, and higher mortality of younger stages, it seems more probable that the overwintering larvae are primarily the F2–F6 stages found in autumn.

4.2. Body growth or shrinkage strategy

Even though larvae may decrease in biomass during winter, this study does not support the premise that most larvae shrink in length. Only 13% of the winter larvae showed negative growth, whereas the majority (87%) of larvae showed no growth or positive growth (Fig. 11). Not decreasing exoskeleton length, perhaps by increasing relative water content, would allow krill larvae the maximum flexibility to increase in body mass when food is available. Variability in growth is expected as individuals exploit small-scale differences in the quality and quantity of food in the water column or under sea-ice over the intermolt period. Although the average size of furcilia stages decreased between autumn and winter, this may not be due to shrinkage in length. Larvae occur as F4–F6 stages in early winter, with F6 being the dominant stage by late winter. If growth rates decreased in early winter, when F4 and F5 larvae were developing to the next stage, then the average size of F6 individuals by late winter would show an apparent decrease. The lower growth rates observed by Ross et al. (2004) are equivalent to only a 0.03–0.18 mm decrease over their average intermolt period (30.6 d). Our different results may be due to the fact that my growth rates were based on furcilia collected from both the undersurface of

sea-ice and from the water column or differences in experimental (uropod vs. telson, preservation issues, etc.) and/or statistical methodology.

The comparison of uropod and telson measurements suggests that estimates of growth based on the telson may give erroneous results; thus, a standardization of methodology is needed to achieve a better understanding of winter growth processes, as pointed out by Nicol (2000). Growth is usually considered to be the change in weight or biomass per unit time. Since weight is proportional to the cube of the length, length is often used as a proxy of growth, especially as it is relatively easy to measure change in length of an individual and not possible to measure a change in weight over time. Given the large variability in dry weight versus length during winter (Fig. 8), however, length alone is not a good indicator of biomass change during this season.

Although my results indicate that most larvae did not shrink in length, some portion of the larval population did appear to be starving and may have combusted body lipid and protein to support metabolism. The greater variability and decrease of length-specific dry weights (Fig. 8) and C and N content in winter compared to that in autumn supports this observation. Clearly the results of the starvation experiment demonstrate that some percentage of the population can survive without eating for at least one month. Larvae did reduce their metabolic rate between autumn and winter (J. Torres, personal communication), so that they required less food. A mass-balance calculation using average winter ingestion, respiration, and egestion rates indicate that C ingestion about equaled C losses in many larvae (K. Daly and J. Torres, unpublished). Nevertheless, more than 30% of individuals in winter growth experiments showed evidence of positive growth and, therefore, must have ingested sufficient food to support both metabolism as well as growth.

4.3. Role of sea-ice

Does an early and long-lasting ice cover provide a dependable food supply and enhanced survival of larval krill? The answer to this question does not appear to be straightforward. Winter sea-ice coverage over the study area and surrounding environs was extensive and similar between years (Fig. 1) and, therefore, not expected to be a factor affecting differences in larval behavior. The timing of sea-ice formation, however, did vary between the two years. Despite the fact that in 2002 first-year sea-ice formed several weeks to 2 months earlier, depending on the location, than in 2001 and that second-year sea-ice had visible accumulations of ice algae, sea-ice did not appear to significantly enhance the food supply for larval krill in either year. Much of the increased biomass in second year sea-ice in 2002 occurred in internal assemblages up inside the sea-ice, which were not accessible to krill. The average concentration of ice algae at the ice–water interface was very low in both winters (0.05 vs. 0.07 $\mu g\,chl\,l^{-1}$). In general it is difficult to make an accurate assessment of the availability of sea-ice biota to krill, however, because, (1) the under-ice surface is highly variable and physically complex, (2) krill can access surface areas under rafted floes or inside brine channels which are not easily sampled, (3) sample collections must be made at the ice–water interface on the spatial scale of feeding krill, and (4) sea-ice biota includes a heterotrophic component that is not assessed by chlorophyll, the most common indicator measured in most studies. Furthermore, assessments based on chlorophyll concentrations in the bottom section of ice cores, which is what is typically reported (see review in Palmisano and Garrison, 1993), often imply relatively high ice algal concentrations, but do not accurately depict the available food supply at the ice–water interface. The sea-ice chlorophyll concentrations reported here were from samples collected by divers from surfaces where krill were feeding. Hence, in spite of the relatively small sample size, they represent the variety of food concentrations exploited by larvae.

Numerous processes influence the location and biomass of ice assemblages (Ackley and Sullivan, 1994). For example, the type, size, and concentration of particulate matter that can be scavenged by forming ice crystals or pumped into unconsolidated ice by wave passage will vary spatially and interannually, as well as ice substructure (e.g., frazil vs. congelation ice), location of ice growth

(e.g., bottom vs. surface-flooding), ice ablation, and deformation processes. Due to low irradiance levels at high latitudes in autumn, such as in Marguerite Bay, ice algae may not be able to accumulate sufficient biomass on the undersurface of sea-ice to support larvae during winter, even when sea-ice forms relatively early. Freezing and melting processes at the ice–water interface during winter also may prevent biomass from accumulating. Instead, the ability of some larvae to survive at least a month without food, as evidenced by the results of the starvation experiment, coupled with opportunistic feeding on microzooplankton and detritus, may sustain much of the population until irradiance levels become sufficient to allow ice algal growth during September. In regions or years when the availability of winter ice biota is greater, there may be increased larval survival. The timing of the ice algal biomass increase during spring, which will be a function of latitude as well as physical characteristics of ice, such as snow cover, may be critical to larval survival if they are severely food limited in winter. Increased solar irradiance in spring also causes ice melt, which will give larvae access to internal ice communities through draining brine channels and sloughing ice at ice edges.

Alternatively, sea-ice at all latitudes may have an indirect effect on larval survival that is not yet appreciated. Ice floes release particulate matter during deformation, such as ridge formation, which could provide additional food if it remains suspended near surface. However, a limited number of chlorophyll and POC/N samples, collected just below or next to ice floes to examine this hypothesis, did not have higher concentrations than those deeper in the water column (data not shown).

Sea-ice, when present, also may provide a more dependable source of food for overwintering larvae in more northern latitudes of the Southern Ocean. Unlike Marguerite Bay larvae, winter furcilia in the Scotia–Weddell seas at 60°S, where irradiance levels are higher and for longer periods of the day, did not show evidence of food limitation in their molting, growth and development (Daly, 1990). For example, F6 larvae continued to develop during August (molting to the juvenile stage), they had a shorter IMP, and higher growth rates than Marguerite Bay larvae (Table 8). The growth rates were derived from changes in the length frequency of larvae collected in June and August in the vicinity of a satellite-tracked ice floe. Even though these rates were not experimentally determined and subject to greater uncertainty, the results are consistent with the experimentally determined molting and development rates, as well as the size of larvae and YO juveniles later in spring. Larvae in offshelf waters of the ACC west of the Antarctic Peninsula may not experience as favorable a food environment during summer and autumn as larvae on-shelf. Individuals advected northeastward in the ACC, however, may obtain enhanced food from sea-ice biota in years when the Scotia Sea is covered by sea-ice, compared with larvae overwintering on the shelf at high latitudes such as Marguerite Bay.

A more rigorous evaluation of the role of sea-ice in the winter survival of larval krill needs to include information on the water-column depth distribution of the larval population in relation to alternative food sources, including sea-ice biota. In one study, winter furcilia were collected throughout the water column down to 1000 m, with the highest densities in the upper 100 m (range: 0.01–63 individuals m^{-3}), while larval densities under sea-ice were on the order of 1000 m^{-2} (Daly and Macaulay, 1991). Frazer et al. (2002b) also reported higher densities of winter larvae in net tows than divers counted under sea-ice. Preliminary results from diver and ROV (Gallager et al., 2002) observations and MOCNESS net samples (Ashjian et al., 2004) during winter 2001 indicate that larvae occurred both on the undersurface of sea-ice and throughout the upper 150 m of the water column. In contrast, during 2002 larvae were much less abundant under sea-ice until mid-September when light levels and biomass of sea-ice biota increased. Instead, larvae appeared to be concentrated in the water column between 5 and 25 m. Even if sea-ice biota is not well developed, sea-ice may provide a refuge from predators (Daly and Macaulay, 1988, 1991). Food acquisition, however, appeared to be a stronger driver than predator avoidance, since some portion of the larval population during 2001, and most of the

larvae during 2002, did not retain a strong fidelity to sea-ice and occurred elsewhere in the water column. A better understanding is needed on the interannual variation of larval distribution in the water column and under sea-ice, the food sources in different habitats, and whether larvae migrate between depths.

5. Summary

An evaluation of the seasonal composition and body characteristics of *E. superba* larvae west of the Antarctic Peninsula indicates that individuals that hatch earlier in the summer and are retained in waters over the shelf are more likely to sustain maximal growth rates and achieve a greater length and weight prior to overwintering. The fact that F4–F6 are the primary stages observed in samples between June and August from different investigations suggests that larvae that have not developed to at least the F4 stage by June probably will not survive. The relatively high mortality of young larvae due to incomplete molting in autumn may have been a harbinger of their eventual decline. Larval krill stage composition, length, and weight, and larval growth and development rates from this study support the finding that larvae were actively feeding and growing during autumn, but were food limited during both winters in the vicinity of Marguerite Bay. Little nutrition was derived from autotrophs during winter; microzooplankton and detritus were the likely food sources, especially in 2001. A comparison of growth methodology also suggests that body length is not a good indicator of "growth" or the body combustion strategy in overwintering larvae. Future winter studies should include dry weight and proximate body composition in addition to length to investigate questions related to body shrinkage.

During this winter study at a relatively high latitude (65–70°S), larval krill employed a variety of overwintering behaviors including, (1) flexible feeding behavior and prey switching (i.e. feeding on algae, microzooplankton, and detritus either on the undersurface of sea-ice or in the water column (2) flexible morphology (i.e. delayed development), (3) flexible physiology (i.e. increased intermolt period and reduced growth) (4) reduced metabolism (J. Torres, personal communication), (5) moderate lipid storage, and (6) ability to withstand starvation for weeks by combusting body C and N. Although much of the larval population showed evidence of a loss in dry weight and body C and N between autumn and winter, about 30% of the larvae also had >2% increase in body length in winter. The large juvenile recruitment in 2001 was likely due to the large number of late stage larvae that were retained on the shelf, the condition of larvae prior to winter, as well as alternative food sources available to krill during winter. The physiological processes underlying population dynamics and the effect of variable overwintering growth rates on recruitment may best be investigated through energetic-based, size-structure models.

Overwintering larval *E. superba* clearly accrue some benefit from their association with sea-ice on an evolutionary level as their presence on the undersurface of ice is a persistent behavior. Nevertheless, furcilia have the flexibility to exploit a number of alternative food sources, such as microzooplankton and detritus, and therefore sea-ice is not the only parameter that must be assessed in order to obtain a mechanistic understanding of factors controlling larval survival. Additional winter studies at different latitudes are needed to fully evaluate the direct and indirect affects of sea-ice on overwintering larval krill.

Acknowledgements

I thank the officers and crew of the R.V. *L.M. Gould* and the R.V.I.B. *N.B. Palmer* and Raytheon Polar Services personnel, particularly Alice Doyle, for project planning and support at sea. I am grateful to Mari Butler, Scott Polk, Kerri Scolardi, Hyoung-Chul Shin, Tracey Sutton, Emily Yam, and Jason Zimmerman for their able assistance at sea and to Jason Zimmerman and Kerri Scolardi for net sample and laboratory analyses. John Klinck and Eileen Hofmann kindly provided CTD data, Chris Fritsen provided water column chlorophyll profiles for autumn 2001, Gabriel Vargo identified the phytoplankton, and S. Bosch the

pilidium larvae. I also thank Meng Zhou, Yiwu Zhu, Ryan Dorland, Dan Mertes, and Joe Smith for collecting the 1m MOCNESS samples. Diver observations and collections were made by Jose Torres, Christian McDonald, Kerri Scolardi, Joel Bellucci, Melanie Parker, and Stian Alesandrini. Finally, I thank two anonymous reviewers for their comments. Funding for this research was supported by NSF grants OPP-9910610 and OPP-0196489. This publication represents GLOBEC contribution #457.

References

Ackley, S.F., Sullivan, C.W., 1994. Physical controls on the development and characteristics of Antarctic sea-ice biological communities—a review and synthesis. Deep-Sea Research I 41, 1583–1604.

Ashjian, C.J., Rosenwaks, G.A., Wiebe, P.H., Davis, C.S., Gallager, S.M., Copley, N.J., Lawson, G.L., Alatalo, P., 2004. Distribution of zooplankton on the continental shelf off Marguerite Bay, Antarctic Peninsula, during austral fall and winter, 2001. Deep-Sea Research II, this issue [doi: 10.1016/j.dsr2.2004.07.025].

Beardsley, R.C., Limeburner, R., Owens, W.B., 2004. Drifter measurements of surface currents near Marguerite Bay on the western Antarctic Peninsula shelf during austral summer and fall, 2001 and 2002. Deep-Sea Research II, this issue [doi: 10.1016/j.dsr2.2004.07.031].

Brinton, E., Huntley, M., Townsend, A.W., 1986. Larvae of *Euphausia superba* in the Scotia Sea and Bransfield Strait in March 1984—development and abundance compared with 1981 larvae. Polar Biology 5, 221–234.

Buchholz, F., 1985. Moult and growth in euphausiids. In: Siegfried, W.R., Condy, P.R., Laws, R.M. (Eds.), Antarctic Nutrient Cycles and Food Webs. Springer, Berlin, pp. 339–345.

Buchholz, F., 1991. Molt cycle and growth of Antarctic krill *Euphausia superba* in the laboratory. Marine Ecology Progress Series 69, 217–229.

Daly, K.L., 1990. Overwintering development, growth, and feeding of larval *Euphausia superba* in the Antarctic marginal ice zone. Limnology and Oceanography 35, 1564–1576.

Daly, K.L., 1998. Physioecology of juvenile Antarctic krill (*Euphausia superba*) during spring in ice-covered seas. Antarctic Research Series 73, 183–198.

Daly, K.L., Macaulay, M.C., 1988. Abundance and distribution of krill in the ice edge zone of the Weddell Sea, austral spring 1983. Deep-Sea Research 35 (1), 21–41.

Daly, K.L., Macaulay, M.C., 1991. Influence of physical and biological mesoscale dynamics on the seasonal distribution and behavior *of Euphausia superba* in the antarctic marginal ice zone. Marine Ecology Progress Series 70, 37 -66.

Endo, Y., Hiroshi, A., Watanuki, Y., Kato, A., Kuroki, M., Nishikawa, J., 2002. Biological characteristics of euphausiids preyed upon by Adélie penguins in relation to sea-ice conditions in Lützow-Holm Bay, Antarctica. Polar Biology 25, 730–738.

Fraser, F.C., 1936. On the development and distribution of young stages of krill (*Euphausia superba*). Discovery Reports 24, 1–192.

Frazer, T.K., Quetin, L.B., Ross, R.M., 2002a. Energetic demands of larval krill, *Euphausia superba*, in winter. Journal of Experimental Marine Biology and Ecology 277, 157–171.

Frazer, T.K., Quetin, L.B., Ross, R.M., 2002b. Abundance, sizes and developmental stages of larval krill, *Euphausia superba*, during winter in ice-covered seas west of the Antarctic Peninsula. Journal of Plankton Research 24, 1067–1077.

Gallager, S., Daly, K., Fisher, K., Lawson, G., Davis, C.S., Ashjian, C., Wiebe, P.H., 2002. Seasonal changes in the association of larval krill with its potential microplankton food resources along the Western Antarctic Peninsula. AGU-OS51A-13, Ocean Sciences Meeting, Feb., Honolulu.

Garrison, D.L., Close, A.R., 1993. Winter ecology of the sea-ice biota in Weddell Sea pack ice. Marine Ecology Progress Series 96, 17–31.

Guzman, O., 1983. Distribution and abundance of Antarctic krill (*Euphausia superba*) in the Bransfield Strait. In: Schnack, S.B. (Ed.), On the biology of *Euphausia superba*. Alfred-Wegener-Institut für Polarund Meeresforschung, Bremerhaven, pp. 169–190.

Hagen, W., Van Vleet, E.S., Kattner, G., 1996. Seasonal lipid storage as overwintering strategy of Antarctic krill. Marine Ecology Progress Series 143, 85–89.

Hagen, W., Kattner, G., Terbrüggen, Van Vleet, E.S., 2001. Lipid metabolism of the Antarctic krill *Euphausia superba* and its ecological implications. Marine Biology 139, 95–104.

Hofmann, E.E., Klinck, J.M., 1998. Thermohaline variability of the waters overlying the west Antarctic Peninsula continental shelf. Antarctic Research Series 75, 67–81.

Hopkins, T.L., Lancraft, T.M., Torres, J.J., Donnelly, J., 1993. Community structure and trophic ecology of zooplankton in the Scotia Sea marginal ice zone in winter (1988). Deep-Sea Research 40, 81–105.

Hoshiai, T., 1985. Autumnal proliferation of ice-algae in Antarctic sea-ice. In: Siegfried, W.R., Condy, P.R., Laws, R.M. (Eds.), Antarctic Nutrient Cycles and Food Webs. Springer, Berlin, pp. 89–92.

Hosie, G.W., Stolp, M., 1989. Krill and zooplankton in the western Prydz Bay region, September–November 1985. Proceedings of the National Institute of Polar Research 2, 34–45.

Huntley, M., Brinton, E., 1991. Mesoscale variation in growth and early development of *Euphausia superba* Dana in the western Bransfield Strait region. Deep-Sea Research 38, 1213–1240.

Ikeda, T., 1984. Development of the larvae of the Antarctic krill (*Euphausia superba* Dana) observed in the laboratory. Journal of Experimental Marine Biology and Ecology 75, 107–117.

Ikeda, T., Dixon, P., 1982. Body shrinkage as a possible over-wintering mechanism of the Antarctic krill, *Euphausia superba* Dana. Journal of Experimental Marine Biology and Ecology 62, 143–151.

Ikeda, T., Thomas, P.G., 1987. Moulting interval and growth of juvenile Antarctic krill (*Euphausia superba*) fed different concentrations of the diatom *Phaeodactylum tricornutum* in the laboratory. Polar Biology 7, 339–343.

Ju, S.-J., Harvey, H.R., 2004. Lipids as markers of nutritional condition and diet in the Antarctic krill *Euphausia superba* and *Euphausia crystallorophias* during austral winter. Deep-Sea Research II, this issue [doi: 10.1016/j.dsr2.2004.08.004].

Kawaguchi, S., Satake, M., 1994. Relationship between recruitment of the Antarctic krill and the degree of ice cover near the South Shetland Islands. Fisheries Science 60 (1), 123–124.

Kittel, W., Jażdżewski, K., 1982. Studies on the larval stages of *Euphausia superba* Dana (Crustacea, Euphausiacea) in the southern Drake Passage and in the Bransfield Strait in February and March 1981 during the BIOMASS-FIBEX expedition. Polish Polar Research 3, 273–280.

Klinck, J.M., Hofmann, E.E., Beardsley, R.C., Salihoglu, B., Howard, S., 2004. Water-mass properties and circulation on the west Antarctic Peninsula Continental Shelf in Austral Fall and Winter 2001. Deep-Sea Research II, this issue [doi: 10.1016/j.dsr2.2004.08.001].

Kolakowski, E., Szyper-Machowska, L., 1989. Seasonal changes of carbohydrate content in Antarctic krill (*Euphausia superba* Dana). Polish Polar Research 10, 133–139.

Kottmeier, S.T., Sullivan, C.W., 1987. Late winter primary production and bacterial production in sea-ice and seawater west of the Antarctic Peninsula. Marine Ecology Progress Series 36, 287–298.

Lawson, G.L., Wiebe, P.H., Ashjian, C.J., Gallager, S.M., Davis, C.S., Warren, J.D., 2004. Acoustically-inferred zooplankton distribution in relation to hydrography west of the Antarctic Peninsula. Deep-Sea Research II, this issue [doi: 10.1016/j.dsr2.2004.07.022].

Lizotte, M.P., 2001. The contribution of sea-ice algae to Antarctic marine primary production. American Zoologist 41, 57–73.

Makarov, R., 1980. Larval development of the Antarctic euphausiids. BIOMASS Handbook 3, 1–13.

Marr, J.W.S., 1962. The natural history and geography of the Antarctic krill (*Euphausia superba* Dana). Discovery Report 32, 33–464.

Marschall, H.P., 1988. The overwintering strategy of Antarctic krill under the pack-ice of the Weddell Sea. Polar Biology 9, 129–135.

McGaffin, A.F., Nicol, S., Ritz, D.A., 2002. Changes in muscle tissue of shrinking Antarctic krill. Polar Biology 25, 180–186.

Melnikov, I.A., Spiridonov, V.A., 1996. Antarctic krill under perennial sea-ice in the western Weddell Sea. Antarctic Science 8, 323–329.

Meyer, B., Saborowski, R., Atkinson, A., Buchholz, F., Bathmann, U., 2002a. Seasonal differences in citrate synthase and digestive enzyme activity in larval and postlarval Antarctic krill, *Euphausia superba*. Marine Biology 141, 855–862.

Meyer, B., Atkinson, A., Stübing, A., Oettl, B., Hagen, W., Bathmann, U.V., 2002b. Feeding and energy budgets of Antarctic krill *Euphausia superba* at the onset of winter. I. Furcilia III larvae. Limnology and Oceanography 47, 943–952.

Meyer, B., Atkinson, A., Blume, B., Bathmann, U.V., 2003. Feeding and energy budgets of larval Antarctic krill *Euphausia superba* in summer. Marine Ecology Progress Series 257, 167 177.

Miller, D.G.M., 1983. Variation in body length measurements of *Euphausia superba* Dana. Polar Biology 2, 17–20.

Nicol, S., 2000. Understanding krill growth and aging: the contribution of experimental studies. Canadian Journal of Fisheries and Aquatic Sciences 57 (Suppl. 3), 168–177.

Nicol, S., Stolp, M., Cochran, T., Geijsel, P., Marschall, J., 1992. Growth and shrinkage of Antarctic krill *Euphausia superba* from the Indian Ocean sector of the Southern Ocean during summer. Marine Ecology Progress Series 89, 175–181.

Pakhomov, E.A., Atkinson, A., Meyer, B., Oettl, B., Bathmann, U., 2004. Daily rations and growth of larval krill *Euphausia superba* in the Eastern Bellingshausen Sea during austral autumn. Deep-Sea Research II, this issue [doi: 10.1016/j.dsr2.2004.08.003].

Palmisano, A.C., Garrison, D.L., 1993. Microorganisms in Antarctic sea-ice. In: Friedmann, E.I. (Ed.), Antarctic Microbiology. Wiley-Liss, New York, pp. 167–218.

Poleck, T.P., Denys, C.J., 1982. Effect of temperature on the molting, growth, and maturation of the Antarctic krill *Euphausia superba* (Crustacea: Euphausiacea) under laboratory conditions. Marine Biology 70, 255–265.

Préezelin, B.B., Hofmann, E.E., Mengelt, C., Klinck, J.M., 2000. The linkage between upper circumpolar deep water (UCDW) and phytoplankton assemblages on the west Antarctic Peninsula continental shelf. Journal of Marine Research 58, 165–202.

Quetin, L.B., Ross, R.M., Clarke, A., 1994. Krill energetics: seasonal and environmental aspects of the physiology of *Euphausia superba*. In: El-Sayed, S.Z. (Ed.), Southern Ocean Ecology: The BIOMASS Perspective. Cambridge University Press, Cambridge, pp. 165–184.

Ross, R.M., Quetin, L.B., 1991. Ecological physiology of larval euphausiids, *Euphausia superba* (Euphausiacea). Memoirs of the Queensland Museum 31, 321–333.

Ross, R.M., Quetin, L.B., Baker, K.S., Vernet, M., Smith, R.C., 2000. Growth limitation in young *Euphausia superba* under field conditions. Limnology and Oceanography 45, 31–43.

Ross, R.M., Quetin, L.B., Newberger, T., Oakes, S.A., 2004. Growth and behavior of larval krill (*Euphausia superba*) under the ice in late winter 2001 west of the Antarctic Peninsula. Deep-Sea Research II, this issue [doi: 10.1016/j.dsr2.2004.07.001].

Siegel, V., 1989. Winter and spring distribution and status of the krill stock in Antarctic Peninsula waters. Archiv furr Fischerie Wissenschaft 39, 45–72.

Siegel, V., Loeb, V., 1995. Recruitment of Antarctic krill *Euphausia superba* and possible causes for its variability. Marine Ecology Progress Series 123, 45–56.

Smetacek, V., Scharek, R., Nöthig, E.-M., 1990. Seasonal and regional variation in the pelagial and its relationship to the life history cycle of krill. In: Kerry, K.R., Hempel, G. (Eds.), Antarctic Ecosystems. Ecological Change and Conservation. Springer, Berlin, pp. 103–114.

Smith, R.C., Dierssen, H.M., Vernet, M., 1996. Phytoplankton biomass and productivity in the western Antarctic Peninsula region. Antarctic Research Series 70, 333–356.

Stübing, D., Hagen, W., Schmidt, K., 2003. On the use of lipid biomarkers in marine food web analyses: An experimental case study on the Antarctic krill, *Euphausia superba*. Limnology and Oceanography 48, 1685–1700.

Sun, S., De La Mare, W., Nicol, S., 1995. The compound eye as an indicator of age and shrinkage in Antarctic krill. Antarctic Science 7 (4), 387–392.

Torres, J.J., Donnelly, J., Hopkins, T.L., Lancraft, T.M., Aarset, A.V., Ainley, D.G., 1994. Proximate composition and overwintering strategies of Antarctic micronektonic Crustacea. Marine Ecology Progress Series 113, 221–232.

Zar, J.H., 1984. Biostatistical Analysis. Prentice-Hall, Englewood Cliffs NJ, 717pp.

ELSEVIER

Deep-Sea Research II 51 (2004) 2169–2184

DEEP-SEA RESEARCH
PART II

www.elsevier.com/locate/dsr2

Growth and behavior of larval krill (*Euphausia superba*) under the ice in late winter 2001 west of the Antarctic Peninsula

Robin M. Ross[a,*], Langdon B. Quetin[a], Timothy Newberger[b], Stephanie A. Oakes[a]

[a] *Marine Science Institute, University of California at Santa Barbara, Santa Barbara, CA 93106, USA*
[b] *Lamont-Doherty Earth Observatory, Columbia University, Palisades, NY 10964, USA*

Accepted 12 July 2004

Abstract

In situ growth rates are one measure of the physiological condition of larval Antarctic krill in winter. During the southern ocean global ecosystem dynamics (SO GLOBEC) research cruise in July/August 2001 aboard the ARSV *Laurence M. Gould* west of Adelaide Island and Marguerite Bay, larval krill were observed in the under-ice habitat. Ten instantaneous growth rate experiments were conducted with larvae collected from the under-ice habitat on the outer shelf, mid-shelf, and just south of Adelaide Island in the mouth of Marguerite Bay. For all experiments, average growth increments for larval krill were about −1.6% per intermolt period, with a median intermolt period of 30.6 d. Larvae were observed feeding on the ice, even though no color was visible in the ice. Pigment (chlorophyll *a* equivalents) content of larvae from three of the sites was measured as an indicator of ingestion of sea-ice microalgae. Pigment values were above those found in starved controls, but only about 20% of maximum possible values. Although feeding, the data suggested that the larval krill were unable to ingest enough food to maintain growth. The results from this first SO GLOBEC winter process cruise were compared to growth rates of larval krill during previous winter cruises that covered all months from late May through September, except for the month of August.
© 2004 Elsevier Ltd. All rights reserved.

1. Introduction

The Southern Ocean Global Ecosystem Dynamics (SO GLOBEC) program has multiple goals, but focuses on understanding the biological–physical interactions impacting the population dynamics of a target species, Antarctic krill (*Euphausia superba*), and its predators. Recruitment success in Antarctic krill is highly variable, as has been documented in many regions of the Southern Ocean (Siegel and Loeb, 1995; Siegel et al., 1998, 2002; Watkins, 1999; Siegel, 2000; Quetin and Ross, 2003). These studies include reports on decade-long time series in two regions west of the Antarctic Peninsula, one at the tip of the peninsula (Siegel and Loeb, 1995) and one between Anvers

*Corresponding author.

0967-0645/$ - see front matter © 2004 Elsevier Ltd. All rights reserved.
doi:10.1016/j.dsr2.2004.07.001

and Adelaide Islands, the Palmer Long-Term Ecological Research study region (Quetin and Ross, 2003). Variation in recruitment leads to significant interannual differences in the population structure, and potentially abundance. The strong correlation between recruitment and various aspects of seasonal sea-ice dynamics has been documented well (Siegel and Loeb, 1995; Quetin and Ross, 2003). Also, differences have been documented in the physiological condition (growth, lipid reserves, condition factor) of larval krill in winter from under the ice and in open water (Ross and Quetin, 1991). The previous results support the concept that sea ice and the associated microbial community provide food resources during a period in larval development when food resources in the water column are low. And as a consequence, variation in the availability of food resources in sea ice may lead to variability in larval survival and consequent recruitment. Thus understanding growth processes in larval krill in winter is a critical aspect of understanding the nature of recruitment and population regulation in Antarctic krill.

A hypothesis widely accepted in discussions about recruitment in larval marine fish is that the survival of a cohort or year class is directly related to growth rates during the pre-recruit period. The underlying concept is that any food limitation simultaneously affects both growth rates and survivorship. The effects of temperature on production of prey and developmental rates of the larvae also often play a role (Ottersen and Loeng, 2000; Pepin, 1991).

In the case of Antarctic krill, sea ice, and the microbial community living on and within the sea ice, is perceived as the winter grazing ground for larval krill when food in the water column is low (Smetacek et al., 1990; Quetin et al., 1996). A lack of sea ice and/or the quantity, quality or availability of the microbial community within the ice may lead to food limitation in larval krill. A reasonable assumption is that slower-growing individuals are more likely to die before recruitment into the adult population than the faster-growing individuals (Pepin, 1989). Pepin's model (1989) predicts that the death of slow-growing individuals is one mechanism of increasing the mean growth rate over time. If this holds true, then variations in growth rates within a year class might be of value in predicting survivorship. Thus understanding seasonal patterns in growth in Antarctic krill could have significant implications for predicting recruitment patterns.

A recent compilation of fall and winter growth data for larval Antarctic krill in waters west of the Antarctic Peninsula documented variability in the pattern of seasonal growth that exceeded interannual variability (Quetin et al., 2003). This multiple-cruise study reported results from three June cruises and two September cruises, with results showing far great variability month to month than year to year within the same month. Other cruises were in fall (April/early May, late May), and mid-winter (late June/early July, July). The growth data were from instantaneous growth rate experiments (IGRs), and showed that the growth increment decreased throughout the fall to low and sometimes negative values in mid-June through early July. By September, growth increments were positive and at their maximum. Mid-winter growth rates were similar to those of larvae maintained on low-food concentrations (Elias, 1990), whereas late winter rates were comparable to those of larvae fed unlimited food supplies (Ikeda, 1984). For these data, a strong correlation existed between daylength at the time of collection and the average growth increment of the larval krill in the experiment. However, no growth data in the late July through August time period were available. Whether low growth increments would continue through the remainder of the winter and increase as a step function in the late winter and early spring or if growth increments would slowly increase through late July and August was unknown. There was also the question of whether the daylength predictor would hold during this late winter period, as there are several alternative explanations for what the daylength parameter represented (Quetin et al., 2003).

In light of the documented winter-season variability in growth rates (Quetin et al., 2003), we need to understand the full scope of the seasonal patterns in growth in addition to the weaker interannual variation if we are to understand the role of growth in larval krill survivorship

nd ultimately recruitment. In this study, we eport on SCUBA diver observations of larval rill in their under-ice habitat, the results of a eries of IGR experiments, and pigment content as n index of ingestion of sea-ice microalgae in arval krill from the same habitat. Some of the bservations and data were obtained during two ce camps or multi-day observations of the same ce floes, enabling us to compare larval krill collections on small time and space scales. This esearch cruise provided the opportunity to obtain nformation on the length and stage composition, nd physiological condition of larval krill during a ime period in winter for which no data exist west of the Antarctic Peninsula. With this information n hand, we can now begin to explore the full range of seasonal and interannual variability in growth nd behavior of larval krill from the pack-ice abitat in winter.

2. Material and methods

Study site: The first winter process cruise for SO GLOBEC took place on board the ARSV *Laurence M. Gould* from 21 July to 1 September 2001. The study region was on the continental shelf, west of the Antarctic Peninsula, from the mid-point of Adelaide Island to just south of Marguerite Bay (Fig. 1). The study area was approximately 160 km^2, with a latitudinal range of 1.65°. Collection of larval krill for experiments and analysis took place between 28 July and 22 August (Table 1).

Collections and observations: Larval krill were collected from under the ice by SCUBA divers with fine-meshed (~680-μm mesh) aquarium nets. Larvae from ten dives were used in instantaneous growth experiments, larvae from six dives were extracted for pigment content, and larvae from six dives were processed for carbon and/or dry mass (Table 1). Ice Station Robert (Dives 6–11) comprised six dives on the same ice floe in the mouth of Marguerite Bay from 5 to 9 August; Ice Station Billy (Dives 13 18) comprised six dives about 100 km to the northwest of Ice Station Robert from 16 to 18 August. In three cases (Dives 12, 13 and 18), larvae were collected during the same dive for both growth and pigment data (Table 1).

Four divers with pairs alternating dives were used throughout the cruise. Observations during each dive included notes on whether krill were present or absent, whether krill were displaying feeding behavior, and their location, e.g. in the water column or associated with a particular surface of ice. Divers distinguished among three ice orientations: floors (upward facing), walls (side facing) or ceilings (downward facing). Maximum depth of over rafting, color of the ice and hardness were also noted. Maximum depth of the rafted ice was determined with a diver's depth gauge. Color of the ice was noted as white (no color), green, yellow or brown, and recorded as evidence of the overall presence or absence of ice algae to the diver's eye. Hardness of the ice was noted as hard or soft. Hard ice could not be penetrated by a diver's finger and had a polished feel. Soft ice could be penetrated to varying depths.

IGR experiments: Immediately after collection, the contents of the aquarium net were gently placed into large insulated buckets of seawater at in situ temperatures and taken back to the ship. Larvae from each collection were randomly selected for subsequent growth experiments. The IGR method was first briefly described as a method to measure field growth rates for krill in short-term (4 d) experiments (adults, Quetin and Ross, 1991; larvae, Ross and Quetin, 1991). Nicol et al. (1992) confirmed the underlying premise that maintenance conditions do not affect the length increment at ecdysis for up to 7 d after collection when in situ water temperatures are 2 °C or less. Further details of the experimental protocol were described in Ross et al. (2000) for late furcilia and juvenile krill ~10–12-month old, and Quetin et al. (2003) for larval krill. Between 83 and 100 randomly selected larvae were individually placed in 1.2-μm filtered seawater in separate 500-ml containers and held at ambient seawater temperatures. At 12-h intervals over the following four days all containers were inspected for molts, and the temperature of the water measured. Average temperature in an experiment ranged from −1.3 to −1.6 °C. Upon molting, the larva was measured for total length, and the larva and its molt were

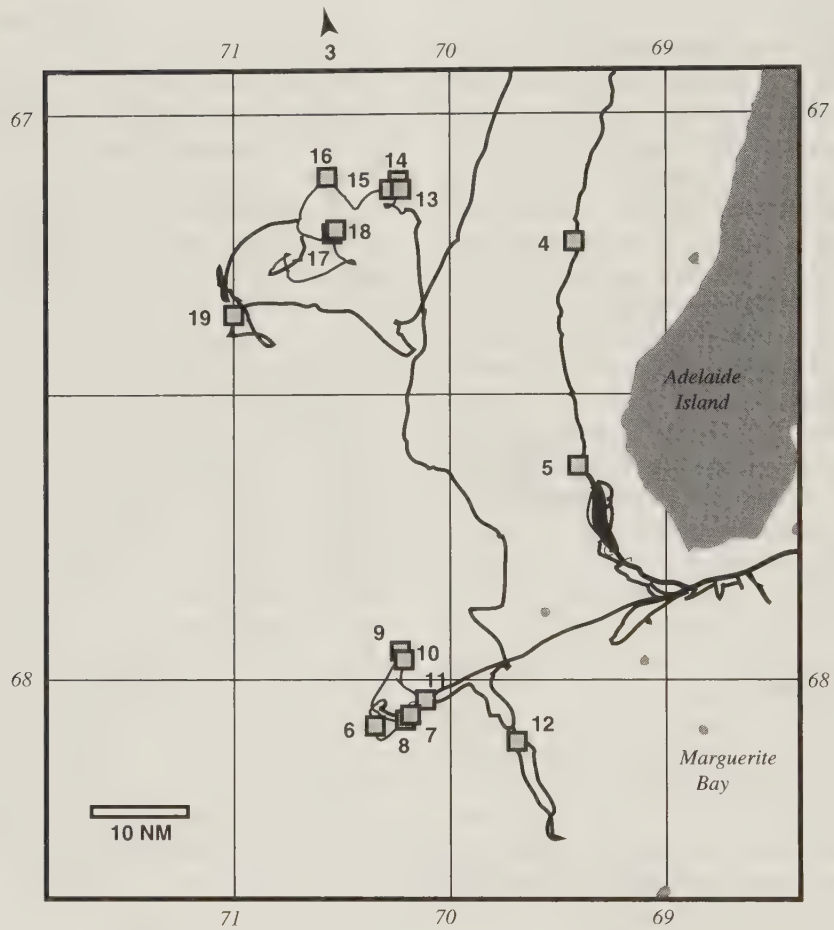

Fig. 1. Southern Ocean GLOBEC study region for ARSV *Laurence M. Gould* 01–06, 29 July to 1 September, and dive number near the symbol for each dive location to show the location of each type of sampling (Table 1). Dives 6–11 were at Ice Station Robert, Dives 13–18 at Ice Station Billy. Cruise track lines between dives at each ice station, e.g. diving from the same floe, are thicker than track lines between single dives on a floe. Dive 3 is off the map, 82 km north–northeast of Dive 16.

preserved together in 10% buffered formalin. At the end of the experiment, total length and stage of all non-molters were determined prior to preservation.

The total length from the tip of the rostrum to the end of the uropods of each larva in the experiment was measured under a dissecting microscope (Standard Length 1; Mauchline, 1980), and the developmental stage was determined according to Fraser (1936). In addition, telson lengths of both molt and larva were measured, and the stage of the molt was determined. The intermolt period (IMP) was estimated as the inverse of the molting frequency per day in the experiment. The growth increment was based on the change in telson length and expressed as percent growth per IMP (% IMP^{-1}). The number of growth increments measured ranged from 11 to 18 for most of the experiments, with 3 and 7 molters each for the other two experiments. The mean, standard deviation, and standard error of the growth increment of all molters were calculated for each experiment. Telson lengths were measured from the side, from mid-bump at the insertion point to the abdomen to the tip, to keep the entire telson length in focus under a dissecting

Table 1
Location from event log and date of collection of larvae for growth experiments (IGR, with number), carbon (C) and dry mass (dwt) determination, and pigment content determination (Pig)

ce tation	Dive	Date	Latitude (°S)	Longitude (°W)	IGR Expt. no.	C/dwt	Pig
–	3	28 Jul	66°22.5′	70°44.7′	1	—	—
–	4	29 Jul	67°13.7′	69°25.5′	2	X	—
–	5	2 Aug	67°35.7′	69°24.9′	3	X	—
Robert	6	5 Aug	68°4.6′	70°21.4′	4	X	—
Robert	7	6 Aug	68°3.8′	70°10.5′	—	—	X
Robert	8	6 Aug	68°3.88′	70°11.6′	—	—	X
Robert	9	8 Aug	67°57.2′	70°13.7′	5	X	—
Robert	10	8 Aug	67°58.5′	70°13.2′	—	—	—
Robert	11	9 Aug	68°2.0′	70°6.8′	—	—	—
–	12	11 Aug	68°6.6′	69°41.3′	6	X	X
Billy	13	16 Aug	67°8.20′	70°14.5′	7	—	X
Billy	14	16 Aug	67°7.50′	70°15.0′	—	—	X
Billy	15	16 Aug	67°7.5′	70°16.2′	—	—	—
Billy	16	17 Aug	67°6.8′	70°34.3′	8	—	—
Billy	17	18 Aug	67°12.7′	70 32.1′		—	—
Billy	18	18 Aug	67°12.5′	70°31.5′	9	—	X
–	19	22 Aug	67°21.4′	71°0.0′	10	X	—

microscope at a magnification so that the telson filled the field of view. The lengths were recorded to the nearest division on the eyepiece micrometer, a precision of ±0.012 mm at the magnifications used. This yielded a precision of ±0.45–0.66% IMP^{-1} for the growth increments in these experiments.

Other investigators have measured the growth increment in IGR experiments from changes in the average uropod length (Nicol et al., 1992; Daly, 2004). Although there are advantages to both measurement types, the results of a cross-calibration study (Nicol's uropod and Quetin and Ross's telson measurements) showed that growth increments of a group of krill followed over time are not significantly different with the two measurements (Hollander, 2001, pers. comm.). Both the relationships between uropod and total length and telson and total length are significant (generally with r^2 of >0.95) but they are not identical. Thus, to compare directly growth increments in % IMP^{-1} derived from telson and uropod measurements, both should be used to estimate a change in the same size measure, such as total length or dry mass or carbon.

Two indices of development were calculated. We calculated the percentage of furcilia stage larvae that advanced to the next larval stage at ecdysis. A developmental stage index (DSI) also characterized the stage composition of each experimental population. Each furcilia stage was assigned a number 'i', 4 for furcilia stage 4, 5 for furcilia stage 5, 6 for furcilia stage 6, and 7 for juveniles, and the DSI is calculated as follows:

$$\mathrm{DSI} = \sum_i \frac{\text{number larvae in stage } i \bullet i}{\text{total number of larvae}}.$$

Length and mass relationships: The relationships between telson length, total length, and wet and dry mass were determined from a group of larvae from Dive 19 maintained in 2-l jars at ambient temperatures for 3.5 d until arrival at Palmer Station. On station, total and telson length of a larva were measured, and then the larva was weighed on a 5-place Mettler balance. Dry mass was determined after 24 h in a 60 °C oven. The range in total length was 6.5–15.0 mm, in wet mass from 2.0 to 21.4 mg, and in dry mass from 0.4 to 5.1 mg. On five dives (Dives 4–6, 9 and 12), larvae collected from under the ice were processed for later determination of dry mass and organic carbon. The stage and total length of the larva were determined, then the individual larva was placed in a pre-weighed aluminum sleeve that had been fired at 450 °C for 2 h. The sleeve was then placed in a hole in an aluminum plate (previously fired at 450 °C for 24 h) in a drying oven. The mass of the larvae was determined on a Cahn Electrobalance, and the elemental analysis was conducted with an elemental analyzer at the Marine Science Institute's Analytical Laboratory, University of California at Santa Barbara.

Pigment content of larvae: The gut fluorescence or pigment content method is specific for the algal component of the diet. The measurement of chlorophyll *a* (chl *a*) and phaeopigments in copepod guts has long been used as an index of phytoplankton ingestion (Mackas and Bohrer, 1976; Dagg, 1993). We used the pigment content of freshly collected larval krill as an index of their

recent feeding history on sea-ice microalgae. Less than a minute after the diver surfaced with larvae for pigment content analysis, groups of larvae were placed in glass vials containing 8 ml of 90% acetone. Five vials of about 15 larvae each were prepared for each collection. Vials were then taken from the ice floe and placed in a freezer for 24 h for extraction of the plant pigment from the larvae. The chl *a* and phaeopigment (phe) content (μg) in the extract were determined according to the method described in Smith et al. (1981) with a Turner Designs digital fluorometer calibrated at the beginning of the cruise. After extraction, the telson lengths of all larvae in a vial were measured. The relationship between telson length and wet mass determined with larvae collected on the cruise was used to estimate the wet mass of each individual. Individual wet masses were summed for the total wet mass of larvae in each vial. The sum of the pigments (chl *a* and phe) in μg chl *a* equivalents (Dagg, 1993) was divided by the total wet mass of the larvae for pigment content in μg $gwwt^{-1}$.

To determine the pigment content of starved larvae, larvae from nine dive collections were held in 1.2 μm filtered seawater for 2–14 d. Two sets of five vials of five larvae each were prepared as described above, one at the end of the starvation period and the second after a further 12 h of starvation. The pigment content was determined as described above.

3. Results

Diving observations: Several observations made by divers were consistent throughout the cruise on each dive. The pack ice rafted to maximum depths of 5–8 m. Over-rafted ice was consistently characterized as white and hard. Color was only observed in the ice at one location (Dive 19) and was recorded as light yellow. No adult krill were seen. On every dive except one, most larval krill were found feeding on floors of the over-rafted ice. On Dive 3 the krill were in aggregations drifting in the water column.

Size and developmental stage: Length frequency distributions (LFD) of the larvae were similar across the study area (Fig. 2), with mean total lengths ranging from 8.77 to 10.23 mm (Table 2, Fig. 3A). However, there were inter-collection differences in the relative dominance of small (7–10 mm) and large (12–15 mm) larvae. The collections grouped into LFDs characterized by either (1) a dominance ($\geqslant 70\%$) of small larvae and a lack of large larvae (Dives 3–5, 9, and 16), or (2) the presence ($>2\%$) of large larvae and a lower percentage (62% of small larvae) (Dives 6, 12, 13, 18, and 19). The remainder of the larvae were 10–12 mm in length. Groups of similar LFDs did not necessarily come from the same geographical location or ice floe. Significant variation in larval size existed on the small temporal and spatial scales present in the ten collections (ANOVA, $F=14.66$, $p \ll 0.001$, $n=974$). This result held at even smaller scales. For example, at Ice Station Billy, the size of larval krill collected from the same ice floe on three dives 1-d apart yielded significantly different size distributions (ANOVA, $F=24.4$, $p \ll 0.001$) (Fig. 3A).

Larval stage distribution paralleled that of the LFD, as larger larvae tended to be more advanced. Larvae were predominantly furcilia stage 6 and juveniles, with a small percent (0–6%) of furcilia stages 4 and 5. The DSI ranged from 6.0 to 6.5 (Table 2, Fig. 3B). Differences in the DSI were due to changes in the relative proportions of furcilia stage 6 and juvenile. The larval stage frequency clustered in two groups: collections dominated by furcilia stage 6 (average 77% furcilia 6, 19% juvenile), and collections with nearly equal proportions (52% furcilia 6, 46% juvenile) (Fig. 4). As with total length, collections from dives on the same floe at Ice Station Billy showed stage development indices at almost the extremes of the range of all collections, 6.5 versus 6.1 (Table 2). In summary, significant variation in length and stage of larvae were found on small space (same ice floe) and time (1 d) scales. This result reinforces the findings of previous researchers that single samples of krill from one area do not provide reliable estimates of either population characteristics (Watkins et al., 1990) or genetic population parameters (Jarman et al., 2002) of krill in that area. Thus, single samples of larval krill taken at different points in time cannot be used to track a

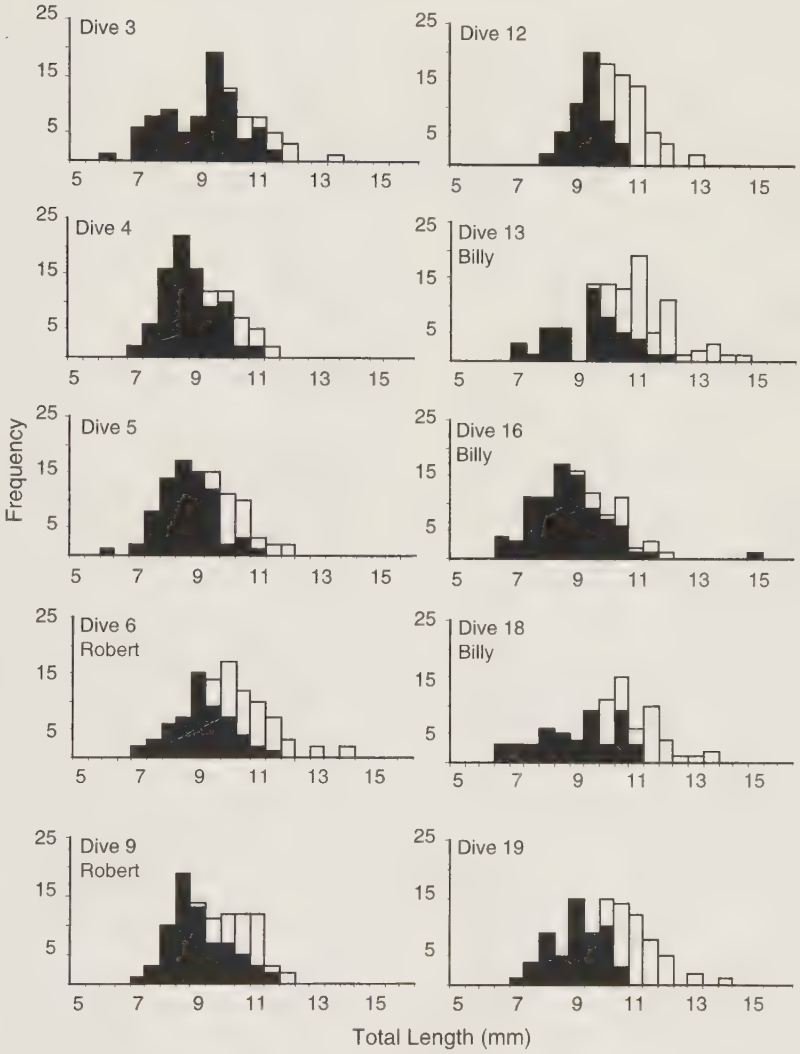

Fig. 2. *E. superba* larvae. Length frequency distributions in IGR experiments in 0.5 mm increments. Length frequency distributions labeled with dive number and Ice Station name if appropriate. Column color indicates proportion of furcilia (black) and juvenile (white) in a length class.

population of larvae over time, and cannot be used to estimate growth rates of larvae in the region.

IGR experiments: In all experiments, average percent growth per IMP was negative (Fig. 5A). The highest average growth increment was found at the farthest north station, and the lowest growth increment at Ice Station Billy. However, there was no significant difference in growth increments determined in the separate experiments (ANOVA, $F=0.91$, $p=0.52$, $n=111$). The mean growth increment in this region in winter 2001 was -1.64% IMP^{-1} (SD = 1.73). Growth increments of the 111 individual molters ranged from $+4.3\%$ to -6.1% IMP^{-1}, with the majority (78%) showing negative growth. Zero growth was observed in 9% of the individuals, and positive growth in 13%. The percentage of individuals showing positive growth varied among experiments, ranging from 0 in several experiments to 38.5% in the experiment with larvae from the site

Table 2
Total length (TL) with standard deviation (SD), developmental stage index (DSI), percent of furcilia stage larvae advancing to the next stage and percent of molters showing positive growth

Ice station	IGR Expt no.	TL (mm) (SD)	DSI	% Adv stage	% Positive growth
—	1	9.22	6.01	33.3	38.5
—	—	(1.42)	—	—	—
—	2	8.82	6.11	0	16.7
—	—	(1.03)	—	—	—
—	3	8.93	6.17	27.3	7.7
—	—	(1.11)	—	—	—
Robert	4	9.69	6.38	25	16.7
—	—	(1.36)	—	—	—
Robert	5	9.26	6.25	14.3	0
—	—	(1.14)	—	—	
—	6	9.92	6.48	0	8.3
—	—	(1.01)	—	—	—
Billy	7	10.23	6.48	50.0	0
—	—	(1.52)	—	—	—
Billy	8	8.77	6.11	0	9.1
—	—	(1.37)	—	—	—
Billy	9	9.70	6.36	0	0
—	—	(1.61)	—	—	—
—	10	9.75	6.44	0	15.4
—	—	(1.35)	—	—	—

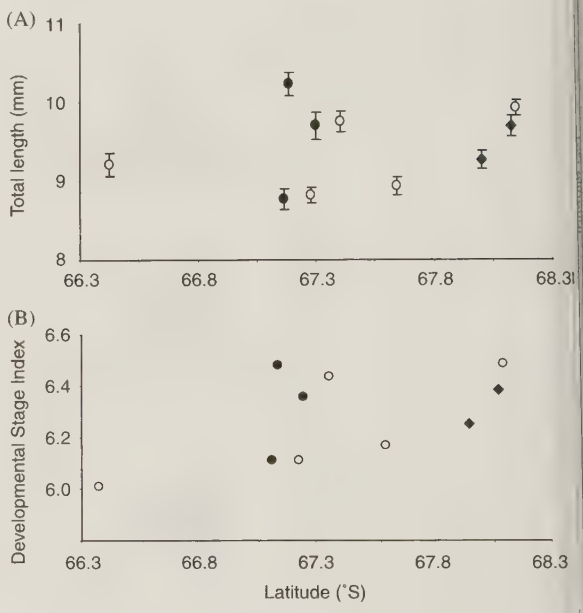

Fig. 3. *E. superba* larvae from the under-ice habitat. (A) Mean total length and standard error. (B) Developmental stage index. Plotted against the latitude of collection: single collections from floes (open circles), Ice Stations Robert (closed diamonds) and Billy (closed circles).

farthest north (Dive 3) (Fig. 1, Table 2). IMPs were generally 22–30 d (Fig. 5B), with a median IMP of 30.6 d.

The relationships derived between telson length (TelL) and different size parameters (total length in mm (TL), wet mass in mg (wwt), dry mass in mg (dwt), and carbon in μg (C)) (Fig. 6) allowed us to estimate growth rates in terms of both length and mass. To estimate growth rates as dry mass, pre- and post-molt telson lengths were used to estimate dry mass of the larva pre- and post-molt. For estimates of growth rates as carbon, pre- and post-molt telson lengths were used to estimate total length, and total length used to estimate carbon content of the larva. The pre- and post-molt estimates were subtracted to estimate the absolute dry mass and carbon change during the IMP for each experiment (Fig. 7A and B). The patterns were similar to those found for the linear growth increment in % IMP^{-1}, with the highest average growth rate at the ice floe farthest north (-0.041 mg dwt IMP^{-1} and -19.43 μg C IMP^{-1}), and the lowest growth rate (-0.155 mg dwt IMP^{-1} and -76.97 μg C IMP^{-1}) found at Ice Station Billy west of Adelaide Island. The median average growth rate was -0.075 mg dwt IMP^{-1} and -35.93 μg C IMP^{-1}. Minor differences in patterns were due to differences in the relationships between telson and total length (linear) and length and dry mass and carbon (power function), and the varying size of the experimental larvae.

The change per IMP was divided by the median IMP to calculate growth in mg dwt d^{-1} and μg C d^{-1} (Table 3). The measured total length, the growth increment (% IMP^{-1}) and median IMP were used to calculate growth rates in mm d^{-1}. Average growth rates for all three measures were calculated for each experiment (Table 3). Dry mass growth rates ranged from -0.0006 to -0.0051 mg dwt d^{-1}, carbon growth rates ranged from -0.295 to -2.515 μg C d^{-1}, and linear growth rates ranged from -0.0021 to -0.0065 mm d^{-1} (Table 3).

The percent of furcilia stage 4, 5 or 6 advancing stage upon molting in an experiment also varied

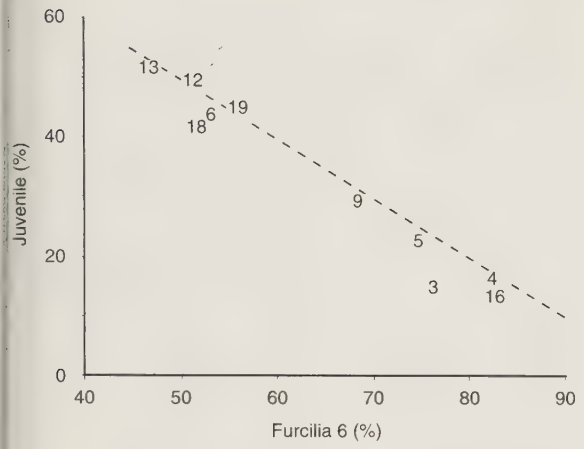

Fig. 4. *E. superba* larvae from the under-ice habitat. Relationship between percent of furcilia stage 6 and percent of juveniles. The number is the dive number.

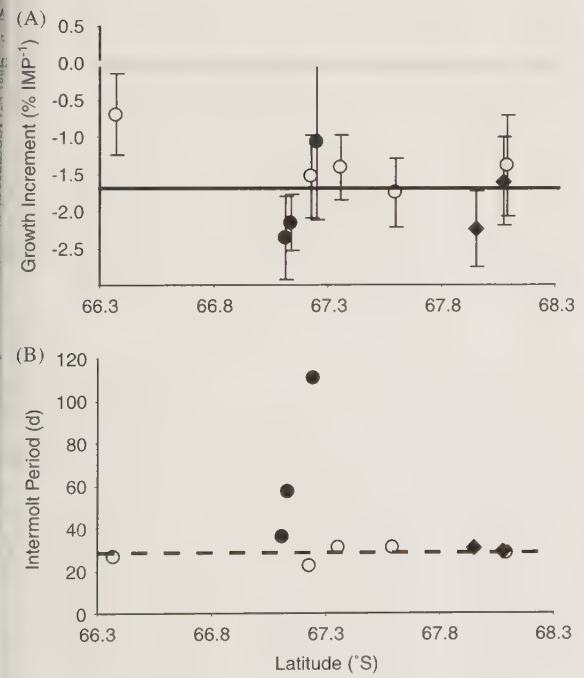

Fig. 5. *E. superba* larvae from the under-ice habitat. (A) Average growth increment (% IMP^{-1}) with standard error. Speckled bar indicates zero growth increment. Solid line is the mean growth increment. (B) IMP (d) with the dotted line indicating the median value. Plotted against the latitude of collection: single collections from floes (open circles), Ice Stations Robert (closed diamonds) and Billy (closed circles).

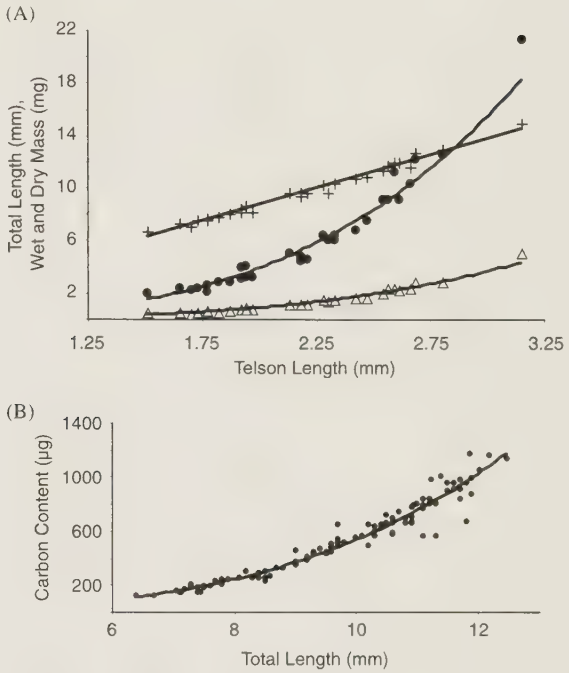

Fig. 6. *E. superba* larvae. Relationships between larval length measurements and other parameters. (A) Telson length (TelL, mm) and total length (TL, mm, +), wet mass (wwt, mg, closed circle) and dry mass (dwt, mg, open triangle). (B) Total length and carbon content (C, µg). The equations derived were: $TL = 5.09\,TelL - 1.4391$, $r^2 = 0.98$ ($n = 30$); $Wwt = 0.365\,TelL^{3.412}$; $Dwt = 0.074\,TelL^{3.554}$, $r^2 = 0.96$ ($n = 31$); and $C = 0.136\,TL^{3.60}$, $r^2 = 0.97$ ($n = 106$).

from 0 ($n = 5$ experiments) to 50% (Table 2). All furcilia 4 and 5 larvae advanced ($n = 4$), whereas only 9% of furcilia 6 advanced to juvenile. Those furcilia that advanced a stage were larger than those that did not (Table 4) (ANOVA, $F = 6.05$, $p = 0.016$), but the growth increments were not significantly different (ANOVA, $F = 0.44$, $p = 0.50$).

Pigment content: Pigment content in the larvae decreased with increasing days of starvation, leveling off at day 5.5 at a value of 0.02 µg $gwwt^{-1}$ for long-term starvation (Fig. 8A). Larvae from Ice Station Robert averaged slightly higher pigment contents than those from Ice Station Billy, but pigment contents of larval krill from different sites were very similar (Fig. 8B). All were 3–8 times greater than long-term starvation levels, although two of the collections showed pigment values similar to 2–3 d starvation levels (Fig. 8A). For the

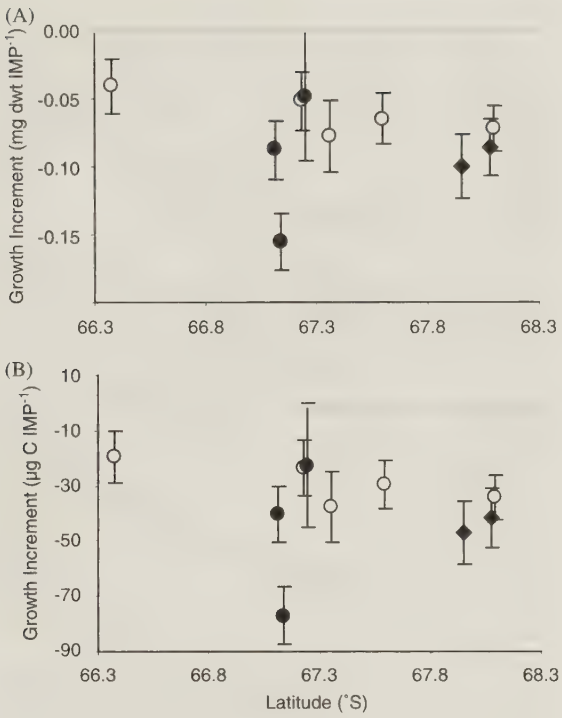

Fig. 7. *E. superba* larvae from the under-ice habitat. Growth increments in dry mass and carbon estimated from IGR experiments. (A) Average dry mass growth increment (mg dwt IMP^{-1}) with standard error. (B) Average carbon growth increment (µg $C IMP^{-1}$) with standard error. Plotted against the latitude of collection: single collections from floes (open circles), Ice Stations Robert (closed diamonds) and Billy (closed circles).

three collections for which both pigment content and growth increment exist, the two parameters do not co-vary.

In separate experiments not reported here, larval krill feeding at maximum ingestion rates at phytoplankton concentrations of $>4\,\mu g$ chl $a\,l^{-1}$ at in situ temperatures reached an average maximum pigment content of approximately $1.0\,\mu g\,gwwt^{-1}$ (S. A. Oakes, unpublished data). This maximum pigment content was 5 times that of the larval krill collected from under the ice during this cruise.

4. Discussion

The combination of diver observations, the results of the growth rate experiments and the pigment content determination allowed us to draw some general conclusions about the physiological status of larval krill from under the pack ice in August 2001. The observations and results describe larval krill from the under-ice surface in areas of moderately over-rafted pack ice, 5–8 m deep, in the winter of 2001. The dominant stages were furcilia stage 6 and juveniles, as has been previously found for late winter and early spring in the Scotia-Weddell Seas (Daly, 1990) and west of the Antarctic Peninsula (Frazer et al., 2002a; Quetin et al., 2003).

Table 3
Daily growth rates in terms of linear dimension (mm of total length), dry mass (mg dwt) and carbon (C) for the 10 instantaneous growth rate experiments: Mean, standard deviation (SD) and number of measurements (n)

Expt.	N	Linear (mm d^{-1})	Dry mass (mg dwt d^{-1})	Dry mass SD	Carbon (µg d^{-1})	Carbon (SD)
1	11	0.0021	−0.0013	0.0022	−0.635	1.043
2	18	−0.0062	−0.0017	0.0029	−0.777	1.383
3	13	−0.0054	−0.0021	0.0022	−0.968	1.043
4	12	−0.0051	−0.0028	0.0023	−1.362	1.135
5	12	−0.0065	−0.0033	0.0027	−1.542	1.284
6	12	−0.0050	−0.0023	0.0019	−1.116	0.913
7	7	−0.0041	−0.0051	0.0018	−2.515	0.894
8	11	−0.0061	−0.0029	0.0023	−1.314	1.087
9	3	−0.0010	−0.0016	0.0027	−0.737	1.277
10	13	−0.0049	−0.0026	0.0031	−1.232	1.533

The median IMP of 30.6 d was used as the molt interval.

Table 4
Total length and growth increment of furcilia 6 stage (F6) larval krill advancing a stage and not advancing a stage at ecdysis

	Mean	SD	*n*
Total Length (mm)			
F6 adv	10.06	0.41	7
F6 no adv	8.95	1.18	71
Growth increment (% IMP^{-1})			
F6 adv	−1.30	2.34	7
F6 no adv	− 1.74	1.74	71

Mean, standard deviation (SD) and number of larval krill. ANOVA: total length, $F=6.05$, $p=0.02$; growth increment, $F=0.44$, $p=0.50$.

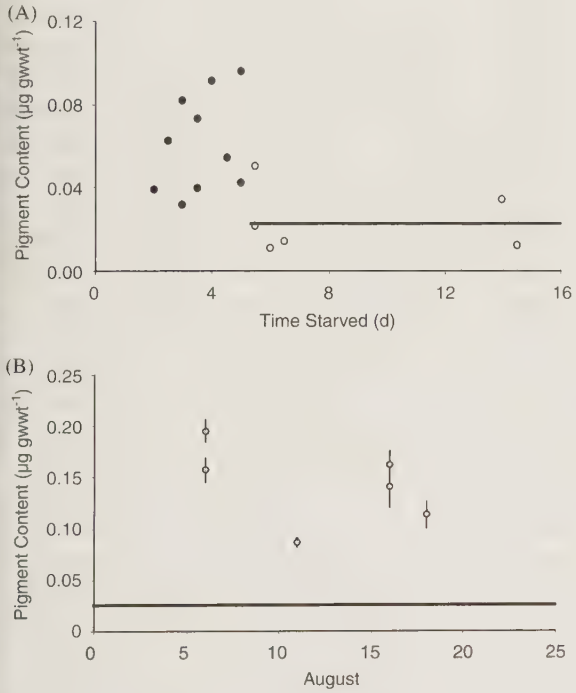

Fig. 8. Pigment content of *E. superba* larvae. (A) Mean pigment content versus days of starvation. Mean is of five subsamples. Horizontal line is the mean of days 5 through 14.5. (B) Pigment content of collections of larval krill from under the ice during August, with standard error. Horizontal line is the mean pigment content after 5–14.5 days of starvation.

Variability in both length frequency and stage frequency was observed on small spatial and temporal scales on the shelf seaward of Marguerite Bay, i.e. within the study region of ~160 km^2 and within an ice station. Biological variation between krill collections from the same area has been demonstrated previously for adult Antarctic krill (Quetin and Ross, 1984; Watkins et al., 1986, 1990). Watkins et al. (1990) found that more than 14 samples of more than 100 individuals were needed to get an unbiased estimate of most population parameters, including length and maturity. We suggest that similar levels of heterogeneity may exist in samples of larval krill. The results imply that growth rate estimates derived from single samples taken at a series of time points are subject to error due to the fact that no one sample gives a good representation of the size of the population. A comparison of size derived from two sets of samples, each taken relatively close in time, may give reasonable large scale results (Ashjian et al., 2004). However, although the difference between average size of larval krill in the winter and fall suggests that growth has occurred (Ashjian et al., 2004), the time scale is large, and we do not know when that growth occurred or under what environmental conditions. We also do not know if mortality has been higher in smaller larval krill, thus shifting the size distribution toward the larger krill without appreciable growth.

IGR experiments are short-term experiments conducted immediately after capture which document in situ growth rates, and have become accepted as the best method to determine growth rates of euphausiids in the field while avoiding the multiple assumptions inherent in following a cohort with length frequency analysis (Nicol, 2000). Determining growth rates of *E. superba* in the laboratory began with Mackintosh (1967) in the early Discovery days, and experimental results became clearer as control of conditions such as food and temperature increased (Poleck and Denys, 1982; Buchholz, 1991) (reviewed in Ross and Quetin, 2003). However, only with the advent of IGR experiments are we able to measure in situ growth rates of individuals. In the molting cycle of *E. superba*, the new exoskeleton is formed several days prior to molting depending on temperatures, and thus for euphausiids that have formed their new exoskeleton prior to collection, the initial growth increment reflects the feeding history prior to collection. The lack of a 'holding' effect is based on this characteristic of the molting cycle. With the

IGR technique, we can document growth rates of the target species over the critical periods.

Average growth increments over the time and space scales surveyed were all negative, i.e. the larvae were shrinking, whether growth was expressed in linear, dry mass or carbon terms. However, shrinkage was relatively low. In linear terms, the median shrinkage in total length ($-0.005\,\mathrm{mm\,d^{-1}}$) would only result in a larva decreasing in total length by about 0.1 mm in a month. The median loss in dry mass was estimated at $0.002\,\mathrm{mg\,dwt\,d^{-1}}$ and in carbon, $1.17\,\mu\mathrm{g\,C\,d^{-1}}$. To place this level of loss in perspective, Daly (2004) found that larvae kept starved, lost $0.009\,\mathrm{mg\,dwt\,d^{-1}}$ and $6.49\,\mu\mathrm{g\,C\,d^{-1}}$. Thus larvae starved in the laboratory lost dry mass and carbon at rates of about 5 times faster than the rates documented for larvae from the under-ice habitat in this region in winter 2001, as estimated from the IGR experiments.

Daly (2004) found that growth rates in larval krill decreased to near zero in both the winters of 2001 and 2002 in the SO GLOBEC study region. Combining the results from both winters, she found that 87% of the larvae in her experiments (total of five experiments for the 2 years) either maintained their size or grew. In this study, based on data from 10 experiments in the winter of 2001 only, the majority of larvae were shrinking, although over one-fifth (22%) were receiving enough food to either maintain their size or grow. What are some of the possible causes of the difference in the distribution of individual growth increments between this study and that of Daly (2004)? One possibility is that the experiments were conducted with larvae from slightly different geographical locations. In the study of Quetin et al. (2003), although the seasonal pattern was stronger than the interannual and within cruise variability, growth rates did vary from site to site within a cruise by 1–3% $\mathrm{IMP^{-1}}$. The results of the present study also show that there is a large variability in the percent of positive individual growth rates in an experiment with location, ranging from 0% to 38.5%, leading to one experiment with an average growth increment that was not significantly different from zero.

Development also appeared to be slow, as only 9% of the furcilia stage 6 that molted advanced to juvenile, a similar result to that of Daly (2004). This result implies that multiple instars within the furcilia 6 stage were the rule and not the exception under these winter conditions. As might be predicted, those furcilia that advanced a stage were larger than those that did not, but the growth increments were the same. Such developmental delays and consequent multiple instars due to slow growth were also found for larval *Euphausia pacifica* in laboratory experiments (Ross, 1981).

Larval krill were coupled to the under-ice habitat in winter 2001, and generally feeding on the floors of over-rafted ice floes, as previously found and described in Frazer et al. (1997, 2002a). Visually, however, the ice surface was white and hard, to all appearances devoid of sea-ice algae. Pigment content of the larvae was used as an index of grazing on sea-ice algae. Two studies indicate that larval krill from under the ice in winter are primarily herbivores. The first was based on the stable isotopic composition of the larvae (Frazer, 1996), and the second on the metabolic O:N ratio (Frazer et al., 2002b). Larval krill also may be grazing on heterotrophic organisms living on the ice surfaces, increasing total food intake by an unknown amount, as protozoans can comprise 6–49% of the biomass in the ice (Garrison, 1991; Palmisano and Garrison, 1993). Garrison and Close (1993) also suggested that the heterotrophic component of the sea-ice microbial community might become increasingly important in the fall and winter, but there was considerable interannual variation. Thus pigment content yields qualitative data on the feeding of these larval krill on sea-ice microalgae alone, but is likely to follow total ingestion if the heterotrophic/autotrophic ratio does not vary substantially and if larval krill are not strongly selective for one group or the other.

In previous studies, larval or juvenile krill from under ice floes in winter or spring have shown higher pigment content than those in this study that averaged $0.15\,\mu\mathrm{g\,gwwt^{-1}}$. Two other data sets exist on pigment content of larval krill in winter from under the ice (Daly, 1990, 2004), and other studies have documented pigment content in

subadult krill in spring (November) (Daly, 1998) and summer (Urbań-Rich et al., 2001). Larval krill in the Scotia-Weddell Seas contained from 4.0 to 11.0 ng pigment per krill, corrected for degradation (Daly, 1990) or about 0.5–2 $\mu g\,gwwt^{-1}$ (our calculation). For subadults (27 mm), during spring in the west of Antarctic Peninsula, pigment content corrected for degradation was equivalent to 0.06 $\mu g\,gwwt^{-1}$ in krill from the water column, but 1.5 $\mu g\,gwwt^{-1}$ in krill from under ice floes (Daly, 1998). In winter 2001, Daly (2004) found that pigment content of larvae was low, and the same whether larvae were from the water column or the under-ice habitat. If we use the estimates of pigment degradation found in Daly (1998) of 9–67%, the average pigment values of larval krill from under the ice in August 2001 would still be at the low end of those found in previous studies. However, pigment content of well-fed larvae (S. A. Oakes, unpublished data) was similar to the maximum values of larval and juvenile krill from under ice floes (Daly, 1990, 1998).

In addition, Perissinotto et al. (2000) measured pigment content in adult krill on three summer cruises. Pigment content, corrected for degradation and assuming that adult krill were about 500 mg wwt, ranged from 0.1 to 7.9 $\mu g\,gwwt^{-1}$, with most values $<0.2\,\mu g\,gwwt^{-1}$. They emphasize that the pigment content tended to correlate well with the chl *a* concentration in the water column, confirming that pigment content can be used as an index of grazing on phytoplankton.

One other issue is that microalgal pigments cannot be used as quantitative tracers of ingestion because the pigments are degraded to a variable extent during the digestive process (Conover et al., 1986; Perissinotto and Pakhomov, 1996; Dagg, 1993; Daly, 1998). This variability may be due, in part, to variations in ingestion rate and nutritional history (Penry and Frost, 1990). We minimized the factor of variable levels of pigment degradation due to temperature and larval condition by comparing pigment content of larvae from under the ice to that of starved and well-fed larvae from the same region and held at in situ temperatures. Although variability may exist in the extent of pigment degradation in larval krill from the field and well-fed larval krill on board the ship, our comparison allowed us to qualitatively evaluate the level of ingestion of sea-ice microalgae.

Pigment content of larval krill associated with the under-ice surface was only about 20% of that of larvae fed high concentrations of phytoplankton (about 4 $\mu g\,l^{-1}$ chl *a*). These results suggested that larvae in the field were not feeding on sea-ice algae at maximum possible ingestion rates. Additional data on the abundance and composition of the sea-ice microbial community, and possible selection by larval krill on that community will contribute to our understanding of the interaction of larval krill with the sea-ice community. At this juncture, the low pigment content and negative growth increments suggested that although larval krill were feeding on the sea-ice microbial community, total intake for most larvae was less than required for both maintenance and growth. However, the larvae were losing dry mass and carbon at rates much less than those of starved larvae, and thus, although food limited from the perspective of being able to grow, they may not have been in danger of starvation.

Comparison to historical data: One of the objectives of this study was to obtain data on growth rates of larval krill in August, a time period for which there was no historical data (Quetin et al., 2003). The low and negative growth increments found in this study appeared to continue the decreasing trend of growth found in early winter in this previous study of growth increments for larvae from the under-ice habitat (Quetin et al., 2003). Growth rates in August in this study were slightly less than those found early in the winter (June/July), and much less than those found in September, as winter turns to spring (Quetin et al., 2003) (Fig. 9A). The results suggest that the rate of increase in growth from late winter progressing into spring is more rapid than the decline in growth rate from fall progressing to winter.

In Quetin et al. (2003), based on 52 experiments from nine fall and winter cruises with larvae from both the water column and the under-ice habitat, daylength appeared to be a good predictor of growth increments. However, growth increments in this study were not correlated with daylength, and were well below the regression line describing the previous relationship between daylength at the

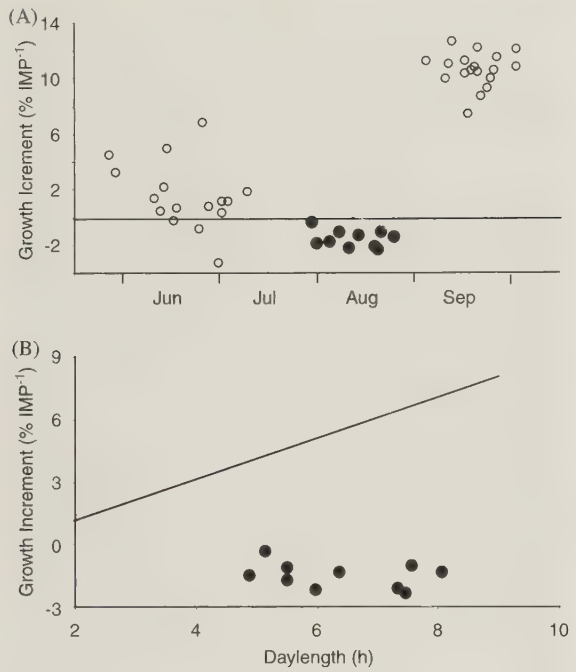

Fig. 9. Comparison to historical growth data on larval krill in winter west of the Antarctic Peninsula. (A) Growth increment versus Julian Day. Open circles are historical data for larval krill from the under-ice habitat only from Quetin et al. (2003), closed circles are the present study. Horizontal line is zero growth. (B) Growth increment versus daylength. Closed circles are data from this study. Line is the linear regression describing the previously found relationship between daylength and growth increment for larvae from both the water column and under the ice in fall and winter (growth increment = 0.984 (daylength in h) –0.868, $r^2 = 0.74$, $n = 49$) (Quetin et al., 2003).

time and place of collection and growth increment (Fig. 9B). Given that this is a single study compared to nine previous cruises, the results suggest that food availability in the late winter of 2001 was anomalously low. However, an alternate explanation involves the differences in the platforms used to collect the data. During this SO GLOBEC cruise, due to the assistance of the RVIB *Nathaniel B. Palmer*, the ARSV *Laurence M. Gould* penetrated further into pack ice in this region in winter than was previously possible. One possibility is that the relationship previously derived is relevant for the fringes and lighter regions of the pack ice, but may not be relevant for the interior. In the interior, the degree of overrafting is greater, and the light penetration to the under-ice habitat is less. Under these conditions, daylength would not represent the light available for sea-ice microalgal production, as was postulated by Quetin et al. (2003). The sequential cruise in August 2002 may help us resolve this discrepancy.

Acknowledgements

We express our appreciation to the Captain and crew of the ARSV *Laurence M. Gould* for their skill and attention to safety during the cruise. Members of the Raytheon support staff also contributed significantly to our ability to conduct research under winter conditions. We would particularly like to mention the contributions of C. Boch and J. Watson, SCUBA divers 'par excellence', who in addition to Quetin and Newberger were essential to the under water observations and collection of larval krill. M. Thimgam was of great assistance in overall cruise sampling. We would also like to thank two anonymous reviewers and an editor for their helpful comments. This research was supported by National Science Foundation, Office of Polar Programs, Grant No. OPP-9909933 to Ross and Quetin. U.S. GLOBEC Contribution No. 458.

References

Ashjian, C.J., Rosenwaks, G.A., Wiebe, P.H., Davis, C.S., Gallager, S.M., Copley, N.J., Lawson, G.L., Alatalo, P., 2004. Distribution of zooplankton on the continental shelf off Marguerite Bay, Antarctic Peninsula, during austral fall and winter, 2001. Deep-Sea Research II, this issue [doi: 10.1016/j.dsr2.2004.07.025].

Buchholz, F., 1991. Moult cycle and growth of Antarctic krill *Euphausia superba* in the laboratory. Marine Ecology Progress Series 69, 217–229.

Conover, R.J., Durvasula, S., Roy, S., Wang, R., 1986. Probable loss of chlorophyll-derived pigments during passage through the gut of zooplankton, and some of the consequences. Limnology and Oceanography 31, 878–887.

Dagg, M.J., 1993. Grazing by the copepod community does not control phytoplankton production in the subartic Pacific Ocean. Progress in Oceanography 32, 163–183.

Daly, K.L., 1990. Overwintering development, growth and feeding of larval *Euphausia superba* in the Antarctic

marginal ice zone. Limnology and Oceanography 35, 1564–1576.

Daly, K.L., 1998. Physioecology of juvenile Antarctic krill (*Euphausia superba*) during spring in ice-covered seas. In: Lizotte, M.P., Arrigo, K.R. (Eds.), Antarctic Sea Ice Biological Processes, Interactions, and Variability. Antarctic Research Series. American Geophysical Union, Washington, DC, pp. 183–198.

Daly, K.L., 2004. Overwintering growth and development of larval *Euphausia superba*: an interannual comparison under varying environmental conditions west of the Antarctic Peninsula. Deep-Sea Research II, this issue [doi: 10.1016/j.dsr2.2004.07.010].

Elias, M.C., 1990. Effects of photoperiod, phytoplankton level and temperature on the growth, development and survival of larval *Euphausia superba* (Dana). Master of Arts in Biology Thesis, University of California, Santa Barbara.

Fraser, F.C., 1936. On the development and distribution of the young stages of krill (*Euphausia superba*). Discovery Reports 14, 1–192.

Frazer, T.K., 1996. Stable isotope composition (δ^{13}C and δ^{15}N) of larval krill, *Euphausia superba*, and two of its potential food sources in winter. Journal of Plankton Research 18, 1413–1426.

Frazer, T.K., Quetin, L.B., Ross, R.M., 1997. Abundance and distribution of larval krill, *Euphausia superba*, associated with annual sea ice in winter. In: Battaglia, B., Valencia, J., Walton, D.W.H. (Eds.), Sixth Biological Symposium. Scientific Committee on Antarctic Research (SCAR), pp. 107–111.

Frazer, T.K., Quetin, L.B., Ross, R.M., 2002a. Abundance, sizes and developmental stages of larval krill, *Euphausia superba*, during winter in ice-covered seas west of the Antarctic Peninsula. Journal of Plankton Research 24, 1067–1077.

Frazer, T.K., Quetin, L.B., Ross, R.M., 2002b. Energetic demands of larval krill, *Euphausia superba*, in winter. Journal of Experimental Marine Biology and Ecology 277, 157–171.

Garrison, D.L., 1991. The biota of Antarctic sea ice. American Zoologist 31, 17–33.

Garrison, D.L., Close, A.R., 1993. Winter ecology of the sea ice biota in Weddell Sea pack ice. Marine Ecology Progress Series 96, 17–31.

Hollander, E., 2001. Investigation of growth measurements for Antarctic krill, *Euphausia superba*. Honors Thesis, University of Tasmania, Australia.

Ikeda, T., 1984. Development of the larvae of the Antarctic krill (*Euphausia superba* Dana) observed in the laboratory. Journal of Experimental Marine Biology and Ecology 75, 107–117.

Jarman, S.N., Elliott, N.G., Nicol, S., McMinn, A., 2002. Genetic differentiation in the Antarctic coastal krill *Euphausia crystallorophias*. Heredity 88, 280–287.

Mackas, D., Bohrer, R., 1976. Fluorescence analysis of zooplankton gut contents and an investigation of diel feeding patterns. Journal of Experimental Marine Biology and Ecology 25, 77–85.

Mackintosh, N.A., 1967. Maintenance of living *Euphausia superba* and frequency of moults. Norsk Hvalfangst-Tidende (The Norwegian Whaling Gazette) 5, 97–102.

Mauchline, J., 1980. Measurement of body length of *Euphausia superba* Dana: BIOMASS Handbook, vol. 4, pp. 4–9. SCAR/SCOR.

Nicol, S., 2000. Understanding krill growth and aging: the contribution of experimental studies. Canadian Journal of Fisheries and Aquatic Sciences 57, 168–177.

Nicol, S., Stolp, M., Cochran, T., Geijsel, P., Marshall, J., 1992. Growth and shrinkage of Antarctic krill (*Euphausia superba* Dana) from the Indian sector of the Southern Ocean during summer. Marine Ecology Progress Series 89, 175–181.

Ottersen, G.B., Loeng, H., 2000. Covariability in early growth and year-class strength of Barents Sea cod, haddock and herring: The environmental link. ICES Journal of Marine Science 57, 339–348.

Palmisano, A.C., Garrison, D.L., 1993. Microorganisms in Antarctic sea ice. In: Friedmann, E.I. (Ed.), Antarctic Microbiology. Wiley-Liss, Inc., New York, pp. 167–218.

Penry, D.L., Frost, B.W., 1990. Re-evaluation of the gut-fullness (gut fluorescence) method for inferring ingestion rates of suspension-feeding copepods. Limnology and Oceanography 35, 1207–1214.

Pepin, P., 1989. Using growth histories to estimate larval fish mortality rates. Rapports et Proces-Verbaux des Réunions, Conseil International Pour L'Exploration de la Mer 191, 324–329.

Pepin, P., 1991. The effect of temperature and size on development and mortality rates of pelagic life history stages of marine fish. Canadian Journal of Fisheries and Aquatic Sciences 48, 503–518.

Perissinotto, R., Pakhomov, E.A., 1996. Gut evacuation rates and pigment destruction in the Antarctic krill *Euphausia superba*. Marine Biology 125, 47–54.

Perissinotto, R., Gurney, L., Pakhomov, E.A., 2000. Contribution of heterotrophic material to diet and energy budget of Antarctic krill, *Euphausia superba*. Marine Biology 136, 129–135.

Poleck, T.P., Denys, C.J., 1982. Effect of temperature on the molting, growth and maturation of the Antarctic *Euphausia superba* (Crustacea: Euphausiacea) under laboratory conditions. Marine Biology 70, 255–265.

Quetin, L.B., Ross, R.M., 1984. School composition of the Antarctic krill, *Euphausia superba*, in the waters west of the Antarctic Peninsula during the austral summer, 1982. Journal of Crustacean Biology 4 (Spec. No. 1), 96–106.

Quetin, L.B., Ross, R.M., 1991. Behavioral and physiological characteristics of the Antarctic krill, *Euphausia superba*. American Zoologist 31, 49–63.

Quetin, L.B., Ross, R.M., 2003. Episodic recruitment in Antarctic krill, *Euphausia superba*, in the Palmer LTER study region. Marine Ecology Progress Series 295, 185–200.

Quetin, L.B., Ross, R.M., Frazer, T.K., Haberman, K.L., 1996. Factors affecting distribution and abundance of

zooplankton, with an emphasis on Antarctic krill, *Euphausia superba*. In: Ross, R.M., Hofmann, E.E., Quetin, L.B. (Eds.), Foundations for Ecological Research West of the Antarctic Peninsula. Antarctic Research Series. American Geophysical Union, Washington, DC, pp. 357–371.

Quetin, L.B., Ross, R.M., Frazer, T.K., Amsler, M.O., Wyatt-Evens, C., Oakes, S.A., 2003. Growth of larval krill, *Euphausia superba*, in fall and winter west of the Antarctic Peninsula. Marine Biology 143, 833–843.

Ross, R.M., 1981. Laboratory culture and development of *Euphausia pacifica*. Limnology and Oceanography 26, 235–246.

Ross, R.M., Quetin, L.B., 1991. Ecological physiology of larval euphausiids, *Euphausia superba* (Euphausiacea). Memoirs of the Queensland Museum 31, 321–333.

Ross, R.M., Quetin, L.B., 2003. Working with living krill—the people and the places. Marine and Freshwater Behavior and Physiology 36, 207–228.

Ross, R.M., Quetin, L.B., Baker, K.S., Vernet, M., Smith, R.C., 2000. Growth limitation in young *Euphausia superba* under field conditions. Limnology and Oceanography 45, 31–43.

Siegel, V., 2000. Krill (Euphausiacea) life history and aspects of population dynamics. Canadian Journal of Fisheries and Aquatic Sciences 57, 130–150.

Siegel, V., Loeb, V., 1995. Recruitment of Antarctic krill (*Euphausia superba*) and possible causes for its variability. Marine Ecology Progress Series 123, 45–56.

Siegel, V., Loeb, V., Gröger, J., 1998. Krill (*Euphausia superba*) density, proportional and absolute recruitment and biomass in the Elephant Island region (Antarctic Peninsula) during the period 1977 to 1997. Polar Biology 19, 393–398.

Siegel, V., Bergström, B., Mühlenhardt-Siegel, U., Thomasson, M., 2002. Demography of krill in the Elephant Island area during summer 2001 and its significance for stock recruitment. Antarctic Science 14, 162–170.

Smetacek, V., Scharek, R., Nothig, E.-M., 1990. Seasonal and regional variation in the pelagial and its relationship to the life history cycle of krill. In: Kerry, K.R., Hempel, G., (Eds.), Antarctic Ecosystems, Ecological Change and Conservation. Symposium on Antarctic Biology (SCAR). Springer, Berlin, pp. 103–114

Smith, R.C., Baker, K.S., Dustan, P., 1981. Fluorometer techniques for measurement of oceanic chlorophyll in the support of remote sensing. La Jolla, California, Scripps Institution of Oceanography, University of California, Ref. 81-17, 14pp.

Urban-Rich, J., Dagg, M., Peterson, J., 2001. Copepod grazing on phytoplankton in the Pacific sector of the Antarctic Polar Front. Deep-Sea Research II 48, 4223–4246.

Watkins, J., 1999. A composite recruitment index to describe interannual changes in the population structure of Antarctic krill at South Georgia. CCAMLR Science 6, 71–84.

Watkins, J.L., Morris, D.J., Ricketts, C., Priddle, J., 1986. Differences between swarms of Antarctic krill and some implications for sampling krill populations. Marine Biology 93, 137–146.

Watkins, J.L., Morris, D.J., Ricketts, C., Murray, A.W.A., 1990. Sampling biological characteristics of krill: effects of heterogeneous nature of swarms. Marine Biology 107, 409–415.

ELSEVIER

Deep-Sea Research II 51 (2004) 2185–2198

DEEP-SEA RESEARCH
PART II

www.elsevier.com/locate/dsr2

Daily rations and growth of larval krill *Euphausia superba* in the Eastern Bellingshausen Sea during austral autumn

E.A. Pakhomov[a,c,*], A. Atkinson[b], B. Meyer[c], B. Oettl[c], U. Bathmann[c]

[a]*Department of Zoology, University of Fort Hare, Private Bag X1314, Alice 5700, South Africa*
[b]*British Antarctic Survey, Natural Environment Research Council, High Cross, Madingley Road, Cambridge CB3 0ET, UK*
[c]*Alfred-Wegener-Institute for Polar and Marine Research, Am Handelshafen 12, D-27515 Bremerhaven, Germany*

Accepted 9 July 2004

Abstract

As the German contribution to the Southern Ocean Global Ocean Ecosystems Dynamics Study (SO GLOBEC), RV *Polarstern* visited the Eastern Bellingshausen Sea between 18 April and 1 May 2001. This paper examines in situ feeding cycles, ingestion rates and growth of larval krill *Euphausia superba*. Larval krill were exceptionally numerous, especially over the shelf break and continental slope: mean 8872 larvae m^{-2}, maximum 30 084 larvae m^{-2}. The developmental stage composition of krill larvae over the shelf was advanced compared to that at continental slope stations, which may have resulted from enhanced food availability over the shelf. Despite the season being late autumn, the feeding activity of larval krill was similar to published summer rates. The intermoult period of larval krill ranged from 6 to 17 days, with daily growth rates reaching 2.2% of body length, 8.7% of body wet mass and 5.7% of body carbon. Daily ingestion rates were 8.5–17.6 μg C ind^{-1} d^{-1} for calyptopis 3 to furcilia 2 and 35.1–57.4 μg C ind^{-1} d^{-1} for furcilia 3–5, and were positively correlated with ambient chlorophyll *a* concentrations. Daily rations showed the same tendency, ranging from 21.5 to 44.5% of body C d^{-1} (calyptopis 3 to furcilia 2) and from 17.8 to 29.2% of body C d^{-1} (furcilia 3–5). Comparison of daily rations between open water and sea ice stations supports the notion that larval krill at low pelagic food supply under the sea ice have to exploit ice biota to sustain their metabolic demands.
© 2004 Elsevier Ltd. All rights reserved.

1. Introduction

Antarctic krill *Euphausia superba* (hereafter "krill") is a keystone species of the Southern Ocean, supporting numerous populations of apex predators, including fish, squid, birds and mammals, as well as a commercial fishery (Knox, 1994). Despite major research efforts starting over a century ago in the Southern Ocean, there are still many gaps in our knowledge of the biology of adult krill and particularly of their larvae (e.g., Miller and Hampton, 1989; Daly, 1990; Ross and Quetin, 1991). Several studies have focused on

*Corresponding author at present address: Department of Earth and Ocean Sciences, University of British Columbia, 6339 Stores Road, Vancouver, British Columbia, Canada V6T 1Z4.
E-mail address: epakhomov@eos.ubc.ca (E.A. Pakhomov).

0967-0645/$ - see front matter © 2004 Elsevier Ltd. All rights reserved.
doi:10.1016/j.dsr2.2004.08.003

larval and adult krill overwintering strategies (e.g., Daly, 1990; Hagen et al., 2001; Atkinson et al., 2002b). There is growing evidence that, due to differences in ecophysiology and biochemistry, larval and adult krill probably adopt "business as usual" and "compromise" (*sensu* Torres et al., 1994) overwintering strategies, respectively (Daly, 1990; Atkinson et al., 2002b; Meyer et al., 2002). After adult spawning in December–March, krill larvae usually grow to furcilia stage 2–3 by autumn (Fraser, 1936; Makarov et al., 1990; Huntley and Brinton, 1991). If larval krill adopt "business as usual" they have to change from a pelagic to an under the sea-ice habitat between summer and winter for continuous feeding, since a pelagic habitat is unlikely able to sustain sufficient food supply during winter (Daly, 1990; Ross and Quetin, 1991; Meyer et al., 2002). To date, only a few studies have addressed the ecophysiology of larval krill. Daily rations of furcilia have been estimated in only three studies: using gut fluorescence during austral winter in the Scotia Sea (Daly, 1990), in vitro incubations in the south-western Lazarev Sea (Meyer et al., 2002), and an energetic approach in the western Bransfield Strait region (Huntley and Brinton, 1991). The values ranged widely from 0.4 to 52% of body $C\,d^{-1}$.

In a study of Gerlache Strait in 1986–87, Huntley and Brinton (1991) suggested that coastal regions along the Antarctic Peninsula may be significant nursery areas for krill larvae and may act as "focal points in krill recruitment". During April–May 2001, a German Southern Ocean Global Ocean Ecosystems Dynamics (SO GLOBEC) cruise in the Eastern Bellingshausen Sea was conducted. Its main objective was to examine interactions between zooplankton and the physical conditions during the autumn transitional period in this suggested krill "nursery area" (Siegel, 1989, 2000). The main aim of this study was to provide information on feeding dynamics of larval krill using the gut fluorescence technique, and to measure its growth.

2. Material and methods

Data were collected during the expedition ANTARKTIS XVIII/5b to the Eastern Bellingshausen Sea on board RV *Polarstern* conducted between 18 April and 1 May 2001 as the German contribution to the field campaign of the SO GLOBEC (Fig. 1; Bathmann, 2002). At each oceanographic station, seawater temperature, salinity and density were measured using a Sea-Bird Electronics SBE 911 conductivity-temperature-depth (CTD) profiler, which was mounted on a Sea-Bird SBE 32 Carousel holding 24 Niskin bottles of 12 l capacity (Strass et al., 2002). Water samples for total chlorophyll *a* (Chl *a*) were collected at eight standard depths: 0, 10, 25, 50, 75, 100, 150 and 200 m (Brichta and Belem, 2002). Chl *a* was extracted from 1000-ml aliquots in 90% aqueous acetone following filtration through GFF Whatman filters for 12 h in the dark at −18 °C. Concentrations were calculated from fluorescence readings on a Turner Design 10AU fluorometer before and after acidification with HCl (Parsons et al., 1984).

2.1. Larval krill sampling and grazing

Larval krill were collected using a Bongo net ($0.5\,m^{-2}$ mouth area, mesh size 300 μm) during vertical tows from 300 m to the surface. Zooplankton samples from one of the net pair were pored through a 300-μm mesh, placed in a plastic bag and immediately transferred to a deep freezer (−80 °C). These samples were used for determination of larval krill abundance and additional measurements of gut fluorescence (see below). Gut pigment content and grazing rates of larval krill were measured from the other net throughout the sampling period at every station. The in situ gut contents were measured either onboard ship by processing from 2 to 6 krill larvae per tube according to developmental stages, including early (calyptopis 3 to furcilia 2) and late stage (3–5) furcilia. In addition, at selected stations gut pigments of different developmental stages were determined using deep-frozen (−80 °C) samples. Deep-frozen samples were thawed in the refrigerator in darkness for several hours, rinsed briefly in deionised water, sorted on ice according to developmental stage and placed (three to five specimens per tube) in 10-ml polypropylene tubes for pigment extraction. The remaining larvae were

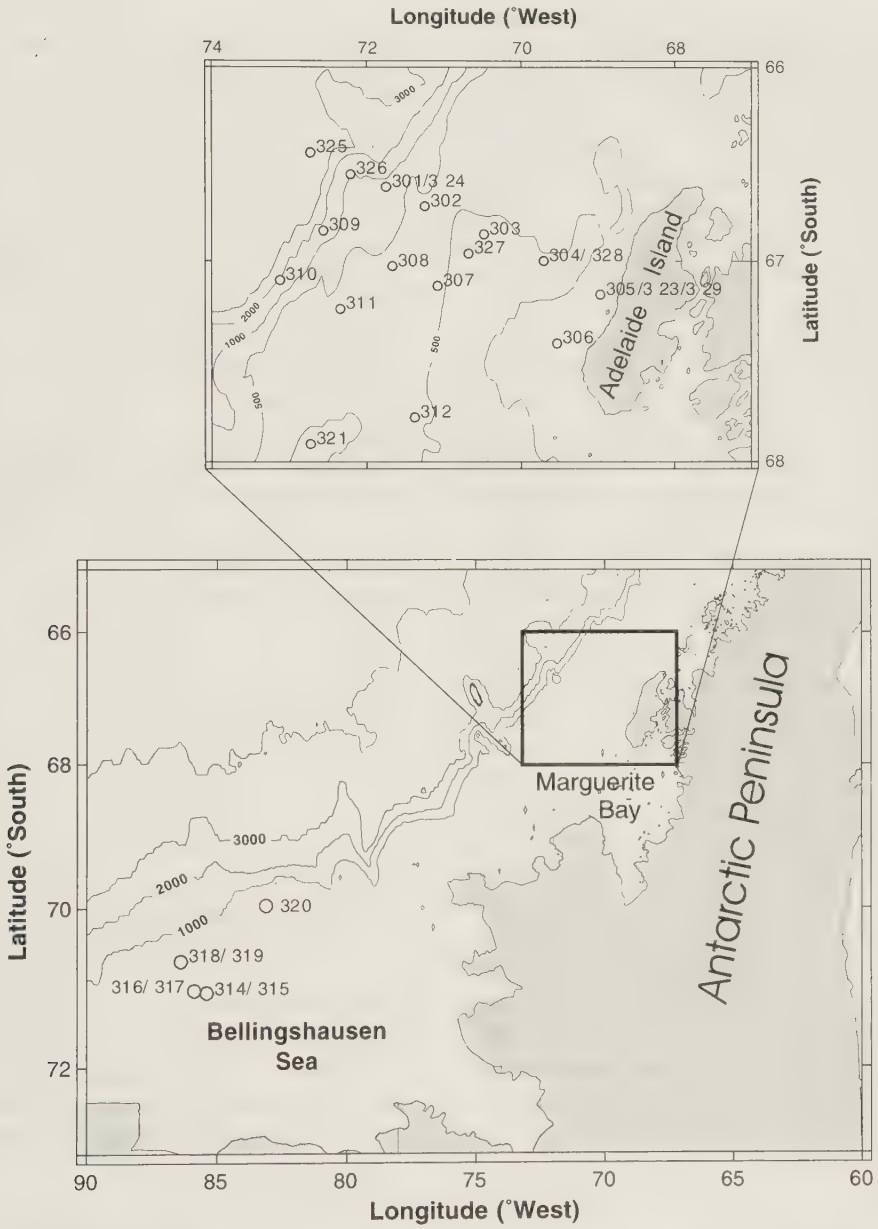

Fig. 1. Location of stations conducted during the ANTARKTIS XVIII/5b cruise to the Eastern Bellingshausen Sea on board RV *Polarstern* between 18 April and 1 May 2001.

counted and their developmental stages were determined.

Gut evacuation rate experiments consisted of in vitro incubations of 70–80 freshly caught specimens in 20-l polyethylene containers filled with surface seawater filtered through 0.2 μm (Milli-Q filtration system) to which non-fluorescent charcoal particles of <100 μm in diameter were added to simulate continuous feeding conditions (Willason and Cox, 1987). The incubations lasted 1.5–2 h, with gut fluorescence measured at 10–15 min intervals for the first hour and at

20–30-min intervals thereafter until the end of the experiment. Prior to each incubation, 5–10 fresh individuals were processed for the measurement of their initial gut pigment content. Gut evacuation rate constants (k, h^{-1}) were then derived from the slope of the regression versus time (Perissinotto and Pakhomov, 1996).

Gut pigment destruction efficiency was estimated using the two-compartment (phytoplankton and grazer) pigment budget approach. For this, freshly caught larvae were first incubated in particle-free seawater for 4–6 h to allow time to empty their guts. 3–5 specimens per jar were then incubated for 1 h in 1-l polyethylene containers containing natural seawater. After 1 h feeding, a comparison of the pigment budgets in the control (without grazers) and experimental containers was carried out. Any significant loss in the pigment budget from the experimental treatment (water + larval krill) was then attributed to gut destruction of phytoplankton pigments (Perissinotto and Pakhomov, 1996). In all experiments, gut pigments were extracted in polyethylene tubes (2–6 individuals per tube, 2–5 replicate tubes) with 10 ml of 90% acetone at −18 °C for 24 h in darkness. After centrifugation at 5000 rpm (1745 × g), the pigment content was measured as for CTD extractions. Pigment contents were then expressed in terms of total pigments (Chl a + phaeopigments) per individual. Where the Chl a:phaeopigment ratio in the gut content was > 0.25, total pigment values were corrected according to Baars and Helling (1985). Background fluorescence was estimated from incubations of krill larvae in filtered seawater for 10–12-h and then subtracted from all gut pigment content data.

Daily ingestion rates (I, ng pigm ind^{-1} d^{-1}) were estimated from the relationship of Perissinotto (1992): $I = kG/(1-b')$, where G is an integrated value over 24 h period of gut pigments (ng pigm ind^{-1} d^{-1}), k is the gut evacuation rate constant (h^{-1}) and b' is efficiency of gut pigment destruction. To convert pigment concentrations into autotrophic carbon (C), we used a mean POC: pigment (Chl a + phaeopigments) ratio of 37.5, obtained at Stations 303 and 320 in the top 100-m water layer (M. Brichta and A. Belem, unpublished).

2.2. Moulting experiments

Three moulting experiments were conducted using larval krill collected gently with a hand-hauled Apstein net in the top 30-m water layer during darkness. One hundred and sixty-four to 174 furcilia (stages 1–6) were immediately transferred to 250- or 500-ml bottles (depending on size, one furcilia per jar) filled with surface seawater. Experiments were run for 2 days in darkness at ambient (0 °C) seawater temperature. At the end of each experiment, each jar was examined and all animals and moults were frozen at −80 °C. The intermoult period was calculated as the inverse of the fraction of the population that moulted per day (Nicol et al., 1992). To determine growth increments, the exopodite of the right uropod was measured on both the moult and the moulted animal using a microscope ocular micrometer. To calculate growth rates, 30 furcilia ranging from stage 1 to 5 were selected from the moulting experiments. Uropod- and total length (from the base of the eye to the tip of telson) were measured for these individuals before determination of their wet mass, dry mass and C and N masses. For dry mass, individual larvae were oven-dried for 36 h at 60 °C in pre-weighed tin capsules and then used for C and N mass measurements in a Carlo Erba 1500 analyser. Growth rates were expressed as the percentage change in uropod length between the postmoult krill and its moult. The percentage change in mass (wet, dry, carbon and nitrogen) was determined using uropod length–body mass regressions. The daily growth rates (d^{-1}) were calculated as the difference between the premoult and postmoult length/mass parameters divided by the intermoult period.

3. Results

3.1. Larval distribution, abundance and composition

Total larval density varied between 4 and 30 084 ind m^{-2} (Table 1). The highest concentrations (> 10 000 ind m^{-2}) were observed near the shelf break and over the continental slope, while

Table 1
E. superba larval abundance estimated using Bongo net during April and May 2001 in the Eastern Bellingshausen Sea

Area, station number	Date, 2001	Sampling depth (m)	Sampling time (local)	Chl-*a* biomass ($mg\,m^{-2}$)	Total larval density ($ind\,m^{-2}$)
Near shelf break, over continental slope					
309	20 Apr	0–300	06:40	110.7	18 984
324	28 Apr	0–300	20:42	44.0	30 084
325	29 Apr	0–300	08:00	16.5	14 164
326	29 Apr	0–300	21:23	15.1	14 544
Mean (±SD)					19 444±7423
Shelf region					
302	18 Apr	0–400	14:28	51.1	1004
304	19 Apr	0–100	01:37	30.3	26 516
305	19 Apr	0–300	06:49	86.2	188
306	19 Apr	0–200	11:00	59.9	4
312	21 Apr	0–300	12:37	130.9	44
323	28 Apr	0–200	06:55	89.9	60
327	30 Apr	0–300	16:21	53.8	1308
328	1 May	0–300	06:26	44.8	7760
329	1 May	0–300	12:45	99.6	680
Mean (±SD)					4174±8730

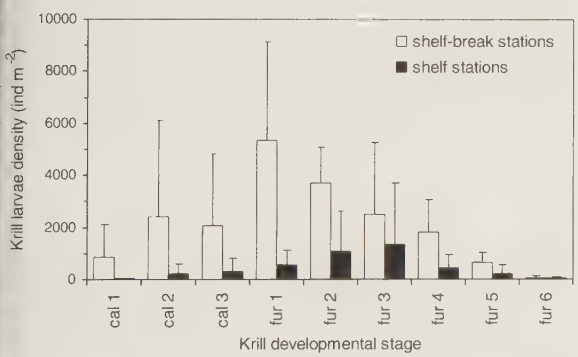

Fig. 2. Larval krill *E. superba* developmental composition in the Eastern Bellingshausen Sea during 18 April to 1 May 2001 according to Bongo net tows. Cal: calyptopis; fur: furcilia. Error bars represent 95% confidence limits.

over the shelf, with the exception of Station 304, larval concentrations did not exceed $8000\,ind\,m^{-2}$ (Table 1). Average larval densities were 4174 and $19\,444\,ind\,m^{-2}$ over the shelf area and near the shelf break, respectively. Krill larvae ranged from calyptopis 1 to furcilia 6. Although the larval composition was not significantly different (Spearman's rank test, $r=0.642$, $n=9$, $P>0.05$) between the shelf and near the shelf break regions, there was a clear tendency toward advanced larval composition over the shelf (Fig. 2). At stations near the shelf break and over the continental slope, furcilia 1 and 2 predominated, accounting on average for 47% of total larvae. Calyptopis 2 and 3 stages contributed on average 23% to total abundance. On stations over the shelf, furcilia 2 and 3 comprised ~60% of total larval abundance (Fig. 2).

3.2. Larval krill feeding dynamics

Individual gut pigment contents of krill larvae ranged widely between and within open-water and ice stations and between different stages (Fig. 3). Daytime gut pigment values were generally lower (occasionally significantly) than nighttime values. Furthermore, 57 and 26% of the variation in gut pigments in the open-ocean stations of early (calyptopis 3 to furcilia 2) and late (furcilia 3–5) furcilia was accounted for by variability in Chl *a* standing stock (Fig. 4). Thus for further analysis all larvae were separated into two age groups (early and late furcilia) and further according to ambient Chl *a* stock (lower or higher than $50\,mg\,m^{-2}$). However, for the ice stations all furcilia were pooled due to small differences in gut pigments among larval stages and the limited number of observations (Fig. 3).

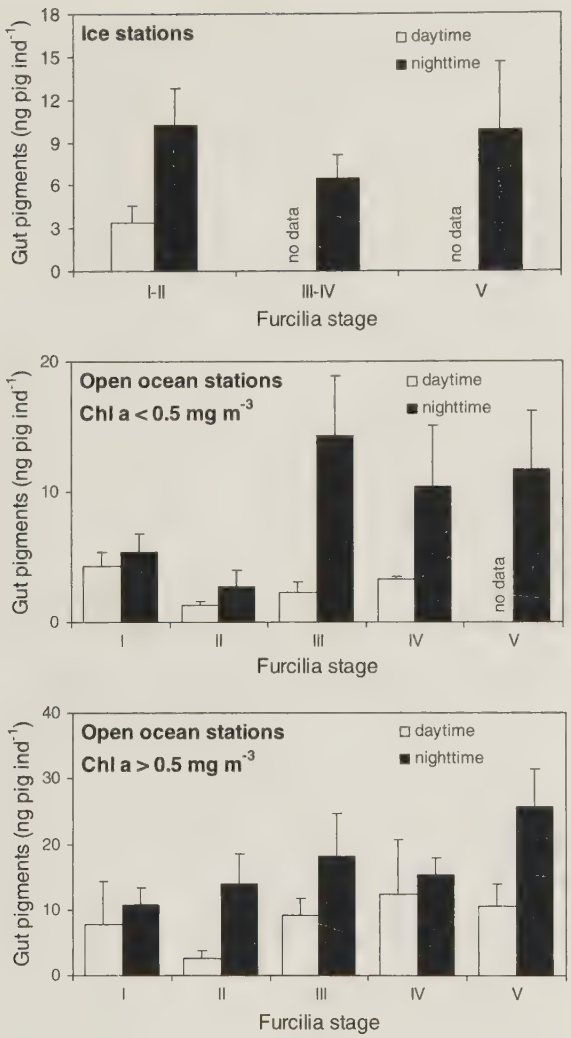

Fig. 3. Gut pigment levels of different developmental stages of larval krill on open water and ice stations. Error bars represent 95% confidence limits.

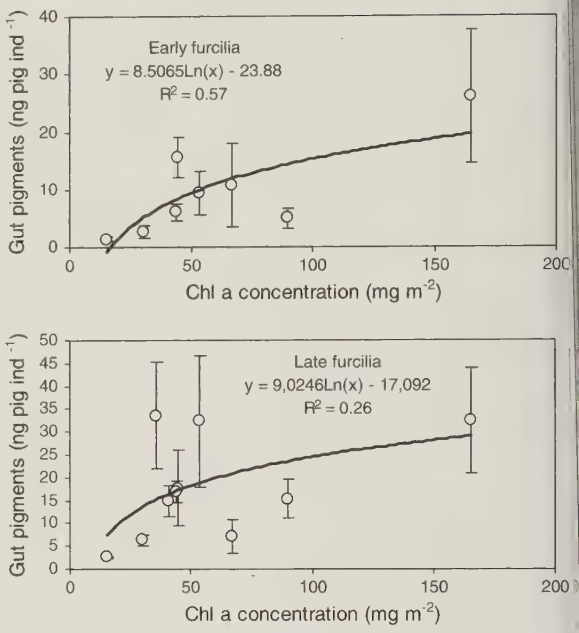
Early furcilia
y = 8.5065Ln(x) - 23.88
R2 = 0.57
Gut pigments (ng pig ind-1)
Chl a concentration (mg m-2)
Late furcilia
y = 9,0246Ln(x) - 17,092
R2 = 0.26
Gut pigments (ng pig ind-1)
Chl a concentration (mg m-2)

Fig. 4. Relationship between gut pigment contents and ambient chlorophyll *a* concentration in early and late furcilia of *E. superba* at nighttime stations in the Eastern Bellingshausen Sea during 18 April to 1 May 2001. *Y*: gut pigments (ng(pig) ind^{-1}); *X*: Chl *a* concentration (mg m^{-2}); Ln: natural logarithm. Error bars represent 95% confidence limits.

No dedicated 24-h stations were conducted during the cruise, so the diel series of in situ gut pigment contents of krill larvae are expressed simply as a composite of all stations separated according to Chl *a* ambient stock (Fig. 5). All data sets show elevated feeding rates at night (Fig. 5). There were approximately 2-fold differences in mean gut pigment contents of each larval group between stations with low and high Chl *a* stock (Fig. 5). Gut clearance rates of larval krill ranged from 0.65 to 1.72 h^{-1}, equivalent to gut passage times of 0.6–1.5 h (Table 2). Gut pigment destruction rates determined on two occasions ranged from 63 to 86% in early furcilia and from 60 to 89% in late furcilia (Table 3).

Daily ingestion rates of larval krill at ice stations were 612 ng pig ind^{-1} d^{-1} or 23 μg C ind^{-1} d^{-1}, equivalent to 16.5% of body C d^{-1}. In open waters, daily ingestion rates of krill furcilia ranged from 226 to 1531 ng pig ind^{-1} d^{-1}, equivalent to 8.5–57 μg C ind^{-1} d^{-1} or 18–45% of body C d^{-1} (Table 4).

3.3. Larval krill morphometrics, moulting and growth rates

Morphometric relationships obtained for the three moulting rate stations are presented in Fig. 6. The biometric parameters of krill furcilia 1–5 are summarised for comparative purposes in Table 5.

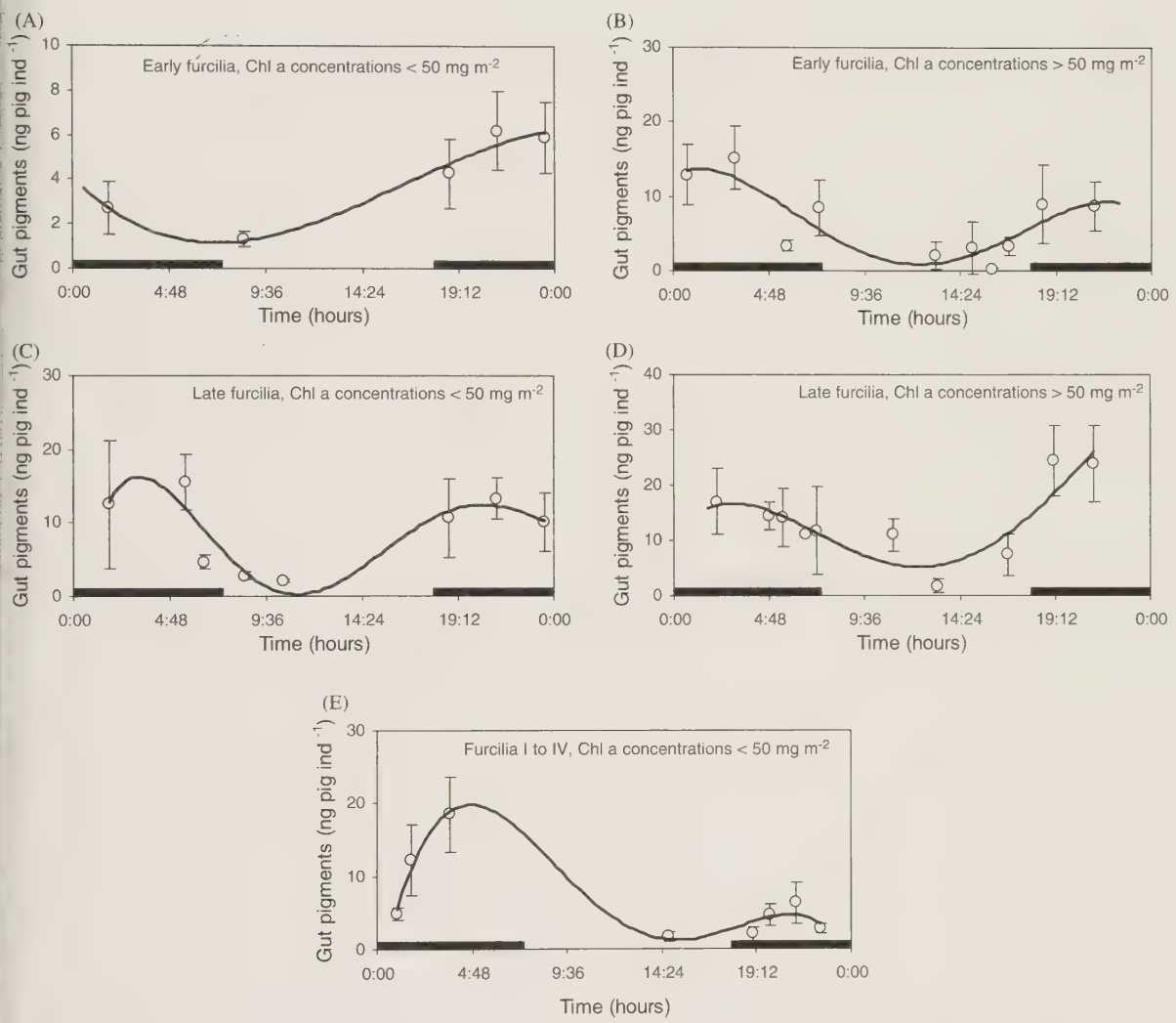

Fig. 5. Diel dynamics in gut pigment contents of larval krill *E. superba* at open water (A–D) and sea ice (E) stations for early and late furcilia at different ambient chlorophyll *a* concentrations in the Eastern Bellingshausen Sea during 18 April to 1 May 2001. Error bars represent 95% confidence limits. Thickening of the horizontal axis indicates the period of darkness.

We stress that variability of mass within each particular stage was high, often reaching one order of magnitude (Table 5).

The intermoult period increased with the developmental stage and was 6–8, 8–15 and 16–17 days for furcilia 3, 4 and 5, respectively (Table 6). The daily growth increments decreased with developmental stage (Table 6). For example, between furcilia 3 and 5 growth increments consistently decreased: from 2–2.2% d^{-1} to 0.7–1.1% d^{-1} based on uropod length, from 7.4–8.7% d^{-1} to 2.4–4.2% d^{-1} for wet mass and from 4.9–5.7% d^{-1} to 1.6–2.7% d^{-1} for carbon mass (Table 6).

4. Discussion

Huntley and Brinton (1991) proposed that certain areas at the Antarctic Peninsula, such as Gerlache Strait, may be hotspots for recruitment

Table 2
E. superba larvae gut clearance parameters and their relationships with ambient Chl *a* concentration (0–200 m) and initial gut pigment content (IGPC)

Station number	Local time (hours)	IGPC (±SD) (ng pig ind^{-1})	Chl-*a* conc. (mg m^{-2})	k (h^{-1})	$1/k$ (h)	R^2 (%)
Early furcilia						
318 (ice)	14:00	3.4±0.4	22.1	0.6564	1.523	39.4
319 (ice)	01:00	12.9±4.9	22.1	1.7255	0.579	69.7
324	20:00	3.4±1.5	44.0	1.1330	0.883	53.8
Late furcilia						
301	01:30	18.5±3.6	40.9	0.7391	1.353	48.7
308	01:00	47.8±4.9	35.8	1.2213	0.819	65.0
316 (ice)	18:50	8.0±0.8	22.7	0.8760	1.141	87.1
324	20:00	17.7±5.0	44.0	1.6750	0.597	54.8
325	08:30	2.0±0.3	16.5	1.4326	0.698	68.0

Table 3
E. superba furcilia: estimation of pigment destruction

Station number	Initial pigment concentration (ng pig l^{-1})	Incubation time (hour)	Pigment ingested (ng pig ind.$^{-1}$)	Pigment recovered (ng pig ind.$^{-1}$)	Destruction efficiency (%)	
					Mean	Range
Early furcilia						
303	2250±825	1	80.8±42.7	18.9±9.4	74.8±9.8	63.5–85.6
Late furcilia						
303	2834±11	1	74.6±35.2	12.3±2.0	80.7±11.8	72.4–89.1
308	2579±30	1	117.5±14.8	40.6±2.2	65.1±6.3	60.6–69.5

of Antarctic krill. The Marguerite Bay area is also a potential hotspot, but with the paucity of studies this far south along the peninsula, this has been conjectural. Therefore, SO GLOBEC targeted this area to study overwintering of krill. Only modest numbers of krill postlarvae were encountered in this area during April and May 2001, either with acoustics or with nets (Atkinson et al., 2002a). However, the abundance of krill larvae was exceptional, with numbers reaching 30 000 ind m^{-2}. Comparable larval krill densities have been observed previously only in Gerlache Strait, Scotia Sea and Prydz Bay region (e.g., Brinton et al., 1986; Huntley and Brinton, 1991; Pakhomov and Karpenko, 1992), while the abundances in the Bransfield Strait and Drake Passage are much lower (Fraser, 1936; Brinton and Townsend, 1984; Brinton et al., 1986; Siegel, 1989; Huntley and Brinton, 1991). Furthermore, this area should clearly be recognised as another "hotspot" in Antarctic krill recruitment along the Antarctic Peninsula. Krill larvae comprised a large proportion of both the abundance and total biomass of the mesozooplankton (S. Schiel, unpublished data), so these early stages of krill may play a major role in the shelf ecosystem of the eastern Bellingshausen Sea.

5. Feeding dynamics

Within the study area, the shelf was greatly affected by Circumpolar Deep Water (Strass et al., 2002; Klinck et al., 2004). Almost all shelf stations

Table 4
Daily consumption rates of larval krill *E. superba* in the Eastern Bellingshausen Sea during late autumn 2001

Region	Chl *a* stock ($mg\,m^{-2}$)	Group	Consumption rates ng (pig) $ind^{-1}\,d^{-1}$	$\mu g\,C\,ind^{-1}\,d^{-1}$	% body $C\,d^{-1}$
Sea ice stations	< 50	All furcilia	619.9	22.9	16.5
Open ocean stations	< 50	Early furcilia	225.7	8.5	21.5
Open ocean stations	< 50	Late furcilia	936.9	35.1	17.8
Open ocean stations	> 50	Early furcilia	470.4	17.6	44.5
Open ocean stations	> 50	Late furcilia	1531.1	57.4	29.2

All furcilia: furcilia 1 to 5; Early furcilia: calyptopis 3 to furcilia 2; Late furcilia: furcilia 3–5.

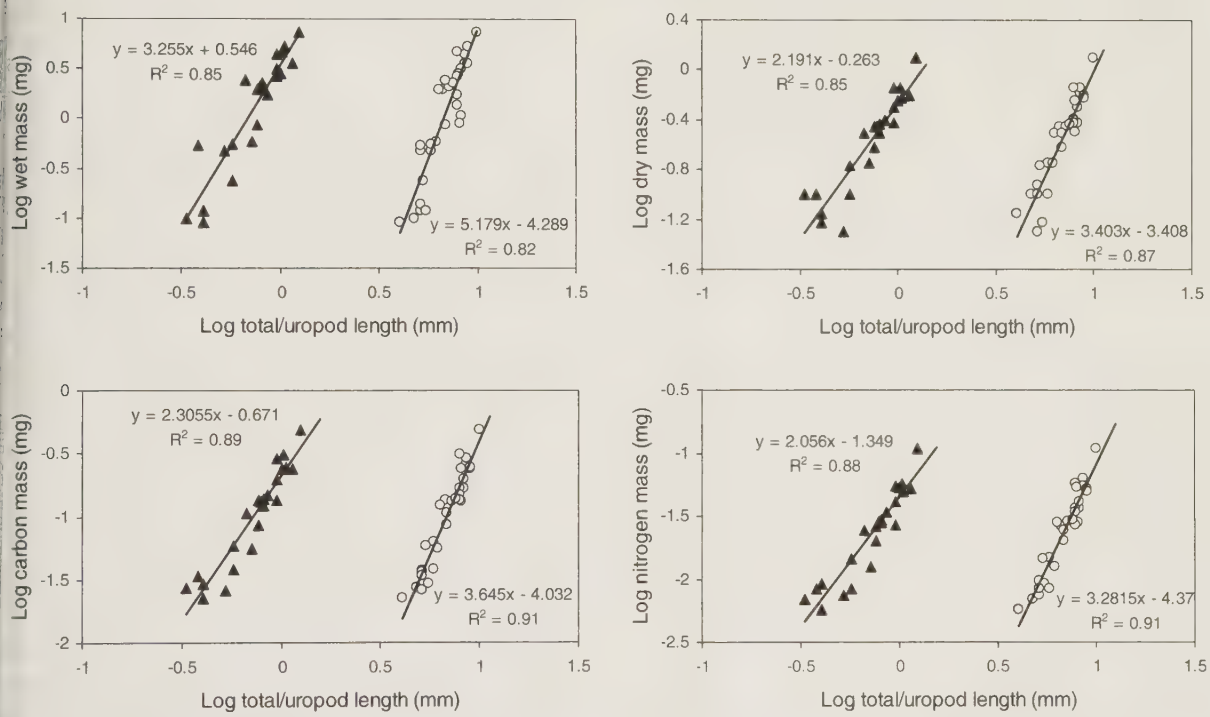
y = 3.255x + 0.546
R² = 0.85
y = 5.179x - 4.289
R² = 0.82
Log wet mass (mg)
Log total/uropod length (mm)
y = 2.191x - 0.263
R² = 0.85
y = 3.403x - 3.408
R² = 0.87
Log dry mass (mg)
Log total/uropod length (mm)
y = 2.3055x - 0.671
R² = 0.89
y = 3.645x - 4.032
R² = 0.91
Log carbon mass (mg)
Log total/uropod length (mm)
y = 2.056x - 1.349
R² = 0.88
y = 3.2815x - 4.37
R² = 0.91
Log nitrogen mass (mg)
Log total/uropod length (mm)

Fig. 6. Relationships between total (open circles) and uropod (filled triangles) lengths and wet, dry, carbon and nitrogen mass of larval krill in the Eastern Bellingshausen Sea during 18 April to 1 May 2001. *Y*: log-transformed wet, dry, carbon or nitrogen furcilia mass (mg); *X*: log-transformed total (open circles) or uropod (filled triangles) furcilia length (mm).

Table 5
Biometrical parameters of *E. superba* furcilia in the Eastern Bellingshausen Sea during late autumn 2001

Stage	Total length (mm)		Wet mass (mg)		Dry mass (mg)		Carbon (μg)		Nitrogen (μg)	
	Mean	Range (*N*)	Mean	Range (*N*)	Mean	Range (*N*)	Mean	Range (*N*)	Mean	Range (*N*)
1	5.04	4.1–5.8 (9)	0.27	0.09–0.55 (8)	0.09	0.05–0.1 (8)	31.2	22.5–37.6 (8)	8.2	5.7–9.8 (8)
2	5.88	5.3–7.2 (13)	0.44	0.24–0.59 (3)	0.18	0.17–0.19 (3)	58.7	55.3–63.1 (3)	13.9	12.6–14.8 (3)
3	7.21	7.2–8.2 (28)	1.76	0.86–2.45 (8)	0.34	0.24–0.41 (8)	132	86.4–168 (8)	28.8	20.2–36.5 (8)
4	8.10	7.9–8.6 (25)	2.35	0.89–3.64 (5)	0.46	0.32–0.65 (5)	183	131–266 (5)	41.0	28.1–62.5 (5)
5	8.77	7.9–10 (16)	4.77	3.15–7.38 (6)	0.74	0.5–1.24 (6)	295	197–494 (6)	60.8	41.4–109 (6)

Table 6
Summary of growth rate experiments (GRE) conducted using larval *E. superba* during April and May 2001 in the Eastern Bellingshausen Sea

Station Number	Date. 2001	Ambient Chl *a* ($mg\,m^{-2}$)	Chl-*a* in containers ($\mu g\,l^{-1}$)	Larval stages	No moulting	IMP (days)	% Change in uropod length	Growth increments during IMP (%, mean ±SD)			
								Wet mass	Dry mass	Carbon	Nitrogen
303	19/04	151.2	2.3	F2-F4 (mostly F4)	17	14	14.4±5.3	56.1±23.1	34.7±13.6	36.8±14.5	32.2±12.5
324	28/04	44.0	1.2*	F1–F2	1	(64)**	11.1	40.9	26.0	27.5	38.7
				F2–F3	1	(32)**	12.0	44.6	28.2	29.9	49.9
				F3–F4	11	8	17.5±3.6	69.7±17.0	42.6±9.7	45.3±10.74	36.7±16.6
				F4–F5	6	15	18.5±7.9	75.9±40.2	45.7±21.9	48.7±23.6	43.4±8.3
				F5–F6	3	17	18.0±5.3	72.1±24.9	43.9±14.1	46.7±15.1	29.5±3.0
328	1/05	44.8	0.65	F3–F4	5	6	11.7±5.6	44.4±23.4	27.7±14.0	29.4±14.9	30.5±9.0
				F4–F5	12	8	10.2±2.7	37.5±11.3	23.8±6.8	25.2±7.2	17.2±8.1
				F5–F6	12	16	10.4±5.5	39.0±22.1	24.5±13.5	25.9±14.3	26.7±9.4

IMP: intermoult period; F1–F2: furcilia 1 to furcilia 2. *Water in the incubation container was enriched from $0.4\,\mu g\,l^{-1}$ ambient Chl *a* concentration by net phytoplankton collected using the Apstein net in the top 25 m. **In brackets are preliminary values due to the limited number of moulted furcilia: data are presented but not discussed.

displayed the typical oceanic vertical water structure, with temperature > 0.5 °C below 100 m depth. A relatively warm and fresh upper mixed layer induced a sharp shallow picnocline, creating favourable conditions (increased vertical stability) for phytoplankton bloom development (Brichta and Belem, 2002). At open-water stations, Chl *a* concentrations in the upper layer ranged from 0.2 to $2.43\,mg\,m^{-3}$ (mean $0.9\,mg\,m^{-3}$) and decreased sharply below 60 m depth. Depth-integrated Chl *a* stocks (0–200 m) varied between 15 and $165\,mg\,m^{-2}$ (Brichta and Belem, 2002). Although no clear pattern in Chl *a* distribution was found, the highest Chl *a* values ($>1\,mg\,m^{-3}$ and $>50\,mg\,m^{-2}$) were observed over the shelf. At the ice stations (Stations 314–318), Chl *a* concentrations were low and never exceeded $0.3\,mg\,m^{-3}$ and $25\,mg\,m^{-2}$ (Brichta and Belem, 2002). Further, the Sea Wide Field Viewing Sensor (SeaWiFS) data confirmed that bloom conditions had persisted here since March 2001 (Belem, 2002). Hence, feeding conditions had probably been good for larval krill in the Eastern Bellingshausen Sea during late summer—autumn 2001.

Larval *E. superba* were feeding actively on the autumn bloom. Their feeding rates were equivalent to those found in summer along the Antarctic Peninsula or in winter under the sea ice in the Scotia-Weddell Seas (Daly, 1990; Huntley and Brinton, 1991). The gut evacuation rates in this study were generally higher than the values of Daly (1990) during winter, but lower than those for *E. crystallorophias* larvae during spring/early summer (Pakhomov and Perissinotto, 1996). A previous study (Perissinotto and Pakhomov, 1996) suggested that gut passage time might co-vary with the initial gut pigment content of krill. This, however, was not observed in this study (see Table 2). There are no gut pigment destruction rates available for larval krill, but our values are broadly similar to those for juvenile krill (Daly, 1998) and for northern hemisphere copepods (Head and Harris, 1992, 1996) but generally lower than values for adult krill (58–98%, Perissinotto and Pakhomov, 1996).

Daily ingestion rates during April and May 2001 in the Eastern Bellingshausen Sea varied between 8.5 and $57.4\,\mu g\,C\,ind^{-1}\,d^{-1}$ and were within the

range (2–67 μg C ind^{-1} d^{-1}) previously reported for furcilia 3–6 (Daly, 1990; Huntley and Brinton, 1991; Meyer et al., 2002). The daily rations estimated in this study were in the higher range of values (< 1–52% of body carbon) reported in the literature and similar to the value (28% of body carbon) estimated from in vitro incubations with high food concentrations (Meyer et al., 2002, 2003).

During our study, the particulate organic carbon (POC) concentration within the top 50 m of the open-water stations was often ~200 μg C l^{-1} (Brichta and Belem, unpublished data). Based on the relationship between the daily ration and food concentration published by Meyer et al. (2002), the average food intake of larval krill would then be equivalent to ~20% of body carbon, similar to our own measured values. In comparison, POC concentrations in the top 50 m water layer at the ice stations generally did not exceed 50 μg C l^{-1} (Brichta and Belem, unpublished data). The calculated daily ration at such carbon concentrations using the same equation will not exceed 2% of body carbon, which is ~8-fold lower than we found using the gut fluorescence method. This suggests that larval krill under the sea ice were either exploiting dense localised food patches or, likely, may have been feeding on ice algae (Meyer et al., 2002).

Physiological measures such as respiration, excretion and growth are useful indicators of the minimum metabolic demands of individuals. During the same cruise, larval krill respiration and ammonia excretion rates also were measured and will be published elsewhere. Preliminary calculations indicate that C and N losses of freshly caught krill furcilia 3–5 were approximately 2% of body C and 1% of body N per day (Meyer and Oettl, 2002), which are close to those obtained for furcilia 3 in the southwestern Lazarev Sea (Meyer et al., 2002). Combining these values with maximal growth rates from Table 6 and assuming an average assimilation efficiency of 0.7 (Conover, 1978), the minimal daily ration would be ~9% (furcilia 3–12%, furcilia 5–7%) of body C and 7% (furcilia 3–10%, furcilia 5 5%) of body N. Daly (1990) reported daily rations ranging from 3 to 52% of body C based on the gut fluorescence method and suggested that a daily ration of 10% was realistic. Our preliminary calculations using the energy budget support this suggestion. However, in this study the gut fluorescence method showed substantially higher (up to 44% of body C d^{-1}) ingestion rates. This may be a result of drawbacks associated with the gut fluorescence technique (Perissinotto and Pakhomov, 1996) but could also imply a decreased assimilation efficiency at high food concentrations. A decrease in assimilation efficiency at high food concentrations is well documented for copepods (Gaudy, 1974). Nevertheless, our findings demonstrate that the feeding rates of larval krill obtained using the gut fluorescence method during autumn in the Eastern Bellingshausen Sea appeared to be close to the maximal reported in in vitro studies in the Lazarev Sea and at Rothera Station (25–30% of body carbon d^{-1}, Meyer et al., 2002, 2003). These values, therefore, are probably a realistic assessment of maximal, food-saturated larval ingestion rates.

Estimating grazing impact of krill larvae was not an aim of this study. However, using average densities of larval krill (Table 1) and pigment ingestion rates (Table 4), the grazing impact exerted by krill larvae alone in the Eastern Bellingshausen Sea during austral autumn of 2001 could be either negligible ($\ll$0.1 of Chl *a* stock d^{-1}) or as high as 25% of Chl *a* stock d^{-1}. This clearly places larval krill among the most important players in carbon cycling of the Eastern Bellingshausen Sea and may explain the general negative correlation between the Chl *a* stock and larval krill densities in the study region.

6. Larval composition, growth and development

The favourable feeding conditions, particularly over the shelf, could be reflected in the larval krill average body length and mass as well as in the developmental composition (Huntley and Brinton, 1991). Indeed, larval lengths (furcilia 3–5) in this study were comparable with those obtained during several summer studies (Fraser, 1936; Brinton and Townsend, 1984; Brinton et al., 1986; Huntley and Brinton, 1991). However, they were 8–17%

smaller than those measured in Gerlache Strait and in laboratory-raised furcilia (Huntley and Brinton, 1991; Ikeda, 1984, respectively). In both of the latter studies, food concentrations were substantially higher than in our study. Our furcilia stages 3–4 were ~6–17% longer than equivalent stages in winter in the Scotia-Weddell area (Daly, 1990). Further, the average dry mass of furcilia in our study is in the upper range of values reported for the Southern Ocean (e.g., Brinton and Townsend, 1984; Daly, 1990; Meyer et al., 2002).

Larval growth and development rates respond to food availability over different timescales (Brinton and Townsend, 1984; Ikeda, 1984). The age structure of larval krill over the shelf during our April–May 2001 study was similar to that in mid-March 1987 in Gerlache Strait (Huntley and Brinton, 1991). A slower seasonal development rate and slightly smaller larvae in our study may be explained by the exceptionally abundant food in Gerlache Strait. On the other hand, their age structure in our study was similar to that in June 1988 (Daly, 1990), so the Marguerite Bay populations were probably intermediate in development between the 1987 Gerlache Strait and the 1988 Weddell-Scotia populations.

Differences in developmental stage composition between slope and shelf stations during April and May 2001 may be a result of the prolonged spawning period (Siegel, 2000) but likely are due to differences in food concentrations between the open-ocean and shelf realms (Brichta and Belem, 2002). Consequently, larvae hatching at the same time but at different places would be exposed to different food concentrations (Huntley and Brinton, 1991). This may explain a discrepancy in larval abundance and composition between the shelf and open-ocean stations in the Eastern Bellingshausen Sea. Although it is not quantified, it is important to note that earlier larval stages (late calyptopis–early furcilia) of krill had higher mortality rates than later stages in all three moulting experiments. Two other research teams working with larval krill independently observed a similar phenomenon during the same cruise. We speculate that the open-ocean "cohort", exposed to lower food concentrations in the past, despite good feeding conditions during the study, was in poorer condition and appeared to have naturally higher mortality rates than their counterparts found over the shelf region. Although very limited, our results on furcilia 1 and 2 intermoult periods and intermoult growth increments presented in Table 6 support this suggestion.

The intermoult periods obtained during this study in the Eastern Bellingshausen Sea were in the range of those previously measured in the laboratory, near Palmer Station and in Gerlache Strait during summer (range 8–17 days, Murano et al., 1979; Ikeda, 1984; Huntley and Brinton, 1991; Ross et al., 2000) and substantially lower than observed under the sea ice during winter and in the Bransfield Strait during late summer (range 20–28 days, Daly, 1990; Huntley and Brinton, 1991). The growth rates estimated in this study were somewhat greater than previously reported (Ikeda, 1984; Ross and Quetin, 1991) and are comparable to values obtained in Gerlache Strait during late summer, near Palmer Station in spring/early summer and in the Scotia-Weddell Seas under the sea ice during winter (~5% of wet mass per day, Daly, 1990; Huntley and Brinton, 1991; Ross et al., 2000). The long-term study near Palmer Station has supported the hypothesis that the secondary production of larval and juvenile Antarctic krill are limited by both food quantity and quality most of the time and only maximal during diatom blooms (Ross et al., 2000). Our study shows that favourable conditions in the Eastern Bellingshausen Sea in late summer/autumn 2001 resulted in an abundant and advanced larval krill population. Furthermore, it appears that feeding and growth rates of larval krill at that time of year were more comparable to summer maximum rates rather than to late summer or winter rates, suggesting that a "business as usual" strategy, with continuous feeding and growth, has been adopted by larval krill (Meyer et al., 2002).

Acknowledgements

We are grateful to the University of Fort Hare (South Africa), the Alfred-Wegener-Institute for Polar and Marine Research (Germany), British Antarctic Survey (UK) and the Alexander von

Humboldt Foundation (Germany) for providing funds and facilities, which allowed us to conduct this study. We are indebted to M. Brichta and A. Belem for allowing us to use unpublished chlorophyll *a* data. The professional and friendly support at sea by the Capitan and the crew of the RV *Polarstern* during the ANTATKTIS XVIII/5b cruise is greatly appreciated. This is publication awi-n11013 of the Alfred-Wegener Institute. This is U.S. GLOBEC contribution no. 459.

References

Atkinson, A., Bathmann, U.V., Blume, B., Oettl, B., Meyer, B., 2002a. Survival strategies of *Euphausia superba* in autumn. Berichte zur Polar- und Meeresforschung 407, 26–34.

Atkinson, A., Meyer, B., Stübing, D., Hagen, W., Schmidt, K., Bathmann, U.V., 2002b. Feeding and energy budgets of Antarctic krill *Euphausia superba* at the onset of winter—II. Juveniles and adults. Limnology and Oceanography 47, 953–966.

Baars, M.A., Helling, G.R., 1985. Methodological problems in the measurements of phytoplankton ingestion rate by gut fluorescence. Hydrobiological Bulletin 19, 81–88.

Bathmann, U. (Ed.), 2002. The expedition ANTARKTIS XVIII/5b of the research vessel "Polarstern" in 2001. Berichte zur Polar- und Meeresforschung 407, 1–98.

Belem, A., 2002. Remote sensing program during the ANTXVIII/5b cruise. Berichte zur Polar- und Meeresforschung 407, 65–67.

Brichta, M., Belem, A., 2002. Chlorophyll-*a*, particulate organic carbon/nitrogen (POC/N) and biogenic silica (Bsi) distribution. Berichte zur Polar- und Meeresforschung 407, 61–64.

Brinton, E., Townsend, A., 1984. Regional relationships between development and growth in larvae of Antarctic krill, *Euphausia superba*, from field samples. Journal of Crustacean Biology 4, 224–246.

Brinton, E., Huntley, M., Townsend, A.W., 1986. Larvae of *Euphausia superba* in the Scotia Sea and Bransfield Strait in March 1984—Development and abundance compared with 1981 larvae. Polar Biology 5, 221–234.

Conover, R.J., 1978. Transformation of organic matter. In: Kinne, O. (Ed.), Marine Ecology. vol. 4. Dynamics. Wiley, New York, pp. 221–499.

Daly, K., 1990. Overwintering development, growth, and feeding of larval *Euphausia superba* in the Antarctic marginal ice zone. Limnology and Oceanography 35, 1564–1576.

Daly, K.L., 1998. Physioecology of juvenile Antarctic krill (*Euphausia superba*) during spring in ice-covered seas. Antarctic Research Series 73, 183–198.

Fraser, F.C., 1936. On the development and distribution of the young stages of krill (*Euphausia superba*). Discovery Reports 14, 1–192.

Gaudy, R., 1974. Feeding for species of pelagic copepods under experimental conditions. Marine Biology 25, 125–141.

Hagen, W., Kattner, G., Terbrüggen, A., Van Vleet, E.S., 2001. Lipid metabolism of the Antarctic krill *Euphausia superba* and its ecological implications. Marine Biology 139, 95–104.

Head, E.J.H., Harris, L.R., 1992. Chlorophyll and carotenoid transformation and destruction by *Calanus* spp. grazing on diatoms. Marine Ecology Progress Series 86, 229–238.

Head, E.J.H., Harris, L.R., 1996. Chlorophyll destruction by *Calanus* spp. grazing on phytoplankton, kinetics, effects of ingestion rate and feeding history, and a mechanistic interpretation. Marine Ecology Progress Series 135, 223–235.

Huntley, M., Brinton, E., 1991. Mesoscale variation in growth and early development of *Euphausia superba* Dana in the western Bransfield Strait region. Deep-Sea Research I 38, 1213–1240.

Ikeda, T., 1984. Development of the larvae of the Antarctic krill (*Euphausia superba* Dana) observed in the laboratory. Journal of Experimental Marine Biology and Ecology 75, 107–117.

Klinck, J.M., Hofmann, E.E., Beardsley, R.C., Salihoglu, B., Howard, S., 2004. Water-mass properties and circulation on the west Antarctic Peninsula Continental Shelf in Austral Fall and Winter 2001. Deep-Sea Research II, this issue [doi:10.1016/j.dsr2.2004.08.001].

Knox, G.A., 1994. The biology of the Southern Ocean. Cambridge University Press, Cambridge.

Makarov, R., Menshenina, L., Spiridonov, V., 1990. Distribution ecology of euphausiid larvae in the Antarctic Peninsula region and adjacent waters. Proceedings of NIPR Symposium on Polar Biology 3, 23–35.

Meyer, B., Atkinson, A., Stübing, D., Oettl, B., Hagen, W., Bathmann, U.V., 2002. Feeding and energy budgets of Antarctic krill *Euphausia superba* at the onset of winter—I. Furcilia III larvae. Limnology and Oceanography 47, 943 952.

Meyer, B., Oettl, B., 2002. Grazing, assimilation and metabolic rates of furcilia. Berichte zur Polar- und Meeresforschung 407, 27–30.

Meyer, B., Atkinson, A., Blume, B., Bathmann, U.V., 2003. Feeding and energy budgets of larval Antarctic krill *Euphausia superba* in summer. Marine Ecology Progress Series 257, 167–178.

Miller, D.G.M., Hampton, I., 1989. Biology and ecology of the Antarctic krill (*Euphausia superba* Dana), a review. BIOMASS Scientific Series 9, 1–166.

Murano, M., Segawa, S., Kato, M., 1979. Moult and growth of the Antarctic krill in laboratory. Transactions of the Tokyo University of Fisheries 3, 99–106.

Nicol, S., Stolp, M., Cochran, T., Geijsel, P., Marshall, J., 1992. Growth and shrinkage of Antarctic krill *Euphausia superba* from the Indian Ocean sector of the Southern Ocean during summer. Marine Ecology Progress Series 89, 175–181.

Pakhomov, E.A., Karpenko, G.P., 1992. Oceanographic conditions of Antarctic krill (*Euphausia superba* Dana) reproduction in the southern part of the Indian Ocean. In: Rzhosnitsky, V.B. (Ed.), Physical Oceanography and Problems of the Biological Productivity. Saint-Petersburg University Press, St Petersburg, pp. 128–135 (in Russian).

Pakhomov, E.A., Perissinotto, R., 1996. Antarctic neritic krill *Euphausia crystallorophias*: Spatio-temporal distribution, growth and grazing rates. Deep-Sea Research I 43, 59–87.

Parsons, T.R., Maita, Y., Lalli, C.M., 1984. A manual of chemical and biological methods for seawater analysis. Pergamon Press, Oxford.

Perissinotto, R., 1992. Mesozooplankton size selectivity and grazing impact on the phytoplankton community of the Prince Edward Archipelago (Southern Ocean). Marine Ecology Progress Series 79, 243–258.

Perissinotto, R., Pakhomov, E.A., 1996. Gut evacuation rates and pigment destruction in the Antarctic krill *Euphausia superba*. Marine Biology 125, 47–54.

Ross, R.M., Quetin, L.B., 1991. Ecological physiology of larval euphausiids, *Euphausia superba* (Euphausiacea). Memoirs of the Queensland Museum 31, 321–333.

Ross, R.M., Quetin, L.B., Baker, K.S., Vernet, M., Smith R.C., 2000. Growth limitation in young *Euphausia superb* under field conditions. Limnology and Oceanography 45 31–43.

Siegel, V., 1989. Winter and spring distribution and status o the krill stock in Antarctic Peninsula waters. Arch Fischereiwiss 39, 45–72.

Siegel, V., 2000. Krill (Euphausiacea) demography and variability in abundance and distribution. Canadian Journal of Fisheries and Aquatic Sciences 57 (Suppl 3) 151–167.

Strass, V., Borth, H., Cisewski, B., Rabe, B., Radke, C., Rinas K., 2002. Hydrographic conditions of the Eastern Bellingshausen Sea ecosystem during austral autumn 2001. Berichte zur Polar- und Meeresforschung 407, 11–16.

Torres, J.J., Donnelly, J., Hopkins, T.L., Lancraft, T.M. Aarset, A.V., Ainley, D.G., 1994. Proximate composition and overwintering strategies of Antarctic micronektonic crustacea. Marine Ecology Progress Series 113, 221–232.

Willason, S.W., Cox, J.L., 1987. Diel feeding, laminarinase activity and phytoplankton consumption by euphausiids. Biological Oceanography 4, 1–24.

ELSEVIER

Deep-Sea Research II 51 (2004) 2199–2214

DEEP-SEA RESEARCH
PART II

www.elsevier.com/locate/dsr2

Lipids as markers of nutritional condition and diet in the Antarctic krill *Euphausia superba* and *Euphausia crystallorophias* during austral winter

Se-Jong Ju, H. Rodger Harvey*

Chesapeake Biological Laboratory, University of Maryland Center for Environmental Science, P.O. Box 38, Solomons, MD 20688, USA

Accepted 10 July 2004

Abstract

To understand the nutritional condition and feeding history of Antarctic krill during winter, *Euphausia superba* and *E. crystallorophias* were collected by MOCNESS during July–August 2001 in Maguerite Bay southeast of Adelaide Island. Total lipid, lipid classes, fatty acids, fatty alcohols and sterols were analyzed in animals among several life stages. Lipids in seston and major copepods representing potential diets were collected from the water column and quantified to compare with krill. Stomach contents also were examined in selected adult krill to provide a visual snapshot of ingested material and comparison with lipid biomarkers. Total lipids in adult *E. crystallorophias* were significantly higher than adult *E. superba* (30.0% and 20.2% of dry weight, respectively). Wax esters were the major storage lipid in *E. crystallorophias*, accounting for over half (mean of 55.9%) of the total lipid in adult animals. In contrast, *E. superba* contained triacylglycerols as the dominant storage lipid in adults (mean of 45.5% of total lipid). Fatty acid and sterol distributions in krill showed minor differences between species and life stages. Larval krill, however, contained higher polyunsaturated fatty acids (PUFA) than sub- and adult krill. While only trace amounts of fatty alcohols were found in *E. superba*, significant amounts were found in *E. crystallorophias*, particularly 14:0 and 16:0, which were major components of wax esters. Results for lipid classes, individual lipids, and stomach content suggest that *E. superba* is less dependent on stored lipid for overwintering than *E. crystallorophias*. *E. superba* are omnivorous, with copepods representing a significant dietary source for adults in winter. Furciliae of both species contain lower levels of lipid storage in winter and feed largely on detritus or organisms associated with ice.
© 2004 Elsevier Ltd. All rights reserved.

1. Introduction

Euphausia superba and *E. crystallorophias* are the dominant krill species in the Antarctic and a key component of the Southern Ocean ecosystem

*Corresponding author. Tel.: +1-410-326-7206; fax: +1-410-326-7341.

E-mail address: harvey@cbl.umces.edu (H.R. Harvey).

0967-0645/$ - see front matter © 2004 Elsevier Ltd. All rights reserved.
doi:10.1016/j.dsr2.2004.08.004

(e.g., Laws, 1985). While *E. crystallorophias* is a neritic species confined to the coastal waters of Antarctica, *E. superba* maintains a wide range around the Antarctic continent and through the Southern Ocean (Falk-Petersen et al., 2000). The general difficulty in accessing Antarctic waters, especially in winter, has lead to conflicting physiological and ecological hypotheses on survival and reproductive strategies of krill. Krill overwintering strategies are of particular interest since they are a major determinant of their condition, survival, recruitment, and population size (Ross and Quetin, 1991; Siegel, 2000; Quetin and Ross, 2001). Although both species are known as herbivores when phytoplankton are abundant, Antarctic krill face extremely low levels of phytoplankton during the long winter with extensive ice cover. Laboratory and field studies have suggested that they may efficiently switch to alternate prey (copepods, ice algae, or detritus) and/or rely on physiological mechanisms, (e.g., reduced metabolism, shrinkage or use of energy reserves) that enable them to survive through the extended period of low food availability (Ikeda and Dixon, 1982; Schnack, 1985; Quetin and Ross, 1991; Torres et al., 1994; Hagen et al., 1996; Quetin et al., 1996). While multiple mechanisms are possible, detailed information is limited.

Lipids are essential biochemical constituents of all organisms, and lipid composition can often be related to taxonomy and physiology. The importance of lipids in krill reproduction (Clark, 1980, 1984; Pond et al., 1995; Virtue et al., 1996) and as a mechanism for energy storage during the winter is well documented (Quetin and Ross, 1991; Hagen et al., 1996). In several cases specific lipids (e.g., long-chain polyunsaturated fatty acids) have been applied to understand trophic relationships (Bottino, 1974; Virtue et al., 1993; Cripps et al., 1999; Cripps and Atkinson, 2000) since such molecules are taxon-specific and obtained solely from their diet. For the predominant species *E. superba*, triacylglycerols are the primary depot lipid (Pond et al., 1995; Hagen et al., 1996; Mayzaud et al., 1998; Hagen et al., 2001). This lipid class also appears as the major energy storage in several Antarctic copepods (Albers et al., 1996), which could represent potential diets. Other Antarctic euphausiids such as *E. crystallorophias* and *Thysanoessa macrura* (see Falk-Petersen et al., 2000) appear to store even higher amounts of lipid reserves, but in the form of wax esters (Bottino 1974; Hagen et al., 1996; Kattner and Hagen 1998; Falk-Petersen et al., 2000; Scott et al., 2002). In addition, Hagen et al. (1996) have suggested that even phospholipids also might serve as storage lipids for *E. superba* and *E. crystallorophias,* which would further elevate their potential energy reserves. Quetin and Ross (1991) first suggested that the lipid concentrations in *E. superba* might not be sufficient to meet the energy requirements during the winter, when food supplies are very low. Atkinson and Snÿder (1997) have further argued that lower levels of lipid deposits in *E. superba* require it to be omnivorous and feed year-round. While *E. crystallorophias* maintains higher levels of lipids as part of their overwintering strategy, it also has been suggested that they may be opportunistic and switch dietary sources during winter (Kattner and Hagen, 1998). Although some studies on lipid class and fatty acid composition of *E. superba* and *E. crystallorophias* have been done in Southern Ocean, little information is available on lipid compositions in these two krill species from the same region at the same time, particularly during austral winter. The objective of this study was to understand further nutritional condition and feeding mechanisms by examining lipid classes, together with detailed information on fatty acids, fatty alcohols and sterols in different life stages during the winter. Collections were made in Marguerite Bay, a biologically rich shelf environment known to support a persistent and large standing stock of krill (Marr, 1962; Lascara et al., 1999). Large populations of top predators, which depend mainly on krill as a food source, also are found in this region (Fraser and Trivelpiece, 1996; Costa and Crocker, 1996, 2004). Because physical features (i.e. sea-ice cover, circulation patterns) in this region may significantly affect the distribution of krill in winter (Hofmann et al., 2002), detailed lipid analysis also was used to address the possibility that *E. superba* shift their habitat from the water column to the ice to take advantage of ice biota during the winter larval stages (Quetin et al., 1996).

2. Materials and methods

2.1. Sampling area and collection

This study is a component of the US Southern Ocean GLOBEC field programs, which consists of multidisciplinary oceanographic research programs focused on Marguerite Bay and environs along the western Antarctic Peninsula (WAP), on board R.V. *L. M. Gould* during late winter from 25 July to 20 August 2001. Patches of adult krill were observed during these field studies in the nearshore areas, especially in areas characterized by variable topography, such as Crystal Sound and near the northern part of Alexander Island (Hofmann et al., 2002 and papers in this DSRII issue). Significant ice cover was often a hindrance, but krill (*E. superba* and *E. crystallorophias*) and adult copepods (*Pareuchaeta antarctica*, *Metridia gerlachei*, and *Calanoides acutus*) were collected in a localized polynya (process St. 5 during LMG01-06 process cruise) at the southeast of Adelaide Island in northern Marguerite Bay using 1 m^2 Multi Opening/Closing Net Environmental Sensing System (MOCNESS) equipped with nine 333 μm mesh nets, with the exception of *E. superba* larvae. *E. superba* larvae were collected by diver under the ice at the sea-ice edge over the shelf break (st.2 during NBP01-04 survey cruise). Stratified sampling observed animals throughout the upper water column (60–200 m), with adults concentrated below the thermocline (ca. 120 m). Krill were sorted by species and size (total length (TL: mm)—length from anterior margin of the eye to the tip of the telson) using a dissecting microscope and individually transferred to pre-combusted 8 ml amber vials. The post-larval *E. superba* were sorted into two distinct size groups of 30–40 and 45–62 mm total length, hereafter termed sub-adults and adults. This maturity grouping based on size corresponds well with previous observations (Siegel, 1987). Water samples were collected from CTD casts (4 m) and filtered through pre-combusted (450 °C, 4–6 h) 47 mm Whatman GF/F (nominal pore size: 0.7 μm) filters for seston lipid analysis. All samples were immediately frozen and stored at −70 °C until analysis onshore-based facilities.

2.2. Lipid extraction and analysis

Before lipid analysis, wet weights of all samples (krill and copepods) were measured by thawing and briefly rinsing with Nano-pure water. A subset of krill and copepod samples was dried at 60°C for 48 h for measurement of water content and used to convert wet weight of animals to dry weight (Fig. 1B). Total lipids were extracted from freshly thawed animals three times with a mixture of CH_2CL_2:MeOH (1:1) in solvent washed 25 mL screw-cap glass/Teflon-lined cap test tubes with probe sonication as previously described (Harvey et al., 1987). A small volume of the three extracts was pooled, the solvent removed by rotary evaporation, and total lipid redissolved in CH_2CL_2:MeOH (2:1). Subsamples of lipid extracts from animals were used for lipid class analysis with the remaining fraction used for measurement of individual lipid components.

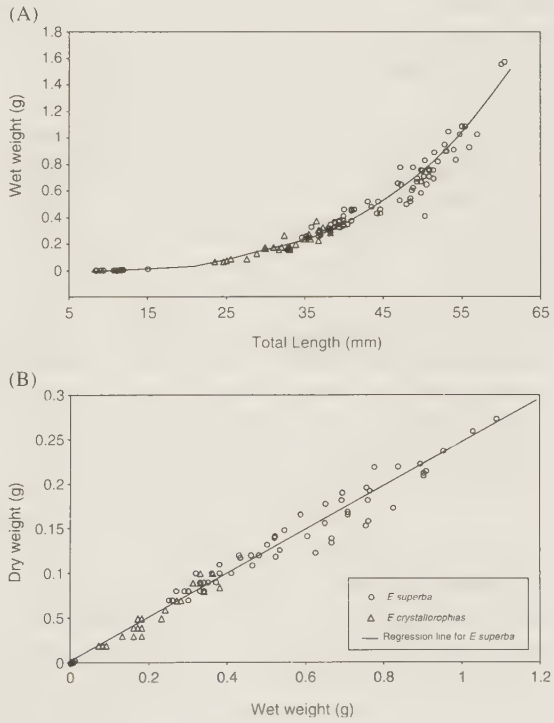

Fig. 1. Relationships between (A) wet animal weight and total length for animals collected and (B) relationship between dry weight and wet weight for *E. superba* and *E. crystallorophias*.

Major lipid class composition was determined by thin-layer chromatography with flame ionization detection (TLC-FID) using an Iatroscan MK-V Analyzer (Volkman et al., 1986b; Ju et al., 1997). Aliquots (1–2 μL) of total extracts were spotted onto replicate S-III Chromarods and developed in hexane: diethyl ether: formic acid (85:15:0.2) for separation of major lipid classes. This solvent system allowed individual neutral lipid classes to be separated in a single development; phospholipids remained at the origin and were not identified individually. Lipid classes were identified and calibrated using a mixture of commercial standards (phosphatidyl choline for phospholipids, cholesterol for cholesterol, nonadecanoic acid for free fatty acids, triolein for triacylglycerol, and stearyl ester for wax esters; Sigma Co.). Peak areas were integrated (HP ChemStation) and quantified using the standard mix run in parallel. Total lipid content was determined by summation of all lipid classes quantified by TLC-FID. Overall precision for total lipid and major classes was ±10% or better.

For quantification of individual components in neutral (alcohols and sterols) and polar (fatty acids) lipid fractions, internal standards (5α-cholestane for neutral and nonadecanoic acid for polar) were added to the remaining fraction (or subsamples) of the total lipid extract. Remaining solvent was dried under N_2 gas and the sample subjected to alkaline hydrolysis using 0.5 N methanolic KOH with gentle heating (at 70 °C) for 30 min. After cooling and addition of water, neutral lipid fractions were partitioned three times with a mixture of hexane:diethyl ether (9:1). The neutral fraction was dried under N_2 gas and treated with 30 μL of bis(trimethylsilyl) trifluoroacetamide (BSTFA) with 25% pyridine at 50 °C for 15 min to convert free alcohols to their corresponding trimethylsilyl (TMS) esters. Polar lipid fractions containing fatty acids were partitioned similarly following acidification to pH 2, dried under N_2 gas, and converted to fatty acid methyl esters (FAMES) by using BF_3–MeOH at 70 °C for 30 min. FAMES were isolated from the final mixture by partitioning into hexane:diethyl ether (9:1). A subsample of FAMES was treated with dimethyl disulfide (DMDS) to determine double bond position of monounsaturated fatty acids (Nichols et al., 1986). Procedural blanks were processed in parallel with samples with similar internal standards. Polar and neutral lipids were quantified by capillary gas chromatography (HP 5890-II GC) equipped with flame ionization detector. Separations were performed with DB-5MS fused silica column (60 m length × 0.32 mm internal diameter × 0.25 m film thickness; J & W Scientific) and hydrogen as carrier gas (e.g. Harvey and McManus, 1991). Samples injected in split less mode at an initial oven temperature 50 °C and an injector temperature 225 °C. Then the oven temperature was ramped at 15 °C min^{-1} to 120 °C and thereafter 4 °C min^{-1} to 300 °C and held at 300 °C for 10 and 20 min for polar and neutral lipids, respectively. All data were processed using a dedicated data system (HP ChemStation Rev. A.07.01—Agilent Tech.) with quantification based on peak area response compared to the internal standards. Structural identification was made utilizing gas chromatography–mass spectrometry (GC–MS; Agilent 6870 GC with Agilent 5973 MSD) operating at 70 eV with mass range acquisition of 10–700 a.m.u. The column and temperature programs for the GC–MS are similar to that described above, with helium used as a carrier gas and injector temperature of 250 °C.

2.3. Statistical analysis

All data were tested before statistical analyses to satisfy assumptions for homogeneity of variances and normality of residuals. If necessary, data were properly transformed to satisfy the assumptions. In order to determine the differences of total lipid content among krill species and life stage, the protracted Fisher's least significant difference (LSD) was used. Multi-regression analysis was used to determine whether length and weight was different between two krill species (Littell et al., 1999). Principle component analysis (PCA) was performed using fatty acid data of all individual krill samples and potential diets for krill using MINITAB statistic software package (Minitab Inc.). Principle component analysis is a multivariate chemometric technique, which allows objective comparisons of large data sets to identify

hose variables, which account for most of the ariance. Component scores were calculated from he first two principal components for each sample or further evaluation.

.4. Stomach content analysis

For the microscopic examination of stomach ontent, frozen krill were thawed and each size roup (i.e. furcilia, sub-adult, and adult) of nimals was dissected to remove their stomachs. Material inside stomachs were carefully examined mong 5–10 individuals using the microscope Olympus BH-2), and their digital images were aken using Hitachi KP-D50 color digital camera ith image software (Optimus Ver. 6.51).

. Results

.1. Length–weight relationships in krill

Wet weights (WW) of both krill species were xponentially related to total length as shown in Fig. 1A. The relationship of WW (g) to TL (mm) were similar between the two species and could be described by

$$\text{WW } E.\ superba = (0.1 \times 10^{-6})\text{TL}^{3.478} \quad (n = 87, r^2 = 0.991),$$

$$\text{WW } E.\ crystallorophias = (0.2 \times 10^{-5})\text{TL}^{3.244} \quad (n = 31, r^2 = 0.915).$$

The relationships were not significantly different between two species (regression analysis; $p > 0.05$) and were similar to previous estimates (Färber-Lorda, 1994; Hofmann and Lascara, 2000, and references therein). Similarly, dry weight and wet weight of individual krill were highly correlated between the two species ($n = 77$ and 26 for *E. superba* and *E. crystallorophias*, respectively; $r^2 > 0.99$ for both) (Fig. 1B).

3.2. Total lipid and lipid class in krill and copepods

Total lipid contents in *E. superba* were ranged from 15% to 30% of dry weight and increased with maturity. *E. crystallorophias*, had significantly higher lipid content than *E. superba* (fisher's LSD at $p = 0.05$; Fig. 2), particularly among adults collected. Lipid content in three copepod species (*P. antarctica*, *M. gerlachei*, and *C. acutus*) collected in Marguarite Bay were also very high at 32%, 23%, and 38% of dry weight, respectively, and similar to *E. crystallorophias*. While triacylglycerols (TG) were dominant storage lipids (>45% of total lipid) in *E. superba*, wax esters (WE) were dominant (>50% of total lipids) in *E. crystallorophias* with no significant ontogenic shift observed. Wax esters were also dominant storage lipids in *P. antarctica* and *C. acutus* (84% and 89% of total lipids, respectively). In *M. gerlachei*, WE and TG were both observed in roughly equal amounts (46% and 32% of total lipids, respectively).

3.3. Fatty acids in krill and their potential diets

Both species of krill contain a wide range of saturated (SFA), monounsaturated (MUFA), polyunsaturated (PUFA), and branched fatty acids ranging from C_{12} to C_{22} (Table 1). Total concentration ranged from 14.0 mg g^{-1} dry weight in furcilia of *E. crystallorophias* to 180.9 ± 32.9 mg g^{-1} in sub-adult *E. superba*. The 16:0, 16:1ω7, 18:1ω9 and ω7, and 20:5ω3 acids were major components in adult krill, with only minor differences observed between species. The 14:0 acid, however, was high (>10% of total fatty acids) only in sub-adult and adult *E. superba*, while the 18:1ω9 was elevated (32.5% of total fatty acids) in adult *E. crystallorophias*. Several branched fatty acids and the major components of calanoid copepod lipids, including the 20:1 and 22:1, were also found in small quantities (<5% of total fatty acids) in krill. The distribution of fatty acids in larval krill was not significantly different from sub-adult and adults, but larval animals did contain much higher levels of PUFA, particularly flagellate markers 18:4ω3 and 22:6ω3 (Graeve et al., 1994; Falk-Petersen et al., 2000) and diatom marker 20:5ω3 (Nichols et al., 1993).

The fatty acid distribution in potential diets (e.g., seston, ice algae, and copepods) for krill and stomach contents of adult *E. superba* are shown in

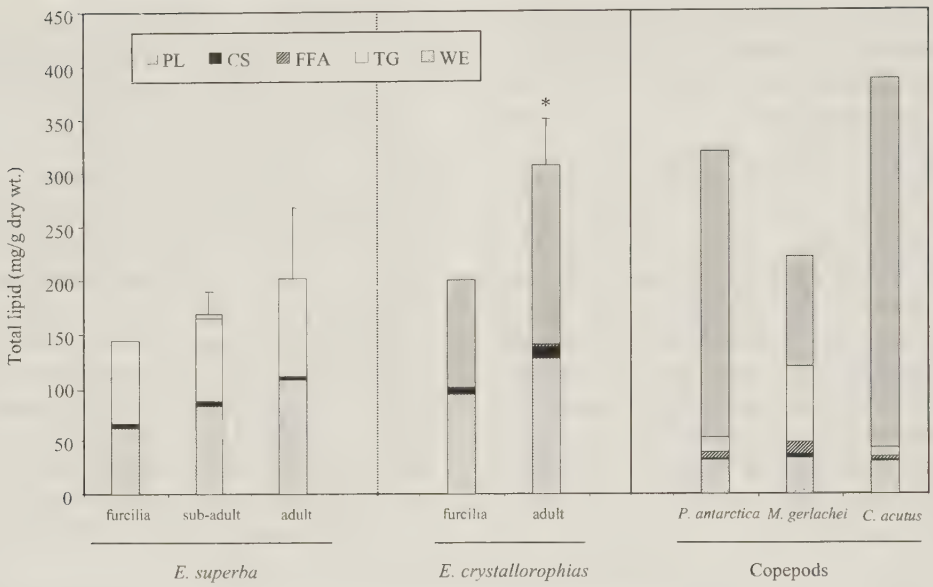

Fig. 2. Total lipid concentration and lipid class composition in Antarctic krill and copepods. *E. superba*—furcilia (TL: 7.1±1.6 mm, $n = 7$), sub-adult (38.1±2.9 mm, $n = 10$), adult (53.9±5.5 mm, $n = 17$); *E. crystallorophias*—furcilia (TL: 7.4±0.3 mm, $n = 10$), adult (33.2±4.7 mm, $n = 14$). *indicates significant differences of total lipid contents between krill species and stages as determined by protected Fisher's LSD test at $p = 0.05$. Data (for furcilia and copepods) without an error bar were from the composite samples.

Table 2. In seston, 16:0, 18:0, 18:1ω9 and ω7, and 22:6ω3 accounted for over 70% of total fatty acids, while 14:0, 16:0, 16:1ω7, 16:4ω1, and 20:5ω3 were major fatty acids (>72% of total fatty acids) in ice algae. The 14:0, 16:0, 16:1ω7, 18:1ω9, and 20:5ω3 were major fatty acids (>65% of total fatty acids) in stomach contents. Three copepod species (*P. antarctica*, *M. gerlachei*, and *C. acutus*) contained fatty acids ranging from C_{14} to C_{22}, with total concentrations 103, 89, and 128 mg g^{-1} dry weight, respectively. Monounsaturated fatty acids (MUFA) were most abundant fatty acid (>60% of total acids) in all copepods, with the major acids comprised of 16:1ω7, 18:1ω9, and 20:1 isomers. In *C. acutus*, the 20:1 and 22:1 fatty acid isomers were significantly higher (33.9% of total fatty acids) than two other copepod species.

Principal component analysis (PCA) was applied to the suite of fatty acids encountered in individual animals as well as potential diets to allow a more robust examination of the relationship among diets and animals. Scores for the first two principle components for fatty acids seen in individual animals and potential diets are shown in Fig. 3. The first principal component (PC) accounted for 30% of the total variation, with the second PC accounting for 18% of the variation. Loadings among individual fatty acids revealed that the first component was mainly due to PUFAs, which accounts for the large displacement of ice algae seen in the positive direction. Negative displacements in the PC 1 were due to the 18:1 isomers (ω7 and ω9). These two acids are common to wax esters, and were the major energy reserve seen *E. crystallorophias* and *P. antarctica* (Fig. 2). Positive (upward) displacement in the PC 2 included MUFAs (e.g., 16:1ω7, 20:1 and 22:1 isomers), which was seen in ice algae and copepods, with negative loadings for saturated acids (e.g., 16:0). Using the suite of fatty acids, it is apparent that adult krill of each species were clearly separate from each other. Furciliae of both species were distinct from adults in PC 1 only. In particular, furcilia of *E. superba* reflect a greater proportion of algal material in their diets apparent by the elevated presence of algal fatty acids

able 1
omposition of fatty acid (% of total fatty acid) in Antarctic Euphausiids

atty acid	*E. superba*			*E. crystallorophias*	
	Furcilia[a]	Sub-adult ($n=9$)	Adult ($n=10$)	Furcilia[a]	Adult ($n=7$)
-Saturates					
2:0	—	0.1±0.0	0.1±0.1	—	0.1±0.2
4:0	8.0	12.3±1.0	11.1±1.8	4.0	1.3±0.7
5:0	0.6	0.3±0.1	0.5±0.1	0.4	0.1±0.0
6:0	22.0	28.9±2.8	27.8±2.2	16.9	18.1±6.0
7:0	0.1	0.1±0.0	0.6±1.3	0.1	Tr
8:0	1.0	1.6±0.3	1.7±0.3	1.1	0.9±0.2
0:0	0.1	0.2±0.1	0.1±0.0	Tr	Tr
2:0	0.1	Tr	Tr	Tr	Tr
Monounsaturates					
4:1ω5	0.2	0.1±0.0	0.1±0.0	0.1	Tr
5:1[b]	0.1	0.1±0.0	0.1±0.1	0.1	0.1±0.2
6:1ω9	0.2	0.1±0.0	0.1±0.0	0.1	0.2±0.3
6:1ω7	4.1	10.5±3.1	7.6±1.8	5.6	10.7±3.2
6:1ω5	0.8	0.5±0.2	0.5±0.1	0.3	0.1±0.1
6:1ω3	0.6	0.1±0.0	0.1±0.0	0.1	Tr
7:1[b]	0.8	0.2±0.1	0.5±0.4	0.2	0.2±0.0
8:1ω9	8.6	14.1±2.5	14.8±2.2	17.1	32.9±2.9
8:1ω7	7.0	7.3±0.8	8.9±1.9	9.6	13.9±1.0
8:1ω5	0.4	0.2±0.1	0.3±0.2	0.3	0.2±0.1
0:1[b]	0.8	1.5±0.2	1.4±0.4	3.8	2.6±0.6
2:1[b]	0.3	0.6±0.4	0.2±0.2	1.4	1.1±1.3
Polyunsaturates					
6:4ω1	1.5	0.4±0.2	0.5±0.2	0.6	Tr
6:2ω4	0.3	0.2±0.1	0.2±0.1	0.2	Tr
6:2ω6	0.7	1.1±0.2	1.2±0.2	0.8	0.7±0.3
8:4ω3	6.7	1.4±0.8	1.7±0.3	2.3	0.2±0.2
8:3ω4	0.4	0.2±0.1	0.2±0.1	0.2	0.1±0.1
8:2[b]	1.2	1.4±0.4	1.8±0.5	1.6	2.5±2.9
0:5ω3	17.1	9.8±1.6	10.7±2.1	18.3	8.1±3.2
0:4ω6	0.4	0.2±0.1	0.2±0.1	0.4	0.1±0.1
0:4ω3	0.2	0.2±0.1	0.1±0.1	0.3	0.1±0.1
0:2ω6	0.1	Tr	0.1±0.0	0.1	Tr
2:6ω3	10.6	3.1±0.7	3.2±1.0	10.7	2.2±0.9
2:5ω6	0.2	0.1±0.1	Tr	0.3	0.1±0.3
2:4ω3	0.4	0.2±0.1	0.1±0.1	0.5	0.1±0.0
Branched					
15:0	0.4	0.3±0.1	0.3±0.1	0.2	0.1±0.1
15:0	0.1	0.2±0.1	0.4±0.3	0.1	0.3±0.3
16:0	0.3	0.1±0.0	0.2±0.1	0.2	Tr
17:0	0.4	0.2±0.0	0.2±0.1	0.3	0.2±0.0
17:0	0.1	0.1±0.0	0.2±0.1	0.1	0.2±0.1
18:0	3.2	2.6±0.5	2.6±0.5	1.4	1.2±0.9
Total % Saturates	32.0	43.4	41.7	22.6	21.6
Total % MUFA	23.8	35.2	34.6	38.8	62.0
Total % PUFA	39.7	18.1	19.8	36.3	14.4
Total % Branched	4.5	3.3	3.9	2.3	2.0
Total FA (mg g^{-1} dry wt.)	141.0	180.9±32.9	146.9±52.9	139.9	165.2±27.1

Branched acids are indicated by *i* (iso) and *a* (anteiso).
[a]Composite samples were used for analysis.
[b]Indicates all isomers combined.

Table 2
Composition of fatty acid (% of total fatty acid) in stomach contents of adult *E. superba* and seston, ice algae, and copepods (potenti diets) from Maguerite Bay

Fatty acids	Stomach content	Seston	Ice algae	Copepods		
				P. antarctica	*M. gerlachei*	*C. acuti*
n-Saturates						
12:0	Tr	0.3	—	—	—	—
14:0	9.5	0.8	18.0	0.6	1.8	4.3
15:0	0.4	0.6	0.5	Tr	0.1	Tr
16:0	20.9	29.3	10.2	4.4	9.3	6.4
17:0	0.1	1.3	0.2	Tr	Tr	Tr
18:0	1.3	16.4	1.7	0.5	2.0	0.4
20:0	0.1	0.5	—	Tr	Tr	Tr
22:0	Tr	0.4	0.1	Tr	Tr	0.2
Monounsaturates						
14:1ω3	0.1	Tr	0.1	0.1	Tr	Tr
15:1[a]	0.1	0.1	0.4	Tr	Tr	Tr
16:1ω9	0.1	0.3	0.3	Tr	0.2	Tr
16:1ω7	8.2	3.8	11.9	25.0	17.6	12.1
16:1ω5	0.4	0.1	0.4	0.2	0.2	0.2
16:1ω3	0.1	0.1	2.6	Tr	0.1	Tr
17:1[a]	0.3	4.6	0.3	0.3	0.1	0.1
18:1ω9	12.8	14.1	3.1	35.2	20.8	9.9
18:1ω7	7.1	6.6	1.4	4.6	5.2	3.9
18:1ω5	0.4	0.2	Tr	0.9	0.4	0.3
20:1[a]	4.6	1.3	—	8.3	13.4	25.0
22:1[a]	2.1	4.0	0.6	Tr	4.1	8.9
Polyunsaturates						
16:4ω1	0.9	0.1	13.4	0.1	0.5	1.6
16:3ω4	0.3	0.1	2.7	0.1	0.4	1.0
16:2ω6	0.8	0.3	1.4	0.5	1.0	1.3
18:4ω3	2.2	0.2	5.4	1.8	0.9	2.0
18:3ω3	0.2	0.2	0.9	Tr	0.2	0.2
18:2[a]	1.4	1.4	1.0	1.7	1.0	1.5
20:5ω3	14.5	2.2	18.5	7.0	10.9	13.2
20:4ω6	0.6	0.1	0.2	0.1	0.3	0.2
20:4ω3	0.3	0.2	0.3	0.2	0.3	0.4
20:2ω6	0.1	1.3	Tr	0.1	0.2	0.4
22:6ω3	6.6	5.0	2.0	4.5	6.5	4.5
22:5ω6	0.4	0.2	—	0.2	0.4	0.3
22:4ω3	0.4	1.6	Tr	0.2	0.3	0.4
Branched						
*i*15:0	0.2	0.3	0.5	0.2	0.2	0.1
*a*15:0	0.1	0.3	0.5	0.4	0.2	0.2
*a*16:0	0.2	0.2	0.7	Tr	Tr	0.1
*i*17:0	0.2	0.3	0.2	0.1	Tr	0.1
*a*17:0	Tr	0.3	0.3	0.2	0.1	0.1
*i*18:0	2.1	1.6	0.3	0.6	1.3	0.9
Total % Saturates	32.4	49.4	30.7	5.7	13.2	11.3
Total % MUFA	36.1	35.1	21.0	76.3	62.1	60.4
Total % PUFA	28.7	12.8	45.8	16.5	22.9	26.8
Total % Branched	2.8	2.7	2.5	1.5	1.8	1.5
Total FA ($mg\,g^{-1}$ dry wt.)	0.2[b]	0.7	11.1	103.2	88.6	128.0

Branched acids are indicated by *i* (iso) and *a* (anteiso);Tr: <0.1%, —: not detected.
[a]Indicates all isomers combined.
[b]Concentration of total fatty acids in stomach contents is mg $individual^{-1}$.

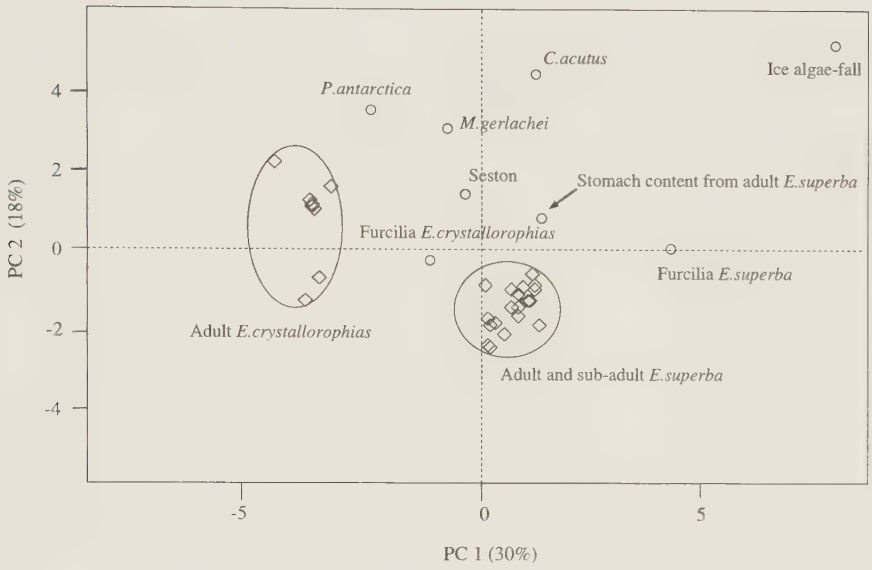

Fig. 3. Two-dimensional PCA score plot of the first two principle components observed for krill and potential diets based on individual fatty acid compositions of all krill and potential diets. Individual adult animals are shown for *E. superba* and *E. crystallorophias* with composite samples used for furcilia and copepods.

compared to sub-adults and adults. Compared to larval animals, adult *E. superba* also appear to be more omnivorous in their feeding pattern as seen from their close grouping to seston. Although it must be cautiously interpreted since it undoubtedly includes some contribution by the animal itself, the fatty acid distribution of stomach contents collected from adult *E. superba* also was closely related to seston and adult animals (Fig. 3). All copepods showed a positive displacement in PC 2 and were well separated from krill as a result of the high content of 20:1 and 22:1 acids. Among the copepods, two copepod species (*P. antarctica* and *M. gerlachei*) were distinct from herbivorous copepod *C. acutus* in PC 1 and also isolated from ice algae.

3.4. Fatty alcohols and sterols in krill and potential diets

The fatty alcohol and sterol distributions of the two krill species are shown in Table 3. Trace amounts of fatty alcohols (less than 0.1 mg g^{-1} dry wt.) were present in *E. superba*, with a greater diversity and higher concentrations present in *E. crystallorophias*. The 14:0 and 16:0 alcohols comprised more than 70% of total fatty alcohols in *E. crystallorophias*, with high amounts of 20:1 also seen in furcilia. The presence of phytol (3, 7, 11, 15-tetramethylhexadec-2-enol), originating from the side chain of chlorophyll *a*, in all krill confirms their consumption of algal related materials (e.g., sedimenting detritus, phytoplankton) or perhaps indirectly by predation of herbivores. Average concentrations of sterols were 2–3 times higher in furcilia (5.84 and 7.31 mg g^{-1} dry wt. for *E. superba* and *E. crystallorophias*, respectively) compared to sub-adult and adult for both krill species. Even though a diverse suite of sterols were present, particularly in furcilia, cholesterol remained the major sterol (more than 76% of total sterols) in all krill with a minor variations between species and maturity (Table 3). The second most abundant sterol was cholesta-5, 24-dien-3β-ol (27Δ5,24), which is produced from phytosterol dealkylation and common to several marine microalgae (Goad 1978; Barrett et al., 1995).

The fatty alcohol and sterol distributions in potential diets for krill (e.g., seston, ice algae, and copepods) and stomach contents were more varied

Table 3
Fatty alcohol and sterol composition (% of total fatty acid) of neutral lipid of Antarctic Euphausiids

Compound	*E. superba*			*E. crystallorophias*	
	Furcilia[a]	Sub-adult ($n=9$)	Adult ($n=10$)	Furcilia[b]	Adult ($n=7$)
n-alcohols					
14:1	—	—	—	0.43	0.04±0.07
14:0	—	—	—	45.26	58.44±4.35
15:0	—	—	—	2.09	1.51±0.47
16:1	—	—	—	2.59	3.31±1.13
16:0	—	29.86±32.69	3.45±9.58	27.35	33.79±2.84
17:0	—	—	—	0.40	0.22±0.08
18:1	—	Tr	—	1.75	0.46±0.29
18:0	—	28.69±18.23	94.50±1.60	4.31	0.16±0.07
20:1	—	—	—	11.45	1.36±1.02
22:1	100	19.23±20.99	2.05±6.49	4.23	0.56±0.38
Total n-alcohols					
(mg g^{-1} dry wt.)	0.09	0.04±0.03	0.05±0.04	53.74	106.59±26.79
Phytol (mg g^{-1} dry wt.)	0.60	0.89±1.26	0.51±0.57	4.92	5.37±2.99
Sterols					
24-norcholesta-5,22-dien-3β-ol (26Δ5,22)	0.25	0.75±0.45	1.79±0.92	0.26	0.92±0.69
Cholesta-5,22-dien-3β-ol (27Δ5,22)	3.58	0.71±0.34	0.49±0.37	3.10	0.51±0.51
5α-cholesta-22-en-3β-ol	—	—	—	0.04	—
Cholesta-5-en-3β-ol (Cholesterol)	76.88	80.93±4.55	85.32±3.85	80.20	85.58±1.95
5α-cholestan-3β-ol (Cholestanol)	1.27	0.08±0.17	1.69±1.03	0.61	0.03±0.04
Cholesta-5,24-dien-3β-ol (27Δ5,24)	17.43	17.52±4.91	10.70±3.20	15.37	12.98±1.58
24-methylcholesta-5,22-dien-3β-ol (28Δ5,22)	0.08	—	—	0.30	—
Cholesta-7-en-3β-ol (27Δ7)	0.37	—	—	0.09	Tr
24-ethylcholesta-5-en-3β-ol (29Δ5)	0.13	—	—	0.08	—
Total sterols (mg g^{-1} dry wt.)	5.84	1.62±0.82	2.88±0.65	7.31	2.97±1.28

[a]Composite samples were used for analysis; Tr: <0.1%, —: not detected.
[b]Fatty alcohols includes all isomers. Minor amounts of some fatty alcohols (15:1, 17:1, 18:2, 20:0, 22:0, and 24:1) in *E. crystallorophias* (0.01–0.06%) and omitted for brevity.

(Table 4). In seston and ice algae, total concentration of fatty alcohols was very low (less than 0.3 mg g^{-1} dry wt.), with dominance of the 14:0, 16:0, and 18:1 alcohols much greater amounts of fatty alcohols were present in copepods (164, 93, and 264 mg g^{-1} dry wt. for *P. antarctica*, *M. gerlachei*, and *C. acutus*, respectively) with significant differences in composition among species. The presence of phytol in all copepods reflects the consumption of algal related materials (e.g., sedimenting detritus, phytoplankton) or indirectly by predation on herbivores, yet very low amounts of phytol were present in seston in the water column at the site of collection. Interestingly, the fatty alcohol distribution in the stomach contents of adult *E. superba* was very similar to that in *C. acutus*, particularly with the appearance of the 20:1 and 22:1 alcohols. The sterol distributions in seston and ice algae showed several sterols present in zooplankton but also much greater diversity (Table 4). Cholesterol remained substantial (42.19% of total sterols) in seston, yet cholesta-5,24-dien-3β-ol (27Δ5,24) was the dominant sterol (59.57% of total sterols) in ice algae and also in *C. acutus* (43.54% of total sterols). Although cholesterol remained the principle sterol in copepods, additional sterols not seen in krill were also present and accounted for a significant fraction

able 4
atty alcohol and sterol composition (% of total fatty acid) of neutral lipids in stomach contents (from adult *E. superba*) and seston, ice lgae, and copepods from study area

ompound	Stomach contents	Seston	Ice algae	Copepods		
				P. antactica	*M. gerlachei*	*C. acutus*
-alcohols						
4:1	—	0.28	—	0.19	0.07	0.01
4:0	10.34	31.88	12.36	30.54	16.27	10.17
5:0	0.99	4.78	6.85	2.68	1.36	0.72
6:1	1.13	1.77	—	4.52	3.51	3.36
6:0	18.96	33.24	28.26	30.00	16.84	13.92
7:1	—	0.27	—	0.19	0.39	1.28
7:0	1.07	1.74	5.77	0.42	0.36	0.14
8:2	0.09	0.15	1.05	0.33	0.20	0.09
8:1	3.62	3.11	3.14	8.46	5.80	3.10
8:0	1.28	10.70	25.08	1.00	0.80	0.65
0:1	45.02	6.54	12.29	14.49	40.00	49.89
0:0	0.58	2.17	—	0.12	0.14	0.16
2:1	16.86	1.82	3.11	7.02	14.16	16.43
2:0	0.07	0.70	2.10	0.05	0.03	0.04
Total n-alcohols						
mg g^{-1} dry wt.)	38.1[a]	0.19	0.30	164.10	93.23	264.35
Phytol (mg g^{-1} dry wt.)	1.25[a]	0.01	2.78	1.40	1.15	1.56
Sterols						
24-norcholesta-5,22-dien-3β-ol (26Δ5,22)	1.15	11.15	2.45	3.70	5.23	1.92
27-nor-24-cholesta-5,22-dien-3β-ol	0.17	4.96	0.32	8.86	0.57	—
Cholesta-5,22-dien-3β-ol (27Δ5,22)	4.71	12.84	9.35	12.90	16.24	10.45
5α-cholesta-22-en-3β-ol	0.34	1.01	0.40	—	—	—
Cholesta-5-en-3β-ol (Cholesterol)	72.27	42.19	13.35	49.37	56.58	42.78
5α-cholestan-3β-ol (Cholestanol)	1.01	1.60	0.40	—	0.77	0.29
Cholesta-5,24-dien-3β-ol (27Δ5,24)	19.10	13.23	59.57	23.04	19.33	43.54
24-methylcholesta-5,22-dien-3β-ol (28Δ5,22)	—	0.93	0.40	—	—	0.48
Cholesta-7-en-3β-ol (27Δ7)	—	1.25	0.59	—	0.63	—
24-methylcholesta-5,24(28)-dien-3β-ol (28Δ5,24(28))	0.69	4.98	7.51	2.10	0.34	0.36
24-methylcholesta-5-en-3β-ol (28Δ5)	—	—	0.38	—	—	0.19
24-ethylcholesta-5,22-dien-3β-ol (29Δ5,22)	—	1.46	0.79	—	—	—
24-ethylcholesta-5-en-3β-ol (29Δ5)	0.55	4.40	1.17	—	—	—
24-ethylcholesta-5,24(28)*Z*-dien-3β-ol (29Δ5,24 (28)Z)	—	—	1.62	—	—	—
4α,23,24-trimethylcholesta-8(14)-en-3β-ol	—	—	1.71	—	—	—
Total sterols (mg g^{-1} dry wt.)	3.27[a]	0.06	1.57	1.47	3.50	1.83

Note: Individual fatty alcohols includes all isomers.
[a]Concentrations of total *n*-alcohols, phytol, and total sterols in stomach contents are mg individual^{-1}.

of the total (Table 4). In copepods, cholesta-5,22-dien-3β-ol (27Δ5,22), cholesterol, and cholesta-5,24-dien-3β-ol (27Δ5,24) in particular were important sterols. Although copepods showed much overlap in sterol distributions, some species differences were apparent, with significantly higher proportion of 27-nor-24-cholesta-5,22-dien-3β-ol and cholesta-5,24-dien-3β-ol (27Δ5,24) were in *P. antarctica* and *C. acutus*, respectively.

3.5. Microscopic examination of stomach contents

Although only limited numbers of krill (4–5 individuals from each life stage of krill) for both

species were used for microscopic examination of stomach contents, visual analysis of krill adults and furcilia showed clear differences in composition (Appendix—supplement in this issue). Furcilia had fuller stomachs and contained smaller particles (including algal fragments), whereas adults contained large amounts of copepod mandibles and body parts. Stomach contents in furcila of both *E. superba* and *E. crystallorophias* were similar, with much detritus and algal fragments. All adult *E. crystallorophias* examined had empty stomachs.

4. Discussion

The lipid dynamics of Antarctic krill are closely linked with their life cycle, particularly reproduction and overwintering (Falk-Petersen et al., 2000 and references therein). This is reflected in the lipid content and class composition, which varied between krill species and among maturity stages. For both species, adults had higher lipid content than furcilia, with *E. superba* containing triacylglycerols as its major energy reserve while wax esters were found in *E. crystallorophias*. Moreover, *E. crystallorophias* has significantly higher total lipid content than *E. superba*. This distinction in lipid composition between two species of krill inhabiting the same environment may reflect their differing reproductive and overwintering strategies. *E. superba* generally shows a major spawning in summer, but can extend its reproduction from late spring through fall (Marr, 1962; Quetin et al., 1994). This time frame allows *E. superba* to feed actively on algae during spring prior to spawning, and thus obtain needed energy for reproduction. In contrast, *E. crystallorophias*, typically spawns in early spring when phytoplankton production is extremely low (Pakhomov and Perissinotto, 1996). Extensive lipid reserves are needed by *E. crystallorophias* to provide the energetic needs for both survivals during the food-limited winter as well as reproduction before the spring bloom. Indeed, we observed significantly higher amounts of total lipid reserved in *E. crystallorophias* compared to *E. superba* in winter, which corresponds with previous observations (Hagen et al., 1996; Kattner and Hagen, 1998). Assuming wax ester mobilization has similar energetic costs as that for triacylglycerol, then the early timing of reproduction for *E. crystallorophias* has the advantage in that larval stages are able to build up sufficient body mass and energy reserves during their first season (Kattner and Hagen 1998; Falk-Petersen et al., 2000).

The increased lipid stores for neutral lipids in *E. crystallorophias* compared to *E. superba* does not appear to extend to phospholipids, which have been shown to provide an important site for lipid reserves in Antarctic krill in addition to their structural role (Hagen et al., 1996). Total phospholipid content in *E. crystallorophias* averaged 126.89 ± 18.94 (mean $\pm$ SD) $\mu g\, g^{-1}$ dry wt. for winter collected animals here, yet adult animals collected in the same area in the fall of 2002 had higher amounts ($187.55 \pm 13.23\, \mu g\, g^{-1}$ dry wt.—Ju and Harvey, unpublished). *E. superba* showed a similar trend, with animals collected in the fall of 2002 containing higher total phospholipids levels ($147.7 \pm 18.84\, \mu g\, g^{-1}$ dry wt.) than animals in winter ($107 \pm 6.69\, \mu g\, g^{-1}$ dry wt.). Although it is difficult to consider these differences in absolute terms given the yearly sampling span, it does indicate that phospholipid reserves, likely phosphatidylcholine, are mobilized along other storage lipids during winter periods for both species (Hagen et al., 1996; Stübing et al., 2003).

While total lipid and major classes provide important energetic information, specific lipid structures can allow insight into diet history (Ederington et al., 1995). Comparisons of animal and available food resources in particular can provide tracers of dietary patterns for adult and furcilia. Although detailed measures of lipid synthesis have not been conducted for krill, the crustacea are well known to lack the ability for *de novo* synthesis of sterols (Goad, 1978) and thus rely on dealkylation of dietary sources for these essential components. Cholesterol is the dominant structure formed, but it is not common to their primary algal diets and thus crustacea such as copepods can convert a number of algal sterols to cholesterol dependent upon the structure encountered (Harvey et al., 1987). Whether via passive adsorption during digestion or perhaps enzymatic

inefficiency, small amounts of dietary sterols remain and provide a means to trace past consumption. Detailed analysis of sterols present in adults and juvenile krill shown here reflect this process, with cholesterol representing the major sterol together with small amounts of a number of sterols obtained from their diets. Minor sterols seen in both adults and younger life stages showed substantial overlap, yet important differences were apparent between furcilia and adults of both species (Table 3). Most notable is that furcilia of both *E. superba* and *E. crystallorophias* contained small amounts of three sterols (28Δ5,22, 27Δ7, 29Δ5) absent from adult tissues, but observed in both seston and ice algae (Tables 3 and 4). These sterols are common to a number of marine algae including diatoms (Barrett et al., 1995, and references therein) and likely originate from feeding of furcilia on ice biota at the ice water interface. One novel sterol common to all krill observed is cholesta-5, 24-dien-3β-ol (27Δ5,24). Although not widely distributed in marine algae (Volkman, 1986a), it has been reported to account for 100% of the sterol seen in the pennate diatom *Nitzchia closterium* and over 94% of total sterols in the centric species *Rhizosolenia setigera* (Barrett et al., 1995). Its common appearance in all krill, the three copepods examined, and its dominance in ice algae suggest that diatoms residing at the ice interface comprise an important fraction of all animal diets and are the major fraction of ice algal material available to furcilia in winter. The importance of ice algae for furcilia is further supported by fatty acid data, which find PUFA's common to diatoms present at over two-fold higher concentrations in furcilia than adult krill of both species. As noted by other authors (Quetin and Ross, 1991; Meyer et al., 2002; Stübing et al., 2003), furcilia do not enter dormancy during winter, and thus the increased PUFA accumulation seen here likely represents continual feeding under ice during winter.

Fatty acids have been used as indices of feeding and metabolism for many crustacea, including krill (Virtue et al., 1996; Hagen et al., 2001). Although several individual fatty acids can be considered as specific markers of food source (e.g., 20:5 for diatoms), many have common origins, which makes assigning a specific source difficult. One illustration of this difficulty is the work of Cripps and Atkinson (2000), who fed copepods to *E. superba* and observed the ratio of PUFA/SFA to increase. They suggested that the ratio could be used as an indicator for carnivory (seen as high values) even though copepods do not synthesize PUFA's and the acids originates from copepod herbivory. In this study, we found that the PUFA/SFA ratio as an index for carnivory seems to hold for copepods, with the carnivore *P. antarctica* known having a higher ratio (2.93) than herbivorous copepod *C. acutus* (2.4) and omnivorous copepod *M. gerlchei* (1.73) (Øresland, 1991; Atkinson, 1995; Pasternak and Schnack-Schiel, 2001). The index was not effective for krill, however, with the ratio for adults (mean 0.5) feeding on copepods lower than that for furciliae (>1.27), which other markers suggested were feeding almost exclusively on ice algae. Others also have suggested that this ratio might not be useful for Antarctic krill because fatty acid compositions are largely dependent on total lipid content of individuals (Kattner and Hagen, 1998; Hagen et al., 2001). Rather than a ratio, we applied PCA to total fatty acid profiles to provide a more robust measure of the relationship among diets and animals. PCA applied to fatty acid profiles nevertheless requires careful interpretation since fatty acid profiles included both dietary information as well as lipid stores which are replaced at varying time scales and include the presence of compositionally stable structural lipids principally as phospholipids (Sargent et al., 1987; Stübing et al., 2003). A further complication is the potential for varied fatty acid composition dependent upon prey and lipid storage; i.e. krill feeding on WE—rich prey (like copepods) may either convert their dietary fatty alcohols to fatty acids as in the case of *E. superba*, or retain them as fatty alcohols for deposition as WE in the case of *E. crystallorophias*. Measures of fatty acids alone would not capture this transfer.

Although small numbers of stomachs were examined, visual analysis of their contents suggested copepods account for a substantial portion of the adult krill diet in winter. Lipid biomarkers present in high levels among copepods include the

20:1 and 22:1 acids, but were not accumulated in adult krill. Similarly low levels were observed by Stübing et al. (2003) in *E. superba* fed a copepod diet under experimental conditions, but they did find high levels of these acids were present in fecal strings produced after copepod feeding. Low assimilation efficiency appears the cause, and explains the absence of these fatty acids in the adult krill collected in winter even though visual and sterol data suggests that copepods can account for a substantial fraction of the diet of *E. superba* in winter. Although qualitative in nature, the presence of a significant fraction of the stomach contents as copepod body parts and mandibles together with sterols information present compelling evidence for copepod consumption in winter. Although no attempts were made to measure abundance, the common presence of significant numbers of copepod mandibles in stomach contents confirms that copepod might account for a significant fraction of adult *E. superba* food resources in winter. Furthermore, it is now well established that *E. superba* can resort to carnivory during periods of phytoplankton shortage (Huntley et al., 1994; Atkinson and Snÿder, 1997; Atkinson et al., 2002). Because copepods contain significant amounts of lipids (Hagen et al., 1993, this study), they also represent an abundant high-energy food source during winter. The observation that total lipid reserves are lower than previously observed for adult animals collected in fall (Atkinson et al., 2002), indicates that *E. superba* in Marguarite Bay relies on carnivory as well as the utilization of energy reserves as an over-wintering strategy. *E. superba* furcilia showed the lowest lipid reserves, supporting the contention by Hagen et al. (2001) that larvae may not survive austral winter with lipid utilization alone. Lipid biomarkers and stomach content analysis of larval krill indicate consumption of ice-associated biota, suggesting they supplement the utilization of lipid reserves by feeding at the ice interface to survive.

This study suggests that post-larval *E. superba* are omnivorous, whereas adult *E. crystallorophias* may not feed actively during austral winter. Thus, for *E. crystallorophias*, lipid reserves seem to play more important roles than feeding for overwintering survival. However, *E. superba* furcilia mainly feed on ice associated biota (including small zooplankton), whereas furcilia of *E. crystallorophias* may feed on any particles (e.g., sedimentin detritus from ice) in water column during winter. In addition to fatty acids, other lipid components including sterols and fatty alcohols appear to integrate over differing time scales, providing important insights into feeding patterns and history for both species of krill.

Acknowledgments

We thank the captain and crew of the *L.M. Gould* and technicians and personnel of Raytheon Polar Services Company for assistance with field collections as well as technical and travel support. We also thank Brenda Yates for help with manuscript preparation. This work was supported by the NSF through the Southern Ocean GLOBEC Program (OPP-9910043). This manuscript is contribution No. 3677 of The University of Maryland Center for Environmental Science and contribution No. 460 of USGLOBEC program.

Appendix A. Supplementary data

The online version of this article contains additional supplementary data containing digital images of stomach contents. Please visit doi:10.1016/j.dsr2.2004.08.004.

References

Albers, C.S., Kattner, G., Hagen, W., 1996. The compositions of wax esters, triacylglycerols and phospholipids in Artic and Antarctic copepods: evidence of energetic adaptations. Marine Chemistry 55, 347–358.

Atkinson, A., 1995. Omnivory and feeding selectivity in 5 copepod species during spring in the Bellingshausen-Sea, Antarctica. Ices Journal of Marine Science 52 (3–4), 385–396.

Atkinson, A., Snÿder, R., 1997. Krill-copepod interactions at South Georgia, Antarctica, I. Omnivory by *Euphausia superba*. Marine Ecology Progress Series 160, 63–76.

Atkinson, A., Meyer, B., Stübing, D., Hagen, W., Schmidt, K., Bathmann, U.V., 2002. Feeding and energy budgets of Antarctic krill *Euphausia superba* at the onset of winter—II. Juveniles and adults. Limnology and Oceanography 47 (4), 953–966.

Barrett, S.M., Volkman, J.K., Dunstan, G.A., 1995. Sterols of 14 species of marine diatoms (Baccillariophyta). Journal of Phycology 31, 360–369.

Bottino, N.R., 1974. The fatty acids of Antarctic phytoplankton and euphausiids. Fatty acid exchange among trophic levels of the Ross Sea. Marine Biology 27, 197–204.

Clark, A., 1980. The biochemical composition of krill *Euphausia superba* Dana from south Georgia. Journal of Experimental Marine Biology and Ecology 43, 221–236.

Clark, A., 1984. Lipid content and composition of Antarctic krill *Euphausia superba* Dana. Journal of Crustacean Biology 4, 285–294.

Costa, D.P., Crocker, D.E., 1996. Marine mammals in the Southern Ocean. In: Ross, R.M., Hofmann, E.E., Quetin, L.B. (Eds.), Foundation for Ecological Research West of the Antarctic Peninsula. Antarctic Research Series, vol. 70. American Geophysical Union, Washington, DC, pp. 287–301.

Cripps, G.C., Atkinson, A., 2000. Fatty acid composition as an indicator of carnivory in Antarctic krill, *Euphausia superba*. Canadian Journal of Fisheries and Aquatic Sciences 57, 31–37.

Cripps, G.C., Watkins, J.L., Hill, H.J., Atkinson, A., 1999. Fatty acid content of Antarctic krill *Euphausia superba* at South Georgia related to regional populations and variations in diet. Marine Ecology Progress Series 181, 177–188.

Ederington, M.C., McManus, G.B., Harvey, H.R., 1995. Trophic transfer of fatty acids, sterols and tritepenoid alcohol between bacteria, a ciliate and the copepod Acartia tonsa. Limnology and Oceanography 40 (5), 860–867.

Falk-Petersen, S., Hagen, W., Kattner, G., Clarke, A., Sargent, J., 2000. Lipids, trophic relationships, and biodiversity in Arctic and Antarctic krill. Canadian Journal of Fisheries and Aquatic Sciences 57, 178–191.

Färber-Lorda, J., 1994. Length-weight relationships and coefficient of condition of *Euphausia superba* and *Thysanoessa macrura* (Crustacea:Euphausiacea) in southwest Indian Ocean during summer. Marine Biology 118, 645–650.

Fraser, W.R., Trivelpiece, W.Z., 1996. Factors controlling the distribution of seabirds: winter-summer heterogeneity in the distribution of Adelie penguin populations. In: Ross, R.M., Hofmann, E.E., Quetin, L.B. (Eds.), Foundation for Ecological Research West of the Antarctic Peninsula Antarctic Research Series, vol. 70. American Geophysical Union, Washington, DC, pp. 257–272.

Goad, L.J., 1978. The sterols of marine invertebrates: composition, biosynthesis and metabolites. In: Scheuer, P.J. (Ed.), Marine Natural Products, vol. 2. Academic Press, New York, pp. 74–172.

Graeve, M., Kattner, G., Hagen, W., 1994. Diet-induced changes in the fatty acid composition of Artic herbivorous copepods: experimental evidence of trophic markers. Journal of Experimental Marine Biology and Ecology 182, 97–110.

Hagen, W., Kattner, G., Graeve, M., 1993. *Calanoides acutus* and *Calanus propinquus*, Antarctic copepods with different lipid storage modes via wax esters or triacyglycerols. Marine Ecology Progress Series 97, 135–142.

Hagen, W., Van Vleet, E.S., Kattner, G., 1996. Seasonal lipid storage as overwintering strategy of Antarctic krill. Marine Ecology Progress Series 134, 85–89.

Hagen, W., Kattner, G., Terbruggen, A., Van Vleet, E.S., 2001. Lipid metabolism of the Antarctic krill *Euphausia superba* and its ecological implications. Marine Biology 139 (1), 95–104.

Harvey, H.R., McManus, G.B., 1991. Marine ciliates as a widespread source of tetrahymanol and hopan-3-ϐ-ol in sediments. Geochemica et Cosmochimica Acta 55, 3387–3390.

Harvey, H.R., Eglinton, G., O'Hara, S.C.M., Corner, E.D.S., 1987. Biotransformation and assimilation of dietary lipids by Calanus feeding on a dinoflagellate. Geochemica et Cosmochimica Acta 51, 3030–3041.

Hofmann, E.E., Lascara, C.M., 2000. Modeling the growth dynamics of Antarctic krill *Euphausia superba*. Marine Ecology Progress Series 194, 219–231.

Hofmann, E.E., Costa, D.P., Daly, K.L., Torres, J.J., Fraser, W.R., 2002. US Southern Ocean Global Ocean Ecosystems Dynamics Program. Oceanography 15 (2), 64–74.

Huntley, M.E., Nordhausen, W., Lopez, M.D.G., 1994. Elemental composition, metabolic-activity and growth of Antarctic krill *Euphausia superba* during winter. Marine Ecology Progress Series 107 (1-2), 23–40.

Ikeda, T., Dixon, P., 1982. Body shrinkage as a possible overwintering mechanism of the Antarctic krill, *Euphausia superba*. Journal of Experimental Marine Biology and Ecology 62, 143–151.

Ju, S-J., Kucklick, J.R., Kozlova, T., Harvey, H.R., 1997. Lipid accumulation and fatty acid composition during maturation of three pelagic fish species in Lake Baikal. Journal of Great Lake Research 23 (3), 241–253.

Kattner, G., Hagen, W., 1998. Lipid metabolism of the Antarctic euphausiid *Euphausia crystallorophias* and its ecological implication. Marine Ecology Progress Series 170, 203–213.

Lascara, C.M., Hofmann, E.E., Ross, R.R., Quetin, L.B., 1999. Seasonal variability in the distribution of Antarctic krill, *Euphausia superba*, west of the Antarctic Peninsula. Deep-Sea Research I 46, 925–949.

Laws, R.M., 1985. The ecology of the Southern Ocean. American Scientist 73, 26–40.

Littell, R.C., Milliken, G.A., Stroup, W.W., Wolfinger, R.D., 1999. SAS System for Mixed Models. SAS Institute Inc., Cary, NC.

Marr, J.W.S., 1962. The natural history and geography of Antarctic krill (*Euphausia superba* Dana). Discovery Report 32, 33–464.

Mayzaud, P., Albessard, E., Cuzin-Roudy, J., 1998. Changes in lipid composition of the Antarctic krill *Euphausia superba* in the Indian sector of the Antarctic Ocean: influence of geographical location, sexual maturity stage and distribution among organs. Marine Ecology Progress Series 173, 149–162.

Meyer, B., Atkinson, A., Stübing, D., Oettl, B., Hagen, W., Bathmann, U.V., 2002. Feeding and energy budgets of Antarctic krill *Euphausia superba* at the onset of winter—I. Furcilia III larvae. Limnology and Oceanography 47 (4), 943–952.

Nichols, P.D., Guckert, J.B., White, D.C., 1986. Determination of monounsaturated fatty acid double-bond position and geometry for microbial monocultures and complex consortia by capillary GC-MS of their dimethyl disulphide adducts. Journal of Microbiological Methods 5, 49–55.

Nichols, D.S., Nichols, P.D., Sullivan, C.W., 1993. Fatty acid, sterol and hydrocarbon composition of Antarctic sea ice diatom communities during spring bloom in McMurdo Sound. Antarctic Science 5 (3), 271–278.

Øresland, V., 1991. Feeding of the carnivorous copepod *Euchaeta antarctica* in Antarctic waters. Marine Ecology Progress Series 78, 41–47.

Pakhomov, E.A., Perissinotto, R., 1996. Antarctic neritic krill Euphausia crystallorophias: spatio-temporal distribution, growth and grazing rates. Deep-Sea Research I 43, 59–87.

Pasternak, A.F., Schnack-Schiel, S.B., 2001. Seasonal feeding patterns of the dominant Antarctic copepods *Calanus propinquus* and *Calanoides acutus* in the Weddell Sea. Polar Biology 24, 771–784.

Pond, D., Watkins, J., Priddle, J., Sargent, J., 1995. Variation in the lipid content and composition of Antarctic krill *Euphausia superba* at South Georgia. Marine Ecology Progress Series 117, 49–57.

Quetin, L.B., Ross, R.M., 1991. Behavioural and physiological characteristics of the Antarctic krill, *Euphausia superba*. American Zoologist 31, 49–63.

Quetin, L.B., Ross, R.M., 2001. Environmental variability and its impact on the reproductive cycle of Antarctic krill. American Zoologist 41 (1), 74–89.

Quetin, L.B., Ross, R.M., Clarke, A., 1994. Krill energetics: seasonal and environmental aspects of the physiology of *Euphausia superba*. In: El-Sayed, S.Z. (Ed.), Southern Ocean Ecology: the BIOMASS Perspective. Cambridge University Press, Cambridge, pp. 165–184.

Quetin, L.B., Ross, R.M., Frazer, T.K., Haberman, K.L., 1996. Factors affecting distribution and abundance of zooplankton, with an emphasis on Antarctic krill, *Euphausia superba*. In: Ross, R.M., Hofmann, E.E., Quetin, L.B. (Eds.), Foundation for Ecological Research West of the Antarctic Peninsula. Antarctic Research Series, vol. 70. American Geophysical Union, Washington, DC, pp. 357–371.

Ross, R.M., Quetin, L.B., 1991. Ecological physiology of larval euphausiids, *Euphausia superba* (Euphausiacea). Memoria. Queensland Museum 31, 321–333.

Sargent, J.R., Parkers, R.J., Mueller-Harvey, I., Henderson R.J., 1987. Lipid biomarkers in marine ecology. In: Sleigh M.A. (Ed.), Microbes in the Sea. Ellis Horwood, Chichester, UK, pp. 491–533.

Schnack, S.B., 1985. Feeding by *Euphausia superba* and copepod species in response to varying concentrations of phytoplankton. In: Siegfried, W.R., Condy, P.R., Laws, R.M. (Eds.), Antarctic Nutrient Cycles and Food Webs. Springer, Berlin, pp. 311–323.

Scott, C.L., Kwasniewski, S., Falk-Petersen, S., Sargent, J.R., 2002. Species differences, origins and functions of fatty alcohols and fatty acids in the wax esters and phospholipids of *Calanus hyperboreus*, *C. glacialis* and *C. finmarchicus* from Arctic waters. Marine Ecology Progress Series 235, 127–134.

Siegel, V., 1987. Age and growth of Antarctic Euphasiacea (Crustacea) under natural conditions. Marine Biology 96, 483–495.

Siegel, V., 2000. Krill (Euphausiacea) demography and variability in abundance and distribution. Canadian Journal of Fisheries and Aquatic Sciences 57, 151–167.

Stübing, D., Hagen, W., Schmict, K., 2003. On the use of lipid biomarkers in marine food web analyses: an experimental case study on the Antarctic krill, *Euphausia superba*. Limnology and Oceanography 48 (4), 1685–1700.

Torres, J.J., Donnelly, J., Hopkins, T.L., Lancraft, T.M., Aarset, A.V., Ainley, D.G., 1994. Proximate composition and overwintering strategies of Antarctic micronektonic crustacea. Marine Ecology Progress Series 113, 221–232.

Virtue, P., Nicol, S., Nichols, P.D., 1993. Changes in the digestive gland of *Euphausia superba* during short-term starvation: lipid class, fatty acid and sterol content and composition. Marine Biology 117, 441–448.

Virtue, P., Nichols, P.D., Nicol, S., Hosie, G.W., 1996. Reproductive trade-off in male Antarctic krill, *Euphausia superba*. Marine Biology 126, 521–527.

Volkman, J.K., 1986a. A review of sterol markers for marine and terrestrial organic matter. Organic Geochemistry 9, 83–99.

Volkman, J.K., Everitt, D.A., Allen, D.I., 1986b. Some analyses of lipid classes in marine organisms, sediments and seawater using thin-layer chromatography-flame ionization detection. Journal of Chromatography 356, 147–162.

ELSEVIER

Deep-Sea Research II 51 (2004) 2215–2224

DEEP-SEA RESEARCH
PART II

www.elsevier.com/locate/dsr2

Condition of *Euphausia crystallorophias* off East Antarctica in winter in comparison to other seasons

S. Nicol[a,*], P. Virtue[b], R. King[a], S.R. Davenport[a], A.F. McGaffin[b], P. Nichols[c]

[a]*Australian Antarctic Division, Channel Highway, Kingston, Tasmania 7050, Australia*
[b]*Institute of Antarctic and Southern Ocean Studies, University of Tasmania, GPO Box 252-50 Hobart, Tasmania 7001, Australia*
[c]*CSIRO, Division of Marine Research, GPO Box 1538, Hobart TAS 7001, Australia*

Accepted 11 July 2004
Available online 18 October 2004

Abstract

Antarctic coastal krill (*Euphausia crystallorophias*) were collected in Austral winter (July/August) 1999 in the Mertz Glacier polynya off the coast of East Antarctica and were compared to krill collected off East Antarctica during summer in 1996 and 2001 and spring 1999. A range of experiments and measurements were conducted to assess their relative condition in winter and summer. Krill collected in winter had pale yellow–green digestive glands, indicating some recent feeding activity. The size of the digestive glands was small relative to those of krill caught in summer. This indicates that feeding had been occurring at low levels during the collection period. Growth rates, measured using the instantaneous growth rate methodology, were close to zero in winter (range −5% to 7% per moult). This was an indication that some food had been available during the period of the moult cycle. Growth rates in spring ranged from −0.5% to +8.7% per moult and from 4% to 12% per moult in the summer. The mean length of the winter moult cycle (68 days) was considerably greater than the measured intermoult period in summer and spring (24–33 days). Lipid levels were low in winter, less than 5% of body weight, compared to summer levels of ~15% (dry weight). Winter krill were richer in wax esters and poorer in polar lipids than specimens collected in summer. Krill in winter were lacking in C16 PUFA that are markers of the phytoplankton diet common in summer krill. Krill caught in the winter had significantly higher levels of 20:1 and 22:1 fatty acids (2.3%) and alcohols (8.1%) than krill sampled in summer (0.2%, 0%), indicating a shift to a carnivorous diet. Results from this study suggest that *E. crystallorophias* respond to low food abundance during the winter through metabolic and physiological processes. These processes were reflected in a decrease in growth rate and a significant increase in the intermoult period. The process of lipid utilisation and switching to a carnivorous/detrital type diet are also overwintering strategies employed by this species.
© 2004 Elsevier Ltd. All rights reserved.

1. Introduction

Euphausia crystallorophias is a key component of the neritic community in the Antarctic coastal

*Corresponding author. Fax: +61-363-323-351.
E-mail address: steve.nicol@aad.gov.au (S. Nicol).

0967-0645/$ - see front matter © 2004 Elsevier Ltd. All rights reserved.
doi:10.1016/j.dsr2.2004.07.002

waters. It is the dominant food source for many carnivorous species including fish, penguins, seabirds and whales in the shelf waters (Nordhausen, 1994; Pakhomov and Perissinotto, 1996), replacing the dominant species, *Euphausia superba*, found in more oceanic waters. *E. crystallorophias* occupies an extreme habitat and is thought to face long periods of food shortage during the ice-covered winter. Investigations into how this species survives these extreme winter conditions have not been previously reported due to the inaccessibility of its neritic habitat.

Theoretical growth curves for *E. crystallorophias* have been generated from length-frequency analyses collected over several seasons off the Antarctic Peninsula and in the south-eastern Weddell Sea (Siegel, 1987) and during austral summer off East Antarctica (Pakhomov and Perissinotto, 1996), and development rates have been measured from the Bransfield Strait (Brinton and Townsend, 1991) and from a fjord population (Kirkwood, 1996). Experimental investigations into the development rate (Ikeda, 1986) and spawning (Harrington and Thomas, 1987) also have been reported.

Understanding how Antarctic euphausiids survive over the winter period of food scarcity has been hampered by the lack of samples collected during autumn, winter and spring and by the lack of accepted techniques that can evaluate their physiological or nutritional condition. Euphausiids in high latitudes are thought to exhibit growth rates that vary greatly with season (Siegel and Nicol, 2000). Generally, these growth rates have been estimated from the analysis of length frequencies from sequential samples throughout a season. For many oceanic species, or for species that inhabit remote or seasonally inaccessible waters, obtaining a seasonal series of samples to estimate growth is difficult. Experimental studies have examined growth rates of a small number of euphausiid species in the laboratory and have provided evidence that all species so far examined possess the ability to shrink in length through moulting in times of food shortage, such as in high-latitude winter (Nicol, 2000). There are also suggestions from length-frequency analysis that such shrinkage might occur in the field, but until recently there has been sparse evidence to support this conjecture (Stepnik, 1982).

The size of the digestive gland in Antarctic krill *E. superba* is a simple indication of the nutritional conditions krill have experienced over a period of about a week (Shin and Nicol 2003a,b). Over longer time periods, the instantaneous growth rate (IGR) technique, which measures the rate at which freshly collected krill are growing (Nicol et al., 1992; Quetin and Ross, 1991), provides information on the timescale of a moult cycle. This technique relies on the assumption that the measured growth rate in captive animals within 5 days of collection reflects the response of krill to conditions experienced within a moult cycle. This technique has been in use for *E. superba* for a number of years now and has yielded results that reflect seasonal (Nicol et al., 2000; Quetin and Ross, 1991), ontogenetic (Nicol et al., 1992), and food-related (Ross et al., 2000) variations in growth rates. Although the size difference between the moulted exoskeleton and the freshly moulted krill has been used as a measure of growth in laboratory studies (Buchholz, 1985; Hosie and Ritz, 1989; Marinovic and Mangel, 1999), there have been no reported results of applying the IGR technique to species other than *E. superba* in the field.

Additional information on the seasonal condition of krill and their dietary history can come from their lipid content and composition (Hagen et al., 1996; Virtue et al., 2000). The lipid content (Littlepage, 1964; Bottino, 1975; Clarke, 1984) and fatty acid composition (Kattner and Hagen, 1998) of *E. crystallorophias* have been previously reported for other regions of the Antarctic. Lipid analysis also provides a method for evaluating diet and to identify food web interactions (Mayzaud et al., 1976; Virtue et al., 1993a, b).

Determining how krill cope with winter conditions requires a novel approach. The use of basic morphometrics measurements combined with growth rate and biochemical data have provided a means to allow interpretation of over-winter strategies in *E. crystallorophias*.

2. Materials and methods

Live *E. crystallorophias* were collected on two occasions from the Mertz Glacier Polynya

66° 23.911'S, 145° 54.123'E and 66° 29.083'S, 146° .711'E) off East Antarctica in winter (22 and 23 f August 1999) using a RMT8 net in the top 00 m of the water column. A second collection of *E. crystallorophias* was made in spring (17 December 1999) at 66° 29.08'S, 146° 0.71'E. A hird collection was made in summer the year fterwards (12 February 2001) at 67° 42.46'S, 77° 2.24'E. Summer adult samples were collected for ipid analysis on two occasions: 18 March 1996 at 6° 03.69'S, 144 29.83'E and 27 December 1999 at 6° 29.08'S, 146° 0.71'E.

2.1. Instantaneous growth rates

Live krill were transferred immediately after capture into individual perforated 250 ml polycarbonate jars that were stacked eight-high in a perforated PVC tube. The tube was then suspended vertically in a 1000 l tank of sea water that was continually being replenished from the Southern Ocean. Up to 130 such tubes could be accommodated in the tank, and the perforations in the jars and tubes ensured an adequate exchange of sea water between the jars and the tank. Each jar was inspected daily to ascertain whether the animal within had moulted. If an animal had moulted then the animal and its moult were collected and frozen in liquid nitrogen to be measured on return to the laboratory. Moulted animals were collected in this fashion for a period of 5–14 days after capture.

The total length of the uropod exopodites was measured on both the left and right sides for both the animal and the moult. Measurements were made with a Leica MZ95 stereomicroscope connected to a Sony DXC-AP colour video camera. The images were analysed with Sigma Scan Pro® image analysis software, and from these measurements the percentage change in uropod length at moult were calculated. Growth rates were expressed separately for each sex as an average for all animals that moulted within the first 5 days after capture.

The intermoult period was calculated from the proportion of the total experimental population moulting per day assuming random moulting. For example, in Winter Experiment A 85 animals moulted in 15 days, equivalent to 5.6 moultings per day. A population of 400 animals (the experimental group minus mortalities) would thus have all moulted in 71.4 days. This approach gave only approximate results as mortalities occurred throughout the course of the experiments.

2.2. Digestive gland

The digestive glands of 100 krill from spring and 29 krill from winter were measured through the carapace along their longest axis. The carapace length was measured from the tip of the rostrum to the posterior notch of the carapace.

2.3. Lipid extraction and analysis

Krill collected for lipid analysis were frozen immediately in liquid nitrogen and maintained at −80 °C until analysed. Samples were quantitatively extracted using the modified Bligh and Dyer (1959) technique as described in Virtue et al. (1993a,b). Six adult individual male and female krill were initially analysed from each site; as there was no significant difference in total lipid content and composition between sexes, adult krill of similar size were then batched and each sample consisted of three whole krill (either male or female) (see Table 3). Total lipid content was determined gravimetrically and a portion of the total lipid extract was analysed for lipid class composition with chromatographic separation coupled with a flame ionization detector (FID) on an Iatroscan Mark V TH 10 (Ackman, 1981). Fatty acids and alcohols were obtained via methylation and saponification of the total lipid fraction as described in Virtue et al. (1993a,b). Gas chromatographic (GC) analyses were performed with a Hewlett Packard 5890 GC as described in Virtue et al. (1993a). GC results are subject to an error of ±5%. For ease of reporting, only a limited data set is tabulated, specifically those addressed in the text and other major fatty acids. Minor components (under 0.5%) and other lipid components not referred to in the results comprised only 13–16% of the total fatty acids (Table 3). The full data set is available from the authors. Gas chromatographic-mass spectrometric

(GC-MS) analyses of selected samples were performed on a Fisons MD 800 GC-MS (Manchester, UK) as described in Virtue et al. (2000).

2.4. Statistical analysis

Statistical analysis of lipid data was performed using 'Statistica' 6.0 (Copyright @Stat Soft Inc 2001). Arcsin square root transformation was used for all percentage data. A Tukey's HSD post hoc test was used, and results are reported using a significance level of 99% unless otherwise stated in the text.

3. Results

The digestive glands of krill collected in spring were larger than digestive glands of similar sized animals collected in winter (Fig. 1). The digestive gland in winter krill occupied an average of 33% of the carapace length, which was a significantly lower percentage than that in summer (63%) ($t=27.96$, 126 DF, $p<0.0001$). Digestive glands of winter krill were uniformly pale yellow–green whereas those from spring and summer were dark green.

Four growth rate experiments were conducted between 1999 and 2001 covering winter, spring and summer (Table 1). These varied in duration from 5 to 15 days. Krill exhibited different growth rates in the winter, spring and summer experiments (Table 2). In winter, adult krill were growing at a rate that was only just positive (0.35% per moult, males and females combined) whereas in spring they were growing at a much faster rate (3.05% per moult). Juveniles in summer were growing at a significantly faster rate than krill in spring or winter. In winter, by day 4 of the IGR experiment the krill began to shrink (mean growth rate became negative). The mean shrinkage rate between days 4 and 15 was −0.83%. The calculated mean intermoult period for adults in winter (68.7–71.4 days) was over double that calculated in spring (33.5 days). The overall adult winter growth rate was between −0.002% and +0.01% of body length per day compared to adult growth rates from spring of 0.11% of body length per day and juvenile summer growth rates of 0.35% of body length per day.

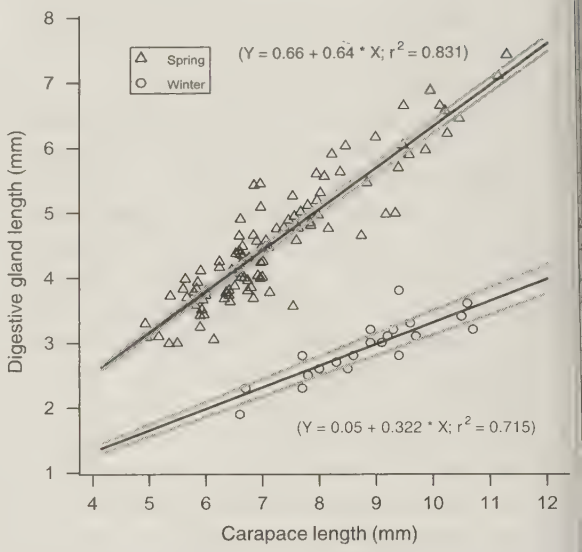

Fig. 1. The relationship between the length of the digestive gland and the carapace length in *E. crystallorophias* in winter and spring. Test for common slopes rejected ($p<0.001$) [$F(1,117)=13.40$]. Test for common y-intercepts accepted ($p=0.923$) [$F(1,117)=0.01$]; common y-intercept ($=-0.075$, SE $=0.194$) not significantly different from zero ($t=-0.39$, $p=0.7$).

Significantly higher total lipid contents were found in summer krill (~15% dry weight), than in winter krill (3–5% dry weight) (Fig. 2) ($F_{2,44}=48.923$, $p<0.0001$). There was no significant difference in total lipid contents between krill collected in summer 1996 and summer 1999 ($p=0.58$). Significant differences were found in the relative levels of wax ester between summer krill of 1999 (20% of total lipid) and summer krill of 1996 (49% of total lipid). Wax ester is thought to be used for long-term storage and utilised during times of low food supply. Winter krill had high relative levels of wax esters (58% of total lipid); however, the absolute levels were much lower than in summer. Conversely, polar lipids were lower in winter krill on a relative basis (40% of total lipid) than summer krill (48–68% of total lipid). As polar lipids are structural components compared with triacylglycerols, which fulfill a storage role, they would be expected to remain more stable throughout the seasons. Negligible

Table 1
Collection dates and sample sizes for *E. crystallorophias* used in the instantaneous growth rate experiments

Location	Collection date	Number of animals in experiment	Duration of experiment (days)	Total number of animals moulting	Number of animals moulting in first 5 days
66° 23.911'S 45° 54.123'E	15/08/1999 (Winter)	415	15	125	38
66°29.083'S 46° 0.711'E	23/08/1999 (Winter)	416	7	54	32
65° 32.1'S 107° 0.15'E	17/12/99 (Spring)	160	9	18	7
67°42.46'S 67°42.24'E	12/2/2001 (Summer)	104	5	21	21

Table 2
Growth rates of *E. crystallorophias* determined from the instantaneous growth rate experiments

Season	Mean uropod length (mm) + standard deviation	Mean initial growth rate (% change in uropod length in first 5 days) + standard deviation	Calculated intermoult period (days)	Growth rate (% change in mean uropod length over entire moult cycle)
Winter ($n=50$)	4.1 (0.43) (Adults)	0.35 (3.85)	71.4 (Expt. A)	−0.002
			68.7 (Expt. B)	0.01
Spring ($n=7$)	4.19 (0.541) (Adults and juveniles)	3.05 (3.17)	33.5	0.11
Summer ($n=14$)	1.98 (0.13) (Juveniles)	8.28 (2.43)	24.0	0.35

[a]Sample sizes may differ from number of animals moulting in Table 1 because damage to uropods can make measurement impossible.
[b]Intermoult periods and overall growth rates for winter experiments expressed separately. Summer krill were significantly smaller than either winter or spring krill (ANOVA, F-value: 134.9, $p < 0.001$, 2 DF). Growth rates differed significantly between seasons: (ANOVA, F-value: 51.109, $p < 0.0001$, 2 DF).

levels of triacylglycerol were detected in all samples (0.1–2% of total lipid). Triacylglycerol is regarded as a short-term storage lipid. Relative levels of free fatty acids were low (0–3%) indicating a high degree of sample integrity. Relative levels of sterol ranged between 0.6% and 3% with summer samples having higher levels than winter samples.

E. crystallorophias contains high levels of omega-3 polyunsaturated fatty acids (PUFA) (30–42% of the total fatty acids), which are characteristic of most species of krill. There were no significant differences in relative levels of PUFA between summer and winter samples (Table 3). PUFA (in particular 20:5(n-3) and 22:6(n-3)) are considered essential fatty acids as they cannot be synthesised by crustaceans. These fatty acids are derived from ingested food. They are, however, as a consequence of being 'essential', conserved and may be of limited use as dietary markers. Krill sampled in winter from all sites had significantly higher relative levels of 20:1 and 22:1 fatty acids. These long-chain monounsaturated fatty acids are typically found in calanoid

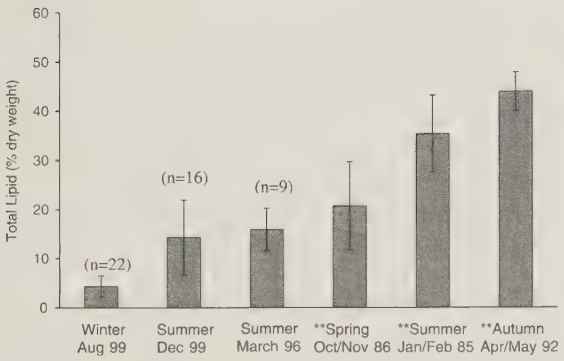

Fig. 2. Lipid content in adult *E. crystallorophias* (mean, SD error bars). Spring 1986, summer 1985, and autumn 1992 data are taken from Kattner and Hagen (1998).

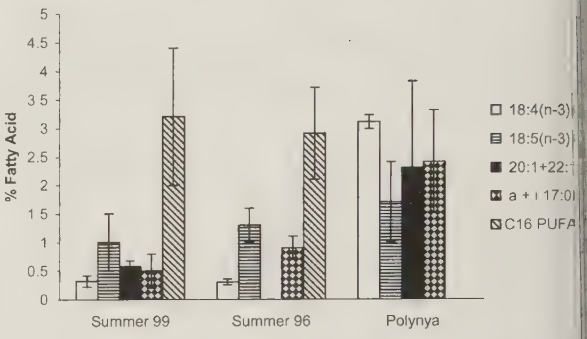

Fig. 3. Selected biomarker fatty acids in *E. crystallorophias* in summer (1996 and 1999) and winter 1999 (mean, SD error bars).

Table 3
Percentage composition ± SD of selected fatty acids and alcohols in *E. crystallorophias* during summer (96 and 99) and winter (99)

	Summer 96 ($n=9$)	Summer 99 ($n=16$)	Winter 99 ($n=22$)
Total lipid (% dry weight)	15.9±4.3	14.3±7.6	4.4±2.1
Fatty Acids			
Sum saturated	13.8±2.3	14.8±3.6	12.5±2.9
*i*15:0	0.0±0.0	0.0±0.0	0.9±0.2
i and *a* 17:0	0.9±0.2	0.5±0.3	2.4±0.9
16:1(*n*-7)	6.2±1.2	4.9±0.8	3.3±0.3
18:1(*n*-9)	34.8±4.2	24.3±5.3	31.3±3.8
18:1(*n*-7)	9.6±1.4	8.4±0.9	9.6±1.8
20:1(*n*-11)	0.0±0.0	0.3±0.1	1.2±0.7
20:1(*n*-9)	0.0±0.0	0.0±0.0	0.4±0.3
22:1(*n*-9)	0.0±0.0	0.1±0.0	0.7±0.2
Sum monounsaturated	50.6±6.8	38.0±7.1	46.5±7.1
16:4(*n*-3)	2.9±0.8	3.2±1.2	0.0±0.0
18:5(*n*-3)	1.3±0.3	1.0±0.5	1.7±0.7
18:4(*n*-3)	0.3±0.1	0.3±0.1	3.1±0.1
18:2(*n*-6)	0.9±0.1	1.4±0.8	2.8±0.6
20:5(*n*-3) EPA	16.8±3.8	21.6±3.9	15.1±1.7
20:4(*n*-3)	0.5±0.2	0.9±0.0	0.6±0.3
22:6(*n*-3) DHA	11.8±3.6	17.5±2.8	14.1±1.7
Sum polyunsaturated	34.5±8.9	45.9±9.3	37.4±5.1
Total 20:1+22:1	0.0±0.0	0.4±0.1	2.3±1.2
Fatty alcohols			
14:0	63.3±4.3	67.2±1.9	63.0±2.3
*i*15:0	0.0±0.0	0.0±0.0	2.4±0.3
15:0	0.0±0.0	0.0±0.0	1.5±0.7
16:0	36.7±1.9	31.9±2.3	24.1±1.6
18:1	0.0±0.0	0.8±0.3	1.2±0.5
20:1(*n*-9)	0.0±0.0	0.0±0.0	4.7±0.6
22:1(*n*-11)	0.0±0.0	0.0±0.0	3.4±1.2

copepods and are considered markers of a carnivorous diet. Some minor fatty acids fluctuated with site. 18:4(*n*-3) was found in all samples, with significantly higher relative levels in winter krill (3%) than summer krill (0.3%). The relative contribution of C18 PUFA of the (*n*-3) family (dinoflagellate and other flagellate markers) was higher in the winter krill. Long-chain monoenoic acids (including 20:1(*n*-9), and 22:1(*n*-11)) (copepod markers) were also higher (2.3%) in winter krill than they were in krill sampled in summer (0.4%) (Fig. 3). One of the diatom fatty acid markers (16:4(*n*-3)) was found in summer krill, and absent in the winter samples. Winter krill had significantly higher amounts of branched fatty acids (considered to be detrital/bacterial markers) than that found in the summer krill. The fatty alcohols in *E. crystallorophias* caught in summer consisted exclusively of the saturated alcohols 14:0 and 16:0 (Table 3). In the winter samples other minor alcohols were detected including *i*15:0 (*iso* branched fatty alcohol), 15:0, 18:1, 20:1 and 22:1(*n*-11). Both long-chained monoenoic acids and alcohols are indicators of carnivorous feeding behaviour.

4. Discussion

E. crystallorophias collected during winter exhibited many characteristics that indicate that it was in a state of reduced biological activity. Feeding was depressed relative to spring and

ummer, and there were indications of a dietary hift from mainly herbivory to omnivory. Also, ery limited growth occurred over an extended ntermoult period, shrinkage occurred after very hort periods of food limitation, and lipid stores ere reduced. These results reflect the low availbility of food in the coastal pelagic zone during ie Antarctic winter.

Elements of the suite of techniques applied to *E. rystallorophias* in this study have been applied ndividually to Antarctic krill *E. superba* and to ome other species of krill in experimental and eld conditions, but this is the first attempt to pply them in an integrated approach to any pecies of krill. The measures are intended to give nformation on different time scales. Measurements of the digestive gland can give information n whether the krill have been feeding in the revious week. Instantaneous growth rate experiments provide information over the period of a noult cycle (Nicol, 2000; Nicol et al., 1992; Ross et l., 2000). Lipid content and composition give ndications of seasonal changes (Hagen, 1999) and f dietary shifts (Virtue et al., 2000). This study as shown that such a suite of measures can rovide complementary results that provide new nsights into how *E. crystallorophias* survives over winter. Of the measures, the digestive gland measurement provides the most clear-cut results, which indicate that feeding intensity is much lower n winter than in spring or summer. It is also the easiest technique to apply. Lipid measurements provided a strong indication of the shift from herbivory in summer to omnivory, including detrital feeding, in winter and also of the loss of storage lipid that accompanies winter food shortage in the pelagic zone. The growth rate experiments indicated that in *E. crystallorophias* the ntermoult period doubles during winter. When coupled with the very low moult increment 0.35%), it strongly suggests that they are not growing and that their reserves are such that they re on the point of shrinkage, should food supplies drop any lower.

In the Indian Ocean sector the distribution of *E. rystallorophias* has been described as highly patchy but related to the distribution of polynyas (Pakhomov and Perissinotto, 1996). Their studies, conducted between 30°E and 90°E during summer months, provide an overview of the population biology of this species. Spawning occurred from October to December and could extend into January. At least four age groups were identified. Theoretical growth curves suggested that growth slows down in adults and that $L\infty$ (the asymptotic length) for females is between 38.1 and 39.2 mm and for males $L\infty$ is between 34.8 and 36 mm. Consequently, the large animals in the current study might not be expected to be growing, although it should be noted that growth is a dynamic process in euphausiids with periods of shrinkage and positive growth occurring in reaction to prevailing environmental conditions in post-larval stages (Marinovic and Mangel, 1999). Estimates of growth derived from length frequencies of samples collected in summer are not necessarily good predictors of seasonal growth patterns.

The only year-round study of *E. crystallorophias* provided some information on the cycle of growth in Admiralty Bay in the South Shetland Islands (Stepnik, 1982). The size structure of this population showed a net increase in size between December and March, remained stable and unimodal between April and July, followed by fluctuations in September and October. Both larger and smaller krill occurred simultaneously the following December. Juveniles were found in summer, males began maturing in April and females began maturing in July. There are very few other studies of the seasonal biology of *E. crystallorophias*. In shelf waters to the west of the Antarctic Peninsula, *E. crystallorophias* were found at depths greater than 50 m during winter (July and August) with no obvious peaking in the depth distribution (Nordhausen, 1994). The population consisted of late larval stages and of adults in the 20–31 mm size group.

There are considerable differences in the lipid content of krill between season and area. Kattner and Hagen (1998) reported summer lipid content of adult *E. crystallorophias* in the Weddell Sea to be almost twice as high as those found in this study (Fig. 2), which may be a reflection of regional food availability. Also, we found major differences in storage lipids in summer-caught krill in different years suggesting inter-annual variability in food abundance.

Spawning by *E. crystallorophias* has been observed in November and December off East Antarctica (Harrington and Thomas, 1987). Eggs of *E. crystallorophias* are neutrally buoyant (Ikeda, 1986). This observation has been used to account for the ability of *E. crystallorophias* to spawn on the continental shelf (Harrington and Thomas, 1987). *E. superba*, in contrast, has negatively buoyant eggs and spawns mainly offshore. The neutral buoyancy of the eggs of *E. crystallorophias* is not thought to result from a high lipid content but rather is due to the presence of a large perivitelline space. Consequently, *E. crystallorophias* are not thought to lose a substantial portion of their lipid during spawning (Harrington and Thomas, 1987). In the Weddell Sea, lipid content of post-larval *E. crystallorophias* reached a maximum in autumn (51.5% of dry mass) and a minimum in spring (6.5% of dry mass) (Kattner and Hagen, 1998). Wax esters were the dominant lipid class, constituting 55.6% of the total lipid in autumn. The early spawning season suggests that *E. crystallorophias* enter spring in a physiological condition that is not so depressed that it inhibits reproduction.

The diet of *E. crystallorophias* is reported to vary seasonally with an omnivorous diet in spring giving way to a largely herbivorous diet in summer (Pakhomov et al., 1999). In the winter, krill are likely to be feeding on other crustaceans as indicated by the levels of wax esters and the long-chain monounsaturated fatty acids and fatty alcohols (typical lipid profiles of copepods and other crustaceans). Some euphausiids, e.g., *Nematobrachion sexspinosus*, can synthesise wax esters from fatty alcohol precursors obtained from a carnivorous diet (Morris and Sargent, 1973). There is evidence of krill feeding on detritus during the winter in this study by the higher levels of branched fatty acids that are characteristic of bacterial fatty acid profiles. Recently Graeve et al. (2002) have reported high percentage levels of 18:4*n*-3 in some cold water macrophytes. In winter, with the absence of C16 PUFA (a typical diatom marker) macrophyte detritus may be a source of 18:4*n*-3 and these branched fatty acids. The daily ration for *E. crystallorophias* was calculated at between 0.08 mg C day^{-1} (or 0.93% of body weight) for adults in December to 0.107 mg C day^{-1} (or 8.69% of body weight) for juveniles. There is also evidence of benthic feeding by *E. crystallorophias* (Kittel and Ligowski, 1980), with 12 of the 37 identifiable algae from stomach contents collected in Admiralty Bay in February being benthic species.

A considerable amount of research effort has been directed towards the question of how krill, particularly *E. superba*, overwinter in the Antarctic. Indeed, SO-GLOBEC has this as one of its main focus areas (GLOBEC, 1999). Suggested overwintering strategies include: shrinkage (Ikeda and Dixon, 1982), lipid storage and metabolism (Hagen et al., 1996), carnivory (Huntley et al., 1994), and metabolic reduction (Torres et al., 1994; Kawaguchi et al., 1986). All of these have been observed, however, and it seems unlikely that any species of krill would use any of the suggested strategies to the exclusion of others. The critical questions become: under what conditions do krill adopt one of these strategies over another, and does dependence on any of them have an effect on subsequent population dynamics. A further question is whether shrinkage occurs to the degree that the size profile of the population is altered, altering our perception of their population dynamics (Nicol, 2000). Further seasonal studies on krill in the Antarctic, using a range of techniques such as those described in this study, will in time allow us to build up a picture of the range of possible overwintering strategies.

Acknowledgements

We thank the officers and crew of the RSV *Aurora Australis*, and all those who have assisted the krill team. Steve Candy and Sam Lake provided statistical expertise and Jacob Virtue is acknowledged for his technical help.

References

Ackman, R.G., 1981. Application of flame ionization detectors to thin layer chromatography on coated quartz rods. Methods in Enzymology 72, 205–252.

Bligh, E.G., Dyer, W., 1959. A rapid method of total lipid extraction and purification. Canadian Journal of Biochemistry and Physiology 37, 911–917.

Bottino, N.R., 1975. Lipid composition of two species of Antarctic krill: *Euphausia superba* and *E. crystallorophias*. Comparative Biochemistry and Physiology 50B, 479–484.

Brinton, E., Townsend, A.W., 1991. Development rates and habitat shifts in the Antarctic neritic euphausiid *Euphausia crystallorophias*, 1986–1987. Deep-Sea Research 38, 1195 1211.

Buchholz, F., 1985. Moult and growth in euphausiids. In: Siegfried, W.R., Condy, P., Laws R.M. (Eds), Antarctic Nutrient Cycles and Food Webs. Proceedings of the 4th Symposium on Antarctic Biology, Springer, Berlin, pp. 339–345.

Clarke, A., 1984. The lipid content and composition of some Antarctic macrozooplankon. British Antarctic Survey Bulletin 63, 57–70.

GLOBEC, 1999. GLOBAL Ocean Ecosystem Dynamics Implementation Plan IGBP Report 47, GLOBEC Report 13. IGBP, Stockholm, Sweden.

Graeve, M., Kattner, G., Wiencke, C., Karsten, U., 2002. Fatty acid composition of Arctic and Antarctic macroalgae: indicator of phylogenetic and trophic relationships. Marine Ecology Progress Series 231, 67–74.

Hagen, W., 1999. Reproductive strategies and energetic adaptations of polar zooplankton. Invertebrate Reproduction and Development 36, 25–34.

Hagen, W., van Vleet, E.S., Kattner, G., 1996. Seasonal lipid storage as overwintering strategy of Antarctic krill. Marine Ecology Progress Series 134, 85–89.

Harrington, S.A., Thomas, P.G., 1987. Observations on spawning by *Euphausia crystallorophias* from waters adjacent to Enderby Land (East Antarctica) and speculations on the early ontogenetic ecology of neritic euphausiids. Polar Biology 7, 93–95.

Hosie, G.W., Ritz, D.A., 1989. Body shrinkage in the subtropical euphausiid *Nyctiphanes australis* G. O. Sars. Journal of Plankton Research 11, 595–598.

Huntley, M.E., Nordhausen, W., et al., 1994. Elemental composition, metabolic activity and growth of Antarctic krill *Euphausia superba* during winter. Marine Ecology Progress Series 107, 23–40.

Ikeda, T., 1986. Preliminary observations on the development of the larvae of *Euphausia crystallorophias* Holt and Tattersall in the laboratory. Memoirs of the National Institute of Polar Research Special Issue 40, 183–186.

Ikeda, T., Dixon, P., 1982. Body shrinkage as a possible overwintering mechanism of the Antarctic krill, *Euphausia superba* Dana. Journal of Experimental Biology and Ecology 62, 143–151.

Kattner, G., Hagen, W., 1998. Lipid metabolism of the Antarctic euphausiid *Euphausia crystallorophias* and its ecological implications. Marine Ecology Progress Series 170, 203–213.

Kawaguchi, K., Ishikawa, S., Matsuda, O., 1986. The overwintering strategy of Antarctic krill (*Euphausia superba* Dana) under the coastal fast ice off the Ongul Islands in Lutzow-Holm Bay, Antarctica. Memoirs of the National Institute of Polar Research Special Issue 44, 67–85.

Kirkwood, J.M., 1996. The developmental rate of *Euphausia crystallorophias* larvae in Ellis Fjord, Vestfold Hills, Antarctica. Polar Biology 16, 527–530.

Kittel, W., Ligowski, R., 1980. Algae found in the food of *Euphausia crystallorophias* (Crustacea). Polish Polar Research 1, 129–137.

Littlepage, J., 1964. Seasonal variation in lipid content of two Antarctic marine crustaceans. In: Carrick, R., Holdgate, M.W., Prevost, J. (Eds), Biologie antarctique, First SCAR Symposium, Paris 2.-8.9.1962. Hermann, Paris, pp. 463–470.

Marinovic, B., Mangel, M., 1999. Krill can shrink as an ecological adaptation to temporarily unfavourable environments. Ecology Letters 2, 338–343.

Mayzaud, P., Eaton, C.A., Ackman, R.G., 1976. The occurrence and distribution of octadecapentaenoic acids in a natural plankton population. A possible food chain index. Lipids 11 (12), 858–862.

Morris, R.J., Sargent, J.R., 1973. Studies of the lipid metabolism of some oceanic crustaceans. Marine Biology 22, 77–83.

Nicol, S., 2000. Understanding krill growth and aging: the contribution of experimental studies. Canadian Journal of Fisheries and Aquatic Sciences 57 (Suppl. 3), 168–177.

Nicol, S., Stolp, M., Cochran, T., Geijsel, P., Marshall, J., 1992. Growth and shrinkage of Antarctic krill *Euphausia superba* from the Indian Ocean sector of the Southern Ocean during summer. Marine Ecology Progress Series 89, 175–181.

Nicol, S., Kitchener, J., King, R., Hosie, G.W., de la Mare, W.K., 2000. Population structure and condition of Antarctic krill (*Euphausia superba*) off East Antarctica (80–150°E) during the Austral summer of 1995/6. Deep-Sea Research II Topical Studies in Oceanography 47, 2465–2488.

Nordhausen, W., 1994. Winter abundance and distribution of *Euphausia superba*, *E. crystallorophias* and *Thysanoessam macrura* in Gerlache Strait and Crystal Sound, Antarctica. Marine Ecology Progress Series, 109, 131–142.

Pakhomov, E.A., Perissinotto, R., 1996. Antarctic neritic krill *Euphausia crystallorophias*: spatio-temporal distribution, growth and grazing rates. Deep-Sea Research I 43, 59–87.

Pakhomov, E.A., Perissinotto, R., Froneman, P.W., 1999. Abundance and trophodynamics of *Euphausia crystallorophias* in the shelf region of the Lazarev Sea during austral spring and summer. Journal of Marine Systems 17, 313–324.

Quetin, L., Ross, R.M., 1991. Behavioural and physiological characteristics of Antarctic krill *Euphausia superba* Dana. American Zoologist 31, 49–63.

Ross, R.M., Quetin, L.B., Vernet, M., Baker, K.S., Smith, R.C., 2000. Growth limitation in young *Euphausia superba* under field conditions. Limnology Oceanography 45, 31–43.

Shin, H.-C., Nicol, S., 2003a. Changes in the digestive gland of Antarctic krill during short term starvation: mass, content of protein and lipid, and digestive enzyme activity. Marine Biology, submitted for publication.

Shin, H.-C., Nicol, S., 2003b. Changes in the digestive gland of juvenile Antarctic krill during a long-term feeding experiment. Marine Biology, submitted for publication.

Siegel, V., 1987. Age and growth of Antarctic Euphausiacea (Crustacea) under natural conditions. Marine Biology 96, 483–495.

Siegel, V., Nicol, S., 2000. Population parameters. In: Everson, I. (Ed.), Krill Biology, Ecology and Fisheries. Blackwell Science, London, pp. 103–149.

Stepnik, R., 1982. All-year population studies of Euphausiacea (Crustacea) in Admiralty Bay (King George Island, South Shetland Islands, Antarctica). Polish Polar Research 3, 49–68.

Torres, J.J., Aarset, A.V., Donnelly, J., Hopkins, T.L., Lancraft, T.M., Ainley, D.G., 1994. Metabolism of Antarctic micronektonic Crustacea as a function of depth of occurrence and season. Marine Ecology Progress Series 113, 221–232.

Virtue, P., Nicol, S., Nichols, P.D., 1993a. Changes in the digestive gland of *Euphausia superba* during short-term starvation: lipid class, fatty acid and sterol content and composition. Marine Biology 117, 441–448.

Virtue, P., Nichols, P.D., Nicol, S., McMinn, A., Sikes, E., 1993b. The lipid composition of *Euphausia superba* Dana in relation to the nutritional value of *Phaeocystis pouchetii* (Hariot) Lagerheim. Antarctic Science 5, 169–177.

Virtue, P., Mayzaud, P., Albessard, E., Nichols, P., 2000. Use of fatty acids as dietary indicators in northern krill (*Meganyctiphanes norvegica*) from northeastern Atlantic, Kattegat, and Mediterranean waters. Canadian Journal Fisheries and Aquatic Science 57, 104–114.

ELSEVIER

Deep-Sea Research II 51 (2004) 2225–2245

DEEP-SEA RESEARCH
PART II

www.elsevier.com/locate/dsr2

Metabolism of Antarctic micronektonic crustacea across a summer ice-edge bloom: respiration, composition, and enzymatic activity

Joseph Donnelly[a], Helena Kawall[b], Stephen P. Geiger[a], Joseph J. Torres[a,*]

[a]*College of Marine Science, University of South Florida, 140 Seventh Avenue South, St. Petersburg, FL 33701, USA*
[b]*Coordenaçào de Biologia-Uniandrade, R. Joào Negrào, 1285—Curitiba/PR—80230 150, Brazil*

Accepted 12 July 2004

Abstract

The Antarctic marginal ice zone is an important oceanic front separating the pack-ice and open-water environments. During summer, the retreating pack ice creates a meltwater lens in the euphotic zone, allowing primary producers and microheterotrophs to flourish in a discrete bloom just seaward of the retreating ice edge that lasts about 60 days. The purpose of the present study was to see if the ice-edge bloom had a discernible effect on the metabolism and physiological condition of Antarctic micronekton similar to that observed in zooplankton species. We also wished to assess the importance of the summer season to species' life cycles. Two major data sets were collected on 25 species in the following taxonomic groups: amphipods, cephalopods, decapods, euphausiids, isopods, mysids, ostracods, and polychaetes. The first data set described the metabolic rates of individuals in areas of the marginal ice zone with widely different levels of chlorophyll biomass to investigate the effect of the ice-edge bloom on metabolism. Additionally, summer metabolic rates were compared with data from other seasons. The second data set detailed the levels of protein, water, ash, RNA and DNA, and the activities of metabolic enzymes (citrate synthase and malate dehydrogenase) to examine the efficacy of biochemical indices as predictive tools for metabolism. Results suggested that the mobility of the micronektonic species eliminated most direct effects of the bloom on metabolism. Individuals captured in very different productivity regimes showed few significant differences in the metabolic indicators listed above. Isolated cases of changes in body composition and enzyme activity, however, implied that longer-term effects of the bloom may be exhibited. Seasonal increases in metabolism from winter to summer were observed in the euphausiids *Euphausia superba, E. triacantha*, and *Thysanoessa macrura* and the amphipod *Vibilia stebbingi*. It was concluded that the seasonal shifts were indicative of a "type 2" or compromise overwintering strategy whereby metabolism drops without an accompanying dormant state. Protein content and MDH activity were found to be the best predictors of respiration rate, while nucleic acid measures only correlated with respiration in immature specimens.
© 2004 Elsevier Ltd. All rights reserved.

*Corresponding author.

0967-0645/$ - see front matter © 2004 Elsevier Ltd. All rights reserved.
doi:10.1016/j.dsr2.2004.07.003

1. Introduction

The Antarctic marginal ice zone (MIZ) is an important oceanic front separating the pack-ice and open-water environments. When sea ice melts in the summer, a low-density meltwater lens is formed over the higher-salinity seawater below, creating a physically stable and nutrient-rich layer seaward of the ice edge. The summer increase in insolation and penetration of light into the layer creates optimal conditions for phytoplankton growth (Sakshaug and Skjoldal, 1989). The resulting ice-edge bloom contributes about 40% of the total annual production in the Southern Ocean (Smith and Sakshaug, 1990). However, it is ephemeral, lasting for approximately 60 days as a rolling wave of high production following the retreating ice edge (Smith and Nelson, 1985). During this period, as the ice progressively melts southward and the phytoplankton bloom moves with it, herbivorous species obtain much of their energy for growth and reproduction for the year.

The short, highly pulsed period of maximum production and the months of extremely low productivity that follow it pose a challenge to longer-lived consumer species with generation times of a year or more. Three types of overwintering strategies were proposed for Antarctic zooplankton and micronekton by Torres et al. (1994b). Type 1, exhibited by some calanoid copepods, is characterized by accumulation of large lipid deposits accompanied by a depressed metabolism (diapause) and sinking of the population maximum to mesopelagic depths (400–1000 m). In the Type 2 strategy, activity and metabolic rates are reduced after the summer season (Quetin and Ross, 1991; Torres et al., 1994a), but no true dormancy is shown. The individuals may show depletion of metabolic reserves (Drits et al., 1993; Torres et al., 1994b) in addition to expanding their spectrum of food items (Daly, 1990; Huntley et al., 1994). The Type 2 strategy has been observed in *Euphausia superba* and hyperiid amphipods such as *Cyllopus lucasii* and *Vibilia stebbingi*. Type 3 is exhibited by decapods and gammarid amphipods, which are opportunistic feeders, and show no difference in metabolic rates or compositional attributes during the winter season.

The purpose of the present study was to see if the ice-edge bloom had a discernible effect on the metabolism and physiological condition of Antarctic micronekton, similar to that observed in zooplankton species (Geiger et al., 2001; Kawall et al., 2001). By definition, micronektonic species are capable of purposeful extended horizontal movement. Their ability to move in and out of areas of higher production might eliminate the obvious effects on metabolic processes. We also wished to assess the importance of the summer season on species' life cycles (cf. Meyer et al., 2002a, b; Atkinson et al., 2002). The following data sets on biomass-dominant micronektonic species were collected: (1) oxygen consumption rates in areas with widely different levels of primary productivity to investigate the effect of the ice-edge bloom, and in addition, providing summer metabolic data for comparison with data from other seasons; and (2) proximate composition (water, ash, protein, lipid, and chitin), RNA and DNA content, and the activities of intermediate metabolic enzymes citrate synthase (CS) and malate dehydrogenase (MDH) to examine the efficacy of biochemical indices as predictive tools for metabolism.

2. Methods

2.1. Collection of specimens

Field work was done in the Weddell Sea vic. 60°S 36°W in late November and December 1993. To assess the location and extent of the spring bloom within the study area, two transects were run while continuously monitoring chlorophyll biomass as in vivo fluorescence (Fig. 1). The first was a west–east transect within the marginal ice zone to examine variability within the core of the bloom. The second was a north–south transect to look at the north–south influence of the bloom. The transect was initiated north of the ice edge where in vivo fluorescence values had dropped to values well below those found in the bloom. From its most northerly point in open water, the transect

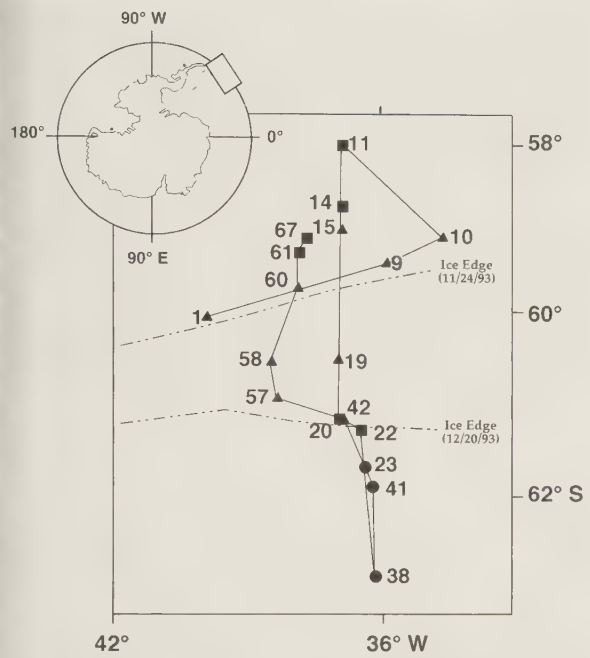

Fig. 1. Cruise track during November–December, 1993 within the MIZ in the northwest Weddell Sea. Station numbers shown depict the first and last for each area within the MIZ: (■) open water, (▲) ice edge, and (●) pack ice.

proceeded through the core of the bloom in the marginal ice zone into the pack ice until the fluorescence signal from the bloom was absent at the southern end. At that point, zonal occupations of 5–6 days were performed in each of three MIZ areas: pack ice, ice edge, and open water. The biological and physical framework of each region was provided by CTD/rosette casts, primary productivity measurements, and chlorophyll biomass determinations (see Kawall et al. (2001) for a more detailed description of the bloom and marginal ice-zone conditions).

Sampling was conducted with two nets, an obliquely towed Tucker trawl (9 m^2 mouth area) and a vertically deployed Plummet net (1 m^2 mouth area). Each net terminated in a blind codend, which maintained the animals in good condition for physiological studies. Specimens for respiration measurements were obtained predominantly from 0–200 m tows, while those frozen for biochemical assays were collected over 0–1000 m.

2.2. Respiratory measurements

On board, organisms were kept in buckets filled with cold (~0°C) sea water, and sorted for respirometry and biochemical assays. Oxygen consumption rates were determined by allowing individuals to deplete the oxygen in sealed, water-jacketed, lucite chambers filled with filtered (0.45 μm) sea water, at a controlled temperature of 0.5 °C. Chambers of different volumes (25–1340 ml) were used to accommodate different-sized specimens. Oxygen partial pressure (PO_2) was continuously monitored with Clark polarographic oxygen electrodes. Electrodes were calibrated before each experimental run with air- and nitrogen-saturated sea water. Data were recorded every minute for a period of 10–20 h using a computer-controlled data-logging system. A graph of oxygen partial pressure versus time was generated, allowing determination of the best slope representing the routine rate. The data acquired in the first hour were discarded because of the increased rates associated with handling stress. The lowest and highest respiratory rates observed for each run were designated the minimum and maximum rates. To control for possible O_2 consumption by microorganisms, one respirometer was kept without a specimen and oxygen partial pressure recorded as in the experimental chambers. No decrease in oxygen was observed in the control runs.

After respiratory measurements were taken, specimens were blotted dry, individually sealed in either plastic freezer bags or polypropylene vials, frozen in liquid nitrogen, and stored in a −80 °C freezer.

2.3. Biochemical assays

Identifications of species, sex, and developmental stage were verified in the laboratory. Individuals were then measured from the tip of the rostrum to the end of the telson (standard length (SL)), weighed (wet mass (WM)), and homogenized in deionized water with a glass tissue grinder followed by an Ultrasonic homogenizer. Dilutions (WM to water) varied from 1:9 in larger animals to 1:24 in smaller individuals. The homogenate was

kept cold (~0 °C) and aliquotted for the biochemical assays. Water content, dry mass (DM), ash-free dry mass (AFDM), and protein were measured using the methods of Donnelly et al. (1990). Lipids were extracted from aliquots using the methods of Bligh and Dyer (1959). Extracts were dried at 30 °C under a flow of nitrogen and total lipid content determined gravimetrically. Hexosamine (= chitin) was measured using the methods of Donnelly et al. (1994), with D-glucosamine hydrochloride as the standard. Nucleic acid (RNA, DNA) contents were measured fluorimetrically following the procedures of Bentle et al. (1981), with bakers' yeast RNA and calf thymus DNA used as standards. CS activities were determined using the methods of Torres and Somero (1988a). MDH activities were determined using the methods of Childress and Somero (1979), with 20 mM $MgCl_2$ being substituted for 20 mM $MgSO_4$.

2.4. Data

Respiratory rates are expressed as µl of oxygen consumed per individual ($\mu l\, O_2\, ind^{-1}\, h^{-1}$) and per milligram wet mass per hour ($\mu l\, O_2\, mg WM^{-1}\, h^{-1}$, $\dot{V}O_2$). Water content is expressed as percent of wet mass (%WM), and ash content as percent of dry mass (%DM). Protein, lipid and hexosamine are expressed as total content ($mg\, ind^{-1}$) and as a mass percent (%WM, %AFDM). Nucleic acids are expressed as total content ($mg\, ind^{-1}$) and as a ratio (RNA:DNA). Enzymatic activity is expressed as µmol of substrate converted to product per min per total WM (International Unit (IU) ind^{-1}) and as activity per gram wet mass ($IU\, g WM^{-1}$).

Oxygen consumption rates and biochemical measures were grouped by size classes within each species. The size classes were created by halving each order of magnitude change in WM (as in Torres et al. (1994a)); i.e., size class 1: 0.0–4.9 mg, size class 2: 5.0–9.9 mg, size class 3: 10.0–49.0 mg, size class 4: 50.0–99.9 mg, size class 5: 100–499.9 mg, size class 6: 500–999.9 mg, and size class 7: 1000–4999.9 mg. All krill length measurements were from the tip of the rostrum to the end of the telson, slightly different from the total length used by Mauchline and Fisher (1969), but used several times previously in the literature (Fraser, 1936; Einarsson, 1945; Nemoto, 1957).

Data are reported as mean ± standard deviation. Means were tested for differences using one-way analysis of variance (ANOVA), and when variances were not homogeneous, a Kruskal–Wallis test (KW) was applied (Zar, 1974). Simple regressions were fitted using the least-squares method. Regressions were compared using analysis of covariance (ANCOVA). The level of significance for all statistical analyses was $p < 0.05$.

3. Results

3.1. Oxygen consumption rates

Routine, maximum and minimum oxygen consumption rates for 23 species are shown in Table 1. Mean $\dot{V}O_2$ ranged from 0.006 in the largest specimens of *Gigantocypris mulleri* to 0.403 in the smallest specimens of *C. lucasii*. Rates for all species fell into two general groups. Species in the first group with mean rates between 0.006 and 0.094 $\mu l\, O_2\, mg\, WM^{-1}\, h^{-1}$ included all the gammarid amphipods; the hyperiid amphipods *Hyperiella antarctica*, *Megalanceola remipes*, *M. stephenseni* and large *Primno macropa*; the cephalopod *Galiteuthis glacialis*; all the decapods except for the smallest size class of *Pasiphaea scotiae*; the mysid *Boreomysis rostrata*; the ostracod *G. mulleri*; and the polychaete *Tomopterus carpenteri*. Species in the second group with mean rates between 0.122 and 0.403 $\mu l\, O_2\, mg\, WM^{-1}\, h^{-1}$ included the hyperiid amphipods *C. lucasii*, *Hyperoche medusarum*, small *P. macropa*, and *V. stebbingi*; small *P. scotiae*; all the euphausiids; and the isopod *Anuropus australis*. All of the mesopelagic species examined (i.e. those with a minimum depth of occurrence > 200 m) fell into the first group, while those species with MDOs < 200 m had representatives in both groups. Mass-specific rates showed an inverse relationship with size in all species examined over multiple size classes. The ratios of maximum to routine rate and maximum to minimum rate were similar for all species, with

Table 1
Oxygen consumption rates for 23 species of invertebrate micronekton

Group / Species	MDO (*m*)	SC (*n*)	SL (mm) [range]	WM (mg)	O_2 consumption rates ($\mu l\, O_2\, mg\, WM^{-1}\, h^{-1}$)			Conversions	
					Routine	Min	Max	DM	AFDM
Amphipods (Gammarid)									
Cyphocaris faueri	40	5 (1)	31.0	467.4	0.082	0.056	0.119	3.38	4.31
C. richardi	340	4 (1)	15.0	54.2	0.081	nd	nd	nd	nd
		5 (10)	25.1 [21.0–31.5]	287.0 (105.2)	0.067 (0.018)	0.034 (0.012)	0.110 (0.037)	4.64	5.99
		6 (3)	34.3 [31.0–36.0]	700.3 (48.0)	0.038 (0.009)	0.019 (0.008)	0.068 (0.030)	2.55	2.93
		7 (1)	40.0	1106.9	0.042	0.023	0.087	2.97	3.39
Cleonardo longipes	Nd	5 (1)	21.5	151.2	0.049	nd	nd	3.94	4.85
Parandania boecki	270	6 (1)	27.0	886.5	0.030	0.019	0.051	6.29	9.17
Amphipods (Hyperiid)									
Cyllopus lucasii	0	3 (1)	11.0	48.1	0.403	0.120	0.630	nd	nd
		4 (5)	13.0 [12.0–14.5]	89.6 (9.0)	0.230 (0.077)	0.123 (0.060)	0.376 (0.146)	5.53	7.08
		5 (10)	18.6 [17.5–22.0]	241.7 (30.0)	0.130 (0.031)	0.065 (0.026)	0.203 (0.054)	4.76	5.96
Hyperiella antarctica	0	4 (1)	11.0	67.2	0.067	0.027	0.126	nd	nd
Hyperoche medusarum	0	4 (1)	11.0	62.1	0.167	0.101	0.246	nd	nd
Megalanceola remipes	100	5 (1)	30.0	418.9	0.042	0.023	0.056	8.41	12.36
M. stephenseni	nd	7 (1)	42.0	4997.1	0.008	0.003	0.013	15.15	25.64
Primno macropa	0	3 (1)	9.5	36.0	0.266	nd	nd	nd	nd
		4 (1)	15.0	94.6	0.094	0.038	0.186	5.26	6.67
Vibilia stebbingi	0	3 (9)	10.7 [8.0–12.0]	38.6 (10.5)	0.321 (0.114)	0.202 (0.093)	0.555 (0.173)	nd	nd
		4 (8)	12.3 [11.0–13.5]	58.4 (5.7)	0.236 (0.051)	0.119 (0.032)	0.404 (0.107)	nd	nd
Cephalopods									
Galiteuthis glacialis	50	5 (2)	17.3[a] [16.0–18.5]	423.7 (70.4)	0.039 (0.003)	0.014 (0.008)	0.065 (0.0002)	13.94	17.93
		6 (6)	24.1[a] [22.0–29.0]	771.6 (135.5)	0.033 (0.009)	0.019 (0.006)	0.055 (0.012)	11.72	14.01
Decapods									
Gennadas kempi	500	7 (2)	52.5 [50.0–55.0]	1839.0 (387.8)	0.037 (0.001)	0.017 (0.008)	0.054 (0.010)	3.28	3.68
Nematocarcinus lanceopes	0	5 (3)	42.8 [38.0–46.0]	308.3 (23.3)	0.073 (0.040)	nd	nd	4.50	5.23
Pasiphaea scotiae	100	5 (2)	35.8 [33.0–38.5]	299.5 (110.4)	0.212 (0.189)	0.128 (0.139)	0.334 (0.249)	3.51	3.85
		6 (1)	47.0	725.5	0.052	0.015	0.096	2.67	2.90
		7 (3)	73.5 [67.0–81.0]	2927.8 (770.8)	0.034 (0.013)	0.018 (0.008)	0.057 (0.024)	3.06	3.31
		8 (1)	100.0	5421.9	0.028	0.019	0.037	2.78	2.98
Petalidium foliaceum	500	6 (1)	43.0	792.2	0.025	0.013	0.036	3.19	3.48
Euphausiids									
Euphausia superba	0	3 (16)	15.7 [12.0–18.0]	31.7 (9.4)	0.291 (0.078)	0.146 (0.084)	0.516 (0.140)	nd	nd
		4 (5)	21.3 [20.0–22.0]	81.2 (14.8)	0.239 (0.046)	0.132 (0.028)	0.375 (0.074)	4.44	5.12
		5 (8)	28.3 [26.0–36.5]	206.3 (114.5)	0.160 (0.018)	0.085 (0.014)	0.250 (0.042)	5.38	6.36
		6 (9)	42.9 [39.0–48.0]	742.0 (102.8)	0.122 (0.025)	0.071 (0.019)	0.177 (0.037)	5.57	6.73
		7 (23)	51.5 [49.0–58.0]	1403.0 (313.1)	0.130 (0.026)	0.086 (0.025)	0.183 (0.032)	4.62	5.42
E. triacantha	0	5 (2)	35.5 [35.0–36.0]	296.0 (3.6)	0.148 (0.022)	0.072 (0.025)	0.215 (0.046)	4.84	5.50
Thysanoessa macrura	100	3 (16)	16.6 [14.5–18.5]	35.7 (7.9)	0.234 (0.072)	0.092 (0.039)	0.415 (0.152)	3.55	4.23
		4 (7)	22.3 [19.0–24.0]	72.3 (14.3)	0.245 (0.069)	0.082 (0.037)	0.389 (0.203)	5.05	6.11
		5 (2)	28.0 [27.0–29.0]	164.4 (10.7)	0.188 (0.020)	0.118 (0.050)	0.337 (0.086)	3.31	3.64
Isopods									
Anuropus australis	100	6 (1)	23.0	528.0	0.214	0.134	0.251	4.51	5.68
Mysids									
Boreomysis rostrata	550	6 (1)	45.0	934.8	0.055	0.022	0.076	2.70	2.85
Ostracods									
Gigantocypris mulleri	500	5 (1)	10.0[b]	431.0	0.020	0.011	0.036	14.39	20.82
		6 (1)	13.0[b]	739.2	0.011	0.005	0.015	14.80	23.00
		7 (4)	17.0[b] [15.0–18.0]	1803.6 (458.8)	0.006 (0.002)	0.003 (0.001)	0.013 (0.007)	12.10	16.41

Table 1 (*continued*)

Group / Species	MDO (*m*)	SC (*n*)	SL (mm) [range]	WM (mg)	O_2 consumption rates ($\mu l\, O_2\, mg\, WM^{-1}\, h^{-1}$) Routine	Min	Max	Conversions DM	AFDM
Polychaetes									
Tomopterus carpenteri	0	5 (3)	36.8 [33.0–39.0]	354.5 (55.5)	0.097 (0.015)	0.056 (0.022)	0.163 (0.015)	9.32	12.65
		6 (2)	47.0 [41.0–53.0]	788.3 (294.2)	0.060 (0.020)	0.030 (0.023)	0.091 (0.007)	8.26	10.71

Values are mean ± standard deviation. Multiply WM-specific rate by conversion factors to yield DM-specific or AFDM-specific rates. Minimum depth of occurrence (MDO) data from Lancraft et al., 1989, 1991). SC = sizeclass, *n* = number of replicates used in determining respiration rates, SL = standard length, WM = wet mass, DM = dry mass, AFDM = ash-free dry mass, nd = no data.

[a]values are mantle length.

[b]values are sphere diameter.

overall means of 1.57 ± 0.19 (range: 1.17–1.98) and 3.25 ± 0.88 (range: 1.88–4.96), respectively.

A total of 61 respiratory runs on *E. superba* of different sexes and developmental stages (Table 2a, b) allowed further investigation of metabolism in this species. Adults were defined as individuals with a total length greater than ~32 mm (Ikeda, 1985). Females carrying spermatophores or eggs were considered separately. As expected, the mean rate value for mass-specific oxygen consumption was significantly higher in immature specimens ($p < 0.003$); however, no differences in mean O_2 consumption rate were observed between any adult group ($p > 0.94$) (Table 2a). The slopes of the regression lines for respiration rate ($\mu l\, O_2\, ind^{-1}\, h^{-1}$, y) vs. WM (mg, x) were also found to be significantly different between immature and adult specimens ($p < 0.00001$) (Table 2b).

Six species were respired in sufficient numbers to allow comparison of metabolism between the different areas of the marginal ice zone (Table 3). No significant differences ($p > 0.40$) in mean VO_2 between areas were found for *Cyphocaris richardi*, *V. stebbingi*, *G. glacialis,* and *Thysanoessa macrura.* Significant differences in mean VO_2 were found between ice-pack and open-water areas in *C. lucasii* and between the ice-pack and edge areas in *E. superba*; however, these were due to differences in specimen size between areas for both these species. In *C. lucasii* there was a clear inverse pattern of decreasing WM and increasing VO_2 from ice-pack to edge to open water. In *E. superba* the size effect was less apparent. While mean WM values were similar between ice-pack and edge areas (647 vs. 616 mg), median values were not (719 vs. 153 mg), indicating a greater number of smaller specimens in the edge group. Examining only *E. superba* specimens greater than size class 3, there were no significant differences in mean VO_2 between areas ($p > 0.83$, mean VO_2 ice:edge:open = 0.150:0.139:0.137).

Regressions of routine rate ($\mu l\, O_2\, ind^{-1}\, h^{-1}$, y) vs. WM (mg, x) within each area for *C. richardi*, *C. lucasii*, *V. stebbingi*, *E. superba* and *T. macrura* were also compared. No significant differences ($p > 0.50$) in either the slope or intercept were found for any species. Consequently, data from all areas were combined to generate regressions of routine rate vs. WM for those species with data over a size range ($n \geq 5$, Table 4). Only *G. mulleri* showed no noticeable change in oxygen consumption rate with increased mass.

3.2. Biochemical measures

Twenty-five species were analyzed for water, ash, protein and nucleic acid content, and the activities of CS and MDH (Table 5). Lipid and hexosamine content were analyzed in 15 of the species, but only on a subsample of specimens. Measures of compositional components (water, ash, protein, lipid, hexosamine) showed a range of values, reflecting differences in species' body type and ecology. Seven species (*Parandania boecki*, *Megalanceola* spp., *G. glacialis*, *Gnathophausia*

Table 2

(a) Biochemical parameters and oxygen consumption rates for *E. superba*. Values are mean ± standard deviation. (b) Regressions ($y = ax^b$) of oxygen consumption and nucleic acids vs. WM, and protein vs. RNA content for *E. superba*

(a)

Sex/developmental stage	*n*	SL (mm) (range)	WM (mg)	Water (%WM)	Ash (%DM)	Protein (%WM)	Protein (%AFDM)	RNA:DNA	CS (IU g WM^{-1})	MDH (IU g WM^{-1})	O_2 consumption rates (µl O_2 mg WM^{-1} h^{-1})		
											Routine	Min	Max
Immature	29	19.0 (12–27)	65.6 (50.0)	81.3 (1.6)	15.5 (2.1)	8.0 (1.5)	59.4 (10.9)	2.09 (0.66)	2.19 (1.18)	31.00 (17.63)	0.253 (0.082)	0.130 (0.070)	0.434 (0.154)
♂	12	48.0 (32–53)	1139.5 (393.7)	78.3 (1.9)	16.1 (3.2)	9.1 (0.8)	50.3 (7.6)	2.65 (0.55)	2.92 (0.77)	99.20 (43.84)	0.126 (0.026)	0.088 (0.020)	0.179 (0.027)
♀	11	47.0 (39–51)	1007.3 (259.5)	80.5 (2.6)	17.4 (1.8)	10.0 (1.8)	62.3 (7.2)	2.45 (1.60)	1.82 (0.68)	83.57 (22.22)	0.121 (0.027)	0.072 (0.029)	0.176 (0.042)
♀ w. spermatophore	7	46.1 (39–52)	970.0 (278.3)	83.3 (1.8)	17.5 (1.1)	9.3 (1.5)	66.9 (5.0)	2.55 (1.74)	1.92 (0.45)	68.19 (32.94)	0.143 (0.023)	0.078 (0.027)	0.204 (0.025)
♀ w. eggs	7	54.7 (50–58)	1720.0 (363.1)	76.4 (1.5)	11.6 (1.5)	9.2 (1.6)	44.2 (8.2)	5.64 (1.91)	2.23 (0.87)	66.23 (13.43)	0.124 (0.022)	0.090 (0.013)	0.168 (0.028)

(b)

Stage	µl O_2 ind^{-1} h^{-1} vs. WM (mg)	RNA (mg) vs. WM (mg)	DNA (mg) vs. WM (mg)	RNA:DNA vs. WM (mg)	Protein (mg) vs. RNA (mg)
Immature (SC 3,4,5)	$y = 0.759x^{0.710\pm0.048}$	$y = 0.015x^{0.907\pm0.062}$	$y = 0.023x^{0.617\pm0.068}$	$y = 0.472x^{0.362\pm0.074}$	$y = 7.854x^{1.091\pm0.075}$
	(0.89, 29, <0.0000)	(0.89, 29, <0.0000)	(0.75, 30, <0.0001)	(0.46, 30, <0.0001)	(0.89, 29, <0.0000)
Adult (SC 6,7)	$y = 0.086x^{1.053\pm0.111}$	$y = 0.017x^{0.816\pm0.287}$	$y = 0.014x^{0.701\pm0.200}$	nc	nc
	(0.75, 32, <0.0001)	(0.20, 34, 0.0077)	(0.27, 35, 0.0013)		

b values are slope ± standard error. Values in parentheses are: correlation coeficient (r^2), *n*, significance level (*p*). SC = sizeclass, nc = no correlation.

Table 3
Oxygen consumption rate and biochemical parameters for six micronekton species from different areas of the MIZ

Species	MIZ area	n	WM (mg)	O_2 consumption rate ($\mu l O_2 mg WM^{-1} h^{-1}$)	Water (%WM)	Ash (%DM)	Protein (%WM)	Protein (%AFDM)	CS (IU g WM^{-1})	MDH (IU g WM^{-1})	RNA:DNA
Cyphocaris richardi	Edge	7	220.8 (114.7)	0.065 (0.020)	81.2 (4.1)	31.0 (9.5)	5.4 (1.7)	39.0 (5.7)	0.99 (0.98)	9.16 (7.86)	3.49 (1.77)
	Open	9	511.9 (325.8)	0.057 (0.021)	66.7 (16.6)	16.7 (5.1)	8.4 (2.4)	31.1 (5.3)	1.67 (0.87)	13.57 (7.80)	4.23 (1.82)
Cyllopus lucasii	Ice	5	240.5 (30.9)	0.130 (0.035)	78.3 (4.6)	19.8 (4.2)	7.6 (0.6)	44.7 (7.6)	2.20 (0.57)	50.63 (4.53)	3.88 (3.38)
	Edge	6	192.4 (80.5)	0.173 (0.083)	80.2 (2.3)	20.2 (1.3)	7.1 (0.7)	45.7 (2.8)	2.82 (0.98)	53.81 (10.09)	3.13 (1.90)
	Open	5	111.2 (80.0)	0.213 (0.082)	80.8 (0.0)	23.6 (1.6)	7.7 (1.1)	51.4 (1.6)	3.50 (1.77)	55.39 (10.70)	4.31 (1.62)
Vibilia stebbingi	Edge	12	44.0 (12.6)	0.275 (0.107)	nd	nd	7.4 (1.8)	nd	1.26 (1.17)	50.98 (27.73)	16.03 (5.32)
	Open	6	56.6 (8.9)	0.297 (0.062)	nd	nd	7.8 (1.5)	nd	0.91 (1.44)	41.10 (33.99)	18.36 (9.22)
Galiteuthis glacialis	Ice	4	750.2 (255.3)	0.032 (0.013)	91.8 (0.4)	18.0 (1.1)	2.8 (0.2)	41.0 (2.1)	1.01 (0.16)	2.40 (0.80)	2.10 (0.20)
	Edge	5	737.6 (119.6)	0.035 (0.008)	91.5 (0.6)	15.1 (1.6)	3.1 (0.3)	42.1 (2.3)	1.09 (0.20)	2.81 (0.85)	1.72 (0.38)
	Open	3	681.3 (256.8)	0.036	91.9 (1.3)	17.3 (2.6)	2.9 (0.9)	42.4 (5.3)	1.09 (0.31)	4.36 (2.31)	2.53 (0.33)
Euphausia superba	Ice	18	647.3 (414.8)	0.146 (0.034)	82.7 (2.1)	17.3 (1.3)	9.0 (1.4)	63.6 (6.6)	2.36 (0.80)	55.46 (26.17)	2.79 (1.38)
	Edge	41	615.5 (698.0)	0.206 (0.062)	78.7 (2.4)	15.8 (3.0)	8.7 (1.3)	55.1 (12.1)	2.31 (0.80)	60.81 (34.61)	2.62 (2.12)
	Open	7	1376.6 (656.2)	0.137 (0.033)	77.8 (2.6)	12.7 (2.9)	8.9 (1.4)	45.5 (8.5)	1.85 (1.25)	73.03 (36.82)	2.73 (0.82)
Thysanoessa macrura	Ice	12	53.0 (24.8)	0.272 (0.083)	80.3	17.7	9.2 (1.0)	56.7	0.06 (0.01)	38.59 (14.74)	2.95 (1.25)
	Edge	14	41.3 (12.2)	0.210 (0.045)	78.6 (1.5)	16.8 (0.5)	9.8 (1.2)	53.0 (4.6)	0.39 (0.54)	37.83 (19.04)	2.16 (0.88)

Values are mean ± standard deviation.

gigas, *G. mulleri*, and *T. carpenteri*) had high water levels (84–93%WM). Except for *G. glacialis*, those species also tended to have the highest ash levels (23–41%DM). Protein ranged from 0.8 to 13.3%WM (19.0–61.4%AFDM) and was highest in euphausiids. Lipid ranged from 1.1 to 29.0%WM (15.2–86.1%AFDM) and, except for *Pasiphaea scotiae* and *G. mulleri*, was highest in deeper-living species. Hexosamine ranged from 0.6 to 2.6%WM (2.2–15.4%AFDM).

Mean values for RNA:DNA ratio ranged from 0.36 to 25.47. For *P. boecki*, *P. macropa* and *Themisto gaudichaudi*, the high ratio values may be related to reproduction. All the specimens of *P. boecki* and *P. macropa* were carrying eggs and the specimen of *T. gaudichaudi* had young in a brood pouch. Elevated ratio values were observed in other specimens that were without visible eggs or young: all *H. antarctica, H. medusarum*, *Megalanceola* spp., and *V. stebbingi*; and several *C. richardi*, *C. lucasii*, *P. scotiae*, *E. superba*, *T. macrura* and *T. carpenteri* specimens. A few specimens with eggs (3 *C. lucasii*, 2 *G. mulleri*) showed no elevation in RNA:DNA ratio.

Mass-specific enzyme activities exhibited both inter- and intraspecific variability. Activities were generally 1–2 orders of magnitude higher in MDH than CS, with mean values ranging from 0.06 to 5.31 for CS and from 0.77 to 88.76 for MDH.

Mass-related changes in biochemical measures were examineud in *C. richardi*, *C. lucasii*, *V. stebbingi*, *G. glacialis*, *P. scotiae*, *E. superba*, *T. macrura*, *G. mulleri* and *T. carpenteri* (Table 4). In all nine species, protein content scaled directly with WM. With the exception of *C. richardi*, no changes in relative composition (%WM, %AFDM) with mass (mg, m) were observed. In *Cyphocaris*, smaller specimens had higher water (%WM, w), ash (%DM, a), and protein (%AFDM, pr), as expressed by the following equations: $w = 194.44\,m^{-0.17\pm0.04}$, $r^2 = 0.60$, $p = 0.0005$; $a = 144.62\,m^{-0.44\pm0.05}$, $r^2 = 0.83$, $p < 0.0000$; $\mathrm{pr} = 60.17\,m^{-0.13\pm0.03}$, $r^2 = 0.57$, $p = 0.0008$. Limited data on lipid and hexosamine precluded statistical testing for any species. It is interesting to note, however, that the lower lipid shown for sizeclass 5 *C. richardi* was from a pregnant specimen whose eggs hatched prior to

Table 4
Regressions of oxygen consumption rate and biochemical parameters vs. WM, and protein vs. RNA content for nine species of micronekton

Species	Misc. parameter vs. WM (mg)									Protein (mg) vs. RNA (mg)
	$\mu l\, O_2\, ind^{-1}\, h^{-1}$	Protein (mg)	RNA (mg)	DNA (mg)	RNA:DNA	CS (IU ind^{-1})	MDH (IU ind^{-1})	CS (IU gWM^{-1})	MDH (IU gWM^{-1})	
Cyphocaris richardi	$y = 0.334x^{0.696\pm0.093}$ (0.81, 15, <0.0000)	$y = 0.020x^{1.211\pm0.124}$ (0.86, 17, <0.0000)	$y = 0.007x^{0.870\pm0.213}$ (0.53, 17, 0.0010)	$y = 0.002x^{0.825\pm0.179}$ (0.59, 17, 0.0003)	nc	$y = 0.0002x^{1.279\pm0.302}$ (0.54, 17, 0.0007)	$y = 0.001x^{1.310\pm0.287}$ (0.58, 17, 0.0003)	nc	nc	$Y = 21.259x^{0.792\pm0.192}$ (0.53, 17, 0.0009)
Cyllopus lucasi	$y = 2.457x^{0.460\pm0.18}$ (0.52, 16, 0.0016)	$y = 0.070x^{1.012\pm0.051}$ (0.97, 16, <0.0000)	$y = 0.010x^{0.864\pm0.255}$ (0.45, 16, 0.0045)	$y = 0.003x^{0.856\pm0.303}$ (0.36, 16, 0.0136)	nc	$y = 0.008x^{0.774\pm0.185}$ (0.57, 15, 0.0011)	$y = 0.055x^{0.992\pm0.079}$ (0.92, 15, <0.0001)	nc	nc	$Y = 13.217x^{0.536\pm0.159}$ (0.45, 16, 0.0045)
Vibilia stebbingi	$y = 1.976x^{0.477\pm0.211}$ (0.25, 17, 0.0391)	$y = 0.068x^{1.019\pm0.213}$ (0.59, 18, 0.0002)	nc	nc	nc	nc	$y = 0.022x^{1.15\pm0.563}$ (0.21, 18, 0.0579)	nc	nc	nc
Galiteuthis glacialis	$y = 0.323x^{0.650\pm0.293}$ (0.45, 8, 0.0685)	$y = 0.010x^{1.168\pm0.166}$ (0.83, 12, <0.0000)	$Y = 0.0002x^{1.345\pm0.256}$ (0.73, 12, 0.0004)	$y = 0.0002x^{1.194\pm0.251}$ (0.69, 12, 0.0008)	nc	$y = 0.0001x^{1.459\pm0.164}$ (0.89, 12, <0.0000)	$y = 0.00004x^{1.641\pm0.396}$ (0.63, 12, 0.0020)	$y = 0.051x^{0.459\pm0.165}$ (0.44, 12, 0.0193)	$y = 0.042x^{0.641\pm0.396}$ (0.21, 12, 0.1372)	$Y = 17.424x^{0.721\pm0.121}$ (0.78, 12, 0.0001)
Pasiphaea scotiae	$y = 0.730x^{0.612\pm0.123}$ (0.86, 6, 0.0075)	$y = 0.066x^{1.008\pm0.044}$ (0.99, 8, <0.0000)	$y = 0.004x^{0.850\pm0.098}$ (0.93, 8, 0.0001)	$y = 0.004x^{0.672\pm0.077}$ (0.94, 7, 0.0003)	$y = 0.599x^{0.262\pm0.062}$ (0.82, 6, 0.0130)	$y = 0.004x^{0.728\pm0.154}$ (0.79, 8, 0.0032)	$y = 0.021x^{0.993\pm0.062}$ (0.98, 8, <0.0000)	$y = 3.861x^{-0.272\pm0.154}$ (0.34, 8, 0.1271)	nc	$y = 50.470x^{1.096\pm0.140}$ (0.91, 8, 0.0002)
Euphausia superba	$y = 0.562x^{0.786\pm0.018}$ (0.97, 61, <0.0000)	$y = 0.062x^{1.059\pm0.012}$ (0.99, 66, <0.0000)	$y = 0.027x^{0.788\pm0.035}$ (0.88, 63, <0.0000)	$y = 0.021x^{0.648\pm0.027}$ (0.90, 65, <0.0000)	$y = 1.197x^{0.117\pm0.039}$ (0.12, 66, 0.0037)	$y = 0.001x^{1.065\pm0.054}$ (0.86, 62, <0.0000)	$y = 0.006x^{1.353\pm0.034}$ (0.96, 66, <0.0000)	nc	$y = 6.494x^{0.353\pm0.035}$ (0.62, 66, <0.0000)	$y = 10.676x^{1.228\pm0.062}$ (0.87, 63, <0.0000)
Thysanoessa macrura	$y = 0.298x^{0.927\pm0.106}$ (0.77, 25, <0.0000)	$y = 0.112x^{0.955\pm0.045}$ (0.94, 28, <0.0000)	$y = 0.004x^{1.081\pm0.176}$ (0.59, 28, <0.0001)	$y = 0.009x^{0.626\pm0.140}$ (0.43, 28, 0.0001)	$y = 0.416x^{0.454\pm0.158}$ (0.24, 28, 0.0079)	nc	$y = 0.015x^{1.203\pm0.208}$ (0.56, 28, <0.0001)	$y = 1.641x^{-0.695\pm0.371}$ (0.13, 26, 0.0732)	nc	$y = 9.052x^{0.487\pm0.088}$ (0.48, 28, <0.0001)
Gigantocypris mulleri	$y = 4.277x^{0.1097\pm0.0680}$ (0.32, 6, 0.2442)	$y = 0.002x^{1.242\pm0.138}$ (0.95, 6, 0.0008)	$y = 0.0002x^{1.120\pm0.263}$ (0.82, 6, 0.0130)	$y = 0.001x^{0.857\pm0.333}$ (0.62, 6, 0.0616)	$y = 0.268x^{0.258\pm0.088}$ (0.68, 6, 0.0434)	nc	$y = 0.0001x^{1.428\pm0.378}$ (0.78, 6, 0.0195)	nc	nc	$y = 25.127x^{0.952\pm0.194}$ (0.86, 6, 0.0080)
Tomopteris carpenteri	$y = 3.256x^{0.397\pm0.224}$ (0.51, 5, 0.1743)	$y = 0.027x^{1.060\pm0.136}$ (0.94, 6, 0.0015)	nd	nd	nd	$y = 0.004x^{0.734\pm0.143}$ (0.87, 6, 0.0069)	$y = 0.002x^{1.115\pm0.422}$ (0.64, 6, 0.0573)	$y = 3.975x^{-0.266\pm0.143}$ (0.46, 6, 0.1369)	nc	nd

b values are slope ± standard error. Values in parentheses as in Table 2b. nc = no correlation, nd = not determined.

Table 5
Biochemical parameters for 25 species of micronekton

Group Species	MDO (m)	SC (n)	WM (mg)	Water (%WM)	Ash (%DM)	Protein (%WM)	Protein (%AFDM)	Lipid (%WM)	Lipid (%AFDM)	Hexosamine (%WM)	Hexosamine (%AFDM)	RNA:DNA	CS ($IU\,gWM^{-1}$)	MDH ($IU\,gWM^{-1}$)
Amphipods (Gammarid)														
Cyphocaris faueri	40	5 (1)	467.4	70.4	21.6	6.5	28.0	12.8	55.2	2.6	11.0	2.54	0.51	18.73
C. richardi	340	4 (1)	54.2	nd	nd	7.5	nd	nd	nd	nd	nd	2.11	3.11	13.12
		5 (11)	275.5 (106.8)	79.0 (5.2)	26.4 (10.1)	5.8 (2.1)	37.3 (6.1)	8.6	49.8	1.3	7.3	4.27 (1.85)	0.95 (0.82)	8.14 (6.86)
		6 (4)	691.4 (43.1)	61.0 (4.7)	12.9 (0.7)	10.3 (1.6)	30.3 (1.4)	21.7 (4.0)	61.3 (5.9)	2.3 (0.4)	6.6 (0.4)	4.69 (0.56)	1.93 (0.68)	16.79 (10.61)
		7 (1)	1106.9	66.3	12.5	7.2	24.3	25.4	86.1	1.6	5.3	2.63	1.46	15.59
Cleonardo longipes	nd	5 (1)	151.2	74.6	18.9	9.3	45.3	nd	nd	nd	nd	1.63	0.60	0.77
Parandania boecki	270	6 (1)	886.5	84.1	31.4	4.6	42.6	5.6	51.3	1.0	8.9	6.41	0.13	5.17
Amphipods (Hyperiid)														
Cyllopus lucasii	0	3 (1)	48.1	nd	nd	9.0	nd	nd	nd	nd	nd	3.87	5.31	68.55
		4 (5)	89.6 (9.0)	82.5 (2.5)	21.5 (4.6)	7.0 (1.0)	50.3 (3.3)	nd	nd	nd	nd	3.44 (2.20)	3.08 (1.49)	49.06 (9.91)
		5 (10)	241.7 (30.0)	78.9 (3.2)	20.4 (2.9)	7.5 (0.5)	45.5 (5.6)	nd	nd	nd	nd	3.86 (2.41)	2.50 (0.85)	54.27 (6.68)
Hyperiella antarctica	0	3 (1)	11.2	nd	nd	10.2	nd	nd	nd	nd	nd	nd	0.59	nd
		4 (1)	67.2	nd	nd	2.8	nd	nd	nd	nd	nd	11.53	1.34	4.25
Hyperoche medusarum	0	4 (1)	62.1	nd	nd	8.0	nd	nd	nd	nd	nd	10.98	2.23	31.30
Megalanceola remipes	100	5 (1)	418.9	88.1	31.9	3.5	43.2	nd	nd	0.6	8.0	9.50	0.20	16.74
M. stephenseni	nd	7 (1)	4997.1	93.4	40.9	1.3	32.6	nd	nd	0.6	15.4	8.55	0.15	1.41
Primno macropa	0	3 (2)	33.5 (3.6)	nd	nd	4.8 (1.7)	nd	nd	nd	nd	nd	25.47 (6.8)	0.39 (0.16)	42.00 (5.39)
		4 (1)	94 6	81.0	21.1	6.3	nd	nd	nd	nd	nd	11.43	0.10	34.35
Themisto gaudichaudi	0	4 (1)	81.5	nd	nd	6.1	nd	nd	nd	nd	nd	5.19	0.18	31.07
Vibilia stebbingi	0	3 (9)	38.6 (10.5)	nd	nd	7.8 (1.8)	nd	nd	nd	nd	nd	15.06 (5.24)	1.42 (1.27)	48.62 (29.14)
		4 (9)	57.7 (5.7)	nd	nd	7.3 (1.7)	nd	nd	nd	nd	nd	18.45 (7.82)	0.87 (1.21)	46.75 (31.26)
Cephalopods														
Galiteuthis glacialis	50	5 (2)	423.7 (70.4)	92.8 (0.8)	18.3 (2.8)	2.3 (0.6)	39.0 (3.5)	2.4	37.0	nd	nd	2.15 (0.42)	0.77 (0.04)	2.70 (1.34)
		6 (10)	788.6 (136.1)	91.4 (0.5)	16.3 (1.9)	3.0 (0.3)	42.4 (2.7)	1.1 (0.2)	15.2 (3.7)	nd	nd	2.03 (0.47)	1.12 (0.16)	3.14 (1.51)
Decapods														
Gennadas kempi	500	7 (2)	1839.0 (387.8)	69.4 (1.1)	11.0 (0.2)	9.0 (0.4)	33.1 (2.8)	14.7 (2.4)	54.0 (6.7)	0.8 (0.2)	2.9 (0.7)	1.09 (0.09)	1.31 (1.19)	15.65 (16.33)
Nematocarcinus lanceopes	0	5 (4)	280.2 (59.6)	77.9 (1.7)	14.1 (1.9)	7.1 (1.0)	37.5 (1.9)	6.8 (0.9)	35.0 (3.0)	0.9 (0.0)	4.6 (0.5)	2.13 (0.38)	1.13 (0.19)	24.57 (5.78)
Pasiphaea scotiae	100	5 (2)	299.5 (110.4)	71.8 (1.8)	8.9 (0.6)	6.9 (0.1)	26.8 (1.5)	nd	nd	nd	nd	2.79 (0.30)	0.94 (0.13)	20.13 (1.09)
		6 (1)	725.5	62.6	7.8	8.0	23.1	29.0	84.2	1.3	3.7	2.79	0.87	22.27
		7 (3)	2927.8 (770.8)	67.2 (3.2)	7.6 (0.6)	6.4 (1.0)	21.1 (2.1)	22.1 (4.2)	69.3 (8.9)	1.0 (0.3)	3.2 (0.8)	5.13 (0.95)	0.28 (0.09)	17.30 (4.80)
		8 (2)	6724.0 (1841.2)	63.8 (1.2)	6.6 (0.3)(0.3)	7.9 (0.5)	23.5 (2.2)	24.2 (0.8)	71.7 (4.9)	1.2 (0.0)	3.6 (0.3)	4.95 (1.60)	0.58 (0.14)	22.70 (1.50)
Petalidium foliaceum	500	6 (1)	792.2	68.7	8.3	7.4	25.9	15.4	53.7	0.7	2.3	0.66	0.57	3.28

Euphausiids														
Euphausia superba	0	3 (17)	31.6 (9.1)	nd	nd	7.3 (1.1)	nd	nd	nd	nd	nd	1.87 (0.70)	1.86 (1.07)	22.14 (12.79)
		4 (5)	81.2 (14.8)	81.1 (3.1)	13.3 (0.1)	9.2 (0.8)	61.4 (23.2)	nd	nd	nd	nd	2.51 (0.57)	3.06 (1.01)	45.26 (10.73)
		5 (8)	206.3 (114.5)	81.1 (3.1)	15.8 (2.7)	9.0 (1.4)	57.1 (9.4)	nd	nd	nd	nd	2.85 (1.23)	2.41 (1.29)	46.96 (17.55)
		6 (9)	742.0 (102.8)	82.1 (2.4)	17.3 (1.4)	8.6 (1.2)	58.5 (5.4)	nd	nd	nd	nd	3.38 (1.31)	2.59 (0.73)	69.75 (33.73)
		7 (27)	1379.7 (299.2)	78.7 (2.5)	15.5 (3.3)	9.7 (1.4)	55.2 (12.2)	nd	nd	nd	nd	2.93 (1.98)	2.24 (0.86)	88.76 (34.03)
E. triacantha	0	5 (2)	296.0 (3.6)	79.4 (0.1)	12.0 (4.3)	9.9 (0.1)	54.6 (2.1)	nd	nd	nd	nd	1.44 (0.30)	1.35 (1.10)	35.73 (0.06)
Thysanoessa macrura	100	3 (18)	35.4 (7.5)	76.9	16.2	9.8	57.7	nd	nd	nd	nd	2.18 (0.92)	0.33 (0.51)	37.49 (18.69)
		4 (8)	71.9 (13.3)	79.8 (0.4)	17.3 (0.3)	9.0 (0.8)	52.7 (4.1)	nd	nd	nd	nd	3.31 (1.19)	0.07 (0.04)	39.74 (12.74)
		5 (2)	164.4 (10.7)	71.1	9.0	8.3 (0.3)	32.4	nd	nd	nd	nd	4.59 (0.68)	0.06 (0.00)	40.06 (18.42)
Isopods														
Anuropus australis	100	6 (1)	528.0	77.8	20.7	5.5	31.3	8.6	49.0	1.3	7.1	0.59	0.02	15.65
Mysids														
Boreomysis rostrata	550	6 (1)	934.8	63.0	5.1	13.3	37.9	20.9	59.5	0.8	2.2	1.06	1.54	36.69
Gnathophausia gigas	500	7 (1)	1274.1	84.8	28.9	2.8	25.7	6.2	57.7	0.8	7.8	0.36	0.02	7.48
Ostracods														
Gigantocypris mulleri	500	5 (1)	431.0	93.1	30.9	1.0	19.9	nd	nd	nd	nd	1.33	0.18	1.25
		6 (1)	739.2	93.3	35.1	0.8	19.0	nd	nd	nd	nd	1.41	0.03	0.91
		7 (4)	1803.6 (458.8)	91.7 (0.6)	25.7 (7.4)	1.3 (0.2)	21.1 (2.9)	1.5 (0.3)	24.9 (3.8)	0.6 (0.1)	10.7 (3.4)	1.87 (0.35)	0.18 (0.15)	2.75 (1.24)
Polychaetes														
Tomopterus carpenteri	0	4 (1)	55.2	nd	nd	4.0	nd	nd	nd	nd	nd	3.15	1.58	4.54
		5 (3)	354.5 (55.5)	89.5 (2.7)	28.5 (8.1)	3.4 (1.2)	45.1 (5.8)	1.5 (0.8)	19.0 (2.8)	nd	nd	10.65	0.77 (0.29)	3.44 (3.35)
		6 (2)	788.3 (294.2)	87.9 (0.9)	22.8 (2.3)	4.7 (0.0)	50.1 (2.7)	1.6	16.8	nd	nd	8.08	0.77 (0.11)	5.58 (0.46)

Values are mean ± standard deviation. MDO = minimum depth of occurrence, SC = sizeclass, n = number of specimens analyzed. nd = no data.

analysis. Nucleic acid content also scaled with WM but not as well or as uniformly as protein content, especially for *C. richardi*, *C. lucasii*, *V. stebbingi* and *T. macrura* where the correlations became weak or non-existent. Strong correlations between RNA:DNA ratio (y) and wm (m) were observed in *P. scotiae* (specimens <6 g), immature *E. superba* (sizeclasses <6, Table 2b) and *G. mulleri*. Species that showed a good correlation between RNA content and mass (*G. glacialis*, *P. scotiae*, *E. superba*, and *G. mulleri*) also showed a similarly strong relationship between protein and RNA content (Table 4). Total enzyme activity ($IU\,ind^{-1}$) also scaled with mass in most species, with MDH showing a better correlation to mass than CS in all but *G. glacialis* and *T. carpenteri*. Mass-specific enzyme activity ($IU\,g\,WM^{-1}$) only showed a correlation with mass in three instances: CS in *G. glacialis* and *T. macrura*; and MDH in *E. superba*.

Biochemical measures were further examined in *E. superba* with respect to sex/developmental stage (Table 2a, b). Within the adult groups, pregnant females had significantly higher mean WM ($p<0.014$) and RNA:DNA ratio ($p<0.003$), and lower mean ash (%DM, $p<0.004$) than males and non-pregnant females. Pregnant females also had significantly lower water (%WM, $p<0.003$) and protein (%AFDM, $p<0.0004$) than non-pregnant females (Table 2a). Mass-specific CS and MDH activities were not significantly different among adults ($p>0.30$). The regressions of protein content, total CS ($IU\,ind^{-1}$) and total MDH ($IU\,ind^{-1}$) vs. WM shown in Table 4 are generally unchanged when immature and adult *E. superba* are considered separately; however, the correlations of both RNA and DNA content with WM as well as that between protein content and RNA content become very weak or non-existent in adult specimens (Table 2b).

Mean values of biochemical measures within different MIZ areas were examined in six species (Table 3). In *C. richardi*, water (%WM) and ash (%DM) levels were higher in the edge area but, as both these parameters scale with mass, the differences were a consequence of specimen size. No differences in any parameter between areas were observed for *C. lucasii*, *V. stebbingi* and *G. glacialis*. In *E. superba*, water level (%WM) was significantly higher in the ice than both the edge and open-water areas ($p<0.001$). Ash level (%DM) was not significantly different between ice and edge areas ($p=0.113$), but was significantly higher in the ice than open-water area ($p=0.0004$). For *E. superba*, individual values for water and ash levels varied only by 1–2% over the size range of specimens examined, and neither was found to scale with mass. In *T. macrura*, mass-specific CS activity ($IU\,g\,WM^{-1}$) was significantly higher in the edge than ice areas ($p=0.0004$). The high standard deviation associated with the mean in the edge sample is a consequence of three very high CS activities. If these three values are excluded from the comparison, mean mass-specific CS activity in the edge area (adjusted $x\pm s.d.=0.13\pm0.04$) is still significantly higher than in the ice area ($p=0.0012$).

3.3. Oxygen consumption vs. biochemical measures

The use of biochemical measures as predictors of metabolic rate was examined by regressing individual oxygen consumption rate ($\mu l\,O_2\,ind^{-1}\,h^{-1}$) against protein, RNA, and DNA content (mg); RNA:DNA ratio; and enzyme activity ($IU\,ind^{-1}$ and $IU\,g\,WM^{-1}$) individually for nine species analyzed over a size range ($n\geqslant5$) and also collectively for all 23 species in the data set (Table 6). Three species (*C. lucasii*, *G. glacialis*, and *G. mulleri*) showed only weak to moderate correlations of individual respiration rate with any biochemical parameter, five species (*C. richardi*, *P. scotiae*, *E. superba*, *T. macrura* and *T. carpenteri*) showed strong correlations between individual respiration rate and at least one parameter, and one species (*V. stebbingi*) failed to show any correlations. Protein content showed the best correlation in *C. richardi*, *P. scotiae*, *E. superba* and *T. macrura*, while MDH activity (total and mass-specific) showed the best correlation in *T. carpenteri*. For *E. superba*, a strong relationship between protein content and individual respiration rate was observed in both juveniles and adults. When all 23 species are considered collectively, protein content (mg) and total MDH activity

Table 6
Regressions of oxygen consumption rate vs. biochemical parameters for nine species of micronekton sampled over a size range

Species	$\mu l\, O_2\, ind^{-1}\, h^{-1}$ vs. :						
	Protein (mg)	RNA (mg)	DNA (mg)	CS ($IU\, ind^{-1}$)	MDH ($IU\, ind^{-1}$)	CS ($IU\, g WM^{-1}$)	MDH ($IU\, g WM^{-1}$)
Cyphocaris richardi	$y = 3.952x^{0.505\pm0.093}$ (0.69, 15, 0.0001)	$y = 18.903x^{0.456\pm0.114}$ (0.55, 15, 0.0014)	$y = 36.758x^{0.513\pm0.123}$ (0.57, 15, 0.0011)	$y = 26.511x^{0.354\pm0.105}$ (0.47, 15, 0.0050)	$y = 13.698x^{0.276\pm0.103}$ (0.35, 15, 0.0200)	nc	nc
Cyllopus lucasi	$y = 9.725x^{0.388\pm0.129}$ (0.39, 16, 0.0094)	$y = 26.944x^{0.292\pm0.107}$ (0.35, 16, 0.0162)	$y = 40.246x^{0.319\pm0.084}$ (0.51, 16, 0.0019)	nc	$y = 10.376x^{0.473\pm0.128}$ (0.45, 15, 0.0059)	nc	nc
Vibilia stebbingi	$y = 8.389x^{0.313\pm0.164}$ (0.19, 17, 0.0761)	nc	nc	nc	nc	nc	nc
Galiteuthis glacialis	$y = 5.328x^{0.485\pm0.218}$ (0.45, 8, 0.0677)	$y = 21.106x^{0.467\pm0.159}$ (0.59, 8, 0.0259)	$y = 27.277x^{0.406\pm0.180}$ (0.46, 8, 0.0653)	$y = 26.033x^{0.399\pm0.187}$ (0.43, 8, 0.0764)	nc	$y = 22.041x^{0.729\pm0.472}$ (0.28, 8, 0.1731)	nc
Pasiphaea scotiae	$y = 3.794x^{0.610\pm0.151}$ (0.80, 6, 0.0156)	$y = 45.516x^{0.545\pm0.210}$ (0.63, 6, 0.0603)	$y = 104.221x^{0.912\pm0.303}$ (0.75, 5, 0.0574)	$y = 79.980x^{0.530\pm0.312}$ (0.42, 6, 0.1652)	$y = 9.967x^{0.558\pm0.172}$ (0.73, 6, 0.0314)	$y = 45.265x^{-0.624\pm0.393}$ (0.39, 6, 0.1882)	nc
Euphausia superba (all)	$y = 4.509x^{0.738\pm0.019}$ (0.96, 61, <0.0000)	$y = 26.123x^{0.899\pm0.053}$ (0.84, 58, <0.0000)	$y = 61.957x^{1.109\pm0.051}$ (0.89, 60, <0.0000)	$y = 66.080x^{0.629\pm0.038}$ (0.83, 57, <0.0000)	$y = 11.357x^{0.555\pm0.020}$ (0.93, 61, <0.0000)	nc	$y = 0.250x^{1.366\pm0.146}$ (0.60, 61, <0.0000)
E. superba (immature)	$y = 5.213x^{0.628\pm0.050}$ (0.85, 29, <0.0000)	$y = 19.716x^{0.705\pm0.060}$ (0.84, 28, <0.0000)	$y = 42.659x^{0.902\pm0.101}$ (0.75, 29, <0.0000)	$y = 28.729x^{0.329\pm0.075}$ (0.42, 29, 0.0001)	$y = 11.242x^{0.430\pm0.045}$ (0.77, 29, <0.0000)	nc	$y = 1.875x^{0.604\pm0.166}$ (0.33, 29, 0.0011)
E. superba (adult)	$y = 2.107x^{0.940\pm0.166}$ (0.71, 32, <0.0000)	nc	$y = 106.309x^{0.443\pm0.153}$ (0.22, 31, 0.0074)	$y = 82.222x^{0.570\pm0.160}$ (0.33, 28, 0.0015)	$y = 21.928x^{0.421\pm0.103}$ (0.36, 32, 0.0003)	nc	nc
Thysanoessa macrura	$y = 2.792x^{0.904\pm0.119}$ (0.72, 25, <0.0000)	$y = 22.978x^{0.524\pm0.108}$ (0.51, 25, 0.0001)	$y = 53.933x^{0.686\pm0.200}$ (0.38, 25, 0.0023)	nc	$y = 8.514x^{0.489\pm0.087}$ (0.58, 25, <0.0001)	$y = 4.872x^{-0.348\pm0.113}$ (0.29, 25, 0.0053)	$y = 3.408x^{0.328\pm0.190}$ (0.11, 25, 0.0980)
Gigantocypris mulleri	$y = 7.249x^{0.096\pm0.060}$ (0.39, 6, 0.1839)	$y = 9.880x^{0.093\pm0.064}$ (0.35, 6, 0.2195)	$y = 10.468x^{0.101\pm0.174}$ (0.32, 6, 0.2423)	$y = 10.586x^{0.096\pm0.043}$ (0.31, 6, 0.2538)	$y = 8.762x^{0.073\pm0.048}$ (0.37, 6, 0.2028)	nc	nc
Tomopterus carpenteri	$y = 15.773x^{0.301\pm0.123}$ (0.67, 5, 0.0921)	nd	nd	$y = 58.522x^{0.437\pm0.187}$ (0.87, 5, 0.0217)	$y = 34.317x^{0.202\pm0.025}$ (0.96, 5, 0.0040)	$y = 47.367x^{0.783\pm0.368}$ (0.58, 5, 0.1368)	$y = 26.831x^{0.283\pm0.028}$ (0.97, 5, 0.0020)
All species[a]	$y = 4.391x^{0.652\pm0.025}$ (0.79, 179, <0.0000)	$y = 27.394x^{0.740\pm0.035}$ (0.73, 174, <0.0000)	$y = 52.016x^{0.578\pm0.042}$ (0.59, 175, <0.0000)	$y = 46.573x^{0.350\pm0.025}$ (0.53, 175, <0.0000)	$y = 10.789x^{0.525\pm0.021}$ (0.78, 178, <0.0000)	nc	$y = 9.301x^{0.317\pm0.053}$ (0.13, 178, <0.0000)

Regressions are also shown using individual values for all species in the data set. Values in parentheses as in Table 2b. nc = no correlation, nd = not determined.
[a]Individual values for all 23 species in the data set.

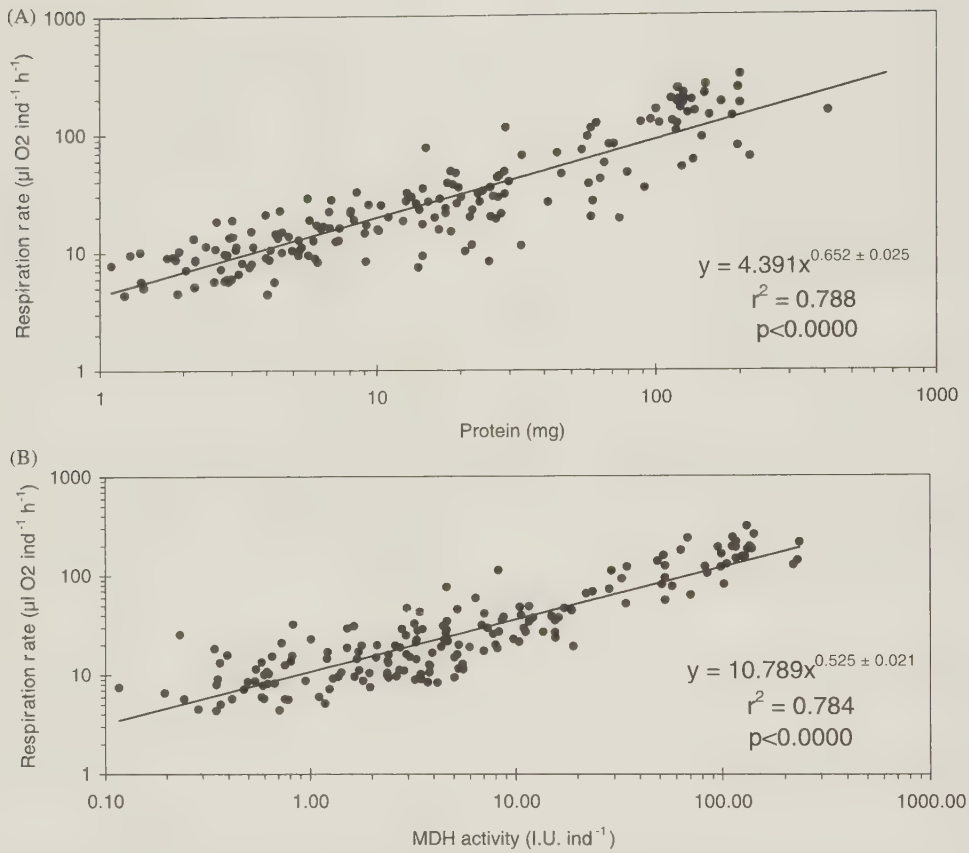

Fig. 2. Log log plot of oxygen consumption rate ($\mu l\, O_2\, ind^{-1}\, h^{-1}$) vs. (A) protein content (mg) and (B) total MDH activity ($IU\, ind^{-1}$) using individual values ($n = 178$) for all species. b = slope ± standard error.

($IU\, ind^{-1}$) show the best correlation to individual respiration rate (Fig. 2).

4. Discussion

4.1. Effects of MIZ area

The absence of significant changes in oxygen consumption rate among specimens from different areas within the marginal ice zone implies that there is little short-term direct influence of the ice-edge bloom on metabolism for micronekton species or that the influence is masked by the mobility of the fauna. Higher levels of water and ash in *E. superba* in the pack-ice area and the higher level of CS activity in *T. macrura* in the ice-edge area suggest that longer-term effects of an individual's distribution with respect to the bloom may be exhibited by changes in proximate composition or metabolic potential. Data on zooplankton from the same cruise showed bloom-related changes in abundance and age structure (Burghart et al., 1999) as well as body compositon (Geiger et al., 2001) for the dominant copepod species, factors that could influence metabolism or chemical composition in micronekton species that were feeding on them. Of the six species examined across MIZ areas in this study, *C. richardi*, *C. lucasii*, *E. superba* and *T. macrura* are omnivorous (Hopkins, 1985; Hopkins and Torres, 1989; Daly, 1990). *V. stebbingi* is a

particulate feeder associated with salps (Madin and Harbison, 1977) and, based on dietary data for other Antarctic squids (Hopkins, 1985), *G. glacialis* is carnivorous. With the exception of *V. stebbingi*, all of the species are highly motile, can actively forage, and take a variety of prey. It is not surprising that physiological parameters for these species remain fairly uniform across the marginal ice zone.

4.2. Effects of season

Metabolic and/or compositional data for 17 of the species examined in this study are available from previous studies. Oxygen consumption rates from this study are similar to other reported summer values (Opalinski and Jazdzewski, 1978; Ikeda and Mitchell, 1982; Hirche, 1983, 1984; Ikeda and Bruce, 1986; Ikeda, 1988). For gammarids, decapods, mysids and ostracods, summer values for oxygen consumption rate were not significantly different from those measured in other seasons (Torres et al., 1994a). Consequently, metabolic data from all seasons were combined to generate regressions of respiration rate ($\mu l\, O_2\, ind^{-1}\, h^{-1}$) vs. WM (mg) for all species in these groups with $n \geqslant 6$ (Table 7). As was observed with the summer data, the giant ostracod *G. mulleri* continued to show no significant correlation ($p > 0.20$) of respiration with mass. Most compositional parameters for species in those groups were also similar between seasons (Clarke and Holmes, 1986; Torres et al., 1994b), the only noticeable exception being higher lipid levels in summer. Elevated summer lipid levels could reflect increases in storage depots during productive times, as well as being associated with egg production (Clarke and Holmes, 1986). The present data set included non-ovigerous females of *Gennadas kempi*, *B. rostatra* and *P. scotiae* (sizeclass 8), as well as ovigerous females of *C. richardi* and *G. mulleri*, so, for at least the latter two species, reproductive influences were important in the observed higher summer lipid levels.

For the hyperiid amphipods *C. lucasii* and *V. stebbingi*, mean respiration rates in summer are higher than those reported for fall and winter by Torres et al. (1994a). While both species show the same trend, differences in mean values are significant only for *V. stebbingi* (summer > winter, $p = 0.0002$; summer > fall, $p = 0.089$). Comparison of regressions of respiration rate ($\mu l\, O_2\, ind^{-1}\, h^{-1}$) vs. WM (mg) for *C. lucasii* between spring, summer, fall (combined) and winter show no significant difference in slopes ($p > 0.5$), but a significantly lower intercept in winter ($p < 0.5$) (Table 7). For *V. stebbingi*, the slope is significantly higher ($p < 0.005$) and the intercept significantly lower ($p < 0.001$) in winter compared to summer, fall combined (Table 7). In contrast, compositional values for the species are similar to winter values reported by Torres et al. (1994b). In that study, changes in proximate composition from fall to winter were attributed to combustion of body components, proposing that a lower salp biomass in the winter (Lancraft et al., 1991) argued against a fall–winter reproductive strategy. While no ovigerous specimens of *V. stebbingi* were observed in the present data set, there were several ovigerous *C. lucasii* specimens collected, indicating a summer reproductive effort.

For euphausiids, the present summer data complete the seasonal coverage on *E. superba* initiated by Torres et al. (1994a, b) and also allow for a summer–winter comparison in *T. macrura*. Mean summer respiration rates for both juvenile (sizeclass < 6) and adult (sizeclass > 5) *E. superba* are not significantly different than values for spring and fall ($p > 0.20$) but are significantly higher than winter rates ($p < 0.0001$). Comparison of the regressions of respiration ($\mu l\, O_2\, ind^{-1}\, h^{-1}$) vs. WM between spring, summer and fall show no significant differences in slope ($p > 0.25$) or intercept ($p > 0.50$). Comparison of the regressions for combined spring, summer, fall vs. winter show that, while the slopes are not significantly different ($p > 0.25$), the elevations of the lines are ($p < 0.001$) (Fig. 3). Consequently, the inclusion of summer respiration data only serves to further support the conclusion of Torres et al. (1994a) of a depressed winter metabolism in *E. superba*. The significant difference in regression slopes observed between juvenile and adult *E. superba* in the present data set is maintained when data from spring, summer, and fall are combined (Table 7). In juveniles, metabolism scales in a conventional way with mass

Table 7
Regression s of oxygen consumption rate ($\mu l\, O_2\, ind^{-1}\, h^{-1}$) vs. WM (mg) for eight species of micronekton

Species	All seasons	Spring–summer–fall seasons	Winter season
Cyphocaris richardi	$y = 0.157x^{0.848\pm0.075}$ (0.85, 24, <0.0000)		
Cyllopus lucasii		$y = 0.955x^{0.644\pm0.097}$ (0.62, 29, <0.0000)	$y = 0.470x^{0.728\pm0.171}$ (0.78, 7, 0.0081)
Vibilia stebbingi		$y = 2.698x^{0.362\pm0.239}$ (0.10, 23, 0.1441)	$y = 0.006x^{1.805\pm0.401}$ (0.74, 9, 0.0028)
Galiteuthis glacialis	$y = 0.578x^{0.614\pm0.125}$ (0.62, 17, 0.0002)		
Gennadas kempi	$y = 0.135x^{0.849\pm0.147}$ (0.89, 6, 0.0045)		
Pasiphaea scotiae	$y = 0.938x^{0.591\pm0.111}$ (0.70, 14, 0.0002)		
Euphausia superba			
All		$y = 0.497x^{0.805\pm0.019}$ (0.95, 88, <0.0000)	$y = 0.211x^{0.803\pm0.018}$ (0.97, 65, <0.0000)
Juvenile		$y = 0.646x^{0.739\pm0.039}$ (0.90, 42, <0.0000)	$y = 0.217x^{0.797\pm0.021}$ (0.97, 47, <0.0000)
Adult		$y = 0.214x^{0.929\pm0.117}$ (0.59, 46, <0.0000)	$y = 0.510x^{0.678\pm0.374}$ (0.17, 18, 0.0888)
Thysanoessa macrura		$y = 0.293x^{0.932\pm0.103}$ (0.77, 26, <0.0000)	$y = 0.309x^{0.824\pm0.075}$ (0.83, 26, <0.0000)

Regressions listed under "all seasons" for species that showed no significant differences in respiration between any season. Spring, fall, and winter data from Torres et al. (1994a). Values in parentheses as in Table 2b.

($b \approx 0.75$; Withers, 1992). In adults, the b-value is slightly higher ($b \approx 0.9$).

For *T. macrura*, mean respiration rates for sizeclasses 4 and 5 are significantly higher in summer than in winter ($p < 0.022$). Mean rates for sizeclass 3 are also higher in summer but not significantly so ($p = 0.22$). Comparison of the regressions of respiration ($\mu l\, O_2\, ind^{-1}\, h^{-1}$) vs. WM in *T. macrura* for summer and winter also shows no significant ($p > 0.10$) difference between slopes, but an unexpected higher intercept in the winter ($p < 0.001$). The higher winter intercept is a consequence of greater variability in respiration values among sizeclass 3 specimens and and the resultant lack of significant difference between seasons in this group. When just sizeclasses 4 and 5 are compared, the slopes remain similar ($p > 0.10$), but the winter intercept is significantly lower ($p < 0.001$). Thus, *T. macrura* also shows a winter metabolic depression, at least in the larger sizeclasses. Respiration rates ($\mu l\, O_2\, mg\, WM^{-1}\, h^{-1}$) for *E. triacantha* also appear higher in the summer vs. the winter, but data on similar-sized specimens are insufficient for statistical comparison.

Trends in water, ash, and protein levels among euphausiids are less consistent. For *E. superba*, summer and winter water levels are similar, both higher than fall values ($p < 0.001$), while ash levels are not significantly different in any season ($p > 0.30$). Protein levels (%WM) are similar in summer and winter, both lower than in fall ($p < 0.0001$). As %AFDM, fall and winter protein levels are the same, both are lower than in summer ($p < 0.005$). Limited sample size precludes statistical comparisons of compositional components for *T. macrura* and *E. triacantha*, but the general patterns for these species mirror that observed in *E. superba*. Lower %WM protein in summer merely reflects changes in water level, while higher %AFDM protein indicates actual increases in organic protein, suggesting increased growth during the productive season. Lipid and protein are the two main compositional components; when combusted, they are replaced by water. It is most likely that the high summer water contents and implied depletion of lipid reserves are a consequence of energy invested in reproduction. *T. macrura* reproduces in the spring (Nordhausen,

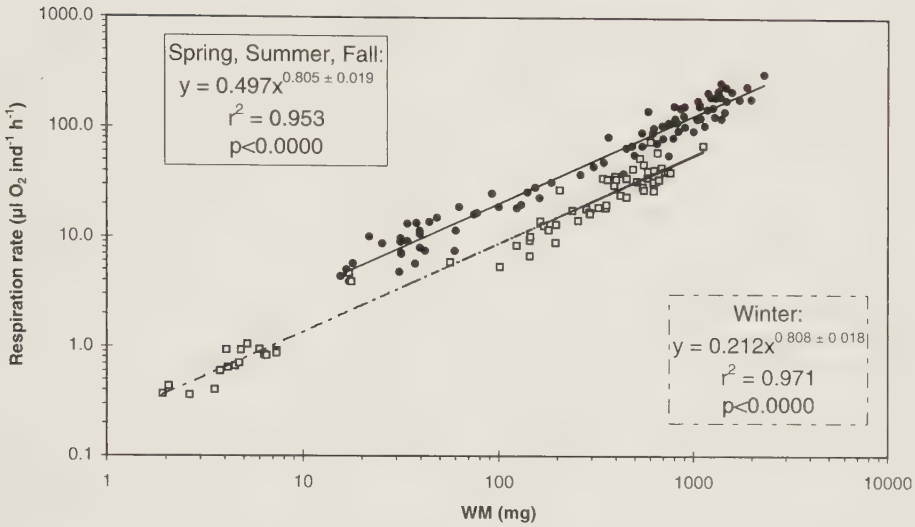

Fig. 3. Log–log plot of oxygen consumption rate ($\mu l\, O_2\, ind^{-1}\, h^{-1}$) vs. WM (mg) for *E. superba* between seasons. (●): combined spring, summer, and fall data; (□): winter data. b = slope ± standard error.

1994) and *E. superba* from mid-November through April (Mauchline, 1980; Quetin et al., 1994).

Following the classification of metabolic strategies proposed by Torres et al. (1994b), summer oxygen consumption rates were higher in all species exhibiting a Type 2 overwintering strategy, while species with a Type 3 overwintering strategy did not show any changes in respiration rate during summer. An increased summer metabolism suggests that the animals are feeding, growing, and in some cases, accumulating energy stores for the winter.

4.3. Biochemical measures as predictors of respiration rate

The use of biochemical indices as predictive tools for growth (Buckley, 1980; Buckley et al., 1984; Mugiya and Oka, 1991; Brightman et al., 1997) and metabolism (Torres and Somero, 1988b; Clarke et al., 1984) is an idea that has been evolving since the early 1980s. The measurement of oxygen consumption rates of aquatic organisms is difficult and time consuming. Similarly, retrieving live animals in excellent condition for respirometry can be difficult, especially when studying animals from great depths or in delicate species such as gelatinous plankton (cf. Ikeda et al., 2000).

Since muscle tissue is the principal metabolizing body component, it is not surprising that oxygen consumption rate ($\mu l\, O_2\, ind^{-1}\, h^{-1}$) scales very strongly with protein content (mg). Furthermore, since protein content was found to scale directly with WM in every species examined , the nature of the respiration vs. protein relationship for a particular species depends mainly on the correlation between respiration rate and mass. For example, *C. richardi*, *P. scotiae*, *E. superba* and *T. macrura* showed strong correlations for both respiration vs. WM and protein vs. WM and, as a consequence, had good respiration vs. protein correlations. In contrast, *V. stebbingi* and *G. mulleri* showed no correlations between respiration and WM and also exhibited no respiration vs. protein correlations. The observation that protein content can be a good indicator of respiratory rate in pelagic organisms was first reported for pelagic crustaceans off Southern California by Childress and Nygaard (1974). Our findings indicate that this predictive relationship is present in Antarctic micronekton as well.

The usefulness of nucleic acids as predictors of respiration rate remains as long as these

components remain coupled to growth and increases in protein, as is the case in juveniles and individuals not generating major energy stores. Examples in the present data set are *G. glacialis*, *P. scotiae* and immmature *E. superba*. In all three species, RNA and DNA content as well as RNA:DNA ratio scaled positively with mass, indicating active growth, and, except in *G. glacialis*, these parameters also scaled positively with respiration rate ($\mu l\, O_2\, ind^{-1}\, h^{-1}$). The lack of correlation between respiration rate and RNA:DNA ratio in *G. glacialis* is likely a consequence of the limited size range of specimens examined and the resultant weak correlation between respiration rate and mass. The finding of elevated RNA:DNA ratios in ovigerous females is consistent with previous studies (Nakata et al., 1994; Saiz et al., 1998). That not all ovigerous specimens had higher relative RNA:DNA ratio values implies that the developmental stage of eggs may also influence measured values. In a study of the copepod *Calanus helgolandicus,* Biegala et al. (1999) found that gonad maturation also resulted in higher RNA:DNA ratios, which could explain the high ratio values observed in non-ovigerous specimens in this study. Furthermore, they found no change in protein content ($\mu g\, ind^{-1}$) during the same period, a finding consistent with the observed lack of correlation between protein and RNA in adult *E. superba* in the present study. Adult *E. superba* males show a weak but definite positive correlation between protein (y, mg) and RNA (x, mg) as expressed by the regression: $y = 35.171x^{0.647\pm0.302}$, $r^2 = 0.32$, $p = 0.057$, but adult females show no correlation at all ($r^2 = 0.02$, $p = 0.49$). Furthermore, the strong correlation observed in juveniles between protein content and RNA content improves when adult males are added to the regression ($y = 10.169x^{1.385\pm0.059}$, $r^2 = 0.94$, $n = 39$, $p < 0.0000$), but weakens when adult females are included instead ($y = 10.007x^{1.200\pm0.066}$, $r^2 = 0.87$, $n = 51$, $p < 0.0000$). Protein content continues to scale positively with WM in adult *E. superba*, but the correlation is stronger in males ($r^2 = 0.96$) than in females ($r^2 = 0.85$). The influence of reproductive activity on nucleic acid measures is also indicated in *C. richardi*, *C. lucasii* and *T. macrura*, all species exhibiting only weak correlations of RNA content vs. WM and protein content vs. RNA content. The very high RNA:DNA ratios found for *V. stebbingi* (8.9–24.0) suggest reproductive effects as well, but growth influences could also be a factor. Since *V. stebbiingi* feed directly on the particulate food collected by their host salp (Madin and Harbison, 1977), they are directly affected by phytoplankton concentrations. Thus RNA:DNA ratio values could be elevated in response to high food availability in the edge and open-water areas.

Mass-specific enzyme activity ($IU\, g\, WM^{-1}$) did not explain much of the variability in individual respiration rate ($\mu l\, O_2\, ind^{-1}\, h^{-1}$) when one was plotted against the other (Table 6). However, mass-specific activity did not scale strongly with mass in most species, and it initially appeared to contrast with that found for fish (Childress and Somero, 1979; Torres and Somero, 1988b). In the present study, entire specimens were homogenized rather than an excised muscle sample, as is normally done with fish. Homogenizing the entire specimen resulted in lower mass-specific enzyme activities but made the results more comparable with smaller species of Crustacea such as copepods, where excising the muscle would be impractical. A recent study (Cullen et al., 2003) using excised sections of abdominal muscle of *E. superba* gave CS activities approximately 5 times higher than those reported here.

Both CS and MDH catalyze reactions in the citric acid cycle serving as proxies for aerobic potential, but MDH also plays other roles; for example, shuttling electrons between the cytosol and mitochndrion, and as such might better represent overall metabolism (Lehninger, 1982). That *E. superba* was the only individual species to exhibit a strong correlation between mass-specific enzyme activity and mass (and consequently respiration rate) may be due to the combined influence of a large sample size, wide specimen size range, and high protein content (45–78%AFDM).

When all the species were considered using mean values for each sizeclass, MDH activity showed a significant positive correlation with respiration rate (Fig. 4). This illustrates a predictive capability of MDH activity for respiration

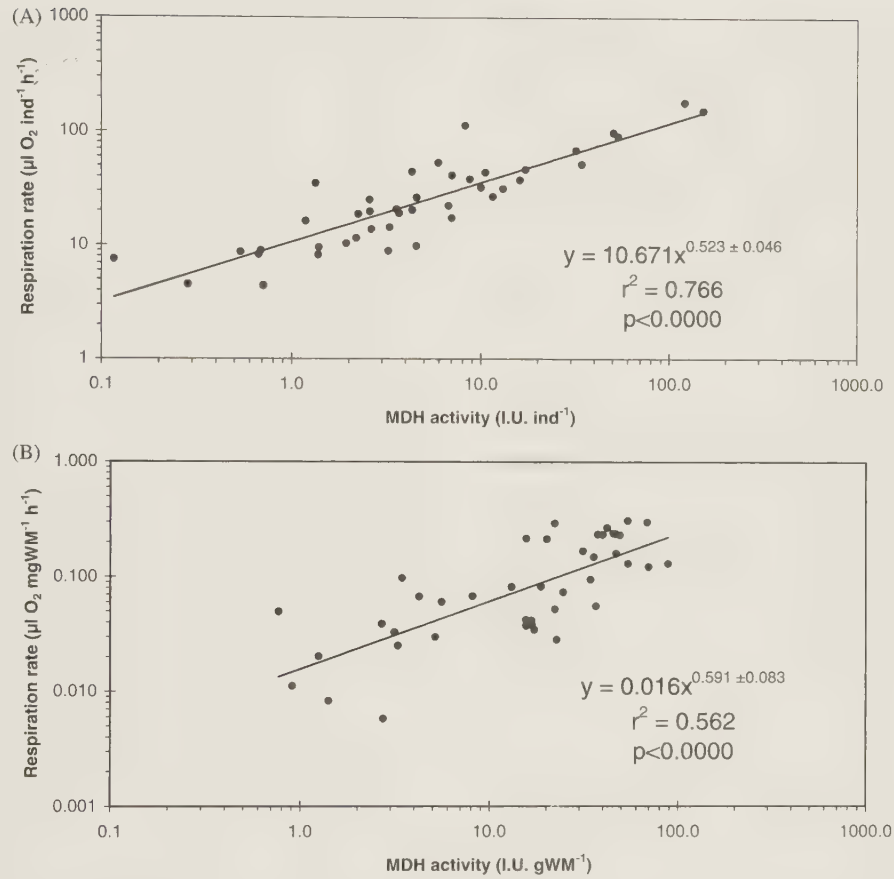

Fig. 4. (A) Log–log plot of individual oxygen consumption rate ($\mu l\, O_2\, ind^{-1}\, h^{-1}$) vs. total MDH activity ($IU\, ind^{-1}$) using sizeclass mean values ($n = 42$) for all species. b = slope ± standard error. (B) Log–log plot of mass-specific oxygen consumption rate ($\mu l\, O_2\, mg\, WM^{-1}\, h^{-1}$) vs. mass-specific MDH activity ($IU\, g\, WM^{-1}$) using sizeclass mean values ($n = 42$) for all species. b = slope ± standard error.

rate in invertebrate micronekton similar to what has been shown for pelagic fishes (Childress and Somero, 1979), making it and protein content the two most effective biochemical proxies for metabolic rate.

Acknowledgements

We thank the captain and crew of the R.V. *Polar Duke* for their expert field assistance. Thanks are also due to Scott Burghart, Tracey Sutton, Liz Clarke, and Teresa Greely for their considerable help with sample collection and processing during the cruise. This study was supported by NSF OPP 9220493 and NSF OPP 9910100, both to J.J. Torres.

References

Atkinson, A., Meyer, B., Stubing, D., Hagen, W., Schmidt, K., Bathmann, U.V., 2002. Feeding and energy budgets of Antarctic krill *Euphausia superba* at the onset of winter—II. Juveniles and adults. Limnology and Oceanography 47, 953–966.

Bentle, L.A., Dutta, S., Metcoff, J., 1981. The sequential enzymatic determination of DNA and RNA. Analytical Biochemistry 116, 5–16.

Biegala, I.C., Harris, R.P., Bergeron, J.P., 1999. ATCase activity, RNA: DNA ratio, gonad development stage, and

egg production in the female copepod *Calanus helgolandicus*. Marine Biology 135, 1–10.

Bligh, E.G., Dyer, W.J., 1959. A rapid method of total lipid extraction and purification. Canadian Journal of Biochemistry and Physiology 37, 911–917.

Brightman, R.I., Torres, J.J., Donnelly, J., Clarke, M.E., 1997. Energetics of larval red drum, *Sciaenops ocellatus*. Part II: Growth and biochemical indicators. Fishery Bulletin US 95, 431 -444.

Buckley, L.J., 1980. Changes in ribonucleic acid, deoxyribonucleic acid, and protein content during ontogenesis in winter flounder, *Pseudopleuronectes americanus*. Fishery Bulletin US 77, 703–709.

Buckley, L.J., Turner, S.I., Halavik, T.A., Smigielski, A.S., Drew, S.M., Laurence, G.C., 1984. Effects of temperature and food availability on growth, survival, and RNA-DNA ratio of larval sand lance (*Ammodytes americanus*). Marine Ecology Progress Series 15, 91 97.

Burghart, S.E., Hopkins, T.L., Vargo, G.A., Torres, J.J., 1999. Effects of a rapidly receding ice edge on the abundance, age structure, and feeding of three dominant calanoid copepods in the Weddell Sea, Antarctica. Polar Biology 22, 279–288.

Childress, J.J., Nygaard, M.H., 1974. Chemical composition and buoyancy of midwater crustaceans as a function of depth of occurrence off southern California. Marine Biology 27, 225–238.

Childress, J.J., Somero, G.N., 1979. Depth-related enzymic activities in muscle, brain, and heart of deep-living pelagic marine teleosts. Marine Biology 52, 273–283.

Clarke, A., Holmes, L.J., 1986. Lipid content and composition of some midwater crustaceans from the Southern Ocean. Journal of Experimental Marine Biology and Ecology 104, 31–51.

Clarke, M.E., Turner, S.I., Halavik, T.A., Smigielski, A.S., Drew, S.M., Laurence, G.C., 1984. Effects of nutrition and temperature on metabolic enzyme activities in larval and juvenile red drum, *Sciaenops ocellatus*, and lane snapper, *Lutjanus synagris*. Marine Biology 112, 31–36.

Cullen, M., Kaufmann, R.S., Lowery, M.S., 2003. Seasonal variation in biochemical indicators of physiological status in *Euphausia superba* from Port Foster, Deception Island, Antarctica. Deep-Sea Research II 50, 1787–1798.

Daly, K.L., 1990. Overwintering development, growth, and feeding of larval *Euphausia superba* in the Antarctic marginal ice zone. Limnology and Oceanography 35, 1564–1576.

Donnelly, J., Torres, J.J., Hopkins, T.L., Lancraft, T.M., 1990. Proximate composition of Antarctic mesopelagic fishes. Marine Biology 106, 13–23.

Donnelly, J., Torres, J.J., Hopkins, T.L., Lancraft, T.M., 1994. Chemical composition of Antarctic zooplankton during austral fall and winter. Polar Biology 14, 171–183.

Drits, A.V., Pasternak, A.F., Kosobokova, K.N., 1993. Feeding, metabolism, and body composition of the Antarctic copepod *Calanus propinquus* Brady with special reference to its life cycle. Polar Biology 13, 13–21.

Einarsson, H., 1945. Euphausiacea I. North Atlantic species Dana Reports 27, 1–85.

Fraser, F.C., 1936. On the development and distribution of the younger stages of krill (*Euphausia superba*). Discovery Reports 14, 3–192.

Geiger, S.P., Kawall, H.G., Torres, J.J., 2001. The effect of the receding ice edge on the condition of copepods in the northwestern Weddell Sea: results from biochemical assays. Hydrobiologia 453/453, 79–90.

Hirche, H.-J., 1983. Excretion and respiration of the Antarctic krill *Euphausia superba*. Polar Biology 1, 205–209.

Hirche, H.-J., 1984. Temperature and metabolism of plankton—I. Respiration of Antarctic zooplankton at different temperatures with a comparison of Antarctic and Nordic krill. Comparative Biochemistry and Physiology 77A, 361–368.

Hopkins, T.L., 1985. Food web of an Antarctic midwater ecosystem. Marine Biology 89, 197–212.

Hopkins, T.L., Torres, J.J., 1989. Midwater food web in the vicinity of a marginal ice zone in the western Weddell Sea. Deep-Sea Research 36, 543–560.

Huntley, M.E., Nordhausen, W., Lopez, M.D.G., 1994. Elemental composition, metabolic activity, and growth of Antarctic krill *Euphausia superba* during winter. Marine Ecology Progress Series 107, 23–40.

Ikeda, T., 1985. Life history of Antarctic krill *Euphausia superba*: a new look from an experimental approach. Bulletin of Marine Science 37, 599–608.

Ikeda, T., 1988. Metabolism and chemical composition of crustaceans from the Antarctic mesopelagic zone. Deep-Sea Research 35, 1991–2002.

Ikeda, T., Bruce, B., 1986. Metabolic activity and elemental composition of krill and other zooplankton from Prydz Bay, Antarctica, during summer (November–December). Marine Biology 92, 545–555.

Ikeda, T., Mitchell, A.W., 1982. Oxygen uptake, ammonia excretion and phosphate excretion by krill and other Antarctic zooplankton in relation to their body size and chemical composition. Marine Biology 71, 283–298.

Ikeda, T., Torres, J.J., Hernandez-Leon, S., Geiger, S.P., 2000. Metabolism. In: Harris, R.P., Wiebe, P.W., Lenz, J., Skjoldal, H.R., Huntley, M.E. (Eds.), Zooplankton Methodology Manual. Academic Press, San Diego, pp. 455–532.

Kawall, H.G., Torres, J.J., Geiger, S.P., 2001. Effects of the ice-edge bloom on the metabolism of copepods in the Weddell Sea, Antarctica. Hydrobiologia 453/454, 67–77.

Lancraft, T.M., Torres, J.J., Hopkins, T.L., 1989. Micronekton and macrozooplankton in the open waters near Antarctic ice edge zones (AMERIEZ 1983 and 1986). Polar Biology 9, 225–233.

Lancraft, T.M., Hopkins, T.L., Torres, J.J., Donnelly, J., 1991. Oceanic micronektonic/macrozooplanktonic community structure and feeding in ice covered Antarctic waters during the winter. Polar Biology 11, 157–167.

Lehninger, A.L., 1982. Principles of Biochemistry. Worth, New York, 1011pp.

Madin, L.P., Harbison, G.R., 1977. The associations of Amphipoda Hyperiidae with gelationous zooplankton. I. Associations with Salpidae. Deep-Sea Research 24, 449–463.

Mauchline, J., 1980. The biology of mysids and euphausiids. Advances in Marine Biology 18, 1–677.

Mauchline, J., Fisher, L.R., 1969. Advances in Marine Biology, vol. 7. The Biology of Euphausiids. Academic Press, London, pp. 1–454.

Meyer, B., Atkinson, A., Stubing, D., Oettl, B., Hagen, W., Bathmann, U.V., 2002a. Feeding and energy budgets of Antarctic krill *Euphausia superba* at the onset of winter-I. Furcilia III larvae. Limnology and Oceanography 47, 943–952.

Meyer, B., Saborowski, R., Atkinson, A., Buchholz, F., Bathmann, U.V., 2002b. Seasonal differences in citrate synthase and digestive enzyme activity in larval and postlarval Antarctic krill, *Euphausia superba*. Marine Biology 141, 855–862.

Mugiya, Y., Oka, H., 1991. Biochemical relationship between otolith and somatic growth in the rainbow trout *Onchorhynchus mykiss*: consequence of starvation, resumed feeding, and diel variations. Fishery Bulletin US 89, 239–245.

Nakata, K., Nakano, H., Kikuchi, H., 1994. Relationship between egg productivity and RNA/DNA ratio in *Paracalanus* sp. in the frontal waters of the Kurshio. Marine Biology 119, 591–596.

Nemoto, T., 1957. Foods of baleen whales in the Northern Pacific. Scientific Report of the Whales Research Institute of Tokyo 14, 149–290.

Nordhausen, W., 1994. Distribution and diel vertical migration of the euphausiid *Thysanoessa macrura* in Gerlache Strait, Antarctica. Polar Biology 14, 219–229.

Opalinski, K.W., Jazdzewski, K., 1978. Respiration of some Antarctic amphipods. Polskie Archiwum Hydrobiologii 25, 643–655.

Quetin, L.B., Ross, R.M., 1991. Behavior and physiological characteristics of the Antarctic krill, *Euphausia superba*. American Zoologist 31, 49–63.

Quetin, L.B., Ross, R.M., Clarke, A., 1994. Krill energetics: seasonal and environmental aspects of the physiology of *Euphausia superba*. In: El-Sayed, S.Z. (Ed.), Southern Ocean Ecology: The BIOMASS Perspective. University Press, Cambridge, pp. 165–184.

Saiz, E., Calbet, A., Fara, A., Berdalet, E., 1998. RNA content of copepods as a tool for determining adult growth rates in the field. Limnology and Oceanography 43, 465–470.

Sakshaug, E., Skjoldal, H.R., 1989. Life at the ice edge. Ambio 18, 60–67.

Smith, W.O., Nelson, D.M., 1985. Phytoplankton bloom produced by a receding ice edge in the Ross Sea: spatial coherence with the density field. Science 227, 163–166.

Smith, W.O., Sakshaug, E., 1990. Polar phytoplankton. In: Smith, .O. (Ed.), Polar Oceanography Part B: Chemistry, Biology, and Geology. Academic Press, San Diego, pp. 477 -525.

Torres, J.J., Somero, G.N., 1988a. Metabolism, enzymic activities, and cold adaptation in Antarctic mesopelagic fishes. Marine Biology 98, 169–180.

Torres, J.J., Somero, G.N., 1988b. Vertical distribution and metabolism in Antarctic mesopelagic fishes. Comparative Biochemistry and Physiology 90B, 521–528.

Torres, J.J., Aarset, A.V., Donnelly, J., Hopkins, T.L., Lancraft, T.M., Ainley, D.G., 1994a. Metabolism of Antarctic micronektonic crustacea as a function of depth of occurrence and season. Marine Ecology Progress Series 113, 207–219.

Torres, J.J., Donnelly, J., Hopkins, T.L., Lancraft, T.M., Aarset, A.V., Ainley, D.G., 1994b. Proximate composition and overwintering strategies of Antarctic micronektonic Crustacea. Marine Ecology Progress Series 113, 221–232.

Withers, P.C., 1992. Comparative Animal Physiology. Saunders, Orlando, 949pp.

Zar, J.H., 1974. Biostatistical Analysis. Prentice Hall, Englewood Cliffs, NJ, 620pp.

ELSEVIER

Deep-Sea Research II 51 (2004) 2247–2260

DEEP-SEA RESEARCH
PART II

www.elsevier.com/locate/dsr2

A krill-dominated micronekton and macrozooplankton community in Croker Passage, Antarctica with an estimate of fish predation

Thomas M. Lancraft[a], Kim R. Reisenbichler[b], Bruce H. Robison[b], Thomas L. Hopkins[c], Joseph J. Torres[c,*]

[a]*Department of Natural Sciences, St. Petersburg College, 6605 5th Avenue North, St. Petersburg, FL 33710, USA*
[b]*Monterey Bay Aquarium Research Institute, 7700 Sandholt Road, Moss Landing, CA 95039-9644, USA*
[c]*College of Marine Science, University of South Florida, 140 7th Avenue South, St. Petersburg, FL 33701-5016, USA*

Accepted 14 July 2004

Abstract

A micronektonic and macrozooplanktonic community was sampled with midwater trawls in the Croker Passage, vic. Antarctic Peninsula. Species composition suggested the area was a faunal transition zone between oceanic and nearshore communities. In a comparison between the study area and two oceanic areas, four of the top five numerically dominant species were identical (*Euphausia superba, Salpa thompsoni, Thysanoessa macrura* and *Sagitta gazellae*). In the nearshore region a mysid (*Antarctomysis ohlinii*) replaced the oceanic chaetognath *Eukrohnia hamata* in numerical ranking. *E. superba* was primarily responsible for the much higher nearshore biomass values when compared with those of oceanic regions (52.6 vs 2.4 3.1 g DM/m^2). The ctenophore *Callianira antarctica*, the mysid *A. ohlinii*, and the pelagic notothenid fish *Pleuragramma antarcticum* were important neritic biomass species. Some oceanic species, notably *S. thompsoni* and the mesopelagic fish *Electrona antarctica*, were also important contributors to total micronektonic biomass. Fish predation by *P. antarcticum* and *E. antarctica* on *E. superba* (assuming constant fish and krill populations through the season that was sampled, the austral fall (90 d), and using our daily consumption values) is estimated at 2.5% and 2.9% of the total krill numbers, respectively, mostly on the juvenile segment of the population.

Krill densities vary considerably in time and space, while available data suggest that pelagic fishes show less seasonal and spatial change. The most likely explanation for those observations is that the fishes are reliably more vulnerable to sampling gear than krill, but it also implies a consistent low level of fish predation on krill throughout the year, particularly on juveniles.
© 2004 Elsevier Ltd. All rights reserved.

*Corresponding author.

0967-0645/$ - see front matter © 2004 Elsevier Ltd. All rights reserved.
doi:10.1016/j.dsr2.2004.07.004

1. Introduction

Descriptions of Antarctic pelagic ecosystem ecology have focused on the shallow-dwelling krill, *Euphausia superba* (e.g. El-Sayed, 1971; Ross et al., 1996; Quetin et al., 1996; Hofmann et al., 1998; Lascara et al., 1999), largely due to its overwhelming dominance in nearshore communities (Hopkins, 1985a, b) and clear importance to the nutrition of birds and mammals (Ainley and DeMaster, 1990; Cherel and Kooyman, 1998; Ainley, 2002). Less is known about Antarctic pelagic communities considered as a whole, particularly the interactions of krill and their micronektonic predators, the relative abundance of macrozooplankton other than krill, and the importance of deeper-living or vertically migrating species (Robison, 2003). Deeper-living macrozooplankton and micronekton contribute substantially to the biomass of open-ocean Antarctic systems, sometimes exceeding krill in abundance (Lancraft et al., 1989, 1991; Pakhomov et al., 1996). Despite big differences in the relative importance of krill and other macrozooplankton from place to place in the seasonal sea-ice zone, regional comparisons of micronekton and macrozooplankton abundance are still quite rare (Piatkowski, 1985a, b; Hopkins and Torres, 1988; Lancraft et al., 1989, 1991; Hopkins et al., 1993 a, b; Pakhomov et al., 1996).

Whether offshore or in continental shelf waters, pelagic species form an important trophic link between apex predators and herbivores. The bottom fauna is inaccessible to many diving species on the Antarctic continental shelf because its typical 500 m depth (Eastman, 1993) is beyond their reach. Thus, because of their pelagic distribution, micronekton are an important source of food for flighted seabirds (Ainley et al., 1991) and shallow diving penguins such as the Gentoo, Adelie, and Chinstrap (Bengtson et al., 1993; Williams, 1995; Ainley, 2002). They also form a significant part of the diet of deeper divers such as emperor penguins (Cherel and Kooyman, 1998), and crabeater, Ross, Weddell and leopard seals (Øritsland, 1977; Lowry et al., 1988).

The present study investigated the micronekton and macrozooplankton community in the upper 1000 m of a nearshore pelagic Antarctic environment to provide a basis for comparisons with offshore systems and to give information on accessibility of micronekton to upper trophic levels. In turn, the study considers fish as intermediate trophic level predators to estimate predation pressure of fishes on krill.

2. Materials and methods

Micronekton and macrozooplankton were sampled during the austral fall (March and April 1983) using a modified opening–closing Tucker trawl off R/V HERO. The sampling site was the island-bound Croker Passage, an area consisting of two deep-water basins (maximum depth = 1200 m) in the Palmer Archipelago just north of Anvers Island, Antarctica (Fig. 1). Brash ice was frequently encountered but most sampling was conducted in open waters.

The trawl had a 4.8 m^2 effective mouth opening and a 6 mm (1.1 cm stretched) mesh (Hopkins, 1985b). It was opened and closed with clock-actuated release mechanisms (Davies and Barham, 1969) with filtration volumes monitored by dial-type flowmeters only when the trawl was open. Depth was estimated by wire angle triangulation during the tow and documented by attached time–depth recorders. While depth control was variable due to unavoidable changes in ship speed, only discrete zone tows were used in this study to better characterize patterns of vertical distribution, biomass, and abundance. Trawling was at speeds between 2 and 3 knots.

Twenty-one discrete tows (12 days and 9 nights) filtered a total of 520 477 m^3 of water, with roughly half being filtered in each diel period. Nearly the entire water column was sampled as 1000 m was the maximum depth of towing (see Table 1 for collection information). The collections were first fixed in a buffered 10% formaldehyde solution and then stored in the laboratory in a 50% isopropyl alcohol solution.

Except for one collection (tow 21) each entire sample was sorted with all micronekton and macrozooplankton (organisms greater than 20 mm) identified, enumerated, and their wet

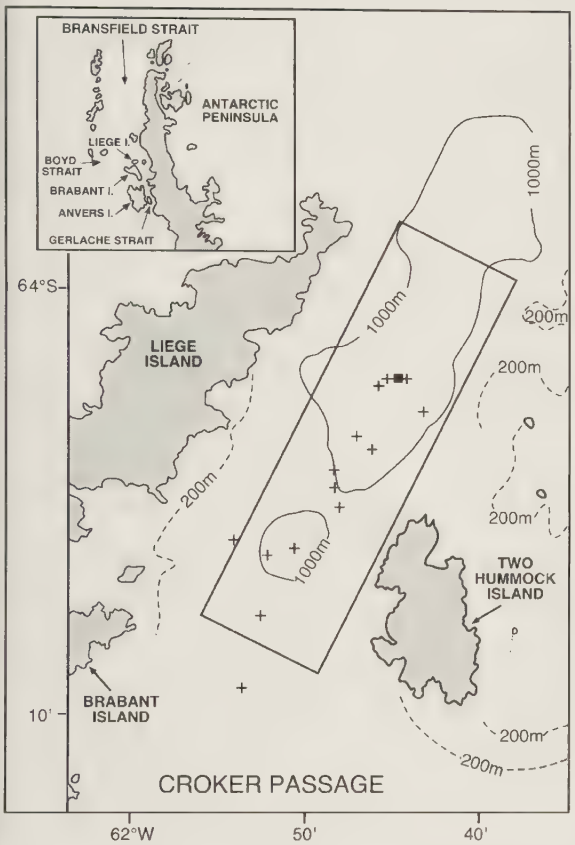

Fig. 1. The study area in Croker Passage. All trawling took place within the rectangle shown. + = XBT profiles. Solid square represents salinity station (8 April 1983).

masses (WM) recorded (±0.001 g). Tow 21 was a large-volume (16 l) shallow night tow consisting primarily of *E. superba*, so a 2-l subsample of the tow was treated as above and then prorated to whole sample values. Because ctenophores do not preserve well, they were counted after each tow, their volume measured, and then were discarded. Tentative identification of the ctenophores indicated that most were *Callianira antarctica* with a few *Beroe* sp. making up the remainder. Some organisms were removed, prior to weighing, for a food web study (Hopkins, 1985a); the weights of these were estimated with length–mass curves (Lancraft, unpubl. data). Wet mass (WM) was converted to dry mass (DM) by subtracting water content. The latter was estimated by drying specimens at 60 °C to constant mass (Donnelly et al., 1990).

For every tow, the biomass/m^3 of each taxon was calculated by dividing its biomass in the sample by the volume of water filtered in that tow. Biomass/m^3 was multiplied by the depth range (in meters) of that tow to yield an integrated biomass over the depth range of the tow. Integrated biomass values for 200 and 1000 m depth strata (mg WM/m^2 and mg DM/m^2) were calculated by summing integrated biomass values for all tows down to those depths (Lancraft et al., 1989). When tows overlapped, a mean was taken for the overlapping strata. Integrated abundance (number/m^2) values were calculated in an identical manner. Daytime catch values were generally lower than those for nighttime catches (Table 2; Fig. 2A and B), suggesting net avoidance was a bias. Nighttime values were therefore used as the best indicators of abundance and biomass.

To estimate the impact of fish predation on *E. superba*, stomach contents were examined in a range of size classes of *Electrona antarctica* and *Pleuragramma antarcticum*, and the number and lengths of krill in the gut contents were noted. While net feeding may be a bias in the determination of pelagic fish diets (Lancraft and Robison, 1980), only krill with obvious signs of digestion were counted in this study, thereby eliminating krill potentially consumed in the trawl cod end. The size of prey and the degree of digestion indicated that most of the fish fed daily. Predation pressure (number krill consumed/day/100 m^2) was estimated for each fish size class by multiplying the number of krill consumed per fish by the abundance of that size class in the total fish population. All size classes for each fish species were then summed to determine the total predation impact by that species on the krill population. Krill biomass consumed (mg DM/day/100 m^2) was estimated by multiplying average lengths of krill prey by their dry masses and treating those values like the abundances. Four hundred specimens of *E. superba* were randomly selected from a variety of tows and measured to determine the spectrum of prey lengths available to fish predation. All krill length measurements were from the tip of the rostrum to the end of the telson, slightly different

Table 1
Data on trawl tows taken during March–April 1983 in Croker Passage

Tow no.	Local time	Date (mm.dd.yy)	Depth (m)	Vol. fil. (m^3)
9	1352–1552 (D)	3.15.83	450–850	38 579
10	2010–2225 (N)	3.15.83	550–820	25 771
11	0210–0430 (N)	3.16.83	630–820	35 744
12	1501–1711 (D)	3.16.83	750–820	35 063
13	2237–0047 (N)	3.16–17.83	775–1000	32 010
14	0406–0551 (N)	3.17.83	300–400	26 362
15	1546–1731 (D)	3.17.83	230–480	25 495
16	2133–2238 (N)	3.18.83	130–200	25 115
17	0958–1024 (D)	4.8.83	0–100	15 114
18	0930–1045 (D)	4.8.83	100–200	21 628
19	1220–1335 (D)	4.8.83	200–300	22 154
20	1558–1708 (D)	4.8.83	340–550	19 460
21	2120–2150 (N)	4.8.83	0–100	8556
22	2300–0013 (N)	4.9.83	200–300	31 142
25	2203–2313 (N)	4.9.83	450–550	18 851
26	0927–1037 (D)	4.10.83	350–550	28 813
27	1237–1347 (D)	4.10.83	480–570	22 009
28	1602–1712 (D)	4.10.83	600–770	18 272
29	2157–2307 (N)	4.10–11.83	550–650	30 178
30	1046–1156 (D)	4.11.83	800–1000	18 365
31	1409–1519 (D)	4.11.83	380–470	21 796
Total day tows				28 6748
Total night tows				23 3729
Total				52 0477

D = day; N = night.

from the total length used by Mauchline and Fisher (1969), but used several times previously in the literature (Fraser, 1936; Einarsson, 1945; Nemoto, 1957). Regressions of size vs. dry mass for *E. superba*, *E. antarctica*, and *P. antarcticum* are reported in Table 4.

3. Results

3.1. Species composition and vertical distribution

Forty-three species of micronekton and macrozooplankton were collected in the Croker Passage (Table 2) during 1983. Single specimens of two other species of fish (*Bathylagus antarcticus* and *Electrona carlsbergi*) (Fig. 3) were collected by trawl tows in a previous cruise to the Croker Passage study area during 1982, bringing fish diversity to a total of 11 species. Except for the notothenid *P. antarcticum*, the liparid *Careproctus georgianus*, and the bathydraconid *Cryodraco antarcticus*, all of the fish were mesopelagic oceanic species. Gammarid amphipods were the second most diverse group with a total of ten species. Cephalopods, because of their avoidance capabilities, were probably under-represented. The mouth area of the net employed during the study was small (4.8 m^2) relative to the most commonly used midwater trawls (RMT-8, 8 m^2, Mother Tucker trawl, 9 m^2, MOC 10, 10 m^2) but was very effective for its size. Comparison of fish lengths with those in other studies (Lancraft et al., 1989, 1991; Pakhomov et al., 1996) showed that the smaller net captured the larger size classes quite well and total biomasses were similar to or greater than those from other reports.

Most of the fauna resided fairly deeply, with abundance peaks centering below 200 m. *E. superba* was a notable exception in that it was

Table 2
Taxonomic composition and diel vertical distribution of Croker passage micronekton and macrozooplankton

Species	*n*	Day range (Peak)	*n*	Night range (Peak)
Fish				
Electrona antarctica	65	230–850 (380–850)	30	130–820(200–400)
Electrona carlsbergi[a]				
Pleuragramma antarcticum	31	230–1000 (500–1000)	48	130–1000(130–200)
Protomyctophum bolini	2	230–480		
Gymnoscopelus nicholsi	1	450–850	2	130–650
Notolepis coatsi			1	450–550
Cyclothone microdon			3	775–1000
Bathylagus antarcticus[a]				
Melanostigma gelatinosum[a]				
Careproctus georgianus[a]				
Cryodraco antarcticus[a]				
Crustaceans				
Euphausia superba	1001	0–850 (0–100)	64787	0–1000(0–100)
Thysanoessa macrura	353	0–1000 (200–1000)	585	130–1000(200–650)
Cyphocaris richardi	108	0–1000 (450–850)	116	130–1000(210–550)
Eurythenes gryllus	10	800–1000	1	775–1000
Eurythenes obesus	1	750–820	1	550–650
Eusirus propeperdentatus	63	230–1000 (350–850)	59	300–1000 (300–820)
Eusirus perdentatus			4	200–300
Eusirus microps	9	230–570	10	130–650
Orchomene plebs	36	230–1000 (230–570)	46	130–1000 (300–400)
Orchomene rossi	11	0–550	20	130–650 (130–200)
Epimeriella macronyx	57	230–850 (450–850)	3	450–650
Parandania boecki	2	750–820	5	775–1000
Themisto gaudichaudi	2	0–300	8	0–300 (0–100)
Pasiphaea scotiae			2	550–650
Antarctomysis ohlinii	866	230–1000 (750–1000)	1201	210–1000 (660–1000)
Antarctomysis maxima			1	550–820
Dactlyamblyops hodgsoni	1	800–1000	5	630–1000
Molluscs				
Galiteuthis glacialis	1	380–470	3	450–1000
Brachioteuthis picta			1	130–200
Alluroteuthis antarcticus			2	550–820
Psychroteuthis glacialis	1	350–550	1	450–550
Macrozooplankton				
Sagitta gazellae	931	0–1000 (860–1000)	972	130–1000 (300–1000)
Sagitta marri	54	450–1000 (750–1000)	48	550–1000 (630–1000)
Eukrohnia hamata	457	200–1000	446	200–1000
Tomopteris carpenteri	54	0–850 (240–470)	29	130–650 (300–400)
Tomopteris septentrionalis	1	450–850		
Salpa thompsoni	4377	0–1000 (200–1000)	3536	0–1000 (0–650)
Callianira Antarctica	178	230–1000	159	0–1000
Atolla wyvillei	1	600–770	4	550–1000
Periphylla periphylla	2	750–1000	2	300–1000
Calycopsis borchgrevinki	16	340–850 (340–550)	5	300–820
Diphyes Antarctica	111	100–850(100–300)	95	130–820 (200–400)

[a]These species were collected in tows not listed in Table 1.

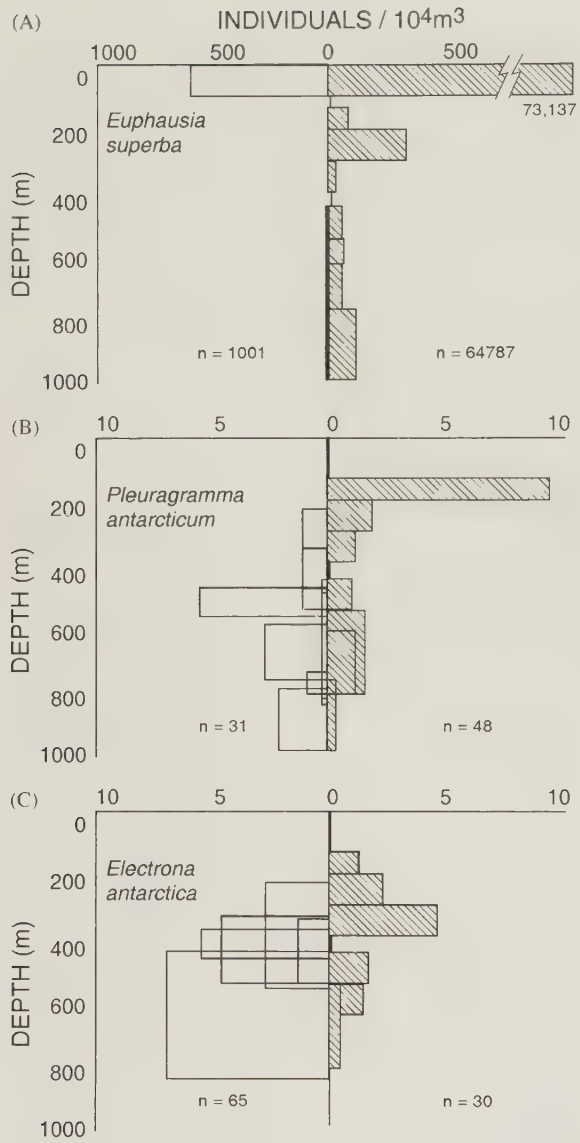

Fig. 2. Diel depth abundance patterns (individuals/10^4 m^3) of *Euphausia superba* (A) and its major fish predators *P. antarcticum* (B) and *Electrona antarctica* (C) in the Croker Passage. Shaded bars are night abundances, n = total number of individuals in day or night samples.

most abundant in the upper 100 m (Fig. 2A). Most of the micronekton and all of the macrozooplankton had wide vertical depth distributions, which, for a few, broadened slightly during the day. Notable deep-living non-migrators were *Thysanoessa macrura* and *Antarctomysis ohlinii*.

The only species exhibiting strong diel vertical migration patterns were the dominant fishes (*P. antarcticum* and *E. antarctica*, Fig. 2B and C). During the night their overall vertical distributions were not significantly different (Kolmogorov–Smirnov test, $p > .05$). However, the nighttime abundance peaks of the fish were separated, with *P. antarcticum* (130–200 m) being more shallowly distributed than *E. antarctica* (200–400 m). The fish also had non-overlapping distributions during the day (Kolmogorov–Smirnov test, $p < .001$). The gammarid amphipod, *Cyphocaris richardi*, and the only tunicate found in the study (*S. thompsoni*) also showed weak diel vertical migration patterns.

3.2. Abundance and biomass

E. superba was the most abundant species in Croker Passage, with an integrated abundance of 787.9 individuals for every square meter of surface (Table 3) in the upper 200 m. Below this depth *E. superba* abundance dropped off precipitously to 8.1/m^2 (difference between integrated 0–200 m and 0–1000 m values), for a total of 796.0/m^2 in the entire sampled water column (0–1000 m). The second most abundant species, *S. thompsoni*, was more evenly distributed with 12.7 individuals/m^2 in the upper 200 m and 7.3/m^2 residing below 200 m, totaling 20.0/m^2 for the 0–1000 m range. The next four numerically subdominant species (*A. ohlinii*, *Sagitta gazellae*, *T. macrura*, and *Eukrohnia hamata*, in order of descending abundance) were all most abundant below 200 m. *E. superba* and the other five species made up 99.5% of the total micronekton and macrozooplankton abundance. *E. superba* alone accounted for 95.5% of all numbers. With *E. superba* excluded, the other five dominant species accounted for 89.3% of the total, while with *E. superba* they account for only 4.0%. This underscores how strongly *E. superba* dominated the Croker Passage community.

Total nighttime dry biomass (Table 3) in the epipelagic zone (0–200 m) was high (48 791 mg DM/m^2) due to the intense concentration of *E. superba* in that zone. The night time dry biomass from the surface to 1000 m for all species was 52 606 mg DM/m^2. Without *E. superba*, biomass values for the 0–200 m and 0–1000 m zones

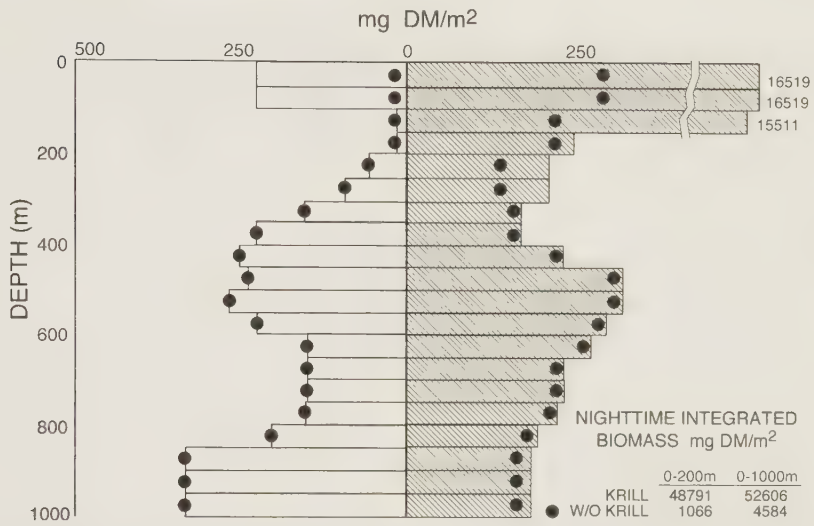

Fig. 3. Croker Passage community biomass (mg DM/m^2), 0–1000 m. Shaded bars are biomasses determined from night tows. Filled circles represent biomass in depth stratum without *Euphausia superba*.

decreased to 1066 and 4584 mg DM/m^2, respectively (Fig. 4). Dense concentrations were evident in the 0–200 m zone on the ship's fathometer during the day as well but our daytime catches were reduced because of gear avoidance.

E. superba was the biomass dominant in the 0–1000 m column, accounting for 91.3% of the total dry mass with 48 022 mg DM/m^2 (Table 3). Ctenophores (mostly *C. antarctica*), *A. ohlinii, S. thompsoni, P. antarcticum*, and *E. antarctica* were the subdominants, in order of decreasing biomass. Wet mass (WM) biomass patterns varied only in the reversal of the ranking of *A. ohlinii* and *S. thompsoni* because of the latter's greater water content.

While *E. superba* dominated the upper 200 m, its dry biomass below 200 m (297 mg DW/m^2; 0–1000 m value minus 0–200 m value) was exceeded by that of the ctenophores (1597 mg DM/m^2), *A. ohlinii* (746 mg DM/m^2) and *P. antarcticum* (307 mg DM/m^2) and was only slightly above that of *E. antarctica* (282 mg DM/m^2) and *S. thompsoni* (223 mg DM/m^2).

3.3. Predation

Stomach contents from a total of 133 specimens of *E. antarctica* and 37 specimens of *P. antarcticum* were examined for krill prey. The two species consumed similar numbers and sizes of krill (Table 4). Average number of krill/stomach (varying from 0.7 to 2.6) increased with fish length. Mean krill prey size ranged from 24.2 to 28.5 mm with the average size also increasing with larger fish. Maximum abundances of krill taken from the trawl were in the 30–32 mm size fraction, with the average being 31.1 mm (Fig. 4). The average size of krill consumed by the fishes was smaller than the mean size of trawl-caught krill, suggesting a positive selection for smaller krill (Fig. 4). The estimated daily consumption of total krill numbers by *E. antarctica* was 0.027%, which translates to 0.017% of the total krill biomass. *P. antarcticum* captured slightly larger krill, ingesting a slightly larger fraction of krill population numbers (0.033%) and higher biomass than *E. antarctica* (0.026%, Table 5).

4. Discussion

The Croker Passage species list was that of a modified open-ocean community (Lancraft et al., 1989, 1991) mixed with nearshore species. Fish diversity was low in contrast to the oceanic Antarctic systems like the Scotia Sea and Weddell

Table 3
Integrated biomass and numerical abundance of Croker Passage micronekton and macrozooplankton

Species	0–200 m			0–1000 m		
	mg DM/m^2	mg WM/m^2	no./1000 m^2	mg DM/m^2	mg WM/m^2	no./1000 m^2
Pisces						
Electrona antarctica	28	91	11	310	990	122
Pleuragramma antarcticum	223	1190	88	530	2834	175
Protomyctophum bolini				2	9	9
Gymnoscopelus nicholsi	16	81	4	26	128	5
Notolepis coatsi				<1	1	6
Cyclothone microdon				1	4	6
Subtotal	267	1362		869	3966	
Euphausiacea						
Euphausia superba	47725	174814	787885	48022	175905	796014
Thysanoessa macrura	24	82	257	75	252	2209
Subtotal	47749	174896		48097	176157	
Amphipoda						
Cyphocaris richardi	7	28	48	87	344	465
Eurythenes gryllus				31	121	6
Eurythenes obesus				<1	1	2
Eusirus propeperdentatus				49	235	262
Eusirus perdentatus				3	15	13
Eusirus microps	<1	2	4	5	26	38
Orchomene plebs	1	2	7	21	56	194
Orchomene rossi	11	28	48	15	40	63
Epimeriella macronyx				<1	3	10
Parandania boecki				14	44	30
Themisto gaudichaudi	1	6	58	1	7	64
Subtotal	20	66		226	892	
Mysidacea						
Antarctomysis ohlinii				746	3720	5053
Antarctomysis maxima				3	16	4
Dactlyamblyops hodgsoni				<1	3	27
Subtotal				749	3739	
Thaliacea						
Salpa thompsoni	346	8450	12665	569	13887	20014
Coelenterata						
Ctenophores	404	4163	220	2001	20627	762
Atolla wyvillei				11	260	16
Periphylla periphylla				5	267	11
Calycopsis borchgrevinki				2	34	20
Diphyes antarctica	<1	21	48	1	74	353
Subtotal	404	4184		2020	21262	
Others						
Galiteuthis glacialis				16	136	17
Brachioteuthis picta	4	34	4	4	34	4
Alluroteuthis antarcticus				15	131	10
Psychroteuthis glacialis				1	11	6
Sagitta gazellae	<1	9	29	33	678	4112

Table 3 (*continued*)

Species	0–200 m			0–1000 m		
	mg DM/m^2	mg WM/m^2	no./1000 m^2	mg DM/m^2	mg WM/m^2	no./1000 m^2
Sagitta marri				<1	4	186
Eukrohnia hamata				2	37	2074
Tomopteris carpenteri	1	4	7	5	35	125
Subtotal	5	47		76	1066	
Total	48791	189005		52606	220969	

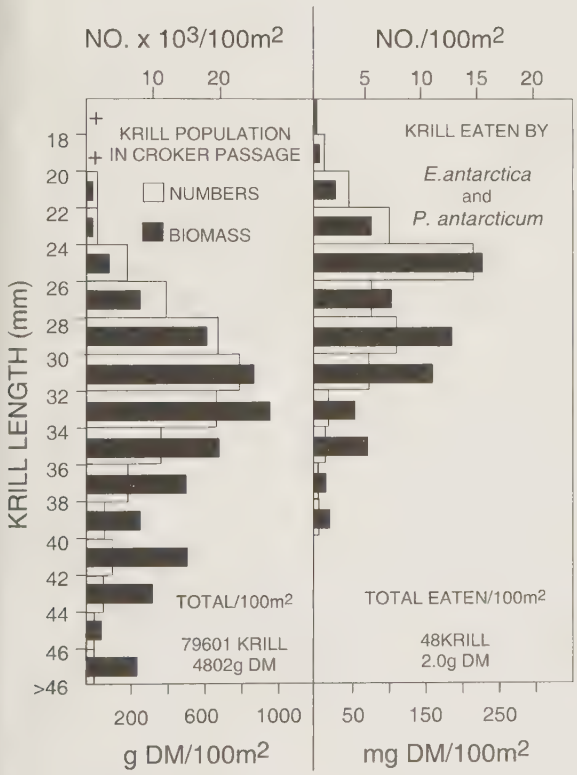

Fig. 4. Comparison of abundance, biomass, and length composition of the total Croker Passage *Euphausia superba* population and the *E. superba* eaten by fish.

Sea (Lancraft et al., 1989, 1991). Mesopelagic species like *B. antarcticus*, myctophids other than *E. antarctica,* and large mesopelagic predatory fish were notably absent or occurred in reduced numbers in Croker Passage. *P. antarcticum*, an endemic pelagic nototheniid, replaced the mesopelagic species in abundance in the nearshore environment, a pattern also observed by Slosarczyk and Cielniaszek (1985) over the Antarctic Peninsula shelf, Williams (1985) in Prydz Bay, and Dewitt (1970) in the Ross Sea.

Restricted circulation from the Bellingshausen Sea over the continental shelf into Croker Passage, as indicated by its lack of a well-developed Upper Circumpolar Deep Water zone (temperatures $>1.5\,^{\circ}C$ at a depth of 200 m, Fig. 5), a water mass typically found in the Bellingshausen Sea and Bransfield Strait (Grelowski and Tokarczyk, 1985; Smith et al., 1999), may exclude the deeper-living oceanic fauna from the Croker Passage. *A. ohlinii*, a robust pelagic mysid completely absent from the mesopelagic zone of oceanic areas (Lancraft et al., 1989, 1991),was abundant in the Croker Passage, suggesting a strong neritic influence. The high diversity and, in some cases, high abundance (*Eusirus propeperdentatus*) of benthopelagic gammarid amphipods also registered the influence of land on the Croker Passage community.

A regional biomass comparison of Antarctic pelagic ecosystems (this study and Lancraft et al., 1989) shows that the most obvious difference was the overwhelming dominance of *E. superba* in the nearshore area (Table 6). Ctenophores (*C. antarctica*) also were more important in Croker Passage, decreasing in the blue water study areas of the Scotia and Weddell Seas. *A. ohlinii* and *P. antarcticum*, both nearshore species, also greatly increased the overall biomass of Croker Passage.

The top five most abundant species in all three regions are the same except for the replacement of

Table 4
Diets of dominant fishes, with comparisons to published information

Fishes			*Euphausia superba*			Daily ration		
Size (*n*)	Size at midrange (mm)	DM (g) at midrange	No./stom. mean (range)	Size (mm) mean (range)	DM (g) in stomach	Daily ration (% DM) This study	Daily ration (% DM) Pakhomov et al. (1996)	Daily ration (% DM) Rowedder (1979)
Electrona antarctica								
60–69 (11)	65	1.190	1.4 (0–2)	24.2 (20–27)	0.045	3.752		
70–79 (45)	75	1.947	1.4 (0–5)	24.5 (19–33)	0.046	2.382		
80–89 (50)	85	2.993	2.2 (0–8)	26.0 (17–39)	0.087	2.916		
90–99 (27)	95	4.387	1.7 (0–5)	26.3 (19–35)	0.070	1.592		
Total (133)		Mean (range)	1.7 (0–8)	25.3 (17–39)	0.062	2.660	1.86 (0.46–3.45)	5
Pleuragramma antarcticum								
<100 (7)	90	1.062	0.7 (0–3)	26.0 (25–27)	0.028	2.616		
101–125 (10)	113	2.323	0.7 (0–4)	27.8 (21–32)	0.034	1.465		
126–150 (10)	139	4.738	2.6 (0–6)	28.0 (15–39)	0.129	2.726		
>150 (10)	160	7.689	2.4 (0–13)	28.5 (17–34)	0.126	1.636		
Total (37)		Mean (range)	1.6 (0 13)	27.6 (15–39)	0.076	2.111	no data	no data

Dry mass of *Electrona antarctica* computed from the length mass regression: y (mass, g) = 0.0000007 × (standard length, mm)$^{3.437}$, $r^2 = 0.954$, $n = 222$. Dry mass of *Pleuragramma antarcticum* computed from the length mass regression: y (mass, g) = 0.0000002 × (standard length, mm)$^{3.441}$, $r^2 = 0.977$, $n = 46$. Dry mass of *Euphausia superba* computed from the length mass regression: y (mass,g) = 0.000006 × (length, mm)$^{3.037}$, $r^2 = 0.978$, $n = 480$.

Table 5
Predation on krill by dominant fishes

Fishes			*Euphausia superba*		
Size (*n*)	% Abund.	No.eaten/d (/100 m^2)	DM eaten/d (g DM/100 m^2)	% total krill population eaten/d	
				(no./100 m^2)	(g DM/100 m^2)
Electrona antarctica					
60–69 (11)	8.42	1.4	0.045		
70–79 (45)	31.58	5.4	0.179		
80–89 (50)	42.11	11.3	0.448		
90–99 (27)	17.89	3.7	0.152		
Total (133)	100	21.8	0.796	0.027	0.017
Pleuragramma antarcticum					
<100 (7)	15.38	1.9	0.075		
101–125 (10)	41.03	5	0.243		
126–150 (10)	19.23	8.8	0.437		
>150 (10)	24.36	10.2	0.535		
Total (37)	100	25.9	1.232	0.033	0.026

Estimates of krill removed from the total population (per 100 m^2) by *Electrona antarctica* and *Pleuragramma antarcticum*. Data on total krill numbers from Fig. 4, masses calculated using regressions in legend of Table 4.

the chaetognath *E. hamata* with the mysid *A. ohlinii* in the Croker Passage (Table 7). The general uniformity of important species in Croker Passage when compared with offshore regions and the notable differences in species composition support the contention that the Croker Passage area is a transition zone between oceanic mesopelagic and nearshore pelagic fauna.

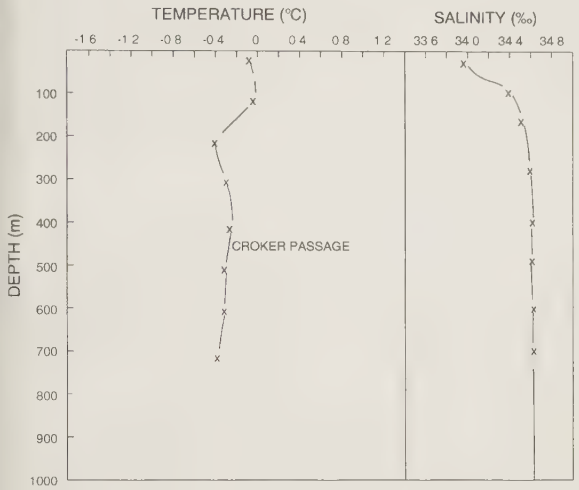

Fig. 5. Hydrographic data from the Croker Passage study area (Hopkins 1985b). Note temperatures below 0 °C at depths of 200 m and greater.

Many estimates of krill biomass in the upper 200 m have been taken from areas north of the study site using nets (Piatkowski, 1985a, b; Siegel, 1986; Worner, 1979, to name only a few) as well as acoustical methods (Rakusa-Suszczewski, 1982; Macaulay et al., 1984; Kalinowski et al., 1985). Our mean abundance of 788 individuals/m^2 falls into the range of previous Antarctic Peninsula studies (Piatkowski, 1985a; Worner, 1979) while our net captured wet biomass values (175 g WM/m^2) are moderate compared to acoustical biomass estimates (Rakusa–Suszczewski, 1982; Macaulay et al., 1984; Kalinowski et al., 1985; Lascara et al., 1999). Using a separate set of oblique tows taken during the same cruise as this study, Hopkins (1985a) estimated the *E. superba* biomass for 0–1000 m at 55 g DM/m^2, a value quite close to ours (48 g DM/m^2) considering the differences in methodology.

Table 6
Regional comparison of biomass (mg DM/m^2) dominants in the 0–1000 m range

Species	Scotia Sea Spring '83	Weddell Sea Fall '86	Croker Passage Fall '83
Euphausiacea			
Euphausia superba	1077	667	48 022
Thysanoessa macrura	15	24	75
Subtotal	1092	691	48 097
Thaliacea			
Salpa thompsoni	1156	159	569
Pisces			
Electrona antarctica	314	273	310
Gymnoscopelus nicholsi	0	0	26
Gymnoscopelus braueri	128	86	0
Gymnoscopelus opisthopterus	81	304	0
Bathylagus antarcticus	216	283	0
Pleuragramma antarcticum	0	0	530
Subtotal	739	946	866
Ctenophora	<1	99	2001
Mysidacea	<1	<1	749
Amphipoda	16	6	226
Others	129	476	98
TOTAL	3132	2377	52 606

Table 7
Regional comparison of top five numerically dominant species (number/m^2)

Scotia Sea	Weddell Sea	Croker Passage
Salpa thompsoni (145.33)	*Euphausia superba* (6.05)	*Euphausia superba* (796.01)
Euphausia superba (4.34)	*Salpa thompsoni* (5.62)	*Salpa thompsoni* (20.01)
Sagitta gazellae (1.88)	*Eukrohnia hamata* (2.73)	*Antarctomysis ohlinii* (5.05)
Thysanoessa macrura (0.91)	*Sagitta gazellae* (2.08)	*Sagitta gazellae* (4.11)
Eukrohnia hamata (0.85)	*Thysanoessa macrura* (1.31)	*Thysanoessa macrura* (2.21)

With few exceptions, during the austral fall in the Croker Passage macrozooplankton and micronekton species were primarily distributed below 200 m as were their zooplankton prey, much of which had migrated to typical winter depths (Hopkins 1985a, b). Of the abundant species, only *E. superba* and, at night, the vertically migrating taxa (*S. thompsoni, E. antarctica,* and *P. antarcticum*) were abundant above 200 m (Table 2). *E. superba* and *S. thompsoni* inhabited the surface waters (salps only at night) to feed mainly on phytoplankton (Hopkins 1985b) while the fish, living just below the krill, are important nocturnal predators on *E. superba* (Dewitt and Hopkins, 1977; Hopkins, 1985a). Kock (1987) suggested that mesopelagic fish, contrary to earlier beliefs (e.g., Laws, 1985), were more important krill predators than cephalopods.

Our values for daily ration of the two dominant fishes agree quite well with numbers available from other studies (Table 4). Both *Electrona* and *Pleuragramma* had mean daily ingestion rates of between 2% and 3% of dry mass (2.66% and 2.11% respectively), whereas Pakhomov et al. (1996) estimated 1.86% for *Electrona*, and Rowedder (1979) estimated 5% for *Electrona* during the summer. An energy budget constructed for the third year of life of *Electrona*, using growth data based on microincremental aging techniques and published respiration measurements, showed excellent agreement (87%) between energy expenditures and an ingestion rate of 2.44% dry mass (Greely et al., 1999), further corroborating the numbers in Table 4. Rowedder (1979) numbers are likely most typical of maximal summer ingestion rates. Both Rowedder (1979) and the present study showed an overwhelming dominance of krill in the diet of fishes, whereas the fishes of Pakhomov et al. (1996) showed a preference for Calanoid copepods. Fishes likely take krill when they are available, switching to copepods when krill are more scarce.

Previous estimates of pelagic fish predation on krill (Kock, 1985; Laws, 1985), based on feeding through half the year, suggest that 15% of the krill population is annually consumed by fish. If winter feeding intensity is near that of summer feeding, then predation impact would be somewhat higher. Information on winter feeding rates is scarce and contradictory, with some indicating slower winter feeding for nototheniids (Chekunova and Naumov, 1982; Linkowski et al., 1983) and mesopelagic fish (Lancraft et al., 1991) while others observed active winter–spring feeding by nototheniids (Daniels, 1982; Tarverdiyeva, 1972). For the present study, assuming constant fish and krill populations through the season that was sampled, the austral fall (90 d), and using our daily consumption values, *E. antarctica* and *P. antarcticum* would ingest 2.5% and 2.9% of the total krill numbers, respectively, just during the fall season. Most of the predation was only on the juvenile segment of the population.

Krill densities vary considerably in time and space (Nast, 1986; Lascara et al., 1999), while available data suggest that pelagic fishes show less seasonal and spatial change (Table 5; Lancraft et al., 1991). What is most likely is that the fishes are reliably more vulnerable to sampling gear than krill, but it also implies a consistent low level of predation pressure by fishes throughout the year, particularly on juvenile krill.

Acknowledgments

Special thanks go to Captain Lenie and the crew of R/V HERO. Without his extensive knowledge of the waters of the Antarctic Peninsula and the crew's unflagging help, this study would not have been possible. This study was supported by NSF Grants DPP-8107510 to T.L. Hopkins and B.H. Robison, DPP-8420562 to T.L. Hopkins and J.J Torres, and OPP 9910100 to J.J. Torres.

References

Ainley, D.G., 2002. The Adelie Penguin. Columbia University Press, New York.

Ainley, D.G., DeMaster, D.P., 1990. The upper trophic levels in polar marine ecosystems. In: Smith, W.O. (Ed.), Polar Oceanography. Part B. Chemistry, Biology, and Geology. Academic Press, San Diego, pp. 599–630.

Ainley, D.G., Fraser, W.R., Smith, W.O., Hopkins, T.L., Torres, J.J., 1991. The structure of upper level pelagic food webs in the Antarctic: effect of phytoplankton distribution. Journal of Marine Systems 2, 111 122.

Bengtson, J.L., Croll, D.A., Goebel, M.E., 1993. Diving behavior of chinstrap penguins at Seal Island. Antarctic Science 5, 9–15.

Chekunova, V.J., Naumov, A.G., 1982. Energy metabolism and food requirements of the marbled Notothenia, Notothenia rossii marmorata. Voprosy Ikthiologie 22, 294–302.

Cherel, Y., Kooyman, G.L., 1998. Food of emperor penguins (*Aptenodytes forsteri*) in the western Ross Sea, Antarctica. Marine Biology 130, 335–344.

Daniels, R.A., 1982. Feeding ecology of some fishes of the Antarctic Peninsula. Fishery Bulletin US 80, 575–588.

Davies, T.E., Barham, E.G., 1969. The Tucker opening-closing micronekton net and its performance in a study of the deep scattering layer. Marine Biology 2, 127–131.

DeWitt, H.H., 1970. The character of the midwater fish fauna of the Ross Sea, Antarctica. In: Holdgate, M.W. (Ed.), Antarctic Ecology, vol. 1. Academic Press, London, pp. 305 -314.

DeWitt, H.H., Hopkins, T.L., 1977. Aspects of the diet of the Antarctic silverfish, Pleuragramma antarcticum. In: Llano, G.A. (Ed.), Adaptations within Antarctic Ecosystems. Smithsonian Institution, Washington, D.C., pp. 557–568.

Donnelly, J., Torres, J.J., Hopkins, T.L., Lancraft, T.M., 1990. Proximate composition of Antarctic mesopelagic fishes. Marine Biology 106, 13–23.

Eastman, J.T., 1993. Antarctic Fish Biology: Evolution in a unique environment. Academic Press, San Diego.

Einarsson, H., 1945. Euphausiacea I. North Atlantic species. Dana Reports 27, 1–85.

El-Sayed, S.Z., 1971. Dynamics of trophic relations in the Southern Ocean. In: Quam, O. (Ed.), Research in the Antarctic. American Association for the Advancement of Science, Washington, D.C., pp. 73–91.

Fraser, F.C., 1936. On the development and distribution of the younger stages of krill (*Euphausia superba*). Discovery Reports 14, 3–192.

Greely, T.M., Gartner, J.V., Torres, J.J., 1999. Age and growth of Electrona antarctica (Pisces: Myctophidae), the dominant mesopelagic fish of the Southern Ocean. Marine Biology 133, 145–158.

Grelowski, A., Tokarczyk, R., 1985. Hydrological conditions in the region of the Bransfield Strait and southern part of the Drake Passage in the period from December 10, 1983 to January 8, 1984. Polish Polar Research 6, 31–41.

Hofmann, E.E., Klinck, J.M., Locarnini, R.A., Fach, B., Murphy, E., 1998. Krill transport in the Scotia Sea and environs. Antarctic Science 10, 406–415.

Hopkins, T.L., 1985a. Food web of an Antarctic midwater ecosystem. Marine Biology 89, 197–212.

Hopkins, T.L., 1985b. The zooplankton community of Croker Passage, Antarctic Peninsula. Polar Biology 4, 161–170.

Hopkins, T.L., Ainley, D.G., Torres, J.J., Lancraft, T.M., 1993. Trophic structure in open waters of the marginal ice zone in the Scotia–Weddell confluence region during spring 1983. Polar Biology 13, 389–397.

Hopkins, T.L., Lancraft, T.M., Torres, J.J., Donnelly, J., 1993. Community structure and trophic ecology of zooplankton in the Scotia Sea marginal ice zone in winter (1988). Deep-Sea Research 40, 81 105.

Hopkins, T.L., Torres, J.J., 1988. The zooplankton community in the vicinity of the ice edge, western Weddell Sea, March 1986. Polar Biology 9, 79–87.

Kalinowski, J., Godlewska, M., Klusek, Z., 1985. Distribution and stock of krill in the Bransfield Strait and Drake Passage during December 1983–January 1984, BIOMASS-SIBEX. Polish Polar Research 6, 151–158.

Kock, K.H., 1985. Krill consumption by Antarctic notothenioid fish. In: Siegfried, M.W.R., Condy, P.R., Laws, R. (Eds.), Antarctic Nutrient Cycles and Food Webs. Springer-Verlag, Berlin, pp. 437–444.

Kock, K.H., 1987. Marine consumers, fish and squid. Environment International 13, 37–45.

Lancraft, T.M., Hopkins, T.L., Torres, J.J., Donnelly, J., 1991. Oceanic micronektonic/macrozooplanktonic community structure and feeding under ice covered Antarctic waters during the winter (AMERIEZ 1988). Polar Biology 11, 157–167.

Lancraft, T.M., Robison, B.H., 1980. Evidence of post-capture ingestion by midwater fishes in trawl nets. Fishery Bulletin US 77, 713–715.

Lancraft, T.M., Torres, J.J., Hopkins, T.L., 1989. Micronekton and macrozooplankton in the open waters near Antarctic ice edge zones (AMERIEZ 1983 and 1986). Polar Biology 9, 225–233.

Lascara, C.M., Hofmann, E.E., Ross, R.M., Quetin, L.B., 1999. Seasonal variability in the distribution of Antarctic

krill, *Euphausia superba*, west of the Antarctic Peninsula. Deep-Sea Research I 46, 951–984.

Laws, R.M., 1985. The ecology of the Southern Ocean. American Scientist 73, 26–40.

Linkowski, T.B., Presler, P., Zukowski, C., 1983. Food habits of nototheniid fishes (Nototheniidae) in Admiralty Bay (King George Island, South Shetland Islands). Polish Polar Research 4, 79–95.

Lowry, L.F., Testa, J.W., Calvert, W., 1988. Notes on winter feeding of crabeater and leopard seals near the Antarctic Peninsula. Polar Biology 8, 475–478.

Macaulay, M.C., English, T.S., Mathisen, O.A., 1984. Acoustic characterization of swarms of Antarctic krill (*Euphausia superba*) from Elephant Island and Bransfield Strait. Journal of Crustacean Biology 4, 16–44.

Mauchline, J., Fisher, L.R., 1969. Advances in Marine Biology, vol. 7. The Biology of Euphausiids. Academic Press, London.

Nast, F., 1986. Changes in krill abundance and in other zooplankton relative to the Weddell–Scotia Confluence around Elephant Island in November 1983, November 1984, and March 1985. Archiv Fischeriewissenschaft 37, 73–94.

Nemoto, T., 1957. Foods of baleen whales in the Northern Pacific. Scientific Reports of the Whales Research Intstitute of Tokyo 14, 149–290.

Øritsland, T., 1977. Food consumption of seals in the Antarctic pack ice. In: Llano, G.A. (Ed.), Adaptations within Antarctic ecosystems. Smithsonian Institution, Washington, D.C., pp. 749–768.

Pakhomov, E.A., Perissinoto, R., McQuaid, C.D., 1996. Prey composition and daily rations of myctophid fishes in the Southern Ocean. Marine Ecology Progress Series 134, 1–14.

Piatkowski, U., 1985a. Maps of the geographical distribution of macrozooplankton in the Atlantic sector of the Southern Ocean. Berichte Polarforschung 22, 1–55.

Piatkowski, U., 1985b. Distribution, abundance, and diurnal migration of macrozooplankton in Antarctic surface waters. Meeresforschung 30, 264–279.

Quetin, L.B., Ross, R.M., Frazer, T.K., Haberman, K.L., 1996. Factors affecting distribution and abundance of zooplankton, with an emphasis on Antarctic krill, *Euphausia superba*. In: Ross, R.M., Hofmann, E.E., Quetin, L.B. (Eds.), Foundations for Ecological Research West of the Antarctic Peninsula. Antarctic Research Series, vol. 70. American Geophysical Union, Washington, D.C., pp. 357–372.

Rakusa-Suszczewski, S., 1982. The relationship between the distribution of plankton biomass and plankton communities in the Drake Passage and the Bransfield Strait (BIOMASS-SIBEX, February–March 1981). Memoirs of the National Institute for Polar Research special issue 27, 77–83.

Robison, B.H., 2003. What drives the diel vertical migrations of Antarctic midwater fish? Journal of the Marine Biological Association of the UK 83, 639–642.

Ross, R.M., Quetin, L.B., Lascara, C.M., 1996. Distribution of krill and dominant zooplankton west of the Antarctic peninsula. In: Ross, R.M., Hofmann, E.E., Quetin, L.B. (Eds.), Foundations for Ecological Research West of the Antarctic Peninsula. Antarctic Research Series, vol. 70. American Geophysical Union, Washington, DC, pp. 199–218.

Rowedder, U., 1979. Feeding ecology of the myctophid, Electrona antarctica (Gunther, 1878) (Teleostei). Meeresforschung 27, 252–263.

Siegel, V., 1986. Structure and composition of the Antarctic krill stock in the Bransfield Strait, Antarctic Peninsula during the second international BIOMASS experiment (SIBEX). Archiv Fischeriewissenschaft 37, 51–72.

Slosarczyk, W., Cielniaszek, Z., 1985. Postlarval and juvenile fish (Pisces, Perciformes, and Myctophiformes) in the Antarctica Peninsula region during BIOMASS/SIBEX, 1983/1984. Polish Polar Research 6, 159–165.

Smith, D.A., Hofmann, E.E., Klinck, J.M., Lascara, C.M., 1999. Hydrography and circulation of the West Antarctic Peninsula continental shelf. Deep-Sea Research I 46, 925–949.

Tarverdiyeva, M.I., 1972. Daily food consumption of the South Georgian cod (Notothenia rossii marmorata) and the Patagonian toothfish (Dissostichus elegenoides Smitt) (family Nototheniidae) in the South Georgia area. Journal of Ichthyology 12, 684–692.

Williams, R., 1985. The potential impact of a krill fishery upon pelagic fish in the Prydz Bay area of Antarctica. Polar Biology 5, 1–4.

Williams, T.D., 1995. The Penguins. Oxford University Press, Oxford.

Worner, F.G., 1979. Zooplankton und Mikronektofange. Archiv Fischeriewissenschaft 30, 40–61.

ELSEVIER

Deep-Sea Research II 51 (2004) 2261–2278

DEEP-SEA RESEARCH
PART II

www.elsevier.com/locate/dsr2

The distribution of seabirds and pinnipeds in Marguerite Bay and their relationship to physical features during austral winter 2001

Erik W. Chapman[a,*], Christine A. Ribic[a], William R. Fraser[b]

[a]*USGS Wisconsin Cooperative Wildlife Research Unit, Department of Wildlife Ecology, University of Wisconsin, Madison, WI 53706, USA*

[b]*Polar Oceans Research Group, P.O. Box 368, Sheridan, MT 59749, USA*

Accepted 9 July 2004

Abstract

The distribution of seabirds and pinnipeds and their relationship to physical oceanographic variables were investigated as part of the US Southern Ocean Global Ocean Ecosystem Dynamics field program along a study grid centered around Marguerite Bay on the west Antarctic Peninsula during late fall (April–May) and winter (July–August), 2001. Sea-ice conditions during the cruises provided an opportunity to compare the relationship among physical oceanographic variables and species distributions before and after the development of pack ice. During the fall cruise before pack ice development, both sea-ice-affiliated species and open-water-affiliated were observed in the area. The most common ice-affiliated species observed at this time were snow petrel (*Pagodroma nivea*, 0.7 individuals km^{-2}) and Antarctic petrel (*Thalassoica antarctica*, 0.2 individuals km^{-2}) and the most common open-water-affiliated species were blue petrel (*Halobaena caerulea*, 0.4 individuals km^{-2}), cape petrel (*Daption capense*, 0.2 individuals km^{-2}), and southern fulmar (*Fulmarus glacialoides*, 0.1 individuals km^{-2}). In addition, Antarctic fur seals (*Arctocephalus gazella*, 0.1 individuals km^{-2}) and crabeater seals (*Lobodon carcinophagus*, 0.4 individuals km^{-2}) were observed in low numbers. Akaike's information criterion was used to assess competing models that predicted predator distributions based on physical oceanographic variables proposed to structure predator distribution in previous research. These analyses indicated that predator distributions were primarily associated with water-mass structure and variability in bottom depth during the fall cruise. Crabeater seal, snow petrel, Antarctic petrel, and southern fulmar had higher densities in Inner Shelf Water, particularly near Alexander Island where a coastal current was present. Blue petrel, kelp gull (*Larus dominicanus*), and southern giant petrel (*Macronectes giganteus*) were positively associated with variability in bottom depth in April–May, suggesting that hydrographic processes influenced by bathymetry may have been important in structuring bird distributions. After the development of pack ice, during July and August, only sea-ice-affiliated species, including snow petrel (1.0 individuals km^{-2}), Antarctic petrel (0.1 individuals km^{-2}), Adélie penguin (*Pygoscelis adeliae*, 0.4 individuals km^{-2}), and crabeater seal (0.3 individuals km^{-2}), were observed. Seabirds

*Corresponding author. CCPO, Crittenton Hall 768, 52nd Street, Norfolk, VA 23529, USA. Tel.: +1-757-377-0482.
E-mail address: chapman@ccpo.odu.edu (E.W. Chapman).

0967-0645/$ - see front matter © 2004 Elsevier Ltd. All rights reserved.
doi:10.1016/j.dsr2.2004.07.005

were primarily associated with sea-ice characteristics (e.g. sea-ice concentration, sea-ice type) rather than the water-column environment later in the winter. Results from this study suggest that the timing and extent of sea-ice development in the fall may influence over-winter predation by seabirds and pinnipeds on zooplankton and fish on the western Antarctic Peninsula. Delays in sea-ice development may allow seabirds and pinnipeds access to biologically important areas such as the Inner Shelf Water for a longer period of time thereby increasing predation on zooplankton and fish.
© 2004 Elsevier Ltd. All rights reserved.

1. Introduction

The close coupling between trophic levels in the Southern Ocean presents a unique opportunity for investigating linkages between physical and biological components of the marine system (Hofmann et al., 2002). The US Southern Ocean Global Ocean Ecosystem Dynamics (US SO GLOBEC) program is a multi-disciplinary effort designed to investigate these linkages by focusing on how krill and other species within the system adapt to austral winter, a critical part of many life cycles. The ultimate goal of the research is to use the understanding of the physical and biological linkages in the marine system to predict the influence of environmental perturbation, such as climate change, through the system to top predators (Hofmann et al., 2002).

Seabirds and marine mammals have been found to be associated with a range of physical variables in the Southern Ocean. In particular, top-predator distributions have been associated with physical properties of the water column (Abrams, 1985; Ainley and Jacobs, 1981; Ainley et al., 1998; Hunt et al., 1992), sea-ice type and concentration (Ainley and Jacobs, 1981; Ainley et al., 1993, 1998; Ribic et al., 1991), and hydrographic structures, such as shelf-slope fronts (Ainley and Jacobs, 1981; Ainley et al., 1998). In near-shore, shallow waters in the Arctic, seabird distributions have been found to be associated with areas where varied bathymetry interacts with currents to form fronts, eddies or upwelling zones (Brown and Gaskin, 1988; Vermeer et al., 1987; Hunt et al., 1998), though associations of this type have not been examined in the Antarctic (Hunt, 1991).

In general, the relationship between predators and physical oceanographic features has been hypothesized to reflect an interaction between species foraging adaptations (Ainley et al., 1993) and prey distribution (Hunt and Schneider, 1987; van Franeker, 1992). The link between seabird distribution and ecosystem characteristics may be particularly strong during late fall and winter in the Antarctic. During this time, seabirds should be continuously associated with foraging habitat as they will not need to be migrating to and from breeding sites. However, little is known about the distribution of seabirds and other top predators and their linkages with oceanographic features in the Southern Ocean during the late fall and winter (Ainley et al., 1994; Fraser and Trivelpiece, 1996; Whitehouse and Veit, 1994). The survey methodology and multi-disciplinary approach of the US SO GLOBEC field program provided an unprecedented opportunity to test competing hypotheses that predict top-predator distributions based on biological and physical variables (Hofmann et al., 2002). The objectives of this paper are to assess the distribution of seabirds and pinnipeds in the US SO GLOBEC study area (see Fig. 1 in Klinck et al., 2004) during two cruises in austral winter 2001 and to describe their associations with environmental structures that have been previously hypothesized to influence predator distributions. Information on relationships with biological factors, linked physical/biological processes, and a discussion of the potential influence of climate change on these linkages will be presented in future papers.

2. Methods

2.1. Cruise tracks

The US SO GLOBEC survey provided multi-disciplinary studies of primary and secondary

biological production, Antarctic krill (*Euphausia superba*) ecology and distribution, hydrography, circulation, and top predators in the region around Marguerite Bay, Antarctica. Two survey cruises were conducted in 2001; one during April–May and the second during July–August. The survey cruises were designed to provide broad-scale studies that complement concurrent process-oriented cruises that focused on specific areas of interest in the same study area. On the survey cruise, seabird and marine mammal observations were made in conjunction with hydrographic, bioacoustical, primary production and nutrient surveys on the R.V.I.B. *Nathaniel B. Palmer*. Results from cetacean surveys are reported in Thiele et al. (2004). The April–May 2001 predator survey was a 23-d effort (88 h during daylight) and covered 938.2 km of trackline (Fig. 1). Little sea ice was present in the study area during this cruise. Weather experienced during the cruise was characterized by periodic northerly gale force winds. Air temperature remained at or near 0 °C until the final two weeks of the cruise, after which it dropped to between −6 and −8 °C. Visibility was often limited by fog and snowfall throughout the cruise. The July–August 2001 survey was a 28-d effort (99 h during daylight) and covered 828.6 km of trackline (Fig. 1). Air temperature was typically below −10 °C and southwesterly winds periodically reached gale force. During this cruise, there was less snowfall, fog, and low-lying clouds than during the April–May cruise.

2.2. Visual survey methods

Predator surveys were conducted while the ship traveled at 4–6 kts, the speed at which a multi-frequency acoustical system was being towed (BIOMAPER-II, Woods Hole Oceanographic Institute, Woods Hole, MA, Lawson et al., 2004). A two-person team was used to survey birds and marine mammals during all daylight hours while the ship was underway. Observers surveyed simultaneously, using hand-held binoculars to scan for animals and to confirm species identifications. One observer used 8× and the other used 10× magnification binoculars so that each observer's survey capabilities complemented the other, maximizing the team's ability to detect and identify animals in varied conditions. Observations were made from the bridge (15 m above sea surface) from sunrise to sunset, except when

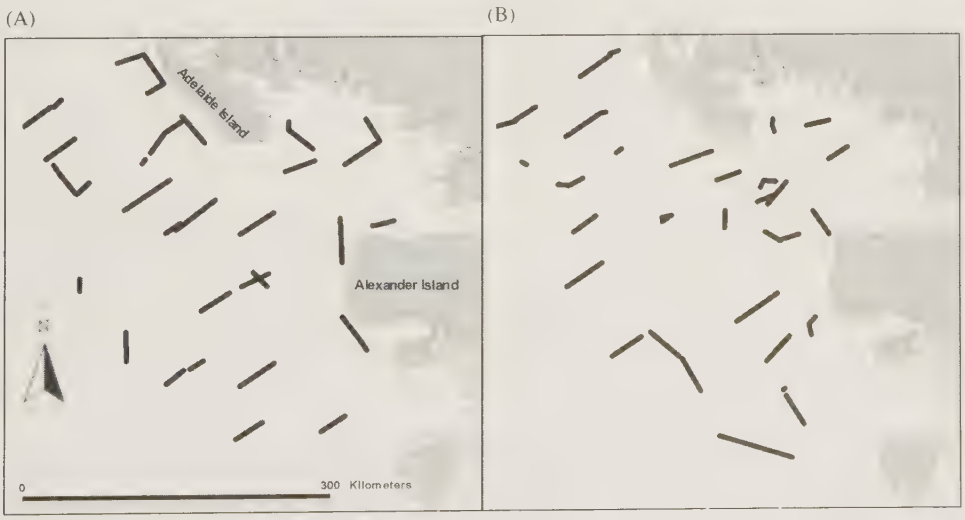

Fig. 1. Predator survey locations in the US SO GLOBEC study area during (A) the April–May and (B) the July–August, 2001 cruise. Survey locations are indicated with black lines. The study area is centered on Marguerite Bay (68°29.5′S, 70°02.3′W) between Alexander and Adelaide Islands which are labeled on map A. Coastline digital data courtesy of the Antarctic Digital Database Version 3.0, Mapping and Geographic Information Centre, British Antarctic Survey.

visibility was <300 m, Beaufort Sea State was >5 (following Ainley et al., 1993), or when the ship was stopped at hydrographic stations. Predator surveys consisted of a continuous 300-m strip transect off the port side of the ship, sweeping from the bow to 90° perpendicular to the ship (Ainley et al., 1993, 1998). Perpendicular distances to animals on the sea ice were determined using a laser range finder (Leica Geovid 7 X 10 BD Binoculars), and distances to flying birds were estimated using a range finder (Heinemann, 1981). A 300-m strip transect width also was used for seal observations (Ribic et al., 1991).

2.3. Data analysis

The continuous strip transects were split into one-half hour segments. For the April–May cruise, 155 one-half hour transects were included in the analysis and the mean length for these transects was 5.2 km (S.D. = 1.5 km). For the July–August cruise, 130 one-half hour transects were analyzed and the mean length for these transects was 4.8 km (S.D. = 0.7 km). The difference in transect lengths between cruises reflected slightly different ship speeds during surveys.

The correlations of bird densities in adjacent transects made during a single day were calculated for days when surveys were conducted for at least three hours, yielding a minimum of five adjacent transects. Using day as a replicate, autocorrelations of bird densities varied from −0.54 to 0.87 for the April–May cruise ($n = 14$ days) and −0.69 to 0.76 for the July–August cruise ($n = 11$ days). Even though there was no significant correlation of bird densities between adjacent transects (using days as replicates: April–May cruise: $r = -0.03$, $df = 14$, $p > 0.05$; July–August cruise: $r = 0.1$, $df = 10$, $p > 0.05$), the error variance in the analyses can be too low if autocorrelation is ignored. This causes variables to be declared significant when, in fact, they are not (Cressie, 1993). Thus, a generalized least-squares approach (described below) was used to adjust for autocorrelation between transects when fitting models.

Seabird densities were calculated using corrections for variation in perceived density resulting from the relative movement of ship and birds (flux, as described in Spear et al., 1992) and with ship-following birds down-weighted (Ainley et al., 1998). Many of the pinnipeds were in the water, which made estimation of numbers of animals difficult and density calculations based on line transect methodology (Lakke, 2001) not possible. Therefore, the presence/absence of pinnipeds was analyzed following Ribic et al. (1991).

2.4. Distributions of species

The number of transects along which each bird or mammal species was seen was tabulated. Although the presence/absence of pinnipeds was used in analyses, densities of pinnipeds were mapped and are considered to be a minimum estimate. Species were categorized as being sea-ice- or open-water-affiliated based on criteria given in Ainley et al. (1994), Ribic et al. (1991), and Woehler et al. (2003). These associations are summarized in Table 1. For spatial representation, the mid-point of the transect was used to map the occurrence of the species in the study area using ArcView Geographical Information Systems (Environmental Systems Research Institute Inc., 1996a)

2.5. Relationships with physical features

We investigated the relationships among predator density or the presence/absence with bathymetry characteristics, surface thermohaline properties, water-column environment, sea-ice structure, distance to breeding colony, and distance to the sea-ice edge. These variables have been hypothesized to affect top-predator distributions in the Antarctic (Ainley et al., 1994, 1998; Ribic et al., 1991). The specific variables used were:

(1) bottom depth and variation in depth for bathymetry (variation in bathymetry was used to detect an association with a bathymetrically controlled physical process);
(2) sea-surface salinity and temperature;
(3) temperature maximum below 200 m and salinity at 50 m for water-column environment;

Table 1
Number of 30-minute transects along which predator species were seen during two cruises to the US SO GLOBEC study area during April–May and July–August, 2001

Species	Habitat affiliation	Cruise	
		April–May	July–August
Emperor penguin (*Aptenodytes forsteri*)	Ice	0	7
Adélie penguin (*Pygoscelis adeliae*)	Ice	0	19
Black-browed albatross (*Diomedia melanophris*)	Open water	0	1
Unidentified albatross (*Diomedia* spp.)	Open water	1	0
Southern giant petrel (*Macronectes giganteus*)	Open water	20	6
Southern fulmar (*Fulmarus galcialoides*)	Open water	91	0
Antarctic petrel (*Thalassoica antarctica*)	Ice	56	21
Cape petrel 'pintado petrel' (*Daption capense*)	Open water	70	0
Snow petrel (*Pagodroma nivea*)	Ice	54	81
Blue petrel (*Halobaena caerulea*)	Open water	64	0
Sooty shearwater (*Puffinus griseus*)	Open water	1	0
Kelp gull 'kelp gull' (*Larus dominicanus*)	Ice	16	0
Antarctic tern (*Sterna vittata*)	Open water	1	0
Imperial cormorant 'blue-eyed shag' (*Phalacrocorax atriceps*)	Open water	1	0
Crabeater seal (*Lobodon carcinophagus*)	Ice	8	19
Leopard seal (*Hydrurga leptonyx*)	Ice	2	0
Weddell seal (*Leptonychotes weddellii*)	Ice	1	2
Antarctic fur seal (*Arctocephalus gazella*)	Ice edge	12	0
Unidentified seal		4	0
Total number of transects		155	130

Note: Habitat affiliation is based on Ainley et al. (1994), Ribic et al. (1991), and Woehler et al. (2003).

(4) distance to sea-ice edge, the presence/absence of sea ice, sea-ice type and sea-ice concentration for sea-ice structure; and
(5) distance to land (a proxy for distance to breeding colonies and other potential roosting sites on land).

Bottom depth for each transect was obtained by interpolating depth values for the mid-point of each transect using high-resolution bathymetry data currently being developed for the study region (T. Bolmer and R. Beardsley, Technical Report, Woods Hole Oceanographic Institute, in prep.). The coefficient of variation of bottom depth was calculated for each transect using depth measurements calculated using the one-minute depth values generated from the ship's continuous, underway system. Average sea-surface temperature (°C) and salinity [practical salinity unit (psu)] were calculated for each transect by averaging the one-minute values obtained from the ship's continuous real-time underway system. In July and August, sea ice prevented accurate measurement of the surface water by the ship's underway systems. Therefore, transect surface salinity and temperature values were not calculated for this cruise. Distance to land was calculated using an algorithm within ArcView Spatial Analyst (Environmental Systems Research Institute Inc., 1996b).

The temperature maximum below 200 m and salinity at 50 m along each transect were calculated using the mid-point of the transect and interpolating between the closest conductivity–temperature–depth (CTD) stations using ArcView Spatial Analyst (Environmental Systems Research Institute Inc., 1996b). Water-mass definitions were based on ranges of temperature maximum below 200 m as described in Smith et al. (1999, 1995), Hofmann and Klink (1998), Orsi et al. (1995), and Prézelin et al. (2004) (Table 2). Based on these definitions and interpolated values from CTD data during the study, transects were assigned to a

Table 2
Definitions of sub-surface waters based on temperature maximum below 200 m ($T_{max\ 200}$) for the US SO GLOBEC study area on the western Antarctic Peninsula during April–May 2001

Sub-surface water mass	Definition	References
ACC	$T_{max\ 200} \geq 1.8\,^{\circ}C$	Orsi et al. (1995)
ACC-derived newly intruded UCDW	$1.5 \leq T_{max\ 200} < 1.8\,^{\circ}C$	Smith et al. (1995)
UCDWB	$1.4 < T_{max\ 200} < 1.5\,^{\circ}C$	Hofmann and Klink (1998), Table II
MUCDW/shelf water	$1.2 \leq T_{max\ 200} \leq 1.4\,^{\circ}C$	Smith et al. (1999), Fig. 8a
InSWB	$1.1 < T_{max\ 200} < 1.2\,^{\circ}C$	Smith et al. (1999), Fig. 8a and b
InSW	$T_{max\ 200} \leq 1.1\,^{\circ}C$	Prézelin et al. (in press)

InSW: Inner Shelf Water; InSWB: Inner Shelf Water Boundary; MUCDW: modified Upper Circumpolar Deep Water; UCDWB: Upper Circumpolar Deep Water Boundary; UCDW: Upper Circumpolar Deep Water; ACC: Antarctic Circumpolar Current.

particular water mass, which was then included in the models as a categorical variable. Because just two transects were in the Antarctic Circumpolar Current (ACC) during the April–May cruise, these were grouped with the Upper Circumpolar Deep Water (UCDW) in the analysis. In the July–August cruise, two transects were in the Inner Shelf Water and these were combined with transects in the Inner Shelf Water Boundary in the analysis. Densities of all species were calculated separately for each water-mass structure and tabulated.

For the April–May 2001 cruise we looked for a relationship between sub-surface water masses and mean sea-surface temperature and salinity values for the transects using a generalized linear model with a Gaussian error structure. This test was not performed for the July–August 2001 cruise because of missing sea-surface temperature and salinity data.

The sea-ice edge was defined during each cruise through visual analysis of weekly sea-ice concentration analyses of satellite imagery (The National/Naval Ice Center, Washington, DC, 2002) combined with our own field observations. When our field observations disagreed with satellite imagery analyses, field observations took precedence over the sea-ice edge definition based on satellite imagery. The sea-ice edge was defined as the transition region where sea ice covered more than 15% of the ocean surface (Zwally et al., 1983). Distance to the sea-ice edge for each transect was then calculated using ArcView Spatial Analyst (Environmental Systems Research Institute Inc., 1996a, b). During the fall cruise, the sea-ice edge occurred just within the study area as the pack ice developed from the south, and nine of the 155 transects were inside the pack ice. The average distance to the sea-ice edge during this cruise was 139.7 km (S.D. = 81.8 km). During the winter cruise, the pack ice had developed well north and west of the study area and all of the survey transects were within the pack ice. The average distance to the sea-ice edge during this cruise was 421.3 km (S.D. = 82.7 km). Because most transects during the April–May cruise were in open water, the presence of sea-ice was used as the sea-ice structure variable for that cruise. Because all of the transects were within the pack ice during the July–August cruise, we defined sea-ice type using the Antarctic Sea-ice Processes and Climate (ASPeCt) sea-ice observation protocol (University of Tasmania, Antarctic CRC, 1998). For analysis, we grouped the sea-ice types into the following categories; new ice (grease, nilas, frazil, pancake) and brash, cake ice, floes (small, medium, large), and vast floes. Sea-ice concentrations in tenths were averaged across each transect for the July–August cruise.

We used generalized linear models to model density or the presence/absence as a function of the physical variables (McCullagh and Nelder, 1989). Both polynomial and linear relationships with physical variables were considered. Models were fit for any species observed in at least 10% of transects within each cruise. Bird density was log-transformed and modeled with a Gaussian error structure. The presence/absence of pinnipeds was modeled with a binomial error structure.

Models composed of variables corresponding to bathymetry, surface thermohaline properties,

water-column environment, and sea-ice structure were developed before analysis commenced (Burnham and Anderson, 1998). Variables with correlations greater than 0.70 were not used in any model to avoid potential problems with multi-colinearity (Weisberg, 1985). Akaike's information criterion (AIC) corrected for sample size was used to select the best model (Burnham and Anderson, 1998). Adjusted-R^2 values (for the Guassian error models) were calculated to assess how much variability was explained by the models. Residual analysis was done to identify influential points using Cook's distance; influential points are points that change the conclusions of the analysis when they are deleted from the data set and the reduced data set is reanalyzed (Cook and Weisberg, 1999). Results from the full data set and the reduced data set are presented when influential points were identified (following Cook and Weisberg, 1999). Significance of the models was assessed at an alpha of 0.05. All models were checked for autocorrelation in the residuals using semivariograms (Cressie, 1993). Spherical semivariograms were used to estimate the error structure, the model was refit using generalized least-squares (Cressie, 1993), and the AIC value recalculated. Analyses were done in S-Plus 2000 (MathSoft, 1999).

3. Results

3.1. Association of sub-surface water masses to surface characteristics

Sea-surface temperature and salinity were associated with distinct sub-surface water masses ($F = 92.2$, df = 3, 151, $p < 0.001$, proportion variance explained = 0.647). All of the sub-surface water masses, with the exception of the ACC, were associated with a particular combination of temperature and salinity ranges (Table 3).

3.2. Distribution of species

Overall, 11 bird and four pinniped species were recorded during the April–May cruise (Table 1). The majority of the individuals seen was from two sea-ice-affiliated species and three open-water-affiliated species (Table 1). Southern fulmar (*Fulmarus galcialoides*), an open-water-affiliated species, was the most common species observed, followed by snow petrel (*Pagodroma nivea*), cape petrel (*Daption capense*), Antarctic petrel (*Thalassoica antarctica*), and blue petrel (*Halobaena caerulea*). Kelp gull (*Larus dominicanus*) and southern giant petrel (*Macronectes giganteus*) also were observed, though in fewer transects. Adélie penguins (*Pygoscelis adeliae*) were present in the area in unknown numbers as individuals were seen hauled out on islands when the ship was off survey effort. Crabeater seals (*Lobodon carcinophagus*) and Antarctic fur seals (*Arctocephalus gazella*) were the most common pinnipeds seen; however, pinnipeds were relatively rare, being seen on fewer than 10% of the transects. There was a concentration of birds and pinnipeds off the northwest shore of Alexander Island (Figs. 2–5).

During the July–August cruise, six bird and two pinniped species were observed (Table 1) in the survey area. Only sea-ice-affiliated species were seen in July–August, reflecting the presence of sea ice on all transects during this cruise (Table 1).

Table 3
Mean sea-surface temperature (°C) and salinity (psu) associated with predator survey transects grouped by sub-surface water-mass location for data collected within the US SO GLOBEC study area during April–May 2001

Surface property	InSW ($n=29$)	InSWB ($n=7$)	MUCDW ($n=41$)	UCDWB ($n=33$)	UCDW ($n=43$)	ACC ($n=2$)
Sea-surface temperature (°C)	−1.22 (.307)	−.495 (.221)	−.945 (.366)	−.867 (.268)	−.929 (.417)	−.861 (.0005)
Sea-surface salinity (psu)	33.17 (.087)	33.24 (.114)	33.47 (.189)	33.69 (.086)	33.66 (.135)	33.73 (.005)

Note: Standard errors are in parentheses. Each water mass was statistically associated with a particular combination of sea-surface temperature and salinity values during this cruise with. The only exception was ACC due to the low sample size. See Table 2 for sub-surface water-mass definitions.
For explanation of abbreviations see Table 2 footnote.

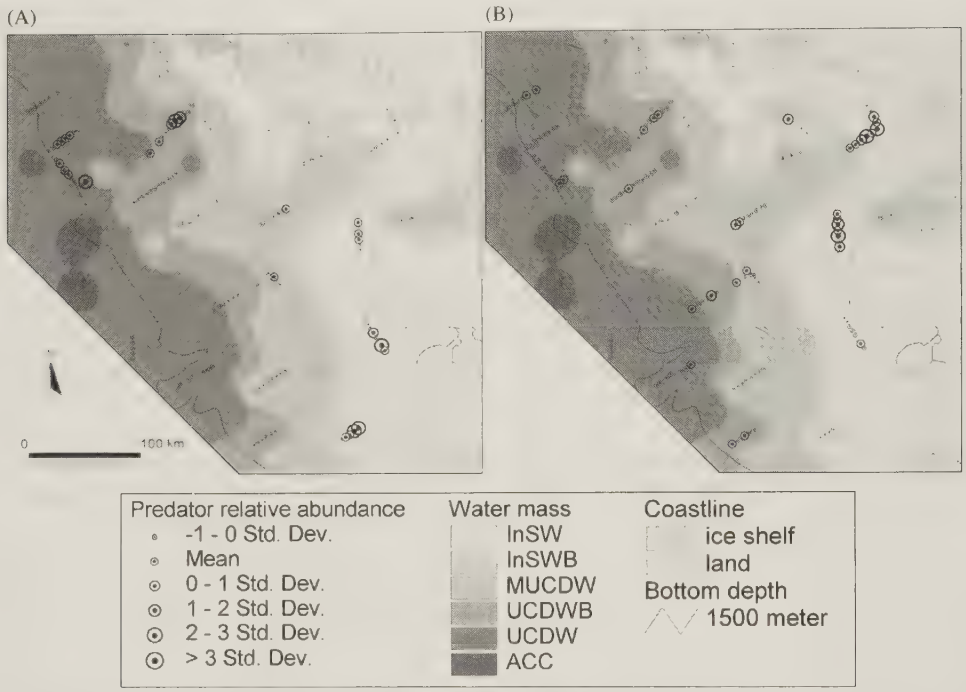

Fig. 2. Relative density for (A) Antarctic petrel (mean density = 0.2 individuals km $^{-2}$) and (B) southern fulmar (mean density = 0.4 individuals km^{-2}) for 30-minute survey transects during the April–May, 20001 cruise. Water-mass locations also are plotted using interpolated values for temperature maximum below 200-m (see Table 2 for water-mass definitions). See Fig. 1 for data source and map location.

Overall bird densities were lower during the July–August cruise than the April–May cruise (Tables 4 and 5). Snow petrel was the most common bird observed, with Antarctic petrel and Adélie penguin the next most frequently observed species. Crabeater seal was the only commonly seen pinniped in the July–August cruise (Table 5). The concentration of birds and mammals around Alexander Island was markedly reduced from that seen during the April–May cruise (Figs. 6 and 7).

3.3. *Relationships with physical variables*

During the April–May cruise, water-mass structure was the most common variable included in the best fitting models (present in best models for four species), followed by the presence of sea ice and bottom depth variation (present in best models for three species) (Table 6). At this time, four of the species were found at their greatest densities within the study area in the Inner Shelf Water or the Inner Shelf Water Boundary (Table 4). Antarctic petrel, snow petrel, and southern fulmar densities were highest over the Inner Shelf Water (Figs. 2 and 3), sometimes dramatically so, while kelp gull densities were highest over the Inner Shelf Water Boundary (Table 4, Fig. 5B). Analysis of surface thermohaline characteristics showed a southwesterly flowing coastal current associated with the Inner Shelf Water during the April–May period (Klinck et al., 2004). The Inner Shelf Water also was characterized by relatively fresh, cold surface water (Table 3) and also was the only water mass in which new sea ice and relatively large numbers of icebergs were observed. Specifically, brash and new sea ice in the vicinity of icebergs were found in the region of the Inner Shelf Water immediately north and west of Alexander Island.

The importance of other physical variables in April–May was species dependent (Table 6). Besides being associated with the Inner Shelf Water, snow petrel densities were highest in areas

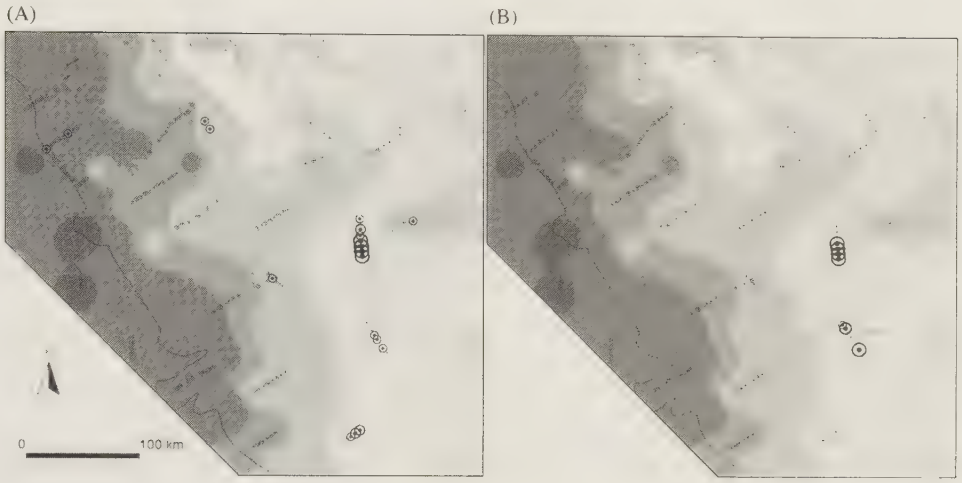

Fig. 3. Relative density for (A) snow petrel (mean density = 0.7 individuals km^{-2}) and (B) crabeater seal (mean density = 0.4 individuals km^{-2}) for 30-minute survey transects during the April–May, 20001 cruise. See Fig. 1 for digital data source and map location. See Fig. 2 for definitions of symbols and water masses.

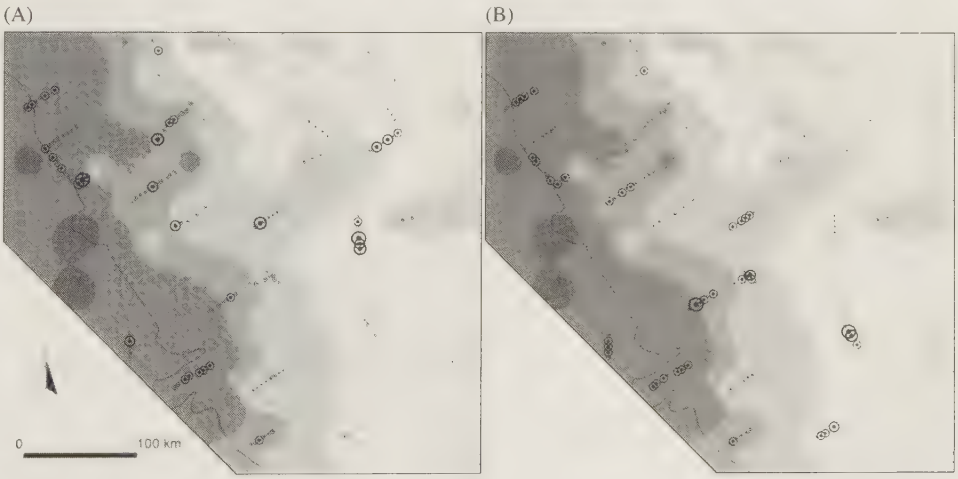

Fig. 4. Relative density for (A) cape petrel (mean density = 0.2 individuals km^{-2}) and (B) blue petrel (mean density = 0.4 individuals km^{-2}) for 30-minute survey transects during the April–May, 20001 cruise. Water-mass locations also are plotted using interpolated values for temperature maximum below 200 m (see Table 2 for water-mass definitions). See Fig. 1 for digital data source and map location. See Fig. 2 for definitions of symbols and water masses.

where sea-surface temperatures were lower and where sea ice was present. The sea-ice concentration where snow petrels were observed was, on average, 0.38. Blue petrel densities were higher where the bottom topography was most variable and in areas farther from land. There was one influential point; when that point was removed, the presence of sea ice was added to the previous model and the adjusted-R^2 increased to 0.175. Transects with higher blue petrel densities and variable bottom topography corresponded to Inner Shelf Water near Alexander Island; otherwise, blue petrel densities were higher in transects farther from land (which occurred in UCDW)

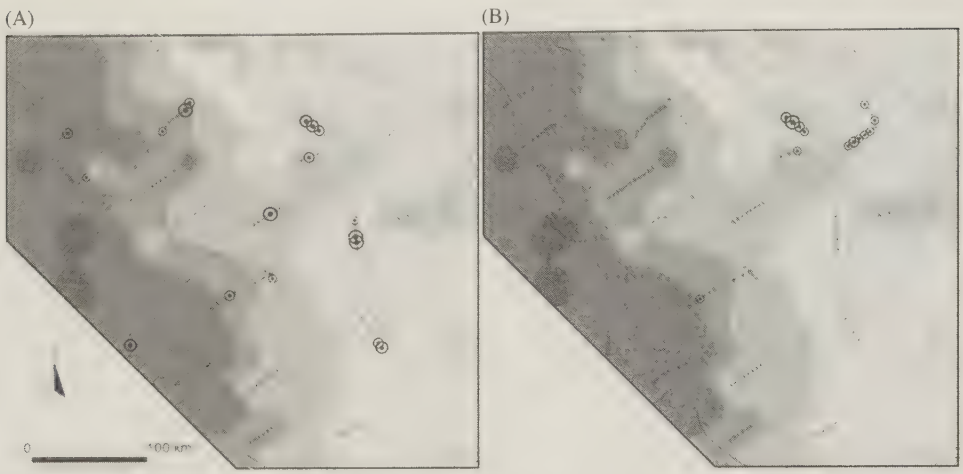

Fig. 5. Relative density for (A) southern giant petrel (mean density = 0.1 individuals km^{-2}) and (B) kelp gull (mean density = 0.1 individuals km^{-2}) for 30-minute survey transects during the April–May, 20001 cruise. See Fig. 1 for digital data source and map location. See Fig. 2 for definitions of symbols and water masses.

Table 4
Average density of top predators (individuals km^{-2}) within each water mass during the April–May 2001 cruise

Species	InSW ($n=29$)	InSWB ($n=7$)	MUCDW ($n=41$)	UCDWB ($n=33$)	UCDW ($n=43$)	ACC ($n=2$)	Overall ($n=155$)
Snow petrel	3.1 (5.7)	0.1 (0.2)	0.2 (0.4)	0.02 (0.1)	0.1 (0.3)	0.0	0.7 (2.7)
Cape petrel	0.3 (0.8)	0.2 (0.4)	0.1 (0.3)	0.1 (0.3)	0.2 (0.4)	0.03	0.2 (0.5)
Southern fulmar	1.2 (2.0)	0.5 (0.5)	0.1 (0.3)	0.3 (0.3)	0.2 (0.3)	0.0	0.4 (1.0)
Antarctic petrel	0.5 (1.1)	0.0 (0.0)	0.04 (0.1)	0.2 (0.6)	0.2 (0.5)	0.0	0.2 (0.6)
Blue petrel	0.4 (1.1)	0.1 (0.3)	0.3 (0.5)	0.3 (0.4)	0.7 (2.1)	0.0	0.4 (1.2)
Southern giant petrel	0.1 (0.2)	0.2 (0.3)	0.1 (0.1)	0.1 (0.2)	0.02 (0.1)	0.0	0.1 (0.2)
Kelp gull	0.4 (0.9)	5.2 (9.5)	0.02 (0.1)	0.02 (0.1)	0.0 (0.0)	0.0	0.3 (2.2)
Total birds	6.0 (6.9)	6.2 (9.4)	0.7 (0.8)	0.9 (0.9)	1.4 (2.2)	0.03	2.2 (4.3)
Antarctic fur seal	0.02 (0.1)	0.2 (0.4)	0.1 (0.1)	0.1 (0.2)	0.1 (0.5)	0.0	0.1 (2.1)
Crabeater seal	2.1 (4.4)	0.0 (0.0)	0.0 (0.0)	0.0 (0.0)	0.0 (0.0)	0.0	0.4 (0.3)
Total seals	2.1 (4.4)	0.2 (0.4)	0.03 (0.2)	0.1 (0.5)	0.1 (0.5)	0.0	0.5 (2.1)

Note: Standard errors are given in parentheses and are presented for water masses in which at least three transects were conducted. The number of transects in a water mass is given by "n".
For explanation of abbreviations see Table 2 footnote.

(Fig. 4B). Higher cape petrel densities were associated with the presence of sea ice. However, this model was influenced by high density in a single transect with brash ice and a sea-ice concentration of 0.57 ice. When this value was removed, water-mass structure was associated with cape petrels; higher densities were found in Inner Shelf Water and UCDW (Table 4, Fig. 4A). Kelp gulls were positively associated with variability in bottom depth as well as with the Inner Shelf Water Boundary. The area where this combination occurred was at the entrance to Marguerite Bay (Fig. 5B) over Marguerite Trough, which is a deep trough extending across the continental shelf (see Klinck et al., 2004). Southern giant petrels were not found to be concentrated in

Table 5
Average density of top predators (individuals km ^{2}) within each water mass during the July–August 2001 cruise

Species	InSW ($n=2$)	InSWB ($n=4$)	MUCDW ($n=49$)	UCDWB ($n=16$)	UCDW ($n=49$)	ACC ($n=10$)	Overall ($n=131$)
Snow petrel	0.0	0.7 (0.7)	0.8 (1.6)	0.8 (1.1)	1.4 (2.7)	1.1 (1.5)	1.0 (2.0)
Antarctic petrel	0.0	0.0 (0.0)	0.03 (0.1)	0.02 (0.1)	0.2 (0.6)	0.1 (0.1)	0.1 (0.4)
Southern giant petrel	0.0	0.0 (0.0)	0.3 (1.3)	0.0 (0.0)	0.01 (0.02)	0.0 (0.0)	0.1 (0.8)
Adélie penguin	0.0	0.0 (0.0)	0.8 (2.4)	0.1 (0.4)	0.1 (0.4)	0.8 (1.8)	0.4 (1.6)
Emperor penguin	0.0	0.4 (0.8)	0.1 (0.4)	0.0 (0.0)	0.04 (0.2)	0.0 (0.0)	0.1 (0.3)
Total birds	0.0	1.1 (1.4)	2.0 (3.3)	0.9 (1.1)	1.7 (3.2)	2.0 (3.3)	1.7 (3.0)
Crabeater seal	0.0	0.8 (1.3)	0.5 (1.2)	0.04 (0.2)	0.1 (0.4)	0.0 (0.0)	0.3 (0.9)
Total seals	0.0	0.8 (1.3)	0.5 (1.2)	0.04 (0.2)	0.1 (0.4)	0.0 (0.0)	0.3 (0.9)

Note: Standard errors are given in parentheses and are presented for water masses in which at least three transects were conducted. The number of transects in a water mass is given by "n".
For explanation of abbreviations see Table 2 footnote.

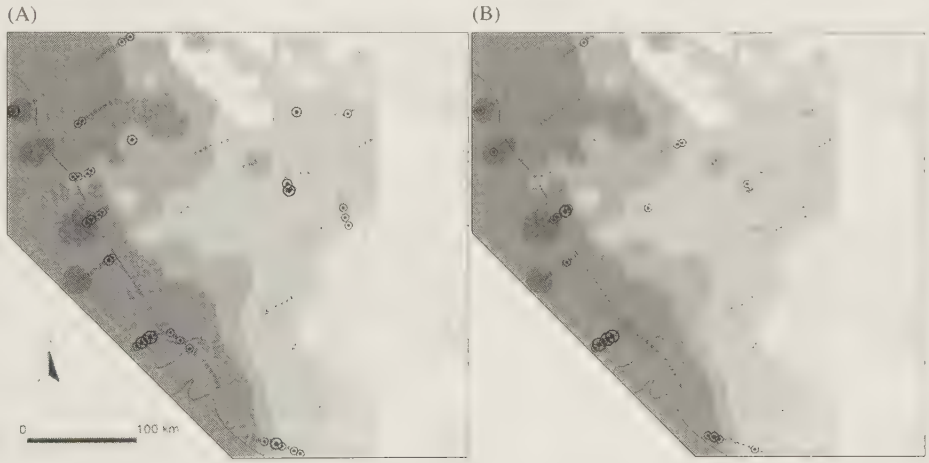

Fig. 6. Relative density for (A) snow petrel (mean density = 1.0 individuals km^{-2}) and (B) Antarctic petrel (mean density = 0.1 individuals km^{-2}) for 30-minute survey transects during the July–August, 2001 cruise. See Fig. 1 for digital data source and map location. See Fig. 2 for definitions of symbols and water masses.

any particular water mass (Fig. 5A). However, this species was found in areas where sea ice was present and where bottom depth variability was higher.

In the July–August cruise, sea-ice structure of some type was the common variable for the best models associated with the bird species (Table 7). Crabeater seals were associated with water-mass structure, specifically modified UCDW/shelf water (Fig. 7B), as well as shallow bottom depths. This combination of modified UCDW/shelf water and shallow bottom depths occurred mainly in the southern portion of the study area and extended from within Marguerite Bay, southwest and offshore to the continental shelf-break (see bathymetry in Fig. 1 of Klinck et al., 2004).

In the July–August cruise, snow petrel abundance showed a nonlinear relationship with ice concentration and salinity at 50 m, peaking at 0.8 coverage and 33.9 psu, respectively, (Table 7). Snow petrel abundance also was highest in new and brash ice and at greater bottom depths

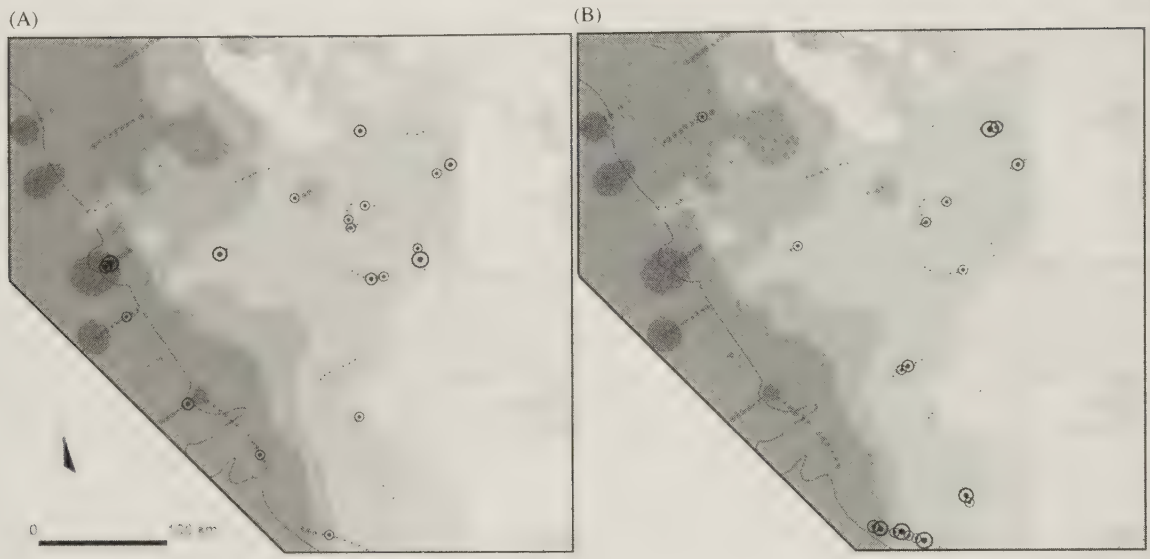

Fig. 7. Relative density for (A) Adélie penguin (mean density = 0.4 individuals km $^{-2}$) and (B) crabeater seal (mean density = 0.3 individuals km $^{-2}$) for 30-minute survey transects during the July August, 2001 cruise. See Fig. 1 for digital data source and map location. See Fig. 2 for definitions of symbols and water masses.

(Table 7). Antarctic petrel density (Fig. 6B) was associated with vast floes, relatively low sea-ice concentration, and deeper waters. Adélie penguin density (Fig. 7A) was associated with newer or light sea-ice types and were found within the pack ice, farther from the sea-ice edge, and in deeper waters within the pack ice.

4. Discussion

4.1. Seabird and pinniped distribution

Overall, the species we encountered in our surveys were typical of the Antarctic seabird and pinniped fall and winter community (Ainley et al., 1993; Whitehouse and Veit, 1994; Woehler et al., 2003). However, during the winter cruise, species abundances were low compared to other studies that took place during the winter (Ainley et al., 1993; Fraser and Ainley, 1986; van Franeker, 1992). The 2001 SO GLOBEC surveys were, on average, over 400 km inside the pack ice while previous winter studies took place within 150 km of the ice edge in both open water and inside the pack ice. Therefore, the differences between the 2001 results and those from previous studies may indicate that seabird densities decrease further inside the pack ice.

Of the seabirds commonly observed in this study, only blue petrel (Watson, 1975) and Antarctic petrel (van Franeker et al., 1999) are known to not breed on the Antarctic Peninsula. Blue petrel is a Sub-Antarctic breeder and is likely only a seasonal migrant into Antarctic waters prior to the development of seasonal pack ice. However, Antarctic petrels are year-round residents of high Antarctic latitudes and were relatively common near Marguerite Bay in the winter (cf. Fig. 6, Table 1). The nearest known Antarctic petrel breeding colony is 1800 km from the SO GLOBEC study area, along the eastern shore of the Weddell Sea (van Franeker et al., 1999). This result could reflect a significant winter migration to the study area, perhaps suggesting that Antarctic petrels are capitalizing on high prey availability near Marguerite Bay during winter. However, it has been speculated that major breeding colonies of Antarctic petrels have yet to be discovered on the Antarctic Peninsula (van Franeker et al., 1999), in which case high densities of this species in winter may represent a lingering association with breeding

Table 6
Variables included in the minimum AIC model for species observed on 10% or more of the transects during April–May 2001

Species	Distance to land (km)	Sea-surface temperature (°C)	Presence of ice	Bottom depth variation (coefficient of variation)	Water-mass structure	Adjusted-R^2	p-Value
Antarctic petrel					InSW 0.53 (1.1)/0.21 (0.5)	0.082	.01
Snow petrel		− −1.22 (0.36)	+ 5.5 (7.5)/ 0.2(0.6)		InSW 3.1 (5.7)/0.2 (0.4)	0.539	<.001
Blue petrel	+ 111.31 (50.94)			+ 0.11 (0.19)		0.091	<.001
Cape petrel			+ 0.5 (1.1)/0.1 (0.3)			0.03	.024
Southern fulmar					InSW 1.2 (2.0)/0.5 (0.5)	0.187	<.001
Kelp gull				+ 0.27 (0.19)	InSWB 5.2 (9.5)/0.4 (0.9)	0.38	<.001
Southern giant petrel			+ 0.16(0.2)/ 0.04(0.2)	+ 0.16 (0.19)		0.05	.006

Note: The sign in the table is the direction of the relationship between the species and the variable (+ - positive, − = negative) in the minimum AIC model. For continuous variables included in the AIC model for each species, the mean and standard error of the variable for transects in the 80th percentile of density values are also given. Where the presence of sea-ice is included in the minimum AIC model, the mean and standard error of species density (individuals km $^{-2}$) when ice is present and when it is not are given [mean (standard error) with ice, mean (standard error) without ice]. When water-mass structure is present in the minimum AIC model, the water mass where the species was most abundant is listed. The mean and standard error for species density (individuals km $^{-2}$) over this water mass and the water mass where the species is second most abundant are also given [mean (standard error) where species is most abundant, mean (standard error) where species is second most abundant]. Adjusted-R^2 and p-values for the models are also given.
For explanation of abbreviations see Table 2 footnote.

Table 7
Variables included in the minimum AIC model for species observed on 10% or more of the transects during July–August 2001

Species	Distance to ice edge (km)	Coded ice	Ice conc. (tenths)	Distance to land (km)	Bottom depth (m)	Water mass	Sal. at 50 m.(psu)	Adjusted-R^2	p-Value
Adélie penguin	− −469.39 (92.37)	New and brash ice 1.7 (4.7)/0.3 (1.2)			+ 1228 (1050)			0.136	<0.001
Antarctic petrel		Vast floe 0.12 (0.44)/0.06 (0.17)	− 8.7 (0.6)		+ 1605 (1248)			0.153	<0.001
Snow petrel		New and brash ice 1.9 (2.1)/1.0 (1.3)	Poly (0.8)	+ 118 (62)			Poly (33.9)	0.198	<0.001
Crabeater seal					− 460 (132)/ 1092 (1049)	MUCDW		0.103	0.013

Note: "Poly" indicates where a polynomial relationship was found for a variable. The value where species abundance was highest is given for these variables where the polynomial relationship was found. The sign in the table is the direction of the relationship between the species and the variable (+ = positive, − = negative) in the minimum AIC model. For continuous variables included in the AIC model for each species, the mean and standard error of the variable for transects in the 80th percentile of density values are also given. For crabeater seals, mean and standard errors are given for continuous variable values when this species was present and when it was not present [mean (standard error) when present/mean (standard error) when not present]. Because the presence/absence of crabeater seals was used in the analysis, no abundance values are given for categorical variables in the minimum AIC model for this species. When coded ice is present in the minimum AIC model, the ice code where the species was most abundant is listed. The mean and standard error for species density (individuals km^{-2}) over this ice type and the ice type where the species is second most abundant are also given [mean (standard error) where species is most abundant/mean (standard error) where species is second most abundant]. Distances to the ice edge within the ice are negative. Adjusted-R^2 and p-values for the models are also given.
For explanation of abbreviations see Table 2 footnote.

colonies. Finally, the loss or reduced density of several species that breed on the Antarctic Peninsula, including cape petrels, southern giant petrels, kelp gulls and southern fulmar, on the July–August surveys suggests the movement of these species north to open water and the ice edge as pack ice develops (Ainley et al., 1993).

4.2. Adélie penguin distribution

Because Antarctic krill is typically the dominant prey choice of Adélie penguins on the Antarctic Peninsula (Ainley, 2003), understanding Adélie penguin distribution and foraging ecology is of particular importance to the SO GLOBEC objectives. On the southern portion of the Antarctic Peninsula, there are three clusters of Adélie penguin breeding colonies centered on Avian Island (67°46′S, 68°54′W), Renaud Island (65°52′S, 66°15′W), and Anvers Island (64°46′S, 64°04′W) with a combined population of 112,400 breeding pairs (Woehler, 1993). The winter movement of this population is poorly understood (Fraser and Trivelpiece, 1996). Although the 2001 surveys did not indicate a concentration of Adélie penguins offshore within Marguerite Bay during either cruise, it is possible that penguins are using near-shore areas not included within the survey area, particularly in late fall. During the April–May cruise, groups of Adélie penguins were observed hauling out on islands just north of Marguerite Bay and the survey area. In addition, results from a concurrent telemetry study found that Adélie penguins generally restrict their movement to near-shore areas during late fall (Fraser, unpublished data). During the July–August cruise, Adélie penguins were observed in our survey grid and telemetry results began to detect a movement of Adélie penguins further north. These observations suggest that Adélie penguins may be foraging near-shore and hauling out on islands prior to the establishment of sea ice and shifting their distribution offshore in winter, presumably in association with the developing pack ice.

4.3. Influence of varied bathymetry

The association of blue petrels, kelp gulls, and southern giant petrels with areas characterized by high bottom depth variability during the fall cruise suggests that bottom topography may be influencing biological processes in the Marguerite Bay region at this time of year. Kelp gulls and southern giant petrels were observed well inshore, which may indicate the presence of bathymetrically controlled fronts, eddies, or upwelling zones; features that seabirds have been associated with in other shallow seas (Russell et al., 1999; Schneider et al., 1987). Blue petrels also were observed further offshore and may be associated with bathymetrically controlled processes near the shelf break as well as features in near-shore areas. During the winter cruise, variation in bathymetry was no longer an important variable in the models, suggesting that sea ice may have prevented access by the top predators to environmental structures (e.g. food) associated with fixed, bathymetric features.

4.4. Influence of water-column environment and pack ice development

Previous research has suggested that seabirds in the Southern Ocean have foraging strategies that are adapted to particular sea-ice habitats (Ainley et al., 1992, 1994; Fraser and Ainley, 1986). Furthermore, it has been suggested that this specialization plays an important role in structuring seabird distributions. The only other study during the austral winter on the Antarctic Peninsula found a dramatic shift in species assemblage and abundance presumably due to the development of the winter pack ice (Whitehouse and Veit, 1994). In this study, the development of sea ice appeared to have influenced a shift in seabird and pinniped species assemblage, abundance, and habitat associations. However, the relative contribution of seasonal changes that co-varied with changes in sea-ice habitat between cruises (e.g. reduced day-length, lower ambient temperatures, large-scale shifts in prey distribution and availability) cannot be assessed with our analysis.

Snow petrel, Antarctic petrel, southern giant petrel, Adélie penguin, and crabeater seal all remained within, or moved into, the study area after the pack ice developed between the April–May and July–August cruises. These results

are consistent with previous studies that have found these species to be associated with pack ice (Ainley et al., 1993; Ribic et al., 1991; van Franeker, 1992; Woehler et al., 2003). The results from this study also are consistent with previous studies that have found lower species abundance in the Southern Ocean in winter presumably because species typically found in open water, such as cape petrel, blue petrel, southern fulmar (Ainley et al., 1994; van Franeker, 1992; Whitehouse and Veit, 1994) and Antarctic fur seal (Ribic et al., 1991), move north as the pack ice develops.

Additionally, the development of sea ice appeared to reduce predator densities in the study area, a finding that contradicts results from a study in the Scotia–Weddell Confluence during the summer that found higher seabird and seal abundance further inside the pack ice than at the sea-ice edge or in open water (van Franeker, 1992). This may reflect a difference in system characteristics between the southern Antarctic Peninsula and the Scotia–Weddell Confluence, or that the SO GLOBEC surveys were conducted further within the pack and during the winter.

Sea-ice characteristics played an important role in structuring seabird and pinniped distributions within the study area during both the April–May and July–August cruises. However, water-column environment and other physical variables were more strongly associated with species distributions during the April–May cruise, prior to the development of pack ice. At this time, the commonly observed species were associated with physical characteristics of the water column. In particular, most species were associated with Inner Shelf Water just north and west of Alexander Island in the vicinity of brash and new sea ice that covered greater than 0.3 of the ocean surface; all of the crabeater seal sightings also were in this area. These results agree with the findings of Burns et al. (2004) that crabeater seals outfitted with Satellite Relay Data Loggers focused their activity in this region just north and west of Alexander Island. In this study, crabeater seals were observed in shallow water, on-shelf areas during the July–August cruise, a result which also agrees with locations of crabeater seals reported in Burns et al. (2004).

Previous analyses of water-column processes and primary production in western Antarctic Peninsula continental shelf waters suggest the important role of sub-surface processes in determining phytoplankton communities in the surface waters in this region (Prézelin et al., 2000, 2004). The results presented in Tables 3 and 6 show that both physical properties and predator distributions were associated with sub-surface water masses, thereby suggesting that sub-surface processes may be influencing physical and biological processes in surface waters during winter on the western Antarctic Peninsula. Alternatively, the distribution of the temperature maximum below 200 m may have served as a proxy for some other variable that is important for structuring predator distribution, rather than indicating the influence of deep water masses on surface biology.

After the sea ice developed, sea-ice characteristics became more useful in predicting species distributions than the water-column environment and also appeared to modify the relationship between top-predator distributions and physical variables for species observed during both cruises. Snow petrels and Antarctic petrels, previously associated with Inner Shelf Water in the April–May cruise, were no longer associated with a particular water mass after pack ice developed. Instead, in the July–August cruise, these species were associated with a combination of sea-ice characteristics and other water-column variables. Additionally, crabeater seals, previously seen concentrated near Alexander Island in the Inner Shelf Water, became more dispersed throughout the study area and were associated with modified UCDW after the pack ice developed.

5. Conclusions

The results from the 2001 austral fall and winter cruises suggest that some of the more abundant seabird and pinniped species distributions are structured by interactions between sea ice and other environmental variables. As a result, the development of pack ice in winter appears to limit access to environmental or ecosystem structures that arise from water-column processes or bathy-

metric influences on water flow. Consequently, predation pressure by birds and pinnipeds in the Southern Ocean during the austral winter may be strongly modified by the timing and extent of the development of pack ice during the winter months. Furthermore, these results suggest a link between top-predator distributions and water-column processes on the western Antarctic Peninsula, at least during austral fall, prior to pack-ice development. A better understanding of the physical–biological processes that are responsible for these patterns awaits further synthesis work combining field and modeling research.

Acknowledgements

We thank Raytheon Polar Services and Edison Chouest for the logistical support that contributed to the success of these cruises. We thank E. Hofmann, E. Woehler, R. Veit, and an anonymous reviewer for their comments on the manuscript. We thank R. Beardsley for his assistance with the R.V.I.B. *Nathaniel B. Palmer*'s underway environmental conditions data set and E. Hofmann and J. Klinck for their help in defining subsurface water masses. Mention of trade names does not constitute endorsement for use. This material is based upon work supported by the National Science Foundation under Grant No. 9910096. This is GLOBEC Contribution No. 464.

References

Abrams, R.W., 1985. Environmental determinants of pelagic seabird distribution in the African sector of the Southern Ocean. Journal of Biogeography 12, 473–492.

Ainley, D.A., 2003. The Adélie Penguin: Bellwether of Climate Change. Columbia University Press, New York, p. 310.

Ainley, D.A., Jacobs, S.S., 1981. Sea-bird affinities for ocean and ice boundaries in the Antarctic. Deep-Sea Research I 28, 1173–1185.

Ainley, D.A., Ribic, C.A., Fraser, W.A., 1992. Does prey preference affect habitat choice in Antarctic seabirds? Marine Ecology Progress Series 90, 207–221.

Ainley, D.A., Ribic, C.A., Spear, L.B., 1993. Species–habitat relationships among Antarctic seabirds: a function of physical or biological factors? The Condor 95, 806–816.

Ainley, D.A., Ribic, C.A., Fraser, W.A., 1994. Ecological structure of migrant and resident seabirds of the Scotia–Weddell Confluence region. Journal of Animal Ecology 63, 347–364.

Ainley, D.A., Jacobs, S.S., Ribic, C.A., Gaffney, I., 1998. Seabird distributions and oceanic features of the Amundsen and southern Bellingshausen seas. Antarctic Science 10, 111–123.

Brown, R.G.B., Gaskin, E.C., 1988. The pelagic ecology of the grey and red-necked phalaropes *Phalaropus fulicarius* and *P. lobatus* in the Bay of Fundy, eastern Canada. Ibis 130, 234–250.

Burnham, K.P., Anderson, D.R., 1998. Model Selection and Inference, a Practical Information-Theoretic Approach. Springer, New York, p. 353.

Burns, J.M., Costa, D.P., Fedak, M.A., Hindell, M.A., Bradshaw, C.J.A., Gales, N.J., McDonald, B., Trumble, S.J., Crocker, D.E., 2004. Winter habitat use and foraging behavior of crabeater seals along the Western Antarctic Peninsula. Deep-Sea Research II, this issue [doi:10.1016/j.dsr2.2004.07.021].

Cook, R.D., Weisberg, S., 1999. Applied Regression Including Computing and Graphics. Wiley, New York, p. 593.

Cressie, N.A.C., 1993. Statistics for Spatial Data, Revised Edition. Wiley, New York, p. 900.

Environmental Systems Research Institute Inc., 1996a. Arc View GIS. Environmental Systems Research Institute Inc., Redlands, CA, p. 340.

Environmental Systems Research Institute Inc., 1996b. Using the Arc View Spatial Analyst. Environmental Systems Research Institute Inc., Redlands, CA, p. 148.

Fraser, W.R., Ainley, D.A., 1986. Ice edge and seabird occurrence in Antarctica. Bioscience 36, 258–263.

Fraser, W.R., Trivelpiece, W.Z., 1996. Factors controlling the distribution of seabirds: winter–summer heterogeneity in the distribution of Adélie penguin populations. Foundations for ecological research west of the Antarctic Peninsula. Antarctic Research Series 70, 257–272.

Heinemann, D., 1981. A range finder for pelagic bird censusing. Journal of Wildlife Management 45, 489–493.

Hofmann, E.E., Klink, J.M., 1998. Thermohaline variability of the waters overlying the west Antarctic Peninsula continental shelf. Ocean, Ice, and Atmosphere: Interactions at the Antarctic Continental Margin Antarctic Research Series 75, 67–81.

Hofmann, E.E., Klinck, J.M., Costa, D.P., Daley, K.L., Torres, J.J., Fraser, W.R., 2002. US Southern Ocean global ocean ecosystems dynamics program. Oceanography 15, 64–74.

Hunt Jr., G.L., 1991. Marine ecology of seabirds in polar oceans. American Zoologist 31, 131–142.

Hunt Jr., G.L., Schneider, D.C., 1987. Scale-dependent processes in the physical and biological environment of marine birds. In: Croxall, J.P. (Ed.), Seabirds: Feeding Ecology and Role Marine Ecosystems. Cambridge University Press, Cambridge, UK, pp. 7–42.

Hunt Jr., G.L., Priddle, J., Whitehouse, M.J., Veit, R.R., Heywood, R.B., 1992. Changes in seabird species abundance near South Georgia during a period of rapid change in sea surface temperature. Antarctic Science 4, 15–22.

Hunt Jr., G.L., Russell, R.W., Coyle, K.O., Weingartner, T., 1998. Comparative foraging ecology of planktivorous auklets in relation to ocean physics and prey availability. Marine Ecology Progress Series 167, 241–259.

Klinck, J.M., Hofmann, E.E., Beardsley, R.C., Salihoglu, B., Howard, S., 2004. Water-mass properties and circulation on the west Antarctic Peninsula continental shelf in austral fall and winter, 2001. Deep-Sea Research II, this issue [doi:10.1016/j.dsr2.2004.08.001].

Lakke, J., 2001. Ice Seal Protocol. National Marine Mammal Laboratory, Seattle, Washington, p. 8 (unpublished document).

Lawson, G.L., Wiebe, P.H., Ashjian, C.J., Gallager, S.M., Davis, C.S., Warren, J.D., 2004. Acoustically-inferred zooplankton distribution in relation to hydrography west of the Antarctic Peninsula. Deep Sea Research II, this issue [doi:10.1016/j.dsr2.2004.07.022].

MathSoft, 1999. S-Plus 2000 User's Guide. Data Analysis Products Division. MathSoft, Seattle, WA, p. 557.

McCullagh, P., Nelder, J.A., 1989. Generalized Linear Models, 2nd Edition. Chapman & Hall, New York, p. 511.

Orsi, A.H., Whitworth III, T., Nowlin Jr., W.D., 1995. On the meridional extent of fronts of the Antarctic Circumpolar Current. Deep-Sea Research I 5, 641–673.

Prézelin, B.B., Hofmann, E.E., Mengelt, C., Klinck, J.M., 2000. The linkage between Upper Circumpolar Deep Water (UCDW) and phytoplankton assemblages on the west Antarctic Peninsula continental shelf. Journal of Marine Research 58, 165–202.

Prézelin, B.B., Hofmann, E.E., Moline, M., Klinck, J.M., 2004. Physical forcing of phytoplankton community structure and primary production in continental shelf waters of the Western Antarctic Peninsula. Journal of Marine Research 62, 419–460.

Ribic, C.A., Ainley, D.G., Fraser, W.R., 1991. Habitat selection by marine mammals in the marginal ice zone. Antarctic Science 3, 181–186.

Russell, R.W., Harrison, N.M., Hunt Jr., G.L., 1999. Foraging at a front: hydrography, zooplankton, and avian planktivory in the northern Bering Sea. Marine Ecology Progress Series 182, 77–93.

Schneider, D., Harrison, N.M., Hunt Jr., G.L., 1987. Variation in the occurrence of marine birds at fronts in the Bering Sea. Estuarine, Coastal and Shelf Science 25, 135–141.

Smith, D.A., Lascara, C.M., Klinck, J.M., Hofmann, E.E., Smith, R.C., 1995. Palmer LTER: Hydrography in the inner shelf region. Antarctic Journal of the United States 30, 258–260.

Smith, D.A., Hofmann, E.E., Klinck, J.M., Lascara, C.M., 1999. Hydrography and circulation of the west Antarctic Peninsula continental shelf. Deep-Sea Research I 45, 925–949.

Spear, L., Nur, N., Ainley, D.G., 1992. Estimating absolute densities of flying seabirds using analyses of relative movement. Auk 109, 385–389.

The National/Naval Ice Center, Washington, DC, 2002. WWW Page, http://www.natice.noaa.gov.

Thiele, D., Chester, E., Moore, S., Širovic, A., Hildebrand, J., Friedlaender, A., 2004. Seasonal variability in whale encounters in the Western Antarctic Peninsula. Deep-Sea Research II, this issue [doi:10.1016/j.dsr2.2004.07.007].

University of Tasmania, Antarctic CRC, 1988. Seaice Version 2.22. University of Tasmania, Antarctic CRC, Hobart, Australia.

van Franeker, J.A., 1992. Top predators for ecosystem events in the confluence zone and marginal ice zone of the Weddell and Scotia Seas, Antarctica, November 1988 to January 1989 EPOS Leg 2. Polar Biology 12, 93–102.

van Franeker, J.A., Gavrilo, M., Mehlum, F., Veit, R.R., Woehler, E.J., 1999. Distribution and abundance of the Antarctic petrel. Waterbirds 22, 14–28.

Vermeer, K., Szabo, I., Greisman, P., 1987. The relationship between plankton-feeding Bonaparte's and Mew Gulls and tidal upwelling at Active Pass, British Columbia. Journal of Plankton Research 9, 483–501.

Watson, G.E., 1975. Birds of the Antarctic and Subantarctic. American Geophysical Union, Washington, DC, pp. 350.

Weisberg, S., 1985. Applied Linear Regression, 2nd Edition. Wiley, New York, p. 324.

Whitehouse, M.J., Veit, R.R., 1994. Distribution and abundance of seabirds and fur seals near the Antarctic Peninsula during the austral winter, 1986. Polar Biology 14, 325–330.

Woehler, E.J., 1993. The Distribution and Abundance of Antarctic and Subantarctic Penguins. Compiled on behalf of the SCAR Bird Biology Subcommittee, Australian Antarctic Division, Kingston, Tasmania, Australia, p. 76.

Woehler, E.J., Raymond, B., Watts, D.J., 2003. Decadal-scale seabird assemblages in Prydz Bay, East Antarctica. Marine Ecology Progress Series 251, 299–310.

Zwally, H.J., Comiso, J.C., Parkinson, C., Campbell, W.J., Carsey, F.D., Gloersen, P., 1983. Antarctic Sea-Ice, 1973–1976: Satellite Passive-Microwave Observations. NASA Special Publication 459, Washington, DC, p. 206.

ELSEVIER

Deep-Sea Research II 51 (2004) 2279–2303

DEEP-SEA RESEARCH
PART II

www.elsevier.com/locate/dsr2

Winter habitat use and foraging behavior of crabeater seals along the Western Antarctic Peninsula

Jennifer M. Burns[a,*], Daniel P. Costa[b], Michael A. Fedak[c], Mark A. Hindell[d], Corey J.A. Bradshaw[d], Nicholas J. Gales[e], Birgitte McDonald[f], Stephen J. Trumble[g], Daniel E. Crocker[f]

[a]*Department of Biological Science, University of Alaska, 3211 Providence Dr., Anchorage, AK 99508, USA*
[b]*Department of Ecology and Evolutionary Biology, University of California Santa Cruz, 100 Shaffer Road, Santa Cruz, CA 95060, USA*
[c]*Gatty Marine Laboratory, Sea Mammal Research Unit, University of St. Andrews, Fife KY16 8LB, Scotland*
[d]*Antarctic Wildlife Research Unit, School of Zoology, University of Tasmania, GPO Box 252-05, Hobart, Tasmania 7001, Australia*
[e]*Australian Antarctic Division, Channel Highway, Kingston Tasmania 7050, Australia*
[f]*Department of Biology, Sonoma State University, 1801 East Cotati Avenue, Rohnert Park, CA 94928, USA*
[g]*School of Fisheries and Ocean Sciences, University of Alaska Fairbanks, Fairbanks, AK 99775, USA*

Accepted 8 July 2004

Abstract

We quantified the winter and spring movement patterns and foraging behavior of adult crabeater seals (*Lobodon carcinophagus*), and the influence of sea ice and bathymetry on their foraging behavior. Thirty-four seals (16 M 18 F) were outfitted with Satellite Relay Data Loggers (SRDLs) in the Marguerite Bay Region of the Antarctic Peninsula (~67°S, 67°W) during the austral winters of 2001 and 2002. Tags transmitted position and dive information for between 4 and 174 days. Overall, winter activity patterns differed significantly from previously reported data collected during the summer: seals in this study dived deeper (92 ± 0.2 m, range 6–713 m) and longer (5.26 min ± 0.6, range 0.2–23.6 min), hauled out during the night rather than the day, and showed seasonal shifts in foraging patterns consistent with foraging on vertically migrating prey. While these patterns were more pronounced in 2001 than in 2002, there were no strong differences in patterns of habitat use between the 2 years. Some animals made long distance movements (furthest movements 664 km to northeast, 1147 km to southwest), but most seals remained within 300 km of their tagging location. Within the Marguerite Bay/Crystal Sound region, seals appeared to favor foraging locations on the continental shelf within the 50 to 450 m depth range, with a tendency to avoid depths of 600 m or greater. In both years, seals remained deep within the pack ice throughout the winter, and did not move into regions with less ice cover. Seals were more likely to be located in shallow water where the bathymetric gradients were greatest, and in areas of higher

*Corresponding author. Tel.: +1-907-786-1527; fax: +1-907-786-4607.
E-mail address: jburns@uaa.alaska.edu (J.M. Burns).

0967-0645/$ - see front matter © 2004 Elsevier Ltd. All rights reserved.
doi:10.1016/j.dsr2.2004.07.021

sea-ice concentration. In combination, these findings suggest that crabeater seals alter their behavior to accommodate seasonal and/or annual fluctuations in seasonal sea ice and associate with bathymetric features likely to concentrate prey patches.
© 2004 Elsevier Ltd. All rights reserved.

1. Introduction

The pack ice region surrounding Antarctica is home to six species of pinnipeds (Antarctic fur seal, *Arctocephalus gazella*, crabeater, *Lobodon carcinophagus*, Weddell, *Leptonychotes weddellii*, Ross, *Ommatophoca rossii*, leopard, *Hydrurga leptonyx*, and Southern elephant, *Mirounga leonina*, seals) that account for much of the world's total pinniped biomass (Laws, 1977, 1985). As a group, these species are among the dominant predators in the Southern Ocean, and as such, changes in their abundance or distribution will likely influence the trophic structure of the Southern Ocean (Laws, 1985; APIS, 1995; Costa and Crocker, 1996; Hofmann et al., 2002). At the same time, shifts in the trophic structure of the Southern Ocean due to natural or anthropogenic impacts can influence the foraging behavior, reproductive success, and survival of these apex predators (Bengtson and Laws, 1985; Testa et al., 1991; Lunn et al., 1994; Guinet et al., 1994). Recent studies have focused on how researchers might use demographic or behavioral changes in apex predators as indications of ecosystem events (Boyd and Murray, 2001; Hindell et al., 2003), and linking shifts in predator and prey dynamics with environmental variability is a key goal of the US Southern Ocean GLOBEC (GLOBal ocean ECosystems dynamics) research program (Hofmann et al., 2002). However, for these efforts to be successful we must have information on how animals locate and utilize the resources available to them, and how such use varies temporally and spatially.

Marine mammals are not randomly distributed throughout the habitat, but instead are concentrated in more productive waters. As a result, predator distributions have been used as indices of resource availability (van Franecker, 1992; Ancel et al., 1992). However, not only do predator distributions track those of their prey, but for many species, regions of highly localized productivity appear critical for reproductive success and population growth (Costa, 1991; Trillmich et al., 1991; Guinet et al., 1994; Trathan et al., 1996; Boyd and Murray, 2001). Within Antarctic waters, higher predator densities are often seen in polynyas and local eddies (Trathan et al., 1993), at frontal systems and thermal layers (Boyd and Arnbom, 1991; Field et al., 2001), near sea mounts and the continental shelf break (McConnell et al., 1992; Guinet et al., 2001), and in association with certain characteristics of the marginal ice zone (Kawaguchi et al., 1986; Trathan et al., 1996; Ichii et al., 1998). Many of these oceanographic features physically aggregate prey, and therefore create areas where predator foraging efficiency can be increased. However, during the Antarctic winter, resident predators face reduced productivity, increased ice cover, altered hydrographic regimes, and concomitant changes in prey abundance and availability. The strategies marine mammals use to survive in this altered foraging landscape are poorly understood, but likely depend on the magnitude of the seasonal fluctuations and the diving capabilities of the predators.

Crabeater seals are well suited for investigations of relationships between seasonal variation in foraging behavior, habitat use, and environmental conditions. Crabeater seals are abundant, year-round residents of the Antarctic pack ice, and they forage primarily on Antarctic krill (*Euphausia superba*) (Laws, 1985). Krill is a patchily distributed prey resource that varies in abundance and energy content due to seasonal shifts in environmental conditions (Siegel, 1988; Sprong and Schalk, 1992; Trathan et al., 1993; Ichii et al., 1998; Lascara et al., 1999). Therefore, crabeater seal behavioral strategies are likely to change seasonally in response to the same factors that influence krill populations. Previous research has indicated that crabeater seal populations are sensitive to environmental fluctuations (Testa et al., 1991; Bester et al., 1995; APIS,

1995; Bengtson and Laws, 1985), and that individuals are often found in areas where krill abundance is higher (Nordøy et al., 1995; McMahon et al., 2002). However, most models of habitat selection rely on ship-based abundance surveys rather than individual movement patterns, and therefore focus on summertime patterns. To date, information on crabeater seal ecology during winter is largely absent.

Here, we characterize the wintertime diving and movement patterns of crabeater seals diving within the Marguerite Bay region of the Western Antarctic Peninsula (Fig. 1), with an emphasis on seasonal and spatial variation. We focus on seasonal shifts in the depth, duration, and timing of dives, and on how bathymetry and ice cover influence habitat use. We then relate seal behavior to data on prey abundance as determined by other Southern Ocean GLOBEC researchers. Our goal throughout is to determine how seals are selecting foraging locations and exploiting prey in a changing landscape. Because of their large numbers and high biomass, crabeater seals are perhaps the largest consumer of krill in the Antarctic (Hewitt and Lipsky, 2002), and information on wintertime foraging tactics is critical for the ecosystem modeling efforts that are an ongoing component of the Southern Ocean GLOBEC program.

2. Methods

2.1. Animal handling

Crabeater seals were captured during four research cruises (23 April–6 June and 21 July–1 September 2001; 7 April–21 May and 29 July–19 September 2002) to the Marguerite Bay Region of the Antarctic Peninsula (~67°S, 67°W) by the *A.S.R.V. Lawrence M. Gould*. Seals were sighted from the bridge, approached on foot or by inflatable boat, and sedated by an intramuscular injection of Telezol (0.8–1.2 mg kg^{-1}, autumn 2001) or Midazolam (0.39–0.84 mg kg^{-1}; Hoffmann–La Roche Inc., NJ, USA, all subsequent cruises). Following induction, animals were restrained manually with a hoop net, and isoflurane

Fig. 1. Location of satellite tags deployed on crabeater seals within the Marguerite Bay study region in 2001 and 2002. Tags deployed in 2001 are indicated by ■, 2002 by ●. Key places mentioned in the text are also indicated, and contour lines are shown at 200 m intervals.

was delivered at 0.5–5% with 4–5 L min^{-1} oxygen flow using a non-rebreathing Bain circuit (LMG-01-04) or a circle rebreathing circuit (LMG 01-06, 02-03, 02-04) via gas mask or intubation (Gales and Mattlin 1998). Once animals were quiescent, morphometric measurements (mass $\pm$0.5 kg, length and girth $\pm$3 cm) were collected and a satellite-relay data logger (SRDL, manufactured by the Sea Mammal Research Unit, University of St. Andrews, Scotland) was attached to the head using Devcon™ 5-min epoxy. After completion of all procedures, animals were allowed to recover from anesthesia and released. All animal handling protocols were authorized under US Marine Mammal Permit #1003-1665-00 and approved by Institutional Animal Care and Use Committees at University of Alaska Anchorage and University of California Santa Cruz.

2.2. Satellite relay data logger programming

The SRDL tags were programmed to collect data on a range of activity patterns. Tags recorded dive depth, start time, duration, and post-dive surface intervals (4 s sampling frequency), and the start time and duration of haulouts. In addition, for each four-h period of the day, tags recorded the percent time the animals spent hauled out, in water (<6 m depth), and diving (activities >6 m depth), the total number of dives made, and the average depth and duration of all dives in that period. Depth was transmitted with a resolution that increased from 3 to 24 m (3 m surface to 50 m; 24 m once dives exceeded 375 m), to a maximum depth reading of 712.5 m. Dive duration was transmitted with a resolution ranging from 6 s for dives shorter than 9 s, to 48 s once dives exceeded 741 s, with a maximum duration of 1413 s. Dive data were transmitted every 45 s when the animals were on the surface at sea, and at 80 s intervals during the first 2 h of each haulout. Tags then cycled 3 h 'off', 2 h 'on' for the remainder of the haulout, with a maximum of 500 transmissions per day. The ARGOS system calculated animal position from received transmissions (Service Argos, 1996). Since positions were time-referenced, it was possible to determine the approximate location of all dives. Additional tag programming details have been previously published (Fedak et al., 2001, 2002). All time variables were collected in Greenwich Mean Time (GMT) and corrected for local time based on the geographic position of the seal at that time (local solar time = GMT + degrees longitude/15).

2.3. Activity patterns and dive frequency

Activity patterns and dive frequencies were determined only for those days when data were received from all 6-h periods. This summary information was then used to determine the percent time that individual seals spent in three different activity states: hauled out, in water but at the surface (<6 m) and diving (>6 m) each day. All proportions were arcsin transformed ($p' = \arcsin\sqrt{p}$) prior to analysis. Linear, mixed-effects, repeated measures analyses were used to determine the impact of period of day and month on the activity patterns of individual seals (SPSS© 11.5). Since light levels changed dramatically across the seasons, not all periods were similar (i.e. light levels 4–8 a.m. were lower in July than October). Therefore month was treated as the primary fixed factor and period was nested within month. Each year was treated separately due to the differential temporal coverage in 2001 (May–November) and 2002 (April–September). We used an autoregressive moving average covariance structure and a random intercept term. Bonferroni adjusted confidence intervals were used to compare the estimated marginal means for the modeled factors (significance assumed at $P<0.05$).

2.4. Haulout patterns

The start and end time of all haulouts was determined, and the average haulout start, end, duration, and interval was then calculated for each seal in each month of the study. The average start and end time of all haulouts was determined using the circular statistics analysis package Oriana 1.0 (Kovach Computing Services, UK), and these data used to test the effect of month and year in a two-way analysis of variance (ANOVA).

2.5. Dive data analysis

To control for the abundance of short and shallow dives, and because dive depth and duration were bimodally distributed, dives were separated into two categories: dives $\leqslant 24$ m and dives >24 m, where 24 m was the minimum value between the two depth distributions. This separation resulted in three positively skewed distributions: depth and duration of dives $\leqslant 24$ m, and depth of dives >24 m. The duration of dives >24 m was normally distributed. All skewed distributions were log-transformed prior to analyses. To remove internal data-processing errors that were present in a few of the 2002 tags, dives that required ascent or descent swim speeds in excess of $6\,m\,s^{-1}$ were removed from the data set. This cutoff speed is more than double the average swim speeds of most phocids (Williams, 2002), making it a highly conservative criterion.

To test for diel and seasonal effects on dive behavior, the average depth and duration of dives were determined for each individual seal in each hour of each month. As with activity patterns, these mean values were analyzed using a linear mixed-effects repeated measures model, with seal as the subject, an autoregressive moving average covariance structure, and a random intercept term. In these analyses, month was treated as the main term, hour was nested within month, and the measure was the mean value for each individual seal for that month and hour. Cases with fewer than five dives were omitted from the analyses, and separate analyses were run for each year and dive category. To identify significant differences within factors marginal means were compared, using Bonferroni adjustments of the confidence intervals to account for the number of internal comparisons (Sokal and Rohlf, 1995). All statistical analyses of dive data were carried out in SPSS 11.5 (SPSS Inc., USA).

2.6. Spatial analysis

Information received from the tags was integrated into Access databases, and exported into Interactive Data Language (IDL 5.0, Research Systems, Inc) and ArcGIS (ESRI, Inc., USA) for analysis. Locations were screened by an iterative forward/backward averaging filter that identified and excluded locations that would require rates of travel greater than $4\,m\,s^{-1}$ (Vincent et al., 2002). The maximum distance traveled was calculated as the difference between the original tagging location and the furthest average daily position.

Habitat-use patterns were assessed by determining the overall percent time that all seals spent in different regions of the study area, and then comparing this usage data with the physical characteristics of the habitat. To determine usage, the study area was divided into 5×5 km ($25\,km^2$) raster grid cells, and the time spent in each grid cell determined by interpolating between locations assuming constant average speed. This allowed us to determine the seal's putative time of entry and exit for each cell along the trajectory. A spatial grain of 5 km was chosen because (1) finer grains (i.e., <5 km) would have made the summary of spatial data (water depth, sea ice concentration) difficult due to the different spatial scale between seal use and sea ice concentration, (2) finer grains would have made it impossible to determine the variance of depth and prevented the use of depth as a covariate in a general linear model, and (3) this scale provided a method of summarizing overall use from all sampled seals within a single spatial unit. Once entry and exit times were determined for each individual animal, the overall percent of time spent in each grid cell was determined for all animals combined, for each month of the study. All routines were processed in IDL (Bradshaw et al., 2002).

To determine if seals were actively selecting regions with particular depth or sea-ice characteristics, we examined the relationship between the percent time spent in each grid cell, and the depth and percent ice concentration. Bathymetry was determined using the ETOPO2 Global 2′ elevations, and there were a mean of 4.8 ETOPO2 bathymetry estimates per 5×5 km grid cell. This allowed both the mean and standard error of the depth per cell to be calculated. Data on the monthly sea-ice concentration were acquired from the Defense Meteorological Satellite Program (DMSP) Special Sensor Microwave/Imager (SSM/I) from the National Snow and Ice Data

Center (NSIDC) in Boulder, Colorado, and the bootstrap algorithm monthly sea-ice concentrations from the F13 instrument (Comiso, 1990) was used to obtain concentrations from 0% (open water) to 100% (closed ice cover) in every 25 km grid cell in the region surrounding Antarctica. Because the grain size for ice was larger than for seal use, 50 km × 50 km grid cells for sea ice were generated from the point data. Polygons of seal habitat usage were then overlaid onto the sea-ice polygons and the mean value of sea ice per grid cell of seal usage was calculated. Thus, many 5 × 5 km grid cells of usage had identical sea-ice concentration estimates (e.g., within cell variance in sea-ice could not be estimated).

Once the mean seafloor depth, most common sea-ice concentration, and the time spent in each grid cell were tabulated, the total time spent for all seals was determined within each pre-defined habitat class. These classes were based on the distribution of habitat types available. For bathymetry, we divided the habitat into 100-m depth classes (e.g., 0–49 m = '0' m class, 50–149 m = '100' m class, etc.), but because seals spent very little time in depth classes ≥700 m, only those classes <700 m were considered. For sea-ice concentration, we summarized the mean monthly sea-ice concentrations into classes of 10% cover (e.g., 0–19% ice cover, thereafter in 10% increments), and so considered a total of nine ice habitat classes. The amount of time that seals spent in each grid was the index of habitat use.

Habitat availability was determined by assuming that the distribution of all sampled seals represented the maximum dispersal capability within a specific time period (e.g., year; month). All grid cells occupied within a specific time period were outlined with a minimum convex polygon (MCP; White and Garrott, 1990). The resulting area was used to define the boundary of the 'available' environmental variable (bathymetry or sea ice) during that time period. For example, selection for sea-ice was determined by comparing the time spent per sea ice class to the mean sea ice available within the MCP area as defined for that month. For these analyses, the MCPs for the 2 years were combined so as to have the largest range of ice types available.

Habitat selection was determined by comparing modified Bonferroni-corrected 95% confidence intervals for the use and availability, as estimated for each depth and sea-ice concentration class (Neu et al., 2002). For each class, the 95% confidence intervals for both the proportion used and availability were calculated as

$$P_i \pm z_{\alpha/2k}\sqrt{\frac{P_i(1-P_i)}{t}},$$

where P_i is the proportion of habitat type i (depth or sea-ice class) used or available, $z_{\alpha/2k}$ is the upper standard normal variate corresponding to a probability tail area of $\alpha/2k$, k is the number of habitat classes, and t is the total number of use hours estimated from the IDL output routines per month (sea-ice) or per year (bathymetry). When the lower 95% confidence interval for use exceeded the upper 95% confidence interval for availability, that habitat class was said to be significantly selected. When the upper 95% confidence interval for availability was less than the lower 95% confidence interval for use, that habitat class was said to be significantly avoided. When the 95% confidence interval for availability fell within the 95% use confidence interval, that habitat type was said to be used randomly with respect to its availability.

To determine if the amount of time that the seals spent in different areas of the habitat varied in response to physical characteristics of the environment, we examined the relationship between the time spent per 5 × 5 km grid cell, the study year, and the mean depth, standard error of depth, sea ice concentration using a generalized linear model (the GENMOD procedure in SAS 6.11 with a Poisson error model and a log link; McCullagh and Nelder, 1989; McMahon et al., 2002). This effort differs from that described above, as it focuses solely on the cells used by seals, and does not address the availability issue. The number of hours crabeater seals spent per grid cell and the mean depth per grid cell were log-transformed to normalize the data and reduce heteroscedasticity. For the estimated sea-ice concentrations, the angular transformation ($x' = \arcsin\sqrt{x}$) was used. The standard error of the depth estimate was used as a surrogate for bathymetric gradient. We chose

the most parsimonious model by examining all months together, and removing variables (year, depth, SE_{depth}, sea-ice) in a stepwise fashion. The change in deviance was assessed using χ^2 comparisons (McMahon et al., 2002). The resulting model was then applied to each winter month separately.

3. Results

3.1. Animal handling and tag performance

During the four Southern Ocean GLOBEC cruises we captured 46 crabeater seals (24 M, 22 F; 14 in 2001, 29 in 2002), and instrumented 34 seals (18 F, 16 M) with SRDLs (Fig. 1, Table 1). Animals ranged in mass from 113 to 413 kg, and all but the smallest female were judged to be 2 years or older based on mass and standard length (Laws et al., 2003). Animals were easily approached, and reacted well to handling procedures (mean handling time 114 ± 7 min). No adverse effects due to anesthesia protocols were noted. Scats collected from ice floes used by seals in 2001 contained only krill, while those from 2002 contained hard parts from both krill and fish, indicating that crabeater seals in the Marguerite Bay region were occasionally supplementing their zooplankton diet with fish.

The SRDL tags transmitted data for between 4 and 174 days (Table 1). In most cases, transmission failure could be attributed to antenna loss, as signal strength decreased and the proportion of successful transmissions declined prior to reception of the last transmission. Because tags deployed in autumn transmitted for longer than those deployed in winter (84.1 ± 14.7 vs. 47.7 ± 6.5 days), and tags deployed in the relatively lighter ice year (2001) lasted longer than those deployed in the heavier ice year (2002) ($72.6.1 \pm 9.4$ vs. 57.2 ± 12.6 days), we hypothesize that failure was due to antenna wear against the ice. When still functioning properly, we received an average of 21 (1–42) positions per day from the tags, of which an average of 15 (1–32) passed through the position screening algorithms. In total, we received information on 104–440 dives in 2001 and 46–751 dives in 2002. Data-processing errors resulted in the removal of 0.97% of the dives from the 2002 record.

3.2. Activity patterns

Overall, seals spent $29.7 \pm 8.8_{(SD)}$% of their time at the surface, 45.2 ± 11.6% diving, and 25.1 ± 14.4% hauled out. While all three activity patterns varied by month and period, the pattern was similar between years (Fig. 2). The proportion of time seals spent at the surface varied by month in both 2001 and 2002 (2001: $F_{6,104.6} = 5.370$, $P < 0.001$; 2002: $F_{6,51.7} = 3.129$, $P = 0.011$), with a decrease as the season progressed and ice formed. In addition, the proportion of time spent at the surface varied by time of day in both years (2001: $F_{35,94.3} = 1.948$, $P = 0.006$; 2002: $F_{35,81.3} = 2.596$, $P < 0.001$). The pattern was similar across months, with seals spending the least amount of time near the surface in midday, and the most at night.

The proportion of time spent hauled out increased significantly as the season progressed in 2001 but not in 2002 (month effect 2001: $F_{6,43.2} = 2.480$, $P = 0.038$; 2002: $F_{6,55.4} = 1.791$, $P = 0.118$). However, time of day significantly influenced time spent hauled out within each month in both study years (Period (month) 2001: $F_{35,87.3} = 2.115$, $P = 0.003$; 2002: $F_{35,102.1} = 2.959$, $P < 0.001$). Haulout was more common in early morning from May to July, and in late afternoon September to November. These effects were not solely due to the long haulout by seal G010 (discussed below) for they persisted when she was excluded from the data set.

The proportion of time spent diving (>6 m) varied by time of day in 2001 and 2002 (2001: $F_{35,125.9} = 3.516$, $P < 0.001$; 2002: $F_{35,105.4} = 2.042$, $P = 0.003$), with a greater proportion of dives around midday from April to June, and around midnight from September to November. Time spent diving also varied by month in 2001 (month: $F_{6,68.4} = 3.636$, $P = 0.003$) largely due to a decline in the proportion of time spent diving in October and November. There was no effect of month in 2002.

The mean number of dives made per day varied by year, month, and period of day. Overall, seals in 2001 made fewer dives than seals in 2002 ($119 \pm 40_{(SD)}$ vs. 188 ± 42 dives day^{-1}, $t_{31} = 4.854$,

Table 1
Summary information on crabeater seals outfitted with SRDL tags, showing sex, mass, and the first and last dates of data transmissio for seal behavior or location

Seal ID	Sex	Mass (kg)	First transmission	Last transmission	Deployment day
G001	Female	—	5/7/2001	10/1/2001	147
G002	Male	287[a]	5/11/2001	10/22/2001	164
G003	Female	258[a]	5/11/2001	10/31/2001	173
G004	Male	342[a]	5/23/2001	8/26/2001	95
G005	Female	293[a]	5/23/2001	9/24/2001	124
G006	Female	413[a]	5/23/2001	9/6/2001	106
G007	Male	287[a]	5/23/2001	10/8/2001	138
G008	Female	355[a]	5/25/2001	6/18/2001	24
G009	Male	179.0	8/2/2001	9/23/2001	52
G010	Female	307.0	8/6/2001	11/29/2001	115
G011	Male	232.0	7/30/2001	11/18/2001	111
G012	Female	288.0	8/6/2001	9/14/2001	39
G013	Male	234.0	8/7/2001	10/24/2001	78
G014	Male	284.0	8/10/2001	11/18/2001	100
G015	Male	234.0	8/15/2001	10/21/2001	67
G016	Female	273.0	8/22/2001	10/18/2001	57
G017	Female	117.5	4/15/2002	5/23/2002	38
G018	Male	156.5	4/15/2002	04/27/02	12
G019	Female	155.5	4/15/2002	4/22/2002	7
G021	Male	270.5	4/17/2002	8/1/2002	106
G022	Female	268.0	4/20/2002	9/17/2002	150
G023	Male	174.0	4/23/2002	6/10/2002	48
G024	Female	256.0	4/27/2002	10/1/2002	157
G026	Female	266.0	4/27/2002	10/24/2002	180
G031	Female	385.0	8/6/2002	9/24/2002	49
G033	Female	267.5	8/6/2002	10/4/2002	59
G034	Female	294.5	8/6/2002	9/17/2002	42
G035	Female	238.0	8/7/2002	8/12/2002	5
G036	Female	207.0	8/7/2002	9/13/2002	37
G038	Male	273.0	8/9/2002	8/20/2002	11
G039	Male	246.5	8/12/2002	10/25/2002	74
G040	Male	301.5	8/13/2002	9/7/2002	25
G041	Male	269.0	8/13/2002	8/25/2002	12
G042	Male	224.0	8/17/2002	10/16/2002	60

[a]Due to equipment failure, mass was calculated based on length and girth following Laws et al. (2003).

$P<0.001$). In both years, month had a significant impact on dive frequency (2001: $F_{6,61.9} = 2.673$, $P = 0.023$; 2002: $F_{6,53.7} = 2.850$, $P = 0.018$), with dive frequency higher in October and November in 2001, and lower in September 2002. While the diel pattern was similar in both years, the time of peak diving activity changed across the months (significant period by month effects 2001: $F_{35,90.1} = 3.202$, $P<0.001$; 2002: $F_{35,89.6} = 2.092$, $P = 0.003$). Dives were more frequent around local noon between April and July, but least frequent around noon from September on. However the pattern was less evident in 2002 than in 2001 (Fig. 3).

3.3. Haulout patterns

During this study crabeater seals hauled out 1440 times. One haulout was unique: adult female G010 hauled out for 607 h from 14 October to 8 November 2001; this behavior likely reflects

parturition and lactation. Other than this single long haulout, most haulouts were shorter than 24 h (mean 8.0±0.7 h, with only eight events lasting longer than 24 h). On average, haulouts occurred once a day (mean interval 26.9±1.7 h). There was no difference in haulout duration or intervals due to month or year. However, the timing of haulouts shifted during the study period. Before midwinter (April–July), seals hauled out in the late afternoon (16:45±0:16), and returned to the ocean in the early morning (3:04±2:00). After midwinter, the pattern shifted, with haulouts starting in the morning and ending in late afternoon (07:17±1:41 to 16:50±0:44; Fig. 4).

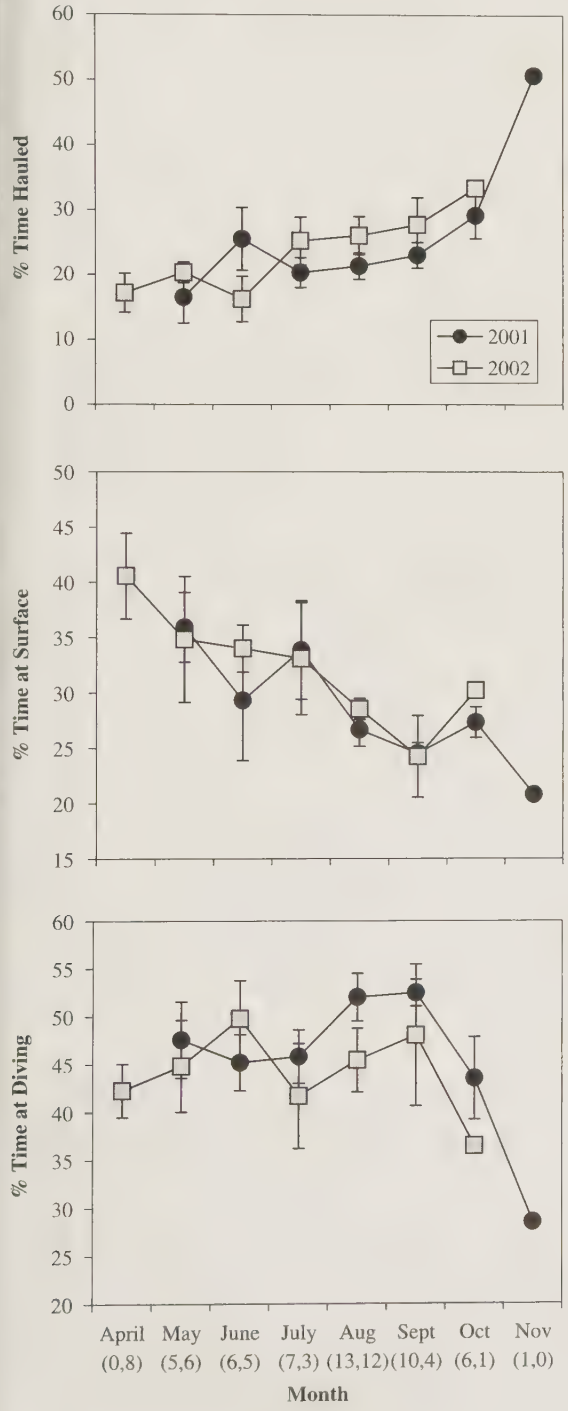

Fig. 2. Activity patterns of crabeater seals by month in 2001 and 2002. (A) mean±SE time spent hauled out per day; (B) mean±SE time spent in the water but at depths shallower than 6 m each day; (C) mean±SE time spent diving per day. Monthly average values were calculated for each seal from only those days in which data were received from all six periods, provided that there were at least 3 days of data in the month. Each individual is represented once per month, and the number of seals is indicated below the month (n_{2001}, n_{2002}). The increase in time spent hauled out in November is associated with the long haulout made by female G010.

3.4. Dive data

For all dives combined, the mean dive depth was 75.8 m±33.9$_{(SD)}$ (range for all dives 6–664.5 m) and the mean dive duration was 4.6 min±1.5 (range 0.2–23.6 min). Because dives longer than 23.6 minutes were assigned this maximum value, it is possible that seals made longer dives. When dives were separated into the two categories (shallow <24 m, or deep >24 m), deeper dives were more common: overall, 65.9% of dives were deeper than 24 m. Individually, the proportion ranged from 57.2–86.3% in 2001 to 10.9–78.4% in 2002.

In general, there was no seasonal or diel influences on the depth or duration of shallow dives. The only exception to this was in 2001, when dive duration varied by month ($F_{6,79.7} = 3.278$, $P = 0.006$), with dives in November significantly shorter than those in May–August. However, the mean difference was generally small (<5 s). Overall, dives averaged 11.0±5.3 m$_{(SD)}$ and 89.5±103.3 s.

In contrast, deeper dives (≥24 m) varied by time of day and season. In both 2001 and 2002 month

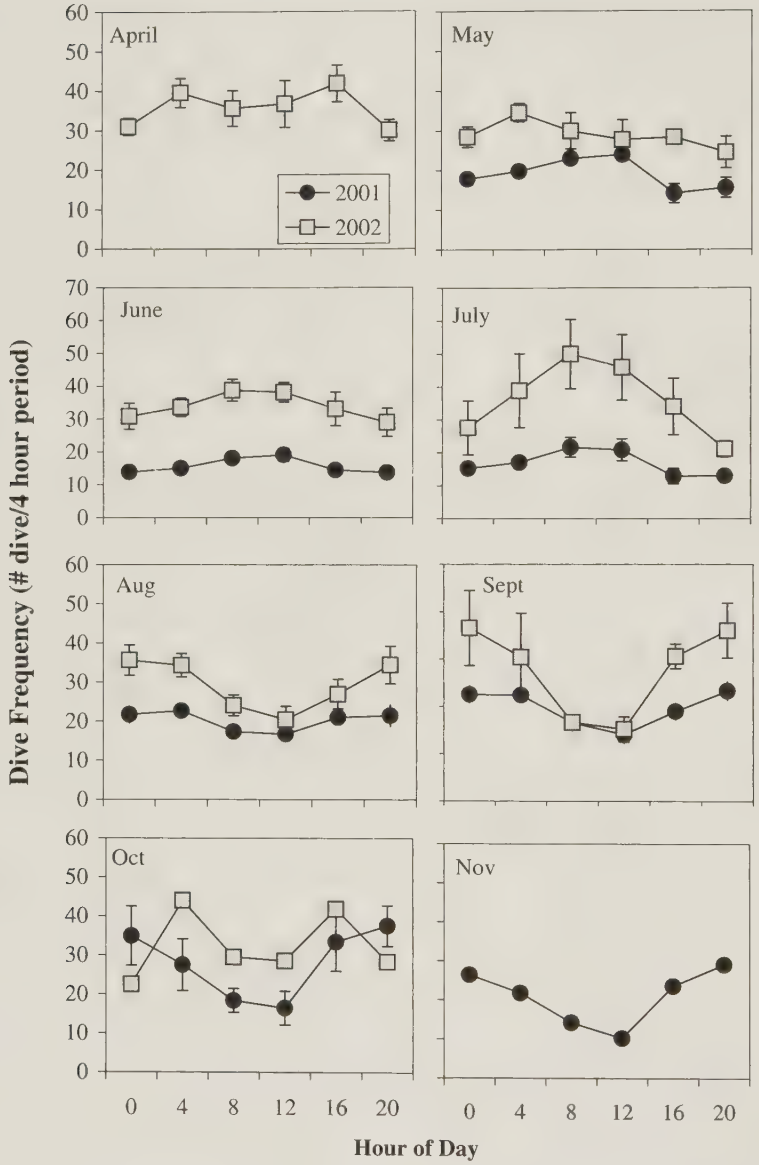

Fig. 3. Monthly mean±SE dive frequency (# dives/4-h period) for seals in 2001 and 2002. Daily averages were calculated for individual seals for those days in which data were received from all six periods. Monthly average values were calculated for each seal from only those days in which data were received from all six periods, provided that there were at least three days of data in the month. Each individual is represented once per month, and the sample sizes are as in Fig. 2.

and hour each accounted for a significant proportion of the overall variation in average depth and duration. Month effects were large: dive depth varied across months by 71% in 2001 and 81% in 2002, and dive duration varied by 94% in 2001 and 83% in 2002 (2001 logDepth $F_{6,83.8} = 4.278$, $P = 0.001$; duration $F_{6,74.4} = 8.889$, $P < 0.001$; 2002 logDepth $F_{6,112.4} = 2.754$, $P = 0.016$; duration $F_{6,104.1} = 2.579$, $P = 0.023$). Post hoc tests demonstrated that average dive depth and duration increased through September, and then decreased in October and November.

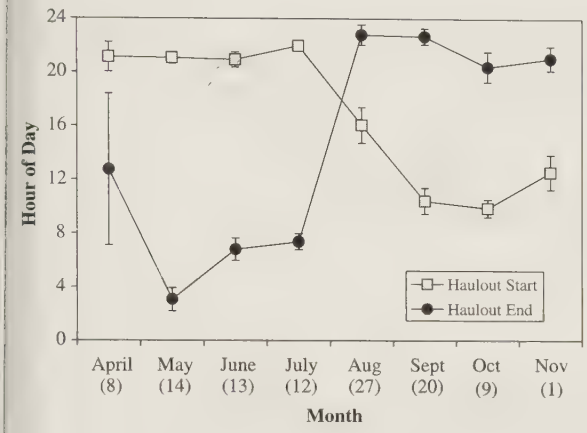

Fig. 4. Haulout patterns for seals in 2001 and 2002 combined showing the average (±SE) time that haulouts began and ended in each month of the study. Sample sizes are the number of seals that hauled out in each month for the two years combined. This number differs from that in Figs. 2 and 5 because haulout information was transmitted separately from diving or summary information.

However, within each month there was also a significant effect of time of day (nested ANOVA, hour by month effect: 2001 logDepth $F_{161,534.4} = 6.512$, $P<0.001$; duration $F_{161,541.4} = 3.5089$, $P<0.001$; 2002 logDepth $F_{161,442.6} = 3.766$, $P<0.001$; duration $F_{161,466.8} = 1.187$, $P = 0.086$). Overall, dives were deeper and longer during midday, with the trend becoming more pronounced as the season progressed from April to September. However, in October and November, dive depth and duration declined, and the diel pattern became less evident. The diel pattern was more evident in 2001 than in 2002, perhaps because dives in 2001 tended to be slightly longer and deeper than those in 2002 (Figs. 5 and 6).

3.5. Movement patterns and spatial analysis

On average, seals remained within 231±40 km of the site where they were tagged, and 26 of the 34 seals (76%) never traveled further than 300 km. However, the remaining seals did make longer movements. In 2001, adult male GG015 moved 1147 km to the southwest (final location 71.337°S, 98.055°W), while in 2002, female G017 traveled 664 km to the northern tip of the Antarctic Peninsula over a period of 30 days (Fig. 7).

Seals that remained within the study region were not distributed randomly throughout their habitat, but instead concentrated their activities in relatively few key areas (Fig. 8). These were the area south of Marguerite Bay off the northwest tip of Alexander Island (approx. 68°S 71°W), the northern portion of LauBeuf Fjord, and in the region of Crystal Sound bounded on the north by the northern end of Lavoisier Island, on the south by the southern end of Hanusse Bay, on the west by Matha Strait, and on the east by longitude 66° 30′W. For example, five seals that were tagged in Lazarev Bay in May 2001 used the Alexander Island region heavily. However, in July these seals, and those tagged in LauBeuf Fjord moved into Crystal Sound, and remained there for the rest of the winter months, along with most of the seals tagged in LauBeuf Fjord, Marguerite Bay, and the outer coast of Adelaide Island. Similarly, in April 2002, eight seals were tagged in Crystal Sound and LauBeuf Fjord, and half of these animals moved south to the same area off the northern tip of Alexander Island that was frequented in 2001. In addition, three seals tagged near Alexander Island and several seals tagged west of Adelaide Island in August later moved into Crystal Sound. Notably, in neither 2001 nor 2002 did seals spend much time the waters of Marguerite Bay proper.

The habitat use vs. availability analyses revealed that the areas where seals were most commonly found were shallower than the habitat as a whole (modified Bonferroni confidence intervals; $P<0.05$ for significance tests). In 2001, seals were found more often than expected in depth classes 0–49, 50–149, 150–249, 250–349, and 350–449 m, and less often than expected in waters of 550–649 m (Table 2). Similarly in 2002, seals were found more often than expected in waters of 50–149, 150–249, 250–349, and 350–449 m, and less often than expected in waters of 550–649 m. When years were pooled, the combined results were identical to those in 2002 (Table 2).

Seals were also non-randomly distributed with respect to sea-ice, but the pattern was less clear due to the changing nature of the sea-ice and the extreme differences in ice cover in 2001 and 2002. When the average concentration of ice was low (<50%), seals selected areas of high ice cover and

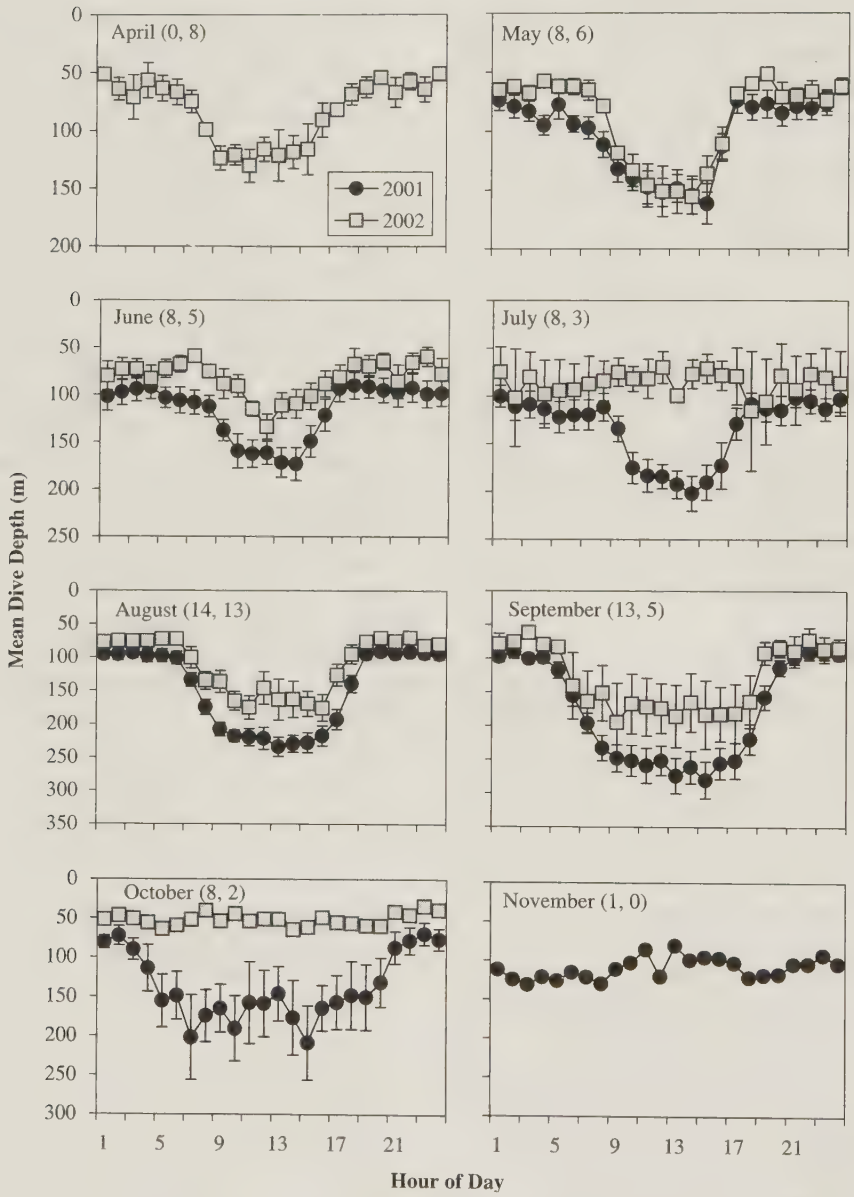

Fig. 5. Mean ± SE dive depth (m) by month and hour for seals in each year of the study. Each individual is represented once per month, and the number of seals is indicated (n_{2001}, n_{2002}). Sample sizes differ from those in Fig. 2 because data were included from all dives without ensuring complete daily coverage.

avoided region of open water. Once ice availability increased, seals remained within ice covered areas. As a result, there was a trend for animals to use areas of medium ice coverage (30–50%) earlier in the winter and to utilize areas of higher coverage (90%) later in the winter. However, in most late-winter months complete ice coverage (100%) was significantly avoided (Table 3).

When we examined how physical features influenced the amount of time seals spent in the areas that they used, we found that the most parsimonious model that predicted crabeater seal

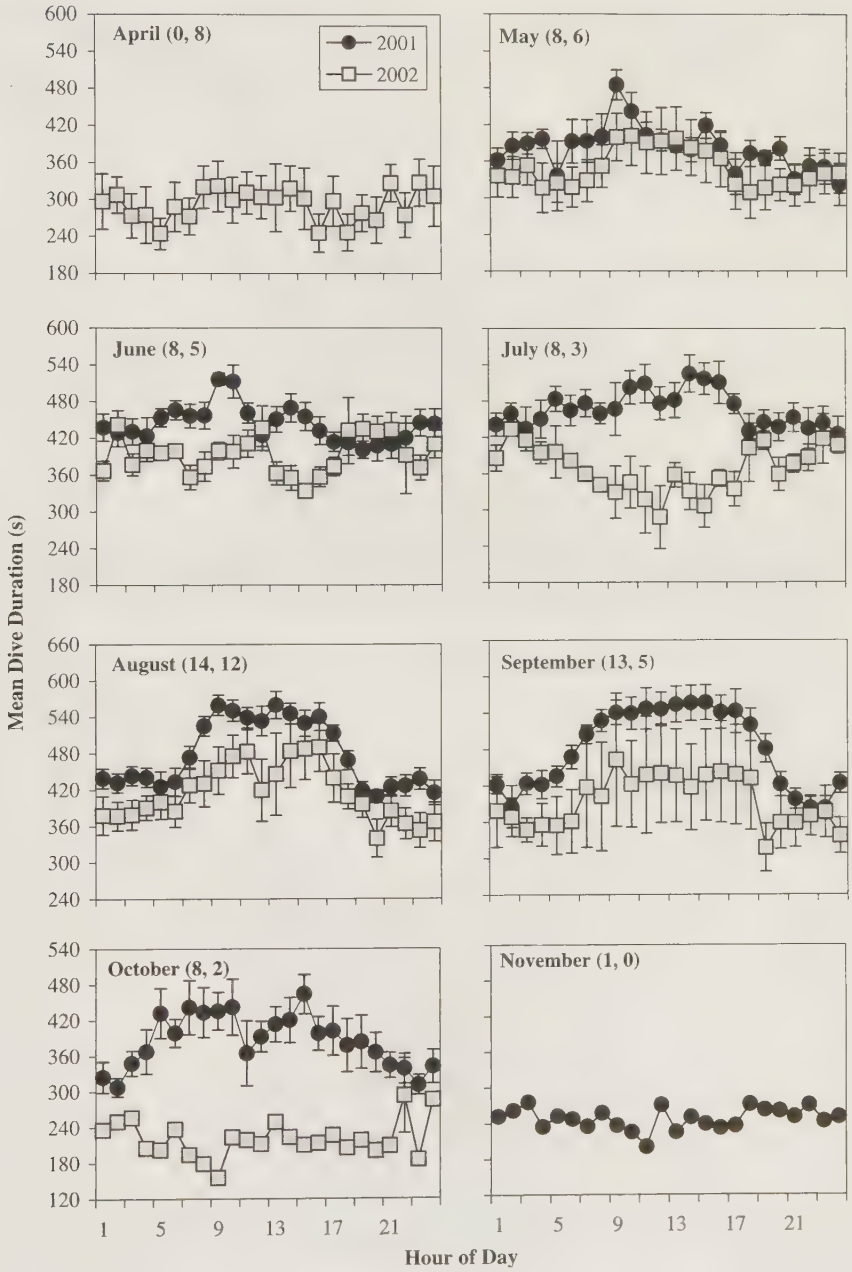

Fig. 6. Mean±SE dive duration (s) by month and hour for seals in each year of the study. Each individual is represented once per month, and the number of seals is indicated (n_{2001}, n_{2002}). Sample sizes differ from those in Fig. 2 because data were included from all dives without ensuring complete daily coverage.

habitat use (time spent per grid cell) was one that incorporated each of the modeled physical variables, but did not separate the 2 years (Table 4). This model was then applied to each month separately. Depending on the month, the relative significance of mean depth, standard error of depth, and mean sea ice concentration changed (Table 5). However, overall, there was a trend for

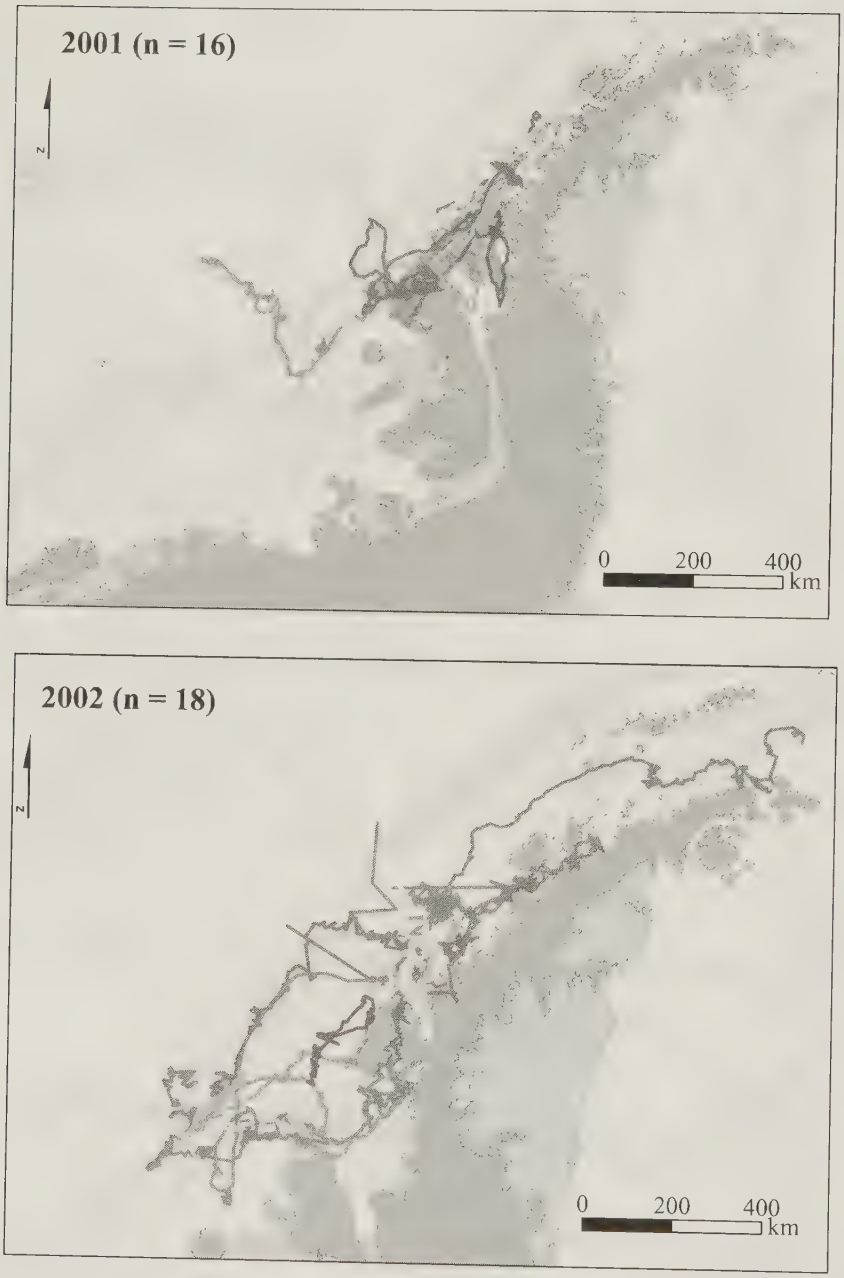

Fig. 7. Movement patterns of individual seals in 2001 and 2002. Lines were drawn between points that passed the location filtering algorithms.

habitat use to be positively related to sea-ice concentrations and standard error of depth, and negatively related to depth. This indicates that, on average, seals were selecting shallower areas, that had higher ice concentration and more varied depth. These results are in fundamental agreement with the results from the habitat selection analyses that used Bonferroni confidence intervals.

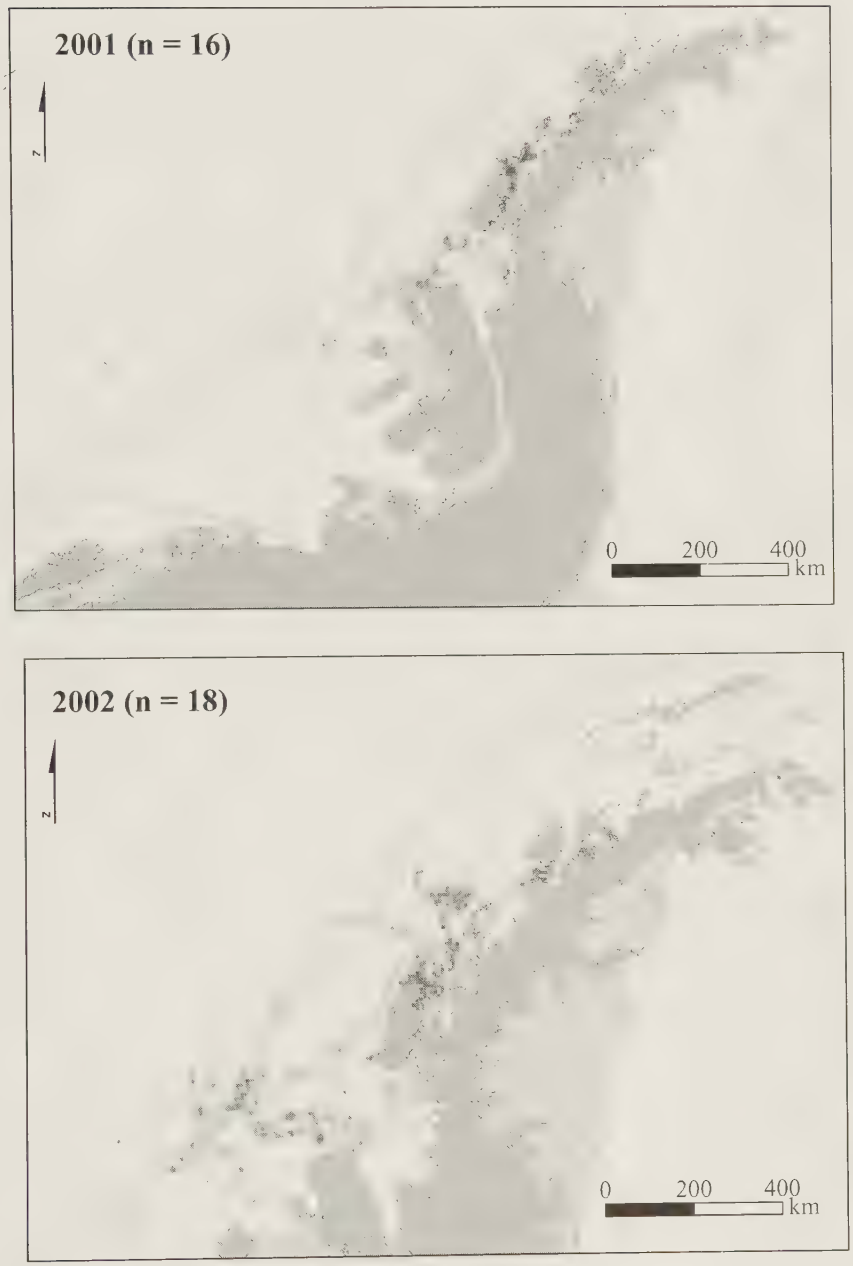

Fig. 8. Habitat use patterns for seals in 2001 and 2002. Deeper colors indicate a greater proportion of time was spent in that area.

4. Discussion

4.1. Diving behavior and activity patterns

Previous studies of crabeater seal diving patterns indicate that they, like most krill predators, primarily focus their foraging in the upper 50 m of the water column (Croxall et al., 1985; Costa et al., 1989; Bengtson and Stewart 1992; Boyd et al., 1994; Nordøy et al., 1995). However, in this study, crabeater seals made dives that were substantially longer and deeper than those in previous studies:

Table 2
Patterns of habitat use and availability for depth class.
Average depth available is the average coverage throughout the habitat, as determined from the ETOPO2 bathymetry data set. Average depth used is the weighted average depth in areas where seals were found, as defined by the annual MCPs. Modified Bonferroni confidence intervals for use and availability were used to assess whether seals were selecting or avoiding regions with particular depth classes (100 m increments from 0 to 600 m; depth bins rounded to nearest 100 m). Values for habitat use include all behavioral states

Year	Avg. depth available (mean ± SD)	Weighted avg. depth used (± SE)	Selection for depth class	Avoidance of depth class
2001	1118.6 ± 1310.7	343.9 ± 44.6	0, 100, 200, 300, 400	600[a]
2002	1118.6 ± 1310.7	512.3 ± 66.0	100, 200, 300, 400	600
2001–2002 combined	1118.6 ± 1310.7	396.6 ± 53.8	100, 200, 300, 400	600

[a]Use of depth classes >600 m was not modeled because of extremely low use of these areas.

Table 3
Patterns of habitat use and availability for sea ice concentration, calculated from monthly seal distribution for both years combined. Ice concentration (%) is the average coverage throughout the habitat, as determined from the NSIDC sea ice dataset. Average ice use is the weighted average ice cover in areas where seals were found (± standard errors). Modified Bonferroni confidence intervals for use and availability were used assess whether seals were selecting or avoiding regions with particular ice densities. Values for habitat use include all behavioral states

Month	Year	Avg. ice concentration available	Weighted avg. ice used	Selection for % class ice cover	Avoidance of % class ice cover
April	2001	—	—	—	—
	2002	14.2 ± 1.6	30.1	40	0
May	2001	8.7 ± 1.0	35.8	30, 40	None
	2002	55.0 ± 2.6	55.8	40, 70	30, 60
June	2001	31.4 ± 1.7	44.6	40, 50, 60	0, 20
	2002	84.6 ± 1.2	70.6	30, 80	90
July	2001	77.0 ± 1.6	73.9	60	80
	2002	89.1 ± 1.1	67.9	50	100
August	2001	88.0 ± 0.9	85.9	90	100
	2002	86.4 ± 1.1	83.7	80	90, 100
September	2001	89.3 ± 0.8	86.9	90	80, 100
	2002	84.4 ± 1.1	90.1	90	80, 100
October	2001	80.1 ± 2.1	85.7	100	None
	2002	84.5 ± 0.9	75.8	60	None

55% of dives were deeper than 50 m, and 34% were deeper than 100 m. Similarly, two-thirds of all dives were longer than 3 min, and almost half (47%) were longer than 5 min. Thus, this study documented the deepest (664 m) and longest (23.6 min) dives ever recorded for crabeater seals, but more importantly, demonstrated that crabeater seals can utilize a much larger portion of the water column than previously recognized.

In part, differences between the diving behavior of seals in this study and those previously conducted are likely due to seasonal differences

Table 4
Results of the generalized linear model relating crabeater seal use (h) to three environmental variables: mean depth, standard error of depth, and sea ice concentration.
The most parsimonious model is Model 2 that included all three environmental variables, but excluded the *year* term. Any removal of the environmental variables resulted in a significant change in the deviance

Model	Variables	Deviance	Deviance/degrees of freedom	Difference in deviance (χ^2_1)	P
1	Year, depth, SE of depth, sea ice concentration	154.45	38.612	0.77	0.382
2	Depth, SE of depth, sea ice concentration	153.68	51.23	84.11	<0.001
3	Depth, sea ice concentration	69.57	34.79	43.76	<0.001
4	Sea ice concentration	25.81	25.81		

Table 5
Results of the monthly generalized linear modeling using GENMOD (SAS 6.11) with a Poisson error model and a log link.
The dependent variable was the $\log_e$-transformed total seal use (h) per $5 \times 5\,km^2$ grid cell. Independent model terms include the $\log_e$-transformed mean depth (D), the untransformed standard error of depth (D_{SE}) and the angular-transformed sea ice concentration (SI). Term coefficients and standard errors (SE) are also shown. Significant terms ($P<0.05$) and terms approaching significance ($P<0.10$) for each monthly model are shown in italics

Month	Scaled deviance	Df	Model significance (P)	Coefficient ± SE	Coefficient P
April	7.64	3595	0.054	*D*:−0.0447±0.0303 D_{SE}: 0.0016±0.0019 *SI: 0.2027±0.1178*	0.1406 0.4101 *0.0852*
May	11.36	31,263	0.0099	*D: −0.0441±0.0188* D_{SE}: −0.0018±0.0012 SI: −0.0162±0.1009	*0.0188* 0.1355 0.8722
June	28.08	31,308	< 0.0001	*D: −0.0755±0.0140* D_{SE}: 0.0012±0.0009 *SI: 0.1981±0.0752*	*< 0.0001* *0.1723* *0.0084*
July	5.86	31,131	0.1187	*D: −0.0487±0.0234* *D_{SE}: 0.0033±0.0015* SI: 0.2420±0.1533	*0.0369* *0.0375* 0.1144
August	44.71	31,496	< 0.0001	*D*: 0.0020±0.0198 *D_{SE}: 0.0050±0.0008* SI: −0.0951±0.1554	0.9216 *< 0.0001* 0.5405
September	29.51	3791	< 0.0001	*D: −0.0845±0.0223* *D_{SE}: 0.0044±0.0009* *SI: 0.6635±0.1920*	*0.0002* *< 0.0001* *0.0005*
October	26.32	3752	< 0.0001	*D: −0.0552±0.0304* *D_{SE}: 0.0075±0.0019* SI: −0.1636±0.2170	*0.0699* *< 0.0001* 0.4508
November	2.71	3221	0.4385	*D*: −0.1813±0.1152 D_{SE}: 0.0086±0.0090 SI: −0.5188±0.4236	0.1156 0.3369 0.2207

in when the studies were carried out. Most studies of krill predators have taken place during summer and fall, when adult krill are abundant in the upper 50 m of the water column, and are generally accessed there (Croxall et al., 1985; Bengtson and Stewart 1992; Hunt et al., 1992; Veit et al., 1993; Boyd et al., 1994). However, during the Southern Ocean GLOBEC cruises, adult krill and large zooplankton were largely absent from the surface waters, and instead were most abundant in deep waters and close to the bottom (Ashjian et al., 2004; Lawson et al., 2004; Zhou and Dorland, 2004). In addition, large zooplankton were less abundant in winter than fall, and more biomass was observed at depth later in the season (Lawson et al., 2004). Crabeater seals were likely diving deep to access these prey resources, and the downward shift in the prey distribution likely explains the increased depth of dives later in the winter. However, fish were also more prevalent in deeper waters, and it is possible that the deeper diving later in the winter reflects an increased reliance on fish as zooplankton biomass declined over winter (Øritsland, 1977; Green and Williams, 1986; Lowry et al., 1988; Lawson et al., 2004). Ongoing studies of crabeater seal diet should help resolve this issue. Regardless of the diet composition, the absence of prey in the upper water column in late fall and early winter likely required crabeater seals to dive deeply in order to access sufficient food resources.

Another notable feature of the diving patterns of crabeater seals in this study was the strong diel pattern in dive depth and duration. From autumn to midwinter, seals were more active during the daylight hours, with dives around midday more frequent, deeper, and longer than those around midnight. This pattern differs substantially from that previously observed, and from the activity patterns of the Antarctic fur seal, another krill specialist. Prior work with both species has indicated that animals generally rest during the day and forage mainly at night when krill are close to the surface and easily accessed (Croxall et al., 1985; Costa et al., 1989; Bengtson and Stewart 1992; Boyd et al., 1994; Nordøy et al., 1995). The pattern we observed more closely resembles that of king and Adélie penguins, which forage at depth during the day and haulout during the night (Kooyman et al., 1992; Wilson et al., 1993). For these species, daytime prey capture rates are higher because birds could more easily capture krill when they were aggregated along the seafloor than when dispersed throughout the water column (Wilson et al., 1993). Similar conditions could be present within Marguerite Bay: krill are known to migrate vertically (Kalinowski, 1978; Tomo, 1983; Siegel et al., 1998), and diel vertical migrations were observed within the coastal fjords frequented by seals (Zhou and Dorland, 2004). In addition, large zooplankton were most abundant and in denser swarms closer to the bottom (Ashjian et al., 2004; Lawson et al., 2004), and previous research has suggested that krill overwinter at depth (Kawaguchi et al., 1986; Gutt and Siegel 1994). In combination it appears likely that crabeater seals were improving foraging success by focusing activities in areas where the seafloor could constrain prey escape movements.

However, this explanation does not account for the seasonal changes in activity patterns. In both 2001 and 2002, seals shifted to daytime haulout and nighttime foraging by the end of August, and from that date forward their behavior was more similar to, although still deeper and longer than, that recorded during summer studies (Bengtson and Stewart, 1992; Nordøy et al., 1995). Possible explanations for this shift include changes in seal diet, prey behavior, or seal foraging tactics. While we cannot assess midwinter diets or prey behaviors directly because there were no late winter cruises, several lines of evidence suggest that this behavioral shift reflects both changes in prey behavior and seal foraging tactics. For example, many vertically migrating prey species descend until the ambient light levels reach some minimum set point (Wilson et al., 1993; Nybakken, 2001; Zhou and Dorland, 2004), and it may be that as day length increased, zooplankton moved into areas of deeper water and became less accessible to foraging seals. Deep troughs and depressions are common in Marguerite Bay and the coastal areas, and may serve as refuges from predation by seals (Zhou and Dorland, 2004). Indeed, as day length and light levels increased, the depth and duration of midday dives also increased, until more than half the dives

were longer than 8 min. Since dives longer than 9 min were followed by extended post dive surface intervals, if krill moved into deeper waters, seals may have switched to nighttime midwater feeding as a result of increased recovery costs associated with such long and deep dives (Fedak and Thompson, 1993).

Alternatively, seals may have switched foraging tactics as a result of increased prey abundance in the surface water in early spring (O'Brien, 1987; Siegel, 1988). Support for this hypothesis comes from the fact that as behavioral patterns shifted, neither dive frequency nor time in water increased, as would be expected if prey were more dispersed or harder to capture (Costa et al., 1989; Trillmich et al., 1991; Boyd et al., 1994). Instead, as light levels increased and nighttime diving became more common, average dive depth and duration declined, and the proportion of time spent hauled out increased. In combination, this suggests that as seals shifted to focus their foraging effort into the upper water column, they were able to obtain sufficient prey with less effort than when foraging at depth (Costa et al., 1989; Boyd et al., 1994). However, deep midday dives did not disappear completely from the behavioral repertoire, indicating that seals within Marguerite Bay continued to utilize deep prey patches even once prey availability in the surface waters increased. Nor does deep, water foraging appear to negatively impact condition. Seals handled in this study were significantly heavier (246 kg) than those handled in March in LauBeuf fjord (Laws et al., 2003) and along Queen Maud Land (182.5 kg; Nordøy et al., 1995), in October off Enderby Land (220 kg; Shaughnessy, 1991), and between late December and early February in the Ross Sea (183.6 kg, M. Castellini pers comm.). This pattern suggests that winter foraging is associated with mass gain, and that seals are lightest at the end of the summer season. Unfortunately, without serial measurements of individuals it is impossible to tell if the above pattern is due to seasonal, annual, or geographic differences.

In combination, these data indicate that crabeater seals, like many Antarctic predators, show seasonal differences in diving patterns, and suggest that differences result from interactions between zooplankton behavior and predator diving capacity. However, not only can diving seals track krill over a much larger segment of the water column than was previously appreciated, they might also influence it. Vertical shifts in zooplankton biomass were not observed farther offshore where seals and other predators were less abundant (Lawson et al., 2004), and within the coastal fjords vertically migrating zooplankton descended further than expected based on light levels alone (Zhou and Dorland, 2004).

4.2. Habitat use patterns

In this study, we found that seals showed habitat selection at both broad- and finer-scales, and with respect to both bathymetric features and ice characteristics. At the broad scale, we identified several areas within the Marguerite Bay area where tagged seals were commonly found in both study years. These regions were the northwest tip of Alexander Island, LauBeuf fjord, and Crystal Sound, all areas where zooplankton abundance was high, bathymetry varied (Lawson et al., 2004; Zhou and Dorland, 2004), and apex predator densities high (Chapman et al., 2004; Thiele et al., 2004; Zhou and Dorland, 2004). While coastal regions were heavily utilized, areas such as the middle of Marguerite Bay, the offshore shelf, and the shelf break were not frequented by seals. During the research cruises, these were regions of lower zooplankton and predator abundance (Ashjian et al., 2004; Chapman et al., 2004; Lawson et al., 2004; Thiele et al., 2004). Thus, crabeater seals, like other aquatic predators appear to be selecting regions of their habitat where prey are locally concentrated (Croxall et al., 1985; McConnell et al., 1992; Wilson et al., 1993; Crocker et al., 2004).

Our next question was whether these areas of local concentration shared particular habitat characteristics that might help explain habitat use patterns at times when information on zooplankton abundance was not available. To address this issue we examined both how seals were distributed with respect to range of habitat types available, and how time spent in areas varied based on the physical characteristics at that

location. The two sets of results were similar and complimentary. We found that areas of local concentration and higher than expected seal usage were characterized by shallower than average bathymetry, bathymetry that was discontinuous, and/or areas with higher than average ice density. One reason that seals might select shallower coastal regions would be to exploit prey residing at or near the bottom that in deeper waters would be less accessible (as discussed above). However, shallower coastal zones could have higher zooplankton abundance due to hydrographic features that serve to retain zooplankton, or to active habitat selection by zooplankton themselves.

Within Marguerite Bay hydrographic features likely play a key role. Drifter studies (Beardsley et al., 2004) identified small gyres off Alexander Island and in LauBeuf fjord that may have retained krill in these areas, and there was a persistent mesoscale cyclonic gyre within Marguerite Bay (Klinck et al., 2004) that may have retained krill inshore (Lawson et al., 2004). Similarly, visual surveys conducted by other researchers (Chapman et al., 2004; Thiele et al., 2004) indicate that seals and seabirds were often seen in association with particular water masses and fronts, areas that may be preferred by krill due to their generally enhanced productivity. Gyres, currents, frontal systems, and varied bathymetry are often associated with increased productivity (McConnell et al., 1992; Ichii et al., 1998; Field et al., 2001), and studies on krill movements and swimming speeds suggest that krill could have been actively selecting these inshore and coastal habitats (Lawson et al., 2004; Zhou and Dorland, 2004). From the predator perspective, relying on foraging areas that are correlated with physical features of the environment offers the significant advantage that they are likely highly predictable. Certainly, regions of high seal abundance and use were remarkably similar across the two study years, and seals made very directed movements between LauBeuf fjord and Alexander Island, suggesting previous familiarity with these regional 'hotspots'.

However, bathymetry and currents are not the only physical variables of importance to crabeater seals. Seasonal changes in sea-ice abundance and distribution impact all marine species, but particularly air breathing predators (Lunn et al., 1994; Costa and Crocker 1996; Ainley et al., 1998). As predicted, seals were not randomly distributed with respect to ice. In both years when ice was scarce, seals used areas of open water, but spent a disproportionate amount of time in areas where sea-ice was present, such as Crystal Sound and the coast along Alexander Island. Then, as the season progressed and ice thickened, seals remained within the pack ice but selected regions with high but not complete ice cover, such as was found in Crystal Sound and off the coast of Adelaide Island. This change in habitat selection criteria as the season progressed likely explains the inconsistent monthly results produced by our generalized linear modeling effort. It also may explain why previous studies on how seals are distributed with respect to ice have produced conflicting results (Gilbert and Erickson, 1977; Joiris, 1991; Bengtson and Stewart, 1992; Bester et al., 1995).

In part, crabeater seals may have been selecting regions with ice cover to improve foraging success. Krill are often associated with ice edges and ice algae (O'Brien, 1987; Stretch et al., 1988; Brierley and Watkins, 2000), and water currents may have retained krill along with ice in Crystal Sound and the coastal fjords (Beardsley et al., 2004; Klinck et al., 2004). However, even though adult krill have been observed to aggregate under the ice during winter (Marschall, 1988; Spiridonov, 1992), they were rarely abundant under the ice surface during the Southern Ocean GLOBEC cruises. Therefore, habitat selection for ice was probably not solely due to ice-related increases in krill density. Instead, our modeling results suggest that seal habitat use patterns reflect the interaction between the seals' reliance on regions of high zooplankton abundance, such as occurred near the bottom, at water mass boundaries, over varied topography, and (perhaps) under stable sea ice, and their need to access air to breath and ice to rest.

As a result, crabeater seal densities in Marguerite Bay did not decline throughout the winter as the pack ice expanded (Bester et al., 1995; Chapman et al., 2004), but instead became locally concentrated in areas of suitable ice, bathymetery, and prey availability. In this, our results are

qualitatively similar to those of Nordøy et al. (1995) who found that crabeater seals near Queen Maud Land spent considerable time in very deep (>2000 m) waters along the shelf break and near seamounts, and McMahon et al. (2002) who found that seals in the Mertz Glacier region (~66°S, 144°E) were associated with shallow water and thick sea ice. Seals in all three studies selected regions of higher than average prey availability, as determined by the local physical and hydrographic conditions. Thus, crabeater seals, like other krill predators, appear to forage at the depths and in areas where prey are locally abundant, and perhaps predictably found, provided that the substrate is suitable for both prey access and haulout (Croxall et al., 1985; Costa et al., 1989; Wilson et al., 1993; Ainley et al., 1998; Guinet et al., 2001). Our challenge now is to determine how seals locate new hot spots, should environmental conditions change.

In this endeavor, we offer one note of caution. Our analysis of habitat selection was based on where seals spent their time, and did not distinguish between time in water and time hauled out. In contrast, visual survey records are biased towards areas where seals haul out, and areas of daytime activities. Because crabeater seals do not always haul out during the day, are capable of extensive use of ice free waters, and can go for long periods without hauling out (23 days for seal G017 in this study), interpretation of overall habitat use patterns based on observational data may be significantly biased. This is particularly true in low ice conditions, when sighting probabilities are low. For example, in fall 2001, tag data indicated that seals were active in LauBeuf Fjord, but few seals were ever sighted there due to the absence of ice suitable for haulout.

Furthermore, interpretation of habitat use patterns also can be confounded by the occurrence of highly seasonal events. For example, one adult female (G010) hauled out for the entire period between 14 October and 8 November 2001, during which time she moved (drifted) farther offshore and over deeper water than any other crabeater seal in the study, and thus 'used' very different habitat classes. This long haulout was coincident with observations by Rothera Base (67° 35S, 68° 10W) personnel of a female crabeater seal that hauled out, gave birth on 11 October and nursed her pup until 6 November (Rothera Base, unpublished science records). In combination with prior research (Shaughnessy and Kerry, 1989; Green et al., 1993), these observations suggest that crabeater seals select highly stable substrates for reproduction, in part due to the long lactation period (approximately 24 days). Further, they indicate that crabeater seal females fast for the entire nursing period. Seasonal models of krill predation by crabeater seals should take the timing and duration of this fasting period into account.

5. Conclusions

Crabeater seals foraging during the winter in the Marguerite Bay region were locally concentrated in areas where adult krill and large zooplankton are abundant, and these regions were characterized by shallower-than-average depths, and greater-than-average ice cover. These findings suggest that seal densities need not decline during winter as more sea ice becomes available, but instead might increase as seals become concentrated in regions with suitable ice concentrations and prey densities. The highly localized habitat use, in combination with the deep diving pattern, likely serves to concentrate predation pressure on adult krill and large zooplankton found in the deeper waters inside the coastal fjords. If seals are able to continue to specialize on krill throughout the winter, then the impact of the crabeater seal population on overwintering krill will be substantial, albeit localized, and may account for much of the observed reduction in larger zooplankton biomass. However, even a small percentage of fish in the diet would reduce the impact on krill populations, and cannot yet be ruled out as an alternative foraging strategy.

Seals in this study did not exploit surface waters at night as has been previously reported, but instead demonstrated a nocturnal haulout pattern, used deeper depths, and possibly included benthic foraging in their repertoire. While wintertime growth and acquisition of lipid reserves suggest that this strategy was effective, as summer

approached, seals returned to daytime haulout and nocturnal foraging. These findings indicate that despite their high degree of specialization on a single prey resource, crabeater seals have the behavioral plasticity to forage successfully under a wide range of environmental conditions. Further, they suggest that there are complex interactions between seal movement and diving patterns, krill abundance and distribution, sea-ice extent and seafloor depth, and seasonal light levels.

Acknowledgements

Our research in the Antarctic could not have been carried out without the able assistance of a splendid group of field and technical assistance: Beth Chittick, Millie Gray and Julie Barnes provided fabulous veterinary support, Ari Friedlander, Carey Kuhn, and Scott Shaffer were intrepid seal handlers, and Phil Lovell provided excellent technical assistance. In addition, the Captain and Crew of the *A.S.R.V. Lawrence M. Gould*, and the science support staff from Raytheon Polar Services worked hard to ensure our success. In particular, we would like to thank Captains Robert Verret and Warren Sanamo, and the crew of the *Gould* for excellent ship handling and operations. Marine Project Coordinators Steve Ager, Alice Doyle, Karl Newyear, and Skip Owens, and marine technicians Josh Spillane, Christian McDonald, Jenny White and Sparky Weisblatt provided excellent support throughout. In addition, we sincerely appreciate the generosity and hospitality of the British Antarctic Survey and the winter-over personnel at Rothera Base who supported us during a week long stay in autumn 2002, during which time we were able to deploy three SRDL tags. We would also like to thank Hoffmann–La Roche Inc., which donated the Midazolam. Finally, we would like to thank the cruise leaders Jose Torres and Peter Wiebe, and all the scientists who participated on the Southern Ocean GLOBEC cruises, who willingly shared ship time and resources so that we all could accomplish our research goals. This research was funded under NSF grants #OPP-0003956 to J.M. Burns and OPP-9981683 to D.P. Costa and D. Crocker. U.S. GLOBEC contribution number is 465.

References

Ainley, D.G., Wilson, R.P., Barton, K.J., Ballard, G., Nur, N., Karl, B., 1998. Diet and foraging effort of Adélie penguins in relation to pack-ice condition in the southern Ross Sea. Polar Biology 20, 311–319.

Ancel, A., Kooyman, G.L., Ponganis, P.J., Gendner, J.P., Lignon, J., Mestre, X., Huin, N., Thorson, P., Robisson, P., Le Maho, Y., 1992. Foraging behavior of emperor penguins as a resource detector in winter and summer. Nature 360, 336–338.

APIS, 1995. Report of Antarctic Pack Ice Seals: Indicators of Environmental Change and Contributors to Carbon Flux.

Ashjian, C.J., Rosenwaks, G.A., Wiebe, P.H., Davis, C.S., Gallager, S.M., Copley, N.J., Lawson, G.L., Alatalo, P., 2004. Distribution of zooplankton on the continental shelf off Marguerite Bay, Antarctic Peninsula, during Austral Fall and Winter, 2001. Deep-Sea Research II, this issue [doi:10.1016/j.dsr2.2004.07.025].

Beardsley, R.C., Limeburner, R., Owens, W.B., 2004. Drifter measurements of surface currents near Marguerite Bay on the western Antarctic Peninsula shelf during austral summer and fall, 2001 and 2002. Deep-Sea Research II, this issue [doi:10.1016/j.dsr2.2004.07.031].

Bengtson, J.L., Laws, R.M., 1985. Trends in crabeater seal age at maturity: an insight into Antarctic marine interactions. In: Siegfried, W.R., Condy, P.R., Laws, R.M. (Eds.), Antarctic Nutrient Cycles and Food Webs. Springer, Berlin, pp. 669–675.

Bengtson, J.L., Stewart, B.S., 1992. Diving and haulout behavior of crabeater seals in the Weddell Sea, Antarctica, during March 1986. Polar Biology 12, 635–644.

Bester, M.N., Erickson, A.W., Ferguson, J.H., 1995. Seasonal change in the distribution and density of seals in the pack ice off Princess Martha Coast, Antarctica. Antarctic Science 7, 357–364.

Boyd, I.L., Arnbom, T.R., 1991. Diving behaviour in relation to water temperature in the southern elephant seal: foraging implications. Polar Biology 11, 259–266.

Boyd, I.L., Murray, A.W.A., 2001. Monitoring a marine ecosystem using responses of upper trophic level predators. Journal of Animal Ecology 70, 747–760.

Boyd, I.L., Arnould, J.P.Y., Barton, T., Croxall, J.P., 1994. Foraging behaviour of Antarctic fur seals during periods of contrasting prey abundance. Journal of Animal Ecology 63, 703–713.

Bradshaw, C.J.A., Hindell, M.A., Michael, K.J., Sumner, M.D., 2002. The optimal spatial scale for the analysis of elephant seal foraging as determined by geo-location in relation to sea surface temperatures. International Council for the Exploration of the Sea Journal of Marine Science 59, 770–781.

Brierley, A.S., Watkins, J.L., 2000. Effects of sea ice cover on the swarming behaviour of Antarctic krill, *Euphausia superba*. Canadian Journal of Fisheries and Aquatic Sciences 57, 24–30.

Chapman, E.W., Ribic, C.A., Fraser, W.R., 2004. The distribution of seabirds and pinnipeds in Marguerite Bay and their relationship to physical features during austral winter 2001. Deep-Sea Research II, this issue [doi:10.1016/j.dsr2.2004.07.005].

Comiso, J.C., 1990. DMSPSSM/I Daily Polar Gridded Sea Ice Concentrations. National Snow and Ice Data Center, Boulder, CO.

Costa, D.P., 1991. Reproductive and foraging energetics of high latitude penguins, albatrosses and pinnipeds: implications for life history patterns. American Zoologist 31, 111–130.

Costa, D.P., Crocker, D.E., 1996. Marine mammals of the Southern Ocean. Antarctic Research Series 70, 287–301.

Costa, D.P., Croxall, J.P., Duck, C.D., 1989. Foraging energetics of Antarctic fur seals in relation to changes in prey availability. Ecology 70, 596–606.

Crocker, D.E., Costa, D.P., Le Boeuf, B.J., Webb, P.M., Houser, D.S., 2004. Impact of El Niño on the foraging behavior of female northern elephant seals. Marine Ecology Progress Series, in press.

Croxall, J.P., Everson, I., Kooyman, G.L., Ricketts, C., Davis, R.W., 1985. Fur seal diving behavior in relation to vertical distribution of krill. Journal of Animal Ecology 54, 1–8.

Fedak, M.A., Thompson, D., 1993. Behavioural and physiological options in diving seals. Symposium of the Zoological Society of London 66, 333–348.

Fedak, M.A., Lovell, P., Grant, S.M., 2001. Two approaches to compressing and interpreting time–depth information as collected by timed depth recorders and satellite linked data loggers. Marine Mammal Science 17, 94–110.

Fedak, M.A., Lovell, P., McConnell, B.J., Hunter, C., 2002. Overcoming the constraints of long range radio telemetry from animals: getting more useful data from smaller packages. Integrative and Comparative Biology 42, 3–10.

Field, I., Hindell, M.A., Slip, D.J., Michael, K., 2001. Foraging strategies of southern elephant seals (*Mirounga leonina*) in relation to frontal zones and water masses. Antarctic Science 13, 371–379.

Gales, N.J., Mattlin, R.H., 1998. Fast, safe, field-portable gas anesthesia for otariids. Marine Mammal Science 14, 355–361.

Gilbert, J.R., Erickson, A.W., 1977. Distribution and abundance of seals in the pack ice of the Pacific sector of the Southern Ocean. In: Llano, G.A. (Ed.), Adaptations Within Antarctic Ecosystems. Smithsonian Institution, Washington, DC, pp. 703–740.

Green, K., Williams, R., 1986. Observations on food remains in faeces of elephant, leopard and crabeater seals. Polar Biology 6, 43–45.

Green, B., Fogerty, A., Libke, K., Newgrain, K., Shaughnessy, P.D., 1993. Aspects of lactation in the crabeater seal (*Lobodon carcinophagus*). Australian Journal of Zoology 41, 203–213.

Guinet, C., Jouventin, P., Georges, J.-Y., 1994. Long term population changes of fur seals *Arctocephalus gazella* and *Arctocephalus tropicalis* on subantarctic (Crozet) and subtropical (St. Paul and Amsterdam) island and their possible relationship to El Niño Southern Oscillation. Antarctic Science 6, 473–478.

Guinet, C., Dubroca, L., Lea, M.A., Goldsworthy, S., Cherel, Y., Duhamel, G., Bonadonna, F., Donnay, J., 2001. Spatial distribution of foraging in female Antarctic fur seals *Arctocephalus gazella* in relation to oceanographic variables: a scale-dependent approach using geographic information systems. Marine Ecology Progress Series 219, 251–264.

Gutt, J., Siegel, V., 1994. Benthopelagic aggregations of krill (*Euphausia superba*) on the deeper shelf of the Weddell Sea (Antarctica). Deep Sea Research 41, 169–178.

Hewitt, R.P., Lipsky, J.D., 2002. Krill. In: Perrin, W.F., Wursig, B., Thewissen, J.G.M. (Eds.), Encyclopedia of Marine Mammals. Academic Press, San Diego, pp. 676–684.

Hindell, M.A., Bradshaw, C.J.A., Harcourt, R.G., Guinet, C., 2003. Ecosystem monitoring: are seals a potential tool for monitoring change in marine systems? In: Gales, N.J., Hindell, M.A., Kirkwood, R. (Eds.), Marine Mammals. Fisheries, Tourism and Management Issues. CSIRO Publishing, Melbourne.

Hofmann, E., Klinck, J.M., Costa, D.P., Daly, K.L., Torres, J.J., Fraser, W.R., 2002. US Southern Ocean Global Ocean Ecosystems Dynamics Program. Oceanography 15, 64–74.

Hunt, G.L., Heinemann, D., Everson, I., 1992. Distribution and predator–prey interactions of macaroni penguins, Antarctic fur seals, and Antarctic krill near Bird Island, South Georgia. Marine Ecology Progress Series 86, 15–30.

Ichii, T., Katayama, K., Obitsu, N., Ishii, H., Naganobu, M., 1998. Occurrence of Antarctic krill (*Euphausia superba*) concentrations in the vicinity of the South Shetland Islands: relationship to environmental parameters. Deep-Sea Research 45, 1235–1262.

Joiris, C.R., 1991. Spring distribution and ecological role of seabirds and marine mammals in the Weddell Sea, Antarctica. Polar Biology 11, 415–424.

Kalinowski, J., 1978. Vertical migration of krill in the region of South Georgia, February–March 1976. Polish Archives of Hydrobiology 25, 573–583.

Kawaguchi, S., Ishikawa, K., Matsuda, O., 1986. The overwintering strategy of Antarctic krill (*Euphausia superba* Dana) under the coastal fast ice off the Ongul Islands in Lutzow–Holm Bay, Antarctica. Memoirs of National Institute of Polar Research (Special Issue) 44, 67–85.

Klinck, J.M., Hofmann, E.E., Beardsley, R.C., Salihoglu, B., Howard, S., 2004. Water-mass properties and circulation on the west Antarctic Peninsula Continental Shelf in Austral Fall and Winter 2001. Deep-Sea Research II, this issue [doi:10.1016/j.dsr2.2004.08.001].

Kooyman, G.L., Cherel, Y., Le Maho, Y., Croxall, J.P., Thorson, P., Ridoux, V., Kooyman, C.A., 1992. Diving behavior and energetics during foraging cycles in king penguins. Ecological Monographs 62, 143–163.

Lascara, C.M., Hofmann, E.E., Ross, R.R., Quetin, L.B., 1999. Seasonal variability in the distribution of Antarctic krill, *Euphausia superba*, West of the Antarctic Peninsula. Deep-Sea Research I 46, 951–984.

Laws, R.M., 1977. The significance of vertebrates in the Antarctic marine ecosystem. In: Llano, G.A. (Ed.), Adaptations Within Antarctic Ecosystems. Smithsonian Institute, Washington, DC, pp. 411–438.

Laws, R.M., 1985. The ecology of the Southern Ocean. American Scientist 73, 26–40.

Laws, R.M., Baird, A., Bryden, M.M., 2003. Size and growth of the crabeater seal *Lobodon carcinophagus* (Mammalia: Carnivora). Journal of Zoology (London) 259, 103–108.

Lawson, G.L., Wiebe, P.H., Ashjian, C.J., Galleger, S.M., Davis, C.S., Warren, J.D., 2004. Acoustically-inferred zooplankton distribution in relation to hydrography west of the Antarctic Peninsula. Deep-Sea Research II, this issue [doi:10.1016/j.dsr2.2004.07.022].

Lowry, L.F., Testa, J.W., Calvert, W., 1988. Winter feeding of crabeater and leopard seals near the Antarctic penninsula. Polar Biology 8, 475 -478.

Lunn, N.J., Boyd, I.L., Croxall, J.P., 1994. Reproductive performance of female Antarctic fur seals: the influence of age, breeding experience, environmental variation and individual quality. Journal of Animal Ecology 63, 827–840.

Marschall, H.P., 1988. The overwintering strategy of the Antarctic krill under the pack-ice of the Weddell Sea. Polar Biology 6, 129–135.

McConnell, B.J., Chambers, C., Fedak, M.A., 1992. Foraging ecology of southern elephant seals in relation to the bathymetry and productivity of the Southern Ocean. Antarctic Science 4, 393–398.

McCullagh, P., Nelder, J.A., 1989. Generalized Linear Models. Chapman & Hall, London, UK.

McMahon, C.R., Hindell, M.A., Dorr, T., Massom, R.A., 2002. Winter distribution and abundance of crabeater seals off George V land, East Antarctica. Antarctic Science 14, 128 -133.

Neu, C.W., Byers, C.R., Peek, J.M., 2002. A technique for analysis of utilization-availability data. Journal of Wildlife Management 38, 541 545.

Nordøy, E.S., Folkow, L.P., Blix, A.S., 1995. Distribution and diving behaviour of crabeater seals (*Lobodon carcinophagus*) off Queen Maud Land. Polar Biology 15, 261–268.

Nybakken, J.W., 2001. Marine Biology, An Ecological Approach. Benjamin Cummings, San Francisco, CA.

O'Brien, D.P., 1987. Direct observations on the behaviour of *Euphausia superba* and *Euphausia crystallorophias* under pack-ice during the Antarctic spring of 1985. Journal of Crustacean Biology 7, 437–448.

Øritsland, T., 1977. Food consumption of seals in the Antarctic pack ice. In: Llano, G.A. (Ed.), Adaptations within Antarctic Ecosystems. Smithsonian Institute, Washington, DC, pp. 749–767.

Service Argos, 1996. User's Manual. Argos/CLS, Landover, MD.

Shaughnessy, P.D., 1991. Immobilisation of crabeater seals *Lobodon carcinophagus*, with ketamine and diazepam Wildlife Research 18, 165–168.

Shaughnessy, P.D., Kerry, K.R., 1989. Crabeater seals *Lobodon carcinophagus* during the breeding season: observations on five groups near Enderby Land, Antarctica. Marine Mammal Science 5, 68–77.

Siegel, V., 1988. A concept of seasonal variation of krill (*Euphausia superba*) distribution and abundance west of the Antarctic Penninsula. In: Sahrhage, D. (Ed.), Antarctic Ocean and Resources Variability. Springer, Berlin pp. 219–230.

Siegel, V., Loeb, V., Gröger, J., 1998. Krill (*Euphausia superba*) density, proportional and absolute recruitment and biomass in the Elephant Island region (Antarctic peninsula) during the period 1977 to 1997. Polar Biology 19, 393–398.

Sokal, R.R., Rohlf, F.J., 1995. Biometry. W.H. Freeman and Company, New York.

Spiridonov, V.A., 1992. Distribution and biological properties of the Antarctic krill *Euphasia superba* Dana during winter Weddell gyre study (WWGS) 1989. Proceedings of the NIPR Symposium on Polar Biology 5, 55–64.

Sprong, I., Schalk, P.H., 1992. Acoustic observations on krill spring–summer migration and patchiness in the northern Weddell Sea. Polar Biology 12, 261–268.

Stretch, J.J., Hamner, P.P., Hamner, W.M., Michel, W.C., Cook, J., Sullivan, C.W., 1988. Foraging behavior of Antarctic krill (*Euphausia superba*) on sea ice microalgae. Marine Ecology Progress Series 44, 131–139.

Testa, J.W., Oehlert, G., Ainley, D.G., Bengtson, J.L., Siniff, D.B., Laws, R.M., Rounsevell, D., 1991. Temporal variability in Antarctic marine ecosystems: periodic fluctuations in the phocid seals. Canadian Journal of Fisheries and Aquatic Sciences 48, 631–639.

Thiele, D., Chester, E., Moore, S., Sirovic, A., Hildebrand, J., Friedlaender, A., 2004. Seasonal variability in whale encounters in the Western Antarctic Peninsula. Deep-Sea Research II, this issue [doi:10.1016/j.dsr2.2004.07.007].

Tomo, A.P., 1983. Study on the diurnal migration of *Euphausia superba* and the formation of shoals. Berichte Zur Polarforschung 4, 191–195.

Trathan, P.N., Priddle, J., Watkins, J.L., Miller, D., Murray, A.W.A., 1993. Spatial variability of Antarctic krill in the relation to mesoscale hydrography. Marine Ecology Progress Series 98, 61–71.

Trathan, P.N., Croxall, J.P., Murphy, E.J., 1996. Dynamics of Antarctic penguin populations in relation to inter-annual variablilty in sea ice distribution. Polar Biology 16, 321–330.

Trillmich, F., Ono, K.A., Costa, D.P., Gentry, R.L., Heath, C.B., Le Boeuf, B.J., Majluf, P., York, A.E., 1991. The effects of El Niño on pinniped populations in the eastern Pacific. In: Trillmich, F., Ono, K.A. (Eds.), Pinnipeds and El Niño. Springer, Berlin, pp. 247–270.

van Franecker, J.A., 1992. Top predators as indicators for ecosystem events in the confluence zone and the marginal ice zone of the Weddell and Scotia Seas, Antarctica, November 1988–January 1989. Polar Biology 12, 93–102.

Veit, R.R., Silverman, E.D., Everson, I., 1993. Aggregation patterns of pelagic predators and their principal prey, Antarctic krill, near South Georgia. Journal of Animal Ecology 62, 551–564.

Vincent, C., McConnell, B.J., Ridoux, V., Fedak, M.A., 2002. Assessment of Argos location accuracy from satellite tags deployed on captive grey seals. Marine Mammal Science 18, 156–166.

White, G.C., Garrott, R.A., 1990. Analysis of Wildlife Radio-Tracking Data. Academic Press, Inc., San Diego.

Williams, T.M., 2002. Swimming. In: Perrin, W.F., Wursig, B., Thewissen, J.G.M. (Eds.), Encyclopedia of Marine Mammals. Academic Press, San Diego, pp. 1213–1222.

Wilson, R.P., Puetz, K., Bost, C.A., Culik, B.M., Bannasch, R., Reins, T., Adelung, D., 1993. Diel dive depth in penguins in relation to diel vertical migration of prey: whose dinner by candlelight? Marine Ecology Progress Series 94, 101 104.

Zhou, M., Dorland, R.D., 2004. Aggregation and vertical migration behavior of *Euphausia superba*. Deep-Sea Research II, this issue [doi:10.1016/j.dsr2.2004.07.009].

ELSEVIER

Deep-Sea Research II 51 (2004) 2305 2310

DEEP-SEA RESEARCH
PART II

www.elsevier.com/locate/dsr2

Do crabeater seals forage cooperatively?

Nicholas J. Gales[a,*], William R. Fraser[b], Daniel P. Costa[c], Colin Southwell[a]

[a]*Australian Antarctic Division, Channel Highway, Kingston, Tasmania 7050, Australia*
[b]*Polar Oceans Research Group, Sheridan, MT, USA*
[c]*Department of Ecology and Evolutionary Biology, 100 Shaffer Road, University of California, Santa Cruz, CA 95060, USA*

Accepted 9 July 2004

Abstract

Crabeater seals are abundant pack-ice predators that feed almost exclusively on krill. They have a circumpolar distribution and are generally sighted hauled out on ice floes alone or in pairs. Here we report our observations of a sighting of 150–200 crabeater seals, which were synchronised in their diving and surfacing behaviour, along with a summary of similar observations from western Antarctica of large groups of crabeater seals in synchronous dive cycles. We report on the low frequency of sightings of such groups during Antarctic pack-ice seal surveys in eastern (Greater) Antarctica. We examine plausible hypotheses to explain these observations, and suggest this behaviour is likely to represent some form of cooperative foraging behaviour, whereby a net advantage in individual energy intake rates is conferred to each seal. Current research on crabeater seal foraging using satellite-linked dive recorders is unlikely to provide sufficiently fine-scale data to examine this hypothesis. Nor will this approach indicate if a seal is foraging with conspecifics. The use of remote or animal-borne camera systems is more likely to provide an insight into fine-scale foraging tactics, as well as the possible, occasional use of cooperative foraging strategies.
© 2004 Elsevier Ltd. All rights reserved.

1. Introduction

Batch feeders are predators that consume a large number of prey, such as krill, in a single feeding event (Heithaus and Dill, 2002). Obligate batch feeders like the mysticetes have evolved anatomical (e.g., baleen plates, throat pleats) and behavioural (e.g., lunge feeding, skim feeding) features to optimise their foraging efficiency through filtering large volumes of water and prey (Croll and Tershy, 2002). Non-whale predators of krill (e.g., seals, penguins, sea birds, fish) have evolved other strategies that generally require the individual predator to move through the prey patch consuming individual or small numbers of prey at a time. The density and behaviour of the prey (particularly predator avoidance) is highly influential on foraging performance. Cooperative, group foraging is one mechanism that could optimise the net energy intake rate of individual predators.

*Corresponding author.

0967-0645/$ - see front matter © 2004 Elsevier Ltd. All rights reserved.
doi:10.1016/j.dsr2.2004.07.006

Crabeater seals, *Lobodon carcinophagus*, are abundant inhabitants of the Antarctic pack-ice zone (Erickson et al., 1973; Kooyman, 1981; Laws, 1984). Their biomass is perhaps greater than any other seal (Erickson and Hanson, 1990), and their specialised foraging behaviour means they are important consumers of krill (Øritsland, 1977; Laws, 1984). Indeed, Hewitt and Lipsky (2002) estimated that crabeater seals consume more krill in the southern ocean than do whales. Many aspects of the foraging ecology of crabeater seals remain to be elucidated, primarily as a result of the inaccessibility of their habitat.

The dentition of crabeater seals is among the most specialised of any mammal. The post-canine teeth of the upper and lower jaw have elaborate cusps that interdigitate when the mouth is closed which, together with other aspects of their cranial anatomy, form an effective sieve to retain captured prey (King, 1961; Kooyman, 1981). Direct observation of crabeater seal feeding behaviour is understandably limited. Racovitza (1900) described apparent filter feeding in crabeater seals with his observation of individual seals swimming, with mouths open, through krill aggregations. Kooyman (1981) cited G.S. Wilson (personal communication) as observing crabeater seals feeding on invertebrates that were attracted to a light on a pier. The seals were capturing their prey one at a time. A different prey capture method has been observed in a few captive seals, which were observed to suck food items into their mouths from distances up to 50 cm (Ross et al., 1976; Klages and Cockroft, 1990). These authors suggested that such a strategy would enable crabeater seals to capture Antarctic krill *Euphausia superba* among the rough habitat on the bottom of ice floes.

Bengtson and Stewart (1992) described the autumn diving behaviour of six crabeater seals, and noted a diel pattern of diving that encompassed depths and times where the animals might encounter krill aggregations. They argued that the pattern of deep dives (100–250 m) during crepuscular periods (twilight), shallow (20–50 m), continuous dives during the night, and haul-out during the day, was responsive to prey movement in the water column, as well as maximising hunting efficiency by foraging in minimum light. Nordøy et al. (1995) reported similar foraging patterns for eight crabeater seals in the late summer, through autumn period, and concluded the behaviour was consistent with that of a specialist krill predator. More recent research efforts including the international initiative of the Antarctic Pack Ice Seal (APIS) Program, and the US Southern Ocean Global Ocean Ecosystems Dynamics Program (SO GLOBEC) (Hofmann et al., 2002; Burns et al., 2004) are providing further insights into the seasonal foraging behaviour of individual, instrumented crabeater seals. These studies are characterising large- and meso-scale spatial and temporal aspects of how crabeater seals interact with their prey, but will not provide an insight into fine-scale foraging strategies, and in particular whether or not crabeater seals forage independently, or in association with others.

The foraging behaviour of another Antarctic krill consumer, the Antarctic fur seal *Arctocephalus gazella*, has been widely reported (e.g., Boyd, 1996, 1999; Goebel et al., 2000). Analyses of many dive records have provided insights into the way this species search and move between krill patches, but it has not been until the recent innovation of using a seal-borne camera that fine-scale foraging tactics have been examined (Hooker et al., 2002). In five of six deployments of the camera, subsurface photographs included the presence of other fur seals. Surface aggregations of fur seals in the vicinity of prey patches have been observed, but this was the first record that the aggregations were maintained, to some extent, at depth (Hooker et al., 2002).

Determining if a group of predators are actually cooperating in their foraging, as opposed to acting independently, requires at least two criteria to be satisfied (modified from Heithaus and Dill, 2002). First, in the context of a batch feeder, there must be a short-term opportunity cost to the individual by not attacking prey immediately while herding. Second, the cooperative strategy must lead to a net increase in energy intake rate compared to feeding independently. The existence of these criteria is difficult to demonstrate methodologically for marine predators, and generally our interpretation of group foraging strategies is constrained to direct

observations. In this paper we report on the behaviour of a large aggregation of foraging crabeater seals that provides some evidence that this species may hunt cooperatively. Further, we examine two extensive sightings data sets to determine how often this species is seen in large groups, along with some notes on group behaviour.

2. Methods

Data are reported from three sources. The first are observations by three of us (NG, WF and DC) from the vessel ARSV *Lawrence M. Gould* (LMG), which, during July and August, was conducting one of four SO GLOBEC cruises in 2001. A broader description of the process and survey SO GLOBEC cruises, and maps can be found in Hofmann et al. (2002, 2004). A component of the planned work on the LMG was the capture and deployment of satellite-linked dive recorders on crabeater seals and daylight observations for seals was maintained from the ship's bridge.

The other sources of data are two extensive crabeater seal sightings datasets, which were examined for information on group size and activity. The first dataset (the APIS dataset) is from the Australian APIS surveys conducted off eastern Antarctica in the period of September to December in the years 1994–1997. The data are all from structured ship-based or aerial ice-seal surveys (C. Southwell, unpublished data). The second dataset (the Fraser dataset) was collected as opportunistic sightings of crabeater seals recorded during research work around Palmer Station, western Antarctica (64° 46′S, 64° 04′W) between 1990 and 2002 (W. Fraser, unpublished data). The data were collected between October and March, with most sightings during December, January and February.

3. Results

On 27 July 2001 at 2030 h a group of 150–200 crabeater seals was encountered by the LMG hauled out along the edge of a large ice floe (approximately 200 m × 100 m) to the west of Adelaide Island, Antarctica at 67° 30′S, 69° 30′W. Ice cover in the area was approximately 8/10th, with surrounding floes being generally smaller and more fragmented. The combination of dark conditions and light snowfall made a more accurate estimation of seal numbers impossible. With the intention of working on one or more of the seals from this group after dawn, the LMG remained close to the ice floe for the rest of the night. At about 0400 h on 28 July 2001, the Captain of the LMG, Mr. Robert Verret, reported that all the seals moved into the water over a period of about half an hour. After dawn, at about 0900 h two of us (NG and DC) went onto the ice floe the seals had been hauled out on and collected 5 fresh faecal samples. These samples consisted almost entirely of krill exoskeletons. At about 1030 h a very large group of crabeater seals was seen from the bridge of the ship in an area of water with about 7/10th ice that was to the fore and portside of the ship. Beyond about 700 m the ice cover was heavier, with no open water being in view. The animals were in the water about 500 m off the bow of the ship (which was still holding position with the starboard side of the ship alongside the floe the seals had hauled out on). The number of seals was similar to the group seen the previous night, so they were assumed to be the same animals. The most notable feature of the behaviour of this group was that their surfacing behaviour was highly synchronised. All seals in the group surfaced very close to each other between the many small floes (ranging mainly from about 2–10 m diameter), and then remained underwater for about 6 min. Subsequent surfacings occurred up to several hundred metres apart. The group was visible at the surface for a period of about 20 s. Although accurate data were not recorded for each dive, the seals were observed from the bridge to continue a highly synchronised, continuous cycle of approximately 6 min dives and 20 s surfacing periods. After about 2 h the group disappeared from view.

During the two cruises of the SO GLOBEC in 2001, satellite-linked dive recorders (SDR) were attached to 16 crabeater seals. These seals had a mean dive depth of 140 m and a mean dive

duration of 7.5 min (Burns et al., 2004). The dive duration of about 6 min that we recorded from the LMG for the synchronously diving group of seals is in close accord to the data from the SDR. Similarly, the 6 min dive cycle is close to the 5.4 min mean dive time for Type III (crepuscular foraging dives) reported by Bengtson and Stewart (1992).

The APIS dataset revealed no sightings of groups comparable to the one seen from the LMG. The total number of crabeater seal sightings was 1990, of which 96% were of single or pairs of animals. The largest group recorded was 15 seals. Most sightings were of animals on ice (98%), but group sizes were not significantly different on ice or in water (t test; $p=0.83$) (C. Southwell, unpublished data).

By contrast to the APIS dataset, only 54% of sightings from the Fraser dataset were of single or pairs of animals, with 23% of groups of 3–10 animals, 14% of 11–100 animals, and 9% of greater than 100 animals. The maximum group size was estimated to be at least 300 seals. Of the 18 sightings of aggregations of greater than 100 seals, three groups of an estimated 128, 155 and 299, respectively, were hauled out on ice floes. A further four groups were milling at the water surface, and 11 groups were feeding. Feeding was used as a category only when krill were seen in association with the seals. Of the feeding groups, four of the aggregations were exhibiting the synchronous diving and surfacing that we observed from the LMG.

4. Discussion

The two datasets are not readily comparable, as one was targeted and the other opportunistic, and the temporal and spatial scales are entirely different. Furthermore, as there appears to be an inverse relationship between pack-ice cover and crabeater seal density (Eklund and Atwood, 1962; Erickson et al., 1973; Bester et al., 1995) comparisons of the surveys may be further confounded. Nevertheless, the presence of substantial sightings of large aggregations of crabeater seals in the Fraser dataset is a dramatic difference. While regular sightings of large aggregations of crabeater seals are not widely reported in the literature (e.g., Kooyman, 1981; Erickson and Hanson, 1990; Bengtson, 2002), they clearly do occur, particularly around western Antarctica. Siniff et al. (1979) surveyed the region on the western Antarctic Peninsula from September through November during 1975, 1976 and 1977. They classified sightings of seals as singles, family groups, mated pairs and concentrations. The last category was generally associated with bays and fast ice, and included two sightings of more than 1000 hauled out crabeater seals. Associated with the large groups on the fast ice, they reported groups of fifty or fewer seals swimming together "surfacing periodically more or less in synchrony." Similarly, Bertram (1940) discusses the sightings of many large groups of crabeater seals by Antarctic expeditions during the early Twentieth Century, many of which were apparently travelling together in the water.

The sighting of the crabeater seals we report from the LMG, and at least 11 of the observations in the Fraser database add to the earlier published accounts, and demonstrate that, at least in western Antarctica, crabeater seals do, on occasions, aggregate in very large numbers. While the mechanisms that lead to such aggregations are unknown, and the functions are likely to be varied (and could include predator avoidance, socialisation and foraging), the sighting of krill in the water in association with the crabeater group sightings reported in the Fraser database and the presence of krill in the seal scats we report indicate that these crabeater seal groups are often associated with aggregations of their primary prey, Antarctic krill.

Given the known patchy distribution of *E. superba* (Miller and Hampton, 1989), a finding of an associated concentration of their predators is perhaps not surprising. The focus of this paper however, is interpreting what the observations of synchrony in surface behaviour suggest.

If the rate at which each crabeater seal was able to capture krill from the patch was independent of the behaviour of the other seals, then we would expect to see no pattern in overall dive cycles within the group. While this non-synchronised

pattern is commonly seen, our observations, on at least six occasions, that these large groups will surface and dive synchronously, for sustained periods, provides compelling evidence of mutually beneficial (cooperative) interactions during each dive. We are not the first to report this type of synchronised diving. Bertram (1940) described his observation of two adult crabeater seals feeding close to his ship. The seals were diving synchronously ("in almost perfect unison"), spending about 3 min submerged and 30 s at the surface. The seals dived vertically, disappearing from view in about 6 m, and resurfacing within about 20 m of where they dived.

This type of cooperative diving may function if a group of crabeater seals was able to herd the prey in order to concentrate and constrain the aggregation to enable more efficient capture rates. We have one observation made by one of us (WF), that such herding occurs. On 2nd March 1995 about 55 crabeater seals were feeding, in open water, directly off the jetty at Palmer Station. By viewing the behaviour from above, the seals were seen to be swimming relatively fast, clockwise, and in unison, around a krill aggregation about 3–5 m below the surface. This behaviour concentrated the patch in the water column and one or more seals would then feed on the patch either by "darting" out from the group into the patch, or by taking krill near the patch's perimeter while maintaining swimming formation.

It is possible that mechanisms other than herding are utilised by groups of crabeater seals. By feeding independently, but simultaneously (within the same dive cycle), a large number of predators within the same krill aggregation may sufficiently disrupt the efficiency of the prey's avoidance strategies to lead to an increase in prey capture rate. Heithaus and Dill (2002) describe such a strategy as bi-product mutualism. It is possible that other krill predators such as the Antarctic fur seal may occasionally utilise similar strategies.

Clearly, crabeater seals do not spend much of their time in large, conspecific aggregations. Indeed, the locations of the large groups of crabeater seals we discuss are limited to the shelf and near-shore waters of the western Antarctic Peninsula. This may reflect some unique physical or bio-oceanographic features of the region, or may simply reflect higher observation effort in near-shore waters. It is likely that the cooperative feeding strategy we suggest only occurs in circumstances where movements of predators and prey are such that a sufficient number of predators are feeding on a particular form (size, shape or density) of krill aggregation that triggers an advantage to such a strategy. Factors such as ice conditions or prey concentrations could lead to such circumstances. Our data suggest that at least 50–100 crabeater seals are required, but there may even be mutual advantages in synchronising the efforts of as few as two seals (Bertram, 1940). In all other circumstance we would expect crabeater seals to utilise a range of fine-scale foraging tactics that are independent of the activity of other predators.

Current research on crabeater seal foraging using satellite-linked dive recorders is unlikely to provide sufficiently fine-scale data to examine this hypothesis. Nor will this approach indicate if a seal is foraging with conspecifics. The use of remote or animal-borne camera systems (e.g., Hooker et al., 2002) is more likely to provide an insight into fine-scale foraging tactics, as well as the possible, occasional use of cooperative foraging strategies.

Acknowledgements

We thank the Captain and Crew of the LMG, and the science support staff from Raytheon Polar Services. This work was supported by NSF Grant #OPP-9981683 to D. Costa and by the Australian Antarctic Division. The Palmer Station data were obtained through long-term funding by the US National Marine Fisheries Service and National Science Foundation Grants 8918324, 9011927, 9103429, 9320115, 9505596 and 9632763. We are grateful for the assistance provided by the more than 20 students and technicians who have assisted the data collection effort over the years, and for the leadership given to the field teams by Brent Houston, Donna Patterson, Eric Holm, Peter Duley and Matt Irinaga. For assistance with the

Australian APIS surveys we thank the expeditioners and crew aboard the Australian research vessel, *Aurora Australis*, during the years 1994–1997. We thank Sarah Robinson for assistance with analysis of the crabeater seal sightings databases. Richard Laws, Marthan Bester and two anonymous reviewers are thanked for comments that improved the manuscript.

References

Bengtson, J.L., 2002. Crabeater Seal *Lobodon carcinophagus*. In: Perrin, W.F., Würsig, B., Thewissen, J.G.M. (Eds.), Encyclopedia of Marine Mammals. Academic Press, San Diego, pp. 302–304.

Bengtson, J.L., Stewart, B.S., 1992. Diving and haulout behaviour of crabeater seals in the Weddell Sea, Antarctica, during March 1986. Polar Biology 12, 635–644.

Bertram, G.C.L., 1940. The biology of the Weddell and crabeater seals, British Grahamland Expedition, 1934–1937. Scientific Reports 1, 1–139.

Bester, M.N., Erickson, A.W., Ferguson, J.W.H., 1995. Seasonal change in the distribution and density of seals in the pack ice off Princess Martha Coast, Antarctica. Antarctic Science 7, 357–364.

Boyd, I., 1996. Temporal scales of foraging in a marine predator. Ecology 77, 426–434.

Boyd, I., 1999. Foraging and provisioning in Antarctic fur seals: interannual variability in time-energy budgets. Behavioural Ecology 10, 198–208.

Burns, J., Costa, D., Fedak, M., Hindell, M., Bradshaw, C., Gales, N., McDonald, B., Trumble, S., Crocker, D., 2004. Winter habitat use and foraging behavior of crabeater seals along the Western Antarctic Peninsula. Deep-Sea Research II, this issue [doi:10.1016/j.dsr2.2004.07.021].

Croll, D.A., Tershy, B.R., 2002. Filter feeding. In: Perrin, W.F., Würsig, B., Thewissen, J.G.M. (Eds.), Encyclopedia of Marine Mammals. Academic Press, San Diego, pp. 428–432.

Eklund, C.R., Atwood, E.L., 1962. A population study of Antarctic seals. Journal of Mammalogy 43, 229–238.

Erickson, A.W., Hanson, M.B., 1990. Continental estimates and population trends of Antarctic ice seals. In: Kerry, K.R., Hempel, G. (Eds.), Antarctic Ecosystems: Ecological Change and Conservation. Springer, Berlin, pp. 253–264.

Erickson, A.W., Gilbert, J.R., Otis, J., 1973. Census of pelagic seals off the Oates and George V Coasts, Antarctica. Antarctic Journal of the United States 8, 191–193.

Goebel, M.E., Costa, D.P., Crocker, D.E., Sterling, J.E., Demer, D.A., 2000. Foraging ranges and dive patterns in relation to bathymetry and time-of-day of Antarctic fur seals, Cape Shirreff, Livingston Island Antarctica. In: Davisons, W., Howard-Williams, C., Broady, P. (Eds.), Antarctic Ecosystems: Models for Wider Ecological Understanding. New Zealand Natural Sciences Press, Christchurch, New Zealand, pp. 47–50.

Heithaus, M.R., Dill, L.M., 2002. Feeding strategies and tactics. In: Perrin, W.F., Würsig, B., Thewissen, J.G.M. (Eds.), Encyclopaedia of Marine Mammals. Academic Press, San Diego, pp. 412–421.

Hewitt, R.P., Lipsky, J.D., 2002. Krill. In: Perrin, W.F., Würsig, B., Thewissen, J.G.M. (Eds.), Encyclopedia of Marine Mammals. Academic Press, San Diego, pp. 676–684.

Hofmann, E.E., Klinck, J.M., Costa, D.P., Daly, K.L., Torres, J.J., Fraser, W.R., 2002. US Southern Ocean Global Ocean Ecosystems Dynamics Program. Oceanography 15, 64–74.

Hofmann, E.E., Wiebe, P.H., Torres, J.J., Costa, D.P., 2004. An overview of the Southern Ocean Global Ocean Ecosystems Dynamics program. Deep-Sea Research II, this issue [doi:10.1016/j.dsr2.2004.08.007].

Hooker, S.K., Boyd, I.L., Jessopp, M., Cox, O., Blackwell, J., Boveng, P.L., Bengtson, J.L., 2002. Monitoring the prey-field of marine predators: combining digital imaging with datalogging tags. Marine Mammal Science 18, 680–697.

King, J.E., 1961. The feeding mechanism and jaws of the crabeater seal (*Lobodon carcinophaga*). Mammalia 25, 462–466.

Klages, N.T.W., Cockroft, V.G., 1990. Feeding behaviour of a captive crabeater seal. Polar Biology 10, 403–404.

Kooyman, G.L., 1981. Crabeater Seal *Lobodon carcinophagus* (Hombron and Jacquinot, 1842). In: Ridgway, S.H., Harrison, R.J. (Eds.), Handbook of Marine Mammals, vol. 2. Seals. Academic Press, London, pp. 221–235.

Laws, R.M., 1984. Seals. In: Laws, R.M. (Ed.), Antarctic Ecology, Vol. 2. Academic Press, London, pp. 621–715.

Miller, D.G., Hampton, I., 1989. Biology and ecology of the Antarctic krill (*Euphausia superba* Dana): a review. BIOMASS Scientific Series 9, 1–166.

Nordøy, E.S., Folkow, L., Blix, A.S., 1995. Distribution and diving behaviour of crabeater seals (*Lobodon carcinophagus*) off Queen Maud Land. Polar Biology 15, 261–268.

Øritsland, T., 1977. Food consumption of seals in the Antarctic pack ice. In: Llano, G.A. (Ed.), Adaptations within Antarctic Ecosystems. Smithsonian Institution, Washington, pp. 749–768.

Racovitza, E.G., 1900. La vie des animaux et des plantes dans l'Antarctique. Bulletine de la Royale Societie Blege de Geographie. Brussels 24, 177–230.

Ross, G.J.B., Ryan, F., Saayman, G.S., Skinner, J., 1976. Observations of two captive crabeater seals *Lobodon carcinophagus* at the Port Elizabeth oceanarium. International Zoo Yearbook 16, 160–164.

Siniff, D.B., Stirling, I., Bengtson, J.L., Reichle, R.A., 1979. Social and reproductive behaviour of crabeater seals (*Lobodon carcinophagus*) during the austral spring. Canadian Journal of Zoology 57, 2243–2255.

ELSEVIER

Deep-Sea Research II 51 (2004) 2311–2325

DEEP-SEA RESEARCH
PART II

www.elsevier.com/locate/dsr2

Seasonal variability in whale encounters in the Western Antarctic Peninsula

Deborah Thiele[a,*], Edwin T. Chester[a], Sue E. Moore[b], Ana Širovic[c], John A. Hildebrand[c], Ari S. Friedlaender[d]

[a]*Whale Ecology Group–Southern Ocean, Deakin University, School of Ecology and Environment, Warrnambool, VIC, Australia*
[b]*NOAA/AFSC/National Marine Mammal Laboratory, Seattle, WA, USA*
[c]*Scripps Institution of Oceanography/MPL, La Jolla, CA, USA*
[d]*Duke University, Nicholas School of the Environment, Durham, NC, USA*

Accepted 14 July 2004

Abstract

Cetacean sighting surveys were conducted as part of nine multidisciplinary research cruises over late summer, autumn and winter of 2 years (2001–2003) during the Southern Ocean Global Ocean Ecosystems (SO GLOBEC) program. Sea-ice cover differed markedly between years, with apparent effects on cetacean distribution. No ice was present until late June in 2001, while the previous winter sea ice never fully retreated (>30% cover) during the 2002 or 2003 summer, thus increasing the proportion of thicker and more complex ice, including multi-year floes. Humpback (237 sightings; 537 individuals) and minke (103 sightings: 267 individuals) whales were the most commonly detected species. Data from seven comparable cruises were used to identify habitat for minke and humpback whales over five geographically distinct spatial divisions in the study area. In all years, both species were predominantly found in near coastal habitat, particularly in the fjords where complex habitat likely concentrated prey. In 2002 and 2003 the presence of sea ice provided additional feeding habitat, and the numbers of minkes (in winter) and humpbacks (late summer and autumn) in the area doubled compared with 2001. Humpbacks in particular were concentrated at the ice boundaries during late summer and autumn, while minke numbers increased in the winter that followed and occupied ice-covered areas along the entire shelf edge. Important resource sites for these species are mainly located in near-coastal areas and are used in all years, but when ice margins exist and intersect with resource sites they attract much larger numbers of animals due to the dynamics between sea ice and prey.
© 2004 Elsevier Ltd. All rights reserved.

1. Introduction

The core objective of the International Whaling Commission's (IWC) collaborative research in the

*Corresponding author. Fax: +61-355-633-462.
E-mail address: dthiele@deakin.edu.au (D. Thiele).

0967-0645/$ - see front matter © 2004 Elsevier Ltd. All rights reserved.
doi:10.1016/j.dsr2.2004.07.007

Antarctic is to investigate how spatial and temporal variability in the physical and biological environment influences cetaceans (IWC 2000). The IWC participated in the Southern Ocean Global Ocean Ecosystems Dynamics (SO GLOBEC) studies in the Western Antarctic Peninsula (WAP) to contribute to this objective. The multidisciplinary framework and scale of the SO GLOBEC program provided a rare opportunity to investigate cetacean patterns of occurrence concomitant with data collected across physical and biological domains.

Programs of cetacean research have been conducted along the Antarctic Peninsula for many years, but most have focused on areas north of the SO GLOBEC study site (Stone and Hamner, 1988; van Franeker, 1992; Pankow and Kock, 2000; Olavierra et al., 2003). Cetacean sightings data have also been collected from the offshore, shelf and fjord regions to the north and west of Marguerite Bay during the austral summer, as part of the United States (US) Long Term Ecological Research (LTER) program (LTER unpublished data) and also on the IWC International Decade of Cetacean Research (IDCR) and Southern Ocean Whale Ecosystem Research (SOWER) circumpolar surveys (Kasamatsu et al., 2000). These surveys included portions of the WAP region (IWC Management Area I 60°W–120°W), in the austral summers of 1982/83, 1989/90, 1993/94, 1999/00, 2000/01 (Branch and Butterworth, 2001). Marguerite Bay has never been surveyed during IWC circumpolar surveys (Branch and Butterworth, 2001; Kasamatsu et al., 2000; Matsuoka et al., 2003). Those IWC surveys rarely approached the shelf in this area, and no cetacean sightings have been reported from the WAP SO GLOBEC study area (Kasamatsu et al., 2000). Reports of cetacean surveys in this region outside the spring and summer seasons or within the pack ice are rare (Joiris, 1991; Aguayo-Lobo, 1994).

Marguerite Bay is located in the central Western Antarctic Peninsula (WAP) (Fig. 1). It is a large embayment open to the continental shelf (~100 nm wide) to the west, abutting a steep shelf slope and waters over 3000 m. The bay is bordered to the north by Adelaide Island, and to the south by Alexander Island. The eastern edge of the bay is the main Peninsular land mass. A coastal fjord system, formed by near-shore islands close to the steep mountains and glaciers of the continent, extends from the east side of Adelaide Island to Anvers Island in the north. Marguerite Bay is bisected in the south by a deep trough (Marguerite Trough) that extends across the shelf in the west and lies along the northern edge of Alexander Island. This trough extends all the way into the bay and ends in a glacier-filled sound (George VI Sound). The overall bathymetric environment of Marguerite Bay is complex, and comprises many shoals, minor troughs and deep holes and ridges. The southern boundary of the Antarctic Circumpolar Current flows in a northwesterly direction against the continental shelf here, causing warm-water intrusions throughout the year (Smith, D. A. et al., 1999).

The combination of complex bathymetry and oceanographic processes in this region produces very high-velocity currents and small gyres in some parts of the bay (Smith et al., 1999, Beardsley et al., 2004), that may concentrate and entrain zooplankton such as krill in particular areas (Lawson et al., 2004; Ashijan et al., 2004). This area was chosen for multidisciplinary research into the physical and biological factors that contribute to enhanced krill growth, reproduction, recruitment and survivorship (Hofmann et al., 2002) for two reasons: unusually high krill production (Lascara et al., 1999) and predictable winter sea-ice cover (Jacobs and Comiso, 1997).

Krill (*Euphausia superba and E. sp.*) form a significant component of baleen whale diet in the Antarctic (Kawamura, 1994), and relationships between the distribution of these predators and that of their prey have been shown at broad (~100 to 1000s of km) spatial scales for the Antarctic (Tynan, 1998; Reid et al., 2000; Thiele et al., 2000; Murase et al., 2002). So far, strong associations between baleen whale and krill distributions have not been shown at smaller (10s of km) spatial scales (Pankow and Kock, 2000; Reid et al., 2000). This may be due to the difficulty of integrating data for predator and prey species that both have patchy distributions (van Franeker et al., 2002). In the Antarctic, the patchiness of whale distributions

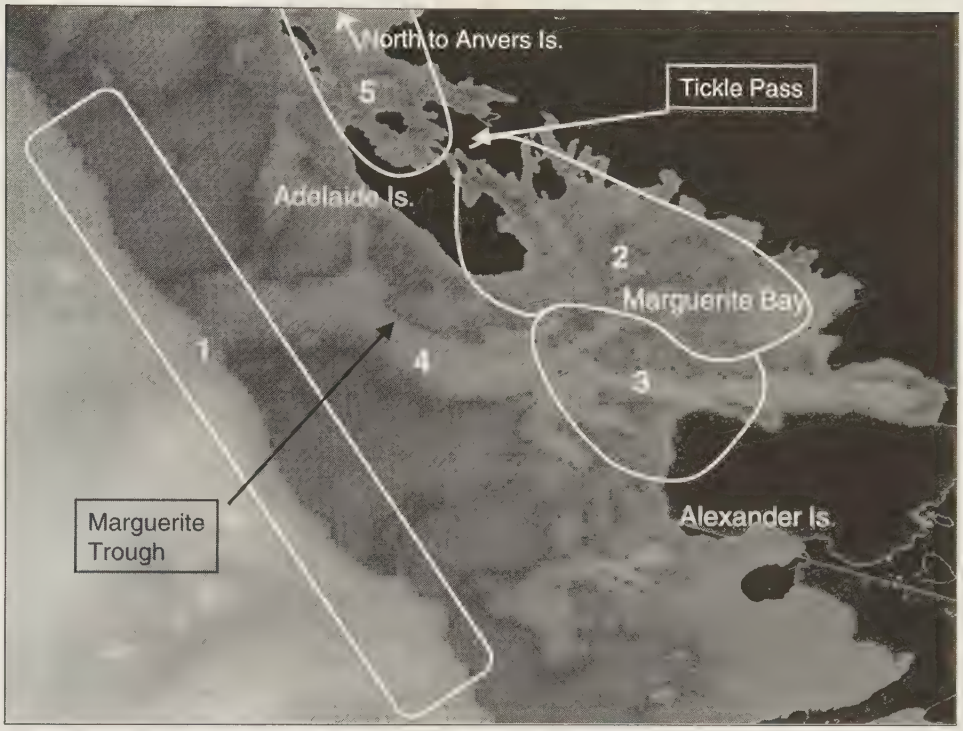

Fig. 1. Study area around Marguerite Bay with bathymetry. Spatial divisions used in analysis: shelf edge (SD 1), inner shelf (SD 2), southern inner shelf (SD 3), outer shelf (SD 4) and coastal fjord area (SD 5).

is further compounded by low densities of many species due to the depletion of populations during commercial whaling.

Krill population dynamics have been linked to variability in sea ice conditions in a number of studies (Fraser and Hofmann, 2003; and summarized in Constable et al., 2003), and winter ice extent is known to affect krill survival and abundance in the following season (Daly, 1990; Siegel and Loeb, 1995; Loeb et al., 1997; Nicol et al., 2000; Constable et al., 2003). High densities of krill, baleen whales and other predators have been observed at 'ice margins' or 'ice edges' (de la Mare, 1997; Ainley et al., 1998; Ferguson et al., 2000; Brierly et al., 2002; van Franeker et al., 2002), and particularly where ice habitat coincides with certain physical features and biological processes such as complex bathymetry, gyres, eddies, warm-water intrusions, high-velocity currents, high productivity, troughs, ridges, slopes, shelf edges, and other features which, alone or in combination, produce upwelling or concentration of nutrients and prey (Daly and Macaulay, 1991; Ribic et al., 1991; Plotz et al., 1991; Ichii et al., 1998; Murase et al., 2002). In general, habitat complexity is reported to result in increased diversity and abundance for many species (Bartholomew et al., 2000). Marguerite Bay and the surrounding area have complex habitat features, as well as a predictably high krill abundance. We therefore expected that significant numbers of baleen whales would be present there, and that the distribution of krill and krill predators would reflect the spatial complexity of the Marguerite Bay area.

Our central objective here was to investigate seasonal changes in distribution and concentration of minke and humpback whales, and to relate this to variability in feeding habitat associated with bathymetric and sea-ice features. Our analyses were focused on minke and humpback whales because they are often found in association with sea ice, and because of the relatively low numbers

of other cetacean species observed. Sea-ice conditions and krill abundance differed greatly between 2001 and 2002 (Ashijan et al., 2004; Lawson et al., 2004), which provided a strong foundation for comparison of cetacean distribution and relative abundance between years.

2. Materials and methods

The SO GLOBEC research program in the WAP was conducted over two years commencing March 2001 and finishing in March 2003 (Table 1). Three sampling protocols were developed for research cruises: survey grid, process studies and mooring deployments (see Hofmann et al., 2004, for detail of cruise tracks and descriptions of survey types). Four survey cruises were conducted aboard the *RVIB Nathaniel B Palmer (NBP)*, comprised of multidisciplinary sampling of the entire study area along pre-determined grid lines except when sea ice made this impossible. Four process cruises were conducted aboard the *RV Laurence M. Gould (LMG)*. At process sites a range of sampling and experimental activities occurred (e.g. seal foraging and tagging (Burns et al., 2004), penguin tagging and diet studies, zooplankton sampling (Lawson et al., 2004). Surveys for cetaceans were conducted whenever the vessel transited between sampling sites. The *RV Laurence M. Gould (LMG)* have also used for three mooring cruises to deploy and retrieve a series of oceanographic and cetacean passive acoustic moorings along the outer shelf and inshore regions. Visual surveys for cetaceans were conducted as the vessel transited through the study area. The *RV Polarstern* conducted one cruise in this study area, but these data have not been used in statistical analyses. Sightings are reported here only to provide seasonal context of humpback whale presence for late April/May 2001, due to the large concentrations seen in southern MB on a single helicopter survey.

2.1. Data collection

One or two trained cetacean observers were placed on each cruise to search along all survey grid lines and transits between process, mooring and other sampling sites (Table 1). Observers searched an arc 180° ahead of the vessel whenever the ship was in transit, usually by naked eye, but sometimes augmented by Fujinon 7×50 binoculars. Zeiss $20\times$ binoculars were used to aid in species identification. Search effort was occasionally interrupted while observers attempted to positively identify species or note unusual sightings. Data were recorded using a laptop computer based sighting program (Wincruz Antarctic[1]) that also logged GPS position, ship course and speed. The Wincruz program catalogued search effort, number of observers on effort, weather and sea-state information (Beaufort sea state, swell height and direction), cetacean sightings (time, ship's position, angle and distance from vessel, species identification, group size, presence of ice) and ancillary data. A group is defined here as two or more cetaceans, broadly coordinating their behavior and direction of movement. Best, high and low estimates of group size were recorded for each sighting, and where more than one observer made an estimate, the final record was arrived at by consensus.

Our goal was to detect cetaceans whenever possible, so search effort was conducted over a broad range of weather conditions. The majority of Antarctic species are medium to large whales, with cues that can be detected in relatively high Beaufort sea states (Thiele et al., 2000). Search effort was terminated when observers determined that visibility was too poor due to some combination of adverse weather conditions that precluded detection of most species (i.e. strong winds, fog, large swell, confused swell, high sea state). Cetaceans were identified to the lowest taxonomic level possible. A positive species identification was made only when there was certainty.

2.2. Data analysis

To compare variability in cetacean distributions across multiple surveys of a geographically

[1]Wincruz Antarctic is a free software program developed by Robert Holland at the Southwest Fisheries Science Centre, La Jolla, USA, for cetacean surveys in the Antarctic. The software is available at http://mmdshare.ucsd.edu/software.html.

Table 1
SO GLOBEC cruises 2001–2003 with cetacean sighting survey data

Vessel/cruise acronym	Cruise dates	Purpose
R/V Laurence M. Gould/LMG 0103	18 March–13 April 2001	Mooring cruise (Initial deployments)
RV Polarstern/AntXVIII5b	14 April–7 May 2001	Survey and ice/krill process cruise
RVIB Nathaniel B. Palmer/NBP 0103	24 April–5 June 2001	Survey cruise
RVIB Nathaniel B. Palmer/NBP 0104	24 July–31 Aug 2001	Survey cruise
R/V Laurence M. Gould/LMG 0201A	6 Feb–3 March 2002	Mooring cruise (Retrieve and deploy)
R/V Laurence M. Gould/LMG 0203	7 April–21 May 2002	Process cruise
RVIB Nathaniel B. Palmer/NBP 0202	9 April–21 May 2002	Survey cruise
RVIB Nathaniel B. Palmer/NBP 0204	31 July–18 Sept 2002	Survey cruise
R/V Laurence M. Gould/LMG 0302	12 Feb–17 March 2003	Final mooring cruise (Retrieval)

complex study area, we: (a) divided the study area into biologically meaningful zones within which total effort was pooled; (b) treated sections of sighting survey effort as statistical samples; (c) adjusted sighting survey counts by the duration of effort within defined spatial divisions; (d) selectively pooled some cruises and areas for separate analyses; (e) separated some cruises completely when they could not easily be used in analyses; and (f) tested hypotheses of independence and homogeneity, rather than for differences in abundance or density.

The study area was divided into four subregions based upon potentially biologically important locations (Fig. 1). These spatial divisions (SD) included: the *shelf edge* (SD 1); the *inner shelf* waters inside Marguerite Bay and around the southern tip of Adelaide Island, generally with depths of 100–400 m (SD 2); the *southern inner-shelf waters* including the mouth and southern part of Marguerite Bay, and Marguerite Trough (SD 3); the outer shelf (SD 4) Additionally, sighting effort was pooled in order to allow adequate overall survey time in the *coastal fjord* area from near Anvers Island in the north (64°00'S), to Tickle Pass at Adelaide Island (SD 5).

Sighting survey effort was not continuous along entire cruise tracks, but occurred only when the vessel was transiting between points during daylight, and where sea and weather conditions did not critically affect visibility. For analysis, survey periods of varying length "on effort" (time spent on visual survey) were treated as independent "shifts". "Off effort" temporal discontinuities allowed shifts to be viewed as samples within each spatial division The fact that the coincidence of timing for each shift with geographic position was not planned addresses concerns about sampling bias (Quinn and Keough, 2002). Shifts were considered separate, or independent, if the end of one recorded survey period was separated by more than one hour from the beginning of the next. Shifts were eliminated or truncated if they did not fit wholly within a particular spatial division. Consequently, sighting data were standardized by the duration of effort for each shift, and then the adjusted counts for each spatial division were summed.

Once adjusted for effort, counts for each "sample" were then grouped within "cells" of a table formed by each combination of cruise and spatial division (Fig. 2). Several cells in Part A (Fig. 2) are empty, as the result of two distinct occurrences, where (1) the cruise track did not cover that combination, or there was little or no effort there, or (2) the combinations did not exist, e.g., because fast ice prevented access to areas during winter 2002 in Marguerite Bay. Sampling effort in a division for each cruise was determined to be significant if it exceeded 5 h in total (~0.2 days): any cell with less than this was counted as missing (only NBP 0104 division 5). Fig. 2 also includes the two cruises (Polarstern AntXVIII5b and LMG 0302) where effort was not directly comparable with the other cruises: these were not used in statistical analyses, but provided

		SPATIAL DIVISION	1	2	3	4	5
A	Summer 2001	LMG 0103					
	Autumn 2001	Polarstern AntXVIII5b	-----	-----	-----	-----	-----
B	Autumn 2001	NBP 0103					
C	Winter 2001	NBP 0104					
D	Summer 2002	LMG 0201A					
E	Autumn 2002	NBP 0202/LMG 0203					
F	Winter 2002	NBP 0204					
	Summer 2003	LMG 0302	-----	-----	-----	-----	-----

Fig. 2. Analysis of whale sightings as table frequencies. Counts (per 24 h) within each voyage by spatial division combination are entered as cell frequencies for statistical analysis (Part A). Cruises with dashes were not included in statistical analyses. Missing cells (missing survey grid data) in the table are due to (1) combinations where there was no significant sampling effort (cells shown crossed), and (2) where no sighting were recorded for a particular combination (dark shaded for humpback whales, diagonally striped for minke whales).

additional supporting data for some locations within the study area.

The presence of zero or missing values (Goodman, 1968) strongly influences the way in which data are analyzed, because too many prevent meaningful hypothesis tests. Here, LMG 0203 and NBP 0202 could be combined because their temporal extents were nearly coincident, and this eliminated a missing cell in the table. The influence of other missing cells on statistical tests was minimized by separating the table into subsets for analysis.

For statistical analyses, sightings (for cruises A–F in Fig. 2) were treated as a multinomial experiment, i.e. counts adjusted for effort were treated as frequencies allocated to each cell within the full table (Ramsey and Schaeffer, 1996). Analysis tested hypotheses using chi-squared statistics for homogeneity or goodness of fit on separable 'sub-tables', with tests of quasi-independence for the full table (Quinn and Keough, 2002). Where there was the potential for compounding error due to repeated tests on the same data, Bonferroni type corrections (Quinn and Keough, 2002) were not deemed necessary because evidence in favour of rejecting null hypotheses was always either very strong or very weak. Specifically, null hypotheses for sub-tables were that across-division patterns of frequencies (i.e. effort-adjusted counts) do not change between cruises. Then, using the additive property of χ^2 statistics (Goodman, 1968), results for the sub tables were combined to test the equivalent null hypothesis for the full table. The prior analysis of sub-tables allowed complex interactions between the spatial and temporal components of observed frequencies to be explored. Because hypothesis tests for independence or homogeneity do not involve directly comparing estimates of, e.g., density between different times or area, the different spatial extents of the divisions to which counts were assigned have no effect on the outcome.

The analyses for humpback and minke whale habitat use were conducted independently both to address different sets of hypotheses and because the patterns of missing values and zero frequencies required tables to be separated and/or pooled differently. Humpbacks were seen throughout most of the study area on four cruises (NBP 0103–Autumn 2001, LMG 0201a–Summer 2002, LMG 0203/NBP 0202–Autumn 2002) so data were combined into a 3×4 cell table with the four SDs around Marguerite Bay. A separate test for homogeneity of frequencies was done for SD 5 for LMG 0201a and LMG 0203/NBP 0202. Sightings for winter cruises were not included in statistical analysis because of the pattern of zero values.

A different approach was taken for minke whales, because they were seen in the study area during all seasons, on all cruises. The zero frequencies (especially in LMG 0103) were addressed by separating the full table by year, then differentially pooling each year across spatial

divisions. This allowed the separate examination and then comparison of the change in the pattern of distribution in each year. Since 2001 and 2002 were very different in terms of extent and timing of pack-ice formation: we hypothesized that pack ice was an important habitat for minke whales, hence we expected the distribution of minkes through the year to respond to pack ice.

Finally, there was the problem of missing survey grid data, for NBP 0204 (in Winter, 2002), because at this time fast ice covered the inner shelf and southern inner shelf (SD 2 and 3) around Marguerite Bay. Hence, for 2001, the shelf edge and outer shelf (SD 1 and 4) were pooled, and SD 2 and 3 also were pooled within each cruise, forming a 2×3 sub-table. The coastal fjord area (SD 5) could not be included because there was no (or very little) effort there for NBP 0103 and NBP 0104 (2001). For 2002, SD 2 and 3 were not included in the sub-table, leaving SD1 and 4, which were largely covered by pack ice by Autumn 2002. A further test was done for SD 2–4 between May 2001 and May 2002.

3. Results

Ten cetacean species (fin whale *Balaenoptera physalus*, sei whale *Balaenoptera borealis*, blue whale *Balaenoptera musculus* sp., minke whale *Balaenoptera bonaerensis and B. acutorostrata sub species*, killer whale *Orcinus orca*, humpback whale *Megaptera novaeangliae*, sperm whale *Physeter macrocephalus*, hourglass dolphin *Lagenorhynchus cruciger*, Ziphiidae and various categories of 'unidentified' cetaceans) were detected on nine cruises (Table 2). Humpback and minke whales were by far the most numerous species.

Overall survey effort was 650 h for the seven statistically analysed cruises (Fig. 3). Total search effort per cell ranged up to 62 h (NBP 0202 SD 4), and total effort per division ranged from 79 (SD 3) to 232 h (SD 4). Additionally, for LMG 0302 there was over 55 h survey effort in the study area . The Polarstern cruise (April/May 2001) conducted only a brief survey of the study area, but did include helicopter survey of the inner shelf (SD 2), where a large concentration of humpbacks was seen. Two cruises ancillary to the analyses, but important for their contribution of additional distribution data are the Polarstern ANTXVII5b and LMG 0302 cruises. Sightings recorded on these cruises were 20 sightings of 90 individual humpbacks (20:90 this is standard notation for recording number of sightings/groups and number of individual whales and will be used from now on in the text), 9:11 minkes (LMG 0302) and 16 sightings of 38 humpbacks, 15 sightings of 28

Table 2
Cetacean species, total number of sightings/groups and individuals for all (nine) SO GLOBEC cruises 2001–2003 south of 60°S

Species (common name)	No. of groups	No. of animals
Humpback whale	356	848
'like' humpback	14	34
Antarctic minke and undetermined minke	137	331
'like' minke whale	17	29
All unidentified cetacean categories	94	198
Killer whale	17	172
Fin whale	3	12
'like' fin whale	9	24
Sei whale	6	30
'like' sei whale	1	3
Ziphiidae	5	15
Hourglass dolphin	4	19
Sperm whale	2	3
'like' blue whale	1	1
Total	666	1719

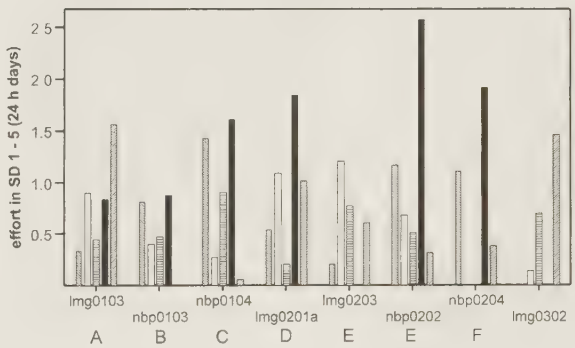

Fig. 3. Effort (24 h day equivalents) for SD 1–5, all cruises except Polarstern (total eight cruises). A–F as per Fig. 2.

minkes (Polarstern). Sighting summaries for all cruises in the analysis (A-F Table 2) include 103 minke sightings of 267 individuals and 237 humpback sightings of 537 individuals; by far the highest proportion of these were in the coastal fjords (SD 5). Sightings corrected for effort were: minkes (87.36:225.26); humpbacks (196.92:423.11).

The overall pattern of distribution of humpback and minke whales is evident in Fig. 4(A)–(E). Humpback whales were detected throughout late summer and autumn of both years. Detections were much higher in 2002 and distribution appeared to follow the position of the pack-ice edge. For example in 2001 humpbacks were concentrated in the inner shelf area (SD 2) (Fig. 4A), while in 2002, although some large groups were found in one area of the inner shelf (SD 2), humpback aggregations were seen in the southern inner shelf area (SD 3) in association with the pack ice margin, with smaller groups scattered over the outer shelf (SD 4) (Fig. 4B). The late summer 2003 cruise (LMG 0302) also recorded the largest concentrations of humpbacks near ice margins in the coastal fjords (SD 5) and in the southern inner shelf, where this intersected the pack ice margin (SD 3) (Fig. 4C). Notably, one pair of humpback whales was seen on 4 August 2002 near Anvers Island (64° 53.15S 64°08.37W).

Minke whales were seen on every survey. During late summer and autumn of 2001 and 2002, most minke whales were found in the coastal fjords (SD 5), although sightings were lower for 2002. During 2001, there were fewer minke sightings on winter surveys, while in 2002 numbers increased during winter and were significantly higher than in 2001. Winter distributions of minke whales were concentrated at two sites: one very close to the shelf edge, and one in the Marguerite Trough. In 2001 most were seen at one location on the shelf edge (Fig. 4D), while in 2002 they occupied a much greater area of the shelf edge (Fig. 4E). Standardizing by effort did not generally affect this pattern of occurrences, i.e. where there were many sightings, there were still many sightings with the correction. Two cruises ancillary to the analyses, but important for additional distribution data are the Polarstern ANTXVII5b and LMG 0302 cruises. Sightings recorded on these cruises were 20:90 humpbacks, 9:11 minkes (LMG 0302) and 16:38 humpbacks, 15:28 minkes (Polarstern). For all cruises in the analysis (Fig. 2) minke sightings with 103 groups and 267 individuals (103:267) and humpback whales are 237 groups and 537 individuals (237:537): by far the highest proportion of these were in the coastal fjords (SD 5). When corrected for effort, i.e. expressed as sightings per day added for each spatial division, the totals are: minkes (87.36:225.26); humpbacks (196.92:423.11) (Fig. 5A–D).

3.1. Humpback whale seasonal occurrence and habitat selection

Humpback whale distribution was restricted to the inner shelf and coastal fjord area in late Summer 2001 (SD 2 and 5). They were detected

Fig. 4. Whale sightings from cetacean sighting surveys in the SO GLOBEC Western Antarctic Peninsula study area. All sightings represented by black filled squares. (A) Humpback whales March 2001–June 2001 (symbol size represents group size for each sighting: groups size categories are 1, 2, 3, 4, 5 or 6 whales). There was no sea ice in the study area until after June 2001. (B) Humpback whales February 2002–May 2002 (symbol size represents group size for each sighting: groups size categories are 1–2, 3–4, 5–6, 7–8, 9–10, 11–12 whales). Sea-ice extent for February 22 2002, 6 May 2002 and 4 June 2002 represented by solid line. May ice extent comprised more than one third brash marginal ice zone at outer edge – diffuse ice edge; while February sea-ice extent had a distinct boundary of sheet ice. (C) Humpback whales LMG 0302 February 2003–March 2003 in the SO GLOBEC Western Antarctic Peninsula (symbol size represents group size for each sighting: groups size categories are 1, 2, 3, 4, 5, 6 whales). Sea-ice extent for cruise period marked with dashed lines. (D) Minke whales July 2001–August 2001 (symbol size represents group size for each sighting: groups size categories 1, 2 or 3 whales). Pre-winter sea-ice extent is shown by a dashed line for comparison with 2002. In both 2001 and 2002 sea ice covered the entire bay and shelf when winter cruises were conducted. Ice thickness, ridging and the percentage of multi year floes changed between years, with 2002 having thicker ice, more ridging and more multi-year floes than 2001. (E) Minke whales August 2002–September 2002 (symbol size represents group size for each sighting: groups size categories are (1, 2, 3 or 4 whales).

only once during winter 2002 Fig. 2: C and F), in the extreme north of the coastal fjord area (SD 5). The hypothesis of non-independence between spatial divisions and the cruises outside winter was thus supported by the lack of sightings on LMG 0103 (Fig. 2): their distribution was restricted to the inner shelf and coastal fjord area in late Summer 2001 (SD 2 and 5).

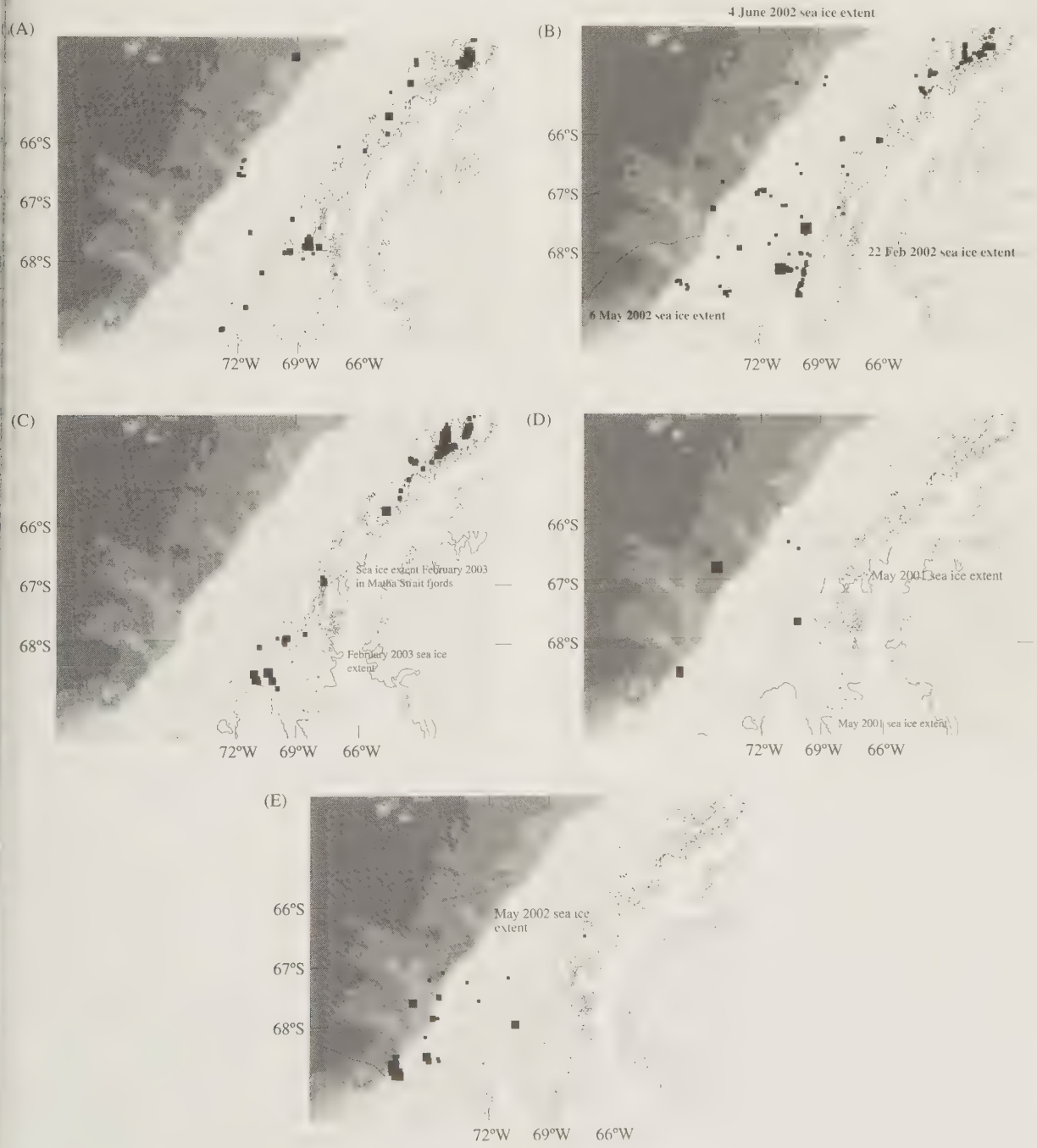

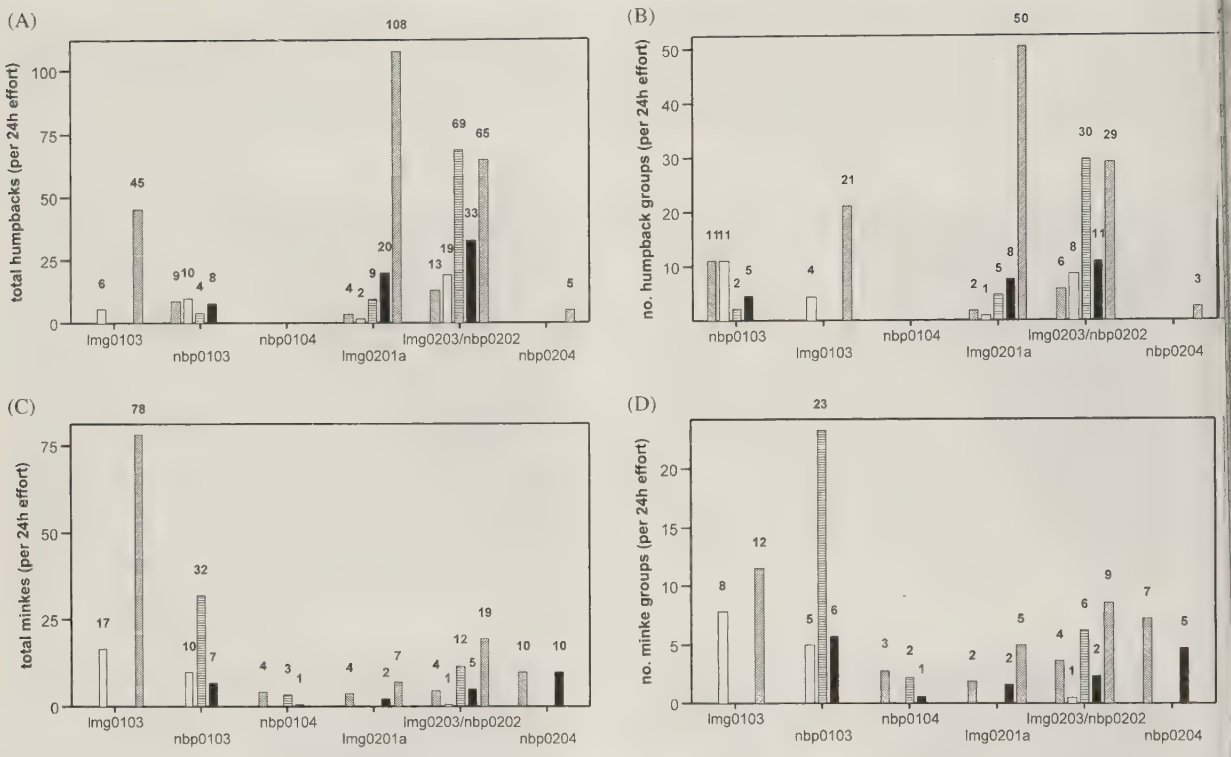

Fig. 5. Individuals and groups in SD 1–5 corrected for effort: (A) total humpbacks (no. individuals), (B) total humpbacks (no. groups), (C) total minkes (no. individuals) and (D) total minkes (no. groups).

Significantly more humpback whales were found in summer 2002 than in autumn 2002 in the coastal fjords (SD 5) ($\chi^2 = 10.79 > \chi^2_{0.001,1}$ for individuals $\chi^2 = 5.726 > \chi^2_{0.05,1}$) for groups. In late summer, the majority of humpbacks were found in the coastal fjords (SD 5) (50.42:107.75), 75% of the total. This is concordant with LMG 0103 at a similar time in 2001 (21.14:45.49) 89% of the total, although for this cruise, humpbacks were seen throughout the coastal fjord area (SD 5). In 2002 they were mainly seen in the far north of SD 5. The Polarstern helicopter surveys confirmed the presence of aggregations of humpback whales (38 individuals in groups of 2–4), near the south east coast of Adelaide Island, and in bays around Anvers Island in early May 2001.

While many humpbacks (33% of individuals) were still found in the coastal fjord area (SD 5) in Autumn 2002 (29.08:64.62), the distribution between divisions was more uniform than in 2001. In Autumn 2002, most (80%) humpbacks were found in SD 5 and the southern inner shelf area (SD 3) (29.65:68.66). This cruise went mainly through and along the edge of pack ice (Fig. 4B), in the inner shelf area (SD 2) and SD 3, and relative densities were much higher here in 2002 (87.77 versus 14.19 individuals) than in the equivalent (ice-free) areas in 2001 (Fig. 4A). The average group size for humpbacks was higher in 2002 and 2003 than in 2001 (Fig. 4A, B).

The test for the 4×3 cell table provided very strong evidence to reject the null hypothesis of independence between the four spatial divisions around Marguerite Bay and the cruises ($\chi^2 = 35.242 > \chi^2_{0.001,6}$ for individuals; $\chi^2 = 24.176 > \chi^2_{0.001,6}$ for groups). Examination of cell expected values showed that this could be attributed to cell differences between LMG 0203/NBP 0202 (Autumn 2002) and both the autumn 2001 and summer 2002 cruises. A test for the table combining both the previous sub-table and the non-missing cells for SD 5 then provided very strong

evidence to reject the null hypothesis of quasi-independence ($\chi^2 = 45.538 > \chi^2_{0.001,7}$ and $\chi^2 = 29.901 > \chi^2_{0.001,7}$ for groups sighted) between spatial divisions and sampling times for humpback whales.

In March 2003 (LMG 0302) large numbers (20 sightings of 90 whales) of humpbacks were again found in the inner shelf, southern inner shelf and coastal fjord areas (SD 2,3 and 5) (there was little effort away from the coast in SD1, on this cruise). More individuals (56, 62%) were observed in the coastal fjords (SD 5); however, this proportion dropped when corrected for effort (28%). Sampling by shift was not strictly comparable with previous cruises: effort in SD 2 was less than the a priori threshold for significance of 0.2, but this was an artifact of an inability to assign shifts as occurring wholly within the spatial divisions used on previous cruises.

3.2. Minke whale seasonal occurrence and habitat selection

By far the largest number of minkes were observed in the coastal fjords (SD 5) on LMG 0103 (18:122, 11.53:78.16 per 24 h effort). This included two large feeding groups encountered in Matha Strait, north of Adelaide Island (~100 animals), which dispersed after several hours. Many fewer minkes were seen on the equivalent cruise in 2002 (LMG 0201a) (Fig. 4), although most were still seen in SD 5. With SD 5 excluded from the 2001 sub-table, there were many zero frequencies for minkes in the full cruise by spatial division table, indicating that minke distributions were relatively localized within the period covered by each cruise. The highest proportion of minke whale sightings occurred in autumn in both 2001 and 2002. 66% and 45% of the overall effort-corrected totals for their respective within-year sub tables.

There was strong evidence to reject the null hypothesis of independence between cruises and spatial division groupings for total individuals seen (for 2001, $\chi^2 = 14.72 > \chi^2_{0.001,2}$; for 2002, $\chi^2 = 22.92 > \chi^2_{0.001,4}$), as well as for number of groups seen for both years (2001, $\chi^2 = 8.881 > \chi^2_{0.001,2}$; 2002, $\chi^2 = 13.78 > \chi^2_{0.001,4}$). The null hypothesis of quasi-independence for the table combining both years was also rejected ($\chi^2 = 9.49 > \chi^2_{0.001,6}$ for total number; $\chi^2 = 22.591 > \chi^2_{0.001,6}$ for groups). The single zero-values in both these tables contributed greatly to this result: i.e., no minkes were in the shelf edge or outer shelf areas (SD 1 and 4) in March 2001, and none were found in the coastal fjords (SD 5) in winter 2002.

The test for independence for the 3×2 complete table for the inner, inner southern and outer shelf (SD 2–4) autumn cruises reused cells from the previous analyses. A statistically significant result would need to be corrected for potentially compounding type I error (Quinn and Keough, 2002); however, there was no evidence that the null hypothesis of independence for spatial divisions across the two years should be rejected, neither for individuals ($\chi^2 = 4.05 < \chi^2_{0.05,2}$), nor groups ($\chi^2 = 0.733 < \chi^2_{0.05,2}$). In other words, the relative distribution of minke whales in and around Marguerite Bay during autumn appears to have been similar in 2001 and 2002 for those spatial divisions, although the densities were higher in 2001.

There were differences in the seasonal pattern of minke whale distribution between years, and the difference in analytical treatment between years is partly due to this. Interannual differences for the combined table were largely due to the large number of minkes found inshore (SD 2, 3) in 2001. However, examining the full data for cruises A–F before it was pooled for statistical tests (Fig. 5C, D) also shows the effect of the high number of minkes seen in SD 5 on LMG 0103, and the missing cells (Fig. 2, Part A), where there was insignificant effort, i.e. no data to be compared with equivalent times or spatial divisions. The most obvious interannual pattern is that minke whales were more dispersed, in pack ice, in winter 2002.

4. Discussion

The ecology of Marguerite Bay is probably influenced both by habitat complexity and by the effects of regional oceanographic and sea ice processes (e.g., Antarctic Circumpolar Current

intrusions onto the MB shelf, timing, nature and extent of sea ice) on the fauna. The marked seasonal and interannual variability in this environment observed over the two years of this study had apparent effects on cetacean distribution in and around the bay.

The results of these surveys showed humpback and minke whales using primarily near-coastal habitat (SD2, 3 and 5) in the late summer and autumn. When sea ice was present, its boundary provided an additional area of concentration, particularly for humpback whales. Both species were found in greater numbers during seasons where a sea ice boundary existed over the inner, and southern inner shelf areas of Marguerite Bay. For humpbacks, this was evident throughout late summer and autumn in years where sea ice was present across the inner shelf (2002 and 2003). Also, in winter, minke whales were found in greater numbers on the shelf in 2002 compared to 2001. The single winter sighting of one pair of humpback whales in the northern part of the coastal fjords in early August of 2002 is notable, since this provides solid evidence that members of this species can remain in this part of the Antarctic during winter. All humpback whales are presumed to migrate out of the Antarctic prior to winter (Dawbin, 1997), yet this has been challenged by Brown et al. (1995) with evidence of possible sex segregated migration off the East coast of Australia. The sex of the pair of humpbacks sighted in winter during this study could not be determined.

Hypothesis tests supported the assumption that whale distributions vary on a seasonal basis and between years. There was complex non-independence in the relationship between sampling location and cruise (or time of year), both within 2001 and 2002 and between cruises compared across the 2 years. Despite strong qualifications because of uncertainty over the effects of any interaction between varying effort and sampling location, spatial and temporal heterogeneity is clearly apparent for both minkes and humpbacks. A component of this is broad, taxon-specific behavior, i.e. the rarity of humpbacks over winter due to migration, and the association of minkes with pack ice in winter. However, it is clear that the distribution of whales changed markedly between years, between spatial divisions, and with the extent and nature of sea-ice cover, and that this likely reflects changes in the distribution and abundance of prey.

In the regions we surveyed, it appears that there are 'resource sites' that are important locations for baleen whale feeding during summer and autumn in years with or without ice. These sites were in the coastal fjord area, particularly Matha Strait and south eastern Adelaide Island; southwest Adelaide Island, north and northwest Alexander Island; the shelf edge; and around the Marguerite Trough. These localities had in common some of the following features: complex bathymetry, high velocity currents, small to medium gyres and eddies (Beardsley et al., 2004). We hypothesize that combinations of these features form a complex habitat that functions to enhance the concentration of zooplankton, and that this explains the strong seasonal and interannual association between these locations and the distribution of humpback and minke whales.

Reports of linkages between marine vertebrate distributions and physical features in the Antarctic, such as oceanographic fronts and gyres, which concentrate prey, also appear in much of the recent literature (Ainley, 1985; de la Mare, 1997; Tynan, 1997, 1998; van Franeker et al., 2002; Thiele et al., 2000; Wilson et al., 2001). Sea-ice processes play an integral role in the lives of Antarctic marine biota, whether they be permanent (e.g., krill, penguins, minke, killer and some other species of whales), or temporary (migrating seabirds and some whales) residents (Tonnessen and Johnsen, 1982; Ainley, 1985; Trathan et al., 1996; Ichii et al., 1998; Nicol et al., 2000; Barbraud et al., 2000; Wilson et al., 2001; Barbraud and Weimerskirch, 2001; Brierley et al., 2002; Murase et al., 2002).

A complex series of events determines sea-ice formation and structure (Allison, 1997). A sea-ice environment that forms relatively rapidly (2001 winter) will be more homogenous than one that has formed over many months (2002). The slower ice cover forms, and the older the ice involved, the more time it is exposed to the destructive effects of sea and weather conditions, and thus more areas will be ridged and broken, creating more diverse

habitats. Krill have been shown to congregate under ridged ice (Eicken, 1992) and concentrations of zooplankton (particularly krill, *E. superba*) have been reported as being significantly higher at some Antarctic ice boundaries (Ichii, 1990; Brierley et al., 2002).

In this study we see that when ice cover is present, as in 2002, resource sites remain important, but ice margins, edges, boundaries, or areas where these intersect with resource sites, attract much larger numbers of animals (particularly, but not exclusively humpbacks); i.e. they become 'enhanced resource sites'.

Examination of cell structure within analysed tables showed significant differences between the groups and the total number of individuals, suggesting that degree of aggregation changes seasonally, and potentially with annual ice conditions. Since baleen whales found in and around ice boundaries were usually engaged in feeding behaviour, aggregation at ice edges or boundaries is probably a manifestation of a direct link between ice as habitat for krill and a trophic response by their predators. In both years of this study, krill predators other than cetaceans (seabirds and seals) were generally found in higher abundance in the same areas as whales (Chapman et al., 2004), providing support for a link between habitat complexity and a greater diversity and abundance of fauna (Eicken, 1992; Bartholomew et al., 2000). The presence of large concentrations of krill predators feeding at sea-ice margins in the study area in 2002 supports the suggestion by Brierley et al. (2002) and others of a strong positive relationship between the sea-ice edge and krill densities.

The distribution of humpback and minke whales on the Antarctic feeding grounds is therefore likely to be influenced by both short and long-term changes in the distribution and dynamics of sea ice. The availability and abundance of baleen whale prey will be affected by variability in sea ice conditions, particularly in regions of the Antarctic where annual sea-ice extent is being reduced or increasing (Zwally et al., 2002). This variability directly influences the population dynamics, distribution and abundance of many krill predators in localized areas, as well as at regional and circum-Antarctic scales (van Franeker, 1992; Trathan et al., 1996; Smith, et al., 1999a,b; Barbaud and Weimerskirch, 2001; Croxall et al., 2002; Kato et al., 2002; Fraser and Hofmann 2003). Similar responses are likely for baleen whale populations that feed in the Antarctic, and therefore the implications of such environmental change need to be considered in the management and conservation of these species in the Southern Ocean.

Acknowledgements

We acknowledge the enthusiasm and support of Eileen Hofmann and Uli Bathmann in this work. The International Whaling Commission, the US SO GLOBEC Steering Committee and the National Science Foundation provided berths, funding for observers and support. A number of IWC observers contributed to the collection of data (Debra Glasgow, Rebecca Pirzl, Francisco Viddi) and deserve mention, as do the passive acoustics personnel and our colleagues from the many disciplines involved in the WAP study. The captains and crew of the RV *Nathaniel B. Palmer*, the RV *Laurence M. Gould* and the RV *Polarstern* must be thanked for their support, professionalism and enthusiasm. Alice Doyle, Andy Nunn and Skip Owen of Raytheon Polar Services have given great assistance to our program, as have all the Raytheon marine support staff. We are grateful for the positive suggestions from two anonymous reviewers as these contributed significantly to improving the manuscript. An unpublished manuscript by B.J. Robson was very useful for analysis, and we thank S. McKay for help with maps.

References

Aguayo-Lobo, A., 1994. Is there a population of minke whale that overwinter among the Antarctic sea-ice? INACH 44, 91–98.

Ainley, D.G., 1985. Biomass of birds and mammals in the Ross Sea. In: Siegfried, W.R., Condy, P.R., Laws, R.M. (Eds.), Antarctic Nutrient Cycles and Food Webs. Springer, Berlin, Heidelberg, pp. 498 515.

Ainley, D.G., Jacobs, S.S., Ribic, C.A., Gaffney, I., 1998. Seabird distribution and oceanic features of the Amundsen

and southern Bellingshausen seas. Antarctic Science 10 (2), 111–123.

Allison, I., 1997. Physical processes determining the Antarctic sea ice environment. Australian Journal of Physics 50, 759–771.

Ashjian, C.J., Rosenwaks, G.A., Wiebe, P.H., Davis, C.S., Gallager, S.M., Copley, N.J., Lawson, G.L., Alatalo, P., 2004. Distribution of zooplankton on the continental shelf off Marguerite Bay, Antarctic Peninsula during Austral Fall and Winter 2001. Deep-Sea Research II, this issue [doi:10.1016/j.dsr2.2004.07.025].

Barbraud, C., Weimerskirch, H., 2001. Emperor penguins and climate change. Nature 411, 183–186.

Barbraud, C., Weimerskirch, H., Guinet, C., Jouventin, P., 2000. Effect of sea-ice extent on adult survival of an Antarctic top predator: the snow petrel *Pagodroma nivea*. Oecologia 125, 483–488.

Bartholomew, A., Diaz, R.J., Cicchetti, G., 2000. New dimensionless indices of structural habitat complexity: predicted and actual effects on a predator's foraging success. Marine Ecology Progress Series 206, 45–58.

Beardsley, R.C., Limeburner, R., Owens, W.B., 2004. Drifter measurements of surface currents near Marguerite Bay on the western Antarctic Peninsula shelf during austral summer and fall, 2001 and 2002. Deep-Sea Research II, this issue [doi:10.1016/j.dsr2.2004.07.031].

Branch, T.A., Butterworth, D.S., 2001. Southern hemisphere minke whales: standardized abundance estimates from the 1978/79 to 1997/98 IDCR-SOWER surveys. Journal of Cetacean Research and Management 3 (2), 143–174.

Brierley, A.S., Fernandes, P.G., Brandon, M.A., Armstrong, F., Millard, N.W., McPhail, S.D., Stevenson, P., Pebody, M., Perrett, J., Squires, M., Bone, D.G., Griffiths, G., 2002. Antarctic krill under sea ice: elevated abundance in a narrow band just south of ice edge. Science 295, 1890–1892.

Brown, M.R., Corkeron, P.J., Hale, P.T., Schultz, K.W., Bryden, M.M., 1995. Evidence for a sex-segregated migration in the humpback whale (*Megaptera novaeangliae*). Proceedings of the Royal Society of London, B 259, 229–234.

Burns, J.M., Costa, D.P., Fedak, M., Bradshaw, C.J.A., Hindell, M.A., McDonald, G., Trumble, S.J., Chittick, E., Gray, M., Gales, N., Barnes, J., Shaffer, S., Kuhn, K., Lovell, P., Crocker, D., 2004. Winter habitat use and foraging behavior of crabeater seals along the Western Antarctic Peninsula. Deep-Sea Research II, this issue [doi:10.1016/j.dsr2.2004.07.021].

Chapman, E.W., Ribic, C.A., Fraser, W.R., 2004. The distribution of seabirds and pinnipeds in Marguerite Bay and their relationship to physical features during austral winter 2001. Deep-Sea Research II, this issue [doi:10.1016/j.dsr2.2004.07.005].

Constable, A.J., Nicol, S., Strutton, P.G., 2003. Southern Ocean productivity in relation to spatial and temporal variation in the physical environment. Journal of Geophysical Research 108 (C4), 8079–8099.

Croxall, J.P., Trathan, P.N., Murphy, E.J., 2002. Environmental change and Antarctic seabird populations. Science 297, 1510–1514.

Daly, K.L., 1990. Overwintering development, growth, and feeding of larval *Euphausia superba* in the Antarctic marginal ice zone. Limnology and Oceanography 35, 1564–1576.

Daly, K.L., Macaulay, M.C., 1991. Influence of physical and biological mesoscale dynamics on the seasonal distribution and behavior of *Euphausia superba* in the Antarctic marginal ice zone. Marine Ecology Progress Series 79, 37–66.

Dawbin, W.H., 1997. Temporal segregation of humpback whales during migration in southern hemisphere waters. Memoirs of the Queensland Museum 42 (1), 105–138.

de la Mare, W.K., 1997. Abrupt mid-twentieth-century decline in Antarctic sea-ice extent from whaling records. Nature 389, 57–60.

Eicken, H., 1992. The role of sea ice in structuring Antarctic ecosystems. Polar Biology 12, 3–13.

Ferguson, S.H., Taylor, M.K., Messier, F., 2000. Influence of sea ice dynamics on habitat selection by polar bears. Ecology 81 (3), 761–772.

Fraser, W.R., Hofmann, E.E., 2003. A predator's perspective on causal links between climate change, physical forcing and ecosystem response. Marine Ecology Progress Series 265, 1–15.

Goodman, L.A., 1968. The analysis of cross classified data: independence, quasi-independence and interactions in contingency tables with or without missing entries. Journal of American Statistical Association 63, 1019–1131.

Hofmann, E.E., Klinck, J.M., Costa, D.P., Daly, K.L., Torres, J.J., Fraser, W.R., 2002. US Southern Ocean Global Ocean Ecosystems Dynamics Program. Oceanography 15 (2), 64–74.

Hofmann, E.E., Wiebe, P.H., Costa, D.P., Torres, J.J., 2004. An overview of the Southern Ocean Global Ocean Ecosystems Dynamics program. Deep-Sea Research II, this issue [doi:10.1016/j.dsr2.2004.08.007].

Ichii, T., 1990. Distribution of Antarctic krill concentrations exploited by Japanese krill trawlers and minke whales. Proceedings of the National Institute of Polar Research Symposium on Polar Biology 3, 36–56.

Ichii, T., Katayama, K., Obitsu, N., Ishii, H., Naganobu, M., 1998. Occurrence of Antarctic krill (Euphausia superba) concentrations in the vicinity of the South Shetland Islands: relationship to environmental parameters. Deep-Sea Research I, 1235–1262.

Jacobs, S.S., Comiso, J.C., 1997. Climate variability in the Amundsen and Bellingshausen Seas. Journal of Climate 10, 697–709.

Joiris, C.R., 1991. Spring distribution and ecological role of seabirds and marine mammals in the Weddell Sea, Antarctica. Polar Biology 11, 415–424.

Kasamatsu, F., Ensor, P., Joyce, G.G., Kimura, N., 2000. Distribution of minke whales in the Bellingshausen and Amundsen Seas (60°W–120°W), with special reference to

environmental/physiographic variables. Fisheries Oceanography 9 (3), 214–223.

Kato, A., Ropert-Coudert, Y., Naito, Y., 2002. Changes in Adélie penguin breeding populations in Lützow-Holm Bay, Antarctica, in relation to sea-ice conditions. Polar Biology 25, 934–938.

Kawamura, A., 1994. A review of baleen whale feeding in the Southern Ocean. Report of the International Whaling Commission 44, 261–271.

Lascara, C.M., Hofmann, E.E., Ross, R.R., Quetin, L.B., 1999. Seasonal variability in the distribution of Antarctic krill, Euphausia superba, west of the Antarctic Peninsula. Deep Sea Research I 46, 925–949.

Lawson, G.L., Wiebe, P.H., Ashjian, C.J., Gallager, S.M., Davis, C.S., Warren, J.D., 2004. Acoustically-inferred zooplankton distribution in relation to hydrography west of the Antarctic Peninsula. Deep-Sea Research II, this issue [doi:10.1016/j.dsr2.2004.07.022].

Loeb, V., Siegel, V., Holm-Hansen, O., Hewitt, R., Fraser, W., Trivelpiece, W., Trivelpiece, S., 1997. Effects of sea-ice extent and krill or salp dominance on the Antarctic food web. Nature 387, 897–900.

Matsuoka, K., Ensor, P., Hakamada, T., Shimada, H., Nishiwaki, S., Kasamatsu, F., Kato, H., 2003. Overview of the minke whale sighting survey in IWC/IDCR and SOWER Antarctic cruises from 1978/79 to 2000/01. Unpublished paper submitted to the International Whaling Commission Scientific Committee May 2003, Berlin, SC/55/For Information 20.

Murase, H., Matsuoka, K., Ichii, T., Nishiwaki, S., 2002. Relationship between the distribution of euphausiids and baleen whales in the Antarctic (35°E–145°W). Polar Biology 25, 135–145.

Nicol, S., Pauly, T., Bindoff, N.L., Wright, S., Thiele, D., Hosie, G.W., Strutton, P.G., Woehler, E., 2000. Ocean circulation off east Antarctic affects ecosystem structure and sea-ice extent. Nature 406, 504–507.

Olavierra, C., Aguayo-Lobo, A., Larrea, A., 2003. Chilean Antarctic Institute (INACH) photo-identification catalogue of Antarctic Peninsula humpback whales (1995–1999). Unpublished paper submitted to the International Whaling Commission Scientific Committee May 2003, Berlin, SC/55/SH13.

Pankow, H., Kock, K-H., 2000. Results of a cetacean sighting survey in the Antarctic Peninsula region in November–December 1996. Unpublished paper submitted to the International Whaling Commission Scientific Committee May 2000, Adelaide, SC/52/E23.

Plotz, J., Weidel, H., Bersch, M., 1991. Winter aggregations of marine mammals and birds in the north-eastern Weddell Sea pack ice. Polar Biology 11, 305–309.

Quinn, G.P., Keough, M.J., 2002. Experimental Design and Data Analysis for Biologists. Cambridge University Press, UK, pp. 537.

Ramsey, F.L., Schafer, D.W., 1996. The Statistical Sleuth: a Course in Methods of Data Analysis. 742pp.

Ribic, C.A., Ainley, D.G., Fraser, W.R., 1991. Habitat selection by marine mammals in the marginal ice zone. Antarctic Science 3 (2), 181–186.

Reid, K., Brierley, A.S., Nevitt, G.A., 2000. An initial examination of relationships between the distribution of whales and Antarctic krill *Euphausia superba* at South Georgia. Journal of Cetacean Research and Management 2 (2), 143–150.

Siegel, V., Loeb, V., 1995. Recruitment of Antarctic krill *Euphausia superba* and possible causes for its variability. Marine Ecology Progress Series 123, 45–56.

Smith, D.A., Hofmann, E.E., Klinck, J.M., Lascara, C.M., 1999a. Hydrography and circulation of the west Antarctic Peninsula continental shelf. Deep Sea Research I 46, 951–984.

Smith, R.C., Ainley, D., Baker, K., Domack, E., Emslie, S., Fraser, W., Kennett, J., Leventer, A., Mosley-Thompson, E., Stammerjohn, S., Vernet, M., 1999b. Marine ecosystem sensitivity to climate change. Bioscience 49 (5), 393–404.

Stone, G.S., Hamner, W.M., 1988. Humpback whales Megaptera novaeangliae and southern right whales *Eubalaena australis* in Gerlache Strait, Antarctica. Polar Record 24 (148), 15–20.

Thiele, D., Chester, E.T., Gill, P.C., 2000. Cetacean distribution off Eastern Antarctica (80°–150°e) during the austral summer of 1995/96. Deep-Sea Research II 47, 2543–2572.

Tonnessen, J.N., Johnsen, A.O., 1982. The History of Modern Whaling. C. Hurst and Co. and Australian National University Press.

Trathan, P.N., Croxall, J.P., Murphy, E.J., 1996. Dynamics of Antarctic penguin populations in relation to inter-annual variability in sea ice distribution. Polar Biology 16, 321–330.

Tynan, C.T., 1997. Cetacean distributions and oceanographic features near the Kerguelen Plateau. Geophysical Research Letters 24 (22), 2793–2796.

Tynan, C.T., 1998. Ecological importance of the Southern Boundary of the Antarctic Circumpolar Current. Nature 392, 708–710.

van Franeker, J.A., 1992. Top predators as indicators for ecosystem events in the confluence zone and marginal ice zone of the Weddell and Scotia Seas, Antarctica, November 1988 to January 1989 (EPOS Leg 2). Polar Biology 12, 93 102.

van Franeker, J.A., van den Brink, N.W., Bathmann, U.V., Pollard, R.T., de Baar, H.J.W., Wolff, W.J., 2002. Responses of seabirds, in particular prions (Pachyptila sp.), to small scale processes in the Antarctic Polar Front. Deep-Sea Research II 49, 3931–3950.

Wilson, P.R., Ainley, D.G., Nur, N., Jacobs, S.S., Barton, K.J., Ballard, G., Comiso, J.C., 2001. Adelie penguin population change in the Pacific sector of Antarctica: relation to sea-ice extent and the Antarctic Circumpolar Current. Marine Ecology Progress Series 213, 301–309.

Zwally, H.J., Comiso, J.C., Parkinson, C.L., Cavalieri, D.J., Gloersen, P., 2002. Variability of Antarctic sea ice 1979–1998. Journal of Geophysical Research 107 (C5, 10), 1029.

ELSEVIER

Deep-Sea Research II 51 (2004) 2327–2344

DEEP-SEA RESEARCH
PART II

www.elsevier.com/locate/dsr2

Seasonality of blue and fin whale calls and the influence of sea ice in the Western Antarctic Peninsula

Ana Širović[a,*], John A. Hildebrand[a], Sean M. Wiggins[a], Mark A. McDonald[b], Sue E. Moore[c], Deborah Thiele[d]

[a]*Scripps Institution of Oceanography, UCSD, La Jolla, CA 92093-0205, USA*
[b]*Whale Acoustics, Bellvue, CO, USA*
[c]*NOAA/AFSC/National Marine Mammal Laboratory, Seattle, WA, USA*
[d]*Deakin University, School of Ecology and Environment, Warrnambool, VIC, Australia*

Accepted 8 July 2004

Abstract

The calling seasonality of blue (*Balaenoptera musculus*) and fin (*B. physalus*) whales was assessed using acoustic data recorded on seven autonomous acoustic recording packages (ARPs) deployed from March 2001 to February 2003 in the Western Antarctic Peninsula. Automatic detection and acoustic power analysis methods were used for determining presence and absence of whale calls. Blue whale calls were detected year round, on average 177 days per year, with peak calling in March and April, and a secondary peak in October and November. Lowest calling rates occurred between June and September, and in December. Fin whale calling rates were seasonal with calls detected between February and June (on average 51 days/year), and peak calling in May. Sea ice formed a month later and retreated a month earlier in 2001 than in 2002 over all recording sites. During the entire deployment period, detected calls of both species of whales showed negative correlation with sea ice concentrations at all sites, suggesting an absence of blue and fin whales in areas covered with sea ice. A conservative density estimate of calling whales from the acoustic data yields 0.43 calling blue whales per 1000 n mi^2 and 1.30 calling fin whales per 1000 n mi^2, which is about one-third higher than the density of blue whales and approximately equal to the density of fin whales estimated from the visual surveys.
© 2004 Elsevier Ltd. All rights reserved.

1. Introduction

Baleen whales were severely depleted throughout Antarctic waters by intense commercial whaling in the first half of the 20th century. Large species such as blue (*Balaenoptera musculus*) and fin (*B. physalus*) whales were the most sought after. It has been estimated that over 360,000 blue whales and 725,000 fin whales were removed from the southern hemisphere by whaling during the 20th century (Clapham and Baker, 2001). Efforts

*Corresponding author. Fax: + 1-858-534-6849
E-mail address: ana@mpl.ucsd.edu (A. Širović).

0967-0645/$ - see front matter © 2004 Elsevier Ltd. All rights reserved.
doi:10.1016/j.dsr2.2004.08.005

to document the status of whale populations in the Western Antarctic Peninsula region have been limited to three cruises simultaneously conducted by up to four vessels under the auspices of the International Whaling Commission during 1982/83, 1989/90, and 1993/94 in Area I (longitude 60°–120°W). These cruises yielded only nine blue whale sightings and 14 fin whale sightings (Branch and Butterworth, 2001). Such alarmingly low sightings suggest either a population in jeopardy, inadequate population assessment methods, or both (Horwood, 1986; IWC, 2001). The need to develop alternative methods of assessing whale populations, such as passive acoustics, has already been established (Clark and Ellison, 1988, 1989; Clark and Fristrup, 1997), but this need is even more important for the Southern Ocean given the considerable expense and logistical constraints of working there (Costa and Crocker, 1996).

Seasonal migrations have been documented, both visually and acoustically, for several baleen whale species (Mackintosh and Wheeler, 1929; Dawbin, 1966; Mackintosh, 1966; Clapham and Mattila, 1990; Katona and Beard, 1990; Mate et al., 1999; Norris et al., 1999; Stafford et al., 1999b). In general, many baleen whales spend summers feeding in productive waters at high latitudes and over-winter in warmer waters at lower latitudes (Mackintosh and Wheeler, 1929; Mackintosh, 1965; Bowen and Siniff, 1999). Whaling records suggest that blue and fin whales migrate seasonally to and from the Southern Ocean (Kellogg, 1929; Brown, 1962; Mackintosh, 1966). Although blue whales have been found close to the ice edge in the austral summer (Kasamatsu et al., 1988), there is little information on their wintering areas (Mackintosh, 1965; Mizroch et al., 1984) and some high latitude areas, such as South Georgia and the North Pacific, may be continuously occupied by blue whales (Kellogg, 1929; Hart, 1935; Curtis et al., 1999; Watkins et al., 2000; Stafford et al., 2001). Fin whales are rarely sighted at the ice edge during the summer and in the winter they appear to calf and breed at low latitudes (Laws, 1961; Brown, 1962).

Aggregations of blue and fin whales have been observed in association with dense patches of euphausiids during the summer and fall in regions with high biological productivity (Croll et al., 1998; Fiedler et al., 1998; Reid et al., 2000; Murase et al., 2002). These regions often have distinguishing characteristics such as complex bathymetry, presence of sharp oceanographic fronts, eddies, and upwelling that can support high phytoplankton and zooplankton biomass (Beklemishev, 1960; Whitehead and Glass, 1985; Reilly and Thayer, 1990; Fiedler et al., 1998; Tynan, 1998). In the highly productive Southern Ocean, sea ice is an additional factor that affects the ecosystem, generally increasing krill productivity in areas of large sea ice fluctuation, thereby also affecting higher trophic predators (Smith and Nelson, 1985; Fraser et al., 1992; Loeb et al., 1997; Nicol et al., 2000; Croxall et al., 2002). The Western Antarctic Peninsula has a distinct, fluctuating sea ice pattern (Stammerjohn and Smith, 1996), which could support high primary productivity, concentrations of Antarctic krill, and higher predators.

Blue and fin whales produce low frequency (< 1 kHz), high intensity (above 180 dB re: 1 μPa at 1 m) calls and are good subjects for acoustic monitoring (Clark, 1990). Whale call detections have been applied to studies of seasonal occurrence and migration since the 1980s (e.g., Clark and Ellison, 1988, 1989; Stafford et al., 1999a; Watkins et al., 2000). Blue whale calls can be distinguished by their relatively long duration (10–20 s) and very low frequency (20–100 Hz) (Cummings and Thompson, 1971; Edds, 1982; McDonald et al., 1995; Stafford et al., 1998). Typically, the calls consist of two to four units that can be either pulsed or tonal in character. Blue whales produce a single call-type with uniform acoustic characteristics around the Antarctic (Ljungblad et al., 1998; Matsuoka et al., 2000; Clark and Fowler, 2001). Fin whale calls have been well documented in the northern hemisphere (Watkins, 1981; Edds, 1988; McDonald et al., 1995). They typically consist of short (1 s duration), repetitive downsweeps, but they show some variation among different geographic locations in the frequency range of the sweep and the intercall interval (Thompson et al., 1992). We are not aware of any previous reports of fin whale call recordings from the Antarctic.

Recent advances in computer technologies have enabled the development of instruments capable of long-term autonomous acoustic sampling (McDonald et al., 1995; Stafford et al., 1999a; Fox et al., 2001; Wiggins, 2003). We took advantage of this developing technology and deployed seven acoustic recording packages (ARPs) near the SO GLOBEC study site in the Western Antarctic Peninsula from March 2001 until February 2003 to monitor for baleen whale calls (Wiggins, 2003). They provided a record of seasonal occurrence of these large euphausiid predators that can be integrated further with the studies of other biotic and abiotic parameters within the SO GLOBEC framework. In this paper we report the first results on the seasonality of blue and fin whale calls from this acoustic monitoring effort.

2. Methods

Seven ARPs were deployed in the Western Antarctic Peninsula from March 2001 to February 2003 (Fig. 1). ARPs are bottom-moored instruments that consist of a data logging system with a 16-bit A/D converter and 36 GB of storage capacity, a hydrophone tethered 10 m above the seafloor-mounted package (sensitivity −198 dB re: 1 Vrms/μPa and a −3 dB low-end roll-off at around 5 Hz), an acoustic release, two ballast weights, batteries, and flotation (Wiggins, 2003). The acoustic data were collected at 500 samples/s with a –6 dB roll-off at 250 Hz, so the effective bandwidth sampled was 5–250 Hz. At this sampling rate, the instruments were capable of recording data for 400 days. The instruments were retrieved in February 2002 for data recovery and battery replacement, then redeployed with final recovery in February 2003. In this paper we refer to the period between March 2001 and February 2002 as the 'first year of deployment', while the 'second year of deployment' refers to February 2002–February 2003.

Two ARPs were located on the continental shelf (sites 7 and 9) at depths of 450 and 870 m. Six ARPs were located on the shelf break; the northernmost (site 1) was at a depth of approximately 1600 m, while the depths of the remaining five

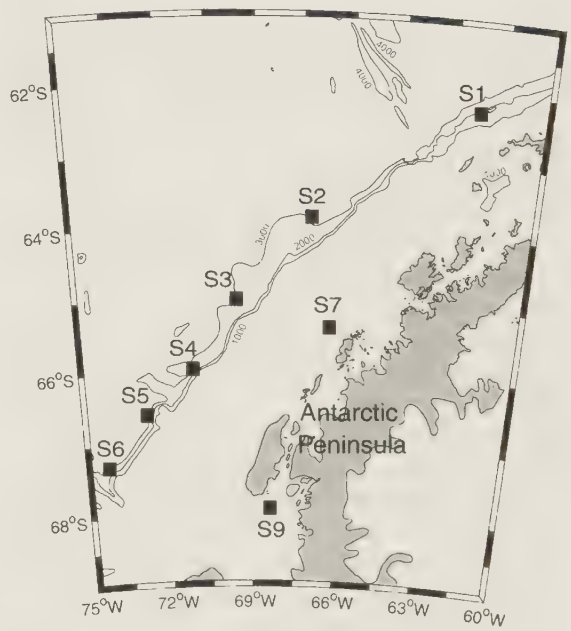

Fig. 1. ARP deployment locations west of the Antarctic Peninsula. The actual locations for ARPs were as follows: S1–62° 16.44' S 62° 10.02' W; S2–63° 50.63' S 67° 08.33' W; S3 64° 59.41' S 69° 28.79' W; S4–65° 58.40' S 71° 04.10' W; S5–66° 34.99' S 72° 41.43' W; S6–67° 18.25' S 74° 10.15' W; S7–65° 22.62' S 66° 28.21' W; S9–67° 54.50' S 68° 23.00' W.

ARPs ranged between 2500 and 3500 m. In this paper, we refer to sites 1 and 2 as 'northern sites', sites 3 and 4 are 'central sites', 5 and 6 are 'southern sites', and 7 and 9 are 'shelf sites.' Distances between neighboring ARPs ranged from 110 to 260 km. Acoustic data for the two northern sites were available for the entire deployment period, data for site 3 were available from July 2001 to February 2002, data for site 4 were available only for the first year of deployment and those for sites 5, 6, 7, and 9 were available only for the second year of deployment.

In order to describe the acoustic characteristics of blue and fin whale calls, we measured beginning and ending frequencies, durations, intercall and intersequence intervals (time between successive call sequences that is shorter than 100 s and is presumably too short to be a surfacing event; only applicable for fin whales), and long intervals (time between successive call series longer than 100 s,

when the calling animal is presumably at the surface) of calls of both species. We used spectrograms of calls with high signal-to-noise ratios from several different times and various sites. We reported the mean and the standard deviation of each property.

We used these measurements to conduct automatic detection of blue and fin whale calls from this large data set using spectrogram correlation (Mellinger and Clark, 2000; Mellinger, 2001). This method cross-correlates the data set spectrogram with an artificial kernel that represents a whale call. The values for two kernels that represented blue and fin whale calls were obtained from the ARP data set as described above. For blue whales, we used a kernel that started with a 9 s flat tone at 27.7 Hz, followed by a 1 s downsweep to 19.5 Hz and another 7 s downsweep to 18.8 Hz. The fin whale call kernel was made to last 1 s and sweep down in frequency from 28 to 15 Hz.

When analyzing data by automatic spectrogram correlation, a detection threshold must be set. Exceeding this threshold for a set period of time (6 s for blues and 0.5 s for fins) triggered a detection event. We initially chose high thresholds to minimize false detections. The detection threshold was iteratively adjusted until the false detection rate was less than 1%. The consequence of a high detection threshold, however, is the omission of calls with low signal-to-noise ratios, which results in an underestimate of the total number of calls. Detected calls were saved as individual WAV files, along with the information on the day and time when the call occurred. Files from days with low call counts (<50) were additionally screened to verify the detections. Of the remaining files, we randomly chose for verification approximately 1000 files for each species' calls to confirm that the false detection rate was $<1\%$. Calling statistics and seasonality were reported for the automatic detection results. We define seasonality (or seasonal calling) as a pattern by which whale calls were present during one part of the year and absent during another continuous period longer than 1 month. Intermittent calling is used to describe a pattern of calling in which there are no periods longer than 1 month during which there are no detected calls. Detection totals for each species and site were combined into 8-day bins for qualitative comparison with sea ice concentrations.

Sound velocity profiles were calculated from XBTs (expendable bathythermographs) deployed in the region. They indicated that the Western Antarctic Peninsula was an upward refracting environment for sound propagation with a relatively shallow (50–150 m) sound channel axis in the summer. Most of the ARPs were in deep water, therefore minimizing reception of very distant (>1000 km) calls. The manual detection range for blue whale calls was determined to be up to 250 km by observing calling sequences produced by the same animal and recorded on multiple instruments. It was then possible to localize on the animal using differences in arrival times of the same call to multiple instruments. Comparison of those calls to automatic detections yielded an automatic detection range of up to 60 km for blue whales, and somewhat less for fin whale calls. It should be noted, however, that the spectrogram correlation method is signal-to-noise dependent and the automatic detection range changes depending on ambient acoustic conditions. During times of high ambient noise the detection range will be diminished. Since the instruments were fairly deep, sea ice formation and melting did not increase the ambient noise in the detected bands and the noise was generally lowered during the periods of ice cover. Therefore the presence of sea ice did not decrease our capability to detect calling whales.

Recordings were also analyzed by comparing the acoustic power in frequency bands characteristic for whale calls, to the power levels of adjacent frequencies. We calculated power spectral density (500-point FFT, 50% overlap, Hanning window) of the entire data set and averaged it over 15 min samples. We determined the ratio of the power in the whale call frequency band to the average power in two adjacent bands where no whale sounds were expected. We assumed linear noise at frequencies around the whale call. For blue whales, we used power at 28 Hz as the calling band and compared it to powers at 15 and 41 Hz as the noise bands. For fin whales, we compared the power at 89 Hz (see Fig. 2B) as the calling band to powers at 80 and 98 Hz as the noise bands. We

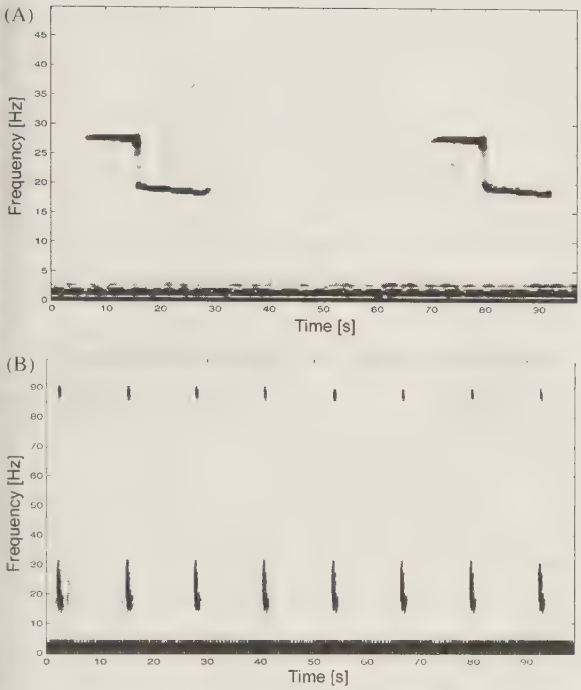

Fig. 2. Spectrograms of (A) Antarctic blue (1500-point FFT, 90% overlap, Hanning window) and (B) fin whale (500-point FFT, 90% overlap, Hanning window) calls recorded in the Western Antarctic Peninsula.

used the higher frequency component of fin whale call to avoid overlap with blue whale calls and because of lower ambient noise at higher frequencies. The range of detection using this method is probably larger than for automatic detections, but it is also a signal-to-noise dependant method. We calculated one-day averages of the signal-to-noise ratios and cross-correlated the results to one-day total automatic detections, and we used a t-test to determine whether the two methods yielded significantly different results.

The nature of the acoustic data enables us to determine only when calling animals are present in the detection area. During periods when no calls are detected, whales may be absent or silent (Stafford et al., 1999b). In this paper, we use call abundance as a proxy for whale abundance. The relationship between the number of calls detected and the number of animals present is not currently understood. We assume that higher calling rates in automatic detection and higher signal-to-noise ratios in acoustic power analysis reflect a greater number of animals present, although seasonal variation in the tendency to call may also be reflected in these data.

In calculations of the average number of days/site that whales were detected during the year, we did not include site 3 (because it did not have a full deployment year of data) nor site 9 (because no blue or fin whale calls were detected). We reported the average number of calls at all sites, normalized by the number of sites recording that month and the number of days with recordings per month for each site, as well as the total number of blue and fin whale call detections for each deployment year. We compared the differences between the 2 years as well as the differences among sites. Also, we cross-correlated in time daily detections at different sites, for indication of blue and fin whale movement between the sites. These time lag analyses were conducted for periods when data were available at all sites (April 2, 2001–February 9, 2002 during the first deployment year and March 1, 2002–February 17, 2003 during the second) and we report the ones that showed clear trends. We did not perform time lag calculations for site 7 because of the low call detection numbers at that site.

Sea ice concentration estimates were made using Special Sensor Microwave/Imager (SSM/I) passive microwave data obtained from the National Snow and Ice Data Center. Derived daily gridded sea ice concentration data sets were generated using the Bootstrap algorithm (Comiso, 1991, updated 2002) and are archived from 1995. Ice concentrations are binned to 25 km square cells in a polar stereographic projection. We extracted daily mean values for 75 km × 75 km areas centered around each ARP using the imaging software *WIM* (Kahru, 2000). Since sites 7 and 9 were less than 75 km from coastline that has snow and ice cover year round, it is likely that the sea ice coverage on these sites is overestimated. We calculated 8-day averages for qualitative comparison to whale call detections. Since daily or weekly samples are not necessarily independent, to determine the number of independent sea ice and whale call samples at each site we calculated the integral time scales

from autocorrelations of the sea ice and whale call detection data. We calculated Pearson's coefficient of correlation between blue and fin whale call detections and sea ice concentrations binned in periods corresponding to the integral time scale. The number of deployment days was divided with the calculated integral time scale to determine the number of independent samples, N, at each site. We used a t-test for testing a null hypothesis that sea ice concentration and the number of blue and fin whale call detections are not related, using significance level $\alpha = 0.05$.

We made minimum density estimates of calling whales. We assumed detection radius of 60 km (32.4 n mi) for both species. Since we know blue whales make calls at regular 62 s intervals, we assumed there were two calling whales present when two calls were detected in less than a minute and we inspected the automatic detection results at each of the sites for sequences of calls with the intercall interval shorter than one minute. For fin whales, we estimated the number of calls that occurred in a 13 s interval. We report the values in number of calling animals/n mi^2 so that they are comparable to the results of visual surveys.

3. Results

The call of the Antarctic blue whale (Ljungblad et al., 1998; Clark and Fowler, 2001) consists of three components and lasts about 18.6 s (Fig. 2A). For our data, on average, the call starts with a tone at 27.7 ± 0.4 Hz that lasts 9.5 ± 1.4 s. The second component is a short, 1.1 ± 0.5 s duration downsweep in frequency from 27.7 ± 0.4 Hz to 19.5 ± 0.4 Hz, and the third component is a slightly downswept 18.9 ± 0.5 Hz tone lasting 8.0 ± 3.0 s (for all measurements, $n = 241$). The calls are produced in sequences and repeated with intercall intervals of 62.3 ± 5.2 s ($n = 316$) and long intervals of 172 ± 48 s ($n = 44$), presumably for breathing.

Fin whales in the Antarctic produce short, 0.7 ± 0.3 s average duration pulsed calls (Fig. 2B). They sweep down from 27.6 ± 2.2 Hz to 14.9 ± 1.3 Hz ($n = 277$). There is an additional, simultaneous pulse centered at 89.2 ± 0.7 Hz with an average bandwidth of 4.5 ± 0.9 Hz ($n = 90$). The calls are repeated at 12.9 ± 0.5 s intercall intervals ($n = 238$) and 29.7 ± 6.5 s intersequence intervals ($n = 32$) over long periods, with long intervals of 140 ± 64 s ($n = 8$), again presumably for breathing.

Calls attributed to blue and fin whales were recorded at seven out of eight sites in the Western Antarctic Peninsula, with no calls from either blue or fin whales detected at site 9 in Marguerite Bay. A total of 258,706 blue whale calls were automatically detected from March 2001 to February 2003 by use of spectrogram correlation. Likewise, 72,194 fin whale calls were detected by spectrogram correlation during this period, although poor performance of the automatic call detection method during periods of intense calling suggests that the total number of fin whale calls in our data was actually higher. On average, blue whale calls were detected on 177 days during a year and fin whale calls were detected on 51 days. There was a significant increase in the number of blue whale call detections at the northern sites (1 and 2) from the first deployment year to the second ($\chi^2 = 432$, $df = 2$, $p < 0.001$; $\chi^2 = 1128$, $df = 2$, $p < 0.001$, respectively). There was also a significant increase in fin whale call detections at the same sites during that period ($\chi^2 = 88$, $df = 2$, $p < 0.001$ at site 1; $\chi^2 = 1295$, $df = 2$, $p < 0.001$ at site 2).

On average for all sites and both years, blue whale calls were detected intermittently year round in the Western Antarctic Peninsula (Fig. 3A). The highest blue whale calling rates were in March and April. Calling decreased in May and was minimal between June and August. There was a secondary peak in calling in October and November. Typically, few calls were detected in December. Fin whale calls showed a strong seasonal presence (Fig. 3B). They were detected from February until June, with the peak in call detections in May. No calls were detected between July and January.

Blue whale calling varied among sites and between deployment years (Fig. 4). Northern sites had intermittent calling during the austral winter of the first deployment year and seasonal calling during the second year. Other sites had a seasonal pattern of blue whale calls throughout their deployment periods. Fewer calls were detected on the shelf sites than on the shelf break sites. The detections at the two northern sites occurred

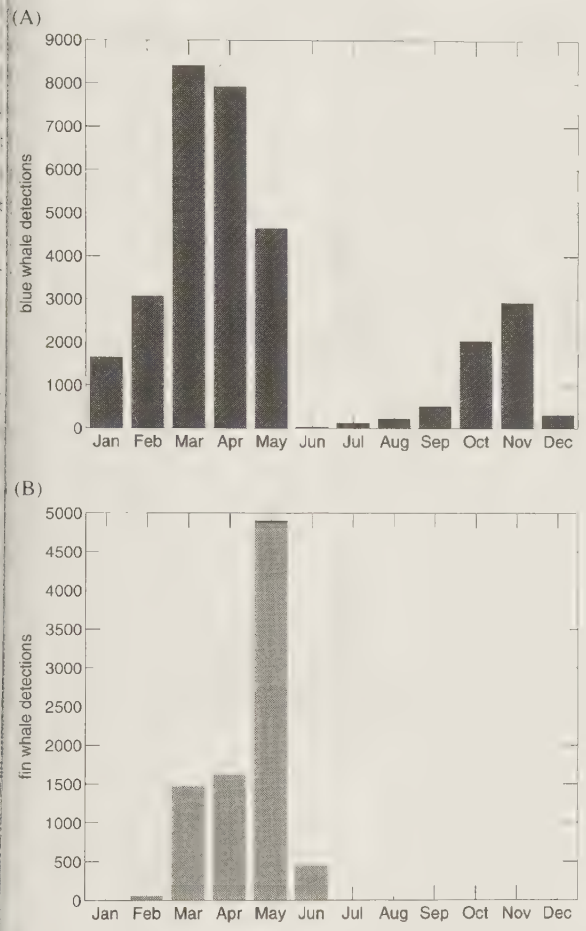

Fig. 3. Monthly averages of the number of blue (A) and fin (B) whale call automatic detections over the whole deployment period, normalized by the number of sites with recordings in a month and the number of days with recordings at each site.

simultaneously during the second year of deployment (Fig. 5). Calls on the two southern sites occurred simultaneously as well, but they lagged the northern sites by 3–4 weeks during the summer, and preceded them by about a month in the spring. The first big increase in the number of detections during austral summer (February–March) 2002 was at the northern sites. Detections increased on the southern sites in April, but in May they were higher at northern sites. In October 2002, the first high detections occurred at the southern sites. In early November the detection peak shifted north, and in late November and early December it returned to the southern sites.

Fin whale calls showed a strong seasonal presence on all sites where calls were detected (Fig. 6). A few calls were detected on site 4 in October and November 2001 (5 and 2 detections, respectively). The highest call counts were at the northern sites. Low detection numbers or no call detections were characteristic of the shelf sites. Peaks in calls were delayed between the two northern sites by about 10 days. In 2002, peaks in calling at northern sites were preceded by calling at southern sites by approximately a month. Fin whale calls were detected on site 6 four days earlier than on site 5. The detections of fin whale calls typically stopped as the sea ice began to form.

The results obtained by the acoustic power analysis were not significantly different from the automatic detection results, except on the shelf site. Results on seasonality of blue whale calls were very consistent between the two methods (Fig. 7). However, there was a slight difference in fin whale presence patterns between the two methods (Fig. 8). Acoustic power method inferred a more continuous presence of fin whales and in some cases about a month longer presence than the automatic detection method. Manual inspection of data during fin whale presence revealed frequent fin whale calling, resulting in a persistent fin whale "noise" band, especially at northern sites, ranging in frequency between 15 and 30 Hz (and around 90 Hz). This band of calling "noise" decreased the signal-to-noise ratio of individual calls, therefore decreasing the number of automatic detections. The acoustic power method was better at detecting the continuous, fin whale calling band signal. This was quite pronounced at the two northern sites. The fin whale calling band (and acoustic power) was stronger at site 1, and fewer fin whale calls were detected there than at site 2, which had a weaker calling band. There were few calls detected at site 7 on the shelf, and these low calling rates caused the acoustic power method to be less robust relative to the automatic call detection method. Even though both methods yielded similar results, it is clear that each method has its advantages and disadvantages and the choice of method should vary depending on the species and their calling intensities. In general, the acoustic power method may be sensitive to more distant calls and provides

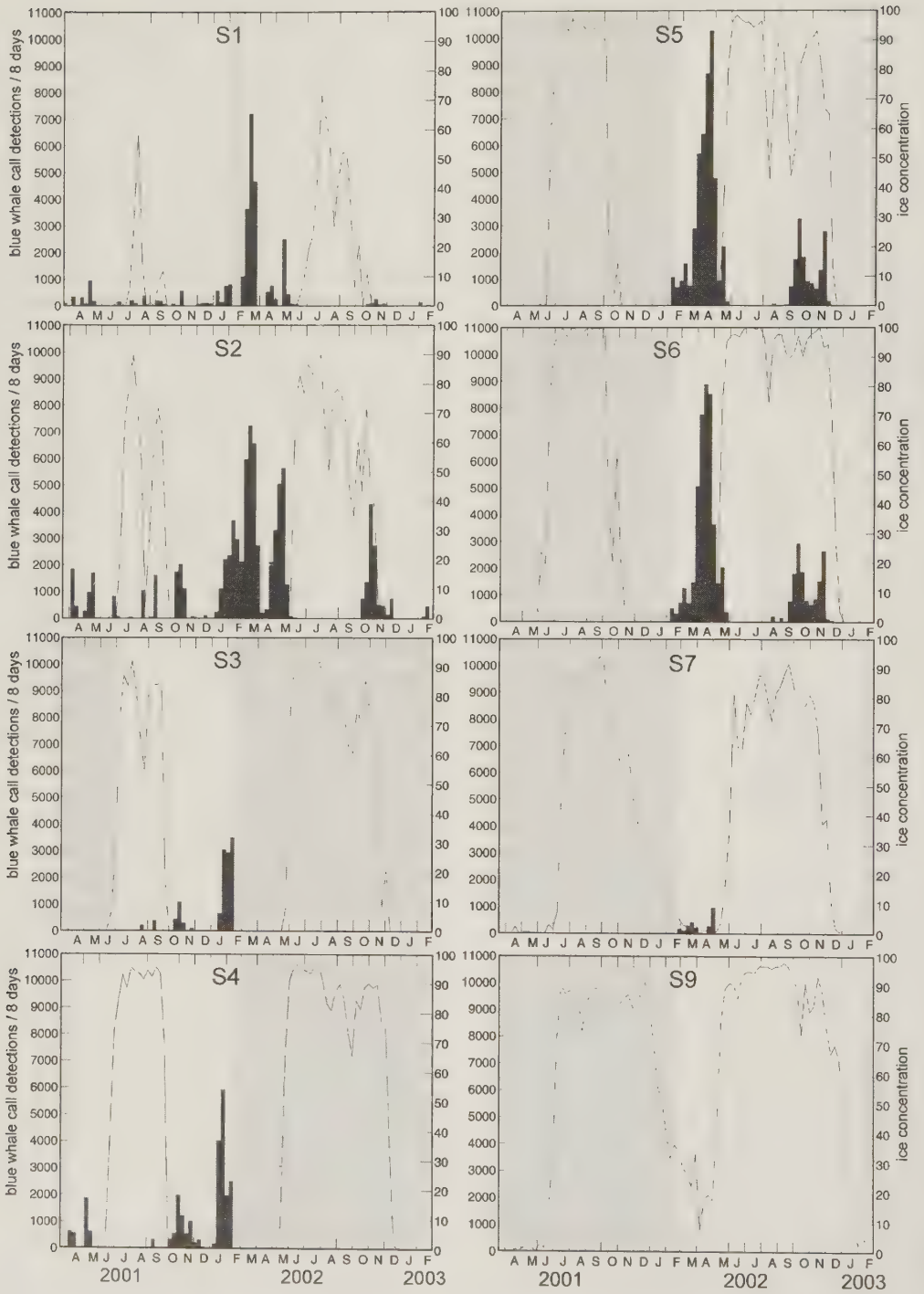

Fig. 4. Blue whale call automatic detections (bars) and sea ice concentration data (line) in 8-day bins for all sites. Gray rectangles represent periods during which there were no acoustic data.

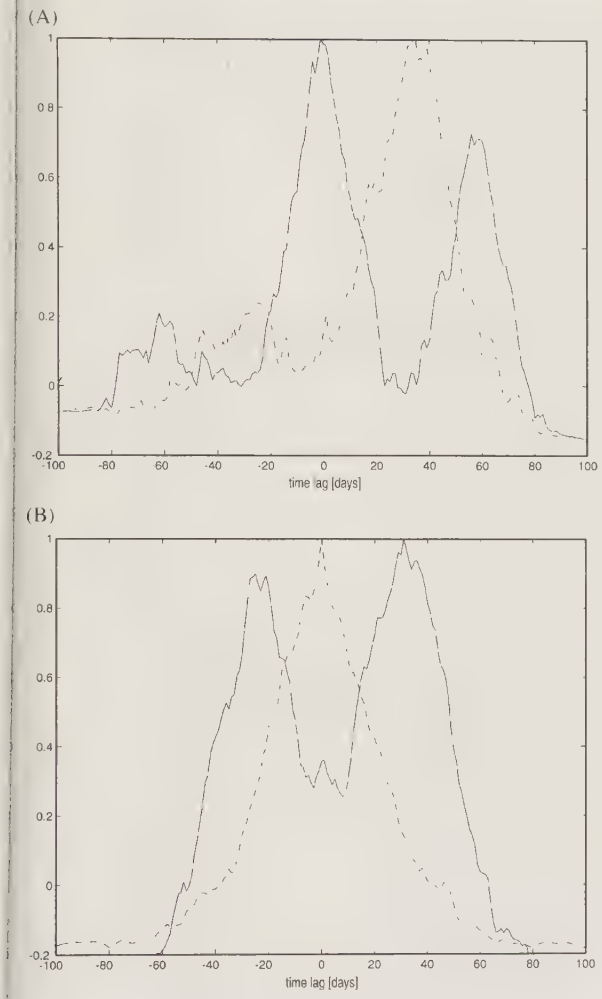

Fig. 5. Time-delayed correlations between blue whale call detections at different sites. (A) Solid: sites 1 and 2; dash-dotted: sites 1 and 5 (both 1 March 02–17 February 03). (B) Solid: sites 2 and 5; dashed: sites 5 and 6 (both 1 March 02–17 February 03).

better results during periods of intense calling, whereas the automatic call detection method is superior for periods of sparse calling and nearby animals.

At some point during the year, sea ice extended over all the instruments during both deployment years (Figs. 4 and 6). On average, sea ice started to form a month earlier and retreated a month later in 2002 than in 2001. As expected, sea ice started forming first on the central and southern sites in May and June, and it fully retreated from these sites in November and December. During at least half of the time, the sea ice cover was over 90% at the southern sites, and over 80% at the central sites. Sea ice at the shelf sites formed approximately at the same time as on the central and southern sites, but the coverage was less than 80% during half of the time. Also, the sea ice never completely melted at those sites between the two years. At northern sites the sea ice formed in June and July and retreated by October or November. The average sea ice concentration during the time of coverage for sites 1 and 2 was 32% and 61%, respectively.

Sea ice concentration had a longer integral time scale for independence of estimates at all sites than call detections from either species, ranging from 8 to 53 days. There was a negative correlation between blue and fin whale calls and sea ice concentration at all sites on these weekly to monthly scales during the entire deployment period, although none of the p-values were statistically significant (Table 1; Figs. 4 and 6). On the annual scale, however, the year with longer sea ice coverage had more whale calls of both species.

While making minimum density estimates, we found one-minute intervals with more than one blue whale call on all the shelf break sites in a given day. Therefore we assumed two blue whales calling at each site on the shelf break, and no blue whales calling at the shelf sites, and obtained a blue whale density of 0.43 calling whales per 1000 n mi^2. To obtain the fin whale calling intensity that we observed on the northern sites, there had to be at least one fin whale calling for every second of the intercall interval, which is 13 s. So we assumed 15 simultaneously calling whales at each of the two northern sites, and no calls at other sites, and obtained a fin whale density of 1.30 calling whales per 1000 n mi^2 over the whole area, or 4.55 calling whales per 1000 n mi^2 at the northern sites.

4. Discussion

Blue whale calls were recorded intermittently year round, while fin whale calls were recorded

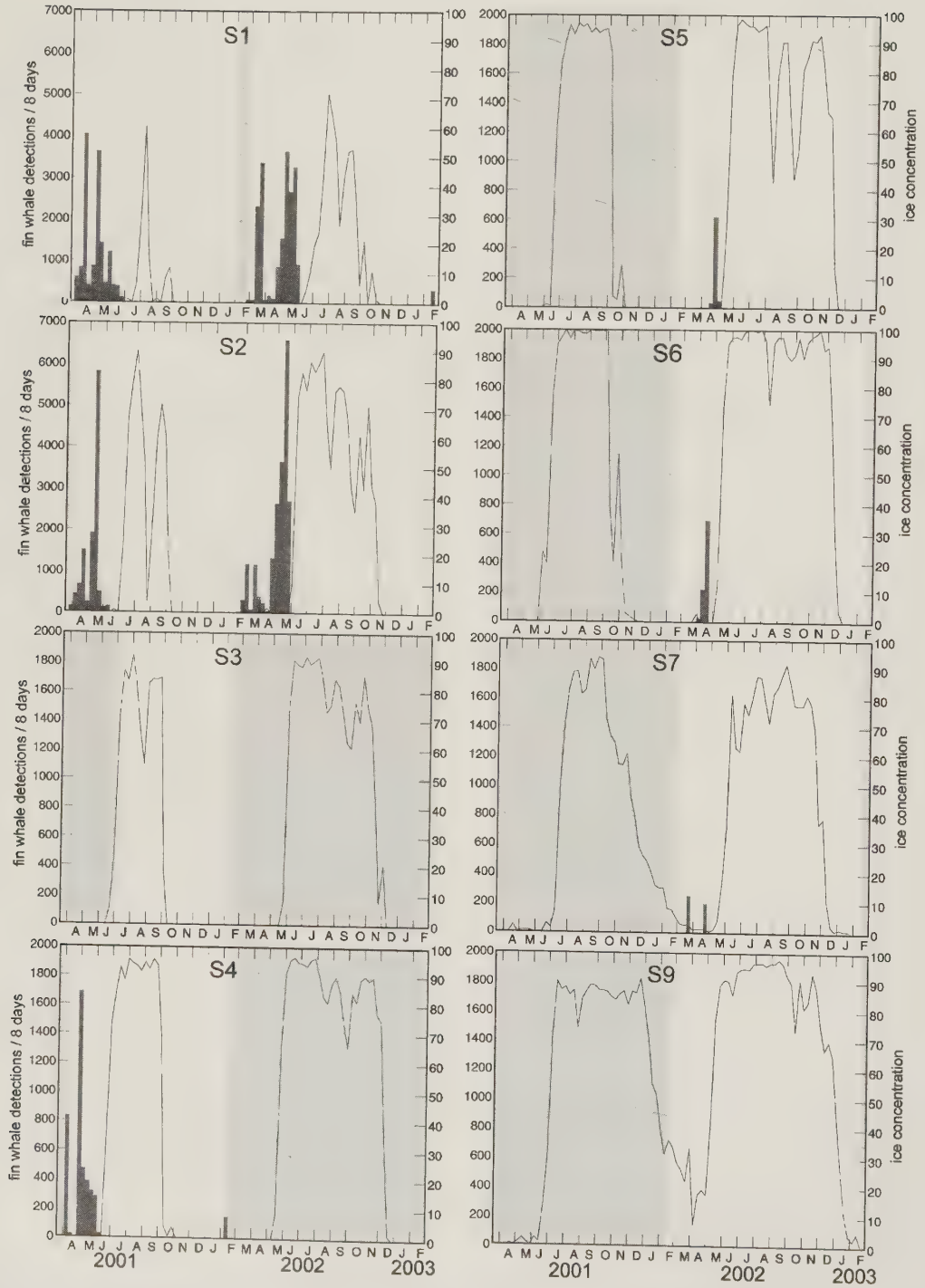

Fig. 6. Fin whale call automatic detections (bars) and sea ice concentration data (line) in 8-day bins for all sites. Gray rectangles represent periods during which there were no acoustic data. Note different scales for automatic detections between northern and all other sites.

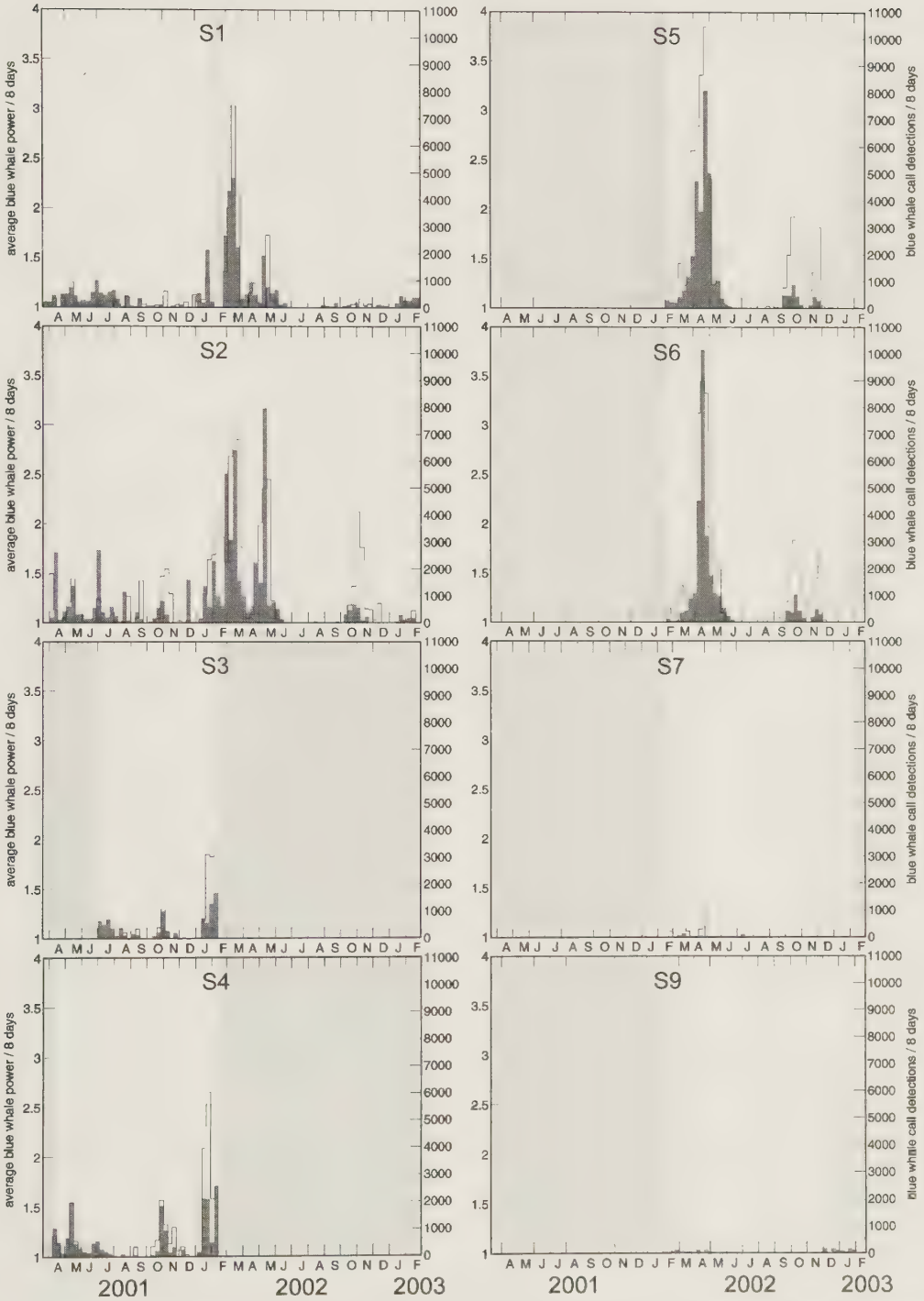
S1
S2
S3
S4
S5
S6
S7
S9
average blue whale power / 8 days
blue whale call detections / 8 days
A M J J A S O N D J F M A M J J A S O N D J F M A M J J A S O N D J F
2001
2002
2003

Fig. 7. Comparison of blue whale seasonality obtained by acoustic power (shaded bars) and automatic detection (clear bars) methods for all sites. Gray rectangles represent periods during which there were no acoustic data.

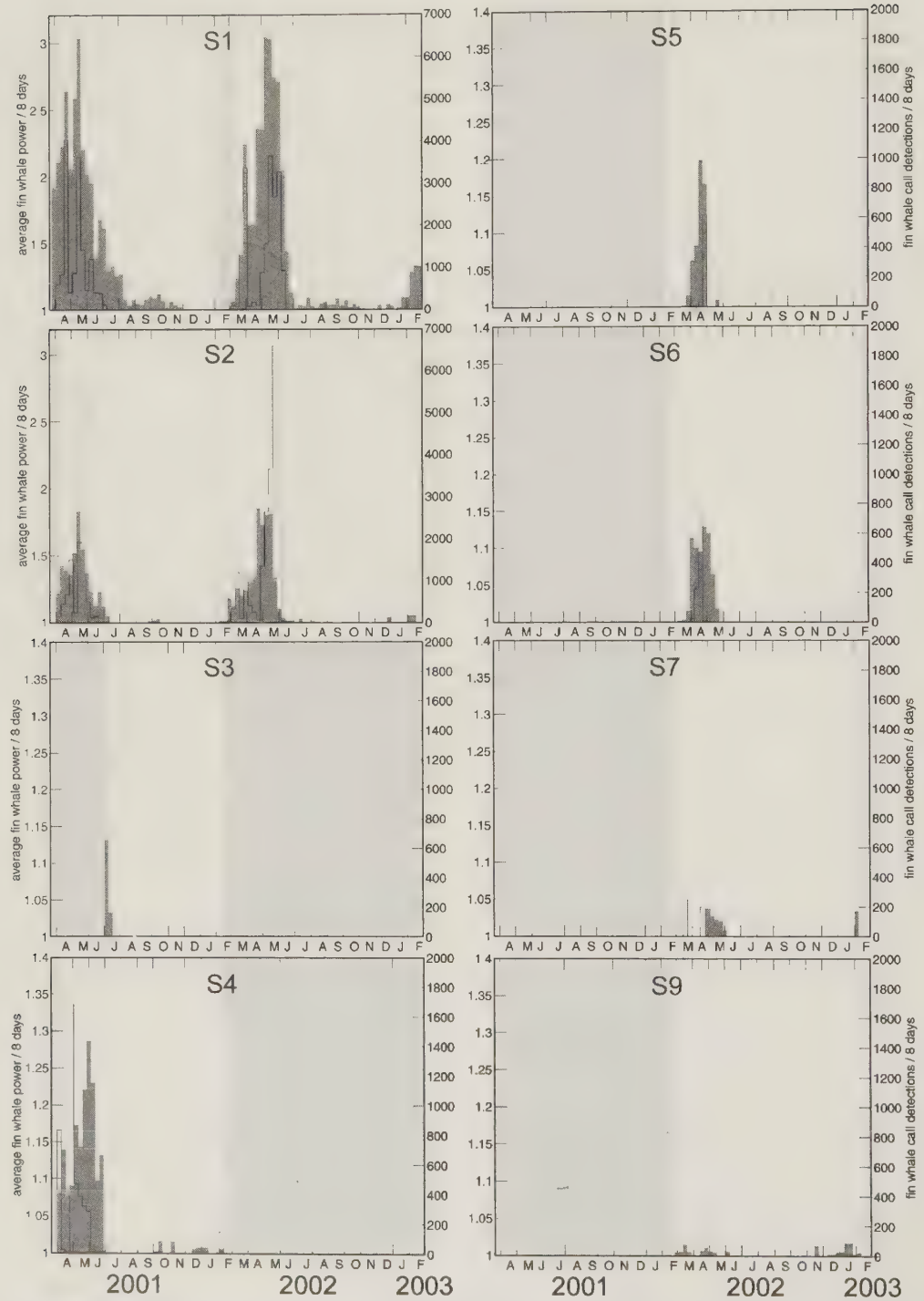

Fig. 8. Comparison of fin whale seasonality obtained by acoustic power (shaded bars) and automatic detection (clear bars) methods for all sites. Gray rectangles represent periods during which there were no acoustic data. Note different scales between northern and all other sites.

Table 1
Correlations between the number of blue and fin whale call detections and sea ice concentrations binned in N-day bins by year (a) and overall (b, when applicable)

(a)

	2001/02					2002/03				
	Blues		Fins			Blues		Fins		
Site	r	p	r	p	N	r	p	r	p	N
1	−0.052	>0.2	−0.163	>0.2	36	−0.225	>0.1	−0.295	>0.05	37
2	−0.321	>0.2	−0.297	>0.2	13	−0.469	>0.1	−0.346	>0.2	11
3	−0.640	>0.1	—	—	7	—	—	—	—	—
4	−0.488	>0.1	−0.379	>0.2	10	—	—	—	—	—
5	—	—	—	—	—	−0.300	>0.2	−0.283	>0.2	8
6	—	—	—	—	—	−0.120	>0.2	−0.207	>0.2	7
7	—	—	—	—	—	−0.461	>0.2	−0.462	>0.2	5

(b)

	Overall				
	Blues		Fins		
Site	r	p	r	p	N
1	−0.253	>0.2	−0.327	>0.1	21
2	−0.394	>0.05	−0.285	>0.2	19

Data for site 9 were not included since there were no whale call detections at that site.

only seasonally in continental slope and shelf waters off the Western Antarctic Peninsula. There was a clear temporal overlap in occurrence, as indicated by simultaneous reception of calls from the two species. More calls of each species were detected in the second year of deployment, which was also a year with longer sea ice coverage. On weekly to monthly time scales, however, whale calls from both species were negatively correlated with sea ice concentrations. Whales may have left the area or stopped calling as the sea ice began to form. The peak in calling for both species occurred about a month later during both years (March–May) than predicted from whaling data (February–March) (Mackintosh and Brown, 1956; Laws, 1961).

It is possible that the differences in the detections of the two species are due to the fact that the area we sampled is not an equally preferred habitat by blue and fin whales (Mackintosh, 1965). The sites on the continental shelf break (1–6) were located along the flowpath of the Antarctic Circumpolar Current (Hofmann et al., 1996). Those were the sites with high call detection rates for both species and they all had periods of open ocean as well as times with sea ice coverage. While blue whales are known to associate with sea ice (Mackintosh, 1965; Kasamatsu et al., 1988), fin whales are not (Mackintosh and Wheeler, 1929) and could be staying farther north. Notably, there were fewer fin whale calls on the southern sites, while blue whale call detections were highest at those sites. Sites 7 and 9, which were both on the continental shelf, had few or no calls from either species. It appears that blue and fin whales did not come onto the continental shelf for long periods of time and probably did not go into Marguerite Bay even at times when the sites were free from sea ice.

While it has been reported in both the northern and the southern hemispheres that blue whales can overwinter at high latitudes (Kellogg, 1929; Clark and Charif, 1998; Watkins et al., 2000; Stafford et al., 2001), Antarctic-type blue whale calls have been detected in the Eastern Tropical Pacific in

July (see Figs. 3A and B in Stafford et al., 1999a). The blue whale calling rate decreased at our instruments between June and August, suggesting that some northward migration may have taken place during the winter. Blue whale calls were detected at northern sites intermittently throughout the winter (June–October) 2001, indicating presence of at least some calling whales. This intermittent calling could be an implication of a time-lagged migration, or that some individuals skip migration. Our data are consistent with the IWC sightings data indicating that blue whale population in the Antarctic does not increase dramatically between November and February (Kasamatsu et al., 1996) and the whaling data showing blue whale presence in September and October (Horwood, 1986).

The cessation of fin whale calls in May is most likely an indication of fin whale migration out of the area, as it coincided with the sea ice formation across all sites. Fin whales did not start calling again before the middle of February. There have been suggestions that fin whales use repetitive calls as reproductive displays (Watkins et al., 1987; Croll et al., 2002) so in spring they could be present off the Western Antarctic Peninsula feeding (Mackintosh and Wheeler, 1929; Gaskin, 1982), but producing few or no calls. Autumn is the onset of their mating season (Laws, 1961) at which time they could start to engage in more frequent calling. Whaling records, however, show a higher proportion of fin whale catches after January (Kellogg, 1929; Mackintosh, 1965), just as the more recent IWC sightings data show increased sightings in January (Kasamatsu et al., 1996), indicating that a late-summer arrival to the Antarctic is a likely explanation for the February start of calling.

While more calls were detected during the year with longer sea ice cover, on shorter time scales sea ice concentration and whale calls were negatively correlated. This negative correlation on a shorter time scale is consistent with previous observations (Mackintosh, 1965), but the lack of significance in most cases could be due to the small independent sample sizes. The big increase in the number of calls between the two deployment years was not expected. It cannot be attributed to population growth because it would imply an increase of more than 30% in 1 year, which is an unrealistic growth rate. This increase in relative abundance could have resulted from the movement of animals from other areas of the Antarctic. However, the whaling and sightings data suggest limited meridional movement (Brown, 1954; Kasamatsu et al., 1996). Or it might be possible the differences between the years were related to the observed differences in sea ice conditions (Fraser et al., 1992; Nicol et al., 2000). Longer acoustic time series with year-round coverage could shed more light on this observation. Also, further comparisons of whale calls with other biological parameters (e.g. krill abundance) could reveal the causes of this increase in relative abundance.

Such comparisons also could further understanding of the apparent movements of these two species of whales. Both blue and fin whale calls were detected sequentially on instruments distributed along the continental shelf break, moving in the southwest–northeast direction. Since blue and fin whales feed in Antarctic waters (Mackintosh and Wheeler, 1929; Kawamura, 1980; Gaskin, 1982; Kawamura, 1994), their movement along the shelf could reflect the seasonality of their prey (Kellogg, 1929; Nemoto, 1957; Springer et al., 1999) and sea ice conditions. For example, the notable decline in blue whale call detections in late December and early January, which would not be predicted from the catch data (Mackintosh and Wheeler, 1929), could indicate that blue whales use a larger area for foraging than the area covered by our acoustic array and they could be further south during this period of low detections. A northeast–southwest movement pattern along the shelf break was especially noticeable from both blue and fin whale calls during the second year of deployment. During the austral summer this movement for both species was from the northern sites towards the southwest, and it reversed towards the northeast in the fall. In spring, blue whale calling occurred first at the southern sites and moved northeast again, but it reversed in late October and returned to the southern sites. There is clearly a bias in this interpretation due to the locations of instruments. However, this movement may be explained by productivity and sea ice

patterns in the area (Siegel, 1988; Holm-Hansen and Mitchell, 1991; Ross and Quentin, 1996; Stammerjohn and Smith, 1996). During autumn, the whales may be moving north as the sea ice begins to form. In the spring, on the other hand, the first high blue whale call detections occurred at the southern sites, during a period when the sea ice cover was still substantial. At this time the whales could be following productivity blooms to the retreating ice edge.

We can make a comparison of whale densities between the acoustic data and visual census. Data from the circumpolar visual surveys conducted by the International Whaling Commission indicate an average density in the Antarctic of 0.32 blue whales per 1000 n mi^2 and 1.59 fin whales per 1000 n mi^2 (Branch and Butterworth, 2001). Minimum density estimates from the acoustic data can be considered conservative because we based them on the automatic detections, which are an underestimate of the total number of calls due to the omission of calls with a low signal-to-noise ratio. Also, we did not take into account gender (McDonald et al., 2001; Croll et al., 2002) or other factors that could affect calling. Still, our blue whale estimate is about one-third higher than the density estimate from visual surveys. Fin whale density values are equal to the values predicted from the visual surveys. In both the blue and fin whale cases presented here, the assumptions were very conservative given the real acoustic data, which indicates that, locally, both species are more abundant than the Antarctic-wide visual estimates predict. The calling ecology of blue and fin whales, however, is not well understood and needs to be explored further before we can interpret acoustic data in terms of blue and fin whale absolute abundance.

5. Conclusion

We have found passive acoustic detections to be a powerful tool for studying blue and fin whale seasonal occurrence in the Western Antarctic Peninsula. Acoustic data can be collected year-round despite the harsh environmental conditions present in the Southern Ocean. Periods of whale presence were revealed over the 24-month deployment period, showing different degrees of seasonality in the presence of both blue and fin whales. These results suggest that acoustic monitoring may be an efficient method of studying these animals in the Southern Ocean.

Our initial analysis has considered only the relationship between the sea ice and blue and fin whale calls. However, sea ice alone is not enough to provide a full explanation of the changes in whale calling and future analyses will include data on other biological and physical factors, which are available from the SO GLOBEC data sets. Knowledge of the behavioral context of calling is limited, despite some suggestions that calling sequences such as those reported here are primarily breeding displays by males (Watkins et al., 1987; McDonald et al., 2001; Croll et al., 2002). Knowledge of the ecology of calling, however, is necessary for understanding the role of calling in the life histories of these species. In addition, to census populations acoustically, data are needed to quantify the number of calling animals at any one time and the proportion of animals present that are calling. A combination of acoustic and behavioral data would enhance our ability to monitor calling whales over large regions and long time periods.

Acknowledgments

This work was supported by NSF Office of Polar Programs grant OPP 99-10007 as part of the SO GLOBEC program, with program guidance by Polly Penhale. We are grateful for the assistance of Raytheon Polar Services marine and science support personnel, the Masters, Officers and crew of ASRV L.M. Gould during cruises LMG01-03, LMG02-01A, and LMG03-02. We also acknowledge National Snow and Ice Data Center for the processing and distribution of sea ice concentration data. We thank Dr. Allan Sauter for assistance with ARP preparation and deployment, Jessica Burtenshaw for her help with sea ice data acquisition, and editor Dr. Daniel Costa and anonymous reviewers for helpful advice on this manuscript. This is U.S. GLOBEC contribution number 468.

References

Beklemishev, C.W., 1960. Southern atmospheric cyclones and the whale feeding grounds of the Antarctic. Nature 187, 530–531.

Bowen, W.D., Siniff, D.B., 1999. Distribution, population biology and feeding ecology of marine mammals. In: Reynolds, III, J.E., Rommel, S.A. (Eds.), Biology of Marine Mammals. Smithsonian Institution Press, pp. 423–484.

Branch, T.A., Butterworth, D.S., 2001. Estimates of abundance south of 60 S for cetacean species sighted frequently on the 1978/79 to 1997/98 IWC/IDCR-SOWER sighting surveys. Journal of Cetacean Research and Management 3, 251–270.

Brown, S.G., 1954. Dispersal in blue and fin whales. Discovery Reports 26, 355–384.

Brown, S.G., 1962. A note on migration of fin whales. Norsk Hvalfangst-Tidende 51, 13–16.

Clapham, P. J., Baker, C. S., 2001. How many whales were killed in the Southern Hemisphere in the 20th century? Report of the International Whaling Commission 53, 3 pp.

Clapham, P.J., Mattila, D.K., 1990. Humpback whale songs as indicators of migration routes. Marine Mammal Science 6, 155–160.

Clark, C.W., Ellison, W.T., 1988. Number and distributions of bowhead whales, *Balaena mysticetus*, based on the 1985 acoustic study off Pt. Barrow, Alaska. Report of the International Whaling Commission 38, 365–370.

Clark, C.W., Ellison, W.T., 1989. Numbers and distribution of bowhead whales, *Balaena mysticetus*, based on the 1986 acoustic study off Pt. Barrow, Alaska. Report of the International Whaling Commission 39, 297–303.

Clark, C.W., 1990. Acoustic behavior of mysticete whales. In: Thomas, J., Kastelein, R. (Eds.), Sensory Abilities of Cetaceans. Plenum Press, New York, pp. 571–583.

Clark, C. W., Charif, R. A., 1998. Acoustic monitoring of large whales to the west of Britain and Ireland using bottom-mounted hydrophone arrays, October 1996—September 1997. JNCC Report No. 281.

Clark, C. W., Fowler, M., 2001. Status of archival and analysis effort of acoustic recordings during SOWER and IWC cruises 1996-2000. Report of the International Whaling Commission SC/53/IA28, 9pp.

Clark, C.W., Fristrup, K.M., 1997. Whales '95: A combined visual and acoustic survey of blue and fin whales off Southern California. Report of the International Whaling Commission 47, 583–600.

Comiso, J., 1991. updated 2002. In: Maslanik, J., Stroeve, J. (Eds.), DMSP SSM/I Daily Polar Gridded Sea Ice Concentrations. Boulder CO, National Snow and Ice Data Center (Digital Media).

Costa, D.P., Crocker, D.E., 1996. Marine mammals of the Southern Ocean. In: Ross, R.M., Hofmann, E.E., Quentin, L.B. (Eds.), Foundations for Ecological Research West of the Antarctic Peninsula, vol. 70. American Geophysical Union, Washington DC, pp. 287–301.

Croll, D.A., Tershy, B.R., Hewitt, R.P., Demer, D.A., Fiedler, P.C., Smith, S.E., Armstrong, W., Popp, J.M., Kiekhefer, T., Lopez, V.R., Urban, J., Gendron, D., 1998. An integrated approach to the foraging ecology of marine birds and mammals. Deep-Sea Research II 45, 1353–1371.

Croll, D.A., Clark, C.W., Acevedo, A., Tershy, B.R., Flores, S., Gedamke, J., Urban, J., 2002. Only male fin whales sing loud songs. Nature 417, 809.

Croxall, J.P., Trathan, P.N., Murphy, E.J., 2002. Environmental change and Antarctic seabird populations. Science 297, 1510–1514.

Cummings, W.C., Thompson, P.O., 1971. Underwater sounds from the blue whale, *Balaenoptera musculus*. The Journal of the Acoustical Society of America 50, 1193–1198.

Curtis, K.R., Howe, B.M., Mercer, J.A., 1999. Low-frequency ambient sound in the North Pacific: long time series observation. The Journal of the Acoustical Society of America 106, 3189–3200.

Dawbin, W.H., 1966. The seasonal migratory cycle of humpback whales. In: Norris, K.S. (Ed.), Whales, Dolphins, and Porpoises. University of California Press, Berkeley, pp. 145–170.

Edds, P.L., 1982. Vocalizations of the blue whale, *Balaenoptera musculus*, in the St. Lawrence River. Journal of Mammalogy 63 (2), 345–347.

Edds, P.L., 1988. Characteristics of finback *Balaenoptera physalus* vocalizations in the St Lawrence estuary. Bioacoustics 1, 131–149.

Fiedler, P.C., Reilly, S.B., Hewitt, R.P., Demer, D., Philbrick, V.A., Smith, S., Armstrong, W., Croll, D.A., Tershy, B.R., Mate, B.R., 1998. Blue whale habitat and prey in the California Channel Islands. Deep-Sea Research II 45, 1781–1801.

Fox, C.G., Matsumoto, H., Lau, T.-K.A., 2001. Monitoring Pacific Ocean seismicity from an autonomous hydrophone array. Journal of Geophysical Research (Solid Earth) 106 (B3), 4183–4206.

Fraser, W.R., Trivelpiece, W.Z., Ainley, D.G., Trivelpiece, S.G., 1992. Increases in Antarctic penguin populations: reduced competition with whales or a loss of sea ice due to environmental warming? Polar Biology 11, 525–531.

Gaskin, D.E., 1982. The Ecology of Whales and Dolphins. Heinemann Educational Books Ltd., London, p. 459.

Hart, T.J., 1935. On the diatoms of the skin film of whales, and their possible bearing on problems of whale movements. Discovery Reports 10, 247–282.

Hofmann, E.E., Klinck, J.M., Lascara, C.M., Smith, D.A., 1996. Water mass distribution and circulation west of the Antarctic Peninsula and including Bransfield Strait. In: Ross, R.M., Hofmann, E.E., Quentin, L.B. (Eds.), Foundations for Ecological Research West of the Antarctic Peninsula, vol 70. American Geophysical Union, Washington, DC, pp. 61–80.

Holm-Hansen, O., Mitchell, B.G., 1991. Spatial and temporal distribution of phytoplankton and primary production in the western Bransfield Strait region. Deep-Sea Research 38, 961–980.

Horwood, J.S., 1986. The distribution of the Southern blue whale in relation to recent estimates of abundance. Scientific Reports of the Whales Research Institute 37, 155–165.

IWC, 2001. Report of the sub-committee on the comprehensive assessment of whale stocks—other stocks. Journal of Cetacean Research and Management 3 (Suppl), 209–228.

Kahru, M., 2000. Windows Image Manager—Image display and analysis program for Microsoft Windows with special features for satellite images, WWW page, http://wimsoft.com.

Kasamatsu, F., Hembree, D., Joyce, G., Tsunoda, L., Rowlett, R., Nakano, T., 1988. Distribution of cetacean sightings in the Antarctic: results obtained from the IWC/IDCR minke whale assessment cruises, 1978/79 to 1983/84. Report of the International Whaling Commission 39, 449 473.

Kasamatsu, F., Joyce, G.G., Ensor, P., Mermoz, J., 1996. Current occurrence of baleen whales in Antarctic waters. Report of the International Whaling Commission 47, 293–304.

Katona, S.K., Beard, J.A., 1990. Population size, migrations and feeding aggregations of the humpback whale (*Megaptera novaeangliae*) in the western North Atlantic Ocean. Report of the International Whaling Commission 12 (Special issue), 295–305.

Kawamura, A., 1980. A review of food of Balaenopterid whales. Scientific reports of the Whales Research Institute 32, 155–197.

Kawamura, A., 1994. A review of baleen whale feeding in the Southern Ocean. Report of the International Whaling Commission 44, 261–271.

Kellogg, R., 1929. What is known of the migrations of some of the whalebone whales. Smithsonian Institution Annual Report 1928, 467–496.

Laws, R.M., 1961. Reproduction, growth and age of southern fin whales. Discovery Reports 31, 327–486.

Ljungblad, D., Clark, C.W., Shimada, H., 1998. A comparison of sounds attributed to pygmy blue whales (*Balaenoptera musculus brevicauda*) recorded south of the Madagascar Plateau and those attributed to 'true' blue whales (*Balaenoptera musculus*) recorded off Antarctica. Report of the International Whaling Commission 49, 439–442.

Loeb, V., Siegel, V., Holm-Hansen, O., Hewitt, R., Fraser, M., Trivelpiece, W., Trivelpiece, S., 1997. Effects of sea-ice extent and krill or salp dominance on the Antarctic food web. Nature 387, 897–900.

Mackintosh, N.A., 1965. The Stocks of Whales. Fishing News (Books) Ltd., London, p. 232.

Mackintosh, N.A., 1966. The distribution of southern blue and fin whales. In: Norris, K.S. (Ed.), Whales, Dolphins, and Porpoises. University of California Press, Berkeley, pp. 125–144.

Mackintosh, N.A., Brown, S.G., 1956. Preliminary estimates of the southern populations of the larger baleen whales. Norsk Hvalfangst-Tidende 45, 469–480.

Mackintosh, N.A., Wheeler, J.F.G., 1929. Southern blue and fin whales. Discovery Reports 1, 257–540.

Mate, B.R., Lagerquist, B.A., Calambokidis, J., 1999. Movements of North Pacific blue whales during the feeding season off Southern California and their southern fall migration. Marine Mammal Science 15, 1246–1257.

Matsuoka, K., Murase, H., Nishiwaki, S., Fukuchi, T., Shimada, H., 2000. Development of a retrievable sonobuoy system for whale sounds recording in polar region. Presented to the IWC Scientific Committee (unpublished), 7pp.

McDonald, M.A., Hildebrand, J.A., Webb, S.C., 1995. Blue and fin whales observed on a seafloor array in the Northeast Pacific. The Journal of the Acoustical Society of America 98, 1–10.

McDonald, M.A., Calambokidis, J., Teranishi, A.M., Hildebrand, J.A., 2001. The acoustic calls of blue whales off California with gender data. The Journal of the Acoustical Society of America 109, 1728–1735.

Mellinger, D. K., 2001. Ishmael 1.0 User's Guide. NOAA Technical Memorandum OAR PMEL-120, available from NOAA/PMEL, 7600 Sand Point Way NE, Seattle, WA 98115-6349

Mellinger, D.K., Clark, C.W., 2000. Recognizing transient low-frequency whale sounds by spectrogram correlation. The Journal of the Acoustical Society of America 107, 3518–3529.

Mizroch, S.A., Rice, D.W., Breiwick, J.M., 1984. The blue whale, *Balaenoptera musculus*. Marine Fisheries Review 46 (4), 15–19.

Murase, H., Matsuoka, K., Ichii, T., Nishiwaki, S., 2002. Relationship between the distribution of euphausiids and baleen whales in the Antarctic (35 E–145W). Polar Biology 25, 135–145.

Nemoto, T., 1957. Foods of baleen whales in the Northern Pacific. Scientific Reports of the Whales Research Institute 12, 33–89.

Nicol, S., Pauly, T., Bindoff, N.L., Wright, S., Thiele, D., Hosie, G.W., Strutton, P.G., Woehler, E., 2000. Ocean circulation off east Antarctica affects ecosystem structure and sea-ice extent. Nature 406, 504–507.

Norris, T.F., McDonald, M., Barlow, J., 1999. Acoustic detections of singing humpback whales (*Megaptera novaeangliae*) in the eastern North Pacific during their northbound migration. The Journal of the Acoustical Society of America 106, 506–514.

Reid, K., Brierley, A.S., Nevitt, G.A., 2000. An initial examination of relationships between the distribution of whales and Antarctic krill *Euphausia superba* at South Georgia. Journal of Cetacean Research and Management 2, 143–149.

Reilly, S.B., Thayer, V.G., 1990. Blue whale (*Balaenoptera musculus*) distribution in the Eastern Tropical Pacific. Marine Mammal Science 6, 265–277.

Ross, R.M., Quentin, L.B., 1996. Distribution of Antarctic krill and dominant zooplankton west of the Antarctic Peninsula. In: Ross, R.M., Hofmann, E.E., Quentin, L.B. (Eds.), Foundation for Ecological Research West of the Antarctic

Peninsula, vol 70. American Geophysical Union, Washington, DC, pp. 199 217.

Siegel, V., 1988. A concept of seasonal variation of krill (*Euphausia superba*) distribution and abundance west of the Antarctic Peninsula. In: Sahrhage, D. (Ed.), Antarctic Ocean and Resources Variability. Springer, Berlin Heidelberg, pp. 219–230.

Smith, W.O., Nelson, D.M., 1985. Phytoplankton bloom produced by a receding ice-edge in the Ross Sea: spatial coherence with the density. Science 277, 163–167.

Springer, A.M., Piatt, J.F., Shuntov, V.P., Van Vliet, G.B., Vladimirov, V.L., Kuzin, A.E., Perlov, A.S., 1999. Marine birds and mammals of the Pacific Subarctic Gyres. Progress in Oceanography 43, 443–487.

Stafford, K.M., Fox, C.G., Clark, D.S., 1998. Long-range acoustic detection and localization of blue whale calls in the northeast Pacific Ocean. The Journal of the Acoustical Society of America 104, 3616–3625.

Stafford, K.M., Nieukirk, S.L., Fox, C.G., 1999a. Low-frequency whale sounds recorded on hydrophones moored in the eastern tropical Pacific. The Journal of the Acoustical Society of America 106, 3687–3698.

Stafford, K.M., Nieukirk, S.L., Fox, C.G., 1999b. An acoustic link between blue whales in the Eastern Tropical Pacific and the Northeast Pacific. Marine Mammal Science 15, 1258–1268.

Stafford, K.M., Nieukirk, S.L., Fox, C.G., 2001. Geographic and seasonal variation of blue whale calls in the North Pacific. Journal of Cetacean Research and Management 3, 65–76.

Stammerjohn, S.E., Smith, R.C., 1996. Spatial and temporal variability of western Antarctic Peninsula sea ice coverage. In: Ross, R.M., Hofmann, E.E., Quentin, L.B. (Eds.), Foundations for Ecological Research West of the Antarctic Peninsula, Vol. 70. American Geophysical Union, Washington DC, pp. 81 104.

Thompson, P., Findley, L.T., Vidal, O., 1992. 20-Hz pulses and other vocalizations of fin whales, *Balaenoptera physalus*, in the Gulf of California, Mexico. The Journal of the Acoustical Society of America 92, 3051–3057.

Tynan, C.T., 1998. Ecological importance of the southern boundary of the Antarctic Circumpolar Current. Nature 392, 708–710.

Watkins, W.A., 1981. Activities and underwater sounds of fin whales. Scientific reports of the Whales Research Institute 33, 83 117.

Watkins, W.A., Tyack, P., Moore, K.E., Bird, J.E., 1987. The 20-Hz signal of finback whales (*Balaenoptera physalus*). The Journal of the Acoustical Society of America 82, 1901 1912.

Watkins, W.A., Daher, M.A., Reppucci, G.M., George, J.E., Martin, D.L., DiMarzio, N.A., Gannon, D.P., 2000. Seasonality and distribution of whale calls in the North Pacific. Oceanography 13, 62–67.

Whitehead, H., Glass, C., 1985. The significance of the Southeast Shoal of the Grand Bank to humpback whales and other cetacean species. Canadian Journal of Zoology 63, 2617–2625.

Wiggins, S., 2003. Autonomous Acoustic Recording Packages (ARPs) for long-term monitoring of whale sounds. Marine Technology Society Journal 37 (2), 13–22.

ANNOUNCING

Interhemispheric Water Exchange in the Atlantic Ocean

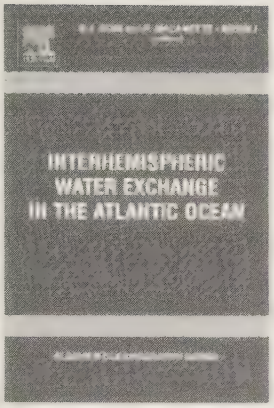

Year 2003
Hardbound
ISBN: 0-444-51267-5
524 pages
EUR 179 / USD 179

Elsevier
Regional Sales Office
Customer Service Department
11830 Westline Industrial Drive
St. Louis, MO 63146, USA
for US customers
Tel: (+1) 800 545 2522
Fax: (+1) 800 535 9935
for customers outside US
Tel: (+1) 800 460 3110
Fax: (+1) 314 453 7095
E-mail: usbkinfo@elsevier.com

Elsevier
Regional Sales Office
Customer Service Department
Linacre House Jordan Hill
Oxford OX2 8DP, UK
Tel: +44 1865 474140
Fax: +44 1865 474141
Email:
amstbkinfo@elsevier.com

ELSEVIER

Elsevier Oceanography Series, Volume 68

Edited by
G.J. Goni, *National Oceanic and Atmospheric Administration, Atlantic Oceanographic and Meteorological Laboratory, Miami, FL, USA*
P.M. Rizzoli, *Massachusetts Institute of Technology, Department of Earth, Atmospheric and Planetary Sciences, Cambridge, MA, USA*

Recent results from modeling and observational studies demonstrate that the tropical Atlantic is a critical region for processes that maintain the meridional overturning circulation, such as cross-equatorial exchanges, and for sea surface temperature variability that impacts on climate variability of the coupled tropical ocean/atmosphere system.

The theme of this book is the inter-hemispheric and inter-gyre exchanges of heat, salt and fresh water, while its goal is to improve the knowledge of the tropical Atlantic dynamics and how it affects the global ocean. A clear understanding of the dynamics of processes that affect the flow of mass and heat between the southern and the northern hemispheres in the upper few hundred meters in the tropical Atlantic and of those associated to the ocean circulation or to surface signals, from decadal, inter-annual to mesoscale periods, becomes necessary to better evaluate their contribution to the interhemispheric mass exchange. These processes are believed to be largely responsible in driving the sea surface temperature, which in turn, is a critical parameter to investigate ocean-atmospheric interactions. Output produced by regional models is also used to complement the observations and to provide additional information on their spatial and temporal variability. The subtropical cells, by bringing water masses subducted in the subtropics to the equator, and zonal currents investigated here contribute to the interhemispheric water exchange.

Special attention is also given to the warm and salty anticyclonic rings shed by the North Brazil Current, which are now known to have a much broader impact, not only on interhemispheric water mass transfer, but also on the environment of remote regions. Observations from different sources are blended together, are used to validate model outputs and are also assimilated into models to obtain a more complete and accurate picture of the oceanic circulation and of its time evolution.

Further information, full contents and ordering details available online at:
www.elsevier.com/locate/isbn/0444512675

ANNOUNCING

Principles and Standards for the Disposal of Long-lived Radioactive Wastes

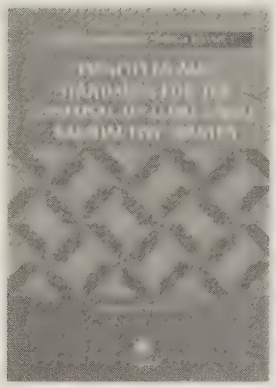

Waste Management Series, 3

By

N. Chapman, *Department of Civil Structural Engineering, University of Sheffield, UK*

C. McCombie, *McCombie Consulting, Switzerland*

This handbook is concerned with developing principles and standards for the safe disposal of solid radioactive wastes by burial deep in the Earth's crust. Radioactive wastes have focussed thinking on long-term environmental protection issues in an unprecedented way. Consequently, the way in which principles and standards are set, and the thinking behind this, is of wider interest than to the nuclear field alone. The issues are not just technical and scientific. There is also a much wider philosophical context to the debate, centering on ethics, human values and the expectations of society.

In this handbook it is intended that all theses issues are brought together, suggesting appropriate ways forward in each area, culminating in a proposed structure for safety regulations. It also aims to provide a detailed discussion of some of the most difficult logical an ethical issues facing those wishing to dispose of long-lived radioactive wastes.

Year 2003 Hardbound

ISBN: 0-08-044192-0

250 pages

Price: EUR 140 / USD 140

Elsevier
Regional Sales Office
Customer Service Department
11830 Westline Industrial Drive
St. Louis, MO 63146, USA
for US customers
Tel: (+1) 800 545 2522
Fax: (+1) 800 535 9935
for customers outside US
Tel: (+1) 800 460 3110
Fax: (+1) 314 453 7095
E-mail: usbkinfo@elsevier.com

Elsevier
Regional Sales Office
Customer Service Department
Linacre House Jordan Hill
Oxford OX2 8DP, UK
Tel: +44 1865 474140
Fax: +44 1865 474141
Email:
amstbkinfo@elsevier.com

Contents

Preface.

1. Introduction.
2. Safety and security issues in deep geological disposal.
3. Ethics.
4. Reversibility and retrievability.
5. Timescales in repository evolution.
6. Performance measures and appropriate standards.
7. Siting requirements within standards.
8. Natural disruptive events and processes.
9. Intrusion by future generations.
10. Monitoring and controlling a repository before and after closure.
11. Preserving records of the existence of a repository.
12. Accounting for uncertainty.
13. Chemotoxicity and radiotoxicity: A common framework?
14. Setting new standards.
15. Conclusions.
16. References.

Appendix I.

Appendix II.

List of Acronyms.

Further information, full contents and ordering details available online at: www.elsevier.com/locate/isbn/0080441920

ELSEVIER

Deep-Sea Research Part II – Instructions to Authors

A more detailed set of instructions can be found in the journal's home page at http://www.elsevier.com/locate/dsr2

1. Submission of Papers

Authors are requested to submit their original manuscript and figures with two copies to the Guest Editor of their Special Issue. Authors should ensure that they submit manuscripts and meet any additional requirements in line with deadlines set by the Guest Editor(s) to ensure that the entire issue can be published in a timely fashion. In most instances, revised manuscripts must be resubmitted within six months of receipt by the author. Failure to do so may lead to additional review, in some instances, rejection of the paper. Submission of a paper implies that it has not been published previously, that it is not under consideration for publication elsewhere, and that if accepted it will not be published elsewhere in the same form, in English or in any other language, without the written consent of the publisher.

2. Manuscript Preparation

General: Manuscripts must be typewritten, double-spaced with wide margins on one side of white paper. Good quality printouts with a font size of 12 or 10 pt are required. The corresponding author should be identified (include a Fax number and E-mail address). Full postal addresses must be given for all co-authors. Authors should consult a recent issue of the journal for style if possible. An electronic copy of the paper should accompany the final version. The Editors reserve the right to adjust style to certain standards of uniformity. Authors should retain a copy of their manuscript since we cannot accept responsibility for damage or loss of papers. Original manuscripts are discarded one month after publication unless the Publisher is asked to return original material after use.

Paper Length: Authors should try to confine the text to no more than 25–30 pages, with a total manuscript length (including figures and tables) of 45–50 pages.

Abstracts: The essential contents of each paper should be recapitulated briefly in an abstract of no more than 500 words at the head of the paper.

Keywords: Please provide up to six subject keywords, plus regional index terms. At least four of the subject keywords should be selected from the *Aquatic Science & Fisheries Thesaurus*. An eletronic version of the Thesaurus can be found at: http://www.csa.com/ helpV3/ ab.html. The Regional terms should be provided as a hierarchical string, eg; USA, California, Monterey Bay.

Text: Follow this order when typing manuscripts: Title, Authors, Affiliations, Abstract, Keywords, Main text, Acknowledgements, Appendix, References, Vitae, Figure Captions and then Tables. The corresponding author should be identified with an asterisk and footnote. All other footnotes (except for table footnotes) should be identified with superscript Arabic numbers.

Units: In general, metric units should be used, preferably the Systeme International (SI). If other units are used (fathoms, F, knots, etc), the metric equivalents must be given in parentheses ( ) or by presenting the dimensionally correct conversion factors as a footnote.

References: All publications cited in the text should be presented in a list of references following the text of the manuscript. In the text refer to the author's name (without initials) and year of publication (e.g. "Since Peterson (1993) has shown that ..." or "This is in agreement with results obtained later (Kramer, 1994)". For three or more authors use the first author followed by "et al.", in the text. The list of references should be arranged alphabetically by authors' names. The manuscript should be carefully checked to ensure that the spelling of authors' names and dates are exactly the same in the text as in the reference list. The title of the journal should not be abbreviated; titles of journals in Russian language should be transliterated and not translated. References should be given in the following form:

Gooday, A.J., Bett, B.J., Shires, R., Lambshead, P.J.D., 1998. Deep-sea benthic foraminiferal species diversity in the NE Atlantic and NW Arabian Sea: a synthesis. Deep-Sea Research Part II 45 (1–3), 165–201.

Hessler, R.R., Wilson, G.D.F., 1983. The origin and biogeography of malacostracan crustaceans in the deep sea. In: Sims, R.W., Price, J.H., Whalley, P.E.S. (Eds.), Evolution, time and space: the emergence of the biosphere. Academic Press. London, pp. 227–254. Thiel, H., 1983. Benthos size classification. Deep-Sea Newsletter 20, 8–11.

References to unpublished literature should be set out in the format detailed below. The following information needs to be provided: Names and initials of all authors., year. Title of work. All other relevant information needed to identify items (e.g., technical report, Ph.D. Thesis, institute, current status, i.e. in press/unpublished, etc).

Marstakas, N., 1990. Relationships of morphological and physicochemical properties of vertisols under Greek climate conditions. Ph.D. Thesis, Agricultural University Athens, unpublished.

Examples of appropriate citation formats for non-text and electronic-only information can be found in the Guide for Authors at the Deep-Sea Research Part II website. However, it is requested that a web site address, or listserver message is given as a reference only where the information is unavailable in a more permanent form. If such sources are given, then please give as complete information as is possible. All references to such material in the text of the article must be supported by a full entry in the bibliography.

Illustrations: All illustrations should be provided in camera-ready form, suitable for reproduction (which may include reduction) without retouching. Photographs, charts and diagrams are all to be referred to as "Figure(s)" and should be numbered consecutively in the order to which they are referred. They should accompany the manuscript, but should not be included within the text. All illustrations should be clearly marked on the back with the figure number and the author's name. All figures are to have a caption. Captions should be supplied on a separate sheet.

Line drawings: Good quality printouts on white paper produced in black ink are required. All lettering, graph lines and points on graphs should be sufficiently large and bold to permit reproduction when the diagram has been reduced to a size suitable for inclusion in the journal. Dye-line prints or photocopies are not suitable for reproduction. Do not use any type of shading on computer-generated illustrations.
Photographs: Original photographs must be supplied as they are to be reproduced (e.g. black and white or colour). If necessary, a scale should be marked on the photograph. Please note that photocopies of photographs are not acceptable. Half-tone illustrations should be kept to a minimum.
Fold-charts: The cost of fold-charts or diagrams must be borne by the author or his institution. *Colour:* Authors will be charged for colour reproduction as follows: €350 (or US$350) for the first page, €175 (or US$175) for subsequent pages.
Submit colour illustrations as original photographs, high-quality computer prints or transparencies, close to the size expected in publication, or as 35 mm slides. Polaroid colour prints are not suitable. If, together with your accepted article, you submit usable colour figures then Elsevier will ensure, at no additional charge, that these figures will appear in colour on the web (e.g., ScienceDirect and other sites) regardless of whether or not these illustrations are reproduced in colour in the printed version. For colour reproduction in print, you will receive information regarding the costs from Elsevier after receipt of your accepted article. For further information on the preparation of electronic artwork, please see *Artwork Instructions*. Please note: Because of technical complications which can arise by converting colour figures to 'grey scale' (for the printed version should you not opt for colour in print) please submit in addition usable black and white prints corresponding to all the colour illustrations.
Tables: Tables should be numbered consecutively and given a suitable caption and each table typed on a separate sheet. Footnotes to tables should be typed below the table and should be referred to by superscript lowercase letters. No vertical rules should be used. Tables should not duplicate results presented elsewhere in the manuscript, (e.g. in graphs).

Authors in Japan kindly note: Upon request Elsevier Japan will provide a list of people who can check and improve the English of an article (*before submission*). Please contact our Tokyo office: Elsevier Japan K.K., 1-9-15 Higashi Azabu, Minato-ku, Tokyo 106-0044, Japan; tel.: +81-3-5561-5032; fax: +81-3-5561-5045; e-mail: jp.info@elsevier.com

3. Electronic Submission
Authors should submit an electronic copy of their paper with the final version of the manuscript. The electronic copy should match the hardcopy exactly. For authors using LaTex, the document style files, as well as the instructions "Preparing articles with LaTex" in the form of a dvi file, can be obtained free of charge from any host on the Comprehensive Tex Archive Network (CTAN) using anonymous ftp. The primary CTAN hosts are ftp.dante.de and ftp.tex.ac.uk. The Elsevier macros are in /pub/tex/macros/latex/contrib/supported/elsevier. These can also be downloaded from the Internet site http://www.tex.ac.uk. Always keep a back up copy of the electronic file for reference and safety. Full details of electronic submission and other formats can be obtained from http://authors.elsevier.com or from Author Support at Elsevier.

4. Proofs
Proofs will be sent to the author (first named author if no corresponding author is identified of multi-authored papers) and should be returned within 48 hours of receipt. Corrections should be restricted to typesetting errors; any others may be charged to the author. Any queries should be answered in full. Please note that authors are urged to check their proofs carefully before return, since the inclusion of late corrections cannot be guaranteed. If authors are expecting to be away from their office when the proofs arrive, arrangements should be made with colleagues for the proofs to be checked in the authors absence. Proofs are to be returned to the Log-in Department, Elsevier, Stover Court, Bampfylde Street, Exeter, Devon EX1 2AH, UK.

5. Offprints
Twenty-five offprints and a copy of the issue will be supplied free of charge to each corresponding author of a paper. Additional offprints can be ordered at a specially reduced rate using the order form sent to the corresponding author after the manuscript has been accepted. Orders for reprints will incur a 50% surcharge.

6. Copyright
All authors must sign the "Transfer of Copyright" agreement before the article can be published. This transfer agreement enables Elsevier Ltd to protect the copyrighted material for the authors, but does not relinquish the author's proprietary rights. The copyright transfer covers the exclusive rights to reproduce and distribute the article, including reprints, photographic reproductions, microfilm or any other reproductions of similar nature and translations. Includes the right to adapt the article for use in conjunction with computer systems and programs, including reproduction or publication in machine-readable form and incorporation in retrieval systems. Authors are responsible for obtaining from the copyright holder permission to reproduce any figures for which copyright exists.

7. Author Enquiries
For enquiries relating to the submission of articles (including electronic submission), the preparation of electronic artwork, the status of accepted articles, author Frequently Asked Questions and any other enquiries relating to Elsevier Science, please consult http://authors.elsevier.com
Contact details for questions arising after acceptance of an article, especially those relating to proofs, are provided when an article is accepted for publication.
Authors can also keep a track on the progress of their accepted article, and setup e-mail alerts informing them of changes to their manuscripts status, by using the "Track a paper" feature of Elsevier's Author gateway (http://authors.elsevier.com).

DEEP-SEA RESEARCH II, Vol. 51, Nos. 17–19

(*Continued from outside back cover*)

		Krill feeding, growth, development, and overwintering studies
M. Zhou and R.D. Dorland	2119	Aggregation and vertical migration behavior of *Euphausia superba*
K.L. Daly	2139	Overwintering growth and development of larval *Euphausia superba*: an interannual comparison under varying environmental conditions west of the Antarctic Peninsula
R.M. Ross, L.B. Quetin, T. Newberger and S.A. Oakes	2169	Growth and behavior of larval krill (*Euphausia superba*) under the ice in late winter 2001 west of the Antarctic Peninsula
E.A. Pakhomov, A. Atkinson, B. Meyer, B. Oettl and U. Bathmann	2185	Daily rations and growth of larval krill *Euphausia superba* in the Eastern Bellingshausen Sea during austral autumn
S.-J. Ju and H.R. Harvey	2199	Lipids as markers of nutritional condition and diet in the Antarctic krill *Euphausia superba* and *Euphausia crystallorophias* during austral winter
S. Nicol, P. Virtue, R. King, S.R. Davenport, A.F. McGaffin and P. Nichols	2215	Condition of *Euphausia crystallorophias* off East Antarctica in winter in comparison to other seasons
J. Donnelly, H. Kawall, S.P. Geiger and J.J. Torres	2225	Metabolism of Antarctic micronektonic crustacea across a summer ice-edge bloom: respiration, composition, and enzymatic activity
		Krill predator studies: seabirds, seals, whales, and midwater fish
T.M. Lancraft, K.R. Reisenbichler, B.H. Robison, T.L. Hopkins and J.J. Torres	2247	A krill-dominated micronekton and macrozooplankton community in Croker Passage, Antarctica with an estimate of fish predation
E.W. Chapman, C.A. Ribic and W.R. Fraser	2261	The distribution of seabirds and pinnipeds in Marguerite Bay and their relationship to physical features during austral winter 2001
J.M. Burns, D.P. Costa, M.A. Fedak, M.A. Hindell, C.J.A. Bradshaw, N.J. Gales, B. McDonald, S.J. Trumble and D.E. Crocker	2279	Winter habitat use and foraging behavior of crabeater seals along the Western Antarctic Peninsula
N.J. Gales, W.R. Fraser, D.P. Costa and C. Southwell	2305	Do crabeater seals forage cooperatively?
D. Thiele, E.T. Chester, S.E. Moore, A. Širovic, J.A. Hildebrand and A.S. Friedlaender	2311	Seasonal variability in whale encounters in the Western Antarctic Peninsula
A. Širović, J.A. Hildebrand, S.M. Wiggins, M.A. McDonald, S.E. Moore and D. Thiele	2327	Seasonality of blue and fin whale calls and the influence of sea ice in the Western Antarctic Peninsula

CONTENTS Direct

This journal is part of **ContentsDirect**, the *free* alerting service which sends tables of contents by e-mail for Elsevier books and journals. You can register for **ContentsDirect** online at: **www.elsevier.com/locate/contentsdirect**

Indexed/abstracted in: *Curr Cont/Agri Bio Env Sci. Cirr Cont/Phys. Chem. Earth Sci, Curr Cont Sci Cit Ind, Res Alert, Global Change, Curr Aware BioSci, Geobase, Ocean Lit Rev, Awuat Sci. Fish Abstr, Meteor, Geoastrophys Abstr*

ISSN 0967–0645

ELSEVIER

DEEP-SEA RESEARCH PART II

Topical Studies in Oceanography

Integrated Ecosystem Studies of Western Antarctic Peninsula Continental Shelf Waters and Related Southern Ocean Regions

Volume 51, Numbers 17–19, 2004

CONTENTS

		Editorial
E.E. Hofmann, P.H. Wiebe, D.P. Costa and J.J. Torres	1921	An overview of the Southern Ocean Global Ocean Ecosystems Dynamics program
		The Physical/Biological Setting
J.M. Klinck, E.E. Hofmann, R.C. Beardsley, B. Salihoglu and S. Howard	1925	Water-mass properties and circulation on the west Antarctic Peninsula Continental Shelf in Austral Fall and Winter 2001
R.C. Beardsley, R. Limeburner and W.B. Owens	1947	Drifter measurements of surface currents near Marguerite Bay on the western Antarctic Peninsula shelf during austral summer and fall, 2001 and 2002
S.L. Howard, J. Hyatt and L. Padman	1965	Mixing in the pycnocline over the western Antarctic Peninsula shelf during Southern Ocean GLOBEC
Y.M. Serebrennikova and K.A. Fanning	1981	Nutrients in the Southern Ocean GLOBEC region: variations, water circulation, and cycling
M.S. Dinniman and J.M. Klinck	2003	A model study of circulation and cross-shelf exchange on the west Antarctic Peninsula continental shelf
D.K. Perovich, B.C. Elder, K.J. Claffey, S. Stammerjohn, R. Smith, S.F. Ackley, H.R. Krouse and A.J. Gow	2023	Winter sea-ice properties in Marguerite Bay, Antarctica
G.L. Lawson, P.H. Wiebe, C.J. Ashjian, S.M. Gallager, C.S. Davis and J.D. Warren	2041	Acoustically-inferred zooplankton distribution in relation to hydrography west of the Antarctic Peninsula
C.J. Ashjian, G.A. Rosenwaks, P.H. Wiebe, C.S. Davis, S.M. Gallager, N.J. Copley, G.L. Lawson and P. Alatalo	2073	Distribution of zooplankton on the continental shelf off Marguerite Bay, Antarctic Peninsula, during Austral Fall and Winter, 2001
M. Zhou, Y. Zhu and J.O. Peterson	2099	In situ growth and mortality of mesozooplankton during the austral fall and winter in Marguerite Bay and its vicinity

(*Continued on inside back cover*)

Visit our home page:
http://www.elsevier.com/locate/dsr2

Printed in Great Britain by Alden Press Ltd., Osney Mead, Oxford OX2 OEF
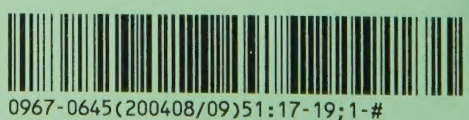
Also available on
SCIENCE DIRECT®
www.sciencedirect.com